**WSRC-TR-95-0057**
Rev.0
September 1995

# Site Geotechnical Services (SGS)

# In-Tank Precipitation Facility (ITP) and H-Tank Farm (HTF) Geotechnical Report (U)

**Site Geotechnical Services Department**

**UNCLASSIFIED**
DOES NOT CONTAIN
UNCLASS. D CONTROLLED
NUCLEAR INFORMATION
ADC & Reviewing Official C.B. Reeves, RO.
(Name and Title)
Date: 9/29/95

**Westinghouse Savannah River Company**
**Savannah River Site**
**Aiken, SC 29808**

PREPARED FOR THE U.S. DEPARTMENT OF ENERGY UNDER CONTRACT DE-AC09-89R18035

SAFETY • RESPONSIBILITY • SECURITY
SRS
SAVANNAH RIVER SITE

## DISCLAIMER

**This report was prepared as an account of work sponsored by an agency of the United States Government. Neither the United States Government nor any agency Thereof, nor any of their employees, makes any warranty, express or implied, or assumes any legal liability or responsibility for the accuracy, completeness, or usefulness of any information, apparatus, product, or process disclosed, or represents that its use would not infringe privately owned rights. Reference herein to any specific commercial product, process, or service by trade name, trademark, manufacturer, or otherwise does not necessarily constitute or imply its endorsement, recommendation, or favoring by the United States Government or any agency thereof. The views and opinions of authors expressed herein do not necessarily state or reflect those of the United States Government or any agency thereof.**

**DISCLAIMER**

**Portions of this document may be illegible in electronic image products. Images are produced from the best available original document.**

WSRC-TR--95-0057-Vol.1

RECEIVED
NOV _ 8 1995
OSTI

Volume 1

*Executive Summary, Table Of Contents, Report, Tables, and Figures*

# In-Tank Precipitation Facility (ITP) and H-Tank Farm (HTF) Geotechnical Report (U) WSRC-TR-95-0057, Rev. 0

**DISCLAIMER**

This report was prepared as an account of work sponsored by an agency of the United States Government. Neither the United States Government nor any agency thereof, nor any of their employees, makes any warranty, express or implied, or assumes any legal liability or responsibility for the accuracy, completeness, or usefulness of any information, apparatus, product, or process disclosed, or represents that its use would not infringe privately owned rights. Reference herein to any specific commercial product, process, or service by trade name, trademark, manufacturer, or otherwise does not necessarily constitute or imply its endorsement, recommendation, or favoring by the United States Government or any agency thereof. The views and opinions of authors expressed herein do not necessarily state or reflect those of the United States Government or any agency thereof.

MASTER

DLC

Project: In-Tank Precipitation (ITP) Facility

Document: WSRC-TR-95-0057, Rev. 0

Title: In-Tank Precipitation Facility (ITP) and H-Tank Farm (HTF) Geotechnical Report (U).

Approvals:

M. R. Lewis, Manager, Geotechnical Engineering, SGS Department — Date 9/28/95

L. A. Salomone, Site Chief Geotechnical Engineer, SGS Department — Date 9/29/95

**Peer Review of Savannah River Site**
**In Tank Precipitation Facility (ITP) and H-Tank Farm (HTF)**
**Geotechnical Investigation**

## Background

In accordance with the memorandum from Mr. Brent J. Gutierrez, US Department of Energy (DOE) Savannah River, dated August 19, 1993, a geotechnical peer review panel was established for the geotechnical investigation at the In Tank Precipitation Facility (ITP) and H-Tank Farm (HTF) Savannah River Site (SRS), South Carolina. Our panel's general assignment was to review the approach, methods, and results of the seismic stability evaluation of the facilities' foundation and embankments performed by DOE, Westinghouse, and Bechtel for the Seismic Safety Issues Resolution Program.

During the period October 1993 through September 1995 six peer review meetings were held. The first two meetings were held at SRS, October 13, 1993, and December 6-7, 1993. Professors Mitchell and Sowers attended an ad hoc program meeting in San Francisco, April 12-13, 1994, which preceded the third peer review meeting held in Atlanta, April 26-27, 1994. The fourth meeting was at SRS, September 27-28, 1994. The fifth and then the final meeting were held in Atlanta, December 20, 1994 and September 11, 1995, respectively. These meetings and resulting correspondence allowed us to adequately review the approach, methods, and results developed throughout this investigation, culminating with our review of the final draft report, "In Tank Precipitation Facility (ITP) and H-Tank Farm (HTF) Geotechnical Report," WSRC-TR-95-0057.

## Review Summary

The specific objectives of our panel were to review (1) characterization of the subsurface, with special attention to the carbonate feature, (2) sampling, (3) testing, (4) interpretation of results, (5) liquefaction potential analyses, (6) settlement estimates, and (7) stability of the fill surrounding the tanks. During the two year duration of this project, we have visited the site, examined outcrops of the upper formations, listened to verbal presentations of the methods adopted, and have been furnished interim reports addressing the objectives of the ITP/ HTF investigation. We have responded verbally in the meetings and in writing to the reports submitted and to the draft of the final report. Our criticisms and comments have been acted upon and many of our recommendations have been incorporated in the final report.

We agree with the approach, methods, and findings presented in the final report. The approach used state-of-the-knowledge and state-of-the-art engineering, with appropriate and reasonably conservative assumptions where needed.

We thank the program engineers and scientists who were very forthright and cooperative with our inquiries and responsive to our reviews. We appreciated this opportunity to serve as peer reviewers for this technically challenging and interesting investigation and look forward to future interaction.

Our joint signature page follows.



W. F. Marcuson, III, Ph.D., P.E.
Chief, Geotechnical Laboratory
Waterways Experiment Station

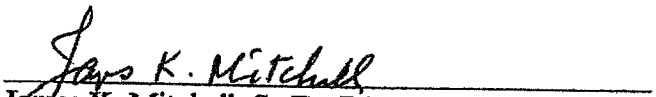

James K. Mitchell, Sc.D., P.E.
Geotechnical Engineer

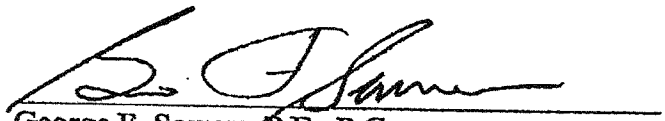

George F. Sowers, P.E., P.G.
Senior Geotechnical Consultant
Law Companies Group, Inc.

**Disclaimer**

This report was prepared as an account of work sponsored by an agency of the United States Government. Neither the United States Government nor any agency thereof, nor any of their employees, makes any warranty, express or implied, or assumes any legal liability or responsibility for the accuracy, completeness, or usefulness of any information, apparatus, product, or process disclosed, or represents that its use would not infringe privately owned rights. Reference herein to any specific commercial product, or process or service by the trade name, trademark, manufacturer, or otherwise, does not necessarily constitute or imply its endorsement, recommendation, or favoring by the United States Government or any agency thereof. The views and opinions of authors expressed herein do not necessarily state or reflect those of the United States Government or any agency thereof.

# EXECUTIVE SUMMARY

A geotechnical study has been completed in H-Area for the In-Tank Precipitation Facility (ITP) and the balance of the H-Area Tank Farm (HTF) at the Savannah River Site (SRS) in South Carolina. The study consisted of subsurface field exploration, field and laboratory testing, and engineering analyses. The purpose of these investigations is to evaluate the overall stability of the H-Area tanks under static and dynamic conditions. The objectives of the study are to define the site-specific geological conditions at ITP and HTF, obtain engineering properties for the assessment of the stability of the native soils and embankment under static and dynamic loads (i.e., slope stability, liquefaction potential, and potential settlements), and derive properties for soil-structure interaction studies. This work was done in compliance with DOE Order 6430.1A (DOE, 1992a).

## Background

The HTF is located in what is called the "General Separations Area" (GSA) of the central part of SRS (see Figure ES-1). It consists of 29 waste storage tanks constructed on relatively level ground (average elevation about 295 to 300 feet, Mean Sea Level (MSL)) within an embankment fill built up to approximately elevation 328 to 335 feet, MSL (hereafter, all elevations are with respect to MSL). The embankment fill slopes are constructed at two horizontal to one vertical.

The original scope of this investigation only included ITP, which is located in the southeast part of HTF (Figure ES-2). However, shortly after the program began, it was expanded to include all of HTF. This report is the culmination of that effort.

## Investigations

The field investigations and testing included the following:

- drilling 27 exploratory boreholes, to a maximum depth of 300 feet, from which samples were retrieved for laboratory testing,
- determining compression and shear wave velocities in three cross-hole geophysical arrays,
- geophysically logging six boreholes,
- completing 37 piezocone penetrometer test soundings, 34 of which were used to determine shear wave velocities using the down-hole technique,
- completing four dilatometer soundings,
- completing one down-hole refraction survey,
- completing one shallow high resolution seismic reflection survey,
- completing two panels of cross-hole seismic tomography and,
- incorporating 101 existing boreholes from previous investigations.

In the laboratory, representative samples of the various strata were classified with respect to their plasticity and gradation characteristics, natural water content, and density. Triaxial and consolidation tests were performed to define the strength and the compressibility of the soils under static loads. The dynamic properties (modulus and damping) of the various subsurface materials

were determined with a series of resonant column and strain-controlled cyclic triaxial tests. An extensive laboratory testing program was also carried out to determine the strength and deformation of the subsurface materials under dynamic loading.

### *Geology and Shallow Stratigraphy*

Eocene and Miocene sediments within the General Separations Area (GSA) (i.e., F-Area, H-Area, and the Burial Grounds) consist of unconsolidated deposits of sands, and silty to clayey sands. Shallow sediments of the Altamaha, Tobacco Road, and Upper Dry Branch Formations are generally silty to clayey sands. Carbonate-rich horizons, of Eocene age, are found sporadically in the lower Dry Branch and underlying Santee Formations. These carbonate horizons are interspersed with sands and clays in a complex manner. In general, these carbonate buildups (layers) appear to be oriented northeast-southwest and parallel the strike of the coastal shoreline at the time of deposition.

The strata of the GSA, inclusive of the HTF area are interrupted by faults and/or slumps that are often found along the flanks of carbonate buildups. The association of faulting with carbonate sediments has three possible explanations. The first suggests raveling and local slumping of the predominately sandy sediments above carbonate buildups where differential dissolutioning and subsequent compaction of the carbonate interval occurred. The second alternative hypothesizes that postdepositional, tectonic faulting fracturing caused preferential dislocation of the strata. The third explanation, which is a combination of the first two, postulates that dissolutioning occcurred along these pre-existing faults in a manner determined by the fault geometry. Based on present information, all three of these mechanisms are plausible.

Weight of rod and occasional rod drops have occurred in calcareous sediments as described in numerous drilling reports for the GSA. Most of these "soft zones" are sediment-filled with a fine-grained sand. Also, the "soft zones" in the Santee/Tinker Formation are commonly associated with silicified "hard grounds," where hard drilling and high penetration resistances are found. It appears that the silicification formed during an unconformity at the end of Santee time, 40-43 million years before present (mybp) in proximity to the ancient water table. Similar hard and soft zones are found at ITP and are related to those described for the GSA.

Exploratory work completed during this investigation, supplemented with information from previous work in the HTF area, disclosed subsurface conditions similar to those encountered in the central part of SRS. However, zones within the structural fill compacted for the embankment around the tanks exhibited lower strengths than expected.

### *Embankment Fill and Slope Stability*

Extensive data were collected for evaluation of the structural fill surrounding the tanks. Fill strengths were determined from field and laboratory investigations. Earth pressures for structural analyses of the outer tank walls are presented in the report. Also, slope stability analyses of the embankment fill were performed for static and dynamic conditions. The results show that the

embankment slopes are stable for static and dynamic conditions with factors of safety greater than 1.5. The predicted slope deformation under the prescribed dynamic loading is negligible.

### *Liquefaction*

The late Eocene Tobacco Road Formation is about 40 million years old and is composed primarily of laminated, gap-graded, clayey sands deposited under alternating marginal marine and fluvial conditions. The clay, consisting of kaolinite and illite minerals, binds the sand grains and appears to have been formed by in situ weathering. The cone penetration test (CPT) tip resistances of this material range from less than 10 tons per square foot (tsf) to 160 tsf, and CPT friction ratios (sleeve resistance divided by tip resistance) range from less than 1% to over 10%. Corresponding Standard Penetration Test (SPT) N-Values range from less than 10 to over 20 blows per foot (bpf). Because of these relatively low penetration values, the potential for seismic liquefaction of the formation was recognized early in the investigation.

Subsequent detailed characterization of the Tobacco Road Formation indicated that its geologic genesis, age, and composition was distinctly different from recently deposited sands and silty sands from which the widely used empirical chart for liquefaction was developed (Seed, Tokimatsu, Harder, and Chung in 1984). Therefore, site-specific correlations and analyses were performed for ITP and HTF.

Five separate approaches were used for evaluating the liquefaction potential of the soils:

- Criteria for clayey soils
- Shear wave velocity
- Performance of old sand deposits
- Strength
- Strain method

For these evaluations, two surface spectra evaluation basis earthquakes (EBE), and one 84th percentile rock spectrum were utilized. The first EBE is a local event, characteristically represented by an earthquake of Magnitude 5 to 6 with a zero-period ground surface acceleration equal to 0.19 g. The second EBE is a distant event, characteristically represented by an earthquake of Magnitude 7.5 with a zero-period ground surface acceleration equal to 0.11 g. The 84th percentile rock motion represents an earthquake of Magnitude 7.5 with a zero period rock acceleration of 0.13 g. The following conclusions are drawn based on the liquefaction analyses:

- Application of the liquefaction criteria for clayey soils to the Tobacco Road and Dry Branch Formations shows that these soils are categorized as non-liquefiable.

- Field testing determined that the average shear wave velocity of the same soils is greater than 900 feet per second. Available empirical charts that relate shear wave velocity to liquefaction performance during earthquakes indicate that for this velocity, liquefaction is not expected to occur.

- Many factors are believed to be the result of soil aging, such as cementation, weathering (which chemically breaks down minerals into clays), increased exposure to low-level seismic shaking, cold bonding, and consolidation. All of these factors tend to increase the liquefaction resistance of sands. In addition, most of these factors tend to increase the CPT and SPT resistances. To study the importance of these factors on liquefaction resistance, the Charleston, South Carolina earthquake of 1886 was reviewed (Arango, Lewis and Kimball, 1994, in press). The results of this review and other studies (BSRI, 1993b), suggest that pre-Holocene deposits have a greater resistance to seismic liquefaction than Holocene (less than 10,000 years old) soil deposits. This conclusion was documented by Youd and Perkins (1978) and more recently in a study by Martin and Clough (1994) for the 1886 Charleston earthquake. Thus, it was concluded that exisitng empirical charts based on Holocene sands would not adequately represent the liquefaction behavior of the soils at HTF and ITP and site-specific relations were required based on strengths determined from laboratory testing.

- Using the strength approach, factors of safety against initial liquefaction were calculated based on a series of undrained, stress-controlled, cyclic triaxial tests. Dynamic stress profiles from three earthquake motions were determined for the foundation soils by ground response analysis using site-specific properties and the computer code SHAKE (Schnabel, Lysmer, and Seed, 1972; Idriss and Sun, 1992). Based on the results of the strength approach, the resulting factors of safety against initial liquefaction indicate the potential for liquefaction is negligible at HTF and ITP.

- The calculated cyclic shear strains induced by the postulated earthquakes at various depths within the Tobacco Road, Dry Branch, and Santee/Tinker Formations were small, near the strain value (threshold strain) required to initiate the generation of pore water pressures. Therefore, based on the strain approach, the potential for liquefaction is negligible.

Thus, the results of all five liquefaction susceptibility methods indicate that for the prescribed motions, the factors of safety against initial liquefaction are high and the potential for liquefaction-induced settlement beneath the tanks is small.

In addition to the deterministic methods, a probabilistic liquefaction hazard assessment was completed for the ITP area. This analysis was based on site-specific soil properties and earthquake motions developed from the EPRI hazard study. The results show the annual hazard for liquefaction is less than $1 \times 10^{-5}$.

### *Expected Tank Settlement*

All of the tanks in H-Area have experienced post-construction settlement. In particular, the four tanks at ITP have experienced approximate total and differential settlements of 1¾ inches and less than ½ inch, respectively, based on current available data. This amount of settlement is also similar to other tanks within HTF.

Future settlement of the tanks may occur in the following ways: (1) dynamic settlement due to a postulated seismic event, and (2) static settlement due to secondary consolidation and increased tank loading during operation for the newer tanks not yet in service. Analyses show that the

potential future tank settlement due to these causes totals about 2½ inches. The dynamic settlement increment (incorporating soil-structure interaction effects) for the ITP tanks due to earthquake motions ranges between 0 to 1½ inches. The future tank settlement increment due to increased fluid level during operation and long-term (over a 30-year time period) settlement of tanks due to secondary consolidation is estimated at 1 inch. When added to the existing settlement, this results in a total tank settlement of 4¼ inches with a differential settlement of less than about 1¾ inches.

The tank settlement results are summarized in the following table.

**Settlement Summary - Realistic Case**

| | *Settlement, inches* | |
|---|---|---|
| *Condition* | *Total* | *Differential* |
| Existing | 1.75 | 0.5 |
| Increased loading and secondary consolidation | 1 | 0.5 |
| Dynamic (liquefaction only, no soft zone compression): | | |
| -Local EBE | 0.2 | 0.1 |
| -Distant EBE | 0.7 | 0.35 |
| -Distant 84th | 1.5 | 0.75 |
| **Maximum Settlement** | **4.25**[1] | **1.75**[1] |

[1] ***Maximum total and differential settlement for tanks equals sum of existing settlement, settlement resulting from increased loading and secondary consolidation, and dynamic settlement from the 84th percentile distant event.***

One-dimensional, free-field dynamic settlement analyses for HTF predict total settlements to be less than 2 inches. These analyses were performed using the 84 percentile rock spectrum and neglected the 2-D effects of the embankment and the tanks.

### *Postulated Worst Case Tank Settlement*

At other facilities within the SRS it has been postulated that the soft zones within the Santee Formation are underconsolidated and could potentially consolidate due to a seismic load with underconsolidation ranging from less than one-half of the overburden pressure to normally loaded (Geotechnical Engineers, Inc., GEI, 1991a and K-Area Soil Stabilization, KASS, 1992). Laboratory and field tests at ITP also indicate the existence of "soft zones" or underconsolidated pockets within the Santee/Tinker Formation. The amount of underconsolidation ranges from about 0.5 to 1.0 of the overburden pressure. Field moisture content data and analytical modeling suggest that the soft zones have an average overconsolidation ratio of about 0.7.

Field evidence at ITP suggests that the soft zones are actually pockets and that the lateral extent of any given pocket is small; for if it were large, significant settlement would have occurred during

the placement of the embankment fill. Previous work at other SRS facilities also suggests that these soft zones are small (U. S. Army Corps of Engineers, COE, 1952a, 1952b; GEI, 1991a; KASS, 1992). Those studies concluded that the underconsolidated zones are small, not interconnected, and average about 6 feet thick with a maximum lateral dimensions less than 50 feet. Geostatistical analyses for ITP indicate that the soft zones have an average thickness of about 4 feet and a maximum lateral dimension of about 10 to 20 feet.

Nevertheless, a hypothetical worst-case settlement analysis was performed assuming that large, laterally continuous soft zones exist below the tanks. The results show that a load transfer to the soft zones due to an earthquake would produce from about 4 to 7 inches of soft zone compression. Analyses that combine dynamic settlement due to earthquake loading (the settlement is due to the dissipation of cyclically induced pore water pressure) with the soft zone compression result in a maximum tank foundation settlement of 5 to 7 inches and a maximum differential (edge to edge) settlement of less than about 2 inches. To these worst case results, the existing and future total and differential settlements must be added, thus resulting in a worst case total tank settlement of 8 to 10 inches and a differential settlement of about 3 inches.

The results are summarized in the table below:

**Settlement Summary - Worst Case**

| | *Settlement, inches* | |
|---|---|---|
| *Condition* | *Total* | *Differential* |
| Existing | 1.75 | 0.5 |
| Increased loading and secondary consolidation | 1 | 0.5 |
| Dynamic (liquefaction and soft zone compression): | | |
| -Local EBE | 5 to 7 | 2 |
| -Distant EBE | 5 to 7 | 2 |
| -Distant 84th | 5 to 7 | 2 |
| **Maximum Settlement** | **8 to 10[1]** | **3[1]** |

[1] Maximum total and differential settlement for tanks equals sum of existing settlement, settlement resulting from increased loading and secondary consolidation, dynamic settlement from liquefaction, and deep-seated settlement from compression of soft zones in the Santee Formation.

## *Summary*

Investigations and analyses of the seismic performance of ITP and HTF soils show that the embankment is stable under both static and dynamic conditions, with acceptable safety factors and negligible deformation for the earthquake motions analyzed. Probabilistic liquefaction assessments show that the Tobacco Road Formation has an annual liquefaction hazard that is less than $1 \times 10^{-5}$. Total tank settlement (including existing settlement) due to the dissipation of cyclically induced

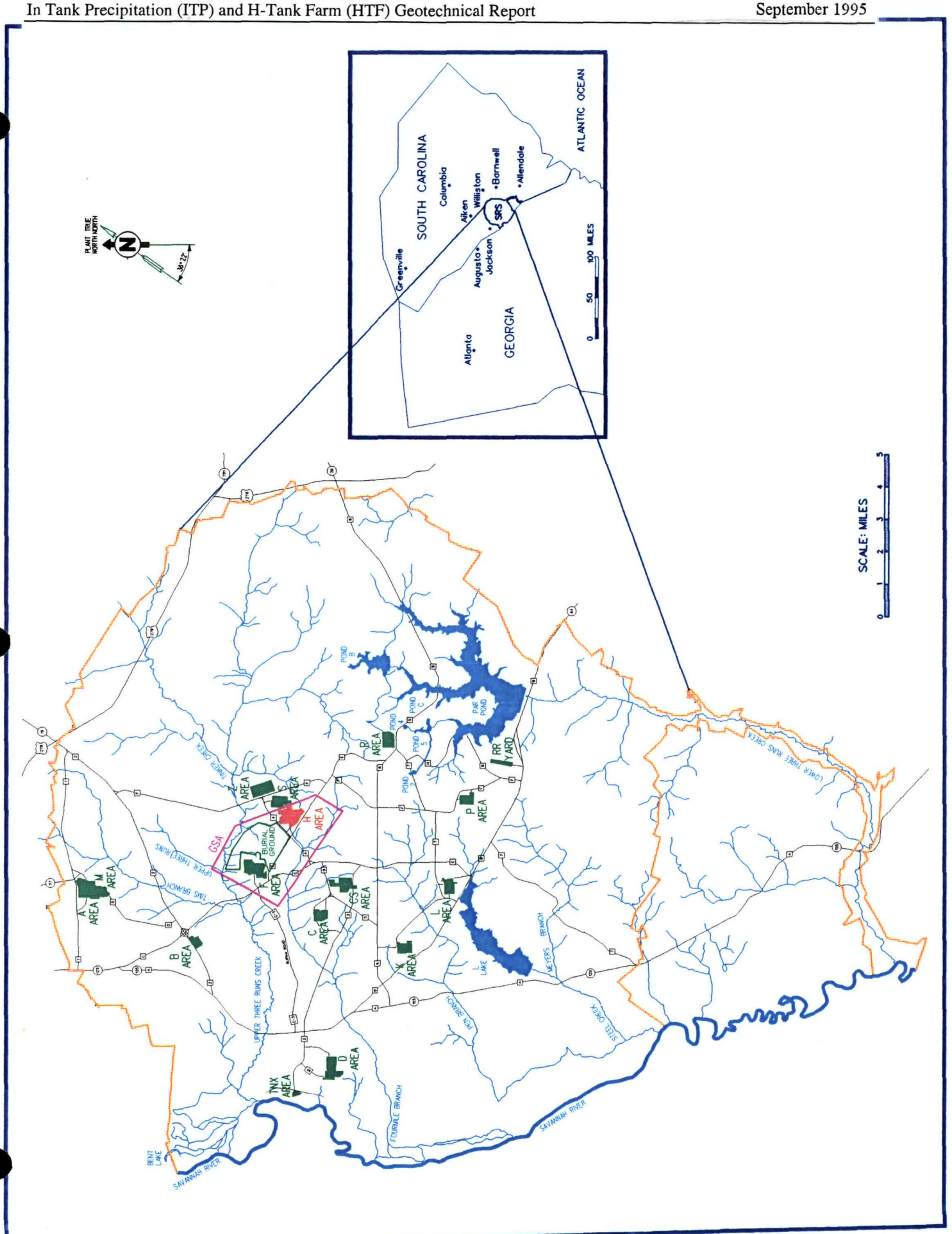


Figure ES-1 Savannah River Site Map

pore water pressures; additional static, long-term loading; and secondary consolidation is expected to be 4¼ inches. The differential settlement is expected to be less than 1¾ inches. Hypothetical worst case settlement analyses show total tank settlement at 8 to 10 inches with a differential settlement of 3 inches.

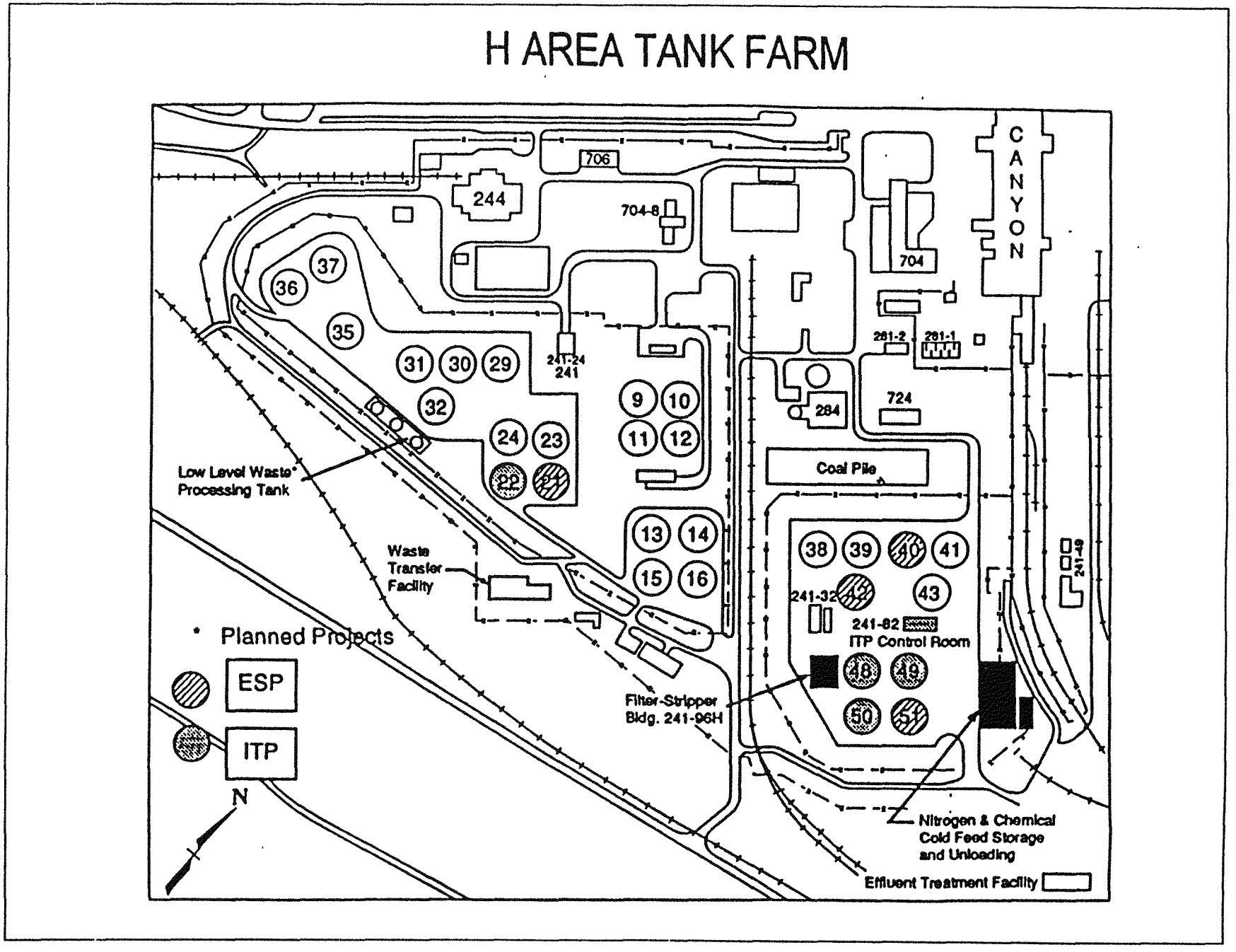


Figure ES-2 H-Area Tank Farm - plan layout.

## TABLE OF CONTENTS

**PEER REVIEW SUMMARY** ..... III

**EXECUTIVE SUMMARY** ..... VI

**LIST OF TABLES** ..... XX

**LIST OF FIGURES** ..... XXII

**LIST OF VOLUMES AND APPENDICES** ..... XXIII

**LIST OF ACRONYMS, SYMBOLS, AND JARGON** ..... XXXIV

**1. INTRODUCTION** ..... 1-1

1.1 Report Organization ..... 1-1
1.2 Background ..... 1-2
1.2.1 Tank Farm ..... 1-2
1.2.2 In-Tank Precipitation ..... 1-3
1.3 Objectives ..... 1-4
1.4 Work Schedule and Personnel ..... 1-4
1.5 Available Geotechnical Information ..... 1-7
1.5.1 Previous Foundation Investigations at ITP ..... 1-7
1.5.1.1 High Level Waste Storage Tanks Nos. 48 through 51," March 22, 1977 ..... 1-7
1.5.1.2 Relocated High Level Waste Storage Tanks Nos. 48 through 51," May, 1978 ..... 1-8
1.5.1.3 In-Tank Precipitation Facility," August 27, 1984a ..... 1-8
1.5.2 Previous Foundation Investigation Reports in the Balance of the HTF ..... 1-8
1.5.2.1 Report of Investigation of Subsidence, Evaporator Building Fill - Building 242-H," (Law, 1962) ..... 1-8
1.5.2.2 Settlement Investigation Of Evaporator Building 242-H," MPMR, 1962 ..... 1-9
1.5.2.3 Areas 200H and 200F Radioactive Waste Storage Tanks, Subsurface Geologic Investigations," (Blume & Associates 1971). ..... 1-9
1.5.2.4 Savannah River Plant Additional Facilities, High Level Waste Storage, 200H," MRWJ, 1974. ..... 1-9
1.5.2.5 New High Level Storage Tank No. 38 Building 241H," MRWJ, 1975a ..... 1-10
1.5.2.6 Building 241H New High Level Waste Storage Tanks Nos. 42 & 43," MRWJ,1975b ..... 1-10
1.5.2.7 Waste Transfer Facility H-Area Savannah River Plant," MRJD, 1984c. ..... 1-10
1.5.2.8 Waste Transfer Facility Revised Location H-Area," Mueser Rutledge, 1985 ..... 1-11
1.5.2.9 TBP Removal Tanks At The F/H Effluent Treatment Facility," Main, 1987. ..... 1-11
1.5.2.10 Tank Farm Space Gain Facility, 200 H-Area," Mueser, Rutledge, 1988a. ..... 1-11
1.5.2.11 ETF Wastewater Collection Tanks F/H Effluent Treatment Facility," Mueser, Rutledge, 1988b. ..... 1-11
1.5.2.12 Nitrogen Storage Tanks And Vaporizer, 200 H-Area," Mueser Rutledge, 1988c. ..... 1-12
1.5.2.13 Replacement High Level Waste Evaporator, Soils Report," Bechtel, 1989. ..... 1-12
1.5.2.14 Report of Geotechnical Exploration WMWE Maintenance Facility Building 241-41H," Westinghouse Environmental 1990. ..... 1-12
1.5.2.15 New Waste Transfer Facility ( NWTF) - Geotechnical Assessment," WSRC, 1993c. ..... 1-12
1.5.2.16 Geotechnical Summary Report For H-DB7," WSRC, 1994e ..... 1-13
1.5.3 Review of Previous Pertinent Liquefaction Potential and Soft Zone Evaluations ..... 1-13
1.5.3.1 Seismic Criteria URS/Blume, 1982 ..... 1-13
1.5.3.2 Barnwell Nuclear Fuel Plant: Dames & Moore, 1968 ..... 1-13
1.5.3.3 Building 221H: Geotechnical Engineers, Inc., 1979 ..... 1-14
1.5.3.4 Defense Waste Processing Facility DWPF, 200-S Area: D'Appolonia, 1979 (b) ..... 1-14
1.5.3.5 Defense Waste Processing Facility, 200-S area: D'Appolonia, 1982 ..... 1-15
1.5.3.6 Defense Waste Processing Facility, 200-S Area: Geotechnical Engineers, Inc., 1983 ..... 1-15
1.5.3.7 Comparison of Seismic Analysis for the 200-H and 200-S Areas: D'Appolonia, 1979 (a) ..... 1-16
1.5.3.8 K Reactor Area: GEI Consultants, 1991a ..... 1-17

1.5.3.9 K-Area Soil Stabilization Program: KASS, 1992 ..... 1-19
1.5.3.10 Replacement Tritium Facility (RTF), Building 233-H BSRI, 1993b ..... 1-20
1.5.3.11 Historical Settlement: WSRC, 1995; Mueser, 1991 ..... 1-22
1.5.4 Summary of the Review ..... 1-22
1.6 Quality Assurance ..... 1-23

**2. SEISMOLOGY AND GEOLOGY ..... 2-1**

2.1 Seismic Evaluations Introduction ..... 2-1
2.2 Summary of Parameters Associated with the Development of the ITP EBE Distant Soil Spectrum. 2-2
2.2.1 Source Parameters ..... 2-2
2.2.2 Structure/Q ..... 2-2
2.2.3 Kappa Bedrock ..... 2-2
2.2.4 Soil Model ..... 2-3
2.3 ITP Median and 84th Percentile Rock Motions ..... 2-3
2.4 Summary ..... 2-3
2.5 Regional Stratigraphy at the SRS ..... 2-4
2.5.1 Cretaceous Sediments ..... 2-4
2.5.2 Tertiary Sediments ..... 2-5
2.5.2.1 Paleocene ..... 2-5
2.5.2.2 Eocene ..... 2-6
2.5.2.3 Younger than Eocene ..... 2-7

**3. SUBSURFACE EXPLORATION ..... 3-1**

3.1 ITP Phase 1 (December 1992 to April 1993) ..... 3-1
3.2 ITP Phase 2 (April 1993 to November 1993) ..... 3-1
3.3 ITP Phase 3 (November 1993 to August 1994) ..... 3-1
3.4 HTF Field Exploration (November 1993 to May 1995) ..... 3-2
3.4.1 Multi-Mode Deep Profiling Program (MMDPP) ..... 3-2
3.5 Field Test Location and Clearance ..... 3-3
3.6 Equipment and Field Test Methods ..... 3-4
3.6.1 Drilling Contractor(s) and Equipment ..... 3-4
3.6.1.1 Graves Environmental Failing 1500 ..... 3-5
3.6.1.2 Graves Environmental AMC Quick Drill Speed Star 275 ..... 3-5
3.6.1.3 Environmental Drilling Services Davy Kent DK-5 ..... 3-5
3.6.2 Standard Penetration Test ..... 3-5
3.6.3 Undisturbed Sampling ..... 3-6
3.6.3.1 Direct Push Shelby Tube ..... 3-7
3.6.3.2 Pitcher Barrel Sampler ..... 3-7
3.6.3.3 Stationary Piston Sampler ..... 3-7
3.6.4 Core Boreholes ..... 3-7
3.6.5 Cased Boreholes ..... 3-8
3.6.5.1 Inclinometer Casing ..... 3-8
3.6.5.2 Steel Casing ..... 3-8
3.6.6 Piezocone Penetrometer Soundings ..... 3-8
3.6.7 Dilatometer Soundings ..... 3-9
3.6.8 Geophysical Borehole Logging ..... 3-9
3.6.8.1 Gamma ..... 3-9
3.6.8.2 Caliper ..... 3-9
3.6.8.3 Spontaneous Potential ..... 3-9
3.6.8.4 Resistivity ..... 3-10
3.6.8.5 Sonic Velocity ..... 3-10
3.6.8.6 Variable Density ..... 3-10
3.6.9 Cross-Hole Seismic Velocity Survey ..... 3-10
3.6.10 Cross-Hole Tomography Survey ..... 3-11

3.6.11 Down-Hole Seismic Refraction Survey ..... 3-12
3.6.12 Borehole, Casing, and Penetration Abandonment ..... 3-12
3.7 Sample Preparation, Handling, Storage, Transportation and Control ..... 3-13

**4. LABORATORY TESTING ..... 4-1**

4.1 Quality Assurance Plan ..... 4-2
4.2 Testing Program ..... 4-2
4.2.1 Static Triaxial Tests ..... 4-3
4.2.2 Strain-Controlled Cyclic Triaxial and Resonant Column Tests ..... 4-3
4.2.3 Stress-Controlled Cyclic Triaxial Tests ..... 4-4
4.2.4 Low-Amplitude Strain Determination ..... 4-4
4.2.5 Volumetric Strain Determination ..... 4-5
4.2.6 Residual Strength Determination ..... 4-5
4.2.7 Mineralogical Analysis ..... 4-5

**5. SUBSURFACE CONDITIONS ..... 5-1**

5.1 Generalized Engineering Profiles of the ITP ..... 5-1
5.1.1 Structural Fill at ITP ..... 5-2
5.1.2 Altamaha Formation or TR1 and TR2 Layers at ITP ..... 5-2
5.1.3 Tobacco Road Formation or TR3 and TR4 Layers at ITP ..... 5-3
5.1.4 Dry Branch Formation or DB1-DB5 Layers at ITP ..... 5-3
5.1.5 Santee Limestone / Tinker Formation or ST layer at ITP ..... 5-4
5.1.6 Green Clay and Congaree Formations ..... 5-6
5.2 Soft Zones at the ITP ..... 5-6
5.2.1 Soft Zone Location, Thickness, and Lateral Extent in the Santee Formation ..... 5-7
5.2.2 Grout Injection Evaluation of Soft Zones ..... 5-9
5.2.3 Potential Voids in Relation to Soft Zone Intervals at ITP ..... 5-9
5.2.4 Investigation of Void Intervals at the ITP ..... 5-10
5.3 Generalized Engineering Profiles of the HTF ..... 5-10
5.3.1 Evaluation of Soft Zones, Voids and Carbonates for the HTF ..... 5-11
5.4 Shallow Faulting at the ITP and HTF ..... 5-12

**6. ENGINEERING PROPERTIES ..... 6-1**

6.1 Dynamic Properties ..... 6-1
6.1.1 Local and Distant Event ITP Evaluation ..... 6-1
6.1.2 84th Percentile Dynamic Analysis for ITP and HTF. ..... 6-2
6.2 Cyclic Strength and Compressibility ..... 6-2
6.2.1 Foreword ..... 6-2
6.2.2 Cyclic Strength ..... 6-3
6.2.2.1 Methodology ..... 6-3
6.2.2.2 Selection of Samples for Testing Program ..... 6-4
6.2.2.3 Laboratory Testing ..... 6-4
6.2.2.4 Derivation of a Site-Specific $k_\sigma$ Factor ..... 6-6
6.2.3 Cyclic Compressibility ..... 6-6
6.2.3.1 Liquefaction Volumetric Strain ..... 6-7
6.2.3.2 Partial Liquefaction Volumetric Strain ..... 6-8
6.2.3.3 Threshold Strain ..... 6-9
6.3 Engineering Properties of Fill Used for Slope Stability Analyses ..... 6-9
6.3.1 In-Tank Precipitation Facility ..... 6-9
6.3.2 H-Area Tank Farm ..... 6-10
6.3.2.1 Effective Stress Properties ..... 6-11
6.3.2.2 Total Stress Properties ..... 6-11

**7. DESIGN CRITERIA AND EVALUATIONS FOR THE ITP ..... 7-1**

7.1 Controlling Earthquake Motions ..... 7-1
7.2 Slope Stability ..... 7-1
7.2.1 Methodology ..... 7-1
7.2.2 Geometry and Stratigraphy Used for Slope Stability Analyses ..... 7-2
7.2.3 Analyses ..... 7-2
7.2.3.1 Static Factors of Safety ..... 7-2
7.2.3.2 Pseudo-Static Factors of Safety ..... 7-3
7.2.3.3 Seismically-Induced Slope Deformations ..... 7-3
7.2.3.4 Reduced Strength Evaluation ..... 7-3
7.2.4 Conclusions ..... 7-4
7.3 Liquefaction and Dynamic Settlement ..... 7-4
7.3.1 Methodology ..... 7-4
7.3.1.1 Clayey Soils ..... 7-4
7.3.1.2 Shear Wave Velocity ..... 7-5
7.3.1.3 Stress Method ..... 7-6
7.3.1.4 Strain Method ..... 7-7
7.3.1.5 Performance of Old Sand Deposits ..... 7-7
7.3.2 Evaluations and Results ..... 7-9
7.3.2.1 Clayey Soils ..... 7-9
7.3.2.2 Shear Wave Velocity Approach ..... 7-10
7.3.2.3 The Stress Method ..... 7-10
7.3.2.3.1 Ground Response Analyses ..... 7-10
7.3.2.3.2 Evaluation of Factors of Safety Against Initial Liquefaction ..... 7-11
7.3.2.4 Strain Approach ..... 7-11
7.3.3 Liquefaction Evaluation: Conclusion ..... 7-13
7.4 Bearing Capacity ..... 7-13
7.4.1 Criteria ..... 7-13
7.4.2 Evaluation and Results ..... 7-13
7.5 Expected Tank Settlement ..... 7-14
7.5.1 Dynamic Settlement Due to Dissipation of Seismically-Induced Pore Water Pressure ..... 7-14
7.5.2 Static Settlement Due to Tank Loading During Operation ..... 7-14
7.5.3 Tank Settlement: Worst Case ..... 7-18
7.5.3.1 Geologic Model: Worst Case ..... 7-18
7.5.3.2 Geotechnical Parameters: Worst Case ..... 7-20
7.5.3.3 Analytical Model: Worst Case ..... 7-20
7.5.3.3.1 Tank Structural Model ..... 7-21
7.5.3.3.2 Soil-Structure Interaction Analysis and Results ..... 7-23
7.5.3.3.3 Settlement Analyses: Simulation of Existing Stress State, Pre-Earthquake Condition ..... 7-24
7.5.3.3.4 Interpolation of Piezocone Data ..... 7-25
7.5.3.3.5 Compression of Soil Layers Upon Pore Water Pressure Dissipation ..... 7-26
7.5.3.3.6 Post-Earthquake Tank Settlement Analysis: Results ..... 7-27
7.5.3.4 Tank Settlement Summary: Worst Case ..... 7-27

**8. ENGINEERING EVALUATIONS FOR THE BALANCE OF THE H-TANK FARM ..... 8-1**

8.1 Controlling Earthquake Motions ..... 8-1
8.2 Evaluation of Slope Stability for the HTF ..... 8-1
8.2.1 General ..... 8-1
8.2.2 Methodology ..... 8-2
8.2.3 Layering of Fill for Slope Stability Analyses ..... 8-2
8.2.4 Analyses ..... 8-3
8.2.4.1 Static Factors of Safety ..... 8-3
8.2.4.2 Pseudo-Static Factors of Safety ..... 8-3
8.2.4.3 Seismically-Induced Slope Deformations ..... 8-3

8.2.5 Conclusions ..... 8-4
8.3 Liquefaction and Dynamic Settlement ..... 8-4
8.4 Bearing Capacity ..... 8-7
8.5 Static Settlement ..... 8-7

**9. PROBABILISTIC LIQUEFACTION ASSESSMENT AT THE IN-TANK PRECIPITATION .. 9-1**

9.1 Introduction ..... 9-1
9.2 Methodology ..... 9-1
9.3 Seismic Models ..... 9-2
9.3.1 Introduction ..... 9-2
9.3.2 Selection of Seismic Hazard Curve ..... 9-3
9.3.3 Selection of Mbar and Dbar ..... 9-3
9.3.4 Spectra and Time History Development ..... 9-4
9.4 Engineering Properties and Parameters ..... 9-6
9.4.1 Shear Wave Velocity ..... 9-6
9.4.2 Strain-Dependent Shear Modulus and Damping ..... 9-6
9.4.3 SPT $(N1)_{60}$ Values ..... 9-7
9.4.4 Cyclic Shear Strength Adjustment Factors ..... 9-9
9.4.4.1 Correction for Over-consolidation ratio of 3.0 ..... 9-10
9.4.4.2 Correction for Sample Disturbance ..... 9-11
9.4.5 Cyclic Shear Strength Magnitude Correction Factors ..... 9-11
9.5 Free-Field Seismic Ground Response Analysis ..... 9-15
9.6 ASHLE Analyses and Results ..... 9-16
9.6.1 Analysis ..... 9-16
9.6.2 Results ..... 9-19
9.6.3 Qualitative Comparison of EPRI and LLNL Hazard ..... 9-19
9.7 Parametric Liquefaction Settlement Analysis ..... 9-20
9.8 Conclusions ..... 9-20

**10. SUMMARY ..... 10-1**

10.1 Soil Spectra ..... 10-1
10.2 Calcareous Lithofacies and Soft Zones ..... 10-1
10.3 Faulting ..... 10-2
10.4 Slope Stability ..... 10-2
10.5 Liquefaction ..... 10-2
10.6 Settlement ..... 10-3
10.7 Bearing Capacity ..... 10-4

**11. CONCLUSIONS AND RECOMMENDATIONS ..... 11-1**

**12. REFERENCES ..... 12-1**

**LIST OF TABLES**


| | |
|---|---|
| Table 3.6-1 | Exploration point summary |
| Table 4.0-1 | Standard laboratory testing procedures |
| Table 4.2-1(a) | Summary of laboratory test results at ITP (static) |
| Table 4.2-1(b) | Summary of laboratory test results at HTF (static) |
| Table 4.2-2 | Summary of consolidation parameters |
| Table 4.2-3 | Summary of cyclic triaxial tests performed at ITP |
| Table 5.2-1 | SPT-N, Atterberg limits, and soil classification for soft zones in the DB4/DB5 layer at the 1977 proposed location of Tank 51 (select data from Mueser et al., 1977) |
| Table 5.2-2 | Consolidation properties and Atterberg limits for soft zones within the DB4/DB5 layer at the 1977 proposed location of Tank 51 (select data from Mueser et al., 1977) |
| Table 5.2-3 | Thickness of soft zones in the Santee Formation at ITP |
| Table 6.0-1(a) | Average material properties at ITP |
| Table 6.0-1(b) | Average material properties at HTF |
| Table 6.1-1 | Recommended damping ratio and modulus reduction relationships with cyclic shear strain |
| Table 6.2-1 | Summary of results of cyclic shear test and index properties of RTF specimens |
| Table 6.2-2 | Comparisons between average engineering properties |
| Table 6.2-3 | Stationary piston sample properties |
| Table 6.2-4 | Normalized cone tip resistances applicable to the laboratory cyclic test specimens |
| Table 6.2-5 | Summary of results of cyclic shear tests and index properties of ITP specimens (1) |
| Table 6.2-6 | Summary of results of cyclic shear tests and index properties of ITP specimens (2) |
| Table 6.2-7 | Results of liquefaction testing of SRS/ITP soils |
| Table 6.2-8 | Parameters from cyclic triaxial tests |
| Table 6.2-9 | Calculation of $K_\sigma$ factor |
| Table 6.2-10 | Summary of data for volumetric strain calculations |
| Table 6.2-11 | Relationship between limiting cyclic shear strain, factor of safety against initial liquefaction, cone tip resistance, and volumetric strain |
| Table 6.3-1 | Best estimate shear strength parameters used in the ITP stability analyses |
| Table 6.3-2 | Best estimate shear strength parameters used in the HTF stability analyses |
| Table 7.2-1 | Summary of critical factors of safety |
| Table 7.3-1 | Average and normalized shear wave velocities for the ITP soil column |
| Table 7.3-2 | Soil profiles for SHAKE analyses, Phase 1 |
| Table 7.3-3 | Soil profiles for SHAKE analyses, Phase 2. |
| Table 7.5-1 | Soil properties used by Mueser et. al. (1984b) for settlement analyses |

| | |
|---|---|
| Table 7.5-2a | Settlement due to soft zone compression, north-south and east-west subsurface cross-sections |
| Table 7.5-2b | Settlement due to soft zone compression, north-south and east-west subsurface cross-sections |
| Table 7.5-3a | Estimated total and differential tank settlements |
| Table 7.5-3b | Estimated total and differential tank settlements |
| Table 8.2-1 | Best estimate shear strength parameters at HTF |
| Table 8.2-2 | Minimum static factors of safety at HTF, effective stress conditions |
| Table 8.2-3 | Minimum static factors of safety at HTF, total stress conditions |
| Table 8.2-4 | Minimum pseudo-static factors of safety at HTF, total stress conditions (0.2g) with 10% strength reduction |
| Table 8.2-5 | Summary of minimum factors of safety at HTF |
| Table 8.3-1 | Comparison of 1-D liquefaction settlements calculated using ITP and GEI dynamic curves for the 84th percentile, non-fill profile at ITP |
| Table 8.3-2 | Summary of 1-D liquefaction settlements calculated for the 84th percentile, fill profile at ITP |
| Table 8.3-3 | Summary of 1-D liquefaction settlements calculated for the 84th percentile, non-fill profile at HTF |
| Table 8.3-4 | Summary of 1-D liquefaction settlements calculated for the 84th percentile, fill profile at HTF |
| Table 8.5-1 | Tank settlement survey schedule |
| Table 9.3-1 | EPRI deaggregation matrix: mean 2.5 Hz spectral velocity of 2.0 cm/s, 5% critical damping magnitude |
| Table 9.3-2 | EPRI mean rock 2.5 Hz spectral velocity for 5% critical damping |
| Table 9.3-3 | Selected 10 points on EPRI hazard curve |
| Table 9.4-1 | Summary of shallow depth shear wave velocities (fps) |
| Table 9.4-2 | Summary of layer thicknesses (ft) |
| Table 9.4-3 | Summary of soil profile & properties, ITP. |
| Table 9.4-4 | Summary of soil profile & properties, Confirmatory Drilling Site (CFD) |
| Table 9.4-5 | Summary of SPT N-value data (TR3 & TR4) |
| Table 9.5-1 | Free field analysis: case combinations |
| Table 9.5-2 | Effective shear stress ratio CSR = $0.65^{*}(\tau_{xy})_{max}/\sigma'_{y}$ from SHAKE analysis Tobacco Road 3/4 |

## LIST OF FIGURES


| | |
|---|---|
| Figure ES-1 | Savannah River Site Map |
| Figure ES-2 | H-Area Tank Farm - plan layout |
| Figure 1.0-1 | Savannah River Site Map |
| Figure 1.0-2 | Aerial photo of ITP |
| Figure 1.0-3 | Aerial photo of HTF. |
| Figure 1.2-1 | H-Area Tank Farm - plan layout |
| Figure 1.2-2 | H-Area Tank Farm - tank details |
| Figure 1.2-3 | Distribution of waste in tanks |
| Figure 1.2-4 | Timeline for construction of ITP tanks |
| Figure 1.2-5 | Photo of mudmat and base slab during ITP tank construction |
| Figure 1.2-6 | Photo of steel liners of ITP tanks during construction |
| Figure 1.2-7 | Timeline for construction of ITP buildings and related facilities |
| Figure 2.1-1 | Comparison of the smoothed 5 percent EBE local and distant event spectra |
| Figure 2.3-1 | ITP/H-area median and 84th percentile rock spectra |
| Figure 2.5-1 | SRS general stratigraphic chart |
| Figure 3.3-1 | In-Tank Precipitation area: Phase 1 field investigation |
| Figure 3.3-2 | In-Tank Precipitation area: Phases 1 and 2 field investigations |
| Figure 3.3-3 | In-Tank Precipitation area: Phases 1, 2, and 3 field investigations |
| Figure 3.4-1 | HTF field investigations |
| Figure 3.4-2 | Shear wave velocities from H-Area, OYO™ logged, deep borehole MMP-2-SB |
| Figure 3.4-3 | Shear wave velocity comparison of OYO™ logged hole, MMP-2-SB, with seismic cone penetrometer measurements from HMMC-B02 and HMMC-C02 |
| Figure 5.0-1 | Typical CPT log with stratigraphy |
| Figure 5.1-1 | Subsurface profile A-A' |
| Figure 5.1-2 | Subsurface profile B-B'. |
| Figure 5.1-3(a) | Idealized cross-section showing mean shear wave velocities, Poisson's ratios, and unit weights for layers at ITP |
| Figure 5.1-3(b) | Idealized cross-section showing mean shear wave velocities, Poisson's ratios, and unit weights for layers at HTF |
| Figure 5.1-4 | Comparison of geologic and engineering nomenclature |
| Figure 5.1-5 | Summary of laboratory data for the ITP fill |
| Figure 5.1-6 | Percent compaction (Modified Proctor) for the ITP fill |
| Figure 5.1-7 | Idealized facies map of the upper Tinker/Santee Formation |
| Figure 5.1-8 | Tank and borehole location map |
| Figure 5.2-1 | Combined thickness map of upper and lower soft zone in the Santee/Tinker formation. |

Figure 5.2-2 CPT tip resistance ($q_c$) versus SPT-N for Tinker/Santee Formation
Figure 5.2-3 CPT tip resistance ($q_c$) versus SPT-N for Dry Branch (DB3) layer
Figure 5.2-4 Distribution of void intervals from CPT data
Figure 5.2-5 H-BOR-50 sampling
Figure 5.3-1 Generalized profiles at HTF - section DD'
Figure 5.3-2 Generalized profiles at HTF - sections EE', FF', and GG'
Figure 5.3-3 Histogram for HTF fill vs. ITP fill
Figure 5.3-4 Histogram for HTF Upland vs. ITP Upland
Figure 5.3-5 Histogram for HTF TR3/4 vs. ITP TR3/4
Figure 5.3-6 Histogram for HTF DB1/3 vs. ITP DB1/3
Figure 5.3-7 Histogram for HTF DB4/5 vs. ITP DB4/5
Figure 5.3-8 Histogram for HTF ST vs. ITP ST.
Figure 5.3-9 Distribution of SPT and CPT for ITP and HTF
Figure 5.3-10 Distribution of soft zones for ITP and HTF
Figure 5.3-11 Map distribution of soft zones, carbonates and voids
Figure 5.3-12 Profile view of soft zones, carbonates, and voids
Figure 5.4-1 Approximate stike line of ITP fault and Santee facies relationship
Figure 5.4-2 Isometric view of TR3/Red Layer and Congaree surface
Figure 6.0-1 Variation of over-consolidation ratio (OCR) with elevation at the ITP facility
Figure 6.1-1 Variation of damping ratio with cyclic shear strain amplitude for upper ITP soils
Figure 6.1-2 Shear modulus reduction with cyclic shear strain amplitude for upper ITP soils
Figure 6.1-3(a) Typical example of cut-off trace from strain controlled dynamic triaxial tests
Figure 6.1-3(b) Typical example of jagged trace from strain controlled dynamic triaxial tests
Figure 6.1-4 Variation of damping ratio with cyclic shear strain modulus (GEI, 1991 B)
Figure 6.1-5 Shear modulus reduction with cyclic shear strain amplitude (GEI, 1991 B)
Figure 6.2-1 Methodology used to develop relationships between cyclic stress ratios in the laboratory and in the field
Figure 6.2-2 Relationship between RTF design curve for stress ratio causing initial liquefaction and $(N_1)_{60}$ values - Comparison with empirical data
Figure 6.2-3 RTF: cyclic triaxial test results (1)
Figure 6.2-4 RTF: cyclic triaxial test results (2)
Figure 6.2-5 Proposed correlation for RTF between modified cone tip resistance and cyclic stress ratio required for initial liquefaction
Figure 6.2-6 Comparison between soil profiles at the RTF and the ITP facilities
Figure 6.2-7 ITP: cyclic triaxial test results

Figure 6.2-8 ITP: cyclic triaxial test results
Figure 6.2-9 ITP: cyclic triaxial test results
Figure 6.2-10 Proposed correlation for ITP between modified cone tip resistance and cyclic stress ratio required for initial liquefaction
Figure 6.2-11 Correlation between percent fines and friction ratio in cone tests
Figure 6.2-12 Proposed correlation for ITP between modified cone tip resistance and friction ratio with the cyclic stress ratio required for initial liquefaction in the field
Figure 6.2-13 Derivation of the $k_\sigma$ factor relating the influence of confining pressure on the cyclic stress ratio in laboratory triaxial tests
Figure 6.2-14 ITP soils: Influence of confining pressure on cyclic triaxial test results (1)
Figure 6.2-15 ITP soils: Influence of confining pressure on cyclic triaxial test results (2)
Figure 6.2-16 ITP soils: Influence of confining pressure on cyclic triaxial test results (3)
Figure 6.2-17 ITP soils: Derivation of a site-specific $K_\sigma$ factor
Figure 6.2-18 Comparison of $K_\sigma$ factors from several sources
Figure 6.2-19 Relationship between cyclic stress ratio, $(N_1)_{60}$ and volumetric strain for saturated clay sands
Figure 6.2-20 Relationship between volumetric strain, induced maximum limiting shear strain, and cone tip penetration resistance
Figure 6.2-21 Relationship between cyclic stress ratio causing initial liquefaction, $(N_1)_{60}$ and limiting shear strain
Figure 6.2-22 Derivation of a relationship between limiting cyclic shear strain and factor of safety against initial liquefaction
Figure 6.2-23 Relationship between factor of safety against initial liquefaction and limiting cyclic shear strain
Figure 6.2-24 Relationship between factor of safety against initial liquefaction and volumetric strain after liquefaction
Figure 6.2-25 Derivation of a relationship between pore water pressure ratio and volumetric strain after liquefaction
Figure 6.2-26 Relationship between factor of safety against initial liquefaction and residual excess pore water pressure ratio
Figure 6.2-27 Volumetric strain expressed as a function of factor of safety against initial liquefaction
Figure 6.2-28 Relationship between cyclic shear strain amplitude, number of cycles, and pore water pressure increase, Tobacco Road Formation
Figure 6.2-29 Relationship between cyclic shear strain amplitude, number of cycles, and pore water pressure increase, Santee Formation
Figure 6-3-1 Slope stability - cross-section 1
Figure 6.3-2 Average CPT tip resistance and variability in the fill at ITP
Figure 6.3-3 Plot plan of HTF area
Figure 6.3-4 Summary of tip resistances for CPTs in north hill area
Figure 6.3-5 Summary of tip resistances for CPTs in east hill area

Figure 6.3-6 Summary of tip resistances for CPTs in west hill area
Figure 6.3-7 Summary of the laboratory data for the HTF fill, excluding ITP
Figure 6.3-8 Relationship between $Q_c$ and friction angle
Figure 6.3-9 Calculated $S_u$ versus depth at ITP
Figure 6.3-10 Calculated $N_k$ versus depth at ITP
Figure 6.3-11 Calculated $S_u$ versus depth for north hill area
Figure 6.3-12 Calculated $S_u$ versus depth for east hill area
Figure 6.3-13 Calculated $S_u$ versus depth for west hill area
Figure 7.2-1 Slope stability - cross-section 1
Figure 7.2-2 Variation of permanent slope displacement with yield acceleration
Figure 7.2-3 Slope stability - cross-section 1 - for reduced strength analyses
Figure 7.3-1 Relationship between plasticity index of fines and cyclic stress ratio causing liquefaction
Figure 7.3-2 Correlation between field liquefaction of sands, penetration resistance, and shear wave velocity
Figure 7.3-3 Correlation between normalized shear wave velocity and cyclic stress ratio causing liquefaction
Figure 7.3-4 Liquefaction potential chart based on shear wave velocity of a sand layer and 20 cycles of strong motion
Figure 7.3-5 Charleston, South Carolina earthquake: Liquefaction/marginal liquefaction data
Figure 7.3-6 Charleston, South Carolina earthquake: No liquefaction/liquefaction data.
Figure 7.3-7 Influence of period of sustained pressure on stress ratio causing 100 percent pore water pressur
Figure 7.3-8 Influence of age on relative strength against liquefaction
Figure 7.3-9(a) Application of Chinese criteria to the clayey soils
Figure 7.3-9(b) Application of Chinese criteria to the clayey soils
Figure 7.3-9(c) Application of Chinese criteria to the clayey soils
Figure 7.3-9(d) Application of Chinese criteria to the clayey soils
Figure 7.3-9(e) Application of Chinese criteria to the clayey soils
Figure 7.3-9(f) Application of Chinese criteria to the clayey soils
Figure 7.3-9(g) Application of Chinese criteria to the clayey soils
Figure 7.3-10 Acceleration, velocity, and displacement time histories: Local earthquake event
Figure 7.3-11 Acceleration, velocity, and displacement time histories: Distant earthquake event
Figure 7.3-12 Acceleration, velocity, and displacement time histories: 84th percentile motion
Figure 7.3-13 Acceleration response spectrum: Local earthquake
Figure 7.3-14 Acceleration response spectrum: Distant earthquake
Figure 7.3-15 Acceleration response spectrum: 84th percentile earthquake

Figure 7.3-16 Subsurface cross-section A used for free-field ground response and settlement analyses
Figure 7.3-17 Subsurface cross-section B used for free-field ground response and settlement analyses
Figure 7.3-18 Relationship between pore pressure buildup and coefficient of volumetric compression - (a) measured; (b) theoretical (Lee and Albaisa, 1974)
Figure 7.5-1 Tank 48: Observed settlements
Figure 7.5-2 Tank 49: Observed settlements
Figure 7.5-3 Tank 50: Observed settlements
Figure 7.5-4 Tank 51: Observed settlements
Figure 7.5-5 Settlement pattern comparison for ITP and DWPF
Figure 7.5-6 Distribution of vertical stress at different stages of tank operation
Figure 7.5-7 Correlation between moisture content and initial void ratio
Figure 7.5-8 Correlation between moisture content and compression ratio
Figure 7.5-9 Tank Type III structure footnote: for Type IIIA tanks, roof is 5 feet thick at the center tapering to 4 feet at edges
Figure 7.5-10 WSRC tank 3D SASSI model for Type IIIA
Figure 7.5-11 Criteria for determination of the equivalent length of the 2D model
Figure 7.5-12 Tank 2D SASSI model for Type IIIA
Figure 7.5-13 Comparison of horizontal transfer functions between 2D and 3D models
Figure 7.5-14 Comparison of vertical transfer functions between 2D and 3D models
Figure 7.5-15 SASSI 2D model of profile AA
Figure 7.5-16 SASSI 2D model of profile BB
Figure 7.5-17 Comparison of SASSI results with free-field SHAKE results for profile AA at the location of column A5
Figure 7.5-18 Comparison of SASSI and SHAKE maximum shear stresses at column A5 for EBE local event
Figure 7.5-19 Comparison of SASSI and SHAKE maximum shear stresses at column A5 for EBE distant event
Figure 7.5-20 Comparison of SASSI SSI results with free-field SHAKE results for profile BB at the location of column B3
Figure 7.5-21 Comparison of SASSI and SHAKE maximum shear stress results at column B3 for EBE local event
Figure 7.5-22 Comparison of SASSI and SHAKE maximum shear stress results at column B3 for EBE distant event
Figure 7.5-23 Maximum horizontal acceleration contours (in g's) for profile AA from SASSI analysis - EBE local event - full tank condition
Figure 7.5-24 Maximum horizontal acceleration contours (in g's) for profile AA from SASSI analysis - EBE local event - empty tank condition
Figure 7.5-25 Maximum horizontal acceleration contours (in g's) for profile AA from SASSI analysis - EBE distant event - full tank condition

Figure 7.5-26 Maximum horizontal acceleration contours (in g's) for profile AA from SASSI analysis - EBE distant event - empty tank condition

Figure 7.5-27 Maximum shear stress contours (ksf) for profile AA from SASSI analysis - EBE local event - full tank condition

Figure 7.5-28 Maximum shear stress contours (ksf) for profile AA from SASSI analysis - EBE local event - empty tank condition

Figure 7.5-29 Maximum shear stress contours (ksf) for profile AA from SASSI analysis - EBE distant event - full tank condition

Figure 7.5-30 Maximum shear stress contours (ksf) for profile AA from SASSI analysis - EBE distant event - empty tank condition

Figure 7.5-31 Maximum horizontal acceleration contours (g's) for profile BB from SASSI analysis - EBE local event - full tank condition

Figure 7.5-32 Maximum horizontal acceleration contours (g's) for profile BB from SASSI analysis - EBE local event - empty tank condition

Figure 7.5-33 Maximum horizontal acceleration contours (g's) for profile BB from SASSI analysis - EBE distant event - full tank condition

Figure 7.5-34 Maximum horizontal acceleration contours (g's) for profile BB from SASSI analysis - EBE distant event - empty tank condition

Figure 7.5-35 Maximum shear stress contours (ksf) for profile BB from SASSI analysis - EBE local event - full tank condition

Figure 7.5-36 Maximum shear stress contours (ksf) for profile BB from SASSI analysis - EBE local event - empty tank condition

Figure 7.5-37 Maximum shear stress contours (ksf) for profile BB from SASSI analysis - EBE distant event - full tank condition

Figure 7.5-38 Maximum shear stress contours (ksf) for profile BB from SASSI analysis - EBE distant event - empty tank condition

Figure 7.5-39 Effective cyclic shear stress ratio contours for profile AA from SASSI analysis - EBE local event, full tanks condition

Figure 7.5-40 Effective cyclic shear stress ratio contours for profile AA from SASSI analysis - EBE distant event, full tanks condition

Figure 7.5-41 Maximum shear strain contours for profile AA form SASSI analysis - EBE local event, full tanks condition

Figure 7.5-42 Maximum shear strain contours for profile AA form SASSI analysis - EBE distant event, full tanks condition

Figure 7.5-43 Effective cyclic shear stress ratio contours for profile BB from SASSI analysis - EBE local event, full tanks condition

Figure 7.5-44 Effective cyclic shear stress ratio contours for profile BB from SASSI analysis - EBE distant event, full tanks condition

Figure 7.5-45 Maximum shear strain contours for profile BB form SASSI analysis - EBE local event, full tanks condition

Figure 7.5-46 Maximum shear strain contours for profile BB from SASSI analysis - EBE distant event, full tanks condition

Figure 7.5-47 Maximum seismic soil bearing demand for Tank 48, profile BB, EBE local event
Figure 7.5-48 Maximum seismic soil bearing demand for Tank 48, profile BB, EBE distant event
Figure 7.5-49 Maximum seismic soil bearing demand for Tank 49, profile AA, EBE local event
Figure 7.5-50 Maximum seismic soil bearing demand for Tank 49, profile AA, EBE distant event
Figure 7.5-51 Maximum seismic soil bearing demand for Tank 49, profile BB, EBE local event
Figure 7.5-52 Maximum seismic soil bearing demand for Tank 49, profile BB, EBE distant event
Figure 7.5-53 Maximum seismic soil bearing demand for Tank 51, profile AA, EBE local event
Figure 7.5-54 Maximum seismic soil bearing demand for Tank 51, profile AA, EBE distant event
Figure 7.5-55 Maximum horizontal acceleration contours (g's) for profile AA from SASSI analysis - 84th percentile motion - full tank condition
Figure 7.5-56 Maximum shear stress contours (ksf) for profile AA from SASSI analysis - 84th percentile motion - full tank condition
Figure 7.5-57 Effective cyclic stress ratio contours for profile AA from SASSI analysis - 84th percentile motion - full tank condition
Figure 7.5-58 Maximum shear strain contours for profile AA from SASSI analysis - 84th percentile motion - full tank condition
Figure 7.5-59 Maximum seismic soil bearing demand for Tank 49, profile AA, $84^{th}$ percentile motion
Figure 7.5-60 Maximum seismic soil bearing demand for Tank 51, profile AA, $84^{th}$ percentile motion
Figure 7.5-61 FLAC discretized elements for profile AA
Figure 7.5-62 Soil layers in FLAC model of profile AA
Figure 7.5-63 FLAC discretized elements for profile BB
Figure 7.5-64 Soil layers in FLAC model of profile BB
Figure 7.5-65 Contours of effective vertical stresses (ksf) for profile AA under full tank condition
Figure 7.5-66 Contours of effective vertical stresses (ksf) for profile AA under empty tank condition
Figure 7.5-67 Orientation of effective principal stresses for profile AA
Figure 7.5-68 Contours of effective vertical stresses (ksf) for profile BB under full tank condition
Figure 7.5-69 Contours of effective vertical stresses (ksf) for profile BB under empty tank condition
Figure 7.5-70 Orientation of effective principal stresses for profile BB.

Figure 7.5-71 Kriged CPT tip resistance for profile AA for tip resistance values less than 50 tsf
Figure 7.5-72 Kriged CPT tip resistance for profile AA for tip resistance values greater than 50 tsf
Figure 7.5-73 Kriged CPT friction ratio for profile AA
Figure 7.5-74 Kriged CPT tip resistance for profile BB for tip resistance values less than 50 tsf
Figure 7.5-75 Kriged CPT tip resistance for profile BB for tip resistance values greater than 50 tsf
Figure 7.5-76 Kriged CPT friction ratio for profile BB
Figure 7.5-77 Cross validation results for borehole SCPT 1
Figure 7.5-78 Cross validation results for borehole SCPT 6B
Figure 7.5-79 Settlement profile for Tank 49, EBE local and distant events, with 4.5 in. compression of soft zones, tank full and empty conditions, profile AA
Figure 7.5-80 Settlement profile for Tank 51, EBE local and distant events, with 4.5 in. compression of soft zones, tank full and empty conditions, profile AA
Figure 7.5-81 Settlement profile for Tank 49, EBE local and distant events, with 7 in. compression of soft zones, tank full and empty conditions, profile AA
Figure 7.5-82 Settlement profile for Tank 51, EBE local and distant events, with 7 in. compression of soft zones, tank full and empty conditions, profile AA
Figure 7.5-83 Settlement profile for Tank 49, EBE local event, with variable compression of soft zones, tank full condition, profile AA
Figure 7.5-84 Settlement profile for Tank 51, EBE local event, with variable compression of soft zones, tank full condition, profile AA
Figure 7.5-85 Settlement profile for Tanks 50 and 51, EBE local event, with variable compression of soft zones, tank full condition, profile CC'
Figure 7.5-86 Settlement profile for Tank 49, 84th percentile motion, with variable compression of soft zones, tank full condition, profile AA
Figure 7.5-87 Settlement profile for Tank 51, 84th percentile motion, with variable compression of soft zones, tank full condition, profile AA
Figure 8.2-1 Slope stability - cross-section 1
Figure 8.2-2 Slope stability - cross-section 2
Figure 8.2-3 Slope stability - cross-section 3
Figure 8.2-4 Slope stability - cross-section 4
Figure 8.2-5 Summary of tip resistances for CPTs in north hill area.
Figure 8.3-1 Cyclic shear stress ratio profile for ITP 1-D liquefaction settlement analysis
Figure 8.3-2 Cyclic shear stress ratio profile for HTF 1-D liquefaction settlement analysis
Figure 8.3-3 Comparison of shear modulus curves developed for ITP with those used by GEI
Figure 8.3-4 Comparison of damping curves developed for ITP with those used by GEI

Figure 8.3-5 Comparison of cyclic stress ratio profiles for the 84th percentile ground motion using ITP and GEI dynamic curves
Figure 8.3-6 Comparison of 1-D liquefaction settlements calculated using ITP and GEI dynamic curves for the 84th percentile, non-fill profile at ITP
Figure 8.3-7 Summary of 1-D liquefaction settlements calculated for the 84th percentile ground motion at ITP
Figure 8.3-8 Summary of 1-D liquefaction settlements calculated for the 84th percentile ground motion at HTF
Figure 8.5-1 Summary of settlements for H-area waste storage tanks
Figure 9.2-1 Contours of equal probability of liquefaction for silty sand - local model (after Liao et al., 1988)
Figure 9.3-1 EPRI and LLNL spectral hazard curves
Figure 9.3-2 EPRI Vogtle rock mean hazard - SV(2.5Hz) = 1.0 cm/sec
Figure 9.3-3 EPRI Vogtle rock mean hazard - SV(2.5Hz) = 2.0 cm/sec
Figure 9.3-4 EPRI Vogtle rock mean hazard - SV(2.5Hz) = 6.0 cm/sec
Figure 9.3-5 EPRI Vogtle rock mean hazard - SV(2.5Hz) = 8.7 cm/sec
Figure 9.3-6 EPRI Vogtle rock mean hazard - SV(2.5Hz) = 16.0 cm/sec
Figure 9.3-7 EPRI Vogtle rock mean hazard - SV(2.5Hz) = 26.0 cm/sec
Figure 9.3-8 EPRI Vogtle rock mean hazard - SV(2.5Hz) = 40.0 cm/sec
Figure 9.3-9 EPRI Vogtle rock mean hazard - SV(2.5Hz) = 90.0 cm/sec
Figure 9.3-10 Functional relationship between Mbar and spectral velocity
Figure 9.3-11 Functional relationship between Mbar and mean annual hazard
Figure 9.3-12 Functional relationship between Dbar and spectral velocity
Figure 9.3-13 Ten acceleration response spectra (5% damping) developed for the rock motion
Figure 9.3-14 Duration envelope function
Figure 9.3-15 Acceleration time history for earthquake motion E01
Figure 9.3-16 Acceleration time history for earthquake motion E02
Figure 9.3-17 Acceleration time history for earthquake motion E03
Figure 9.3-18 Acceleration time history for earthquake motion E04
Figure 9.3-19 Acceleration time history for earthquake motion E05
Figure 9.3-20 Acceleration time history for earthquake motion E06
Figure 9.3-21 Acceleration time history for earthquake motion E07
Figure 9.3-22 Acceleration time history for earthquake motion E08
Figure 9.3-23 Acceleration time history for earthquake motion E09
Figure 9.3-24 Acceleration time history for earthquake motion E010
Figure 9.3-25 Acceleration response spectra for earthquake motion E01
Figure 9.3-26 Acceleration response spectra for earthquake motion E02
Figure 9.3-27 Acceleration response spectra for earthquake motion E03
Figure 9.3-28 Acceleration response spectra for earthquake motion E04

Figure 9.3-29 Acceleration response spectra for earthquake motion E05
Figure 9.3-30 Acceleration response spectra for earthquake motion E06
Figure 9.3-31 Acceleration response spectra for earthquake motion E07
Figure 9.3-32 Acceleration response spectra for earthquake motion E08
Figure 9.3-33 Acceleration response spectra for earthquake motion E09
Figure 9.3-34 Acceleration response spectra for earthquake motion E10
Figure 9.4-1 CPT soundings and SPT boreholes used in probabalistic liquefaction hazard evaluation
Figure 9.4-2 Shallow shear wave velocity profiles at ITP from seismic cone penetrometer
Figure 9.4-3 Comparison of deep shear wave velocity profiles used in dynamic analysis
Figure 9.4-4 Map showing 2 OYO™ logged, deep core borings
Figure 9.4-5 Measured $(N_1)_{60}$ values for ITP
Figure 9.4-6 Simulated $(N_1)_{60}$ values for ITP
Figure 9.4-7 Measured and simulated $(N_1)_{60}$ values for ITP
Figure 9.4-8 Histogram of measured $(N_1)_{60}$ values - Tobacco Road 3/4
Figure 9.4-9 Histogram of simulated $(N_1)_{60}$ values - Tobacco Road 3/4.
Figure 9.4-10 Histogram of combined (measured and simulated) $(N_1)_{60}$ values - Tobacco Road 3/4
Figure 9.4-11 Relationships between stress ratio causing liquefaction and $(N1_1)_{60}$ values for sands and silty sands in M =7 1/2 earthquakes. (after Seeds et al., 1985)
Figure 9.4-12 Relationship between stress ratio causing liquefaction and cone tip resistance for sands and silty sands. (after DeAlba and Seed, 1986)
Figure 9.4-13 Relationship between combined correction factor Cr and over-consolidation ratio. (after Seed, Arango and Chan, 1975)
Figure 9.4-14 Comparison of earthquake magnitude correction factors from various sources
Figure 9.4-15 Liquefaction data: field vs. laboratory
Figure 9.5-1 Effect of frequency content of input motion on the effective cyclic stress ratio (CSR) - Tobacco Road 3/4, Soil Profile CPT11
Figure 9.5-2 Relative histogram for effective shear stress ratio - Tobacco Road 3/4, earthquake EO1. Mean = 0.0078, Standard deviation = 0.0019
Figure 9.5-3 Relative histogram for effective shear stress ratio - Tobacco Road 3/4, earthquake EO2 - Mean = 0.0119, Standard deviation 0.0018
Figure 9.5-4 Relative histogram for effective shear stress ratio - Tobacco Road 3/4, earthquake EO3 - Mean = 0.022, Standard deviation = 0.0054
Figure 9.5-5 Relative histogram for effective shear stress ratio - Tobacco Road 3/4, earthquake EO4 - Mean = 0.0333 Standard deviation = 0.0082
Figure 9.5-6 Relative histogram for effective shear stress ratio - Tobacco Road 3/4, Earthquake E05 - Mean = 0.0564, Standard deviation = 0.0124

Figure 9.5-7 Relative histogram for effective shear stress ratio - Tobacco Road 3/4, earthquake EO6 - Mean = 0.0752, Standard deviation = 0.0116

Figure 9.5-8 Relative histogram for effective shear stress ratio - Tobacco Road 3/4, earthquake EO7 - Mean = 0.117, standard deviation = 0.021

Figure 9.5-9 Relative histogram for effective shear stress ratio - Tobacco Road 3/4, earthquake EO8 - Mean = 0.155, Standard deviation = 0.036

Figure 9.5-10 Relative histogram for effective shear stress ratio - Tobacco Road 3/4, earthquake EO9 - Mean 0.205, Standard deviation 0.048

Figure 9.5-11 Relative histogram for effective shear stress ratio - Tobacco Road 3/4, earthquake E10 - Mean 0.262, Standard deviation 0.0424

Figure 9.6-1 Flow chart for ASHLE Methodology

Figure 9.6-2 Annual liquefaction hazard computed by ASHLE

## LIST OF VOLUMES AND APPENDICES

| | |
|---|---|
| Volume 1 | Text, Tables and Figures |
| Volume 2 | Appendices A, B, C and D |
| Volume 3 | Final Report, Phase I and II, Cone Penetrometer Studies |
| Volume 4 | Laboratory Test Results, Phase I |
| Volume 5 | Laboratory Test Results, Phase II, Vol. 1 of 2 |
| Volume 6 | Laboratory Test Results, Phase II, Vol. 2 of 2 |
| Volume 7 | Ebasco Geophysical Report |

## LIST OF ACRONYMS, SYMBOLS, AND JARGON

| | |
|---|---|
| AASHO | American Association of State and Highway Officials |
| AASHTO | American Association of State and Highway Transportation Officials |
| AF | Adjustment Factor |
| $a_{max}$ | Peak horizontal ground acceleration |
| ARA | Applied Research Associates |
| arkosic | A sandstone or sand containing more than 25% feldspar |
| ASHLE | Advanced Seismic Hazard/Liquefaction Evaluation |
| ASTM | American Society for Testing Materials |
| B-value | Pore pressure parameter for isotropic loading (an indication of saturation) |
| bioclastic | Sediments consisting of fragmental organic remains |
| biomoldic | Composed of, or containing shell molds |
| BLUE | Best Linear Unbiased Estimate |
| BNI | Bechtel National, Inc. |
| bpf | blows per foot |
| BSRI | Bechtel Savannah River, Inc. |
| c | Total cohesion |
| c' | Effective cohesion |
| calcareous | containing calcium carbonate |
| calcilutite | A limestone made up of calcareous rock flour |
| Cambrian | Geological Period from 570 mybp to 500 mybp |
| carbonate | A compound containing the radical $CO_3^{+2}$ |
| CCNY | City College of New York |
| $C_c$ | Compression Index |
| CD | Consolidated Drained Triaxial Test |
| Cenozoic | Geological Era from 65 mybp to present |
| cf | cubic feet |
| CH | Highly plastic clay |
| clastic | Consisting of fragments of rock that have been transported |
| Cn | Vertical Effective Stress Normalization Factor for SPT-N |
| COE | Corps of Engineers |
| COR | Corrected tip resistance for pore pressure induced behind the cone tip. |
| CPS | Cycles per second, Hz |
| CPT | Cone Penetrometer Test |
| $C_r$ | Correction factor to adjust CTX results to field conditions (liquefaction) |
| $C_r$ | Recompression Index (static settlement) |
| Cretaceous | Geological Period from 136 mybp to 65 mybp |
| cristobalite | polymorphous quartz ($Si0_2$) |

| | |
|---|---|
| CSR | Cyclic Stress Ratio |
| CSRN | Cyclic Stress Ratio normalized to one ton per square foot |
| CTX | Cyclic Triaxial Shear Testing |
| CU | Consolidated Undrained Triaxial Test |
| Cv | Coefficient of Consolidation |
| CWP | Circulating Water Pipeline |
| d(50) | Mean grain size |
| DB1 | Dry Branch Layer 1 |
| DB1/DB3 | Dry Branch Layers 1 through 3 |
| DB2 | Dry Branch Layer2 |
| DB3 | Dry Branch Layer3 |
| DB4 | Dry Branch Layer4 |
| DB4/DB5 | Dry Branch Layers 4 through 5 |
| DB5 | Dry Branch Layer 5 |
| DBE | Design Basis Earthquake |
| deltaic | Of or produced by deltas |
| Devonian | Geological Period from 395 mybp to 345 mybp |
| DMT | Dilatometer soundings |
| DOE | Department of Energy |
| $D_r$ | Relative density |
| DWPF | Defense Waste Processing Facility |
| EBE | Evaluation basis earthquake |
| echinoid | One of a group of invertebrates including sea urchins and their allies |
| EDS | Environmental Drilling Services |
| El | Elevation relative to Mean Sea Level |
| $e_o$ | Initial void ratio |
| Eocence | Geological Epoch from 38 mybp to 54 mybp |
| EPRI | Electric Power Research Institute |
| ESP | Extended Sludge Processing |
| facies | General appearance of one part of a rock or sedimentary body |
| feldspar | A group of common aluminum-silicate, rock-forming minerals |
| feldspathic | Containing feldspar |
| FLAC | Fast Lagrangian Analysis of Continua |
| fluvial | Produced by river action |
| fps | feet per second |
| fr | CPT friction ratio |
| FS | Factor of Safety |
| g | Acceleration of gravity |

| | |
|---|---|
| G | Shear Modulus |
| G&HES | Geotechnical & Hydraulic Engineering Services |
| G/Gmax | Shear Modulus Ratio |
| GEI | Geotechnical Engineers, Inc. |
| glauconite | A green mineral closely related to the micas, commonly of marine origin |
| GM | Geometric Mean |
| Gmax | Low strain shear modulus |
| GSA | General Separations Area |
| GWT | Groundwater table |
| H | Layer thickness |
| HHW | High Heat Waste |
| HLW | High Level Waste |
| Holocene | Geological Epoch from 10,000 years to present |
| HTF | H-Area Tank Farm |
| Hz | Hertz, cycles per second |
| ID | Inside diameter |
| ITP | In-Tank Precipitation Facility |
| Jurassic | Geological Period from 190 mybp to 136 mybp |
| kaolin | A common hydrous, aluminum silicate, clay mineral |
| kaolinitic | Of or containing kaolin |
| KASS | K-Area Soil Stabilization |
| kcf | Kips per cubic foot |
| kip | 1000 pounds |
| km | Kilometer |
| $k_{max}$ | Maximum average acceleration |
| $k_\sigma$ | Vertical effective stress reduction factor |
| ksf | Kips per square foot |
| $k_y$ | Seismic yield coefficient |
| L | Length |
| LHW | Low Heat Waste |
| LLNL | Lawrence Livermore National Laboratory |
| lignite | A brown-black, low grade coal |
| lignitic | Containing lignite |
| lithofacies | The rock record of any sedimentary environment |
| LL | Liquid limit |
| m/sec | Meters per second |
| MAH | Mean annual hazard |
| MC | Moisture content |
| Mesozoic | Geological Era from 225 mybp to 65 mybp |

| | |
|---|---|
| MH | High plasticity silt |
| micaceous | Containing mica |
| micrite | A limestone with a very fine, subcrystalline texture |
| Miocene | Geological Epoch from 26 mybp to 7 mybp |
| Mississippian | Geological Period from 345 mybp to 325 mybp |
| ML | Low plasticity silt |
| mm | Millimeter |
| MMDPP | Multi-Mode Deep Profiling Program |
| MPMR | Moran, Proctor, Mueser & Rutledge |
| MRJD | Mueser, Rutledge, Johnston, & DeSimone |
| MRWJ | Mueser, Rutledge, Wentworth, & Johnston |
| MSF | Magnitude scaling factor |
| MSL | Mean sea level, ft |
| muscovite | A transparent to translucent mica |
| $m_v$ | Coefficient of compressibility |
| $m_{v0}$ | Coefficient of compressibility at low confining pressure |
| $M_w$ | Moment magnitude |
| mybp | million years before present |
| $N_1$ | SPT N-value normalized to 1 tsf |
| $N_k$ | Cone bearing factor |
| $N_L$ | Number of cycles to liquefaction |
| NRC | Nuclear Regulatory Commission |
| NWTF | New Waste Transfer Facility |
| OCR | Overconsolidation ratio |
| OD | Outside Diameter |
| Oligocene | Geological Epoch from 38 mybp to 26 mybp |
| Ordovician | Geological Period from 500 mybp to 430 mybp |
| P | P-wave, compressional seismic wave |
| p-q | stress path strength parameters |
| P/S-CPT | Piezo-seismic CPT |
| Paleocene | Geological Epoch from 65 mybp to 54 mybp |
| Paleozoic | Geological Era from 570 mybp to 225 mybp |
| PB | Pitcher barrel |
| $p_c$ | Preconsolidation pressure |
| pcf | pounds per cubic foot |
| Pennsylvanian | Geological Period from 325 mybp to 280 mybp |
| Permian | Geological Period from 280 mybp to 225 mybp |
| pga | Peak ground acceleration |
| PI | Plasticity index |

| | |
|---|---|
| PL | Plastic limit |
| Pleistocene | Geological Epoch from 2.5 mybp to 10,000 years before present |
| Pliocene | Geological Epoch from 7 mybp to 2.5 mybp |
| Precambrian | Geological Era before 570 mybp |
| PS | Piston sample |
| PSI | Pounds per square inch |
| psf | pounds per square foot |
| PSV | Pseudospectral velocity |
| PVC | Polyvinyl Chloride |
| Q | Crustal structure |
| QA | Quality assurance |
| $q_c$ | CPT tip resistance |
| Quaternary | Geological Period from 2.5 mybp to present |
| RBOF | Receiving Basin for Offsite Fuel |
| RCA | Radiologically Controlled Areas |
| Recent | Geological Epoch from 10,000 years to present (i.e., Holocene) |
| RSA | Rock spectral acceleration |
| RTF | Replacement Tritium Facility |
| $r_u$ | Pore water pressure ratio = $\Delta u/\sigma_0'$ |
| RVT | Random vibratory theory |
| Sa-g | Spectral Acceleration in g |
| SASSI | System for Analysis of Soil Structure Interaction |
| SC | Clayey Sand |
| SCPT | Seismic cone penetrometer test |
| SGS | Site Geotechnical Services |
| siliciclastic | Composed predominately of clastic sediments rich in silica |
| Silurian | Geological Period from 430 mybp to 395 mybp |
| SM | Silty Sand |
| SP | Poorly graded sand |
| SPT | Standard Penetration Test |
| SRP | Savannah River Plant |
| SRP | Standard Review Plan |
| SRS | Savannah River Site |
| SSE | Safe Shutdown Earthquake |
| SSI | Soil structure interaction |
| SSIRP | Seismic Safety Issue Resolution Program |
| ST | Santee/Tinker Formation |
| ST | Shelby tube (soil sampling) |
| st. dev. | standard deviation |

| | |
|---|---|
| STD | Standard |
| $S_u$ | Undrained shear strength |
| T | Time |
| terrigenous | Deposited in or on the earth's crust |
| Tertiary | Geological Period from 65 mybp to 2.5 mybp |
| Tomography | Cross-hole velocity imaging |
| TR1 | Tobacco Road Layer 1 |
| TR2 | Tobacco Road Layer 2 |
| TR3 | Tobacco Road Layer 3 |
| TR3/TR4 | Tobacco Road Layers 3 through 4 |
| TR4 | Tobacco Road Layer 4 |
| Triassic | Geological Period from 225 mybp to 190 mybp |
| TSEP | Tank Seismic Expert Panel |
| tsf | tons per square foot |
| TX | Triaxial |
| UCB | University of California, Berkeley |
| UCRL | University California Research Laboratory |
| UD | Undisturbed |
| UG | Underground |
| $u_r$ | Residual pore water pressure |
| US | United States |
| USACOE | United States Army Corps of Engineers |
| USGS | United States Geological Survey |
| USNRC | U. S. Nuclear Regulatory Commission |
| UU | Unconsolidated Undrained TriaxialTest |
| V | Volume |
| $V_s$ | S-wave velocity |
| Vugular porosity | Porosity due to vugs (cavity) in calcareous rock |
| WC | Water content (moisture content) |
| WSRC | Westinghouse Savannah River Company |
| $(N_1)_{60}$ | SPT N-value normalized to 1 tsf and 60% max. hammer energy ratio |
| $(q_c)_1$ | CPT tip resistance normalized to 1 ton per square foot |
| (U) | Unclassified |
| $(V_s)_1$ | S-wave velocity normalized to 1 ton per square foot |
| $\delta_n$ | Change in shape parallel to length |
| $\Delta p$ | Change in load or applied load |
| $\delta_s$ | Change in shape perpendicular to length |
| $\Delta S$ | Settlement |
| $\Delta u$ | Change in pore water pressure |

| | |
|---|---|
| $\Delta u/\sigma_{3c}$ | Pore pressure ratio |
| $\Delta V/V$ | Volumetric strain |
| $\varepsilon_v$ | Volumetric strain |
| $\varepsilon da$ | Axial strain = $\delta_n/L$ |
| $\phi$ | Total friction angle |
| $\phi'$ | Effective friction angle |
| $\gamma$ | Shear strain or cyclic shear strain = $\delta_s/L$ |
| $\gamma$ | Unit weight of soil |
| $\gamma_e$, $\gamma_t$ | Limiting shear strain |
| $\sigma'_{con}$ | Effective confining stress = $\sigma'3c$ |
| $\sigma dp$ | Pulsating applied vertical stress |
| $\sigma dp/2\sigma_{3c}$ | Laboratory pulsating stress ratio |
| $\sigma'$, $\sigma_v'$ | Effective vertical stress |
| $\sigma'_{3c}$ | Effective confining stress in triaxial testing apparatus |
| $\sigma_o'$ | Initial effective vertical stress |
| $\sigma_{vo}$ | Initial total vertical stress |
| $\tau$ | Shear stress |
| $\tau/\sigma_o'$ | Cyclic stress ratio |
| $\upsilon$ | Poisson's ratio |

# 1. INTRODUCTION

A geotechnical program has been completed in H-Area for the In-Tank Precipitation Facility (ITP) and the balance of the H-Area Tank Farm (HTF) at the Savannah River Site (SRS) in South Carolina (see Figure 1.0-1). The program consisted of a literature search for relevant technical data, field explorations, field and laboratory testing, and analyses. The geotechnical program was developed in compliance with DOE Order 6430.1A (DOE, 1992a) and the "Guidance for Geotechnical Studies, DOE Non-Reactor Nuclear Facilities Under Cognizance of the Defense Program." The geotechnical program is one of the three initiated by the H-Area/ITP Seismic Safety Issue Resolution Program (SSIRP) Plan Westinghouse Savannah River Company ((WSRC), 1994a) to resolve the seismic safety issues for the H-Area Tank Farm and ITP facilities. The other two programs, structural and safety, are not addressed herein. Aerial photos of the ITP and HTF are provided in Figure 1.0-2 and 1.0-3, respectively.

Primarily due to scheduling, but also due to funding, this report focuses on the ITP Facility. Thus, the bulk of the analyses described have been performed for the area immediately around and near the ITP. The geotechnical strategy was to perform analyses for ITP and apply the results to the HTF by comparing subsurface conditions at ITP with those in the balance of the HTF. This document presents the results of the investigations and geotechnical engineering analyses for the ITP and the HTF.

## 1.1 Report Organization

This report consists of seven volumes. Volume 1 contains the executive summary, summarizes the field and laboratory investigations, and presents the engineering evaluations and the overall conclusions. Volume 2 contains the preliminary results of the geostatistical study performed by Georgia Institute of Technology, sampling and testing procedures, and field borehole logs. Volume 3 contains the cone penetrometer and dilatometer soundings. Volumes 4, 5, and 6 contain the laboratory test results. Volume 7 contains the geophysical report including the cross- hole velocity surveys and the down-hole refraction surveys.

Volume 1 is organized as follows:

- Section 1: Introduction
- Section 2: Seismology and geology
- Section 3: Subsurface exploration
- Section 4: Laboratory testing
- Section 5: Subsurface conditions
- Section 6: Engineering properties,
- Section 7: Design criteria and evaluations for the ITP

- Section 8: Engineering evaluation for the balance of the HTF
- Section 9: Probabilistic Liquefaction Assessment at the ITP
- Section 10: Summary
- Section 11: Conclusions and recommendations
- Section 12: References
- Tables
- Figures

## 1.2 Background

The initial phases of geotechnical characterization at the H-Tank Farm, undertaken in 1992, focused on the ITP. The site-specific geotechnical characterization and analyses addressed three areas of concern: (1) slope stability of the waste tank embankment; (2) potential liquefaction in zones of loose, saturated, sandy soils; and (3) potential deep subsidence of "soft zones." The 1992 effort concluded that additional subsurface characterization and geotechnical and structural analyses were required before concerns could be adequately addressed regarding slope stability, liquefaction, or subsidence of unstable zones and their effect on the surface structures. As a result, the geotechnical program was developed and implemented within the SSIRP.

### *1.2.1 Tank Farm*

A total of 51 high-level radioactive waste tanks have been, or are in use, at SRS. Twenty-nine of these tanks are located in the H-Area Tank Farm shown in Figure 1.2-1 and the remainder are in the F-Area Tank Farm. The tanks were built of carbon steel and reinforced concrete, following four different designs as illustrated in Figure 1.2-2. The most recent design (Type III) consists of a full-height, secondary tank. Type III tanks are further subdivided into Type IIIA. Type IIIA tanks have more reinforcing steel in the concrete vaults than Type III and also have a moderately inclined roof. Two designs (Types I and II) have 5-foot-high secondary pans. Type IV tanks are prestressed concrete and have a single steel wall. The ITP evaluation focused on the Type IIIA tanks.

All 12 Type I tanks, 3 of 4 Type II, and 5 of 8 Type IV waste tanks are inactive (Figure 1.2-3). Ten of these inactive tanks (1F, 9-12H, 13-16H and 20F) have known cracks and the level of the liquid waste in them has either been reduced below the cracks or all ejector-pumpable liquid has been removed, leaving a small solid residue. The cracked tanks are identified by an asterisk in Figure 1.2-3. Tank 241-916H in H-Area has been completely emptied. There are three different forms of waste: concentrated saltcake resulting from evaporation operations, sludge, and supernate. The present content level of each tank is also illustrated in Figure 1.2-3.

### *1.2.2 In-Tank Precipitation*

The ITP Facility shown in Figure 1.2-1 is located in the southeast portion of the H-Area Tank Farm. The facility processes salt and supernate waste from the waste tanks in preparation for final transfer and treatment at the Defense Waste Processing Facility (DWPF). The ITP process is a precipitation/adsorption reaction. The resultant precipitate slurry is continuously pumped to a filter cell and filtered. The filtrate is collected, stripped of benzene, sampled, and pumped to the Saltstone Facility to be incorporated into a cement/flyash matrix.

Included with the ITP Facility are Waste Storage Tanks 48 (241-48H), 49 (241-49H), and 50 (241-50H), each 95 feet in diameter and 40 feet high; the Filter Stripper Building (241-96H); the Cold Feed Complex (241-32H); the Control Room (241-82H); and an additional waste storage tank, Tank 22 (241-22H), located to the west in the H-Area Tank Farm. Tank 51, located east of Tank 50, is not part of the ITP Facility.

Construction of the ITP storage tanks was initiated in 1978 and lasted 4 years. A timeline of the tank construction is provided in Figure 1.2-4. Each tank is composed of a stress-relieved primary liner, with a secondary liner, a center column, and a flat roof. Tanks 48 through 51 are arranged in a square pattern spaced approximately 35 feet apart, edge-to-edge. The tanks are founded in natural soil at about elevation 286 feet. The original ground surface was about elevation 300 feet. The sides of each of the tanks are surrounded with an embankment of structural fill built up to a surface elevation of about 328 feet, leaving the tank tops exposed. The slopes of the embankment are covered with a rock gabion and the embankment top is surfaced with asphalt. The area surrounding the tank tops serves as a utility area for equipment, service, and facility operations.

Tank construction began by excavating to elevation 286 feet, then pouring a 4-inch-thick concrete working mat. A double-wall concrete tank foundation was then formed and poured (Figure 1.2-5). The primary tank bottom was then welded while suspended and set into place on the foundation walls. Placement of the truss supports and roof plates followed completion of the primary and secondary wall liners (Figure 1.2-6). Two-and-one-half-foot-thick concrete outer walls were then formed and poured, followed by construction of the concrete slab top. At its thickest point in the center, the top slab is 5 feet thick.

Utilities were placed following the construction of the tanks. As utilities were installed, backfill was placed against the tank walls. Once completed, the fill was topped off with a basecourse and asphalt cap.

Records for the construction of the other facilities within the ITP area are not as complete as those for the tanks. A timeline of the construction of buildings and other related facilities for ITP is provided in Figure 1.2-7. Construction began for the Filter Stripper Building in 1986. The structure was located 25 feet west of Tank 48 by placing a sliver fill against the west side of the existing embankment to increase the area of the embankment top, bringing the building foundation to the same level as the top of the tanks. Thus, the east side of the Filter Stripper Building is supported on fill placed during the tank construction, while the west side is supported on newer fill.

Over the next year-and-a-half, construction of the Filter Stripper Building continued with pouring the foundation, constructing the shell, and installing the equipment. The foundation consists of a 3-foot-thick mat to support the filtrate holding tanks and spread footings to support the building structure. The building was completed in the early part of 1988. The loading under the filtrate holding tank is estimated at 2.7 kips per square foot (ksf) and is 1 ksf under the mat.

The Control Room, constructed on top of the embankment to the north of Tank 49, is supported on 7-foot-square footings exerting an average bearing pressure of about 1.8 ksf. The Cold Feed Complex was constructed at the toe of the embankment and consists of a truck unloading facility, a railroad track, a substation, and several chemical and water storage tanks. These structures were built at approximately the same time as the Filter Stripper Building.

## 1.3 Objectives

The purpose of the investigation was to obtain geotechnical information to evaluate the seismic performance of the foundation materials and the embankments under and around the ITP and apply the results to the balance of the HTF. The geotechnical engineering objectives of the investigation were to: (1) define the subsurface stratigraphy, (2) obtain representative engineering properties of the subsurface and embankment materials, (3) assess the behavior of the subsurface materials and embankments under static and dynamic loads, (4) derive properties for seismic soil-structure interaction analysis, (5) evaluate the lateral and vertical extent of soft zones within the Santee/Tinker Formation, and (6) determine potential settlement at the tank foundation level. To this end, five major areas of study and analyses were completed and are presented in this report:

- Seismology and geology,
- Seismic stability and deformation of embankments,
- Liquefaction susceptibility and settlement of foundation soils,
- Deep-seated settlement due to soft zones (Santee/Tinker Formation), and
- Probabilistic liquefaction assessment.

## 1.4 Work Schedule and Personnel

Site Geotechnical Services (SGS) was requested to provide support for the ITP project in the Fall of 1992. A Phase 1 field investigation was initiated in December 1992 and was completed in April 1993. The results were presented in a preliminary assessment report in March 1993 Bechtel River Savnannah River, Inc.((BSRI), 1993a).

The Phase 2 field investigation began in April 1993. In July 1993, the ITP investigation program was temporarily interrupted due to lack of funding. In October of 1993, the program was reactivated and modified to eventually include all of H-Area Tank Farm. As a result, additional field work (Phase 3 for ITP and the HTF field exploration) and analyses were planned.

Periodic reviews of the effort were conducted by outside subject matter experts. These experts provided independent technical oversight during the program. The experts are:

**Seismology and Ground Motion**

- Robin McGuire, Ph.D., Risk Engineering, Inc.
- Ken Campbell, Ph.D., EQE

**Geology**

- Mat Matthews, Texaco

**Geotechnical Engineering**

- William F. Marcuson, Ph.D., Director of the Geotechnical Laboratory, U.S. Army Corps of Engineers' Waterways Experiment Station
- James K Mitchell, Sc.D., P.E., Private Consultant and Professor, Virginia Polytechnic Institute
- George F. Sowers, P.E., P.G., Senior Consultant and Senior Vice President, Law Companies Group, Inc.

An intensive review was conducted by the geotechnical engineering panel, which was established as a peer review panel early in the project.

The first meeting of the geotechnical Peer Review panel was held at the SRS in October 1993. In November 1993, the SSIRP plan was developed and issued under the management of the WSRC High Level Waste Division. With the issuance of the SSIRP plan, field work and analyses began in December 1993. A second geotechnical peer review meeting was held in December 1993.

In January 1994, Revision 1 of the SSIRP was issued. In early April 1994, an ad hoc meeting was held in San Francisco with the project team, A. Cornell, and C. Constantino, to discuss the liquefaction probability analysis. Also in attendance were two of the three geotechnical peer reviewers and DOE. In late April 1994, the third geotechnical peer review meeting was held in Atlanta.

The Phase 3 investigation and engineering analyses were completed in early summer 1994 and a summary report was issued in July 1994. From August through October 1994, work on the final geotechnical report and the HTF Phase 1 field investigation were stopped due to lack of funding.

In September and November 1994, Revisions 1 and 2 of the geotechnical summary report were issued. In late September 1994, the fourth geotechnical peer review meeting was held at SRS. Also, in November 1994, Revision 2 of the SSIRP was issued and limited funding restored. As a result, engineering analyses that had stopped were re-activated and the efforts to prepare this report initiated. In mid-December 1994 and mid-September 1995, additional geotechnical peer review meetings were held in Atlanta. At each meeting, the previous meeting's comments were discussed

with the peer reviewers. Generally, all of the comments have either been resolved and/or incorporated in the program to the satisfaction of the Geotechnical Peer Review Panel.

The first meeting was held with the Senior Seismic Advisory Panel in December 1994. This panel was established by WSRC for the purpose of providing advice to WSRC on the approach and analytical treatment of seismic issues sitewide. The panel concurs with the conclusions regarding liquefaction tank settlement and embankment stability. Details of their assessment and findings are contained in Appendix D.

All work was performed by SGS with additional support from Bechtel National, Incorporated (BNI), Geotechnical & Hydraulic Engineering Services (G&HES) in San Francisco. Personnel and responsibilities were:

- Dr. Jerome Morin, Manager HLW Engineering: program manager for the SSIRP
- Mr. Lawrence A. Salomone, WSRC Chief Geotechnical Engineer, Manager of SGS, Savannah River Site: responsible for all geotechnical, geologic, and seismologic work and project review.
- Dr. Ignacio Arango, Manager, Geotechnical Engineering, G&HES, San Francisco: overall technical direction of the BNI geotechnical program.
- Dr. Farhang Ostadan, Chief Soils Engineer, G&HES, San Francisco: project geotechnical engineer.
- Mr. Michael R. Lewis, Manager, Geotechnical Engineering, SGS, Savannah River Site: overall technical direction of the SGS geotechnical program.
- Mr. Matthew Maryak, Manager, Site Characterization, SGS, Savannah River Site: overall technical direction of the SGS geologic and seismologic program.
- Dr. Steven F. Bartlett, SGS Geotechnical Engineering Lead: engineering analyses.
- Mr. Frank H. Syms, SGS Geological Engineering Lead: geology and field work.

Other staff assigned to the project included the following:

- Field Work: P. F. Brown as field supervisor, P.L. Chau, G.A. Day, S. Desai, C. Doolittle, W. J. Rabe, C. M. Rothammer, L. B. Triplett;
- Laboratory Work: J. T. Cameron, G. H. Glos, Da-Min Ho, R. Luna, S. Sammadar;
- Geology: R. Aadland, S. F. Bartlett, R. Cumbest, S. E. Lewis, V. Price, A. Stieve, F. H. Syms, D. Wyatt;
- Seismology: R. C. Lee;
- Engineering Evaluations: W. R. Albin, S. F. Bartlett, J. T. Cameron, N. Deng, M. A. Durrani, G. H. Glos, Da-Min Ho, J. Lydon, S. M. Mamoon, R. Oberoi, T. Liu, W. J. Rabe, E. Strassburger;

- Report Preparation: M. R. Lewis, F. H. Syms, S. F. Barlett, J. T. Cameron, W. J. Rabe, T. E. Ross, R. C. Lee, A. L. Stieve, M. J. Hasek, P. L. Chau, C. M. Rothammer, P. F. Brown, G. H. Glos, I. Arango, F. Ostadon, V. Price;
- Quality Assurance: J. Bergamyer, T. Harrison, J. Haff, G. Gilbody;
- Support Staff: D. Ahearn, J. Bollinger, H. S. Cooper, E. R. De Leon, C. L Duggins, M. M. Finn, R. V. Gutierrez, T. I. Mote, M. D. Quero, A. Q. Resayo, S. Q. Smoak, S. F. Vick.

## 1.5 Available Geotechnical Information

The H-Area has been the subject of several geotechnical and geological investigations since the inception of SRS in the early 1950s. Early studies at SRS were undertaken by the COE in 1951 and 1952 to broadly identify subsurface conditions, perform subsurface grouting beneath critical structures, and map surficial soils and drainage patterns of the SRS.

During these early studies, the COE identified discrete horizons in the subsurface that were either particularly loose, soft, and/or contained potential voids of various sizes. These zones were related to leaching of carbonate horizons as described in later sections of this report. Geologic and hydrologic studies also identified several shallow surface depressions that were believed to be related to the carbonate deposits. Nine surface depressions were mapped by the COE in 1952 within H-Area. Subsequent geotechnical investigations at the SRS have been made at important structures to characterize the subsurface profiles, identify loose or soft zones and/or possible voids, and improve foundation conditions by grouting when deemed necessary.

### *1.5.1 Previous Foundation Investigations at ITP*

Prior to construction of ITP, (which began in 1978), at least three geotechnical investigations were performed by Mueser, Rutledge, Wentworth and Johnson (MRWJ) (MRWJ, 1977, 1978, 1984a).

#### *1.5.1.1 "High Level Waste Storage Tank Nos. 48 through 51," March 22, 1977*

The initial phase of this investigation included 15 boreholes extending to depths of between 80 to 195.3 feet and one piezometer to a depth of 45.5 feet below the then existing ground surface elevation of 300 feet. Standard Penetration Test (SPT) boreholes were made and undisturbed sampling was performed. Laboratory tests on undisturbed samples recovered from these boreholes disclosed the existence of a deep layer of compressible clay. The clay was encountered near the northern half of the 1977 proposed location for Tank 51 as shown in Figure 5.1-8. As a result, the configuration of the four tanks was changed to their present location.

Five additional boreholes were made to determine the subsurface conditions beneath the alternate Tank 51 location. These boreholes were extended to depths of from 161.5 to 181.5 feet. Three of the boreholes encountered calcareous materials, two of which were noted as having excessive grout takes.

#### *1.5.1.2 "Relocated High Level Waste Storage Tank Nos. 48 through 51," May, 1978*

Five additional boreholes were drilled at the current locations of Tanks 48 and 51. Rod drops, fluid loss, and high grout takes were recorded in three of the boreholes. Approximately 2 inches of total settlement under static loads was predicted for Tanks 48, 49, and 50. The predicted total and differential settlements for Tank 51 are 4.5 and 2 inches, respectively.

#### *1.5.1.3 "In-Tank Precipitation Facility," August 27, 1984a*

Five boreholes were made near the southeast toe of the embankment, extending to depths of up to 201.5 feet. Field density tests performed on the embankment fill in areas surrounding the Filter Stripper Building showed that approximately half of the lower 5 feet of the original embankment fill was compacted to less than 95 percent of the Modified Proctor laboratory dry density (Section 5.1.1). The boreholes also disclosed the presence of calcareous material at depth (Section 5.3).

### *1.5.2 Previous Foundation Investigation Reports in the Balance of the HTF*

The subsurface conditions in the balance of the HTF have been extensively investigated in a manner similar to the investigations performed at ITP. Foundation reports, pre- and post-construction, were reviewed and utilized for the comparison of the subsurface conditions and for the engineering analyses. A list and brief description of these previous reports are provided in the following sections.

#### *1.5.2.1 "Report of Investigation of Subsidence, Evaporator Building Fill - Building 242-H," Law, 1962*

This investigation was made to determine the continuing subsidence of the Evaporator Building and adjoining fill for the new waste storage facilities in the 200 area of the Savannah River Plant. The report incorporates data gathered by Moran, Proctor, Mueser and Rutledge (MPMR), Consulting Engineers.

A summary of the report's conclusions follows. The fill beneath the Evaporator Building was placed under the continuous supervision of the contractor and engineers for DuPont. The fill met the specification for 95% compaction of the Modified American Association of State and Highway Officials (AASHO) (now called American Association of State and Highway Transportation Officials (AASHTO)). However, because of a possible error in the control standard, the compaction percentages in the test reports may be 2 or 3% too high. Tests indicated extensive zones in the fill having densities well below the specified 95%. The concrete maintenance slab beneath the fill settled from 1 to over 4.5 inches and possibly 4 to 11 inches. Tank bottoms settled 1 to 1.5 inches by May 1962. The Evaporator Building settled an average of over 8 inches from October 1961 to July 1962. Voids or pockets of extreme looseness were found in the fill in a number of borings. Over 7000 gallons of water were placed in one boring without filling the hole. The bottom 10 to 12 feet of the fill is almost saturated. Analyses of settlement based on Law

Engineering and Moran, Proctor, Mueser, and Rutledge test data show that consolidation and settlement of a fill compacted as loosely as the recent density tests indicate could account for one-fourth of the observed subsidence. Settlement analyses based on the virgin soil indicate that only a fraction of the observed settlement might have come from that source. Internal erosion of the fill is believed to be occurring from: rat-hole-like passages in the virgin soil down to the cavities in the calcareous formation, and piping into (1) leaking conduits, (2) the loose vermiculite fill around each tank, and (3) pervious strata in the foundation or pipes or loose zones developed by dewatering in adjacent sites. The geologic conditions at the site and the design of the structure are conducive to internal erosion of soil. The manner in which the settlements have occurred, the presence of voids or soft spots in the fill, and the unexplained settlements are both direct and indirect evidence of soil erosion.

#### *1.5.2.2 "Settlement Investigation of Evaporator Building 242-H," MPMR, 1962*

Six undisturbed sample borings and one auger boring were drilled to determine the cause or causes of settlement of the 242-H Building. Loss of drilling fluid into the fill occurred in three borings, one taking 1000 cubic feet. The tank mat was placed 5 feet above natural groundwater, yet the lower portion of the fill became saturated because of perched water trapped by the working mud mat. Approximately 50% of all observations both in construction control and post-construction are less than the specified minimum 95% Modified Proctor dry density. Construction control tests show that 85% of the tests fell within the specification limits indicating good water content control. Settlement is due to the gradual adsorption of moisture by loose pockets of fill. Computations indicate that had all of the fill been compacted to the minimum requirement, settlements would have been less than 5 inches. Computations based on laboratory tests indicate a 10-inch total average settlement for the 242-H Building only is due to increase in moisture content. The average observed settlement to June 8, 1962, attributable to the fill, is about 7.7 inches. Underpinning of the building was recommended.

#### *1.5.2.3 "Areas 200H and 200F Radioactive Waste Storage Tanks, Subsurface Geologic Investigations," Blume & Associates 1971*

The purpose of this report was to determine the geotechnical properties and boundary conditions necessary for Phase II earthquake analysis of the underground radioactive waste storage tanks.

For this investigation two borings were drilled to depths of 250 feet and 255 feet. Elastic modulus, density, shear strength, and identification tests were performed. P and S waves were measured from steel cased drill holes.

#### *1.5.2.4 "Savannah River Plant Additional Facilities, High Level Waste Storage, 200H," MRWJ, 1974*

Seven borings and one piezometer hole were made to investigate the subsurface conditions at the location of the proposed tanks. Boring depths ranged from 80 to 180 feet. This soil investigation

was for the construction of high level waste storage Tanks 35, 36, 37, and 38 (renumbered 38, 39, 40, and 41). One borehole found a large void in the calcareous zone on the west end of the project. This zone did not extend eastward under the other proposed tanks and is not believed to represent a threat to the foundation; however, additional deep borings are recommended. Settlement may be up to 3 inches at the center of the tank group. The bearing capacity is ample to support the tanks and surrounding embankment. The groundwater level is well below the foundation level and should not affect construction. Potential settlement relative to the tanks of the Control House and Evaporator House located on or near the top of the embankment fill should be considered in the design.

#### *1.5.2.5 "New High Level Storage Tank No. 38 Building 241H," MRWJ, 1975a*

Two borings were drilled in the western half of the proposed location of Tank 38 to determine if a void area found in a previous investigation existed here. The two borings were drilled more than 30 feet below the void zone encountered in boring 12H-1. Both borings encountered calcareous material at and below the encountered void zone in 12H-1. The driller reported encountering a thin soft area in boring 12H-18, but attempts to sample this material were unsuccessful. However, it was concluded that the soils beneath the area of Tank 38 are capable of providing proper support for the proposed structure.

#### *1.5.2.6 "Building 241H New High Level Waste Storage Tank Nos. 42 & 43," MRWJ, 1975b*

Two borings were drilled to a depth of 180 feet at this location. Information collected during the investigation for Tanks 35 through 38 (renumbered 38 through 41) was also used with this analysis. The tank subgrade is underlain by stiff clay averaging 18 feet thick, which is underlain by sand and clayey sands to a depth of 170 feet. The piezometric surface was measured at 17 feet below tank subgrade. No zones of calcareous material, voids, and soft or loose soil were encountered in either of the borings beneath the proposed tanks. MRWJ concluded that the clay soil at subgrade was more than adequate to support the tank loading. Static settlement of these tanks were estimated using the recompression curve of the underlying cohesive soils. Uniform tank settlements of less than 2.5 inches were anticipated within a few months after the tank loads and backfill had been applied. It was concluded that this amount of settlement should not affect the structures.

#### *1.5.2.7 "Waste Transfer Facility H-Area Savannah River Plant," MRJD, 1984c*

This report discusses this geotechnical investigation to determine settlement and bearing capacity, slope stability, and construction methodology. Two undisturbed and two dry sample borings were drilled in the area. The undisturbed borings were drilled to 201.5 feet to investigate the presence of voids or leached zones as well as the presence and nature of the lower clay stratum typically encountered in H-area. The dry sample borings were drilled to 54 and 57 feet, respectively, for the installation of piezometers. The groundwater table is as much as 23 feet above the base of the

deeper pump pits. Circulation of drilling fluid was lost in MR-107U at elevation 153 feet, the elevation of the first sample of calcareous sand. Low SPT blow counts were noted and loss of drilling mud indicated that some leaching of calcareous material has occurred. No rod drops or voids were encountered. Settlements were estimated to be less than 1 inch for this facility.

#### *1.5.2.8 "Waste Transfer Facility Revised Location H-Area," Mueser Rutledge, 1985*

The facility was moved because of cost considerations. Two split-spoon borings were drilled to a depth of 101.5 feet to investigate the subsurface conditions and to determine allowable bearing capacities. Maximum settlement would be 1 inch or less. The excavation, shoring, and slope stability were the most critical aspects of the project due to the high groundwater table.

#### *1.5.2.9 "TBP Removal Tanks at The F/H Effluent Treatment Facility," Main, 1987*

Organic materials found in the foundation excavation of two adjacent 450,000-gallon wastewater feed tanks prompted the project engineer to request this investigation. Three borings were drilled to depths of 20 feet to evaluate the subgrade for the construction of four 10-foot-diameter by 10-foot-tall tanks and associated equipment. These are temporary facilities until the start-up of a permanent Effluent Treatment Facility (ETF) Organic Removal Facility. Eighteen inches of organic material considered as unsuitable was removed from below these tanks. Groundwater levels range from 10 to 30 feet below surface grade. A modulus of subgrade reaction of 100 pounds per square inch (psi) applies to these site soils. The allowable design soil bearing capacity ranges from 3000 to 4000 pounds per square foot (psf) , this bearing design capacity settlement was 1/2 to 3/4 inch after old fill removal and replacement.

#### *1.5.2.10 "Tank Farm Space Gain Facility, 200 H-Area," Mueser Rutledge, 1988a*

Based on the review of existing data, a field program of two borings and the installation of one piezometer was undertaken. Midsummer groundwater elevation was around 270 feet, and the maximum water table elevation was projected at 280 feet (10 feet below foundation subgrade). The old fill, approximately 8 feet thick, was unsuitable for the heavy foundation load. Therefore, the foundation should be supported directly on the stratum C1 stiff clay, which has an allowable net bearing capacity of 3 tons per square foot (tsf). Due to concerns of differential settlement below gravity drain lines, all of the fill in the area would be removed and verified as the subgrade was uncovered.

#### *1.5.2.11 "ETF Wastewater Collection Tanks F/H Effluent Treatment Facility," Mueser Rutledge, 1988b*

This investigation was initiated when organics and loose sand was exposed at the bearing level of these tanks in an adjacent trench. Seven, continuous, split-spoon sample borings were drilled around the perimeter of the existing tanks to depths from 12 to 24 feet. Since most of the fill was

removed prior to placement of the mud mat and tank slab, or replaced with construction grade fill, the existing bearing soils appear suitable for support of the tanks.

### *1.5.2.12 "Nitrogen Storage Tanks and Vaporizer, 200 H-Area," Mueser Rutledge 1988c*

The purpose of this report was to investigate the foundation conditions for the Nitrogen Storage Tanks and Vaporizer. Six test pits were dug to determine fill thickness.

Typical fill depths ranged from 1.5 to 3 feet deep with 5-foot depths in utility trenches. No records are available to confirm that the existing fills were placed in a controlled manner. Therefore, the fill should be removed beneath slabs and footings, and bearing established directly on undisturbed soils.

### *1.5.2.13 "Replacement High Level Waste Evaporator, Soils Report," Bechtel, 1989*

The soil investigation consisted of 10 soil borings ranging in depth from 31.5 to 76.5 feet, with laboratory testing and recommendations for mat, raft, or footing foundations. Liquefaction potential is low for earthquakes of magnitudes of 7.5 or less inducing ground accelerations as high as 0.2g. Settlements will be 0.5 inch or less.

### *1.5.2.14 "Report of Geotechnical Exploration WMWE Maintenance Facility Building 241-41H," Westinghouse Environmental 1990*

The purpose of the investigation was to assess the subsurface condition based on borings in the building area, and to provide foundation, earthwork, and liquefaction design and construction recommendations. The investigation included drilling four standard penetration borings ranging in depth from 38.5 to 50.0 feet and performing laboratory tests.

The investigation indicated that the soil was suitable for a shallow foundation with an allowable bearing pressure of 2500 psf. Footings designed in accordance with these guidelines were expected to settle less than about 1 inch. Calculations indicate that for a magnitude 7.5 earthquake, portions of the soils encountered would be susceptible to liquefaction for ground accelerations exceeding about 0.15g.

### *1.5.2.15 "New Waste Transfer Facility (NWTF) - Geotechnical Assessment," WSRC, 1993c*

The report is primarily concerned with liquefaction-induced settlements and the possible presence of deep "loose" zones within the Santee Formation. The results indicate that the soils encountered are competent and that liquefaction due to the Design Basis Earthquake (DBE) will not occur. The resulting dynamic settlements due to the DBE will be less than 1 inch. Based on available boreholes and seismic piezocone penetration tests, the deep "loose" zones found in other investigations in H-Area are not present at the NWTF with any significant thickness or extent. The

maximum settlement at the foundation level of the NWTF due to collapse of these zones will be less than 2 inches.

#### *1.5.2.16 "Geotechnical Summary Report For H-DB7," WSRC, 1994e*

This investigation consisted of three borings to depths ranging from 26.5 to 40.0 feet. Sinco™ Slope Inclinometer casing was installed in two holes to monitor lateral slope movement. Groundwater was not detected in any of the three borings. Over 5 weeks of monitoring, no significant lateral movement was measured in the inclinometers. Factors of safety are near to or less than 1.0 beneath the enclosure building column footings and against deep-seated slope failure.

### *1.5.3 Review of Previous Pertinent Liquefaction Potential and Soft Zone Evaluations*

A project file document for investigations within the SRS disclosed the existence of other reports that address the liquefaction potential of the Tobacco Road Formation (named the Barnwell Formation in older reports) and soft zones within the Santee/Tinker Formation (named Santee Formation and the McBean Formation in older reports). Pertinent excerpts from these studies are presented below.

#### *1.5.3.1 Seismic Criteria: URS/Blume, 1982*

Regarding the general properties of the Barnwell Formation, the report states:

> "This ... would appear to indicate that, although some liquefaction of recent alluvium might occur in a Bowman event (M=7 earthquake at a distance of 90 km producing a 'mean plus one' surface peak acceleration at the site of 0.2 g), liquefaction of even the Pleistocene alluvium ... is unlikely, and the probability of liquefaction in even the cleaner, saturated portions of the Hawthorn and Barnwell formations is negligible because of their age and because they have been subject to at least some overconsolidation."

#### *1.5.3.2 Barnwell Nuclear Fuel Plant: Dames & Moore, 1968*

This study is quoted by URS/Blume (1982) page 236:

> "Cyclic triaxial tests were conducted, and a Cr correction factor of 0.55 was used. No allowance [was made] for sample disturbance, for age, and for probable overconsolidation. The study concluded that the Barnwell formation (depth between 40 feet and 70 feet) at the site was potentially susceptible to liquefaction. Analyses conducted for a surface peak ground acceleration of 0.2 g showed a minimum factor of safety against initial liquefaction of about 1.2. It was recommended that the site grade should be raised 15 feet to achieve a minimum factor of safety of 1.5."

### *1.5.3.3 Building 221H: Geotechnical Engineers, Inc., 1979*

This study is quoted by URS/Blume (1982) pages 239 - 240:

> "Analyses based on results of cyclic triaxial tests (no allowances for sample disturbance nor overconsolidation) showed a factor of safety of 1.25 against development of strains of the order of 1 percent for a surface peak acceleration of 0.2 g."

### *1.5.3.4 Defense Waste Processing Facilit), 200-S Area: D'Appolonia, 1979b*

The DWPF in 200-S Area is located approximately 3600 feet northeast of ITP. The overall subsurface profile and consistency of the Tobacco Road Formation soils are similar.

Analyses conducted by D'Appolonia were based on a peak ground horizontal acceleration equal to 0.26 g based on SPT N-values and Seed et al. (1971) empirical chart for liquefaction. Analyses were also based on the results of 19 cyclic triaxial test specimens trimmed from undisturbed samples (fines content between 5 and 19 percent). After correcting the laboratory test results for the effects of membrane compliance, the following correction factors were applied: test boundary conditions, multi-directional shaking; loss of pre-straining effects due to disturbance, and effect of sustained consolidation pressure. The net correction factor varied between 0.80 and 0.95 for the laboratory test results corrected for membrane compliance.

The consultants concluded that:

> "As noted in D'Appolonia's original report, the analytical results depend largely on the value of the correction coefficient Cr considered to be applicable. The value of Cr was selected to account for the effects of previous seismic history and two-dimensional shaking. While the effects of previous shaking, most of which are probably lost in the sampling process, were considered to increase Cr by 25 to 50 percent, the effects of overconsolidation were ignored for the following reasons:
>
> (1) The overconsolidation ratio (OCR) is unknown, and estimates of its value are highly speculative; there is no firm evidence that the DWPF site is overconsolidated to any significant extent.
>
> (2) The effects of heavy overconsolidation would be expected to be reflected in the SPT resistance which, however, is often in the low range of 5 to 15
>
> (3) The loss of the effects of overconsolidation in sample recovery is much more prevalent in dense and very dense soils than in loose and medium dense soils as exist at the DWPF site.
>
> Given the apparent looseness of the Barnwell soils at the DWPF site, the low penetration resistance, the highly uncertain OCR, and the lack of historical precedent of the USNRC accepting Cr much greater than 0.70 for similar sites, it was believed that Cr much greater than 0.80 could not be successfully defended in a formal review process. Accordingly, it was D'Appolonia's opinion that under the current guidelines and criteria associated with the

licensing of commercial nuclear facilities, the site could be found acceptable only after extensive remedial measures were undertaken."

### *1.5.3.5 Defense Waste Processing Facility, 200-S Area: D'Appolonia, 1982*

D'Appolonia reanalyzed the liquefaction potential of the site studied in 1979 with the following conclusion:

"For the cases analyzed in which the Design Basis Earthquake peak horizontal ground acceleration was taken to be 0.20 g, the methodology based on SPT resistance provides the most conservative assessment of cyclic liquefaction potential of the Barnwell soils. The minimum factor of safety, averaged over the three acceleration records used in the analysis, is approximately 1.3 on the basis of laboratory cyclic triaxial test data using Cr=0.80.

As these minimum factors of safety pertain to sands located at depths of 50 to 70 feet below the ground surface, these sands are overlain by more resistive soils, and the annual probability of seismic-induced liquefaction is acceptably low (less than $2x10^{-4}$), the DWPF site is considered to provide adequate resistance against ground failure due to cyclic liquefaction for a seismic event associated with a peak horizontal ground acceleration of 0.20 g."

### *1.5.3.6 Defense Waste Processing Facility, 200-S Area: Geotechnical Engineers, Inc., 1983*

A second team of consultants was retained by DuPont to review the 1979 D'Appolonia data. The team's conclusions follow:

"The potential for ground failure (liquefaction and/or cyclic mobility) was evaluated using both empirical and analytical methods.

The analysis of ground failure using the SPT approach has indicated that limited pockets of soil do not meet established ground failure criterion [sic]. However, the occurrence of low SPT values was random and represents a small percentage of the soils beneath the site. Thus, the SPT data indicates that there is an adequate margin of safety against ground failure.

The potential for the occurrence of cyclic mobility (deformations during earthquake) was evaluated by two methods. The analyses based on stress-controlled cyclic triaxial tests indicated that a factor of safety against the development of significant cyclic strains (5 percent peak to peak) was at least 2.1.

For interpreting these laboratory tests as they relate to field behavior, it is necessary to correct these results to account for sample disturbance, which tends to eliminate the strengthening effects on in-situ properties of overconsolidation ratio (OCR), of geologic age of the deposit, and of previous seismic history. In addition, corrections need to be included to account for differences between in-situ stresses during an earthquake and stresses in the laboratory.

For the DWPF analysis, the effects of geologic age (cementation) and previous seismic shaking have been conservatively combined into a correction factor of 1.5. The analysis of preconsolidation yields a conservative correction factor of 1.4. The correction factor used for the state of stress in the cyclic triaxial test is 0.65 and a correction factor of 0.9 was applied for the impact of two-directional shaking during an earthquake. This produces a net correction factor of 1.23 (1.5 x 1.4 x 0.65 x 0.90).

Using the estimated correction factor of 1.23, the predicted cyclic shear strength ratio (cyclic stress ratio producing 5 percent double amplitude strain) is 0.32 (1.23 x 0.26). For the soils between El 200 and 250, the range of the average cyclic shear stress ratio produced by the DBE is 0.13 to 0.15. Thus, the computed factor of safety against cyclic mobility is 2.1 to 2.5. The correction factors used were intended to represent the best state-of-the-art estimate, but it should be recognized that selection of these factors involves a considerable degree of judgment. It is believed, however, that any other correction factors that one might reasonably choose would result in satisfactory factors of safety against cyclic mobility for the DWPF site.

Some of the data measured in the stress-controlled cyclic triaxial tests was re-analyzed using the strain approach developed by Dobry et al. This analysis indicated that only limited pore pressures (on the order of 0 to 15 percent of the effective stress) are likely to develop during the DBE. Pore pressures of this magnitude will result in very small cyclic strains and do not affect the undrained shear strength of the soil.

Hence, all of the analyses performed for the DWPF site indicate that there is an adequate margin of safety against the occurrence of liquefaction (dynamic bearing capacity failure) and cyclic mobility (the development of significant strains).

The above findings are further supported by the qualitative assessment of worldwide ground failures by Youd and Perkins (1978). These authors have correlated the occurrence of earthquake-induced ground failures with the geological origin of the soils involved. These data show that cohesionless deposits of sand of the Pre-Pleistocene epoch deposited in a coastal zone have a very low likelihood of being susceptible of earthquake-induced ground failure. In fact, ground failures in even the most susceptible type of soil deposits (Continental deposits in river channels, flood plains, deltas) are generally limited to deposits of the Pleistocene epoch or more recent. Youd and Perkins also point out that for water table depths greater than about 33 feet, the likelihood of ground failure occurring is low. At the DWPF site, the groundwater level in the Barnwell formation ranges from 30 to 50 feet below the ground surface.

Thus, it is concluded that there is overwhelming evidence that the DWPF soils will not experience a liquefaction failure or deform significantly during the DBE."

### *1.5.3.7 Comparison of Seismic Analysis for the 200-H and 200-S Areas: D'Appolonia, 1979a*

Page 10 of the report summarizes the conclusions derived from the comparative study as follows:

"Analyses for the H-Area conducted by Geotechnical Engineers and for the S-Area conducted by D'Appolonia are similar in that each used an analytical profile (largely based on cross-hole seismic surveys) which was analyzed under an acceleration time history through the computer program SHAKE. Geotechnical Engineers used a single time history whose peak ground acceleration was scaled to 0.20 g; D'Appolonia used three time histories whose peak accelerations were scaled to 0.26 g. Despite differences in analytical profiles and excitations, the two analyses were in basic agreement when the results of both were scaled to the higher ground acceleration. Therefore, it is our judgment that the predicted seismic responses (accelerations and stresses) of the H and S-Areas are essentially the same.

Although the soil classifications of the various soils types are basically the same for the two areas, they may actually differ, such that the S-Area has thicker layers of silty sand in the absence of clay layers. Second, SPT resistance and cross-hole seismic surveys indicate the sands in the S-Area may be looser than those in the H-Area. Third, cyclic triaxial and torsional tests indicate that the specimens taken from the S-Area exhibited significantly higher cyclic strains than did specimens taken from H-Area (note that the cyclic testing was not identical for the two areas).

Thus, despite the similar seismic responses (in terms of stresses and accelerations) that would be expected for the H and S-Areas, soil deformation (i.e., settlements of buildings) may be expected to be greater for the S-Area. It should be noted that D'Appolonia is in agreement with Geotechnical Engineers in the latter's assertion that these soils cannot truly liquefy under earthquake loadings, when the term liquefaction is synonymous with complete loss of strength accompanied by flow. On the basis of D'Appolonia cyclic tests, however, under a SSE (Safe Shutdown Earthquake) peak ground acceleration of 0.26 g, there is the potential for high 'cyclic mobility' meaning the temporary loss of strength and the development of significant cyclic strains with the potential consequences of damage to structures."

### *1.5.3.8 K Reactor Area: GEI Consultants, 1991a*

Pages 36 and 37 of the report summarize the conclusions derived from the study:

"A geotechnical investigation related to seismic issues was performed for the K-Area of the Savannah River Site (SRS) in the period June 1990 to February 1991. The investigation included borings to obtain split-spoon and undisturbed soil samples, cone penetration test (CPT) soundings, in situ shear wave velocity measurements, laboratory testing, and analyses.

Explorations in the K-Area indicated that soils within 200 feet of the ground surface consist primarily of clayey sands, silty sands, and clean sands. In approximately 50 percent of the borings and cone soundings performed for this investigation, a zone of low penetration resistance, rod drops, and/or drilling fluid loss was encountered at depths ranging from about 115 to 145 feet below the ground surface. These zones are referred to as soft zones in this report. Thickness of soft zones ranged from 3 to 15 feet and the areal distribution of soft

zones was erratic. Based on an array of closely spaced CPT's performed at the site, the shorter lateral dimension of soft zones did not appear to exceed 15 feet. Based on all available information, the soft zones appear to be elongated, 'channel-like' features occupying about 10 to 15 percent of the soil volume between depths of 115 and 145 below the ground surface.

Continuous sampling of soft zones was performed in several borings, and, in each case, soil was recovered from the soft zones. The boring information, and detailed CPT logs, indicate that soft zones consist of soil rather than open water-filled cavities. Apparently the soft zones consist of soils that have been altered over a long period of geologic time and are now subjected to relatively low effective stresses as a result of arching in denser soils above and to the sides of the soft zones. The alteration process is believed to be removal of calcium carbonate from the soil by ground water dissolution. Calcium carbonate still exists in soils at the site, primarily between depths of 125 and 145 feet below the ground surface. However, based on available information, the rate of solutioning is so slow that additional solutioning is not expected to adversely affect structures at the site for the remaining life of the reactor.

In this report, the critical layer is defined as the 30-foot-thick layer in which soft zones were encountered. The soil in the critical layer that surrounds soft zones is referred to as 'matrix material.'

Analyses were performed to estimate ground surface settlements that could occur in the K-Area as a result of a design earthquake. The design earthquake used in the analyses was that defined by the U.S. Nuclear Regulatory Commission's Guide 1.60 horizontal spectrum shape anchored at 0.20 g zero period acceleration. The computer program SHAKE was used to compute maximum cyclic shear strains in a 200-foot-thick model of soil layers, with the earthquake motion input at the ground surface. Maximum shear moduli used in the analyses were based on the results of down-hole and cross-hole shear wave velocity measurements. Relationships between degradation of shear moduli and strain, and relationships between damping ratio and strain, were based on the results of laboratory tests performed for this investigation.

Based on the SHAKE analyses, the computed maximum seismic shear strain in the critical layer was about 0.1 percent. Maximum shear strains in other layers were less than 0.1 percent. Based on laboratory test data, pore pressure increases in the matrix material are expected to be about 14 percent of the existing effective stress in the material. Thus, arching provided by the matrix material is not expected to change as a result of the design earthquake. In addition, based on low strain levels and low pore pressure increases estimated for design earthquake loading, the potential for 'liquefaction' of soils at the site is negligible. Liquefaction analysis based on Standard Penetration Test blow counts also indicates no potential for liquefaction.

Ground surface settlements were estimated by correlating volumetric strains of soil layers with shear strains computed from the SHAKE analyses. Data relating volumetric strains to cyclic

strains was obtained from laboratory tests performed by GEI on soils from K and other SRS areas. Results of the analyses indicate that the average settlement of the ground surface due to design earthquake loading will be about 1.4 inches.

Differential settlements of the ground surface were estimated using empirical methods for predicting surface settlements caused by soft ground tunneling. The computed maximum differential settlement of the ground surface due to design earthquake loading was 1/2200 or about 0.06 inch per 10 feet. This computed differential settlement was based on a best estimate shear wave velocity of 1,000 feet/second (fps) for the critical layer. For a lower bound estimate shear wave velocity of 750 fps for the critical layer, the computed maximum differential settlements was 1/1,200 or about 0.10 inch per 10 feet. Computed differential settlements of the ground surface resulting from design earthquake loading are well below the range of typical allowable differential settlements for structures.

In summary, the results of the geotechnical investigations indicated that the design earthquake will induce negligible settlements in the foundation soils of the K-Area reactor and cooling water reservoir both in areas that were and were not grouted in 1951."

### *1.5.3.9 K-Area Soil Stabilization Program: KASS, 1992*

The technical findings and conclusions regarding soft zones are as follows:

"Both the Corps of Engineers (COE) 1951-52 program and the KASS Program revealed that soft zones (intervals of low resistance to penetration) are not interconnected, average about 6 feet in thickness, and have an average lateral extent of less than 50 feet in any direction.

Soft zones comprise less than 10 percent of the area that was grouted based on the distribution of holes taking more than 300 cubic feet of grout per hole during the COE and KASS Programs.

Based on an average thickness of soft zones of six feet in the grout zone and the fact that less than 10% of the grout holes in K-Area encountered a soft zone, it is estimated that less than one percent of the soil volume beneath K-Area will accept a significant amount of grout (i.e. more than 300 cf per hole).

The soft zones follow an apparent NE-SW trend; however; the trend is not established well enough for precise prediction of soft zones locations.

Site specific exploration and independent analytical studies have indicated that the previous upper-bound estimate of soft zone compression of 42 inches is unduly conservative. Maximum compression due to complete collapse of the soil arches of the worst case soft zone encountered in the KASS Program, is calculated conservatively as 17 inches.

Potential pipe settlement resulting from 17 inches of compression for both the upper bound soft zone width of 35 feet (plane strain condition), and the upper bound diameter for a circular soft

zone of 50 feet (axisymmetric conditions), is estimated to be less than 1.5 inches. The corresponding pipe flexural strain is less than 0.008%.

The results of the analysis of induced pore pressures from a Design Basis Earthquake (DBE) and a seismic event with accelerations 50 percent greater than the DBE showed that the arching effect will be maintained. Resulting CWP settlement will be 2.4 and 3.8 inches, respectively, and the corresponding pipe strains will be 0.005% and 0.0065%, respectively, for a continuous (plane strain) soft zone 50 feet wide."

### *1.5.3.10 Replacement Tritium Facility, Building 233-H: BSRI, 1993b*

Pages 2, 3 and 4 of the executive summary summarize the conclusions derived from the study regarding the liquefaction potential of the Tobacco Road soils:

"The Tobacco Road formation is a 37-million-year-old deposit composed primarily of laminated gap-graded, clayey sands deposited under alternating marginal marine and fluvial conditions. The clay, consisting of kaolinite and illite minerals, binds the sand grains and appears to have been formed in place by weathering. The Standard Penetration Test N-value of this material varies with depth, but at depths of between about 40 and 70 feet below ground surface, N-values range between 4 and 12 blows per foot. Thus, questions about the seismic liquefaction potential of the formation were asked early in the investigation.

The detailed characterization of the Tobacco Road Formation soils made it clear that their geologic genesis, age, and composition were radically different from the recently deposited sands and silty sands that constitute the database on which the widely used empirical chart for liquefaction evaluation developed by Seed, Tokimatsu, Harder, and Chung in 1984 is based. To define the cyclic strength of the Tobacco Road Formation soils, therefore, and in the absence of empirical liquefaction case histories for this type of soil, a series of laboratory undrained cyclic triaxial tests were carried out.

Four separate approaches were used for the evaluation of the liquefaction potential of the Tobacco Road Formation soils:

1. Strength method
2. Strain method
3. Shear wave velocity comparison
4. Chinese criteria for clayey soil

For the purposes of these evaluations, two earthquake ground motions were postulated (i.e., Design Basis Earthquakes): a local event, characteristically represented by earthquakes of Magnitude 5 to 6 and a zero-period acceleration at the site equal to 0.19 g; and a distant event, characteristically represented by earthquakes of Magnitude 7.5 and a zero-period acceleration at the site equal to 0.10 g. Four accelerograms representative of the postulated ground motions

were used in conjunction with a typical soil profile of the site to calculate both the cyclic stresses and strains developed by these motions at the depths of interest. The ground response analyses were done using the computer code SHAKE developed by Schnabel, Lysmer, and Seed in 1972.

Using the strength approach, the factors of safety against initial liquefaction, the pore water pressure increases due to shaking, and the resulting settlements upon dissipation of the excess pore water pressure were calculated at each of the over two hundred locations within the Tobacco Road formation where N-value information was available. Factors of safety against initial liquefaction ranging between 1.4 and 4.0 were calculated. Estimated settlements ranged from zero to less than one inch.

For comparative purposes, the factors of safety against initial liquefaction and the settlements upon excess pore water pressure dissipation were also calculated adopting cyclic strengths obtained from the empirical chart, which as noted above, applies to younger and weaker clean sands and silty sands. For this comparative evaluation, an average strength was obtained for the upper and lower zones of the formation based on an average N-value for each of the two zones. In this case, the minimum factors of safety against initial liquefaction calculated for the upper and lower zones were 1.4 and 1.0, respectively, and the maximum calculated settlement was under 1.5 inches.

From the application of the strain approach, the cyclic shear strains induced by the postulated earthquakes at various depths within the Tobacco Road formation were calculated to be small, near the threshold value required to initiate the generation of pore water pressures; hence, no potential for liquefaction is indicated, based on this method.

Field testing determined that the shear wave velocity of Tobacco Road formation soils is in excess of 900 fps. Available empirical charts relating shear wave velocity to sand performance during earthquakes would indicate that for this velocity, liquefaction is not expected to occur even for earthquake motions of longer durations and higher acceleration levels than the postulated earthquakes.

Finally, applying the Chinese liquefaction criteria for clayey soils to the soils of the Tobacco Road formation shows that these soils fall in the category non-liquefiable.

To summarize, the results of the four separate liquefaction potential analyses indicated that for the prescribed motions, the factors of safety against initial liquefaction and loss of strength are high, and that the potential settlement of the ground beneath the structure caused by potential liquefaction of the Tobacco Road Formation is small, not greater than one inch.

Sediments in the Santee Formation consist of mixed carbonate deposits, and silty and clayey sands. Dissolutioning since Eocene times of the calcareous materials has resulted in a fine-grained skeletal sediment with high porosity. This process has resulted in the formation of underconsolidated sediments or 'soft zones' which can persist indefinitely, if the overlying sediments are able to bridge the underconsolidated zone (i.e., 'arching effect').

Geological considerations indicate that the Santee Formation at the RTF site should be expected to differ in geometric characteristics and overall conditions from those at other locations within the SRS. While 'soft zones' were also encountered at the RTF site in the Santee Formation, they were comparatively thinner and less frequent than at other locations within the SRS. More importantly, consolidation test data on materials from the Santee interval and overlying soils demonstrated that the soil profile at the site is overconsolidated and that no stress transfers or 'arches' have developed. Thus, potential compression of the Santee Formation due to seismic events can only be the result of the dissipation of seismically induced pore water pressures. The amplitude of the cyclic shear strains derived from the ground response analyses that were used in conjunction with strain/pore pressure generation data for clean sands indicate that the excess pore water pressure ratio increase generated within the Santee Formation should be less than 20 percent, which upon dissipation would imply less than one-half inch compression of these soils. This compression would in turn imply settlement of the structure of not more than this value.

In summary, field and laboratory investigations (and all analyses) provided the necessary information on the foundation stratigraphy and foundation material engineering properties. These analyses demonstrated that for the Design Basis Earthquakes (DBEs) prescribed for this facility, both the Tobacco Road and the Santee Formation soils will perform within acceptable limits. This results in high factors of safety against initial seismic liquefaction (i.e., 100 percent pore pressure response in laboratory undrained cyclic triaxial tests) and minimal overall settlements, less than 1.5 inches, calculated for the RTF (Tobacco Road Formation contributes less than one inch; Santee Formation contributes less than one-half inch; other formations do not contribute to settlement)."

#### *1.5.3.11 Historical Settlemen: WSRC, 1995; Mueser, 1991*

A literature search of available settlement data was done for this evaluation. Results from the H-Area Tank Farm and the Defense Waste Processing Facility (DWPF) were tabulated, reviewed, and utilized as part of this report (Section 7.5 of this report).

### *1.5.4 Summary of the Review*

In summary, the conclusions reached by various consultants based on extensive field and laboratory investigations and current state-of-the-art analyses are:

The Tobacco Road and Dry Branch Formations soils have sufficient strength to resist liquefaction and/or cyclic mobility associated with two earthquakes: (1) a moment magnitude 7.5 (distance 110 km) producing site acceleration of about 0.11g; and (2) a moment magnitude 5.0 (distance < 25 km) producing site acceleration of about 0.2g.

Soft zones are small, isolated, not laterally continuous and generally less than 10 feet thick.

Compression of the soft zones due to various earthquakes, of the size and magnitude of the current earthquake motions used in this report, is expected to be small.

## 1.6 Quality Assurance

Quality-related activities performed by the WSRC organizations during the Geotechnical Investigations were controlled in accordance with the WSRC QA Program (WSRC, 1990). Design activities performed by BNI and testing activities performed by LAW Engineering were accomplished in accordance with their respective QA plans.

SGS QA provided quality oversight of all quality-related project activities. SGS QA oversight activities included reviewing and approving the ITP Geotechnical Program Plan, BNI's QA Plan, and LAW Engineering's technical procedures, QA plan, and QA procedures; reviewing and approving SGS Quality Inspection Plans for drilling activities; and monitoring field, sample handling, testing laboratory, and design activities. SGS QA participated in the readiness reviews performed to qualify the LAW Engineering and University of California, Berkeley (UCB) testing laboratories before starting testing activities. SGS QA also provided full-time QA oversight of the stress-controlled cyclic triaxial tests and associated activities performed at UCB. SGS QA performed a surveillance of calculations completed by BNI. In addition, the QA organizations of BNI and LAW Engineering ensured compliance to their respective QA plans through the performance of surveillances and reviews.

# 2. SEISMOLOGY AND GEOLOGY

## 2.1 Seismic Evaluations Introduction

The SSIRP Plan (WSRC, 1994a) specifies using the Replacement Tritium Facility (RTF) earthquake spectra (derived from spectra developed for the K-Reactor) as the ITP evaluation basis earthquake (EBE) for geotechnical evaluations (Figure 2.1-1). In parallel with geotechnical tasks, ground motion studies (Lee, 1994) were conducted to compare different distant event design basis motions between the ITP, RTF, and K-Reactor. These comparisons were made to understand the sensitivity of the EBE to earthquake source parameters and crustal and soil structure assumptions.

The ITP EBE spectra consist of local and distant spectra. The local spectrum was derived from a deterministic-type NRC Standard Review Plan approach (USNRC, 1990) and then scaled to probabilistically derived values (i.e., $2 \times 10^{-4}$ annual probability of exceedance) contained in DOE-STD-1024 (DOE, 1992b). The distant event spectrum was also derived per NRC Standard Review Plan guidance, but remained unscaled.

The primary issue addressed in the ground motion studies was the adequacy of the distant ITP EBE spectrum. Following DOE guidelines (Bandyopadhyay, 1994), the adequacy of the distant EBE spectrum was judged by comparison to site-specific, 84th percentile rock spectrum from an 1886 Charleston-type earthquake. Comparisons were also made to SRS uniform hazard spectra and published eastern U.S. ground motion attenuation regressions (Lee, 1994). Based on the results of these studies, the ITP EBE distant spectrum was found to be about the 60th percentile of deterministic ground motions for a repeat of the 1886 Charleston earthquake. Ultimately, to meet DOE requirements (Bandyopadhyay, 1994), and the acceptance criteria defined by DOE-STD-1024, the 84th percentile deterministic spectrum and the local EBE spectrum were recommended for the final geotechnical analysis. Since the geotechnical work was completed (WSRC, 1994d) using the EBE spectra (local and distant) specified by the SSIRP, additional liquefaction and selected settlement analyses were required to determine the impact of the 84th percentile distant motion.

In addition to the ground motion specifications described above, DOE (1995) requested further analysis using a 5 to 10 Hz probabilistic-scaled earthquake spectrum. This task was problematic because of the wide variations in Electric Power Research Institute (EPRI) and Lawrence Livermore National Laboratory (LLNL)/SRS hazard results. Based on consistent spectral values between EPRI and LLNL median rock uniform hazard spectra for plant Vogtle (DOE, 1995), a recommendation was made to scale to median values at the $10^{-5}$ hazard level. Using average values of magnitude and distance derived from the hazard studies (M6.1, 80 km), a rock spectrum was derived. DOE (1995) showed that both the median 1-2.5 and 5-10 Hz spectral scaling factors were consistent with the scaled spectral shape. This spectrum was also recommended for liquefaction and settlement analysis.

## 2.2 Summary of Parameters Associated with the Development of the ITP EBE Distant Soil Spectrum

The EBE distant event soil spectrum was previously derived for K-Reactor (Geomatrix, 1991) using Random Vibration Theory (RVT) modeling of the source and path in combination with SHAKE (Schnabel et al., 1972) or equivalent analysis for the soil column as described in the following sections.

### *2.2.1 Source Parameters*

A moment magnitude ($M_w$)=7.5 earthquake at a distant of 120 kilometers (km) with a stress drop of 150 bars was used to derive a rock response spectral shape. This shape was scaled to a higher peak ground acceleration corresponding to a source distance of 110 km. The magnitude and stress drop source parameters are above or in the upper range of values considered median for a repeat of the 1886 Charleston earthquake. The source distance of 110-120 km is closer than the 145 km distance of the 1886 epicenter.

### *2.2.2 Structure/Q*

A Coastal Plain specific Q model and seismic crustal structure were used to model ground motions, and are considered median models. Geometrical spreading from the Coastal Plain crustal model was found to be about the same as a half-space ,1/R spreading model (R < 100 km).

### *2.2.3 Kappa Bedrock*

The Kappa (bedrock attenuation) factor is a median value based on ranges presented in the literature. There are no site-specific data available to provide constraints on Kappa. Bedrock P-wave velocity is constrained by basement refraction velocities. Basement S-wave velocities are developed using a Poisson solid relationship ($\sigma = 0.25$). The geometry of the Triassic basin is constrained by seismic reflection data and a one-dimensional model approximation is used to determine ground motion effects of the basin. The model suggests that the presence of the basin in the K-Reactor ground motion model does not significantly alter the spectra with respect to its application for ITP.

### *2.2.4 Soil Model*

The ITP model uses an average of ITP shallow S-wave velocity ($V_s$) coupled with a deeper $V^s$ profile measured at the Pen Branch Fault Confirmatory Drilling Site. The deep Vs profile is significantly faster than the assumed profile originally used for K-Area. However, comparisons of shallow (less than 200 feet) dynamic properties indicate that the K-Reactor is a stiffer site with less damping than the ITP site.

## 2.3 ITP Median and 84th Percentile Rock Motions

Median and 84th percentile rock spectra for ITP are shown in Figure 2.3-1 (Lee, 1994). The distant controlling median spectrum represents a $M_w$ 7.5 earthquake at a conservative distance of 120 km combined with a median stress drop of 100 bars. The 84th percentile rock motions are derived by using the recently developed EPRI frequency-dependent standard error (Toro et al., 1994).

A rock spectrum for K-Reactor is not available from the Geomatrix (1991) work. Consequently, an approximation of that spectrum was developed. Figure 2.3-1 compares the Random Vibratory Theory rock motions using Geomatrix (1991) source parameters (i.e., Mw 7.5, stress drop 150 bars, and distance of 120 km) versus ITP median and 84th percentile rock motions.

Median motions for a repeat of the 1886 Charleston earthquake were derived that produce significantly less rock motion than the EBE rock spectrum. This indicates that the EBE spectrum is higher than the median. The 84th percentile spectrum, derived from ITP median site spectrum and conservative frequency-dependent scaling parameters for US mid-continent crustal structure, is higher than the EBE rock spectrum.

Until the performance/hazard guidelines are issued (DOE, 1994), WSRC (1994c), it is recommended that engineering evaluations of foundations use the scaled local and 84th percentile deterministic spectra for evaluations.

## 2.4 Summary

A review of the technical basis for the H-Area EBE spectra was conducted together with an overview of the history of recent spectra development at SRS (Lee, 1994). Based on H-Area studies, application of the ITP EBE distant earthquake spectrum at H-Area provides motions that are more conservative than median, but does not meet the DOE (Bandyopadhyay, 1994) requirements of an 84th percentile motion. Therefore, it was recommended that the ITP be evaluated using the local EBE spectra scaled to a peak ground acceleration of 0.19 g ($2 \times 10^{-4}$ probability of exceedance) and the 84th percentile spectrum ($1 \times 10^{-4}$ probability of exceedance, EPRI at 1 to 2.5 hertz).

## 2.5 Regional Stratigraphy at the SRS

Basement lithologies at the SRS consist primarily of crystalline igneous and metamorphic rocks, possible Late Precambrian to Late Paleozoic age, and of Early to Middle Mesozoic (Triassic to Jurassic) rocks that occur in isolated, fault-bounded basins either exposed within the crystalline belts or buried beneath the coastal plain sediments (WSRC, 1994b).

The Coastal Plain stratigraphic section is divided into several formations and groups based principally on age and lithology. Sediments range in age from Late Cretaceous through Tertiary. The lithostratigraphic sequence at the General Separations Area (GSA) is composed mostly of terrigenous clastic sediments interspersed with carbonate-rich clastic sediments and limestones. The clastic facies consist of gravel, pebbly sand, clayey sand, silt, clay, and sandy clay. The calcareous facies consist of calcareous sand and mud, limestone, sandy limestone, and sandy and muddy limestone. These Cretaceous through Tertiary sediments are described in the following sections and depicted in Figure 2.5-1, beginning with the deepest formations and progressing to the surficial sediments.

### *2.5.1 Cretaceous Sediments*

The Cape Fear Formation is the basal unit of the Coastal Plain stratigraphic section and is composed of poorly sorted, silty-to-clayey quartz sand and interbedded clay. The sand is arkosic in places. Muscovite and iron sulfide are also present. The Cape Fear Formation is more indurated than the other Cretaceous formations because of the high clay content and abundance of cristobalite in the sediment matrix. Sand is commonly medium-grained, but ranges from very fine to coarse-grained. Pebbly zones are present in many parts of the section.

The Cape Fear Formation is about 30 feet thick at the northwestern SRS boundary and thickens to more than 180 feet near the southeastern boundary. The environment of deposition has been interpreted as upper delta plain (Prowell et al., 1985).

The Middendorf Formation unconformably overlies the Cape Fear Formation with a sharp, distinct contact. This formation is dominantly a medium to coarse-grained quartz sand with moderate to good sorting. Pebbly zones are common as well as clay clasts. Some parts of the unit are feldspathic, micaceous, and lignitic zones. The sand of the Middendorf Formation is much cleaner and less indurated than sand in the Cape Fear Formation. Cross-bedding is well developed in the lower part of the section in some areas. A clay layer up to 80 feet thick forms the top of the formation. Another clay-rich zone is present near the middle of the formation in places at SRS. In the northern part of SRS, the formation is highly colored and composed mostly of sand. The thick clay bodies observed downdip within SRS are missing in the north, although clay interbeds up to 2 feet in thickness are present.

The formation is approximately 130 feet thick near the northwestern boundary of SRS and thickens to more than 180 feet near the southeastern boundary. The Middendorf Formation at SRS was probably deposited in fluvial and deltaic environments (Prowell et al., 1985).

The Black Creek Formation is composed of sand, silt, and clay. The upper part of the formation is mostly clay and silt, while the lower part consists of silty micaceous sand. Sorting is generally moderate to poor. The sand is micaceous and becomes lignitic in the central and southwestern parts of the SRS. Layers of pebbles and clay clasts are common. Feldspathic zones are present. The upper, clayey, silty section of the Black Creek Formation is divided into three lithofacies, each trending across SRS from southwest to northeast. The northwestern lithofacies is a massive 20 to 40 feet thick clay that is highly oxidized. The Black Creek Formation in the central part of SRS is dominantly dark to light, micaceous silty sand with thin interbeds of clay. The southeastern lithofacies is also fine-grained and consists mostly of dark clay interlaminated with silt. Dark, fine- to medium-grained, fining-upward sand is present within the unit. Iron sulfides are common.

The Black Creek Formation is about 110 feet thick at the northwestern boundary of SRS and thickens to more than 250 feet near the southeastern boundary of the site. Most of the Black Creek Formation was probably deposited in a lower delta plain environment, except for the light-colored sand in the northwestern part of SRS, which was probably deposited in an upper delta plain environment.

The Peedee Formation is dark, glauconitic, fine-grained sand and silt with marine fossils (dinoflagellates). The deposits in the vicinity of SRS are referred to as the Steel Creek Member of the Peedee Formation. The lower part of the Steel Creek Member is sandy with a pebble-rich zone at its base suggesting a basal unconformity. This lower section consists of poorly to well-sorted, fine- to coarse-grained quartz sand and silty sand and is very micaceous in places. The upper part of the Steel Creek Member is a clay that varies from more than 50 feet to less than 3 feet in thickness at SRS. Fining upward sands are interbedded with the clay in some areas. Steel Creek Member probably formed in an upper delta plain environment in the southwest and in a lower delta plain in the northeast. It is about 110 feet thick at the northwestern SRS boundary and 130 feet thick at the southeastern boundary.

### *2.5.2 Tertiary Sediments*

#### *2.5.2.1 Paleocene*

The Sawdust Landing Formation, the lowermost Paleocene unit, rests unconformably on Cretaceous sediments and consists mostly of yellow, orange, tan and gray, poorly sorted, micaceous, silty, and clayey quartz sand interbedded with gray clay. It is locally feldspathic and iron sulfide and lignite are common in the darker sections.

The overlying Lang Syne Formation consists of dark gray and black lignitic clay and poorly to moderately sorted, micaceous, lignitic, silty quartz sand and pebbly sand. Glauconite is common in the southeastern part of the unit. Feldspar occurs locally and iron sulfide and cristobalite are common in the darker colored part of the unit.

The Snapp Formation, the uppermost Paleocene unit, consists typically of light gray, tan, orange, and yellow, medium-to coarse-grained quartz sand and pebbly sand interbedded with kaolinitic clay. Dark muscovite and lignite-bearing sand is less common. The Snapp in the northwest part of SRS is a less silty, better sorted sand with thinner clay interbeds.

The depositional environment for Paleocene unit grades from upper to lower delta plain (deltaic) and marginal marine from northwest to southeast across SRS.

### *2.5.2.2 Eocene*

The Fourmile Formation of Fallaw and Price (1992) is a tan, orange, yellow, brown, and white, fine to coarse, moderately well-sorted, loose sand. Pebbly zones are common. Clay layers are characteristically found near the middle and top of the unit. It is characteristically about 30 feet thick at SRS. The presence of glauconite and dinoflagellate assemblages suggest a shallow marine environment of deposition.

The Congaree Formation unconformably overlies the Fourmile Formation and consists of well sorted, well rounded, and fine- to coarse-grained quartz sand. Thin clay laminae occur throughout the formation, but are more common in the lower part. In some areas a thin clay-rich glauconite-bearing layer separates the Congaree from the underlying Fourmile Formation. Pebble layers, clay clasts, and glauconite are locally present. Both siliceous and calcareous cement have been observed in the upper part of the Congaree Formation at SRS. The unit increases in thickness from about 60 feet on the northwest to about 80 feet in the southeast, and is interpreted as a shallow marine environment of deposition.

The Warley Hill Member (Fallaw and Price, 1995) overlies the Congaree Formation. It consists of variable clay, clayey sand, and silty fine-to medium-grained quartz sand and locally contains glauconite. Thickness varies from a few inches to 15 feet. The Warley Hill is sometimes included in the informal hydrostratigraphic unit known as the "green clay."

The Tinker-Santee-Blue Bluff Formation overlies the Warley Hill interval and includes three distinct lithofacies. The light colored, moderately to well sorted, fine to coarse, sometimes calcareous quartz sands that predominate towards the north and northwestern parts of SRS have been termed the Tinker Formation (Fallaw and Price, 1995). The amount of calcareous material within the Tinker Formation increases from northwest to southeast across SRS and grades into the Santee Limestone towards the southeast. The Santee Limestone consists of cream-colored, micritic to shelly, partially indurated to indurated, biomoldic limestone, indicative of an open, unrestricted shallow marine environment. To the southwest, the Blue Bluff unit consists of clayey and silty, laminated, calcilutite, calcareous clays and calcareous quartz sands indicating a more restricted environment and a more proximal position to a siliciclastic source. Previously, the Tinker-Santee-Blue Bluff interval was termed the McBean Formation or McBean Member of the Lisbon Formation, or the Santee Formation (Siple,1967; Colquhoun et al., 1983; Prowell, et. al., 1985).

The Clinchfield Formation overlies the Tinker Formation and consists of fine- to coarse-grained, locally calcareous, quartz sand. An indurated, bioclastic and biomoldic, glauconitic limestone facies, commonly containing abundant echinoid fragments (Periarchis lyelli), is designated as the Utley Limestone Member. The amount of calcareous material increases downdip (i.e., to the southeast). This formation has not identified in the ITP/HTF area.

The Dry Branch Formation overlies the Clinchfield Formation. The Dry Branch Formation has been subdivided into the Griffins Landing, Twiggs Clay, and the Irwinton Sand Members. The Griffins Landing Member is a distinctive carbonate-bearing facies that interfingers with the Twiggs Clay Member which consists of clay beds of variable thickness interbedded with clayey sand. The Griffins Landing is characterized by the presence of Crassostrea gigantissima often found in growth positions. These carbonate occurrences are discontinuous and probably represent oyster beds developed in a back barrier or transitional environment, and the clays probably represent marsh and tidal flat deposits. The Irwinton Sand Member contains moderately-to well-sorted quartz sand, locally interlaminated with clay. In general, the Irwinton Sand generally maintains a superior stratigraphic position to Twiggs Clay and the Griffins Landing Members. The entire formation thickens from about 50 feet near the northwestern boundary of SRS to approximately 80 feet to the southeast.

The Tobacco Road Formation conformably overlies the Dry Branch Formation. A coarse layer that may contain a flat pebble conglomerate is characteristic at the contact point between the two formations. The formation typically contains moderately- to poorly-sorted, red, brown to variegated purple and orange, quartz sand with clay stringers. Trace fossils, especially burrows of Ophiomorpha, are locally abundant. Pebble layers and muscovite are distributed locally throughout the formation. A heavy mineral concentration, sometimes present at this boundary, may produce radioactivity that assists in identifying the contact on gamma-ray logs.

### *2.5.2.3 Younger than Eocene*

The 'Upland Unit' is an informal stratigraphic term that has been applied to local deposits that outcrop at higher elevations in the coastal plain of southwestern South Carolina (Nystrom and Willoughby 1982; Nystrom et al. 1986). Units in a similar stratigraphic position in Georgia are usually called the Altamaha Formation (Dall and Harris 1892 [fide Huddleston, 1988]). Outcrops and surface exposures are very common in the SRS area. Dark red, brown, orange, poorly sorted clayey to silty sand locally contains lenses and layers of conglomerate, pebbly sand and clay. Cross bedding and white flecks that may be weathered feldspar are locally common. The Upland Unit, locally up to 70 feet thick, is generally fluvial and forms a scoured, erosional surface on the Tobacco Road Formation. The age of this unit has not been definitively determined, and correlation with similar deposits in the region is not yet clear. Prowell, et. al. (1985) and Nystrom et al. (1986) have proposed a Miocene age. Work in progress (Colquhoun 1994) suggests that at least in part, the age of sediments in this interval may be as old as Late Eocene.

# 3. SUBSURFACE EXPLORATION

Subsurface information in the ITP and the remainder of the HTF is available from pre-construction boreholes drilled for the initial tank foundation investigations and from the following recently completed exploratory phases. Each phase, as well as the equipment, test methods, and general field procedures, are summarized in the following sections.

## 3.1 ITP Phase 1 (December 1992 to April 1993)

A series of SPT boreholes and Seismic Piezocone Penetration Test soundings (CPT) were performed around the facility to develop preliminary subsurface characterization and perform a preliminary engineering analysis. SPT boreholes and CPT probes were paired so that a site-specific comparison of results could be obtained. This allowed the CPT to be utilized as the primary exploration tool in areas where soil extraction by sampling was not practical. SPT sampling was performed continuously to derive correlations between SPT N-values and CPT parameters. Soil samples collected from SPT boreholes were tested for classification purposes. Four Flat Plate Dilatometer (DMT) soundings, located near selected boreholes and CPT probe locations, and grout injection tests in two areas were also performed in Phase 1.

## 3.2 ITP Phase 2 (April 1993 to November 1993)

Phase 2 was initiated to investigate areas of potential concern identified in the Phase 1 investigation and to collect information to support detailed engineering analyses. Exploratory techniques consisted of collecting high-quality undisturbed soil samples for laboratory testing, performing cross-hole shear wave velocity surveys to confirm downhole techniques, obtaining core samples from the grout injected test area, and carrying out geophysical borehole logging as described in Section 3.6.8 to supplement the geologic characterization.

## 3.3 ITP Phase 3 (November 1993 to August 1994)

The objectives of the work in Phase 3 were to obtain additional information about the structural embankment fill and the soft zones within the lower Dry Branch and upper Santee/Tinker Formations, to characterize potential faults, and to confirm the western boundary of the carbonate deposit. Investigative techniques used included: surface seismic surveys, soil coring and downhole geophysical logging, undisturbed sampling of soft zones, and of the structural embankment fill, and one SPT borehole.

In summary, the preconstruction and combined Phases 1 through 3 explorations for ITP have resulted in the following to date:

- 20 CPTs
- 4 DMTs
- 5 SPT boreholes

- 6 undisturbed sample boreholes
- 2 undisturbed sample/core boreholes
- 8 core boreholes
- 5 straight drill holes ( to complete cross hole arrays)
- 34 review of preconstruction soil boreholes
- 3 cross-hole seismic surveys
- 1 downhole seismic refraction survey consisting of 3 separate lines
- 1 shallow high resolution seismic reflection survey, consisting of 4 separate lines
- 1 grout injection test at two locations

Figures 3.3-1 through 3.3-3 show locations of the exploratory work completed at the site as summarized above. In addition, a seismic tomographic survey is in progress around Tank 51. The Tank 51 results will be included in a future issue to this report.

## 3.4 HTF Field Exploration (November 1993 to May 1995)

The H-Area Tank Farm investigation involved a single phase which commenced concurrently with the ITP Phase 3 field work. The intent of the HTF exploration program is to apply the same techniques as used for the ITP investigation and perform a reconnaissance of the structural fill and subsurface soils across the balance of the HTF. The results of the HTF exploration will be compared with the ITP investigation by completing statistical and preliminary engineering analyses.

The initial location of exploratory points were in the ITP area. The investigation was expanded to cover the remainder of the tank farm. During this period of investigation, other ongoing SRS site subsurface characterization initiatives included the H-Tank Farm area. These included the seismic reflection survey program and Multi-Mode Deep Profiling Program (MMDPP). The latter involved a core boring, located immediately south and approximately mid point of the tank farm area.

In summary, H-Tank Farm exploration resulted in the following to date:

- 17 CPTs
- 1 core borehole
- Review of 67 existing boreholes
- 1 cross-hole tomography survey

Figure 3.4-1 shows locations of the exploratory work completed at the site as summarized above.

### *3.4.1 Multi-Mode Deep Profiling Program*

The MMDPP was initiated in October 1994 to obtain lithostratigraphic, geophysical, and shear and compressional velocity information extending from the surface to basement rock. Techniques

involved continuous core borings to define stratigraphic intervals, lithologies, and depth to basement rock; geophysical logging including nuclear logs to further define soil lithologies, elastic properties and densities; and downhole suspension logs to obtain shear and compressional wave velocities.

Three primary sites were selected for exploration based upon existing information, basement rock type, and proximity to critical facilities. The three sites selected included:

- A-Area (MMP-4-SB), located in the northern portion of SRS adjacent to well cluster P-30; basement rock relatively shallow and consisting of penetratively deformed mafic and ultramafic rocks.
- K-Area (MMP-3-SB), located on the southeast side of K-Area adjacent to well cluster P-25; basement rock consisting of Triassic-Jurassic clastic sediments.
- H-Area (MMP-2-SB), located mid-point and immediately south of H tank farm; basement rock consisting of amphibolite and gneiss.

The MMP-2-SB boring was utilized for obtaining site-specific information relating the depth to basement and shear wave velocities from basement to surface for the H-Area (refer to Figure 3.4-2). Shear and compressional wave velocity surveys were performed by Agbabian Associates. Measurements were made in the open borehole using a OYO™ Model 170, Suspension Logger which directly measures an average velocity over a 3.28 foot high section of the borehole wall. The digital records were analyzed to define picks for wave travel times and velocities calculated. Two seismic cone penetrometer soundings were also pushed approximately 20 feet from the deep boring to obtain downhole velocities in the shallow subsurface. These downhole velocities were compared to the suspension velocities for consistency (Figure 3.4-3).

## 3.5 Field Test Location and Clearance

The selection of the borehole locations, CPT probes, and other field work was governed by the following factors:

- Facility layout
- Data coverage
- Existing data
- Type of data required
- Under-and-above ground interferences
- Operations
- Radiological (RCA) versus non-radiological area

Approval of the selected location for the field work was preceded by a series of steps as summarized below (the organization responsible for each step is noted in parentheses):

- Selection of general area based upon the factors listed above (Geotechnical Engineering)
- Preliminary interference research (Construction Layout)

- Ground penetrating radar survey (Operations Department)
- Preparation of design change form (Geotechnical Engineering)
- Preparation of work package (Construction Engineering)
- Process control (Operation Department)
- Excavation permitting (Construction Engineering)
- Work clearance permitting (Operations Department)
- Area operational review (Operations Department)
- Field survey (Construction Layout)
- Hand excavation of top 6 feet to verify clearance from utilities (Construction Craft Department)
- Radiological work control (Health Protection)

This detailed routine was essential to safe field operations. A field team from Geotechnical and Construction Engineering was required to effectively coordinate the entire process. Any obstacles encountered in any step during this process required the relocation of the proposed borehole or penetration location and therefore the re-initiation of the process.

## 3.6 Equipment and Field Test Methods

Table 3.6-1 provides information on sampling methods and general information pertaining to completed boreholes and depths for each of the three ITP field exploration phases. All equipment used in the field investigations met applicable ASTM standards and site standards and procedures as listed below:

- K-SPC-G-00004 - Stationary Piston Sampling (WSRC, 1993b)
- K-SPC-G-00003 - Handling, Storage and Shipment of Soil Samples (WSRC, 1993a)
- K-SPC-G-00010 - H-Area CPT and DPT Services, Rev. 1, WSRC (1994f)
- 3Q5 Manual - Hydrogeologic Data Collection, WSRC (1992)
- ASTM D2488-90 - Description and Identification of Soils (Visual-Manual Procedure)
- ASTM D4428-84 - Crosshole Seismic Testing
- ASTM D3441-86 - Deep, Quasi-Static, Cone and Friction-Cone Penetration Test
- ASTM D1586-84 - Penetration Test and Split-Barrel Sampling of Soils
- ASTM D4452-85 - X-Ray Radiography of Soil Samples
- ASTM D1587-83 - Thin-walled Tube Sampling of Soils
- ASTM D4220-89 - Preserving and Transporting Soil Samples

### *3.6.1 Drilling Contractor(s) and Equipment*

In general, the same drilling contractors and equipment used for recently completed investigations at the SRS, such as for the RTF, were used for this investigation. Graves Environmental, Inc., performed all drilling and sampling with the exception of borehole H-BOR-29, which was performed by Environmental Drilling Services (EDS). This borehole involved only undisturbed sampling. All drillers involved with the drilling and sampling activities were experienced and also

had been involved with the RTF investigation program, where extensive undisturbed sampling was performed. The drilling equipment utilized are described in the following sections.

#### *3.6.1.1 Graves Environmental Failing 1500*

The Failing 1500 drill rig is gas-driven with a 40-foot mast. The rig has a 23-foot Kelly assembly which allows for a 20-foot stroke and is capable of mud rotary, augering, and rotary coring techniques. The drill string is controlled by the Kelly arrangement, as well as by a mechanical winch.

#### *3.6.1.2 Graves Environmental AMC Quick Drill Speed Star 275*

This is a truck-mounted, gas-driven rig with a 35-foot mast. This rig also has a 23-foot chain-driven Kelly which allows a 20-foot stroke and is capable of mud rotary, augering and rotary coring techniques. This rig was cleared for use in Radiologically-Controlled Areas (RCA) and performed primarily undisturbed sampling.

#### *3.6.1.3 Environmental Drilling Services Davy Kent DK-5*

This is a truck-mounted rig with a 30-foot mast. The rig uses augers or mud rotary and was primarily used for the undisturbed sampling of H-BOR-29, since the rig was cleared for use in the RCA. General use of this rig included drilling through mud mats for CPT probes and reaming and installing inclinometer casings.

### *3.6.2 Standard Penetration Test*

Continuous SPTs were performed in five boreholes ( H-SPT-1, H-SPT-14, H-SPT-18, H-SPT-20, and H-BOR-23.3). Continuous SPT testing was performed by driving the split spoon sampler 18 inches (unless refusal was met), retrieving the sampler, reaming the 18-inch sampled interval, then performing the next SPT.

Tests were performed in accordance with ASTM D1586-84 using a standard 24-inch long by 2-inch outside diameter (OD), unlined, split-spoon sampler with a 2-foot bleeder and check valve located above the sampler, NX drill stem, and a 140-lb safety hammer. SPT N-values were determined by adding the number of blows required to drive the split-spoon sampler the last 12 inches of the standard 18-inch drive.

The general test procedure, as noted in sequence, is outlined below:

1. Split spoon is lowered into nominal 4-inch diameter borehole
2. Depth is checked and any rod settlement noted
3. Six-inch intervals, totaling 18 inches, are marked on the drill rod above the turntable
4. Sampler is driven by blows applied using a 30-inch stroke with the rope wrapped twice over the cathead
5. Sampler retrieved and recovery noted
6. Sampled interval reamed out to nominal 4 inches

7. Process repeated

Prior to each SPT test, the Geotechnical Oversight verified that the spoon was properly assembled, making sure the bleeder and check valve were clean and the drive shoe was in good condition. The Graves Environmental Failing 1500 was used for all SPT boreholes with the exception of H-SPT-1 (a 50-foot-deep borehole within the RCA) and H-SPT-14 (a 200-foot-deep borehole within the RCA) which required the AMC Quickdrill Speedstar (refer to Figure 3.3-3 for SPT borehole locations)

### *3.6.3 Undisturbed Sampling*

Undisturbed soil samples were obtained for laboratory testing in Phases 2 and 3 of the investigation program in boreholes H-BOR-2, H-BOR-12, H-BOR-23, H-BOR-23.3, H-BOR-29, H-BOR-34, H-BOR-50, and H-BOR-54. The selection of the sampling interval was based on the results of the Phase I program and depended on:

- Low CPT tip resistance
- Low SPT N-value
- Low fines content (based on field observations)
- Preliminary stratigraphy

Sampling equipment used included direct push shelby tubes, pitcher barrel samplers, and stationary piston samplers. The selection of the sampler used depended on the soil type, the type of testing to be done, and on the existing SPT and/or CPT information.

A sampling plan was developed for each borehole. In general, boreholes which were planned for undisturbed sampling were limited to undisturbed sampling only, with no SPTs being performed. If any SPTs or additional coring, was performed, it was done in the bottom portion of the borehole, after all undisturbed sampling had been completed.

Drilling requirements for undisturbed sampling boreholes required that fluid pressures be kept as low as practical, while maintaining fluid return up the borehole. Drill bits with side discharge, or, in the case of tricone bits, with bottom deflectors, were required for reaming and advancing the borehole. In the event of loss of circulation, the hole was reamed and cased to no closer than 5 feet above the next sample interval.

Details of the methods of undisturbed sampling employed are described in the following sections.

#### *3.6.3.1 Direct Push Shelby Tube*

Direct push Shelby tubes were used for sampling cohesive soil layers and dense sands. The shelby tubes used were either brass or galvanized steel with a 3 inch OD, 0.065 inch wall thickness, and a length of 30 inches. Sampling was performed in accordance with ASTM D1587.

Drilling was accomplished by mud rotary methods to the predetermined sampling depth. The drill stem was then tripped out and the bit removed. The Shelby tube head with a ball check valve was then attached and lowered to the bottom of the borehole. Borehole depth was checked against the drilled depth and noted. The maximum push length was marked on the drill stem and the rod hydraulically advanced a full 24 inches or until 600 psi hydraulic pressure was reached. Once the advance was made, the tube was allowed to sit for 5 minutes. When ready to retrieve the sample, the drill string was rotated about 90 degrees to shear the sample off the surrounding soil.

When each sample was brought out of the borehole, the bottom and top were capped with plastic slip-on caps. If a gap was noted between the bottom tube edge and sample, a filler material was placed in the gap prior to placing the cap. Details of final sample preparation are provided in Section 3.7.

#### *3.6.3.2 Pitcher Barrel Sampler*

The pitcher barrel sampler consists of a rotating outer barrel with a leading cutting edge, and a non-rotating inner barrel with a smooth leading edge the same as a standard Shelby Tube. The pitcher barrel sampler was generally used in conditions where cemented layers, interbedded with softer layers, were encountered. The sampling procedure and the field preparation of samples are the same as described above for Shelby Tubes.

#### *3.6.3.3 Stationary Piston Sampler*

Soil samples were obtained with the stationary piston sampler at those locations where it was desired to recover high-quality undisturbed specimens for delicate strength and compressibility testing. A detailed specification covering all activities associated with piston sampling was issued. This specification was a modification of the field procedure produced for the RTF field investigation in 1993. Generic Specification K-SPC-G-00004, Stationary Piston Sampling, is provided in Volume 2, Appendix B.

### *3.6.4 Core Boreholes*

Coring was primarily utilized in Phase 2 to investigate the grout assessment area. Coring was also used in the Phase 3 investigation to obtain stratigraphic information in the area immediately around Tank 51 and the area where tomographic surveys are in progress. (The results of the tomographic survey were not available for this revision.) The coring utilized a mud rotary system which employed a 94-mm, single tube inner barrel with a polyethylene or steel catcher. The inner barrel was 5 feet long and core runs were generally 5 feet in length.

### *3.6.5 Cased Boreholes*

#### *3.6.5.1 Inclinometer Casing*

A total of 12 boreholes (4 separate cross-hole locations) were cased with inclinometer casing for cross-hole testing. However, one array (near CPT-20 on the east side of ITP) was abandoned due to casing collapse, which probably occurred during grouting. A cross-hole array consists of 3 cased holes in a straight line spaced 10 feet apart. Installation was per ASTM D4428. The inclinometer casing used was a 2.74-inch inside diameter polyvinyl chloride (ID PVC) in 20-foot lengths, with 4 slots, oriented 90 degrees from one another. Casing segments were joined together by a coupler glued and pop-riveted to the casing. Tape was wrapped around the coupling to prevent grout intrusion.

During installation, a nominal 5-inch diameter hole was reamed to 5 feet below the target depth to serve as a rat hole to accommodate sloughing. Any room remaining at the bottom of the hole, prior to lowering the PVC casing, was filled with pea gravel to support the PVC casing. Once the PVC casing was lowered into the borehole, the annulus was tremie-grouted. See Figure 3.3-3 for locations of the 3 cross-hole arrays (Arrays 1, 12, and 23).

#### *3.6.5.2 Steel Casing*

Steel casing was installed in five boreholes (H-BOR-34, H-BOR-44, H-BOR-50, H-BOR-54, and HTF-B1). These boreholes were reamed to a nominal 8-inch diameter prior to casing installation, for tomographic surveys. The steel casing was 6-inch ID with threaded outer couplings used to connect each 20-foot length. To improve the cement bond, the casing was sand-blasted prior to installation to remove any milling oils or finishes. Once the casing was lowered into the borehole, the annulus was tremie-grouted in one continuous stage.

### *3.6.6 Piezocone Penetrometer Soundings*

CPT, including seismic (SCPT), were performed in accordance with ASTM D 3441. In general, all CPTs included shear wave velocity surveys at 3-foot intervals. Applied Research Associates (ARA) under contract to Ebasco performed all CPT field and data processing activities. Target depths were based upon the estimated elevation of the top of the Congaree Formation, which at ITP averages about elevation 120 feet. However, actual depths varied, depending upon ground surface elevations and subsurface conditions. Refusal was defined as a tip stress of 1800 psi or reaching the capacity of the hydraulic push system.

The CPT was used in all phases of the exploration program because of the relatively quick and clean operation, which is of significant importance in RCAs and because of its ability to provide a continuous soil profile, which is important when defining the extent of soft or loose soil zones. During the Phase 1 investigation, a CPT probe was pushed adjacent (9- to 10-foot lateral distance) to each SPT borehole and selected undisturbed sample boreholes. These data pairs were then used

to correlate CPT and SPT results, and CPT and laboratory testing results. The CPT was also used as an exploratory tool in RCAs to allow for increased coverage in the ITP area. Refer to Figure 3.3-3 for CPT locations.

### *3.6.7 Dilatometer Soundings*

Four flat plate DMTs were pushed to obtain additional information of in-situ stress and compressibility properties. Three of the four DMTs were pushed adjacent to SPT/CPT data pairs. The fourth was pushed adjacent to a CPT probe. The DMT soundings were performed by ARA utilizing the CPT rig. The tests were carried out in accordance with ASTM Subcommittee 18.02 "Suggested Method for Performing the Flat Plate Dilatometer Test". Typically, the DMT readings were taken at 5-foot intervals. Damage to the membrane attached to the DMT blade was common and required the probe to be returned to the surface, repaired, and re-pushed. Refer to Figure 3.3-3 for DMT locations.

### *3.6.8 Geophysical Borehole Logging*

Geophysical logging was performed on boreholes H-BOR-44, H-BOR-34, H-BOR-50, H-BOR-54, and HTF-B1. These holes were later cased for tomographic surveys. The geophysical logging included gamma, caliper, spontaneous potential, resistivity, and sonic methods prior to casing installation and variable density logging after casing installation. The geophysical logs provided additional information about the lithology and physical properties of the soil column. All logging was performed by the United States Geological Survey (USGS). Brief descriptions of the information obtained from each geophysical logging method are provided in the following sections.

#### *3.6.8.1 Gamma*

Gamma logs were used to obtain basic lithologic properties. Specifically, this type of log is used to estimate the sand to clay ratio, since clays generally contain a higher percentage of radioactive potassium and thorium than sand. Because the gamma log measures natural radiation in soils, an indication of the relative proportion of the two soil constituents can be obtained.

#### *3.6.8.2 Caliper*

The caliper was used to measure the borehole diameter deviation from the drilled diameter. This provides information about layers which may have washed out or reduced in diameter due to squeezing or sloughing.

#### *3.6.8.3 Spontaneous Potential*

The spontaneous potential log was used to further identify more permeable zones versus clayey layers and the boundaries between them. This information was used, along with the gamma measurements, to help define lithologies.

#### *3.6.8.4 Resistivity*

The resistivity log provides information about the resistance of the formation materials to an applied electric potential. This information can be used in conjunction with the gamma log and the spontaneous potential log to verify lithologic boundaries as well as to determine variations of dissolved salts in the groundwater column.

#### *3.6.8.5 Sonic Velocity*

The sonic velocity log was used to measure the acoustic properties of the soil column. The measured amplitudes and attenuation were used to calibrate the seismic reflection and tomographic surveys. The sonic tool utilizes an energy source to create an acoustical wave which is transmitted directly into the borehole wall and the wave propagation through the material is measured. The signal received includes compressional, shear, fluid, and Stonely waves. The tool is designed to first detect the compressional wave so that compressional velocities are more clearly defined. These velocities are then used to create synthetic compressional wave profiles which can be used to correlate depth intervals with the time records of surface reflection surveys.

#### *3.6.8.6 Variable Density*

The variable density log was used as an indicator of the grout to casing bond for the 6-inch steel casings installed for tomography surveys. The tool is calibrated for an assumed density of the steel casing and grout encasement. The tool then measures variations against this density by changes in the acoustical wave velocities very similar to the sonic log as described in Section 3.6.8.5. Where velocities are high, a high relative density indicates a good bond between the casing and grout. Where velocities are low, a separation between the casing and grout, or the absence of grout, is indicated.

### *3.6.9 Cross-Hole Seismic Velocity Survey*

Cross-hole testing was used to measure cross-hole shear wave velocities between boreholes. This testing was performed by Ebasco as part of the cone penetrometer and geophysical contract. Cross-hole testing was performed in accordance with ASTM D4428. The testing was performed primarily for comparison and confirmation of the downhole shear wave velocity surveys obtained from the seismic cone penetrometer.

Three cross-hole arrays were located around the ITP to provide coverage on both the east and west sides of the facility and the embankment fill. Each array consisted of three cased boreholes spaced 10 feet apart. The first array (Array 12) was located on the west side of the embankment (near borehole H-SPT-14) and extended to a depth of 200 feet. The second (Array 1) was located immediately south of ITP Filter Stripper Building on top of the embankment fill (near borehole H-SPT-1), and extended to a depth of 50 feet. The third array (Array 23) was located on the east side

of the Cold Feed Complex, off the embankment (near borehole H-SPT-23), and extended to a depth a 200 feet. See Figure 3.3-3 for cross-hole locations (Array 1, Array 12 and Array 23).

Each array utilized boreholes which had previously served as SPT boreholes and undisturbed (UD) boreholes. SPT boreholes performed during the Phase 1 investigation were cased for cross-hole testing during the Phase 2 operations. Once UD sampling in one of the adjacent array boreholes was accomplished, the borehole was reamed and cased. If the remaining array borehole was not needed for further sampling, the borehole was straight drilled to depth and cased completing the array.

In general the survey was completed with a Bison model 1465-1 hydraulic shear wave source which was capable of applying reversible vertical impacts to the cased borehole wall. The reversal technique was used to reverse the polarity and thus clarify the shear wave arrival. In the lower portions of Array 12 and 23 some of the casings were slightly deformed, making it impossible to use the Bison source. In this case, a Wappa air gun manufactured by OYO™ Geospace was used as the source. The Wappa was not the preferred source and was only used when the Bison could not be. The geophone arrangement consisted of three geophones arranged orthogonally, one in the vertical, and two in the horizontal position. The geophones were positioned in the borehole via pneumatic packers. The testing procedure consisted of installing the geophone package in two adjacent boreholes and the source in the third borehole. Testing was then performed on 3- to 5-foot intervals down and back up the array. The source and receivers were then switched and the testing repeated. The equipment and procedure used to complete the survey is detailed in Volume 7.

### *3.6.10 Cross-Hole Tomography Survey*

Cross-hole tomographic surveys were performed around Tank 51 between boreholes H-BOR-50, H-BOR-34 and H-BOR-54, resulting in two panels with H-BOR-34 being a common hole for each panel. The surveys were performed under two separate contracts so that different acoustic energy sources could be used. Processing of the tomographic information was completed just prior to this report and the interpretation is not included herein. The following paragraphs describe the techniques that were employed.

The Earth Sciences Department at Lawrence Berkeley Laboratory acquired cross-hole seismic data using a high resolution, piezoelectric p-wave source in H-BOR-50 and a six element hydrophone string in H-BOR-54 and a 24 element hydrophone string in H-BOR-34. Data were acquired with this instrumentation at 1/2 meter intervals for both the source and receivers from the water table depth (approximately 20 ft) to the bottom of the holes (approximately 300 ft). The source was swept from 500 to 4000 Hz with a 25 sweep stack to produce each record. With these parameters, 500 to 3000 Hz bandwidth signals were received by the hydrophone strings for ray paths above and below that carbonate - soft zone interval. However, ray paths that intersected the carbonate soft zone interval were not received producing shadow zones in the first arrival information.

Tomographic imaging was also conducted by Southwest Research Institute and Tomoseis Inc. Tomoseis Inc. employed a low frequency piezoelectric source in H-BOR-34 with a six-level hydrophone string in H-BOR-50. This configuration was chosen to reverse the source receiver relationship used by Lawrence Berkeley Laboratory in order to verify their results. The piezoelectric source was swept from 250 to 1500 Hz and stacked 10 times for each record. The p-wave information acquired with this instrumentation produced the same results as Lawrence Berkeley Laboratory's configuration, with excellent transmission in all areas except rays that intersect the carbonate - soft zone interval. Southwest Research Institute instrumented H-BOR-34 with a kilo-joule sparker, impulsive source with a 24 level hydrophone string in H-BOR-54 and a three component clamping receiver in H-BOR-50.

At the time of this report, tomographic data processing was incomplete. Additional field work is scheduled to obtain further information in the shadow zones.

### *3.6.11 Downhole Seismic Refraction Survey*

Thick sections of carbonate and associated soft zones were mapped on the east side of ITP. Due to the existence of above-and below-grade interferences, including the structural embankment, mapping was limited to a narrow area east of the Cold Feed complex. Since the top of the carbonate was known from several boreholes, a downhole seismic refraction technique was used to define the extent of the carbonate.

The technique involves introducing a wave energy directly into the carbonate which was expected to have an unusually high velocity contrast with respect to the surrounding unconsolidated sediments. This technique, however, was also limited by the existence of interferences, because the survey required lines of geophones to be strung out to considerable distances.

The refraction survey was generally successful in delineating the carbonate extent in the southeast side of the ITP area. Delineating the extent of the carbonate in the vicinity of the tanks was based solely upon existing borehole data. See Figures 3.3-2 and 3.3-3 for the layout of the refraction tests and Figure 5.1-7 for the mapped area of the carbonate facies.

### *3.6.12 Borehole, Casing, and Penetration Abandonment*

Abandonment of boreholes and CPTs was performed per WSRC Manual 3Q5, Hydrogeologic Data Collection (WSRC, 1992) Chapters 6, 9, and 10. The standard grout mix consisted of the following:

- One sack Type 1 Portland Cement (94 lb sack)
- Two pounds of dry sodium bentonite
- 6.5-7.5 gallons of potable water

In general, all boreholes were abandoned immediately upon completion of testing, except those which were cased for further testing or held open for downhole geophysical logging. The

exploratory core boreholes in the grout assessment area remained open until all holes cored in the Phase 2 investigation were complete. This was to prevent the abandonment grout from contaminating the grout injected as part of the test.

Grouting was accomplished via the tremie method. The grout pipe was lowered to the bottom of the borehole and grout was injected until the borehole fluid was displaced and grout returned to the surface. Several times, the operation was temporarily halted until the next day to allow the injected grout to set before additional grout was added. All boreholes were grouted to the surface and topped off until the column remained static.

Casings installed included PVC for inclinometers, and 6-inch steel casing. To date all inclinometer casings have been abandoned. The five geologically logged boreholes are cased with steel casing and remain open for tomographic surveys. Abandonment of these boreholes will be deferred until further testing is no longer required. Casings were abandoned following the procedures for uncased boreholes. The same grout mix and tremie method were applied. Casings were abandoned in place and were cut off flush with the ground surface.

## 3.7 Sample Preparation, Handling, Storage, Transportation, and Control

Requirements for sample preparation (Vol. 2, App. B), handling, storage, transportation, and documentation were delineated within specification K-SPC-G-00003, "Handling , Storage and Shipment of Soil Samples". Specific requirements for preparation of Stationary Piston samples were delineated within specification K-SPC-G-00004 (Vol. 2, App. B), "Stationary Piston Sampling".

In general, all undisturbed samples were prepared and handled in the same manner. All undisturbed sample tubes were checked for conformance with ASTM D1587 . In the case of stationary piston tubes, the tubes were verified for conformance with specification K-SPC-G-00004, Stationary Piston Sampling, and weighed. Tubes that did not conform were rejected. All undisturbed soil samples were maintained in a temperature-controlled storage area, free from vibration. Each sample was maintained in a vertical position at all times.

A sample storage area was established near the site. Access to samples was limited to geotechnical personnel only and was controlled by lock and key. The undisturbed samples were maintained in vertical tube boxes capable of holding four tubes as prescribed by ASTM D 4220. Each box was equipped with a lid which was kept locked. The storage area was maintained between 60 and 70 degrees Fahrenheit. The temperature was continuously recorded with a calibrated temperature recorder.

Once the samples were obtained and the tubes returned to the sample storage area, the samples were trimmed, measured, and sealed. Plastic caps were placed over both ends of each tube, then taped and each tube labeled. Stationary Piston samples were X-rayed per ASTM D 4452 prior to shipment for laboratory testing at the University of California, Berkeley (UCB). Upon arrival at UCB the piston samples were again X-rayed using the same technique as that used for the pre-

shipment X-rays, so the pre- and post-transportation X-rays could be compared to determine if sample disturbance occurred.

For SPT boreholes, a sample was collected from the top and bottom of the sample spoon. If a material change occurred within the sample, additional samples were collected, as appropriate. Samples were placed in 8-ounce glass jars. The tops were closed tightly, wrapped, sealed with electrical tape, and samples were labeled on both the jar and the lid.

Core samples were placed in partitioned plastic boxes. Each box was 2 feet wide and could accommodate 10 feet of core (five 2-foot-long rows). Core samples were eventually sent to the site core laboratory for logging.

All undisturbed soil samples selected for testing, excluding the stationary piston samples chosen for testing at UCB, were turned over to Law Engineering for transporting to the laboratory in Atlanta. All tube samples tested by Law Engineering in Atlanta were transported in tube boxes and were maintained in a vertical position.

Stationary piston samples selected for testing at UCB were transported in tube boxes to the Atlanta airport by SGS geotechnical and QA personnel. The samples were loaded into passenger seats, strapped in a vertical position, and accompanied by SGS geotechnical and QA personnel. Upon arrival in San Francisco, the samples were then turned over to Law Engineering personnel who accompanied the samples to UCB. Chain-of-custody protocol was maintained throughout the process of transporting the samples from the sample storage area to the soils laboratory at UCB. A log was maintained during all phases of storage and transportation to document transportation and storage conditions.

# 4. LABORATORY TESTING

Laboratory testing was performed for the ITP investigation in parallel with the field investigation described in the preceding section. The objective of the laboratory testing program was to characterize the physical and engineering properties of the site soils for design purposes. Specifically, the laboratory program was designed to determine:

- Index properties, including classification, moisture content, unit weight, plasticity, and grain size distribution
- Static strength in undrained and drained triaxial compression
- Consolidation properties,
- Compaction characteristics
- Dynamic properties and cyclic strength, and
- Mineralogical composition using X-ray diffraction techniques

The Phase 1 laboratory work was performed by Ebasco Services, Inc. and consisted primarily of classification tests. The majority of the Phase 2 laboratory testing for ITP was performed by Law Engineering of Atlanta, Georgia. Law subcontracted with UCB for specialized dynamic testing and X-ray diffraction analysis. QC Services of Hayward, California also subcontracted with Law to perform post-transport X-ray of the undisturbed samples shipped to UCB for dynamic testing. Ebasco Services, Inc. was retained to perform pre-transport X-rays of the same set of undisturbed samples. A number of consolidation tests performed by MRWJ in 1976 were also used to establish consolidation properties for the ITP soils.

Table 4.0-1 lists the standards and procedures used to perform the recent laboratory work for ITP. The individual static laboratory test results for ITP are presented in Volumes 4 and 5 and the individual dynamic test results and the X-ray diffraction summary for ITP provided in Volume 6 of this report. X-ray films of undisturbed samples (pre- and post-transport) and laboratory test results performed for previous projects within the HTF are available in the project files at SRS.

In general, the selection of samples for laboratory testing at ITP was based on the soil classification from the field borehole logs and on the preliminary subsurface profile developed as part of the Phase 1 exploration (BSRI, 1993a). Reassignment of testing, when necessary, was based on observations made in the laboratory.

## 4.1 Quality Assurance Plan

The Law Engineering QA Manager was responsible for ensuring the quality of laboratory testing activities at the Law Engineering test laboratory in Atlanta and the Department of Civil Engineering test laboratory at UCB. Testing activities included sample handling and storage, sample chain-of-custody integrity, procedure development, software verification, validation, and control, calibration of test equipment, testing, and data recording. An SGS QA engineer was assigned to the UCB test laboratory to oversee quality control activities and to monitor the performance of the stress-controlled cyclic triaxial tests and associated testing activities. Technical oversight at UCB was provided by BNI. Periodic QA oversight by SGS QA and technical oversight by BNI at Law's Atlanta laboratory and at UCB.

## 4.2 Testing Program

A summary of the laboratory testing performed at ITP is given below. The numbers in parentheses indicate the number of test results obtained from previously reported tests at the HTF.

- Visual classification in the laboratory and natural moisture content determinations on nearly all soil samples
- 170 (103) sets of Atterberg Limits
- 217 (19) specific gravity tests
- 234 (80) grain size analyses
- 17 (8) unconsolidated-undrained triaxial (TX-UU) strength tests
- 20 consolidated-drained triaxial (TX-CD) strength tests
- 42 (11) consolidated-undrained triaxial (TX-CU) strength tests
- 31 (20) one-dimensional consolidation tests
- 10 clay mineralogical examinations of Tobacco Road and Santee soils by X-ray diffraction
- 9 resonant column and 9 (2) strain-controlled cyclic triaxial tests for evaluating shear moduli and damping ratios
- 24 undrained stress-controlled cyclic triaxial tests
- 11 threshold (low amplitude) strain tests
- 27 post-liquefaction volumetric strain determinations

Table 4.2-1(a) and 4.2-1(b) summarize the static test results at the ITP and the balance of the HTF, respectively. Table 4.2-2 summarizes the results of all current and previous consolidation tests. The dry density, water content, and initial void ratio reported in Table 4.2-2 denote values obtained from the field prior to saturation. The final column in Table 4.2-2, labeled "Quality is poor," identifies consolidation test results that were poor or questionable based on inspection of their void ratio versus load curve.. These poor quality tests were excluded from the average material properties reported in Section 6. Additional Atterberg limit tests were carried out on the fraction of soil passing the No. 200 sieve for selected samples in order to determine the plasticity of the fines. As discussed in Ishihara (1993), soils that have highly plastic fines are less susceptible to liquefaction. These test results are also included in Table 4.2-1(a). Table 4.2-3 summarizes the dynamic tests performed by sample ID, type, and number of tests. The results of these tests,

together with laboratory tests results from other areas at SRS and field performance data, formed the basis for the representative soil properties as given in Section 6.

In general, all tests for the ITP were performed in accordance with the standards and procedures listed in Table 4.0-1. Specific deviations, or enhancements for testing on the ITP soils, to those listed in Table 4.0-1 are provided in the following sections.

### *4.2.1 Static Triaxial Tests*

Static triaxial tests for ITP were performed to determine the shear strength and elastic moduli of the material over a range of confining stresses for both total and effective stress conditions. Unconsolidated-undrained (TX-UU) and consolidated-undrained (TX-CU) tests were performed in accordance with ASTM D2850 and ASTM D4767, respectively. Consolidated-drained tests were performed in accordance with the Corps of Engineers standard EM 1110-2-1906 (USACOE, 1970). Sample volume change measurements were also recorded in the drained tests so that dilation angles of the various soil formations could be determined for use in the finite difference analyses. All consolidated-undrained and consolidated-drained tests were consolidated isotropically to the effective overburden stress with back-pressure saturation to a B-value (pore pressure parameter) of 0.95 or greater. These test results are reported in Volume 5. The failure strains reported in Table 4.2-1 are defined as the strain at which the deviator stress peaks or a maximum of 15% stress, whichever is less.

### *4.2.2 Strain-Controlled Cyclic Triaxial and Resonant Column Tests*

Strain-controlled cyclic triaxial compression tests and resonant column tests for ITP were performed in accordance with specification K-SPC-G-00001 to determine the dynamic shear modulus and damping ratio of selected soil samples. Strain-controlled cyclic triaxial tests were performed at varying confining pressures over a strain range of $1x10^{-4}$ to $5x10^{-3}$ in./in. Resonant column tests were performed over a strain range of $1x10^{-6}$ to $1x10^{-4}$ in./in. All tests were performed under isotropically consolidated, undrained stress conditions. To develop the final design curves for the shallow (<200 feet deep) sediments, the strain-controlled cyclic triaxial test information obtained from the current investigation was augmented with test results from investigations conducted at RTF. The results are given in Volume 6.

### *4.2.3 Stress-Controlled Cyclic Triaxial Tests*

Thirty-five stress-controlled cyclic triaxial tests for ITP were performed in accordance with test procedure TP-2-ITP (Vol. 2, App. B), which is a modification of the U. S. Army Corps of Engineers specification EM 1110-2-1906 for determining the liquefaction potential and shear strength of soils under earthquake loading. Twenty-four of the tests were for liquefaction evaluation and eleven tests were for low-amplitude strain determination.

Test specimens were mounted on one of three loading frames of the CKC (Clarence K. Chan) testing system and the testing software (Georobot, version 5.2) was initiated. Internal vacuum was then released and replaced by external chamber pressure, after which the specimen was back-pressure saturated to a B-value of 0.95 or greater, and consolidated to the desired isotropic effective initial confining stress. The uniform, stress-controlled cyclic testing was performed under undrained conditions at a frequency of one cycle/second (one hertz). The cell pressure, the effective confining pressure, the axial cyclic load, and the axial strain of the samples were continuously recorded. A videotape of selected cyclic testing and sample preparation was made by Bechtel at UCB and resides in the SRS project files. Failure was defined as either the pore pressure equal to the confining pressure or the double amplitude strain exceeding 10%.

### *4.2.4 Low-Amplitude Strain Determination*

Eleven low-amplitude cyclic tests were performed for the ITP to establish the relationship between shear strain and pore pressure ratio at small strain levels. Because the triaxial testing equipment is only capable of applying relatively large strains, it has a significant degree of compliance, particularly at high confining stresses. The compliance of each system used for low-amplitude strain evaluation was determined using a stiff aluminum sample of known modulus. Further explanation of the procedures used to perform the tests are presented in TP-2-ITP (see Vol. 2, App. B and Vol. 6). The results of the low-amplitude strain evaluation tests are presented in Volume 6. Volumetric Strain Determination

### *4.2.5 Volumetric Strain Determination*

Volumetric strain tests were performed for the ITP to assist in evaluating the magnitude and rate of volume change due to reconsolidation that might be expected following pore pressure generation. The tests were performed on samples immediately after either liquefaction or low-amplitude cyclic loading was completed. This simply involved restoring free drainage to the samples and recording the subsequent changes in volume and height under the applied isotropic confining stress as a function of time. A total of 27 volumetric strain tests were performed (22 on liquefaction specimens and 5 on low-amplitude cyclic specimens) per test procedure ITP-2-ITP (see Vol. 2, App. B).

### *4.2.6 Residual Strength Determination*

Two post-liquefaction undrained residual strength tests were performed for the ITP to assess the stress-strain characteristics of the Tobacco Road soils after they had been liquefied. The test consisted of monotonic, axial compressive loading under undrained conditions as described in TP-2-ITP (see Vol. 2, App. B). The tests were performed immediately after the samples had been liquefied without allowing the pore pressure that had developed under cyclic loading to dissipate. The results of the residual strength tests are presented in Volume 6.

### *4.2.7 Mineralogical Analysis*

The mineralogical analysis used X-ray diffraction on 10 selected specimens that had been used previously for cyclic triaxial testing. The X-ray diffraction tests indicated that, while most of the specimens were composed primarily of quartz and kaolinite, several (belonging to the Santee Formation) contained significant quantities of both carbonates and smectites.

# 5. SUBSURFACE CONDITIONS

The subsurface conditions were determined from the field exploration program described in Section 3.

The sediments in the upper 100 feet of the profile at ITP are predominately sandy soils (SM, SC, SP-SM, SW-SP) with thin interbeds of silt, clayey sand, and clay. These sandy soils are underlain by a complex sequence of interbedded clayey sands, highly plastic clays, calcareous sands, muds, and limestone that extend to a depth of approximately 175 feet below ground surface. Below this depth, dense sands with some clay units predominate to bedrock, which is approximately 960 feet below ground surface. Groundwater in this area shows slight seasonal fluctuations, but averages about El. 275 feet, which is approximately 20 to 25 feet below natural ground surface (≈ El. 300 feet) and 55 feet below the top of the ITP embankment (≈ El. 330 feet).

In developing generalized profiles at ITP and HTF for liquefaction and subsequent settlement calculations, careful attention was given to developing layering that preserved important changes in the strength, compressibility, and fines content of the foundation soils. For engineering analyses, soil profiles were stratified using soil descriptions from the field logs and tip, friction ratio, and pore pressure signatures from the CPT data. The adopted nomenclature followed a simple numerical system with layer numbers increasing from top to bottom within each interpreted geological formation. For example, Figure 5.0-1 is a typical CPT log. Layers that were initially interpreted to be in the Tobacco Road Formation were labeled TR1 through TR4, from top to bottom, respectively. Layers in the Dry Branch Formation were labeled DB1 through DB5, respectively. The Santee/Tinker Formation, because of its lateral and vertical variability, was difficult to layer and was not further subdivided. This formation is labeled as the ST layer elsewhere in this report. The GC layer is the green clay, which is an informal stratigraphic interval at the SRS and characteristically consists of a stiff, green to gray clay or clayey silt that overlies the dense sands of the Congaree Formation.

## 5.1 Generalized Engineering Profiles of the ITP

Figures 5.1-1 and 5.1-2 are subsurface cross-sections beneath the ITP tanks. Figure 5.1-1 is a north-south section (SRS coordinate grid) beneath Tanks 49 and 51 and Figure 5.1-2 is an east-west section beneath Tanks 48 and 49. (These cross sections are also referred to as Profiles AA' and BB', respectively, herein.) These profiles were prepared by correlating CPT tip resistances and friction ratios, SPT N-values, and field soil descriptions and projecting these data a few feet to the profile line.

As laboratory results became available, engineering properties (Table 6.0-1(a) and 6.0-1(b)) were assigned to the layering of the profile. Also, because of their similarities from the laboratory test results, the TR3 and TR4 layers were combined into a TR3/TR4 layer. Likewise layers DB1 through DB3 were combined into a DB1/DB3 layer (Tables 6.0-1(a and b)). Generalized average elevation, Poisson's ratio, total unit weight, and shear wave velocities for each of these layers are

shown in Figure 5.1-3(a) and 5.1-3(b) for ITP and HTF and are also tabulated in Table 6.0-1(a) and 6.0-1(b), respectively.

Stratification for engineering analyses was completed prior to the finalization of the geological interpretation; thus, there are minor differences between the geologic and engineering nomenclature. Figure 5.1-4 compares the geological units with the layering developed for engineering modeling. Of most note, the TR1 and TR2 layers were later identified as the Altamaha Formation (upland unit) and are not part of the Tobacco Road Formation, as originally proposed by the engineering nomenclature.

### *5.1.1 Structural Fill at ITP*

The structural fill at ITP extends approximately between elevations 330 to 286 feet and surrounds the ITP tanks and supports the Filter Stripper Building (Figures 5.1-1 and 5.1-2). The fill material is a relatively uniform, clayey sand (SC). Figure 5.1-5 shows the variation of the liquid and plastic limits, moisture content, fines content, and laboratory-determined undrained strength with elevation. The structural fill is characterized by a layer of moderate CPT tip resistances (mean $q_c$ = 48 tsf) and high friction ratios (mean fr = 8 %) (Table 6.0-1(a)). SPT N-values in the fill range from 10 to 99 bpf and average 25 bpf. Shear wave velocities range from 702 to 1462 feet per second (fps) and average 1,059 fps (Figure 5.1-3(a)).

Six of the seven CPT soundings pushed in the structural fill revealed a 2-foot-thick zone of lower penetration resistance near the base of the fill (labeled Fill 2 in Figure 5.1-5), a few feet above the tank mudmat elevation of 286 feet. A review of the construction compaction records showed that this zone is apparently undercompacted (Figure 5.1-6). (There were insufficient field test results obtained on this weaker zone to provide average SPT N-values or CPT tip resistance and friction ratios.) Details of how this zone was modeled for slope stability analysis are given in Section 7.2.

### *5.1.2 Altamaha Formation or TR1 and TR2 Layers at ITP*

At ITP, the Altamaha Formation was divided into two layers. The upper Altamaha Formation (TR1 layer) is generally more cohesive and less dense than the lower Altamaha Formation (TR2 layer).

Soils in the TR1 layer are typically reddish-brown to purple clayey sands (SC) with some mottled purple and brown clay (CH) and silty sand (SM). This layer has an average thickness of 27 feet (Figure 5.1-3(a)) and is characterized by a zone of moderate CPT tip resistances (mean $q_c$ = 57 tsf) and relatively high friction ratios (mean fr = 5 % ) (Table 6.0-1(a)). SPT N-values in this same layer range from 9 to 65 bpf and average 27 bpf. Shear wave velocities range from 680 fps to 1744 fps and average 1187 fps (Figure 5.1-3(a)).

The soils of the TR2 layer are denser and cleaner than those of the overlying TR1 layer, as seen by the significant increase in tip resistance and decrease in pore pressure generation on the CPT logs

(Figure 5.0-1). The TR2 sediments are dense, silty sands (SM) with interbeds of poorly-graded sand (SP), clayey sand (SC), and silt (ML). CPT logs for this layer show relatively high tip resistances (mean $q_c$ = 168 tsf), moderately low friction ratios (mean fr = 1 %), and no significant generation of excess pore pressure above hydrostatic pressure. SPT N-values in the TR2 layer range from 9 to 53 bpf and average 31 bpf. Shear wave velocities in this layer range from 810 fps to 3,564 fps and average 1,226 fps (Figure 5.1-3(a)). The TR2 layer averages 12 feet in thickness; however, because of obvious thickness changes across ITP, it appears that the TR2 layer has been eroded or cut by the overlying TR1 layer (Figures 5.1-1 and 5.1-2). Also, the TR2 layer rests uncomformably on the underlying Tobacco Road Formation (Fallaw and Price, 1995).

### *5.1.3 Tobacco Road Formation or TR3 and TR4 Layers at ITP*

At ITP, the Tobacco Road Formation was stratified into two layers: TR3 and TR4. These layers appear to be correlative with the upper Tobacco Road and lower Tobacco Road, respectively, described in the geotechnical investigation at the Replacement Tritium Facility (BSRI, 1993b). The upper contact of the TR3 layer is defined by a marked decrease in CPT tip resistance and an increase in both the friction ratio and pore pressure measurements. CPT signatures of the TR4 layer are similar to those of TR3, but show a slight increase in tip resistance and decrease in both the friction ratio and pore pressure generation, indicating that the TR4 layer is denser and more free draining than the overlying TR3 layer (Figure 5.0-1).

Because of similar material properties determined from laboratory testing, the TR3 and TR4 layers were later combined into the TR3/TR4 layer (Table 6.0-1(a)). This combined layer averages about 23 feet thick and consists of mottled red, brown, tan, and white clayey sand (SC) with some interbeds of clayey, silty sand (SC-SM, SM). Kaolinite is the predominate clay mineral in the Tobacco Road Formation (Law, 1994). The TR3/TR4 layer is seen on the CPT logs as a zone having moderate CPT tip resistances (mean $q_c$ = 52 tsf) and moderate friction ratios (mean fr = 3%) (Table 6.0-1(a)). SPT N-values in this layer range from 4 to 29 bpf and average 15 bpf. Shear wave velocities in this same layer range from 809 fps to 1,657 fps and average 1,193 fps (Figure 5.1-3(a)).

### *5.1.4 Dry Branch Formation or DB1-DB5 Layers at ITP*

At ITP, the DB1 through DB3 layers comprise the Irwinton Sand Member of the Dry Branch Formation. The DB1 and DB3 layers are a dense, brown to reddish-brown, poorly-graded sand with some silt (SP-SM, SM). The DB2 layer is a 5- to 10-foot-thick layer of silty sand to clayey sand (SM, SC) in the Irwinton Sand that is traceable across ITP. The DB2 layer is noted on the CPT logs by a zone of lower CPT tip resistance and the generation of pore pressures above hydrostatic pressure. Because of similar material properties, the predominately sandy soils of the DB1 through DB3 layers were ultimately combined into the DB1/DB3 layer (Table 6.0-1(a)). This combined layer averages about 28 feet in thickness. On the CPT logs, the DB1/DB3 layer is

seen as a zone of variable, but generally high CPT tip resistances (mean $q_c$ = 174 tsf) and low friction ratios (mean fr = 1%) (Table 6.0-1(a)). SPT N-values in this layer range from 5 to 99 bpf and average 32 bpf. Shear wave velocities in this same layer range from 665 fps to 1,680 fps and average 1,128 fps (Figure 5.1-3(a)).

The DB4 and DB5 layers comprise the tan clay and Griffins Landing Members of the Dry Branch Formation, respectively. In general, the soils in this interval are much more plastic than the overlying Irwinton Sand (DB1/DB3) and the underlying Santee/Tinker Formation (ST). X-ray diffraction tests show that smectite is the predominant clay mineral in the lower Dry Branch Formation (Law, 1994). Soils in the DB4/DB5 layer range from highly plastic clays (CH) to clayey sands (SC) to silty sands and sandy silts (SM and ML). On soil logs and in core samples, the DB4 layer is seen as a non-calcareous to slightly calcareous, alternating layers of brown, tan, and white, clayey sand (SC) that interfingers with brown to tan, highly plastic clay (CH). The DB5 layer usually has a lighter color and is more silty than the overlying DB4 layer. It is calcareous in some places, especially on the eastern side of ITP tanks. The soils in the DB5 layer are often described as a light olive-green to gray silt (ML) to plastic silt (MH) with varying amounts of clay (CH) and weathered shell fragments.

Underneath ITP tanks, the DB4/DB5 interval is about 14 to 28 feet thick and markedly thickens to the east of Tank 49. The marked thickening of a compressible clay in this area caused Mueser (1977) to abandon the 1977 proposed location of Tank 51 due to concerns of possible differential settlement. The tank sites were later repositioned to their present locations (Figure 5.1-8).

The DB4 layer has moderate to low tip resistances (mean $q_c$ = 48 tsf) and moderate friction ratios (mean fr = 2 % ) (Table 6.0-1(a)). SPT N-values in this layer range from 8 to 30 bpf and average 17 bpf. Shear wave velocities range from 595 fps to 1,309 fps and average 978 fps (Figure 5.1-3(a)). Like the DB4 layer, the DB5 layer is characterized by a zone of moderate to low tip resistances (mean $q_c$ = 50 tsf) and moderate friction ratios (mean fr = 2 %). SPT N-values in this layer range from 7 to 43 bpf and average 20 bpf. Shear wave velocities range from 546 fps to 1,691 fps and average 1,055 fps (Figure 5.1-3(a)).

### *5.1.5 Santee Limestone / Tinker Formation or ST layer at ITP*

The Santee/Tinker interval (ST layer) at ITP averages about 54 feet thick and is found approximately 120 feet below natural ground surface. The contact between the Santee/Tinker Formation and the overlying Dry Branch Formation is seen on the CPT logs as a sharp decrease in the pore pressure measurement. The ST interval is characterized by thin, alternating layers of low and high CPT tip resistances (mean $q_c$ = 111 tsf) and friction ratios (mean fr = 1 %) (Table 6.0-1(a)). SPT-N values in the ST layer range from 0 to 109 bpf and average 58 bpf. Shear wave velocities range from 333 fps to 4,426 fps and average 1,251 fps (Figure 5.1-3(a)).

The Santee/Tinker interval at ITP is depositionally complex and highly variable in both its lithology and material properties. The ITP tanks appear to be located above a transition zone where the Santee Limestone has interfingered or laterally grades into the predominately clayey and silty sands of the Tinker Formation. Characteristically, CPT soundings in the ST layer show a pronounced sawtooth trace due to large variations in the CPT tip resistances over relatively small vertical intervals (Figure 5.0-1). This highly variable pattern suggests interfingering of alternating lenses of clayey and silty sands with more resistant, silica-cemented sediments and less resistant, calcareous sediments, and appears to be a result of rapid lateral and vertical changes in the nature of the materials originally deposited in this interval.

Three distinct lithofacies appear in the upper Santee/Tinker interval in the vicinity of ITP: (1) moldic limestone facies, (2) sandy/silty facies with varying amounts of shell fragments and carbonate sands, and (3) slightly calcareous to non-calcareous, silty to clay sandy facies. (For future reference, these facies will be referred to as Facies 1, 2, and 3, respectively.) Facies 1 predominates on the eastern side of ITP (Figure 5.1-7). To the west and north, the mainly calcareous sediments transition to predominately non-calcareous clayey and silty sands of Facies 3. In this transition zone, the sandy sediments and clastic carbonates of Facies 2 are interfingered with Facies 1 and 3.

Facies 1 was encountered in boreholes H-SPT-20, H-BOR-22, H-BOR-42, H-BOR-43, H-BOR 45, H-BOR 46, H-BOR-47, and H-BOR-50 at elevations 184.5, 153, 180, 170, 176.6, 179, 175.5 and 146 feet, respectively (Figure 5.1-7). Cone penetrometer soundings H-CPT-20, H-CPT-20.1, and H-CPT-20.2 also refused at elevations 186, 185, and 189 feet, respectively, which closely corresponds with the elevations where limestone was encountered in adjacent H-BOR-42, H-BOR-43, H-BOR-45, and H-BOR-47. Much of the limestone is fully lithified with abundant moldic porosity from the fossil molds. Thin, silicified shell layers are also observed in the Santee/Tinker interval.

Facies 2 is localized along a northeast-southwest trending band that roughly parallels the margins of Facies 1 (Figure 5.1-7). Most of the low penetration resistances and drilling fluid losses noted in the Upper Santee/Tinker Formation at ITP occur in Facies 2. The soils in this facies are described as poorly graded, silty and clayey sands and sandy silts with varying amounts of shell fragments and some cemented material. The sand is typically fine-grained, subangular, and well to moderately-sorted quartz. Small percentages of glauconite typically give these sands a light olive-green color.

Facies 2 has its greatest thickness at the cluster of boreholes around H-CPT-23, where a marked decrease in penetration resistance in this layer occurs from elevation 165 to 190 feet. (This is approximately the same interval where limestone was encountered in other nearby boreholes.) CPT tip resistances in H-CPT-23 decrease to an average of 18 tsf in this zone compared to the 135 tsf found in that same interval at nearby H-CPT-20. Also, circulation losses were noted in this same interval in all boreholes near H-CPT-23. Facies 2 is also present near H-CPT-26 in a 10-foot-thick horizon extending from 165 to 175 feet. CPT resistances at this location are generally

below 15 tsf and the soils is described in adjacent H-BOR-50 as a calcareous sand. In that same borehole, shell hash and limestone are noted immediately below the calcareous sand. The adjacent Mueser borehole, 241-12H-45, describes circulation loss and a trace of shells in a calcareous sand and silt which extends from elevation 169 to 152.5 feet.

Facies 3 is predominately non-calcareous and is present to the north and west of a line that roughly extends between H-CPT-5 and H-CPT-30. CPT tip resistances generally increase to above 100 tsf, indicating that the Santee/Tinker sediments in the area are much denser. Soil recovered in H-BOR-29 is described as a clayey sand (SC) with 70 percent fine to medium-grained sand and 30 percent fines of medium to high plasticity.

### *5.1.6 Green Clay and Congaree Formations*

The green clay is an informal stratigraphic name at SRS for stiff, green to gray clays, silts, and clayey sands that are commonly found in the base of the Tinker Formation or within the underlying Warley Hill Formation. In a few of the deeper boreholes at ITP, the top of the green clay was encountered as a 5- to 10-foot-thick, gray to greenish gray, sandy clay and silt with some fine quartz sand at about elevation 120 to 125 feet (Figure 5.1-2). None of the CPT soundings penetrated deep enough to encounter the green clay. Results of the cross-hole seismic survey indicate that shear wave velocity in this layer averages 1,325 fps.

Only a few of the boreholes were advanced deep enough to encounter the sands of the Congaree Formation at ITP. It is described as a dense, brown, poorly graded, quartz sand. The cross-hole shear wave velocities in this layer averages 1,550 fps.

## 5.2 Soft Zones at the ITP

Weight of rod and occasional rod drops have been described in numerous drilling reports for monitoring wells and geotechnical borings located in the central part of the SRS. Early subsurface investigations performed by the U. S. Corps of Engineers frequently described these zones as soft zones, or even voids, and numerous subsequent subsurface investigations have described these same conditions at the SRS. These soft zones typically occur in the carbonate-bearing sediments of the Santee Limestone, Utley Limestone (not present at ITP), and the Griffins Landing Member of the lower Dry Branch Formation. The prevailing assumption about the origin of these soft zones is dissolutioning of carbonate-rich, clastic sediments, resulting in vugular porosity (open pore space). When drilling these zones, the drill rod meets little shear resistance and drops (WSRC, 1994b). However, much of the time, recovery of soil in the sampler precludes the zone from being characterized as a void.

At ITP, soft zones (i.e., SPT-N $\leq$ 5 bpf or CPT tip resistance $\leq$ 15 tsf) are generally restricted to the lower Dry Branch Formation (DB4/DB5 layer) and the Santee/Tinker Formation (ST layer). The soft zones in the lower Dry Branch Formation (DB4/DB5 layer) are generally found on the eastern side of the ITP near the cluster of boreholes drilled at the 1977 proposed location of Tank

51 (Figure 5.1-8). Table 5.2-1 summarizes the SPT blow count and soil properties for the cluster of borings in this area. Mueser (1977) described this interval as "extensive deposits of highly plastic clays." The thickness of this soft layer varies between 20 feet in borehole 241-12H-31 to 30 feet in borehole 241-12H-33 and penetration of the Shelby tube or split-spoon sampler under weight of rod occurred throughout a substantial thickness of this interval. A similar soft zone is found near the eastern half of the present location of Tank 51 near boreholes 241-12H-44, 241-12H45, 241-12H48, and H-CPT-26.

Consolidation properties of the DB4/DB5 layer show that the highly plastic clays (CH) are compressible, but on average, are normally consolidated to slightly overconsolidated (Table 5.2-2). This conclusion is consistent with Mueser (1977) in discussing the consolidation state of the DB4/DB5 layer near the 1977 proposed location of Tank 51: "Of the 12 consolidation tests performed within the highly compressible zone, five were underconsolidated to an average of 70 percent of existing overburden stresses, two were normally consolidated, and five were preconsolidated to only 0.5 to 1.5 tons per square foot above existing overburden stresses. As these deposits have been in place for millions of years, preconsolidation stresses less than existing overburden stresses are not reasonable for undisturbed materials." Furthermore, the tank settlement data compiled in this report (Sections 7.5 and 8.5) show that these plastic soils behaved as preconsolidated sediments when the ITP embankment was placed. Thus, it was concluded that the soft zones in the DB4/DB5 layer pose no significant settlement threat to the ITP tanks (Section 7.5).

Underconsolidated zones are also present in the predominately sandy soils of the Santee/Tinker Formation. Often, in conjunction with these soft zones, intervals of hard drilling, high penetration values (SPT-N > 50 bpf), and high tip resistances ($q_c$ > 200 tsf) were also found in the Santee/Tinker Formation. The hard zones appear to be a result of silicified and/or carbonate-cemented sediments that typically cap or are interlayered with the soft zones. As part of the seismic qualification of the ITP tanks, it was postulated that these hard zones may be arching over pockets of leached calcareous material, thereby allowing the residual, underconsolidated material to persist through geologic time without compressing under the full weight of the effective overburden pressure. It was further postulated that a soft zone of sufficient dimensions might produce an undetermined amount of deep-seated subsidence, if an earthquake of sufficient severity could collapse the arch and transfer full overburden stresses to the underconsolidated zone, thus compressing it.

### *5.2.1 Soft Zone Location, Thickness, and Lateral Extent in the Santee Formation*

To determine the size and location of the soft zones in the Santee Formation at ITP for engineering analyses, CPT and SPT logs were reviewed for all intervals meeting the following criteria: (1) CPT $q_c \leq 15$ tsf or (2) SPT-N $\leq 5$. This review showed that the soft zones are typically found within Facies 2 along the flanks of the moldic limestone of Facies 1 (Figure 5.1-7). CPT and SPT

intervals meeting the soft zone criteria are given in Table 5.2-3 and contoured in Figure 5.2-1. In cross-sectional view, the soft zones were found to be concentrated in two horizons that dip about 2 degrees to the west. This dip parallels the dip of the overlying strata, suggesting that the occurrence of the soft zones is not random, but is stratigraphically controlled. Near the ITP tanks, the upper horizon has a maximum thickness of about 10 to 15 feet and is typically found between elevations 160 to 175 feet (about 110 feet below the tank mudmat). The lower horizon is thinner, less continuous, and has a maximum thickness of about 5 feet. It is typically found between elevations 133 to 138 feet. The thickness reported in Table 5.2-3 and contoured in Figure 5.2-1 represent the combined thickness of the upper and lower horizons.

Although the soft zones in Facies 2 of the Santee/Tinker Formation parallel the moldic limestone in a 100-to 200-foot-wide band, penetration resistances found within this facies are highly variable in both the vertical and lateral directions. Thus, based on data from the existing borings, the soft zones appear to occur as discontinuous pockets, lenses, or stringers within Facies 2. The high degree of variability in penetration resistance is probably a result of rapid lateral and vertical changes in the carbonate deposits and subsequent diagenetic changes such as dissolutioning/ solutioning and silicification.

Geostatistical variography (Journel and Huijbregts, 1978) performed on the Santee/Tinker Formation shows that the soft zones are relatively thin (less than 4 feet on average) and are not laterally continuous for distances greater than a few tens of feet (Rouhani et al., 1995). To perform the variography, all available CPT and SPT data were converted into three categories: soft, intermediate, and hard (Rouhani et al., 1995). Intervals meeting the soft zone criteria were categorized as soft. Intermediate zones were defined as $15 < qc \leq 40$ tsf for the CPT data and $5 < N \leq 10$ for the SPT data. Hard zones were defined as $qc > 40$ tsf and $N > 10$, respectively. Figures A1 - A5 (Vol. 2, App. A) show the results for the soft zone criteria. The vertical variograms for the CPT and SPT data show an average soft zones thickness of about 2 to 4 feet (Figures A1 and A2, respectively). Directional horizontal variography was also conducted along a northeast-southwest trend which parallels the longitudinal axis of Facies 2 (Figure 5.1-7). Three directional angles of N30E, N45E, and N60E were tested (Figures A3 - A5, respectively). None of these cases indicate any discernible lateral correlation on a scale that equals or exceeds the average borehole spacing, which is approximately 35 feet. Thus, if lateral continuity of the soft zones in the Santee/Tinker Formation does exist at ITP, it must be smaller than 35 feet (Rouhani et al., 1995), on average, and is probably on the order of 10 to 20 feet.

To check the conclusions of the geostatistical analyses, penetration resistances from paired CPT-SPT boreholes were also analyzed, The CPT tip resistances, $q_c$, and SPT N-values were paired by elevation for all CPT and SPT boreholes that are separated by approximately 10 feet (or less) horizontal distance. In pairing the CPT data with the SPT N-values, measurements of $q_c$ were averaged over a 2-foot interval, starting 6 inches above the top of the SPT sampling interval. Figure 5.2-2 shows poor lateral correlation, even for these closely spaced boreholes and indicates large heterogeneity in penetration resistance over relatively short horizontal distances. In contrast,

and for comparative purposes, this same process was repeated for the overlying Irwinton Sand (i.e., DB3 layer). Figure 5.2-3 shows some correlation, indicating that the DB3 layer is more homogeneous and laterally continuous than the ST layer.

### *5.2.2 Grout Injection Evaluation of Soft Zones*

To test the potential grout take of the soft zones at the ITP, a grout injection test was performed as part of the Phase 1 exploration. H-CPT-20 and H-CPT-28 were chosen as test areas because of the different subsurface conditions noted above the carbonate bearing stratum. Because of the extensive evaluation of the K-Area Soil Stabilization Program (KASS) program, the test was designed as similarly as possible to the drilling and grouting operations of the KASS program.

At the H-CPT-20 location, 835 cubic feet of grout was injected during the testing and abandonment. At the H-CPT-28 location, 3,253 cubic feet of grout was injected. Subsequent subsurface exploration and coring during Phases 2 and 3 found no grout near the H-CPT-28 location. This suggests that grout can migrate a considerable distance from the injection point in these carbonate sediments.

Due to the scope of this evaluation, a separate report (WSRC-TR-950127) has been issued to detail the investigation and results.

### *5.2.3 Potential Voids in Relation to Soft Zone Intervals at ITP*

As mentioned earlier, observed soft zones are a typical occurrence within the lower Dry Branch and Santee Formations, especially when very soft carbonate sediments are present. Numerous foundation reports across the SRS also make note of voids where drilling indicates rapid advance of the drill string, loss of fluid circulation, or rod drop during sampling. Numerous scenarios such as the weight of the drill rod exceeding the shear strength of the soil, the drill fluid pressure hydrofracturing the soil mass resulting in fluid loss, or the fluid pressure jetting ahead of the drill bit and washing away the interval, thus leaving an artificial void can cause these conditions.

Based upon a void criteria of CPT $q_c \leq 3$ tsf, CPT sleeve $\leq 1$ tsf, and piezocone pore pressure measurements approximately equal to hydrostatic pressure, all CPT soundings from the ITP investigation were evaluated for intervals meeting these criteria. Five CPT soundings measured relatively thin intervals of potential void (Figure 5.2-4). With the exception of SCPT-01, all CPT soundings meeting these conditions were limited to the eastern side of the ITP, where carbonate sediments are present. The interval at which these conditions are noted corresponds to the top of the Santee Limestone (Facies 1) and the bordering Facies 2. Individual thicknesses of potential void range from 0.5 feet to 4.3 feet thick (Figure 5.2-4). The greatest cumulative thickness occurs in H-CPT-28, which is located off the southeastern corner of the ITP embankment. At this location, four separate intervals (1 inch, 51 inches, 1 inch and 10 inches) result in a total of 63 inches (Figure 5.2-4).

It is impossible to determine the lateral extent of a possible void from the existing borehole data. However, it is possible to generalize about a maximum likely dimension using the statistical analyses previously provided. Because the void criteria are more restrictive than the soft zone criteria (i.e., the void criteria are a subset of the soft zone criteria), generalizations about the lateral extent of soft zones also applies to potential void. As previously noted, statistical analyses of the upper Santee Formation suggests that the maximum lateral dimension of a soft zone is no greater than 35 feet and is probably between 10 and 20 feet. This is also true for the maximum lateral dimension of a potential void.

### *5.2.4 Investigation of Void Intervals at the ITP*

An attempt was made during the ITP Phase 3 investigation to sample an interval meeting the void criteria to see if it contains loose sand. This effort involved drilling H-BOR-50 adjacent to H-CPT-26 where two potential void intervals were found between elevations 170 and 165 feet. H-BOR-50 was advanced without sampling through the structural fill to a depth of 40 feet. The boring was then continuously cored with a 94-mm core system to a depth of 145 feet (elevation 181 feet ) or 11.5 feet above the upper most void interval. The hole was reamed to elevation 180 feet and six Shelby tubes continuously pushed to elevation 168.8 feet. The first five tubes had 100 percent recovery of a silty to clayey sand that is typical of DB4 /DB5 soils. The sixth Shelby tube was intended to penetrate the potential void. The tube was advanced a total of 10 inches before the hydraulic pressure exceeded 1,000 psi and the push was discontinued. Once the tube was retrieved, the bottom of the tube was crushed and no material was recovered. Because of the obviously dense layer, the sampling system was then changed to the 94-mm core system. Coring resumed at elevation 167.5 and a 48-inch run was made which extended through the next void interval at elevation 166.5. (See Figure 5.2-5 for sampling intervals of H-BOR-50 and the corresponding tip resistance encountered in H-CPT-26.) Recovery from this core run was 31.5 inches of sandy soil, which is about average recovery in SRS sediments for the 94-mm core system. Thus, because of the potential for poor recovery from this system, it is difficult to determine if the missing 16.5 inches represents a void or poor recovery.

An attempt to resample the void interval was made in an adjacent boring H-BOR-51, however, the first Shelby tube was lost in the hole. Attempts to recover it were unsuccessful and the boring was abandoned.

## 5.3 Generalized Engineering Profiles of the HTF

Four generalized profiles were constructed to represent the stratigraphy for the balance of the tank farm (see Figures 5.3-1 and 5.3-2). Stratigraphic layering was delineated based on CPT and based on boring information. Boring and CPT data were projected perpendicular to the section lines. Maintaining consistency with the two ITP-specific sections, the new sections are referred to as sections DD, EE, FF, and GG and are described as follows:

- Section DD H-Tank Farm - Long Axis Section (Figure 5.3-1) represents a profile line made through the longitudinal axis of the tank farm. The southeast end originates in the ITP area and terminates at the western end of the tank farm embankment. This section extends from the structural fill to basement rock. Two deep borings, extending to basement, were used for defining stratigraphy below the green clay.
- Section EE H-Tank Farm - ITP N-S Extension (Figure 5.3-2) is an extension of the ITP section AA' through the northern embankment (North Hill). The stratigraphy is limited to the engineering layering above the green clay.
- Section FF H-Tank Farm - North Hill E-W Section (Figure 5.3-2) represents a profile line through the northern embankment extending across the midwestern portion of the tank farm. The stratigraphy is limited to the engineering layering above the green clay.
- Section GG H-Tank Farm - Old Hill N-S Section (Figure 5.3-2) represents a section made through the old hill of the tank farm. The section originates off the embankment at NWTF, extends north through the midwestern portion of the tank farm, and terminates at the Receiving Basin for Offsite Fuels (RBOF). The stratigraphy is limited to the engineering layering above the green clay.

The engineering stratigraphy defined for the ITP (Section 5.1) was applied to CPT and borehole data compiled for the balance of the HTF. CPT signatures in both areas are comparable, demonstrating the similarity of foundation soils in the HTF with those previously investigated at ITP. For example, histogram plots of the natural log of CPT tip resistance, by layer, are presented in Figures 5.3-3 to 5.3-8 for HTF and ITP. The log distribution and average of CPT tip resistance ($q_c$) values are quite similar, indicating that the soil has about the same density in both areas. However, the left-skewed distribution for the Santee/Tinker Formation at ITP (Figure 5.3-8) also suggests that soft zones are more prevelant at ITP than in the remainder of the HTF. Figures 5.3-11 and 5.3-12 also show that soft zones, carbonates, and potential voids appear to be more predominate in the ITP area.

Generalized average elevation, Poisson's ratio, total unit weight, and shear wave velocities for each of these layers in the HTF are shown in Figure 5.1-3(b) and tabulated in Table 6.0-1(b).

### *5.3.1 Evaluation of Soft Zones, Voids, and Carbonates for the HTF*

Boring and CPT data (SPT N-values and $q_c$) pertinent to the HTF were reviewed, applying the same soft zone and void criteria as described for ITP. Further, all boring logs contained within the reports listed in Section 1.5 were reviewed for indications of positive reaction to HCL and notes of shell fragments and/or carbonate sediments. This information was then entered into 3-D modeling software so that various data types could be displayed by color to determine spatial relationships. As seen in Figure 5.3-9, the distribution of data across the HTF is not as dense as that obtained at ITP. Therefore, it is important to use the experience gained from the extensive characterization and engineering analyses at ITP and apply this knowledge to the HTF, as the data warrant.

Figure 5.3-10 shows soft zones are present in the remainder of HTF. These zones occur in the same horizons as found at ITP (Figure 5.3-12). Also, as seen in Figures 5.3-11 and 5.3-12, the relationship between carbonates and soft zones appears to be analogous to that of ITP. Based on a review of all subsurface information obtained in the HTF, it is concluded that the subsurface conditions in the remaining HTFs are no worse than in the ITP; and may actually be slightly better due to lesser amounts of carbonate and associated soft zones.

## 5.4 Shallow Faulting at the ITP and HTF

Concurrently, there are no faults classified as active at SRS or in the immediate vicinity (40 km radius). There are several inactive subsurface faults rooted in the crystalline rock beneath the SRS. One such fault, the Pen Branch fault, has been extensively studied and is known to be a very old structure, posing no seismic hazard threat (Stieve et al., 1995; Stephenson and Stieve, 1992; Stieve et al., 1991; Price et al., 1989). Other faults have not been studied as extensively, but investigators suggest that they are not seismogenic nor significantly large structures and do not deform very young sediments. Still other potential faults in the subsurface are known to exist, but the documentation of their age and lateral extent is very limited.

Faults in the GSA of SRS are commonly observed along the flanks of carbonate buildup (Aadland et al., 1991). There are three possible mechanisms that explain the relation between faulting and the distribution of the carbonate buildup. The first mechanism suggests that non-tectonic faulting occurred due to slumping of the overlying sediments above carbonate buildups as dissolution progressed within, or along the fringes, of the carbonate body. In this mechanism, consolidation of the leached residual sediment occurred under lithostatic load, causing an thinning of the stratigraphic column in the carbonate section (WSRC, 1994b). Above the zone of dissolutioning, a general loosening of the overlying sediments may have also occurred as these predominately sandy materials raveled, relaxed, and subsided. For example, Siple (1967) speculated that dissolutioning of calcareous material in the Santee Limestone occurred at the SRS, causing subsidence or slumping of overlying beds and the formation of shallow surface depressions. He noted that voids and loosely compacted sediments were encountered during well drilling and that large amounts of cement grout were used to stabilize the subsurface before construction of heavy structures. The second mechanism consists of small-scale faulting and folding of the Coastal Plain sediments by Tertiary tectonic activity. Several regional basement structures have been interpreted as uplifts or gentle folds and may be indicative of continued crustal movement in the Miocene age. Because of a marked strength contrast between the more rigid limestone and the adjacent, softer, unconsolidated sediments, a series of secondary faults may have formed along the fringes of carbonate bodies when basement faulting was refracted as it propagated to the surface. The last mechanism is simply a combination of the first two mechanisms. In this mechanism, local disruption of confining clay layers along tectonic fault planes may have removed barriers to groundwater migration and exacerbated the amount of leaching and subsequent slumping in pre-existing, fault-controlled orientations (WSRC, 1994b).

During the subsurface exploration of the ITP, stratigraphic offsets were detected between closely spaced CPT soundings and SPT borings. These offsets are thought to be either minor faults or slump features whose geometry and extent with depth is unknown. In the shallow profile, the offsets have displaced strata of the Dry Branch and Tobacco Road Formations, suggesting that most of the deformation is post-Tobacco Road (i.e., post late Eocene). Because the surficial unit at ITP (i.e., Miocene upland unit) is geologically complex and has been disturbed and reworked by construction activities, it is difficult to determine if the offsets have displaced this unit and thus further constrain the latest episode of movement.

The major offset feature at ITP appears to occur near the margins of the Santee Limestone. The exact location of the potential faulting or slumping is difficult to interpret, but probably occurred somewhere between the eastern edge of ITP embankment and the Cold Feeds Facility along the boundary of Facies 1 and 2 (Figure 5.4-1). Also, Figure 5.4-1 shows the elevation of the top of the Tobacco Road Formation (TR3 layer) in parentheses next to each CPT sounding. These data show that the Tobacco Road Formation on the eastern side of ITP, where underlying carbonate is present, is approximately 20 to 30 feet higher than on the western side, where underlying carbonate is mainly absent. This further suggests possible dissolutioning of the calcareous sediments along the fringes of the carbonate body (i.e., Facies 1 and 2) and subsequent slumping of the overlying Tobacco Road Formation on the western side of ITP as carbonate was removed to form Facies 3.

Some secondary faulting, or minor slumping, is also suggested at ITP between H-CPT-16 and H-CPT-31, between H-CPT-11 and H-CPT-6, and between H-CPT-6 and H-CPT-30 (Figure 5.4-1). These minor offsets have been interpreted as a series of east-west trendings, secondary or accommodating faults that strike roughly perpendicular to the western margin of the carbonate body (Figure 5.4-1). Maximum vertical displacement on any of these faults is about 10 to 15 feet.

Unfortunately, the amount of borehole data at ITP decreases with depth (i.e., most borings and CPT soundings are less than 200 feet deep), making it difficult to determine if geological formations below the carbonate have been displaced. For example, the green clay in Figure 5.1-2 does not appear to be offset more than a few feet, suggesting that inferred vertical displacement is mainly restricted to the shallow profile at ITP. However, because deep geological control is somewhat limited in this area, it is difficult to preclude the presence of deeper faulting. Seismic reflection data suggest that faulted or anomalous zones inferred in the deep ITP profile correspond with possible shallow faults mapped by borehole data in the Tobacco Road and Dry Branch Formations (WSRC, 1994b).

As part of the H-Area characterization, a large scale map of select subsurface horizons was prepared (Figure 5.4-2). Both geotechnical and geological well drilling data were combined to maximize the data density. Two specific, mappable horizons were chosen. The uppermost horizon corresponds to a "red" horizon described in the well boring logs. This horizon also correlates to the top of the Tobacco Road Formation (TR3 layer) in the geotechnical logs. The lower horizon correlates to the top of the Congaree Formation (i.e., bottom of green clay). From this data, structural contour and isopach maps were constructed for each horizon. For presentation

purposes, a combined isometric surface map of H-Area is included (Figure 5.4-2). As interpreted from this map, the vertical relief or offset shaded on the upper surface (top of Tobacco Road Formation) is also visible on the lower surface (top of Congaree Formation). This shaded surface corresponds to the north-south trending fault mapped along the boundaries of Facies 1 at ITP (Figure 5.4-1). The similarity of these two surfaces suggests that the shallow faulting in the ITP area has been influenced by deeper faulting, which extends below the carbonate sediments and into the Congaree Formation. However, some differences between the two surfaces are also apparent and depositional and dissolutioning processes may have also played a role in producing the relief.

Any further interpretation of faulting with depth is speculative at this time, but the ongoing seismic reflection program may provide the required information for interpreting these features to depths below the green clay.

# 6. ENGINEERING PROPERTIES

Engineering properties for ITP and the balance of the HTF were derived using laboratory test data gathered for the current and previous investigations in the HTF, previously established empirical relationships, and engineering judgment. Table 6.0-1(a) and 6.0-1(b) contain average static material properties used in engineering evaluations at ITP and HTF, respectively. OCRs are presented in Figure 6.0-1. Special laboratory testing and analyses involved with determining dynamic properties are discussed in Section 6.1 below. Dynamic strength and compressibility are presented in Section 6.2. Strength parameters used for slope stability evaluations are presented in Section 6.3. Further discussion relating to static compressibility properties of the subsurface soils are discussed and summarized in Sections 7.5 and 8.5 for ITP and HTF, respectively.

## 6.1 Dynamic Properties

Idealized soil profiles for ground response evaluations with best estimates of layer thicknesses, total unit weights, and shear wave velocities are presented in Figures 5.1-3(a) and 5.1-3(b) for ITP and HTF, respectively. A dynamic evaluation was performed at ITP for the local and distant EBE using deconvolution techniques which bring ground motions from the ground surface to a depth of 170 feet. Dynamic soil properties below a depth of 170 feet were therefore not required for this portion of the analysis. Subsequently, ITP and HTF were evaluated for 84th percentile ground motions using convolution techniques which bring the ground motions up from bedrock. The dynamic soil properties used for the local and distant events (EBE) and for the 84th percentile motions are discussed separately below.

### *6.1.1 Local and Distant Event ITP Evaluation*

The shear modulus reduction with cyclic strain amplitude and damping ratio versus cyclic strain amplitude relationships were derived by combining test results from the RTF and ITP investigations. The test results were subdivided into fill and in-situ soil. Each group was sorted by shear strain, then both the shear modulus reduction with cyclic strain amplitude and damping ratio versus cyclic strain amplitude relationships were plotted as running averages of every four sequential values. The recommended relationships were then selected by hand-smoothing the running average curves.

The damping ratio versus cyclic strain amplitude curves are shown in Figure 6.1-1 both for fill and the upper (less than 170-foot depth) foundation soils at ITP. The modulus reduction versus cyclic strain amplitude for fill and the upper foundation soils from the ITP site are shown in Figure 6.1-2. Also plotted in these figures are the relationships proposed by Seed and Idriss (1970).

Recommended values of damping ratio and shear modulus reduction with shear strain amplitude for the uppermost approximately 170 feet of subsurface soils are provided in Table 6.1-1.

The above relationships of damping ratio/cyclic strain amplitude and shear modulus reduction/cyclic strain amplitude were used exclusively for the local and distant ITP dynamic analyses (reported in Section 7.3) which employed deconvolution techniques to determine earthquake-induced strains in the upper 170 feet. Dynamic soil properties for the deeper soil deposits were not required to perform these analyses.

Upon review of the strain-controlled triaxial test results, it was observed that the hysteresis loops of axial strain versus deviatoric load from a number of the ITP tests had been cut off at high strains. In addition, some of the test results used from previous projects showed jagged traces on the axial strain versus deviatoric load plots. Figures 6.1-3(a) and 6.1-3(b) show typical examples of the cutoff and jagged traces, respectively. Currently, Professor K. Stokoe (under separate contract) is reviewing this data, as well as all other sitewide dynamic property data, and will be presenting his conclusions regarding sitewide dynamic soil property recommendations in a future report. As a precautionary measure, however, the average curves for damping and shear modulus reduction for ITP were recalculated excluding the questionable tests which had been cut off at high strains. The resulting shear modulus reduction with cyclic strain amplitude and damping ratio versus cyclic strain amplitude relationships were essentially identical to the curves derived using all the data. Therefore, the recommended values indicated in Figures 6.1-1 and 6.1-2, and in Table 6.1-1, were unaltered.

### *6.1.2 84th Percentile Dynamic Analysis for ITP and HTF*

For the 84th percentile ground motion evaluations at ITP and HTF, convolution techniques were employed which required dynamic soil properties down to bedrock (approximately 1,000 feet deep). For these analyses, the dynamic strength properties were modeled using the relationships of damping ratio and shear modulus reduction versus cyclic strain amplitude developed by GEI (1991b) for the K-Reactor area. For these analyses, GEI curves were used in the upper 170 feet as well as the deeper deposits and are presented in Figures 6.1-4 and 6.1-5, for damping ratio and shear modulus reduction, respectively. Parametric analyses comparing the ground response utilizing GEI and WSRC developed dynamic properties are presented in Section 9.

## 6.2 Cyclic Strength and Compressibility

### *6.2.1 Foreword*

It was shown in Section 5 that the soils of the Tobacco Road and of Dry Branch Formations consist of materials which, because of their geologic genesis, age, and composition, are radically different from the sands and silty sands that constitute the database for the widely used empirical chart for liquefaction evaluations proposed by Seed, Tokimatsu, Harder, and Chung (1984). To define the cyclic strength of these formations soils, and to supplement limited empirical data, a comprehensive laboratory testing program was carried out. The methodology and the step-by-step procedure followed in the derivation of cyclic strength and volumetric strain are presented below.

Because of the considerable depth within the stratigraphic soil column at the site, the cyclic shear strains that seismic ground motions induce in the Santee/Tinker Formations soils are small. The strains are near the threshold amplitude level required to start the process of excess pore water pressure generation. The methodology and procedures to analyze pore water pressure generation, and compression mechanisms of the Santee/Tinker Formation soils are also presented below.

### *6.2.2 Cyclic Strength*

#### *6.2.2.1 Methodology*

The steps required to modify the relationship between the laboratory pulsating stress ratio ($\sigma_{dp}/2\sigma_{3C}$) and number of cycles to reach initial liquefaction ($N_L$) to the field cyclic shear stress ratio ($\tau/\sigma_0'$) and the penetration resistance $(N_1)_{60}$ are schematically presented in Figure 6.2-1. In this report, initial liquefaction is understood to mean the stage of a test in the laboratory or of the soil in the field at which the pore water pressure ratio ($r_u$) induced by the cyclic loading reaches a value equal to the initial effective confining pressure in the laboratory, or the initial effective overburden pressure in the field ($\sigma_0'$) and is designated as:

initial liquefaction, pore water pressure ratio $r_u = 100\% = \Delta u/\sigma_0'$

Recent studies carried out for the RTF at the site (BSRI, 1993b) developed the cyclic strength-normalized standard penetration resistance blow count $(N_1)_{60}$ relationship shown in Figure 6.2-2. A similar relationship for the Tobacco Road/Dry Branch soils at ITP is required for the current studies. But, since at the latter facility, the CPT rather than the SPT was more widely used in the subsurface characterization efforts, a cyclic strength-cone tip-friction ratio relationship is more desirable. To achieve this result, the following two-step methodology was adopted:

1. Based on data from Tobacco Road soils at the RTF, obtain a field cyclic strength versus cone tip resistance relationship which also reflects fines content.
2. Incorporate in the relation developed in Step 1 the results from Tobacco Road and Dry Branch soils from ITP.

The work involved in Step 1 is described below. The work corresponding to Step 2 is presented in Sections 6.2.2.2 and 6.2.2.3.

For the RTF facility, 17 triaxial test specimens were selected for the cyclic testing. Table 6.2-1 from BSRI (1993b) summarizes the cyclic test data, together with pertinent sample identifications. Cyclic strength data corrected for field conditions are presented in graphical format in Figures 6.2-3 and 6.2-4 for the Lower and Upper Tobacco Road soils, respectively. Numbers in the notes at the top of the figure are the average tip resistance for the tube sample(s) from which the specimens were obtained. From these figures and from Table 6.2-1, the following information can be summarized:

| Soil Layer at RTF | Normalized Cone Tip Resistance, $(q_c)_1$, tons/ft$^2$ | Fines % | Field Cyclic Strength $\tau/\sigma_o'$ |
|---|---|---|---|
| Upper Tobacco Road | 9.5 | 28.7 | 0.167 |
| Upper Tobacco Road | 20.8 | 19.5 | 0.138 |
| Lower Tobacco Road | 24.4 | 9.6 | 0.095 |
| Lower Tobacco Road | 35.2 | 15.7 | 0.135 |
| Lower Tobacco Road | 51.7 | 10.8 | 0.115 |

These data are superimposed to the cyclic strength-cone tip resistance proposed by Seed, Idriss, and Arango (1983) in Figure 6.2-5. Dashed boundary lines shown were based on considerations of the fines content, and the trends proposed by the authors for clean Holocene sands (shaded band). Figure 6.2-5, which is the end-result of Step 1 is the desired relationship between field cyclic strength, normalized cone tip resistance, and fines content for the Tobacco Road soils at RTF.

### *6.2.2.2 Selection of Samples for Testing Program*

Figure 6.2-6 compares the stratigraphic soil columns under both the RTF and ITP. The figure also indicates that in geologic terms, the Upper Tobacco Road at the RTF is equivalent to the TR3 layer at ITP. Similarly, the Lower Tobacco Road is equivalent to TR4 layer. Table 6.2-2 summarizes engineering properties of the various materials at the site for the two facilities.

Selection of samples for use in the laboratory testing program at ITP was based on the following considerations:

- Low cone tip resistance
- Low fines content (based on field observations)
- Low volumetric change due to sampling
- Sample uniformity
- Minimum disturbance (based on visual examinations of X-ray photos)

Table 6.2-3 summarizes the stationary piston samples selected for the cyclic laboratory testing program, while Table 6.2-4 shows corresponding normalized values of the cone tip resistance for the selected samples.

### *6.2.2.3 Laboratory Testing*

Classification (grain size and plasticity data) for each of the 18 specimens tested is presented in Table 6.2-5. Included in Table 6.2.5 are test results of Atterberg limits performed on the material passing a US No. 200 sieve. These tests were performed to determine the nature of the clay size

material. The corresponding Unified Soil Classification designation, together with test conditions and partial test results, are presented in Table 6.2-6. Cyclic stress ratios obtained in the laboratory tests at the stages of initial liquefaction, and after 5- and 10- percent double amplitude strains are summarized in Table 6.2-7. In Table 6.2-6, the laboratory-obtained cyclic strength ratios at the stage of initial liquefaction are modified for differences between laboratory cyclic triaxial and field sample shear conditions by the factor $C_r$. The results are further normalized to a uniform effective overburden pressure equal to 1 tsf by the factor $k_\sigma$. The numerical value of $C_r$ was conservatively taken equal to 0.64, based on the values recommended by Seed, Arango, and Chan (1975) for an overconsolidation ratio of 2. The pressure normalizing factor, $k_\sigma$, was obtained from the laboratory tests performed for this project, as described in Section 6.2.2.4.

The field cyclic stress ratios shown in the last column of Table 6.2-6, and the number of cycles to reach initial liquefaction, shown in the same table, have been combined graphically in Figures 6.2-7 through 6.2-9, grouped according to fines content. Also shown in the figures for each of the curves drawn are the average normalized cone tip resistance, average fines content, and cyclic stress ratio corresponding to the stage of initial liquefaction at 15 cycles.

The five curves shown in Figures 6.2-7 through 6.2-9 provide five sets of values of cyclic stress ratio, normalized cone tip resistance, and fines content. These ITP data sets are, in turn superimposed on the corresponding RTF data shown in Figure 6.2-5, to produce Figure 6.2-10. This figure is, therefore, the result of the 35 cyclic triaxial tests performed for the two facilities at the site.

The cyclic strength of the Tobacco and Dry Branch soils at any location can now be predicted with Figure 6.2-10, if the cone tip resistance and the fines content of the soil are known. Because the fines content can only be estimated by observation of a sample, or obtained from laboratory tests, it is desirable to devise a means to obtain this soil parameter by a simple field exploratory method such as the cone penetration test. Figure 6.2-11 is a compilation of the data gathered regarding laboratory-obtained fines content and friction ratio measured by the CPT at ITP. From the best-fit mean curve, the following correlation between the friction ratio and fines content is adopted:

| Fines % | Friction Ratio |
|---|---|
| 0 | 0 |
| 10 | 0.5 |
| 15 | 1 |
| 22.5 | 3 |
| 30 | 6 |

The above correlation has been introduced to the data in Figure 6.2-10 to produce the cyclic strength, tip resistance, and friction ratio relationship shown in Figure 6.2-12. This is the cyclic strength relationship adopted for the liquefaction evaluations at ITP.

In summary, the cyclic stress ratio data plotted in Figure 6.2-10 show a strong tendency to increase with increasing fines content; hence, it is clear that the fines content of the Tobacco Road and Dry Branch sediments have an important influence on liquefaction resistance. This conclusion is consistent with other field and laboratory studies that conclude that silty sands are generally more resistant to liquefaction and ground deformation than clean sands for the same penetration resistance or relative density (Tokimatsu and Yoshimi, 1984; Seed et al., 1984; Seed and Harder, 1990; ASCE, 1994; Bartlett and Youd, 1995). Also, the data in Figure 6.2-10 show that $q_{c1}$ values tend to decrease with increasing fines content, suggesting that for these sediments, sands with a significant amount of fines show a more plastic behavior (i.e., less resistance to shear). Thus, it can be concluded that for the silty and clayey sands at ITP, lower penetration resistance is not necessarily indicative of a decrease in liquefaction resistance; lower penetration resistance may actually be a result of an increasing clay content which produces a higher resistance to liquefaction as shown in Figure 6.2-10.

#### *6.2.2.4 Derivation of a Site-Specific $k_\sigma$ Factor*

The procedure recommended by Harder (1988) to quantify the effect of confining pressure on the cyclic stress to cause initial liquefaction in cyclic triaxial tests is schematically presented in Figure 6.2-13. The ratio between the cyclic stress ratio required for initial liquefaction under an initial confining pressure $\sigma'_{3c}$ relative to that under a confining pressure of 1 tsf is called $k_\sigma$.

Data from 24 cyclic triaxial tests performed for ITP are shown in Table 6.2-8 and Figures 6.2-14 through 6.2-16. Cyclic stress ratios for initial liquefaction after 15 cycles of loading were obtained from these figures and plotted at the corresponding confining pressures in Figure 6.2-17, following Harder's (1988) approach. Values of the cyclic stress required for initial liquefaction in 15 cycles under an initial confining pressure of 1 tsf extrapolated from these curves are 0.21, 0.26, and 0.17 for TR3, TR4, and DB1/3 layers, respectively. With these values, the calculation of the $k_\sigma$ factors can then proceed, as shown in Table 6.2-9. The values obtained are plotted in Figure 6.2-18 which for comparative purposes also show data from Harder (1988) and Koester (1992). (Note: It appears that three separate curves can be drawn through the data shown in Figure 6.2-18, one curve for TR3, TR4, and DB1/3 layers, respectively. However, because the data are somewhat limited and the TR3 and TR4 layers were combined into one layer TR3/4 for evaluation purposes. Only one site-specific $k_\sigma$ relation was ultimately adopted.)

### *6.2.3 Cyclic Compressibility*

The magnitude of the volumetric strains that can be expected to follow the dissipation of excess pore water pressures during cyclic loading was studied by Lee and Albeisa (1974). Their studies led to the conclusion that if liquefaction does not develop, the resulting volumetric strains in clean sands are always likely to be less than 1 percent, but that if liquefaction does develop, the resulting strains may be up to 2 or 3 percent or perhaps even greater for loose clean sands. They also found

that the amount of reconsolidation volumetric strains for nonliquefaction conditions increases with decreasing density and increasing excess pore water pressure generated by the cyclic loading.

In 1984, Tatsuoka, Sasaki, and Yamada found that the amount of settlement can be significantly affected by the maximum shear strain developed in the soil. Tokimatsu and Seed (1984) combined the results of prior investigations with their results on the subject and produced the proposed tentative relationship between cyclic stress ratio, $(N_1)_{60}$, and volumetric strain for saturated clean sands shown in Figure 6.2-19.

The relationship shown in Figure 6.2-19 is not useful to the current evaluation because the HTF site is characterized by cone penetration data rather than SPT data. Furthermore, the graph applies to clean sands, and its applicability to the clayey materials encountered at the site is questionable.

To overcome these difficulties, it was decided to develop a site-specific volumetric strain relationship by performing post-liquefaction laboratory testing and relating the test results to the in situ CPT characteristics of the original samples.

### *6.2.3.1 Liquefaction Volumetric Strain*

Axial, shear, and post liquefaction volumetric strains measured in 24 stress-controlled tests performed on samples from ITP site are summarized in Table 6.2-10. The table also provides the cyclic stress ratio, the number of cycles to initial liquefaction, and the in situ normalized cone tip resistance, $q_{c1}$. The data from the table are plotted in Figure 6.2-20 which also shows the inferred average maximum, or limiting, shear strain relationships. The volumetric strain can be read off the figure if the cone tip resistance and the limiting shear strain to which the earthquake will subject the soil at the given location are known. A method to estimate the limiting shear strain if the factor of safety against initial liquefaction is known is presented below.

The relationship between normalized blow count $(N_1)_{60}$, level of cyclic stress, and limiting shear strain proposed by Tokimatsu and Seed (1984) is shown in Figure 6.2-21. From this, it is seen that for a factor of safety against initial liquefaction equal to 1.0, the limiting shear strain is about 3 percent (clean sands). A similar value was suggested by Ishihara (1993), who reported values between 2.5 and 3.5 percent.

The limiting shear strains at the time of initial liquefaction calculated from the cyclic triaxial tests on the ITP soils ranged between 1.1 and 8.2 percent, with a mean value of 3.0 percent. These results show that for a condition of initial liquefaction (i.e., when the factor of safety has a value of 1), the limiting shear strains observed in the ITP tests agree with the trends for sands and silty sands reported by Tokimatsu and Seed and by Ishihara. It is reasonable to assume that the limiting shear strains at other values of the factor of safety against initial liquefaction of the ITP soils would also be similar to the corresponding values reported by the same quoted references for sands and silty sands. Limiting values of shear strains at various factors of safety against initial liquefaction can be derived as shown in Figure 6.2-22. For example, a sand with an $(N1)_{60}$ value of 22 represented by Point B would have a cyclic strength represented by a cyclic stress ratio equal

to 0.24. Such a sand, under an earthquake inducing a cyclic stress ratio of 0.30 would have a factor of safety against initial liquefaction equal to 0.24/0.30, or 0.8, which defines point B. Point C would be obtained in a similar way. Points C and B define the relationship between $(N1)_{60}$ and the cyclic stress ratio that results on a factor of safety against initial liquefaction equal to 0.8. Projection of this curve to the upper part of Figure 6.2-22 shows that for this condition, the limiting shear strain is equal to 9 percent. Limiting shear strains for other values of factor of safety can be obtained in a similar way, and the results plotted as shown in Figure 6.2-23.

Volumetric strain data from the laboratory tests shown in Figure 6.2-20, the corresponding sample field cone tip penetration resistance from Table 6.2-4, and the relationship between the factor of safety against initial liquefaction and limiting shear strain in Figure 6.2-23 are combined in Table 6.2-11, and plotted in Figure 6.2-24. For ITP soils, the volumetric strain after liquefaction can be obtained from this figure at any field location if the factor of safety against liquefaction and the in situ cone tip resistance are known.

### *6.2.3.2 Partial Liquefaction Volumetric Strain*

For partial liquefaction (i.e., $r_u < 100\%$), the model (and relation developed) representing the mechanism of pore pressure generation during cyclic loading (Figure 6.2-25) was used along with the relation between the factor of safety against initial liquefaction and residual excess pore water pressure ratio ($r_u$) (Figure 6.2-26). The data shown in Figure 6.2-26 were obtained from Marcuson, Hynes, and Franklin (1990), Tokimatsu and Yoshimi (1983), Ishihara (1985), Tokimatsu and Seed (1984), and laboratory tests results from the RTF and ITP programs. A conservative upper bound curve enveloping all available data was adopted for the ITP evaluations (Figure 6.2-26). Recompression ratios ($C_r / (1+e_0)$) from the nine consolidation tests performed on Dry Branch and Tobacco Road Formations soils were used to determine the average recompression ratio of 0.0092 for these soils. Using this value, the relation between factor of safety and excess pore water pressure ratio, $r_u$, given in Figure 6.2-26, the volumetric strain equation given in Figure 6.2-25, and the relation between factors of safety and volumetric strain for partial liquefaction can be determined. For example, if the factor of safety against liquefaction is computed to be 1.2, then $r_u = 0.63$ (Figure 6.2-26). The volumetric strain is then computed by the equation shown in Figure 6.2-25 as:

$$\Delta V/V = 0.0092 \log [(1/(1-0.63)] \times 100\% = 0.40\ \%$$

The results are summarized, together with the previous results shown in Figure 6.2-24, to produce the volumetric strain versus factor of safety design curves in Figure 6.2-27 for the site soils. It should be noted from Figure 6.2-26 that for factors of safety (FS) $\leq 1.15$, the excess pore water pressure ratio is conservatively assumed to be equal to 100%. For the analyses in Section 7.3, liquefaction was assumed to occur for all values of FS $\leq 1.15$.

It is important to note that the partial liquefaction volumetric strain computed in the above example compares favorably to the liquefaction volumetric strain calculated for factors of safety

approximately equal to 1 (i.e., FS ≈ 1). For example, for a CPT $q_{c1}$ value of 50 tsf ( which is considered less likely to liquefy) and a factor of safety against liquefaction of 1.0, the calculated liquefaction volumetric strain is 0.69% (Table 6.2-11). This result is very close to the partial liquefaction result of 0.64%, which is also at the threshold of liquefaction. Therefore, the two methodologies to determine volumetric strain produce compatible results for FS ≈ 1.

#### *6.2.3.3 Threshold Strain*

Representative samples of the Tobacco Road and Santee/Tinker Formations were trimmed for low-amplitude stress-controlled cyclic triaxial laboratory tests. A total of 11 specimens, 3 from the Tobacco Road, and 8 from the Santee/Tinker Formation, were tested under isotropic consolidation pressures ranging between 2 tsf and 7.5 tsf. The objectives of this testing program were to obtain the threshold strain for these materials, and also to evaluate the rate of pore water pressure increase resulting from the repeated application of strains. Threshold strain is the lowest amplitude cyclic shear strain that is necessary for a soil to trigger the pore water pressure generation under cyclic loading.

The laboratory test results are shown in Figures 6.2-28 and 6.2-29. These results show that at cyclic shear strains between $10^{-2}$ and $10^{-1}$ percent, $r_u$ values range from near 0 to about 0.2 for the Santee/Tinker Formation and from near 0 to about 0.3 for the Tobacco Road Formation.

## 6.3 Engineering Properties of Fill Used for Slope Stability Analyses

### *6.3.1 In-Tank Precipitation Facility*

The stratigraphy used in the stability analyses for ITP is based on the exploratory boreholes, CPTs, and review of the construction data. The field exploration relevant to the stability analyses included 7 CPTs and two SPT boreholes.

The slope is composed of approximately 40 feet of fill. A review of construction data indicated a thin zone (approximately 2 feet thick) of softer material located at the base of the fill, as noted previously by Mueser (1984a). This was confirmed by 6 of the 7 CPT soundings located along the edge of the slope. This material is identified as Fill 2 in the cross-section (Figure 6.3-1). The overlying material, while not homogeneous, was considered to act as a single unit (Fill 1). Underlying the embankment fill is the Tobacco Road Formation. There was no indication of a perched water table within the fill.

The average CPT tip resistance and its variation with depth within the fill is shown in Figure 6.3-2 for ITP. Figure 5.1-5 shows the variation with depth of liquid and plastic limits, water content, percent fines, and undrained shear strength for the fill at ITP. Total shear strength parameters were derived from Consolidated Undrained (CU) and Unconsolidated Undrained (UU) Triaxial Test results. Effective strength parameters were derived from Consolidated Drained (CD) and CU test results for the majority of the fill material. The effective shear strength parameters for

the Fill 2 material were determined by relating the ratio of total shear strength parameters for Fill 1 and Fill 2 to the tangent of the effective friction angles of Fill 1 and Fill 2. The total and effective stress shear strength parameters used in the analyses for the various materials are given in Table 6.3-1.

### *6.3.2 H-Area Tank Farm*

The CPT results for evaluation of the remaining HTF were grouped by area for comparison purposes. The areas are designated as North, East and West hills, as shown in Figure 6.3-3. The summary of CPT tip resistances for the North, East and West hills are provided in Figures 6.3-4, 6.3-5, and 6.3-6, respectively. Figure 6.3-7 shows the variation with depth of liquid and plastic limits, water content, percent fines, and undrained shear strength for the remaining fill at HTF.

The North hill was identified as the most critical (weakest) portion of HTF by comparing the geometric means (GM), of each grouping. The GM is defined as:

$$GM = \exp\frac{\sum \ln(q_{c_i})}{n}$$

where $qc_i$ is the CPT tip resistance at point i, and n is the total number of points at which $q_c$ is recorded. As for ITP a weaker fill zone was encountered near the base of the fill approximately 3 feet thick and the stability analysis therefore included two distinct layers for the stability analysis.

The effective and total shear strength parameters used for the slope stability evaluation of the HTF were established using the CPT results correlated to laboratory strength results. The effective and total shear strength parameters were then estimated for each area using the steps outlined below.

#### *6.3.2.1 Effective Stress Properties*

The effective strength was determined using the relationship between the average CPT tip resistance and average effective overburden pressure versus effective friction angle, as proposed by Robertson and Campanella (1983), and as shown in Figure 6.3-8.

For the upper fill the average effective overburden stress, $\sigma_o$' is assumed to be equal to the product of the average fill depth of 20 feet and the average unit weight of the fill (128 pcf), resulting in a value of 1.28 tsf. For the lower weaker zone, the average effective overburden stress is assumed to be equal to the product of the average fill depth of 36 feet and the average unit weight of the fill (128 pcf), resulting in a value of 2.32 tsf. Note the groundwater table is well below the base of the fill.

The resulting effective strength parameters used for evaluation of the HTF slopes are summarized in Table 6.3-2.

### *6.3.2.2 Total Stress Properties*

The total stress soil properties used in slope stability evaluation for the remaining HTF slopes were determined using the following methodology:

1. Establish that the fill at ITP and HTF are similar by comparing the CPT results of HTF with those at ITP.

2. Determine the relationship between the average CPT tip resistance, $q_c$, and the shear strength, Su, at ITP utilizing the laboratory test results at ITP and the following relationship:

$$N_k = \frac{q_c - \sigma_{vo}}{S_u} \qquad \text{[Kulhawy and Mayne, 1990]}$$

   where $\sigma_{vo}$ is the total overburden stress, and $S_u$ is the undrained shear strength. The variation of shear strength with depth at ITP is given in Figure 6.3-9. The calculated variation of $N_k$ versus depth at ITP is given in Figure 6.3-10.

3. Assuming that this variation of $N_k$ with depth at ITP applies for all fill in HTF, calculate the shear strength versus depth variation by applying the equation in item 2 above to the CPT tip values recorded for HTF. The calculated variation of $S_u$ with depth is given in Figures 6.3-11, 6.3-12, and 6.3-13 for the North, East and West hills, respectively.

4. Use this shear strength versus depth relationship for the slope stability analyses.

The above methodology was applied for the HTF fill in general; however, the CPT tip resistances in the fill immediately north of ITP indicated a softer zone at the base of the fill. The total stress shear strength for this weaker zone was estimated by equating the ratio of the tangent of the friction angles of the general fill and the weaker fill to the ratio of the undrained shear strength of the two fills, and solving for the undrained shear strength of the weaker fill material. The equation is presented below:

$$\frac{\tan(\phi)_{\text{general fill}}}{\tan(\phi)_{\text{weaker fill}}} = \frac{Su_{\text{general fill}}}{Su_{\text{weaker fill}}}$$

where the friction angles $\phi_{\text{general fill}}$ and $\phi_{\text{weaker fill}}$ are derived using the method presented in Section 6.3.2.1, and the $Su_{\text{general}}$ is the average $S_u$ determined for the soils north of ITP. The resulting total strength parameters used for evaluation of the HTF slopes are summarized in Table 6.3-2.

# 7. DESIGN CRITERIA AND EVALUATIONS FOR THE ITP

The analyses described in the following sections were performed in accordance with applicable DOE standards and guides. Where no standard or guide existed, criteria were developed according to standard engineering practice. The criteria were reviewed and approved by DOE.

## 7.1 Controlling Earthquake Motions

The controlling earthquakes used for the geotechnical evaluations were defined as noted below (WSRC, 1994c). The EBEs consist of the two following surface spectral shapes:

- A median local spectral shape, magnitude ($M_w$) = 5, scaled to 0.19 g;
- A distant Charleston event, magnitude ($M_w$)=7.5, scaled to a peak ground acceleration of 0.11 g;

Following analysis of the distant Charleston event (Lee, 1994), a more conservative spectrum was recommended:

- 84th percentile rock spectral shape, Magnitude ($M_w$) = 7.5, scaled to 0.13 g.

## 7.2 Slope Stability

The criteria for evaluating slope stability are:

| Condition | Required Factor of Safety | Methodology |
|---|---|---|
| Static | 1.5 | Circular and wedge surfaces utilizing modified Bishop and Janbu methods, using laboratory-derived strengths. |
| Dynamic | Evaluation to be based on slope deformation | Pseudo-static utilizing procedure by Makdisi and Seed (1978), with horizontal acceleration of 0.2 g and vertical acceleration of 0.08 g, using laboratory-derived strength. |

### *7.2.1 Methodology*

The stability of the slopes surrounding Tanks 48 through 51 was evaluated using limit equilibrium techniques for static and pseudo-static conditions. SRS computer program Geoslope (SRS, 1988) was used in the analysis. Geoslope generates random failure surfaces based on either given entry or exit failure zone locations. Random, circular and wedge-shaped failure surfaces were considered. Circular surfaces were analyzed using the Modified Bishop's method. Random and wedge-shaped surfaces were analyzed using Janbu's method.

Each slope was initially evaluated for static steady state conditions using effective shear strength parameters. For pseudo-static analyses, total strength parameters were used. In addition to a 0.2g

horizontal pseudo-static load, a vertical component equal to 40 % of the horizontal component was simultaneously applied (in both upward and downward vertical directions) to the critical failure surface for the analyses.

### *7.2.2 Geometry and Stratigraphy Used for Slope Stability Analyses*

The slopes were modeled using three typical cases that represent the various slopes and loading configurations present: the first cross-section is typical of the west slope at the Filter Stripper Building; the second is typical of areas between the tanks; and the third is typical of the east and south slopes at tank locations. All slopes are gabion-faced; however, the gabions were conservatively not modeled in the analyses. The slope geometry was based on a series of five field surveys. For this report only Cross-Section 1 is reported (Figure 6.3-1), since this section results in the lowest safety factors computed.

Cross-Section 1 is typical of the west slope at the Filter Stripper Building. The Filter Stripper Building is located on top of the west slope, approximately 37 feet from the crest (Figure 6.3-1). The largest loads from the building are created by two large tanks located near the center of the building. The tanks are approximately 42 feet by 30 feet oriented with the long axis parallel to the slope. The maximum load induced by these tanks is approximately 2700 psf. The maximum load for Tanks 48 through 51 was estimated to be 4,000 psf. These tanks are founded at the base of the fill, at about elevation 286 feet (Figure 6.3-1). As a result they have no impact on the slope stability of the fill.

Groundwater monitoring wells were installed at the south end of the HTF in early 1986. The water table has been generally constant at elevation 275 feet for approximately the last five years. No perched water tables were found within the fill. Nearly the entire top of the fill is covered with asphalt surface paving. Drainage is provided and storm sewers are present within the fill. These factors combine to minimize the opportunity for water to enter and be retained within the embankment.

Best estimate soil properties were used for the evaluation of each cross-section. Soil properties were derived from review of field CPT and SPT results, and laboratory test data, and are explained in further detail in Section 6.3. In general, the data used to evaluate the individual slope cross-sections were extracted from the boreholes and CPT soundings nearest the slope. The stratigraphy used for the ITP evaluation is depicted in Figure 6.3-1.

### *7.2.3 Analyses*

#### *7.2.3.1 Static Factors of Safety*

The minimum calculated values of FS are given in Table 7.2-1, and shown, along with the failure surfaces, on Figure 7.2-1, for Cross-Section 1. Using effective shear strength values resulted in the

lowest factor of safety of 1.9 for a shallow toe circle as shown on Figure 7.2-1. Factors of safety utilizing total stress strengths resulted in safety factors in excess of 2.0. In all cases the computed factor of safety is above the minimum required of 1.5. It should be noted that no sloughing failures of any kind have been recorded for the embankment fill for the entire H-Area Tank Farm, which includes the ITP area.

### *7.2.3.2 Pseudo-Static Factors of Safety*

For pseudo-static analysis, a horizontal acceleration of 0.2 g was used. (The maximum peak ground acceleration (pga) for the EBEs is 0.19 g.) A vertical acceleration of 0.08 g, which is equivalent to 40 % of the horizontal acceleration, was also incorporated in the analysis in both the upward (+) and downward (-) vertical directions. In addition, the fill shear strength was reduced by 10 percent to account for seismic straining. The resulting factor of safety for Cross-Section 1 is 1.7 (Figure 7.2-1 and Table 7.2-1) for the critical failure surface, which is wedge shaped.

Yield accelerations were also calculated for each cross-section. The yield acceleration ($k_y$) is defined as the pseudo-static acceleration required to produce a factor of safety equal to 1.0. The calculated yield accelerations for each cross-section were 0.6 g, and greater, as given in Table 7.2-1.

### *7.2.3.3 Seismically-Induced Slope Deformations*

Earthquake-induced slope deformations were estimated following the method proposed by Makdisi and Seed (1978). Average accelerations within the embankment were obtained from the two-dimensional response analysis program SASSI (Ostadan, 1988). The acceleration ($k_{max}$) determined for the slope from this analysis (see Section 7.5.3.3.2 and Figure 7.5-31) was approximately 0.2 g. The minimum yield acceleration ($k_y$) for the slope was calculated to be 0.6 g, as discussed previously. The ratio of the yield acceleration to the maximum crest acceleration ($k_y/k_{max}$) is therefore 3.0. The resulting seismically-induced deformation (see Figure 7.2-2) is negligible. Note that determination of the yield acceleration is performed only as an aid to estimate deformation and does not imply that the embankments are capable of sustaining the yield acceleration.

### *7.2.3.4 Reduced Strength Evaluation*

Pseudo-static stability analyses were also carried out assuming arbitrarily reduced shear strength for the fill material. The strength of layer Fill 1 was reduced from 3,785 psf to 1,800 psf and the strength of layer Fill 2 was reduced from 1,703 psf to 1,000 psf. The resulting pseudo-static FS was calculated to be 1.03 occurring along the wedge-shaped failure surface shown on Figure 7.2-3. Since the factor of safety is nearly 1.0, the ratio of the yield acceleration to the maximum crest acceleration ($k_y/k_{max}$) is also about 1.0, resulting in negligible slope deformations (see Figure 7.2-2).

Stability analyses were also performed assuming that the earthquake loading reduces the undrained strength of the TR1 layer, below the water table, to a strength equal to 100 psf. The analysis considered a wedge-type failure passing through the TR1 material in Cross-Section 1, which had the lowest FS under other loading conditions. The minimum calculated FS for the assumed strength was 1.4, as shown in Figure 7.2-3. Note that the residual shear strength corresponding to an $(N_1)_{60}$ value of 14 (the approximate mean $(N_1)_{60}$ for TR1) range from about 400 to 800 psf (Seed and Harder, 1990).

### *7.2.4 Conclusions*

The slopes analyzed have safety factors greater than 1.5 under static and pseudo-static conditions. Under the earthquake loadings analyzed, seismically-induced deformations are estimated to be negligible. Reduced strength analyses show that for the conditions analyzed, calculated safety factors are a minimum of 1.0 with most being higher, and the predicted deformations are negligible.

## 7.3 Liquefaction and Dynamic Settlement

### *7.3.1 Methodology*

The liquefaction susceptibility of the subsurface materials at the ITP site was evaluated using both qualitative and quantitative approaches. These included the shear wave velocity approach, the criteria for clayey soils, the strength and the strain approaches, and finally comparisons of the performance of old age sand deposits in past earthquakes.

Free-field settlement is a result of dissipation of excess pore water pressures due to seismic loading. For the analysis at ITP, the amount of compression expected as a result of this pore water pressure dissipation was estimated based on the laboratory volumetric and threshold strain test results. To accomplish these studies, the extensive field and laboratory program described in previous sections were conducted.

#### *7.3.1.1 Clayey Soils*

Methodology to assess liquefaction potential for clayey soils has been formulated by Wang (1979), (relating liquid limit, water content, and clay content to liquefaction potential and modified for laboratory testing conditions in the United States by Koester and Franklin (1985)), have been applied in this evaluation.

Both laboratory tests and field performance data have shown that the great majority of clayey soils will not liquefy during earthquakes. Criteria to express these observations have been formulated by Wang (1979) and extended to the laboratory conditions in the United States by Koester and Franklin (1985). As defined by Wang (1979), clay sizes are soil particles less than 0.005 mm.

The criteria state that clayey soils which satisfy all of the three following conditions should be judged to be vulnerable to liquefaction or serious loss of strength:

- Laboratory-determined water content (increased by 2 percent) greater than 90 percent of the laboratory-determined liquid limit (increased by 1 percent)
- Liquid limit (increased by 1 percent) is less than 35 percent
- Clay content (<0.005 mm)(decreased by 5 percent) is less than 15 percent

In his recent Rankine Lecture, Ishihara (1993) pointed out that the nature of the fines is just as, if not more, important than amount of fines in its effect on liquefaction potential. Figure 7.3-1 shows the relationship between the plasticity index of the material passing a U.S. No. 200 sieve size (fines) and the cyclic stress ratio causing 5 percent double amplitude strain in 20 cycles. As the figure indicates, the higher plasticity soils are less susceptible to cyclic strain during earthquake shaking.

The geologic and mineralogical investigations performed during this investigation showed that the soils from the Tobacco Road Formation characteristically consist of clayey sands, with almost no silt-size particles, and that the clay material is predominantly a mixture of kaolinite and illite. It was considered appropriate, therefore, that the liquefaction potential of these materials be also assessed based on the empirical criteria for clayey soils, as formulated by Wang and expanded by Koester and Franklin.

### *7.3.1.2 Shear Wave Velocity*

For this evaluation, shear wave velocity methodologies from three investigations have been used. They are:

- Seed, Idriss and Arango (1983)
- Kayen, et al. (1992)
- Stokoe, et al. (1988)

Attempts to relate shear wave velocity to liquefaction susceptibility using empirical data have been pursued by several investigators. For example, Seed, Idriss, and Arango (1983) concluded that: "Liquefaction will never occur in any earthquake if the shear wave velocity in the upper 50 feet of soil exceeds about 1200 fps" (Figure 7.3-2). This conclusion was based on the consideration of the cyclic shear stresses (and corresponding shear moduli) required to induce liquefaction in the field. Similarly, Kayen et al. (1992) and Stokoe et al. (1988) compiled field data obtained in recent earthquakes which show relationships between cyclic stress ratio and normalized shear wave velocity, and between shear wave velocity and maximum ground surface acceleration, respectively. These relationships separate sands into groups which are susceptible or non-susceptible to liquefaction (Figures 7.3-3 and 7.3-4).

### *7.3.1.3 Stress Method*

The stress method is based on a comparison of the ratio of dynamic soil strength as derived from cyclic triaxial laboratory test results to the induced stress of the earthquake as derived from ground response analyses. That ratio is referred to as the FS against liquefaction. For FS ≤ 1.15, the resulting dynamic settlement is computed based on volumetric strain determination from laboratory undrained cyclic triaxial tests, assuming 100 percent pore pressure generation. For FS > 1.15, the resulting dynamic settlement is based on re-compression determined from laboratory consolidation tests and a unique relationship between FS and partial pore pressure buildup (See Figure 6.2-26).

The common method to evaluate the seismic liquefaction potential of a soil deposit is the strength approach. Essentially, the approach consists of calculating cyclic stresses at various depths caused by the earthquake motions and comparing these stresses with the cyclic strengths of the soil. The factor of safety against initial liquefaction is then defined as the ratio between the available strength and the induced stress.

The simplified liquefaction potential evaluation procedure presented by Seed and Idriss (1971) and by Seed, Idriss, and Arango (1983) provides two choices for the determination of the cyclic strength of a soil. Strength is either obtained based on empirical data relating an in situ soil property, such as the normalized blow count $N_1$ from the SPT, the normalized CPT tip resistance, $(q_c)_1$, or the normalized shear wave velocity $(V_s)_1$, to the cyclic stress known to have induced liquefaction in previous earthquakes, or it is determined based on the results of stress-controlled undrained cyclic triaxial tests in the laboratory. The induced stress may be calculated based on ground response considerations, or with the aid of the simplified formula proposed by Seed and Idriss in 1971.

For the current evaluation and studies, the decision was made to obtain the cyclic strength of the soils at the ITP site from the results of the laboratory cyclic triaxial tests, rather than from an empirical chart. It was also decided to obtain the cyclic stresses induced by the EBE from ground response analyses rather than from simplified formulas. Reasons for these decisions follow.

Considerable effort has been spent in the past (BSRI, 1993b; Arango, Lewis, and Kimball 1995, in press) to investigate the geologic origin, and the geotechnical characteristics of the sands which constitute the database for the preparation of the empirical chart for liquefaction potential evaluations proposed by Seed et al., (1984). These efforts showed that the soil deposits represented in the chart are young, Quaternary age, in most cases belonging to the Holocene period, and that in all cases for which the sand gradation was reported, the soils in question consist of clean sands or silty sands (no clayey sands have been reported to have liquefied). The review demonstrated that the genesis and the characteristics of the soils on which the empirical liquefaction chart is based are entirely different from the origin and composition of the soils at the ITP site. Furthermore, because the features that are different (amount and nature of fines, age, and structure) are known to have an important influence on the cyclic strength of a soil, it was concluded that the empirical liquefaction chart could not truly represent the strength of the

Tobacco Road Formation soils. Therefore, for the purposes of this study, the cyclic strengths are derived from the results of the cyclic laboratory triaxial tests (Section 6.2).

Simplified procedures to calculate the values of the cyclic stresses induced by a given ground motion rely only on the value of the prescribed maximum ground surface acceleration, irrespective of the duration of the motion and of its frequency content. For this evaluation, two earthquakes with distant and well defined durations and spectra were prescribed. For this reason, it was considered necessary to calculate the stresses induced in the ground by these motions by ground response analyses, rather than by the simplified formula.

#### *7.3.1.4 Strain Method*

A comparison of strain developed in the soil due to the earthquake motions with the strain levels developed in the laboratory (Figures 6.2-28 and 6.2-29), relating the number of strain cycles and the corresponding increase in pore pressure ratio, will be made.

The fundamental importance of cyclic shear straining on the pore water pressure development of undrained sands and its importance in the evaluation of the potential for seismic liquefaction have been well recognized (Martin, Finn, and Seed, 1975; Dobry et al., 1982). For the current evaluations, the cyclic shear strains induced by the earthquake motions at various depths within the Tobacco Road Dry Branch and Santee/Tinker Formations were compared with the threshold cyclic strain required to induce pore pressure buildup.

#### *7.3.1.5 Performance of Old Sand Deposits*

In its present form, the so-called empirical chart for liquefaction potential evaluation developed by Seed et al., (1984) has gained acceptance by the profession worldwide. Successful application of the chart to case histories of liquefaction and non-liquefaction not included in the development of the chart are abundant in the literature. However, based on the comprehensive review of the data included in the chart, in all cases the liquefied sands are recent alluvial, beach, or deltaic deposits, and the materials themselves are granular clean sands, with silty fines in some cases. In fact, little documentation of liquefaction in deposits older than about 10,000 years appears to exist. In spite of that, engineers have been applying Seed et al.'s (1984) empirical relationships to assess liquefaction potential for both young and old deposits alike, even though recognition that an old sand deposit will exhibit more resistance to liquefaction than a younger deposit goes as far back as Youd and Hoose (1977), and Seed (1979a). It is also useful to recall that the liquefaction resistance is a small strain property, whereas, the SPT N-value results from a large strain measurement.

Many factors are believed to be the result of aging of a soil deposit, such as cementation, weathering (which chemically breaks down minerals into clays), increased exposure to low-level seismic shaking, cold bonding, and consolidation. All of these factors tend to increase the liquefaction resistance of sands. In addition to increasing liquefaction resistance, most of these

factors probably increase, to some degree, the CPT and SPT resistances. To study the aging effect on liquefaction resistance, attention was directed to reviewing data from the Charleston, South Carolina earthquake of 1886 (Arango, Lewis and Kimball, 1994, in press). The results of this analysis, along with studies that have been done on site (BSRI, 1993b), suggest that older soil deposits (older than Holocene age, i.e., 10,000 years) have a greater resistance to seismic liquefaction than young (less than 10,000 years old) soil deposits. This has also been documented by Youd and Perkins (1978) and more recently in a study by Martin and Clough (1994) which investigated liquefaction and non-liquefaction as a result of the 1886 Charleston earthquake. The pattern of increased strength with time, in particular, for the clean sands representing the Charleston case histories, is clear, indicating that geologically older sand deposits do indeed have a greater resistance to liquefaction than young sands. The conclusion is drawn, therefore that the FS against initial liquefaction based on charts reflecting experience with Holocene deposits do not adequately reflect the expected behavior of the soils at HTF and ITP.

To study the aging effect on liquefaction resistance, attention was directed to reviewing data from the Charleston, South Carolina earthquake of 1886 (Arango, Lewis, and Kimball, 1995 in press). This event took place in a setting with a multitude of liquefiable deposits of various ages, ranging from Holocene to greater than one million years. The results of their analysis, along with studies that have been done on site (BSRI, 1993b), suggest that older soil deposits (older than Holocene age, i.e., 10,000 years) have a greater resistance to seismic liquefaction than young (less than 10,000 years old) soil deposits. This has also been recently documented in a study by Martin and Clough (1994) who investigated liquefaction and non-liquefaction as a result of the 1886 Charleston earthquake.

Eight documented cases of liquefaction at locations underlain by recent fluvial deposits were considered in this study. Conditions prevailing at those locations at the time of the earthquake are more difficult to predict than at the locations of older deposits. This is because even today, surface topography at the former sites is actively changing. In spite of this greater uncertainty, the combination of average penetration resistance and cyclic stress ratios induced by the earthquake that did not result in liquefaction (five sites) or caused marginal liquefaction (three sites) at the eight locations with young fluvial deposits are shown in Figure 7.3-5. For the sites of marginal liquefaction, the average penetration resistance $(N_1)_{60}$ value was 18, and the average induced cyclic stress ratio was 0.54. For the sites of no liquefaction, the average penetration resistance was again 18 and the average induced cyclic stress ratio was 0.43.

The strength of the young deposits is also shown to be greater than that derived from the curve for clean sands by Seed et al. It can also be observed that the boundary line representing the maximum values of cyclic stress ratio that was tolerated by the older sands (line 1 in Figure 7.3.5) is higher than that corresponding to the younger deposits (line 2 in Figure 7.3.5).

Figure 7.3-6 presents the combination of average penetration resistance and cyclic stress ratio induced by the 1886 Charleston earthquake that resulted in liquefaction or marginal liquefaction at 28 sites around the Charleston area. The plot is based on the assumption of a peak meizoseismal

acceleration of 0.5 g for the 1886 Charleston earthquake. A low boundary curve for the minimum cyclic stress ratio (cyclic strength) required to cause liquefaction shows that the cyclic stress to cause liquefaction is greater than for young, clean sands.

Similarly, Figure 7.3-5 presents the combination of average penetration resistance and cyclic stress ratio induced by the 1886 Charleston earthquake that did not result in liquefaction or cause marginal liquefaction at 35 sites around the Charleston area. An upper boundary curve shows the maximum values of the stress ratio (cyclic strength) that were tolerated by the soil without widespread liquefaction.

The conclusions reached by reviewing these two figures are that the sands in the Charleston area, which are about 100,000 to 200,000 years old, have significantly higher (about twice as much) cyclic strengths (i.e., greater resistance to liquefaction) than the younger Holocene sands which are depicted by the clean sand curve shown on each figure.

Data documenting the rate of cyclic strength gain with length of time under sustained loading was presented by Seed (1979a) as reproduced in Figure 7.3-7. This figure shows that for lengths of time in excess of about 200 years, the average strength gain flattens to about 1.8 times the strength at deposition. It follows then that Holocene deposits (less than about 10,000 years old) would have a strength which would be about 80 percent higher than their strength at the time of deposition. It also follows that a deposit of T years old would have a cyclic strength given by the expression:

$$\text{Strength, after T years} = \text{Strength, after 10,000 years} \times \frac{\text{Gain from Figure 7.3-7}}{1.8}$$

Based on this, the data points shown in Figure 7.3-7 were replotted as shown in Figure 7.3-8. Superimposed on this figure are the strength gains corresponding to the sands from the Charleston area (about 100,000 to 200,000 years old), and the Tobacco Road sands (about 37 million years old) at SRS.

The pattern of increased strength with time (i.e., aging) is apparent in Figure 7.3-8, in particular for the clean sands representing the Charleston case histories, indicating that geologically older sand deposits do indeed have a greater resistance to liquefaction than implied by the empirical chart of Seed et al., (1984). More importantly, the laboratory-obtained cyclic strength of the old Miocene sand, reflecting the combined effects of fines and aging, falls within this pattern. Thus, laboratory testing is shown to provide reasonable strength results not only for young sands, but also for sands belonging to older deposits.

### *7.3.2 Evaluations and Results*

#### *7.3.2.1 Clayey Soils*

Liquid and plastic limits, plasticity index, natural water content and percent clay for 125 samples from the HTF were selected to check their liquefaction potential according to the criteria for clayey soils. Test data are summarized and plotted in Figures 7.3-9a through 7.3-9g. By inspection, the

application of the criteria to the individual sample for which complete data are available show that the vulnerability of the clayey sands to seismic liquefaction is negligible in the HTF.

The average plasticity index of the -200 material for the TR3/TR4 formation is 101 percent (see Table 6.0-1(a)), which, by extrapolation of Figure 7.3-1, would indicate over a two fold increase in liquefaction resistance over non plastic soils. Similarly, the other soil formations in the HTF have plasticity indices of the fines generally exceeding 50 percent, indicating that all the soils at HTF are naturally resistant to liquefaction.

### *7.3.2.2 Shear Wave Velocity Approach*

The geophysical surveys carried out at ITP site yield the average and normalized shear wave velocity values for the various soil layers given in Table 7.3-1. Based on this data and with reference to Figures 7.3-2 through 7.3-5, the following is concluded:

1. Seed et al.'s chart (Figure 7.3-2) indicates that materials between depths of 50 - 100 feet with an average shear wave velocity equal to about 1100 fps would have a cyclic stress ratio resistance against liquefaction of 0.33. Maximum expected cyclic stress ratios at the site in the event of the EBE are less than 0.15 and less than 0.10 for the 84th percentile motion which is well below 0.33. Thus, the liquefaction potential at this site is nonexistent.

2. The normalized shear wave velocities presented in Table 7.3-1 used in combination with Kayen et al.'s chart (Figure 7.3-3) show that Tobacco Road soils (TR1 through TR4) with normalized velocities between 250 m/sec (820 fps) and 270 m/sec (885 fps) would require a cyclic stress ratio in excess of 0.40 to liquefy. Similarly, the Dry Branch soils (DB1 through DB5) with lower normalized shear wave velocities of about 200 m/sec (656 fps) would require cyclic stress ratios which are much greater than the cyclic ratio expected to be generated by the earthquake motions for liquefaction to occur. Therefore, no liquefaction is predicted by this method.

3. Stokoe et al.'s chart (Figure 7.3-4) would show that for shear wave velocities greater than 500 fps, the required ground acceleration that causes liquefaction is 0.25 g. At ITP, shear wave velocities are twice this value, and the maximum expected peak ground acceleration (0.19 g) is lower than the quoted value. Therefore, this criterion precludes liquefaction at the site.

In conclusion, the observations made by Seed, Idriss, and Arango (1983), Kayen et al., (1992), and Stokoe et al., (1988) indicate liquefaction at ITP site will not occur for the earthquake motions analyzed.

### *7.3.2.3 The Stress Method*

#### 7.3.2.3.1 Ground Response Analyses

The magnitude of both the cyclic shear stress ratios and the cyclic shear strains imposed by the EBE and the 84th percentile motion at various locations within the soil profile were calculated by performing ground response analyses by means of the one-dimensional response analysis computer code SHAKE (Schnabel, Lysmer, and Seed, 1972; Idriss and Sun, 1992). Consistent with the development of these spectra (see Section 2), the EBE motions were prescribed at the ground surface at the top of the Tobacco Road. The 84th percentile motion was prescribed as a basement motion at an approximate depth of 1000± feet. Appropriate acceleration time histories (Figures 7.3-10 through 7.3-12) compatible with the spectra of the EBE (Figures 7.3-13 and 7.3-14) and the 84th percentile motion (Figure 7.3-15) were generated, as input to the SHAKE analyses.

Based on the generalized profiles described in Section 5, a total of seven soil columns were analyzed, as depicted in Figures 7.3-16 (Columns A2, A4, A5, and A6) and 7.3-17 (Columns B1, B3, and B4). While the soil column for both Profiles AA' and BB' were considered with the EBE, only the soil columns in Profile AA' were analyzed for the 84th percentile motion. Details on the geometry, unit weights, and shear wave velocities adopted for the profiles are provided in Tables 7.3-2 and 7.3-3. For the soil layers down to the Congaree formation, site-specific strain-dependent shear modulus and damping properties shown in Figures 6.1-1 and 6.1-2 were used. For the deeper soil layers, in conjunction with the 84th percentile input motion, degradation properties developed by GEI (1991b) and shown in Figures 6.1-4 and 6.1-5 were used.

#### 7.3.2.3.2 Evaluation of Factors of Safety Against Initial Liquefaction

The cyclic shear stresses calculated from the response analyses were compared with the cyclic strengths as measured in the laboratory and the factors of safety against the initial liquefaction were calculated for each soil column at a 2-foot depth interval. The values of the factors of safety are as follows:

- Local Event >1.4
- Distant Event >1.4
- 84th Percentile Event >1.4, with localized lenses in the range 1.2 to 1.4

These results indicate that liquefaction will not occur at ITP for the earthquake motions analyzed, since the computed safety factors are not only greater than 1.0, but also greater than the design criteria of 1.15.

#### *7.3.2.4 Strain Approach*

Effective shear strains in the soil columns corresponding to the Santee/Tinker Formation were obtained from the results of soil column ground response analyses. The resulting maximum effective shear strain for the local EBE, the distant EBE, and the distant 84th is 0.01, 0.02, and 0.03 percent, respectively. These strain levels were compared with laboratory data relating the number of strain cycles and the corresponding increase in pore water pressure ratios, Figure

6.2-29. For all seven soil columns analyzed, a maximum excess pore water pressure ratio of less than 0.12 is estimated.

Laboratory shake table tests carried out by several investigators show that the threshold pore water pressure ratio necessary to cause damage effects to foundations (loss of bearing capacity and subsequent settlement) is much higher than this value. For example, in the Shake table tests carried out by De Alba (1975), it was observed that no perceptible movement of the footings of his models occurred until the excess pore water pressure ratio reached about 0.9. Yoshimi and Tokimatsu (1977) also experimenting with models in a shake table found that complete liquefaction was imminent once a pore pressure ratio of 0.6 was achieved. The authors wrote that "it is interesting to note that the excess pore water pressure ratio of about 0.6 seems to correspond to a critical condition where liquefaction failure is imminent, i.e., both the shear strain and the pore water pressure begin to increase abruptly during undrained shear tests."

Lee and Albeisa (1974) determined the volumetric strains due to reconsolidation of samples which had been subjected to excess hydrostatic pore pressure increases caused by cyclic loading or static loading. These studies showed that the important factors controlling the compressibility on reconsolidation were the grain size of the soil, the density of the soil, and the peak pore pressure ratio reached during the test. Further discussion on this issue was presented by Seed, Martin, and Lysmer (1975) as summarized below.

"For low values of pore pressure ratio, however, the data indicates that neither grain size nor relative density have a large influence on the coefficient of compressibility defined by the expression:

$$m_v = \frac{d\varepsilon_v}{d\sigma'}$$

where $d\varepsilon_v$ is the change in volumetric strain corresponding to a small change in effective pressure $d\sigma'$. For such low pore pressure ratios, values of $m_v$ typically range between about $1 \times 10^{-6}$ and $2 \times 10^{-6}$ $ft^2/lb$ for average densities and grain sizes of sandy soils.

However, for pore pressure ratios larger than 0.6, the values of $m_v$ were found to be influenced to a great extent by the relative density. Figure 7.3-18,(a) shows measured variations of the normalized coefficient of volume compressibility, i.e., the ratio of $m_v$ to $m_{vo}$, where $m_{vo}$ is the coefficient of volume compressibility at low pore pressure, for different relative densities. It may be seen that at low pore pressure ratios, the effect is small.

For pore pressure ratios of 0.9, however, it was found that $m_v$ increased by a factor of 5 to 10 for loose sands and by a factor of 3 for dense sands. In order to use this information in a pore pressure dissipation analysis, an analytical expression for the increase in compressibility with pore pressure ratio and relative density was derived as follows:

$$\frac{m_v}{m_{vo}} = \frac{e^{AxB}}{1 + Ax^B + \frac{1}{2}A^2x^{2B}}$$

where $x = \frac{\Delta u}{\sigma_{3c}}$, is the pore pressure ratio, $A = 5 \cdot (1.5 - D_r)$, and $B = 3 \cdot (2)^{-2Dr}$.

This expression is shown in graphical form in Figure 7.3-18,(b) for different values of the relative density $D_r$. The pattern of curves expressed by the equation is very similar to that shown in Figure 7.3-18,(a) for the original test data."

Both of these figures show that for pore water pressure ratios below 0.4, the compressibility of the sand is essentially equal to that at very low pore water pressure ratios. It is only for pore water pressure ratios greater than 0.4 when the compressibility noticeably increases. On this basis, it is concluded that liquefaction will not take place in the Santee/Tinker Formation during the EBEs and the 84th percentile motions.

### *7.3.3 Liquefaction Evaluation: Conclusion*

Several independent approaches to define the seismic liquefaction susceptibility of the Tobacco Road and Dry Branch Formation soils have been presented above. In all cases, the results show that for the prescribed EBEs and the 84th percentile motion, the factor of safety against initial liquefaction is high, and therefore, liquefaction will not occur.

## 7.4 Bearing Capacity

### *7.4.1 Criteria*

For bearing capacity analysis, the criteria are:

| Condition | Required FS | Methodology |
|---|---|---|
| Static | 3 | Conventional Terzaghi bearing capacity analysis (Terzaghi and Peck, 1967) |
| Dynamic | 2 | Conventional Terzaghi bearing capacity analysis (Terzaghi and Peck, 1967) |

### *7.4.2 Evaluation and Results*

The bearing capacity of the ITP tanks and Filter Stripper Building was evaluated utilizing standard practice, as outlined in Terzaghi and Peck (1967). Strength parameters utilized were based on laboratory and field test results and are given in Table 6.0-1. The results show that static safety factors are much higher than the criterion of 3.0 for the ITP tanks and the Filter Stripper Building.

The dynamic incremental increase in bearing pressure resulting from the design ground motions was less than 0.5 ksf. Resulting dynamic factors of safety for the ITP tanks were therefore all in excess of the criterion of 2.0.

## 7.5 Expected Tank Settlement

Future settlement at ITP Tanks may occur in the following ways: (1) dynamic settlement due to dissipation of seismically-induced pore pressures, and (2) static settlement due to tank loading during operation and secondary consolidation. Each will be discussed in the following sections.

### *7.5.1 Dynamic Settlement Due to Dissipation of Seismically-Induced Pore Water Pressure*

As the results discussed in Section 7.3.2 show, seismic liquefaction will not occur at ITP. However, partial pore pressure buildup and subsequent dissipation and settlement will take place as a result of the earthquake motions. These settlements were estimated based on the laboratory volumetric and threshold strain test results.

For the Tobacco Road and Dry Branch Formations, 28 stress-controlled cyclic triaxial tests were performed, including 4 low-amplitude, stress-controlled, triaxial tests. The field and laboratory data provided the means to derive the relationship between cyclic shear strength and cone tip resistance shown in Figure 6.2-12. These results, along with the volumetric strain test results, were used to develop a relationship between the factor of safety and volumetric strain. For factors of safety greater than 1.15, the volumetric strains due to dissipation of pore water pressure increases were calculated based on recompression properties of the materials as determined by the laboratory consolidation tests. The relationship shown in Figure 6.2-27 was used to compute post-earthquake settlement for the Tobacco Road and Dry Branch Formations.

For the Santee/Tinker Formation, seven low-amplitude stress-controlled cyclic triaxial tests were carried out. The results presented in Figure 6.2-29 show the relationship between induced pore water pressure and repeated cyclic strains of various amplitudes. The compression which results from the pore pressure dissipation was computed from the consolidation properties of the materials.

The partial contributions of the settlement due to the dissipation of pore water pressure in the soils of the Tobacco Road/Dry Branch, and the Santee/Tinker Formations were calculated. Figures 7.3-16 and 7.3-17 summarize the calculated settlements for the seven free field soil columns examined in this evaluation. The results show that total dynamic settlements range from near zero to about 0.2 inches for the local EBE; from 0.4 to about 0.7 inches for the distant EBE; and from about 0.75 to 1.5 inches for the distant 84th percentile motion. Further, based on the range of these calculated values, the dynamic differential settlement is expected to be about one half of the total.

### *7.5.2 Static Settlement Due to Tank Loading During Operation*

ITP Tanks 48, 49, 50, and 51 were constructed between 1978 and 1982. Fluid levels and tank settlement have been monitored regularly. To date, these tanks have experienced (on average) 1¾ inches of total settlement and ½ inch of differential settlement (Figures 7.5-1 through 7.5-4). This section discusses the additional expected static settlement which may occur from filling the tanks to

their maximum design capacity, and from long-term settlement. Ultimately, the predicted static settlement was determined by assessing historic tank settlement data in H-Area and settlement evaluations from the nearby DWPF in S-Area (Mueser, 1984b), as discussed below.

Observed tank settlements at ITP are smaller than the values that can be calculated from consolidation test data. For example, 1½ to 2 feet of settlement is predicted if the average compressibility properties ($C_c$ and $C_r$) and consolidation state (OCR) given in Table 6.0-1(a) (non-parenthetical values) are used. On the contrary, the post-construction settlement monitoring at ITP shows only (on average) about 1¾ inches of post-construction settlement. This suggests that the consolidation parameters determined solely from laboratory testing (Table 6.0-1(a)) are overly conservative.

Peck (1954, 1977) emphasizes some of the pitfalls encountered when trying to predict settlement based solely on laboratory test data. He stresses the use of field performance data, when available, or other simple methods, especially when soils that are poorly understood or highly variable are involved. In discussing the settlement predictions for 3 nuclear power plants founded on stiff clays, Peck (1977) discusses the impact of sample disturbance.

> "Overconservatism may also enter into the calculations made by the geotechnical engineer of the amount of settlement to be expected. This has been demonstrated in the design of three nuclear power plants at sites underlain by deposits of stiff to hard clay. In each instance, straightforward taking of samples, presumably by good techniques, straightforward performance of consolidation tests, and standard methods of computation and analysis led to predicted settlements on the order of 12 to 15 inches (305-381 mm). These settlements were considered far too great by any criteria and alternatives were proposed such as pile foundations, pier foundations, or stress reduction by major excavations. Although it was realized that disturbance has a profound effect on the compressibility of stiff clays, conservatism suggested that the consolidation tests be interpreted in a textbook manner and that the preconsolidation load, also greatly influenced by disturbance, should be judged by the usual procedures on the basis of the pressure-void ratio curves."

> "At each site a careful study of the geology indicated that a high degree of precompression was at least probable. Additional techniques were used to judge the overconsolidation ratio. The relationship between c/p ratio and the plasticity index for normally loaded clays was invoked to determine the value of consolidation pressure corresponding to the measured undrained shear strength. In each instance, it was found that the preconsolidation load indicated in this manner was appreciably greater than that derived from the consolidation tests. This is not surprising, because the undrained shear strength is less influence by disturbance than are the consolidation characteristics (Peck, 1977)."

In discussing the settlement predictions for Safeway Store Inc. in Salt Lake City, Peck (1954) emphasizes the need to use field performance data, especially for soils that are highly variable. The Safeway site was founded on heterogeneous deposits of sand, silt, and clay. Theoretical settlement predictions, based on laboratory test data, had overestimated observed settlements.

> "The study has indicated that the clay is precompressed to the extent that the settlements predicted on a theoretical basis are much too large, and that the real settlements will be of such

> a nature that satisfactory behavior can be assured. Fortunately, because of excellent case histories available, it is not necessary to base decisions upon theoretical considerations but rather upon observed facts (Peck, 1954)."

Fortunately, the geology, consolidation state, and compression indices of the SRS soils have been thoroughly reviewed and discussed by other investigators at nearby facilities, and ultimately, field performance data were selected over laboratory data to estimate settlement performance. This is best illustrated at the SRS by reviewing the settlement predictions for the Defense Waste Processing Facility (DWPF) in S-Area (Mueser, 1984b).

D'Appolonia (1982) performed an extensive field and laboratory investigation of the soils in the Tobacco Road and Dry Branch Formations for the preliminary safety analysis of DWPF. The compiled data included conventional and undisturbed sample boreholes, piezometers, pressuremeter tests, cross hole seismic tests, cone penetrometer tests, and laboratory testing. Using laboratory-determined compressibility parameters, D'Appolonia concluded that the clay layers within the Tobacco Road and Dry Branch Formations were normally consolidated and predicted in excess of 12 inches of total settlement for the DWPF mat foundation. Because of these large predicted settlements, D'Appolonia recommended precompression of the foundations soils by dewatering and designing the DWPF structure to withstand large differential settlements (Richards, 1982).

However, at the request of DuPont, Mueser was asked to review the preconsolidation state of the soils at DWPF. Based on tank settlement data in H-Area (Tanks 38 through 42), Mueser concluded that the soils in both S-Area and H-Area were overconsolidated and that any settlement of the DWPF foundation would occur on the recompression part of the consolidation curve (Richards, 1982). An additional consulting engineer, R. M. Pyke, was also requested to review D'Appolonia's findings (in Glisson, 1982). Pyke made the following comments about the apparent consolidation state of the S-Area soils:

- The geological history suggests that the soil profile is overconsolidated. George Siple, in a conversation with Pyke, estimated that 50 to 100 feet of overburden may have been removed from the site.

- Data from consolidation tests made of samples from H- and S-Areas indicate preconsolidation. Some of the samples have enough fines to give a good curve definition of preconsolidation. (From these results, Pyke found OCR ranging from 1 to 5.2. He recommended that 2 be used as a representative value.)

- Shear wave velocity measurements from geophysical logs are inconsistent with the assumption of normal consolidation.

To resolve the differences between the settlement predictions, meetings were held between D'Appolonia, Mueser, and DuPont on September 8, 1982 and September 23, 1982 (Edinger, 1982). In the latter meeting, Mueser presented an expanded summary of all consolidation tests and loading versus time plots for Tanks 38 through 42 in H-Area (Note: Tanks 38 through 42 are just north of the ITP facility) . Mueser had used these data to estimate approximately 3.5 inches of

recompression settlement under the DWPF structure. As a result of these meetings, D'Appolonia agreed that the settlements under DWPF should be determined from moduli computed from observed tank settlements in H-Area. They revised their original DWPF total settlement estimates to about 3 to 5 inches of total settlement. Furthermore, D'Appolonia agreed that the geotechnical report on DWPF should avoid characterizing the soils as "normally consolidated." They maintained, however, that the high moduli have only been confirmed for loadings up to 4 kips per square foot and for structures where soil disturbance is small.

A pre-construction heave and post-construction settlement monitoring program was initiated at DWPF in June of 1984. Excavation was completed by October of 1984 and the full structural loads were essentially in place by January, 1988. In the last progress report of this program, Mueser (July, 1991) reported: "The total cumulative settlement of the mat from November 1984, the date of the mat placement, through April 1991 varied from 2.2 inches to 2.7 inches in the northern section of the building where the heaviest loads were applied and 1.3 to 2.0 inches in the southern section." In addition, recent settlement measurements taken in April 1994 confirm these results. Thus, the settlement data collected from post-construction monitoring at DWPF shows good agreement with the settlement predictions of Mueser (Edinger, 1982; Mueser, 1984b); hence giving credence to the correctness of the applied consolidation parameters. Table 7.5-1 lists these consolidation parameters (Mueser, 1984b).

The measured settlements at DWPF and ITP are compared on Figure 7.5-5. Shown on the figure are load and settlement versus log of time since the beginning of construction for two typical settlement markers at DWPF (Points 18 and 35) and the average settlement for ITP Tank 48. The results show remarkably consistent behavior for the applied loads. Thus, it is concluded that the soil profile at ITP, just like the DWPF profile, is overconsolidated and large, continuous soft zones do not exist under the structures; otherwise large settlements would have already occurred.

The parameters listed in Table 7.5-1 were used by this investigation to calculate the future, static, ITP tank settlement. Although not developed specifically for ITP tanks, these parameters are deemed appropriate because they were obtained from tank settlement performance data in H - Area at nearby Tanks 38 through 42. When these parameters are applied and all soil layers are treated in recompression (as indicated in Figure 6.0-1), about 3-1/3 inches of post-construction settlement is predicted compared to the measured settlement of 1¾ inches. Thus, based on actual observed movement, all recompression indices were decreased by the ratio of predicted to measured movement (i.e., 1.9). The adjusted recompression indices are shown in parenthesis in Table 7.5-1.

Classical one-dimensional consolidation theory was then used to compute the future settlement resulting from filling the tanks to maximum operating capacity. The increase of vertical pressure for the soil layer was calculated using Boussinesq theory (Figure 7.5-6). The predicted additional settlement due to filling the tanks to their maximum capacity is about 0.4 inches (this value has already been decreased by a factor of 1.9). For long-term settlement, the loading history of the tanks was estimated using the settlement data collected between May 1978 and April 1994 (Figures 7.5-1 through 7.5-4). Long-term settlement for the lifetime of the tanks (i.e., 30 years) is

calculated to be about 0.3 inches. However for conservatism, the predicted static total future tank settlement due to tank loading during operation and secondary consolidation is estimated to be 1 inch. It is further expected that additional differential settlement of about ½ of the total settlement will occur. In summary, the expected settlement of Tanks 48 through 51 due to earthquake motions, increased loading during operation, and long-term secondary consolidation is as follows:

| | *Settlement, inches* | |
|---|---|---|
| *Condition* | *Total* | *Differential* |
| Existing | 1.75 | 0.5 |
| Increased loading and secondary consolidation | 1 | 0.5 |
| Dynamic: | | |
| -Local EBE | 0.2 | 0.1 |
| -Distant EBE | 0.7 | 0.35 |
| -Distant 84th | 1.5 | 0.75 |

Thus, for the recommended 84th percentile ground motion, the total tank settlement will be about 4¼ inches with a differential settlement of about 1¾ inches.

### *7.5.3 Tank Settlement: "Worst Case"*

At other areas within the SRS, it has been assumed that the Santee/Tinker formation, or zones within it, are underconsolidated. The estimated amount of underconsolidation has ranged from less than half of the overburden pressure to normally loaded (GEI, 1991a and KASS, 1992). Laboratory and field tests at ITP do indicate the existence of soft zones or underconsolidated pockets within the Santee/Tinker formation. The sections that follow describe the geologic models and geotechnical parameters used to characterize the soft zones and describe the analytical models used to predict tank settlement for the given earthquake motions.

#### *7.5.3.1 Geologic Model: Worst Case*

Site-specific investigations at ITP have revealed that soft zones within the Santee/Tinker Formation are found at depths approximately 130 to 170 feet below natural ground surface (about 110 to 150 feet below the foundations of the ITP tanks). These soft zones act as local, underconsolidated pockets with overburden stresses arching around the underconsolidated zones. Because the soft zones have formed over a considerable period of time (late-Eocene, or about 40 mybp) and have survived for millions of years and have apparently persisted through several pre-historic earthquakes, it is reasonable to assume that for all practical purposes, they are of no engineering concern to the dynamic stability of the ITP tanks.

However, settlement analyses have been done at other SRS facilities assuming that these underconsolidated zones are "arched" by more competent material and that the arch is broken during an earthquake (KASS, 1992). In those evaluations, very conservative subsurface conditions were assumed concerning the potential width, depth, and extent of the soft zones within the surrounding matrix material. Two basic methodologies were used to calculate the potential amount of surface settlement following a postulated collapse during an earthquake: (1) analogies to both soft-ground tunneling and coal mining (GEI, 1991a) and (2) numerical modeling (KASS, 1992). The analyses suggest that the matrix sandy soils are incapable of arching zones larger than about 50 feet in diameter.

Geostatistical analyses of the subsurface penetration data at ITP suggest that the soft zones in the Santee/Tinker Formation are not laterally continuous for more than a few tens of feet (Section 5.2.1). However, due to the observed high lateral variability, it is impossible to preclude that some larger zones may exist. Also, the soft zones appear to be concentrated in two distinct stratigraphic horizons that roughly parallel the dip of the overlying strata, suggesting that the occurrence of the soft zones is not random, but is depositionally controlled. Thus, for the dynamic settlement evaluation of ITP, a conservative estimate of the possible maximum thickness and lateral extent of the soft zones was made based on the contouring of the penetration data meeting the soft zone criteria (Section 5.2.1 and Figure 5.2-1).

At the beginning of the project, two subsurface profiles had been developed: Profile AA', a north-south section through Tanks 49 and 51; and Profile BB', an east-west section through Tanks 48 and 49 (Figures 5.1-1 and 5.1-2). However, based on further refinement of the geologic model (Figures 5.2-1, 5.3-11, and 5.3-12), a 10 to 15-foot-thick soft zone was interpreted under Tank 51 in Facies 2 of the Santee/Tinker Formation (Figure 5.1-7). Also, a 10-foot-thick soft zone was suggested under the northwest corner of Tank 50 (Figure 5.2-1). Along Profile BB', no appreciable thickness of soft zones was found under Tanks 48 and 49 (Figure 5.2-1).

The initial dynamic settlement modeling was done assuming a constant soft zone thickness of 10 and 15 feet (Section 7.5.3.4). However, as the development of the geological model proceeded, it became clear that a variable thickness representation of the soft zones was more realistic. Also, because the soft zone thickness was greatest under Tank 51, an east-west profile line through Tanks 50 and 51 was developed and named Profile CC' (Figure 5.2.1). The east-west orientation of Profile CC' was chosen because the majority of the soft zones within the Santee/Tinker Formation are apparently found beneath Tanks 50 and 51.

Profiles AA' and CC' were analyzed with a variable soft zone thickness as shown in Figure 5.2.1 and tabulated in Tables 7.5-2 (a) and 7.5-2(b), respectively. Also, a ten and a fifteen-foot-thick uniform soft zone was modeled. For these analyses, it was assumed that the entire soft zone thickness was underconsolidated and that a complete transfer of effective vertical stress would occur after the earthquake (i.e., the arch would break). As discussed in the following section, post-earthquake compressions at depth using best-estimate values of the compressibility and consolidation state of the soft zone material and analytical modeling were used to estimate the

resulting differential settlement by numerically propagating the deep-seated compressions to the tank foundation level.

### *7.5.3.2 Geotechnical Parameters: Worst Case*

To complete this numerical analysis, a best estimate OCR of 0.7 was used for the soft zones (Figure 6.0-1). Also, numerous moisture content data were tabulated for the soft zones and matrix material. These data showed an average moisture content for the soft zones and matrix material of 44.3 percent and 30.2 percent, respectively. These average values were then used with a site-specific void ratio versus moisture content relation to estimate average void ratios of 1.285 and 0.928, respectively, for the soft zone and matrix material (Figure 7.5-7). Also, a site-specific compression ratio ($C_c/(1+e_0)$) versus moisture content relation (Figure 7.5-8) was used to estimate an average compression ratio of 0.24 for the soft zone material. This compression ratio, in conjunction with an OCR of 0.7 and the soft zone thickness, H, were used to compute soft zone compression at depth utilizing the following equation:

$$S = (H/(1+e_o))\ C_c \log ((p_c+\Delta p)/p_c) = (H/(1+ e_o))\ C_c \log (OCR^{-1})$$

where S is the compression at depth, $p_c$ is the preconsolidation pressure, and $\Delta p$ is the applied load to bring the soil to a normally consolidated state.

The soft zone compressions at depth of 4.5 and 7 inches (Table 7.5-3(a)) Profiles AA' and BB', respectively) were based on a constant soft zone thickness of 10 and 15 feet, respectively and were calculated using the above equation. A variable soft zone thickness model was also analyzed for Profiles AA' and CC' for the local EBE and 84th Percentile event assuming full tank conditions. The soft zone thickness and post-earthquake compression at depth (H and $\Delta S$) used in these analyses are given in Tables 7.5-2(a) and 7.5-2(b). The analytical model used to perform these analyses is discussed in the following sections and the results are summarized in Sections 7.5.3.3.6 and 7.5.3.4.

### *7.5.3.3 Analytical Model: Worst Case*

The seismic structural evaluations of the ITP tanks require an evaluation of both total and differential settlements. The method for evaluating settlement was selected so that important aspects of the site stratigraphy and soil properties, as well as configurations of the ITP tanks and properties, are considered in the evaluation.

In some previous studies at SRS, the settlement analysis was based on free-field modeling (e.g., RTF), i.e., the structural total and differential settlement were estimated based on the free-field soil column models. Instead, for settlement analyses of the ITP tanks, a methodology was selected which is more elaborate because:

- The soil properties vary within each formation. The effect of the soil in-homogeneity, especially in the lateral direction, needs to be included in the settlement analysis.

- The ITP tanks are buried within an embankment, and the tank foundation settlement may be influenced by the settlement of the berm around the tanks.
- In addition to the soil-tank interaction effects, tank-to-tank interaction may also influence the magnitude of the seismic stresses in the supporting soil foundation.
- The stratigraphy at the ITP site (see Figures 5.1-1 and 5.1-3) with layers having varying thickness in lateral direction differs from that which assumes a horizontally layered site, as normally considered in a one-dimensional soil column settlement analysis approach.
- The ITP tanks may be full or empty depending on their operational schedule. Soil stresses may be affected by the effect of fluid inertia.
- Deformation of the soft zones and settlement of the layers above the soft zones needs to be considered.
- In addition to the tank settlement, the seismic soil pressure demand under the tank foundation and the acceleration responses on the berm are required. These responses are used in subsequent structural evaluation of the tanks and stability of the slopes of the berms.

The methodology consists of developing the structural models of the tanks, performing seismic soil-structure interaction analysis, simulating in-situ stress conditions, and finally, computing the final settlement from the post-earthquake settlement analysis. These steps are outlined as follows.

#### 7.5.3.3.1 Tank Structural Model

A structural model of the tank was required to perform the soil-structure interaction (SSI) analysis. Although the tanks in the H-Area Tank Farm are different in type and capacity, the four tanks at ITP are known to be of Type IIIA. A section view of the Type III tank is shown in Figure 7.5-9. This is a concrete cylindrical structure 95 feet in diameter and approximately 40 feet in height, with a concrete column at the center. The base slab is flat with 3 ft-7 in. thickness. The roof slab is flat in the Type III tank, but in the Type IIIA tank, the slab is 5 feet thick at the center tapering to 4 feet at the edges.

A three-dimensional dynamic model of the tank was developed by WSRC for structural evaluation. This model is shown in Figure 7.5-10. The fluid mass representing the contents of the tank was modeled using a beam stick model. The fluid mass was distributed to the base slab as well as to the top slab based on the impulsive action of the mass. In the vertical direction, single-degree-of-freedom oscillators were used to model the fluid mass. The oscillators are directly connected to the base slab. The base slab, the shell, and the roof slab were modeled using plate elements.

Both the SSI and the soil deformation analyses are performed using two-dimensional (2D) models. For this reason, a conversion was made from the three-dimensional (3D) to an equivalent 2D structural model. The equivalent length of the 2D model was obtained based on in-house civil/structural design guide (Bechtel, 1992), as shown in Figure 7.5-11. Using these criteria, the full width of the tank structure is retained in the 2D model, thereby the configuration of the tank within the berm and the spacing between the tanks are maintained. As shown in Figure 7.5-11, the width of 95 feet, equivalent to the tank diameter, is maintained and a depth of L = 80.75 feet is

calculated for conversion of the mass and stiffness properties from the 3D to the 2D model. In the 2D model, beam elements are used to model the tank structure. The mass and stiffness of the 3D model were converted to an equivalent 2D model following the steps shown below:

1. All lumped mass points were divided by the scaling factor L

2. All distributed mass values using weight/mass density in the 3D model were adjusted proportionally according to the ratio of the total mass between the 2D and the 3D model in the respective structural component

3. An additional rotational mass was added at the basemat model of the 2D model to preserve the compatibility of rotational inertia between the 3D and 2D models

4. The stiffness properties of the beam models representing the roof slab, shell, center column, base slab, and the beam stick representing the fluid in the 2D model were adjusted step-by-step to match the predominant frequencies of the 3D model.

Frequency response comparisons were made between each respective component pair of the 2D and 3D models to ensure full compatibility of dynamic properties between them. These consisted of:

- Comparisons of the responses of the roof slab assuming fixed boundary conditions around the edge

- Comparisons of the fixed base responses of the roof slab with the center columns attached to the slab

- Comparisons of the fixed base responses of the entire structure consisting of roof slab, center column, shell, base slab, and fluid masses.

The resultant 2D structural model is shown in Figure 7.5-12.

A final response comparison of the 2D and 3D models was made using the soil spring approach. Assuming a circular foundation (diameter of 95 feet) on the surface of an elastic half space (shear wave velocity of 1000 fps), dynamic stiffness and damping coefficients of the soil-foundation system were calculated. These coefficients in the form of spring and dashpots were added to the base of the 3D model. The model was then analyzed under both horizontal and vertical excitation. Similarly, the 2D model with scaled-down spring and dashpot coefficients was analyzed. The results, in terms of acceleration amplification functions at a point in the center of the roof slab, are compared in Figures 7.5-13 and 7.5-14, for the horizontal and vertical directions, respectively.

As shown in these figures, the 2D model replicates the dynamic properties of the 3D model with some deviations at higher modes. The effect of these deviations at higher frequencies is expected to be insignificant considering the overall response.

7.5.3.3.2 Soil-Structure Interaction Analysis and Results

The SSI analyses were performed using the computer program SASSI (Ostadan 1988). The two design soil Profiles AA' (north-south section) and BB' (east-west section) described in Section 5.1 were used in the analysis. The SASSI models for Profiles AA' and BB' are shown in Figures 7.5-15 and 7.5-16, respectively. In Profile AA', Tanks 49 and 51 are modeled, and in Profile BB', Tanks 48 and 50 are considered. The stratigraphy extends to the Congaree Formation. The SSI analyses were performed for three earthquake motions: the EBE ground motions (local and distant events) and one motion representing the 84th percentile, all described in Sections 7.1 and 7.5. Consistent with the development of the ground motions, the local and distant time histories were prescribed at the grade level at the top of the Tobacco Road in the free-field. The 84th percentile time history was prescribed as a basement motion at a depth of approximately 1,000 feet. Strain-compatible soil properties obtained from the free-field analyses were used in the respective SSI analyses. Both full and empty tank conditions were considered. A total of nine SSI cases were analyzed as shown below. Note, no SSI analyses was performed for Profile CC'.

| Input Motion | SSI Cases Analyzed<br>Soil Profile | |
|---|---|---|
| | AA' | BB' |
| EBE-local | tanks full/tanks empty | tanks full/tanks empty |
| EBE-distant | tanks full/tanks empty | tanks full/tanks empty |
| 84th percentile motion | tanks full | ---- |

To evaluate the SSI effects on the maximum shear stresses in the soil layers below the tank foundation, a comparison was made between the free-field SHAKE results and SASSI SSI results for both soil Profiles AA' and BB'. For Profile AA', a soil column designated as A5 (see Figure 7.5-17) was selected for this comparison. The maximum shear stresses are compared in Figures 7.5-18 and 7.5-19 for the local and distant motions, respectively. Similarly, for Profile BB', a soil column designated as B3 (see Figure 7.5-20) was selected. The SSI results are compared with the free-field results in Figures 7.5-21 and 7.5-22 for local and distant motions, respectively.

As shown in these figures, SSI and free-field results are comparable, and differences up to 30 percent can be observed. These differences are mostly in the limited depth range of the Dry Branch formation. Depending on the layer and the SSI case considered, SSI results can be larger or smaller than the free-field results. The differences are due to soil-tank interaction effects and to non-horizontal layering of the soil under the tanks. No comparison of the stress results were made for the 84th percentile motion.

The results of SSI analyses for Profile AA' in terms of maximum acceleration and maximum shear stress contours for EBE are shown in Figures 7.5-23 through 7.5-30. Similarly, the results for Profile BB' are shown in Figures 7.5-31 through 7.5-38. The analysis shows almost no significant amplification in terms of acceleration in the embankment fill. These results are used in connection with the stability evaluation of the embankments and the settlement of the soil layers below the tank foundation.

The results in terms of maximum cyclic stress ratios (CSR) and maximum shear strain profiles AA' and BB' under full tank conditions for the EBE are shown in Figures 7.5-39 through 7.5-46. The results in terms of soil pressure demand under Tanks 48, 49, and 51 for both local and distant motions are shown in Figures 7.5-47 through 7.5-54. In every case the maximum increase in dynamic bearing pressure is less than 0.5 ksf, resulting in no impact on the existing bearing capacity of the tanks.

Similarly, the SSI results for the 84th percentile motion are shown in Figures 7.5-55 through 7.5-60 in terms of contours of maximum acceleration, maximum shear stress, maximum cyclic stress ratios, maximum shear strain, and soil pressure under the tanks for Profile AA'. These results are similar to the EBE in that no significant amplification of maximum acceleration occurs in the embankment and the increase in dynamic bearing pressure is less than 0.5 ksf.

7.5.3.3.3 Settlement Analyses: Simulation of Existing Stress State, Pre-Earthquake Condition

Settlement analyses were performed using the computer program FLAC (1991). The program is capable of handling large strain deformations, non-linear soil properties, and soil-structure interaction effects. For the analyses, the existing pre-earthquake stress conditions in the field must be simulated. The FLAC models and the associated subsurface soil layers and soft zones are shown in Figures 7.5-61 and 7.5-62 for Profile AA' and in Figures 7.5-63 and 7.5-64 for Profile BB'. The soft zones were modeled based on the information presented in Section 5.2. The 2D structural models of the tanks were also used in the FLAC models and both empty and full tank conditions considered. The soil properties used in the FLAC analysis are shown in Table 6.0-1(a). Low strength properties were assigned to the soft zone elements. The non-linear soil behavior was modeled using the Mohr-Coloumb Constitutive Law. The FLAC analyses was carried out in steps beginning with the successive placement of the soil layers from Congaree to Tobacco Road; the placement of the fill layer, and the placement of the tank models. In the model for Profile BB', the Filter Stripper Building weight was also considered. To analyze Profile CC', a separate model was not developed. Rather, the east-west model for Profile BB' was utilized with variable soft zone compressions (for Profile CC') as discussed in Section 7.5.3 and given on Table 7.5-2.

The FLAC results in terms of contours of effective vertical stresses for Profile AA' for full and empty tank conditions are shown in Figures 7.5-65 and 7.5-66. The results in terms of orientation of principal stresses for the full tank condition are shown in Figure 7.5-67. This figure illustrates the soil arching effect around and above the soft zone. The stresses are about 65 to 75 percent of

the overburden pressure, thus corroborating previous conclusions related to the OCR. Similarly, the results for Profile BB' are shown in Figures 7.5-68 through 7.5-70.

It should be noted that upon placement of the fill and tank structures in the FLAC model, the computed settlement is in the range of 1.5 to 2.5 inches which is in agreement with measured settlements for Tanks 48 through 51 (in the range of 1.5 to 2 inches, see Figures 7.5-1 to 7.5-4). The agreement between the calculated and the observed settlements corroborates the model (methodology, soil parameters, and properties) used for the analyses.

The pre-earthquake FLAC analysis results, along with the piezocone data (see Section 7.5.3.3.4), are used in conjunction with the shear stresses induced by the evaluation basis earthquakes (from the SASSI analyses) to determine the settlement resulting from the dissipation of the excess pore water pressure (using a post-earthquake FLAC analysis, Section 7.5.3.3.5).

#### 7.5.3.3.4 Interpolation of Piezocone Data

Ordinary kriging (Journel and Huijbregts, 1978) was used to interpolate CPT tip resistances, $q_c$, and friction ratio, fr, along Profiles AA' and BB' for dynamic settlement analysis (Rouhani et al., 1995). Kriging is a geostatistical interpolation method which uses spatial models (variograms) to determine best estimates at an unmeasured point. Kriging was selected as the preferred method of interpolation because it is a best, linear, unbiased estimator (blue). It also uses an empirical model of the observed spatial correlation (i.e., variogram) to determine the interpolation weights, thus preserving any spatial structure present in the actual data.

Prior to kriging, a series of vertical and horizontal variograms were created for each of the layers shown in Figures 5.1-1 and 5.1-2. The developed variograms were then used to perform a 3-D, kriged interpolation to the FLAC mesh for Profiles AA' and BB' (Figures 7.5-61 and 7.5-63, respectively). The 3-D interpolation was done layer by layer, using the CPT data (Volume 3).

Contours of the kriged values of $q_c$ and fr are given in Figures 7.5-71 through 7.5-76 for Profiles AA' and BB'. Figures 7.5-71 and 7.5-74 presents contoured results for zones having $10 \leq q_c < 50$ tsf for Profiles AA' and BB', respectively. Figures 7.5-72 and 7.5-75 show contoured results of $q_c > 50$ tsf for these same profiles, respectively. Figure 7.5-73 and 7.5-76 are contours of fr for the same profiles.

To check the "reasonableness" of the kriging algorithm, a cross-validation test was performed (Rouhani et al., 1995). In cross-validation, one CPT borehole is removed from the CPT data set and kriging is done without the selected borehole. The predicted or kriged values at the location of the removed borehole are then compared with the actual values to judge the quality of fit. For example, Figures 7.5-77 and 7.5-78 show cross-validation results for SCPT1 and SCPT6B. Based on these figures, it appears that kriged estimates are reasonable for layers above elevation 220 feet, which encompasses the primary layers of concern for liquefaction and dynamic settlement analyses.

7.5.3.3.5 Compression of Soil Layers Upon Pore Water Pressure Dissipation

The settlement of the soil layers presented in Section 7.3 was based on analyses of one-dimensional soil columns at the locations where cone penetration logs data are readily available. These free-field settlements did not include the contribution due to soft zone compression. The estimation of the tank settlement accounting for variations of soil properties in the lateral direction, and the compression of each soil element (see Figures 7.5-62 and 7.5-64) upon dissipation of excess pore pressure was done using the following steps:

1. The kriged tip resistance and friction ratio values for each soil element were retrieved (see Section 7.5.3.3.4)

2. Using the cone tip and friction ratio for each soil element, the cyclic shear strength were obtained from Figure 6.2-12. The cyclic shear strength for each element was corrected for the earthquake magnitude as follows (Seed and Idriss, 1982):

| | |
|---|---|
| EBE local | $r_m = 1.3$ |
| EBE Distant | $r_m = 1.0$ |
| 84th percentile motion | $r_m = 1.0$ |

3. From the contours of seismic shear stress induced (Section 7.5.3.3.2) and the contours of effective vertical stress (Section 7.5.3.3.3), the effective stress ratios were computed for each element in the FLAC model representing soil layers below ground water in the Tobacco Road and Dry Branch Formations. For elements in the Santee/Tinker Formation, effective seismic shear strains were retrieved from the SASSI analysis results

4. Knowing the cyclic shear strength ratios (capacity) from Step 2 and the shear stress ratios (demand) from Step 3, the factors of safety are computed for all soil elements in the Tobacco Road and Dry Branch Formations

5. From the factors of safety (Step 4) and cone tip resistances (Step 1) for each element, the volumetric strain is obtained using Figure 6.2-27. Knowing the height of the soil element and the volumetric strain, the settlement of each element is computed. These settlement values were used as input loading in the FLAC post-earthquake analysis (see Section 7.5.3.3.6)

6. For soil elements in the Santee/Tinker Formation, the effective shear strain from the SASSI analysis were used in conjunction with the laboratory test results from the Santee/Tinker Formation shown in Figure 6.2-29 to compute the pore water pressure ratio generated by the cyclic loading. Depending on the earthquake magnitude, the curves corresponding to 10, 20, and 15 (interpolation between the two curves) number of cycles were used in conjunction with the EBE local, distant and 84th percentile motions, respectively. From these, and with the consolidation properties of the Santee/Tinker Formation, the settlement at each element level was calculated. These settlement values were prescribed at the respective nodal points in the post-earthquake FLAC analysis.

7.5.3.3.6 Post-Earthquake Tank Settlement Analysis: Results

Using the nodal settlement values (see Section 7.5.3.3.5) and compression of the soft zones discussed in Section 7.3.3, a series of FLAC analyses were performed to compute the total and differential tank settlement profiles. Structural models of the tanks under full and empty conditions in the pre-earthquake FLAC model were retained. Maintaining the stress field obtained from pre-earthquake FLAC analysis, the soil elements in the Tobacco Road, Dry Branch, and the Santee/Tinker Formations were subjected to nodal displacements. The nodal points corresponding to the soft zones were also simultaneously subjected to compression. The results for Profiles AA' and BB' for constant soft zone compressions of 4.5 and 7 inches are shown in Table 7.5-3(a). Settlement plots under the Tanks 49 and 51 in Profile AA' for constant soft zone compressions of 4.5 and 7 inches are shown in Figures 7.5-79 through 7.5-82. Settlement plots for tanks in Profile BB' are not given, since they have much less settlement, but show similar settlement patterns.

The results for Profile AA' and CC' for variable soft zone compression are shown in Table 7.5-3(b). Settlement plots under Tanks 49 and 51 in Profile AA' and for Tanks 50 and 51 for Profile CC' for variable soft zone thickness and the 84th percentile ground motion are shown in Figures 7.5-83 through 7.5-87. As shown in all of these results, while total settlement of up to 5 to 7 inches may occur, differential settlement (edge-to-edge) is limited to less than about 2 inches.

In interpretation of the settlement results, it should be noted that two-dimensional plane-strain models were used in the FLAC analyses. In such models, the thickness of soft zones is assumed to be continuous in the horizontal plane perpendicular to the FLAC profile, thus neglecting the beneficial arching effect in this third dimension.

### *7.5.3.4 Tank Settlement Summary: Worst Case*

Total and differential settlements of the tanks at ITP due to dissipation of excess pore pressure and potential compression of the soft zones as a result of the EBEs and the 84th percentile motion were computed. The results, given on Tables 7.5-3a and 7.5-3b, cover a wide variety of conditions postulated at ITP. The analysis method incorporated site specific soil properties allowing for lateral in-homogeneity of soil layers and soil-structure interaction effects. However, the analytical method was plane strain and is therefore conservative. In areas where soft zones were indicated by the borehole data (Sections 5.2.1 and 7.5.3.1), these zones were assumed to be laterally continuous, underconsolidated, and were compressed using full effective vertical stresses (i.e., no post-earthquake arching was assumed).

These worst case analyses assumed a soft zone thickness of up to 15 feet thick, resulting in a maximum soft zone compression at depth of 7 inches. Based on this result, estimated total settlements at the tank foundation level range up to 5 inches for variable soft zone thicknesses and up to 7 inches for a constant soft zone thickness of 15 feet thick. However, in all cases reported, the maximum differential settlement across an half-width of a tank (i.e., center to edge) is about 1 inch (Table 7.5-3(b), or about 2 inches across a full tank diameter (i.e., edge to edge).

# 8. ENGINEERING EVALUATIONS FOR THE BALANCE OF THE H - TANK FARM

## 8.1 Controlling Earthquake Motions

The 84th percentile rock spectrum developed for ITP was used for the seismic evaluation of the HTF (Figure 2.3-1). From this spectrum, a compatible time history was generated (Figure 7.3-12) and the resulting motion was convolved from bedrock to the ground surface using the computer program SHAKE (Schnabel, Lysmer, and Seed, 1972; Idriss and Sun, 1992). The dynamic shear stress profile as a function of depth was calculated from the SHAKE output and used in the one-dimensional (1D) liquefaction analyses described in Section 8.3.

## 8.2 Evaluation of Slope Stability for the HTF

### *8.2.1 General*

For fill evaluation purposes, the tank farm was divided into three locales arbitrarily designated the North, East, and West Hills. Statistical review of the CPT data revealed that the fill north of the ITP tanks has the lowest shear strength in the balance of the HTF. See Section 6.3.2 for the statistical model used. This data, developed in Section 6, was used as an enveloping case for all areas. The stability of slopes was evaluated using the methodology described in Section 7.2.1, except no random failure surfaces were generated and no vertical acceleration component was applied since it results in no affect on the computed safety factors.

The slopes were modeled using four cross-sections that represent the various slopes and loading configurations present: the first cross-section is typical of the majority of the slopes and included the Control Building (241-82H); the second cross-section is typical of the notched slope located east of Tanks 41 and Tank 43; the third cross-section is typical of the highest slope located east of Tanks 21 and Tank 22; and the fourth cross-section is typical of the slopes immediately opposite of the tanks. All slopes are gabion-faced; however to be conservative, the gabions were not modeled in the analyses. The slope geometry and loading conditions were visually verified in the field. The cross-sections are shown in Figures 8.2-1 through 8.2-4. Each cross-section shows the approximate locations of the lowest FS failure surfaces for static and pseudo-static conditions.

- Cross-Section 1 (Figure 8.2-1) is typical of the slope at the Control Building (241-82H). The Control Building is located on top of the slope, 25 feet back from the crest. The building loads are simulated by a uniform load of 700 psf over the building footprint. The maximum load for the tanks was estimated to be 4,000 psf. These tanks are founded at the base of the fill, at about elevation 286 feet.

- Cross-Section 2 (Figure 8.2-2) is typical of the notched slope located east of Tanks 41 and 43. Here the toe of the slope was removed and replaced by an approximately 17-foot-high retaining

wall. The notched width is approximately 52 feet. The slope then extends back from the top of the retaining wall to the crest of the slope at a 2:1 (H:V) inclination.

- Cross-Section 3 (Figure 8.2-3) is typical of the longer slope located east of Tanks 21 and 22. The vertical slope height along this portion of the hill is approximately 43 feet. This represents the highest slope in the tank farm.
- Cross-Section 4 (Figure 8.2-4) is typical of the slopes immediately opposite of the tanks where potential failure services could only extend back a limited distance before encountering a tank wall.

Groundwater monitoring wells were installed at the south end of the HTF in early 1986. The water table has been generally constant at Elevation 275 feet for approximately the last five years. No perched water tables were found within the fill. Nearly the entire top of the fill is covered with asphalt surface paving. Drainage is provided and storm sewers are present within the fill. These factors combine to minimize the opportunity for water to enter and be retained within the embankment.

### *8.2.2 Methodology*

SRS computer Program GEOSLOPE (SRS, 1988) was used in the analysis of the cross-sections described previously. The program is described in Section 7.2.1.

Each cross-section was evaluated for static steady-state conditions using total and effective shear strength parameters and for pseudo-static conditions using total stress shear strength parameters reduced by 10 % (Makdisi, 1977). The minimum acceptable static and pseudo-static factor of safety were 1.5 (Huang, 1983) and 1.15 (Seed, 1979b).

Circular failure surfaces were computed using the Modified Bishop method. Wedge-shaped failure surfaces were analyzed using Janbu's method. The factor of safety is defined as the ratio of the resisting forces divided by the driving forces.

As with ITP, a pseudo-static horizontal load of 0.2 g was applied to the critical (lowest factor of safety) failure surface to simulate the effects of earthquake loading.

### *8.2.3 Layering of Fill for Slope Stability Analyses*

The stratigraphy used in the stability analysis of the slope is based on the 10 CPTs pushed in the hill north of the ITP Area.

The geologic formation underlying the HTF is the Altamaha Formation, commonly referred to as the "Upland unit". For a further discussion of geology and development of shear strength parameters, see Sections 5 and 6, respectively. Formations located deeper than the Altamaha Formation are too deep to significantly affect slope stability.

The shear strength parameters were developed in Section 6.3. The layers designated Tobacco Road Formation 1 (TR-1) and Tobacco Road Formation 2 (TR-2) used in the ITP analysis in Section 7.2 are equivalent to the Upland 1 and Upland 2 layers at the HTF. The shear strength parameters used for the HTF analysis are given in Table 8.2-1

The fill is a relatively uniform clayey sand (Unified Classification SC), approximately 40 feet thick. A soft zone approximately 3 feet thick was encountered at the base of the fill similar to that found at ITP. The average CPT tip resistances for the weaker portions of the HTF (plus and minus 1 standard deviation) versus depth are plotted in Figure 8.2-5. Note that the tip resistance in Figure 8.2-5 are somewhat lower than those encountered at ITP (Figure 6.3-2).

### *8.2.4 Analyses*

#### *8.2.4.1 Static Factors of Safety*

All cross-sections were analyzed using total and effective shear strength parameters using the strength properties of the weakest fill encountered in the HTF. For static analyses, results assuming both effective and total shear strength parameters of the fill are reported in terms of minimum FS in Tables 8.2-2 and 8.2-3.

For the effective stress analysis, Cross-sections 1, 3, and 4 have adequate FS for the assumed conditions (see Table 8.2-2). Cross-section 2 displays unacceptably low FS.

For the total stress analysis, all cross sections have adequate FS for the assumed conditions (see Table 8.2-3).

#### *8.2.4.2 Pseudo-Static Factors of Safety*

Table 8.2-4 shows the minimum pseudo-static FS for a design horizontal acceleration of 0.2 g. Total stress strength parameters were reduced by 10 % to account for strain softening of the material during a seismic event (Makdisi, 1977). All cross sections analyzed have adequate FS for pseudo-static conditions.

#### *8.2.4.3 Seismically-Induced Slope Deformations*

As for ITP, earthquake-induced slope deformations were estimated following the method proposed by Makdisi and Seed (1978) using the same maximum crest acceleration, $k_{max}$, of 0.2 g. The minimum yield acceleration ($k_y$) for the HTF slopes was calculated to be 0.45 g. The ratio of the yield acceleration to the maximum crest acceleration ($k_y/k_{max}$) is therefore 2.75. The resulting seismically-induced deformation is negligible. As for the analysis performed for ITP, it should be noted that determination of the yield acceleration is performed only as an aid to estimate deformation and does not imply that the embankments are capable of sustaining the yield acceleration.

### *8.2.5 Conclusions*

Stability evaluations have been performed for the HTF slopes using the best estimate soil and loading conditions. To evaluate long-term static conditions, both total and effective stress soil strength parameters were used in the analysis. Short-term, or earthquake loading conditions, were evaluated using total stress strength parameters because dynamic pore pressures are unknown.

Effective stress parameters were derived from combining laboratory test results from CD and CU tests with pore pressure measurements. Total stress parameters were derived from combining laboratory test results of UU and CU tests with pore pressure measurements.

The groundwater is well below the fill and the surface of the fill is paved, there is very little potential for the fill to become saturated. Based on review of previous construction and recent laboratory test records, the fill has remained at nearly the same moisture content as when it was originally placed. Therefore, it is in an unsaturated state, and will remain so given the low groundwater level, the relatively low permeability of the fill material, and the surface cover.

It is therefore concluded that pore water pressures will not change appreciably during loading, for either the long-term or short-term case, and total stress strength parameters are more applicable than effective stress strength parameters for evaluating all loading cases of the HTF slopes.

As indicated in Table 8.2-5, the total stress analyses for the static and dynamic evaluations of the HTF slopes exceed the required minimum FS. Therefore, all slopes in HTF are considered stable under the present conditions. In the unlikely event that a significant portion of a slope at the HTF become saturated over an extended period of time, analyses indicate that all slope configurations are acceptably stable with FS of 1.4, or greater, except for the notched cross-section 3, which has an unacceptable FS of about 1.1. Because of the low potential for significant saturation to occur within the fill, it is judged that no remedial measures are necessary at this time.

## 8.3 Liquefaction and Dynamic Settlement

The primary strategy for evaluating the liquefaction susceptibility and settlement hazard at HTF is to compare the subsurface conditions at HTF with those found at ITP. If the HTF field investigation uncovered subsurface conditions that are similar to (or better than) those found at ITP, then the detailed 2D settlement analysis performed for the ITP tanks (Section 7.5) would not be necessary for HTF. This is based on the premise that the 2D settlement calculations performed for ITP will reasonably approximate those expected at HTF and thus are directly applicable for differential settlement evaluations of tanks located within HTF.

The CPT soundings performed for HTF show penetration resistances in the shallow strata that are similar to those of ITP (Section 5.3). Prior liquefaction analysis for ITP (Section 7.5) indicates that the TR3/TR4 layer is the layer with the lowest factor of safety against liquefaction. A

comparison of the CPT tip resistances for HTF and ITP for this layer shows a geometric mean and log normal distribution which are very similar (Figure 5.3-5). This suggests that the TR3/TR4 layer is relatively uniform throughout the southern part of H - Area. Based on this similarity, one can conclude a priori that liquefaction settlements for HTF will be similar to those of ITP.

However, as an additional check that the calculated liquefaction settlements at ITP and HTF are similar, a series of 1D liquefaction settlement analyses were performed using both ITP and HTF CPT soundings. If from these analyses, if it is found that the 1D liquefaction settlements for ITP and HTF are indeed similar, then the 2D differential settlements calculated in Section 7.5 are also applicable to HTF and the 2D settlement analysis for HTF could be precluded. The remainder of this section discusses the methodology used in calculating the 1D liquefaction settlement analysis for ITP and HTF.

The cyclic shear stress ratio and cyclic shear strain in the soil profile at ITP and HTF were calculated from SHAKE output using the 84th percentile compatible time history as the input motion (Section 8.1). Shallow shear wave velocity profiles (depth < 175 feet) were defined for both ITP and HTF based on average layer shear wave velocities from the appropriate SCPT's (Figures 5.1-3(a) and 5.1-3(b), respectively). For the deep shear wave velocity profile (depth > 175 feet), only one uncased borehole was drilled to basement rock in H-Area. This deep borehole, MMP-2-SB, is located just outside the southwest perimeter fence in the central part of the HTF (Figure 3.4-1). Shear wave velocities at this locale were logged through approximately 1,000 feet of unconsolidated, coastal plain sediments using the OYO™ suspension logger (Figure 3.4-2). The shallow ITP and HTF shear wave velocity profiles of Figures 5.1-3(a) and 5.1-3(b) were coupled with the deep profile at a depth of approximately 175 feet below ground surface (i.e., top of green clay). These composite profiles were used in the subsequent SHAKE analyses.

Because some of the SCPT soundings are located on top of the ITP and HTF embankment, while others were located at the base, cyclic shear stress ratio profiles were needed for both fill and non-fill cases. The shear wave velocity profiles described previously were used for the fill case in the SHAKE analysis. The shear wave velocity profiles used for the non-fill case were identical to those of the fill case, except that the fill layer was removed from the profile prior to performing the SHAKE analysis. The resulting cyclic stress ratio profiles for the fill and non-fill cases at ITP and HTF are presented in Figures 8.3-1 and 8.3-2, respectively. The ITP cyclic stress profiles (fill and non-fill) were completed using shear modulus and damping curves developed specifically for ITP for the shallow profile and similar curves proposed by Geotechnical Engineers Inc. (GEI, 1991b) at K - Reactor for the deep profile (Figures 8.3-3 and 8.3-4). Note that the GEI curves are really a suite of curves whose shear modulus and damping values are a function of confining pressure or depth below the ground surface. For HTF SHAKE analyses, the GEI curves were used for both the shallow and deep profile. For all cases, 5 percent spectral damping was assumed.

Peer reviewers raised the question about the sensitivity of the SHAKE and liquefaction settlement results to the inputted shear modulus and damping curves. This question stems from observed differences in the ITP damping curves when compared with the GEI curves (Figures 8.3-3 and 8.3-

4). Most notably, the ITP damping curves for the fill and non-fill indicate relatively high damping at low strain when compared to the GEI curves (Figure 8.3-4). Thus, it was reasoned that the higher damping values of the ITP curves may diminish ground motion in the shallow profile, thereby reducing the cyclic stresses and decreasing the calculated dynamic settlement. To assess this potential impact, two cases of shear modulus and damping curves were used in the SHAKE calculations for the ITP non-fill profile. Case 1 used the ITP modulus and damping curves for the shallow profile (i.e., for depths < 175 feet) and the appropriate GEI curves (1991b) for the deep profile. For Case 2, the GEI curves were used for both the shallow and deep profile. For both cases, 5 percent spectral damping was assumed. Figure 8.3-5 presents the results of this sensitivity analysis in terms of cyclic stress ratios. On average, the cyclic stress ratios for Case 2 are about 4 to 5 percent higher than those of Case 1. Liquefaction settlement analysis were also completed for these same profiles according to the methodology described below. The results for Cases 1 and 2 are shown in Figure 8.3-6 and tabulated in Table 8.3-1 for the ITP soundings without embankment fill. This table shows that the average liquefaction settlement increases by about 18 percent (0.025 feet) for Case 2. It was decided to use the GEI shear modulus and damping curves for the subsequent HTF liquefaction analysis, because they provide a slightly more conservative estimate of total settlement.

The 1D liquefaction susceptibility and settlement analysis for ITP and HTF used the general procedure outlined in Section 7.3.1.3. Using the liquefaction susceptibility curves shown in Figure 6.2-12, values of FS against liquefaction were calculated at each depth increment of the CPT sounding. The resulting volumetric strains due to complete liquefaction (i.e., FS 1.15) and partial liquefaction ($1.15 < FS \leq 2.2$) were accumulated throughout the profile for all soils below the water table and above the tan clay (i.e., above the DB4/DB5 layer). Figures 8.3-7 and 8.3-8 present the liquefaction settlement results for the ITP and HTF CPT's, respectively. These same results are tabulated in Tables 8.3-1 through 8.3-4.

Because the ITP non-fill CPT soundings (Table 8.3-1, Case 2) and the HTF non-fill CPT soundings (Table 8.3-3) were analyzed using GEI modulus and damping curves exclusively, one can make a direct comparison of these data. The average liquefaction settlement for the ITP non-fill CPT soundings is 0.1622 feet with a standard deviation of 0.1444 feet (Table 8.3-1). Likewise the average liquefaction settlement for the HTF non-fill CPT soundings is 0.1705 feet with a standard deviation of 0.1009 feet (Table 8.3-3). Thus, it was concluded that the average liquefaction settlement for the 84th percentile rock motion will be about 0.16 to 0.17 feet or 2 about inches. However, in these 1D settlement analyses, no allowance was made for possible 2D effects such as stress redistribution and arching; instead, all settlement at depth was assumed to propagate unmitigated to the surface. This 1D method will produce more conservative estimates of liquefaction settlement when compared with the 2D settlement analyses reported in Section 7.5.

In summary, the results of the 1D settlement analyses indicate that the subsurface soils at HTF and ITP have very similar penetration resistances and liquefaction settlement behavior. Hence, any dynamic settlement analyses (either 1D or 2D) performed for ITP is directly applicable to HTF.

## 8.4 Bearing Capacity

The bearing capacity of the H-Area tanks and Building 241-42H was evaluated utilizing standard practice, as outlined in Terzaghi and Peck (1967). Strength parameters utilized were based on laboratory and field test results and are given in Table 6.0-1(a). The results show that static FS is much higher than the criterion of 3.0 for the H-Area tanks and the Control Building.

Similarly, the dynamic incremental increase resulting from the design ground motions is less than 0.5 ksf. Resulting dynamic factors of safety for the H-Area tanks are all in excess of the criterion of 2.0.

## 8.5 Static Settlement

An extensive review was made of existing survey settlement data for the H-Area storage tanks by WSRC (1995). A summary of the tank settlements is presented in Table 8.5-1 and Figure 8.5-1.

Settlement surveys performed for Tanks 38 through 43 and Tanks 48 through 51 are historically complete and began well before these tanks were loaded with waste. However, a complete history of tank settlement is unavailable for 19 of the 29 tanks. Table 8.5-1 shows that after initial loading, gaps in the settlement surveys occur for periods ranging from 14 years to 20 years. The surveys for Tanks 29 through 32 were not begun until about 18 to 20 years after initial loading of the tanks, resulting in a total survey period of only about 3.3 years.

Figure 8.5-1 shows settlements for all 29 of the H-Area tanks. The maximum settlement that occurred during a survey period is shown with the cumulative settlement for all surveys performed for each tank. The actual cumulative settlement may be greater than indicated, as many survey records are incomplete. Consequently, the cumulative settlement serves as the minimum settlement that has occurred as of the survey performed on 15 March 1994. A maximum settlement that exceeds the cumulative settlement indicates the tank has rebounded during either a previous or subsequent survey period.

Also shown in Figure 8.5-1 are the estimated 30-year additional settlement and 30-year total settlement for each tank. In a few cases, an absolute settlement trend is eclipsed by insufficient survey information. Future settlement was estimated by extrapolating the most recent 1.5 to 6 years of settlement data. For most of the tanks, the waste volume has been fairly constant over the past 1.5 to 6 years. The initial loading of the waste storage tanks began from about 10 to 38 years ago. Given current tank loads, the upper bound for the projected 30-year additional settlement for 27 of the tanks is about 0.5 inch with Tanks 41 and 42 estimated at 0.75 inches.

The 30-year total settlement for Tank Nos. 35 and higher is estimated to range from about 1.5 to 2.75 inches, although the true total settlements for Tanks 35, 36, and 37 may be greater than indicated. The 30-year total settlement of Tanks 9 through 32, based on the field performance of Tank Nos. 38 and higher, and considering survey deficiencies, is estimated at 2.5 inches. Summarily, a 30 year total estimated settlement for 27 of the tanks is about 2.5 inches with Tanks 40 and 41 estimated to be about 2.75 inches.

# 9. PROBABILISTIC LIQUEFACTION ASSESSMENT AT THE ITP

## 9.1 Introduction

An evaluation of the liquefaction potential was performed using deterministic qualitative and quantitative procedures as outlined in Section 7.3. In that evaluation, best estimate soil properties, along with the EBE and the 84 percentile ground motions, were used in the analyses. Since the evaluation was based on deterministic methods, the effect of variability in soil properties and in earthquake motions on the liquefaction potential could not be integrated into the analysis. The purpose of the probabilistic evaluation presented here is to incorporate the effects of variation of the most significant soil properties and earthquake parameters and to evaluate the annual liquefaction hazard at the ITP site.

The evaluation is based on site-specific (ITP) subsurface data, the EPRI 1993 seismic hazard study (EPRI 1993) and a recently developed methodology for liquefaction hazard evaluation.

## 9.2 Methodology

The recently developed Advanced Seismic Hazard/Liquefaction Evaluation (ASHLE) method (Bechtel, 1991, Ostadan et al., 1991; Arango, I. and Ostadan, F., 1995) was used for the evaluation. In this method, the probability of liquefaction at a given site is obtained from

$$P_E(L) = P[L|E]\,P[E]$$

where $P_E$ (L) is the overall probability of liquefaction during the earthquake E; P[L|E] is the conditional probability of liquefaction given that earthquake E occurs; and P[E] is the probability that earthquake E occurs. The total overall probability of liquefaction is obtained by summing over all possible earthquakes:

$$P[L] = \sum_E P[L|E]\,P[E]$$

The ASHLE methodology used models for conditional probability of liquefaction developed by Liao, et al. (1988). The models were developed based on statistical analyses (logit analysis followed by likelihood maximization) of a data catalog consisting of 278 observed cases of liquefaction/no liquefaction in Holocene deposits during 40 earthquakes. The Liao model, known as the local model for silty sands, shown in Figure 9.2-1, was used as the basis for this evaluation. From this model, the probability of liquefaction can be obtained once the normalized SPT blow-count data $(N_1)_{60}$, and the normalized cyclic stress ratio (CSRN) are known. The normalized cyclic stress ratio is obtained from

$$CSRN = 0.65\,\frac{\tau_{max}}{\bar{\sigma}'_v}$$

where $\tau_{max}$ is the maximum seismic shear stress in the soil layer under consideration and $\sigma'_v$ is the corresponding effective overburden pressure. The normalization of CSRN is performed to correct for the magnitude (duration) of the earthquake motion, as will be discussed in Section 9.4.

For ASHLE analysis, in addition to the earthquake models, the normalized SPT blow-count data ($(N_1)_{60}$) and the normalized cyclic stress ratios (CSRN) for each level of the earthquake motion are required as input. The derivation of the input parameters is discussed in Sections 9.3, 9.4, and 9.5, while a more detailed description of the ASHLE computational steps is presented in Section 9.6.

## 9.3 Seismic Models

### *9.3.1 Introduction*

The current baselines for SRS seismic hazard are described in investigations conducted for EPRI and the DOE (EPRI, 1986; McCann, 1989) and for the NRC and DOE (LLNL, 1989, Savy, 1993). Discussion of expert elicitation and hazard methodologies and comparison of the results are contained in the Seismology Report (WSRC, 1994c). Briefly, methodologies employed for evaluation of rock hazard are equivalent. Any differences in estimated hazard are a result of differing opinions on seismic zonation, ground motion attenuation, differences in activity rates, and selection of maximum magnitude for the host seismic zones. The SRS studies show significant differences in the mean and median rock hazards. Application of the EPRI and LLNL hazard studies requires selection of one of the hazard curves or a more complicated combination of the studies (e.g., DOE-STD-1024).

In the course of investigating LLNL hazard studies for the nuclear plant Vogtle (DOE, 1995), consistent spectral values between EPRI and LLNL median rock uniform hazard spectra were discovered. The primary difference between the LLNL Plant Vogtle and LLNL SRS rock hazard is the result of differing assessments of the rate of seismicity in the SRS area sources (Kimball, personal communication). The differing assessments were probably related to the interest in the possible capability of the Pen Branch fault at the time of the LLNL SRS study. Since that study was completed, the Pen Branch fault has been assessed not to be capable (Stieve et al., 1994). Variability in the median and mean SRS rock hazard is now significantly reduced by application of the Plant Vogtle hazard results.

Both the EPRI and the LLNL (known as the LLNL 93 study) mean rock spectral hazard curves at 1.0 Hz and 2.5 Hz are shown in Figure 9.3-1. As shown in this figure, while the differences between the 1.0 Hz and the 2.5 Hz hazard curves are insignificant in each study, the LLNL results predict 3 to 4 times higher hazard compared to the EPRI results. The differences in these two results have been the subject of additional ongoing studies. For this liquefaction hazard evaluation, the EPRI data were used in the formulation. However, the impact of using LLNL data has been qualitatively assessed, (See Section 9.6.3).

### *9.3.2 Selection of Seismic Hazard Curve*

Use of the 2.5 Hz spectral hazard curve for liquefaction hazard evaluation was prompted from the results of an independent study by Costantino (1994). In that study, a series of seismic free-field ground response analyses were performed using a total of 32 time histories (real and artificial). The effect of frequency content of the input motion on the cyclic stress ratios induced in the Tobacco Road Soils was thoroughly examined using both high pass and low pass band filters on the input motion. The study concluded that "the important characteristic of the input rock outcrop motion which controls the development of the induced shear stresses in the Tobacco Road Soils is the low frequency content of this motion as measured by the average spectral acceleration from 1 to 3 Hz $[(S_a)_{1\text{-}3}]$."

Based on the finding of that study, it was decided that for the purpose of determining the CSRs in the Tobacco Road soil layers, the 2.5 Hz spectral Hazard Curves should be used as a basis to generate the artificial ground motions for the liquefaction hazard evaluation. The validity of Costantino's conclusion was also confirmed for the ITP site as will be discussed in Section 9.5. Thus, the 2.5 Hz EPRI hazard curve was used for this evaluation.

### *9.3.3 Selection of $M_{bar}$ and $D_{bar}$*

A point on the seismic hazard curve, shown in Figure 9.3-1, defines the annual probability of exceedance at a given ground motion level. This probability is calculated as the summation of the occurrences of ground motion exceedances over a range of source magnitudes and distances. Through a hazard deaggregation process, the explicit contributions to the total hazard may be obtained and displayed in space as earthquake magnitude and distance interval bins. A typical example is the deaggregation matrix for the 2.5 Hz (5 % critical damping) spectral velocity of 2.0 centimeters per second, as tabulated in the EPRI data (Table 9.3-1)

The central magnitude and distance bin values shown in the brackets are those given in the EPRI data file. Except for the last bin, the central magnitude values are the average of the bin ranges. The central distance values are nearly the mass center values (i.e., square root of $[0.5(r_0^2+r_1^2)]$), of the annulus represented by the distance radii $r_0$ and $r_1$, where $r_0$ and $r_1$ are the bin ranges of the distance as shown above for each bin. Explicitly, the distance intervals and the central distance values used in the EPRI deaggregation matrices are given in the Draft Regulatory Guide DG-1015, "Identification and Characterization of Seismic Sources, Deterministic Source Earthquakes, and Ground Motion," dated November 1992. As discussed in this reference, a controlling magnitude and distance are defined as probability-weighted central magnitude and distance corresponding to the given point on the hazard curve:

$$\text{Mbar} = \Sigma_m \Sigma_d \; m \, P_{md} \; / \; \Sigma_m \Sigma_d \, P_{md}$$

$$\log [\text{Dbar}] = \Sigma_m \Sigma_d \; \log [d] \, P_{md} \; / \; \Sigma_m \Sigma_d \, P_{md}$$

where $P_{md}$ is the relative contribution to hazard for each bin centered at magnitude 'm' and distance 'd'. For the above deaggregation matrix for 2.0 cm/s, the Mbar and Dbar values determined from

the above formulae, are 5.95 and 104.21 km, respectively. For other spectral velocities, Mbar and Dbar, along with the corresponding hazard, can be obtained from the EPRI data in Table 9.3-2.

Note that the Mbar values are described as being body wave magnitudes and the distance units are in kilometers, both as used in the EPRI study. The contribution of magnitude/distance bins to annual hazard for each of the eight spectral velocities are depicted in Figures 9.3-2 through 9.3-9 for the EPRI mean hazard data.

For subsequent steps, it was necessary to specify Mbar and Dbar at hazard levels or ground motion levels. Therefore, it was necessary to fit an equation (a polynomial function) to the Mbar and Dbar values to allow for such functionality.

The Polynomial fits to EPRI's Mbar and Dbar values as a function of pseudospectral velocity (PSV, in cm/s) or mean annual hazard (MAH) are as follows:

$$\text{Mbar(PSV)} = 5.7693 + 0.31483 \times \ln(\text{PSV}) - 0.025343 \times (\ln(\text{PSV}))^2$$

$$\text{Mbar(MAH)} = 4.2520 - 0.32933 \times \ln(\text{MAH}) - 0.011291 \times (\ln(\text{MAH}))^2$$

$$\text{Dbar(PSV)} = 115.86 - 10.582 \times \ln(\text{PSV}) - 1.9906 \times (\ln(\text{PSV}))^2$$

$$\text{Dbar(MAH)} = 174.18 + 9.9720 \times \ln(\text{MAH}) + 0.0071233 \times (\ln(\text{MAH}))^2$$

These functions are plotted and compared with the eight Mbar and Dbar EPRI data points in Figures 9.3-10 through 9.3-12.

In these figures, the EPRI hazard curve extends from 1 to 90 cm/s. Ten points spanning this range were selected such they are approximately equally spaced in a logarithmic scale. Using the above equations, the 10 (Mbar, Dbar) pairs are obtained and shown on Table 9.3-3.

For the above Mbar and Dbar pairs, rock acceleration response spectra were developed using region-appropriate seismic data. The resulting spectra were scaled so that the 2.5 Hz spectral amplitude matched that of the corresponding hazard curve point. Spectra development is discussed in the following section.

### *9.3.4 Spectra and Time History Development*

While there is a number of spectral attenuation relations and methodologies that could have been employed to develop the spectra, it was decided to be as consistent as possible with methodologies previously used for the SRS-ITP facility. For this reason, the computer program RASCAL (see Silva et al., 1987) was used. This program uses random vibration theory (RVT) to calculate peak acceleration, velocity, and response spectra for specified earthquake source and propagation path parameters (Boore, 1983).

Ten spectral shapes were generated using RASCAL with Mbar, Dbar, and the source and propagation parameters provided by Lee (1995) as listed below:

| | |
|---|---|
| Stress drop | 100 bars |
| Medium density at the source | 2.8 gm/cc |
| Source depth | 15 km |
| Shear wave velocity | 4 km/s |
| Quality factor, Q | 190 |
| Control frequency for Q factor | 1 Hz |
| Exponential constant for Q | 0.94 |
| Spectral damping | 5% |
| Fmax corner frequency | 0 Hz |
| Kappa | 0.006 sec |

As RASCAL uses Mw and the Mbar values obtained from the EPRI deaggregation matrices are body wave magnitudes (Mbar), it was necessary to convert the Mbar magnitudes to Mw magnitudes. One such relation between Mbar and Mw was made available by WSRC (EPRI, 1993):

$$Mbar = -10.23 + 6.105\ Mw - 0.7632\ M^2w + 0.03436\ M^3w$$

from which the following values are obtained:

**Conversion of $m_b$ to Mw for the 10 Mbar Points**

| Mbar ($M_b$) | Mbar (Mw) |
|---|---|
| 5.77 | 5.26 |
| 5.91 | 5.42 |
| 6.06 | 5.60 |
| 6.19 | 5.77 |
| 6.30 | 5.93 |
| 6.40 | 6.08 |
| 6.49 | 6.23 |
| 6.56 | 6.35 |
| 6.62 | 6.46 |
| 6.67 | 6.55 |

Figure 9.3-13 presents the 10 resultant scaled RASCAL spectra labeled E01 through E10. The spectra have been individually scaled so that the spectral values at 2.5 Hz maintain the appropriate spectral velocity, as defined by the EPRI mean 2.5 Hz spectral hazard curve. These spectra constitute the rock motion target spectra for which spectra-compatible time histories are generated for ground response analyses.

It may be noted that some of the target spectra in Figure 9.3-13 are high. For example, the spectrum with the 2.5 Hz spectral velocity of 90 cm/s requires a spectral acceleration greater than 4.3 g. However, the hazard level corresponding to these ground motions is about $3.5 \times 10^{-7}$, an extremely rare event.

The generation of spectrum-compatible time histories was performed by CCNY and were checked by WSRC according to the duration criteria given by ASCE 4-86 (ASCE, 1986) (see Figure 9.3-14) and the NRC Standard Review Plan (USNRC, 1990b). The acceleration time histories and their spectrum matching characteristics labeled as E01 through E10 are shown in Figures 9.3-15 through 9.3-34.

## 9.4 Engineering Properties and Parameters

For ground response analyses and liquefaction hazard evaluation, the soil properties consisting of the low-strain shear wave velocity, strain-dependent shear modulus and damping, and the insitu SPT blow-count data are required. Each is discussed in the following sections.

### *9.4.1 Shear Wave Velocity*

Low-strain shear wave velocity measurements from 10 SCPTs were used as input for the free-field seismic ground response analyses. The locations of the selected SCPTs are shown in Figure 9.4.1. These 10 SCPTs were selected over other nearby SCPTs because they were pushed deep enough to penetrate the Santee Formation and their locations are somewhat evenly scattered across the ITP site. A composite shear wave velocity profile for the 10 SCPTs is shown in Figure 9.4.2. Table 9.4.1 presents the average shear wave velocity, by layer, for these SCPTs, while Table 9.4.2 gives their respective layer thicknesses. Ultimately, the average shear wave velocities presented in Table 9.4.1 and the layer thicknesses reported in Table 9.4.2 were used in the ground response analyses to represent the variability of shear wave velocity in the upper 170 feet of the ITP subsurface profile.

To define the deep shear wave velocity profile (i.e., below 170 feet to basement rock), two P- and $S_H$-wave logged boreholes (Figure 9.4.3, Tables 9.4.3 and 9.4.4 ) were used from the central part of the SRS. These deep, uncased boreholes were drilled and logged by the OYO™ suspension logger through approximately 1,000 feet of unconsolidated coastal plain sediments and were completed in metamorphic basement rock. The two boreholes are: MMP-2-SB, which is just outside the southwest fence of the central part of the HTF (Figure 9.4-4), and CFD-18, which is from the confirmatory drill site about 3-4 miles south of H-Area .

To construct a complete shear wave velocity profile for ground response analyses, the deep shear wave velocity profiles from MMP-2-SB and CFD-18 were coupled with the 10 shallow SCPTs. The deep and shallow profiles were randomly selected, paired and used in the Monte Carlo type analyses described in Section 9.5.

### *9.4.2 Strain-Dependent Shear Modulus and Damping*

For these analyses GEI curves were used in the upper 170 feet as well as the deeper deposits and are presented in Figures 6.1-4 and 6.1-5, for damping ratio and shear modulus reduction, respectively.

### *9.4.3 SPT $(N1)_{60}$ Values*

The conditional probability of the liquefaction model discussed in Section 9.2 requires the normalized SPT blow count, $(N_1)_{60}$, as a measure of the soil's resistance to liquefaction.

Deterministic analyses show that the Tobacco Road Formation (i.e., TR3/TR4 layer) has the lowest FS against liquefaction (Section 7.3). Hence, the probabilistic liquefaction hazard analysis was restricted to SPT N-values from this layer.

Available boreholes at the ITP Facility include SPT boreholes drilled by WSRC as part of this investigation and by Mueser during the original foundation investigation discussed in Section 1.5. Four SPT boreholes were continuously split-spoon sampled by WSRC: H-SPT-14, H-SPT-18, H-SPT-20, and H-BOR-23.3 (Figure 9.4-5). However, because of numerous buried pipelines and other interferences, none of these newer boreholes were drilled in close proximity to the ITP tanks, but were located around the perimeter of the ITP facility at the base of the embankment (Figure 9.4-1). The WSRC boreholes were completed under a rigorous quality assurance program, which included prior measurement of the energy delivered to the safety hammer. (The hammer energy ratio was measured to be approximately 60 percent of the theoretical maximum (BSRI, 1993b).) Other SPT boreholes completed by Mueser at ITP include all boreholes beginning with a 241-12H prefix shown in Figure 9.4-1. Eight of these boreholes are located underneath the ITP tanks, which make the use of these data highly desirable for defining the subsurface conditions directly underneath the tanks. However, uncorrected SPT N-values from the Mueser boreholes have limited direct use for liquefaction susceptibility analyses, because the hammer type and hammer energy calibration, if performed, were not documented by Mueser.

To incorporate the Mueser SPT-N values in the geostatistical simulation described subsequently, an estimate of the efficiency of Mueser's hammer was needed. A review of all the SPT N-value data at ITP showed that Mueser's SPT N-values are 1.6 times higher, on average, than those performed by WSRC in the layer of interest (i.e., Tobacco Road Formation). This difference suggests that Mueser's hammer was less efficient, having an hammer energy ratio of approximately 37.5 percent (i.e., 60 percent / 1.6 = 37.5 percent). Hence, all Mueser SPT N-values were divided by 1.6 to convert these uncorrected SPT N-values to $N_{60}$ values. Subsequently, all $N_{60}$ values from Mueser and WSRC boreholes were normalized to $(N_1)_{60}$ using the relation:

$$(N_1)_{60} = N_{60}\, C_N$$

Where:

$$C_N = \sqrt{1/\sigma_o'}$$

$N_{60}$ is the blow count corrected to 60 % hammer energy and $\sigma_o'$ is the effective overburden pressure in tsf.

Several WSRC CPT's are also available near the ITP tanks (Figure 9.4-1); however, the use of this data is also somewhat problematic, because the probabilistic liquefaction model used in

ASHLE requires $(N_1)_{60}$ values as input. Normalized CPT tip resistances, $q_{c_1}$, were converted to $(N_1)_{60}$ values for all CPT's prior to simulation using the following relationship:

$$\left(q_{c_1}\right) = C_q \times q_c$$

Where $C_q=1.63(\sigma_v')^{-0.69983}$ is a best fit of the CPT relationship reported by Seed, Idriss, and Arango (1983). This was done using site-specific, regression formulas developed for each layer from using paired data from CPT and SPT boreholes.

One of the primary questions raised by the peer reviewers during the early phases of the ITP investigation was the sensitivity of the liquefaction results to potentially high variability in the subsurface soils at ITP. The liquefaction susceptibility and dynamic settlement analyses completed in Section 7.3 were done using best-estimate soil properties. The soil properties (e.g., CPT $q_{c1}$ and friction ratio) were interpolated (i.e., kriged) to a finite difference mesh to complete the liquefaction settlement analysis (Section 7.5.3.3.4). Kriging, like other interpolation schemes, tends to reduce or smooth variability by the local averaging that takes place. Thus, to better preserve and statistically model any local heterogeneity that may be near the ITP tanks, it was decided to perform a 3 dimensional geostatistical simulation of $(N_1)_{60}$ values underneath the tanks using all available penetration data (Rouhani et al., 1995). Geostatistical simulation was chosen over kriging for two reasons:

(1) In kriging, the goal is to provide a best local estimate, z*(u) of each unsampled value z(u). The statistical structure of estimated values, however, are quite different from the originally measured values. The spatial averaging tends to remove the true variability of measured values, which provides images that have been smoothed by the averaging. In simulation, the goal is to generate equally likely outcomes that have the same statistical structure as the original data. Therefore, the resulting global features (i.e., texture) and statistics of the simulated values, z(l), take precedence over local accuracy. The resulting images have the same texture as the real data and preserve local variability (Deutsch and Journel, 1992).

(2) For a given set of local data and conditioning statistics, kriging uses an interpolation algorithm which provides a single numerical model which is "best" in some local accuracy sense. Whereas, simulation provides many alternative numerical models, each of which is a good representation of the reality in some global sense. Hence, simulated results can be treated as equally-likely outcomes in Monte Carlo type analyses (Deutsch and Journel, 1992).

Four $(N_1)_{60}$ boreholes were geostatistically simulated, one for each of the four tanks (Figure 9.4-6) using all available penetration data (WSRC, Mueser, and CPT). Figure 9.4-7 shows the simulated results from Figure 9.4-6 superimposed on the measured $(N_1)_{60}$ values from Figure 9.4-5. In general, the simulated $(N_1)_{60}$ values appear to agree with the measured data both in trend with depth and in the amount of scatter, suggesting that a reasonable simulation has been performed. The measured, simulated, and combined $(N1)_{60}$ values for the Tobacco Road Formation (i.e., TR3/TR4 layer) are presented in Table 9.4-5. The histograms for these data and the fitted normal

distributions are shown in Figures 9.4-8 through 9.4-10. All three sets of $(N_1)_{60}$ values (measured, simulated, and combined) were used in the ASHLE analysis to investigate the sensitivity of the final results to the simulated values.

### *9.4.4 Cyclic Shear Strength Adjustment Factors*

As described in Section 9.4.2, the conditional probability of liquefaction models developed by Liao et al. (1988) are based on the statistical analysis of field data corresponding to Holocene deposits. For application to the ITP site, the model was modified to reflect the increased cyclic shear strength of the soils due to age, which includes adjustments for overconsolidation and sample disturbance. Those adjustments are discussed in the sections that follow.

The conservative, site-specific relationship between cyclic shear strength and cone tip resistance shown in Figure 6.2-12 is based on the laboratory testing of the ITP soil samples. The curves are normalized to a confining pressure of 1 tsf and an earthquake magnitude of 7.5. In addition, the curves are based on an overconsolidation ratio of 2 and no correction for sample disturbance.

An interpolated curve corresponding to 22.5 percent fines content (average for TR3 and TR4) is shown in Figure 6.2-12. To compare this curve with the curve developed by Seed et al. (1985) for Holocene deposits shown in Figure 9.4-11 it is necessary to express the CSRN in terms of normalized SPT N blow-count $(N_1)_{60}$, rather than in terms of normalized cone tip resistance $q_{c1}$. To this end, a site-specific relationship was developed relating $q_{c1}$ to $(N_1)_{60}$ for the Tobacco Road Formation as follows:

$$(N_1)_{60} = 0.285\ q_{c1} - 2.1399$$

or alternatively,

$$q_{c1} = 3.509\ (N_1)_{60} + 7.508$$

Based on this empirical relationship, the following tabulation can be prepared:

**Cyclic Stress Ratio for 22.5 Percent Fines**

| $q_{c1}$ (tsf) | $(N_1)_{60}$ | CSRN (1) (Figure 9.4-12) | CSRN (2) (Figure 6.2-12) | Ratio 2/1 |
|---|---|---|---|---|
| 20 | 3.6 | 0.10 | 0.145 | 1.45 |
| 30 | 6.4 | 0.13 | 0.182 | 1.40 |
| 40 | 9.3 | 0.162 | 0.216 | 1.33 |
| 50 | 12.1 | 0.192 | 0.250 | 1.30 |
| 60 | 15.0 | 0.23 | 0.300 | 1.30 |
| 70 | 17.8 | 0.28 | 0.360 | 1.29 |
| | | | Average | 1.35 |

As tabulated, the ratio of the increase in strength from the Seed Holocene curve to the site specific ITP curve is about 1.35. As further evidence of this strength gain, Seed and DeAlba (1986) derived the relationship between field CSR and modified cone tip resistance shown in Figure 9.4-12. A similar comparison of the stress ratio from Figure 9.4-11 with the conservative site-specific ITP values presented in Figure 6.2-12 results in the following ratio of strengths:

**Cyclic Stress Ratio for 22.5 Percent Fines**

| $q_{c1}$ (tsf) | CSRN (1) (Figure 9.4-12) | CSRN (2) (Figure 6.2-12) | Ratio 2/1 |
|---|---|---|---|
| 20 | 0.105 | 0.145 | 1.38 |
| 30 | 0.135 | 0.182 | 1.35 |
| 40 | 0.170 | 0.216 | 1.27 |
| 50 | 0.200 | 0.250 | 1.25 |
| 60 | 0.235 | 0.300 | 1.28 |
| 70 | 0.275 | 0.360 | 1.31 |
| | | Average | 1.31 |

Thus, confirming the cyclic strength curve adopted for the ITP site specific evaluation based on a conservative interpretation of the laboratory data shows it to be higher than the Holocene curve by a factor of about 1.35

### *9.4.4.1 Correction for Over-Consolidation Ratio of 3.0*

A modification to Liao's data is required to account for the effect of overconsolidation (i.e., the $C_r$ factors). As shown in Figure 9.4-13, an appropriate value for $C_r$, accounting for three-dimensional shaking effects is 0.64 for a conservative overconsolidation ratio estimate of 2 for the SRS site. Best estimate value of OCR for TR3 and TR4 at the SRS is 3 (see Figure 6.0-1), for which Figure 9.4-13 gives in $C_r = 0.70$. The corresponding correction factor for Liao's model would then be:

$$\frac{0.70}{0.64} = 1.09$$

#### *9.4.4.2 Correction for Sample Disturbance*

It is well established that sample disturbance affects the laboratory-derived estimate of cyclic shear strength of soil deposits. Strength losses of up to 30 % can be realized (Singh, Seed, and Chan, 1979). Currently, to be conservative, the effect of sample disturbance is ignored. If disturbance effects are taken into account as recommended by Singh et al. (1979), the corresponding correction factor to Liao's model is 1.3.

The combined correction factor to apply to Liao's model would vary from 1.35 (Section 9.4.4.1) to:

$$1.35 \times \frac{0.70}{0.64} \times 1.3 = 1.92, \text{ say } 1.9$$

For the subsequent liquefaction hazard assessment, both cyclic strength factors, 1.35 and 1.9, are used in the ASHLE analyses.

### *9.4.5 Cyclic Shear Strength Magnitude Correction Factors*

The magnitude scaling factors (MSF) developed by Seed and Idriss (1982) have been widely used. They are based on laboratory test data and statistical studies relating the number of significant strong motion cycles to earthquake magnitude. The reliability of these factors, however, has never been confirmed. Since publication of the magnitude correction factor by Seed and Idriss in 1982 which is based on laboratory data, several other studies have been performed which are based on various approaches including energy concepts (Arango, 1994), statistical (Loertscher, 1994), and seismologic (Ambraseys, 1988). They all suggest that the Seed and Idriss MSF are very conservative (overestimate the damaging effect) for small to moderate earthquakes (magnitudes less than 7) and underestimate the damaging effects for large earthquakes (magnitudes greater than 8). A comparison of the various relationships is shown in Figure 9.4-14. As shown in this figure, the curve recommended by Arango is in close agreement with that recommended by Ambraseys, both of which are more conservative than Loertscher. For the probabilistic liquefaction hazard evaluation, the magnitude correction factors derived by Arango were adopted. For free field settlement estimates utilizing the ten probabilistic motions, both the Seed and Idriss and Arango MSF were utilized. Arango's derivation is summarized below.

> "The maximum distance at which earthquake-induced liquefaction has occurred has been studied by several investigators including Kuribayashi and Tatsuoka (1975), Youd (1977), Davis and Berril (1983), Seed et al. (1984), and Carter and Seed (1988). Based on 125 case histories from places throughout the world, maximum distances for observed liquefaction as reported by Carter and Seed are

| *Earthquake Magnitude* | *Maximum Distance (km) for Observed Liquefaction* |
|---|---|
| 5.0 | 5 |
| 5.5 | 20 |
| 6.5 | 75 |
| 7.5 | 230 |
| 8.0 | 400 |
| 8.25 | 500 |

Presumably, soil deposits liquefying at great distances must consist of very loose sand. Davis and Berril (1983) considered these deposits to be near the ground surface with an SPT-N value somewhere between 1 and 5. Seed et al. (1984) suggest an $(N_1)_{60}$ value of about 4. Such loose deposits would probably be at a relative density somewhere between 30 and 40 percent which appears to be the loosest state encountered in young alluvial plain and lake deposits in nature.

Carter and Seed (1988) estimated the minimum ground accelerations for which liquefaction has been induced by earthquake shaking, as summarized below:

| *Earthquake Magnitude* | *Minimum Acceleration (g)* |
|---|---|
| 5.5 | 0.12 |
| 6.0 | 0.08 |
| 6.5 | 0.06 |
| 7.0 | 0.05 |
| 7.5 | 0.04 |
| 8.0 | 0.03 |
| 8.25 | 0.025 |

The values of the minimum accelerations were obtained by averaging the results of attenuation relationships presented by Orphal and Lahoud (1974), McGuire (1977), Cornell et al. (1979), Donovan and Bornstein (1974), Iwasaki et al. (1978), McGuire (1978), Battis (1981), and Hasegawa et al. (1981).

Based on the results of investigations carried out by Arango (1994), it was concluded that there does not seem to be any significant effect of the loading frequency on the pore pressure generation in stress-controlled tests. The magnitude of the stress ratio itself (which can be related to an equivalent acceleration level under field conditions) is the one variable controlling the number of cycles required to induce 100-percent pore pressure in a sand at a given density.

It was also shown in the same investigations that the kinetic energy of the earthquake waves depends on both the level of acceleration and the frequency, f, (or period, T) of the motion. Also, that the minimum unit energy required for liquefaction to take place in the field, for the magnitudes and distances considered, is nearly constant. Because the pore water pressure generation under repeated stress cycles is independent of the frequency of the loading, it followes that for the very loose deposits located at large distances, the following approximations are justified:

$$\left[(KE)_{M=Mi}\right] \times N_{Mi} = \left[(KE)_{M=Mi+1}\right] \times N_{Mi+1};$$

$$KE \propto (aT)^2 = (a/f)^2 \approx a^2;$$

$$\left[a^2 N\right]_{M=Mi} = \left[a^2 N\right]_{M=Mi+1};$$

$$N_{Mi} = N_{Mi+1} \times \frac{a^2{}_{M=Mi+1}}{a^2{}_{M=Mi}}$$

where KE stands for kinetic energy per cycle; M, $M_i$, $M_{i+1}$ are earthquake magnitudes; and $N_{Mi}$, $N_{Mi+1}$ are the numbers of stress cycles.

For the acceleration values obtained by Carter and Seed (1988), and the number of cycles usually accepted as being representative of magnitude 7.5 earthquakes ($N \propto 15$):

$$N_{Mi} = 15 \frac{a^2{}_{M=7.5}}{a^2{}_{M=Mi}}$$

Therefore, for other magnitudes:

| *Magnitude* (M) | *a* (g) | N |
|---|---|---|
| 5.5 | 0.12 | 1.5 |
| 6.0 | 0.08 | 4 |
| 7.0 | 0.05 | 10 |
| 7.5 | 0.04 | 15 |
| 8.0 | 0.03 | 27 |
| 8.25 | 0.025 | 40 |

The pairs of acceleration, a (g) and number of cycles N, from this table can be considered to be the field relationship between stress ratio and number of cycles required to reach 100-percent pore water pressure in a very loose sand deposit with $(N_1)_{60} \propto 4$. Field curves for denser soil deposits can be obtained using the empirical data for clean sands presented by Seed et al. (1984), and the relationship between $(N_1)_{60}$ and relative density, Tokimatsu and Seed (1984).

Seed et al.'s (1975) studies to derive the equivalent number of uniform stress cycles from irregular time histories, and the correlations of cyclic stress ratios causing liquefaction in different earthquakes developed by Seed and Idriss (1982) were based on the simple shear test data reproduced in Figure 9.4-15. Superimposed on this figure for comparative purposes are the field curves derived in this investigation for relative densities of 35 percent and 50 percent. It can be seen that the shapes of the field and the laboratory curves are similar, and that for a relative density of about 50 percent, the field-based curve implies stronger resistance against liquefaction for 15 or fewer cycles of loading.

To derive the cyclic strength required to reach liquefaction in the field under various magnitude earthquakes, Seed and Idriss (1982) suggested that the shape of the curve corresponding to 68-percent relative density (Figure 9.4-15) be taken as representative of the cyclic behavior of any sand. They further suggested 15 as the number of cycles corresponding to a magnitude 7.5 earthquake. Then, the relative values of the stress ratio required to cause liquefaction under any other number of cycles (or equivalently earthquakes) were expressed as the ratios of the ordinates of this curve, relative to the ordinate corresponding to 15 cycles. Thus, they found:

*Laboratory-Based Data*
*(Seed and Idriss, 1982)*

| *Earthquake Magnitude* | *Number of Representative Cycles* | *Relative Strength Against Liquefaction* |
|---|---|---|
| 8.5 | 26 | 0.89 |
| 7.5 | 15 | 1.00 |
| 6.75 | 10 | 1.13 |
| 6.0 | 5-6 | 1.32 |
| 5.25 | 2-3 | 1.50 |

Field-based data shown in Figure 9.4-15, on the other hand, suggest the following values:

*Energy-Based Data*
*(Arango, 1994)*

| *Earthquake Magnitude* | *Number of Representative Cycles* | *Relative Strength Against Liquefaction* |
|---|---|---|
| 8.25 | 40 | 0.63 |
| 8.0 | 27 | 0.75 |
| 7.5 | 15 | 1.00 |
| 7.0 | 10 | 1.25 |
| 6.0 | 4 | 2.00 |
| 5.5 | 1.5 | 3.00 |

In a study performed in 1988, Ambrasey's derived relative strength values by analyzing liquefaction data organized in groups corresponding to different earthquake magnitudes. His regression analyses defined bounding curves between cases of liquefaction and no liquefaction, and therefore, were not associated with any probability level. From those curves, relative strengths (i.e., MSF) were derived as follows:

| *Earthquake Magnitude* | *Relative Strength* |
|---|---|
| 8.5 | 0.44 |
| 8.0 | 0.67 |
| 7.5 | 1.00 |
| 7.0 | 1.30 |
| 6.0 | 2.20 |
| 5.5 | 2.86 |

A more rigorous look at the liquefaction data base using logistic approaches was recently reported by Loertscher (1994). Independent variables used by the author were the normalized blow count $(N_1)_{60}$, the CSR, and the earthquake magnitude. An equation was developed which relates the logit i.e., the odds of liquefaction (p) to no liquefaction (1-p), [logit p = ln p - ln (1-p)], to the three independent variables. Thus, the equation makes it possible to predict the probability of liquefaction occurrence. Curves with different probabilities of liquefaction were developed for various earthquake magnitudes. For a 32 percent probability of liquefaction, the author derived the following MSF to be used with the strength chart proposed by Seed et al. (1984).

***Magnitude Scaling Factors from Logistic Analyses by Loertscher (1994) (32-percent probability of misclassification)***

| *Earthquake Magnitude* | *Relative Strength* |
|---|---|
| 8.5 | 0.62 |
| 8.0 | 0.77 |
| 7.5 | 1.00 |
| 7.0 | 1.34 |
| 6.0 | 2.79 |
| 5.5 | 4.46 |

Figure 9.4-14 compares the relative strengths as derived by Seed and Idriss (1982); Ambraseys (1983); Loertscher (1994); and Arango (1994).

## 9.5 Free-Field Seismic Ground Response Analysis

Free-field ground response analyses were performed using the computer program SHAKE, (Idriss et al., 1992). In all SHAKE runs, the input motion was prescribed as outcrop at a depth of 960 feet below ground surface, corresponding to the top of rock in H-Area (See Section 5.0). Prior to these analyses, the effect of frequency content of input motion on the calculated CSR was investigated. For this evaluation, the shallow soil column associated with CPT 11 and the average shear wave velocity obtained for H-area was subjected to successive ground motions filtered at frequencies cutoffs of 60 Hz, 15 Hz, 5 Hz, and 3 Hz. The ground motions utilized were the ten time histories (E1 through E10) developed for the probabilistic analyses. The results in terms of cyclic stress ratio versus frequency are shown in Figure 9.5-1. As shown in this figure, the CSRs

are not significantly affected by the frequency contents of the input motion beyond 3 Hz, thereby, confirming the conclusion reached by Costantino (1994) for the RTF site.

Response analyses would theoretically include 10 soil columns (for the upper layers), two shear wave velocity profiles (for the deep soil layers), and 10 acceleration time histories, for a total of 200 separate computer runs. To reduce this number for each input motion, a total of 8 soil columns were randomly selected from the set of 10 soil columns: half of these were combined with the shear wave velocity profile associated with the confirmatory drilling site (Borehole CFD-18) and the other half were combined with the shear wave velocity profile obtained from the H-Area (Borehole MMP-2-SB). Table 9.5-1 shows the soil column cases analyzed, where E01 represents the lowest intensity motion (see Figures 9.3-15 and 9.3-25) and E-10 represents the largest intensity (see Figures 9.3-24 and 9.3-34). With this random selection, the number of SHAKE runs was reduced to 80. The results of the SHAKE analyses in terms of effective CSR at two depths within the TR3 and TR4 layers (the critical layer for liquefaction) were obtained. The effective CSR is defined as

$$CSR = 0.65 \times \frac{\tau_{max}}{\sigma'_v}$$

where $\tau_{max}$ is the maximum induced shear stress and $\sigma'_v$ is the initial effective overburden pressure at the depth where $\tau_{max}$ is computed. The SHAKE analyses results are shown in Table 9.5-2. The mean values of the results corresponding to each time history were calculated assuming both a normal and a lognormal distribution of the CSRs. The histograms of the CSRs corresponding to each input motion (E1 through E10) are shown in Figures 9.5-2 through 9.5-11.

## 9.6 ASHLE Analyses and Results

### *9.6.1 Analysis*

For application to ITP, the program ASHLE was modified to incorporate the following features.

1. Read in deaggregated seismic hazard data from both the EPRI spectral hazard curves. These data eliminate the need to perform seismic hazard analysis in ASHLE.

2. Read in the CSR for each level of input motion that were obtained from the free-field seismic response analysis (see Section 9.5).

3. Provide an option for correction of cyclic stress ratio (CSR) to the corresponding normalized cyclic stress ratio using the magnitude correction factor ($r_m$) from Arango (1994). The following relationship is used:

$$CSRN = CSR/r_m$$

4. Provide an option to use an adjustment factor (AF) to apply to cyclic stress ratio as discussed in Section 9.4. The following relationship is used:

$$SRN_{SRS\text{-}ITP} = CSRN_{Holocene} \times AF$$

Having obtained all the necessary input data, the modified ASHLE program follows the steps shown below to compute the liquefaction hazard.

Given an evaluation of the probability of liquefaction conditional upon the occurrence of a seismic event, $P[L|E_i]$, and given the annual probability that that seismic event occurs, $P[E_i]$, ASHLE computes the joint probability, the annual probability of liquefaction, by summing over all events $E_i$:

$$P[L] = \sum_i P[L|E_i] * P[E_i]$$

Conventional seismic hazard evaluations consider the annual probability of exceeding a given ground motion level v by $P[V>v]$ where V for the current study is the mean 2.5 Hz rock spectral velocity for 5 % critical damping. A hazard curve is defined by a discrete set of $v_i$ values, such that the hazard curve is given by $P[V>v_i]$.

Basically, each point along the hazard curve is the composite contribution of all seismic sources as represented by modeled magnitude frequency and spatial distribution. The uncertainty in the seismic input is modeled by considering various weighted contributions of different seismic model and ground motion attenuation parameters and/or their distributions. During the hazard calculation, the hazard contribution within specified magnitude intervals and distance intervals may be deaggregated (such that the hazard at a given ground motion level may be deaggregated) forming a deaggregation matrix for ground motion $v_i$, $P[V>v_i, m_j, r_k]$ where $m_j$ and $r_k$ are representative central values of the magnitude and distance bins, respectively. It may be noted that:

$$P[V > v_i] \approx \sum_m \sum_r P[V > v_i, m_j, r_k]$$

For the modified ASHLE methodology, the sum over distance r is no longer necessary since the 10 rock motions developed have included the effect of distance in the computation. For each ground motion, $v_i$, deaggregation over magnitude, $P[V>v_i, m_j]$, is used where:

$$P[V > v_i, m_j] \approx \sum_r P[V > v_i, m_j, r_k]$$

What is required for the liquefaction hazard estimation is the probability of a given ground motion level for which the Liao conditional probability of liquefaction can be determined. Seismic hazard, however, is presented as a probability of exceedance. What can be determined from the seismic hazard curve, however, is the probability of the occurrence of a ground motion level within a given interval, say between $v_i$ and $v_{i+1}$:

$$P[v_{i+1}>V>v_i] = P[V>v_i] - P[V>v_{i+1}]$$

The seismic hazard matrix that quantifies probability of exceedance, may be operated upon, as shown above, to develop a seismic hazard matrix that quantifies probabilities of ground motion intervals:

$$P[v_{i+1}>V>v_i, m_j] = P[V>v_i, m_j] - P[V>v_{i+1}, m_j]$$

In ASHLE, it is assumed that the ground motion interval $v_{i+1} > V > v_i$ may be represented by a central value $\bar{v}_i$, which is defined as the log mean of the bounding values, or

$$\bar{v}_i = \exp\left(\left(\ln(v_i) + \ln(v_{i+1})\right) / 2\right)$$

so that from the two equations above a deaggregation matrix that approximates an annual probability of occurrence can be obtained.

$$P\left[V = \bar{v}_i, m_j\right] = P\left[v_{i+1} > V > v_i, m_j\right]$$

The ground motion $\bar{v}_i$ is used as input into the CSRN function, and subsequently into the Liao conditional probability:

$$P\left[L|CSRN\left(\bar{v}_i, m_j\right), (N_1)_{60}\right]$$

In Section 9.5, the relationship between the CSR($\bar{v}_i$), and the intensity of ground motion, $v_i$, specifically for the Tobacco Road was established. The normalized CSR function is determined by the MSF $r_m$:

$$CSRN\left(\bar{v}_i, m_j\right) = CSR\left(\bar{v}_i\right) / r_m\left(m_j\right)$$

Therefore, the probability of liquefaction is the joint conditional probability of liquefaction given a seismic event and the annual probability of that event, summed over all events:

$$P[L] = \sum_{i,j} P\left[L \mid CSRN\left(\bar{v}_i, m_j\right), (N_1)_{60}\right] * P\left[V = \bar{v}_i, m_j\right]$$

The above equation is the primary formulation used in the ASHLE methodology. In addition to the above relationship, additional features that were incorporated into the program include;

1. Use of statistical distributions of the site-specific CSR function are also allowed. Several model runs were performed to develop the SRS site-specific CSR as a function of input ground motion, as well as a single one-to-one mapping of input ground motion with an equally-weighted distribution set;
2. Further, mean and log-mean statistics were performed on the modeling results to allow for consideration of normal and log normal distributions, where weights are normal distribution probabilities on the value or log value, as appropriate. Hence, upon choice of the desired distribution (discrete, normal, or log normal), an additional summation is added to the preceding equation to consider the weighted ($[W_{CSRN}]_k$) hazard contribution by the chosen distribution of CSR values; and

3. Similar to that for CSR, discrete, normal, or log normal distributions of the blow-count, $(N_1)_{60}$, values were considered. Similarly, an additional summation is added to the relation in the preceding equation to consider the weighted ($[W_{N160}]_l$) hazard contribution by the chosen distribution of $(N_1)_{60}$ values.

The options described above lead to a generalization of the liquefaction hazard formulation in:

$$P[L] = \sum_{i,j,k,l} P\left[L|CSRN_k\left(\bar{v}_i, m_j\right), \left((N_1)_{60}\right)\right] * P\left[V = \bar{v}_i, m_j\right] * [W_{CSRN}]_k * [W_{N160}]$$

Note, that the weights $[W_{CSRN}]_k$ and $[W_{N160}]_l$ each must sum to 1.0. This equation is the basis for computing the liquefaction hazard at the site. The numerical steps discussed above in the ASHLE program are shown in Figure 9.6-1.

### *9.6.2 Results*

Using the EPRI deaggregated hazard data corresponding to 2.5 Hz hazard curves, the normalized SPT $(N_1)_{60}$ data (histogram, normal, and lognormal distributions) presented in Section 9.4, the CSRs (histograms, normal, and lognormal distributions) discussed in Section 9.5, a series of ASHLE analyses were performed. The results are shown in Figure 9.6-2. As shown in this figure, the results are not sensitive to the use of either measured, simulated, or combined $(N_1)_{60}$ data. The results change, however, from $5x10^{-6}$ to approximate to $2.5x10^{-6}$ once the shear strength factor changes from 1.35 to 1.9. The cluster of nine data points shown in each group of results in Figure 9.6-2 is due to the combination of various cases from three distributions of CSR and $(N_1)_{60}$ data (histogram, normal, and lognormal distributions) indicating the liquefaction hazard is insensitive to statistical characterization of CSR and $(N_1)_{60}$ values.

### *9.6.3 Qualitative Comparison of EPRI and LLNL Hazard*

The LLNL seismic hazard data were not used rigorously for liquefaction hazard evaluation. However, based on the hazard curves presented in Figure 9.3-1 and for the same spectral velocity, the LLNL results show a seismic hazard level approximately 3 to 4 times higher than the EPRI results. It is expected that for a given spectral velocity, the Mbar and Dbar from the two studies would result in different spectral shapes. The differences are expected to be very small with the frequency range of interest (1 to 3 Hz) when the spectra are scaled up to the respective 2.5 Hz velocity level. Therefore, given the linear relationship between the annual liquefaction hazard and the seismic hazard, an increase from 3 to 4 times in liquefaction hazard is expected if LLNL hazard data is used. Using the shear strength factor of 1.0 and the results shown in Figure 9.6-2, the LLNL seismic hazard is expected to result in a liquefaction probability in the range of $6 \times 10^{-6}$ to less than $1 \times 10^{-5}$.

## 9.7 Parametric Liquefaction Settlement Analysis

Deterministic liquefaction settlement analyses were also completed for the 10 response spectra (Figure 9.3-13) using the results of the 80 SHAKE analyses and their respective CPT soundings

(Table 9.5-1). The goal of the parametric study was to determine at what level of ground motion does liquefaction settlement become potentially large enough so as to pose a potential danger to the ITP tanks.

Consistent with the combinations given in Table 9.5-1, liquefaction settlement analyses were performed on the respective CPT soundings using the 1-D liquefaction settlement methodology described in Section 8.3. Different cases were analyzed using the MSF discussed in Section 9.4.5 and the combined shear strength correction factors of 1.35 and 1.9 (Sections 9.4.4.1 and 9.4.4.2). In all but the most conservative case (i.e., Seed and Idriss MSF and shear strength correction of 1.35), these analyses show that liquefaction is triggered by ground motion that equals or exceeds that represented by E07. However, at this level of motion, liquefaction settlement appears to be acceptably small (a few inches or less). Also, in all but the most conservative case, unacceptably large liquefaction settlement does not occur until ground motion equals or exceeds that represented by E08.

In addition, a deterministic liquefaction analysis utilizing a 5 to 10 Hz, probabilistic-scaled, earthquake spectrum shows that liquefaction will not occur. This spectrum was determined by a combination of the EPRI and LLNL 94 hazard studies (Section 2.1) and meets the recommendation for a PC4 seismic criteria (DOE, 1995).

## 9.8 Conclusions

Utilizing the EPRI hazard curve at a frequency of 2.5 Hz and site-specific as well as simulated $(N_1)_{60}$ data, the probabilistic liquefaction hazard analyses shows the probability of liquefaction is less than $1 \times 10^{-5}$, which meets the performance goal ($1 \times 10^{-5}$) for Performance Category (PC-4) (DOE, 1993a).

Deterministic free-field liquefaction analysis using the 84th percentile ground motion shows that average settlements for ITP and HTF are both about 2 inches.

Best-estimate deterministic liquefaction analyses for ITP using the 10 probabilistic-based earthquakes shows the threshold for liquefaction to be between earthquake E07 and E08, depending on the input assumptions. These same analyses show that liquefaction will not occur for a PC4 event.

Thus, both deterministic and probabilistic liquefaction analyses for ITP and HTF meet PC-4 performance goals.

# 10. SUMMARY

Field, laboratory, field performance data, geological, seismological, and geotechnical engineering investigations have been completed which provide the necessary data for evaluating the performance of the subsurface soil materials around and beneath ITP and the HTF under both static and dynamic loads. The subsurface conditions were characterized based on a series of investigations which included: boreholes, cone penetrometers, dilatometer soundings, geophysical surveys, cross-hole seismic surveys, surface seismic surveys, field performance data, laboratory testing and utilizing data from previous studies at the SRS. The results of these evaluations, together with geotechnical engineering analyses, are presented in this report and are summarized as follows.

## 10.1 Soil Spectra

The ITP project was initiated based on the use of the EBE spectra providing the same level of conservatism as that applied at K-Reactor. The EBE spectra were based on prior evaluations conducted for the RTF using site-specific K-Reactor spectra and spectral scaling prescribed by DOE-STD-1024 (DOE, 1992b) (Section 2.1). In a parallel investigation with the ITP and HTF geotechnical tasks, an assessment was made of differences in site response between K-Reactor and ITP. These differences, together with a concern over the degree of conservatism of the longer period portion of the distant EBE spectrum, resulted in a new analysis of the distant spectrum. The EBE distant spectrum was compared to the ITP site-specific distant 50th and 84th percentile predicted motions. These spectra indicated that the EBE distant spectrum is in excess of the 50th percentile and less than the 84th percentile deterministic ground motions (the EBE distant rock spectrum is approximately the 60th percentile of the deterministic motion) (Section 2.3).

Until new performance/hazard guidelines are issued (DOE-STD-1023, DOE, 1994), the scaled local and 84th percentile deterministic spectra are recommended for engineering evaluations of foundation materials. Evaluations of structures are to use envelopes of the scaled local and 84th percentile deterministic spectra (Section 2.4).

## 10.2 Calcareous Lithofacies and Soft Zones

The calcareous lithofacies in the GSA is discontinuous, but confined to three distinct stratigraphic horizons of different ages and depositional settings (Section 2.5). The carbonate buildups appear to be oriented northeast-southwest, paralleling the strike of the coastal shoreline at the time of deposition.

The soft zones encountered during drilling typically occur in the carbonate-rich sediments in the Santee Limestone, Utley Limestone, and Griffins Landing Member of the Dry Branch Formation (Section 5.2). They are associated with, and commonly occur below, well-cemented silicified units (hard grounds). The hard grounds and underlying soft zones were probably formed in the time

frame of the development of the unconformity at the end of Santee time (40-43 mybp), in proximity to the water table existing at the time. It appears that the soft zones are sediment-filled, most likely with fine-grained sand. It is believed that the soft zones are small (averaging about 2 to 4 feet in thickness and 10 to 20 feet in lateral extent), not connected, and of limited lateral extent (Section 5.2). Also, areas of vugular porosity (void areas or suspect zones) may exist. At six CPT locations in the HTF, CPT signatures ($q_c$<3 tsf, $f_r$<1 tsf and near-hydrostatic pore pressure), indicating possible void or suspect zones were noted. In all cases, however, shear wave velocities indicated the size of the suspect zones are limited.

## 10.3 Faulting

Detailed stratigraphic data suggests vertical displacement of the ITP profile near the carbonate body found on the eastern side of ITP (Section 5.4). Similar faulting has also been observed in the GSA near other carbonate bodies. The association of these features with carbonate sediments has three possible causal mechanisms. The first alternative suggests unraveling and local slumping of the sediments above carbonate buildups where differential dissolutioning and subsequent compaction of the carbonate interval occurred. The second alternative postulates that Eocene or post-Eocene faulting caused preferential dissolutioning of carbonate and increased displacement along these faults in a pre-determined manner. The third mechanism is a combination of the first two. All three alternatives appear plausible at this time near ITP (Section 5.4).

## 10.4 Slope Stability

Slope stability analyses for the embankment fill were completed for static and pseudo-static conditions. The results of the analyses show that the embankment slopes are stable under all conditions analyzed. Predicted deformations of the slopes are negligible. Reduced-strength analysis shows the slopes will remain stable far beyond EBE events (Section 7.2).

## 10.5 Liquefaction

The liquefaction potential of the soils at the site was evaluated both qualitatively and quantitatively (Section 7.3). The results showed that neither the Tobacco Road nor Dry Branch Formations are susceptible to liquefaction for the EBE or the 84th percentile motion distant spectrum. Measured shear wave velocities, grain size, and plasticity results from each formation show that potential for seismic liquefaction is very low. Quantitatively, both the stress and strain approaches (Sections 7.3.2.3 and 7.3.2.4, respectively) show that the potential for seismic liquefaction in the Tobacco Road, Dry Branch, and Santee/Tinker Formations is negligible.

For the soils underlying ITP, cyclic shear strengths determined from the laboratory test program show an increase in liquefaction resistance with increasing fines content. Also, CPT penetration resistances in these same intervals show a tendency to decrease with increasing fines content,

suggesting that sands with a significant amount of fines also exhibit a more plastic behavior (i.e., less resistance to shear). Thus, it was concluded that lower penetration resistances typically found in the Tobacco Road sands at ITP are not necessarily indicative of a decrease in liquefaction resistance. On the contrary, these zones of lower penetration resistance probably result from an increase in clay content, which has been shown by the testing program to produce a higher resistance to liquefaction (Section 6.2.2.3).

The probabilistic liquefaction hazard analysis has shown that the annual probability of liquefaction at ITP is low, ranging from $1 \times 10^{-6}$ to $1 \times 10^{-5}$ (Section 9.6.2). Statistical analyses also show that the soils in the balance of HTF are very similar to those at ITP (Section 5.3) and have about the same liquefaction susceptibility (Section 8.3). Thus like ITP, the probability of liquefaction in the HTF is also low.

## 10.6 Settlement

An assessment of tank settlement was performed using actual measured performance data. Based on evaluation of this data and analyses, it is concluded the soils at ITP and the HTF are overconsolidated and large continuous soft zones do not exist (Sections 7.5.2 and 5.3). Thus, tank foundation settlement was evaluated considering dynamic settlements due to all three ground motions, additional static settlement due to fluid loading in the tanks during operation, and long-term secondary settlement (Section 7.5). Thus, the existing tank settlement and computed best-estimate results are summarized below:

| | *Settlement, inches* | |
|---|---|---|
| *Condition* | *Total* | *Differential* |
| Existing | 1.75 | 0.5 |
| Increased loading and secondary consolidation | 1 | 0.5 |
| Dynamic: | | |
| -Local EBE | 0.2 | 0.1 |
| -Distant EBE | 0.7 | 0.35 |
| -Distant 84$^{th}$ | 1.5 | 0.75 |

Therefore, for the recommended 84th percentile ground motion, the total tank settlement will be about 4¼ inches with a differential settlement (edge to edge) of 1¾ inches (Section 7.5.2).

## 10.7 Bearing Capacity

Both static and dynamic FS against bearing capacity failure for the tanks were all in excess of the evaluation basis criteria (Section 7.4). Thus, bearing capacity failure of the tanks is not expected for the conditions analyzed.

# 11. CONCLUSIONS AND RECOMMENDATIONS

The combined seismically-induced total settlement expected to be caused by the EBE and the 84th percentile motion for the H-area tanks, taking all of the investigated strata into account, is about 4¼ inches with a differential settlement of 1¾ inches. However, it is recommended that subsequent structural analyses be performed using a differential settlement across the tanks of 2 inches.

No additional characterization or analysis is recommended. It is recommended, however, that all tanks in the HTF continue to be periodically monitored for settlement. Settlement results should be compiled and reviewed by competent geotechnical and structural engineers. Trigger values of settlement (static and dynamic) should be established to signal when additional analysis and/or action should be initiated.

## 12. REFERENCES

Aadland, R.K., M.K. Harris, C.M. Lewis, T.F. Gaughan, and T.M. Westbrook, (1991), "Hydrostratigraphy of the General Separations Area, Savannah River Site (SRS), South Carolina," USDOE Report WSRC-RP-91-13, Savannah River Laboratory, Aiken, SC.

Ambraseys, N. N. (1988), "Engineering Seismology," Earthquake Engineering and Structural Dynamics, Vol. 17.

Arango, I., Lewis, M. R., and Kimball, J. K. (1994, in press) "Seismic Liquefaction-Field Performance Data and the SPT: Review and Commentary on Their Bases and Limitations."

Arango, I., (1994), "Methodology for Liquefaction Potential Evaluation of Sites East of the Rockies," Bechtel Corporation, Technical Grant, June.

Arango, I. and F. Ostadan, (1995), "Qualification of Liquefaction Hazard and Its Application to Risk Assessment and Urban Zoning," 5th International Conference on Seismic Zonation, Nice, France, October.

ASCE, 1986, American Society of Civil Engineers Standard 4-86, "Seismic Analysis of Safety-Related Nuclear Structures and Commentary on Standard for Seismic Analysis of Safety Related Nuclear Structures," September, 1986.

ASCE, 1994, Ground Failures Under Seismic Conditions, Geotechnical Special Publication No. 44, published by American Society of Civil Engineers, 345 East 47th Street, New York, New York, 261 p.

ASTM (1988), American Society for Testing and Materials Annual Book of ASTM Standards, Vol. 4.08 Soil and Rock, Building Stones; Geotextiles.

Bandyopadhyay, K., (1994), "Savannah River ITP Justification for Continued Operations and Evaluation Basis Ground Motion," Letter from Kamel Bandyopadhyay to Dinesh Gupta 9/14/94, 4pp.

Bartlett, S. F., and Youd, T. L., (1995), "Empirical Prediction of Liquefaction-Induced Lateral Spread," Journal of Geotechnical Engineering, Vol. 121, No. 4, Apr. 1995.

Battis, J., (1981) "Regional Modification of Acceleration Functions," Bulletin of the Seismological Society of America, Vol. No. 71, pp. 1309-1321.

Bechtel, (1989) "Replacement High Level Waste Evaporator," October 27.

Bechtel Corporation (1991), Advanced Seismic Hazard/Liquefaction Evaluation (ASHLE), San Francisco, California.

Bechtel (1992) "Civil-Structural Design Guide, Seismic Analysis of Structures and Equipment for Nuclear Power Plants," Design Guide C-104, Rev. 0, December, 1992.

Bechtel Savannah River, Inc. (1993a), "Savannah River Site, H-Area In-Tank Precipitation Facility, Geotechnical Investigation Report, Preliminary Assessment (U)," March, 1993.

Bechtel Savannah River, Inc. (1993b), "Savannah River Site, Replacement Tritium Facility (RTF-Bldg. 233H) Geotechnical Investigation (U)," WSRC-RP-93-606, April, 1993.

Bishop, A.W., and Henkel, D.J., (1957) The Measurement of Soil Properties in the Triaxial Test. Edward Arnold (Publishers) Limited, London.

Blume, John A., & Associates, (1971) "Savannah River Plant Areas 200H and 200F Radioactive Waste Storage Tanks, Subsurface Geologic Investigations," August, 1971.

Boore, D. M., (1983), Stochastic Simulation of High-Frequency Ground Motions based on Seismological Models of the Radiated Spectra. Bull. Seism. Soc. Am., v.73, n. 6, 1856-1894.

Boore, D. M., (1985), The Effect of Finite Bandwidth on Seismic Scaling Relationships. Submitted for Publication in the Proceedings of the 5th Ewing Symposium, Harriman, New York.

Carter, D. P. and H. B. Seed, (1988), "Liquefaction Potential of Sand Deposits Under Low Levels of Excitation," Report No. UCB/EERC-88/11, August. College of Engineering, University of California, Berkeley, California, page 119.

Chan, C.K., (1993), "GEOROBOT Program," Rev. 0, Version 5.2, Feb. 17, 1993.

Colquhoun, D. J., J. Rine, D. Siron, M. P. Segall, M. P. Katuna, and A. D. Cohen, (1994), Sedimentology and Stratigraphy of the Upland Unit: Final Report, SCUREF Cooperative Agreement Task Order No. 119.

Colquhoun, D. J., Woollen, I.D., Van Nieuwenhuise, D.S., Padgett, G.G., Oldham, R.W., Boyland, D.C., Bishop, J.W., and Howell, P.D., (1983), "Surface and Subsurface Stratigraphy, Structure and Aquifers of the South Carolina Coastal Plain," Report to the South Carolina Department of Health and Environmental Control, Ground Water Protection Division, Office of the Governor, State of SC.

Constantino, C. J., (1994), "Results of Recent Sensitivity Studies for the Savannah River RTF Site Subjected to the Loma Prieta and Artificially Generated Rock Outcrop Time Histories," Letter to J. Kimball from C. Costantino, January 27, 1994.

Constantino, C. J., E. Heymsfield, and Y. T. Gu, (1991), "Site Specie Estimate of Surface Ground Motions for the K-Reactor Site, Savannah River Plant," Report No. CEERC-91-003, Department of Civil Engineering, City College of New York, New York.

Cornell, C. A., and A. F. Shakal, (1979), "Seismic Motion and Response Prediction Alternatives," Journal of Earthquake Engineering and Structural Dynamics, No. 7, pp. 295-315.

D'Appolonia (1982), "Balance of Plant Geotechnical Report, Defense Waste Processing Facility 200-S Area Savannah River Plant South Carolina," Project No. 76-372, Jan., 1982.

D'Appolonia (1979a), "Site Comparison Report, Defense Waste Processing Facility Savannah River Plant," Project No. 76-372-K3, Oct., 1979.

D'Appolonia, (1979b) "Defense Waste Processing Facility, Area 200-S."

Dall, W. H., and G. D. Harris, (1892), "Correlation Papers Neocene," U. S. Geological Survey Bulletin 84, pp. 107-111.

Dames & Moore (1968) "Report, Preliminary foundation investigation, Barnwell Nuclear Fuel Plant," Allied Chemical Corporation, in Bechtel Corporation Barnwell Nuclear Fuel Plant Safety Analysis Report, Appendix D.

Davis, R. O. and J. B. Berril, (1983),"Comparison of a Liquefaction Theory with Field Observations," Geotechnique, Vol. 33, No. 4, pp. 455-460.

De Alba, P., (1975), "Determination of Soil Liquefaction Characteristics by a Large-Scale Test." University of California, Berkeley.

Department of Energy (1990), "Design and Evaluation Guidelines for Department of Energy Facilities Subject to Natural Phenomena Hazards," UCRL-15910, June, 1990.

Department of Energy (1992a), "Guidance for Geotechnical Studies, Systematic Evaluation Program," Department of Energy Non-Reactor Nuclear Facilities Under Cognizance of Defense Program, DOE Order 6430.1A October, 1992.

Department of Energy (1992b), General Design Criteria, DOE Standard 1024. "Guidelines for Use of Probabilistic Seismic Hazard Curves at Department of Energy Sites," Washington, D.C.

Department of Energy (1993), "Seismic Design and Evaluation Guidelines for the Department of Energy High-Level Waste Storage Tanks and Appurtenances," Department of Nuclear Energy, Brookhaven National Laboratory, Associated Universities, Inc. Upton, New York, Developed under DOE contract # DE-AC02-76H00016.

Department of Energy (1993a), "Natural Phenomena Hazards Mitigation," DOE Order 5480.28, January 15, 1993.

Department of Energy (1994), Natural Phenomena Hazards Assessment Criteria, Draft DOE Standard 1023. Washington, D.C., November, 1994.

Department of Energy (1995), Revised Performance Category 4 Seismic Acceptance Criteria, letter from S.D. Richardson to A.B. Scott, 12/27/94, 15p. Includes attachment of letter from J. Kimball to R. Erickson on Evaluation Basis Earthquake for Savannah River Site H Tank Farm/In-Tank Precipitation Facility.

Deutsch, C.V., and Journel, A.G., (1992) "Geostatistical Software Library and User's Guide," Oxford University Press.

Dobry, R., R. S. Ladd, F.Y. Yokel, R.M. Chung, and D. Powell, (1982) "Prediction of Pore Water Pressure Buildup and Liquefaction of Sands During Earthquakes by the Cyclic Strain Method," NBS Building Science Series 138, U.S. Department of Commerce, National Bureau of Standards, July, 1982.

Donovan, N. C. and A. E. Bornstein, (1974), "Uncertainties in Seismic Risk Procedures," Journal of the Geotechnical Engineering Division, ASCE, Vol. 104, pp. 869-887.

Edinger, P. H., (1982), "Memorandum, re: Defense Waste Processing Facility, Savannah River Plant," September 23, 1982 in S - Area Correspondence File.

Electric Power Research Institute (EPRI), 1986. "Seismic Hazard and Methodology for the Central and Eastern United States," EPRI Technical Report NP-4726-A, 11 Volumes.

Electric Power Research Institute (EPRI), 1993. "Guidelines for determining design basis ground motions," EPRI Technical Report TR-102293, November 1993.

Fallaw, W. C., and V. Price, (1992), "Outline of Stratigraphy at the Savannah River Site," in W. C. Fallaw and V. Price, eds., 1992, Carolina Geological Society Field Trip Guidebook, November 13-15, 1992, Geological Investigations of the Central Savannah River Area, South Carolina and Georgia, U. S. Department of Energy and South Carolina Geological Survey, p. CGS-92-B-II-1-33.

Fallaw, W. C., and V. Price, (1995), Stratigraphy of the Savannah River Site and vicinity, Southeastern Geology (in press).

FLAC - (1991) Fast Lagrangian Analysis of Continua, Computer Program FLAC - Itasca Consulting Group Inc., Minneapolis, Minnesota.

Geomatrix (1991). Ground motion following selection of SRS design basis earthquake and associated deterministic approach, WSRC subcontract AA20210S.

Geotechnical Engineers Inc. (1991a), "K Reactor Area, Geotechnical Investigation for Seismic Issues—Technical Evaluation," WSRC TR-91-47, March, 1991.

Geotechnical Engineers Inc. (1991b), "Recommended Dynamic Properties for Depths Up to 900 Feet, K Area," Project 90282, Letter to M. Elwyn Wingo, June, 1991.

Geotechnical Engineers, Inc., (1983) "Defense Waste Processing Facility-PSAR-Liquefaction and Cyclic Mobility Potential."

Geotechnical Engineers, Inc., (1979) "Evaluation of Dynamic Soil Properties and Liquefaction Potential, Building 221-H, Savannah River Plant, Aiken, South Carolina:" Unpublished Report.

Glisson, A. L., (1982), "Memorandum, re: Project 9S1780 - Savannah River Plant - 200 S Area, Defense Waste Processing Facility - Sludge Plant, DA 600 - Site Investigation - Meeting Notes," September, 8, 1982 in S - Area Correspondence File.

Harder, L. F. Jr., (1988), "Use of Penetration Tests to Determine the Cyclic Loading Resistance of Gravely Soils During Earthquake Shaking," Ph.D. Dissertation, University of California, Berkeley, California.

Hasegawa, H. S., P. W. Basham, and M. J. Berry, (1981), "Attenuation Relations for Strong Seismic Ground Motion," Bulletin of the Seismological Society of America, Vol. No. 71, pp. 2071-2095.

Huang, Y.H., (1983), "Stability Analysis of Earth Slopes," Van Nostrand Reinhold.

Huddlestun, P. F., (1988), "A Revision of the Lithostratigraphic Units of the Coastal Plain of Georgia, the Miocene through Holocene," Georgia Geologic Survey Bulletin 104, p. 162.

Idriss I. M . and Sun J. I. (1992), "User's Manual for SHAKE 91," University of California, Davis, November, 1992.

Ishihara, (1993), "Liquefaction and Flow Failure During Earthquakes," Geotechnique 43, No. 3, pp 351-415.

Ishihara, K., (1985), "Stability of Natural Deposits During Earthquakes," Proceedings of the Eleventh International Conference on Soil Mechanics and Foundation Engineering.

Iwasaki, T., T. Katayama, K. Kawashima, and M. Saeki, (1978), "Statistical Analysis of Strong Motion Acceleration Records Obtained in Japan," Proceedings of the Second International Conference on Microzonation, San Francisco, Vol. 2, pp. 705-716.

Journel, A.G., and Huijbregts, C.J., (1978), "Mining Geostatistics," London Academic Press.

KASS (1992), "K-Area Soil Stabilization Program, Geotechnical Evaluation." WSRC TR-92-299 July.

Kayen, R. E., J. K. Mitchell, R. B. Seed, A. Lodge, S. Nishio, and R. Coutinno (1992), "Evaluation of SPT-CPT- and Shear Wave-Based Methods for Liquefaction Potential Assessment Using Loma Prieta Data," Proceedings from the Fourth Japan - U. S. Workshop on Earthquake Resistance Design of Lifetime Facilities and Counter Measures for Soil Liquefaction, Volume 1,

Koester, J. P. , and A. G. Franklin (1985), "Current Methodologies for Assessing the Potential for Earthquake-Induced Liquefaction in Soils," NUREG/CR-430, U. S. Regulatory Commission, Washington, D. C.

Koester, J.P. (1992), " Cyclic Strength And Pore Pressure Generation Characteristics Of Fine-Grained Soils," Ph.D. Thesis, University of Colorado, Boulder, CO.

Kuribayashi, E., and F. Tatsuoka, (1975), "Brief Review of Liquefaction During Earthquakes in Japan," Soils and Foundations, Vol. 15, No. 4, December, pp. 81-92.

Kulhawy, F.H., and Mayne, P.W., (1990), "Manual on Estimating Soil Properties for Foundation Design," prepared by Cornell University, New York for Electrical Power Research Institute, Report EL-6800.

Law Engineering Testing Company, (1962), "Report of Investigation of Subsidence, Evaporator Building Fill, - Waste Storage and Evaporation Building 242H, Savannah River Plant," Atomic Energy Commission Job No. 3089, July 9, 1962.

Lawrence Livermore National Laboratory (LLNL), 1989. "Seismic Hazard Characterization of 69 Plant Sites East of the Rocky Mountains," UCID-21517, U.S. Nuclear Regulatory Commission Report, NUREG/CR5250, by D.L. Bernreuter, J.B. Savy, R.W. Mensing, J.C. Chen, and B.C. Davis.Lee, R.C. (1994). "Update of H-Area Seismic Design Basis - Rev. 1", WSRC-TR-94-0528, 91 p.

Lee, K.L., and Albaisa, A. (1974), "Earthquake Induced Settlement in Saturated Sands," Journal of the Soil Mechanics and Foundations Division, ASCE 100(GT4):387-406.

Lee, R., Fax Transmittal to Bechtel Including Input Data for RASCAL to Generate 84 Percentile Rock Motion, December 28, 1994.

Lee, R. (1994), "H-Area Seismology Summary and General Overview," Westinghouse Savannah River Company Technical Report, WSRC-TR-94-0529, Revision 1.

Lee, R., Fax Transmittal to Bechtel Including the Relationship Between the Body Wave and Moment Magnitudes, January 3, 1995.

Lewis, M. R., Interoffice Memorandum to F. Ostadan, Probabilistic Analysis Time Histories, Bechtel San Francisc Office, File No. ECSD-SGS-95-0081, February 21, 1995.

Liao, S. S. C., D. Veneziano, and R. V. Whitman, (1988), "Regression Models for Evaluating Liquefaction Probability," Journal of Geotechnical Engineering, ASCE, Vol. 114, No. 4, pp. 389-411.

Loertscher, T. (1994), "Magnitude Scaling Factors for Analysis of Liquefaction Hazard," Doctoral Dessertation, Department of Civil Engineering, Brigham University, Provo, Utah.

Logan, W.R., and Euler, G.M. (1989), "Geology and Ground-Water resources of Allendale, Bamberg, and Barnwell Counties and Part of Aiken County South Carolina," State of South Carolina Water Resources Commission, Report No. 155.

Main, C.T., Inc., (1987), "Savannah River Plant TBP Removal Tanks at the F/H Effluent Treatment Facility," Rev. 0, Project S2872, December 10, 1987.

Marcuson III, W. F., M. E. Hynes, and A. G. Franklin, (1990), "Evaluation and Use of Residual Strength in Seismic Safety Analysis of Embankments," Earthquake Spectra, Volume 6, Number 3.

Martin, G. R., W. L. Finn, and H. B. Seed, (1975), "Fundamentals of Liquefaction Under Cyclic Loading," Journal of the Geotechnical Engineering Division, ASCE, Volume 101, Number 5, Proc. Paper 11284, May, 1975.

Martin, J. R., and Clough, G. W. (1994), "Seismic Parameters From Liquefaction Evidence," Journal of Geotechnical Engineering, ASCE Vol. 120, No. 8, August, 1994.

Makdisi and Seed (1978), "A Simplified Procedure for Estimating Earthquake Induced Deformations in Dams and Embankments," EERC-77/19.

McCann, M.W., (1989), Probabilistic Seismic Hazard Evaluation for the Savannah River Site, Aiken, SC, Jack Benjamin and Associates.

McGuire, R. K. (1977), "Seismic Design Spectra and Mapping Procedures Using Hazard Analyses Based Directly on Oscillator Response," Journal of Earthquake Engineering and Structural Dynamics, No. 5, pp. 211-234.

McGuire, R. K., (1978), "Seismic Ground Motion Parameter Relations," Journal of the Geotechnical Engineering Division, ASCE, Vol. 104, pp. 481-490.

Moran, Proctor, Mueser & Rutledge, Consulting Engineers (1962), "Settlement Investigation of Evaporator Building 242-H, Savannah River Plant, Atomic Energy Commission," June, 1962.

Mueser, Rutledge, Wentworth & Johnston (1974), "Savannah River Plant Additional Facilities, High Level Waste Storage, 200H," (Tanks 35-38 - Renumbered 38-41), January 22, 1974.

Mueser, Rutledge, Wentworth & Johnston Consulting Engineers (1975a), "New High Level Storage Tank No. 38, Bldg. 241H," SRP, September 24, 1975.

Mueser, Rutledge, Wentworth & Johnston Consulting Engineers (1975b), "Building 241H New High Level Waste Storage Tanks Nos. 42 & 43 Savannah River Plant," September 23, 1975.

Mueser, Rutledge, Wentworth, and Johnston (1977), "Building 241-H, New High Level Waste Storage Tanks Nos. 48 through 51," Savannah River Plant, Report, March 22, 1977.

Mueser, Rutledge, Johnston, and DeSimone (1978), "Building 241-H, New High Level Waste Storage Tanks Nos. 50 and 51," Savannah River Plant, Report, May 23, 1978.

Mueser, Rutledge, Johnston, and DeSimone (1984a), "In-Tank Precipitation Facility H-Area Savannah River Plant," Savannah River Plant, Report, Aug. 27, 1984.

Mueser, Rutledge, Johnston, and DeSimone (1984b), "Geotechnical Report, Design and Construction, Defense Waste Processing Facility, 200-S Area, Savannah River Plant," Aug. 7, 1984.

Mueser, Rutledge, Johnston & Desimone Consulting Engineers (1984c), "Waste Transfer Facility H-Area Savannah River Plant," Sept. 17, 1984.

Mueser Rutledge Consulting Engineers (1985), "Waste Transfer Facility Revised Location H-Area, Savannah River Plant, (MR-108, MR-109)," July 11, 1985.

Mueser Rutledge Consulting Engineers (1988a), "Tank Farm Space Gain Facility, 200 H-Area, Savannah River Plant (H-152, H-154)," September 9, 1988.

Mueser Rutledge Consulting Engineers (1988b), "ETF Wastewater Collection Tanks, F/H Effluent Treatment Facility 200H Area," SRP, June 21, 1988.

Mueser Rutledge Consulting Engineers (1988c), "Nitrogen Storage Tanks and Vaporizer, 200 H-Area, Savannah River Plant, " August 4, 1988.

Mueser Rutledge Consulting Engineers (1991), "Progress Report No. 10, Vitrification Building, Design Area S221, Settlement Monitoring Program, Defense Waste Processing Facility, Savannah River Site, 200-S Area."

Nystrom, P. G., and R. H. Willoughby (1982), "Geological Investigations Related to the Mining of the Kaolin District, Aiken County, South Carolina," South Carolina Geological Survey, 1982 Carolina Geological Society Field Trip Guidebook, p. 183.

Nystrom, P. G., Jr., R. H. Willoughby, and L. E. Kite (1986), "Cretaceous-Tertiary Stratigraphy of the Upper Edge of the Coastal Plain between North Augusta and Lexington, South Carolina," Carolina Geological Survey Field Trip Guidebook 1982, South Carolina Geological Survey, Columbia, South Carolina, pp. 80-113.

Orphal, D. L. and J. A. Lahoud (1974), "Prediction of Peak Ground Motion from Earthquakes," Bulletin of the Seismological Society of America, No. 64, pp. 1563-1574.

Ostadan, F. (1988), Soil-Structure Interaction Analysis (SASSI) - Computer Program, Bechtel Western Power Corporation, San Francisco, CA.

Ostadan, F., I. Arango, J. Litehiser, and J. Marrone, (1991), "Liquefaction Hazard Evaluation, 11th SMiRT Conference, Tokyo, Japan, 1991.

Ostadan, F., J. Marrone, J. Litehiser, and I. Arango, (1991), "Liquefaction Hazard Evaluation: Methodology and Application," 3rd U. S. Conference on Lifeline Earthquake Engineering, Los Angeles, CA, August, 1991.

Peck, R.B. (1954), "Report on Foundation Conditions, Distribution Center for Safeway Stores, Inc., Salt Lake City, Utah," Judgment in Geotechnical Engineering, Ed. Dunnicliff and Deere, BiTech Publisher Ltd., Vancouver, B.C, 1991.

Peck, R.B. (1977), "Pitfalls of Overconservatism in Geotechnical Engineering," Judgment in Geotechnical Engineering, Ed. Dunnicliff and Deere, BiTech Publisher Ltd., Vancouver, B.C, 1991.

Prowell, D. C., R. A. Christopher, L. E. Edwards, L. M. Bybell, and H. E. Gill (1985), "Geologic Section of the Updip Coastal Plain from Central Georgia to Western South Carolina," U. S. Geological Survey Miscellaneous Field Studies Map MF-1737, p. 11.

Richards, E. A. (1982), "Memorandum, re: Review of Soil Properties - H - Area, Savannah River Plant," August 31, 1982, in S - Area correspondence File, 1982.

Robertson, P.K., and Campanella, R.G. (1983), "Interpretation of Cone Penetrometer Tests - Part 1 (Sand)," Canadian Geotechnical Journal, Vol. 20, No. 4, pp. 734-745.

Rouhani, S., Lin, Y.P., and Bartlett, S.F. (1995), "H-Area/ITP Geostatistical Assessment of In-Situ and Engineering Properties," Final Technical Report, ERDA Project No. 93044, Sponsored by Site Geotechnical Services, Westinghouse Savannah River Company, Aiken, SC.

Savy, J.B. (1993), "Seismic Hazard Characterizations at the DOE", Savannah River Site (SRS), Status Report," September 27, 1993, 175 p.

Schnabel, P. B., Lysmer J. and Seed H. B. (1972), "SHAKE—A Computer Program For Earthquake Response Analysis of Horizontally Layered Sites," Report No. EERC 72-12, University of California, Berkeley, Dec, 1972.

Seed, H. B., P. P. Martin, and J. Lysmer, (1975), "The Generation and Dissipation of Pore Water Pressures During Soil Liquefaction." Report No. EERC 75-26, College of Engineering, University of California, Berkeley, CA.

Seed, H. B. (1979a), "Soil Liquefaction and Cyclic Mobility Evaluation for Level Ground During Earthquakes," Journal of Geotechnical Engineering Division, ASCE, Volume 105, Number 2, February, 1979.

Seed, H.B. (1979b) "Considerations in the Earthquake Resistance Design of Earth and Rockfill Dams," 19th Rankine Lecture.

Seed, H. B., I. Arango, and C. K. Chan (1975), "Evaluation of Soil Liquefaction Potential During Earthquakes," Report EERC 75-28, Earthquake Engineering Research Center, University of California, Berkeley, CA.

Seed, H. B., and I. M. Idriss, (1971), "Simplified Procedure for Evaluating Soil Liquefaction Potential," Journal Soil Mechanics and Foundation Division, ASCE, Volume 97, Number 9, 1971.

Seed, H. B., and I. M. Idriss (1970), "Soil Moduli and Damping Factors for Dynamic Response Analyses," Report EERC 70-10, College of Engineering, University of California, Berkeley, CA.

Seed, R. B., Idriss, I. M. and Arango, I. (1983), "Evaluation of Liquefaction Potential Using Field Performance Data," Journal of Geotechnical Engineering Division, ASCE, Volume 97, Number 3.

Seed, R. B., and Harder, L. F. Jr. (1990), "SPT-Based Analysis of Cyclic Pore Pressure Generation and Undrained Residual Strength," H. Bolton Seed Memorial Symposium Proceedings, Vol. 2., Vancouver, B.C., Canada.

Seed, H. B., Tokimatsu, K., Harder, L. F., and Chung, R. M. (1984), "The Influence of SPT Procedures on Soil Liquefaction Resistance Evaluations," Report No. UCB/EERC-84/15, Earthquake Engineering Research Center, University of California, Berkeley, CA, Oct., 1984.

Seed, H. B. and P. De Alba (1986), "Use of SPT and CPT Tests for Evaluating the Liquefaction Resistance of Soils," Proceedings of Specialty Conference on the Use of In Situ Tests in Geotechnical Engineering, ASCE, Geotech Special Publication No. 6, Blacksburg, Virginia, June, 1986.

Seed, H. B. and I. M. Idriss (1982), "Ground Motions and Soil Liquefaction During Earthquakes," Earthquake Engineering Research Institute, Monograph Series, page 134.

Seed, H. B., S. Singh, and C. K. Chan (1979), "Undisturbed Sampling and Cyclic Load Testing of Sands," Report No. UCB/EERC-79/33, University of California, Berkeley, CA.

Silva, W. J. and K. Lee (1987), WES RASCAL Code for Synthesizing Earthquake Ground Motions. Report 24, State-of-the-Art for Assessing Earthquake Hazards in the United States, Misc. Paper S-73-1, U. S. Army Engineer Waterways Experiment Station, page 120.

Siple, G. E. (1967) "Geology and Ground Water of the Savannah River Plant and Vicinity, South Carolina," U.S. Geological Survey Water Paper 1841.

SRS (1988) Computer Program, DEMAP K113M-1, Geoslope, Version 4.2.

Stieve, A.L., C. Coruh, and J. Costain (1994). Confirmatory Drilling Project Final Report, WSRC-RP-94-0136.

Stokoe, K. H., G. R. Rix, I. Sanches, R. D. Andrus, and Y. J. Mok (1988), "Liquefaction of Gravely soils During the 1983 Borah Peak, Idaho Earthquake," Proceedings of the Ninth World Conference On Earthquake Engineering, Tokyo, Japan, Volume III, August.

Tatsuoka, F., T. Sasaki, and S. Yamada, (1984), "Settlement in Saturated Sand Induced by Cyclic Undrained Simple Shear," Proceedings of the Eighth World Conference on Earthquake Engineering, San Francisco, CA.

Terzaghi, K., and Peck, R. (1967), "Soil Mechanics in Engineering Practice," John Wiley & Sons, New York., NY.

Tokimatsu, K., and H. B. Seed (1984), "Simplified Procedures for the Evaluation of Settlements in Clean Sands," Report No. UCB/EERC-84/16, College of Engineering, University of California, Berkeley, CA, October, 1984.

Tokimatsu K., and Yoshimi Y. (1984), "Criteria of Soil Liquefaction with SPT and Fines Content," Proceedings of the Eighth World Conference on Earthquake Engineering, Vol. III, July 21-28, 1984, San Francisco, California, published by Prentice-Hall, Inc., Englewood Cliffs, New Jersey, NJ.

Tokimatsu, K., and Y. Yoshimi (1983), "Empirical Correlation of Soil Liquefaction Based on SPT N-Value and Fines Content," Journal Soil Mechanics and Foundation Division, Volume 23, Number 4.

Toro, G.R., N.A. Abrahamson, and J.F. Schneider (1994). Engineering Model of Strong Ground Motions from Earthquakes in the Central and Eastern United States," submitted to Earthquake Spectra, March, 1994.

URS/John A. Blume and Associates, Engineers (1982). Update of Seismic Criteria for the Savannah River Plant, Vol. 1 of 2, Geotechnical: URS/JAB 8144, 293 pp.

US Army Corps of Engineers (1970), "Engineering Manual EM 1110-2-1906," Appendix X, November, 1970.

US Army Corps of Engineers, Charleston District (COE) (1952a), "Geologic Engineering Investigations, Savannah River Plant," Volumes 1 and 2, Waterways Experiment Station, Vicksburg, MS.

US Army Corps of Engineers, Charleston District (COE) (1952b), "Foundation Grouting Operations, Savannah River Plant," Volumes 1 and 2, Waterways Experiment Station, Vicksburg, MS.

US Nuclear Regulatory Commission (1990a), Standard Review Plan, Office of Nuclear Reactor Regulation, NUREG-0800, Rev. 2, 2.5.2 "Vibratory Ground Motion," Washington, D.C., 15 p.

US Nuclear Regulatory Commission (1990b), Standard Review Plan, Office of Nuclear Reactor Regulation, NUREG-0800, Rev. 2, 3.7.1 "Seismic Design Parameters," Washington, D.C.

U. S. Nuclear Regulatory Commission (1992), Draft Regulatory Guide DG-1015, "Identification and Characterization of Seismic Sources, Deterministic Source Earthquakes, and Ground Motion," November, 1992.

Wang, W. (1979), "Some Findings in Liquefaction," Water Conservancy and Hydroelectric Power Scientific Research Institute, Beijing, China, August.

Westinghouse Environmental and Geotechnical Services, Inc. (1990), "Report of Geotechnical Exploration, WMWE Maintenance Facility Building (241-41H)," Westinghouse Project No. 4136-90-543 #2, July 20, 1990.

WSRC 1Q Manual (1990), "Westinghouse Savannah River Company Quality Assurance Manual," August 31, 1990.

WSRC 3Q-5 Manual (1992), "Hydrogeologic Data Collection (U)," October 1, 1992.

WSRC (1993a), "Generic Specification for Handling, Storage, and Shipment of Soil Samples," Spec. K-SPC-G-00003, Rev. 0, May 10, 1993.

WSRC (1993b), "Generic Specification for Stationary Piston Sampling," Spec. K-SPC-G-00004, Rev. 0, May 10, 1993.

WSRC (1993c), Site Geotechnical Services, "New Waste Transfer Facility (NWTF) - Geotechnical Assessment," December, 1993.

WSRC HLW-ENG-930017 (1994a), "H-Area/ITP Seismic Safety Issue Resolution Program Plan," Rev. 1, Jan. 31, 1994.

WSRC (1994b), "Geological Characterization in the Vicinity of the In-Tank Precipitation Facility (U)," Rev. 0.

WSRC (1994c), "H-Area Seismology Summary and General Overview," Rev. 1, December, 1994.

WSRC (1994d), "In Tank Processing (ITP) Geotechnical Summary Report (U)," WSRC-TR-94-0389, Rev. 2, November, 1994.

WSRC (1994e), Site Geotechnical Services, "Geotechnical Summary Report for HDB-7", October 17, 1994.

WSRC (1994f), Specification K-SPC-G-00010, "H-Area CPT and DPT Services", Rev. 1, September 30, 1994.

WSRC (1995), "Settlement Summary of Waste Tanks in H-Area Tank Farm," Rev. 0, January 11, K-ESR-H-00002.

Yoshimi, Y. K. and K. Tokimatsu (1977), "Settlement of Buildings on Saturated Sands During Earthquakes," Soils and Foundations, JSSMFE, Volume 17, No. 1, pages 23-38.

Youd, T. L, (1977), Discussion on paper entitled "Brief Review of Liquefaction during Earthquakes in Japan," Soils and Foundations, Vol. 17, No. 1, pp. 82-85.

Youd, T. L., and Hoose, S. N. (1977), "Liquefaction Susceptibility and Geologic Setting," Proceedings, 6th World Conference on Earthquake Engineering, New Delhi, India, Vol. 6, pp. 37-42.

Youd, T. L., and Perkins, M. (1978), "Mapping Liquefaction Induced Ground Failure Potential," Journal of the Geotechnical Engineering Division, ASCE 104(GT4):433-446.

# TABLES

ITP EXPLORATION POINT SUMMARY

Project: ITP Facility - Phase 1
Location: H-Area

| Borehole ID | Phase | Type | Northing | Easting | Surface El. (feet) | Tot. Depth (feet) | Grout Take ($ft^3$) | Remarks |
|---|---|---|---|---|---|---|---|---|
| | | | | **RCA** | | | | |
| H-SPT-1 | 1 | SPT | 70863.97 | 62512.00 | 327.72 | 51.0 | 18.7 | Cross-hole testing location, (Array 1) |
| H-SPT-14 | 1 | SPT | 70941.51 | 62384.82 | 300.69 | 196.2 | 61.6 | Cross-hole testing location, (Array 12) |
| H-CPT-1 | 1 | SCPTU | 70843.97 | 62532.00 | 326.83 | 200.5 | * | |
| H-CPT-5 | 1 | SCPTU | 70797.30 | 62667.40 | 326.08 | 203.0 | * | |
| H-CPT-6B | 1 | SCPTU | 70903.41 | 62783.01 | 328.17 | 148.0 | * | |
| H-CPT-10 | 1 | SCPTU | 71002.02 | 62554.29 | 328.41 | 139.5 | * | |
| H-CPT-11 | 1 | CPTU | 70885.10 | 62767.43 | 327.87 | 42.0 | * | Refused on mud mat, repushed Phase II |
| H-CPT-14 | 1 | SCPTU | 70935.99 | 62375.16 | 300.09 | 163.5 | * | |
| DMT-14 | 1 | DMT | 70930.51 | 62384.82 | 300.44 | 116.0 | * | |
| | | | | **NON-RCA** | | | | |
| H-SPT-18 | 1 | SPT | 70601.00 | 62667.50 | 298.50 | 210.0 | * | Converted to monitoring well |
| HSPT18.1 | 1 | SPT | 70601.00 | 62657.50 | 298.43 | 162.5 | * | Converted to monitoring well |
| H-SPT-20 | 1 | SPT | 70853.54 | 63057.89 | 294.24 | 184.5 | 44.8 | |
| H-CPT-18 | 1 | SCPTU | 70601.00 | 62657.50 | 298.32 | 174.5 | * | |
| H-CPT-20 | 1 | SCPTU | 70843.86 | 63059.62 | 294.24 | 108.5 | 835.0 | Drilled out for grout injection test |
| H-CPT201 | 1 | SCPTU | 70835.00 | 63051.50 | 294.31 | 111.0 | * | |
| H-CPT202 | 1 | SCPTU | 70848.00 | 63076.50 | 294.11 | 105.5 | * | |
| H-CPT-23 | 1 | SCPTU | 70970.68 | 63017.30 | 296.59 | 138.0 | * | |
| H-CPT-28 | 1 | CPTU | 70611.74 | 62897.94 | 300.56 | 136.5 | 3253.0 | Drilled out for grout injection test |
| H-CPT282 | 1 | SCPTU | 70611.74 | 62908.00 | 300.42 | 124.0 | * | |
| DMT-18 | 1 | DMT | 70601.00 | 62637.50 | 298.25 | 102.2 | * | |
| DMT-20 | 1 | DMT | 70850.85 | 63069.34 | 294.19 | 71.3 | * | |
| DMT-28 | 1 | DMT | 70611.74 | 62872.90 | 300.14 | 122.0 | * | |
| | | | | | TOTAL | 3010.2 | | |

**SPT** - Standard Penetration Test Borehole **SCPTU** - Seismic Piezo CPT **CPTU** - Piezo CPT **DMT** - Dilatometer
**UD** - Undisturbed Sampling **CORE** - Continuous Coring **FISHTAIL** - Straight drill, no sampling

* No Significant grout takes for CPT's or DMT's.
**Holes were cased for tomography study.

Table 3.6-1 Exploration point summary (p1/3).

ITP EXPLORATION POINT SUMMARY

Project: ITP Facility - Phase 2
Location: H-Area

| Borehole ID | Phase | Type | Northing | Easting | Surface El. (feet) | Tot. Depth (feet) | Grout Take ($ft^3$) | |
|---|---|---|---|---|---|---|---|---|
| | | | | **RCA** | | | | |
| H-BOR-2 | 2 | UD | 70853.97 | 62512.00 | 330.00 | 220.2 | 71.3 | Cross-hole testing location, (Array1) |
| H-BOR-3 | 2 | FISHTAIL | 70843.97 | 62512.00 | 327.70 | 50.0 | 20.1 | Cross-hole testing location, (Array1) |
| H-BOR-12 | 2 | UD | 70961.51 | 62384.82 | 300.00 | 200.5 | 36.4 | Cross-hole testing location, (Array12) |
| H-BOR-13 | 2 | FISHTAIL | 70951.51 | 62384.82 | 300.35 | 205.0 | 43.4 | Cross-hole testing location, (Array12) |
| H-BOR-29 | 2 | UD | 70999.00 | 62805.00 | 328.55 | 208.5 | 43.4 | |
| H-SPT-11 | 2 | CORE | 70885.10 | 62757.43 | 328.03 | 96.0 | 23.3 | |
| H-CPT-7 | 2 | SCPTU | 71030.17 | 62612.85 | 328.76 | 210.0 | * | |
| H-CPT-11 | 2 | CPTU | 70885.10 | 62767.43 | 327.87 | 200.0 | * | |
| H-CPT-16 | 2 | SCPTU | 70733.84 | 62426.06 | 297.57 | 109.5 | * | |
| H-CPT-26 | 2 | SCPTU | 70764.00 | 62805.00 | 326.13 | 173.5 | * | |
| H-CPT-29 | 2 | SCPTU | 71113.00 | 62681.30 | 334.43 | 200.0 | * | |
| H-CPT-30 | 2 | SCPTU | 70989.00 | 62805.00 | 328.49 | 205.0 | * | |
| H-CPT-31 | 2 | SCPTU | 70785.00 | 62537.00 | 326.08 | 137.0 | * | |
| | | | | **NON-RCA** | | | | |
| H-BOR-21 | 2 | CORE | 70862.90 | 63054.21 | 294.20 | 200.0 | 147.0 | Cross-hole casing collapsed, new location selected |
| H-BOR-22 | 2 | FISHTAIL | 70872.25 | 63050.70 | 294.50 | 200.0 | 140.0 | Cross-hole casing collapsed, new location selected |
| H-BOR-23 | 2 | UD | 70960.25 | 63020.79 | 296.59 | 212.0 | 50.0 | Cross-hole testing location, (Array 23) |
| HBOR23.1 | 2 | UD | 70970.25 | 63020.79 | 300.56 | 125.0 | 38.7 | Cross-hole testing location, (Array 23) |
| HBOR23.2 | 2 | SPT | 70980.25 | 63020.79 | 300.56 | 205.0 | 42.7 | Cross-hole testing location, (Array 23) |
| H-BOR-42 | 2 | CORE | 70610.00 | 62920.00 | 300.60 | 154.0 | 130.5 | Communication between H-BOR-42 and H-BOR-47 |
| H-BOR-43 | 2 | CORE | 70641.58 | 62885.27 | 300.33 | 198.5 | 610.6 | |
| H-BOR-45 | 2 | CORE | 70635.67 | 62905.02 | 300.52 | 131.0 | 25.2 | |
| H-BOR-46 | 2 | CORE | 70613.00 | 62940.00 | 300.30 | 125.0 | 26.2 | |
| H-BOR-47 | 2 | CORE | 70615.28 | 62901.48 | 300.50 | 140.0 | 1687.5 | Communication between H-BOR-42 and H-BOR-47 |
| H-CPT-25 | 2 | SCPTU | 71197.74 | 62998.40 | 296.20 | 154.0 | * | |
| H-CPT-32 | 2 | SCPTU | 71419.43 | 61819.39 | 322.24 | 69.0 | * | |
| H-CPT32B | 2 | SCPTU | 71419.43 | 61819.39 | 322.24 | 190.0 | * | |
| H-CPT-34 | 2 | SCPTU | 71390.77 | 61693.69 | 322.20 | 212.0 | * | |
| H-CPT-37 | 2 | SCPTU | 71642.00 | 61616.00 | 322.76 | 189.0 | * | |
| H-CPT-38 | 2 | SCPTU | 71637.68 | 61820.88 | 322.44 | 207.5 | * | |
| | | | | | TOTAL | 4927.2 | | |

**SPT** - Standard Penetration Test Borehole **SCPTU** - Seismic Piezo CPT **CPTU** - Piezo CPT **DMT** - Dilatometer
**UD** - Undisturbed Sampling **CORE** - Continuous Coring **FISHTAIL** - Straight drill, no sampling

* No Significant grout takes for CPT's or DMT's.
**Holes were cased for tomography study.

Table 3.6-1 Exploration point summary (p2/3).

ITP EXPLORATION POINT SUMMARY

Project: ITP Facility - Phase 3
Location: H-Area

| Borehole ID | Phase | Type | Northing | Easting | Surface El. (feet) | Tot. Depth (feet) | Grout Take ($ft^3$) | |
|---|---|---|---|---|---|---|---|---|
| | | | | **RCA** | | | | |
| H-BOR-34 | 3 | UD/SPT/CORE | 70885.10 | 62747.43 | 326.00 | 300.5 | ** | Cased for tomography study |
| H-BOR-50 | 3 | UD/CORE | 70761.17 | 62805.00 | 326.07 | 300.0 | ** | Cased for tomography study |
| H-BOR-51 | 3 | UD/SPT/CORE | 70768.00 | 62811.00 | 326.10 | 153.9 | 264.0 | Communication between H-BOR-51 and H-BOR-50 |
| H-BOR-54 | 3 | UD/CORE | 70794.80 | 62667.40 | 326.10 | 300.0 | ** | Cased for tomography study |
| | | | | **NON-RCA** | | | | |
| HBOR23.3 | 3 | SPT | 70970.25 | 63015.79 | 295.22 | 205.0 | 112.0 | |
| H-BOR-44 | 3 | UD/SPT/CORE | 70662.00 | 62885.00 | 300.20 | 305.0 | ** | Cased for tomography study |
| | | | | | TOTAL | 1564.4 | | |

**SPT** - Standard Penetration Test Borehole **SCPTU** - Seismic Piezo CPT **CPTU** - Piezo CPT **DMT** - Dilatometer
**UD** - Undisturbed Sampling **CORE** - Continuous Coring **FISHTAIL** - Straight drill, no sampling

* No Significant grout takes for CPT's or DMT's.
**Holes were cased for tomography study.

Table 3.6-1 Exploration point summary (p3/3).

| *Test Description* | *Procedure* |
|---|---|
| Handling, storage, and shipment of soil samples | TP-1-ITP |
| Stress Controlled Cyclic Triaxial Testing, Volumetric Strain, Residual Strength Determination and Low Amplitude Cyclic Stress Controlled Triaxial Testing | TP-2-ITP |
| Determination of Soil Mineralogy using X-ray Diffraction | TP-3-ITP |
| Determining the Dry and Wet Densities of Soil Volume Contained in Thin Wall Tube Samples | TP-4A-ITP |
| Sample Extrusion and Preparation | TP-5A-ITP |
| Stationary piston sampling | K-SPC-G-00004 |
| Dry preparation of soil samples for particle size analysis and determination of soil constants | ASTM D421-85 |
| Particle size analysis | ASTM D422-63 |
| Specific gravity of soils | ASTM D854-92 |
| Amount of material in soils finer than the No. 200 sieve | ASTM 1140-92 |
| Laboratory determination of moisture content of soil, rock, and soil-aggregate mixtures | ASTM D2216-92 |
| Liquid limit, plastic limit and plasticity of soils | ASTM D4318-93 |
| Wet preparation of soil | ASTM D2217-85 |
| Classification of soils for engineering purposes | ASTM D2487-93 |
| Description of soils (visual-manual procedure) | ASTM D2488-93 |
| Unconfined compressive strength of cohesive soil | ASTM D2166-91 |
| One-dimensional consolidation properties of soils | ASTM D2435-90 |
| Direct shear test of soil under consolidated drained conditions | ASTM D3080-90 |
| Modulus and damping of soils by resonant column method | ASTM D4015-92 |
| Consolidated-undrained triaxial compression test on cohesive soils | ASTM D4767-88 |
| Unconsolidated, undrained strength of cohesive soils | ASTM D2850-87 |
| Consolidated-drained triaxial tests | EM-1110-2-1906 |

Table 4.0-1 Standard laboratory testing procedures.

| SAMPLE IDENTIFICATION | | | | | CLASSIFICATION PROPERTIES | | | | | | | | PHYSICAL PROPERTIES | | | | | | | | | | | | | | |
|---|---|---|---|---|---|---|---|---|---|---|---|---|---|---|---|---|---|---|---|---|---|---|---|---|---|---|---|
| | | | | | | | | | Atterberg Limits | | | | | | | | | | Static Strength | | | | Consolidation | | | | |
| | | | | | | | | | Liquid | Plas. | Liquid | Plas. | | Natural | Insitu | Insitu | | | | | | | | | | | |
| Layer | Boring No. | Sample No. | Top Depth (feet) | Top Elev. (feet) | USCS Group Symbol | Sand (%) | Fines (%) | Clay %<.005mm | Limit on portion <No. 40 (%) | Index on portion <No. 40 (%) | Limit on portion <-200 (%) | Index on portion <-200 (%) | Specific Gravity | Water Content (%) | Dry Density (pcf) | Wet Density (pcf) | Void Ratio | Test Type | Max. Deviator Stress (ksf) | Confining Stress (ksf) | Strain at Failure (%) | Overburden Stress (ksf) | Precon. Stress (ksf) | Compress. Index Cc | Recomp. Index Cr | Comp. Coef. Cv |
| TR1 | H-BOR-12 | ST1 | 8.3 | 291.7 | SC | 68 | 32 | 29 | 98 | 56 | | | 2.66 | 23.1 | 98.9 | 121.7 | 0.679 | UU | 1.35 | 1.01 | 15 | 1.00 | | | | |
| TR1 | H-BOR-12 | ST2 | 13 | 287 | | | | | | | | | | 20.2 | 95.3 | 114.6 | 0.749 | | | | | 1.56 | 8.4 | 0.24 | 0.01 | 2.2 |
| TR1 | H-BOR-12 | ST2 | 13.4 | 286.6 | SC | 70 | 30 | 27 | 86 | 54 | | | 2.67 | 21.4 | 97.3 | 118.1 | 0.713 | CD | 3.05 | | 10 | 1.61 | | | | |
| TR1 | H-BOR-12 | ST2 | 14 | 286 | | 72 | 28 | 25 | | | 144 | 101 | 2.66 | 20.9 | 97.4 | 117.8 | 0.705 | CD | 4.86 | | 15 | 1.68 | | | | |
| TR1 | H-BOR-12 | ST2 | 14.5 | 285.5 | SC | 70 | 30 | 26 | 104 | 71 | | | 2.66 | 23.6 | 95.3 | 117.8 | 0.742 | CD | 7.92 | | 15 | 1.74 | | | | |
| TR1 | H-BOR-12 | ST3 | 18 | 282 | SC | 73 | 25 | 19 | 100 | 61 | | | 2.67 | 25.5 | 94.5 | 118.6 | 0.763 | CU | 1.45 | 2.11 | 15 | 2.16 | | | | |
| TR1 | H-BOR-12 | ST3 | 18.5 | 281.5 | | 68 | 29 | 22 | | | 152 | 98 | 2.71 | 22.2 | 97.6 | 119.3 | 0.734 | CU | 3.19 | 3.46 | 15 | 2.22 | | | | |
| TR1 | H-BOR-12 | ST3 | 19.1 | 280.9 | SC | 76 | 24 | 20 | 78 | 59 | | | 2.68 | 19.3 | 99.7 | 118.9 | 0.677 | CU | 4.75 | 6.91 | 15 | 2.29 | | | | |
| TR1 | H-BOR-12 | PS2 | 27.3 | 272.7 | | | | | | | | | 2.7 | 26.2 | 96.6 | 121.9 | | | | | | 2.96 | | | | |
| TR1 | H-BOR-12 | PS2 | 28 | 272 | SC | 64 | 36 | 28 | 91 | 61 | | | 2.74 | 25.8 | 93.2 | 117.2 | 0.808 | UU | 2.11 | 3.17 | 10 | 3.00 | | | | |
| TR1 | H-BOR-12 | PS2 | 28.5 | 271.5 | | | | | | | | | | 26.6 | 94.1 | 119.1 | 0.7912 | | | | | 3.03 | 7.5 | 0.25 | 0.02 | 2.3 |
| TR2 | H-BOR-12 | ST5 | 44 | 256 | | 82 | 18 | 9 | | | 70 | 31 | 2.66 | 26.7 | 97.1 | 123.0 | 0.71 | CD | 5.6 | | 9.5 | 3.96 | | | | |
| TR2 | H-BOR-12 | ST5 | 44.5 | 255.5 | | | | | | | | | | 28.2 | 93.8 | 120.3 | 0.7703 | | | | | 3.99 | 8.5 | 0.1 | 0.02 | 1 |
| TR2 | H-BOR-12 | ST7 | 58 | 242 | SP-SC | 92 | 8 | 7 | 36 | 16 | | | 2.69 | | | | | | | | | 4.80 | | | | |
| TR3/TR4 | H-BOR-12 | PS3 | 62.8 | 237.3 | SC | 79 | 21 | 17 | 45 | 25 | | | 2.7 | 18.6 | 109.35 | 129.7 | 0.555 | UU | 3.71 | 4.32 | 15 | 5.08 | | | | |
| TR3/TR4 | H-BOR-12 | PS3 | 63.3 | 236.8 | SC | 77 | 23 | 18 | 44 | 25 | | | 2.67 | 18.4 | 110.1 | 130.4 | 0.497 | UU | 4.35 | 8.64 | 15 | 5.11 | | | | |
| TR3/TR4 | H-BOR-12 | PS3 | 63.8 | 236.3 | | | | | | | | | 2.67 | 19.05 | 105.9 | 126.1 | 0.553 | | | | | 5.14 | 10 | 0.09 | 0.01 | 3.4 |
| TR3/TR4 | H-BOR-12 | PS5 | 70.7 | 229.3 | | | | | | | | | | 21.4 | 105 | 127.5 | | | | | | 5.56 | | | | |
| TR3/TR4 | H-BOR-12 | PS5 | 70.8 | 229.2 | SC | 78 | 22 | 17 | 53 | 30 | 119 | 81 | 2.69 | 19.7 | 112.8 | 135.0 | | STX | | | | 5.57 | | | | |
| TR3/TR4 | H-BOR-12 | PS5 | 71.4 | 228.6 | SC | 72 | 28 | 21 | 51 | 27 | 172 | 130 | 2.7 | 19.7 | 105.2 | 125.9 | | STX | | | | 5.60 | | | | |
| TR3/TR4 | H-BOR-12 | PS5 | 72 | 228 | SC | 72 | 28 | 22 | 48 | 26 | 180 | 139 | 2.71 | 25 | 99.8 | 124.8 | | STX | | | | 5.64 | | | | |
| TR3/TR4 | H-BOR-12 | PS5 | 75 | 225 | SC | 83 | 17 | 14 | 39 | 15 | | | 2.7 | 20.85 | 105.65 | 127.7 | 0.613 | CD | 6.43 | | 12.5 | 5.82 | | | | |
| TR3/TR4 | H-BOR-12 | PS6 | 75.5 | 224.5 | | 87 | 13 | 12 | | | 164 | 126 | 2.72 | 19.6 | 105.9 | 126.7 | 0.603 | CD | 7.45 | | 15 | 5.85 | | | | |
| TR3/TR4 | H-BOR-12 | PS6 | 76.1 | 223.9 | SC | 86 | 14 | 12 | 47 | 28 | | | 2.7 | 17.3 | 106.9 | 125.4 | 0.577 | CD | 19.39 | | 15 | 5.89 | | | | |
| TR3/TR4 | H-BOR-12 | ST8 | 81 | 219 | | 85 | 15 | 15 | | | 167 | 122 | 2.67 | 21.9 | 103.5 | 126.2 | 0.611 | RC | | | | 6.18 | | | | |
| TR3/TR4 | H-BOR-12 | ST8 | 81.5 | 218.5 | SC | 84 | 16 | 15 | 34 | 11 | | | 2.7 | 22 | 104.9 | 128.0 | 0.606 | CTXP | | | | 6.21 | | | | |
| DB1/DB3 | H-BOR-12 | ST9 | 85.3 | 214.7 | SC | 80 | 20 | 19 | 42 | 20 | | | 2.69 | 26.3 | 91.9 | 116.1 | 0.827 | CD | 8.15 | | 15 | 6.44 | | | | |
| DB1/DB3 | H-BOR-12 | ST9 | 85.8 | 214.2 | | 88 | 12 | 12 | | | 173 | 120 | 2.7 | 25.1 | 97.2 | 121.6 | 0.733 | CD | 14.6 | | 15 | 6.47 | | | | |
| DB1/DB3 | H-BOR-12 | ST9 | 86.2 | 213.8 | | 88 | 12 | 10 | | | | | 2.74 | 26 | 97.5 | 122.9 | 0.755 | CD | 21.5 | | 15 | 6.49 | | | | |
| DB1/DB3 | H-BOR-12 | PS7 | 92.8 | 207.2 | SC | 83 | 17 | 16 | 39 | 24 | 152 | 112 | 2.66 | 23.75 | 102.15 | 126.4 | | STX | | | | 6.89 | | | | |
| DB1/DB3 | H-BOR-12 | PS7 | 93.4 | 206.6 | SC | 83 | 17 | 17 | 39 | 15 | 173 | 132 | 2.68 | 24.1 | 101.4 | 125.8 | | STX | | | | 6.92 | | | | |
| DB1/DB3 | H-BOR-12 | PS7 | 94 | 206 | SC | 84 | 16 | 15 | 39 | 16 | 174 | 135 | 2.69 | 24.3 | 100 | 124.3 | | STX | | | | 6.96 | | | | |
| DB4 | H-BOR-12 | ST12 | 119 | 181 | SC | 77 | 23 | 18 | 117 | 99 | | | 2.63 | 34.9 | 86.55 | 116.8 | 0.852 | CD | 3.09 | | 10 | 8.46 | | | | |
| DB4 | H-BOR-12 | ST12 | 119.5 | 180.5 | SC | 66 | 34 | 29 | 130 | 108 | | | 2.63 | 37.8 | 83.3 | 114.8 | 0.972 | CD | 12.24 | | 3.5 | 8.49 | | | | |
| DB4 | H-BOR-12 | PS9 | 120.1 | 179.9 | | 50 | 50 | 41 | | | 154 | 128 | 2.62 | 39.9 | 79.7 | 111.5 | 1.051 | CD | 3.36 | | 2.5 | 8.53 | | | | |
| DB4 | H-BOR-12 | ST13 | 126.5 | 173.5 | | | | | | | | | | 53.6 | 70.5 | 108.3 | | | | | | 8.91 | | | | |
| DB4 | H-BOR-12 | ST13 | 129.1 | 170.9 | CH | 18 | 82 | 74 | 155 | 125 | | | 2.71 | 66.1 | 57.9 | 96.2 | 1.9219 | | | | | 9.07 | 9.8 | 0.75 | 0.16 | 0.1 |
| ST | H-BOR-12 | ST15 | 143.3 | 156.7 | | | | | | | | | 2.67 | | | | | | | | | 9.92 | | | | |
| ST | H-BOR-12 | ST15 | 143.8 | 156.3 | SP-SC | 92 | 8 | 6 | 87 | 72 | | | 2.66 | 19.5 | 94.6 | 113.0 | 0.754 | CTXP | | | | 9.94 | | | | |
| ST | H-BOR-12 | ST15 | 144.3 | 155.7 | | 86 | 14 | 6 | | | 166 | 127 | | 21 | 95.9 | 116.0 | 0.739 | RC | | | | 9.98 | | | | |
| ST | H-BOR-12 | ST16 | 151.5 | 148.5 | SC | 70 | 30 | 27 | 43 | 23 | | | 2.65 | 26.7 | 95.4 | 120.9 | 0.7341 | | | | | 10.41 | 11 | 0 13 | 0.01 | 2.5 |
| ST | H-BOR-12 | ST19 | 172.8 | 127.2 | | | | | | | | | | 27.1 | 95.8 | 121.8 | | | | | | 11.69 | | | | |
| ST | H-BOR-12 | ST19 | 173.2 | 126.8 | SC | 84 | 16 | 13 | 32 | 9 | | | 2.71 | 25.9 | 97.9 | 123.3 | 0.728 | | | | | 11.71 | 8.5 | 0.09 | 0.01 | 0.65 |
| ST | H-BOR-12 | ST20 | 179.3 | 120.8 | SC | 75 | 25 | 20 | 32 | 13 | | | 2.65 | 30.7 | 87 | 113.7 | 0.8259 | | | | | 12.07 | 1.2 | 0.19 | 0.02 | 0.8 |
| ST | H-BOR-12 | ST21 | 186.3 | 113.7 | | 78 | 22 | 21 | | | 93 | 67 | 2.67 | 24.7 | 98.2 | 122.5 | | | | | | 12.50 | | | | |
| FILL | H-BOR-2 | ST2 | 39.3 | 290.8 | SC | 53 | 45 | 34 | 57 | 29 | | | 2.68 | 23.2 | 100.4 | 123.7 | 0.666 | UU | 1.22 | 4.75 | 15 | 4.70 | | | | |
| FILL | H-BOR-2 | ST2 | 39.8 | 290.3 | | | | | | | | | 2.68 | 19.1 | 106.8 | 127.2 | 0.567 | | | | | 4.76 | 7.5 | 0 11 | 0.01 | 4.5 |
| TR1 | H-BOR-2 | ST3 | 51.1 | 278.9 | | 47 | 53 | 38 | | | 109 | 80 | 2.63 | | | | | | | | | 6.13 | | | | |

UU - Unconsolidated-Undrained  CD - Consolidated-Drained  CU - Consolidated-Undrained  STX - Stress-Controlled Cylic Triaxial  CTXP - Strain-Controlled Cyclic Triaxial  RC - Resonant Column

Table 4.2-1(a)  Summary of laboratory test results at ITP (Static p1/8).

| SAMPLE IDENTIFICATION | | | | | CLASSIFICATION PROPERTIES | | | | | | | | PHYSICAL PROPERTIES | | | | | | | | | | | | |
|---|---|---|---|---|---|---|---|---|---|---|---|---|---|---|---|---|---|---|---|---|---|---|---|---|---|
| | | | | | | | | | Atterberg Limits | | | | | | | | | Static Strength | | | Consolidation | | | | |
| | | | | | | | | | Liquid | Plas. | Liquid | Plas. | | Natural | Insitu | Insitu | | | | | | | | | |
| Layer | Boring | Sample | Top | Top | USCS | Sand | Fines | Clay | Limit | Index | Limit | Index | Specific | Water | Dry | Wet | Void | Test | Max. Deviator | Confining | Strain | Overburden | Precon. | Compress. | Recomp. | Comp. |
| | No. | No. | Depth | Elev. | Group | (%) | (%) | %<.005mm | on portion <No. 40 | | on portion <-200 | | Gravity | Content | Density | Density | Ratio | Type | Stress | Stress | at Failure | Stress | Stress | Index | Index | Coef. |
| | | | (feet) | (feet) | Symbol | | | | (%) | (%) | (%) | (%) | | (%) | (pcf) | (pcf) | | | (ksf) | (ksf) | (%) | (ksf) | (ksf) | Cc | Cr | Cv |
| TR1 | H-BOR-2 | ST3 | 51.5 | 278.5 | CH | 43 | 57 | 43 | 59 | 38 | | | 2.62 | | | | | | | | | 6 18 | | | | |
| TR1 | H-BOR-2 | ST3 | 51.9 | 278.1 | | | | | | | | | | 20.2 | 102.1 | 122.7 | 0.6203 | | | | | 6.23 | 10 | 0.17 | 0.02 | 1.4 |
| TR1 | H-BOR-2 | ST3 | 52.3 | 277.7 | SC | 52 | 48 | 37 | 60 | 35 | | | 2.65 | 24.3 | 96.7 | 120.2 | 0.712 | UU | 3.21 | 5.76 | 15 | 6.26 | | | | |
| TR3/TR4 | H-BOR-2 | PS4 | 91.2 | 238.8 | SC | 67 | 33 | 24 | 49 | 33 | 125 | 82 | 2.67 | 21.45 | 105.15 | 127.7 | | STX | | | | 8.59 | | | | |
| TR3/TR4 | H-BOR-2 | PS4 | 91.8 | 238.2 | SC | 66 | 34 | 24 | 47 | 31 | 123 | 82 | 2.68 | 20.9 | 106.4 | 128.6 | | STX | | | | 8.63 | | | | |
| TR3/TR4 | H-BOR-2 | PS5 | 94.1 | 235.9 | SC | 73 | 27 | 22 | 45 | 28 | 151 | 105 | 2.65 | 23.45 | 101.85 | 125.7 | | STX | | | | 8.77 | | | | |
| TR3/TR4 | H-BOR-2 | PS5 | 94.7 | 235.3 | SC | 70 | 30 | 28 | 52 | 31 | 187 | 152 | 2.7 | 27.4 | 95.8 | 122.0 | | STX | | | | 8.80 | | | | |
| TR3/TR4 | H-BOR-2 | PS5 | 95.2 | 234.8 | SC | 74 | 26 | 20 | | | | | | 25.2 | 91.9 | 115.1 | | STX | | | | 8.83 | | | | |
| TR3/TR4 | H-BOR-2 | PS5 | 95.3 | 234.7 | | | | | 51 | 34 | 179 | 136 | 2.63 | | | | | | | | | 8.84 | | | | |
| TR3/TR4 | H-BOR-2 | PS6 | 97 | 233 | SC | 78 | 22 | 18 | 46 | 28 | 186 | 144 | 2.66 | 24.45 | 100.5 | 125.1 | | STX | | | | 8.94 | | | | |
| TR3/TR4 | H-BOR-2 | PS6 | 97.6 | 232.4 | SC | 80 | 20 | 19 | 48 | 29 | 182 | 128 | 2.64 | 22.8 | 102.7 | 126.1 | | STX | | | | 8.98 | | | | |
| TR3/TR4 | H-BOR-2 | PS6 | 98.2 | 231.8 | SC | 81 | 19 | 17 | 51 | 31 | 192 | 156 | 2.67 | 21.6 | 104.5 | 127.1 | | STX | | | | 9.01 | | | | |
| TR3/TR4 | H-BOR-2 | ST4 | 110.2 | 219.8 | | 90 | 10 | 10 | | | 196 | 141 | 2.66 | 26.6 | 90.5 | 114.6 | 0.835 | CD | 12.1 | | 11 | 9.73 | | | | |
| TR3/TR4 | H-BOR-2 | ST4 | 110.7 | 219.3 | SC | 87 | 13 | 11 | | | | | 2.69 | 28.1 | 94.5 | 121.1 | 0.778 | CD | 26.6 | | 15 | 9.76 | | | | |
| DB1/DB3 | H-BOR-2 | ST5 | 120 | 210 | | | | | | | | | 2.69 | 24.1 | 100 | 124.1 | 0.6793 | | | | | 10.32 | 6 | 0.1 | 0.01 | 3.1 |
| DB1/DB3 | H-BOR-2 | ST5 | 120.4 | 209.6 | | 87 | 13 | 12 | | | | | | | | | | | | | | 10.34 | | | | |
| DB1/DB3 | H-BOR-2 | ST5 | 120.9 | 209.1 | | 91 | 9 | 8 | | | 80 | 60 | 2.73 | 21.3 | 95.1 | 115.4 | | CTXP | | | | 10.37 | | | | |
| DB1/DB3 | H-BOR-2 | ST6 | 136.3 | 193.8 | | 83 | 14 | 11 | | | 149 | 119 | 2.61 | 31.1 | 101 | 132.4 | | | | | | 11.29 | | | | |
| DB1/DB3 | H-BOR-2 | PS7 | 142 | 188 | SC | 86.5 | 12.5 | 9 | 55 | 39 | | | 2.68 | 19.5 | 105.2 | 125.7 | | | | | | 11.64 | | | | |
| DB4 | H-BOR-2 | PS8 | 144.8 | 185.2 | | | | | | | | | | 31.1 | 92.3 | 121.0 | | | | | | 11.81 | | | | |
| DB4 | H-BOR-2 | PS8 | 144.9 | 185.1 | | | | | | | | | | 41.5 | 78.2 | 110.7 | 1.163 | CTXP | | | | 11.81 | | | | |
| DB4 | H-BOR-2 | PS8 | 145.1 | 184.9 | | | | | | | | | | 23.1 | 84.9 | 104.5 | 0.9926 | | | | | 11.83 | 8 | 0 24 | 0.04 | 0.6 |
| DB4 | H-BOR-2 | PS8 | 145.5 | 184.5 | SC | 79 | 21 | 20 | 139 | 113 | | | 2.71 | | | | | | | | | 11.85 | | | | |
| DB4 | H-BOR-2 | PS8 | 146 | 184 | | 39 | 61 | 53 | | | 231 | 179 | 2.67 | | | | | | | | | 11.88 | | | | |
| ST | H-BOR-2 | ST9 | 162.4 | 167.6 | SP | 97 | 3 | 3 | | | 148 | 121 | 2.64 | 16.7 | 105.9 | 123.6 | | | | | | 12.86 | | | | |
| ST | H-BOR-2 | ST10 | 167.6 | 162.4 | | 91 | 9 | 8 | | | | | 2.64 | 24 6 | 95.6 | 119.1 | 0.724 | CD | 8.69 | | 8 | 13.18 | | | | |
| ST | H-BOR-2 | ST10 | 168.1 | 161.9 | | 89 | 11 | 9 | | | | | 2.64 | 25.1 | 94 | 117.6 | 0.753 | CD | 15.9 | | 13 | 13.21 | | | | |
| ST | H-BOR-2 | PS11 | 170.4 | 159.6 | SC | 78 | 22 | 18 | 47 | 29 | 104 | 66 | 2.71 | 48.7 | 78.5 | 116.7 | | STX | | | | 13.34 | | | | |
| ST | H-BOR-2 | PS12 | 173 | 157 | | | | | | | | | | 29.3 | 90.3 | 116.8 | | | | | | 13.50 | | | | |
| ST | H-BOR-2 | PS12 | 174.5 | 155.5 | SC | 74 | 26 | 18 | 43 | 19 | | | 2.66 | 29.3 | 89.6 | 115.9 | 0.8533 | | | | | 13.59 | 15 | 0.2 | 0.01 | 2 |
| ST | H-BOR-2 | PS13 | 175.1 | 154.9 | SC | 59 | 40 | 37 | 47 | 23 | 97 | 56 | 2.72 | 37.35 | 79 | 108.5 | | STX | | | | 13.63 | | | | |
| ST | H-BOR-2 | PS13 | 175.7 | 154.3 | SC | 79 | 21 | 20 | 48 | 24 | 115 | 74 | 2.73 | 31.6 | 89.2 | 117.4 | | STX | | | | 13.66 | | | | |
| ST | H-BOR-2 | PS13 | 176.3 | 153.7 | SM | 73 | 27 | 23 | 47 | 15 | 110 | 64 | 2.74 | 46.5 | 72.8 | 106.7 | | STX | | | | 13.70 | | | | |
| ST | H-BOR-2 | PS14 | 178.1 | 151.9 | SC | 79 | 21 | 19 | 45 | 20 | 169 | 128 | 2.67 | 57.05 | 70.65 | 111.0 | | STX | | | | 13.81 | | | | |
| ST | H-BOR-2 | PS14 | 178.7 | 151.3 | SC | 54 | 42 | 39 | 90 | 59 | 180 | 129 | 2.72 | 80.3 | 54 | 97.4 | | STX | | | | 13.84 | | | | |
| ST | H-BOR-2 | PS14 | 179.5 | 150.5 | | 79 | 21 | 18 | | | | | 2.62 | | | | | STX | | | | 13.89 | | | | |
| ST | H-BOR-2 | ST11 | 184 | 146 | | 80 | 20 | 14 | | | 169 | 134 | 2.69 | 36.9 | 82.8 | 113.4 | 1.029 | CD | 12.45 | | 15 | 14 16 | | | | |
| ST | H-BOR-2 | ST11 | 184.5 | 145.5 | SC | 83 | 17 | 10 | 35 | 12 | | | 2.65 | 30 5 | 91.9 | 119.9 | 0.801 | CD | 19.48 | | 15 | 14.19 | | | | |
| ST | H-BOR-2 | ST13 | 193 | 137 | SC | 80 | 20 | 12 | 37 | 13 | | | 2.68 | 26.2 | 96.6 | 121.9 | 0 7319 | | | | | 14.70 | 25 | 0 15 | 0.01 | 3 |
| ST | H-BOR-2 | ST13 | 193.5 | 136.5 | | | | | | | | | | 26 2 | 94.5 | 119.3 | | | | | | 14.73 | | | | |
| ST | H-BOR-2 | ST14 | 200.5 | 129.5 | | 89 | 11 | 7 | | | 127 | 101 | 2.67 | 29.5 | 92.9 | 120 3 | 0.794 | CD | 9.57 | | 12.5 | 15.15 | | | | |
| ST | H-BOR-2 | ST14 | 201 | 129 | | 89 | 11 | 6 | | | | | 2.7 | 28.5 | 92 9 | 119.4 | 0.813 | CD | 17.08 | | 11.5 | 15.18 | | | | |
| ST | H-BOR-2 | ST14 | 201.6 | 128.4 | | 84 | 16 | 15 | | | 171 | 140 | 2 7 | 28.7 | 92.3 | 118 8 | 0.826 | CD | 19.83 | | 13 5 | 15.22 | | | | |
| ST | H-BOR-2 | ST15 | 207.3 | 122.8 | SC | 60 | 40 | 28 | 45 | 23 | | | 2.66 | 23.1 | 101 1 | 124 5 | | | | | | 15.55 | | | | |
| TR3/TR4 | H-BOR-23 | PS1 | 28.7 | 267.9 | | | | | | | | | | 20.8 | 83.8 | 101.2 | | | | | | 2.84 | | | | |
| TR3/TR4 | H-BOR-23 | PS1 | 28.9 | 267.7 | SC | 78 | 22 | 16 | 41 | 26 | | | 2.67 | 20 3 | 107.2 | 129.0 | 0.556 | RC | | | | 2.85 | | | | |
| TR3/TR4 | H-BOR-23 | PS1 | 29.5 | 267.1 | SC | 80 | 20 | 17 | 38 | 21 | | | 2 7 | 21.3 | 103 3 | 125 3 | 0.614 | CTXP | | | | 2.88 | | | | |
| TR3/TR4 | H-BOR-23 | PS2 | 33.3 | 263 3 | SC | 68 | 32 | 24 | 47 | 31 | 124 | 78 | 2 63 | 21 2 | 104 2 | 126 3 | | STX | | | | 3 11 | | | | |

UU - Unconsolidated-Undrained  CD - Consolidated-Drained  CU - Consolidated-Undrained  STX - Stress-Controlled Cylic Triaxial  CTXP - Strain-Controlled Cyclic Triaxial  RC - Resonant Column

Table 4.2-1(a)  Summary of laboratory test results at ITP (Static p2/8).

| SAMPLE IDENTIFICATION | | | | | CLASSIFICATION PROPERTIES | | | | | | | | PHYSICAL PROPERTIES | | | | | | | | | | | | | |
|---|---|---|---|---|---|---|---|---|---|---|---|---|---|---|---|---|---|---|---|---|---|---|---|---|---|---|
| | | | | | | | | | Atterberg Limits | | | | | | | | | | Static Strength | | | | Consolidation | | | |
| | | | | | | | | | Liquid | Plas. | Liquid | Plas. | | Natural | Insitu | Insitu | | | | | | | | | | |
| Layer | Boring No. | Sample No. | Top Depth (feet) | Top Elev. (feet) | USCS Group Symbol | Sand (%) | Fines (%) | Clay %<.005mm | Limit on portion <No. 40 (%) | Index on portion <No. 40 (%) | Limit on portion <-200 (%) | Index on portion <-200 (%) | Specific Gravity | Water Content (%) | Dry Density (pcf) | Wet Density (pcf) | Void Ratio | Test Type | Max. Deviator Stress (ksf) | Confining Stress (ksf) | Strain at Failure (%) | Overburden Stress (ksf) | Precon. Stress (ksf) | Compress. Index Cc | Recomp. Index Cr | Comp. Coef. Cv |
| TR3/TR4 | H-BOR-23 | PS2 | 33.9 | 262.7 | SC | 64 | 36 | 25 | 49 | 26 | 117 | 73 | 2.7 | 21.7 | 103.1 | 125.5 | | STX | | | | 3.15 | | | | |
| TR3/TR4 | H-BOR-23 | PS2 | 34.5 | 262.1 | SC | 67 | 33 | 23 | 44 | 26 | 115 | 74 | 2.71 | 22.2 | 100.4 | 122.7 | | STX | | | | 3.18 | | | | |
| TR3/TR4 | H-BOR-23 | PS3 | 40.2 | 256.4 | SC | 79 | 21 | 18 | 44 | 20 | 163 | 125 | 2.63 | 20.6 | 105.35 | 127.1 | | STX | | | | 3.53 | | | | |
| TR3/TR4 | H-BOR-23 | PS3 | 40.8 | 255.8 | SC | 81 | 19 | 17 | 46 | 29 | 191 | 152 | 2.65 | 20.2 | 104.1 | 125.1 | | STX | | | | 3.56 | | | | |
| TR3/TR4 | H-BOR-23 | PS3 | 41.4 | 255.2 | SC | 82.5 | 17 | 14 | 50 | 26 | 178 | 145 | 2.68 | 21.5 | 103.5 | 125.8 | | STX | | | | 3.60 | | | | |
| TR3/TR4 | H-BOR-23 | ST2 | 43.4 | 253.2 | | 86 | 14 | 12 | | | 168 | 125 | 2.66 | 22 | 99.7 | 121.6 | 0.666 | CU | 3.81 | 3.89 | 15 | 3.72 | | | | |
| TR3/TR4 | H-BOR-23 | ST2 | 43.9 | 252.7 | SC | 86 | 14 | 12 | 41 | 19 | | | 2.71 | 21.6 | 100.3 | 122.0 | 0.687 | CU | 7.86 | 15.47 | 15 | 3.75 | | | | |
| DB1/DB3 | H-BOR-23 | ST3 | 50.5 | 246.1 | | 89 | 11 | 4 | | | | | 2.68 | | | | | | | | | 4.14 | | | | |
| DB1/DB3 | H-BOR-23 | ST4 | 55.1 | 241.5 | SP-SC | 92 | 8 | 7 | 27 | 8 | | | 2.69 | 24.7 | 98.8 | 123.2 | 0.698 | CTXP | | | | 4.42 | | | | |
| DB1/DB3 | H-BOR-23 | ST4 | 55.7 | 240.9 | | 92 | 8 | 7 | | | 127 | 86 | 2.68 | 22.7 | 97.8 | 120.0 | 0.712 | RC | | | | 4.46 | | | | |
| DB1/DB3 | H-BOR-23 | ST5 | 60.6 | 236 | SC | 84 | 16 | 14 | 49 | 30 | | | 2.67 | 23.4 | 97.7 | 120.6 | 0.706 | CD | 5.15 | | 15 | 4.75 | | | | |
| DB1/DB3 | H-BOR-23 | ST5 | 61.1 | 235.5 | | 90.5 | 9.5 | 8 | | | 178 | 138 | 2.7 | 22.7 | 96.4 | 118.3 | 0.729 | CD | 9.63 | | 15 | 4.78 | | | | |
| DB1/DB3 | H-BOR-23 | ST6 | 65 | 231.6 | SP-SC | 94 | 6 | 6 | 112 | 73 | | | 2.64 | 24.8 | 98.4 | 122.8 | 0.6749 | | | | | 5.01 | 9 | 0.08 | 0.01 | 3.5 |
| DB1/DB3 | H-BOR-23 | ST6 | 65.8 | 230.8 | | | | | | | | | | 21.8 | 100.7 | 122.7 | | | | | | 5.06 | | | | |
| DB4 | H-BOR-23 | PS4 | 83.8 | 212.8 | SC | 72 | 28 | 22 | 90 | 70 | 201 | 163 | 2.71 | 25 | 97.4 | 121.8 | | STX | | | | 6.14 | | | | |
| DB4 | H-BOR-23 | PS4 | 84.5 | 212.1 | SC | 83 | 17 | 14 | 90 | 70 | 193 | 145 | 2.74 | 24.7 | 96.3 | 120.1 | | STX | | | | 6.18 | | | | |
| DB4 | H-BOR-23 | PS4 | 85 | 211.6 | SW-SC | 89 | 11 | 10 | 61 | 46 | 229 | 200 | 2.64 | 25.2 | 90.9 | 113.8 | | STX | | | | 6.21 | | | | |
| DB5 | H-BOR-23 | PS5 | 95.7 | 200.9 | | | | | | | | | | 35.5 | 81.1 | 109.9 | | | | | | 6.86 | | | | |
| DB5 | H-BOR-23 | PS5 | 96.9 | 199.7 | SC | 55 | 45 | 28 | 66 | 50 | | | 2.68 | 35.5 | 74 | 100.3 | 1.2609 | | | | | 6.93 | 10 | 0.6 | 0.04 | 2.6 |
| ST | H-BOR-23 | PB4 | 119.3 | 177.3 | | 77.5 | 22 | 12 | | | 110 | 85 | 2.65 | 29.15 | 91.25 | 117.8 | 1.0298 | | | | | 8.27 | 6 | 0.37 | 0.04 | 1.8 |
| ST | H-BOR-23 | PB8 | 142 | 154.6 | GP-GC | 27 | 12 | 5 | 29 | 13 | | | 2.72 | | | | | | | | | 9.63 | | | | |
| ST | H-BOR-23 | PB9 | 148.4 | 148.2 | | 81 | 11 | 6 | | | | | 2.68 | 13.9 | 95.3 | 108.5 | | | | | | 10.02 | | | | |
| ST | H-BOR-23 | PB11 | 158.9 | 137.7 | | 68 | 32 | 15 | | | | | 2.56 | 51.6 | 66.1 | 100.2 | 1.4177 | | | | | 10.65 | 17 | 0.46 | 0.03 | 0.9 |
| ST | H-BOR-23 | PB11 | 159.4 | 137.2 | | | | | | | | | | 42.4 | 70.4 | 100.2 | | | | | | 10.68 | | | | |
| ST | H-BOR-23 | PB12 | 164.9 | 131.7 | | 79 | 21 | 18 | | | 138 | 97 | 2.67 | 27 | 93.3 | 118.5 | 0.786 | CD | 11.13 | | 11 | 11.01 | | | | |
| ST | H-BOR-23 | PB14 | 175.7 | 120.9 | | | | | | | | | | 30.8 | 89.2 | 116.7 | | | | | | 11.66 | | | | |
| ST | H-BOR-23 | PB14 | 176.2 | 120.4 | SC | 48 | 52 | 21 | 47 | 23 | | | 2.65 | 33.8 | 85.8 | 114.8 | 0.9281 | | | | | 11.69 | 28 | 0.29 | 0.01 | 0.5 |
| FILL | H-BOR-34 | ST1 | 30.5 | 295.5 | SC | 56.9 | 39.1 | 32.0 | 57 | 35 | | | 2.69 | 20.2 | 105.4 | 126.7 | 0.593 | UU | 3.17 | 3.60 | 15.0 | | | | | |
| FILL | H-BOR-34 | ST2 | 37.0 | 289.0 | SC | 61.8 | 38.2 | 33.0 | 60 | 38 | | | 2.68 | 16.9 | 112.4 | 131.4 | 0.489 | UU | 3.04 | 4.32 | | | | | | |
| FILL | H-BOR-34 | ST3 | 39.0 | 287.0 | SC | 55.0 | 45.0 | 40.0 | 41 | 22 | | | 2.70 | 27 | 102.4 | 130.0 | 0.647 | UU | 1.89 | 4.75 | 15.0 | | | | | |
| DB5 | H-BOR-50 | ST5 | 154.5 | 171.6 | SP-SM | 91.9 | 8.1 | 8.0 | 32 | 7 | | | 2.70 | 37 | 82.8 | 113.4 | 1.035 | CD | 13.59 | | 15.0 | | | | | |
| DB5 | H-BOR-50 | ST5 | 155.0 | 171.1 | SC | 55.0 | 45.0 | 36.0 | 52 | 34 | | | | 35.6 | 87.35 | 118.4 | 0.977 | CD | 17.02 | | 8.0 | 12.40 | 0.70 | 0.47 | 0.01 | 0.03 |
| FILL | H-BOR-54 | ST1 | 10.0 | 316.1 | SC | 61.9 | 37.1 | 29.0 | 50 | 30 | | | 2.65 | 19.9 | 105.8 | 126.9 | 0.564 | UU | 2.29 | 1.30 | 15.0 | | | | | |
| FILL | H-BOR-54 | ST2 | 15.0 | 311.1 | SC | 55.9 | 42.0 | 37.0 | 81 | 56 | | | 2.66 | 18.1 | 107.7 | 127.2 | 0.535 | UU | 4.00 | 1.83 | 4.4 | | | | | |
| FILL | H-BOR-54 | ST3 | 20.0 | 306.1 | SC | 59.0 | 41.0 | 38.0 | 62 | 41 | | | 2.64 | 17.6 | 108.1 | 127.1 | 0.53 | UU | 4.65 | 2.51 | 15.0 | | | | | |
| FILL | H-BOR-54 | ST4 | 25.0 | 301.1 | SC | 49.9 | 49.1 | 44.0 | 55 | 30 | | | 2.69 | 18.1 | 109.5 | 129.3 | 0.511 | UU | 3.98 | 3.10 | 15.0 | | | | | |
| FILL | H-BOR-54 | ST5 | 30.0 | 296.1 | SC | 57.9 | 39.1 | 36.0 | 56 | 28 | | | 2.69 | 16.4 | 108.3 | 126.1 | 0.527 | UU | 5.17 | 3.70 | 15.0 | | | | | |
| FILL | H-BOR-54 | ST6 | 35.0 | 291.1 | SC | 50.9 | 47.1 | 43.0 | 54 | 36 | | | 2.65 | 17.7 | 111.2 | 130.9 | 0.487 | UU | 6.39 | 4.20 | 15.0 | | | | | |
| FILL | H-BOR-54 | ST7 | 39.0 | 287.1 | SC | 52.9 | 47.1 | 41.0 | 61 | 40 | | | 2.65 | 20.9 | 101.6 | 122.8 | 0.629 | UU | 3.41 | 4.80 | 15.0 | | | | | |
| TR3/TR4 | HBOR23.3 | SS19 | 37.0 | 258.2 | SC | 70.5 | 28.5 | 19.0 | 41 | 22 | | | | 19.8 | | | | | | | | | | | | |
| DB1/DB3 | HBOR23.3 | ST1 | 49.0 | 246.2 | | 88.0 | 12.0 | 11.0 | | | | | 2.67 | 25.5 | 93.9 | 117.8 | 0.775 | CD | 7.78 | | 10.0 | | | | | |
| DB1/DB3 | HBOR23.3 | ST1 | 49.5 | 245.7 | SC | 77.9 | 22.1 | 18.0 | 44 | 23 | | | | 25.9 | 95.5 | 120.2 | 0.746 | CD | 10.09 | | 15.0 | | | | | |
| DB1/DB3 | HBOR23.3 | ST1 | 50.0 | 245.2 | | | | | | | | | | 25.7 | 98.2 | 123.4 | 0.697 | | | | | 4.10 | 2.00 | 0.12 | 0.01 | 0.40 |
| DB1/DB3 | HBOR23.3 | ST1 | 55 6 | 239.6 | SP-SC | 94.0 | 6.0 | 5.0 | 33 | 10 | | | | 27.1 | | | | | | | | | | | | |
| DB1/DB3 | HBOR23.3 | SS34 | 61.0 | 234.2 | SP-SC | 89.5 | 10.5 | 10.5 | 34 | 16 | | | | 28.5 | | | | | | | | | | | | |
| DB1/DB3 | HBOR23.3 | SS35 | 62.5 | 232.7 | SP-SM | 89.0 | 11.0 | 10.5 | 33 | 9 | | | | 25.7 | | | | | | | | | | | | |
| DB1/DB3 | HBOR23.3 | ST2 | 64.0 | 231.2 | SP-SC | 90.0 | 10.0 | 10.0 | 34 | 17 | | | 2.69 | 26 | 94.7 | 119.3 | 0.774 | CD | 9.04 | | 15.0 | | | | | |
| DB1/DB3 | HBOR23.3 | ST2 | 64.5 | 230.7 | SP-SC | 90.0 | 10.0 | 9.5 | 34 | 13 | | | | 22.6 | 100.3 | 123.0 | 0 674 | CD | 12.68 | | 15.0 | | | | | |

UU - Unconsolidated-Undrained  CD - Consolidated-Drained  CU - Consolidated-Undrained  STX - Stress-Controlled Cylic Triaxial  CTXP - Strain-Controlled Cyclic Triaxial  RC - Resonant Column

Table 4.2-1(a)  Summary of laboratory test results at ITP (Static p3/8).

| SAMPLE IDENTIFICATION | | | | | CLASSIFICATION PROPERTIES | | | | | | | | PHYSICAL PROPERTIES | | | | | | | | | | | | | |
|---|---|---|---|---|---|---|---|---|---|---|---|---|---|---|---|---|---|---|---|---|---|---|---|---|---|---|
| | | | | | | | | | Atterberg Limits | | | | | | | | | | | | | | Consolidation | | | |
| | | | | | | | | | Liquid | Plas. | Liquid | Plas. | | Natural | Insitu | Insitu | | | Static Strength | | | | | | | |
| Layer | Boring No. | Sample No. | Top Depth | Top Elev. | USCS Group | Sand (%) | Fines (%) | Clay %<.005mm | Limit on portion <No. 40 | Index | Limit on portion <-200 | Index | Specific Gravity | Water Content | Dry Density | Wet Density | Void Ratio | Test Type | Max. Deviator Stress | Confining Stress | Strain at Failure | Overburden Stress | Precon. Stress | Compress. Index | Recomp. Index | Comp. Coef. |
| | | | (feet) | (feet) | Symbol | | | | (%) | (%) | | | | (%) | (pcf) | (pcf) | | | (ksf) | (ksf) | (%) | (ksf) | (ksf) | Cc | Cr | Cv |
| DB1/DB3 | HBOR23.3 | ST2 | 65.0 | 230.2 | | | | | | | | | | 25.4 | 95.6 | 119.9 | 0.75 | | | | | 5.20 | 2.20 | 0.16 | 0.01 | 0.45 |
| DB1/DB3 | HBOR23.3 | SS40 | 71.5 | 223.7 | | 94.0 | 6.0 | 6.0 | | | | | | 20.2 | | | | | | | | | | | | |
| DB1/DB3 | HBOR23.3 | SS43 | 76.0 | 219.2 | | 92.0 | 8.0 | 6.0 | | | | | | 21.6 | | | | | | | | | | | | |
| DB1/DB3 | HBOR23.3 | SS44 | 77.5 | 217.7 | SC | 87.4 | 12.6 | 12.0 | 36 | 14 | | | | 27.3 | | | | | | | | | | | | |
| DB5 | HBOR23.3 | SS53 | 91.0 | 204.2 | SC | 61.8 | 25.2 | 22.0 | 84 | 65 | | | | 39.1 | | | | | | | | | | | | |
| ST | HBOR23.3 | SS65 | 109.0 | 186.2 | CH | 41.9 | 58.1 | 45.0 | 128 | 100 | | | | 78.9 | | | | | | | | | | | | |
| ST | HBOR23.3 | SS66 | 110.5 | 184.7 | SC | 54.9 | 45.1 | 37.0 | 144 | 120 | | | | 27.2 | | | | | | | | | | | | |
| ST | HBOR23.3 | SS67 | 112.0 | 183.2 | SM | 60.9 | 12.0 | 9.0 | 45 | 10 | | | | 27.3 | | | | | | | | | | | | |
| FILL | H-BOR-29 | ST1 | 10.4 | 318.2 | SC | 66 | 34 | 28 | 100 | 67 | | | 2.66 | 23.2 | 100 | 123.2 | 0.661 | UU | 1.44 | 1.3 | 15 | 1.24 | | | | |
| FILL | H-BOR-29 | ST2 | 15.4 | 313.2 | SC | 64 | 36 | 28 | 60 | 36 | | | 2.66 | 19.4 | 105.6 | 126.1 | 0.573 | RC | | | | 1.84 | | | | |
| FILL | H-BOR-29 | ST3 | 20 | 308.6 | SC | 64 | 33 | 28 | 73 | 42 | | | 2.66 | 19.1 | 103 | 122.7 | 0.618 | CU | 2.6 | 2.12 | 15 | 2.39 | | | | |
| FILL | H-BOR-29 | ST3 | 20.6 | 308 | | 59 | 40 | 38 | | | 144 | 100 | 2.67 | 20.8 | 102.2 | 123.5 | 0.63 | CU | 3.92 | 4.04 | 15 | 2.47 | | | | |
| FILL | H-BOR-29 | ST3 | 21.2 | 307.4 | | | | | | | | | | 20.5 | 97 | 116.9 | 0.7119 | | | | | 2.54 | 5.1 | 0.22 | 0.01 | 2. |
| FILL | H-BOR-29 | ST4 | 25 | 303.6 | | 59 | 41 | 36 | | | 110 | 65 | 2.66 | 19.8 | 95 | 113.8 | 0.747 | RC | | | | 2.99 | | | | |
| FILL | H-BOR-29 | ST4 | 25.7 | 302.9 | SC | 54 | 46 | 39 | 55 | 32 | | | 2.6 | 23.5 | 95.9 | 118.4 | 0.731 | CTXP | | | | 3.08 | | | | |
| FILL | H-BOR-29 | ST5 | 30.6 | 298 | | 51 | 49 | 43 | | | 96 | 57 | 2.68 | 20 | 99.5 | 119.4 | 0.681 | CD | 5.77 | | 15 | 3.67 | | | | |
| FILL | H-BOR-29 | ST5 | 31.1 | 297.5 | SC | 53 | 47 | 39 | 55 | 29 | | | 2.72 | 19.5 | 97.4 | 116.4 | 0.743 | CD | 8.19 | | 15 | 3.73 | | | | |
| FILL | H-BOR-29 | ST6 | 35.4 | 293.2 | | | | | | | | | | 16.9 | 89.8 | 105.0 | 0.8492 | | | | | 4.24 | 2.7 | 0.22 | 0.03 | 1.85 |
| FILL | H-BOR-29 | ST6 | 35.8 | 292.8 | SC | 72 | 28 | 22 | 57 | 37 | | | 2.66 | 14.9 | 111.8 | 128.5 | 0.485 | CU | 4.68 | 8.64 | 15 | 4.29 | | | | |
| FILL | H-BOR-29 | ST6 | 36.3 | 292.3 | | 66 | 32 | 28 | | | 110 | 74 | 2.65 | 14.6 | 113.4 | 130.0 | 0.459 | CU | 4.65 | 4.32 | 15 | 4.35 | | | | |
| FILL | H-BOR-29 | ST6 | 36.8 | 291.8 | SC | 66 | 32 | 28 | 64 | 43 | | | 2.66 | 21.9 | 103.9 | 126.7 | 0.599 | CU | 1.24 | 2.16 | 15 | 4.41 | | | | |
| TR1 | H-BOR-29 | ST7 | 41.1 | 287.5 | SC | 61 | 39 | 32 | 45 | 29 | | | 2.67 | 16.6 | 109 | 127.1 | 0.552 | CU | 4.4 | 4.32 | 15 | 4.93 | | | | |
| TR1 | H-BOR-29 | ST7 | 41.6 | 287 | | 60.5 | 39 | 35 | | | 89 | 67 | 2.7 | 15.2 | 115.2 | 132.7 | 0.447 | CU | 12.21 | 8.64 | 15 | 4.99 | | | | |
| TR1 | H-BOR-29 | ST9 | 46.1 | 282.5 | SC | 68 | 32 | 25 | 60 | 37 | | | 2.63 | 17.3 | 97.3 | 114.1 | 0.687 | CU | 5.24 | 12.95 | 15 | 5.53 | | | | |
| TR1 | H-BOR-29 | PS2 | 53.7 | 274.9 | SC | 76.5 | 23 | 18 | 101 | 72 | 162 | 122 | 2.69 | 20.7 | 101.8 | 122.9 | | STX | | | | 6.25 | | | | |
| TR1 | H-BOR-29 | ST11 | 59.3 | 269.3 | | 71 | 28 | 23 | | | 169 | 127 | 2.64 | 19 | 101.3 | 120.5 | 0.627 | CU | 5.16 | 6.33 | 15 | 6.59 | | | | |
| TR1 | H-BOR-29 | ST11 | 59.9 | 268.7 | SC | 72 | 25 | 18 | 97 | 71 | | | 2.62 | 15.1 | 102.4 | 117.9 | 0.598 | CU | 3.76 | 3.17 | 15 | 6.62 | | | | |
| TR1 | H-BOR-29 | PS4 | 64 | 264.6 | | | | | | | | | | 31.5 | 92.6 | 121.8 | | | | | | 6.87 | | | | |
| TR1 | H-BOR-29 | PS4 | 65.5 | 263.1 | CH | 4 | 96 | 80 | 92 | 58 | | | 2.67 | 31.5 | 89.3 | 117.4 | 0.8665 | | | | | 6.96 | 17 | 0.27 | 0.03 | 1.5 |
| TR1 | H-BOR-29 | PS5 | 67 | 261.6 | SC | 78 | 21 | 18 | 89 | 66 | | | 2.67 | 19.9 | 104.6 | 125.4 | 0.591 | CD | 17.63 | | 11 | 7.05 | | | | |
| TR1 | H-BOR-29 | PS5 | 67.5 | 261.1 | SC | 80 | 20 | 17 | 104 | 79 | | | 2.68 | 20.1 | 100.5 | 120.7 | 0.665 | CD | 5.64 | | 15 | 7.08 | | | | |
| TR1 | H-BOR-29 | PS5 | 68 | 260.6 | | 67.5 | 32 | 28 | | | 150 | 111 | 2.67 | 21.6 | 102.1 | 124.2 | 0.633 | CD | 18.06 | | 15 | 7.11 | | | | |
| TR3/TR4 | H-BOR-29 | PS7 | 90.5 | 238.1 | SC | 70 | 30 | 21 | 49 | 30 | 106 | 66 | 2.68 | 22.7 | 104.35 | 128.0 | | STX | | | | 8.46 | | | | |
| TR3/TR4 | H-BOR-29 | PS7 | 91.1 | 237.5 | SC | 63 | 37 | 23 | 48 | 30 | 121 | 84 | 2.63 | 22.3 | 105.2 | 128.7 | | STX | | | | 8.50 | | | | |
| TR3/TR4 | H-BOR-29 | PS7 | 91.7 | 236.9 | SC | 68 | 32 | 21 | 47 | 27 | 106 | 66 | 2.65 | 20.6 | 58.8 | 70.9 | | STX | | | | 8.53 | | | | |
| TR3/TR4 | H-BOR-29 | PS8 | 92 | 236.6 | | | | | | | | | | 17.9 | 112.1 | 132.2 | | | | | | 8.55 | | | | |
| TR3/TR4 | H-BOR-29 | PS8 | 92.3 | 236.3 | SC | 73 | 27 | 19 | 51 | 28 | | | 2.68 | 14.8 | 113 | 129.7 | 0.481 | CU | 4.37 | 4.32 | 15 | 8.57 | | | | |
| TR3/TR4 | H-BOR-29 | PS8 | 92.8 | 235.8 | | 71 | 29 | 19 | | | 109 | 76 | 2.7 | 18.3 | 110 | 130.1 | 0.533 | CU | 4.22 | 8.63 | 12 | 8.60 | | | | |
| TR3/TR4 | H-BOR-29 | PS8 | 93.4 | 235.2 | SC | 77 | 23 | 19 | 46 | 31 | | | 2.68 | 20.6 | 106.4 | 128.3 | 0.572 | CU | 5.16 | 12.97 | 15 | 8.63 | | | | |
| TR3/TR4 | H-BOR-29 | PS9 | 95.8 | 232.8 | | | | | | | | | | 25.55 | 97.6 | 122.5 | 0.796 | | | | | 8.78 | 8 | 0.21 | 0.03 | 1.8 |
| TR3/TR4 | H-BOR-29 | PS9 | 96 | 232.6 | SC | 74 | 26 | 20 | 53 | 27 | | | 2.69 | 25.2 | 98.4 | 123.2 | 0.706 | CD | 4.8 | | 10 | 8.79 | | | | |
| TR3/TR4 | H-BOR-29 | PS9 | 96.6 | 232 | | 78 | 22 | 18 | | | 167 | 128 | 2.72 | 22.7 | 103 | 126.4 | 0.649 | CD | 9.25 | | 15 | 8.83 | | | | |
| TR3/TR4 | H-BOR-29 | PS9 | 97.1 | 231.5 | SC | 79 | 21 | 18 | 46 | 25 | | | 2.74 | 21.5 | 103.8 | 126.1 | 0.647 | CD | 17 | | 15 | 8.86 | | | | |
| DB1/DB3 | H-BOR-29 | ST18 | 121.8 | 206.8 | | 94 | 6 | 5 | | | 201 | 169 | 2.68 | 23.3 | 101.1 | 124.7 | 0.642 | CD | 7.4 | | 6.5 | 10.34 | | | | |
| DB1/DB3 | H-BOR-29 | ST18 | 122.5 | 206.1 | | 96 | 4 | 3 | | | | | 2.66 | 22.6 | 101.5 | 124.4 | 0.649 | CD | 8.02 | | 6.5 | 10.38 | | | | |
| DB4 | H-BOR-29 | PS10 | 140.1 | 188.5 | | | | | | | | | | 27.3 | 96.7 | 123.1 | | | | | | 11.44 | | | | |
| DB4 | H-BOR-29 | PS10 | 141.1 | 187.5 | SC | 88 | 12 | 11 | 46 | 25 | | | 2.73 | 27.3 | 96.5 | 122.8 | 0.7679 | RC | | | | 11 50 | 6 | 0.18 | 0.01 | 0.85 |
| DB5 | H-BOR-29 | PS12 | 150 | 178 6 | | | | | 112 | 91 | | | 2.7 | 61.05 | 64.15 | 103.3 | 1.444 | CTXP | | | | 12 03 | | | | |

UU - Unconsolidated-Undrained CD - Consolidated-Drained CU - Consolidated-Undrained STX - Stress-Controlled Cylic Triaxial CTXP - Strain-Controlled Cyclic Triaxial RC - Resonant Column

Table 4.2-1(a) Summary of laboratory test results at ITP (Static p4/8).

| SAMPLE IDENTIFICATION | | | | | CLASSIFICATION PROPERTIES | | | | | | | | PHYSICAL PROPERTIES | | | | | | | | | | | | | |
|---|---|---|---|---|---|---|---|---|---|---|---|---|---|---|---|---|---|---|---|---|---|---|---|---|---|---|
| | | | | | | | | | Atterberg Limits | | | | | | | | | | Static Strength | | | | Consolidation | | | |
| Layer | Boring No. | Sample No. | Top Depth (feet) | Top Elev. (feet) | USCS Group Symbol | Sand (%) | Fines (%) | Clay %<.005mm | Liquid Limit on portion <No. 40 (%) | Plas. Index (%) | Liquid Limit on portion <-200 (%) | Plas. Index (%) | Specific Gravity | Natural Water Content (%) | Insitu Dry Density (pcf) | Insitu Wet Density (pcf) | Void Ratio | Test Type | Max. Deviator Stress (ksf) | Confining Stress (ksf) | Strain at Failure (%) | Overburden Stress (ksf) | Precon. Stress (ksf) | Compress. Index Cc | Recomp. Index Cr | Comp. Coef. Cv |
| DB5 | H-BOR-29 | PS12 | 150.4 | 178 2 | | | | | | | | | | 92.8 | 47.2 | 91.0 | 2.571 | | | | | 12.05 | 14 | 1.92 | 0.25 | 0.25 |
| DB5 | H-BOR-29 | PS12 | 150.7 | 177.9 | | 13 | 87 | 73 | | | 205 | 172 | 2.69 | 68.4 | 57.7 | 97.2 | 1.91 | RC | | | | 12.07 | | | | |
| DB5 | H-BOR-29 | PS12 | 151.3 | 177.3 | | 50 | 50 | 42 | | | | | | | | | | | | | | 12.11 | | | | |
| DB5 | H-BOR-29 | ST20 | 155.1 | 173.5 | | 28 | 72 | 61 | | | 190 | 132 | 2.71 | 69.1 | 56.8 | 96.0 | 1.979 | CD | 3.95 | | 5 | 12.34 | | | | |
| ST | H-BOR-29 | ST22 | 178.9 | 149.7 | | 85 | 15 | 13 | 39 | 18 | | | 2.69 | 27.6 | 93.85 | 119.8 | 0.8454 | | | | | 13.76 | 7.5 | 0.23 | 0.04 | 0.9 |
| ST | H-BOR-29 | ST24 | 197.5 | 131.1 | | 59 | 41 | 19 | | | 89 | 64 | 2.72 | 35 | 87.6 | 118.3 | 0.94 | RC | | | | 14.88 | | | | |
| ST | H-BOR-29 | ST24 | 198.1 | 130.5 | | 65 | 35 | 8 | | | | | 2.69 | 44.9 | 71.4 | 103.5 | 1.352 | CTXP | | | | 14.92 | | | | |
| ST | H-BOR-29 | ST24 | 198.7 | 129.9 | | | | | | | | | | 32.3 | 89.9 | 118.9 | 0.8679 | | | | | 14.95 | 6 | 0.15 | 0.02 | 0.35 |
| FILL | H-SPT-1 | SS5 | 12 | 315.7 | SC | 64.3 | 34.7 | | 57 | 31 | | | | | | | | | | | | 1.44 | | | | |
| FILL | H-SPT-1 | SS6 | 13.5 | 314.2 | | | | | | | 100 | 54 | | | | | | | | | | 1.62 | | | | |
| FILL | H-SPT-1 | SS10 | 19.5 | 308.2 | SC | 54.5 | 43.5 | | 66 | 34 | | | | | | | | | | | | 2.34 | | | | |
| FILL | H-SPT-1 | SS17 | 30 | 297.7 | SC | 53.6 | 44.4 | | 47 | 20 | | | | | | | | | | | | 3.60 | | | | |
| FILL | H-SPT-1 | SS19 | 33 | 294.7 | | | | | | | 92 | 52 | | | | | | | | | | 3.96 | | | | |
| FILL | H-SPT-1 | SS20 | 34.5 | 293.2 | SC | 63.5 | 35.5 | | 43 | 20 | | | | | | | | | | | | 4.14 | | | | |
| FILL | H-SPT-1 | SS23 | 39 | 288.7 | SC | 62.6 | 36.4 | | 34 | 16 | | | | | | | | | | | | 4.68 | | | | |
| FILL | H-SPT-1 | SS25 | 42 | 285.7 | | | | | | | 81 | 57 | | | | | | | | | | 5.04 | | | | |
| TR1 | H-SPT-1 | SS26 | 43.5 | 284.2 | SC | 65 | 35 | 12.9 | 47 | 21 | | | 2.68 | 15.8 | | | | | | | | 5.22 | | | | |
| TR1 | H-SPT-1 | SS28 | 46.5 | 281.2 | CH | 31.7 | 68.3 | | 65 | 37 | | | | | | | | | | | | 5.58 | | | | |
| TR1 | H-SPT-1 | SS29 | 48 | 279.7 | CH | 50 | 50 | 24.3 | 58 | 32 | | | 2.68 | 20.6 | | | | | | | | 5.76 | | | | |
| TR1 | H-SPT-1 | SS30 | 49.5 | 278.2 | | | | | | | 102 | 58 | | | | | | | | | | 5.94 | | | | |
| TR1 | H-SPT-14 | SS2 | 7.5 | 293.2 | SC | 67 | 33 | | 85 | 51 | | | | | | | | | | | | 0.90 | | | | |
| TR1 | H-SPT-14 | SS3 | 9 | 291.7 | | | | | | | | | | 15.5 | | | | | | | | 1.08 | | | | |
| TR1 | H-SPT-14 | SS5 | 12 | 288.7 | SC | 67.1 | 32.9 | 8 | 85 | 49 | 112 | 58 | 2.7 | 17 | | | | | | | | 1.44 | | | | |
| TR1 | H-SPT-14 | SS6 | 13.5 | 287.2 | | | | | | | | | | 16.4 | | | | | | | | 1.62 | | | | |
| TR1 | H-SPT-14 | SS7 | 15 | 285.7 | | | | | | | | | | 17 | | | | | | | | 1.80 | | | | |
| TR1 | H-SPT-14 | SS8 | 16.5 | 284.2 | | | | | | | | | | 15.4 | | | | | | | | 1.98 | | | | |
| TR1 | H-SPT-14 | SS9 | 18 | 282.7 | SC | 72 | 28 | | 88 | 53 | | | | | | | | | | | | 2.16 | | | | |
| TR1 | H-SPT-14 | SS10 | 19.5 | 281.2 | | | | | | | | | | 21.3 | | | | | | | | 2.34 | | | | |
| TR1 | H-SPT-14 | SS11 | 21 | 279.7 | SC | 54.3 | 45.7 | 7.2 | 53 | 28 | 83 | 45 | 2.68 | 23.2 | | | | | | | | 2.52 | | | | |
| TR1 | H-SPT-14 | SS12 | 22.5 | 278.2 | | | | | | | 103 | 60 | | 24.7 | | | | | | | | 2.70 | | | | |
| TR1 | H-SPT-14 | SS13 | 24 | 276.7 | | | | | | | | | | 24.4 | | | | | | | | 2.80 | | | | |
| TR1 | H-SPT-14 | SS14 | 25.5 | 275.2 | SC | 61.2 | 36.1 | 8.4 | 52 | 27 | 103 | 60 | 2.72 | 22 | | | | | | | | 2.89 | | | | |
| TR1 | H-SPT-14 | SS18 | 31.5 | 269.2 | | 74 | 26 | | | | | | 2.7 | 24 | | | | | | | | 3.25 | | | | |
| TR1 | H-SPT-14 | SS20 | 34.5 | 266.2 | | 79 | 21 | | | | | | 2.75 | 21 | | | | | | | | 3.43 | | | | |
| TR2 | H-SPT-14 | SS21 | 37 | 263.7 | | 88 | 12 | | | | | | 2.71 | 23 | | | | | | | | 3.58 | | | | |
| TR2 | H-SPT-14 | SS26 | 44.5 | 256.2 | | 81 | 18 | | | | | | | | | | | | | | | 4.03 | | | | |
| TR2 | H-SPT-14 | SS29 | 49.5 | 251.2 | | 84 | 16 | | | | | | 2.69 | 25 | | | | | | | | 4.33 | | | | |
| TR2 | H-SPT-14 | SS32 | 54 | 246.7 | | 89 | 11 | | | | | | 2.7 | 25 | | | | | | | | 4.60 | | | | |
| TR2 | H-SPT-14 | SS34 | 57 | 243.7 | | 90.8 | 9.2 | | | | | | 2.73 | 23 | | | | | | | | 4.78 | | | | |
| TR3/TR4 | H-SPT-14 | SS37 | 61.5 | 239.2 | SC | 77 | 23 | 2.5 | 36 | 14 | 96 | 52 | 2.72 | 21 | | | | | | | | 5.05 | | | | |
| TR3/TR4 | H-SPT-14 | SS38 | 63 | 237.7 | | | | | | | | | | 24.2 | | | | | | | | 5.14 | | | | |
| TR3/TR4 | H-SPT-14 | SS39 | 64.5 | 236.2 | | | | | | | | | | 23 | | | | | | | | 5.23 | | | | |
| TR3/TR4 | H-SPT-14 | SS40 | 66 | 234.7 | SM | 72 | 28 | | 42 | 16 | | | | | | | | | | | | 5 32 | | | | |
| TR3/TR4 | H-SPT-14 | SS41 | 67.5 | 233.2 | | | | | | | | | | 24 5 | | | | | | | | 5.41 | | | | |
| TR3/TR4 | H-SPT-14 | SS42 | 69 | 231.7 | SC | 72.3 | 27.3 | 3.6 | 40 | 18 | 81 | 43 | 2 68 | 23 | | | | | | | | 5.50 | | | | |
| TR3/TR4 | H-SPT-14 | SS45 | 73.5 | 227.2 | | 81 | 19 | | | | | | | | | | | | | | | 5.77 | | | | |
| TR3/TR4 | H-SPT-14 | SS45 | 75.5 | 225.2 | | | | | 43 | 19 | | | | | | | | | | | | 5.89 | | | | |
| TR3/TR4 | H-SPT-14 | SS46 | 76 | 224 7 | | | | | | | | | | 20 6 | | | | | | | | 5.92 | | | | |

UU - Unconsolidated-Undrained CD - Consolidated-Drained CU - Consolidated-Undrained STX - Stress-Controlled Cylic Triaxial CTXP - Strain-Controlled Cyclic Triaxial RC - Resonant Column

Table 4.2-1(a) Summary of laboratory test results at ITP (Static p5/8).

| SAMPLE IDENTIFICATION | | | | | CLASSIFICATION PROPERTIES | | | | | | | | | PHYSICAL PROPERTIES | | | | | | | | | | | | | |
|---|---|---|---|---|---|---|---|---|---|---|---|---|---|---|---|---|---|---|---|---|---|---|---|---|---|---|---|
| | | | | | | | | | Atterberg Limits | | | | | | | | | | | | | | | | | | |
| | | | | | | | | | Liquid | Plas. | Liquid | Plas. | | | Insitu | Insitu | | | | | | | | | | | |
| Layer | Boring | Sample | Top | Top | USCS | Sand | Fines | Clay | Limit | Index | Limit | Index | Specific | Natural Water | Dry | Wet | Void | Test | Static Strength Max. Deviator | Confining | Strain | Overburden | Precon. | Compress. | Recomp. | Comp. |
| | No. | No. | Depth | Elev. | Group | (%) | (%) | %<.005mm | on portion <No. 40 | | on portion <-200 | | Gravity | Content | Density | Density | Ratio | Type | Stress | Stress | at Failure | Stress | Stress | Index | Index | Coef. |
| | | | (feet) | (feet) | Symbol | | | | (%) | (%) | (%) | (%) | | (%) | (pcf) | (pcf) | | | (ksf) | (ksf) | (%) | (ksf) | (ksf) | Cc | Cr | Cv |
| TR3/TR4 | H-SPT-14 | SS47 | 77.5 | 223.2 | | 85.4 | 14.3 | 0.8 | | | 127 | 55 | 2.71 | 22 | | | | | | | | 6.01 | | | | |
| TR3/TR4 | H-SPT-14 | SS49 | 80.5 | 220.2 | | 85 | 15 | | | | | | 2.72 | 25.8 | | | | | | | | 6.19 | | | | |
| TR3/TR4 | H-SPT-14 | SS51 | 83.5 | 217.2 | | 82.2 | 17.8 | 2.1 | | | 129 | 84 | 2.74 | 27.1 | | | | | | | | 6.37 | | | | |
| DB1/DB3 | H-SPT-14 | SS52 | 85 | 215.7 | | | | | | | | | | 22.7 | | | | | | | | 6.46 | | | | |
| DB1/DB3 | H-SPT-14 | SS53 | 86.5 | 214.2 | | 89 | 11 | | | | | | | | | | | | | | | 6.55 | | | | |
| DB1/DB3 | H-SPT-14 | SS55 | 89.5 | 211.2 | | 93.4 | 6.6 | | | | | | 2.74 | 23.5 | | | | | | | | 6.73 | | | | |
| DB1/DB3 | H-SPT-14 | SS57 | 92.5 | 208.2 | | 90 | 10 | | | | | | | | | | | | | | | 6.91 | | | | |
| DB1/DB3 | H-SPT-14 | SS58 | 94 | 206.7 | | | | | | | | | | 27.8 | | | | | | | | 7.00 | | | | |
| DB1/DB3 | H-SPT-14 | SS59 | 95.5 | 205.2 | | 83 | 17 | 1.6 | | | 133 | 84 | 2.72 | 26.1 | | | | | | | | 7.09 | | | | |
| DB1/DB3 | H-SPT-14 | SS61 | 98.5 | 202.2 | | 89 | 11 | | | | | | 2.72 | 30.4 | | | | | | | | 7.27 | | | | |
| DB1/DB3 | H-SPT-14 | SS63 | 101.5 | 199.2 | | 94.3 | 5.7 | | | | | | | | | | | | | | | 7.45 | | | | |
| DB1/DB3 | H-SPT-14 | SS67 | 107.5 | 193.2 | | 92.1 | 7.9 | | | | | | 2.71 | 21.2 | | | | | | | | 7.81 | | | | |
| DB1/DB3 | H-SPT-14 | SS70 | 112 | 188.7 | | 92 | 7 | | | | | | | | | | | | | | | 8.08 | | | | |
| DB1/DB3 | H-SPT-14 | SS72 | 115 | 185.7 | | | | | | | | | | 38.1 | | | | | | | | 8.26 | | | | |
| DB1/DB3 | H-SPT-14 | SS73 | 116.5 | 184.2 | | 83.5 | 13.6 | 1.3 | | | 137 | 100 | 2.69 | 22.6 | | | | | | | | 8.35 | | | | |
| DB1/DB3 | H-SPT-14 | SS74 | 118 | 182.7 | | 80.8 | 13.6 | 1.4 | | | 98 | 70 | 2.71 | 26.6 | | | | | | | | 8.44 | | | | |
| DB4 | H-SPT-14 | SS75 | 119.5 | 181.2 | | | | | | | | | | 28.8 | | | | | | | | 8.53 | | | | |
| DB4 | H-SPT-14 | SS76 | 121 | 179.7 | | | | | | | | | | 31.1 | | | | | | | | 8.62 | | | | |
| DB4 | H-SPT-14 | SS77 | 122.5 | 178.2 | SC | 72.4 | 27.6 | 6.8 | 69 | 46 | 162 | 124 | 2.71 | 32.2 | | | | | | | | 8.71 | | | | |
| DB4 | H-SPT-14 | SS78 | 124 | 176.7 | SC | 57 | 43 | | 78 | 54 | | | | | | | | | | | | 8.80 | | | | |
| DB4 | H-SPT-14 | SS81 | 128.5 | 172.2 | | | | | | | | | | 75.1 | | | | | | | | 9.07 | | | | |
| DB4 | H-SPT-14 | SS82 | 130 | 170.7 | | 31.5 | 68.5 | 31.8 | | | 124 | 81 | 2.75 | 63 | | | | | | | | 9.16 | | | | |
| DB4 | H-SPT-14 | SS83 | 131.5 | 169.2 | SC | 77.7 | 22.2 | 4.5 | 56 | 31 | 135 | 96 | 2.68 | 36 | | | | | | | | 9.25 | | | | |
| DB4 | H-SPT-14 | SS84 | 133 | 167.7 | | | | | | | | | | 37 | | | | | | | | 9.34 | | | | |
| DB4 | H-SPT-14 | SS85 | 134.5 | 166.2 | | 94 | 6 | | | | | | 2.7 | 30.2 | | | | | | | | 9.43 | | | | |
| ST | H-SPT-14 | SS86 | 136 | 164.7 | | 86.3 | 13.7 | 1 | | | 117 | 79 | 2.68 | 28 | | | | | | | | 9.52 | | | | |
| ST | H-SPT-14 | SS87 | 137.5 | 163.2 | | | | | | | | | | 35.6 | | | | | | | | 9.61 | | | | |
| ST | H-SPT-14 | SS88 | 139 | 161.7 | | 93.9 | 6.1 | | | | | | 2.73 | 23 | | | | | | | | 9.70 | | | | |
| ST | H-SPT-14 | SS89 | 140.5 | 160.2 | | | | | | | | | | 19.7 | | | | | | | | 9.79 | | | | |
| ST | H-SPT-14 | SS90 | 142 | 158.7 | SC | 58.9 | 41.1 | 13.1 | 50 | 24 | 100 | 54 | 2.77 | 48 | | | | | | | | 9.88 | | | | |
| ST | H-SPT-14 | SS91 | 143.5 | 157.2 | | | | | | | | | | 29.6 | | | | | | | | 9.97 | | | | |
| ST | H-SPT-14 | SS92 | 145 | 155.7 | | 72 | 26 | | | | | | | 33 | | | | | | | | 10.06 | | | | |
| ST | H-SPT-14 | SS100 | 157 | 143.7 | | 83 | 17 | | | | | | | 28.1 | | | | | | | | 10.78 | | | | |
| ST | H-SPT-14 | SS104 | 163 | 137.7 | | 86 | 14 | | | | | | 2.71 | 27.6 | | | | | | | | 11.14 | | | | |
| ST | H-SPT-14 | SS108 | 169 | 131.7 | | 82 | 18 | | | | | | | 25.4 | | | | | | | | 11.50 | | | | |
| ST | H-SPT-14 | SS110 | 172 | 128.7 | | 90.5 | 9.5 | | | | | | | 24.1 | | | | | | | | 11.68 | | | | |
| ST | H-SPT-14 | SS113 | 176.5 | 124.2 | SC | 63 | 37 | 9.4 | 45 | 22 | 99 | 63 | 2.73 | 26 | | | | | | | | 11.95 | | | | |
| ST | H-SPT-14 | SS114 | 178 | 122.7 | | | | | | | | | | 27.7 | | | | | | | | 12.04 | | | | |
| ST | H-SPT-14 | SS116 | 181 | 119.7 | SC | 70 | 29 | | 56 | 36 | | | | | | | | | | | | 12.22 | | | | |
| FILL | H-SPT-18 | SS2 | 7.5 | 291 | SC | 57.8 | 41.2 | | 52 | 25 | | | | | | | | | | | | 0.90 | | | | |
| FILL | H-SPT-18 | SS3 | 10.5 | 288 | | | | | | | 65 | 25 | | | | | | | | | | 1.26 | | | | |
| FILL | H-SPT-18 | SS5 | 12 | 286.5 | | | | | | | 67 | 25 | | | | | | | | | | 1.44 | | | | |
| FILL | H-SPT-18 | SS7 | 15 | 283.5 | SC | 58.1 | 41.9 | 19 | 50 | 24 | | | 2.63 | 16.2 | | | | | | | | 1.80 | | | | |
| TR1 | H-SPT-18 | SS10 | 19.5 | 279 | SM | 58.6 | 41.4 | | 80 | 42 | | | | | | | | | | | | 2.34 | | | | |
| TR1 | H-SPT-18 | SS13 | 24 | 274.5 | SM | 72.7 | 26.3 | | 73 | 35 | | | | | | | | | | | | 2.67 | | | | |
| TR1 | H-SPT-18 | SS15 | 27 | 271.5 | SC | 59.3 | 40.7 | 15.9 | 50 | 26 | | | 2.74 | 21.6 | | | | | | | | 2.85 | | | | |
| TR1 | H-SPT-18 | SS17 | 30 | 268.5 | | | | | | | 97 | 57 | | | | | | | | | | 3.03 | | | | |
| TR1 | H-SPT-18 | SS18 | 31.5 | 267 | SC | 70.9 | 29.1 | | 45 | 26 | | | | | | | | | | | | 3.12 | | | | |

UU - Unconsolidated-Undrained CD - Consolidated-Drained CU - Consolidated-Undrained STX - Stress-Controlled Cylic Triaxial CTXP - Strain-Controlled Cyclic Triaxial RC - Resonant Column

Table 4.2-1(a) Summary of laboratory test results at ITP (Static p6/8).

| SAMPLE IDENTIFICATION | | | | | CLASSIFICATION PROPERTIES | | | | | | | | PHYSICAL PROPERTIES | | | | | | | | | | | | | |
|---|---|---|---|---|---|---|---|---|---|---|---|---|---|---|---|---|---|---|---|---|---|---|---|---|---|---|
| | | | | | | | | | Atterberg Limits | | | | | | | | | | Static Strength | | | Consolidation | | | | |
| | | | | | | | | | Liquid | Plas. | Liquid | Plas. | | Natural | Insitu | Insitu | | | | | | | | | | |
| Layer | Boring No. | Sample No. | Top Depth | Top Elev. | USCS Group | Sand (%) | Fines (%) | Clay %<.005mm | Limit on portion <No. 40 | Index | Limit on portion <-200 | Index | Specific Gravity | Water Content | Dry Density | Wet Density | Void Ratio | Test Type | Max. Deviator Stress | Confining Stress | Strain at Failure | Overburden Stress | Precon. Stress | Compress. Index | Recomp. Index | Comp. Coef. |
| | | | (feet) | (feet) | Symbol | | | | (%) | (%) | (%) | (%) | | (%) | (pcf) | (pcf) | | | (ksf) | (ksf) | (%) | (ksf) | (ksf) | Cc | Cr | Cv |
| TR1 | H-SPT-18 | SS20 | 34.5 | 264 | CH | 15.3 | 84.7 | | 99 | 62 | | | 2.61 | 32.8 | | | | | | | | 3.30 | | | | |
| TR1 | H-SPT-18 | SS21 | 36 | 262.5 | | | | | | | 106 | 65 | | | | | | | | | | 3.39 | | | | |
| TR1 | H-SPT-18 | SS22 | 37.5 | 261 | CH | 46.7 | 53.3 | 15 | 58 | 34 | | | 2.66 | 26 2 | | | | | | | | 3.48 | | | | |
| TR2 | H-SPT-18 | SS24 | 40.5 | 258 | SC | 68.8 | 31.2 | | 34 | 14 | | | | | | | | | | | | 3.66 | | | | |
| TR2 | H-SPT-18 | SS25 | 42 | 256.5 | | | | | | | 80 | 42 | | | | | | | | | | 3.75 | | | | |
| TR2 | H-SPT-18 | SS26 | 43.5 | 255 | | 76.9 | 23.1 | 3.6 | | | | | 2.63 | 25.3 | | | | | | | | 3.84 | | | | |
| TR2 | H-SPT-18 | SS28 | 46.5 | 252 | | 79.2 | 20.8 | | | | | | 2.62 | 19.1 | | | | | | | | 4.02 | | | | |
| TR2 | H-SPT-18 | SS30 | 49.5 | 249 | | 81.9 | 18 1 | | | | | | | | | | | | | | | 4.20 | | | | |
| TR2 | H-SPT-18 | SS32 | 52.5 | 246 | | 86.8 | 13 2 | | | | | | | | | | | | | | | 4.38 | | | | |
| TR2 | H-SPT-18 | SS34 | 55.5 | 243 | | 86.4 | 13.6 | | | | | | | | | | | | | | | 4.56 | | | | |
| TR2 | H-SPT-18 | SS37 | 60 | 238.5 | | 90 | 10 | | | | | | 2.63 | | | | | | | | | 4.83 | | | | |
| TR2 | H-SPT-18 | SS39 | 63 | 235.5 | | 90 | 10 | | | | | | | | | | | | | | | 5.01 | | | | |
| TR2 | H-SPT-18 | SS43 | 69 | 229.5 | | 70 | 30 | | | | | | | | | | | | | | | 5.37 | | | | |
| TR3/TR4 | H-SPT-18 | SS45 | 72 | 226.5 | | 80 | 20 | | | | | | | | | | | | | | | 5.55 | | | | |
| TR3/TR4 | H-SPT-18 | SS50 | 79.5 | 219 | SC | 77.1 | 22.9 | 4.7 | 44 | 22 | | | 2.6 | 15.8 | | | | | | | | 6.00 | | | | |
| TR3/TR4 | H-SPT-18 | SS51 | 81 | 217.5 | | | | | | | 106 | 60 | | | | | | | | | | 6.09 | | | | |
| TR3/TR4 | H-SPT-18 | SS52 | 82.5 | 216 | | | | | | | 117 | 71 | | | | | | | | | | 6.18 | | | | |
| TR3/TR4 | H-SPT-18 | SS58 | 91.5 | 207 | SC | 76.3 | 21.7 | | 44 | 18 | | | | | | | | | | | | 6.72 | | | | |
| TR3/TR4 | H-SPT-18 | SS59 | 93 | 205.5 | | 84.6 | 15.4 | | | | | | | | | | | | | | | 6.81 | | | | |
| DB1/DB3 | H-SPT-18 | SS68 | 106.5 | 192 | | 89.9 | 10.1 | | | | | | 2.64 | 25.9 | | | | | | | | 7.62 | | | | |
| DB1/DB3 | H-SPT-18 | SS77 | 120 | 178.5 | | 90.3 | 8.7 | | | | | | | | | | | | | | | 8.43 | | | | |
| DB1/DB3 | H-SPT-18 | SS79 | 123 | 175.5 | SC | 76.1 | 23.9 | | 75 | 53 | | | | | | | | | | | | 8.61 | | | | |
| DB1/DB3 | H-SPT-18 | SS80 | 124.5 | 174 | | | | | | | 143 | 108 | | | | | | | | | | 8.70 | | | | |
| DB4 | H-SPT-18 | SS81 | 126 | 172.5 | CH | 24.8 | 75.2 | 36.9 | 90 | 66 | | | 2.5 | 58.8 | | | | | | | | 8.79 | | | | |
| DB5 | H-SPT-18 | SS85 | 132 | 166.5 | MH | 29.4 | 70.6 | 46.6 | 74 | 23 | | | 2.47 | 70.6 | | | | | | | | 9.15 | | | | |
| DB5 | H-SPT-18 | SS86 | 133.5 | 165 | | | | | | | 91 | 28 | | | | | | | | | | 9.24 | | | | |
| DB5 | H-SPT-18 | SS88 | 136.5 | 162 | | 70.3 | 28.2 | 7.6 | | | | | 2.52 | 41.2 | | | | | | | | 9.42 | | | | |
| DB5 | H-SPT-18 | SS90 | 139.5 | 159 | | 77.8 | 22.2 | | | | | | | | | | | | | | | 9.60 | | | | |
| DB5 | H-SPT-18 | SS94 | 145.5 | 153 | | 81.5 | 18.5 | | | | | | | | | | | | | | | 9.96 | | | | |
| ST | H-SPT-18 | SS95 | 147 | 151.5 | | 90.6 | 9.4 | | | | | | | | | | | | | | | 10.05 | | | | |
| ST | H-SPT-18 | SS97 | 150 | 148 5 | | 85.7 | 14.3 | 2.5 | | | | | 2.59 | 32.4 | | | | | | | | 10.23 | | | | |
| ST | H-SPT-18 | SS99 | 162.5 | 136 | | 86.7 | 13.3 | | | | | | | | | | | | | | | 10.98 | | | | |
| ST | H-SPT-18 | SS104 | 170 | 128.5 | | 81 | 19 | | | | | | 2.6 | 33.1 | | | | | | | | 11.43 | | | | |
| ST | H-SPT-18 | SS108 | 176 | 122.5 | | 89.8 | 10.2 | | | | | | | | | | | | | | | 11.79 | | | | |
| ST | H-SPT-18 | SS110 | 179 | 119.5 | SC | 65.8 | 34.2 | | 38 | 17 | | | | | | | | | | | | 11.97 | | | | |
| ST | H-SPT-18 | SS111 | 180.5 | 118 | | | | | | | 85 | 50 | | | | | | | | | | 12.06 | | | | |
| ST | H-SPT-18 | SS112 | 182 | 116.5 | | | | | | | 69 | 42 | | | | | | | | | | 12.15 | | | | |
| ST | H-SPT-18 | SS113 | 183.5 | 115 | CH | 35.4 | 64.6 | 34.5 | 76 | 53 | | | 2.55 | 34.6 | | | | | | | | 12.24 | | | | |
| TR2 | H-SPT-20 | SS6 | 13.5 | 280.7 | | | | | | | 62 | 31 | | | | | | | | | | 1 62 | | | | |
| TR2 | H-SPT-20 | SS7 | 15 | 279.2 | SC | 79.6 | 20.4 | | 27 | 11 | | | | | | | | | | | | 1 80 | | | | |
| TR2 | H-SPT-20 | SS10 | 19.5 | 274.7 | | | | | | | 79 | 41 | | | | | | | | | | 2.15 | | | | |
| TR2 | H-SPT-20 | SS11 | 21 | 273.2 | SC | 84 | 16 | 2.7 | 40 | 20 | | | 2.62 | 17.8 | | | | | | | | 2.24 | | | | |
| TR3/TR4 | H-SPT-20 | SS13 | 24 | 270 2 | | 69.9 | 30.1 | | | | | | | | | | | | | | | 2.42 | | | | |
| TR3/TR4 | H-SPT-20 | SS17 | 30 | 264.2 | SC | 67 | 32 | 13.2 | 40 | 18 | | | 2.67 | 23 6 | | | | | | | | 2.78 | | | | |
| TR3/TR4 | H-SPT-20 | SS18 | 31.5 | 262.7 | | | | | | | 95 | 53 | | | | | | | | | | 2.87 | | | | |
| TR3/TR4 | H-SPT-20 | SS20 | 34.5 | 259.7 | SC | 77.4 | 22.6 | | 40 | 17 | | | | | | | | | | | | 3 05 | | | | |
| TR3/TR4 | H-SPT-20 | SS23 | 39 | 255 2 | | 86 | 14 | | | | | | | | | | | | | | | 3.32 | | | | |
| TR3/TR4 | H-SPT-20 | SS26 | 43.5 | 250.7 | | 84 | 16 | 3.7 | | | | | 2 66 | 25.3 | | | | | | | | 3 59 | | | | |

UU - Unconsolidated-Undrained CD - Consolidated-Drained CU - Consolidated-Undrained STX - Stress-Controlled Cylic Triaxial CTXP - Strain-Controlled Cyclic Triaxial RC - Resonant Column

Table 4.2-1(a) Summary of laboratory test results at ITP (Static p7/8).

| SAMPLE IDENTIFICATION | | | | | CLASSIFICATION PROPERTIES | | | | | | | | PHYSICAL PROPERTIES | | | | | | | | | | | | | |
|---|---|---|---|---|---|---|---|---|---|---|---|---|---|---|---|---|---|---|---|---|---|---|---|---|---|---|
| | | | | | | | | | Atterberg Limits | | | | | | | | | | | Static Strength | | | | Consolidation | | | | |
| | | | | | | | | | Liquid | Plas. | Liquid | Plas. | | Natural | Insitu | Insitu | | | | | | | | | | | |
| Layer | Boring | Sample | Top | Top | USCS | Sand | Fines | Clay | Limit | Index | Limit | Index | Specific | Water | Dry | Wet | Void | Test | Max. Deviator | Confining | Strain | Overburden | Precon. | Compress. | Recomp. | Comp. |
| | No. | No. | Depth | Elev. | Group | (%) | (%) | %<.005mm | on portion <No. 40 | | on portion <-200 | | Gravity | Content | Density | Density | Ratio | Type | Stress | Stress | at Failure | Stress | Stress | Index | Index | Coef. |
| | | | (feet) | (feet) | Symbol | | | | (%) | (%) | (%) | (%) | | (%) | (pcf) | (pcf) | | | (ksf) | (ksf) | (%) | (ksf) | (ksf) | Cc | Cr | Cv |
| DB1/DB3 | H-SPT-20 | SS28 | 46.5 | 247.7 | | 92.1 | 7.9 | | | | | | | | | | | | | | | 3.77 | | | | |
| DB1/DB3 | H-SPT-20 | SS34 | 55.5 | 238.7 | SM | 84 | 16 | 3 | 37 | 12 | | | 2.65 | 27.3 | | | | | | | | 4.31 | | | | |
| DB1/DB3 | H-SPT-20 | SS37 | 60 | 234.2 | | 93.3 | 6.7 | | | | | | | | | | | | | | | 4.58 | | | | |
| DB1/DB3 | H-SPT-20 | SS43 | 69 | 225.2 | | 94.3 | 5.7 | | | | | | | | | | | | | | | 5.12 | | | | |
| DB1/DB3 | H-SPT-20 | SS46 | 73.5 | 220.7 | | 95.1 | 4.9 | | | | | | | | | | | | | | | 5.39 | | | | |
| DB4 | H-SPT-20 | SS48 | 76.5 | 217.7 | | 85.7 | 14.3 | | | | | | | | | | | | | | | 5.57 | | | | |
| DB4 | H-SPT-20 | SS53 | 84 | 210.2 | SC | 68 | 32 | 10.8 | 48 | 24 | | | 2.67 | 39.7 | | | | | | | | 6.02 | | | | |
| DB4 | H-SPT-20 | SS55 | 87 | 207.2 | | 89.1 | 9.9 | | | | | | | | | | | | | | | 6.20 | | | | |
| DB5 | H-SPT-20 | SS59 | 93 | 201.2 | | 55 | 45 | 18.1 | | | | | 2.66 | 42.3 | | | | | | | | 6.56 | | | | |
| DB5 | H-SPT-20 | SS60 | 94.5 | 199.7 | | | | | | | 95 | 62 | | | | | | | | | | 6.65 | | | | |
| DB5 | H-SPT-20 | SS61 | 96 | 198.2 | CH | 40.5 | 59.5 | | 62 | 44 | | | | | | | | | | | | 6.74 | | | | |
| DB5 | H-SPT-20 | SS64 | 100.5 | 193.7 | CH | 39.3 | 60.7 | | 55 | 36 | | | | | | | | | | | | 7.01 | | | | |
| DB5 | H-SPT-20 | SS67 | 105 | 189.2 | | | | | | | 75 | 48 | | | | | | | | | | 7.28 | | | | |
| DB5 | H-SPT-20 | SS68 | 106.5 | 187.7 | CH | 22 | 78 | 48.8 | 78 | 53 | | | 2.65 | 30.6 | | | | | | | | 7.37 | | | | |
| ST | H-SPT-20 | SS69 | 108 | 186.2 | | | | | | | 31 | 10 | | | | | | | | | | 7.46 | | | | |
| ST | H-SPT-20 | SS71 | 111 | 183.2 | | 68.3 | 25.7 | | | | | | | | | | | | | | | 7.64 | | | | |
| ST | H-SPT-20 | SS75 | 117 | 177.2 | | | | | | | 22 | 4 | | | | | | | | | | 8.00 | | | | |
| ST | H-SPT-20 | SS78 | 121.5 | 172.7 | | 66 | 26 | 2.6 | | | | | 2.71 | 12.2 | | | | | | | | 8.27 | | | | |
| ST | H-SPT-20 | SS79 | 123 | 171.2 | | 61.9 | 21.1 | | | | | | | | | | | | | | | 8.36 | | | | |
| ST | H-SPT-20 | SS81 | 126 | 168.2 | | 57.3 | 30.7 | | | | | | | | | | | | | | | 8.54 | | | | |
| ST | H-SPT-20 | SS89 | 138 | 156.2 | | 44 | 21 | | | | | | | | | | | | | | | 9.26 | | | | |
| ST | H-SPT-20 | SS92 | 142.5 | 151.7 | | 63.4 | 31.6 | | | | | | | | | | | | | | | 9.53 | | | | |
| ST | H-SPT-20 | SS96 | 148.5 | 145.7 | SC | 54.9 | 37.1 | | 26 | 9 | | | | | | | | | | | | 9.89 | | | | |
| ST | H-SPT-20 | SS98 | 151.5 | 142.7 | | 68.5 | 29.5 | | | | | | | | | | | | | | | 10.07 | | | | |
| ST | H-SPT-20 | SS103 | 159 | 135.2 | | 74.9 | 25.1 | | | | | | | | | | | | | | | 10.52 | | | | |
| ST | H-SPT-20 | SS108 | 166.5 | 127.7 | | 84 | 16 | 4.7 | | | | | 2.61 | 28.1 | | | | | | | | 10.97 | | | | |
| ST | H-SPT-20 | SS112 | 172.5 | 121.7 | | 83.2 | 16.8 | | | | | | | | | | | | | | | 11.33 | | | | |
| ST | H-SPT-20 | SS114 | 175.5 | 118.7 | ML | 47.5 | 52.5 | | 40 | 10 | | | | | | | | | | | | 11.51 | | | | |
| ST | H-SPT-20 | SS115 | 177 | 117.2 | | | | | | | 65 | 31 | | | | | | | | | | 11.60 | | | | |
| ST | H-SPT-20 | SS117 | 180 | 114.2 | CH | 7 | 93 | 48.5 | 62 | 38 | | | 2.64 | 38.1 | | | | | | | | 11.78 | | | | |
| TR2 | HBOR23.1 | ST3 | 17.5 | 283.1 | SC | 79 | 21 | 18 | 44 | 25 | | | 2.69 | 17.4 | 110 | 129.1 | 0.527 | CU | 3.57 | 2.12 | 9.5 | 2.10 | | | | |
| TR2 | HBOR23.1 | ST3 | 18 | 282.6 | | 79 | 21 | 18 | | | 84 | 49 | 2.66 | 18 | 110.1 | 129.9 | 0.509 | CU | 7.7 | 8.64 | 15 | 2.16 | | | | |
| TR2 | HBOR23.1 | PS1 | 28.9 | 271.7 | SC | 76 | 24 | 19 | 42 | 23 | 128 | 90 | 2.61 | 20.25 | 107.9 | 129.7 | | STX | | | | 3.09 | | | | |
| DB5 | HBOR23.1 | PS2 | 95.7 | 204.9 | | | | | | | | | | 32.1 | 83 | 109.6 | | | | | | 7.09 | | | | |
| DB5 | HBOR23.1 | PS2 | 97.3 | 203.3 | SC | 56 | 44 | 30 | 80 | 62 | | | 2.71 | 32.1 | 84.4 | 111.5 | 1.0044 | | | | | 7.19 | 19 | 0.45 | 0.03 | 2.8 |
| DB5 | HSPT18.1 | SS4 | 144.5 | 153.9 | | 89 | 11 | | | | | | | 28 | | | | | | | | 9.90 | | | | |
| ST | HSPT18.1 | SS10 | 153.5 | 144.9 | | 84 | 16 | | | | | | | 27.6 | | | | | | | | 10.44 | | | | |
| ST | HSPT18.1 | SS12 | 156.5 | 141.9 | | 84.1 | 15.9 | 1 | | | | | 2.61 | 29.4 | | | | | | | | 10.62 | | | | |
| ST | HSPT18.1 | SS14 | 159.5 | 138.9 | SP-SC | 89.7 | 10.3 | 0 | 86 | 60 | | | 2.64 | 27.6 | | | | | | | | 10.80 | | | | |

UU - Unconsolidated-Undrained CD - Consolidated-Drained CU - Consolidated-Undrained STX - Stress-Controlled Cylic Triaxial CTXP - Strain-Controlled Cyclic Triaxial RC - Resonant Column

Table 4.2-1(a) Summary of laboratory test results at ITP (Static p8/8).

| Map Name | Location | Sample Depth (feet) | Sample Elevation (feet) | Stratum | USCS | WD CALC PCF | MC | Atterberg Limits | | | | Sieve Analyses | | | | | | Sg | Consolidation Properties | | | | | | | | Shear Strength (deviatoric stress) | | | | | | | | pH |
|---|---|---|---|---|---|---|---|---|---|---|---|---|---|---|---|---|---|---|---|---|---|---|---|---|---|---|---|---|---|---|---|---|---|---|
| | | | | | | | | LL (%) | PI (%) | LL200 (%) | PI200 (%) | > # 4 < # 200 | < # 200 | D10 (mm) | D30 (mm) | D50 (mm) | D60 (mm) | | eo | Sri (%) | MCI (%) | Po (tsf) | Pc (tsf) | OCR | Cc | Cr | PP (tsf) | UC (tsf) | UU (tsf) | CD (tsf) | CU (tsf) | S3 (tsf) | ΘO (%) | MCI (%) | |
| H-INC-1 | HDB-7 | 6.0 | 324.0 | FILL | SC | | | 73 | 53 | | | | | | | | | | | | | | | | | | | | | | | | | |
| H-INC-1 | HDB-7 | 7.5 | 322.5 | FILL | SC | | | | | | | | | | | | | | | | | | | | | | | | | | | | | |
| H-INC-1 | HDB-7 | 9.0 | 321.0 | FILL | | | | | | | | | | | | | | | | | | | | | | | | | | | | | | |
| H-INC-1 | HDB-7 | 11.0 | 319.0 | FILL | SC | | 32.6 | 80 | 52 | | | 63.9 | 34.1 | | | | | | | | | | | | | | | | | | | | | |
| H-INC-1 | HDB-7 | 12.5 | 317.5 | FILL | SC | | | | | | | | | | | | | | | | | | | | | | | | | | | | | |
| H-INC-1 | HDB-7 | 14.0 | 316.0 | FILL | SC | | 17.5 | 45 | 25 | | | 70.9 | 27.1 | | | | | | | | | | | | | | | | | | | | | |
| H-INC-1 | HDB-7 | 15.5 | 314.5 | FILL | SC | | 19.1 | 52 | 31 | | | | | | | | | | | | | | | | | | | | | | | | | |
| H-INC-1 | HDB-7 | 17.0 | 313.0 | FILL | SC | | | | | | | | | | | | | | | | | | | | | | | | | | | | | |
| H-INC-1 | HDB-7 | 18.5 | 311.5 | FILL | SC | | | | | | | 58.9 | 38.1 | | | | | | | | | | | | | | | | | | | | | |
| H-INC-1 | HDB-7 | 20.0 | 310.0 | FILL | SC | | | | | | | 52.9 | 46.1 | | | | | | | | | | | | | | | | | | | | | |
| H-INC-1 | HDB-7 | 21.5 | 308.5 | FILL | | | | | | | | | | | | | | | | | | | | | | | | | | | | | | |
| H-INC-1 | HDB-7 | 23.5 | 306.5 | FILL | SW-SM | | 22.6 | 36 | 22 | | | 60.8 | 39.2 | | | | | | | | | | | | | | | | | | | | | |
| H-INC-1 | HDB-7 | 25.0 | 305.0 | FILL | | | | | | | | | | | | | | | | | | | | | | | | | | | | | | |
| H-INC-1 | HDB-7 | 27.5 | 302.5 | FILL | SC | | | | | | | | | | | | | | | | | | | | | | | | | | | | | |
| H-INC-1 | HDB-7 | 29.0 | 301.0 | FILL | CL | | 22.7 | 54 | 34 | | | 59.8 | 39.2 | | | | | | | | | | | | | | | | | | | | | |
| H-INC-1 | HDB-7 | 30.5 | 299.5 | FILL | SC | | 36.9 | 46 | 28 | | | 76.8 | 21.2 | | | | | | | | | | | | | | | | | | | | | |
| H-INC-1 | HDB-7 | 32.0 | 298.0 | FILL | SC | | | | | | | | | | | | | | | | | | | | | | | | | | | | | |
| H-INC-1 | HDB-7 | 33.5 | 296.5 | FILL | SC | | | | | | | | | | | | | | | | | | | | | | | | | | | | | |
| H-INC-1 | HDB-7 | 35.0 | 295.0 | FILL | SC | | 21.1 | 49 | 26 | | | 61.8 | 37.2 | | | | | | | | | | | | | | | | | | | | | |
| H-INC-1 | HDB-7 | 36.5 | 293.5 | FILL | SC | | | | | | | | | | | | | | | | | | | | | | | | | | | | | |
| H-INC-1 | HDB-7 | 38.0 | 292.0 | FILL | SC | | | | | | | | | | | | | | | | | | | | | | | | | | | | | |
| H-INC-1 | HDB-7 | 41.0 | 289.0 | FILL | SC | | 31.6 | 75 | 47 | | | 45.9 | 54.1 | | | | | | | | | | | | | | | | | | | | | |
| H-INC-1 | HDB-7 | 48.5 | 281.5 | FILL | SC | | 27.9 | 62 | 37 | | | 45.9 | 48.1 | | | | | | | | | | | | | | | | | | | | | |
| H-INC-2 | HDB-7 | 6.0 | 311.2 | FILL | SC | | 20.2 | 56 | 34 | | | 47.0 | 51.0 | | | | | | | | | | | | | | | | | | | | | |
| H-INC-2 | HDB-7 | 7.5 | 309.7 | FILL | SC | | 19.0 | 56 | 32 | | | 50.9 | 46.1 | | | | | | | | | | | | | | | | | | | | | |
| H-INC-2 | HDB-7 | 9.0 | 308.2 | FILL | SM | | 16.3 | 59 | 36 | | | 58.9 | 41.1 | | | | | | | | | | | | | | | | | | | | | |
| H-INC-2 | HDB-7 | 10.5 | 306.7 | FILL | SC | | | | | | | | | | | | | | | | | | | | | | | | | | | | | |
| H-INC-2 | HDB-7 | 12.0 | 305.2 | FILL | SC | | 17.9 | 57 | 27 | | | 60.9 | 37.1 | | | | | | | | | | | | | | | | | | | | | |
| H-INC-2 | HDB-7 | 12.5 | 304.7 | FILL | | | | 67 | 31 | | | | | | | | | | | | | | | | | | | | | | | | | |
| H-INC-2 | HDB-7 | 13.5 | 303.7 | FILL | SC | | | | | | | | | | | | | | | | | | | | | | | | | | | | | |
| H-INC-2 | HDB-7 | 15.0 | 302.2 | FILL | SC | | 15.6 | 52 | 33 | | | 55.9 | 40.1 | | | | | | | | | | | | | | | | | | | | | |
| H-INC-2 | HDB-7 | 16.5 | 300.7 | FILL | SC | | 19.7 | 54 | 31 | | | 40.9 | 52.1 | | | | | | | | | | | | | | | | | | | | | |
| H-INC-2 | HDB-7 | 18.0 | 299.2 | FILL | SC/SM | | | | | | | | | | | | | | | | | | | | | | | | | | | | | |
| H-INC-2 | HDB-7 | 19.0 | 298.2 | FILL | | | 11.4 | 28 | 15 | | | 59.9 | 39.1 | | | | | | | | | | | | | | | | | | | | | |
| H-INC-2 | HDB-7 | 19.5 | 297.7 | FILL | SC | | 12.8 | 35 | 22 | | | 59.9 | 40.1 | | | | | | | | | | | | | | | | | | | | | |
| H-INC-2 | HDB-7 | 21.0 | 296.2 | FILL | SC | | 15.1 | 43 | 25 | | | 58.9 | 41.1 | | | | | | | | | | | | | | | | | | | | | |
| H-INC-2 | HDB-7 | 22.5 | 294.7 | FILL | SC | | 13.4 | 44 | 26 | | | 62.9 | 37.1 | | | | | | | | | | | | | | | | | | | | | |
| H-INC-2 | HDB-7 | 24.0 | 293.2 | FILL | SC | | 14.1 | 48 | 22 | | | 53.9 | 44.1 | | | | | | | | | | | | | | | | | | | | | |
| H-INC-2 | HDB-7 | 25.5 | 291.7 | FILL | SC | | | | | | | | | | | | | | | | | | | | | | | | | | | | | |
| H-INC-2 | HDB-7 | 30.0 | 287.2 | FILL | SC | | 21.4 | | | | | 50.0 | 50.0 | | | | | | | | | | | | | | | | | | | | | |
| H-INC-2 | HDB-7 | 34.0 | 283.2 | FILL | SC | | 20.9 | 56 | 29 | | | 58.0 | 42.0 | | | | | | | | | | | | | | | | | | | | | |
| H-INC-3 | HDB-7 | 6.0 | 302.4 | FILL | SM | | 5.5 | 34 | 18 | | | 68.9 | 29.1 | | | | | | | | | | | | | | | | | | | | | |
| H-INC-3 | HDB-7 | 6.4 | 302.0 | FILL | | | | 22 | 7 | | | 62.9 | 30.1 | | | | | | | | | | | | | | | | | | | | | |
| H-INC-3 | HDB-7 | 7.0 | 301.4 | FILL | | | 8.2 | | | | | | | | | | | | | | | | | | | | | | | | | | | |
| H-INC-3 | HDB-7 | 7.5 | 300.9 | FILL | SC | | | | | | | | | | | | | | | | | | | | | | | | | | | | | |
| H-INC-3 | HDB-7 | 9.0 | 299.4 | FILL | SC | | | 38 | 21 | | | | | | | | | | | | | | | | | | | | | | | | | |
| H-INC-3 | HDB-7 | 10.5 | 297.9 | FILL | SC | | 12.7 | 31 | 18 | | | 65.9 | 32.1 | | | | | | | | | | | | | | | | | | | | | |
| H-INC-3 | HDB-7 | 11.0 | 297.4 | FILL | SC | | 17.2 | 41 | 24 | | | 55.9 | 44.1 | | | | | | | | | | | | | | | | | | | | | |
| H-INC-3 | HDB-7 | 12.5 | 295.9 | FILL | SC | | 16.4 | 49 | 33 | | | 56.9 | 43.1 | | | | | | | | | | | | | | | | | | | | | |
| H-INC-3 | HDB-7 | 14.0 | 294.4 | FILL | SC | | 16.2 | 44 | 25 | | | 58.9 | 41.1 | | | | | | | | | | | | | | | | | | | | | |
| H-INC-3 | HDB-7 | 15.5 | 292.9 | FILL | SC | | | | | | | | | | | | | | | | | | | | | | | | | | | | | |
| H-INC-3 | HDB-7 | 17.0 | 291.4 | FILL | SC | | | | | | | | | | | | | | | | | | | | | | | | | | | | | |
| H-INC-3 | HDB-7 | 18.5 | 289.9 | FILL | SC | | 19.2 | 64 | 32 | | | 48.9 | 51.1 | | | | | | | | | | | | | | | | | | | | | |
| H-INC-3 | HDB-7 | 20.0 | 288.4 | FILL | SC | | 20.1 | 90 | 48 | | | 47.0 | 53.0 | | | | | | | | | | | | | | | | | | | | | |
| H-INC-3 | HDB-7 | 25.0 | 283.4 | FILL | SC | | | | | | | | | | | | | | | | | | | | | | | | | | | | | |
| 241-12H-16 | HLWS Tanks, 241-H | 10.9 | 290.5 | UPLAND | CM | | 19.0 | | | 52.0 | 12.0 | | | | | | | 2.68 | 0.678 | 74.6 | 18.9 | 0.8 | 7.9 | 9.9 | 0.19 | 0.011 | | | | | 3.37 | 0.55 | | 19.0 | |
| 241-12H-16 | HLWS Tanks, 241-H | 21.5 | 279.9 | UPLAND | CM | | 17.0 | | | | | | | | | | | | | | | | | | | | | | | | 2.26 | 1.05 | | 17.0 | |



Table 4.2-1(b) Summary of laboratory test results at HTF (Static p1/6).

| Map Name | Location | Sample Depth (feet) | Sample Elevation (feet) | Stratum | USCS | WD CALC PCF | MC | Atterberg Limits | | | | Sieve Analyses | | | | | | Sg | Consolidation Properties | | | | | | | | Shear Strength (deviatoric stress) | | | | | | | pH |
|---|---|---|---|---|---|---|---|---|---|---|---|---|---|---|---|---|---|---|---|---|---|---|---|---|---|---|---|---|---|---|---|---|---|
| | | | | | | | | LL (%) | PI (%) | LL200 (%) | PI200 (%) | > # 4 < # 200 | < # 200 | D10 (mm) | D30 (mm) | D50 (mm) | D60 (mm) | | eo | Sri (%) | MCi (%) | Po (tsf) | Pc (tsf) | OCR | Cc | Cr | PP (tsf) | UC (tsf) | UU (tsf) | CD (tsf) | CU (tsf) | S3 (tsf) | eO (%) | MCf (%) | |
| 241-12H-16 | HLWS Tanks, 241-H | 30 0 | 271 4 | UPLAND | CM | | 26 0 | | | | | | | | | | | | | | | | | | | | | | | | | | |
| 241-12H-16 | HLWS Tanks, 241-H | 40 0 | 261 4 | UPLAND | SC | | 24 0 | 27.0 | 7 0 | | | | | | | | | | | | | | | | | | | | | 2 86 | 1 38 | | 26 0 | |
| 241-12H-16 | HLWS Tanks, 241-H | 40 3 | 261 1 | UPLAND | SC | | 22 6 | | | | | | | | | | | | | | | | | | | | | | | 3 31 | 1 63 | | 25 0 | |
| 241-12H-16 | HLWS Tanks, 241-H | 49 8 | 251 6 | UPLAND | SC | | 23 0 | | | 97 0 | 59 0 | | | | | | | 2 58 | 0 698 | 83 6 | 22 6 | 2 3 | 7 2 | 3 1 | 0 24 | 0 027 | | | | | | | | | |
| 241-12H-16 | HLWS Tanks, 241-H | 50 0 | 251 4 | UPLAND | CH&SC | | 24 2 | | | | | | | | | | | 2 60 | 0 686 | 91 6 | 24 2 | 2 6 | 9 2 | 3 5 | 0 25 | 0 060 | | | | | | | | | |
| 241-12H-16 | HLWS Tanks, 241-H | 59 7 | 241 7 | UPLAND | SC | | 22 0 | | | | | | | | | | | | | | | | | | | | | | | | | | | |
| 241-12H-16 | HLWS Tanks, 241-H | 80 0 | 221 4 | TR3/TR4 | SC | | 19 0 | | | | | | | | | | | | | | | | | | | | | | | | | | | |
| 241-12H-16 | HLWS Tanks, 241-H | 91 0 | 210 4 | DB1/DB3 | S | | 18 0 | | | | | | | | | | | | | | | | | | | | | | | | | | | |
| 241-12H-16 | HLWS Tanks, 241-H | 122 2 | 179 2 | DB4/DB5 | SC | | 30 7 | | | | | | | | | | | 2 70 | 0 892 | 92 8 | 30 7 | 5 0 | 8 2 | 1 6 | 0 28 | 0 055 | | | | | | | | | |
| 241-12H-16 | HLWS Tanks, 241-H | 122.3 | 179 1 | DB4/DB5 | SC | | 25 0 | | | 94 0 | 51 0 | | | | | | | | | | | | | | | | | | | | | | | |
| 241-12H-16 | HLWS Tanks, 241-H | 140 3 | 161 1 | ST | SC | | 25 0 | | | | | | | | | | | | | | | | | | | | | | | | | | | |
| 241-12H-17 | HLWS Tanks, 241-H | 5 8 | 295.7 | FILL | CM | | 18 0 | 44 0 | 21 0 | | | | | | | | | | | | | | | | | | | | | | | | | |
| 241-12H-17 | HLWS Tanks, 241-H | 15.8 | 285.7 | UPLAND | CM | | 24 0 | 65 0 | 40 0 | | | | | | | | | | | | | | | | | | | | | | | | | |
| 241-12H-5 | HLWS, Area 200 | 13 6 | 288 3 | UPLAND | SC | | 19 0 | | | | | | | | | | | | | | | | | | | | 1 77 | | | | 0 00 | 4 0 | 20 0 | |
| 241-12H-5 | HLWS, Area 200 | 18 7 | 283 2 | UPLAND | SC | | 20 0 | | | | | | | | | | | | | | | | | | | | 2 37 | | | | 0 00 | 2 0 | 19 0 | |
| 241-12H-5 | HLWS, Area 200 | 24 0 | 277 9 | UPLAND | CL&SC | | 22.0 | 43 2 | 18 6 | | | | | | | | | 2 66 | 0 697 | 86 4 | 22 6 | 1 5 | 10 0 | 6 6 | 0 23 | 0 037 | 2 34 | | | | 0 00 | 3 0 | 24 0 | |
| 241-12H-5 | HLWS, Area 200 | 28 9 | 273 0 | UPLAND | CH | | 26 0 | 98 0 | 62 2 | | | | | | | | | | | | | | | | | | 2 31 | | | | 0 00 | 4 0 | 23 0 | |
| 241-12H-5 | HLWS, Area 200 | 33 9 | 268.0 | UPLAND | SC&CH | | 27.0 | 117.0 | 74.3 | | | | | | | | | 2 79 | 1 192 | 88 8 | 37 9 | 2 1 | 11.0 | 5 4 | 0 50 | 0 145 | 0 65 | | | | 0 00 | 1 0 | 27 0 | |
| 241-12H-5 | HLWS, Area 200 | 68 9 | 233 0 | TR3/TR4 | CL | | 20 0 | 34 6 | 14 9 | | | | | | | | | 2 71 | 0 645 | 84 4 | 20 1 | 3 1 | 8 8 | 2 8 | 0 25 | 0 033 | 2 35 | | | | 0 00 | 4 0 | 20 0 | |
| 241-12H-5 | HLWS, Area 200 | 73 9 | 228 0 | TR3/TR4 | SC | | 22.0 | 33 8 | 11 0 | | | | | | | | | | | | | | | | | | | | | | | | | |
| 241-12H-6 | HLWS, Area 200 | 24.1 | 277 0 | UPLAND | CH | | 18 0 | 54 8 | 31 4 | | | | | | | | | 2 72 | 0 612 | 80 2 | 18 0 | 1 5 | 9 4 | 6 2 | 0 17 | 0 047 | 1 79 | | | | 0 00 | 4 0 | 18 0 | |
| 241-12H-6 | HLWS, Area 200 | 24.3 | 276.8 | UPLAND | | | 17 1 | | | | | | | | | | | 2 73 | 0 605 | | 17 1 | 1 5 | 9 1 | 6 1 | 0 17 | 0 040 | | | | | | | | |
| 241-12H-6 | HLWS, Area 200 | 29 0 | 272.1 | UPLAND | SC | | 20 0 | | | | | | | | | | | | | | | | | | | | 1 28 | | | | 0 00 | 3 0 | 20 0 | |
| 241-12H-6 | HLWS, Area 200 | 34 0 | 267 1 | UPLAND | SC | | 20 0 | | | | | | | | | | | | | | | | | | | | 0 85 | | | | 0 00 | 3 0 | 20 0 | |
| 241-12H-6 | HLWS, Area 200 | 38 9 | 262.2 | UPLAND | SC | | 22 0 | | | | | | | | | | | | | | | | | | | | 0 83 | | | | 0 00 | 2 0 | 20 0 | |
| 241-12H-6 | HLWS, Area 200 | 43 9 | 257.2 | UPLAND | SC&CH | | 23 0 | 87 5 | 53 5 | | | | | | | | | 2 72 | 1 172 | 98 4 | 42 4 | 2 1 | 5 6 | 2 7 | 0 48 | 0 120 | | | | | | | | |
| 241-12H-6 | HLWS, Area 200 | 49 0 | 252.1 | UPLAND | SC | | 25 0 | | | | | | | | | | | | | | | | | | | | | | | | | | | |
| 241-12H-6 | HLWS, Area 200 | 79 0 | 222.1 | TR3/TR4 | SC&CH | | 18 0 | 64.8 | 32 1 | | | | | | | | | | 0 547 | 87 9 | 17 8 | 3 1 | 8 7 | 2 8 | 0 17 | 0 023 | | | | | | | | |
| 241-12H-6 | HLWS, Area 200 | 84 0 | 217 1 | TR3/TR4 | SC | | 20 0 | | | | | | | | | | | | | | | | | | | | | | | | | | | |
| 241-12H-7 | HLWS, Area 200 | 14 0 | 287 5 | UPLAND | SC | | 17 6 | | | | | | | | | | | | | | | | | | | | | | | 2 04 | 0 51 | | 17 6 | |
| 241-12H-7 | HLWS, Area 200 | 29 0 | 272 5 | UPLAND | SC&CL | | | | | | | | | | | | | | | | | | | | | | | | | | | | | |
| 241-12H-7 | HLWS, Area 200 | 34 0 | 267 5 | UPLAND | SC | | 18 4 | | | | | | | | | | | | | | | | | | | | | | | 2 63 | 1 16 | | 18 4 | |
| 241-12H-7 | HLWS, Area 200 | 39 0 | 262.5 | UPLAND | CL | | | | | | | | | | | | | | | | | | | | | | | | | | | | | |
| 241-12H-7 | HLWS, Area 200 | 44 0 | 257 5 | UPLAND | CL&SC | | | | | | | | | | | | | | | | | | | | | | | | | | | | | |
| 241-12H-7 | HLWS, Area 200 | 49 0 | 252 5 | UPLAND | SC | | | | | | | | | | | | | | | | | | | | | | | | | | | | | |
| 241-12H-7 | HLWS, Area 200 | 59 0 | 242 5 | UPLAND | SC | | | | | | | | | | | | | | | | | | | | | | | | | | | | | |
| 241-12H-7 | HLWS, Area 200 | 74 0 | 227 5 | TR3/TR4 | SC&CL | | | | | | | | | | | | | | | | | | | | | | | | | | | | | |
| H-8-1 | Evap Bldg 242-H | 5 0 | 317 0 | FILL | SM | | | | | 40 0 | 15 0 | | 34 | | 0 026 | 0 310 | 0 420 | | | | | | | | | | | | | | | | | |
| H-8-1 | Evap Bldg 242-H | 5 0 | 317 0 | FILL | SM | | | 33 0 | 14 0 | | | | | | | | | | | | | | | | | | | | | | | | | |
| H-8-1 | Evap Bldg 242-H | 17 5 | 304 5 | FILL | SC | | | 40 0 | 12 0 | | | | 30 | | 0 074 | 0 340 | 0 530 | | | | | | | | | | | | | | | | | |
| H-8-1 | Evap Bldg 242-H | 30 0 | 292 0 | FILL | SC | | | | | 37 0 | 15 0 | | 38 | | | 0 180 | 0 280 | | | | | | | | | | | | | | | | | |
| H-8-1 | Evap Bldg 242-H | 30 0 | 292 0 | FILL | SC | | | 34 0 | 14 0 | | | | | | | | | | | | | | | | | | | | | | | | | |
| H-8-1 | Evap Bldg 242-H | 40 8 | 281 3 | FILL | SG | 129 9 | 17 6 | | | | | | | | | | | | | | | | | | 0 09 | | | | | | | | | |
| B-10 | RHLWE, 200-H Area | 5 0 | 292.7 | FILL | | | 17 4 | | | | | | | | | | | | | | | | | | | | | | | | | | | |
| B-10 | RHLWE, 200-H Area | 7 5 | 290 2 | FILL | | | 13 7 | | | | | | | | | | | | | | | | | | | | | | | | | | | |
| B-10 | RHLWE, 200-H Area | 10 0 | 287 7 | FILL | | | 18 8 | | | | | | | | | | | | | | | | | | | | | | | | | | | |
| B-10 | RHLWE, 200-H Area | 12.5 | 285.2 | FILL | | | 17 1 | | | | | | | | | | | | | | | | | | | | | | | | | | | |
| B-10 | RHLWE, 200-H Area | 15 0 | 282.7 | FILL | | | 17 4 | 41 0 | 14 0 | | | | 41 | | | | | | | | | | | | | | | | | | | | | |
| B-10 ¶ | RHLWE, 200-H Area | 20 0 | 277 7 | UPLAND | | | 19 4 | | | | | | | | | | | | | | | | | | | | | | | | | | | |
| B-10 | RHLWE, 200-H Area | 30 0 | 267 7 | UPLAND | | | 14 1 | | | | | | | | | | | | | | | | | | | | | | | | | | | |
| B-10 | RHLWE, 200-H Area | 40 0 | 257 7 | UPLAND | | | 28 4 | | | | | | | | | | | | | | | | | | | | | | | | | | | |
| B-10 | RHLWE, 200-H Area | 50 0 | 247 7 | TR3/TR4 | | | 27 4 | | | | | | | | | | | | | | | | | | | | | | | | | | | |
| B-10 | RHLWE, 200-H Area | 56 5 | 241 2 | TR3/TR4 | | | | 29 0 | 3 0 | | | | 16 | | | | | | | | | | | | | | | | | | | | | |
| B-10 | RHLWE, 200-H Area | 65 0 | 232.7 | TR3/TR4 | | | 27 4 | | | | | | | | | | | | | | | | | | | | | | | | | | | |
| H-8-3 | Evap Bldg 242-H | 5.5 | 316.5 | FILL | SC | | | 37 0 | 12 0 | | | | | | | | | | | | | | | | | | | | | | | | | |
| H-8-3 | Evap Bldg 242-H | 10 5 | 311 5 | FILL | SC | | | 34 0 | 11 0 | | | | | | | | | | | | | | | | | | | | | | | | | |
| H-8-3 | Evap Bldg 242-H | 20.5 | 301 5 | FILL | SC | | | 37.0 | 13 0 | | | | | | | | | | | | | | | | | | | | | | | | | |
| H-8-3 | Evap Bldg 242-H | 25.5 | 296.5 | FILL | SC | | | 38 0 | 13.0 | | | | | | | | | | | | | | | | | | | | | | | | | |
| H-8-3 | Evap. Bldg. 242-H | 30.5 | 291 5 | FILL | SC | | | 36 0 | 11 0 | | | | | | | | | | | | | | | | | | | | | | | | | |

Table 4.2-1(b) Summary of laboratory test results at HTF (Static p2/6).

| Map Name | Location | Sample Depth (feet) | Sample Elevation (feet) | Stratum | USCS | WD CALC PCF | MC | Atterberg Limits | | | | Sieve Analyses | | | | | | | Consolidation Properties | | | | | | | | Shear Strength (deviatoric stress) | | | | | | | pH |
|---|---|---|---|---|---|---|---|---|---|---|---|---|---|---|---|---|---|---|---|---|---|---|---|---|---|---|---|---|---|---|---|---|---|
| | | | | | | | | LL (%) | PI (%) | LL200 (%) | PI200 (%) | > # 4 < # 200 | < # 200 | D10 (mm) | D30 (mm) | D50 (mm) | D60 (mm) | Sg | eo | Sri (%) | MCi (%) | Po (tsf) | Pc (tsf) | OCR | Cc | Cr | PP (tsf) | UC (tsf) | UU (tsf) | CD (tsf) | CU (tsf) | S3 (tsf) | BO (%) | MCi (%) | |
| H-8-3 | Evap. Bldg. 242-H | 33.8 | 288.3 | FILL | SC | 122.0 | 18.2 | | | | | | | | | | | | | | | | | | 0.22 | | | | | | | | |
| H-8-3 | Evap. Bldg. 242-H | 45.5 | 276.5 | UPLAND | CL | | | 45.0 | 21.0 | | | | | | | | | | | | | | | | | | | | | | | | |
| H-8-3 | Evap. Bldg. 242-H | 45.5 | 276.5 | UPLAND | CL | | | 46.0 | 15.0 | | | | | | | | | | | | | | | | | | | | | | | | |
| H-8-3 | Evap. Bldg. 242-H | 45.5 | 276.5 | UPLAND | CL | | | | | 48.0 | 14.0 | | | | | | | | | | | | | | | | | | | | | | |
| B-5 | RHLWE, 200-H Area | 2.5 | 294.2 | FILL | | | 11.8 | | | | | | | | | | | | | | | | | | | | | | | | | | |
| B-5 | RHLWE, 200-H Area | 7.5 | 289.2 | FILL | | | 12.5 | | | | | | | | | | | | | | | | | | | | | | | | | | |
| B-5 | RHLWE, 200-H Area | 12.5 | 284.2 | FILL | | | 15.0 | | | | | | | | | | | | | | | | | | | | | | | | | | |
| B-5 | RHLWE, 200-H Area | 20.0 | 276.7 | UPLAND | | 122.1 | 11.4 | 47.0 | 4.0 | | | | 19 | | | | | | | | | | | | | | 0.56 | | | | | | |
| B-5 | RHLWE, 200-H Area | 25.0 | 271.7 | UPLAND | | | 12.6 | | | | | | | | | | | | | | | | | | | | | | | | | | |
| B-5 | RHLWE, 200-H Area | 28.0 | 268.7 | UPLAND | | | 16.0 | | | | | | | | | | | | | | | | | | | | | | | | | | |
| B-5 | RHLWE, 200-H Area | 35.0 | 261.7 | UPLAND | | | 15.0 | | | | | | | | | | | | | | | | | | | | | | | | | | |
| B-6 | RHLWE, 200-H Area | 5.0 | 291.1 | FILL | | | 17.8 | | | | | | | | | | | | | | | | | | | | | | | | | | |
| B-6 | RHLWE, 200-H Area | 10.0 | 286.1 | FILL | | | 21.8 | | | | | | | | | | | | | | | | | | | | | | | | | | |
| B-7 | RHLWE, 200-H Area | 5.0 | 293.8 | FILL | | | 16.7 | | | | | | | | | | | | | | | | | | | | | | | | | | |
| B-7 | RHLWE, 200-H Area | 10.0 | 288.8 | FILL | | 125.1 | 17.6 | | | | | | | | | | | | | | | | | | | | 0.72 | | | | | | |
| B-7 | RHLWE, 200-H Area | 11.0 | 287.8 | FILL | SM | 128.4 | 15.9 | | | | | | | | | | | | | | | | | | | | | | | 2.04 | 0.26 | | 15.9 |
| B-7 | RHLWE, 200-H Area | 11.0 | 287.8 | FILL | SM | | | | | | | | | | | | | | | | | | | | | | | | | 2.00 | 0.51 | | |
| B-7 | RHLWE, 200-H Area | 11.0 | 287.8 | FILL | SM | | | | | | | | | | | | | | | | | | | | | | | | | 1.97 | 0.75 | | |
| B-7 | RHLWE, 200-H Area | 15.0 | 283.8 | FILL | | | 15.9 | | | | | | | | | | | | | | | | | | | | | | | | | | |
| B-8 | RHLWE, 200-H Area | 5.0 | 312.1 | FILL | | | 15.7 | | | | | | | | | | | | | | | | | | | | | | | | | | |
| B-8 | RHLWE, 200-H Area | 10.0 | 307.1 | FILL | | 128.7 | 15.4 | 34.0 | 13.0 | | | | 62 | | | | | 2.63 | | | | | | | | | 1.15 | | | | | | |
| B-8 | RHLWE, 200-H Area | 15.0 | 302.1 | FILL | | | 18.3 | | | | | | | | | | | | | | | | | | | | | | | | | | |
| B-9 | RHLWE, 200-H Area | 2.5 | 295.8 | FILL | | | 12.1 | | | | | | | | | | | | | | | | | | | | | | | | | | |
| B-9 | RHLWE, 200-H Area | 5.0 | 293.3 | FILL | | | 16.5 | | | | | | | | | | | | | | | | | | | | | | | | | | |
| B-9 | RHLWE, 200-H Area | 7.5 | 290.8 | FILL | | | 17.0 | | | | | | | | | | | | | | | | | | | | | | | | | | |
| B-9 | RHLWE, 200-H Area | 10.0 | 288.3 | FILL | | 118.7 | 17.4 | 47.0 | 13.0 | | | | 43 | | | | | | | | | | | | | | 1.28 | | | | | | |
| B-9 | RHLWE, 200-H Area | 15.0 | 283.3 | FILL | | | 21.7 | | | | | | | | | | | | | | | | | | | | | | | | | | |
| B-9 | RHLWE, 200-H Area | 20.0 | 278.3 | UPLAND | | | 22.3 | | | | | | | | | | | | | | | | | | | | | | | | | | |
| B-9 | RHLWE, 200-H Area | 25.0 | 273.3 | UPLAND | | | 19.1 | | | | | | | | | | | | | | | | | | | | | | | | | | |
| B-9 | RHLWE, 200-H Area | 35.0 | 263.3 | UPLAND | | | 17.3 | | | | | | | | | | | | | | | | | | | | | | | | | | |
| B-9 | RHLWE, 200-H Area | 45.0 | 253.3 | UPLAND | | 119.5 | 23.2 | 41.0 | 14.0 | | | | 21 | | | | | 2.66 | | | | | | | | | 1.49 | | | | | | |
| B-9 | RHLWE, 200-H Area | 55.0 | 243.3 | TR3/TR4 | | | 23.7 | | | | | | | | | | | | | | | | | | | | | | | | | | |
| B-9 | RHLWE, 200-H Area | 65.0 | 233.3 | TR3/TR4 | | | 21.5 | | | | | | | | | | | | | | | | | | | | | | | | | | |
| B-9 | RHLWE, 200-H Area | 75.0 | 223.3 | DB1/DB3 | | | 25.2 | | | | | | | | | | | | | | | | | | | | | | | | | | |
| DH-2 | Waste Tanks, 200-H | 55.0 | 225.4 | TR3/TR4 | CL | 123.4 | 24.0 | 37.0 | 16.0 | | | | 24 | | 0.089 | 0.150 | 0.190 | 2.78 | | | | | | | | | 2.18 | | | | 0.00 | 6.9 | 24.0 | |
| DH-2 | Waste Tanks, 200-H | 90.0 | 190.4 | DB4/DB5 | SM | | 32.1 | 27.0 | 9.0 | | | | 14 | | | | | | | | | | | | | | | | | | | | |
| DH-2 | Waste Tanks, 200-H | 130.0 | 150.4 | ST | SC | | 26.9 | | | | | | 43 | | | | | | | | | | | | | | | | | | | | |
| DH-2 | Waste Tanks, 200-H | 150.0 | 130.4 | ST | SM | | 24.8 | | | | | | 19 | | | | | | | | | | | | | | | | | | | | |
| DH-3 | Waste Tanks, 200-H | 45.0 | 275.3 | UPLAND | SC | | 20.0 | 41.0 | 17.0 | | | | 43 | | | | | | | | | | | | | | | | | | | | |
| DH-3 | Waste Tanks, 200-H | 60.0 | 260.3 | UPLAND | CL | 128.6 | 16.0 | 83.0 | 58.0 | | | | 16 | 0.007 | 0.480 | 0.680 | 0.805 | 2.72 | | | | | | | | | 1.74 | | | | 0.00 | 10.0 | 16.0 | |
| DH-3 | Waste Tanks, 200-H | 85.0 | 235.3 | UPLAND | SP-SM | | 23.0 | | | | | | 10 | | | | | | | | | | | | | | | | | | | | |
| DH-3 | Waste Tanks, 200-H | 95.0 | 225.3 | TR3/TR4 | SM | | 25.1 | 48.0 | 20.0 | | | | 30 | | | | | | | | | | | | | | | | | | | | |
| DH-3 | Waste Tanks, 200-H | 130.0 | 190.3 | DB1/DB3 | SW-SM | | 25.2 | | | | | | 12 | | | | | | | | | | | | | | | | | | | | |
| H-154U | TF Space Gain Facility | 10.5 | 287.4 | FILL | MH | | 35.8 | 63.0 | 27.0 | | | | | | | | | | | | | | | | | | | | | 2.34 | 0.58 | 13.3 | 29.5 | |
| H-154U | TF Space Gain Facility | 10.8 | 287.1 | FILL | MH | | 30.3 | | | | | | | | | | | 2.73 | 0.963 | 85.8 | 30.3 | 0.6 | 5.9 | 9.5 | 0.25 | 0.054 | | | | | | | | |
| H-154U | TF Space Gain Facility | 13.8 | 284.5 | FILL | MH | | 25.0 | | | | | | | | | | | 2.69 | 0.738 | 90.9 | 25.0 | 0.9 | 4.3 | 4.9 | 0.21 | 0.045 | | | | | | | | |
| H-154U | TF Space Gain Facility | 13.7 | 284.2 | FILL | MH | | 29.4 | 61.0 | 25.0 | | | 22.8 | 77 | | | | | | | | | | | | | | | | | | | | |
| H-154U | TF Space Gain Facility | 17.2 | 280.7 | UPLAND | SC | | 18.9 | 60.0 | 31.0 | | | 61.5 | 39 | | | 0.240 | 0.305 | | | | | | | | | | | | | | | | |
| H-154U | TF Space Gain Facility | 27.0 | 270.9 | UPLAND | CH | | 20.4 | | | | | | | | | | | | | | | | | | | | | | | 3.33 | 1.37 | 4.5 | 25.9 | |
| H-154U | TF Space Gain Facility | 28.6 | 269.3 | UPLAND | SC | | 21.2 | | | | | 58.4 | 42 | | | 0.165 | 0.220 | | | | | | | | | | | | | | | | |
| H-154U | TF Space Gain Facility | 72.1 | 225.8 | DB1/DB3 | SC | | 21.4 | 61.0 | 33.0 | | | 67.1 | 33 | | | 0.240 | 0.400 | | | | | | | | | | | | | | | | |
| HMP-1 | Evap. Bldg. 242-H | 6.0 | 316.6 | FILL | F | 132.5 | 16.4 | 83.0 | 57.0 | | | | 12 | | | | | | | | | | | | | | | | | | | | |
| HMP-1 | Evap. Bldg. 242-H | 14.5 | 308.1 | FILL | F | | 14.6 | | | | | | 37 | | | | | | | | | | | | | | | | | | | | |
| HMP-1 | Evap. Bldg. 242-H | 18.5 | 304.1 | FILL | F | 118.1 | 17.0 | 59.0 | 38.0 | | | | 46 | | | | | | | | | | | | | | | | | | | | |
| HMP-1 | Evap. Bldg. 242-H | 24.5 | 298.1 | FILL | F | 125.1 | 15.8 | 67.0 | 44.0 | | | | 51 | | | | | | | | | | | | | | | | | | | | |
| HMP-1 | Evap. Bldg. 242-H | 32.5 | 290.1 | FILL | F | 129.5 | 19.2 | | | | | | 31 | | | | | | | | | | | | | | | | | | | | |
| HMP-1 | Evap. Bldg. 242-H | 35.5 | 287.1 | FILL | F | 132.7 | 16.5 | 68.0 | 46.0 | | | | 36 | | | | | | | | | | | | | | | | | | | | |
| HMP-1 | Evap. Bldg. 242-H | 40.5 | 282.1 | FILL | F | 128.9 | 17.3 | | | | | | 42 | | | | | | | | | | | | | | | | | | | | |
| HMP-2 | Evap. Bldg. 242-H | 2.0 | 319.8 | FILL | F | 111.8 | 18.4 | | | | | | | | | | | | | | | | | | | | | | | | | | |

Table 4.2-1(b) Summary of laboratory test results at HTF (Static p3/6).

| Map Name | Location | Sample Depth (feet) | Sample Elevation (feet) | Stratum | USCS | WD CALC PCF | MC | Atterberg Limits | | | | Sieve Analyses | | | | | | Sg | Consolidation Properties | | | | | | | | Shear Strength (deviatoric stress) | | | | | | | pH |
|---|---|---|---|---|---|---|---|---|---|---|---|---|---|---|---|---|---|---|---|---|---|---|---|---|---|---|---|---|---|---|---|---|---|
| | | | | | | | | LL (%) | PI (%) | LL200 (%) | PI200 (%) | > # 4 < # 200 | < # 200 | D10 (mm) | D30 (mm) | D50 (mm) | D60 (mm) | | eo | Sri (%) | MCI (%) | Po (tsf) | Pc (tsf) | OCR | Cc | Cr | PP (tsf) | UC (tsf) | UU (tsf) | CD (tsf) | CU (tsf) | S3 (tsf) | EO (%) | MCI (%) | |
| HMP-2 | Evap. Bldg. 242-H | 3.5 | 318.3 | FILL | F | 112.8 | 22.9 | | | | | | | | | | | | | | | | | | | | | | | | | | |
| HMP-2 | Evap. Bldg. 242-H | 6.0 | 315.8 | FILL | F | 129.2 | 18.5 | 66.0 | 35.0 | | | | 37 | | | | | | | | | | | | | | | | | | | | |
| HMP-2 | Evap. Bldg. 242-H | 8.0 | 313.8 | FILL | F | 129.3 | 16.6 | | | | | | | | | | | | | | | | | | | | | | | | | | |
| HMP-2 | Evap. Bldg. 242-H | 10.0 | 311.8 | FILL | F | 126.6 | 18.0 | | | | | | | | | | | | | | | | | | | | | | | | | | |
| HMP-2 | Evap. Bldg. 242-H | 11.5 | 310.3 | FILL | F | 133.6 | 15.0 | | | | | | | | | | | | | | | | | | | | | | | | | | |
| HMP-2 | Evap. Bldg. 242-H | 13.5 | 308.3 | FILL | F | 132.2 | 16.3 | | | | | | | | | | | | | | | | | | | | | | | | | | |
| HMP-2 | Evap. Bldg. 242-H | 15.5 | 306.3 | FILL | F | 129.8 | 17.8 | 70.0 | 43.0 | | | | 39 | | | | | | | | | | | | | | | | | | | | |
| HMP-2 | Evap. Bldg. 242-H | 17.0 | 304.8 | FILL | F | 122.3 | 19.9 | | | | | | | | | | | | | | | | | | | | | | | | | | |
| HMP-2 | Evap. Bldg. 242-H | 20.0 | 301.8 | FILL | F | 126.0 | 20.0 | | | | | | | | | | | | | | | | | | | | | | | | | | |
| HMP-2 | Evap. Bldg. 242-H | 21.5 | 300.3 | FILL | F | 126.4 | 17.4 | | | | | | | | | | | | | | | | | | | | | | | | | | |
| HMP-2 | Evap. Bldg. 242-H | 23.0 | 298.8 | FILL | F | 122.4 | 17.8 | | | | | | | | | | | | | | | | | | | | | | | | | | |
| HMP-2 | Evap. Bldg. 242-H | 24.5 | 297.3 | FILL | F | 130.1 | 15.5 | | | | | | | | | | | | | | | | | | | | | | | | | | |
| HMP-2 | Evap. Bldg. 242-H | 26.0 | 295.8 | FILL | F | 126.3 | 18.3 | 68.0 | 42.0 | | | | 44 | | | | | | | | | | | | | | | | | | | | |
| HMP-2 | Evap. Bldg. 242-H | 27.5 | 294.3 | FILL | F | 126.8 | 17.1 | | | | | | | | | | | | | | | | | | | | | | | | | | |
| HMP-2 | Evap. Bldg. 242-H | 29.0 | 292.8 | FILL | F | 134.2 | 14.7 | | | | | | | | | | | | | | | | | | | | | | | | | | |
| HMP-2 | Evap. Bldg. 242-H | 30.5 | 291.3 | FILL | F | 134.9 | 13.4 | | | | | | | | | | | | | | | | | | | | | | | | | | |
| HMP-2 | Evap. Bldg. 242-H | 32.0 | 289.8 | FILL | F | 126.8 | 19.6 | | | | | | | | | | | | | | | | | | | | | | | | | | |
| HMP-2 | Evap. Bldg. 242-H | 33.5 | 288.3 | FILL | F | 135.6 | 15.9 | 61.0 | 37.0 | | | | 34 | | | | | | | | | | | | | | | | | | | | |
| HMP-2 | Evap. Bldg. 242-H | 38.5 | 283.3 | FILL | F | 125.7 | 20.9 | | | | | | | | | | | | | | | | | | | | | | | | | | |
| HMP-2 | Evap. Bldg. 242-H | 40.0 | 281.8 | FILL | F | 129.8 | 19.6 | | | | | | | | | | | | | | | | | | | | | | | | | | |
| HMP-3 | Evap. Bldg. 242-H | 2.0 | 320.1 | FILL | F | 103.1 | 19.9 | | | | | | | | | | | | | | | | | | | | | | | | | | |
| HMP-3 | Evap. Bldg. 242-H | 4.0 | 318.1 | FILL | F | 107.7 | 19.3 | | | | | | | | | | | | | | | | | | | | | | | | | | |
| HMP-3 | Evap. Bldg. 242-H | 6.0 | 316.1 | FILL | F | 117.1 | 19.5 | 89.0 | 61.0 | | | | 36 | | | | | | | | | | | | | | | | | | | | |
| HMP-3 | Evap. Bldg. 242-H | 7.8 | 314.3 | FILL | F | 116.8 | 18.9 | | | | | | | | | | | | | | | | | | | | | | | | | | |
| HMP-3 | Evap. Bldg. 242-H | 8.0 | 314.1 | FILL | F | 126.0 | 18.3 | | | | | | | | | | | | | | | | | | | | | 1.57 | | | 0.42 | 16.0 | 18.3 | |
| HMP-3 | Evap. Bldg. 242-H | 8.1 | 314.0 | FILL | F | 119.4 | 18.5 | | | | | | | | | | | | | | | | | | | | | | | | | | |
| HMP-3 | Evap. Bldg. 242-H | 8.8 | 313.3 | FILL | F | 131.6 | 15.2 | | | | | | | | | | | | | | | | | | | | | | | | | | |
| HMP-3 | Evap. Bldg. 242-H | 10.0 | 312.1 | FILL | F | 105.2 | 17.2 | | | | | | | | | | | | | | | | | | | | | | | | | | |
| HMP-3 | Evap. Bldg. 242-H | 12.0 | 310.1 | FILL | F | 127.4 | 16.7 | | | | | | | | | | | | | | | | | | | | | | | | | | |
| HMP-3 | Evap. Bldg. 242-H | 14.0 | 308.1 | FILL | F | 128.0 | 18.6 | | | | | | | | | | | | | | | | | | | | | | | | | | |
| HMP-3 | Evap. Bldg. 242-H | 14.8 | 307.3 | FILL | F | 127.2 | 20.9 | | | | | | | | | | | | | | | | | | | | | | | | | | |
| HMP-3 | Evap. Bldg. 242-H | 15.1 | 307.0 | FILL | F | 129.2 | 17.7 | | | | | | | | | | | | | | | | | | | | | | | | | | |
| HMP-3 | Evap. Bldg. 242-H | 15.4 | 306.7 | FILL | F | 123.9 | 20.5 | | | | | | | | | | | | | | | | | | | | | | | | | | |
| HMP-3 | Evap. Bldg. 242-H | 15.8 | 306.3 | FILL | F | 128.9 | 18.3 | | | | | | | | | | | | | | | | | | | | | | | | | | |
| HMP-3 | Evap. Bldg. 242-H | 17.0 | 305.1 | FILL | F | 123.7 | 18.9 | | | | | | | | | | | | | | | | | | | | | | | | | | |
| HMP-3 | Evap. Bldg. 242-H | 17.0 | 305.1 | FILL | F | 125.6 | 21.7 | | | | | | | | | | | | | | | | | | | | | 1.64 | | | 0.86 | 13.0 | 21.7 | |
| HMP-3 | Evap. Bldg. 242-H | 18.5 | 303.6 | FILL | F | 125.2 | 17.7 | | | | | | | | | | | | | | | | | | | | | | | | | | |
| HMP-3 | Evap. Bldg. 242-H | 20.0 | 302.1 | FILL | F | 121.7 | 19.1 | | | | | | | | | | | | | | | | | | | | | | | | | | |
| HMP-3 | Evap. Bldg. 242-H | 20.8 | 301.3 | FILL | F | 126.6 | 17.3 | | | | | | | | | | | | | | | | | | | | | | | | | | |
| HMP-3 | Evap. Bldg. 242-H | 21.1 | 301.0 | FILL | F | 124.7 | 14.6 | | | | | | | | | | | | | | | | | | | | | | | | | | |
| HMP-3 | Evap. Bldg. 242-H | 21.4 | 300.7 | FILL | F | 126.2 | 15.0 | | | | | | | | | | | | | | | | | | | | | | | | | | |
| HMP-3 | Evap. Bldg. 242-H | 21.8 | 300.3 | FILL | F | 126.4 | 14.9 | | | | | | | | | | | | | | | | | | | | | | | | | | |
| HMP-3 | Evap. Bldg. 242-H | 23.0 | 299.1 | FILL | F | 128.3 | 17.7 | | | | | | | | | | | | | | | | | | | | | | | | | | |
| HMP-3 | Evap. Bldg. 242-H | 24.5 | 297.6 | FILL | F | 133.9 | 15.6 | 74.0 | 52.0 | | | | 37 | | | | | | | | | | | | | | | | | | | | |
| HMP-3 | Evap. Bldg. 242-H | 26.0 | 296.1 | FILL | F | 137.6 | 15.3 | | | | | | | | | | | | | | | | | | | | | | | | | | |
| HMP-3 | Evap. Bldg. 242-H | 26.5 | 295.6 | FILL | F | 127.5 | 18.9 | | | | | | | | | | | | | | | | | | | | | | | | | | |
| HMP-3 | Evap. Bldg. 242-H | 26.8 | 295.3 | FILL | F | 132.5 | 18.7 | | | | | | | | | | | | | | | | | | | | | | | | | | |
| HMP-3 | Evap. Bldg. 242-H | 27.1 | 295.0 | FILL | F | 133.5 | 13.9 | | | | | | | | | | | | | | | | | | | | | | | | | | |
| HMP-3 | Evap. Bldg. 242-H | 27.8 | 294.3 | FILL | F | 131.9 | 15.4 | | | | | | | | | | | | | | | | | | | | | | | | | | |
| HMP-3 | Evap. Bldg. 242-H | 29.0 | 293.1 | FILL | F | 140.2 | 14.6 | | | | | | | | | | | | | | | | | | | | | | | | | | |
| HMP-3 | Evap. Bldg. 242-H | 30.5 | 291.6 | FILL | F | 136.2 | 15.8 | | | | | | | | | | | | | | | | | | | | | | | | | | |
| HMP-3 | Evap. Bldg. 242-H | 30.5 | 291.6 | FILL | F | 128.6 | 13.6 | | | | | | | | | | | | | | | | | | | | | 7.00 | | | 1.58 | 13.4 | 13.6 | |
| HMP-3 | Evap. Bldg. 242-H | 31.3 | 290.8 | FILL | F | 132.6 | 16.0 | | | | | | | | | | | | | | | | | | | | | | | | | | |
| HMP-3 | Evap. Bldg. 242-H | 31.6 | 290.5 | FILL | F | 130.7 | 15.5 | | | | | | | | | | | | | | | | | | | | | | | | | | |
| HMP-3 | Evap. Bldg. 242-H | 31.9 | 290.2 | FILL | F | 133.5 | 14.9 | | | | | | | | | | | | | | | | | | | | | | | | | | |
| HMP-3 | Evap. Bldg. 242-H | 32.3 | 289.8 | FILL | F | 136.3 | 16.5 | | | | | | | | | | | | | | | | | | | | | | | | | | |
| HMP-3 | Evap. Bldg. 242-H | 33.5 | 288.6 | FILL | F | 135.2 | 17.8 | | | | | | | | | | | | | | | | | | | | | | | | | | |
| HMP-3 | Evap. Bldg. 242-H | 35.0 | 287.1 | FILL | F | 137.3 | 15.4 | 55.0 | 37.0 | | | | 46 | | | | | | | | | | | | | | | | | | | | |
| HMP-3 | Evap. Bldg. 242-H | 36.6 | 285.6 | FILL | F | 132.8 | 12.6 | | | | | | | | | | | | | | | | | | | | | | | | | | |

Table 4.2-1(b) Summary of laboratory test results at HTF (Static p4/6).

| Map Name | Location | Sample Depth (feet) | Sample Elevation (feet) | Stratum | USCS | WD CALC PCF | MC | Atterberg Limits | | | | Sieve Analyses | | | | | | Sg | Consolidation Properties | | | | | | | | Shear Strength (deviatoric stress) | | | | | | | pH |
|---|---|---|---|---|---|---|---|---|---|---|---|---|---|---|---|---|---|---|---|---|---|---|---|---|---|---|---|---|---|---|---|---|---|
| | | | | | | | | LL (%) | PI (%) | LL200 (%) | PI200 (%) | > # 4 < # 200 | < # 200 | D10 (mm) | D30 (mm) | D50 (mm) | D60 (mm) | | eo | Sri (%) | MCI (%) | Po (tsf) | Pc (tsf) | OCR | Cc | Cr | PP (tsf) | UC (tsf) | UU (tsf) | CD (tsf) | CU (tsf) | S3 (tsf) | eO (%) | MCI (%) | |
| HMP-3 | Evap. Bldg. 242-H | 36.5 | 285.6 | FILL | F | 141.8 | 13.9 | | | | | | | | | | | | | | | | | | | | | | | | | | |
| HMP-3 | Evap. Bldg. 242-H | 36.8 | 285.3 | FILL | F | 136.5 | 18.1 | | | | | | | | | | | | | | | | | | | | | | | | | | |
| HMP-3 | Evap. Bldg. 242-H | 37.1 | 285.0 | FILL | F | 136.0 | 18.3 | | | | | | | | | | | | | | | | | | | | | | | | | | |
| HMP-3 | Evap. Bldg. 242-H | 38.0 | 284.1 | FILL | F | 136.0 | 18.3 | | | | | | | | | | | | | | | | | | | | | | | | | | |
| HMP-3 | Evap. Bldg. 242-H | 39.5 | 282.6 | FILL | F | 137.6 | 17.1 | | | | | | | | | | | | | | | | | | | | | | | | | | |
| HMP-3 | Evap. Bldg. 242-H | 39.5 | 282.6 | FILL | F | 133.8 | 18.2 | | | | | | | | | | | | | | | | | | | | | | | | | | |
| HMP-3 | Evap. Bldg. 242-H | 42.6 | 279.6 | UPLAND | CL | | 21.2 | | | | | | | | | | | | | | | | | | | | | 6.04 | | | 2.06 | 13.3 | 18.2 | |
| HMP-3 | Evap. Bldg. 242-H | 45.6 | 276.5 | UPLAND | CL | | 30.6 | | | | | | | | | | | | | | | | | | | | | 4.09 | | | 2.23 | 8.9 | 21.2 | |
| HMP-3 | Evap. Bldg. 242-H | 46.2 | 275.9 | UPLAND | CL | | 30.0 | 61.0 | 30.7 | | | | | | | | | 2.72 | 0.839 | 97.2 | 30.0 | 3.0 | 11.8 | 3.9 | 0.38 | 0.064 | | | 3.27 | | | 2.39 | 7.1 | 30.6 | |
| HMP-3 | Evap. Bldg. 242-H | 51.5 | 270.6 | UPLAND | SM&C | | 24.6 | | | | | | | | | | | | | | | | | | | | | | | | | | |
| HMP-3 | Evap. Bldg. 242-H | 56.0 | 266.1 | UPLAND | CL | | 26.3 | | | | | | | | | | | | | | | | | | | | | 3.58 | | | 2.65 | 8.0 | 24.6 | |
| HMP-3 | Evap. Bldg. 242-H | 56.1 | 266.0 | UPLAND | CL | | 26.1 | 64.7 | 48.1 | | | | | | | | | 2.69 | 0.703 | 98.3 | 25.8 | 1.9 | 7.3 | 3.9 | 0.27 | 0.070 | | | 2.36 | | | 2.91 | 11.6 | 26.3 | |
| HMP-3 | Evap. Bldg. 242-H | 66.4 | 255.7 | UPLAND | ML | | 24.7 | 45.8 | 25.9 | | | | | | | | | 2.69 | 0.814 | 92.0 | 27.8 | 2.1 | 6.0 | 2.9 | 0.26 | 0.046 | | | | | | | | | |
| HMP-4 | Evap. Bldg. 242-H | 2.0 | 319.8 | FILL | F | | 19.0 | | | | | | | | | | | | | | | | | | | | | | | | | | |
| HMP-4 | Evap. Bldg. 242-H | 4.0 | 317.8 | FILL | F | | 18.4 | | | | | | | | | | | | | | | | | | | | | | | | | | |
| HMP-4 | Evap. Bldg. 242-H | 6.0 | 315.8 | FILL | F | | 20.0 | | | | | | | | | | | | | | | | | | | | | | | | | | |
| HMP-4 | Evap. Bldg. 242-H | 8.0 | 313.8 | FILL | F | | 17.8 | | | | | | | | | | | | | | | | | | | | | | | | | | |
| HMP-4 | Evap. Bldg. 242-H | 10.0 | 311.8 | FILL | F | | 17.7 | 73.0 | 56.0 | | | | 35 | | | | | | | | | | | | | | | | | | | | |
| HMP-4 | Evap. Bldg. 242-H | 12.0 | 309.8 | FILL | F | | 16.5 | | | | | | | | | | | | | | | | | | | | | | | | | | |
| HMP-4 | Evap. Bldg. 242-H | 14.0 | 307.8 | FILL | F | | 20.2 | | | | | | | | | | | | | | | | | | | | | | | | | | |
| HMP-4 | Evap. Bldg. 242-H | 16.0 | 305.8 | FILL | F | | 17.8 | 55.0 | 39.0 | | | | 37 | | | | | | | | | | | | | | | | | | | | |
| HMP-4 | Evap. Bldg. 242-H | 18.0 | 303.8 | FILL | F | | 17.2 | | | | | | | | | | | | | | | | | | | | | | | | | | |
| HMP-4 | Evap. Bldg. 242-H | 20.0 | 301.8 | FILL | F | | 16.0 | | | | | | | | | | | | | | | | | | | | | | | | | | |
| HMP-4 | Evap. Bldg. 242-H | 22.0 | 299.8 | FILL | F | | 17.0 | | | | | | | | | | | | | | | | | | | | | | | | | | |
| HMP-4 | Evap. Bldg. 242-H | 24.0 | 297.8 | FILL | F | | 20.8 | | | | | | | | | | | | | | | | | | | | | | | | | | |
| HMP-4 | Evap. Bldg. 242-H | 26.0 | 295.8 | FILL | F | | 40.7 | 64.0 | 46.0 | | | | 43 | | | | | | | | | | | | | | | | | | | | |
| HMP-4 | Evap. Bldg. 242-H | 28.0 | 293.8 | FILL | F | | 25.0 | | | | | | | | | | | | | | | | | | | | | | | | | | |
| HMP-4 | Evap. Bldg. 242-H | 30.0 | 291.8 | FILL | F | | 20.3 | | | | | | | | | | | | | | | | | | | | | | | | | | |
| HMP-4 | Evap. Bldg. 242-H | 32.0 | 289.8 | FILL | F | | 16.7 | | | | | | | | | | | | | | | | | | | | | | | | | | |
| HMP-4 | Evap. Bldg. 242-H | 34.0 | 287.8 | FILL | F | | 17.7 | | | | | | | | | | | | | | | | | | | | | | | | | | |
| HMP-4 | Evap. Bldg. 242-H | 36.0 | 285.8 | FILL | F | | 19.7 | 65.0 | 45.0 | | | | 43 | | | | | | | | | | | | | | | | | | | | |
| HMP-4 | Evap. Bldg. 242-H | 38.0 | 283.8 | FILL | F | | 19.9 | | | | | | | | | | | | | | | | | | | | | | | | | | |
| HMP-4 | Evap. Bldg. 242-H | 40.0 | 281.8 | FILL | F | | 19.2 | | | | | | | | | | | | | | | | | | | | | | | | | | |
| HMP-5 | Evap. Bldg. 242-H | 2.0 | 320.3 | FILL | F | | 17.5 | | | | | | | | | | | | | | | | | | | | | | | | | | |
| HMP-5 | Evap. Bldg. 242-H | 3.5 | 318.8 | FILL | F | | 19.0 | | | | | | | | | | | | | | | | | | | | | | | | | | |
| HMP-5 | Evap. Bldg. 242-H | 5.5 | 316.8 | FILL | F | | 18.1 | | | | | | | | | | | | | | | | | | | | | | | | | | |
| HMP-5 | Evap. Bldg. 242-H | 7.5 | 314.8 | FILL | F | | 18.3 | 89.0 | 63.0 | | | | 38 | | | | | | | | | | | | | | | | | | | | |
| HMP-5 | Evap. Bldg. 242-H | 9.5 | 312.8 | FILL | F | | 16.6 | | | | | | | | | | | | | | | | | | | | | | | | | | |
| HMP-5 | Evap. Bldg. 242-H | 11.0 | 311.3 | FILL | F | | 17.3 | | | | | | | | | | | | | | | | | | | | | | | | | | |
| HMP-5 | Evap. Bldg. 242-H | 12.5 | 309.8 | FILL | F | | 22.5 | | | | | | | | | | | | | | | | | | | | | | | | | | |
| HMP-5 | Evap. Bldg. 242-H | 14.0 | 308.3 | FILL | F | | 17.7 | | | | | | | | | | | | | | | | | | | | | | | | | | |
| HMP-5 | Evap. Bldg. 242-H | 15.5 | 306.8 | FILL | F | | 17.0 | 69.0 | 49.0 | | | | 35 | | | | | | | | | | | | | | | | | | | | |
| HMP-5 | Evap. Bldg. 242-H | 17.0 | 305.3 | FILL | F | | 21.0 | | | | | | | | | | | | | | | | | | | | | | | | | | |
| HMP-5 | Evap. Bldg. 242-H | 18.5 | 303.8 | FILL | F | | 19.7 | | | | | | | | | | | | | | | | | | | | | | | | | | |
| HMP-5 | Evap. Bldg. 242-H | 20.0 | 302.3 | FILL | F | | 21.2 | | | | | | | | | | | | | | | | | | | | | | | | | | |
| HMP-5 | Evap. Bldg. 242-H | 21.5 | 300.8 | FILL | F | | 19.0 | | | | | | | | | | | | | | | | | | | | | | | | | | |
| HMP-5 | Evap. Bldg. 242-H | 24.5 | 297.8 | FILL | F | | 19.5 | | | | | | | | | | | | | | | | | | | | | | | | | | |
| HMP-5 | Evap. Bldg. 242-H | 26.0 | 296.3 | FILL | F | | 19.2 | 58.0 | 37.0 | | | | 41 | | | | | | | | | | | | | | | | | | | | |
| HMP-5 | Evap. Bldg. 242-H | 27.5 | 294.8 | FILL | F | | 20.2 | | | | | | | | | | | | | | | | | | | | | | | | | | |
| HMP-5 | Evap. Bldg. 242-H | 30.5 | 291.8 | FILL | F | | 23.1 | | | | | | | | | | | | | | | | | | | | | | | | | | |
| HMP-5 | Evap. Bldg. 242-H | 32.5 | 289.8 | FILL | F | | 19.5 | | | | | | | | | | | | | | | | | | | | | | | | | | |
| HMP-5 | Evap. Bldg. 242-H | 34.0 | 288.3 | FILL | F | | 21.3 | | | | | | | | | | | | | | | | | | | | | | | | | | |
| HMP-5 | Evap. Bldg. 242-H | 35.5 | 286.8 | FILL | F | | 23.1 | 68.0 | 45.0 | | | | 46 | | | | | | | | | | | | | | | | | | | | |
| HMP-5 | Evap. Bldg. 242-H | 37.0 | 285.3 | FILL | F | | 19.1 | | | | | | | | | | | | | | | | | | | | | | | | | | |
| HMP-5 | Evap. Bldg. 242-H | 38.5 | 283.8 | FILL | F | | 20.8 | | | | | | | | | | | | | | | | | | | | | | | | | | |
| HMP-5 | Evap. Bldg. 242-H | 39.5 | 282.8 | FILL | F | | 22.8 | | | | | | | | | | | | | | | | | | | | | | | | | | |
| HMP-6 | Evap. Bldg. 242-H | 2.0 | 319.9 | FILL | F | 109.7 | 20.6 | | | | | | | | | | | | | | | | | | | | | | | | | | |
| HMP-6 | Evap. Bldg. 242-H | 4.0 | 317.9 | FILL | F | 122.1 | 20.9 | | | | | | | | | | | | | | | | | | | | | | | | | | |
| HMP-6 | Evap. Bldg. 242-H | 6.0 | 315.9 | FILL | F | 128.2 | 16.1 | | | | | | | | | | | | | | | | | | | | | | | | | | |

Table 4.2-1(b) Summary of laboratory test results at HTF (Static p5/6).

| Map Name | Location | Sample Depth (feet) | Sample Elevation (feet) | Stratum | USCS | WD CALC PCF | MC | Atterberg Limits | | | | Sieve Analyses | | | | | | Sg | Consolidation Properties | | | | | | | Shear Strength (deviatoric stress) | | | | | | | | pH |
|---|---|---|---|---|---|---|---|---|---|---|---|---|---|---|---|---|---|---|---|---|---|---|---|---|---|---|---|---|---|---|---|---|---|---|
| | | | | | | | | LL (%) | PI (%) | LL200 (%) | PI200 (%) | > # 4 < # 200 | < # 200 | D10 (mm) | D30 (mm) | D50 (mm) | D60 (mm) | | eo | Sri (%) | MCI (%) | Po (tsf) | Pc (tsf) | OCR | Cc | Cr | PP (tsf) | UC (tsf) | UU (tsf) | CD (tsf) | CU (tsf) | S3 (tsf) | eO (%) | MCI (%) | |
| HMP-6 | Evap. Bldg. 242-H | 8.0 | 313.9 | FILL | F | 129.1 | 16.7 | 87.0 | 63.0 | | | | 61 | | | | | | | | | | | | | | | | | | | | | |
| HMP-6 | Evap. Bldg. 242-H | 10.0 | 311.9 | FILL | F | 130.0 | 16.9 | | | | | | | | | | | | | | | | | | | | | | | | | | | |
| HMP-6 | Evap. Bldg. 242-H | 12.0 | 309.9 | FILL | F | 128.0 | 19.4 | | | | | | | | | | | | | | | | | | | | | | | | | | | |
| HMP-6 | Evap. Bldg. 242-H | 14.0 | 307.9 | FILL | F | 129.9 | 18.4 | | | | | | | | | | | | | | | | | | | | | | | | | | | |
| HMP-6 | Evap. Bldg. 242-H | 16.0 | 305.9 | FILL | F | 123.3 | 22.3 | 103.0 | 72.0 | | | | 31 | | | | | | | | | | | | | | | | | | | | | |
| HMP-6 | Evap. Bldg. 242-H | 17.5 | 304.4 | FILL | F | 127.1 | 18.8 | | | | | | | | | | | | | | | | | | | | | | | | | | | |
| HMP-6 | Evap. Bldg. 242-H | 19.0 | 302.9 | FILL | F | 130.2 | 20.6 | | | | | | | | | | | | | | | | | | | | | | | | | | | |
| HMP-6 | Evap. Bldg. 242-H | 20.5 | 301.4 | FILL | F | 131.8 | 16.3 | | | | | | | | | | | | | | | | | | | | | | | | | | | |
| HMP-6 | Evap. Bldg. 242-H | 22.0 | 299.9 | FILL | F | 131.8 | 15.1 | | | | | | | | | | | | | | | | | | | | | | | | | | | |
| HMP-6 | Evap. Bldg. 242-H | 23.5 | 298.4 | FILL | F | 112.5 | 19.1 | | | | | | | | | | | | | | | | | | | | | | | | | | | |
| HMP-6 | Evap. Bldg. 242-H | 25.0 | 296.9 | FILL | F | 131.3 | 16.9 | 72.0 | 49.0 | | | | 45 | | | | | | | | | | | | | | | | | | | | | |
| HMP-6 | Evap. Bldg. 242-H | 26.5 | 295.4 | FILL | F | 128.4 | 19.1 | | | | | | | | | | | | | | | | | | | | | | | | | | | |
| HMP-6 | Evap. Bldg. 242-H | 28.0 | 293.9 | FILL | F | 137.4 | 15.5 | | | | | | | | | | | | | | | | | | | | | | | | | | | |
| HMP-6 | Evap. Bldg. 242-H | 29.5 | 292.4 | FILL | F | 139.1 | 15.9 | | | | | | | | | | | | | | | | | | | | | | | | | | | |
| HMP-6 | Evap. Bldg. 242-H | 31.0 | 290.9 | FILL | F | 136.0 | 14.5 | | | | | | | | | | | | | | | | | | | | | | | | | | | |
| HMP-6 | Evap. Bldg. 242-H | 32.5 | 289.4 | FILL | F | 133.5 | 19.0 | | | | | | | | | | | | | | | | | | | | | | | | | | | |
| HMP-6 | Evap. Bldg. 242-H | 34.0 | 287.9 | FILL | F | 133.4 | 19.3 | | | | | | | | | | | | | | | | | | | | | | | | | | | |
| HMP-6 | Evap. Bldg. 242-H | 35.5 | 286.4 | FILL | F | 133.7 | 19.8 | 69.0 | 41.0 | | | | | | | | | | | | | | | | | | | | | | | | | |
| HMP-6 | Evap. Bldg. 242-H | 37.0 | 284.9 | FILL | F | 137.7 | 16.5 | | | | | | | | | | | | | | | | | | | | | | | | | | | |
| HMP-6 | Evap. Bldg. 242-H | 38.5 | 283.4 | FILL | F | 136.1 | 19.5 | | | | | | | | | | | | | | | | | | | | | | | | | | | |
| HMP-6 | Evap. Bldg. 242-H | 40.0 | 281.9 | FILL | F | 133.7 | 18.1 | | | | | | | | | | | | | | | | | | | | | | | | | | | |
| HMP-7A | Evap. Bldg. 242-H | | | FILL | F/SC | | | 70.0 | 51.0 | | | | 36 | | | 0.200 | 0.300 | | | | | | | | | | | | | | | | | |
| | Evap. Bldg. 242-H | 1.5 | | FILL | SM | | | | | 47.0 | 27.0 | | 35 | | 0.010 | 0.270 | 0.390 | | | | | | | | | | | | | | | | | |
| | Evap. Bldg. 242-H | 1.5 | | FILL | SM | | | 32.0 | 16.0 | | | | | | | | | | | | | | | | | | | | | | | | | |
| | Evap. Bldg. 242-H | 2.0 | | FILL | SM | 118.8 | 21.0 | | | | | | | | | | | | | | | | | | 0.19 | | | | | | | | | |
| | Evap. Bldg. 242-H | 4.0 | | FILL | SC | 123.2 | 18.4 | | | | | | | | | | | | | | | | | | 0.14 | | | | | | | | | |

Table 4.2-1(b) Summary of laboratory test results at HTF (Static p6/6).

| SAMPLE IDENTIFICATION | | | | | CLASSIFICATION PROPERTIES | | | | | | | | | | | | | | | | | | |
|---|---|---|---|---|---|---|---|---|---|---|---|---|---|---|---|---|---|---|---|---|---|---|---|
| | | | | | | Gradation | | | Atterberg Limits | | | | | | | Effective | Effective | | | | | | |
| Source/Date | Boring No | Sample No | Top Depth (ft) | Top Elevation (ft) | USCS Group Symbol | Sand (%) | Silt (%) | Clay (%<0 005mm) | Liquid Limit (%) | Plasticity Index (%) | Dry Density (pcf) | Water Content (%) | Initial Void Ratio | Specific Gravity | Precon. Stress (ksf) | Overburden Stress (ksf) | Overcon. Ratio OCR | Comp. Index Cc | Comp. Ratio Cc/(1+e) | Recomp Index Cr | Recomp Ratio Cr/(1+e) | Coef of Consol Cv (ft^2/day) | Quality If Poor |
| **FILL** | | | | | | | | | | | | | | | | | | | | | | | |
| LAW 9/93 | H-BOR-29 | ST 3 | 21 2 | 307 4 | SC | 67 | 5 | 28 | 73 | 42 | 97 | 20 5 | 0 7119 | 2 66 | 5 1 | 2 4 | 2 1 | 0 22 | 0 129 | 0 01 | 0 006 | 2 00 | |
| LAW 9/93 | H BOR-29 | ST 6 | 35 4 | 293 2 | SC | 72 | 6 | 22 | 57 | 37 | 89 8 | 16 9 | 0 8492 | 2 66 | 3 0 | 4 2 | 0 7 | 0 22 | 0 119 | 0 03 | 0 016 | 1 85 | |
| LAW 9/93 | H-BOR-2 | ST 2 | 39 8 | 290 3 | SC | 55 | 11 | 34 | 57 | 29 | 106 8 | 19 1 | 0 567 | 2 63 | 7 5 | 4 7 | 1 6 | 0 11 | 0 070 | 0 01 | 0 006 | 4 50 | |
| **TOBACCO ROAD - TR1** | | | | | | | | | | | | | | | | | | | | | | | |
| LAW 9/93 | H-BOR-12 | ST 2 | 13 0 | 287 0 | SC | 70 | 3 | 27 | 86 | 54 | 95 3 | 20 2 | 0 749 | 2 67 | 8 4 | 1 6 | 5 4 | 0 24 | 0 137 | 0 01 | 0 006 | 2 20 | Poor |
| LAW 9/93 | H-BOR-2 | ST 3 | 51 9 | 278 1 | SC | 52 | 11 | 37 | 60 | 35 | 102 1 | 20 2 | 0 6203 | 2 65 | 10 0 | 6 1 | 1 6 | 0 17 | 0 105 | 0 02 | 0 012 | 1 40 | |
| LAW 9/93 | H-BOR-12 | PS 2 | 28 5 | 271 5 | SC | 64 | 8 | 28 | 91 | 61 | 94 1 | 26 6 | 0 7912 | 2 70 | 7 5 | 3 1 | 2 4 | 0 25 | 0 140 | 0 02 | 0 011 | 2 30 | |
| LAW 9/93 | H-BOR-29 | PS 4 | 65 5 | 263 1 | CH | 4 | 16 | 80 | 92 | 58 | 89 3 | 31 5 | 0 8665 | 2 67 | 17 0 | 7 1 | 2 4 | 0 27 | 0 145 | 0 03 | 0 016 | 1 50 | |
| MRW&J 9/76 | 27U | 15U | 52 0 | 249 1 | CH | | | | 98 | 59 | 80 | 37 3 | 1 137 | 2 75 | 20 6 | 4 8 | 4 3 | 0 51 | 0 239 | 0 13 | 0 061 | 0 20 | |
| **TOBACCO ROAD - TR2** | | | | | | | | | | | | | | | | | | | | | | | |
| MRW&J 9/76 | 22U | 9U | 32 5 | 269 4 | MH | | | | 68 | 33 | 85 | 27 2 | 0 983 | 2 70 | 20 4 | 3 6 | 5 7 | 0 31 | 0 156 | 0 08 | 0 040 | 0 07 | |
| LAW 9/93 | H-BOR-12 | ST 5 | 44 5 | 255 5 | SP-SC | 82 | 9 | 9 | | | 93 8 | 28 2 | 0 7703 | 2 66 | 8 5 | 4 1 | 2 1 | 0 10 | 0 056 | 0 02 | 0 011 | 1 00 | Poor |
| **TOBACCO ROAD - TR3/TR4** | | | | | | | | | | | | | | | | | | | | | | | |
| MRW&J 9/76 | 40U | 13U | 59 0 | 241 3 | SC | | | | 33 | 13 | 104 | 20 2 | 0 640 | 2 73 | 15 6 | 5 4 | 2 9 | 0 20 | 0 122 | 0 04 | 0 024 | 1 69 | |
| LAW 9/93 | H BOR-12 | PS 3 | 62 8 | 237 3 | SC | 77 | 5 | 18 | 44 | 19 | 105 9 | 19 7 | 0 592 | 2 63 | 10 0 | 5 3 | 1 9 | 0 09 | 0 057 | 0 01 | 0 006 | 3 40 | |
| LAW 9/93 | H-BOR-29 | PS 9 | 95 8 | 232 8 | SC | 78 | 5 | 17 | 53 | 27 | 93 5 | 28 | 0 796 | 2 69 | 8 0 | 9 0 | 0 9 | 0 21 | 0 117 | 0 03 | 0 017 | 1 80 | |
| **DRY BRANCH - DB1/DB3** | | | | | | | | | | | | | | | | | | | | | | | |
| LAW 9/93 | HBOR23 3 | ST 1 | 50 0 | 245 2 | SC | 79 | 3 | 18 | 44 | 23 | 98 2 | 25 7 | 0 6981 | 2 67 | 2 0 | 4 2 | 0 5 | 0 12 | 0 072 | 0 01 | 0 007 | 0 40 | Poor |
| LAW 9/93 | HBOR23 3 | ST 2 | 65 0 | 230 2 | SC | 90 | 0 | 10 | 34 | 13 | 95 6 | 25 4 | 0 7509 | 2 68 | 2 2 | 5 1 | 0 4 | 0 16 | 0 089 | 0 01 | 0 005 | 0 45 | Poor |
| MRW&J 9/76 | 43U | 9U | 116 5 | 183 4 | SC | | | | 64 | 18 | 78 | 44 6 | 1 162 | 2 71 | 23 4 | 9 2 | 2 5 | 0 57 | 0 264 | 0 09 | 0 040 | 0 13 | |
| LAW 9/93 | H-BOR-23 | ST 6 | 65 0 | 231 6 | SP-SC | 94 | 0 | 6 | 112 | 73 | 98 4 | 24 8 | 0 6749 | 2 64 | 9 0 | 5 4 | 1 7 | 0 08 | 0 048 | 0 01 | 0 006 | 3 50 | |
| LAW 9/93 | H-BOR-2 | ST 5 | 120 0 | 210 0 | SP-SM | 87 | 1 | 12 | | | 100 | 24 1 | 0 6793 | 2 72 | 6 0 | 10 5 | 0 6 | 0 10 | 0 060 | 0 01 | 0 006 | 3 10 | Poor |
| **DRY BRANCH - DB4** | | | | | | | | | | | | | | | | | | | | | | | |
| LAW 9/93 | H-BOR-29 | PS 10 | 141 1 | 187 5 | SC | 87 | 2 | 11 | 46 | 21 | 99 5 | 25 | 0 7128 | 2 73 | 6 0 | 11 7 | 0 5 | 0 18 | 0 105 | 0 01 | 0 006 | 0 85 | |
| LAW 9/93 | H-BOR-2 | PS 8 | 145 1 | 184 9 | CH | 79 | 1 | 20 | 139 | 26 | 84 9 | 23 1 | 0 9926 | 2 71 | 8 0 | 12 0 | 0 7 | 0 24 | 0 120 | 0 04 | 0 020 | 0 60 | Poor |
| LAW 9/93 | H-BOR-12 | PS10 | 129 1 | 170 9 | CH | 18 | 8 | 74 | 155 | 125 | 57 9 | 66 1 | 1 9219 | 2 67 | 9 8 | 9 2 | 1 1 | 0 75 | 0 257 | 0 16 | 0 055 | 0 10 | |
| **DRY BRANCH - DB4/DB5** | | | | | | | | | | | | | | | | | | | | | | | |
| MRW&J 9/76 | 30U | 27U | 112 3 | 186 0 | SC | | | | 64 | 25 | 69 | 51 0 | 1 529 | 2 78 | 7 8 | 9 0 | 0 9 | 0 64 | 0 253 | 0 14 | 0 055 | 1 00 | |
| MRW&J 9/76 | 33U | 8U | 113 0 | 184 8 | CH | | | | 96 | 64 | 55 | 69 0 | 2 110 | 2 72 | 11 6 | 8 6 | 1 3 | 1 30 | 0 418 | 0 21 | 0 068 | 0 17 | |
| MRW&J 9/76 | 35U | 9U | 118 3 | 181 8 | CH | | | | 80 | 52 | 73 | 44 4 | 1 329 | 2 74 | 9 4 | 9 2 | 1 0 | 0 59 | 0 253 | 0 09 | 0 039 | 0 34 | |
| MRW&J 9/76 | 40U | 29U | 121 0 | 179 3 | CH | | | | 120 | 91 | 60 | 62 2 | 1 997 | 2 86 | 10 0 | 9 4 | 1 1 | 1 08 | 0 360 | 0 26 | 0 087 | 0 02 | |
| MRW&J 9/76 | 35U | 11U | 122 3 | 177 8 | CH | | | | 125 | 99 | 56 | 77 9 | 1 976 | 2 69 | 6 6 | 9 4 | 0 7 | 1 48 | 0 497 | 0 23 | 0 077 | 0 01 | |
| MRW&J 9/76 | 33U | 12U | 120 3 | 177 5 | SC | | | | 52 | 32 | 66 | 38 6 | 1 545 | 2 71 | 4 6 | 9 0 | 0 5 | 0 62 | 0 244 | 0 08 | 0 031 | 0 74 | |
| MRW&J 9/76 | 30U | 29U | 121 6 | 176 7 | CH | | | | 141 | 107 | 46 | 107 5 | 2 714 | 2 74 | 6 8 | 9 6 | 0 7 | 1 87 | 0 504 | 0 28 | 0 075 | 0 02 | |
| MRW&J 9/76 | 35U | 13U | 126 3 | 173 8 | CH | | | | 121 | 93 | 61 | 65 9 | 1 856 | 2 78 | 10 8 | 9 6 | 1 1 | 1 30 | 0 455 | 0 20 | 0 070 | 0 06 | |
| MRW&J 9/76 | 35U | 15U | 130 3 | 169 6 | CH | | | | 59 | 37 | 81 | 34 3 | 1 054 | 2 68 | 10 4 | 9 6 | 1 1 | 0 47 | 0 229 | 0 09 | 0 044 | 0 62 | |
| MRW&J 9/76 | 27U | 33U | 135 3 | 165 8 | MH | | | | 114 | 64 | 67 | 54 1 | 1 447 | 2 61 | 25 0 | 10 0 | 2 5 | 1 00 | 0 409 | 0 26 | 0 106 | 0 33 | |
| MRW&J 9/76 | 35U | 17U | 134 3 | 165 8 | CH | | | | 153 | 118 | 53 | 82 2 | 2 349 | 2 82 | 9 4 | 9 8 | 1 0 | 1 80 | 0 537 | 0 32 | 0 096 | 0 03 | |
| **DRY BRANCH - DB5** | | | | | | | | | | | | | | | | | | | | | | | |
| LAW 9/93 | H-BOR-23 | PS 5 | 95 7 | 200 9 | SC | 55 | 18 | 27 | 66 | 50 | 74 | 35 5 | 1 261 | 2 68 | 10 0 | 7 3 | 1 4 | 0 60 | 0 265 | 0 04 | 0 018 | 2 60 | |
| LAW 9/93 | H-BOR-29 | PS 12 | 150 4 | 178 2 | SC | | | | 112 | 91 | 47 2 | 92 8 | 2 571 | 2 70 | 14 0 | 12 2 | 1 1 | 1 92 | 0 538 | 0 25 | 0 070 | 0 25 | |
| LAW 9/93 | HBOR23 1 | PS 2 | 97 3 | 203 3 | SC | 56 | 14 | 30 | 80 | 18 | 84 4 | 32 1 | 1 004 | 2 61 | 19 0 | 7 2 | 2 6 | 0 45 | 0 225 | 0 03 | 0 015 | 2 80 | |
| **SANTEE** | | | | | | | | | | | | | | | | | | | | | | | |
| LAW 9/93 | H-BOR-50 | ST 5 | 155 0 | 171 1 | SC | 54 | 9 | 37 | 52 | 34 | 73 8 | 47 7 | 1 285 | 2 70 | 0 7 | 12 4 | 0 1 | 0 47 | 0 206 | 0 01 | 0 002 | 0 03 | Poor |
| MRW&J 9/76 | 35U | 19U | 137 8 | 162 3 | SC | | | | 124 | 95 | 88 | 30 7 | 0 922 | 2 72 | 11 8 | 10 0 | 1 2 | 0 28 | 0 146 | 0 04 | 0 021 | 1 00 | |
| MRW&J 9/76 | 35U | 21U | 142 0 | 158 1 | SC | | | | 75 | 54 | 89 | 32 3 | 0 865 | 2 67 | 11 8 | 10 2 | 1 2 | 0 26 | 0 139 | 0 04 | 0 021 | 0 64 | |
| MRW&J 9/76 | 30U | 34U | 140 6 | 157 7 | CH | | | | 147 | 116 | 50 | 94 9 | 2 444 | 2 78 | 9 2 | 10 4 | 0 9 | 1 51 | 0 438 | 0 31 | 0 090 | 0 01 | |
| LAW 9/93 | H-BOR-23 | PB 4 | 119 3 | 177 3 | SC | 78 | 10 | 12 | | | 81 5 | 35 8 | 1 030 | 2 65 | 6 0 | 8 6 | 0 7 | 0 37 | 0 182 | 0 04 | 0 020 | 1 80 | |
| LAW 9/93 | H-BOR-2 | PS 12 | 174 5 | 155 5 | SC | 74 | 8 | 18 | 43 | 19 | 89 6 | 29 3 | 0 853 | 2 66 | 15 0 | 13 7 | 1 1 | 0 20 | 0 108 | 0 01 | 0 005 | 2 00 | |
| LAW 9/93 | H-BOR-29 | ST 22 | 178 9 | 149 7 | SC | 85 | 3 | 12 | 39 | 18 | 91 | 29 1 | 0 845 | 2 69 | 7 5 | 13 9 | 0 5 | 0 23 | 0 125 | 0 04 | 0 022 | 0 90 | Poor |
| LAW 9/93 | H-BOR-12 | ST 16 | 151 5 | 148 5 | SC | 70 | 3 | 27 | 43 | 23 | 95 4 | 26 7 | 0 734 | 2 66 | 11 0 | 10 6 | 1 0 | 0 13 | 0 075 | 0 01 | 0 006 | 2 50 | |
| LAW 9/93 | H-BOR-23 | PB 11 | 158 9 | 137 7 | SM | 68 | 17 | 15 | | | 66 1 | 51 6 | 1 418 | 2 56 | 17 0 | 11 0 | 1 5 | 0 46 | 0 190 | 0 03 | 0 012 | 0 90 | |
| LAW 9/93 | H-BOR-2 | ST 13 | 193 0 | 137 0 | SC | 80 | 8 | 12 | 37 | 13 | 96 6 | 26 2 | 0 732 | 2 68 | 25 0 | 14 9 | 1 7 | 0 15 | 0 087 | 0 01 | 0 006 | 3 00 | |
| LAW 9/93 | H-BOR-29 | ST 24 | 198 7 | 129 9 | SM | 61 | 20 | 19 | 89 | 64 | 89 9 | 32 3 | 0 868 | 2 69 | 6 0 | 15 1 | 0 4 | 0 15 | 0 080 | 0 02 | 0 011 | 0 35 | Poor |
| LAW 9/93 | H-BOR-12 | ST 19 | 173 2 | 126 8 | SC | 84 | 3 | 13 | 32 | 9 | 97 9 | 25 9 | 0 728 | 2 71 | 8 5 | 11 8 | 0 7 | 0 09 | 0 052 | 0 01 | 0 006 | 0 65 | Poor |
| LAW 9/93 | H-BOR-12 | ST 20 | 179 3 | 120 8 | SC | 75 | 5 | 20 | 32 | 13 | 90 6 | 31 2 | 0 826 | 2 65 | 1 2 | 12 2 | 0 1 | 0 19 | 0 104 | 0 02 | 0 011 | 0 80 | Poor |
| LAW 9/93 | H-BOR-23 | PB 14 | 176 2 | 120 4 | CL | 48 | 31 | 21 | 47 | 23 | 85 8 | 33 8 | 0 928 | 2 65 | 28 0 | 12 0 | 2 3 | 0 29 | 0 160 | 0 01 | 0 005 | 0 50 | |

Table 4.2-2 Summary of consolidation parameters.

| Boring No. | Sample No. | Top Depth (ft) | Top Elev. (ft) | Dynamic Tests (per Sample) | | | | |
|---|---|---|---|---|---|---|---|---|
| | | | | Stress Control Liquefaction | Stress Control Low-Strain | Strain Control | Volumetric Strain | Resonant Column |
| **STRUCTURAL FILL** | | | | | | | | |
| HBOR29 | ST2 | 15 | 313.4 | | | | | 1 |
| H-BOR-29 | ST 4 | 25 | 303.6 | | | 1 | | 1 |
| **TOBACCO ROAD - TR1** | | | | | | | | |
| H-BOR-29 | PS 2 | 53.7 | 274.9 | 1 | | | 1 | |
| **TOBACCO ROAD - TR2** | | | | | | | | |
| HBOR23.1 | PS1 | 28.9 | 271.7 | | 1 | | | |
| **TOBACCO ROAD - TR3/TR4** | | | | | | | | |
| H-BOR-23 | PS 1 | 28.7 | 267.9 | | | 1 | | 1 |
| H-BOR-23 | PS 2 | 33.3 | 263.3 | 3 | | | 1 | |
| H-BOR-23 | PS 3 | 40.2 | 256.4 | 3 | | | 3 | |
| H-BOR-2 | PS 4 | 91.2 | 238.8 | 2 | | | 2 | |
| H-BOR-29 | PS-7 | 91.1 | 237.5 | | 3 | | 2 | |
| H-BOR-2 | PS 5 | 94.1 | 235.9 | 3 | | | 3 | |
| H-BOR-2 | PS 6 | 97 | 233 | 3 | | | 3 | |
| H-BOR-12 | PS 5 | 70.8 | 229.2 | 3 | | | 3 | |
| H-BOR-12 | ST 8 | 80 | 220 | | | 1 | | 1 |
| **DRY BRANCH - DB1/DB3** | | | | | | | | |
| H-BOR-23 | ST 4 | 55 | 241.6 | | | 1 | | 1 |
| H-BOR-2 | ST 5 | 120 | 210 | | | 1 | | |
| H-BOR-12 | PS 7 | 92.8 | 207.2 | 3 | | | 3 | |
| **DRY BRANCH - DB4** | | | | | | | | |
| H-BOR-23 | PS 4 | 83.8 | 212.8 | 3 | | | 3 | |
| HBOR29 | PS10 | 140 | 188.5 | | | | | 1 |
| H-BOR-2 | PS 8 | 144.9 | 185.1 | | | 1 | | |
| **DRY BRANCH - DB5** | | | | | | | | |
| H-BOR-29 | PS 12 | 150.1 | 178.5 | | | 1 | | 1 |
| **SANTEE** | | | | | | | | |
| H-BOR-2 | PS-11 | 170.4 | 159.6 | | 1 | | | |
| H-BOR-12 | ST 15 | 143 | 157 | | | 1 | | 1 |
| H-BOR-2 | PS13 | 175.0 | 154.9 | | 3 | | | |
| H-BOR-2 | PS14 | 178.0 | 152 | | 3 | | 3 | |
| H-BOR-29 | ST 24 | 197.1 | 131.5 | | | 1 | | 1 |
| | | | **TOTAL** | 24 | 11 | 9 | 27 | 9 |

Table 4.2-3 Summary of cyclic triaxial tests performed at ITP.

| Boring | Elev., MSL (ft) | SPT N-Value (bpf) | Lab* Sample Elev., MSL (ft) | Lab Sample Number | PI (%) | LL (%) | Soil Classi-fication |
|---|---|---|---|---|---|---|---|
| 12H30 | 188.3 | 0 | 186.0 | 27U | 24.7 | 64.0 | SC |
| 12H30 | 173.3 | 0 | 177.1 | 29U | 106.7 | 140.5 | CH |
| 12H30** | 173.3 | 0 | 177.1 | 29U | 95.3 | 143.9 | |
| 12H30 | 163.3 | 4 | 157.0 | 34U | 115.9 | 146.7 | SC |
| 12H30** | 163.3 | 4 | 157.0 | 34U | 118.8 | 181.0 | |
| 12H31 | 178.5 | 4 | 180.5 | 13U | 61.3 | 84.4 | CH |
| 12H31 | 174.5 | 0 | 176.5 | 15U | 77.8 | 100.4 | CH |
| 12H31 | 170.5 | 2 | 168.5 | 19U | 55.8 | 77.6 | CH |
| 12H31** | 170.5 | 2 | 168.5 | 19U | 103.3 | 128.8 | SC |
| 12H33 | 183.8 | 0 | 184.5 | 8U | 64.4 | 96.4 | CH |
| 12H33 | 175.8 | 0 | 176.8 | 12U | 32.0 | 52.2 | SC |
| 12H35 | 184.1 | 0 | 182.1 | 9U | 52.1 | 79.7 | CH |
| 12H35 | 180.1 | 0 | 178.1 | 11U | 99.2 | 125.0 | CH |
| 12H35 | 176.1 | 0 | 174.1 | 13U | 92.3 | 120.6 | CH |
| 12H35 | 172.1 | 0 | 170.1 | 15U | 37.0 | 59.1 | CH |
| 12H35 | 168.1 | 0 | 166.1 | 17U | 118.2 | 153.4 | CH |
| 12H35 | 164.1 | 0 | 162.1 | 19U | 95.0 | 124.3 | SC |
| 12H37 | 179.8 | 0 | 177.8 | 12U | 69.7 | 93.8 | CH |
| 12H37 | 175.8 | 0 | 173.8 | 14U | 98.8 | 134.0 | CH |
| 12H37 | 171.8 | 0 | 169.8 | 16U | 56.0 | 76.8 | SC |
| 12H44*** | 176.0 | 3 | 177.0 | 11D | 118 | 136 | CH |

* Lab sample = undisturbed sample taken in the interval just above or just below where the split spoon sample was taken.
** Two sets of Atterberg limits were performed on the same sample.
*** Values taken from plot on plate #2 of Mueser et al. (1978).

Table 5.2-1 SPT-N, Atterberg limits, and soil classification for soft zones in the DB4/DB5 layer at the 1977 proposed location of Tank 51 (select data from Mueser et. al., 1977).

| Borehole | Elev(ft) | $e_o$ | OCR | $C_c$ | $C_r$ | LL (%) | PI (%) | Class. |
|---|---|---|---|---|---|---|---|---|
| HBOR23.1 | 203.3 | 1 | 2.6 | 0.45 | 0.03 | 80 | 18 | SC |
| 12H-30U | 186.0 | 1.529 | 0.9 | 0.64 | 0.14 | 64 | 25 | SC |
| 12H-30U | 176.7 | 2.714 | 0.7 | 1.87 | 0.28 | 141 | 107 | CH |
| 12H-33U | 184.8 | 2.110 | 1.3 | 1.30 | 0.21 | 96 | 64 | SC |
| 12H-33U | 177.5 | 1.545 | 0.5 | 0.62 | 0.08 | 52 | 32 | CH |
| 12H-35U | 177.8 | 1.976 | 0.7 | 1.48 | 0.23 | 125 | 99 | CH |
| 12H-35U | 173.8 | 1.856 | 1.1 | 1.30 | 0.20 | 121 | 93 | CH |
| 12H-35U | 169.6 | 1.054 | 1.1 | 0.47 | 0.09 | 59 | 37 | CH |
| 12H-35U | 165.8 | 2.349 | 1.0 | 1.80 | 0.32 | 153 | 118 | CH |
| AVERAGE | ----- | 1.793 | 1.10 | 1.103 | 0.176 | 99 | 66 | -- |

In selecting the data that met the soft zone criteria, CPT tip stresses in adjacent CPT soundings were average through a two-foot interval, starting 6 inches above the sampling elevation. For the Mueser et al. (1977) data, SPT N values were reviewed for the intervals just above and below the interval where the undisturbed sample was taken. Only those data having N ≤ 5 in the above and below intervals are tabulated.

Table 5.2-2 Consolidation properties and Atterberg limits for soft zones within the DB4/DB5 layer at the 1977 proposed location of Tank 51 (select data from Mueser et. al., 1977).

| Boring | Northing (ft) | Easting (ft) | Thickness (ft) | Notes: |
|---|---|---|---|---|
| H-CPT-1 | 70844 | 62532 | 8 | 114 CPT readings @ 0.069 feet per reading in Santee Formation |
| H-CPT-5 | 70797 | 62667 | 4 | 4 ft @ elev 129 to 133 |
| H-CPT-7 | 71030 | 62613 | 1 | 1 ft @ elev 145 |
| H-CPT-11 | 70885 | 62768 | 0 | no unusual conditions to elev 128 |
| H-CPT-14 | 70936 | 62375 | 0 | no unusual conditions to elev 137 |
| H-CPT-18 | 70601 | 62658 | 0 | no unusual conditions to elev 130 |
| H-CPT-23 | 70971 | 63017 | 13 | 13 ft @ elev 176 to 189 |
| H-CPT-25 | 71197 | 62998 | 6 | 6 ft @ elev 146 to 152 |
| H-CPT-26 | 70764 | 62805 | 12 | 2 ft @ elev 174 to 176 (DB5); 10 ft @ elev 164 to 174 ( - |
| H-CPT-28 | 70612 | 62898 | 6 | 5 ft @ elev 168 to 174: 1 ft @ elev 165 to 166 |
| H-CPT-29 | 71113 | 62681 | 0 | no unusual conditions to elev 135 |
| H-CPT-30 | 70989 | 62805 | 0 | no unusual conditions to elev 123 |
| H-SPT-14 | 70941 | 62384 | 1 | adjacent H-BOR-13 has 6 inch WR @ elevs 102 and 155 |
| H-SPT-18 | 70601 | 62667 | 4.5 | 4.5 ft @ elev 146 to 150.5 |
| H-SPT-20 | 70854 | 63058 | 0 | no unusual conditions to elev 110 |
| 12H16 | 71185 | 62535 | 0 | no unusual conditions |
| 12H20 | 70976 | 62498 | 1 | 12 inch WR @ depth 139 |
| 12H21 | 70967 | 62636 | 1 | N = 5 @ depth 164 |
| 12H22 | 70956 | 62730 | 0 | no unusual conditions to depth 194 |
| 12H23 | 70956 | 62850 | 10 | N = 5 @ depth 140; N = 3 @ depth 155 |
| 12H27 | 70945 | 62793 | 10 | 4 WRs from depth 150 to 160 |
| 12H30 | 70956 | 62900 | 15 | 2 WRs from depth 145 to 160 |
| 12H31 | 71006 | 62850 | 15 | low N at depth 140, 145, and 155 to 160 |
| 12H32 | 70906 | 62850 | 0 | no unusual conditions to depth 166.5 |
| 12H33 | 71006 | 62900 | 4.5 | WR from depth 122 to 1126.5 |

Table 5.2-3 Thickness of soft zones in the Santee formation at ITP.

| DESCRIPTION | FILL | TR1 | TR2 | TR3/TR4 | DB1/DB3 | DB4 | DB5 | ST |
|---|---|---|---|---|---|---|---|---|
| | AVG | AVG | AVG | AVG | AVG | AVG | AVG | AVG |
| SPT N-VALUE | 25 | 27 | 31 | 15 | 32 | 17 | 20 | 58 |
| SHEAR WAVE VELOCITY, ft/s | 1059 | 1187 | 1226 | 1193 | 1128 | 978 | 1055 | 1251 |
| CONE TIP RESISTANCE, Qc, tsf | 48 | 57 | 168 | 52 | 174 | 48 | 50 | 111 |
| FRICTION RATIO | 8 | 5 | 1 | 3 | 1 | 2 | 2 | 1 |
| Qc/N | 1.9 | 2.1 | 5.4 | 3.5 | 5.4 | 2.8 | 2.5 | 1.9 |
| PERCENT FINES (<.074mm) | 40 | 38 | 17 | 23 | 11 | 34 | 45 | 25 |
| PERCENT SILT | 8 | 16 | 7 | 9 | 3 | 10 | 13 | 12 |
| PERCENT CLAY (<.002mm) | 32 | 22 | 10 | 14 | 8 | 24 | 32 | 13 |
| PLASTICITY INDEX, % | 34 | 47 | 18 | 25 | 23 | 67 | 47 | 31 |
| LIQUID LIMIT, % | 58 | 76 | 37 | 45 | 45 | 90 | 70 | 55 |
| PLASTICITY INDEX (-200 MATERIAL), % | 57 | 79 | 47 | 101 | 110 | 140 | 88 | 78 |
| LIQUID LIMIT (-200 MATERIAL), % | 96 | 120 | 84 | 144 | 148 | 179 | 131 | 112 |
| DRY DENSITY, pcf | 104 | 99 | 104 | 102 | 98 | 85 | 72 | 88 |
| WATER CONTENT, % | 19 | 22 | 22 | 22 | 25 | 39 | 47 | 32 |
| WET DENSITY, pcf | 124 | 121 | 126 | 125 | 122 | 114 | 105 | 116 |
| SPECIFIC GRAVITY | 2.67 | 2.68 | 2.66 | 2.68 | 2.69 | 2.68 | 2.65 | 2.67 |
| VOID RATIO | 0.609 | 0.684 | 0.629 | 0.625 | 0.719 | 1.103 | 1.523 | 0.876 |
| AT-REST LAT. EARTH PRESS. COEFF | 0.40 | 0.44 | 0.52 | 0.46 | 0.44 | 0.78 | 0.52 | 0.44 |
| OVERCONSOLIDATION RATIO | 1.48 | 3.02 | 4.29 | 1.89 | 2.10 | 0.95 | 1.26 | 1.26 |
| COMPRESSION INDEX[1] | 0.18 (0.18) | 0.25 (0.23) | 0.51 (0.10) | 0.17 (0.15) | 0.33 (0.12) | 0.72 | 1.14 | 0.42 |
| RE-COMPRESSION INDEX[1] | 0.02 (0.02) | 0.04 (0.02) | 0.13 (0.02) | 0.03 (0.02) | 0.05 (0.01) | 0.13 | 0.19 | 0.06 |
| COEFF. OF CONSOLIDATION, ft2/day | 2.78 | 1.32 | 0.20 | 2.30 | 1.82 | 0.53 | 0.68 | 1.27 |
| TOTAL COHESION, ksf | 2.5 | 1.1 | 1.5 | 1.9 | - | - | - | - |
| TOTAL FRICTION ANGLE, deg | 0 | 16 | 23 | 13 | - | - | - | - |
| EFFECTIVE COHESION, ksf | 0 | 0 | 0 | 0 | 0 | 0 | 0 | 0 |
| EFFECTIVE FRICTION ANGLE, deg | 37 | 34 | 29 | 33 | 34 | 13 | 29 | 34 |
| DILATION ANGLE, deg | 1.6 | 1.7 | 1.7 | 1.7 | 3.8 | 3.8 | 3.8 | 1.3 |

1 Values reported are from consolidation test results. Settlement estimates used in analyses are based on empirical data (field measurements), indicated in parentheses.

Table 6.0-1(a) Average material properties at ITP.

| DESCRIPTION | FILL | UPLAND | TR3/TR4 | DB1/DB3 | DB4/DB5 | ST |
|---|---|---|---|---|---|---|
| | AVG | AVG | AVG | AVG | AVG | AVG |
| SPT N-VALUE | 25 | 28 | 22 | 32 | 30 | 53 |
| SHEAR WAVE VELOCITY, ft/s | 1044 | 1151 | 1153 | 1211 | 1020 | 1210 |
| CONE TIP RESISTANCE, Qc, tsf | 34 | 98 | 45 | 210 | 58 | 123 |
| FRICTION RATIO | 5 8 | 3.3 | 3 1 | 0.7 | 2.0 | 1 6 |
| Qc/N | 1 4 | 3.5 | 2.0 | 6.6 | 1.9 | 2.3 |
| PERCENT FINES (<.074mm) | 41 | 27 | 23 | 22 | 14 | 31 |
| PLASTICITY INDEX, % | 31 | 32 | 16 | 33 | 9 | - |
| LIQUID LIMIT, % | 54 | 60 | 41 | 61 | 27 | - |
| PLASTICITY INDEX (-200 MATERIAL), % | 15 | 28 | - | - | 51 | - |
| LIQUID LIMIT (-200 MATERIAL), % | 39 | 66 | - | - | 94 | - |
| DRY DENSITY, pcf | 109 | 106 | 100 | - | - | - |
| WATER CONTENT, % | 18 | 21 | 23 | 22 | 29 | 26 |
| WET DENSITY, pcf | 128 | 123 | 123 | - | - | - |
| SPECIFIC GRAVITY | 2.68 | 2.69 | 2.75 | - | 2.70 | - |
| VOID RATIO | 0.851 | 0.791 | 0.596 | - | 0 892 | - |
| OVERCONSOLIDATION RATIO | 7.20 | 4.90 | 2.80 | - | 1.60 | - |
| COMPRESSION INDEX | 0.19 | 0.29 | 0.21 | - | 0.28 | - |
| RE-COMPRESSION INDEX | 0.05 | 0.06 | 0.03 | - | 0 06 | - |
| TOTAL COHESION, ksf | 1.5 | 1.5 | - | - | - | - |

Table 6.0-1(b) Average material properties at HTF.

| Formation | Shear Strain % | G/Gmax | Damping Ratio % |
|---|---|---|---|
| NONFILL | 0.0001 | 1 | 2.1 |
| " | 0.0003 | 1 | 2.1 |
| " | 0.001 | 0.99 | 2.4 |
| " | 0.003 | 0.96 | 3.1 |
| " | 0.01 | 0.84 | 5 |
| " | 0.03 | 0.68 | 7.2 |
| " | 0.1 | 0.375 | 15 |
| " | 0.3 | 0.22 | 20.6 |
| " | 1 | 0.091 | 24.4 |
| FILL | 0.0001 | 1 | 2.1 |
| " | 0.0003 | 1 | 2.1 |
| " | 0.001 | 0.97 | 2.9 |
| " | 0.002 | 0.95 | 4 |
| " | 0.003 | 0.91 | 5 |
| " | 0.01 | 0.73 | 8.06 |
| " | 0.03 | 0.54 | 12.3 |
| " | 0.1 | 0.345 | 16.47 |
| " | 0.3 | 0.19 | 21.18 |
| " | 1 | 0.07 | 24.41 |

Table 6.1-1 Recommended damping ratio and modulus reduction relationships with cyclic shear strain.

| Boring No. | Sample No. | Specimen No. | Formation | Classification | Sigma 3c (ksf) | Cyclic Stress Ratio (Lab.) | Number of Cycles to Initial Liquefaction | K sigma | Stress Ratio (Norm.) | Cr | Stress Ratio (Field) | Fines (%) |
|---|---|---|---|---|---|---|---|---|---|---|---|---|
| B14 | PS10 | 2T | L.T.R. | SC | 6.3 | 0.210 | 9 | 0.89 | 0.236 | 0.64 | 0.151 | 16.8 |
| B14 | PS10 | 2B | L.T.R. | SM | 6.3 | 0.150 | 48 | 0.89 | 0.169 | 0.64 | 0.108 | 16.1 |
| B16 | PS8 | 3T | L.T.R. | SC | 6.3 | 0.200 | 6 | 0.89 | 0.225 | 0.64 | 0.144 | 19.1 |
| B16 | PS8 | 3B | L.T.R. | SM | 6.3 | 0.150 | 447 | 0.89 | 0.169 | 0.64 | 0.108 | 16.8 |
| B16 | PS10 | 4T | L.T.R. | SM | 6.3 | 0.177 | 21 | 0.89 | 0.199 | 0.64 | 0.127 | 18.3 |
| B16 | PS12 | 1T | L.T.R. | SP-SC | 6.3 | 0.210 | 2 | 0.89 | 0.236 | 0.64 | 0.151 | 7.6 |
| B16 | PS13 | 11T | L.T.R. | SC | 6.3 | 0.225 | 1 | 0.89 | 0.253 | 0.64 | 0.162 | 12.3 |
| B16 | PS13 | 11M | L.T.R. | SP-SM | 6.3 | 0.190 | 2 | 0.89 | 0.213 | 0.64 | 0.137 | 9.4 |
| B16 | PS13 | 11B | L.T.R. | SP-SM | 6.3 | 0.166 | 15 | 0.89 | 0.187 | 0.64 | 0.119 | 10.8 |
| B13B | PS2 | QCT | L.T.R. | SP-SM | 6.3 | 0.155 | 3 | 0.89 | 0.174 | 0.64 | 0.111 | 9.7 |
| B13B | PS2 | QCB | L.T.R. | SP-SM | 6.3 | 0.117 | 99 | 0.89 | 0.131 | 0.64 | 0.084 | 9.5 |
| B16 | PS4 | 8T | U.T.R. | SC | 4.2 | 0.210 | 257 | 0.94 | 0.223 | 0.64 | 0.143 | 32.6 |
| B16 | PS4 | 8M | U.T.R. | SC | 4.2 | 0.250 | 11 | 0.94 | 0.266 | 0.64 | 0.170 | 28.7 |
| B16 | PS4 | 8B | U.T.R. | SC | 4.2 | 0.220 | 16 | 0.94 | 0.234 | 0.64 | 0.150 | 24.8 |
| B16 | PS5 | 9T | U.T.R. | SC | 4.2 | 0.190 | 41 | 0.94 | 0.202 | 0.64 | 0.129 | 18.4 |
| B16 | PS5 | 9M | U.T.R. | SC | 4.2 | 0.240 | 7 | 0.94 | 0.255 | 0.64 | 0.163 | 20.8 |
| B16 | PS5 | 9B | U.T.R. | SC | 4.2 | 0.225 | 4 | 0.94 | 0.239 | 0.64 | 0.153 | 16.3 |

Table 6.2-1 Summary of results of cyclic shear test and index properties of RTF specimens.

| Description | RTF Soils | | | | ITP Soils | | | | |
|---|---|---|---|---|---|---|---|---|---|
| | Structural Fill | Upper Tobacco | Lower Tobacco | Upper Dry Branch | Fill | TR | TR2 | TR3/4 | DB1/3 |
| | | | | | | | | | |
| SPT N-value | 43 | 16 | 12 | 12 | 25 | 27 | 31 | 15 | 32 |
| Water Content, % | 14 | 22.1 | 27.0 | 27 | 19 | 22 | 22 | 22 | 25 |
| Wet Density, pcf | 125 | 122 | 122 | 122 | 124 | 121 | 126 | 125 | 122 |
| Liquid Limit, % | NP | 44 | 35 | 35 | 58 | 76 | 37 | 45 | 45 |
| Plasticity Index, % | NP | 20 | 10 | 10 | 34 | 47 | 18 | 25 | 23 |
| Fines, % | 10.7 | 25.4 | 17 | 17 | 40 | 38 | 17 | 23 | 11 |
| Cohesion, ksf | 0 | 0 | 0 | 0 | 2.5 | 1.1 | 1.5 | 1.9 | --- |
| Friction Angle, deg. | 46.5 | 33.5 | 33.5 | 33.5 | 0 | 16 | 23 | 13 | --- |
| Eff. Cohesion, ksf | 0 | 0 | 0 | 0 | 0 | 0 | 0 | 0 | 0 |
| Eff. Friction Angle, deg. | 38.5 | 33.5 | 33.5 | 33.5 | 37 | 34 | 29 | 33 | 34 |
| Compression Index | 0.051 | 0.24 | 0.183 | 0.183 | 0.18 | 0.23 | 0.1 | 0.15 | 0.12 |
| Recompression Index | 0.006 | 0.016 | 0.012 | 0.012 | 0.02 | 0.02 | 0.02 | 0.02 | 0.01 |
| Shear Wave Velocity, fps | 1,000 | 1,125 | 1,125 | 1,125 | 1,059 | 1,187 | 1,226 | 1,193 | 1,128 |

Table 6.2-2 Comparisons between average engineering properties.

| Boring No. | Sample No. | Depth (ft.) | Test Type | Volume Change at Sampling (%) | Tip Resistance (qc)1 (tsf) | Fines Content | |
|---|---|---|---|---|---|---|---|
| | | | | | | Field (1) (%) | Lab (2) (%) |
| H-BOR-2 | PS-4 | 91.2-93.2 | Strength Tests | 0.05 | 5.7 | 30 | 33 |
| H-BOR-2 | PS-5 | 94.1-96.1 | | 0.76 | 9.7 | 30 | 27.3 |
| H-BOR-2 | PS-6 | 97.0-98.9 | | 0.1 | 7.7 | 30 | 20.3 |
| H-BOR-12 | PS-5 | 70.7-72.5 | | -0.66 | 14 | 50 | 25.3 |
| H-BOR-12 | PS-7 | 92.8-94.6 | | -1.33 | 19.8 | 15 | 17 |
| H-BOR-23 | PS-2 | 33.3-35.1 | | 1.75 | 18 | 30 | 33 |
| H-BOR-23 | PS-3 | 40.2-42.1 | | 0.77 | 17.3 | 30 | 18.7 |
| H-BOR-23 | PS-4 | 83.8-85.7 | | -0.13 | 10.1 | 10 | 18.7 |
| H-BOR-29 | PS-2 | 53.7-55.5 | | 3.16 | 21.4 | 30 - 40 | 23 |
| H-BOR-23.1 | PS-1 | 28.9-30.8 | Strain Tests | 1.26 | 30.9 | - | 24 |
| H-BOR-2 | PS-13 | 175-177 | | -1.76 | 6.4 | 20 | 29.3 |
| H-BOR-2 | PS-14 | 178-180 | | 3.91 | 9.5 | 20 | 28 |
| H-BOR-2 | PS-11 | 169.8-171.2 | | -3 | 23.3 | 10 | 22 |
| H-BOR-29 | PS-7 | 90.5-92.3 | | 0.15 | 26.3 | 20 | 33 |

(1) Estimated by field engineer in the field boring log.

(2) As reported by the UC Berkeley laboratory.

Table 6.2-3 Stationary piston sample properties.

| Boring No. | Sample No. | Depth (ft) | Depth to GWT (ft) | Formation (Tentative) | Total Stress (ksf) | Effective Stress (ksf) | Static Water Pressure (ksf) | CPT Data | | | |
|---|---|---|---|---|---|---|---|---|---|---|---|
| | | | | | | | | Qc, tsf | | Cn | (Qc)1 (tsf) |
| | | | | | | | | Range | Average | | |
| H-BOR-2 | PS-4 | 91.2 | 55 | TR3 | 11.4 | 9.14 | 2.26 | 11.27-16.08 | 14.2 | 0.34 | 4.8 |
| H-BOR-2 | PS-5 | 94.1 | 55 | TR3 | 11.76 | 9.32 | 2.44 | 21.51-34.81 | 24.3 | 0.33 | 8.0 |
| H-BOR-2 | PS-6 | 97 | 55 | TR3 | 12.13 | 9.5 | 2.63 | 15.9-23.23 | 19.3 | 0.33 | 6.4 |
| H-BOR-12 | PS-5 | 70.7 | 25 | TR3 | 8.84 | 5.98 | 2.86 | 25.44-39.06 | 30.4 | 0.46 | 14.0 |
| H-BOR-23 | PS-2 | 33.3 | 25 | TR3 | 4.16 | 3.64 | 0.52 | 18.57-41.75 | 27.6 | 0.65 | 18.0 |
| H-BOR-23 | PS-3 | 40.2 | 25 | TR3 | 5.03 | 4.08 | 0.95 | 18.45-36.43 | 28 | 0.62 | 17.3 |
| H-BOR-29 | PS-2 | 53.7 | 55 | TR1 | 6.71 | 6.71 | 0 | 39.76-67.09 | 50.9 | 0.42 | 21.4 |

**NOTES:**

**1. Total and effective stresses were calculated based on a total unit weight of 0.125 ksf.**

**2. The tip resistance Qc shown were corrected values from digitized tabulations.**

Table 6.2-4 Normalized cone tip resistances applicable to the laboratory cyclic test specimens.

| Specimen No. | Formation | Dry Density (pcf) | Fines, % Silt | Clay | Total | d(50) (mm) | Atterberg Limits Liquid Limit | Plastic Limit | Plasticity Index | -200 Atterberg Limits Liquid Limit | Plastic Limit | Plasticity Index |
|---|---|---|---|---|---|---|---|---|---|---|---|---|
| 23/2/T | TR3 | 106.6 | 9 | 24 | 33 | 0.1 | 47 | 16 | 31 | 124 | 46 | 78 |
| 23/2/M | TR3 | 104.6 | 11 | 25 | 36 | 0.09 | 49 | 23 | 26 | 117 | 44 | 73 |
| 23/2/B | TR3 | 102.0 | 10 | 23 | 33 | 0.1 | 44 | 18 | 26 | 115 | 41 | 74 |
| 23/3/T | TR3 | 105.9 | 3 | 18 | 21 | 0.17 | 44 | 24 | 20 | 163 | 38 | 125 |
| 23/3/M | TR3 | 104.7 | 2 | 17 | 19 | 0.22 | 46 | 17 | 29 | 191 | 39 | 152 |
| 23/3/B | TR3 | 104.3 | 2 | 14 | 16 | 0.22 | 50 | 24 | 26 | 178 | 33 | 145 |
| 29/2/T | TR1 | 106.3 | 5 | 18 | 23 | 0.67 | 101 | 29 | 72 | 162 | 40 | 122 |
| 2/4/T | TR3 | 106.9 | 10 | 23 | 33 | 0.1 | 49 | 16 | 33 | 125 | 43 | 82 |
| 2/4/M | TR3 | 108.9 | 10 | 24 | 34 | 0.11 | 47 | 16 | 31 | 123 | 41 | 82 |
| 2/5/T | TR3 | 106.4 | 5 | 22 | 27 | 0.14 | 45 | 17 | 28 | 151 | 46 | 105 |
| 2/5/M | TR3 | 97.8 | 3 | 27 | 30 | 0.13 | 52 | 21 | 31 | 187 | 35 | 152 |
| 2/5/B | TR3 | 93.2 | 5 | 20 | 25 | 0.13 | 51 | 17 | 34 | 179 | 43 | 136 |
| 2/6/T | TR3 | 102.0 | 4 | 18 | 22 | 0.16 | 46 | 18 | 28 | 186 | 42 | 144 |
| 2/6/M | TR3 | 105.0 | 1 | 19 | 20 | 0.19 | 48 | 19 | 29 | 182 | 54 | 128 |
| 2/6/B | TR3 | 106.5 | 2 | 17 | 19 | 0.2 | 51 | 20 | 31 | 192 | 36 | 156 |
| 12/5/T | TR3 | 114.6 | 6 | 16 | 22 | 0.3 | 53 | 23 | 30 | 119 | 38 | 81 |
| 12/5/M | TR3 | 106.8 | 7 | 20 | 27 | 0.14 | 51 | 24 | 27 | 172 | 42 | 130 |
| 12/5/B | TR3 | 100.7 | 5 | 22 | 27 | 0.13 | 48 | 22 | 26 | 180 | 41 | 139 |
| | (Average) | 104.6 | 5.6 | 20.4 | 25.9 | 0.2 | 51.2 | 20.2 | 31.0 | 158.1 | 41.2 | 116.9 |

Table 6.2-5 Summary of results of cyclic shear tests and index properties of ITP specimens (1).

| Boring No. | Sample No. | Specimen No. | Formation | Classification | Sigma 3c (ksf) | Cyclic Stress Ratio (Lab.) | Number of Cycles to Initial Liquefaction | K sigma | Stress Ratio (Norm.) | Cr | Stress Ratio (Field) |
|---|---|---|---|---|---|---|---|---|---|---|---|
| H-BOR-23 | PS-2 | 23/2/T | TR3 | SC | 8.4 | 0.171 | 24 | 0.86 | 0.199 | 0.64 | 0.127 |
| H-BOR-23 | PS-2 | 23/2/M | TR3 | SC | 8.4 | 0.212 | 9 | 0.86 | 0.247 | 0.64 | 0.158 |
| H-BOR-23 | PS-2 | 23/2/B | TR3 | SC | 8.4 | 0.232 | 4 | 0.86 | 0.270 | 0.64 | 0.173 |
| H-BOR-23 | PS-3 | 23/3/T | TR3 | SC | 4.2 | 0.225 | 7 | 0.94 | 0.239 | 0.64 | 0.153 |
| H-BOR-23 | PS-3 | 23/3/M | TR3 | SC | 4.2 | 0.185 | 19 | 0.94 | 0.197 | 0.64 | 0.126 |
| H-BOR-23 | PS-3 | 23/3/B | TR3 | SC | 4.2 | 0.168 | 39 | 0.94 | 0.179 | 0.64 | 0.114 |
| H-BOR-29 | PS-2 | 29/2/T | TR1 | SC | 15.7 | 0.167 | 16 | 0.79 | 0.211 | 0.64 | 0.135 |
| H-BOR-2 | PS-4 | 2/4/T | TR3 | SC | 10.4 | 0.134 | >450 | 0.83 | 0.161 | 0.64 | 0.103 |
| H-BOR-2 | PS-4 | 2/4/M | TR3 | SC | 10.4 | 0.207 | 39 | 0.83 | 0.249 | 0.64 | 0.160 |
| H-BOR-2 | PS-5 | 2/5/T | TR3 | SC | 10.4 | 0.229 | 6 | 0.83 | 0.276 | 0.64 | 0.177 |
| H-BOR-2 | PS-5 | 2/5/M | TR3 | SC | 10.4 | 0.207 | 20 | 0.83 | 0.249 | 0.64 | 0.160 |
| H-BOR-2 | PS-5 | 2/5/B | TR3 | SC | 10.4 | 0.250 | 5 | 0.83 | 0.301 | 0.64 | 0.193 |
| H-BOR-2 | PS-6 | 2/6/T | TR3 | SC | 15.7 | 0.223 | 4 | 0.79 | 0.282 | 0.64 | 0.181 |
| H-BOR-2 | PS-6 | 2/6/M | TR3 | SC | 15.5 | 0.214 | 6 | 0.79 | 0.271 | 0.64 | 0.173 |
| H-BOR-2 | PS-6 | 2/6/B | TR3 | SC | 15.1 | 0.196 | 9 | 0.79 | 0.248 | 0.64 | 0.159 |
| H-BOR-12 | PS-5 | 12/5/T | TR3 | SM-SC | 6.3 | 0.246 | 7 | 0.89 | 0.276 | 0.64 | 0.177 |
| H-BOR-12 | PS-5 | 12/5/M | TR3 | SM-SC | 6.3 | 0.220 | 18 | 0.89 | 0.247 | 0.64 | 0.158 |
| H-BOR-12 | PS-5 | 12/5/B | TR3 | SM-SC | 6.3 | 0.215 | 78 | 0.89 | 0.242 | 0.64 | 0.155 |

NOTES: 1. Site-specific Values of K sigma derived from lab. testing were used.
2. Dry densities, shown on next page, were measured after specimen saturation and consolication.

Table 6.2-6 Summary of results of cyclic shear tests and index properties of ITP specimens (2).

| | Initial Conditions | | Initial Liquefaction | | $\varepsilon_{da}$= 5 % | | $\varepsilon_{da}$= 10 % | |
|---|---|---|---|---|---|---|---|---|
| Test | $\sigma'_{con}$ (kPa) | B-value | N (cycles) | CSR | N (cycles) | CSR | N (cycles) | CSR |
| B2P4T | 500 | 0.97 | >450 | .134 | N/A | N/A | N/A | N/A |
| B2P4M | 500 | 0.99 | 39 | .207 | 70 | .203 | N/A | N/A |
| B2P5T | 500 | 0.97 | 6 | .229 | 10 | .230 | 15 | .234 |
| B2P5M | 500 | 0.98 | 20 | .207 | 27 | .208 | N/A | N/A |
| B2P5B | 500 | 0.98 | 5 | .250 | 7 | .252 | 10 | .254 |
| B2P6T | 750 | 0.95 | 4 | .223 | 4 | .223 | N/A | N/A |
| B2P6M | 743 | 0.97 | 6 | .214 | 6 | .214 | 8 | .214 |
| B2P6B | 725 | 0.98 | 9 | .196 | 10 | .196 | N/A | N/A |
| B12P5T | 300 | 0.96 | 7 | .246 | 26 | .246 | N/A | N/A |
| B12P5M | 300 | 0.96 | 18 | .220 | N/A | N/A | N/A | N/A |
| B12P5B | 300 | 0.95 | 78 | .215 | N/A | N/A | N/A | N/A |
| B12P7T | 375 | 0.98 | 8 | .173 | 12 | .173 | N/A | N/A |
| B12P7M | 375 | 0.96 | 20 | .152 | 24 | .152 | 35 | .152 |
| B12P7B | 375 | 0.96 | 8 | .196 | 9 | .196 | 15 | .196 |
| B23P2T | 400 | 0.97 | 24 | .171 | 33 | .175 | 39 | .175 |
| B23P2M | 400 | 0.98 | 9 | .212 | 9 | .212 | N/A | N/A |
| B23P2B | 400 | 0.97 | 4 | .232 | 3 | .232 | 5 | .232 |
| B23P3T | 200 | 0.99 | 7 | .225 | 12 | .225 | 17 | .228 |
| B23P3M | 200 | 0.96 | 19 | .185 | 24 | .185 | N/A | N/A |
| B23P3B | 200 | 0.98 | 39 | .168 | 56 | .172 | 67 | .175 |
| B23P4T | 750 | 0.98 | 11 | .177 | 17 | .177 | N/A | N/A |
| B23P4M | 700 | 0.96 | 6 | .215 | 3 | .215 | 5 | .215 |
| B23P4B | 750 | 0.98 | 11 | .147 | 9 | .145 | 11 | .147 |
| B29P2T | 750 | 0.97 | 16 | .167 | 17 | .167 | N/A | N/A |

Table 6.2-7 Results of liquefaction testing of SRS/ITP soils.

| Boring No. | Sample No. | Specimen No. | Formation | Classi-fication | Effective Sigma 3c (ksf) | Cyclic Stress Ratio (Lab.) | Number of Cycles to Initial Liquefaction |
|---|---|---|---|---|---|---|---|
| | | | | | | | |
| H-BOR-23 | PS-2 | 23/2/T | TR3 | SC | 8.4 | 0.171 | 24 |
| H-BOR-23 | PS-2 | 23/2/M | TR3 | SC | 8.4 | 0.212 | 9 |
| H-BOR-23 | PS-2 | 23/2/B | TR3 | SC | 8.4 | 0.232 | 4 |
| H-BOR-23 | PS-3 | 23/3/T | TR3 | SC | 4.2 | 0.225 | 7 |
| H-BOR-23 | PS-3 | 23/3/M | TR3 | SC | 4.2 | 0.185 | 19 |
| H-BOR-23 | PS-3 | 23/3/B | TR3 | SC | 4.2 | 0.168 | 39 |
| H-BOR-29 | PS-2 | 29/2/T | TR3 | SC | 15.7 | 0.167 | 16 |
| | | | | | | | |
| | | | | | | | |
| | | | | | | | |
| H-BOR-2 | PS-4 | 2/4/T | TR4 | SC | 10.4 | 0.134 | >450 |
| H-BOR-2 | PS-4 | 2/4/M | TR4 | SC | 10.4 | 0.207 | 39 |
| H-BOR-2 | PS-5 | 2/5/T | TR4 | SC | 10.4 | 0.229 | 6 |
| H-BOR-2 | PS-5 | 2/5/M | TR4 | SC | 10.4 | 0.207 | 20 |
| H-BOR-2 | PS-5 | 2/5/B | TR4 | SC | 10.4 | 0.250 | 5 |
| H-BOR-2 | PS-6 | 2/6/T | TR4 | SC | 15.7 | 0.223 | 4 |
| H-BOR-2 | PS-6 | 2/6/M | TR4 | SC | 15.5 | 0.214 | 6 |
| H-BOR-2 | PS-6 | 2/6/B | TR4 | SC | 15.1 | 0.196 | 9 |
| H-BOR-12 | PS-5 | 12/5/T | TR4 | SM-SC | 6.3 | 0.246 | 7 |
| H-BOR-12 | PS-5 | 12/5/M | TR4 | SM-SC | 6.3 | 0.220 | 18 |
| H-BOR-12 | PS-5 | 12/5/B | TR4 | SM-SC | 6.3 | 0.215 | 78 |
| | | | | | | | |
| | | | | | | | |
| H-BOR-12 | PS-7 | 12/7/T | DB1-3 | SC | 7.8 | 0.173 | 8 |
| H-BOR-12 | PS-7 | 12/7/M | DB1-3 | SC | 7.8 | 0.152 | 20 |
| H-BOR-12 | PS-7 | 12/7/B | DB1-3 | SC | 7.8 | 0.196 | 8 |
| H-BOR-23 | PS-4 | 23/4/T | DB1-3 | SC | 15.7 | 0.177 | 11 |
| H-BOR-23 | PS-4 | 23/4/M | DB1-3 | SC | 14.6 | 0.215 | 6 |
| H-BOR-23 | PS-4 | 23/4/B | DB1-3 | SP-SC | 15.7 | 0.147 | 11 |
| | | | | | | | |

NOTES:
1. Reference - UC Berkeley Test Results, Oct. 25, 1993
2. Conversion of units for Sigma 3 - 1 ksf = 47.88 kpa
   (e.g. 500 kpa = 10.4 ksf)

Table 6.2-8 Parameters from cyclic triaxial tests.

| Formation | Cyclic Stress Ratio (1) | Initial Effective Confining Pressure tsf | Cyclic Stress Ratio (2) | Ksigma |
|---|---|---|---|---|
| | | | | |
| Tobacco Road 3 | 0.196 | 2.1 | 0.21 | 0.93 |
| | 0.185 | 4.2 | | 0.88 |
| | 0.17 | 7.85 | | 0.81 |
| | | | | |
| Tobacco Road 4 | 0.225 | 3.15 | 0.26 | 0.86 |
| | 0.209 | 5.2 | | 0.8 |
| | 0.19 | 7.7 | | 0.73 |
| | | | | |
| Dry Branch 1/3 | 0.16 | 3.9 | 0.17 | 0.94 |
| | 0.148 | 7.65 | | 0.87 |

(1) Initial Liquefaction in 15 Cycles
(2) Initial Liquefaction in 15 Cycles, Initial Confining Pressure equal to 1 tsf

Table 6.2-9 Calculation of Kσ factor.

| Test No. | Specimen No. | Formation | CSR | Number Cycles | Pore Pres Ratio | Axial Strain p-p, % | Shear Strain, % | Volumetic Strain, % | (qc)1 tsf | Type of Test |
|---|---|---|---|---|---|---|---|---|---|---|
| 1 | B2P4T | TR3 | 0.134 | >450 | 0.52 | 0.2 | 0.2 | 0.27 | 5.7 | A |
| 2 | B2P4M | TR3 | 0.207 | 39 | 1 | 9.1 | 6.8 | 2.6 | 5.7 | A |
| 3 | B2P5T | TR3 | 0.229 | 6 | 1 | 15.3 | 11.5 | 3.2 | 9.7 | A |
| 4 | B2P5M | TR3 | 0.207 | 20 | 1 | 8.6 | 6.5 | 2.6 | 9.7 | A |
| 5 | B2P5B | TR3 | 0.25 | 5 | 1 | 15.9 | 11.9 | 3.2 | 9.7 | A |
| 6 | B2P6T | TR3 | 0.223 | 4 | 1 | 9.9 | 7.4 | 2.1 | 7.7 | A |
| 7 | B2P6M | TR3 | 0.214 | 6 | 1 | 17.7 | 13.3 | 4.3 | 7.7 | A |
| 8 | B2P6B | TR3 | 0.196 | 9 | 1 | 9.4 | 7.1 | 2.6 | 7.7 | A |
| 9 | B12P5T | TR3 | 0.246 | 7 | 1 | 8.8 | 6.6 | 2.4 | 14 | A |
| 10 | B12P5M | TR3 | 0.22 | 18 | 1 | 1.5 | 1.1 | 0.8 | 14 | A |
| 11 | B12P5B | TR3 | 0.215 | 78 | 1 | 0.8 | 0.6 | 0.6 | 14 | A |
| 15 | B23P2T | TR3 | 0.171 | 24 | 1 | 13 | 9.8 | 3.9 | 18 | A |
| 16 | B23P3T | TR3 | 0.225 | 7 | 1 | 18.6 | 14.0 | 3.7 | 17.3 | A |
| 17 | B23P3M | TR3 | 0.185 | 19 | 1 | 9.6 | 7.2 | 1 | 17.3 | A |
| 18 | B23P3B | TR3 | 0.168 | 39 | 1 | 14.7 | 11.0 | 3.1 | 17.3 | A |
| 22 | B29P2T | TR1 | 0.167 | 16 | 1 | 7 | 5.3 | 2.6 | 21.4 | A |
| 26 | B29P7T | TR3 | 0.1 | 20 | 0.13 | 0.04 | 0.0 | 0.06 | 26.3 | B |
| 27 | B29P7B | TR3 | 0.15 | 20 | 0.31 | 0.078 | 0.1 | 0.18 | 26.3 | B |
| | | | | | | | | | | |
| 12 | B12P7T | D.B. | 0.173 | 8 | 1 | 9.5 | 7.1 | 2.6 | 19.8 | A |
| 13 | B12P7M | D.B. | 0.152 | 20 | 1 | 16.8 | 12.6 | 4 | 19.8 | A |
| 14 | B12P7B | D.B. | 0.196 | 8 | 1 | 18.6 | 14.0 | 4 | 19.8 | A |
| 19 | B23P4T | D.B. | 0.177 | 11 | 1 | 8 | 6.0 | 2.8 | 10.1 | A |
| 20 | B23P4M | D.B. | 0.215 | 6 | 1 | 13 | 9.8 | 3.6 | 10.1 | A |
| 21 | B23P4B | D.B. | 0.147 | 11 | 1 | 16.5 | 12.4 | 4.2 | 10.1 | A |
| | | | | | | | | | | |
| 25 | B2P14T | SANTEE | 0.1 | 20 | 0.25 | 0.067 | 0.1 | 0.24 | 9.5 | B |
| 26 | B2P14M | SANTEE | 0.12 | 20 | 0.21 | 0.133 | 0.1 | 0.31 | 9.5 | B |
| 27 | B2P14B | SANTEE | 0.1 | 20 | 0.17 | 0.057 | 0.0 | 0.11 | 9.5 | B |

A -- Regular Stress-controlled cyclic triaxial test.
B -- Low-amplitude cyclic triaxial test.

Table 6.2-10 Summary of data for volumetric strain calculations.

| (Qc)1 tsf | FS>1.15 | FS=1.0 (γ=3%) | FS=0.8 (γ=9%) | FS=0.6 (γ=16%) |
|---|---|---|---|---|
| | Volumetric Strain | | | |
| 10 | <1 | 1.61 | 2.88 | 4.65 |
| 20 | <1 | 1.38 | 2.64 | 4.4 |
| 30 | <1 | 1.15 | 2.4 | 4.16 |
| 50 | <1 | 0.69 | 1.92 | 3.65 |

Table 6.2-11 Relationship between limiting cyclic shear strain, factor of safety against initial liquefaction, cone tip resistance and volumetric strain.

| | | | *Effective Stress* | | *Total Stress* | |
|---|---|---|---|---|---|---|
| *Layer* | *Thickness* | *Unit Wt. (Pcf)* | *$\phi'$ (deg.)* | *C' (Psf)* | *$\phi$ (deg.)* | *C (Psf)* |
| Fill 1 | 38 | 121 | 37 | 0.0 | 0 | 3785 |
| Fill 2 | 2 | 115 | 19 | 0.0 | 0 | 1703 |
| TR-1 | 16 | 121 | 34 | 0.0 | 16 | 1100 |
| TR-2 | 20 | 126 | 29 | 0.0 | 23 | 1500 |
| TR-3 | 20 | 124 | 30 | 0.0 | 13 | 1900 |

C = Cohesion $\phi$ = Angle of Internal Friction

Table 6.3-1 Best estimate shear strength parameters used in the ITP stability analyses.

| *Area* | *Undrained Shear Strength, Su (psf)* | *Effective Friction Angle (degrees)* |
|---|---|---|
| **General** | 2400[1] | 32 |
| **Weak Zone at Base of Fill** | 1550 | 22 |

[1]Average over total depth

Table 6.3-2 Best estimate shear strength parameters used in the HTF stability analyses.

| | *CROSS-SECTION 1* | *CROSS-SECTION 2* | *CROSS-SECTION 3* |
|---|---|---|---|
| **Static Effective Stress** | **1.9** | **1.9** | **1.9** |
| **Static Total Stress** | **2.6** | **4.2** | **4.2** |
| **Pseudo-static** | **1.7** | **2.4** | **2.2** |
| **Yield Acceleration (g)** | **0.6** | **0.7** | **0.6** |

Table 7.2-1 Summary of critical factors of safety.

| Formation | Depth to middle of layer (ft) | Avg. Shear Wave (ft/sec) | Normalized Velocity (ft/sec) | (m/sec) |
|---|---|---|---|---|
| Fill | | — | — | — |
| Tobacco Road 1 | 59 | 1187 | 878 | 268 |
| Tobacco Road 2 | 81 | 1226 | 866 | 264 |
| Tobacco Road 3/4 | 98 | 1193 | 818 | 249 |
| Dry Branch 1/3 | 125 | 1128 | 741 | 226 |
| Dry Branch 4 | 145 | 978 | 626 | 191 |
| Dry Branch 5 | 158 | 1055 | 667 | 203 |

Table 7.3-1 Average and normalized shear wave velocities for the ITP soil column.

| Profile No : | A1 | A2 | A3 | A4 | A5 | A6 | B1 | B2 | B3 | B4 | No. of | | |
|---|---|---|---|---|---|---|---|---|---|---|---|---|---|
| Location : | (See Note) | H-CPT-29 | (See Note) | H-CPT-26 | H-CPT-6B | H-CPT-30 | H-CPT-14 | (See Note) | (See Note) | H-CPT-23 | Sublayers | γ | Vs |
| Layer Name | Layer Thickness (ft) | | | | | | | | | | | (kcf) | (fps) |
| | | | | | | | | | | | | | |
| Structural Fill | 16 | 47 | 27 | 42 | 40.5 | 44.5 | 6 | 29.5 | 42 | 8 | 2 | 0.122 | 1078 |
| TR1 | 8 | 35 | 8 | 3.5 | 40 | 31.5 | 27 | 23 | 33.5 | 3 | 3 | 0.121 | 1194 |
| TR2 | 27 | 15 | 24 | 23.5 | 21 | 14 | 27 | 22.5 | 11 | 17 | 2 | 0.122 | 1212 |
| TR3/TR4 | 24 | 24 | 23 | 23 | 20 | 21 | 25 | 24.5 | 22 | 21 | 2 | 0.126 | 1192 |
| DB1-DB3 | 31 | 35 | 33 | 34 | 35 | 33 | 35 | 34 | 33 | 33 | 2 | 0.123 | 1126 |
| DB4 | 12 | 1 | 13 | 14 | 4.5 | 4.5 | 7 | 7 | 7 | 7 | 1 | 0.113 | 968 |
| DB5 | 14 | 3.5 | 15 | 14 | 14 | 21 | 8 | 10.5 | 19.5 | 15 | 1 | 0.104 | 1046 |
| Santee | 50 | 49 | 54 | 57.5 | 34 | 40.5 | 43 | 41.5 | 37.5 | 70 | 3 | 0.117 | 1201 |
| Green Clay | 5 | 11 | 7 | 9 | 10 | 10 | 7 | 7.5 | 8 | 9 | 1 | 0.117 | 1325 |
| Congaree | 19 | 21 | 19 | 19 | 21 | 21 | 26 | 25 | 24 | 26 | 2 | 0.125 | 1550 |
| First Submerged Sublayer : | 5 | 4 | 6 | 6 | 4 | 4 | 5 | 4 | 4 | 7 | | | |
| Total Depth | 206 0 | 241.5 | 223.0 | 239.5 | 240.0 | 241.0 | 211.0 | 225.0 | 237.5 | 209.0 | | | |

NOTES:
Profiles A3, A4, A5, A6 and B3 are under the tanks.
Profiles A1, A2, B1, B2 and B4 are in the free-field.
Profile A1 is at the left end of Section A.
Profile A3 is in the middle of road on left side of Section A.
Profile B2 is in the mid-point of left slope in Section B.
Profile B3 is in the middle of the two tanks in Section B.

Table 7.3-2 Soil profiles for SHAKE analyses, Phase 1.

| Profile No.: | A1 | A2 | A3 | A4 | A5 | A6 | No. of | Sublayer | | | Degrad. |
|---|---|---|---|---|---|---|---|---|---|---|---|
| Location: | (See Note) | H-CPT-29 | (See Note) | H-CPT-26 | H-CPT-68 | H-CPT-30 | Sublayers | Numbers | $\gamma$ | $\bar{V}s$ | Curve |
| Layer Name | Layer Thickness (ft) | | | | | | | | (kcf) | (fps) | Type |
| Structural Fill | 16 | 47 | 27 | 42 | 40.5 | 44.5 | 2 | 1,2 | 0.124 | 1059 | 1 |
| TR1 | 8 | 35 | 8 | 3.5 | 40 | 31.5 | 3 | 3,4,5 | 0.121 | 1187 | 2 |
| TR2 | 27 | 15 | 24 | 23.5 | 21 | 14 | 2 | 6,7 | 0.126 | 1226 | 2 |
| TR3 | 24 | 24 | 23 | 23 | 20 | 21 | 2 | 8,9 | 0.125 | 1193 | 2 |
| DB1-DB3 | 31 | 35 | 33 | 34 | 35 | 33 | 2 | 10,11 | 0.122 | 1128 | 2 |
| DB4 | 12 | 1 | 13 | 14 | 4.5 | 4.5 | 1 | 12 | 0.114 | 978 | 2 |
| DB5 | 14 | 3.5 | 15 | 14 | 14 | 21 | 1 | 13 | 0.105 | 1055 | 2 |
| Santee | 50 | 49 | 54 | 57.5 | 34 | 40.5 | 3 | 14,15,16 | 0.116 | 1251 | 2 |
| Green Clay | 5 | 11 | 7 | 9 | 10 | 10 | 1 | 17 | 0.116 | 1325 | 2 |
| Congaree | 90 | 90 | 90 | 90 | 90 | 90 | 4 | 18,19,20,21 | 0.125 | 1340 | 2 |
| | 20 | 20 | 20 | 20 | 20 | 20 | 1 | 22 | 0.125 | 1370 | 3 |
| Clay | 12 | 12 | 12 | 12 | 12 | 12 | 1 | 23 | 0.125 | 1550 | 3 |
| | 58 | 58 | 58 | 58 | 58 | 58 | 2 | 24,25 | 0.125 | 1770 | 3 |
| | 70 | 70 | 70 | 70 | 70 | 70 | 2 | 26,27 | 0.125 | 2150 | 3 |
| | 170 | 170 | 170 | 170 | 170 | 170 | 3 | 28,29,30 | 0.125 | 2270 | 3,4 |
| Clay | 58 | 58 | 58 | 58 | 58 | 58 | 1 | 31 | 0.125 | 2640 | 4 |
| | 132 | 132 | 132 | 132 | 132 | 132 | 2 | 32,33 | 0.125 | 2450 | 4 |
| | 130 | 130 | 130 | 130 | 130 | 130 | 2 | 34,35 | 0.125 | 2630 | 4 |
| | 50 | 50 | 50 | 50 | 50 | 50 | 1 | 36 | 0.125 | 3080 | 4 |
| Bedrock | - | - | - | - | - | - | - | 37 | 0.150 | 8000 | - |
| First Submerged Sublayer: | 5 | 4 | 6 | 6 | 4 | 4 | | | | | |
| Total Depth | 977.0 | 1010.5 | 994.0 | 1010.5 | 1009.0 | 1010.0 | | | | | |

NOTES:
Profiles A3, A4, A5 and A6 are under the tanks.
Profiles A1 and A2 are in the free-field.
Profile A1 is at the left end of Section A.
Profile A3 is in the middle of road on left side of Section A

Table 7.3-3 Soil profiles for SHAKE analyses, Phase 2.

| Stratum | Unit Weight (pcf) | Average water content (%) | Compression Index ($C_c$) | Recompression Index ($C_r$) | Initial Void Ratio ($e_o$) |
|---|---|---|---|---|---|
| S1 (Tobacco Road) | 130 | 21 | --- | 0.009 (0.0047) | 0.56 |
| S2 (Tobacco Road) | 128 | 22 | ___ | 0.008 (0.0042) | 0.59 |
| S2b (Dry Branch) | 128 | 22 | --- | 0.009 (0.0047) | 0.59 |
| C2 (Tan Clay) | 106 | 53 | 0.85* | 0.070 (0.0368) | 1.4 |
| S3a (Santee) | 127 | 23 | ___ | 0.009 (0.0047) | 0.62 |

* This value is only recommended for the CH soils in the C2 stratum that are found to be normally consolidated.

Numbers in parentheses are recompression indices reduced by a factor of 1.9.

Table 7.5-1 Soil properties used by Mueser et. al. (1984b) for settlement analyses.

Table 7.5-2(a) Profile A-A'

**Soft Zone Compression**
**(North - South Section through Centers of Tanks 51 and 49)**

| Point | Location | H (ft) | ΔS (ft) |
|---|---|---|---|
| A | Centerline Tank 51 | 15 | 0.56 |
| B | 25' South of Centerline of Tank 51 | 10 | 0.37 |
| C | Southern Edge of Tank 51 | 9 | 0.33 |
| D | 100' South of Southern Edge of Tank 51 | 8 | 0.30 |
| E | 25' North of Centerline of Tank 51 | 10 | 0.37 |
| F | Northern Edge of Tank 51 | 7 | 0.26 |
| G | 30' North of Northern Edge of Tank 51 | 5 | 0.19 |
| H | Centerline of Tank 49 | 0 | 0.00 |

Table 7.5-2(b) Profile C-C'

**Soft Zone Compression**
**(West - East Section through Centers of Tanks 50 and 51)**

| Point | Location | H (ft) | ΔS (ft) |
|---|---|---|---|
| A | 25' West of Western Edge of Tank 50 | 6 | 0.22 |
| B | Western Edge of Tank 50 | 5 | 0.19 |
| C | Centerline of Tank 50 | 5 | 0.19 |
| D | Eastern Edge of Tank 50 | 7 | 0.26 |
| E | Western Edge of Tank 51 | 9 | 0.33 |
| F | Centerline of Tank 51 | 15 | 0.56 |
| G | Eastern Edge of Tank 51 | 10 | 0.37 |
| H | 50' East of Eastern Edge of Tank 51 | 7 | 0.26 |

Table 7.5-2 Settlement due to soft zone compression, north-south and east-west subsurface cross-sections.

Table 7.5-3(a)

| Soft Zone Compression (In) | Seismic Event | Tank Loading Condition | Maximum Differential and Total Settlements (inches) | | | |
|---|---|---|---|---|---|---|
| | | | Profile AA' | | Profile BB' | |
| | | | Tank 51 | Tank 49 | Tank 48 | Tank 49 |
| 4.5 | Local | Empty | 0.35 (4.33) | 0.25 (0.38) | 0.01 (0.11) | 0.28 (0.34) |
| | | Full | 0.14 (4.35) | 0.28 (0.42) | 0.03 (0.08) | 0.52 (0.76) |
| | Distant | Empty | 0.28 (4.24) | 0.28 (0.41) | 0.04 (0.11) | 0.28 (0.34) |
| | | Full | 0.14 (4.37) | 0.27 (0.42) | 0.02 (0.08) | 0.53 (0.77) |
| 7.0 | Local | Empty | 0.78 (6.78) | 0.31 (0.48) | 0.02 (0.19) | 0.34 (0.34) |
| | | Full | 0.22 (6.81) | 0.28 (0.42) | 0.03 (0.14) | 0.60 (0.79) |
| | Distant | Empty | 0.68 (6.64) | 0.36 (0.52) | 0.05 (0.19) | 0.35 (0.34) |
| | | Full | 0.14 (6.86) | 0.28 (0.42) | 0.02 (0.14) | 0.60 (0.79) |

Table 7.5-3(b)

| Soft Zone Compression (In) | Seismic Event | Tank Loading Condition | Maximum Differential and Total Settlements (inches) | | | |
|---|---|---|---|---|---|---|
| | | | Profile AA' | | Profile CC' | |
| | | | Tank 51 | Tank 49 | Tank 50 | Tank 51 |
| Variable | Local | Full | 0.29 (4.09) | 0.48 (0.9) | 1.01 (3.7) | 0.59 (5.01) |
| Variable | 84% Motion | Full | 0.3 (4.22) | 0.7 (1.49) | --- | --- |

Notes: Numbers in parentheses are total settlements
Differential settlements (unparenthesized) are measured between center and edge of tank, (See Figures 7.5-81 to 7.5-84 for actual settlement profile).
Reported differential and total settlements are from dissipation of excess pore water pressure in all soil layers plus deep subsidence from soft zones.

Table 7.5-3 Estimated differential and total tank settlements.

| | | | Effective Stress | | Total Stress | |
|---|---|---|---|---|---|---|
| Layer | Thickness | Unit Wt. (Pcf) | "ϕ'" (deg.) | "C'" (Psf) | "ϕ" (deg.) | "C" (Psf) |
| Fill 1 | 37 | 121 | 32 | 0 | 0 | 2400 |
| Fill 2 | 3 | 121 | 22 | 0 | 0 | 1500 |
| "upland" 1 | 30 | 121 | 34 | 0 | 16 | 1100 |
| "upland" 2 | +40 | 126 | 29 | 0 | 23 | 1500 |

C = Cohesion  ϕ = Angle of Internal Friction

Table 8.2-1 Best estimate shear strength parameters at HTF.

| Methodology | Cross-section 1 | Cross-section 2 | Cross-section 3 | Cross-section 4 |
|---|---|---|---|---|
| Circular | 1.6 | 1.1 | 1.6 | 1.6 |
| Wedge | 1.6 | 1.1 | 2.0 | 1.6 |

Table 8.2-2 Minimum static factors of safety at HTF, effective stress conditions.

| Methodology | Cross-section 1 | Cross-section 2 | Cross-section 3 | Cross-section 4 |
|---|---|---|---|---|
| Circular | 2.8 | 2.6 | 2.9 | 2.9 |
| Wedge | 2.6 | 2.3 | 2.8 | 3.0 |

Table 8.2-3 Minimum static factors of safety at HTF, total stress conditions.

| Methodology | Cross-section 1 | Cross-section 2 | Cross-section 3 | Cross-section 4 |
|---|---|---|---|---|
| Circular | 1.6 | 1.6 | 1.6 | 1.7 |
| Wedge | 1.6 | 1.6 | 1.6 | 1.6 |

Table 8.2-4 Minimum pseudo-static factors of safety at HTF, total stress conditions (0.2g) with 10% strength reduction.

| | CROSS-SECTION 1 | CROSS-SECTION 2 | CROSS-SECTION 3 | CROSS-SECTION 4 |
|---|---|---|---|---|
| Static Effective Stress | 1.6 | 1.1 | 1.6 | 1.6 |
| Static Total Stress | 2.6 | 2.3 | 2.8 | 2.9 |
| Pseudo-dynamic 0.2 g (H) | 1.6 | 1.6 | 1.6 | 1.6 |

Table 8.2-5 Summary of minimum factors of safety at HTF.

| ITP 84TH Liquefaction Analyses | | | | | |
|---|---|---|---|---|---|
| OCR = 2.0, Disturbance = 1.0, MSF = 1 for M = 7.5 | | | | | |
| | | | | | |
| Dynamic Profile | CPT | Liquefaction | Liquefaction | Increase | |
| | Sounding | Settlement (ft) | Settlement (ft) | Settlement (ft) | |
| | | (Case 1) | (Case 2) | (Case 2 - Case 1) | |
| | | | | | |
| 84TH NON-FILL PROFILE | CPT 14 | 0.2174 | 0.2578 | 0.0404 | |
| 84TH NON-FILL PROFILE | CPT 16 | 0.2483 | 0.3004 | 0.0521 | |
| 84TH NON-FILL PROFILE | CPT 18 | 0.3229 | 0.3788 | 0.0559 | |
| 84TH NON-FILL PROFILE | CPT 20 | 0.0076 | 0.0097 | 0.0021 | |
| 84TH NON-FILL PROFILE | CPT 20-1 | 0.1263 | 0.1428 | 0.0165 | |
| 84TH NON-FILL PROFILE | CPT 20-2 | 0.0513 | 0.0591 | 0.0078 | |
| 84TH NON-FILL PROFILE | CPT 23 | 0.0362 | 0.0432 | 0.0070 | |
| 84TH NON-FILL PROFILE | CPT 25 | 0.0851 | 0.1011 | 0.0160 | |
| 84TH NON-FILL PROFILE | CPT 28 | 0.1205 | 0.1394 | 0.0189 | |
| 84TH NON-FILL PROFILE | CPT 28-2 | 0.1593 | 0.1898 | 0.0305 | |
| | | | | | |
| | average | 0.1375 | 0.1622 | 0.0247 | |
| | st. dev | 0.1215 | 0.1444 | 0.0233 | |
| | | | | | |
| Case 1 = 84th non-fiill profiles (without structural fill) using WSRC modulus and daming curves for shallow profile above green clay and GEI modulus and damping curves for deep profile. | | | | | |
| Case 2 = 84th non-fill profiles (without structural fill) using GEI modulus and damping curves for entire profile. | | | | | |

Table 8.3-1 Comparison of 1-D liquefaction settlements calculated using ITP and GEI dynamic curves for the 84th percentile, non-fill profile at ITP.

| ITP 84TH Liquefaction Analyses | | | | | | |
|---|---|---|---|---|---|---|
| OCR = 2.0, Disturbance = 1.0, MSF = 1 for M = 7.5 | | | | | | |
| | | | | | | |
| Dynamic Profile | CPT | Liquefaction | | | | |
| | Sounding | Settlement (ft) | | | | |
| | | (Case 1) | | | | |
| | | | | | | |
| 84TH FILL PROFILE | CPT 29 | 0.2047 | | | | |
| 84TH FILL PROFILE | CPT 30 | 0.0976 | | | | |
| 84TH FILL PROFILE | CPT 31 | 0.1422 | | | | |
| 84TH FILL PROFILE | CPT 5 | 0.0779 | | | | |
| 84TH FILL PROFILE | CPT 6B | 0.0526 | | | | |
| 84TH FILL PROFILE | CPT 7 | 0.2686 | | | | |
| 84TH FILL PROFILE | CPT 1 | 0.2951 | | | | |
| 84TH FILL PROFILE | CPT 10 | 0.0919 | | | | |
| 84TH FILL PROFILE | CPT 11 | 0.0874 | | | | |
| 84TH FILL PROFILE | CPT 26 | 0.1298 | | | | |
| | | | | | | |
| | average | 0.1448 | | | | |
| | st. dev | 0.0837 | | | | |
| | | | | | | |
| Case 1 = 84th non-fiill profiles (without structural fill) using WSRC modulus and daming curves for shallow profile above green clay and GEI modulus and damping curves for deep profile. | | | | | | |

Table 8.3-2 Summary of 1-D liquefaction settlements calculated for the 84th percentile, fill profile at ITP.

| HTF 84TH Liquefaction Analyses | | | | | | |
|---|---|---|---|---|---|---|
| OCR = 2.0, Disturbance = 1.0, MSF = 1 for M = 7.5 | | | | | | |
| | | | | | | |
| Dynamic Profile | CPT | Liquefaction | | | | |
| | Sounding | Settlement (ft) | | | | |
| | | (Case 2) | | | | |
| | | | | | | |
| 84TH NON-FILL PROFILE | H-NWT-C4 | 0.3180 | | | | |
| 84TH NON-FILL PROFILE | HCEVP1 | 0.1528 | | | | |
| 84TH NON-FILL PROFILE | HCEVP5 | 0.1549 | | | | |
| 84TH NON-FILL PROFILE | HCEVP10 | 0.1017 | | | | |
| 84TH NON-FILL PROFILE | HTF-C14 | 0.3127 | | | | |
| 84TH NON-FILL PROFILE | HTF-C15 | 0.2707 | | | | |
| 84TH NON-FILL PROFILE | HTF-C16 | 0.1399 | | | | |
| 84TH NON-FILL PROFILE | HTF-C17 | 0.1445 | | | | |
| 84TH NON-FILL PROFILE | HTF-C18 | 0.1096 | | | | |
| 84TH NON-FILL PROFILE | HTF-C19 | 0.0000 | | | | |
| | | | | | | |
| | average | 0.1705 | | | | |
| | st. dev | 0.1009 | | | | |
| | | | | | | |
| Case 2 = 84th non-fiill profiles (without structural fill) using GEI modulus and damping curves for the entire profile. | | | | | | |

Table 8.3-3 Summary of 1-D liquefaction settlements calculated for the 84th percentile, non-fill profile at HTF.

| HTF 84TH Liquefaction Analyses | | | | | | |
|---|---|---|---|---|---|---|
| OCR = 2.0, Disturbance = 1.0, MSF = 1 for M = 7.5 | | | | | | |
| | | | | | | |
| Dynamic Profile | CPT | Liquefaction | | | | |
| | Sounding | Settlement (ft) | | | | |
| | | (Case 2) | | | | |
| | | | | | | |
| 84TH FILL PROFILE | H-CPT-32 | 0.0762 | | | | |
| 84TH FILL PROFILE | H-CPT-34 | 0.0491 | | | | |
| 84TH FILL PROFILE | H-CPT-37 | 0.0925 | | | | |
| 84TH FILL PROFILE | H-CPT-38 | 0.1001 | | | | |
| 84TH FILL PROFILE | HTF-C05 | 0.0439 | | | | |
| 84TH FILL PROFILE | HTF-C06 | 0.0621 | | | | |
| 84TH FILL PROFILE | HTF-C07 | 0.0833 | | | | |
| 84TH FILL PROFILE | HTF-C08 | 0.0468 | | | | |
| 84TH FILL PROFILE | HTF-C09 | 0.1318 | | | | |
| 84TH FILL PROFILE | HTF-C13 | 0.2442 | | | | |
| | | | | | | |
| | average | 0.0930 | | | | |
| | st. dev | 0.0598 | | | | |
| | | | | | | |
| Case 2 = 84th non-fiill profiles (without structural fill) using GEI modulus and damping curves for the entire profile. | | | | | | |

Table 8.3-4 Summary of 1-D liquefaction settlements calculated for the 84th percentile, fill profile at HTF.

| Tank Number | First Survey Period | | Second Survey Period | | Survey Off-Period (yrs) | Third Survey Period | | Survey Off-Period (yrs) | Initial Tank Loading Date | Time Since Loading (yrs) | Off-Periods as Percent of Loading Time |
|---|---|---|---|---|---|---|---|---|---|---|---|
| | from | to | from | to | | from | to | | | | |
| 9 | 02/09/59 | 05/21/73 | 11/15/91 | 03/15/94 | 18.5 | | | | 11/57 | 37.5 | 52.7 |
| 10 | 02/09/59 | 05/21/73 | 11/15/91 | 03/15/94 | 18.5 | | | | 11/57 | 37.5 | 52.7 |
| 11 | 02/09/59 | 05/21/73 | 11/15/91 | 03/15/94 | 18.5 | | | | 11/57 | 37.5 | 52.7 |
| 12 | 02/09/59 | 05/21/73 | 11/15/91 | 03/15/94 | 18.5 | | | | 11/57 | 37.5 | 52.7 |
| 13 | 11/30/56 | 02/21/73 | 11/15/91 | 03/15/94 | 18.7 | | | | 11/57 | 37.5 | 50.0 |
| 14 | 11/30/56 | 02/21/73 | 11/15/91 | 03/15/94 | 18.7 | | | | 11/57 | 37.5 | 50.0 |
| 15 | 11/30/56 | 02/21/73 | 11/15/91 | 03/15/94 | 18.7 | | | | 10/60 | 34.6 | 54.2 |
| 16 | 11/30/56 | 02/21/73 | 11/15/91 | 03/15/94 | 18.7 | | | | 06/59 | 35.9 | 52.1 |
| 21 | 03/04/63 | 04/24/73 | 11/15/91 | 03/15/94 | 18.6 | | | | 10/61 | 33.6 | 59.5 |
| 22 | 03/04/63 | 04/24/73 | 11/15/91 | 03/15/94 | 18.6 | | | | 01/64 | 31.3 | 59.2 |
| 23 | 03/04/63 | 04/24/73 | 11/15/91 | 03/15/94 | 18.6 | | | | 04/63 | 32.1 | 57.9 |
| 24 | 03/04/63 | 04/24/73 | 11/15/91 | 03/15/94 | 18.6 | | | | 04/63 | 32.1 | 57.9 |
| 29 | 11/15/91 | 03/15/94 | | | 20.3 | | | | 08/71 | 23.7 | 85.4 |
| 30 | 11/15/91 | 03/15/94 | | | 17.9 | | | | 01/74 | 21.3 | 83.8 |
| 31 | 11/15/91 | 03/15/94 | | | 19.6 | | | | 04/72 | 23.1 | 85.0 |
| 32 | 11/15/91 | 09/15/93 | | | 20.2 | | | | 09/71 | 23.7 | 85.4 |
| 35 | 10/28/74 | 05/03/76 | 06/03/76 | 11/17/77 | 0.1 | 11/15/91 | 03/15/94 | 14.0 | 03/77 | 18.2 | 77.5 |
| 36 | 11/06/74 | 06/30/76 | 11/16/76 | 11/17/77 | 0.4 | 11/15/91 | 03/15/94 | 14.0 | 01/78 | 17.3 | 83.0 |
| 37 | 11/20/74 | 06/17/76 | 10/14/76 | 11/17/77 | 0.3 | 11/15/91 | 03/15/94 | 14.0 | 01/78 | 17.3 | 82.6 |
| 38 | 09/18/78 | 03/15/94 | | | none | | | | 09/81 | 13.7 | 0.0 |
| 39 | 09/18/78 | 03/15/94 | | | none | | | | 02/82 | 13.2 | 0.0 |
| 40 | 11/09/78 | 03/15/94 | | | none | | | | 07/85 | 9.8 | 0.0 |
| 41 | 11/09/78 | 03/15/94 | | | none | | | | 01/82 | 13.3 | 0.0 |
| 42 | 09/18/78 | 03/15/94 | | | none | | | | 03/82 | 13.2 | 0.0 |
| 43 | 02/23/79 | 03/15/94 | | | none | | | | 04/82 | 13.1 | 0.0 |
| 48 | 05/09/78 | 05/28/80 | 02/22/80 | 03/15/94 | none | | | | 01/83 | 12.3 | 0.0 |
| 49 | 04/22/80 | 03/15/94 | | | none | | | | 02/83 | 12.2 | 0.0 |
| 50 | 05/09/78 | 05/28/80 | 02/22/80 | 03/15/94 | none | | | | 02/83 | 12.2 | 0.0 |
| 51 | 05/09/78 | 05/28/80 | 05/28/80 | 03/15/94 | none | | | | 07/85 | 9.8 | 0.0 |

Table 8.5-1 Tank settlement survey schedule.

| Distance (km) | 5.0 - 5.5 [5.25] | 5.5 - 6.0 [5.75] | 6.0 - 6.5 [6.25] | 6.5 - 7.0 [6.75] | > 7.0 [7.25] |
|---|---|---|---|---|---|
| 0 - 25 [16.7] | $4.94 \times 10^{-05}$ | $2.21 \times 10^{-05}$ | $5.98 \times 10^{-06}$ | $8.21 \times 10^{-07}$ | $3.70 \times 10^{-08}$ |
| 25 - 50 [38.9] | $5.89 \times 10^{-05}$ | $5.46 \times 10^{-05}$ | $1.78 \times 10^{-05}$ | $2.42 \times 10^{-06}$ | $1.17 \times 10^{-07}$ |
| 50 - 100 [77.8] | $4.58 \times 10^{-05}$ | $1.03 \times 10^{-04}$ | $5.67 \times 10^{-05}$ | $1.27 \times 10^{-05}$ | $8.28 \times 10^{-07}$ |
| 100 - 150 [126] | $1.86 \times 10^{-05}$ | $1.12 \times 10^{-04}$ | $9.04 \times 10^{-05}$ | $3.08 \times 10^{-05}$ | $3.57 \times 10^{-06}$ |
| 150 - 200 [176] | $6.57 \times 10^{-06}$ | $9.27 \times 10^{-05}$ | $9.83 \times 10^{-05}$ | $3.56 \times 10^{-05}$ | $5.83 \times 10^{-06}$ |
| > 200 [226] | $1.57 \times 10^{-06}$ | $6.59 \times 10^{-05}$ | $1.15 \times 10^{-04}$ | $2.83 \times 10^{-05}$ | $3.21 \times 10^{-06}$ |

Table 9.3-1 EPRI Deaggregation Matrix: Mean 2.5 Hz Spectral Velocity of 2.0 cm/s, 5% Critical Damping Magnitude

| Spectral Velocity (cm/s) | Annual Hazard | Mbar ($m_b$) | Dbar (km) |
|---|---|---|---|
| 1 | $2.920 \times 10^{-3}$ | 5.79 | 117.75 |
| 2 | $1.140 \times 10^{-3}$ | 5.95 | 104.21 |
| 6 | $2.090 \times 10^{-4}$ | 6.23 | 91.05 |
| 8.672 | $1.035 \times 10^{-4}$ | 6.34 | 83.58 |
| 16.01 | $3.210 \times 10^{-5}$ | 6.46 | 74.13 |
| 26 | $1.040 \times 10^{-5}$ | 6.54 | 60.40 |
| 40 | $3.440 \times 10^{-6}$ | 6.59 | 47.18 |
| 90.02 | $3.510 \times 10^{-7}$ | 6.66 | 28.49 |

Table 9.3-2 EPRI Mean Rock 2.5 Hz Spectral Velocity for 5% Critical Damping

| PSV (cm/s) @ 2.5 Hz | Mean Annual Hazard | Mbar ($m_b$) | Dbar (km) |
|---|---|---|---|
| 1 | $2.831 \times 10^{-3}$ | 5.77 | 115.86 |
| 1.6 | $1.635 \times 10^{-3}$ | 5.91 | 110.45 |
| 2.7 | $7.982 \times 10^{-4}$ | 6.06 | 103.39 |
| 4.5 | $3.559 \times 10^{-4}$ | 6.19 | 95.44 |
| 7.4 | $1.464 \times 10^{-4}$ | 6.30 | 86.71 |
| 12 | $5.602 \times 10^{-5}$ | 6.40 | 77.27 |
| 20 | $1.831 \times 10^{-5}$ | 6.49 | 66.29 |
| 33 | $5.518 \times 10^{-6}$ | 6.56 | 54.52 |
| 55 | $1.461 \times 10^{-6}$ | 6.62 | 41.49 |
| 90 | $3.669 \times 10^{-7}$ | 6.67 | 27.94 |

Table 9.3-3 Selected 10 Points on EPRI Hazard Curve

| CPT | FILL | TR1 | TR2 | TR3/4 | DB1/3 | DB4 | DB5 | ST | GC* |
|---|---|---|---|---|---|---|---|---|---|
| Depth Range (ft) | - | 0-27 | 27-38.6 | 38.6-61.5 | 61.5-89.2 | 89.2-100.7 | 100.7-111.1 | 111.1-165.3 | 165.3-170 |
| CPT 1 | 1129 | 1176 | 1499 | 976 | 795 | 757 | 867 | 824 | 1325 |
| CPT 5 | 975 | 1461 | 1302 | 1304 | 1183 | 977 | 1000 | 1134 | 1325 |
| CPT 7 | 1086 | 1196 | 1110 | 1258 | 1155 | 1055 | - | 1041 | 1325 |
| CPT 11 | - | 1085 | 1119 | 1222 | 1206 | 1092 | 1457 | 1780 | 1325 |
| CPT 14 | - | 1086 | 982 | 1363 | 1076 | 682 | - | 1409 | 1325 |
| CPT 18 | 1175 | 1379 | 1122 | 1308 | 1361 | 1236 | 1152 | 1178 | 1325 |
| CPT 25 | - | 1269 | 1132 | 1132 | 831 | 747 | - | 1223 | 1325 |
| CPT 26 | 1024 | 1331 | 1126 | 1167 | 951 | 909 | 800 | 2278 | 1325 |
| CPT 29 | 976 | 1129 | 1112 | 1042 | 1365 | 1166 | - | 1469 | 1325 |
| CPT 30 | 1034 | 1167 | 922 | 1080 | 1137 | 1087 | 888 | 953 | 1325 |

Notes: CPT - Cone Penetration Probe.
TR - Tobacco Road
DB - Dry Branch
ST - Santee
GC - Green Clay

*** Interpreted from ITP Phase II (Calc. No. II-1)**

Table 9.4-1 Summary of Shallow Depth Shear Wave Velocities (fps)

| CPT | FILL | TR1 | TR2 | TR3/4 | DB1/3 | DB4 | DB5 |
|---|---|---|---|---|---|---|---|
| CPT 1 | 41.33 | 14.70 | 27.32 | 23.65 | 32.15 | 9.20 | 8.00 |
| CPT 5 | 40.83 | 25.00 | 15.10 | 22.00 | 35.80 | 6.95 | 10.30 |
| CPT 7 | 40.76 | 29.70 | 19.60 | 24.20 | 31.40 | 24.10 | - |
| CPT 11 | 42.13 | 29.80 | 18.00 | 22.45 | 32.40 | 8.05 | 14.55 |
| CPT 14 | 6.09 | 28.10 | 25.70 | 23.95 | 34.55 | 15.70 | - |
| CPT 18 | 10.29 | 22.70 | 30.70 | 26.60 | 28.05 | 5.45 | 15.30 |
| CPT 25 | - | 32.75 | 25.35 | 20.80 | 24.70 | 8.60 | - |
| CPT 26 | 35.78 | 11.10 | 20.60 | 23.10 | 32.90 | 15.45 | 16.20 |
| CPT 29 | 43.78 | 35.20 | 16.20 | 24.10 | 34.80 | 4.45 | - |
| CPT 30 | 40.84 | 33.60 | 12.35 | 21.70 | 31.00 | 6.20 | 20.80 |

Notes: CPT - Cone Penetration Probe.
TR - Tobacco Road
DB - Dry Branch

Table 9.4-2 Summary, of Layer Thickness (ft)

| Depth Interval (ft) | Poisson's Ratio | Total Unit Wt. (pcf) | Shear Wave Vel. (fps) |
|---|---|---|---|
| 170-260 | 0.47 | 125 | 1340 |
| 260-280 | 0.47 | 125 | 1370 |
| 280-292 | 0.47 | 125 | 1550 |
| 292-350 | 0.47 | 125 | 1770 |
| 350-420 | 0.47 | 125 | 2150 |
| 420-590 | 0.47 | 125 | 2270 |
| 590-648 | 0.47 | 125 | 2640 |
| 648-780 | 0.47 | 125 | 2450 |
| 780-910 | 0.47 | 125 | 2630 |
| 910-960 | 0.47 | 125 | 3080 |
| below 960 | 0.47 | 125 | 8000 |

Table 9.4-3 Summary of Soil Profile & Properties, ITP

| Depth Interval (ft) | Poisson's Ratio | Total Unit Wt. (pcf) | Shear Wave Vel. (fps) |
|---|---|---|---|
| 200-300 | 0.47 | 125 | 1496 |
| 300-500 | 0.47 | 125 | 1843 |
| 500-550 | 0.47 | 125 | 2374 |
| 550-840 | 0.47 | 125 | 3040 |
| 840-960 | 0.47 | 125 | 3273 |
| below 960 | 0.47 | 125 | 8000 |

Table 9.4-4 Summary of soil profile & properties, Confirmatory Drilling Site (CFD).

| Data Points | Location (1) | $(N_1)_{60}$ Values |
|---|---|---|
| Measured (Total=50) | H-SPT-14 | 9.8, 10.4, 6.7, 7.8, 7.7, 7.7, 7.0, 7.0, 8.1, 14.3, 13.6, 12.4, 11.2, 10.0 |
| | H-SPT-18 | 9.5, 17.1, 10.5, 9.3, 8.1, 8.6, 9.1 |
| | H-SPT-20 | 15.5, 8.4, 9.2, 9.8, 8.9, 8.7, 6.3, 6.9, 6.1, 8.3, 7.5, 9.5, 9.5, 13.6 |
| | H-SPT-23.3 | 9.0, 5.6, 4.8, 3.1, 4.6, 3.8, 4.5, 2.2, 2.9, 3.6, 3.6, 3.5, 4.9, 3.5, 4.8 |
| | | |
| Simulated (Total=21) | Tank 48 - 51 | 5.4, 6.6, 5.2, 8.8, 11.4, 11.2 |
| | | 12.0, 15.1, 8.3, 2.9, 5.3, 7.6, 10.0 |
| | | 16.9, 3.4, 1.5, 4.2, 4.1, 6.9 |
| | | 5.5, 6.9 |
| | | |
| Combined (Total=71) | | 9.8, 10.4, 6.7, 7.8, 7.7, 7.7, 7.0, 7.0, 8.1, 14.3, 13.6, 12.4, 11.2, 10.0 |
| | | 9.5, 17.1, 10.5, 9.3, 8.1, 8.6, 9.1 |
| | | 15.5, 8.4, 9.2, 9.8, 8.9, 8.7, 6.3, 6.9, 6.1, 8.3, 7.5, 9.5, 9.5, 13.6 |
| | | 9.0, 5.6, 4.8, 3.1, 4.6, 3.8, 4.5, 2.2, 2.9, 3.6, 3.6, 3.5, 4.9, 3.5, 4.8 |
| | | 5.4, 6.6, 5.2, 8.8, 11.4, 11.2 |
| | | 12.0, 15.1, 8.3, 2.9, 5.3, 7.6, 10.0 |
| | | 16.9, 3.4, 1.5, 4.2, 4.1, 6.9 |
| | | 5.5, 6.9 |

**Note: (1) See Figure 4.1.**

Table 9.4-5 Summary of SPT N-value data (TR3 & TR4).

| CASE No. | Earthquake No. | CPT No. | Deep Soil Profile | CASE No. | Earthquake No. | CPT No. | Deep Soil Profile |
|---|---|---|---|---|---|---|---|
| 1 | E01 | CPT01 | H-Area | 41 | E06 | CPT01 | CFD |
| 2 | E01 | CPT07 | CFD | 42 | E06 | CPT05 | H-Area |
| 3 | E01 | CPT11 | H-Area | 43 | E06 | CPT11 | H-Area |
| 4 | E01 | CPT18 | H-Area | 44 | E06 | CPT14 | H-Area |
| 5 | E01 | CPT25 | CFD | 45 | E06 | CPT18 | CFD |
| 6 | E01 | CPT26 | CFD | 46 | E06 | CPT25 | CFD |
| 7 | E01 | CPT29 | H-Area | 47 | E06 | CPT26 | CFD |
| 8 | E01 | CPT30 | CFD | 48 | E06 | CPT29 | H-Area |
| 9 | E02 | CPT01 | H-Area | 49 | E07 | CPT01 | H-Area |
| 10 | E02 | CPT05 | H-Area | 50 | E07 | CPT07 | CFD |
| 11 | E02 | CPT07 | H-Area | 51 | E07 | CPT11 | CFD |
| 12 | E02 | CPT11 | CFD | 52 | E07 | CPT14 | H-Area |
| 13 | E02 | CPT18 | CFD | 53 | E07 | CPT18 | CFD |
| 14 | E02 | CPT26 | CFD | 54 | E07 | CPT25 | H-Area |
| 15 | E02 | CPT29 | CFD | 55 | E07 | CPT26 | CFD |
| 16 | E02 | CPT30 | H-Area | 56 | E07 | CPT30 | H-Area |
| 17 | E03 | CPT01 | H-Area | 57 | E08 | CPT01 | H-Area |
| 18 | E03 | CPT07 | CFD | 58 | E08 | CPT05 | H-Area |
| 19 | E03 | CPT11 | CFD | 59 | E08 | CPT07 | CFD |
| 20 | E03 | CPT14 | H-Area | 60 | E08 | CPT11 | H-Area |
| 21 | E03 | CPT18 | H-Area | 61 | E08 | CPT18 | CFD |
| 22 | E03 | CPT25 | CFD | 62 | E08 | CPT25 | CFD |
| 23 | E03 | CPT29 | H-Area | 63 | E08 | CPT29 | H-Area |
| 24 | E03 | CPT30 | CFD | 64 | E08 | CPT30 | CFD |
| 25 | E04 | CPT05 | H-Area | 65 | E09 | CPT01 | CFD |
| 26 | E04 | CPT07 | CFD | 66 | E09 | CPT05 | H-Area |
| 27 | E04 | CPT11 | CFD | 67 | E09 | CPT07 | H-Area |
| 28 | E04 | CPT14 | H-Area | 68 | E09 | CPT11 | H-Area |
| 29 | E04 | CPT18 | CFD | 69 | E09 | CPT14 | H-Area |
| 30 | E04 | CPT25 | CFD | 70 | E09 | CPT18 | CFD |
| 31 | E04 | CPT29 | H-Area | 71 | E09 | CPT29 | CFD |
| 32 | E04 | CPT30 | H-Area | 72 | E09 | CPT30 | CFD |
| 33 | E05 | CPT01 | CFD | 73 | E10 | CPT05 | CFD |
| 34 | E05 | CPT05 | H-Area | 74 | E10 | CPT11 | CFD |
| 35 | E05 | CPT07 | CFD | 75 | E10 | CPT14 | CFD |
| 36 | E05 | CPT11 | H-Area | 76 | E10 | CPT18 | H-Area |
| 37 | E05 | CPT14 | H-Area | 77 | E10 | CPT25 | H-Area |
| 38 | E05 | CPT18 | H-Area | 78 | E10 | CPT26 | H-Area |
| 39 | E05 | CPT25 | CFD | 79 | E10 | CPT29 | H-Area |
| 40 | E05 | CPT29 | CFD | 80 | E10 | CPT30 | CFD |

Table 9.5-1 Free field analysis: case combinations.

| Deep Soil Profile | Case | Earthquake No. | | | | | | | | | |
|---|---|---|---|---|---|---|---|---|---|---|---|
| | | E01 | E02 | E03 | E04 | E05 | E06 | E07 | E08 | E09 | E10 |
| H-Area | C01-D1 | 0.0079 | 0.0105 | 0.0181 | 0.0278 | 0.0442 | 0.0713 | 0.0860 | 0.1190 | 0.1928 | 0.3401 |
| | C01-D2 | 0.0067 | 0.0099 | 0.0175 | 0.0273 | 0.0441 | 0.0735 | 0.0840 | 0.1198 | 0.1926 | 0.3419 |
| | C02-D1 | 0.0063 | 0.0127 | 0.0333 | 0.0482 | 0.0519 | 0.0605 | 0.1203 | 0.1526 | 0.1859 | 0.2897 |
| | C02-D2 | 0.0059 | 0.0122 | 0.0293 | 0.0449 | 0.0500 | 0.0634 | 0.1277 | 0.1486 | 0.1820 | 0.3005 |
| | C03-D1 | 0.0097 | 0.0115 | 0.0252 | 0.0281 | 0.0723 | 0.0894 | 0.1617 | 0.1577 | 0.2226 | 0.1994 |
| | C03-D2 | 0.0085 | 0.0110 | 0.0230 | 0.0299 | 0.0708 | 0.0888 | 0.1466 | 0.1444 | 0.2128 | 0.2094 |
| | C04-D1 | 0.0060 | 0.0115 | 0.0193 | 0.0266 | 0.0640 | 0.0616 | 0.0983 | 0.1365 | 0.1975 | 0.2711 |
| | C04-D2 | 0.0063 | 0.0116 | 0.0177 | 0.0269 | 0.0588 | 0.0694 | 0.0988 | 0.1314 | 0.1920 | 0.2673 |
| CFD | C01-D1 | 0.0075 | 0.0111 | 0.0192 | 0.0261 | 0.0468 | 0.0679 | 0.1129 | 0.1417 | 0.1462 | 0.2510 |
| | C01-D2 | 0.0061 | 0.0111 | 0.0172 | 0.0263 | 0.0435 | 0.0689 | 0.1140 | 0.1328 | 0.1487 | 0.2586 |
| | C02-D1 | 0.0123 | 0.0158 | 0.0211 | 0.0277 | 0.0469 | 0.0909 | 0.1110 | 0.2318 | 0.3287 | 0.2750 |
| | C02-D2 | 0.0113 | 0.0166 | 0.0203 | 0.0266 | 0.0454 | 0.0770 | 0.1133 | 0.2265 | 0.3125 | 0.2756 |
| | C03-D1 | 0.0091 | 0.0127 | 0.0291 | 0.0383 | 0.0800 | 0.0970 | 0.1442 | 0.1942 | 0.2205 | 0.2494 |
| | C03-D2 | 0.0081 | 0.0116 | 0.0297 | 0.0357 | 0.0790 | 0.0893 | 0.1377 | 0.1968 | 0.2002 | 0.2528 |
| | C04-D1 | 0.0070 | 0.0105 | 0.0170 | 0.0472 | 0.0513 | 0.0700 | 0.1082 | 0.1211 | 0.1757 | 0.2043 |
| | C04-D2 | 0.0063 | 0.0103 | 0.0154 | 0.0446 | 0.0530 | 0.0635 | 0.1109 | 0.1194 | 0.1742 | 0.2062 |
| No. of Samples, N | | 16 | 16 | 16 | 16 | 16 | 16 | 16 | 16 | 16 | 16 |
| Mean (Normal) | | 0.0078 | 0.0119 | 0.0220 | 0.0333 | 0.0564 | 0.0752 | 0.1172 | 0.1546 | 0.2053 | 0.2620 |
| S.D. (Normal) | | 0.0019 | 0.0018 | 0.0054 | 0.0082 | 0.0124 | 0.0116 | 0.0210 | 0.0362 | 0.0483 | 0.0424 |
| Mean.(Log Normal) | | -4.8782 | -4.4403 | -3.8436 | -3.4312 | -2.8983 | -2.5998 | -2.1596 | -1.8913 | -1.6070 | -1.3524 |
| S.D.(Log Normal) | | 0.2230 | 0.1380 | 0.2328 | 0.2308 | 0.2086 | 0.1508 | 0.1784 | 0.2165 | 0.2109 | 0.1623 |

Note: The mean and S.D. values for log-normal distributions are calculated with respect to natural log values.

Table 9.5-2 Effective Shear Stress Ratio CSR = $0.65^{*}(\tau_{xy})_{max}/\sigma'_{y}$From SHAKE Analysis Tobacco Road 3/4

# FIGURES

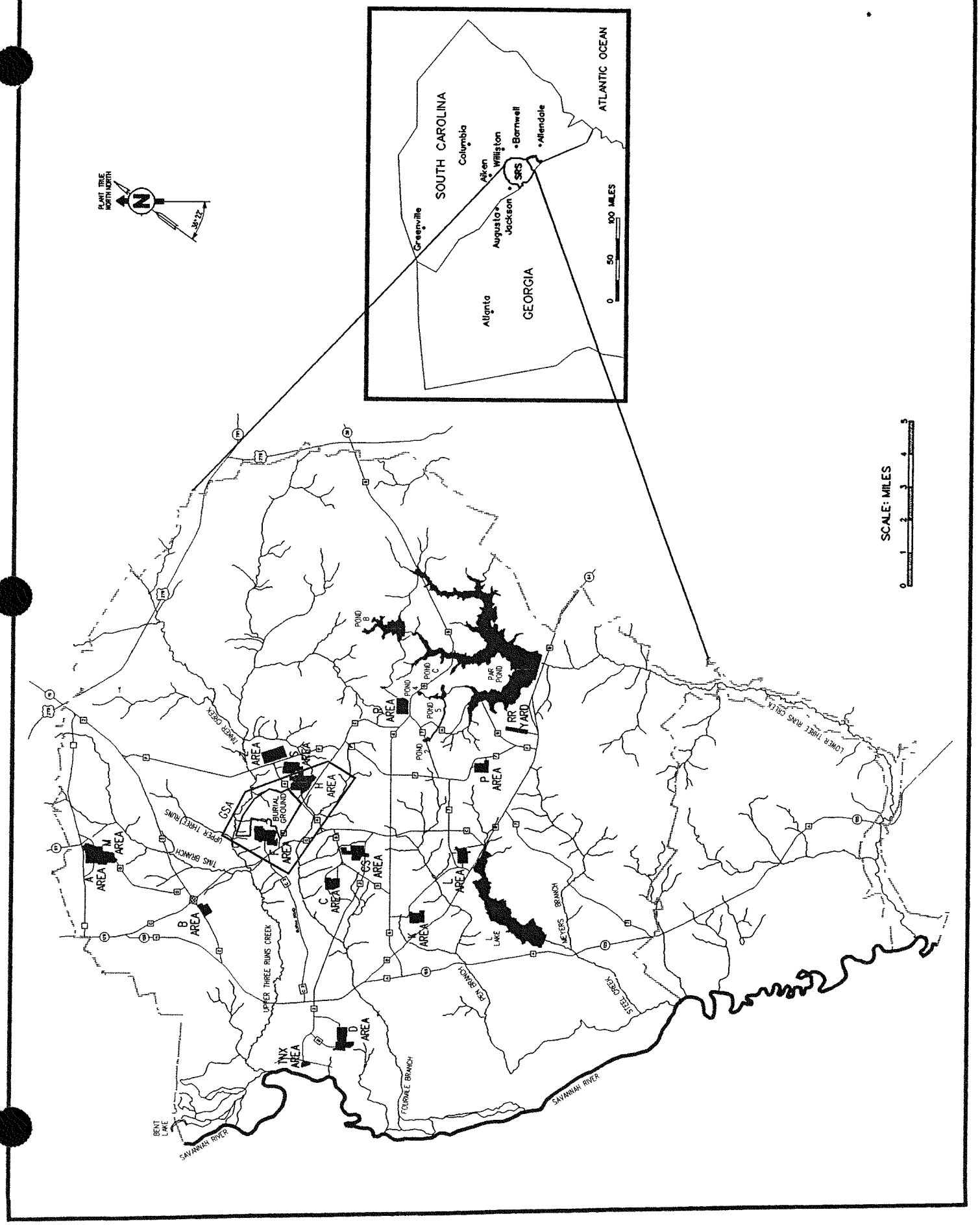


Figure 1.0-1 Savannah River Site Map.

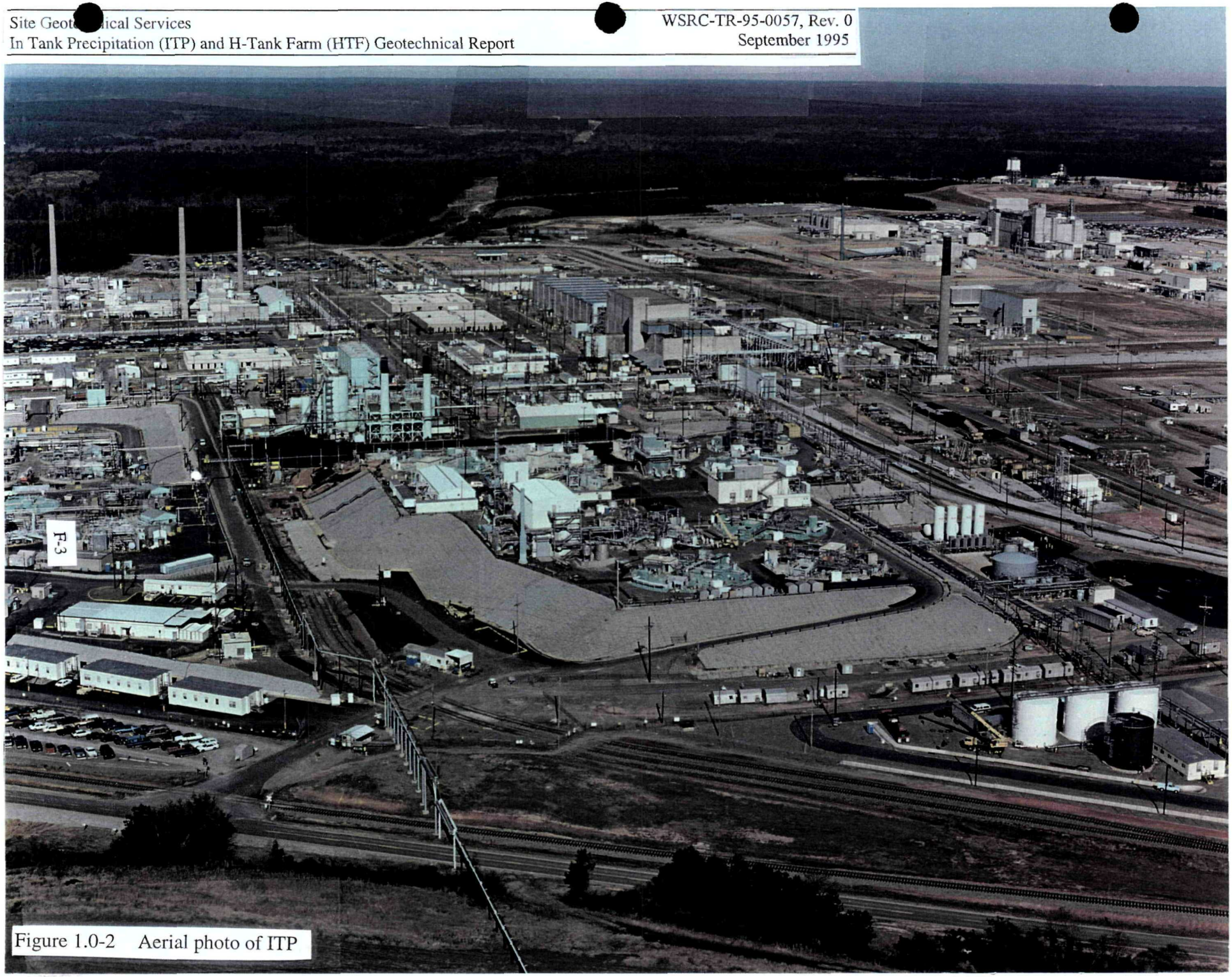

F-3

Figure 1.0-2 Aerial photo of ITP





Figure 1.0-3 Aerial photo of HTF

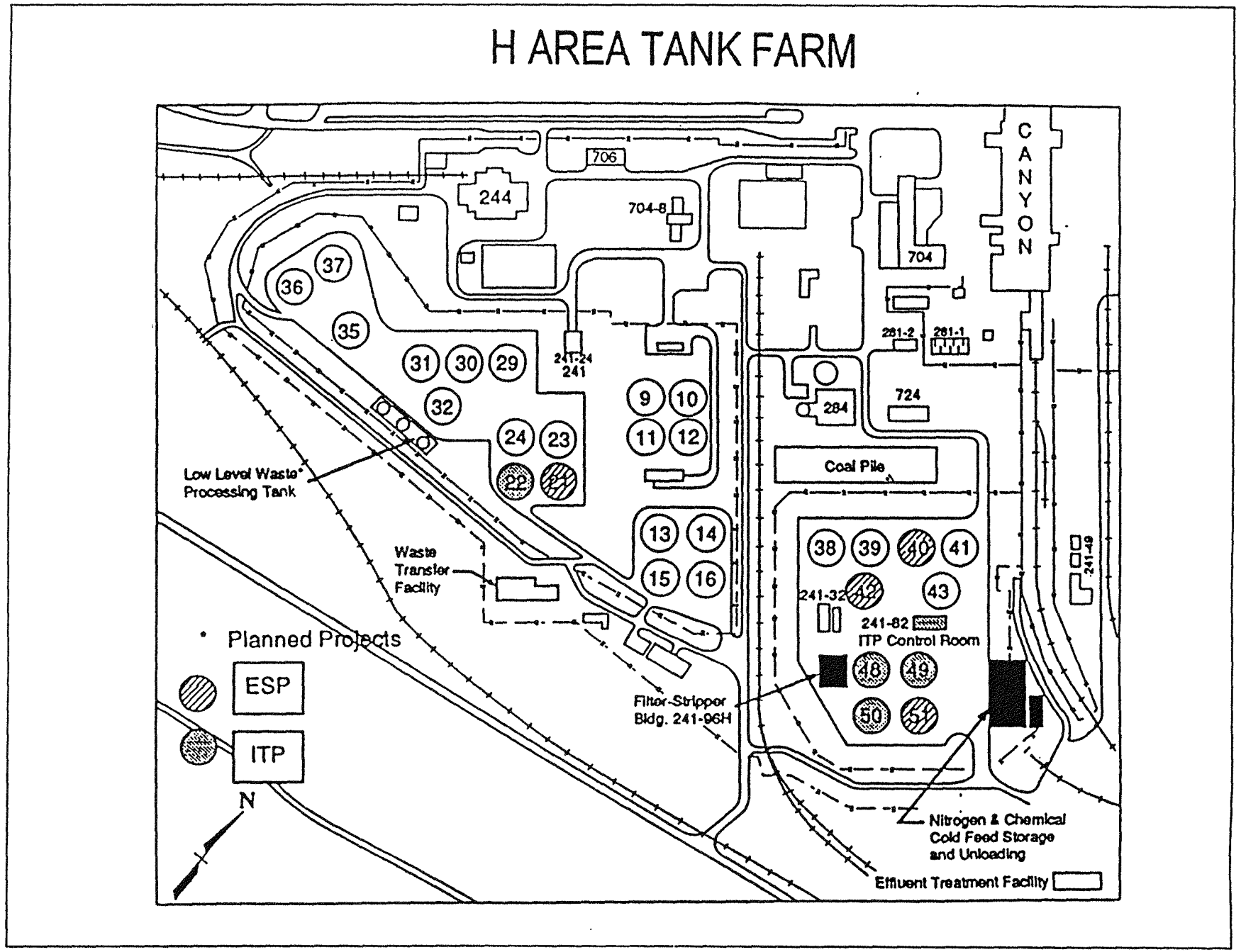


Figure 1.2-1 H-Area Tank Farm - plan layout.

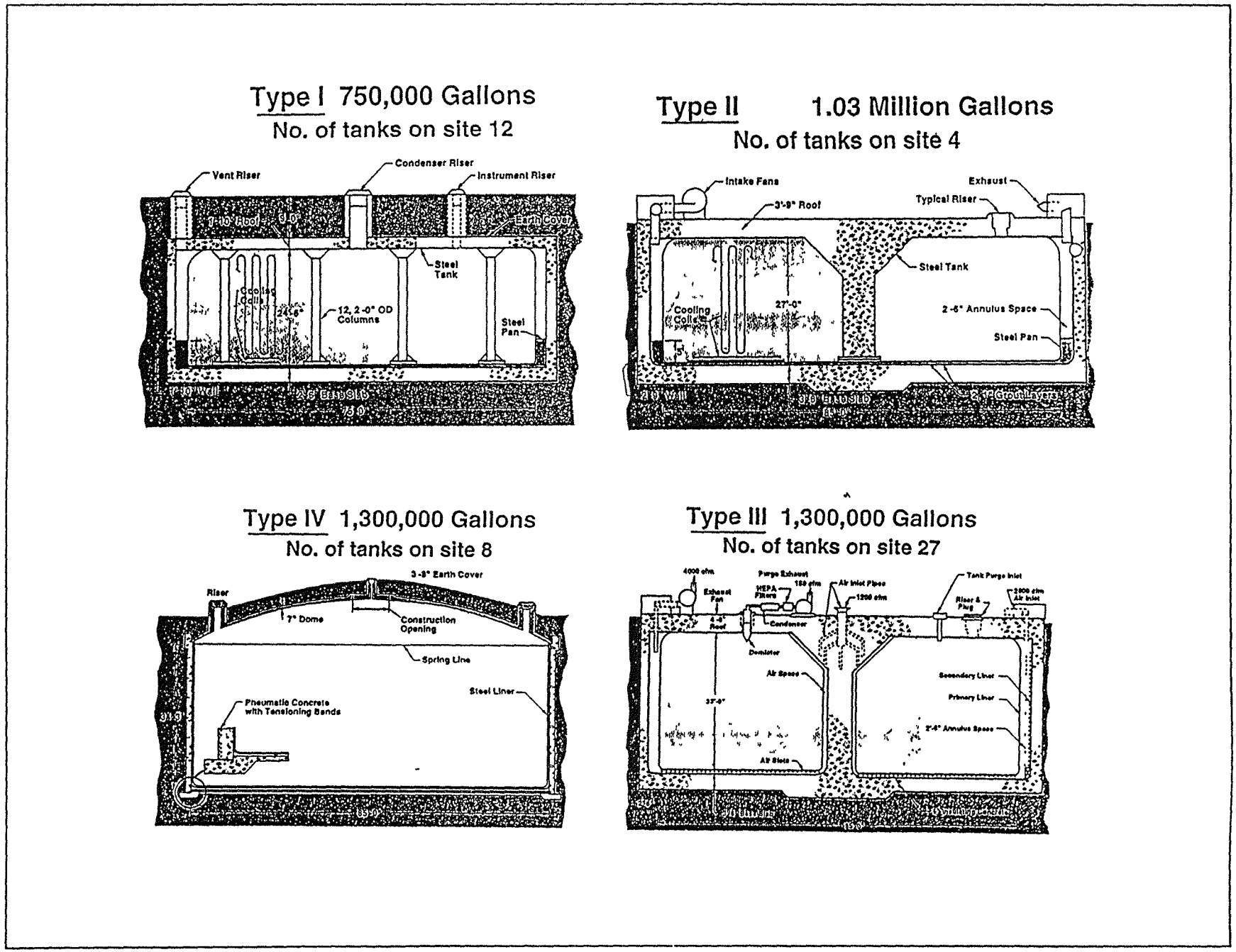


Figure 1.2-2 H-Area Tank Farm - tank details.

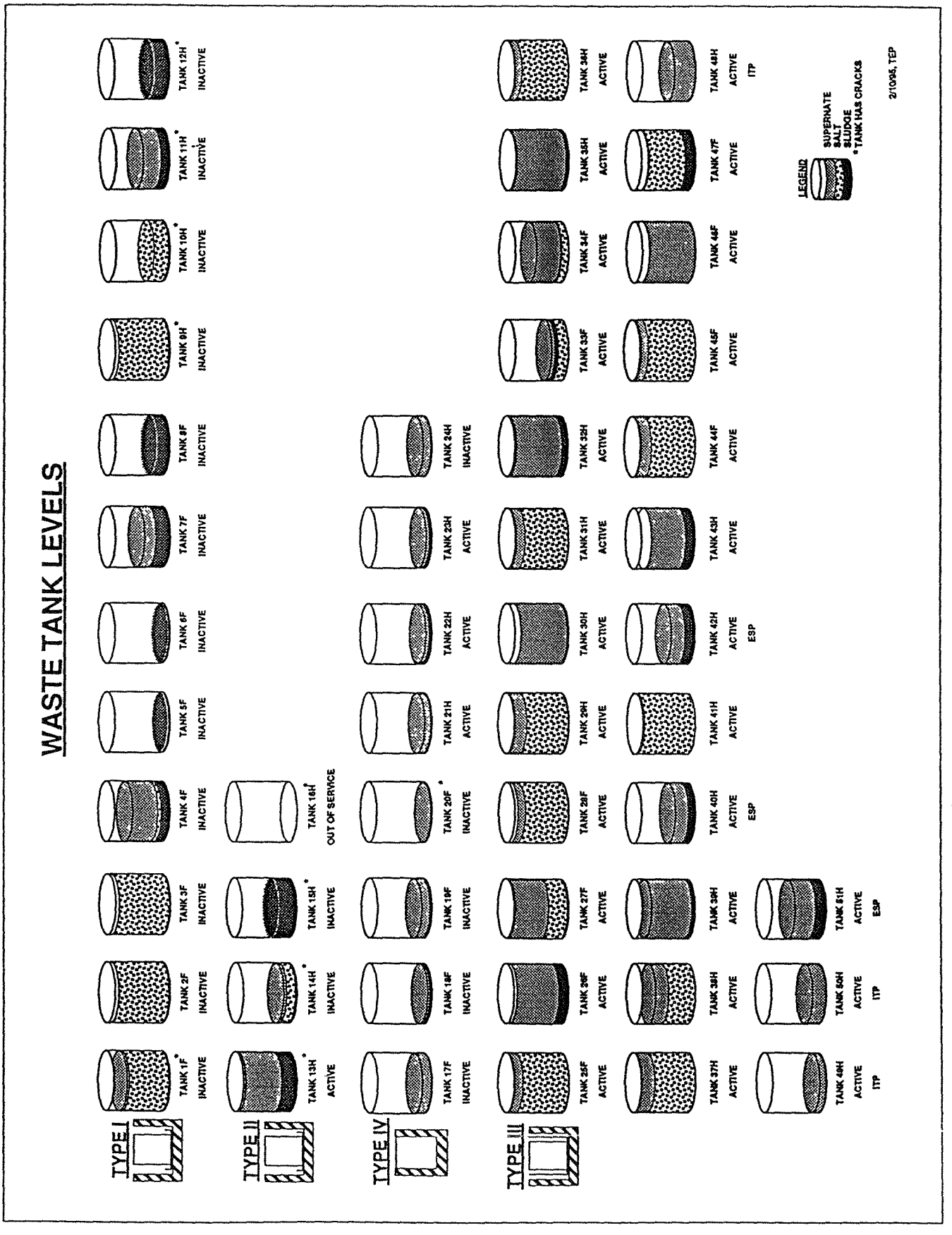


Figure 1.2-3 Distribution of waste in tanks.

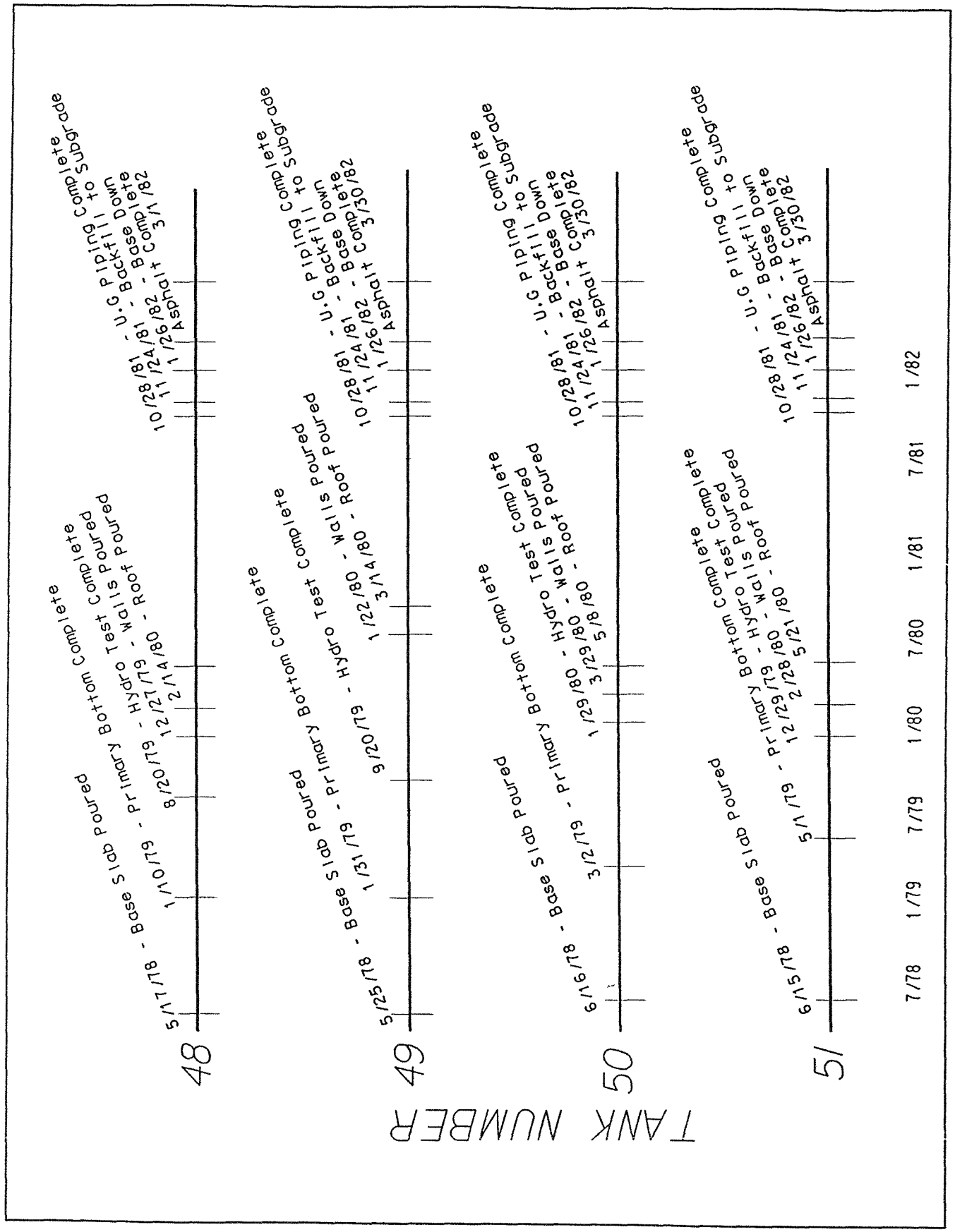


Figure 1.2-4 Timeline for construction of ITP tanks.

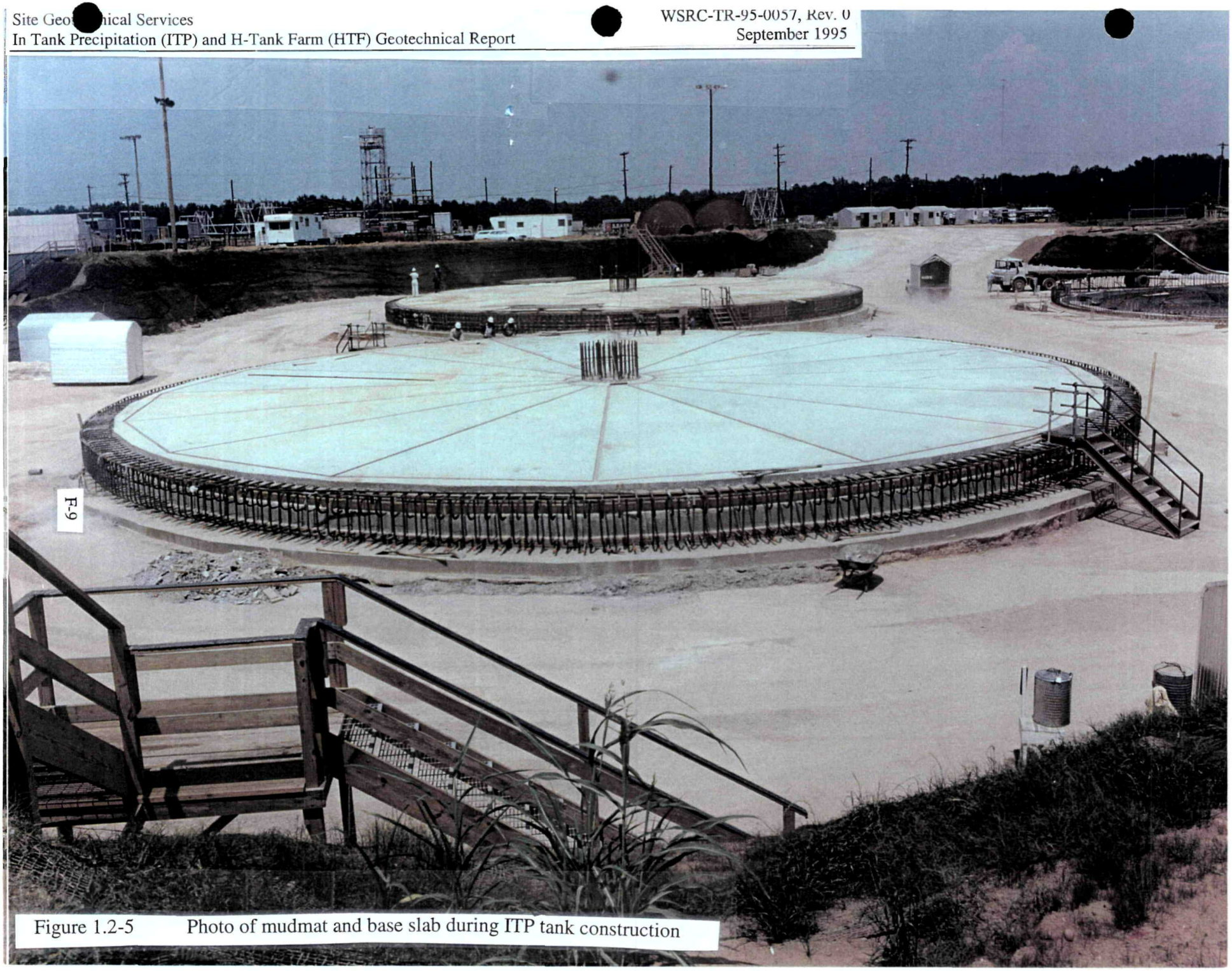



Figure 1.2-5 Photo of mudmat and base slab during ITP tank construction




Figure 1.2-6 Photo of steel liners of ITP tanks during construction

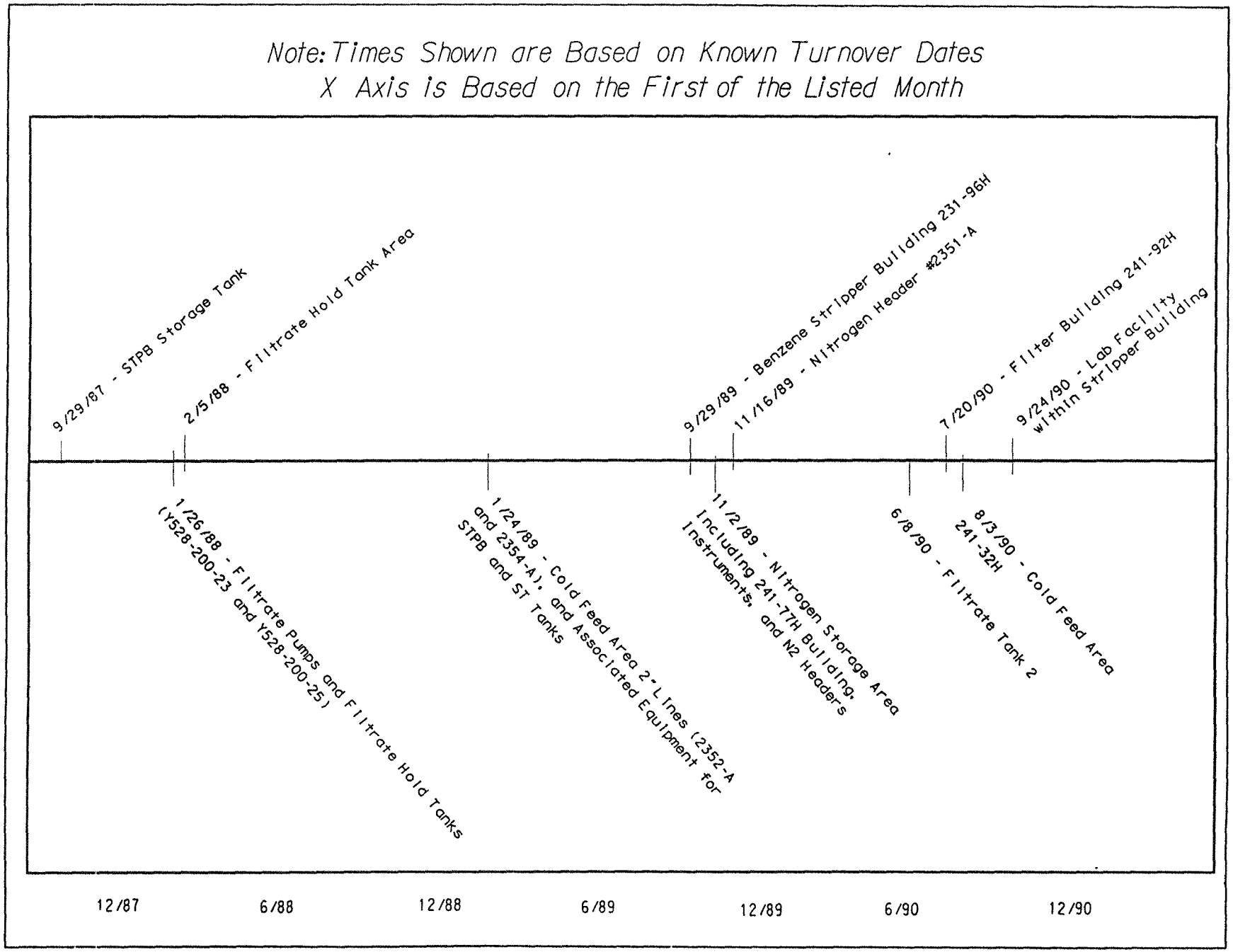


Figure 1.2-7 Timeline for construction of ITP buildings and related facilities.

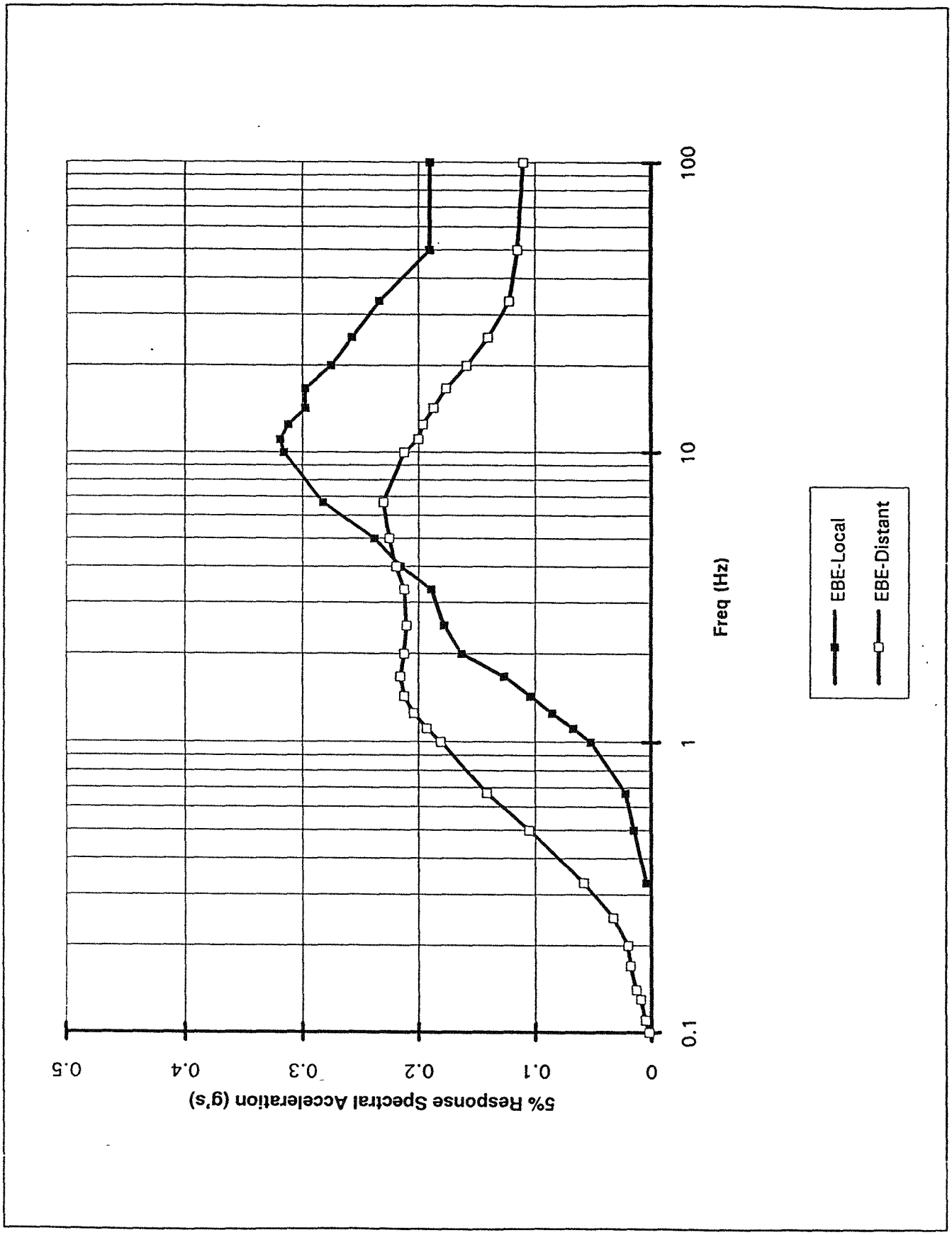


Figure 2.1-1 Comparison of the smoothed five percent EBE local and distant event spectra.

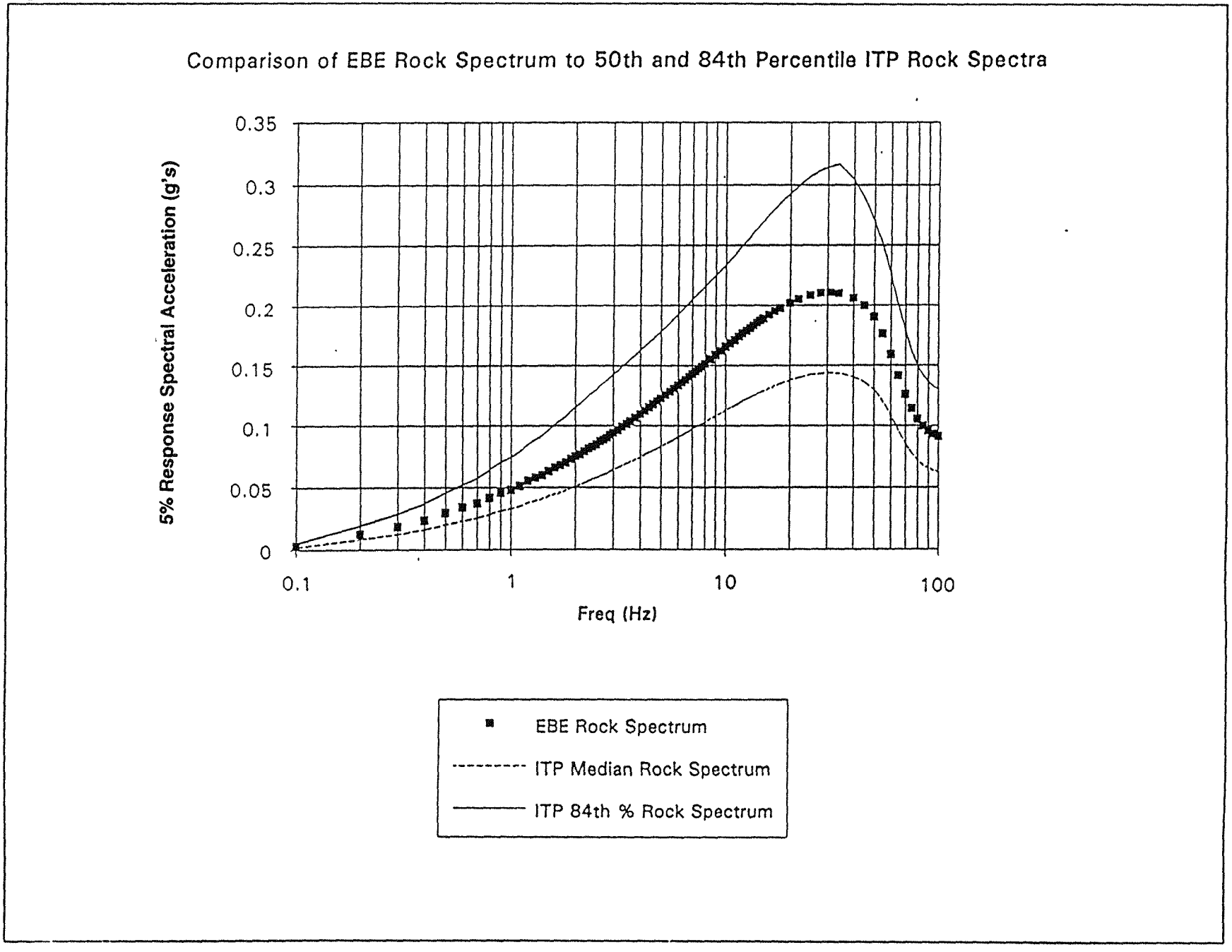


Figure 2.3-1 ITP/H-area median and 84th percentile rock spectra.

| Age | | Group | Formation | | Lithology |
|---|---|---|---|---|---|
| Tertiary | Miocene? | Barnwell Group | "Upland Unit" | | Clayey, silty sands, conglomerates, pebbly sands, and clays, clay clasts common |
| | Late Eocene | | Tobacco Road Sand | | Red, purple, and orange, poorly to well-sorted sand and clayey sand with abundant clay laminae |
| | | | Dry Branch Formation | Irwinton Sand Member, Griffins Landing Member | Tan, yellow, and orange, poorly to well-sorted sand with tan and gray layers near base; calcareous sands and clays and limestone in lower part downdip |
| | | | Clinchfield Formation | | Bimoldic limestone, calcareous sand and clay, and tan and yellow sand |
| | Middle Eocene | Orangeburg Group | Santee Limestone | Utley Tinker Blue Bluff Warley Hill Member | Micriitic, calcarenitic, shelly limestone, and calcareous sands; interbedded yellow and tan sands and clays; green clay and glauconitic sand near base |
| | Early Eocene | | Congaree Formation | | Yellow, orange, tan, and greenish-gray, fine to coarse, well-sorted sand, thin clay laminae common |
| | | | Fourmile Formation | | Tan, yellow, fine to medium, moderately sorted quartz sand with clay layers |
| | Paleocene | Black Mingo Group | Snapp Formation | | Light gray, silty sand interbedded with gray clay |
| | | | Lang Syne Formation | | Light gray, tan medium to coarse quartz sand interbedded with kaolinitic clay |
| | | | Ellenton Member, Sawdust Landing Formation | | Black and gray, lignitic, pyritic sand and interbedded clays with silt and sand laminae |
| Late Cretaceous | Maestrichtian | Lumbee Group | Steel Creek Member, Peedee Formation | | Gray and tan, slightly to moderately clayey sand; gray red, purple, and orange clays common in upper part |
| | Campanian | | Black Creek Formation | | Tan and light to dark gray sand; dark clays common in middle and oxidized clays at top |
| | Santonian | | Middendorf Formation | | Tan and gray, slightly to moderately clayey sand; gray red, and purple clays near top |
| | | | Cape Fear Formation | | Gray, clayey sand with some conglomerates, and sandy clay; moderately to well indurated |
| Late Triassic | | Newark Supergroup | | | Boulder conglomerate, red, arkosic, poorly sorted sandstone and red shale |
| Paleozoic and Cryptozoic (?) | | "crystallines" | | | Biotite gneiss, mica schist, amphibolite, chlorite schist, and granitoid rocks |

Figure 2.5-1 SRS general stratigraphic chart.

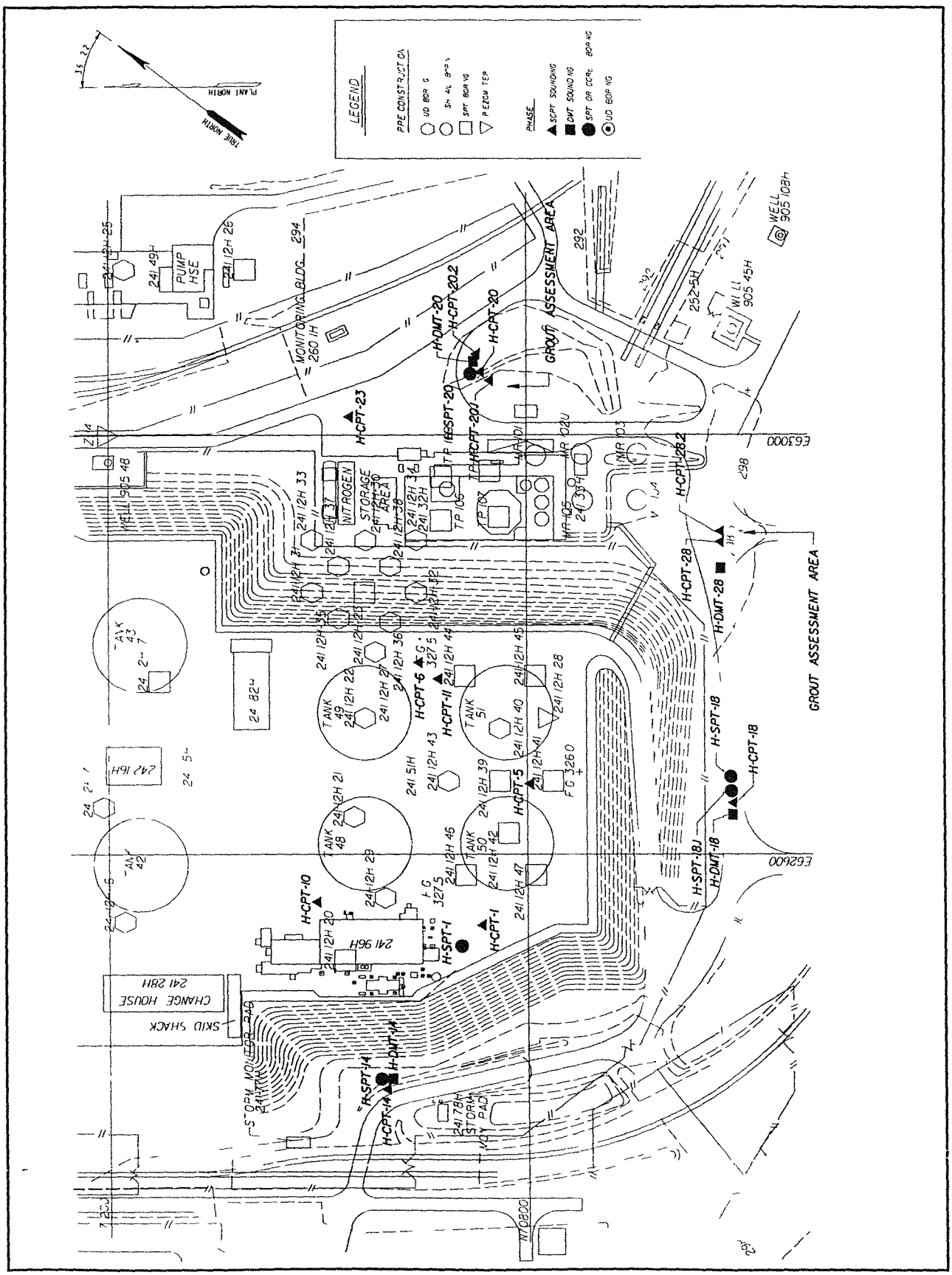


Figure 3.3-1 In-Tank Precipitation area: Phase 1 field investigation.

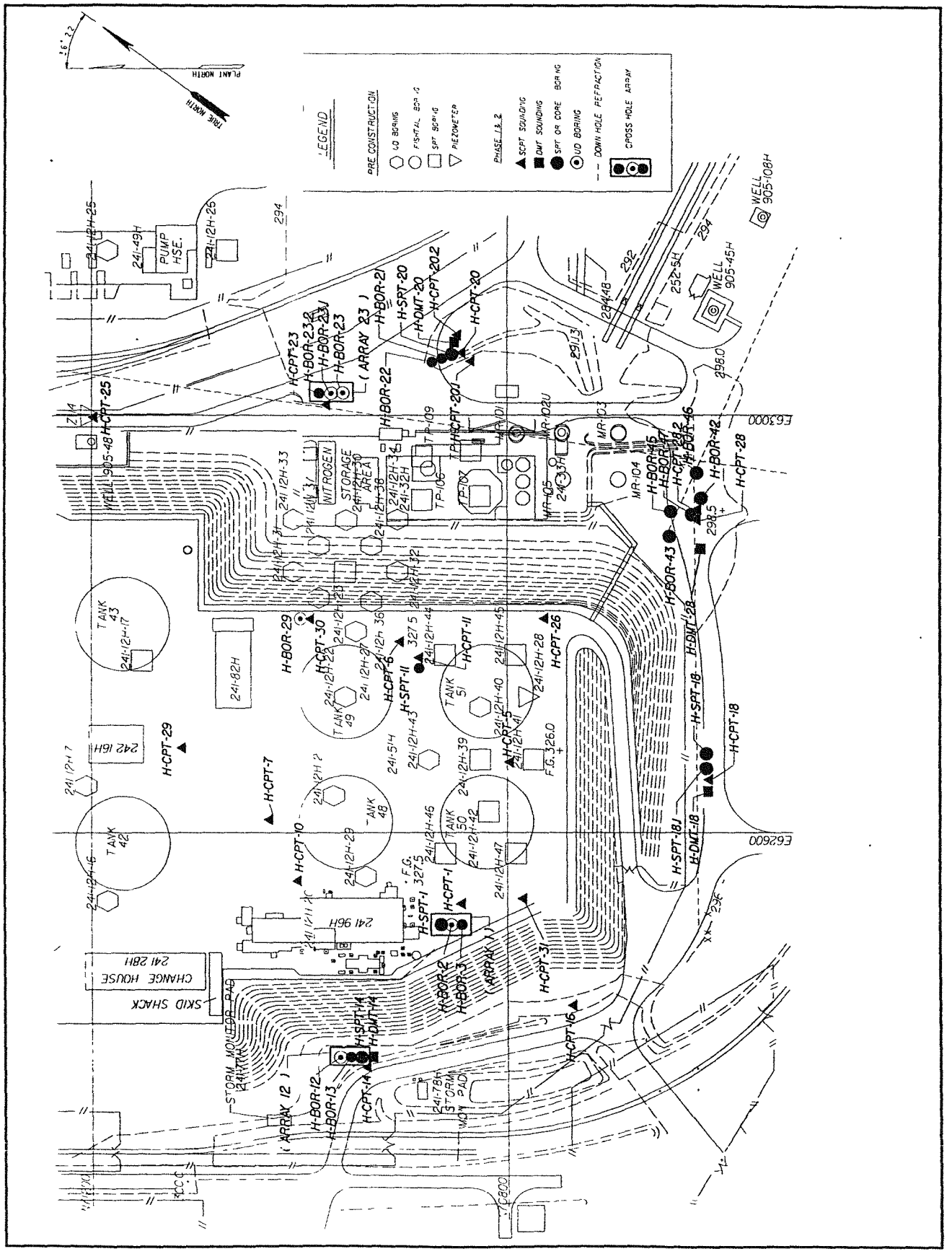


Figure 3.3-2 In-Tank Precipitation area: Phases 1 and 2 field investigations.

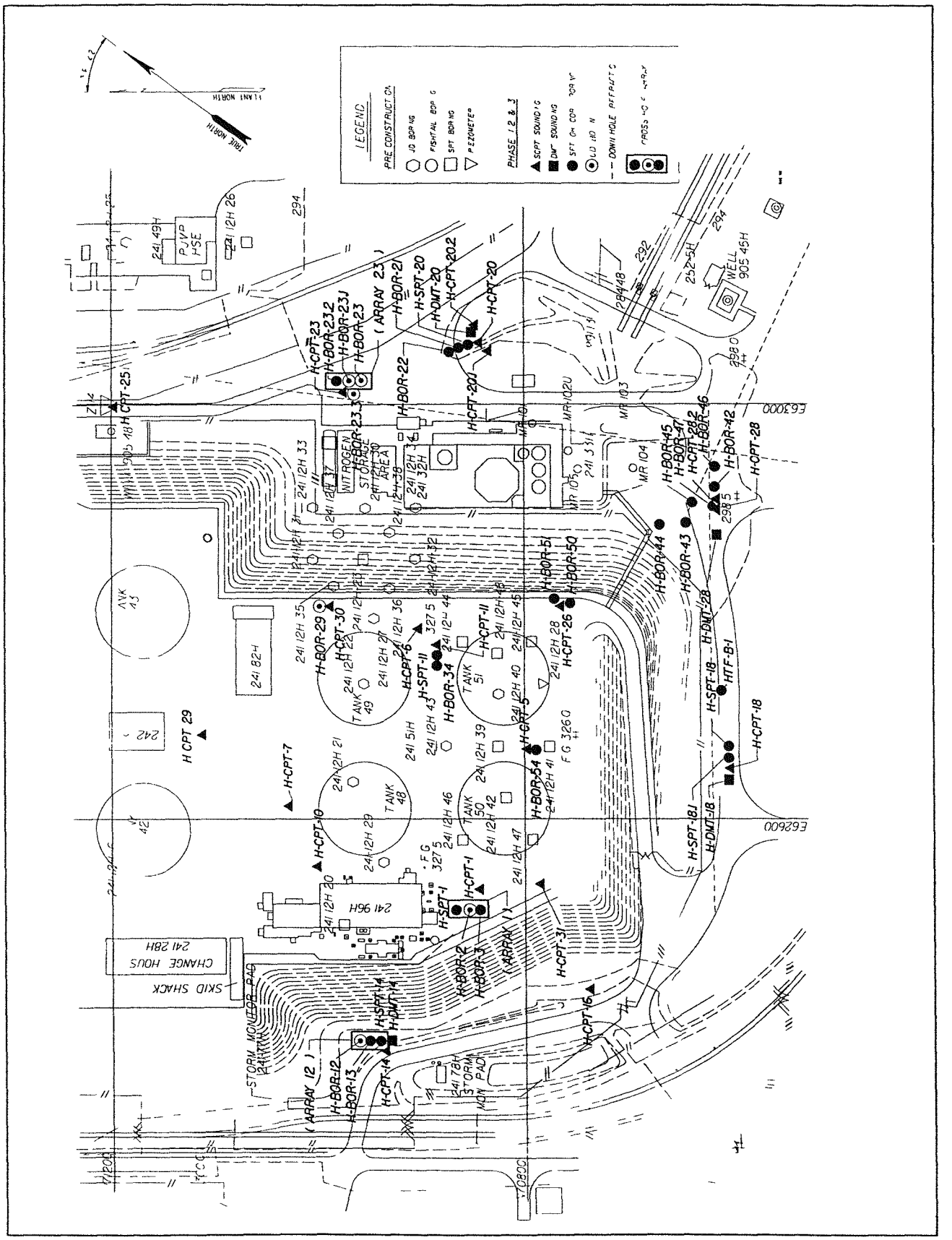


Figure 3.3-3 In-Tank Precipitation area: Phases 1, 2, and 3 field investigations.

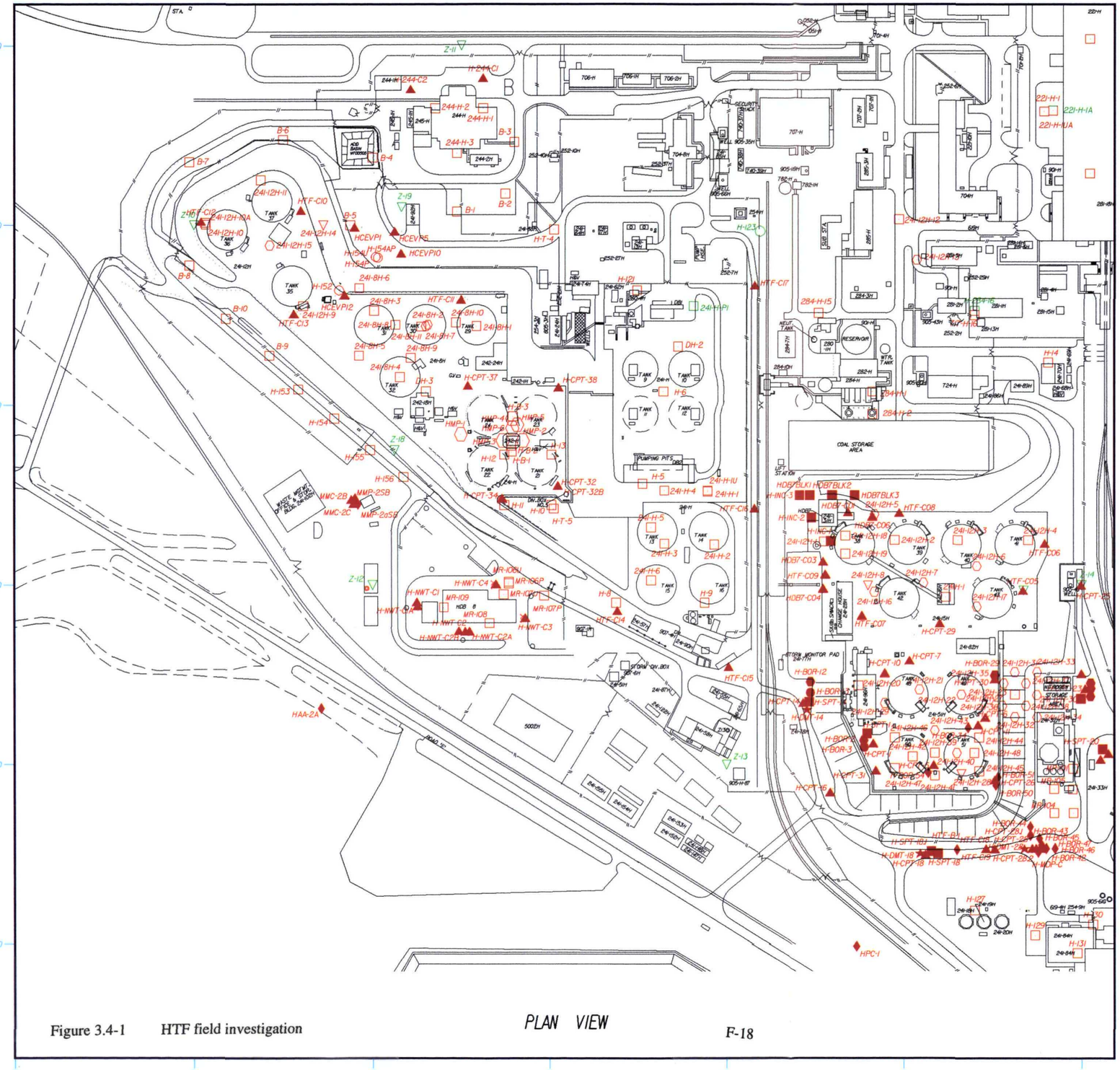


Figure 3.4-1 HTF field investigation

PLAN VIEW



LEGEND

PRE-1990

- SPLIT-SPOON BORING
- UNDISTURBED BORING
- CONE PENETROMETER
- PIEZOMETER
- FISHTAIL BORING
- SPLIT-SPOON BORING (BORING LOG UNACCOUNTED)
- UNDISTURBED BORING (BORING LOG UNACCOUNTED)
- FISHTAIL BORING (BORING LOG UNACCOUNTED)
- PIEZOMETER (BORING LOG UNACCOUNTED)

POST-1990

- SPLIT-SPOON BORING
- UNDISTURBED BORING
- CONE PENETROMETER
- FISHTAIL BORING
- CORE BORING
- DILATOMETER

NOTES

1. BORING SYMBOLS AREA SELECTED BASED ON EXISTING INFORMATION PERTAINING TO SAMPLING.
2. GROUT HOLES WHICH WERE SAMPLED ARE REPORTED ON THIS DRAWING BASED ON THE SAMPLE TECHNIQUE.

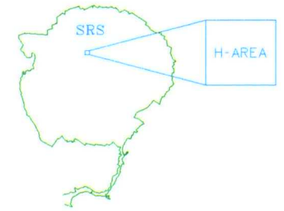


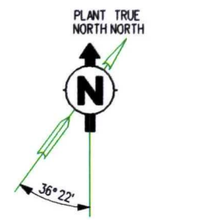





| DWG NO. | REV. NO. | REV. DATE | AREA |
|---|---|---|---|
| G03220 | 0 | 9-27-95 | H-AREA |

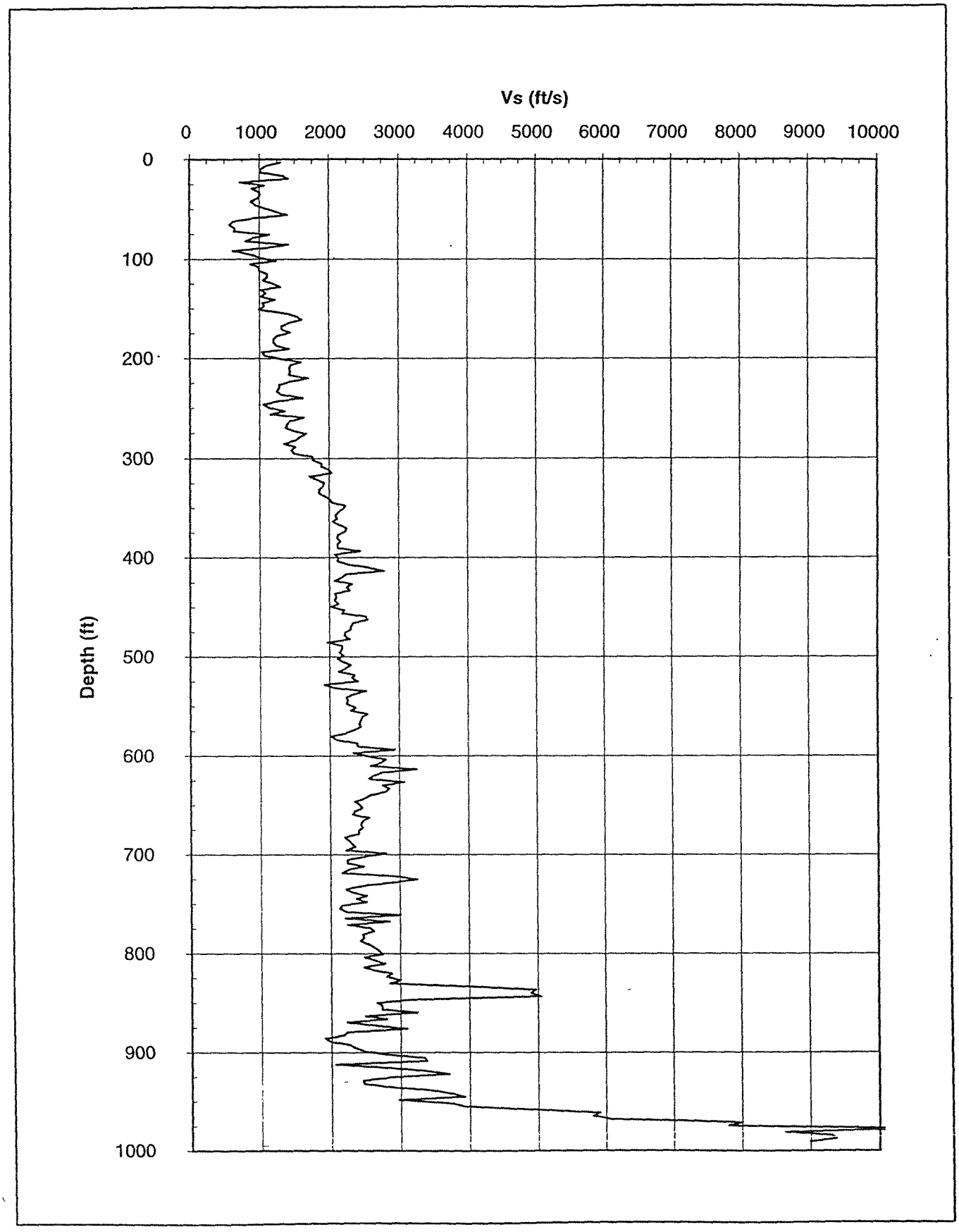


Figure 3.4-2 Shear wave velocities from H-Area, OYO™ logged, deep borehole MMP-2-SB.

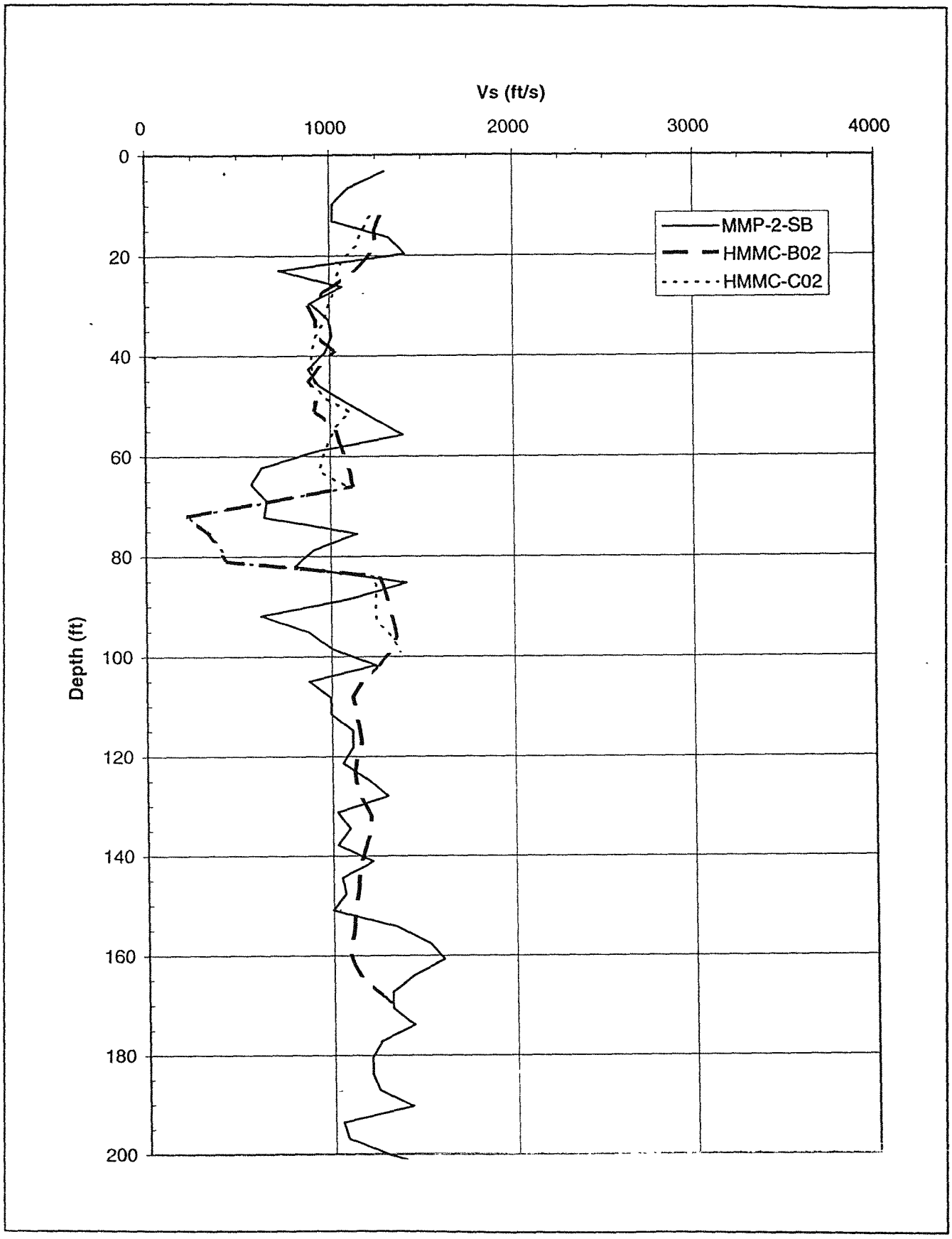


Figure 3.4-3 Shear wave velocity comparison of OYO™ logged hole, MMP-2-SB, with seismic cone penetrometer measurements from HMMC-B02 and HMMC-C02.

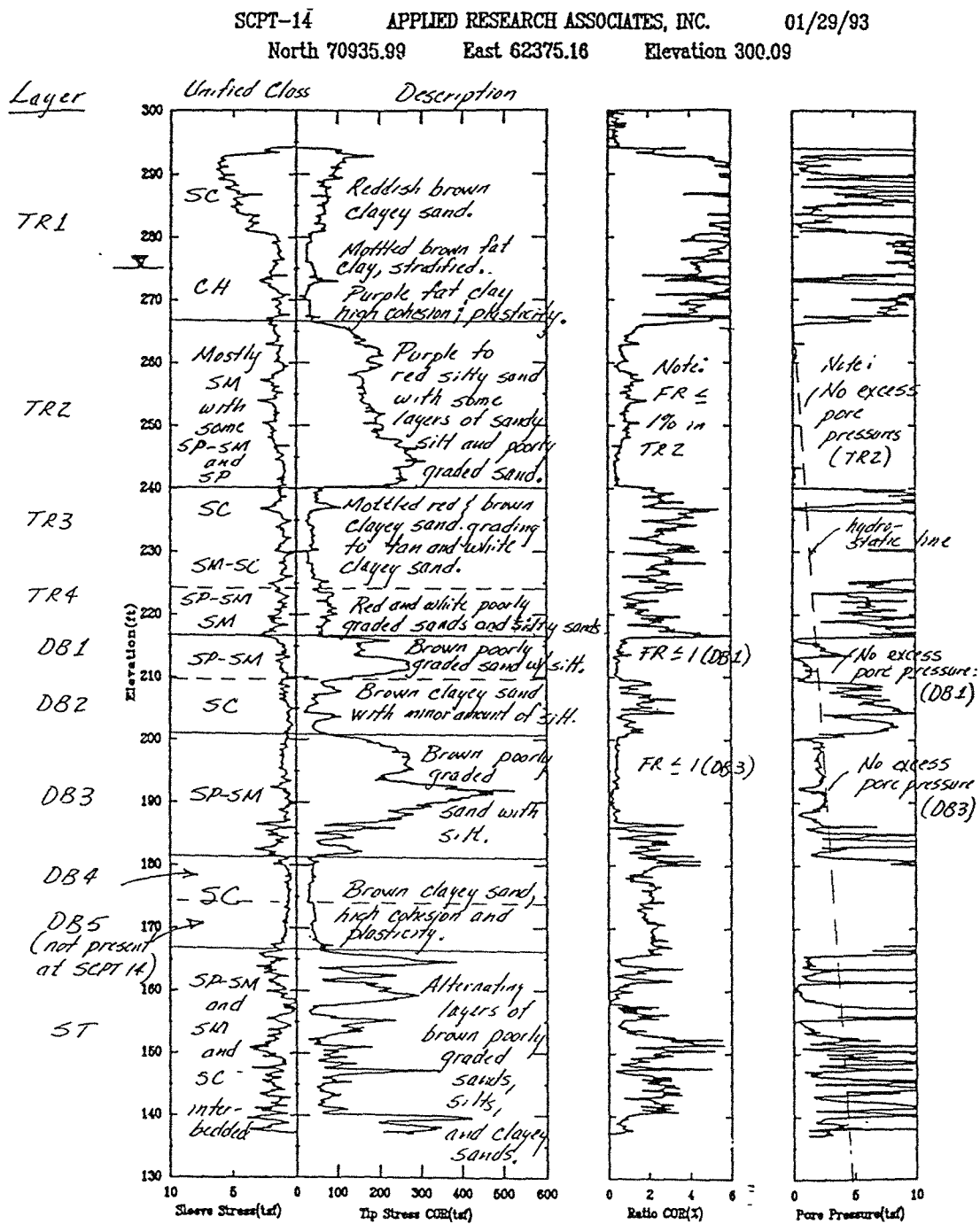


Figure 5.0-1 Typical CPT log with stratigraphy.

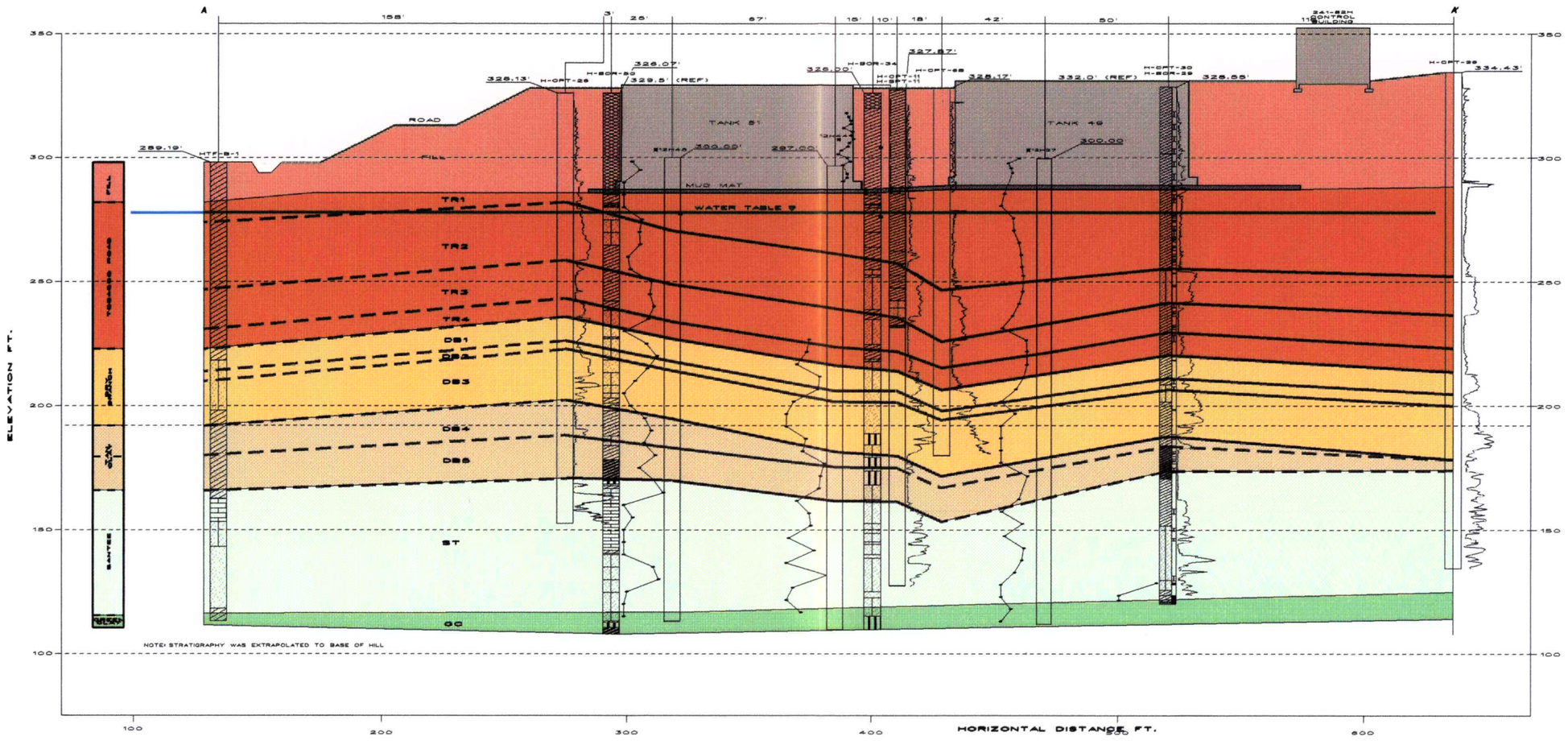


# ITP GEOTECHNICAL PROFILE N - S SECTION A - A'

**NOTES:**

1. THIS SECTION REPRESENTS AN INTERPRETATION OF THE MATERIALS UNDERLYING THE ITP FACILITY.
2. THE PROFILE IS A STRAIGHT LINE SECTION WITH DATA POINTS PROJECTED PERPENDICULAR.
3. THIS SECTION IS SHOWN AT A TRUE SCALE (H = V).
4. THIS SECTION DOES NOT SHOW ALL ABOVE AND BELOW GROUND STRUCTURES.
5. PRE-CONSTRUCTION BORINGS PRESENTED.
6. FACILITIES SHOWN ON THIS DRAWING ARE INTENDED TO PROVIDE RELATIVE LOCATION AND MAY NOT BE EXACTLY CORRECT IN DETAIL OR SHAPE.
7. SCALES:

SPT N-VALUES: 50 25 0 blows/ft
TIP RESISTANCE: 0 300 600 tons/sq ft

**LEGEND**

**SOIL DESCRIPTION**

- CLAYEY SAND (SC)
- SILTY SAND / NARROWLY GRADED SAND WITH SILT (SM/SP-SM)
- FAT CLAY (CH)
- SILTY SAND WITH GRAVEL
- NARROWLY GRADED SAND (SP)
- SILT (ML)
- SILT WITH SAND, SANDY SILT (ML)
- SANDY LEAN CLAY (CL)
- WELL GRADED SAND WITH CLAY (SW)
- SILTY CLAYEY SAND
- POORLY GRADED SAND WITH CLAY (SP-SC)
- CLAYEY SAND TO SANDY CLAY
- LIMESTONE (LS)
- GROUT
- CALCAREOUS SANDSTONE WITH POORLY GRADED SAND
- LIMESTONE IN SILT MATRIX

**SAMPLE TYPE**

- SHELBY TUBE
- SP — STATIONARY POSITION
- SPLIT SPOON
- PITCHER BARREL
- INTERPRETED WATER TABLE
- MEASURED BORING FLUID LEVEL
- PRE-CONSTRUCTION BORING

0 25 50 ft
SCALE

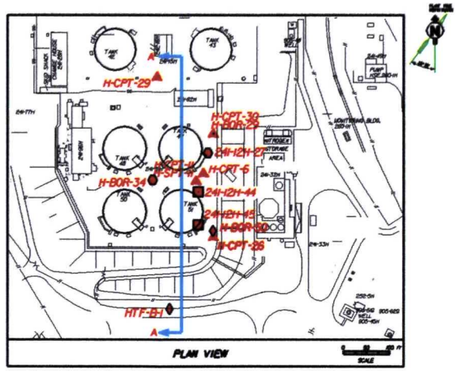


| DWG. NO. | REV. NO. | REV. DATE | DIV. |
|---|---|---|---|
| CCTH7817 | 1 | 2-23-95 | H-AREA |

Figure 5.1-1 Subsurface profile A-A'.

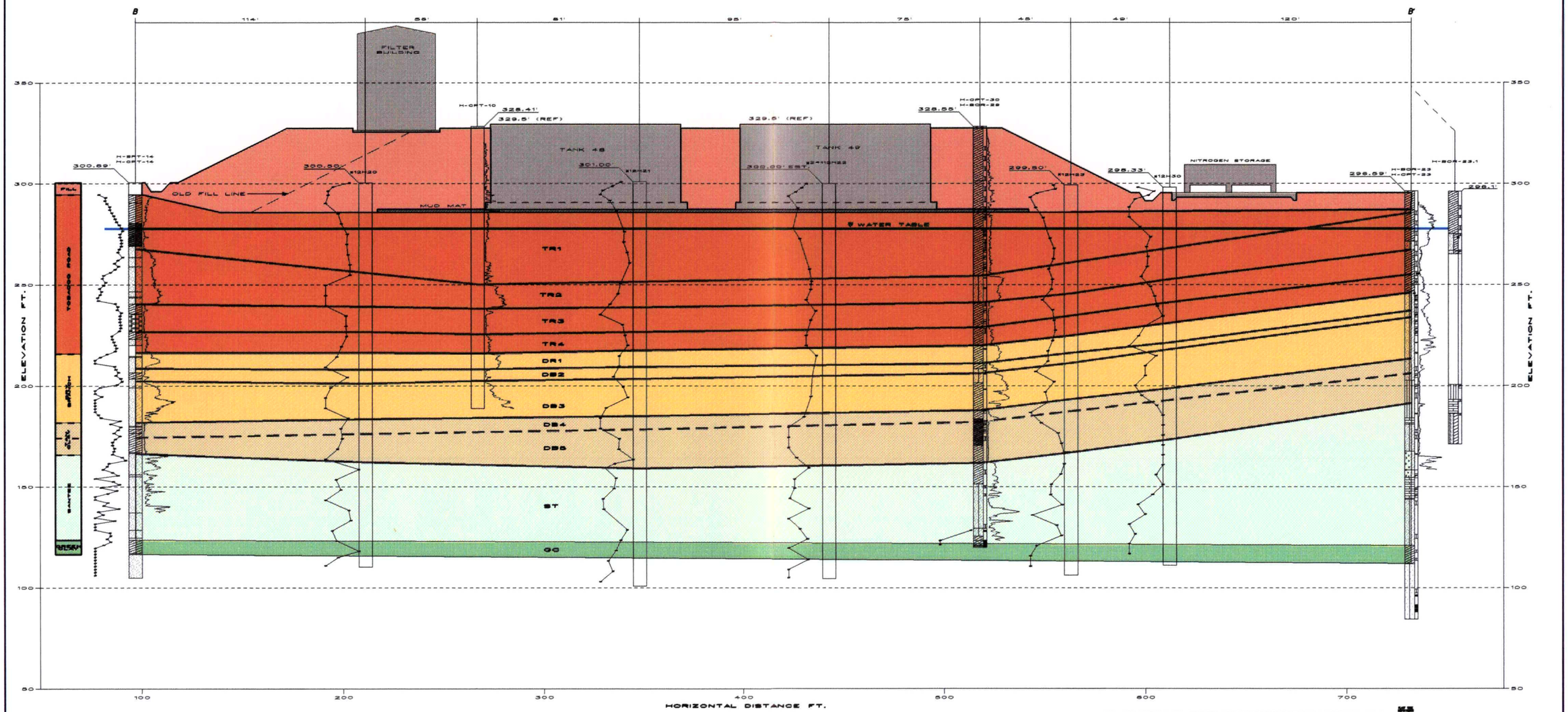


# ITP GEOTECHNICAL PROFILE E - W SECTION B-B'

**NOTES:**

1. THIS SECTION REPRESENTS AN INTERPRETATION OF THE MATERIALS UNDERLYING THE ITP FACILITY.
2. THE PROFILE IS A STRAIGHT LINE SECTION WITH DATA POINTS PROJECTED PERPENDICULAR.
3. THIS SECTION IS SHOWN AT A TRUE SCALE (H = V).
4. THIS SECTION DOES NOT SHOW ALL ABOVE AND BELOW GROUND STRUCTURES.
5. PRE-CONSTRUCTION BORINGS PRESENTED.
6. FACILITIES SHOWN ON THIS DRAWING ARE INTENDED TO PROVIDE RELATIVE LOCATION AND MAY NOT BE EXACTLY CORRECT IN DETAIL OR SHAPE.
7. SCALES:

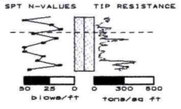


**LEGEND**

SOIL DESCRIPTION
- CLAYEY SAND (SC)
- SILTY SAND / NARROWLY GRADED SAND WITH SILT (SM/SP-SM)
- FAT CLAY (CH)
- SILTY SAND WITH GRAVEL
- NARROWLY GRADED SAND (SP)
- SILT (ML)
- SILT WITH SAND, SANDY SILT (ML)
- SANDY LEAN CLAY (CL)
- WELL GRADED SAND (SW)
- SILTY CLAYEY SAND
- POORLY GRADED SAND WITH CLAY (SP-SC)
- CLAYEY SAND TO SANDY CLAY
- LIMESTONE (LS)
- GROUT
- CALCAREOUS SANDSTONE WITH POORLY GRADED SAND
- LIMESTONE IN SILT MATRIX

SAMPLE TYPE
- SHELBY TUBE
- STATIONARY POSITION
- SPLIT SPOON
- PITCHER BARREL

- INTERPRETED WATER TABLE
- MEASURED BORING FLUID LEVEL
- PRE-CONSTRUCTION BORING

0 25 50 ft
SCALE

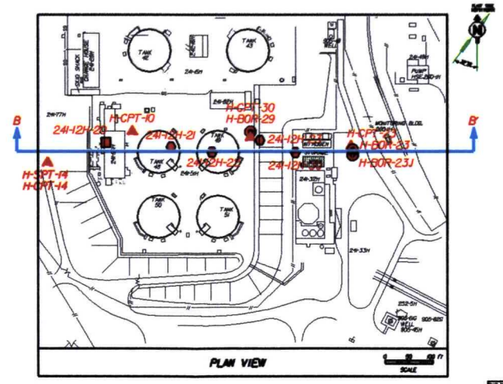


Figure 5.1-2 Subsurface profile B-B'.

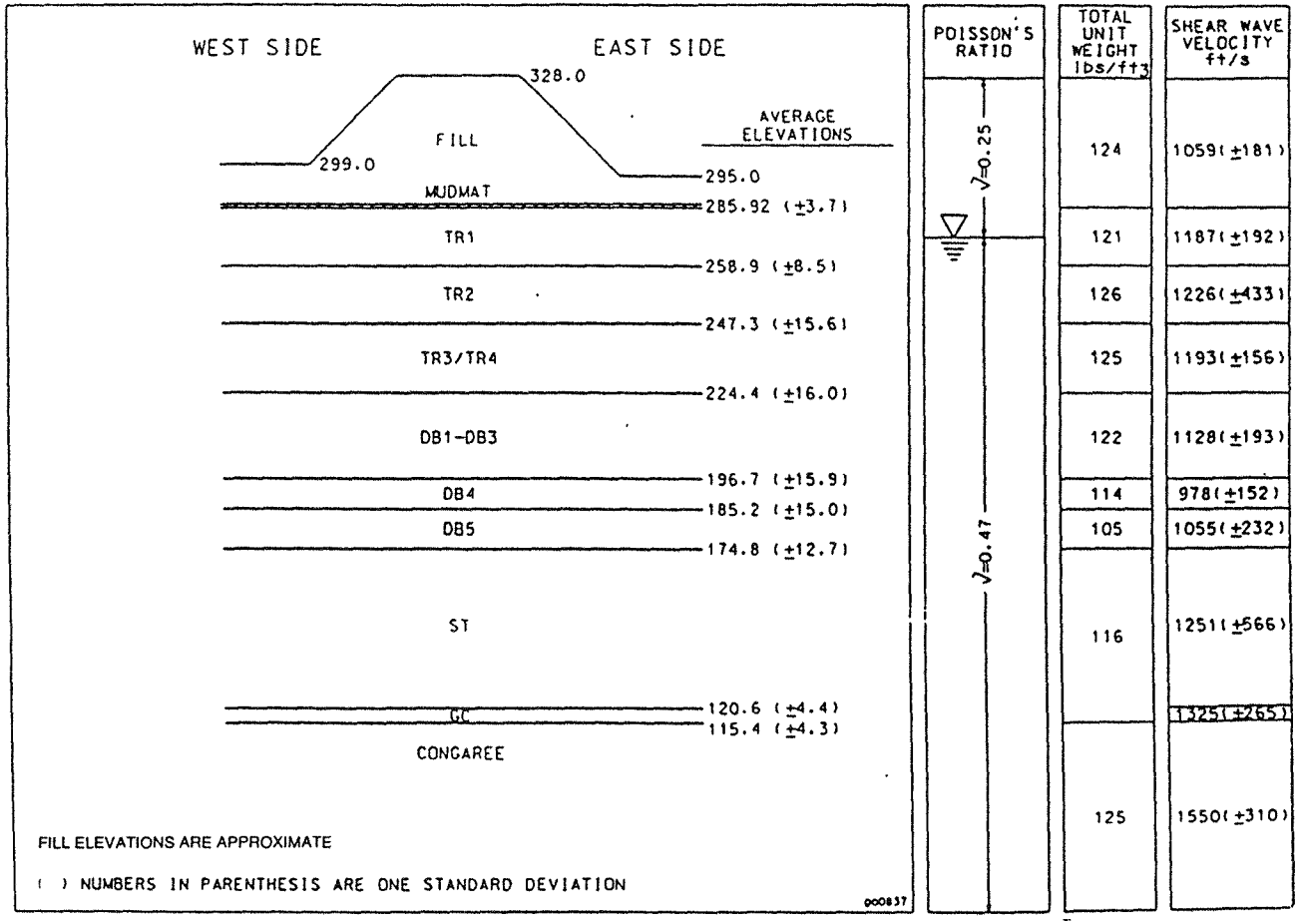


Figure 5.1-3(a) Idealized cross-section showing mean shear wave velocities, Poisson's ratios, and unit weights for layers at ITP.

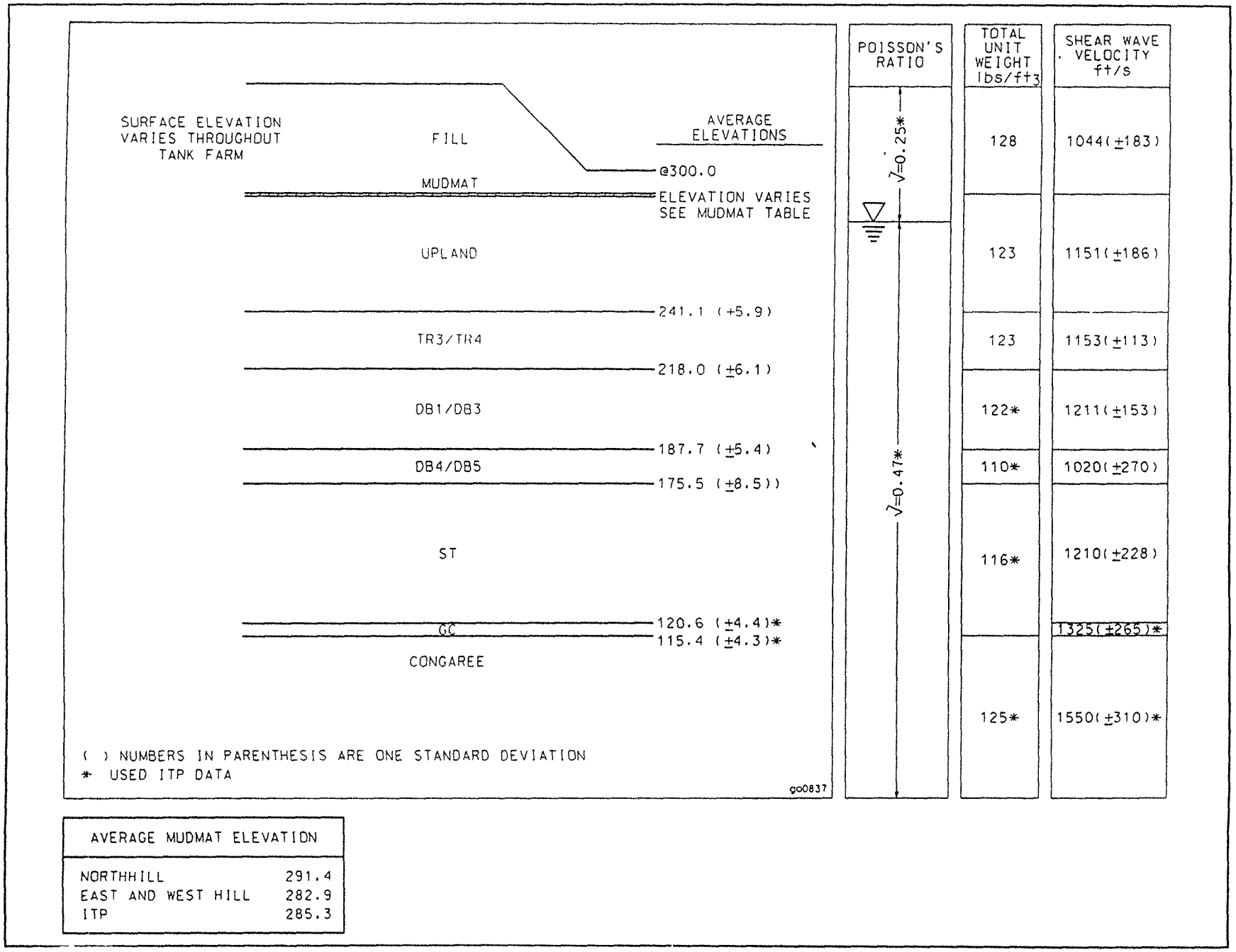


| AVERAGE MUDMAT ELEVATION | |
|---|---|
| NORTHHILL | 291.4 |
| EAST AND WEST HILL | 282.9 |
| ITP | 285.3 |

Figure 5.1-3(b) Idealized cross-section showing mean shear wave velocities, Poisson's ratios, and unit weights for layers at HTF.

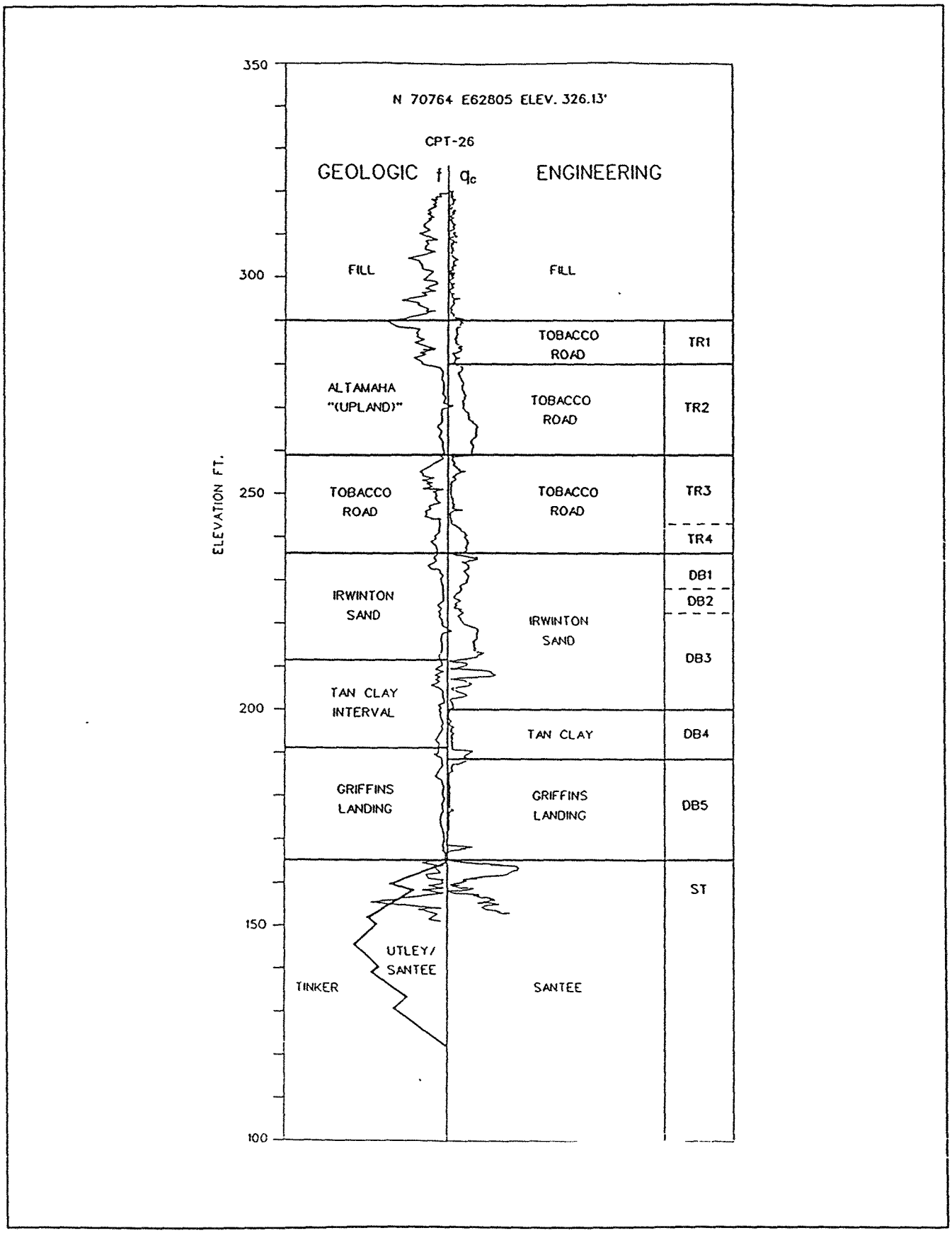


Figure 5.1-4 Comparison of geologic and engineering nomenclature.

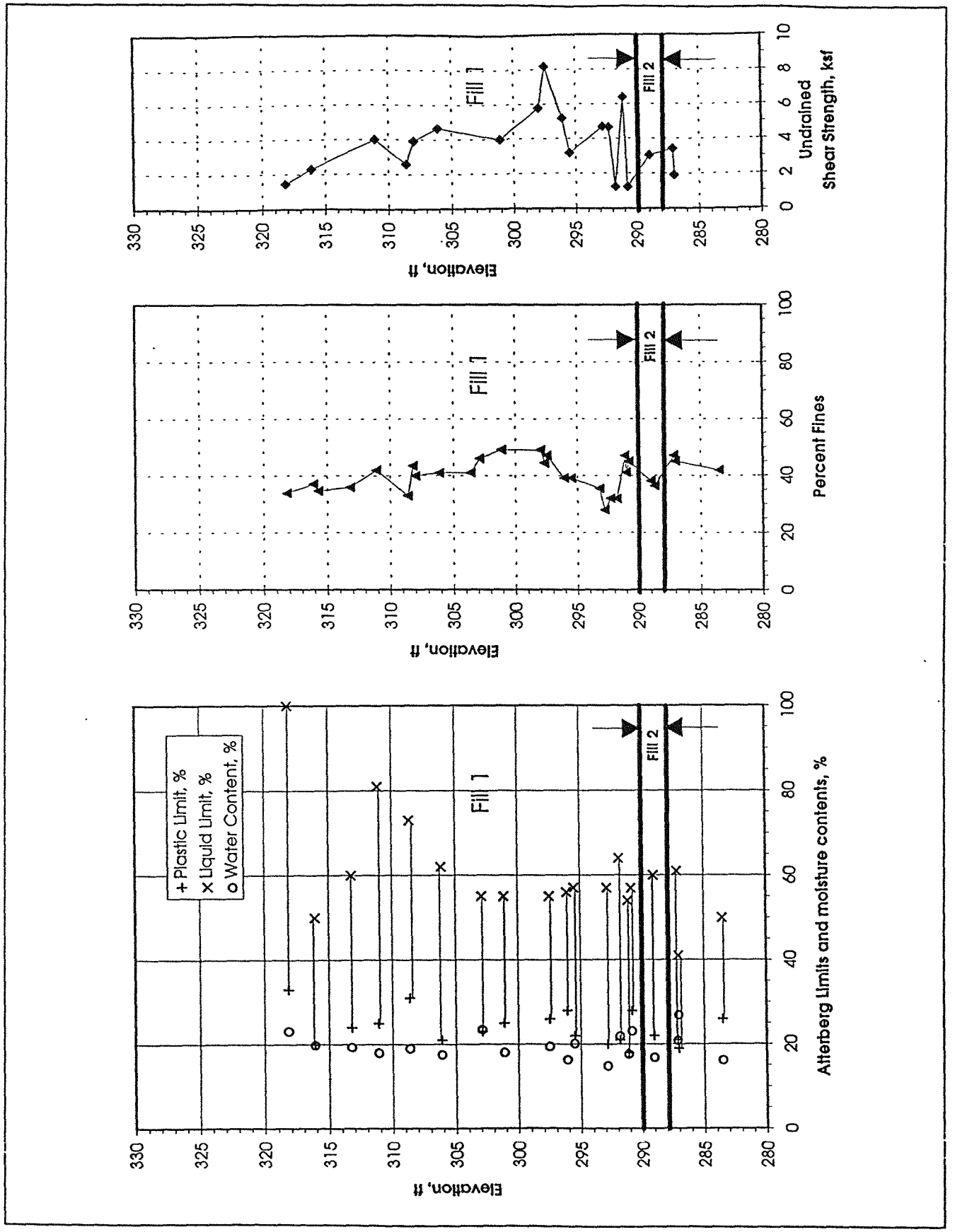


Figure 5.1-5 Summary of laboratory data for the ITP fill.

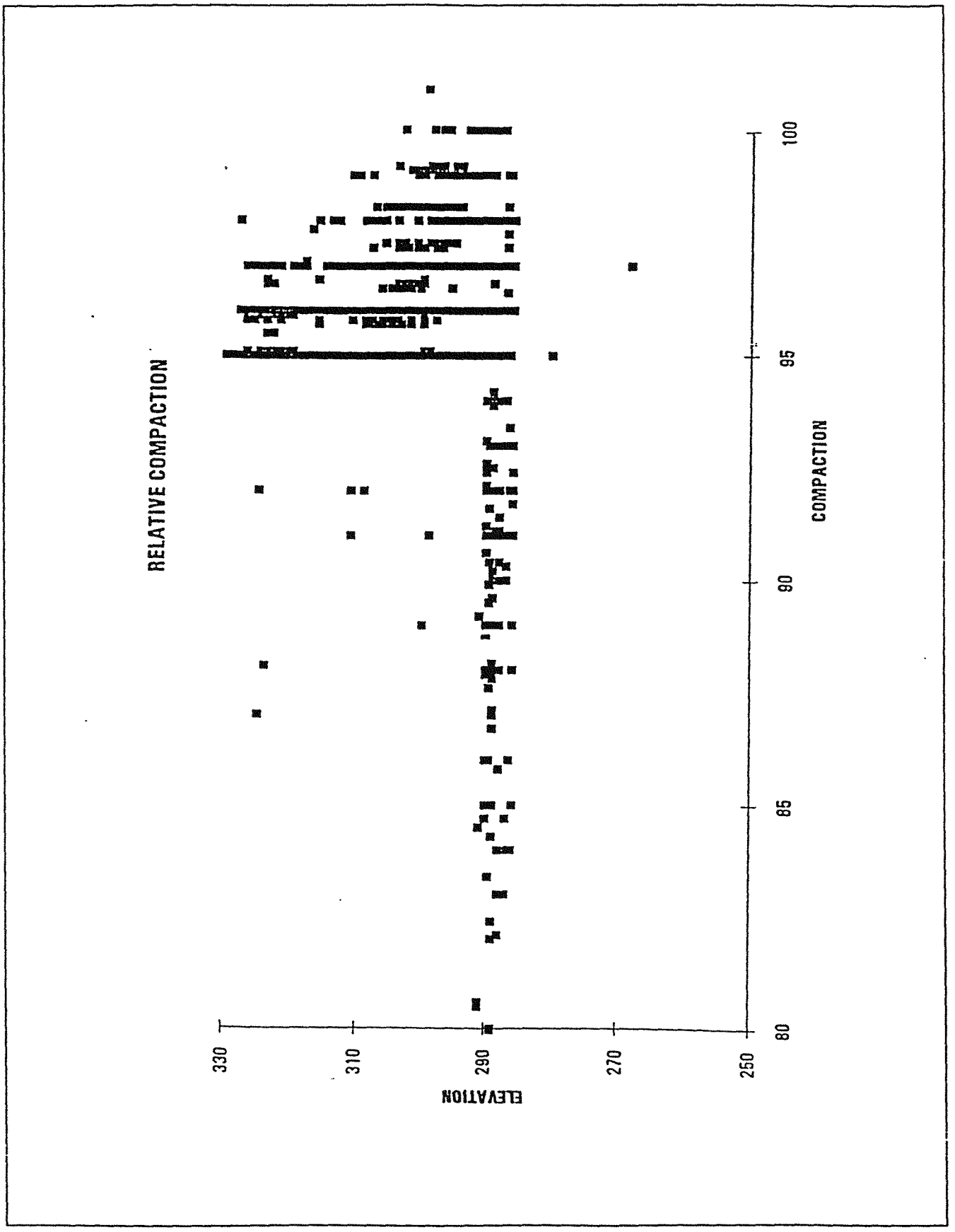


Figure 5.1-6 Percent compaction (Modified Proctor) for the ITP fill.

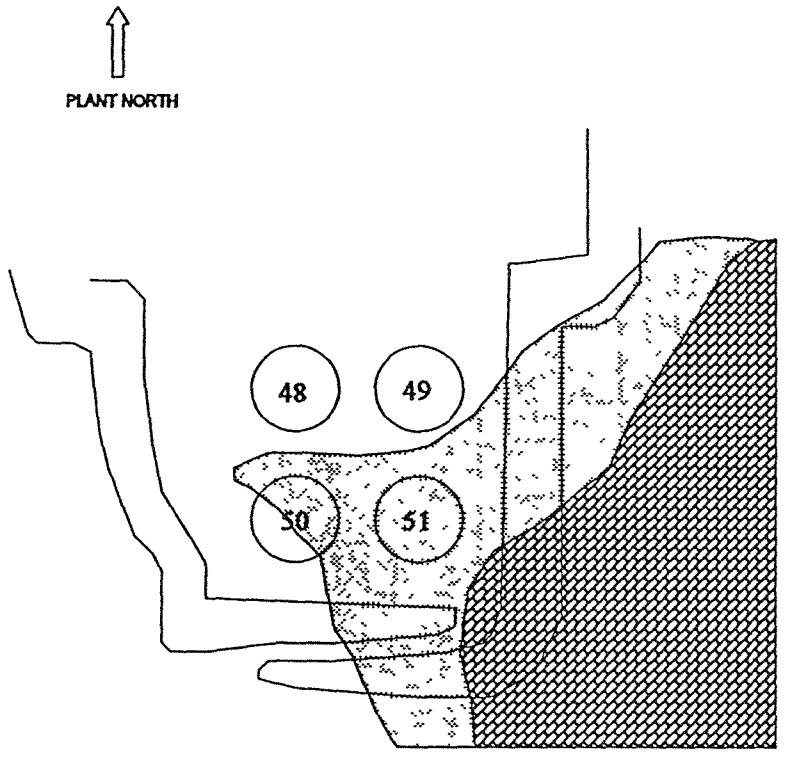


Note: Tank diameter = 95 feet.

LEGEND

MOLDIC LIMESTONE FACIES (FACIES 1)

SANDY/SILTY FACIES WITH SHELL FRAGMENTS AND CARBONATE SANDS (FACIES 2)

SLIGHTLY CALCAREOUS TO NON-CALCAREOUS CLAYEY TO SILTY SANDY FACIES (FACIES 3)

NOTE: The facies boundaries shown on this figure are approximate and inferred from borehole and CPT soundings

Figure 5.1-7 Idealized facies map of the upper Tinker/Santee formation.

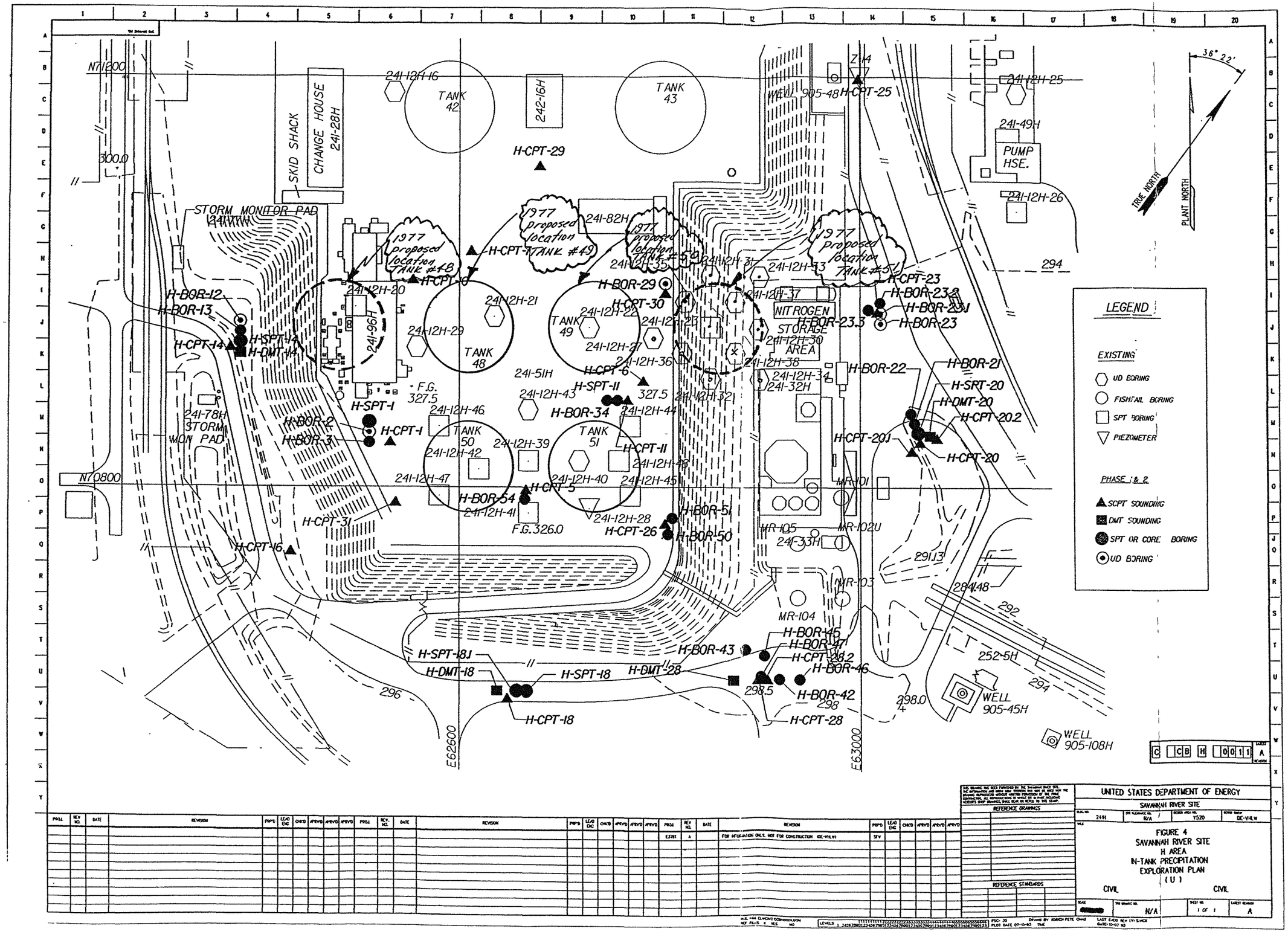


Figure 5.1-8 Tank and borehole location map.

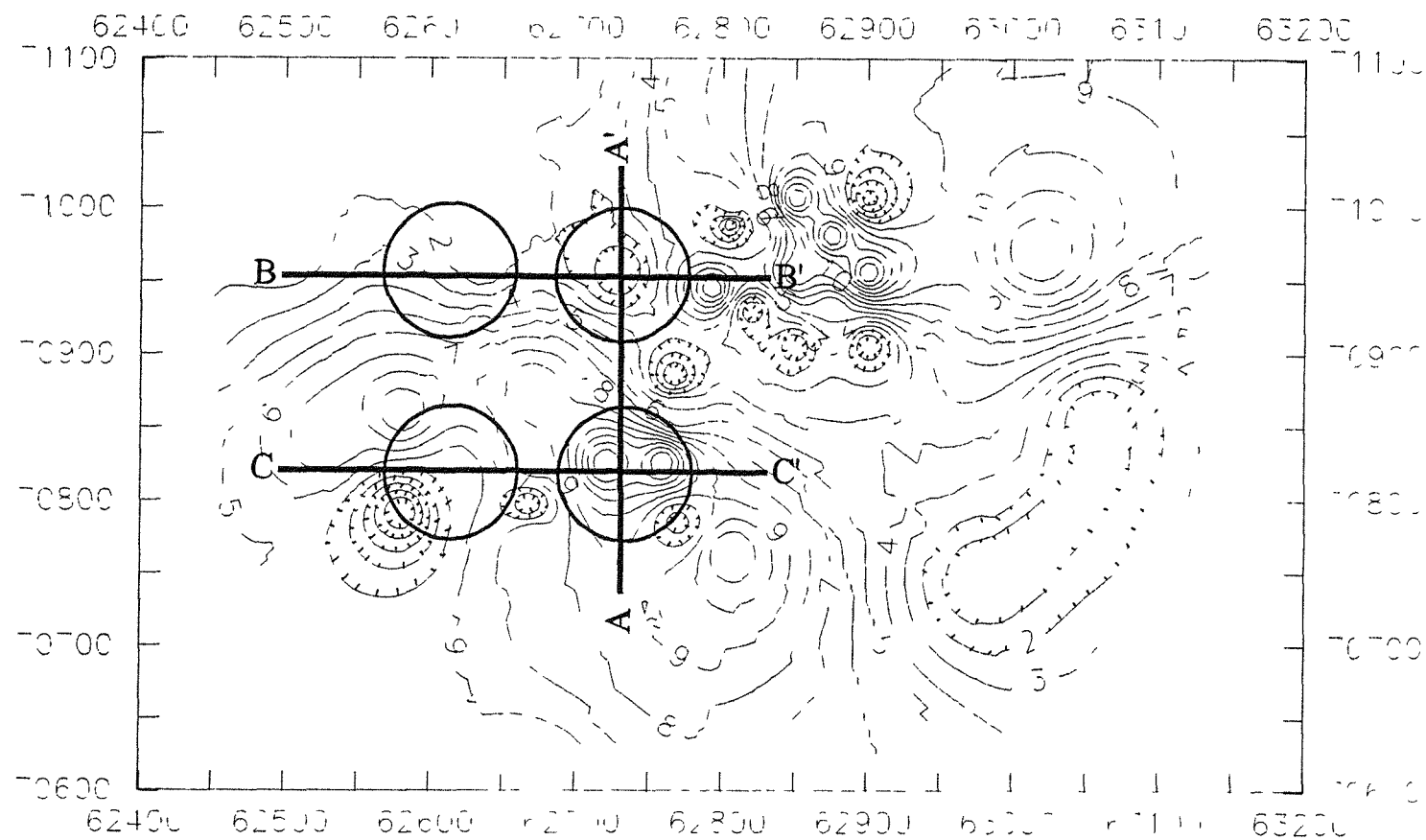


Figure 5.2-1 Combined thickness map of upper and lower soft zone in the Santee/Tinker formation.

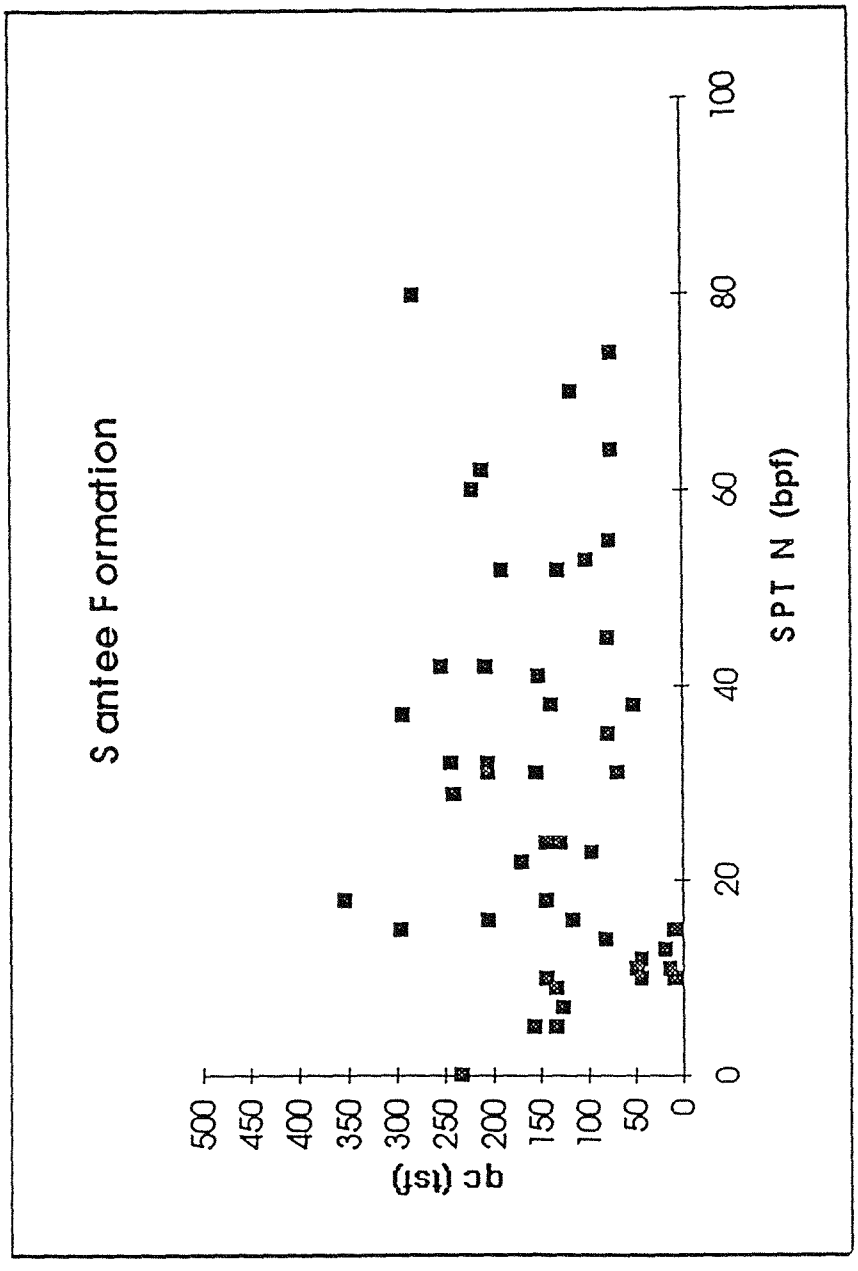


Figure 5.2-2 CPT tip resistance ($q_c$) versus SPT-N for Tinker/Santee formation.

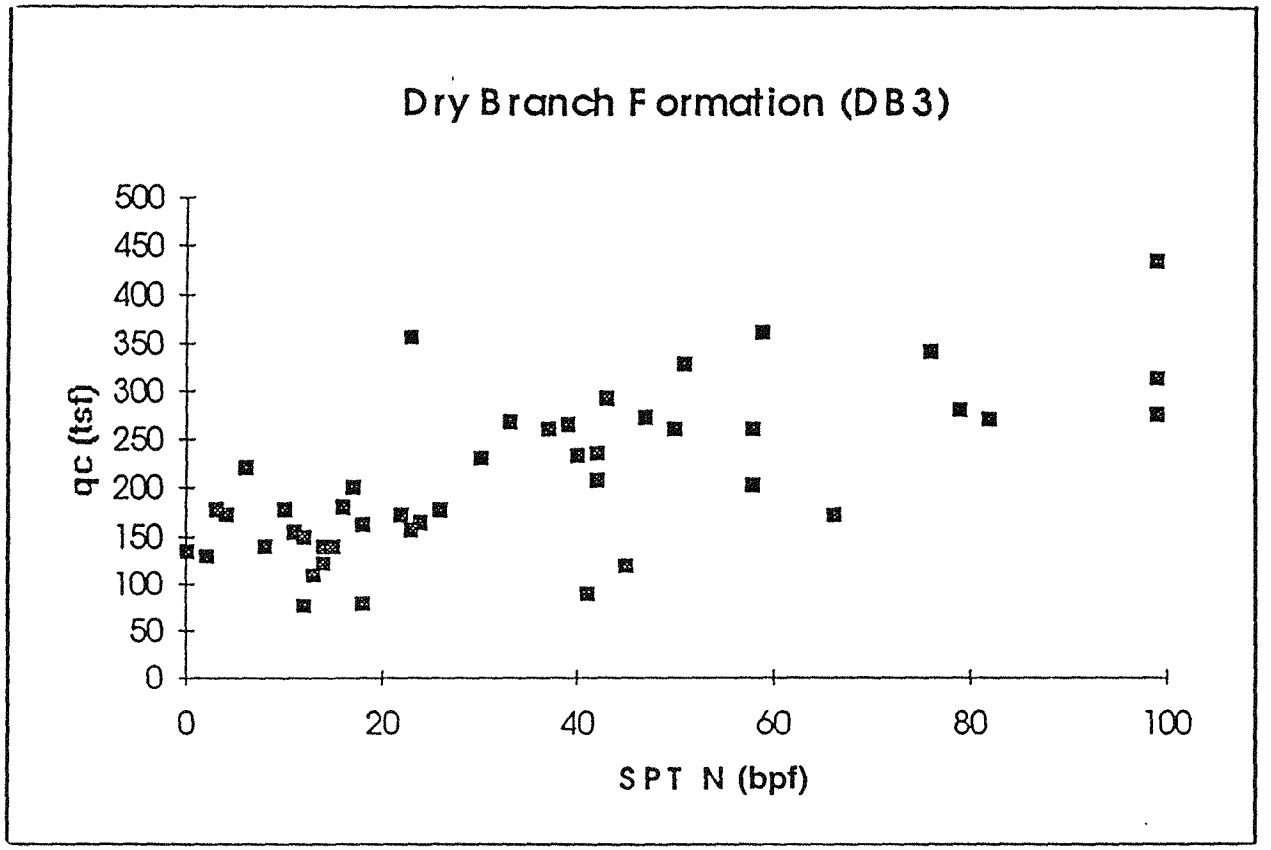


Figure 5.2-3 CPT tip resistance ($q_c$) versus SPT-N for Dry Branch (DB3) layer.

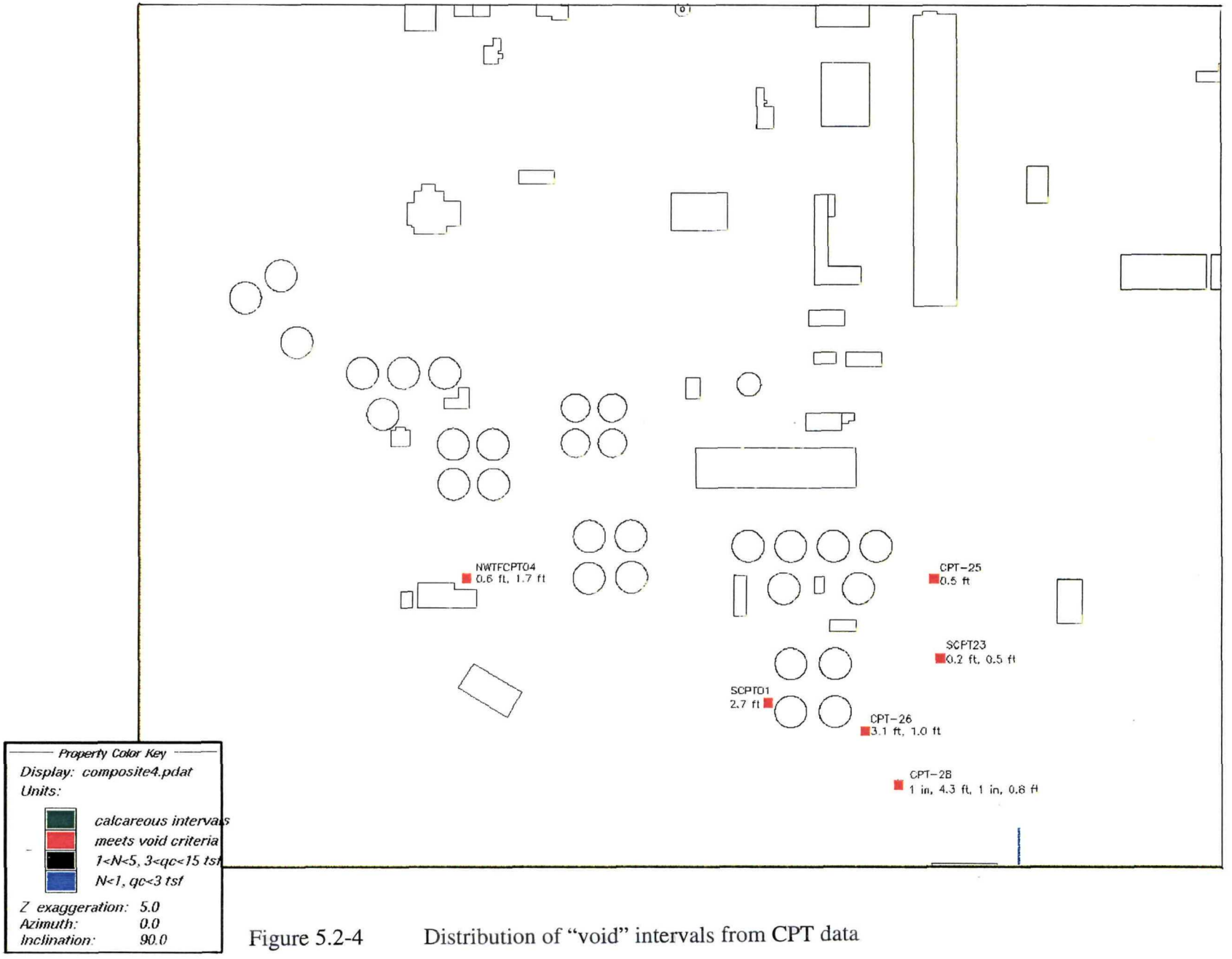


Figure 5.2-4 Distribution of "void" intervals from CPT data

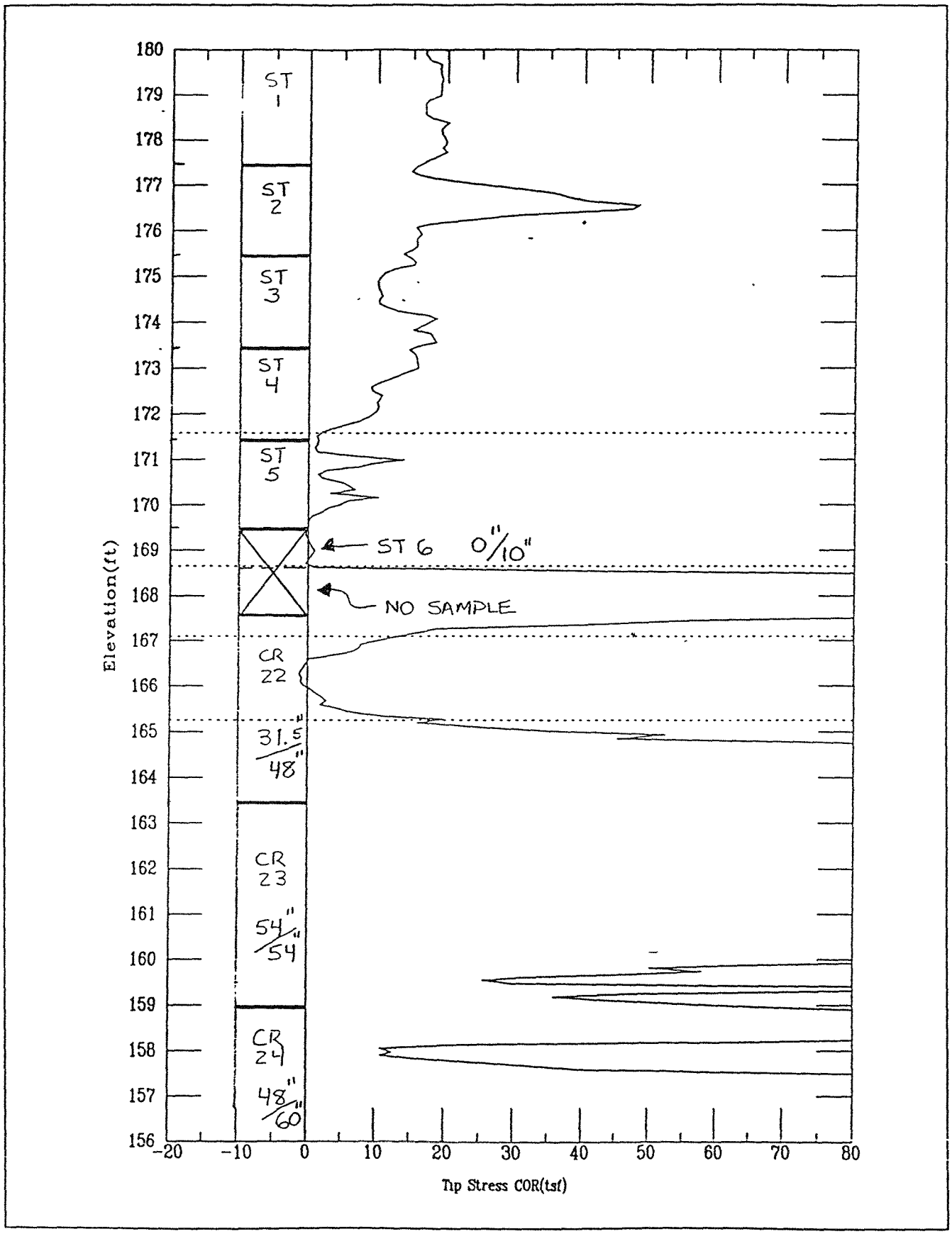


Figure 5.2-5 H-BOR-50 sampling intervals.

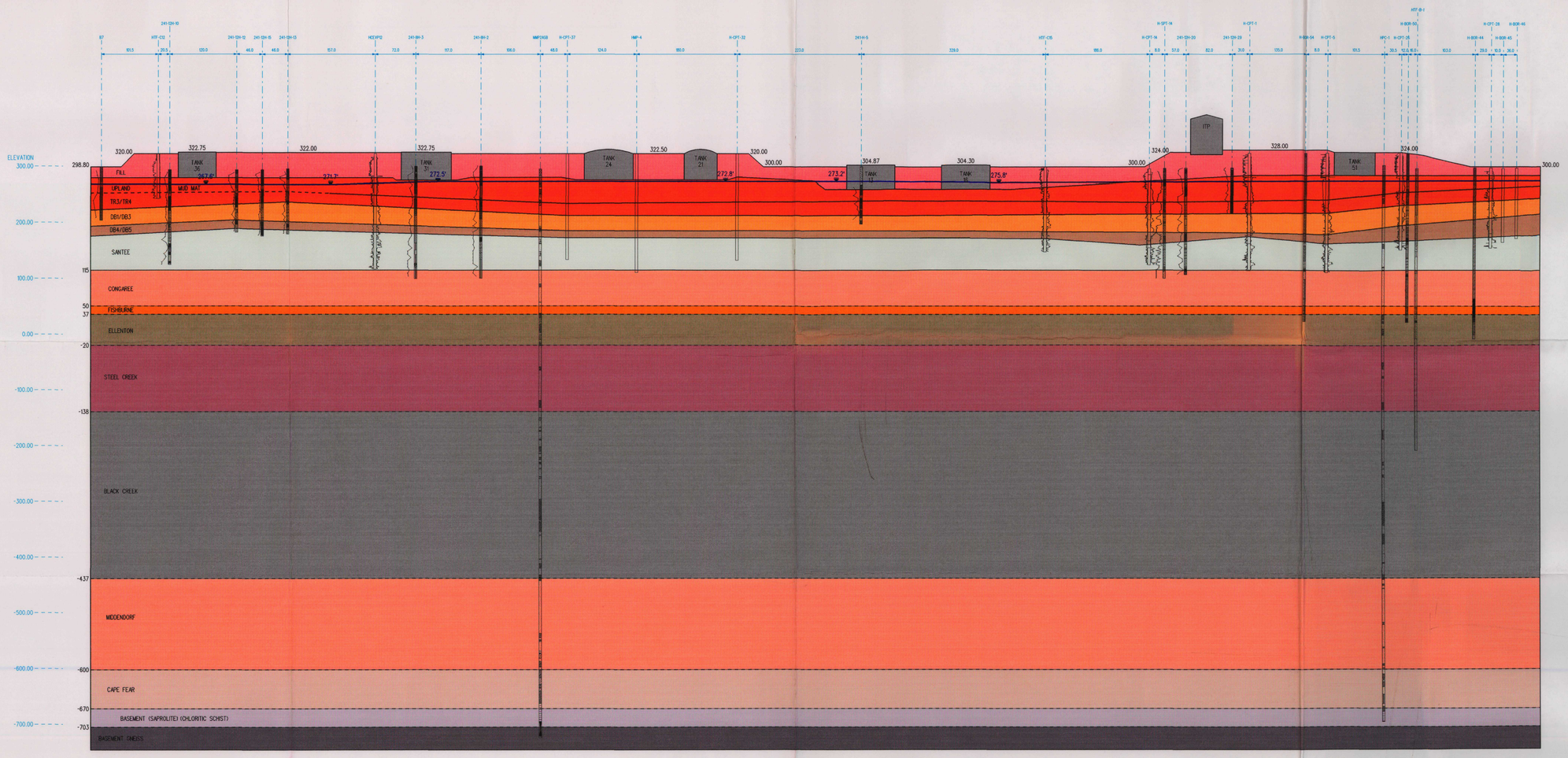


GEOTECHNICAL PROFILE SECTION D-D'

NOTES:

1. THIS SECTION REPRESENTS AN INTERPRETATION OF THE MATERIALS UNDERLYING THE ITP AND HTF FACILITY.
2. THE PROFILE IS A STRAIGHT LINE SECTION WITH DATA POINTS PROJECTED PERPENDICULAR.
3. THIS SECTION IS SHOWN AT A TRUE SCALE (H = V).
4. THIS SECTION DOES NOT SHOW ALL ABOVE AND BELOW GROUND STRUCTURES.
5. PRE-CONSTRUCTION BORINGS PRESENTED.
6. FACILITIES SHOWN ON THIS DRAWING ARE INTENDED TO PROVIDE RELATIVE LOCATION AND MAY NOT BE EXACTLY CORRECT IN DETAIL OR SHAPE.
7. ALL DIMENSIONS ARE FOR REFERENCE ONLY.
8. WATER LEVELS TAKEN FROM THE SAVANNAH RIVER SITE'S GROUNDWATER MONITORING PROGRAM SECOND QUARTER 1994 (U).
9. BORINGS AND CONE PENETROMETER SOUNDINGS ON THIS DRAWING ARE FOR ILLUSTRATION ONLY. FOR DETAILED LITHOLOGIC, N-VALUE, TIP RESISTANCE AND FRICTION RATIO INFORMATION REFER TO APPENDIX C FOR BORING LOGS AND VOLUME 3 FOR CONE PENETROMETERS.

LEGEND

SOIL DESCRIPTION

- CLAYEY SAND (SC)
- SILTY SAND / NARROWLY GRADED SAND WITH SILT (SM/SP-SM)
- FAT CLAY (CH)
- SILTY SAND WITH GRAVEL
- NARROWLY GRADED SAND (SP)
- SILT (ML)
- SILT WITH SAND, SANDY SILT (ML)
- SANDY LEAN CLAY (CL)
- WELL GRADED SAND WITH CLAY (SW)
- SILTY CLAYEY SAND
- POORLY GRADED SAND WITH CLAY (SP-SC)
- CLAYEY SAND TO SANDY CLAY
- LIMESTONE (LS)
- GROUT
- CALCAREOUS SANDSTONE WITH POORLY GRADED SAND
- LIMESTONE IN SILT MATRIX

SAMPLE TYPE

- SHELBY TUBE
- P — STATIONARY POSITION
- SPLIT SPOON
- PITCHER BARREL

- INTERPRETED WATER TABLE
- MEASURED BORING FLUID LEVEL
- PRE-CONSTRUCTION BORING




Figure 5.3-1
Generalized profiles at HTF
Section DD'
F-36

| DWG NO. | REV. NO. | REV. DATE | AREA |
|---|---|---|---|
| SH3222 | 0 | 9-28-95 | H-AREA |

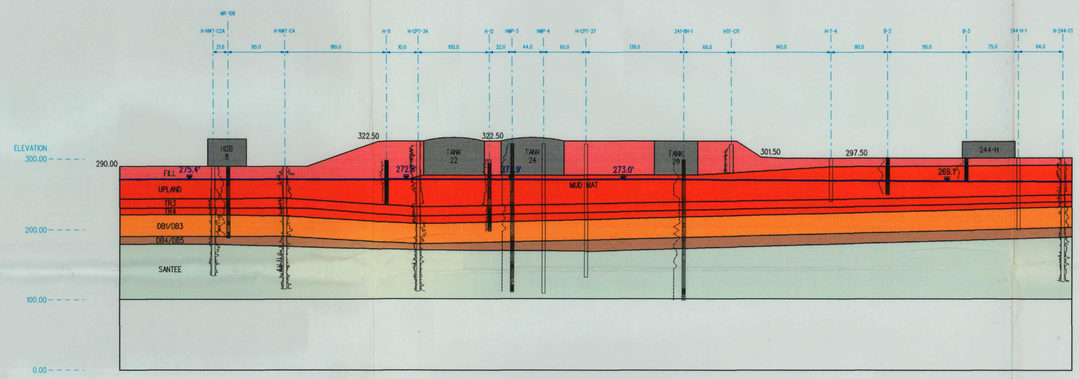


GEOTECHNICAL PROFILE NORTH-SOUTH SECTION G-G'

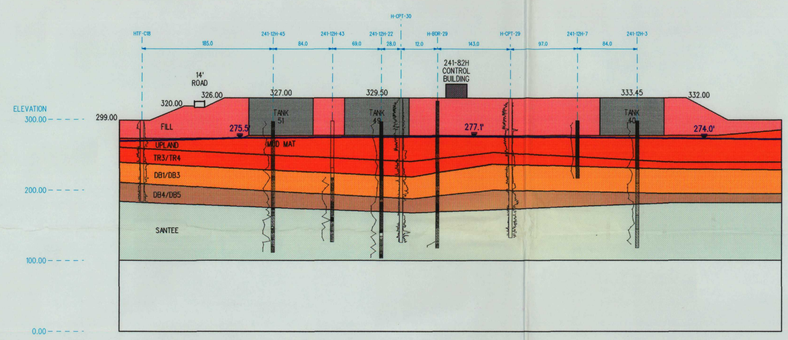


GEOTECHNICAL PROFILE NORTH-SOUTH SECTION E-E'

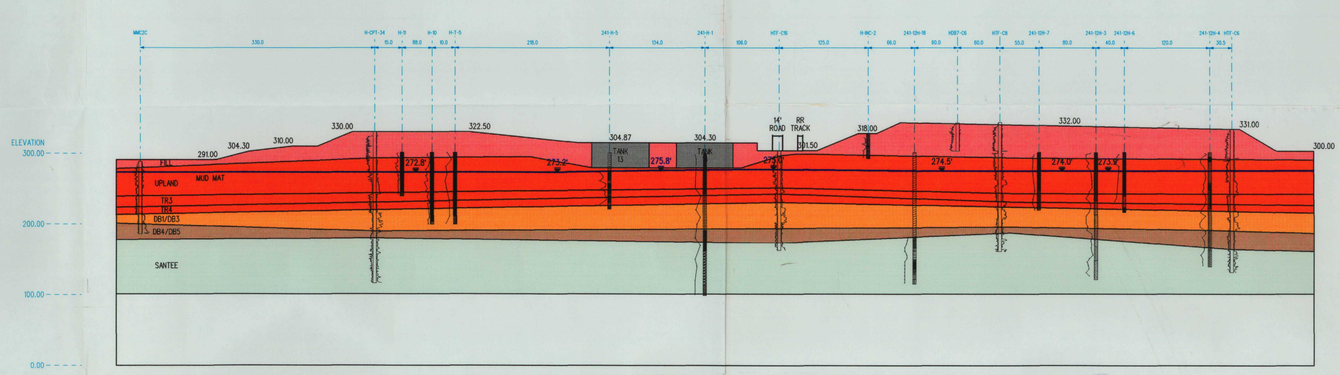


GEOTECHNICAL PROFILE WEST-EAST SECTION F-F'

NOTES:

1. THIS SECTION REPRESENTS AN INTERPRETATION OF THE MATERIALS UNDERLYING THE ITP AND HTF FACILITY.
2. THE PROFILE IS A STRAIGHT LINE SECTION WITH DATA POINTS PROJECTED PERPENDICULAR.
3. THIS SECTION IS SHOWN AT A TRUE SCALE (H = V).
4. THIS SECTION DOES NOT SHOW ALL ABOVE AND BELOW GROUND STRUCTURES.
5. PRE-CONSTRUCTION BORINGS PRESENTED.
6. FACILITIES SHOWN ON THIS DRAWING ARE INTENDED TO PROVIDE RELATIVE LOCATION AND MAY NOT BE EXACTLY CORRECT IN DETAIL OR SHAPE.
7. ALL DIMENSIONS ARE FOR REFERENCE ONLY.
8. WATER LEVELS TAKEN FROM THE SAVANNAH RIVER SITE'S GROUNDWATER MONITORING PROGRAM SECOND QUARTER 1994 (U).
9. BORINGS AND CONE PENETROMETER SOUNDINGS ON THIS DRAWING ARE FOR ILLUSTRATION ONLY. FOR DETAILED LITHOLOGIC, N-VALUE, TIP RESISTANCE AND FRICTION RATIO INFORMATION REFER TO APPENDIX C FOR BORING LOGS AND VOLUME 3 FOR CONE PENETROMETERS.

LEGEND

SOIL DESCRIPTION

- CLAYEY SAND (SC)
- SILTY SAND / NARROWLY GRADED SAND WITH SILT (SM/SP-SM)
- FAT CLAY (CH)
- SILTY SAND WITH GRAVEL
- NARROWLY GRADED SAND (SP)
- SILT (ML)
- SILT WITH SAND, SANDY SILT (ML)
- SANDY LEAN CLAY (CL)
- WELL GRADED SAND WITH CLAY (SW)
- SILTY CLAYEY SAND
- POORLY GRADED SAND WITH CLAY (SP-SC)
- CLAYEY SAND TO SANDY CLAY
- LIMESTONE (LS)
- GROUT
- CALCAREOUS SANDSTONE WITH POORLY GRADED SAND
- LIMESTONE IN SILT MATRIX

SAMPLE TYPE

- SHELBY TUBE
- P — STATIONARY POSITION
- SPLIT SPOON
- PITCHER BARREL

- INTERPRETED WATER TABLE
- MEASURED BORING FLUID LEVEL
- PRE-CONSTRUCTION BORING

0 100 200 300 400
SCALE: FEET

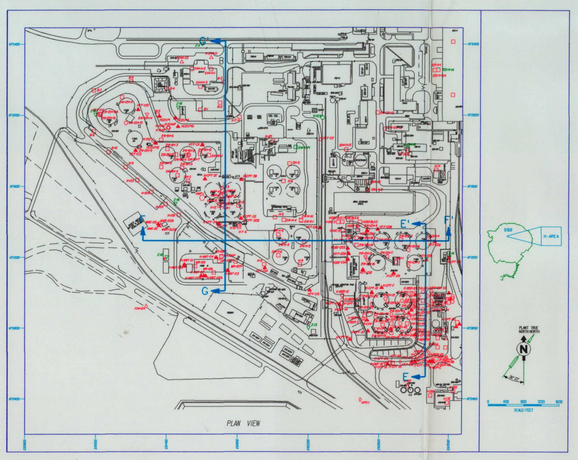


**Figure 5.3-2**
**Generalized profiles at HTF**
**Sections EE', FF' and GG'**
**F-37**

| DWG NO. | REV. NO. | REV. DATE | AREA |
|---|---|---|---|
| SH3223 | 0 | 9-28-95 | H-AREA |

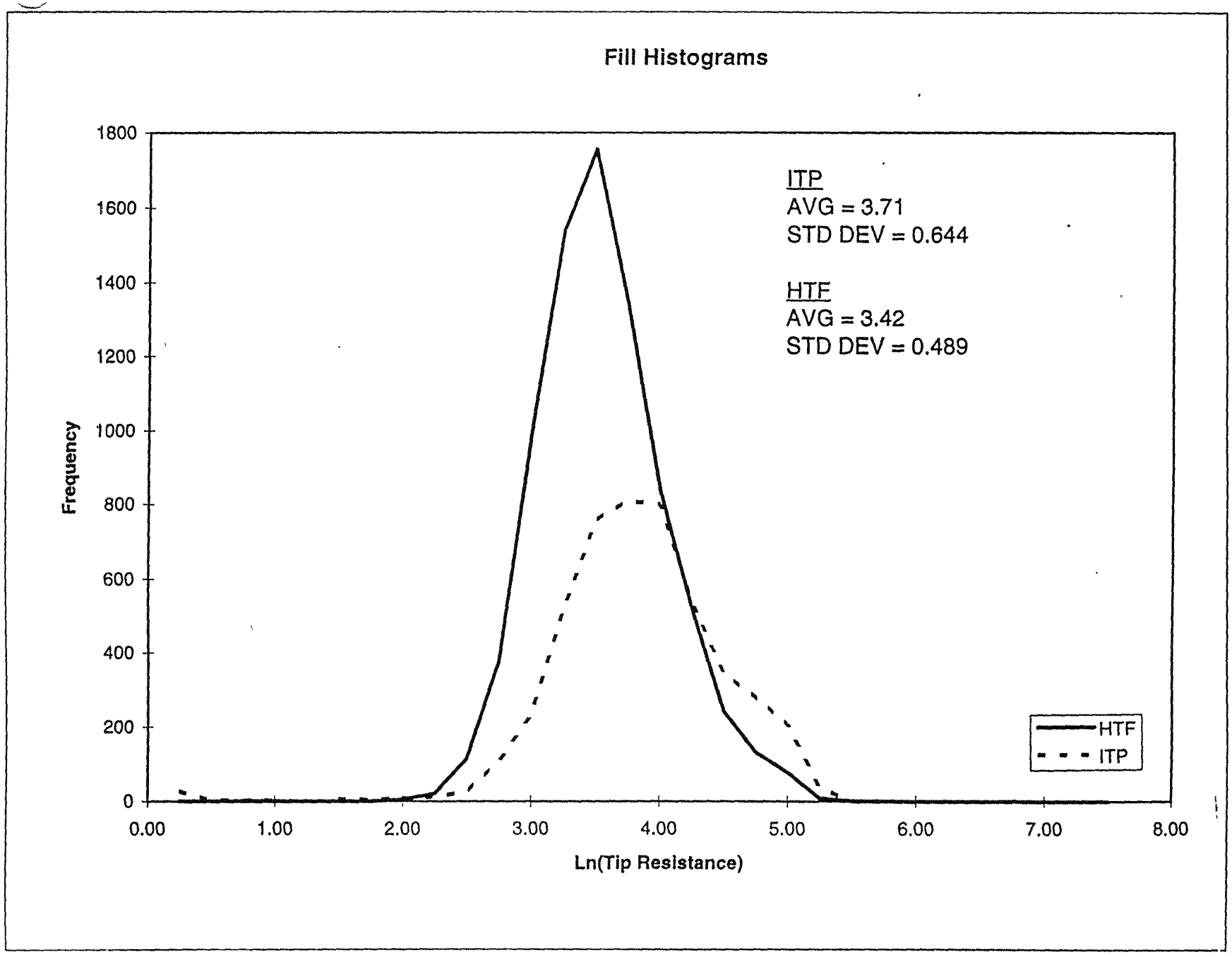


Figure 5 3-3 Histogram for HTF fill vs. ITP fill.

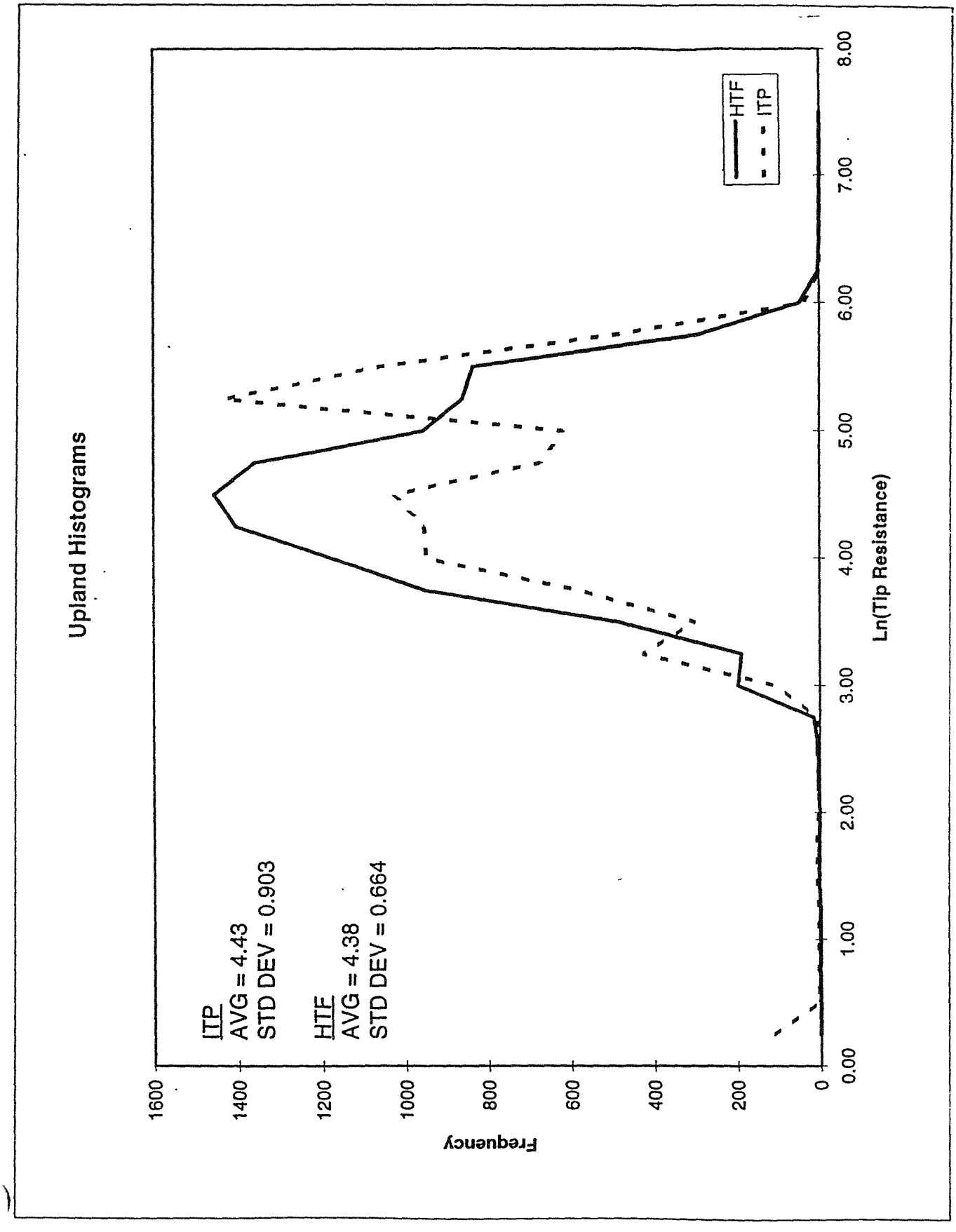


Figure 5.3-4 Histogram for HTF Upland vs. ITP Upland.

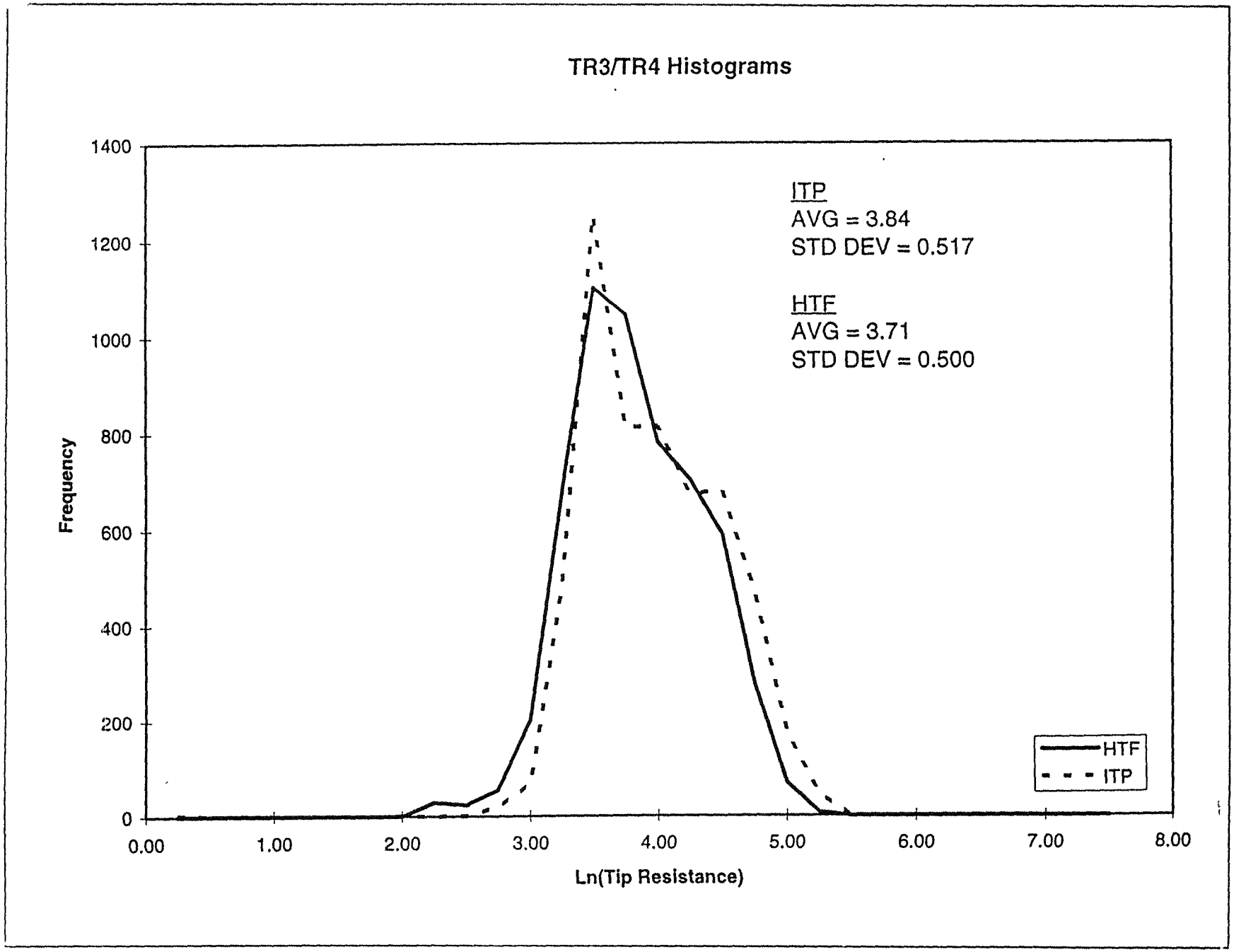


Figure 5.3-5 Histogram for HTF TR3/4 vs. ITP TR3/4.

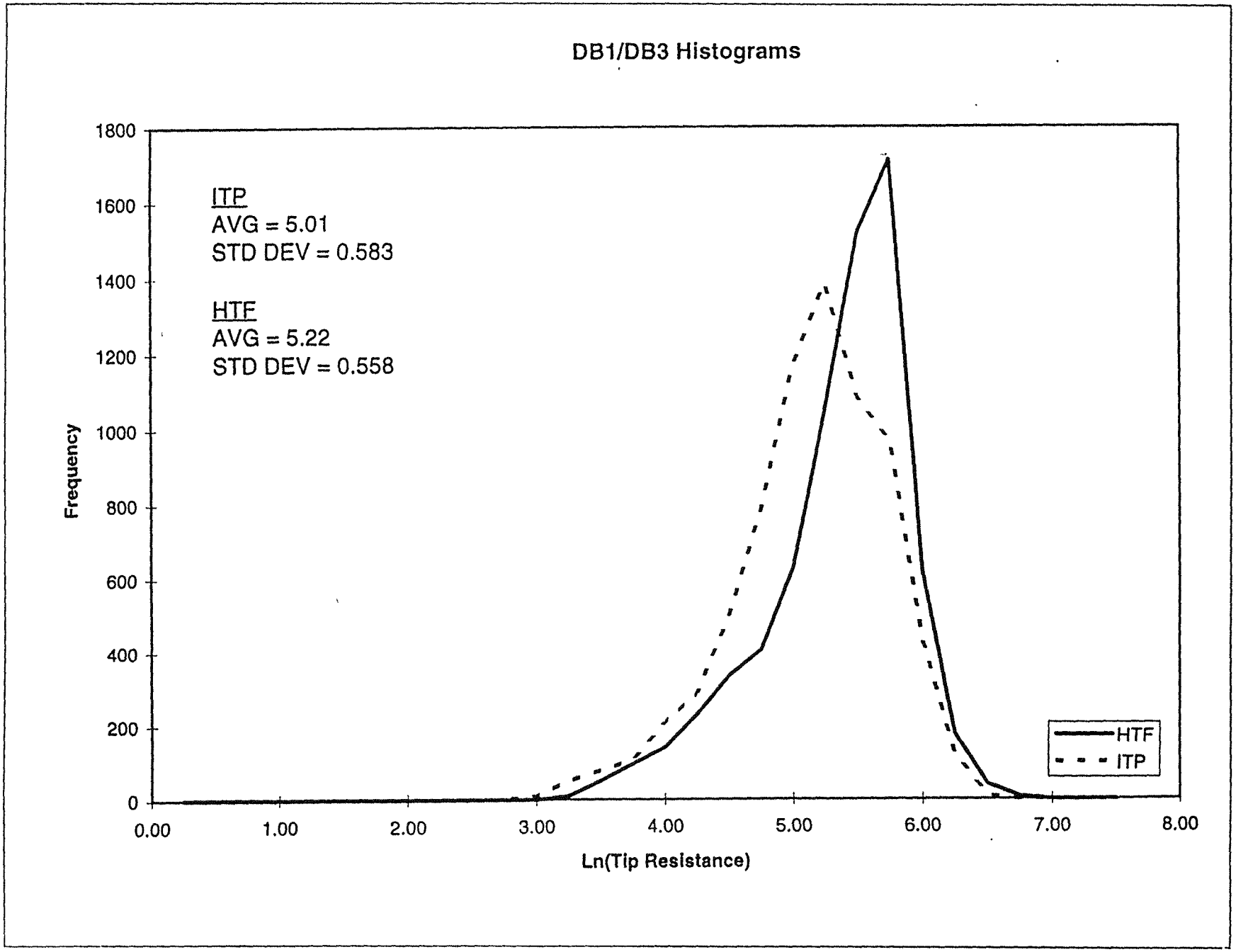


Figure 5.3-6 Histogram for HTF DB1/3 vs. ITP DB1/3.

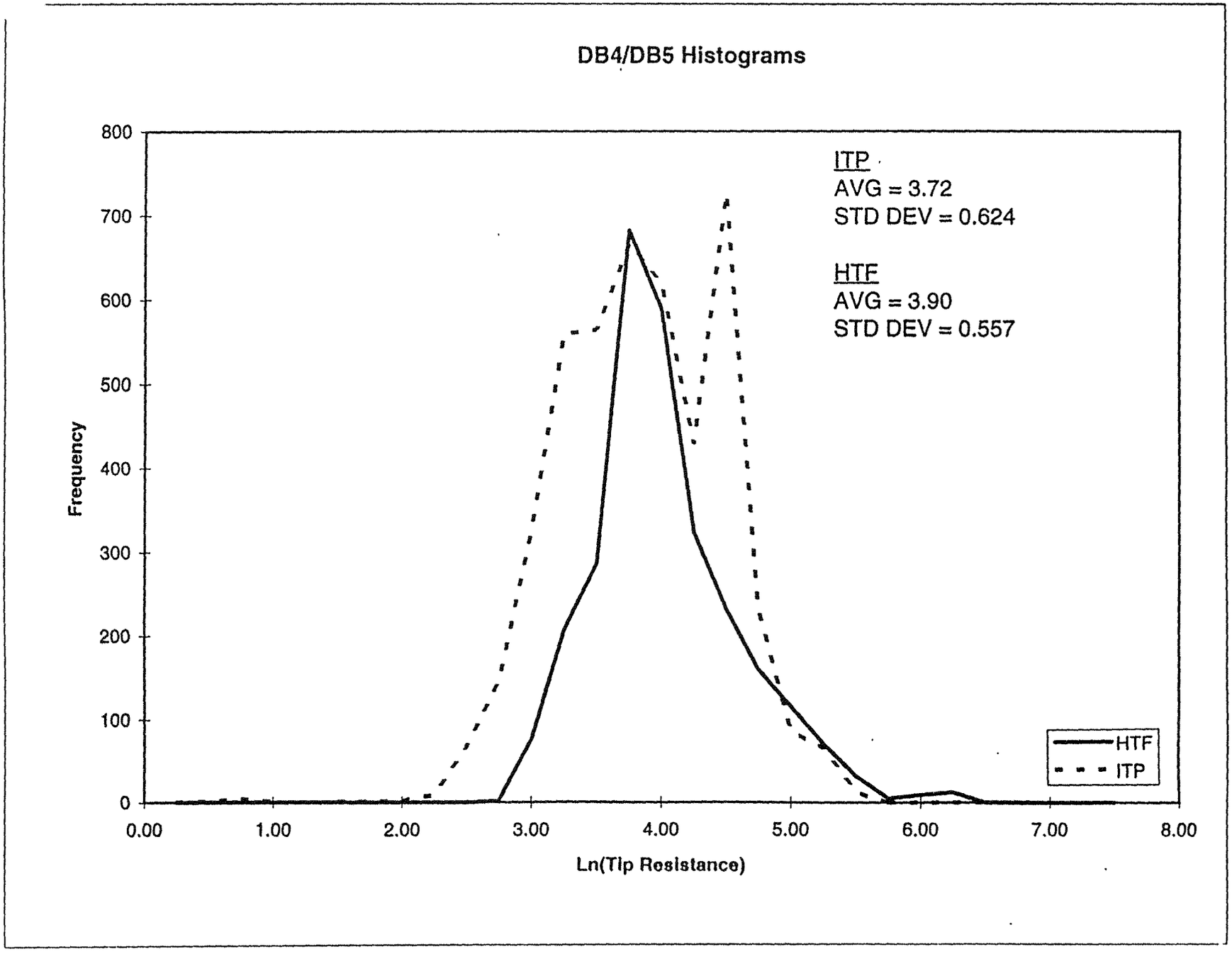


Figure 5.3-7 Histogram for HTF DB4/5 vs. ITP DB4/5.

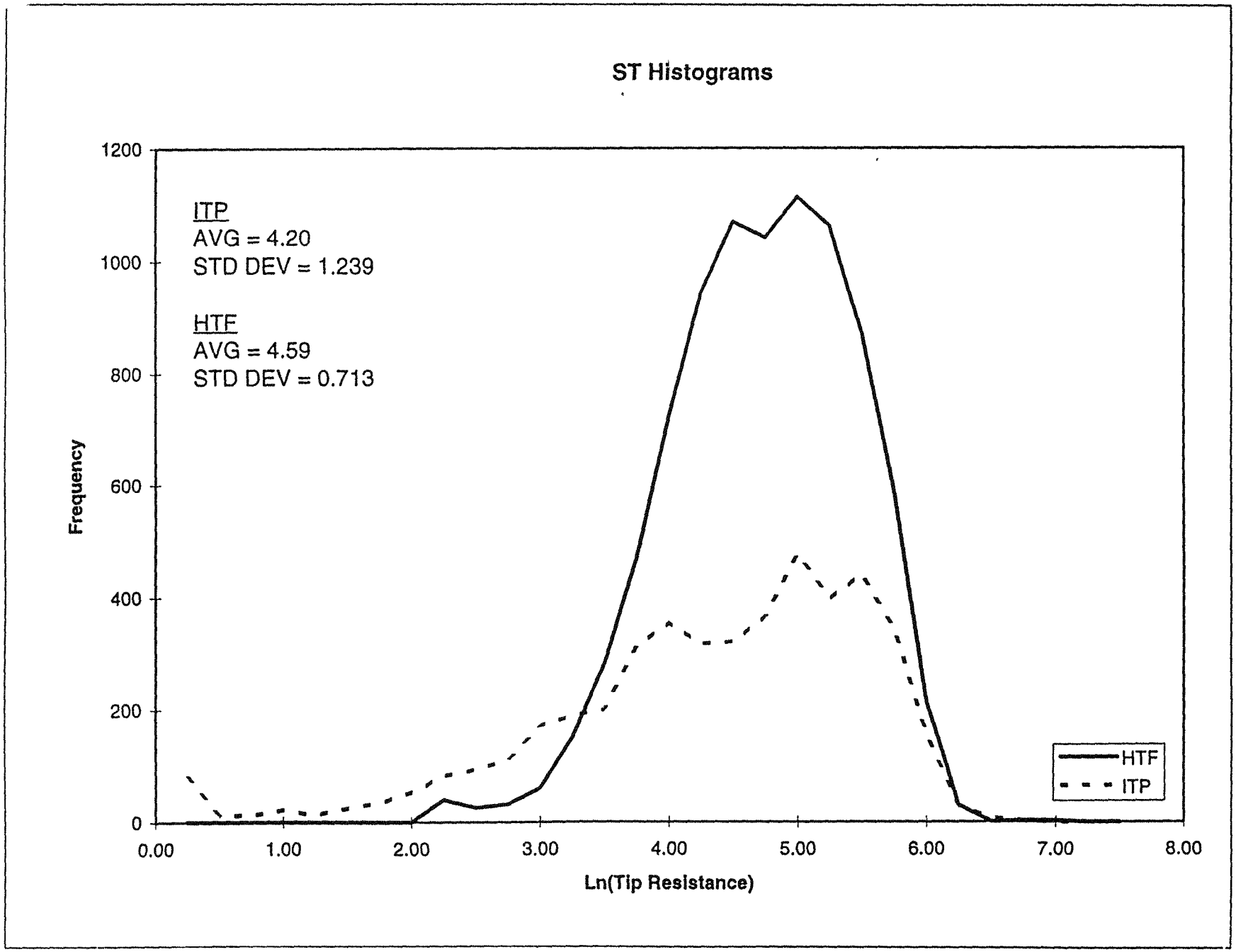


Figure 5 3-8 Histogram for HTF ST vs. ITP ST.

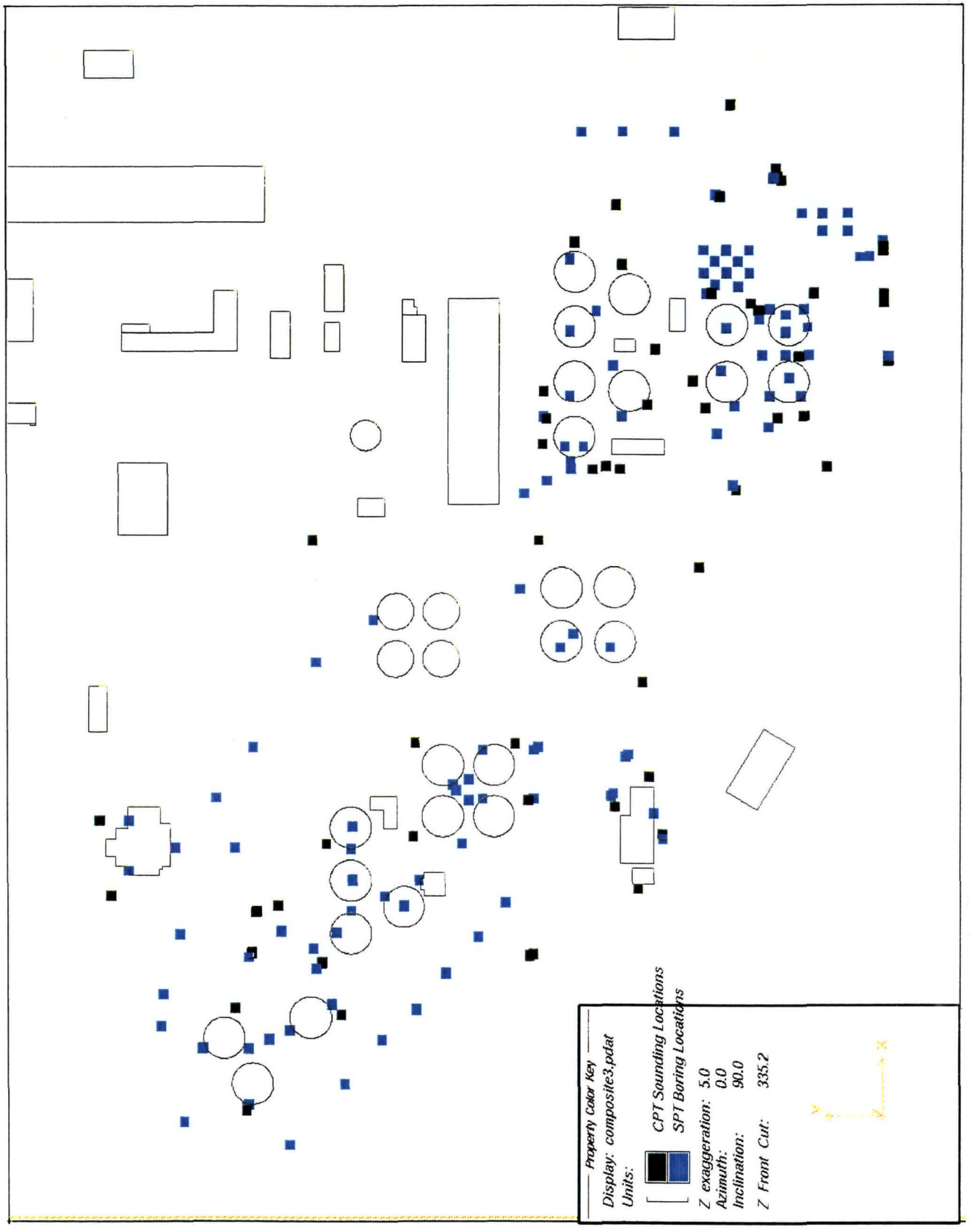


Figure 5.3-9 Distribution of SPT and CPT for ITP and HTF

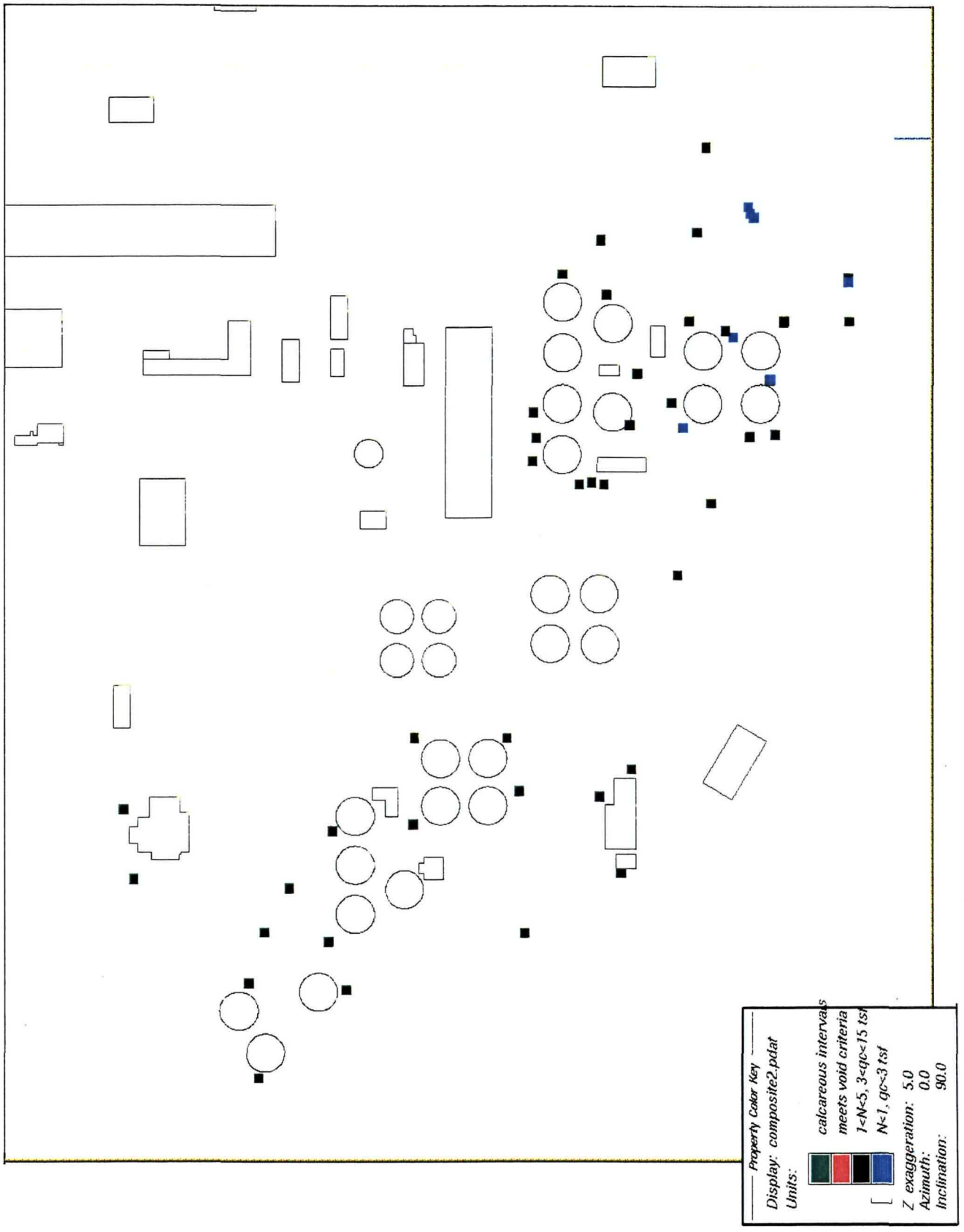


Figure 5.3-10 Distribution of soft zones for ITP and HTF

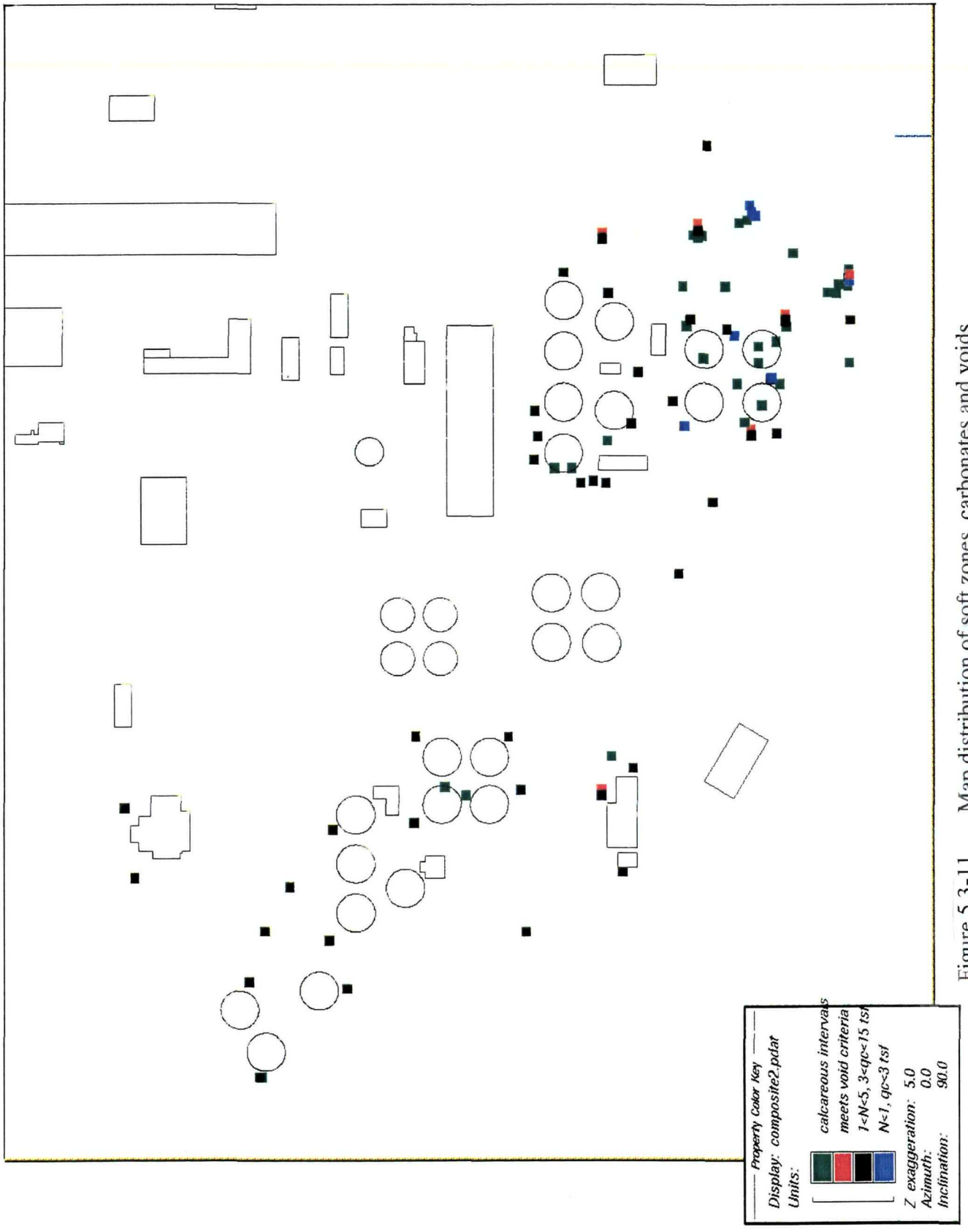


Figure 5.3-11 Map distribution of soft zones, carbonates and voids

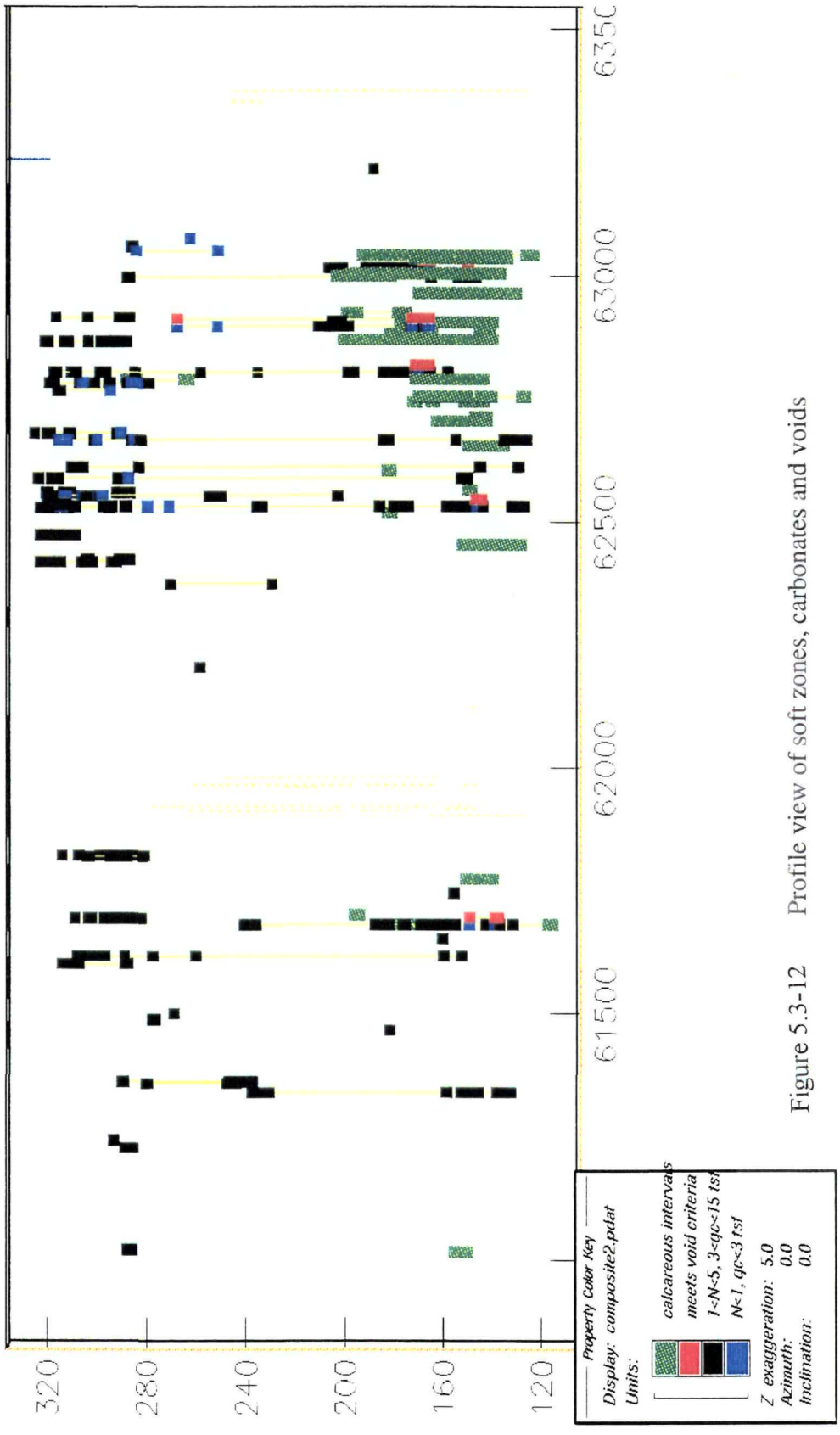


Figure 5.3-12 Profile view of soft zones, carbonates and voids

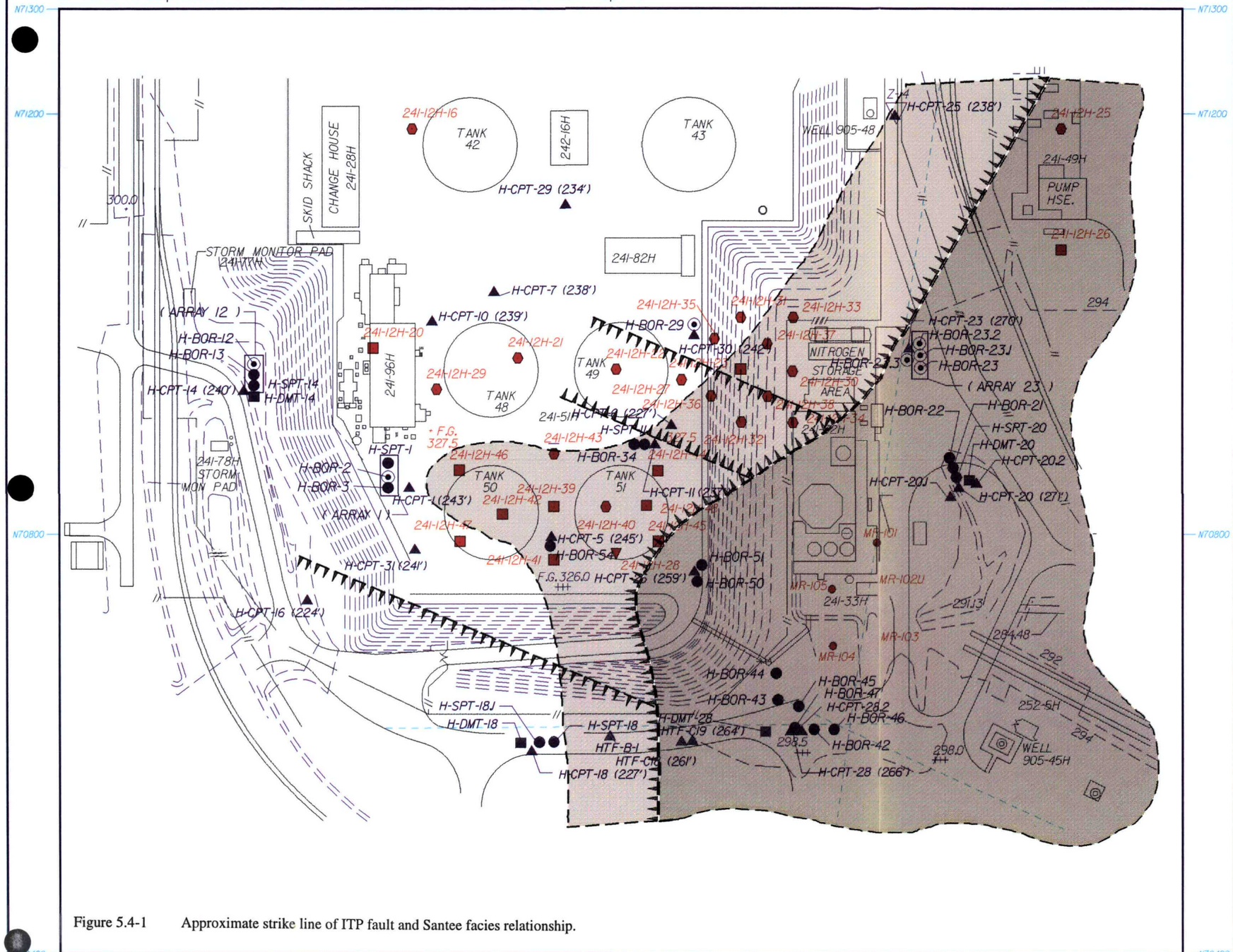


Figure 5.4-1 Approximate strike line of ITP fault and Santee facies relationship.

LEGEND

PRE-CONSTRUCTION

- UD BORING
- FISHTAIL BORING
- SPT BORING
- PIEZOMETER

PHASE 1,2 & 3

- SCPT SOUNDING (NUMBER IN PARENTHESES ARE ELEVATIONS OF THE TOP OF TOBACCO RD. FM)
- DMT SOUNDING
- SPT OR CORE BORING
- UD BORING
- – – DOWN-HOLE REFRACTION
- MOLDIC LIMESTONE (FACIES 1)
- SANDY/SILTY FACIES WITH SHELL FRAGMENTS AND CARBONATE SANDS (FACIES 2)
- SLIGHTLY TO NON CALCAREOUS SILTY/CLAYEY SANDS (FACIES 3)
- INFERRED FAULT

NOTE :
THE FACIES BOUNDARIES SHOWN ON THE FIGURE ARE APPROXIMATE AND AND INFERRED FROM BOREHOLE AND CPT DATA.

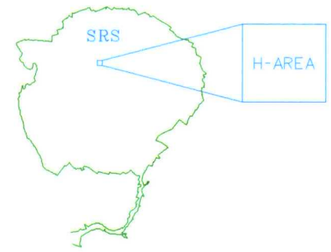


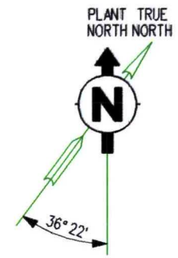


0 50 100 150 200
SCALE: FEET

| DWG NO. | REV. NO. | REV. DATE | AREA |
|---|---|---|---|
| GH3221 | 0 | 9-27-95 | H-AREA |

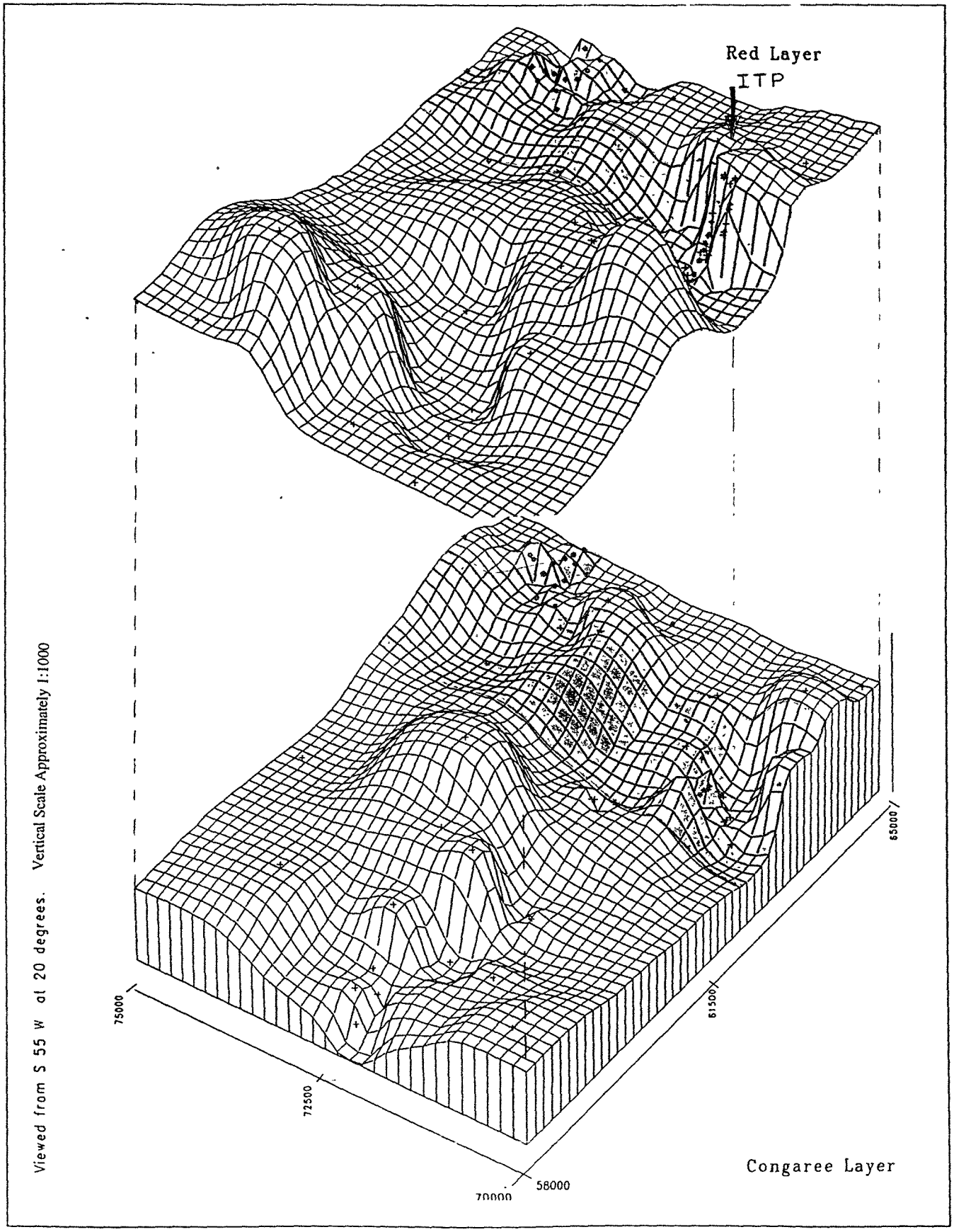


Figure 5.4-2 Isometric view of TR3/Red Layer and Congaree surface.

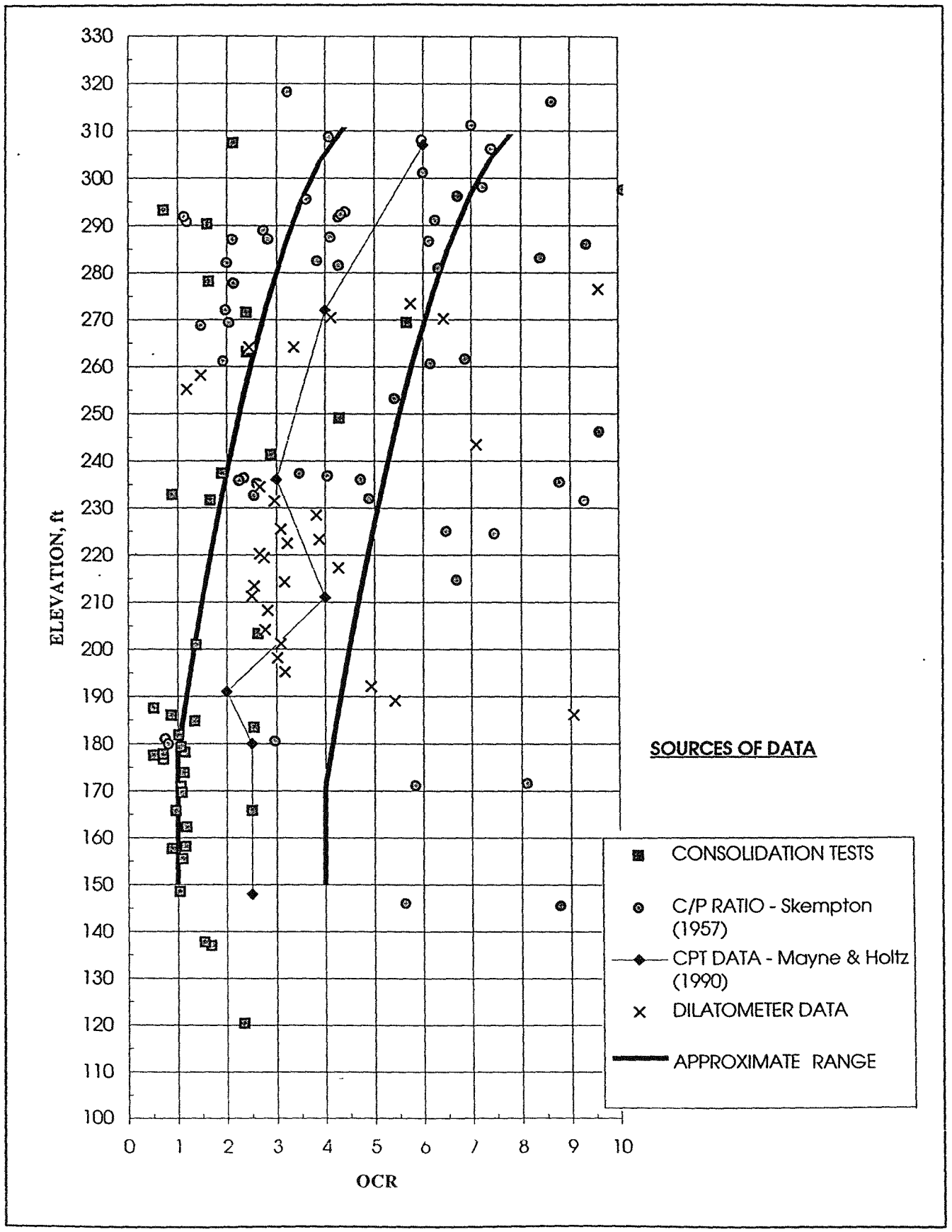


Figure 6.0-1 Variation of overconsolidation ratio (OCR) with elevation at the ITP facility.

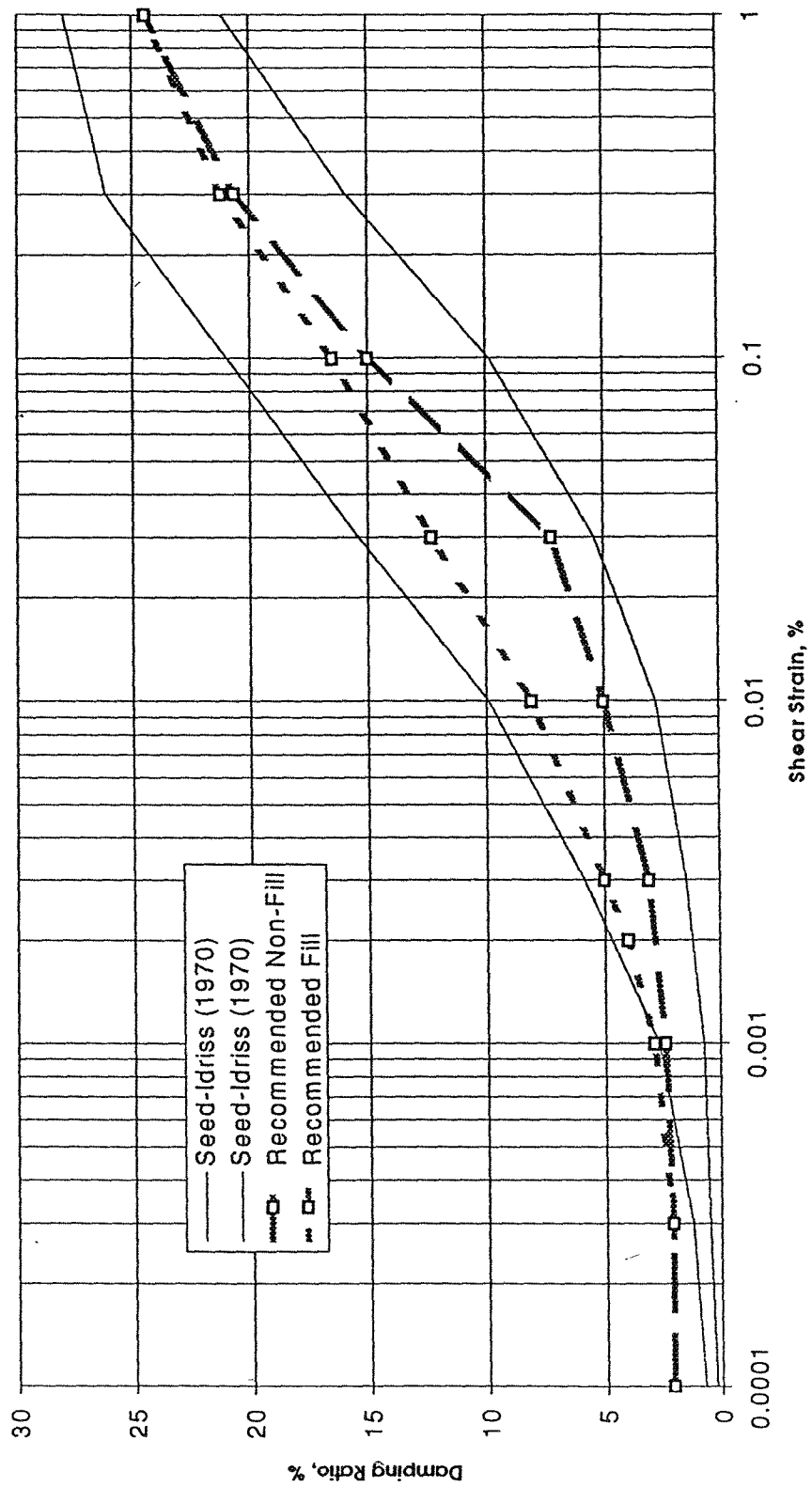


Figure 6.1.1 Variation of damping ratio with cyclic shear strain amplitude for upper ITP soils.

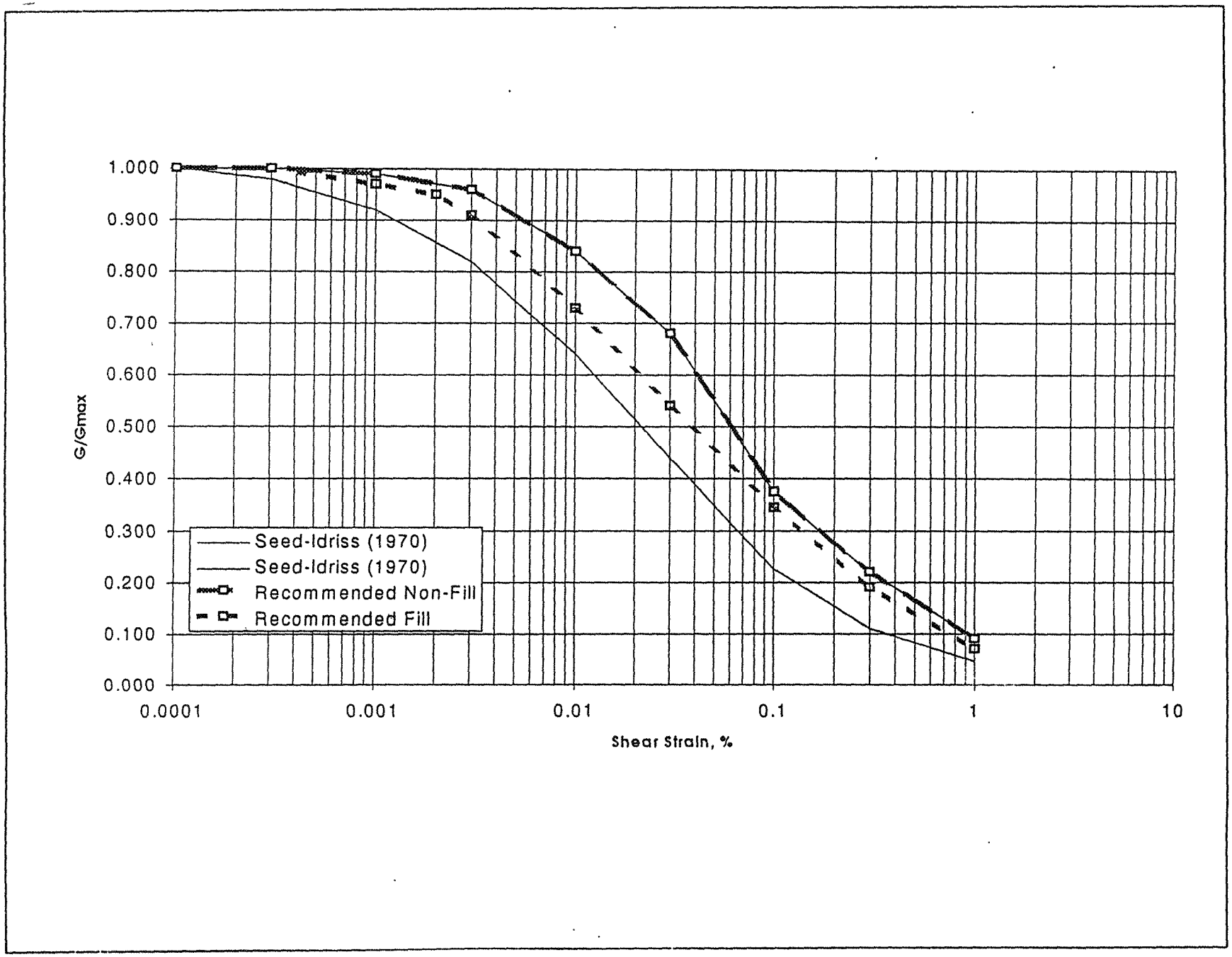


Figure 6.1-2 Shear modulus reduction with cyclic shear strain amplitude for upper ITP soils.

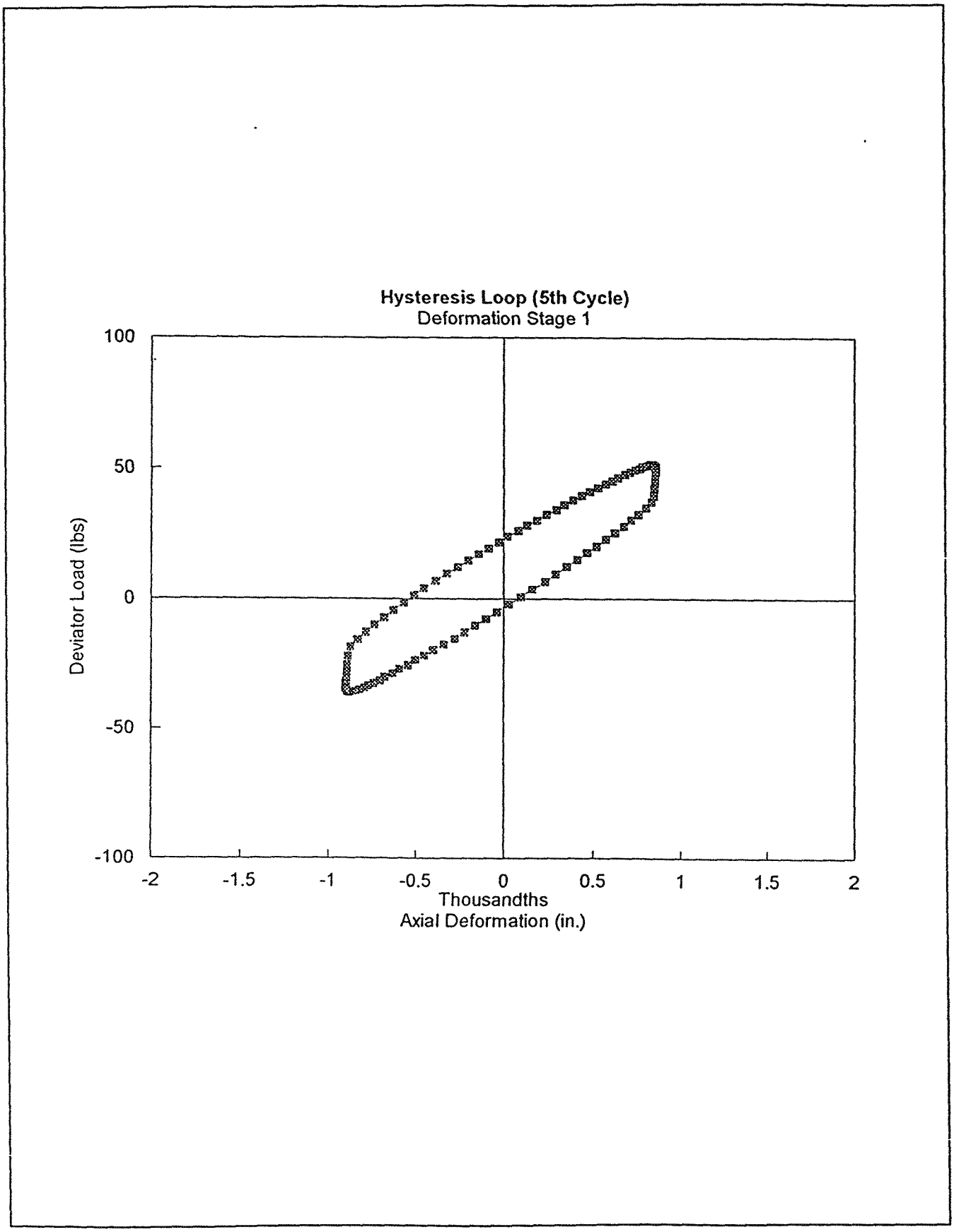


Figure 6.1-3(a) Typical example of cut-off trace from strain controlled dynamic triaxial tests.

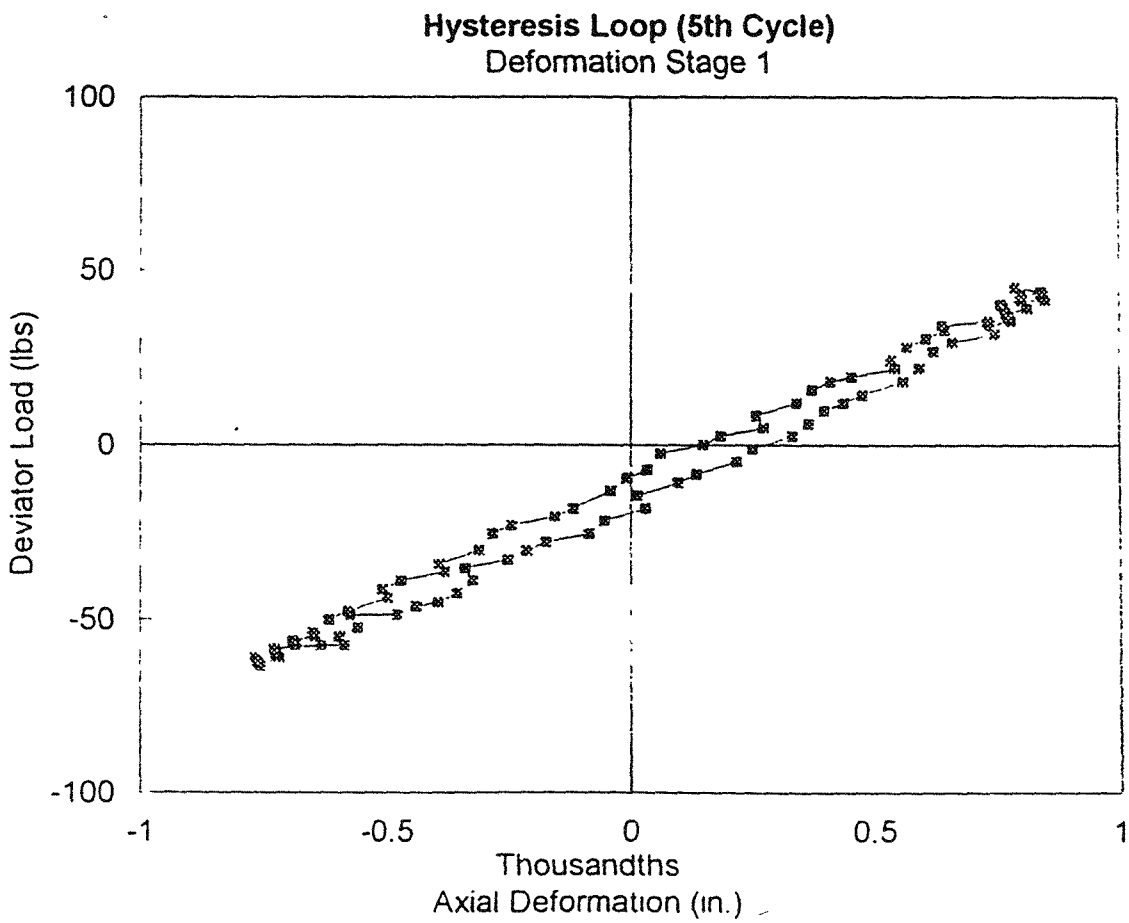


Figure 6.1-3(b) Typical example of jagged trace from strain controlled dynamic triaxial tests.

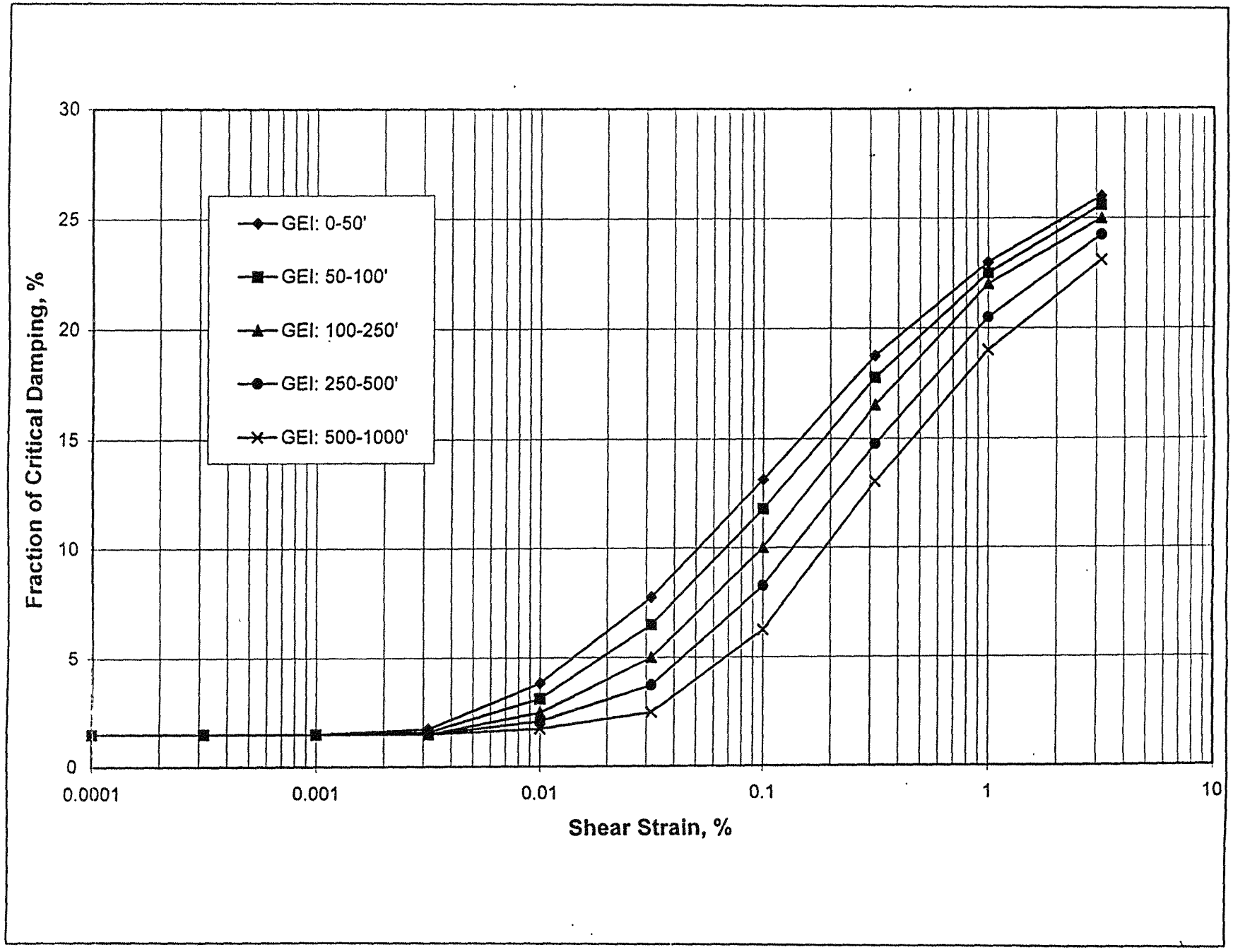


Figure 6.1-4 Variation of damping ratio with cyclic shear strain modulus (GEI, 1991 B).

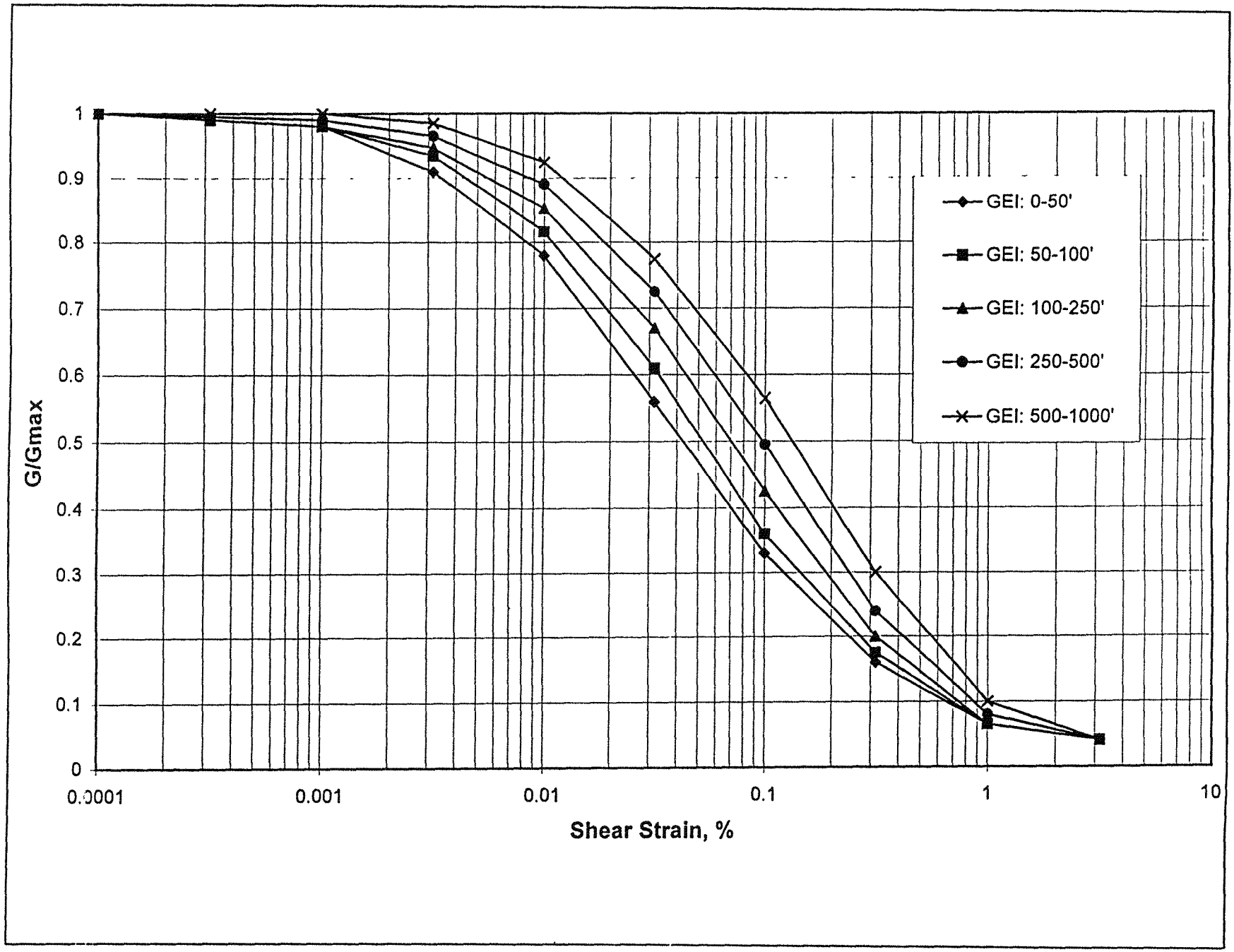


Figure 6.1-5 Shear modulus reduction with cyclic shear strain amplitude (GEI, 1991 B).

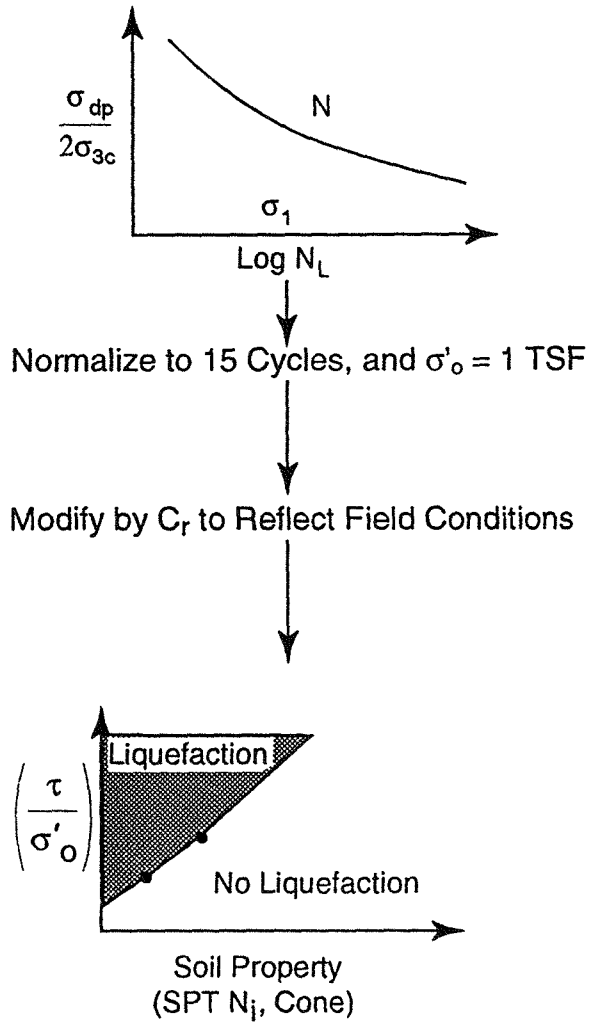


Figure 6.2-1 Methodology used to develop relationships between cyclic stress ratios in the laboratory and in the field.

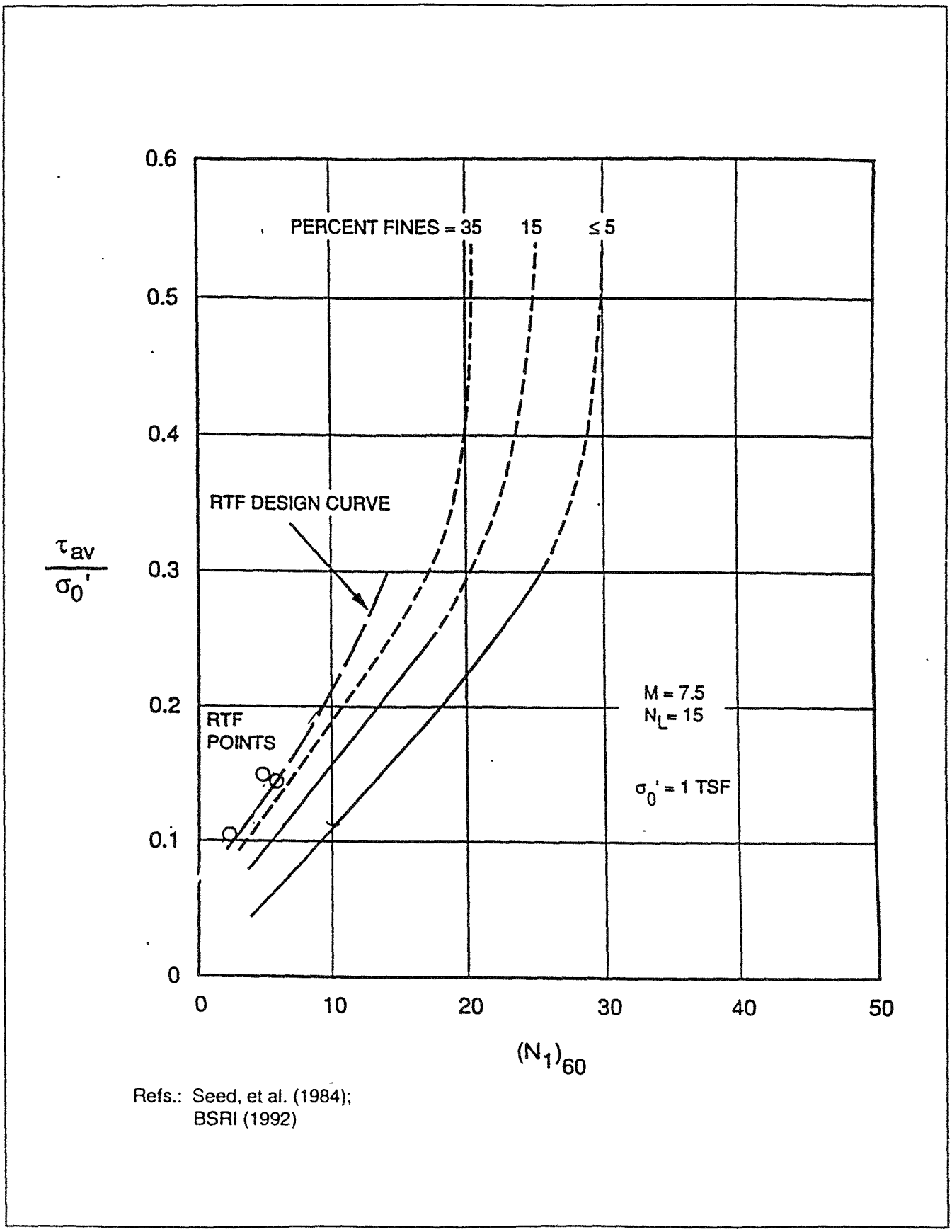


Figure 6.2-2 Relationship between RTF design curve for stress ratio causing initial liquefaction and $(N_1)_{60}$ values. Comparison with empirical data.

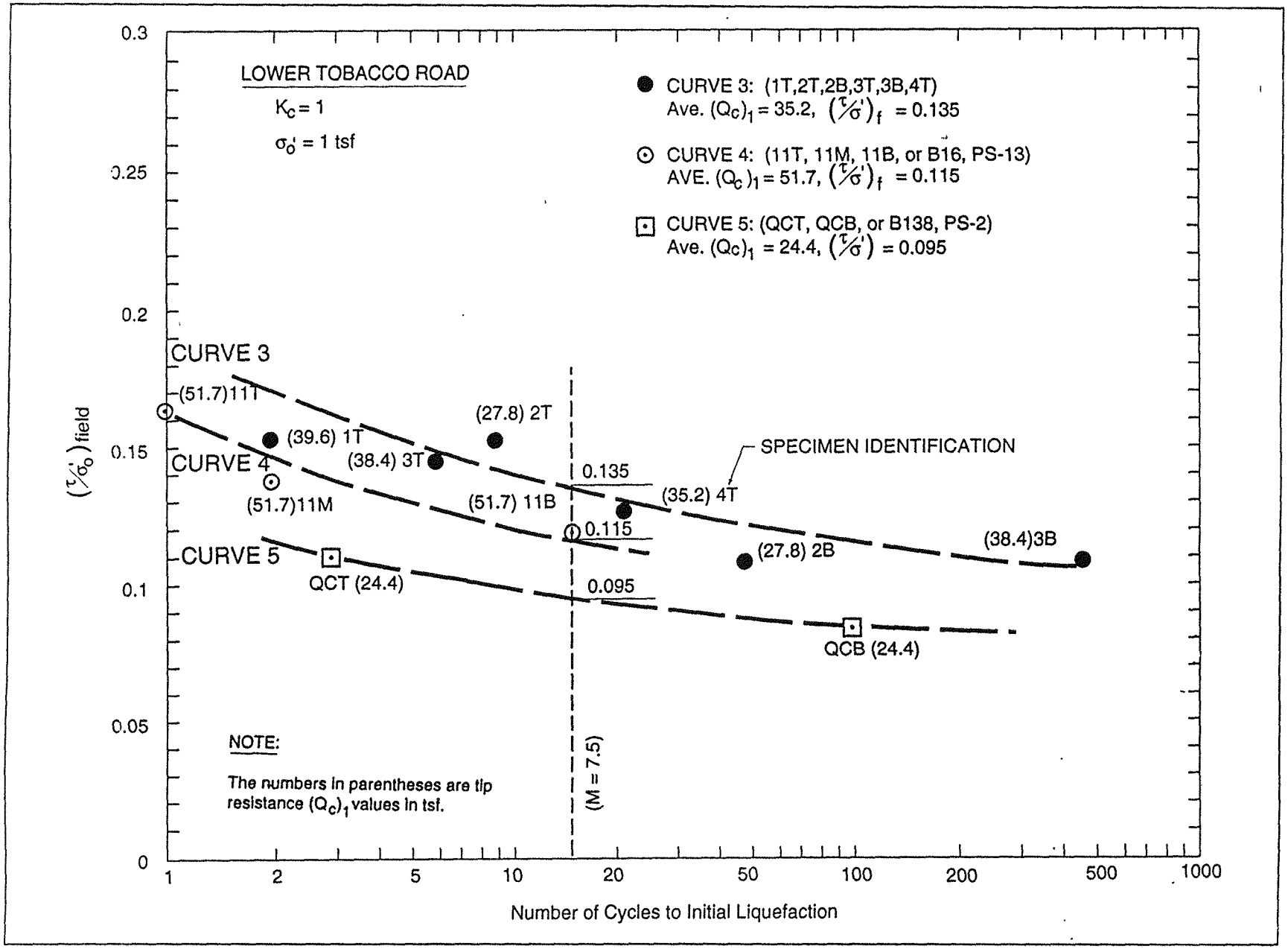


Figure 6.2-3 RTF: cyclic triaxial test results (1).

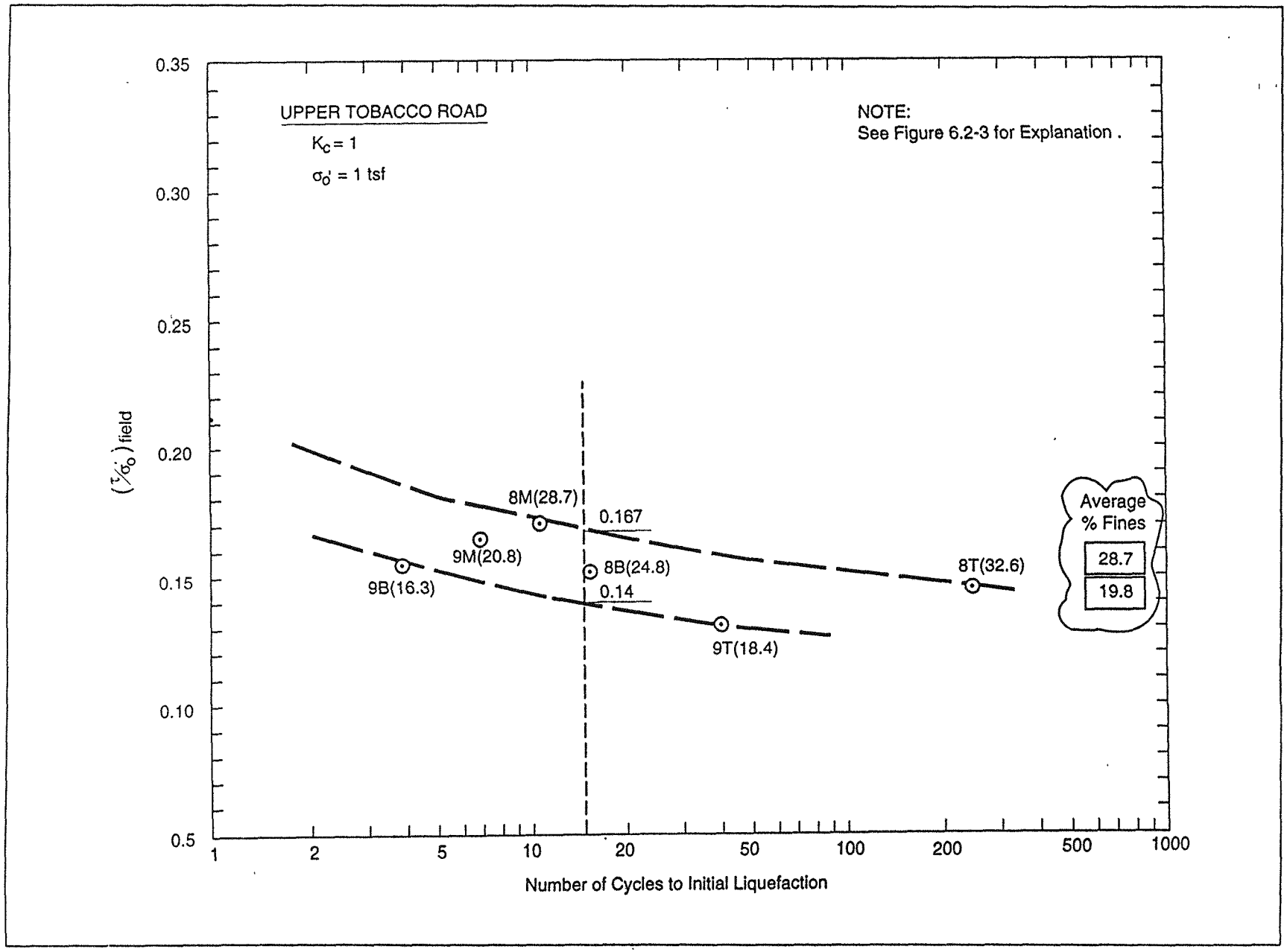


Figure 6.2-4 RTF: cyclic triaxial test results (2).

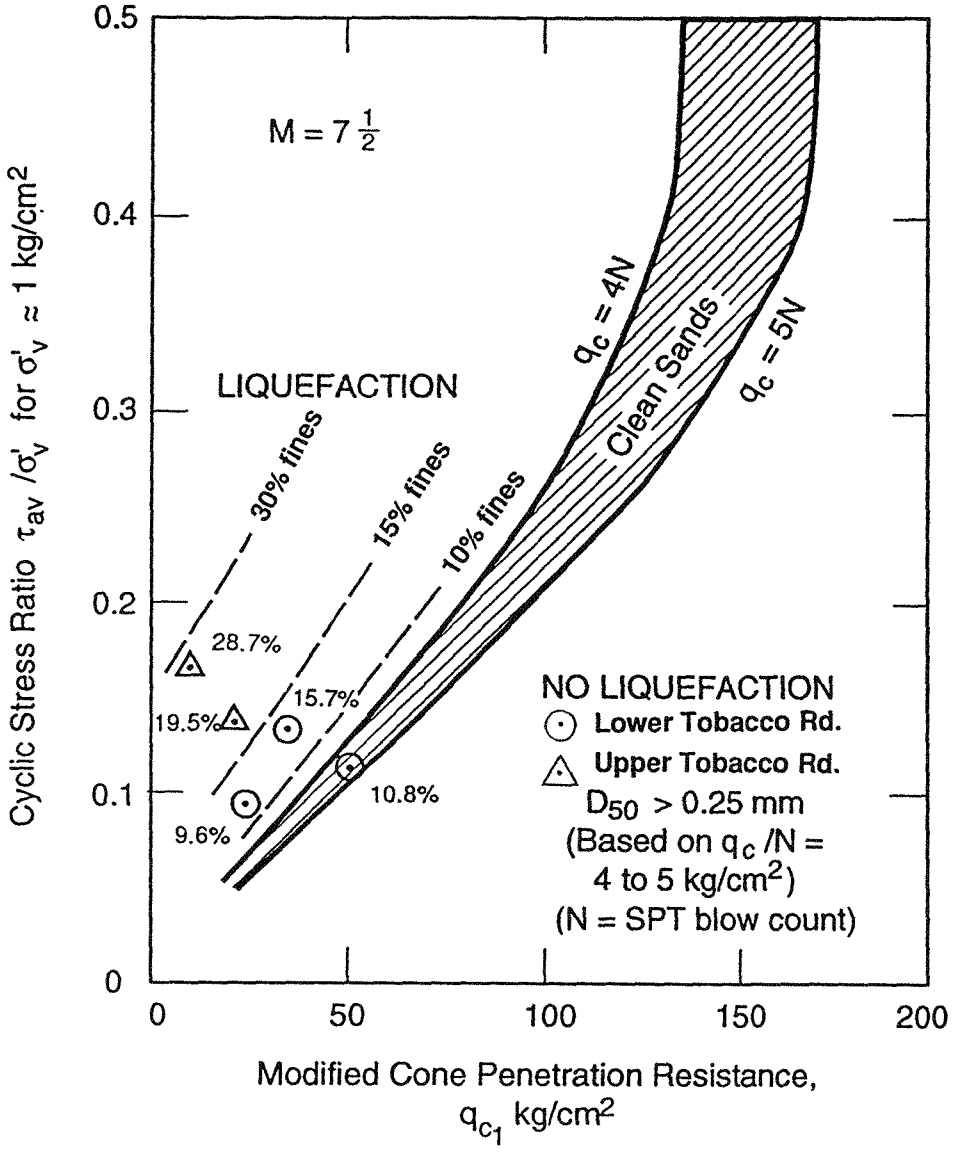


Ref.: Seed et al., 1983

Figure 6.2-5 Proposed correlation for RTF between modified cone tip resistance and cyclic stress ratio required for initial liquefaction.

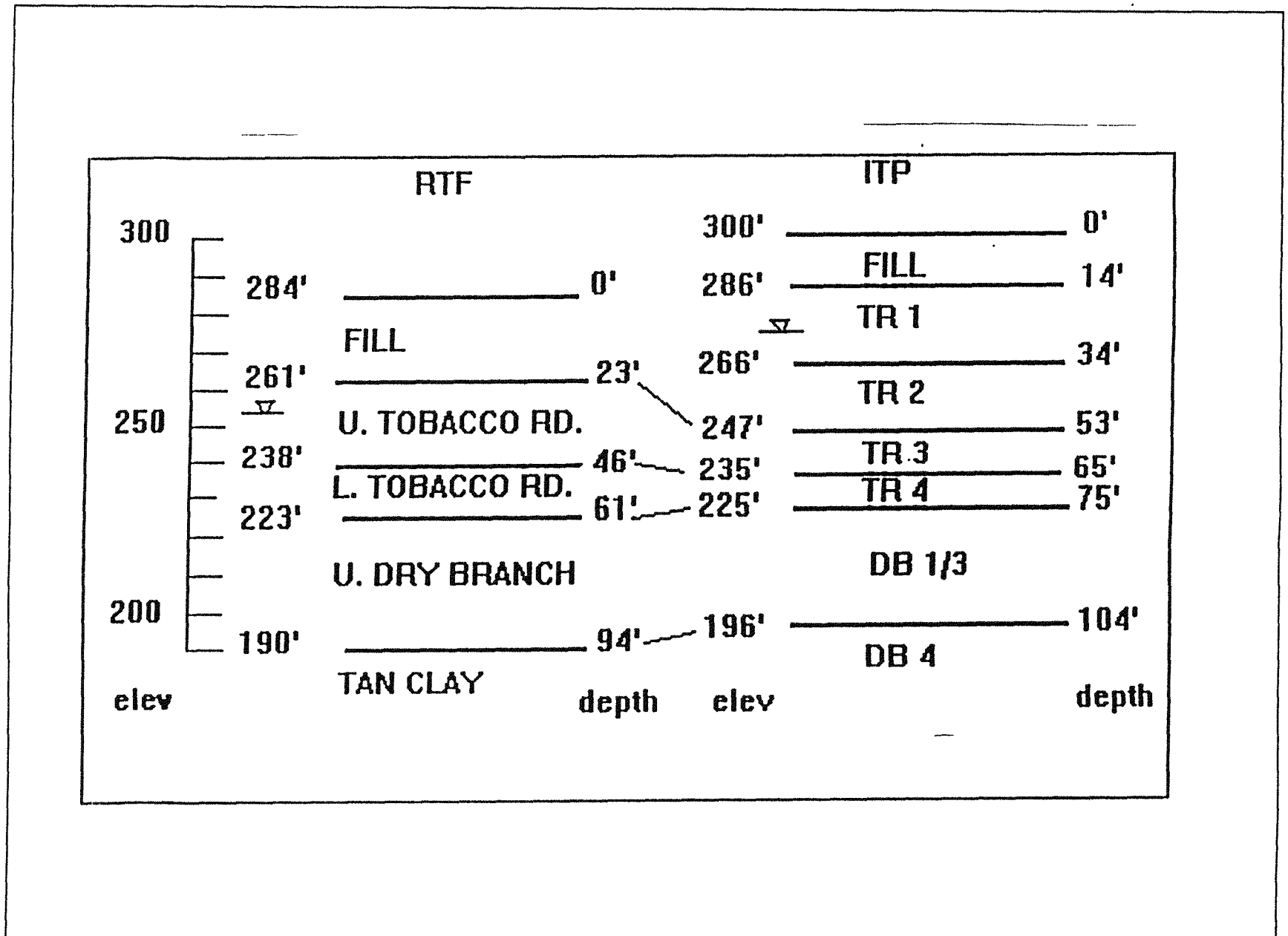


Figure 6.2-6 Comparison between soil profiles at the RTF and the ITP facilities.

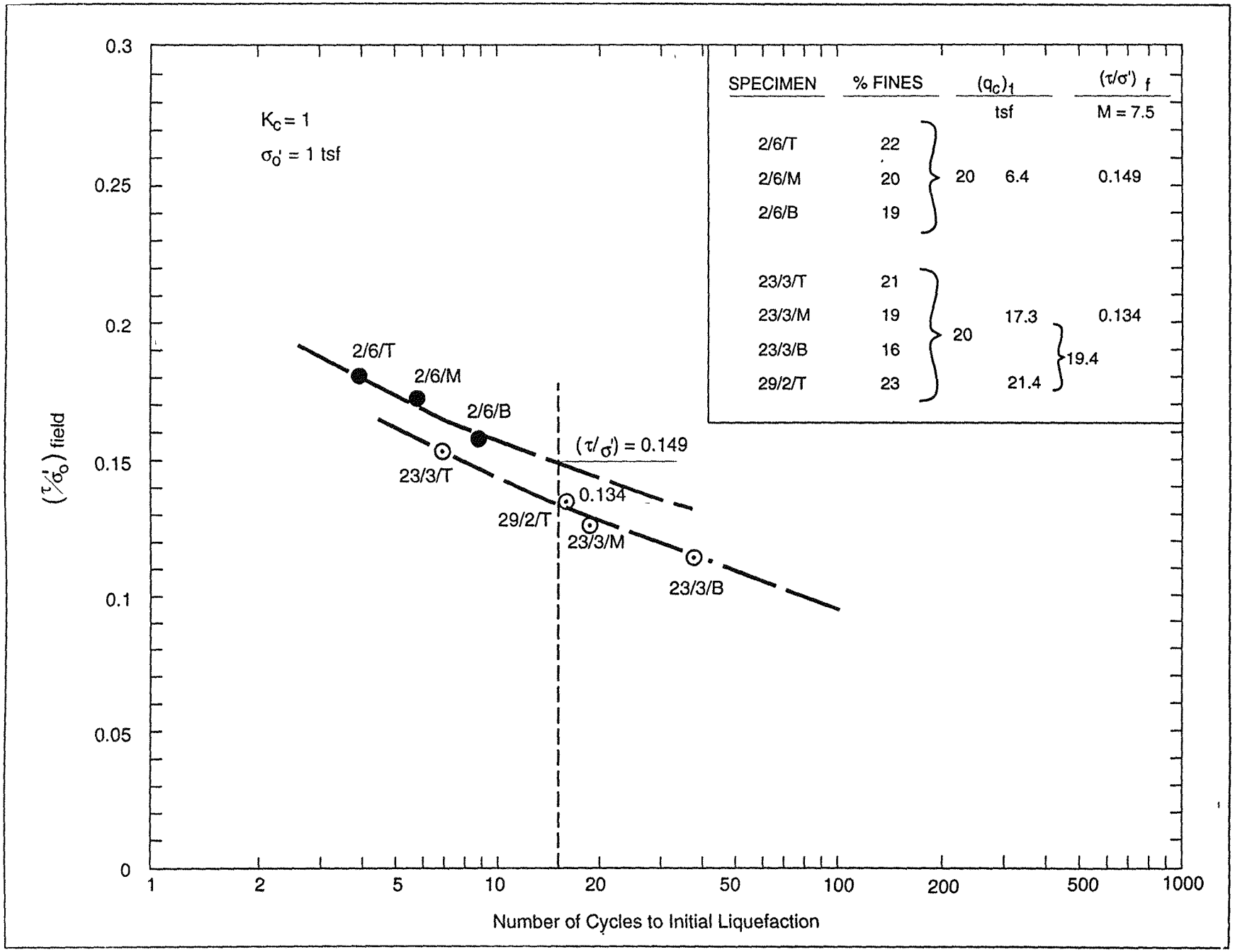


Figure 6.2-7 ITP: cyclic triaxial test results.

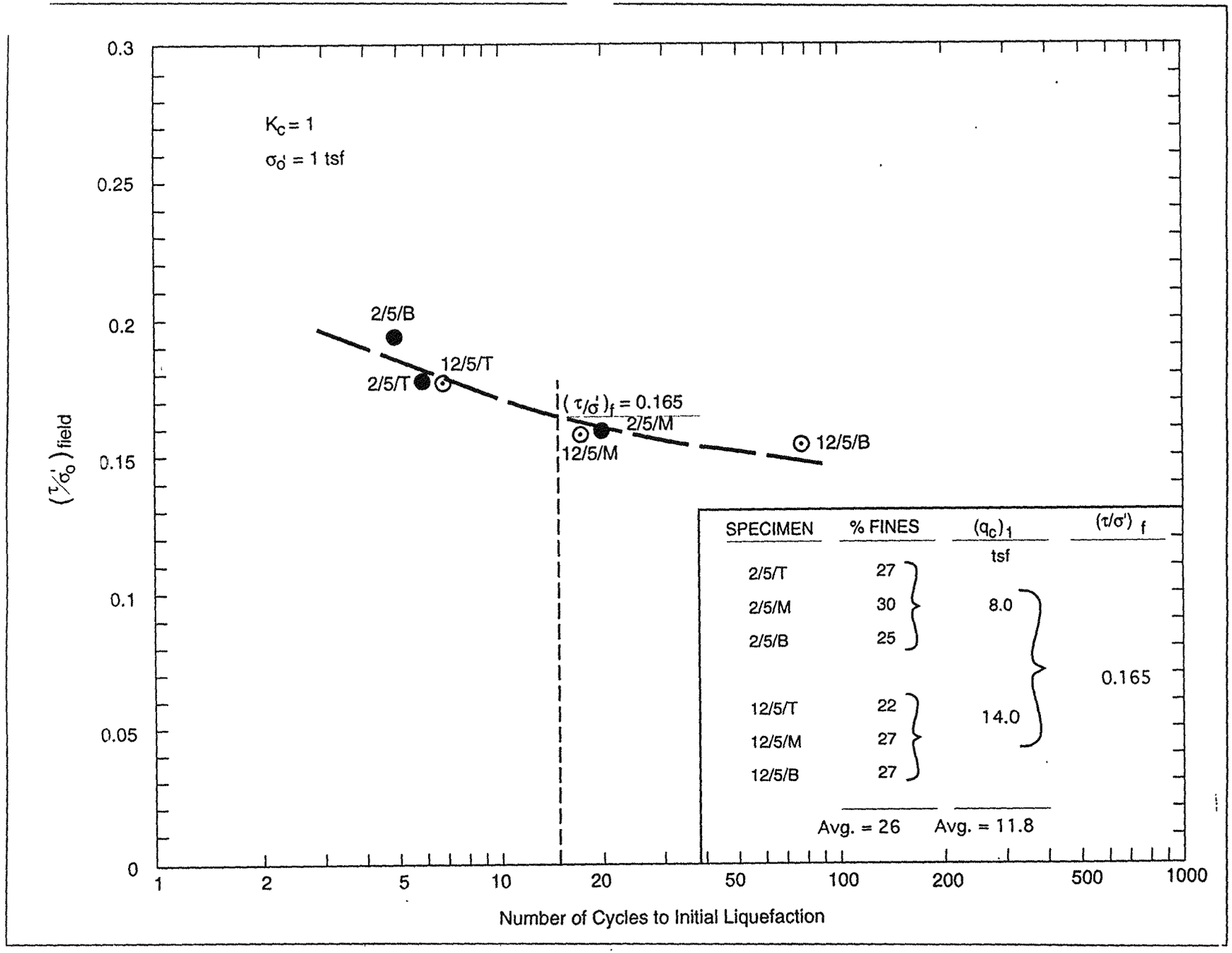


Figure 6.2-8 ITP: cyclic triaxial test results.

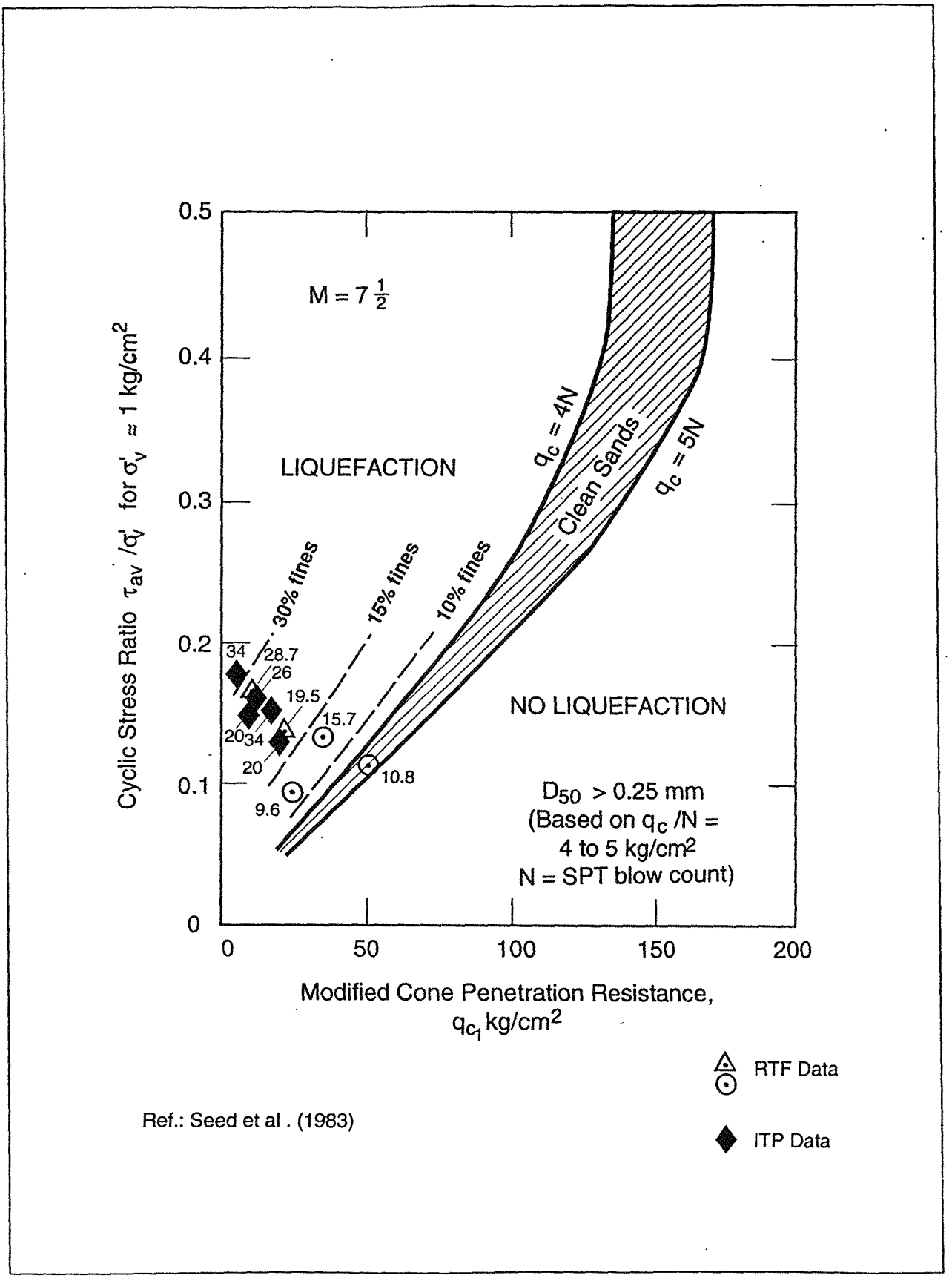


Figure 6.2-10 Proposed correlation for ITP between modified cone tip resistance and cyclic stress ratio required for initial liquefaction.

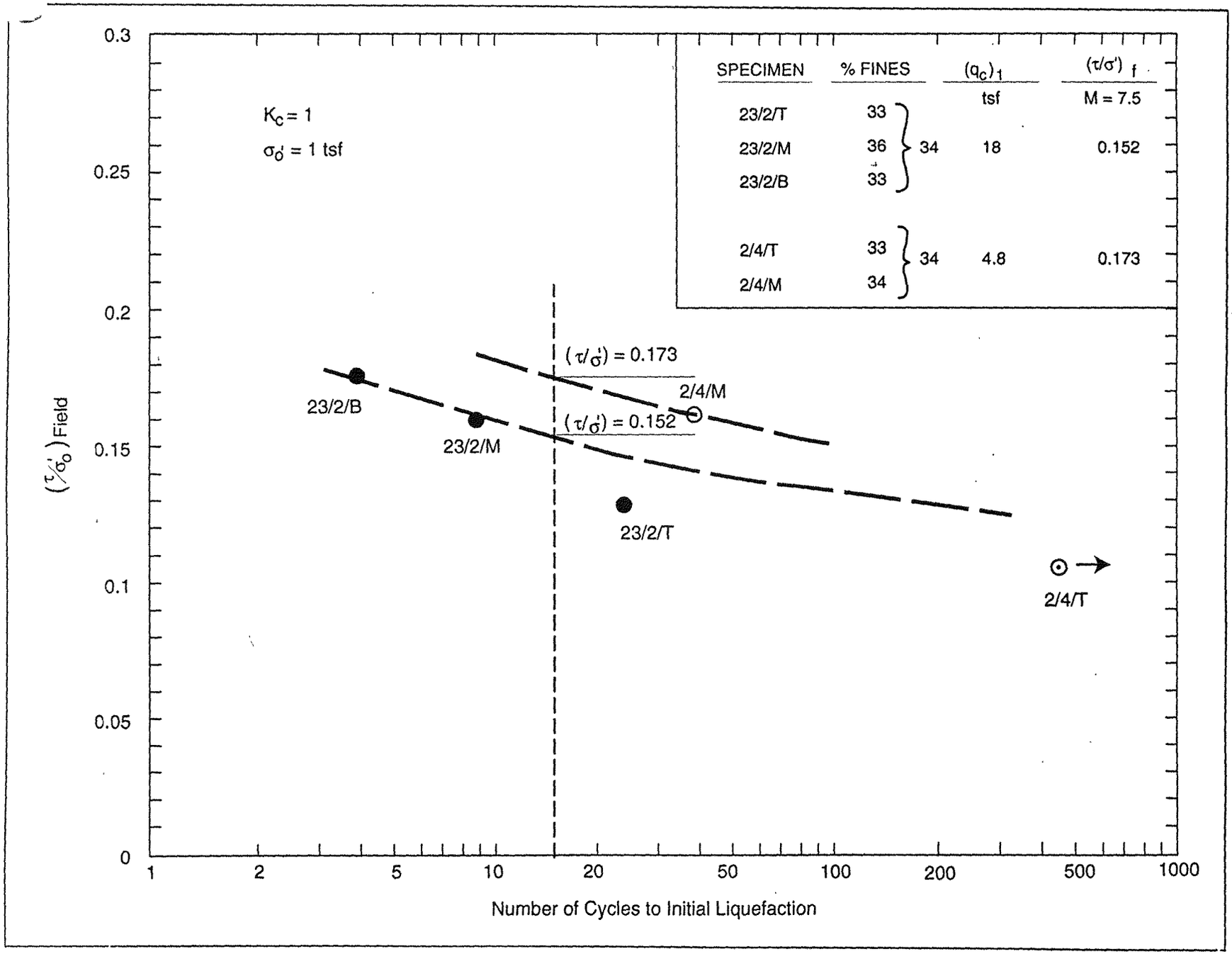


Figure 6.2-9 ITP cyclic triaxial test results.

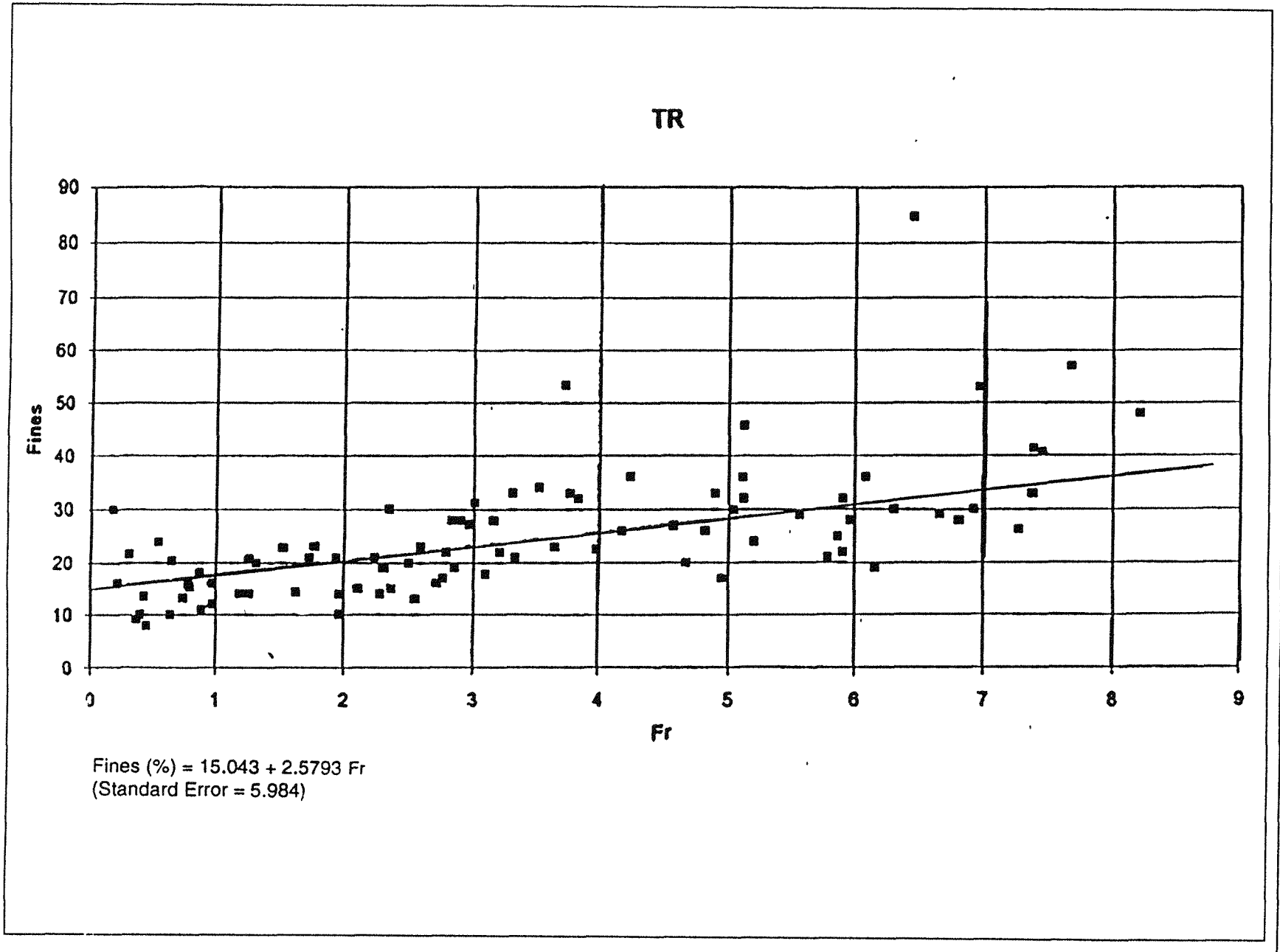


Figure 6.2-11 Correlation between percent fines and friction ration in cone tests.

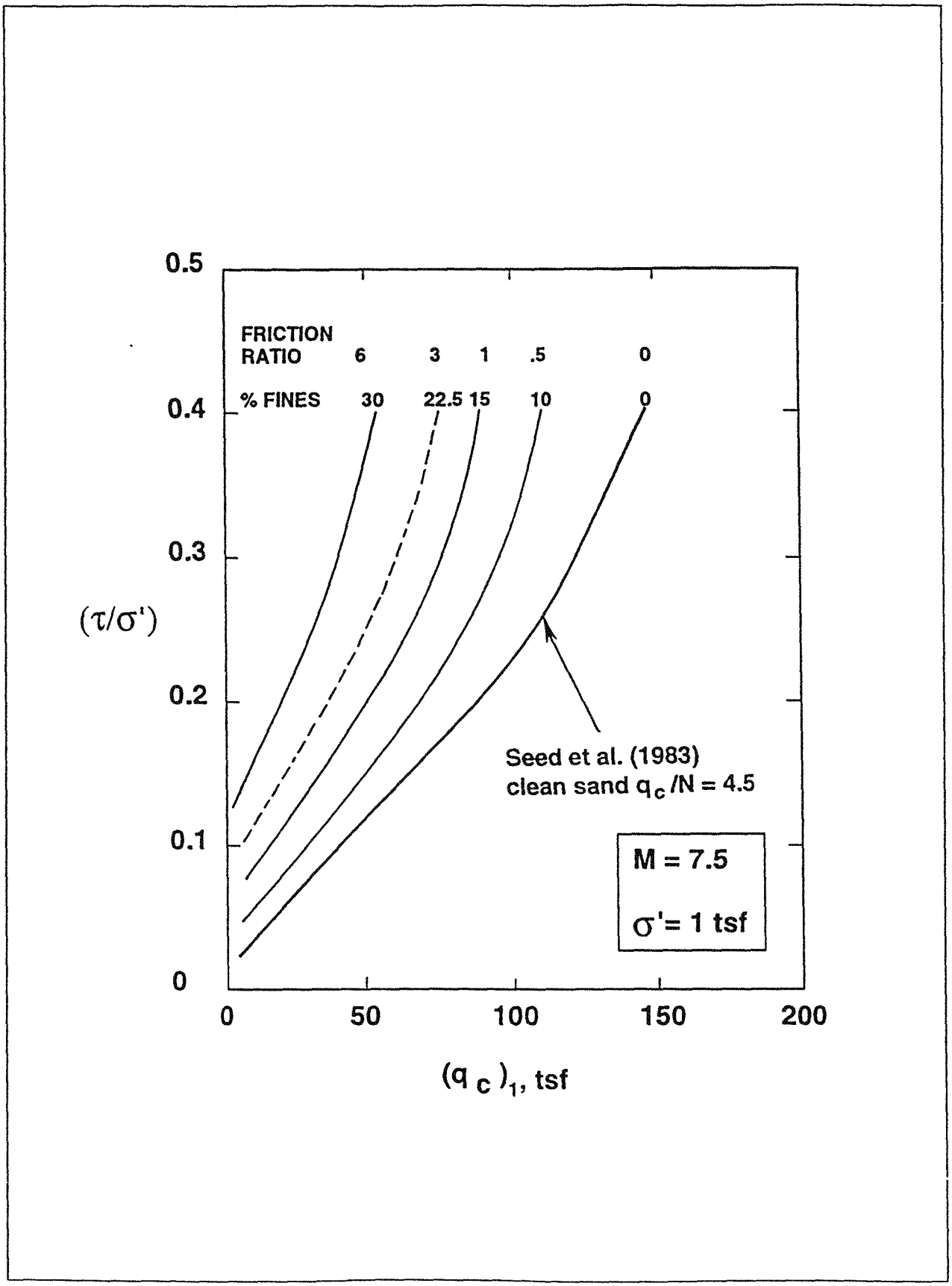


Figure 6.2-12 Proposed correlation for ITP between modified cone tip resistance and friction ratio with the cyclic stress ratio required for initial liquefaction in the field.

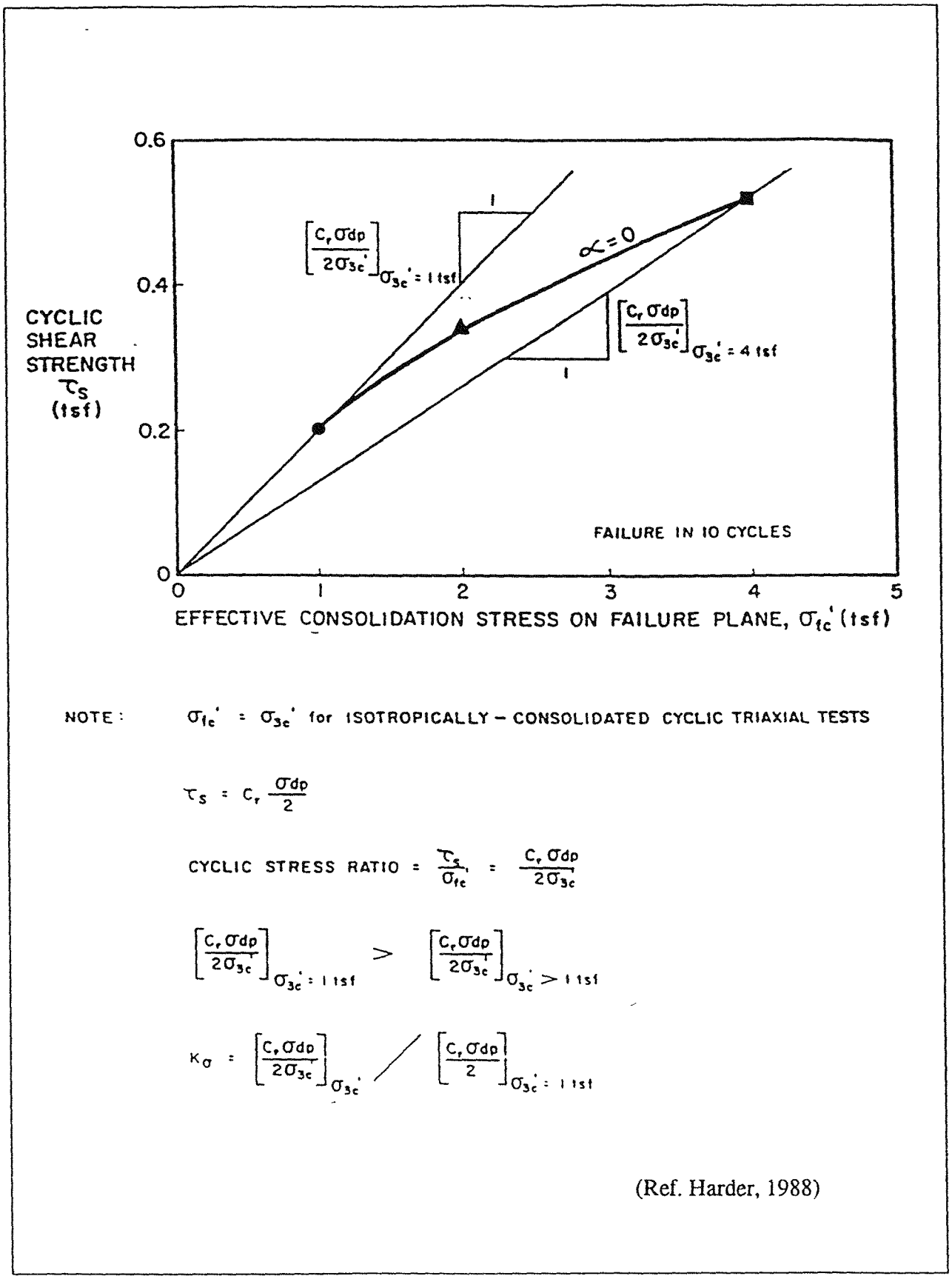


Figure 6.2-13 Derivation of the $k_\sigma$ factor relating the influence of confining pressure on the cyclic stress ratio in laboratory triaxial tests.

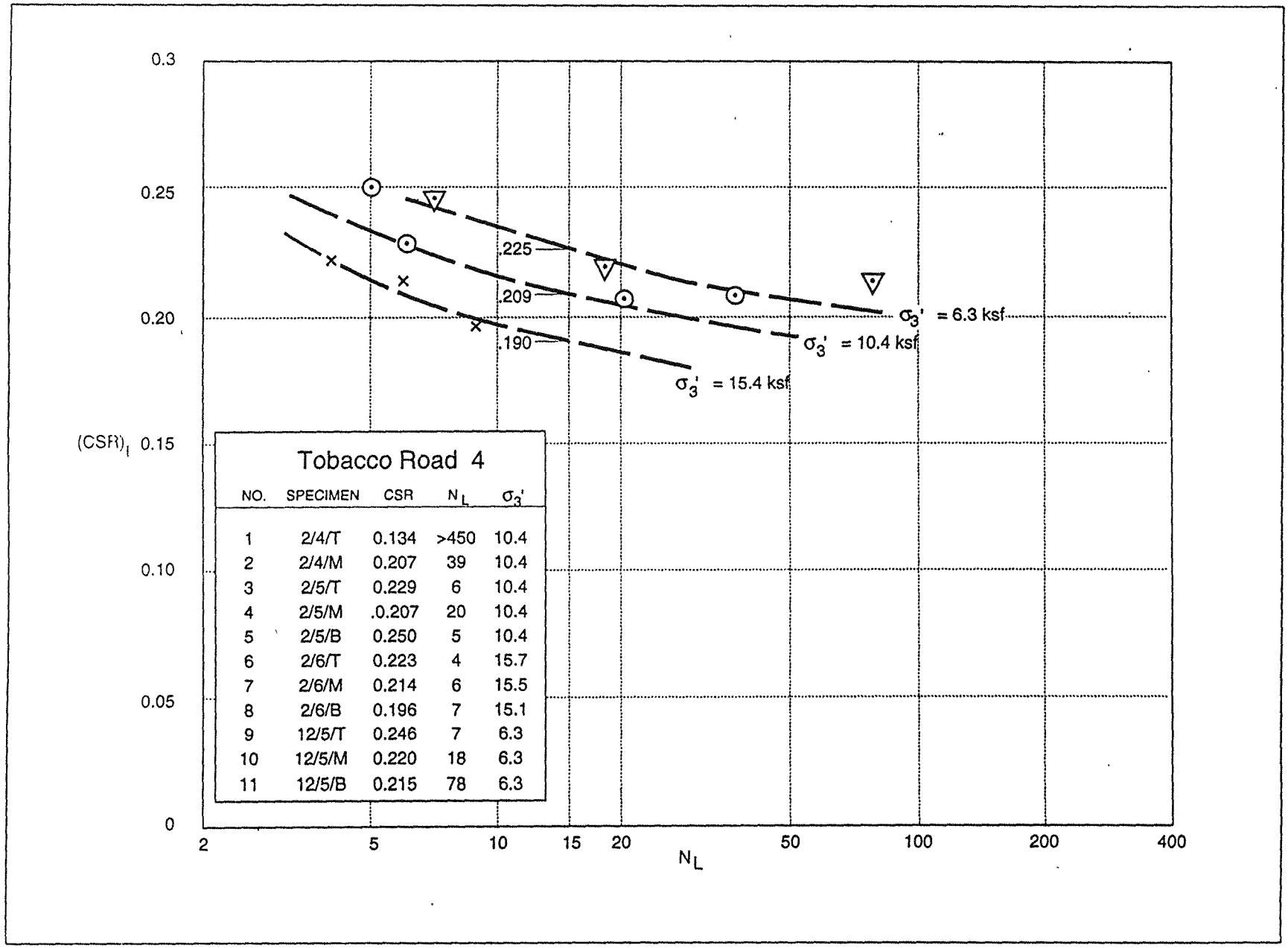


Figure 6.2-14 ITP soils: Influence of confining pressure on cyclic triaxial test results (1).

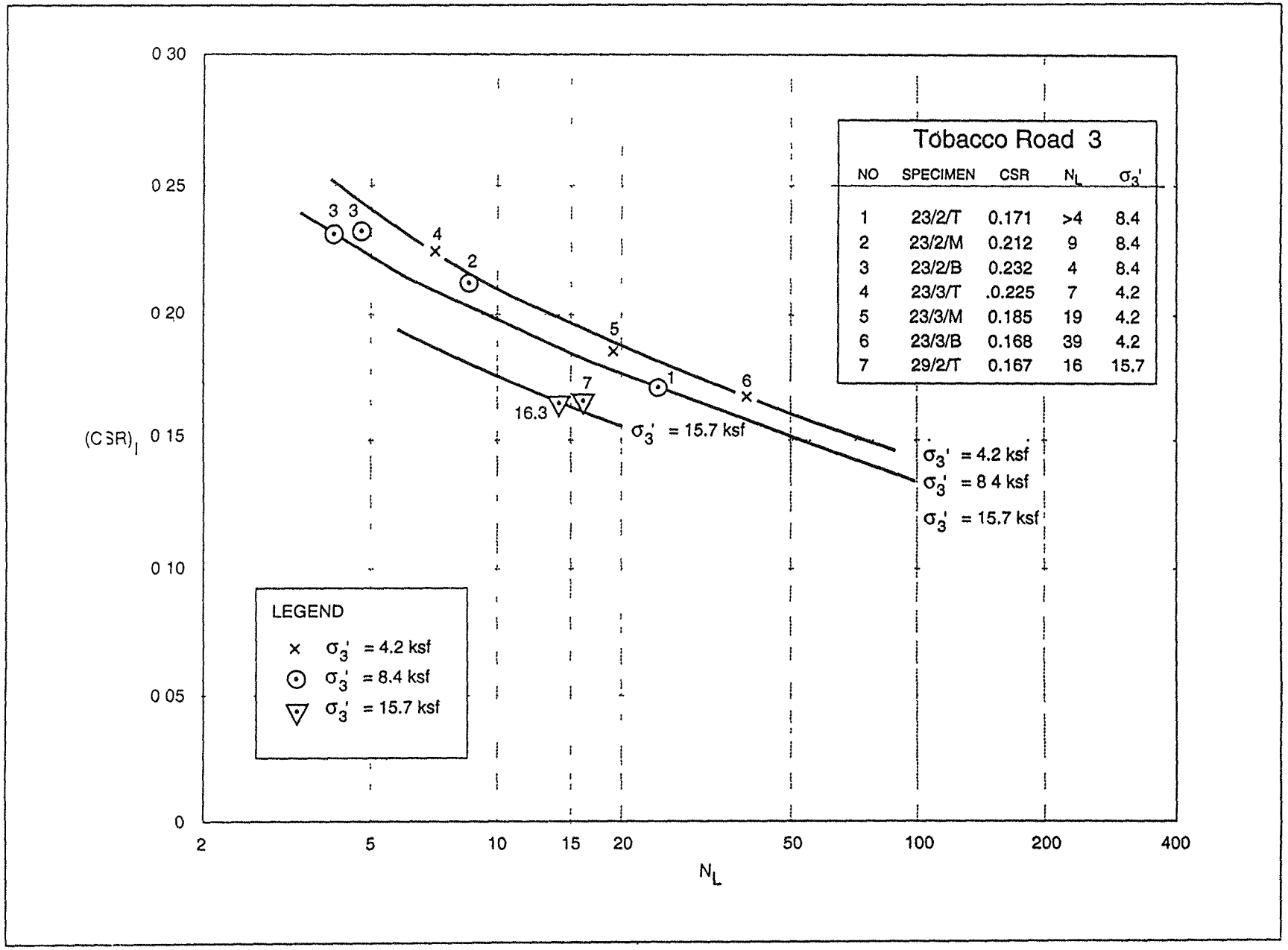


Figure 6.2-15 ITP soils: Influence of confining pressure on cyclic triaxial test results (2).

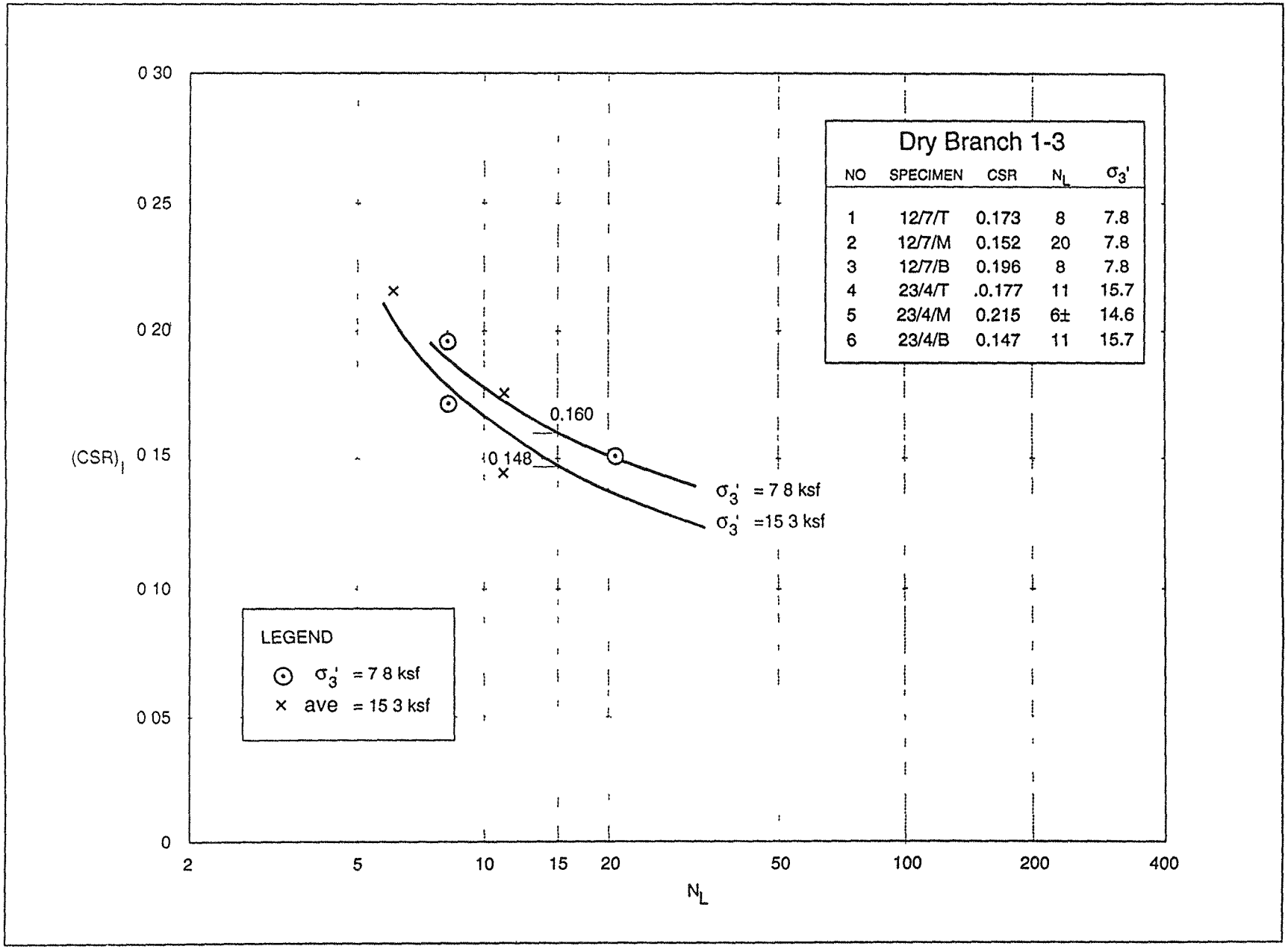


Figure 6.2-16 ITP soils: Influence of confining pressure on cyclic triaxial test results (3).

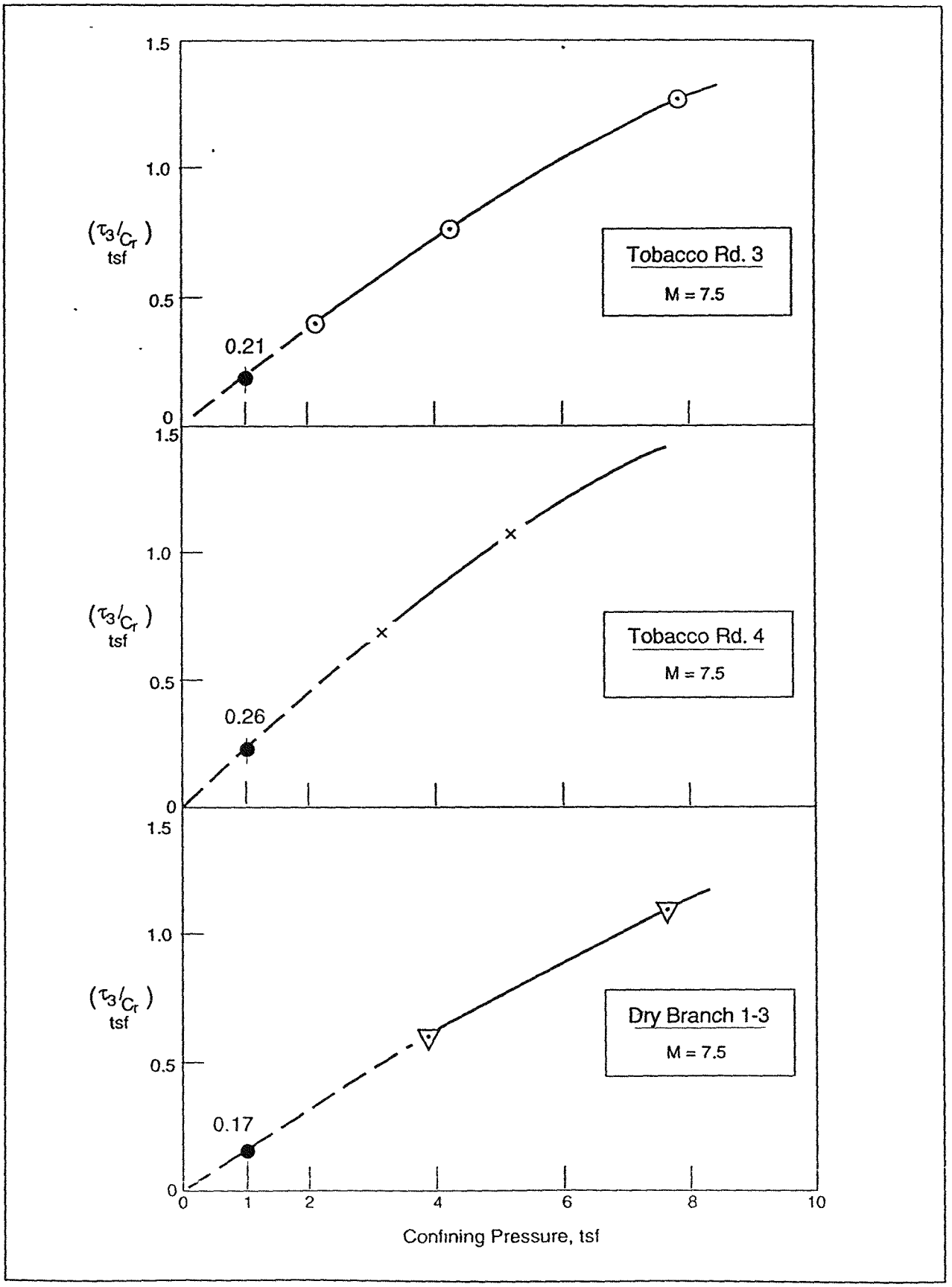


Figure 6.2-17 ITP soils: Derivation of a site-specific Kσ factor.

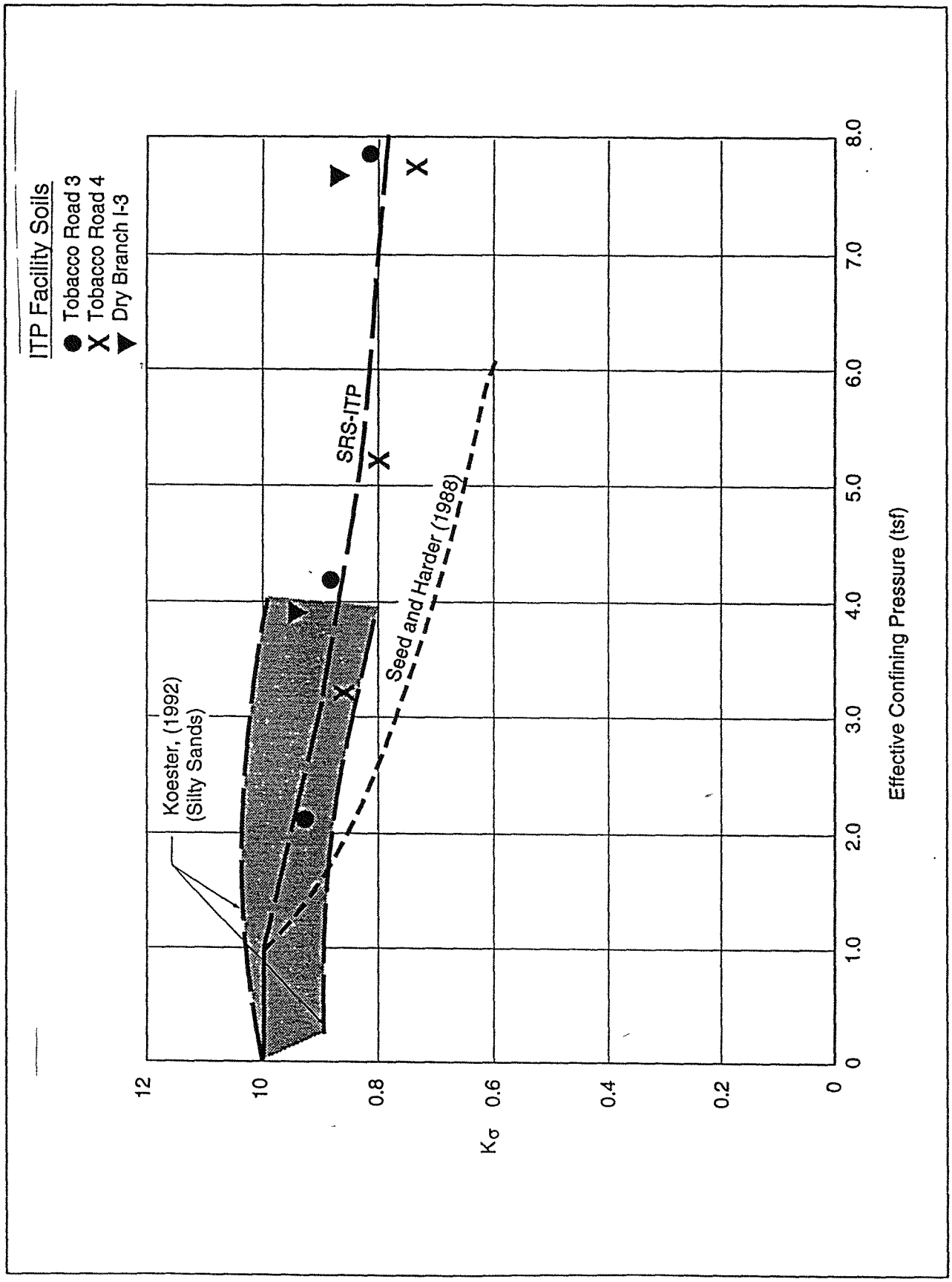


Figure 6.2-18 Comparison of Kσ factors from several sources.

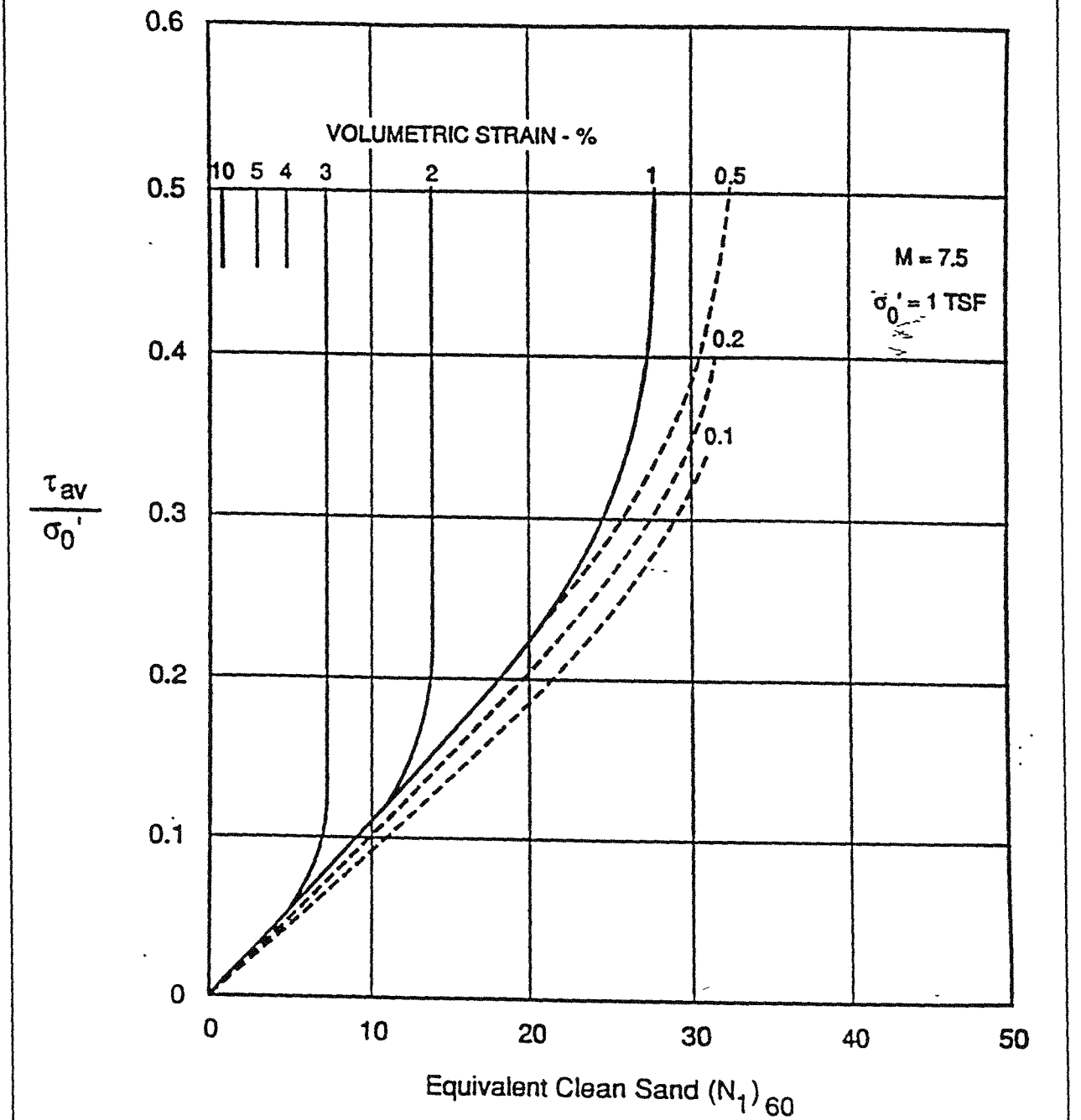


Ref.: Tokimatsu and Seed (1984)

Figure 6.2-19 Relationship between cyclic stress ratio, $(N_1)_{60}$ and volumetric strain for saturated clay sands.

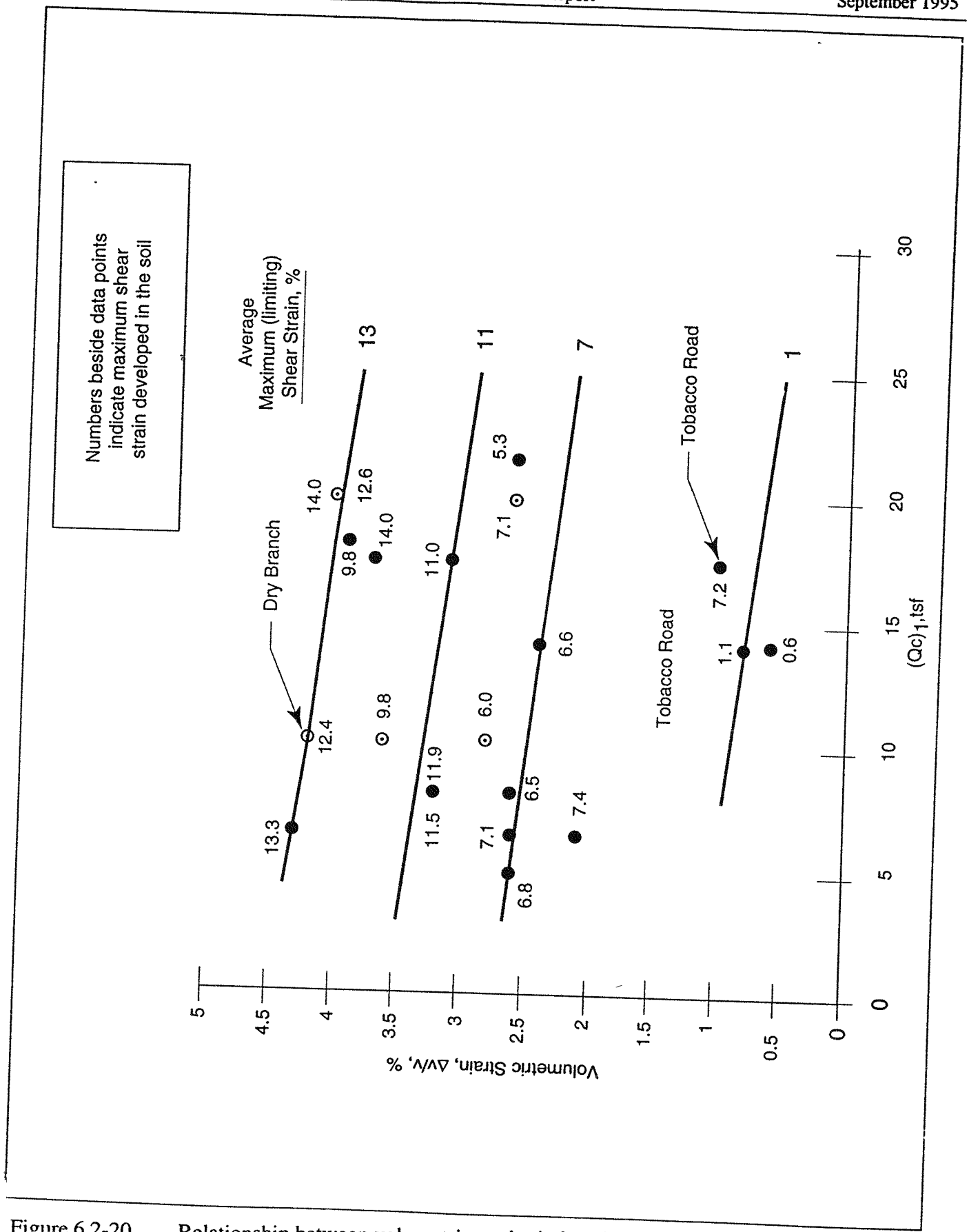


Figure 6.2-20 Relationship between volumetric strain, induced maximum limiting shear strain, and cone tip penetration resistance.

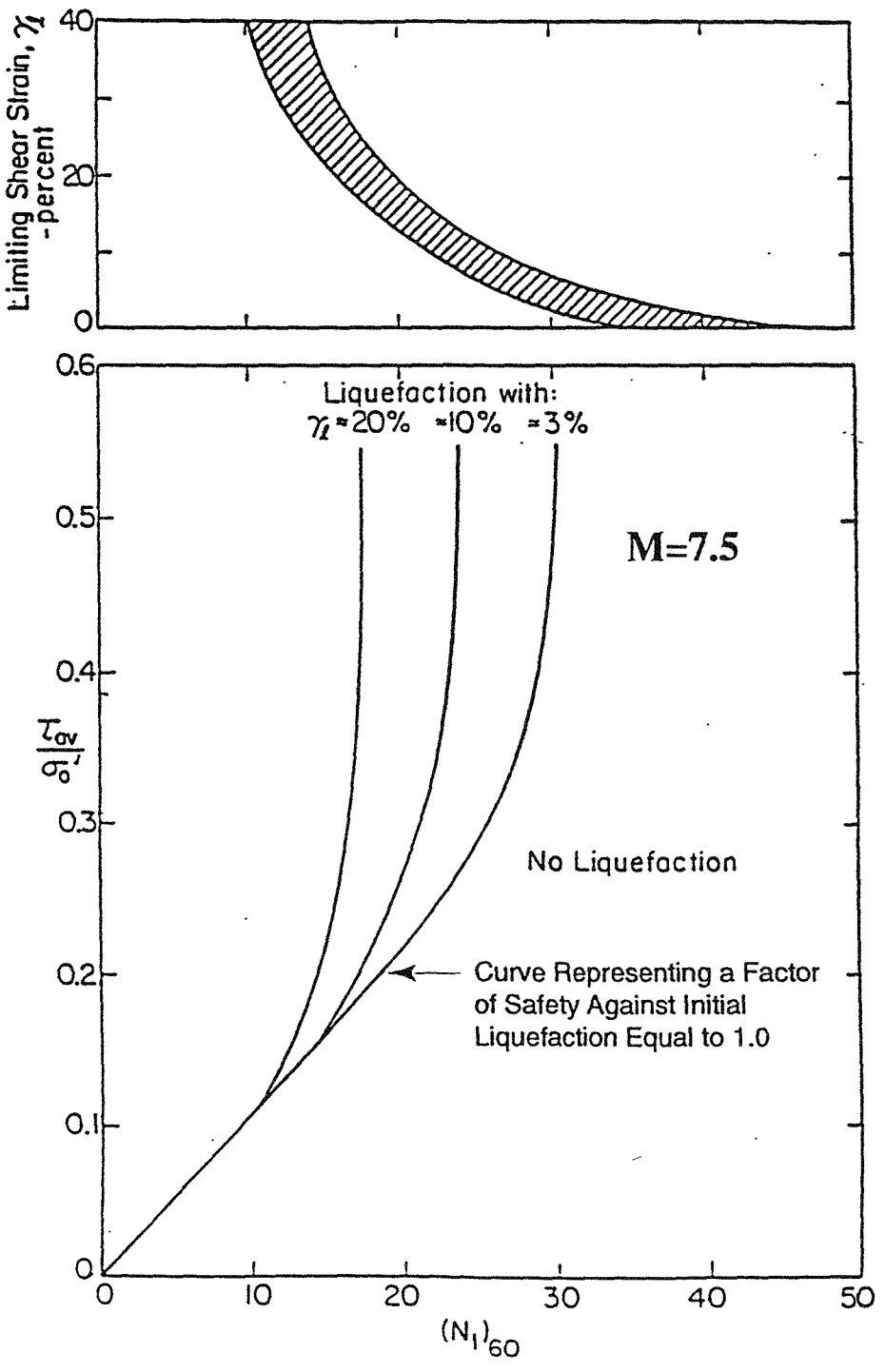


Figure 6.2-21 Relationship between cyclic stress ratio causing initial liquefaction, $(N_1)_{60}$ and limiting shear strain.

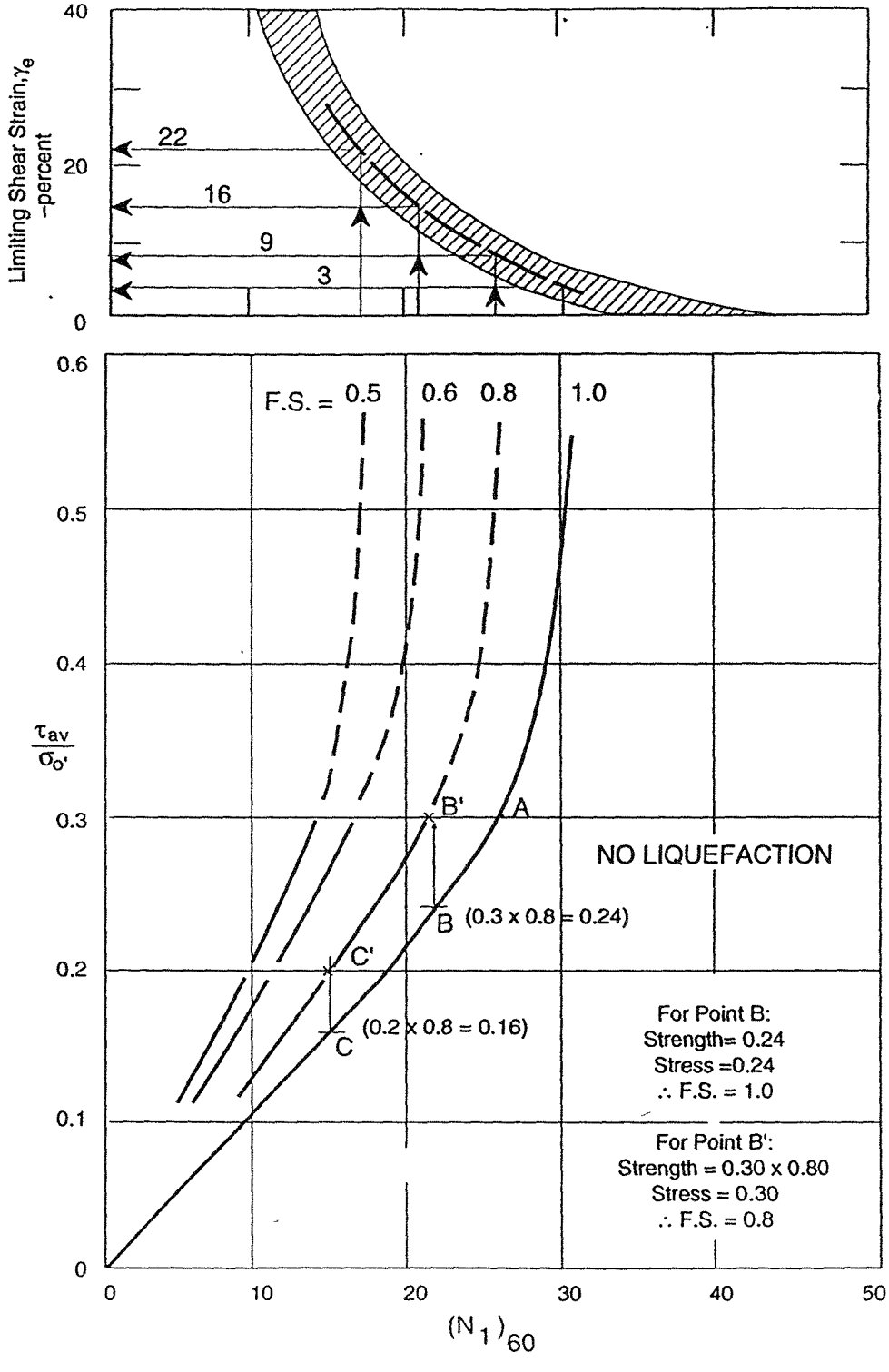


Figure 6.2-22 Derivation of a relationship between limiting cyclic shear strain and factor of safety against initial liquefaction.

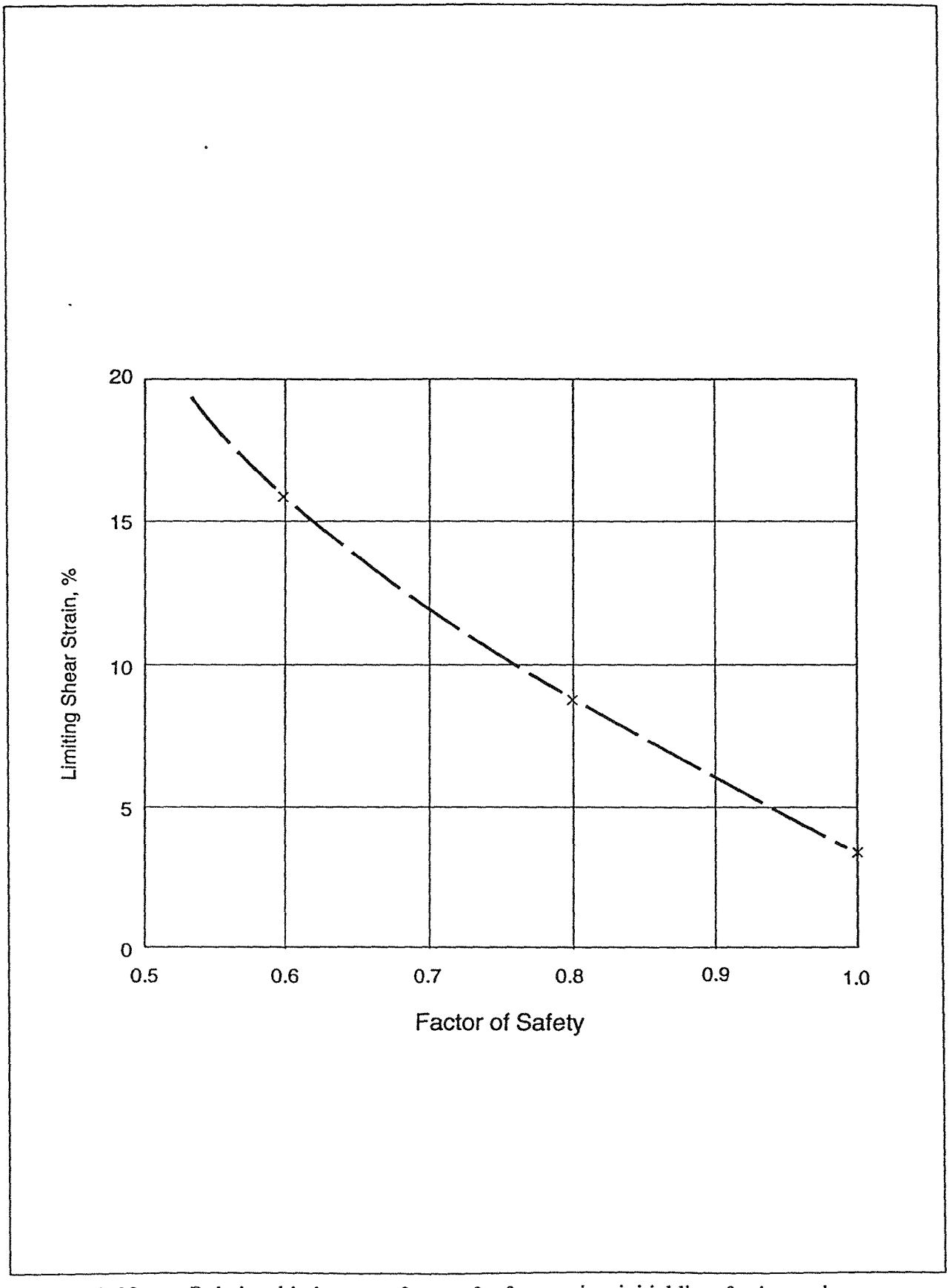


Figure 6.2-23 Relationship between factor of safety against initial liquefaction and limiting cyclic shear strain.

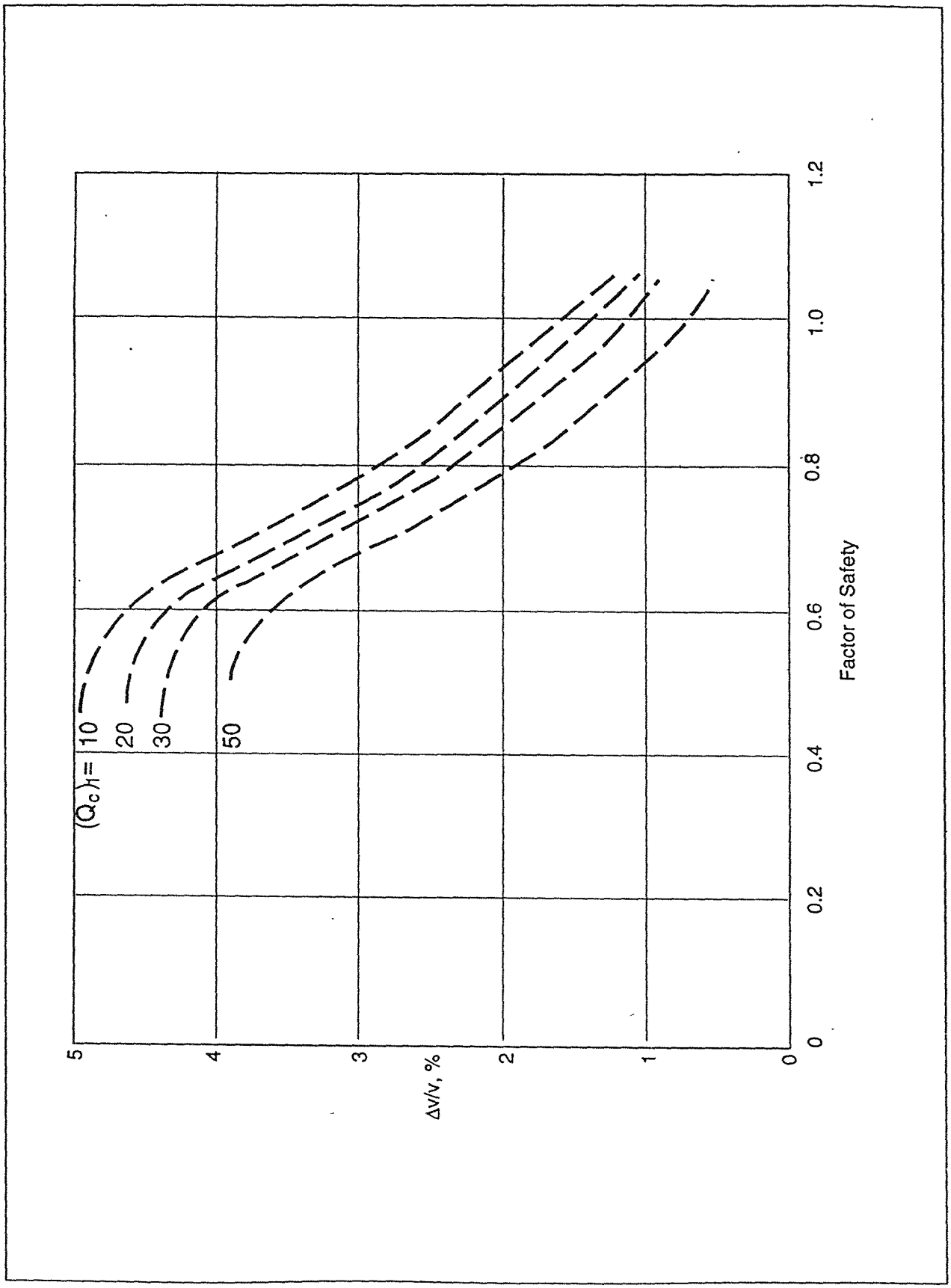


Figure 6.2-24 Relationship between factor of safety against initial liquefaction and volumetric strain after liquefaction.

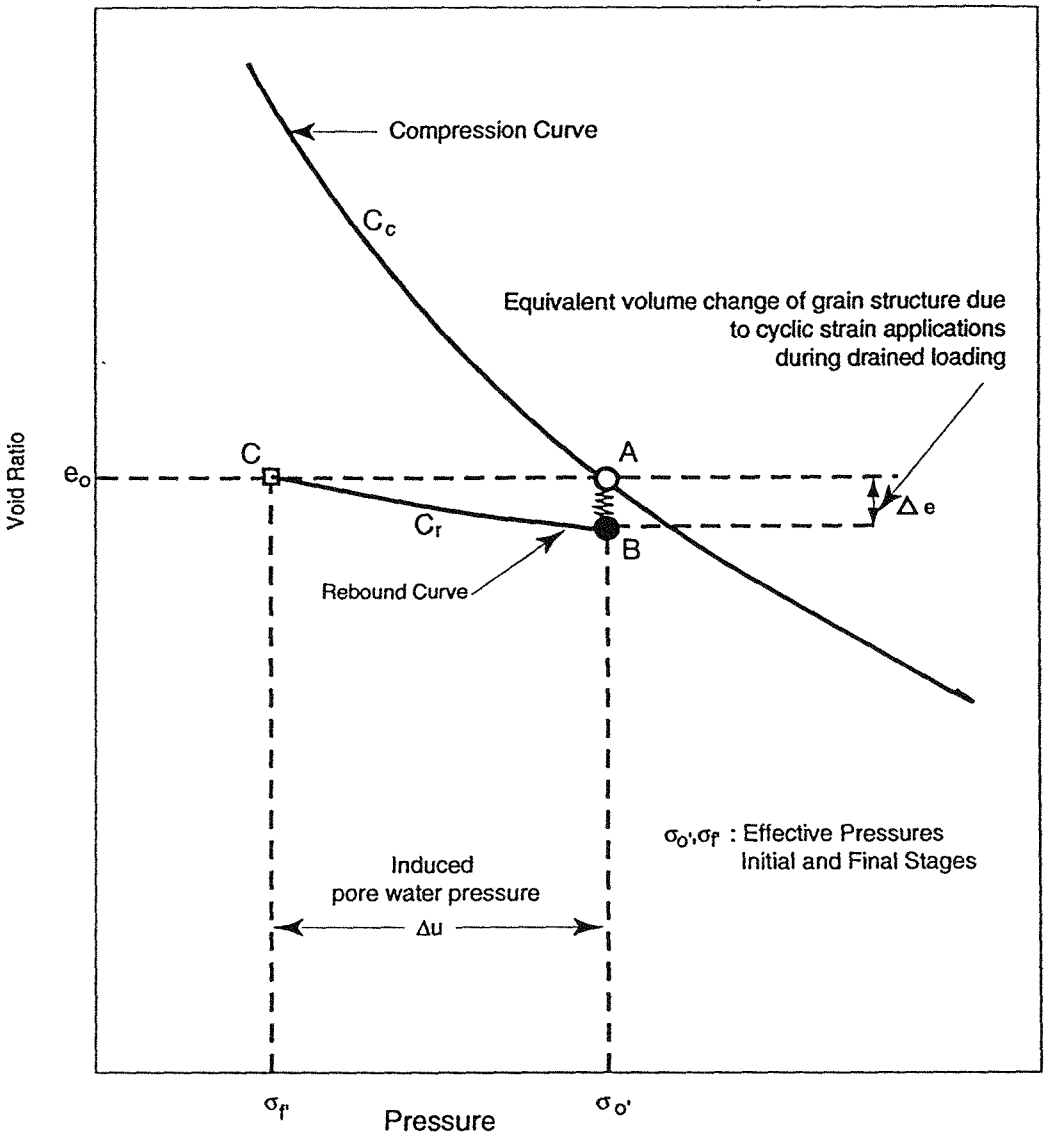


Ref.: Seed, Arango, Chan, 1975

$$\frac{\Delta V}{V} = \frac{\Delta H}{H} = \frac{C_r}{1+e_o} \log \frac{(\sigma_o' - \Delta U) + \Delta U}{\sigma_o' - \Delta U}$$

$$= \frac{C_r}{1+e_o} \log \frac{\sigma_o'}{\sigma_o' - \Delta U}$$

$$= \frac{C_r}{1+e_o} \log \frac{1}{1 - \Delta U/\sigma_o'} = \frac{C_r}{1+e_o} \log \frac{1}{1-r_u}$$

Figure 6.2-25 Derivation of a relationship between pore water pressure ratio and volumetric strain after liquefaction.

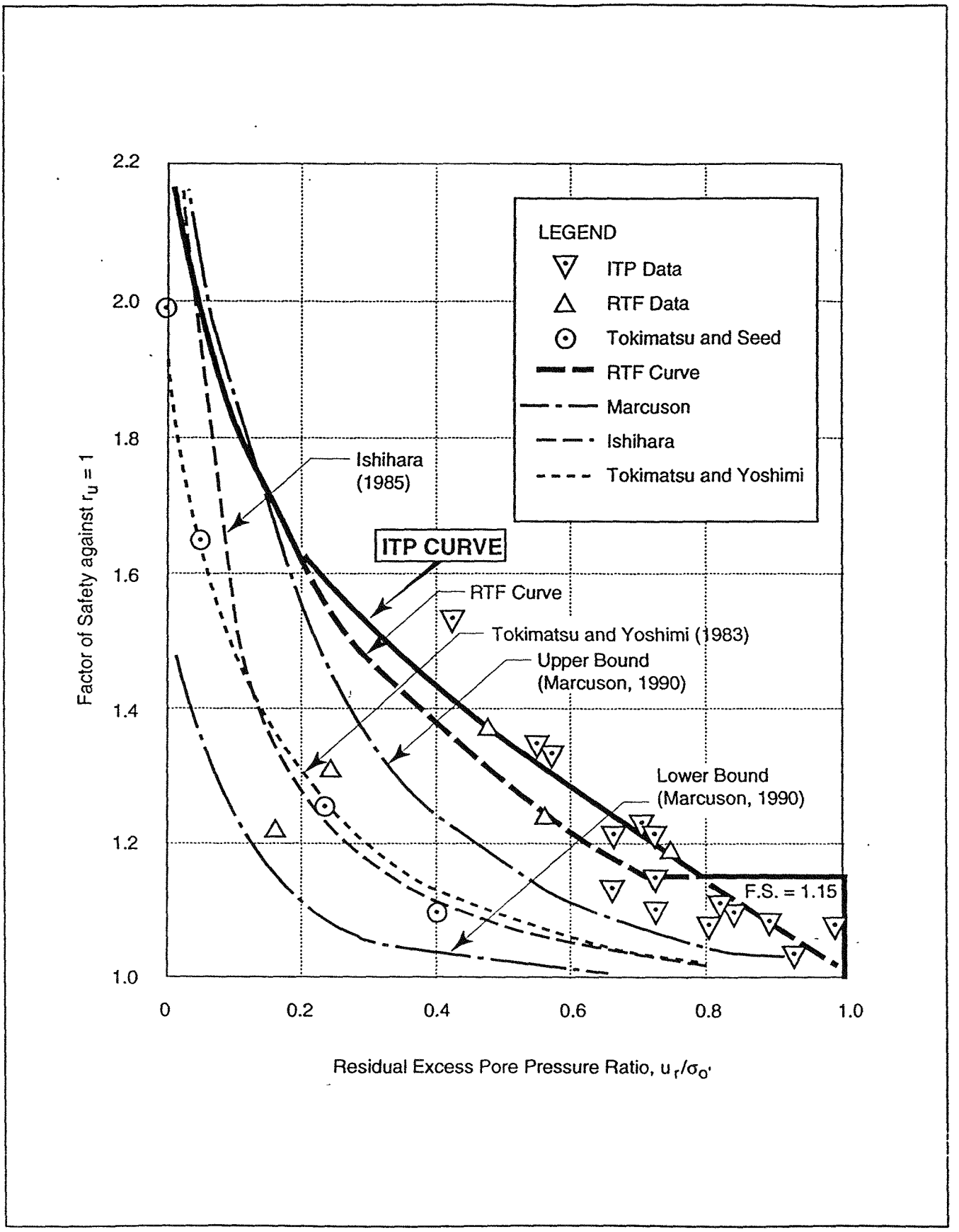


Figure 6.2-26 Relationship between factor of safety against initial liquefaction and residual excess pore water pressure ratio.

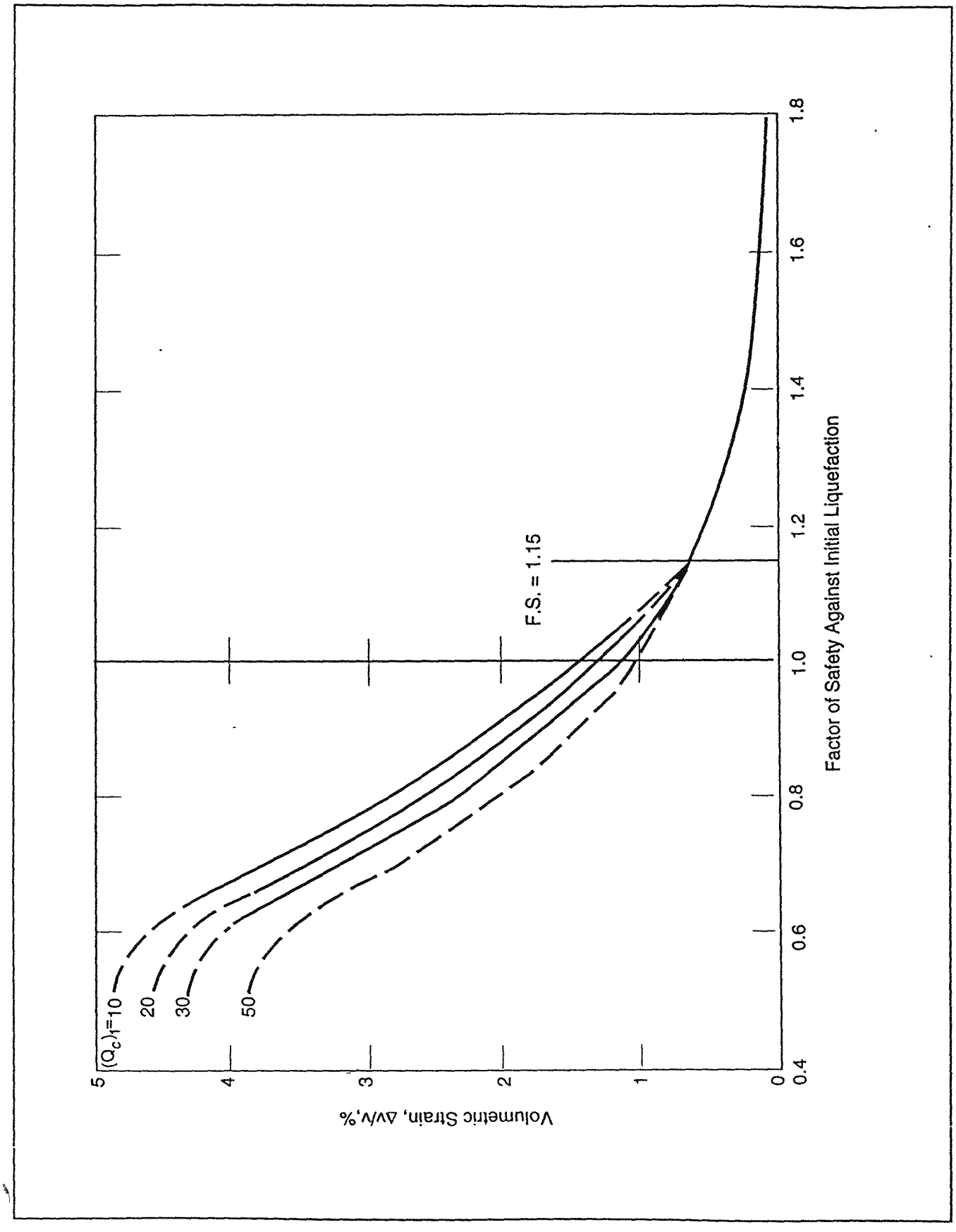


Figure 6.2-27 Volumetric strain expressed as a function of factor of safety against initial liquefaction.

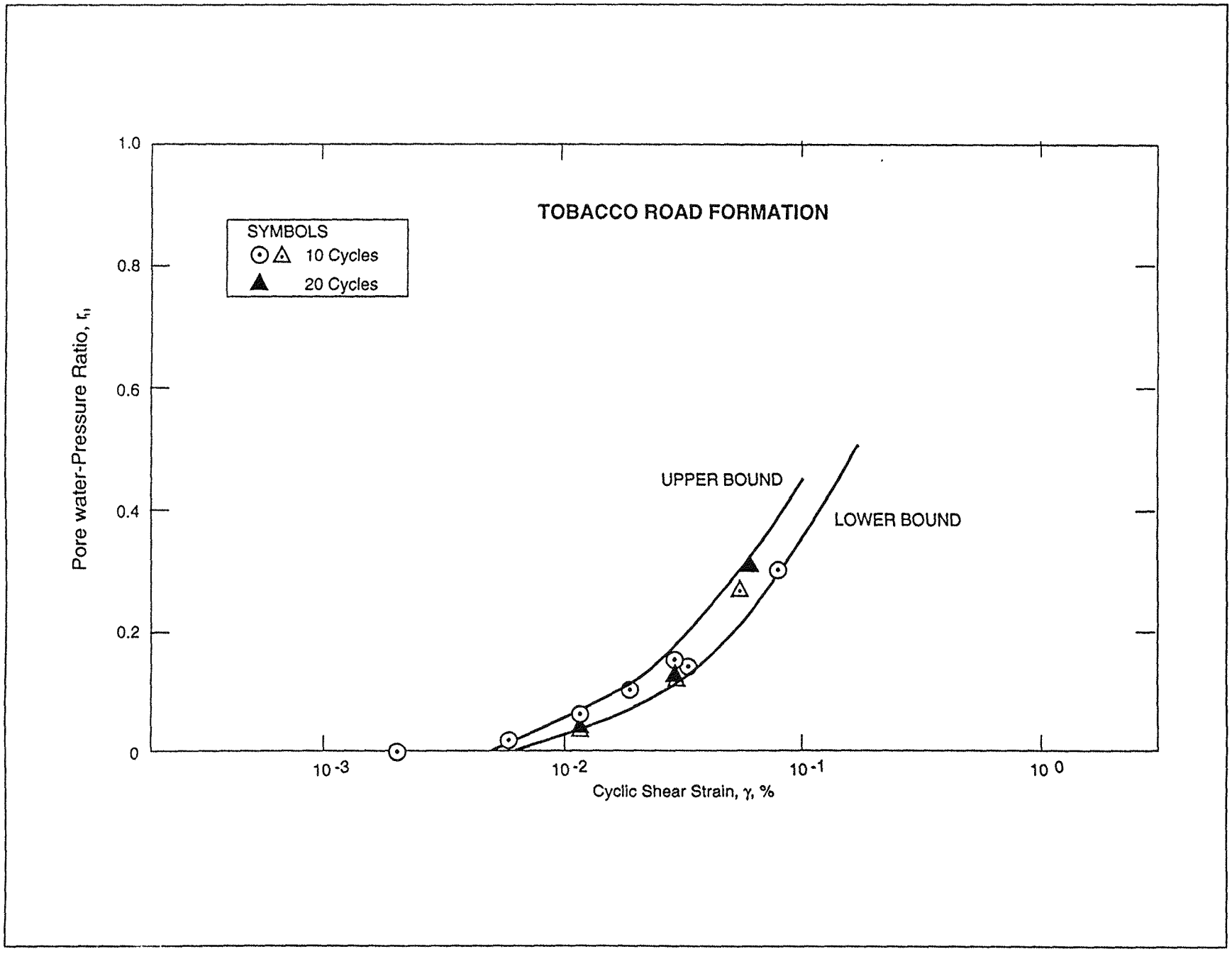


Figure 6.2-28 Relationship between cyclic shear strain amplitude, number of cycles, and pore water pressure increase, Tobacco Road formation.

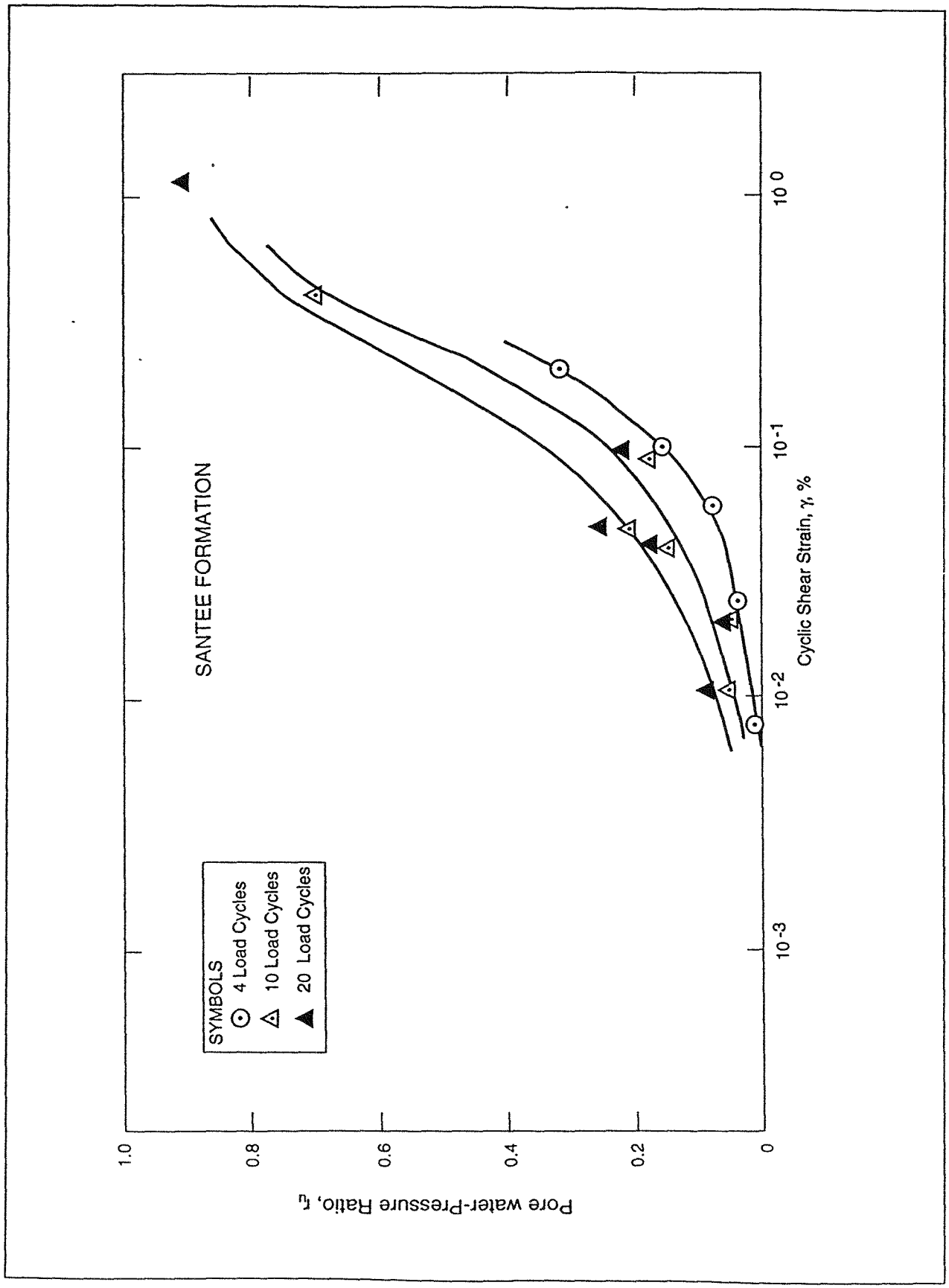


Figure 6.2-29 Relationship between cyclic shear strain amplitude, number of cycles, and pore water pressure increase, Santee formation.

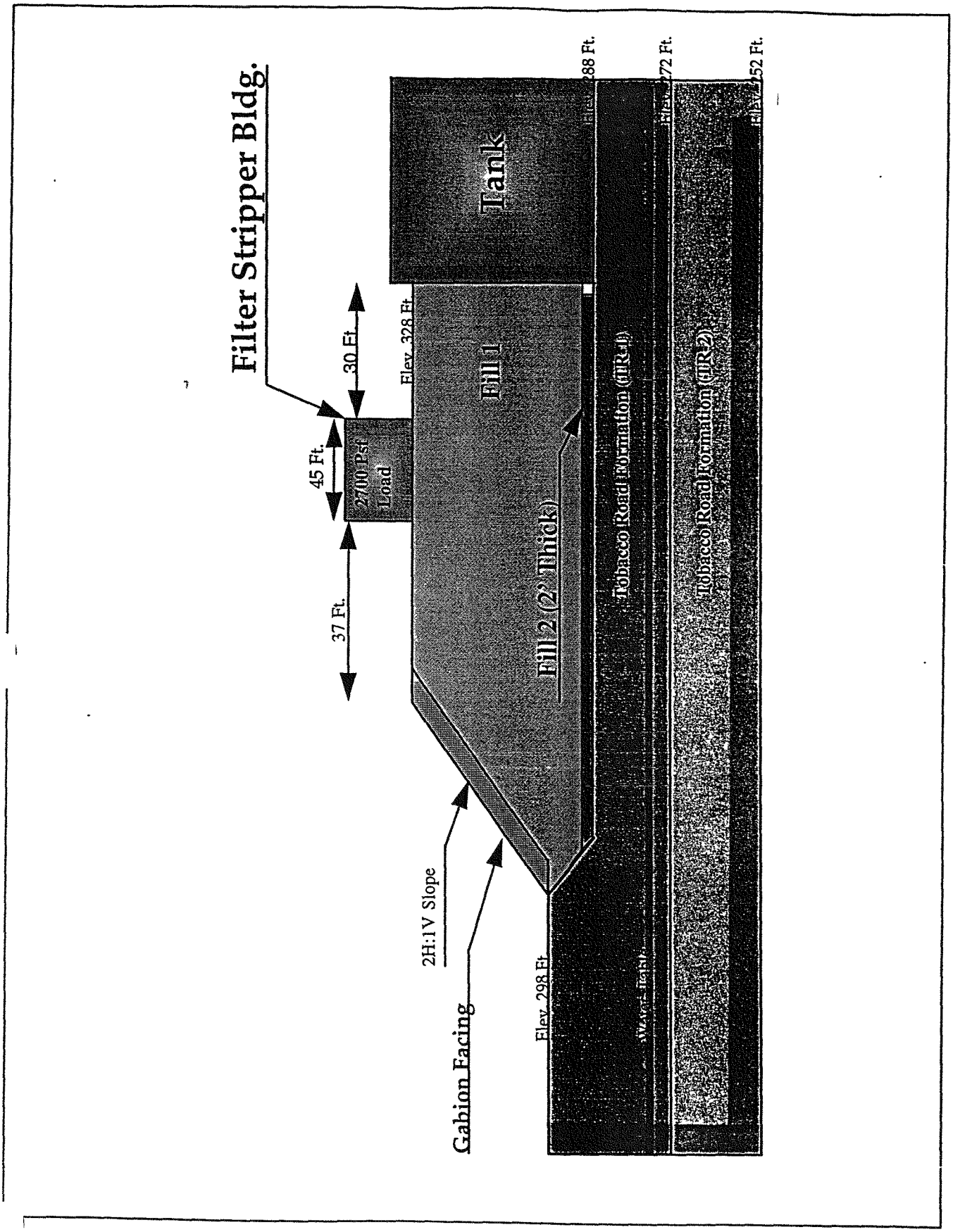


Figure 6-3-1 Slope stability - cross-section 1.

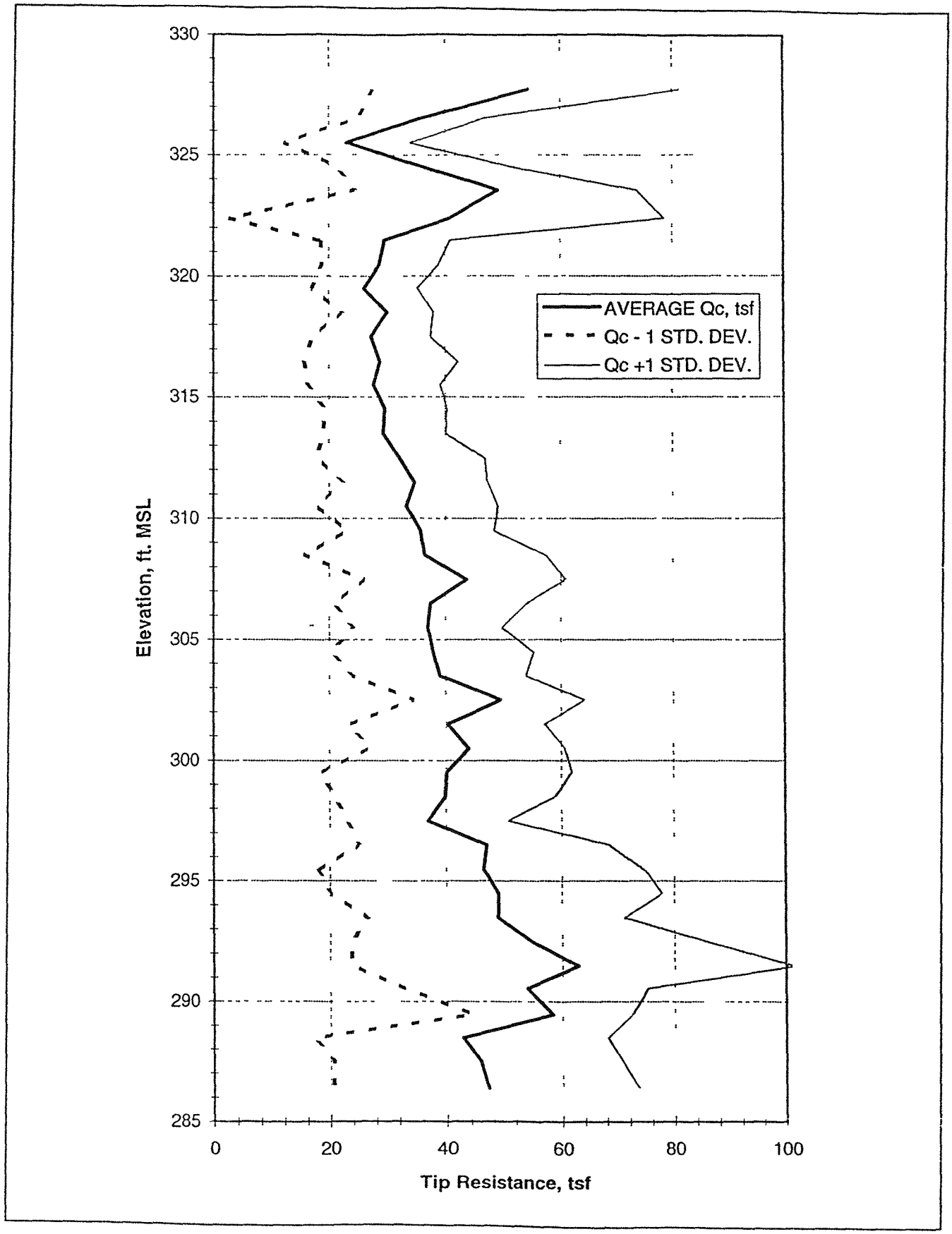


Figure 6.3-2 Average CPT tip resistance and variability in the fill at ITP.

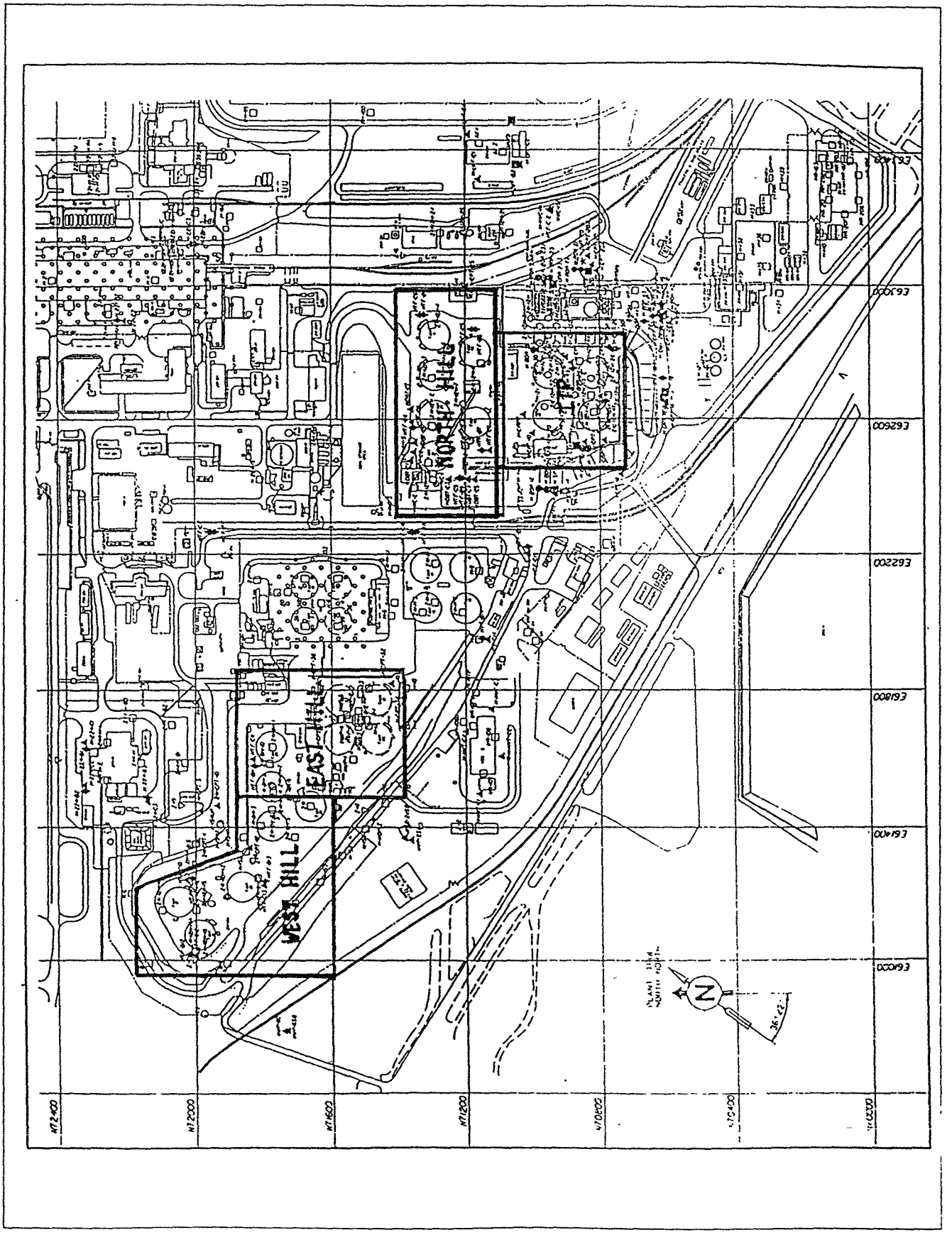


Figure 6.3-3 Plot plan of HTF area.

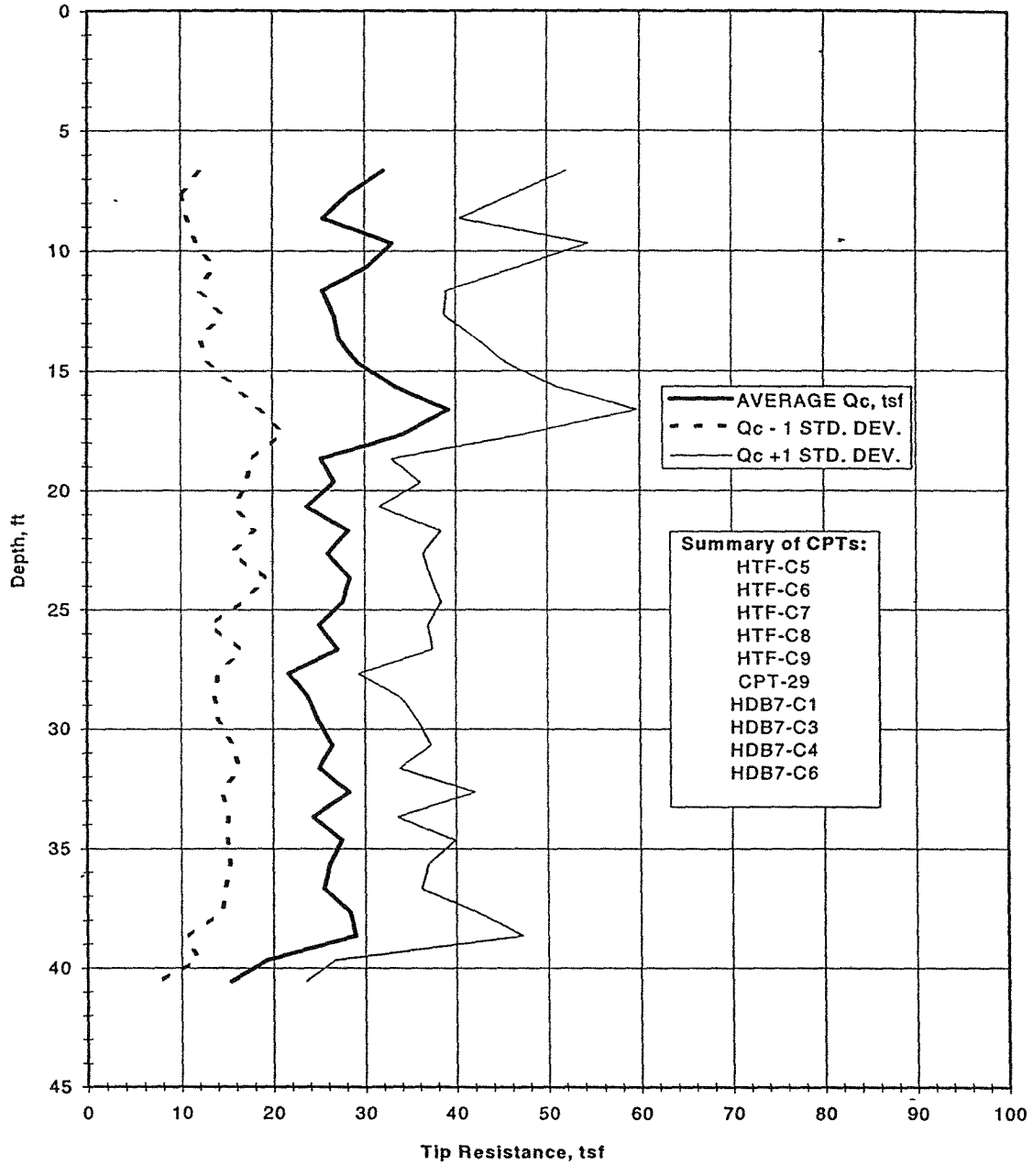


Figure 6.3-4 Summary of tip resistances for CPTs in north hill area.

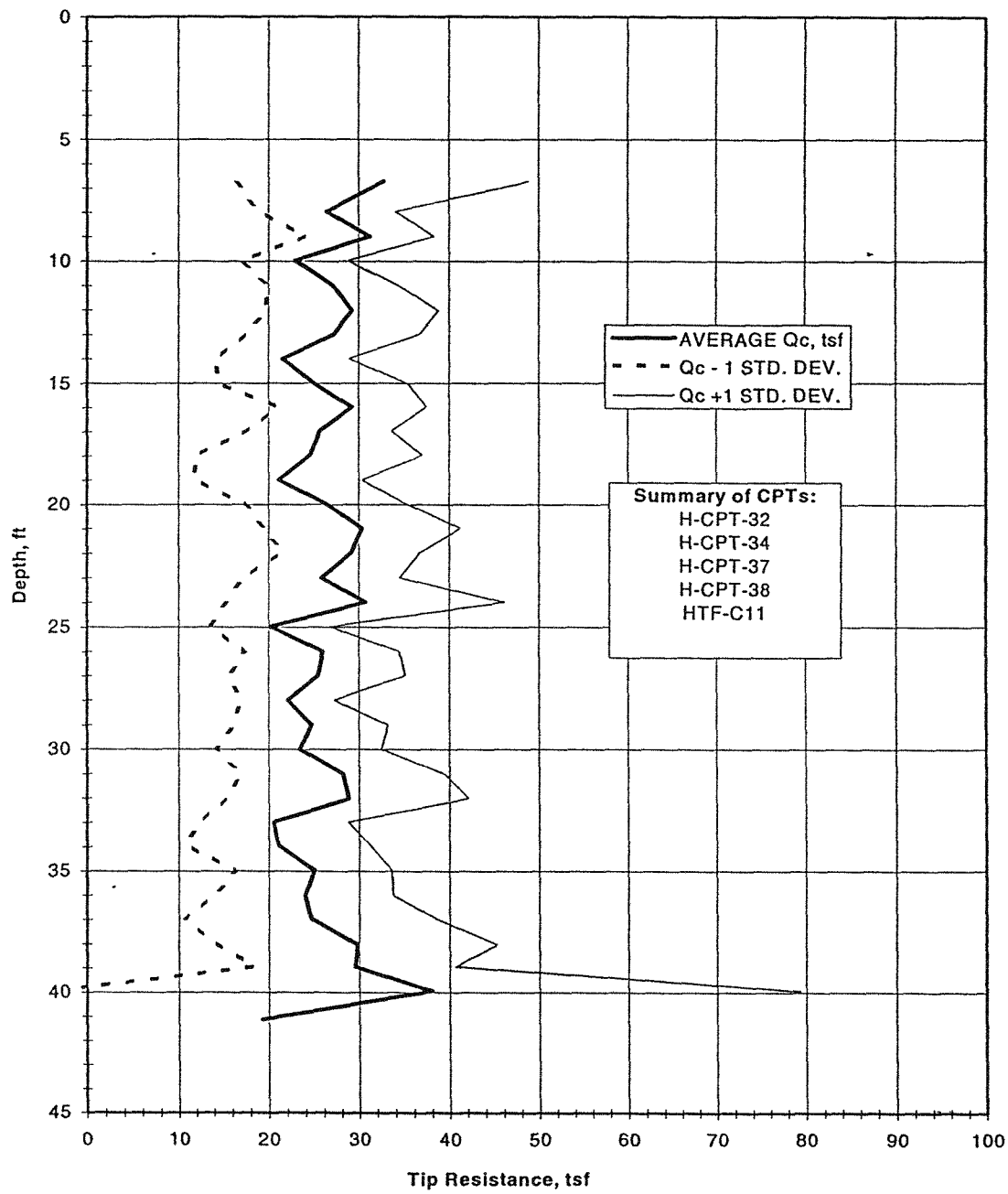


Figure 6.3-5 Summary of tip resistances for CPTs in east hill area.

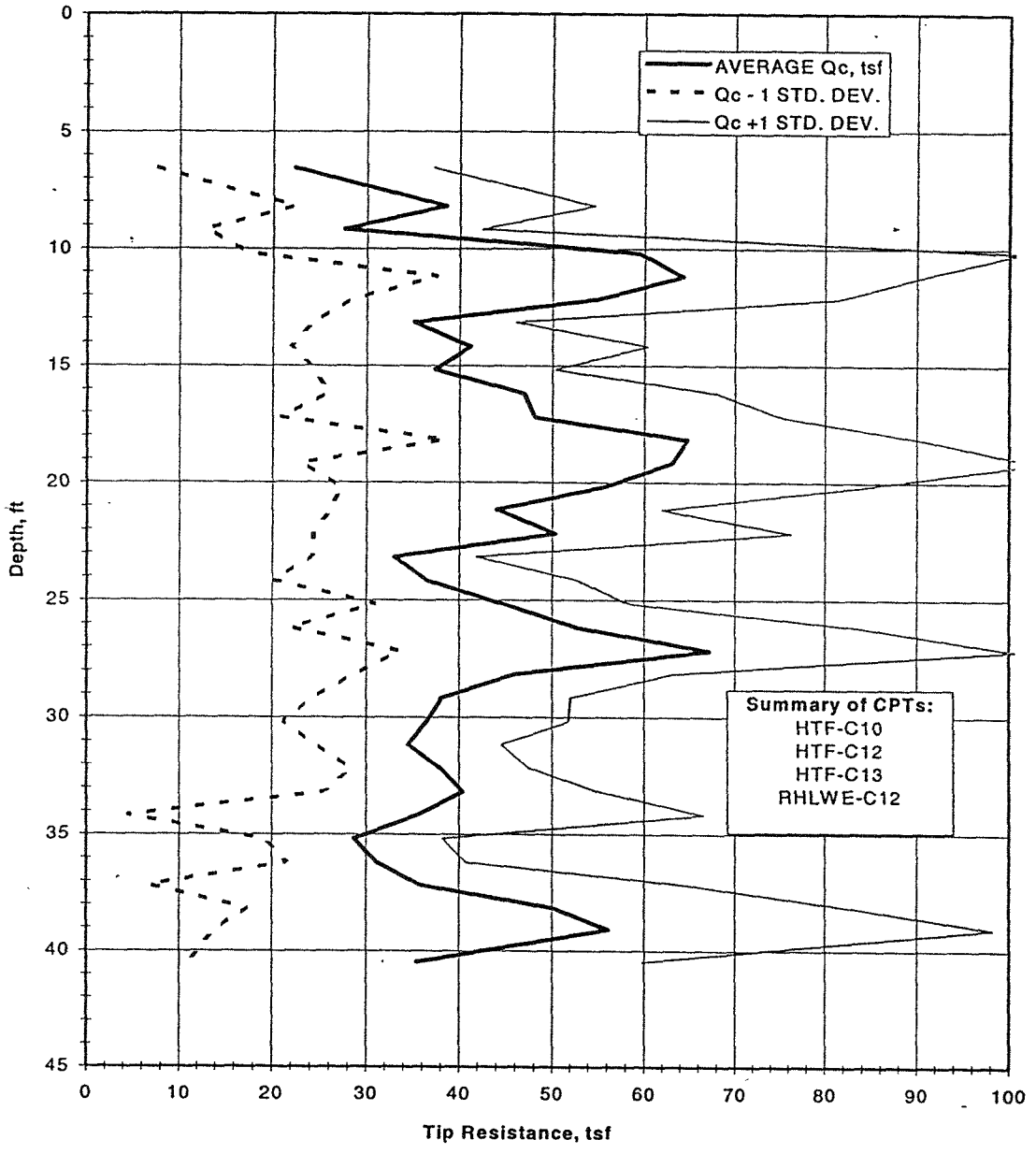


Figure 6.3-6 Summary of tip resistances for CPTs in west hill area.

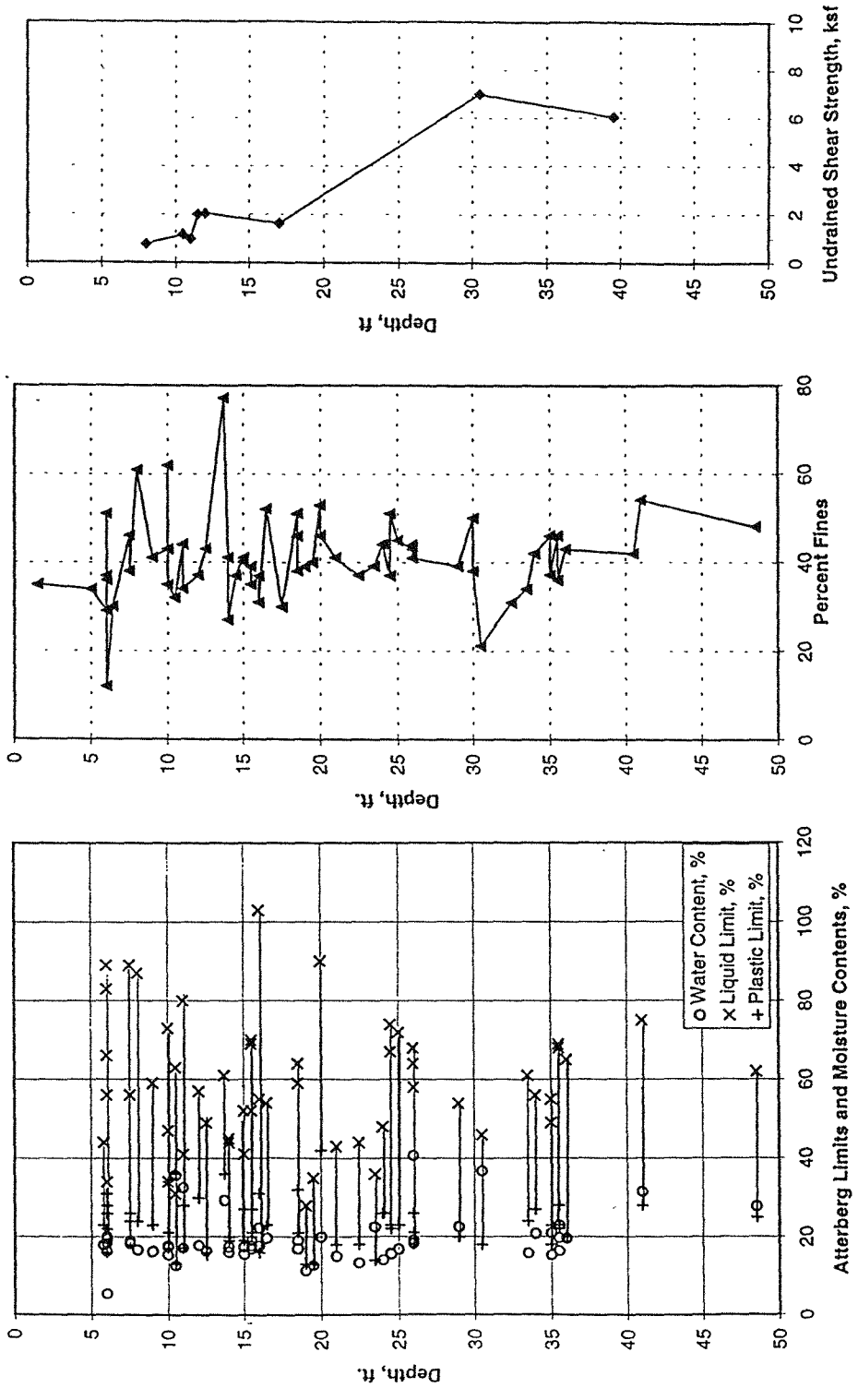


Figure 6.3-7 Summary of the laboratory data for the ITTF fill, excluding ITP.

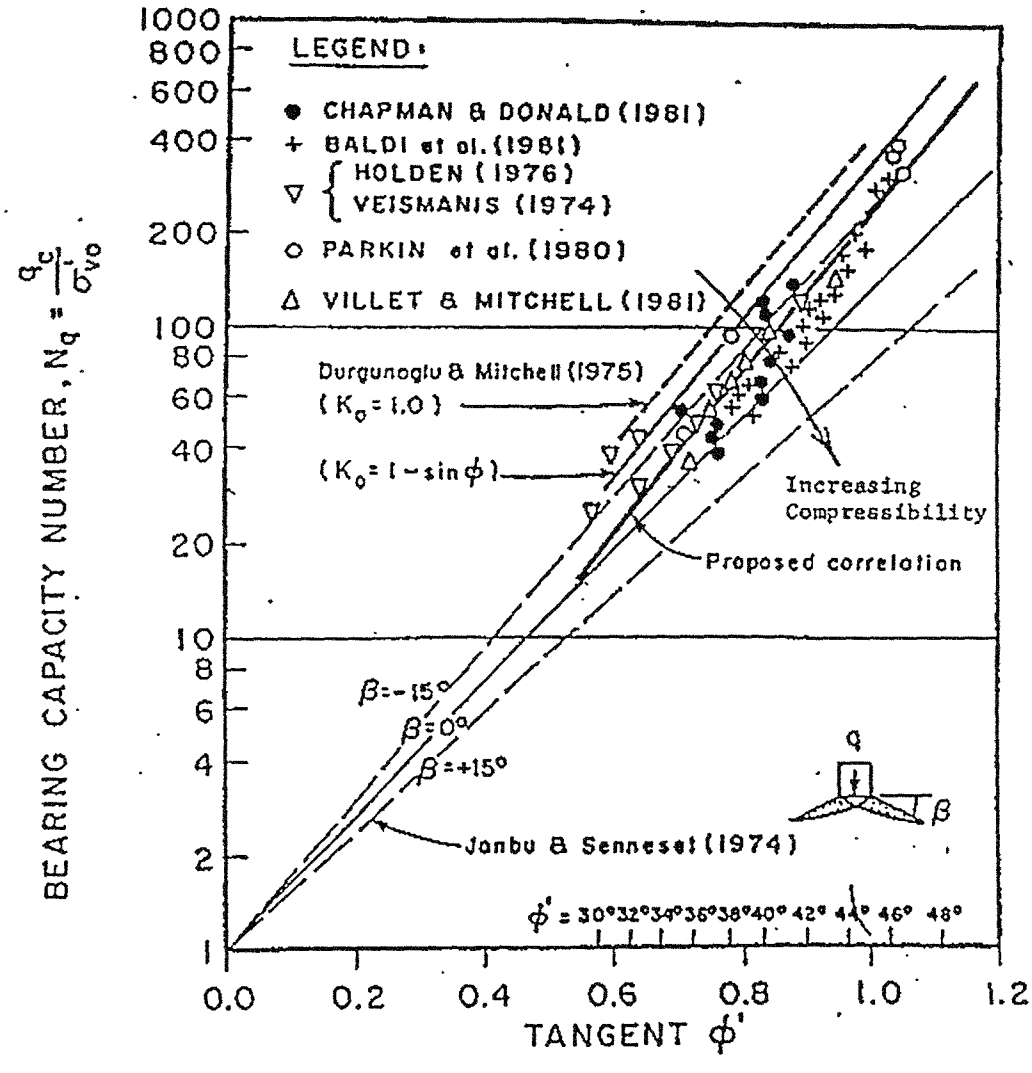


Figure 6.3-8 Relationship between $Q_c$ and friction angle.

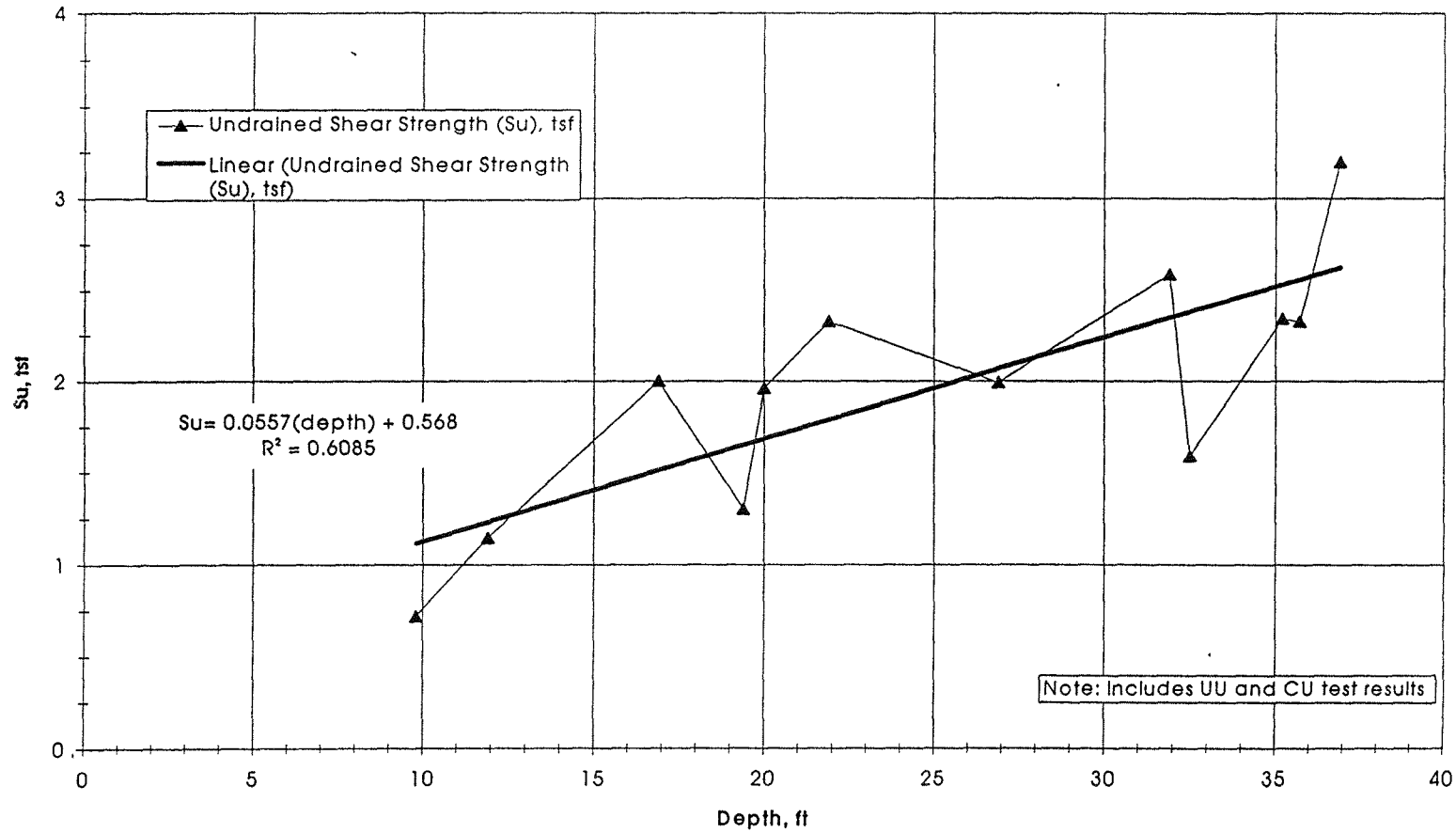


Figure 6.3-9 Calculated $S_u$ versus depth at ITP.

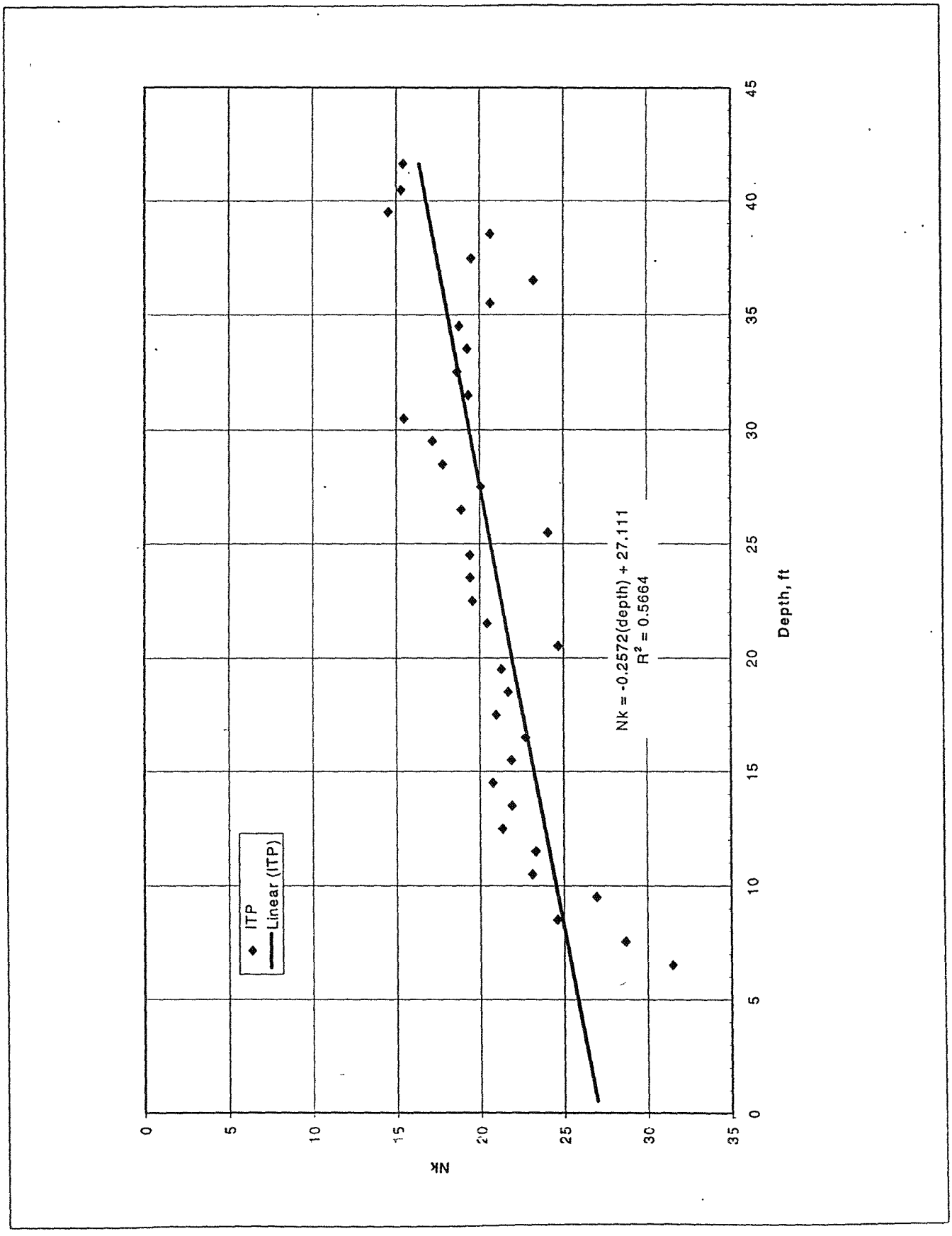


Figure 6.3-10 Calculated $N_k$ versus depth at ITP.

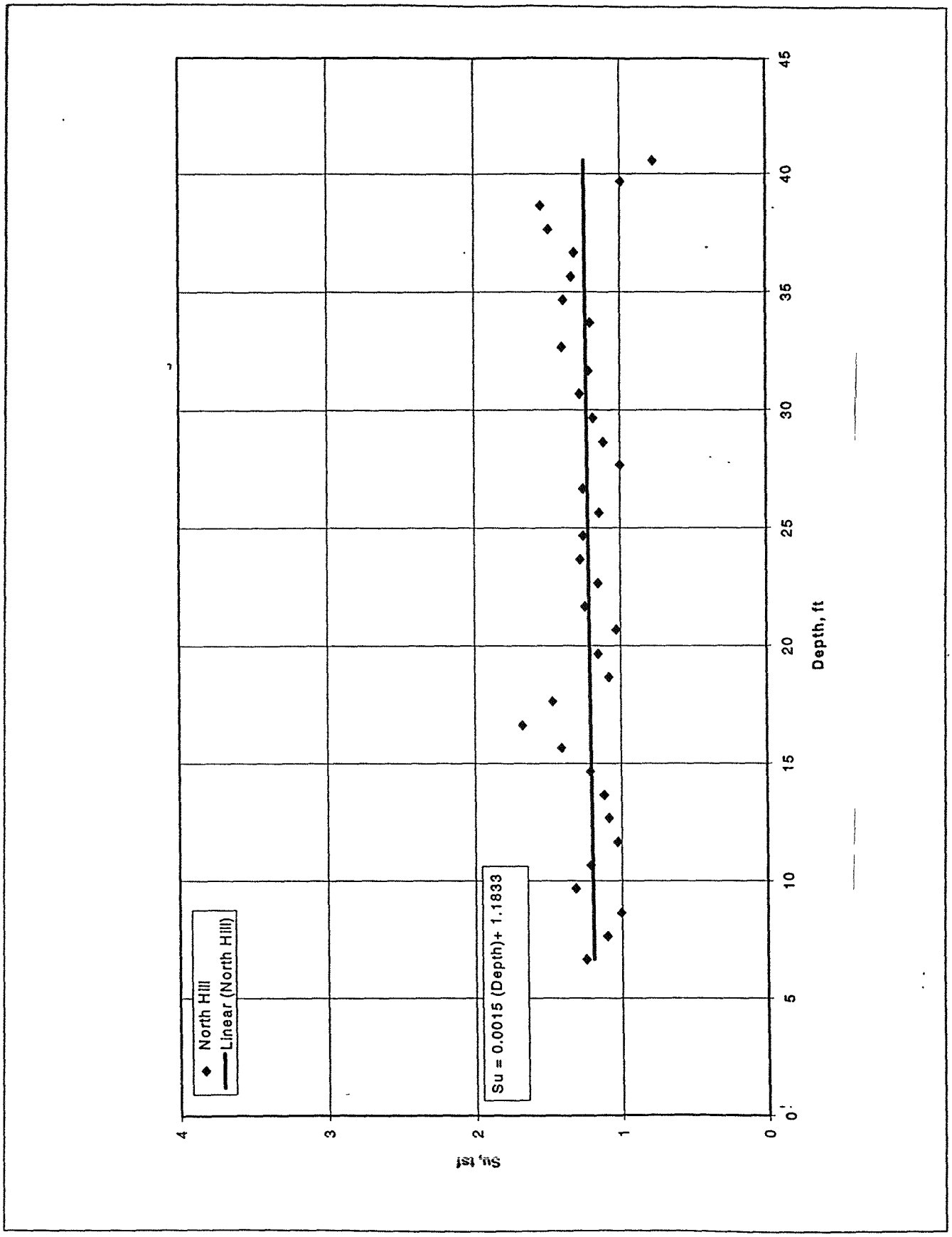


Figure 6.3-11 Calculated $S_u$ versus depth for north hill area.

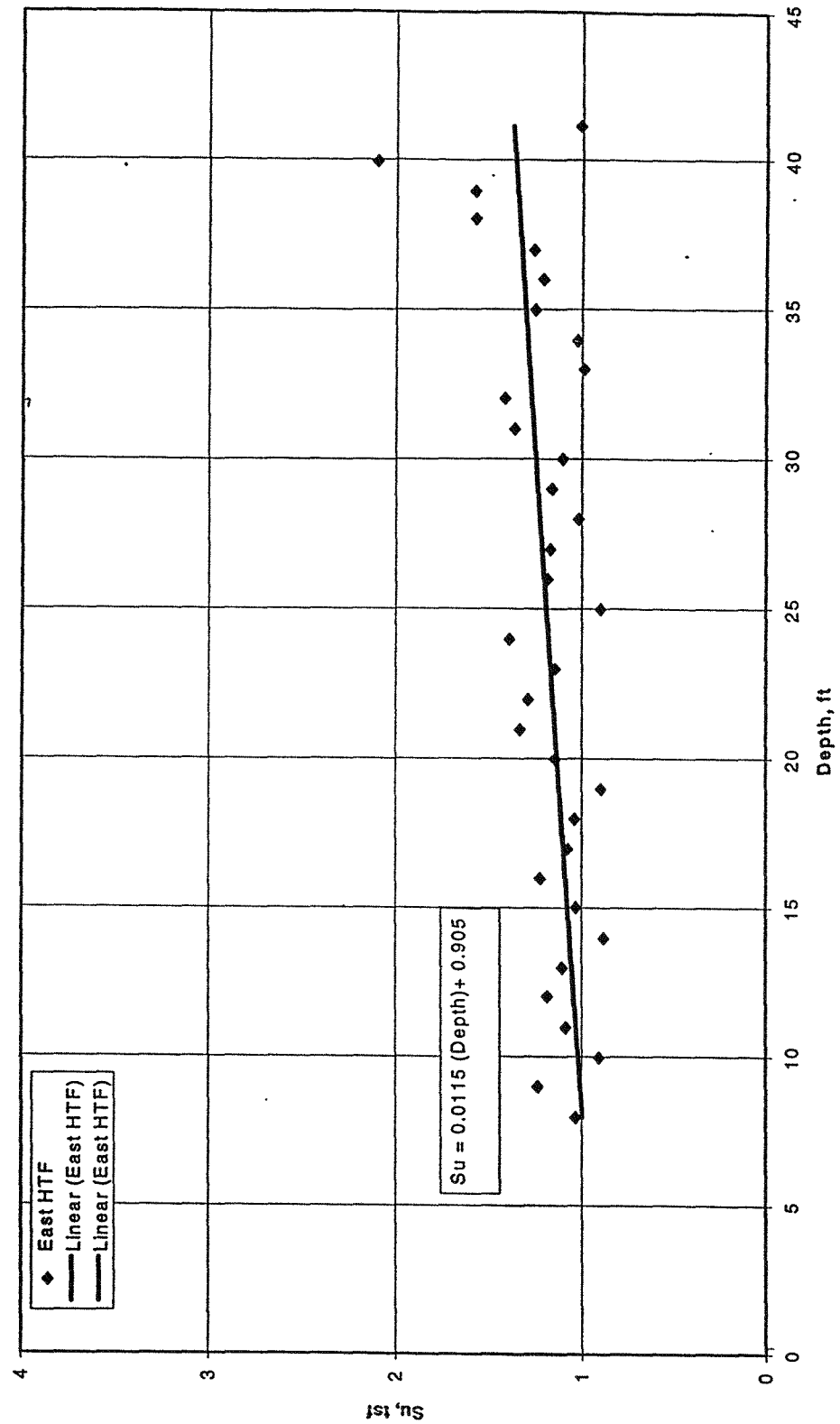


Figure 6.3-12 Calculated $S_u$ versus depth for east hill area.

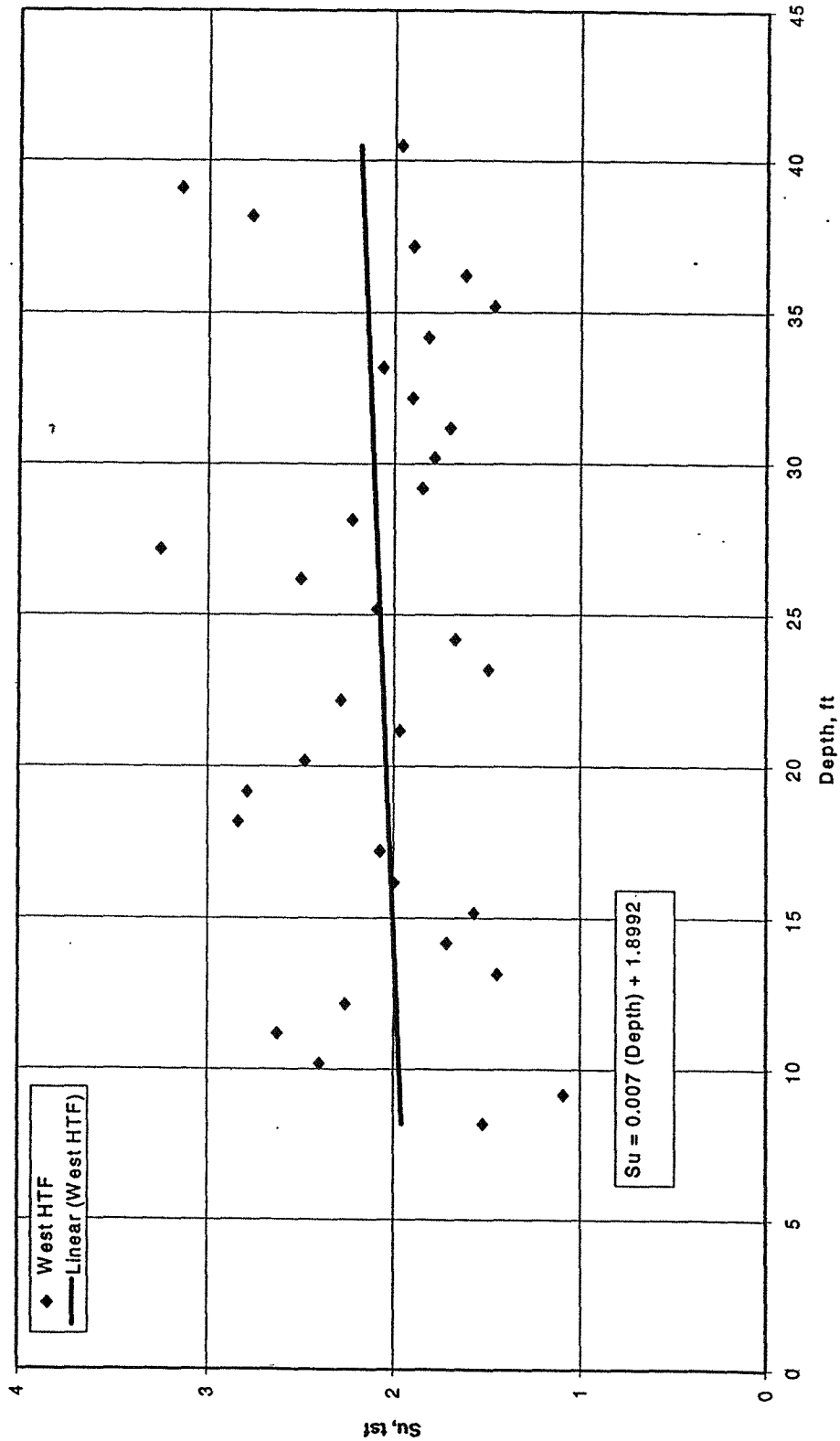


Figure 6.3-13 Calculated $S_u$ versus depth for west hill area.

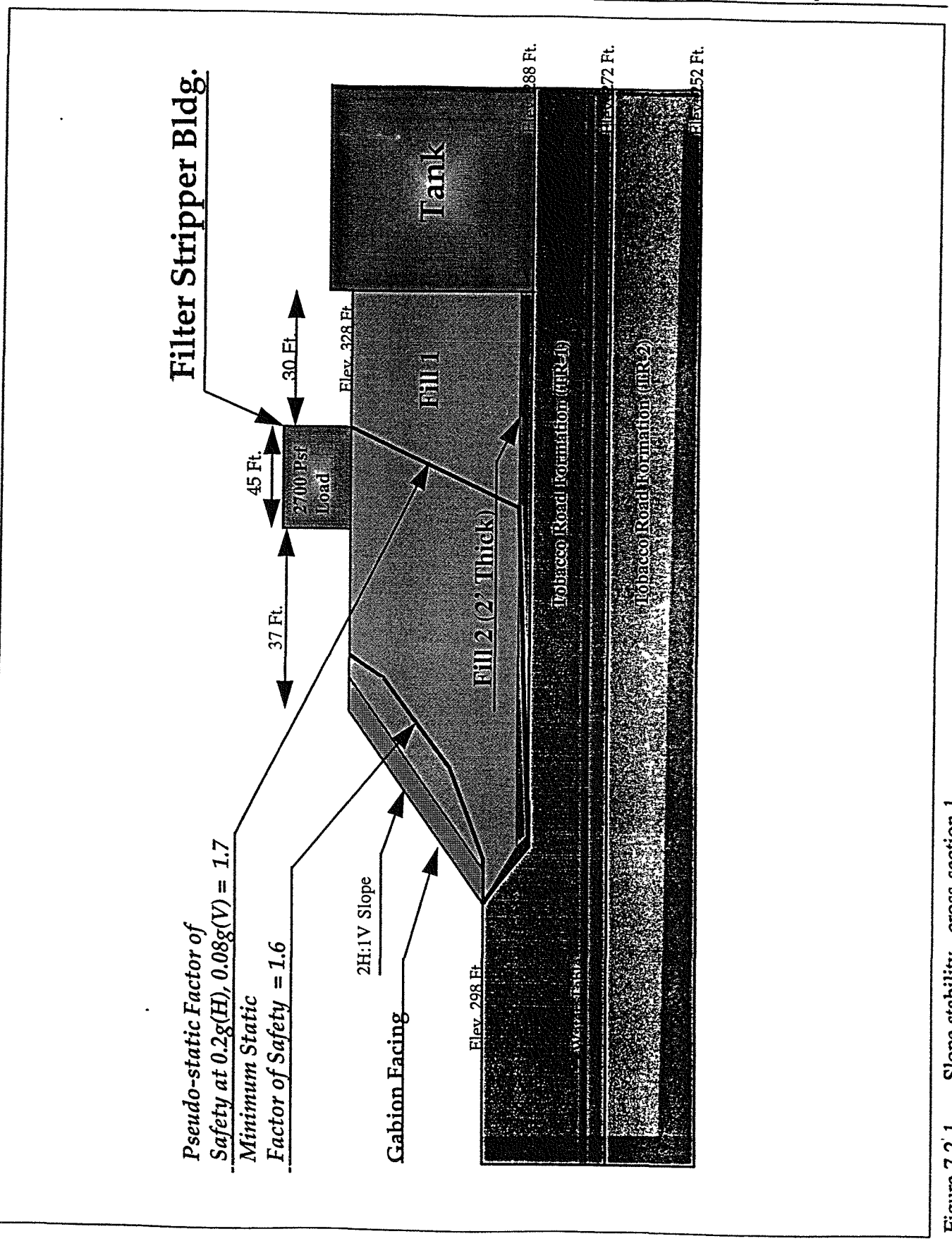


Figure 7.2-1 Slope stability - cross-section 1.

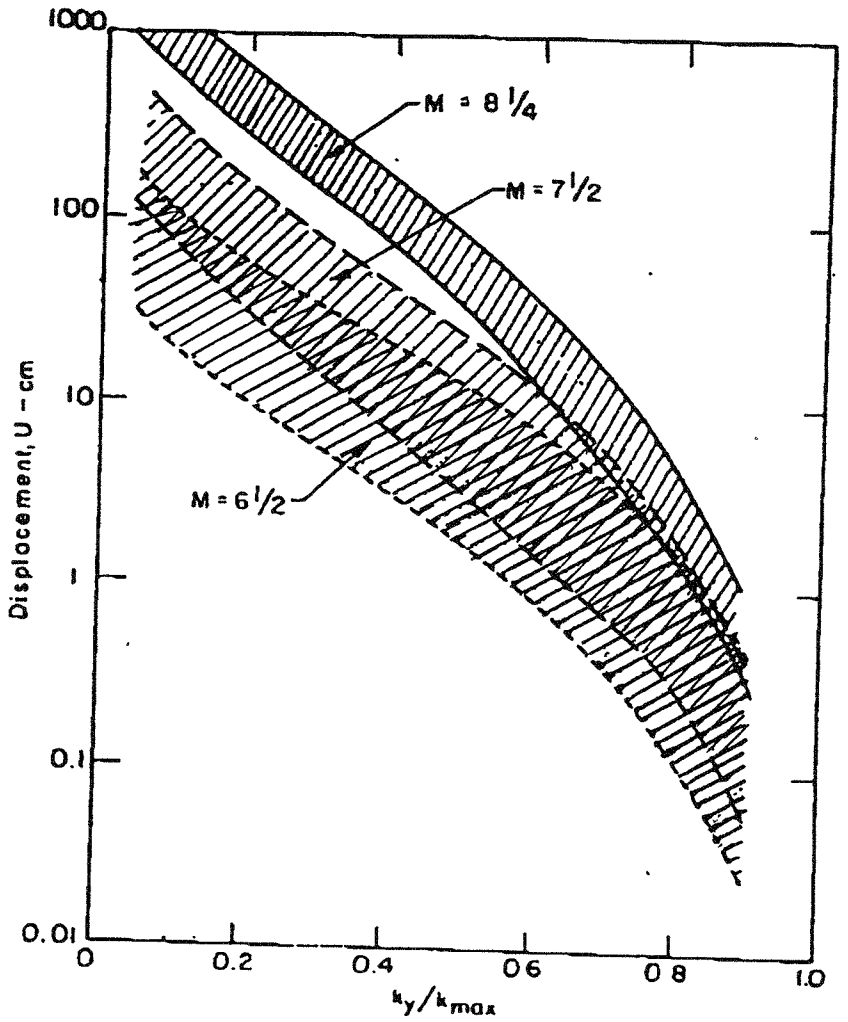


Figure 7.2-2 Variation of permanent slope displacement with yield acceleration.

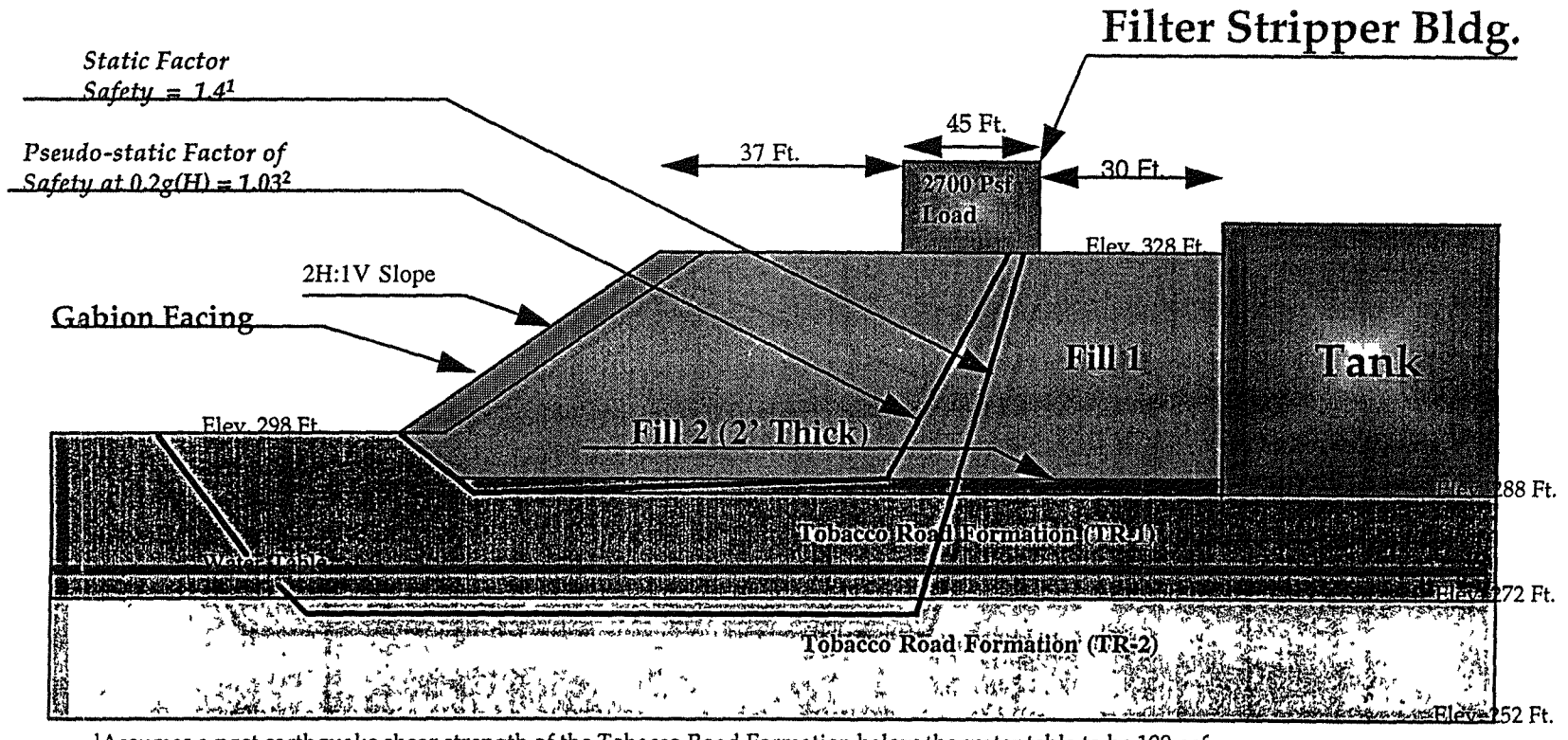


[1]Assumes a post earthquake shear strength of the Tobacco Road Formation below the water table to be 100 psf.
[2]Assumes an arbitrarily reduced shear strength for the Fill 1 and Fill 2 material.

Figure 7.2-3 Slope stability - cross section 1 - for reduced strength analyses.

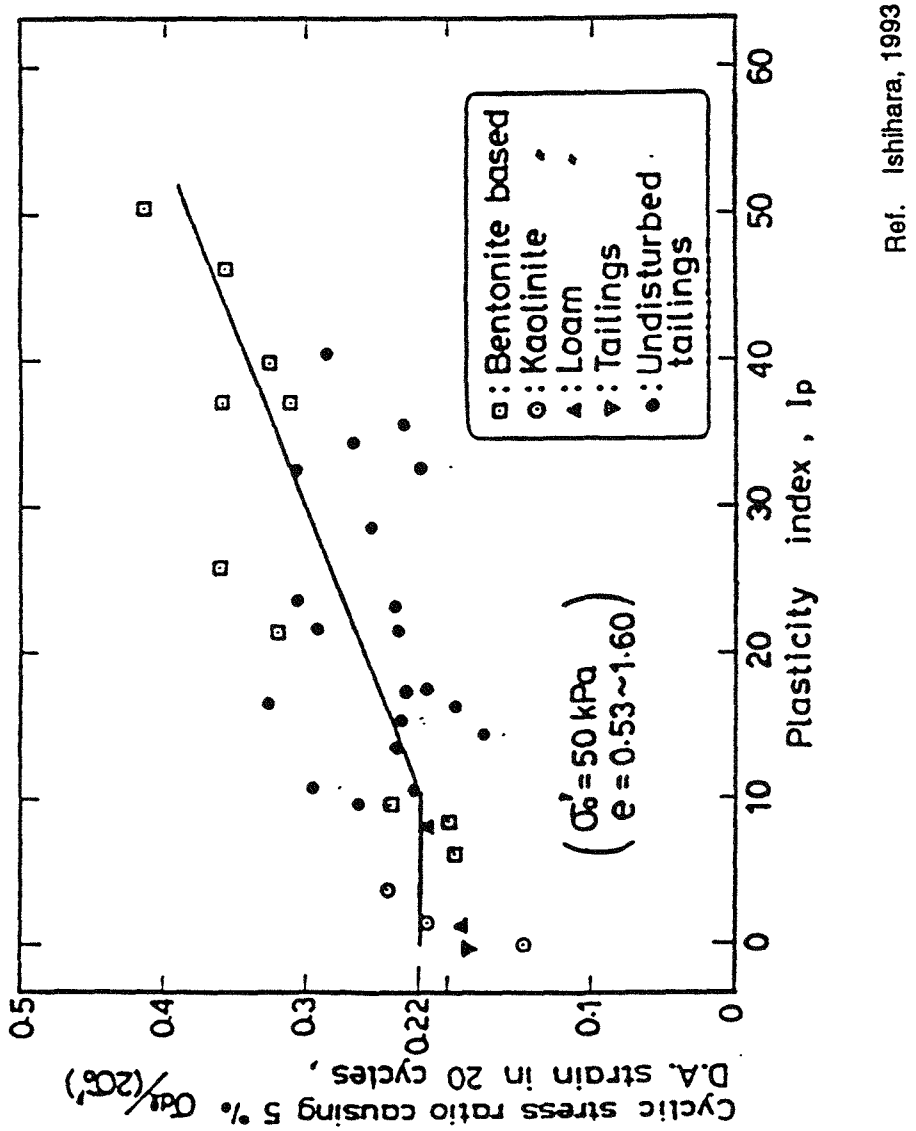


Figure 7.3-1 Relationship between plasticity index of fines and cyclic stress ratio causing liquefaction.

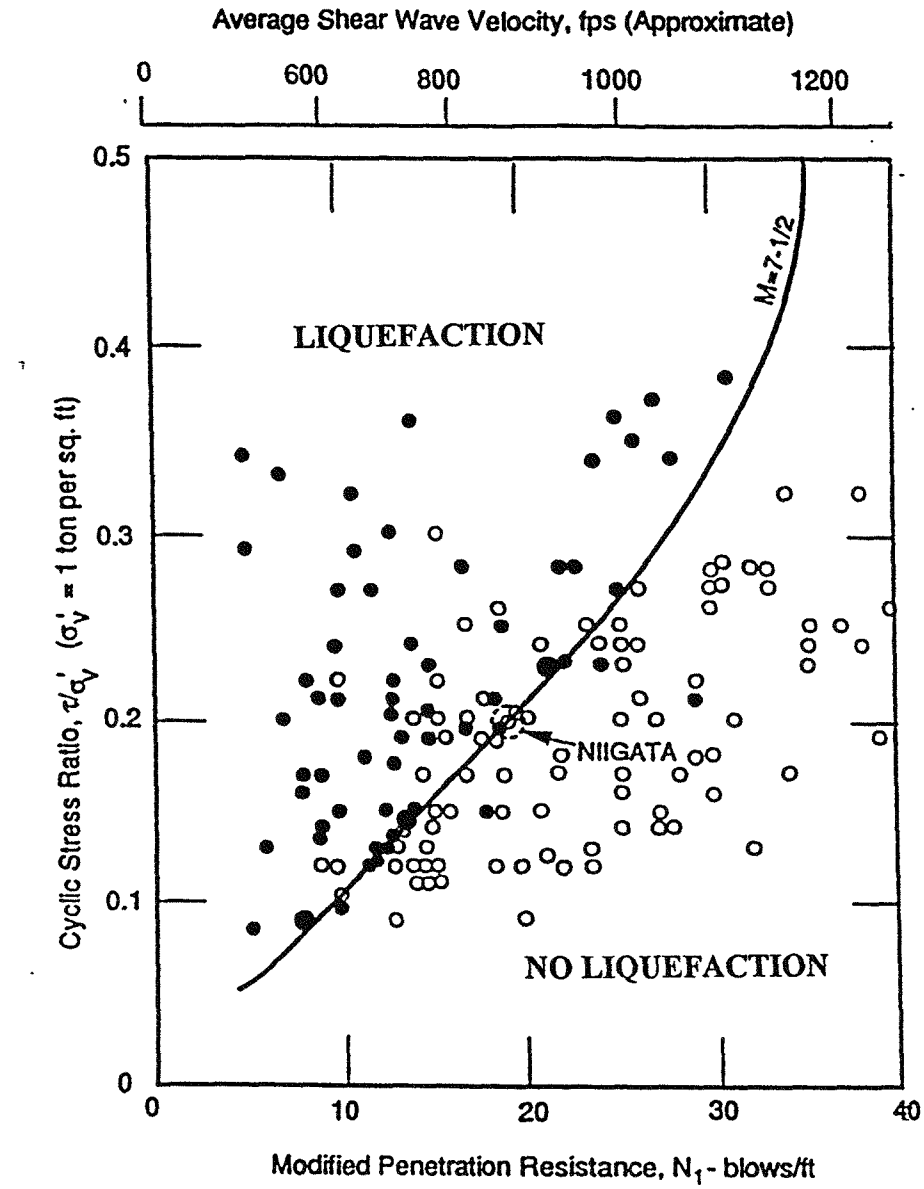


Ref.: Seed, Idriss, and Arango, (1983)

**LEGEND**

- ● Limits set by Chinese Code (1974)
- • Liquefaction
- ○ No Liquefaction

Figure 7.3-2 Correlation between field liquefaction of sands, penetration resistance, and shear wave velocity.

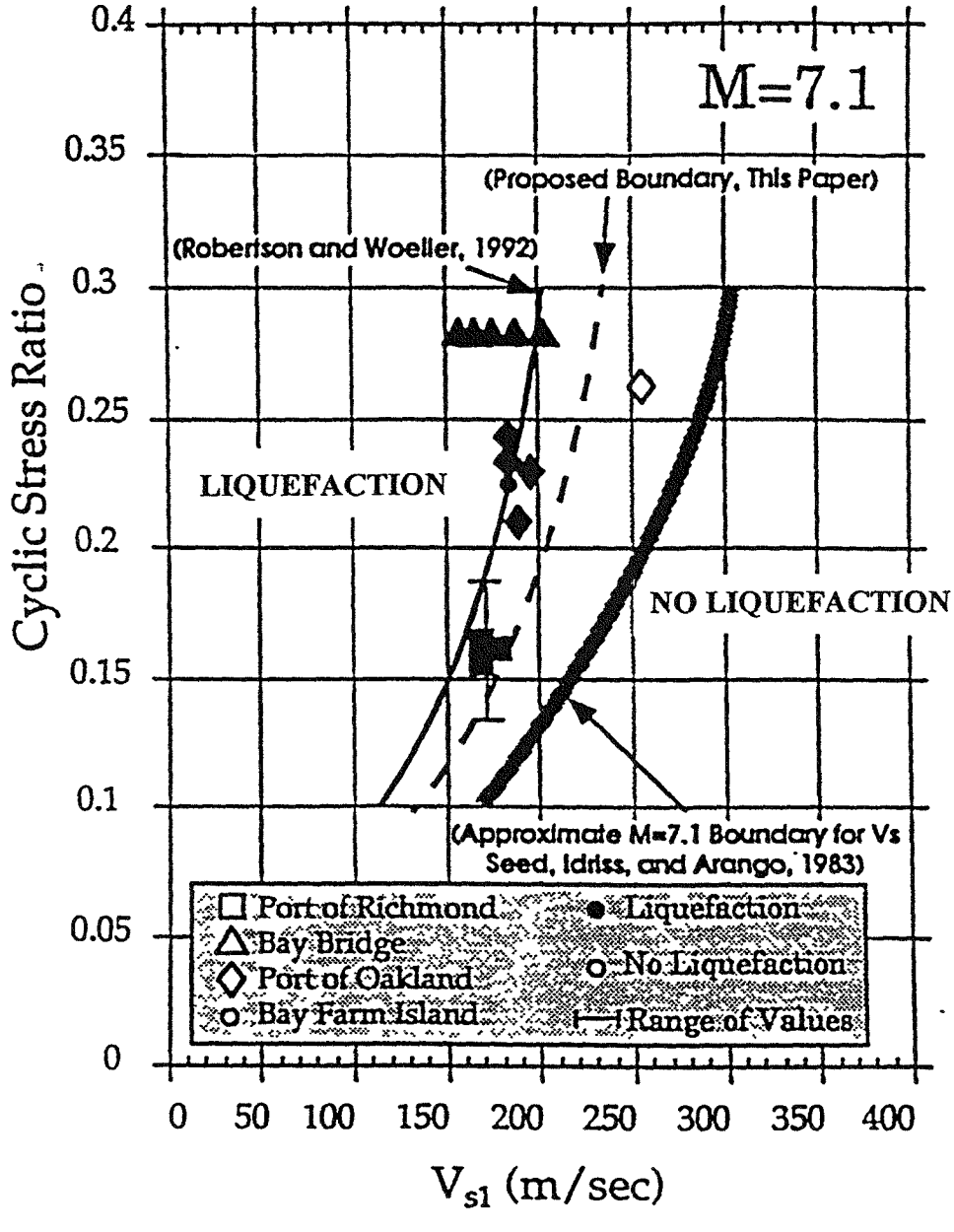


Ref.: Kayen et al. (1992)

Figure 7.3-3 Correlation between normalized shear wave velocity and cyclic stress ratio causing liquefaction.

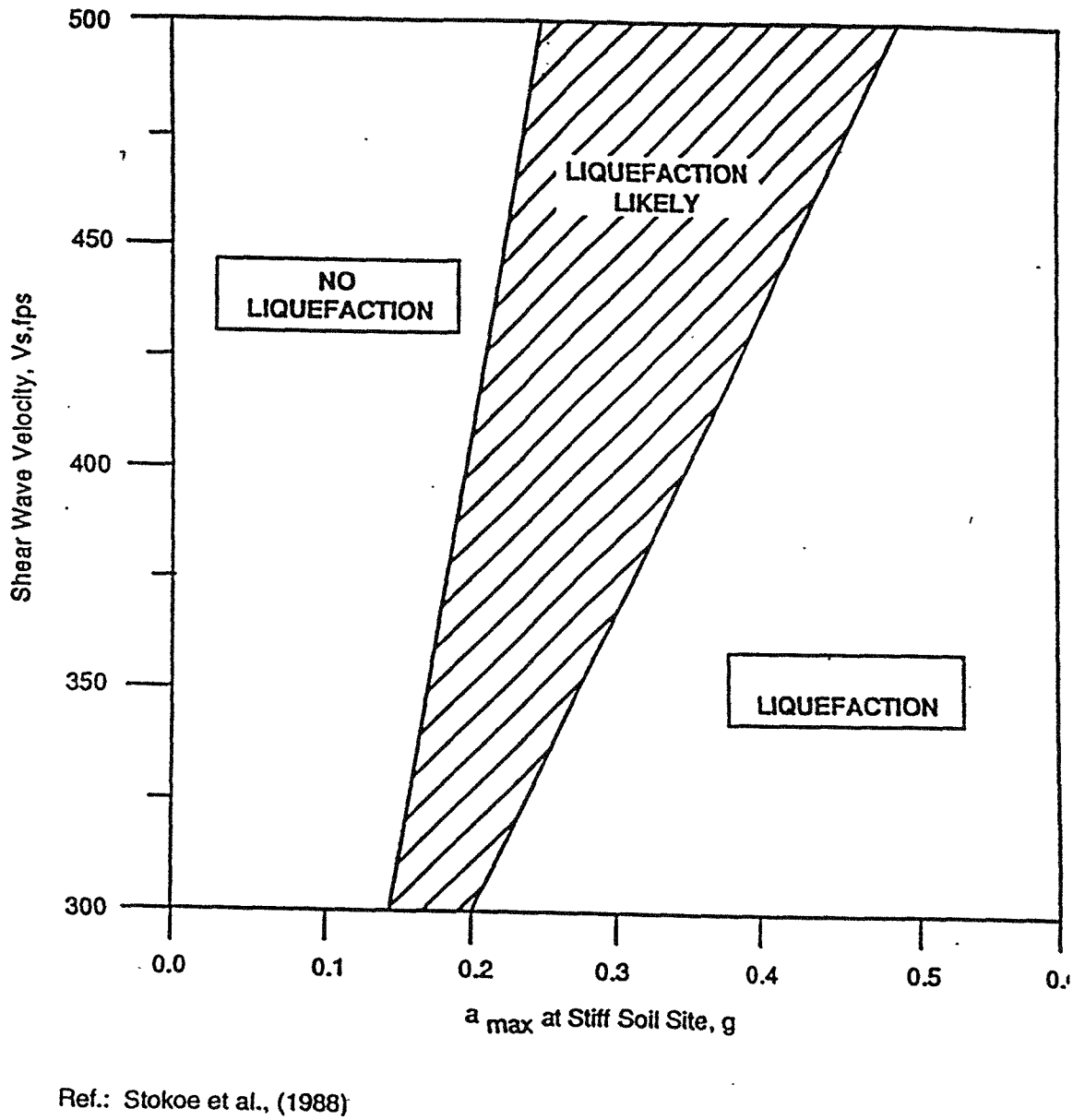


Ref.: Stokoe et al., (1988)

Figure 7.3-4 Liquefaction potential chart based on shear wave velocity of a sand layer and 20 cycles of strong motion.

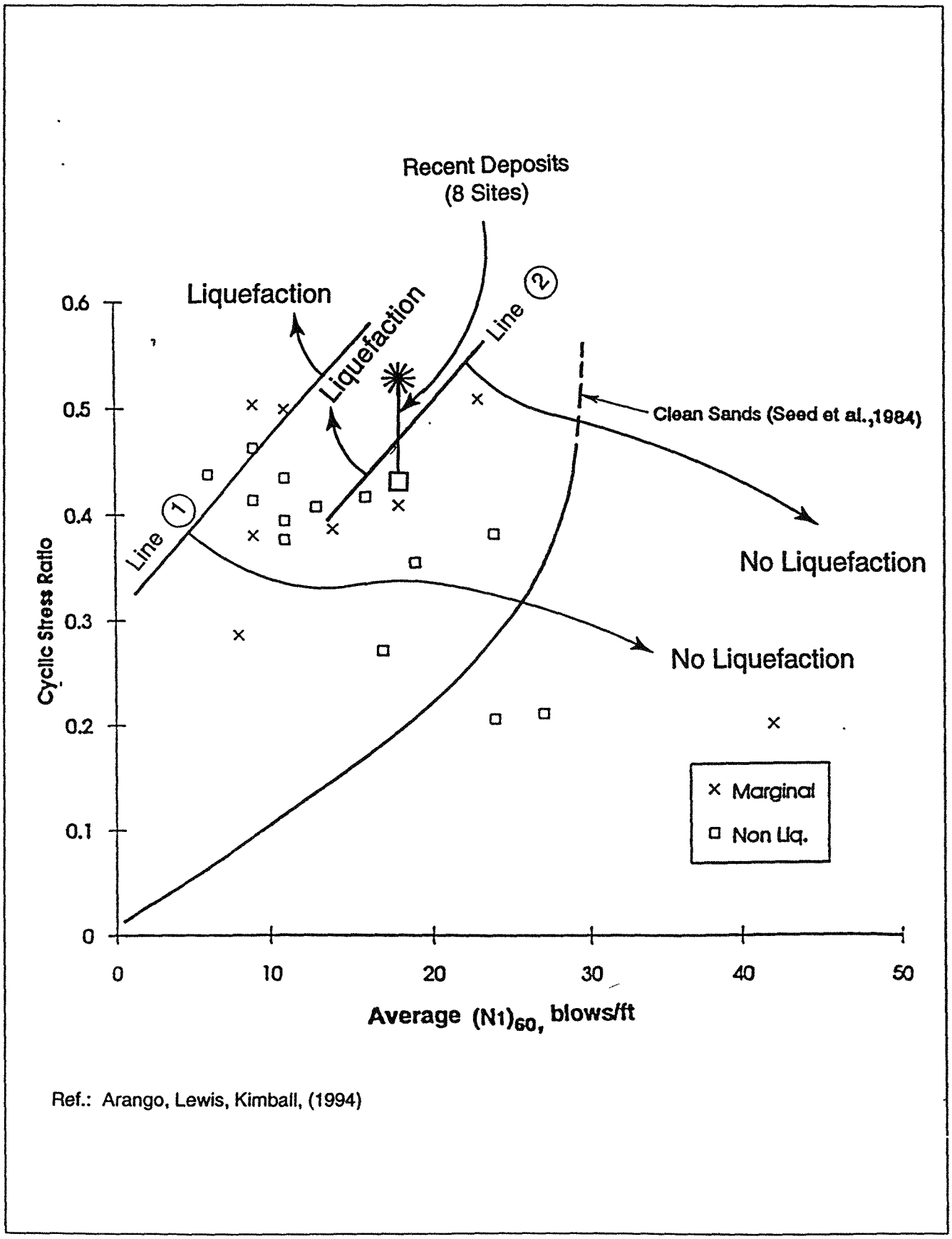


Figure 7.3-5 Charleston, South Carolina earthquake: Liquefaction/marginal liquefaction data.

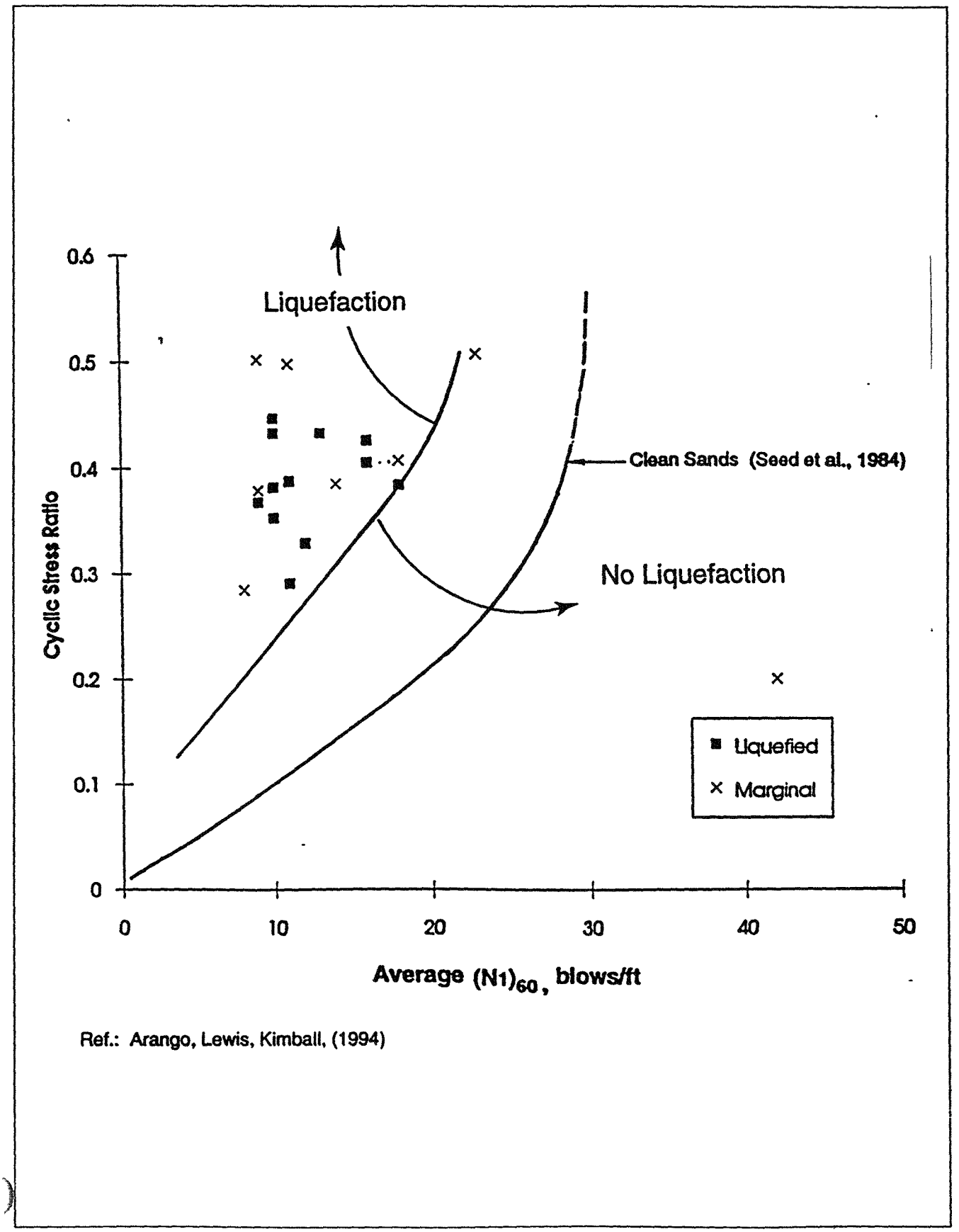


Figure 7.3-6 Charleston, South Carolina earthquake: No liquefaction/liquefaction data.

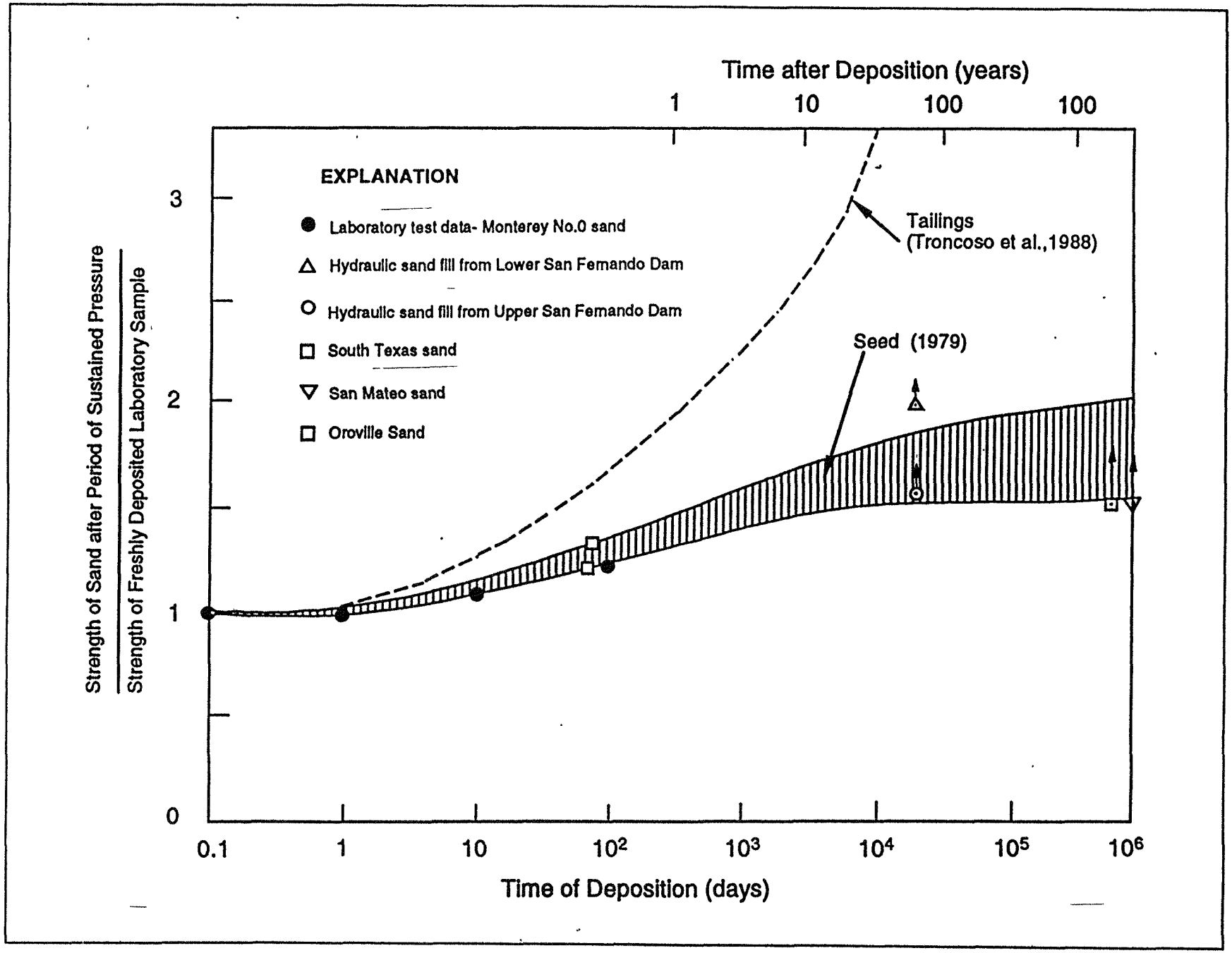


Figure 7.3-7 Influence of period of sustained pressure on stress ratio causing 100 percent pore water pressure.

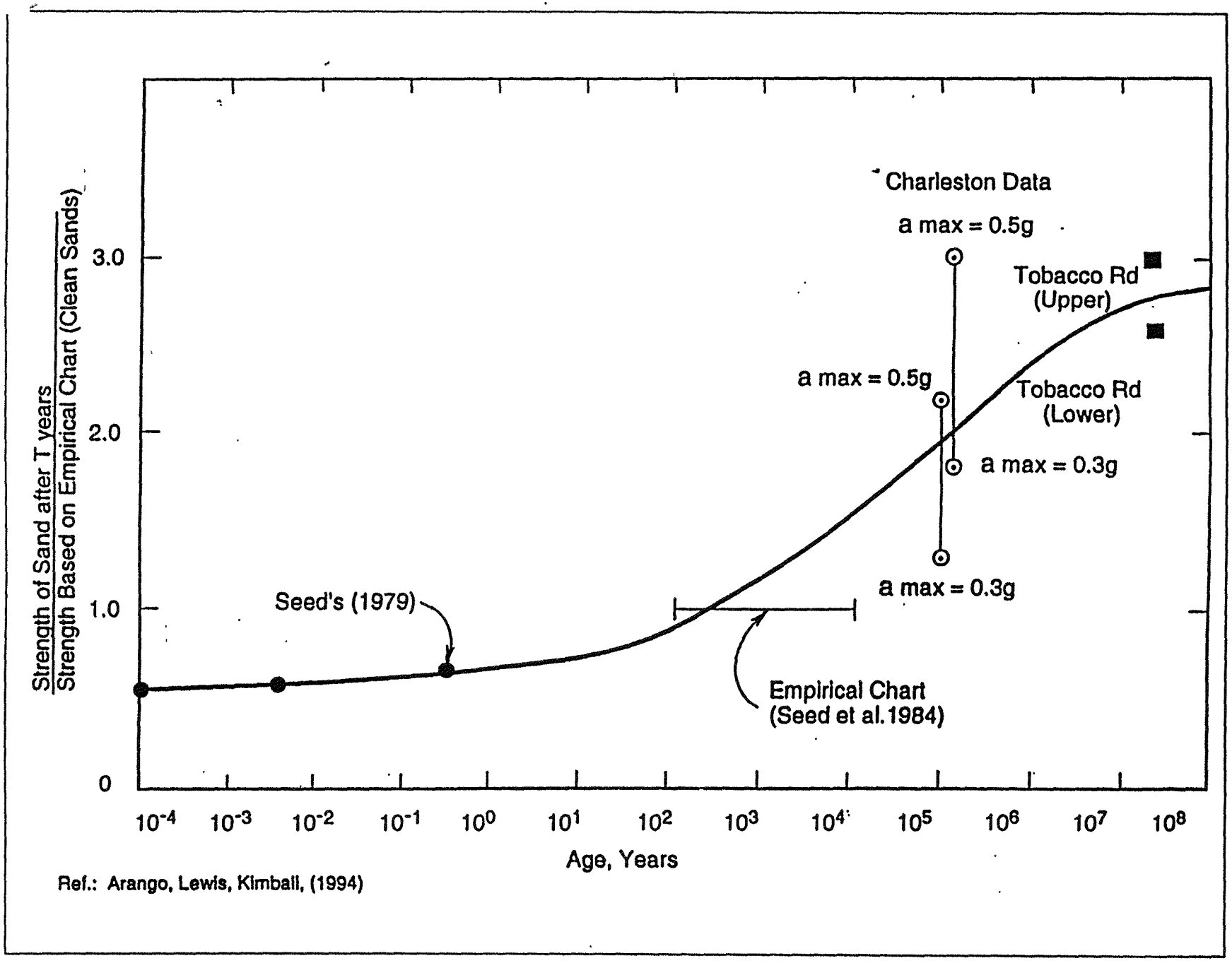


Figure 7.3-8 Influence of age on relative strength against liquefaction.

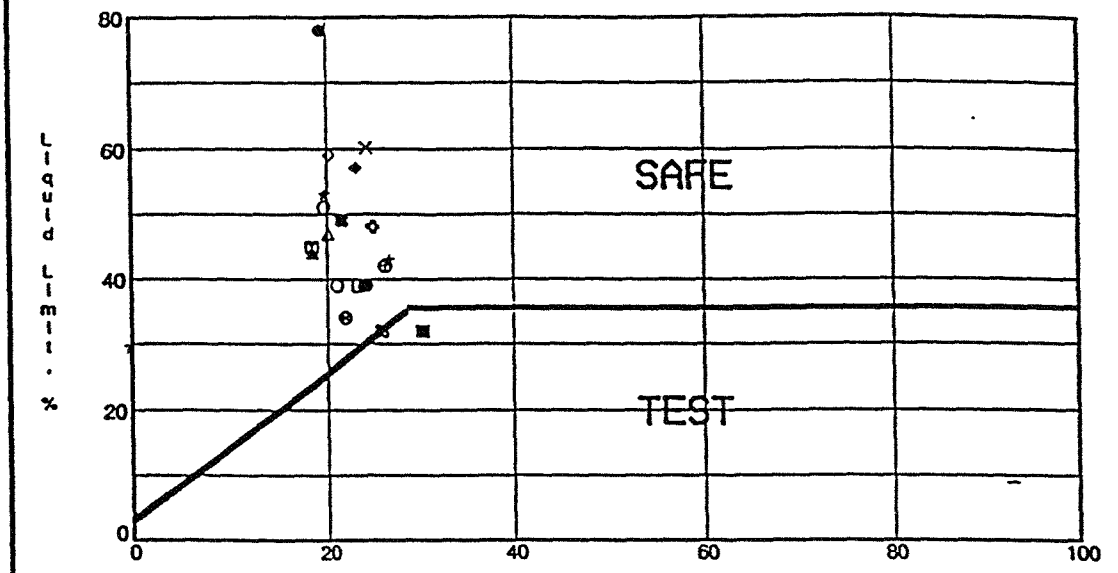


| Specimen ID | Depth, ft | LL | PI | PL | WC | %Clay |
|---|---|---|---|---|---|---|
| H-BOR-12 | 19.1 | 78 | 59 | 19 | 19 | 20.0 |
| H-BOR-12 | 62.8 | 45 | 25 | 20 | 18 | 17.0 |
| H-BOR-12 | 63.3 | 44 | 25 | 19 | 18 | 18.0 |
| H-BOR-12 | 70.8 | 53 | 30 | 23 | 20 | 17.0 |
| H-BOR-12 | 71.4 | 51 | 27 | 24 | 20 | 21.0 |
| H-BOR-12 | 72.0 | 48 | 26 | 22 | 25 | 22.0 |
| H-BOR-12 | 75.0 | 39 | 15 | 24 | 21 | 14.0 |
| H-BOR-12 | 76.1 | 47 | 28 | 19 | 20 | 12.0 |
| H-BOR-12 | 81.5 | 34 | 11 | 23 | 22 | 15.0 |
| H-BOR-12 | 85.3 | 42 | 20 | 22 | 26 | 19.0 |
| H-BOR-12 | 92.8 | 39 | 24 | 15 | 24 | 16.0 |
| H-BOR-12 | 93.4 | 39 | 15 | 24 | 24 | 17.0 |
| H-BOR-12 | 94.0 | 39 | 16 | 23 | 24 | 15.0 |
| H-BOR-12 | 151.5 | 43 | 23 | 20 | 27 | 27.0 |
| H-BOR-12 | 173.2 | 32 | 9 | 23 | 26 | 13.0 |
| H-BOR-12 | 179.3 | 32 | 13 | 19 | 30 | 20.0 |
| H-BOR-2 | 39.3 | 57 | 29 | 28 | 23 | 34.0 |
| H-BOR-2 | 51.5 | 59 | 38 | 21 | 20 | 43.0 |
| H-BOR-2 | 52.3 | 60 | 35 | 25 | 24 | 37.0 |
| H-BOR-2 | 91.2 | 49 | 33 | 16 | 22 | 24.0 |

PROJECT ITP Facility - itp - JOB NO. E3781
DATE 3/23/94

CHINESE CRITERIA FOR CLAYEY SOILS

CHINESE

Westinghouse Savannah River Company
Aiken, South Carolina

Figure 7.3-9(a) Application of Chinese criteria to the clayey soils.

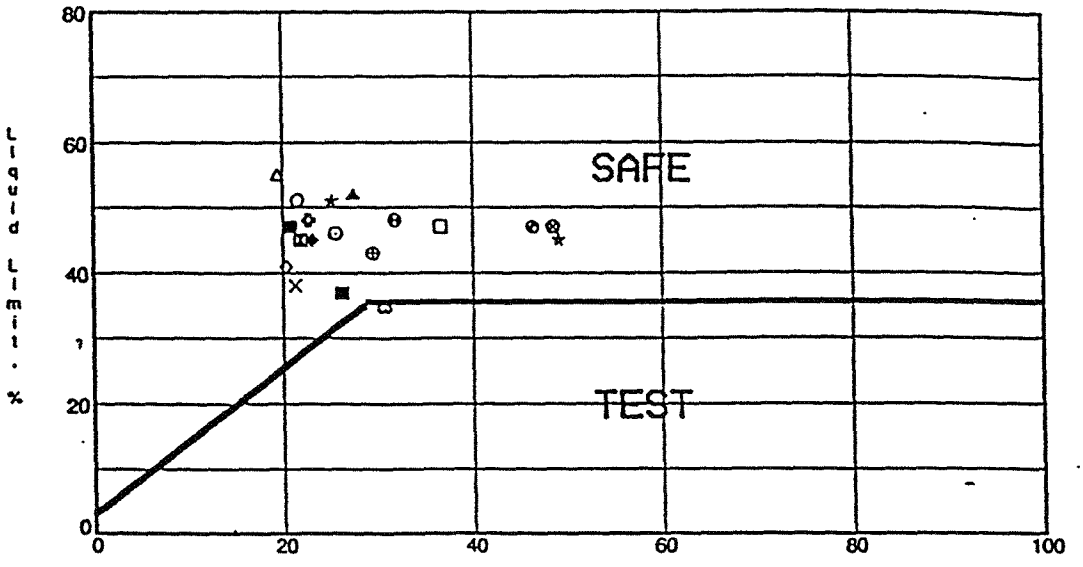


| | Specimen ID | Depth, ft | LL | PI | PL | WC | %Clay |
|---|---|---|---|---|---|---|---|
| ● | H-BOR-2 | 91.8 | 47 | 31 | 16 | 21 | 24.0 |
| ⊠ | H-BOR-2 | 94.1 | 45 | 28 | 17 | 22 | 22.0 |
| ▲ | H-BOR-2 | 94.7 | 52 | 31 | 21 | 27 | 28.0 |
| ★ | H-BOR-2 | 95.3 | 51 | 34 | 17 | 25 | |
| ⊙ | H-BOR-2 | 97.0 | 46 | 28 | 18 | 26 | 18.0 |
| ⊕ | H-BOR-2 | 97.6 | 48 | 29 | 19 | 23 | 19.0 |
| ○ | H-BOR-2 | 98.2 | 51 | 31 | 20 | 22 | 17.0 |
| △ | H-BOR-2 | 142.0 | 55 | 39 | 16 | 20 | 9.0 |
| ⊗ | H-BOR-2 | 170.4 | 47 | 29 | 18 | 49 | 18.0 |
| ⊕ | H-BOR-2 | 174.5 | 43 | 19 | 24 | 29 | 18.0 |
| □ | H-BOR-2 | 175.1 | 47 | 23 | 24 | 37 | 37.0 |
| ⊖ | H-BOR-2 | 175.7 | 48 | 24 | 24 | 32 | 20.0 |
| ⊗ | H-BOR-2 | 176.3 | 47 | 15 | 32 | 47 | 23.0 |
| ★ | H-BOR-2 | 178.1 | 45 | 20 | 25 | 49 | 19.0 |
| ⊠ | H-BOR-2 | 184.5 | 35 | 12 | 23 | 31 | 10.0 |
| ■ | H-BOR-2 | 193.0 | 37 | 13 | 24 | 26 | 12.0 |
| ◆ | H-BOR-2 | 207.3 | 45 | 23 | 22 | 23 | 28.0 |
| ◇ | H-BOR-23 | 28.9 | 41 | 26 | 15 | 20 | 16.0 |
| × | H-BOR-23 | 29.5 | 38 | 21 | 17 | 21 | 17.0 |
| ■ | H-BOR-23 | 33.3 | 47 | 31 | 16 | 21 | 24.0 |

PROJECT ITP Facility - itp -
JOB NO. E3781
DATE 3/23/94

CHINESE CRITERIA FOR CLAYEY SOILS

CHINESE

Westinghouse Savannah River Company
Aiken, South Carolina

Figure 7.3-9(b) Application of Chinese criteria to the clayey soils.

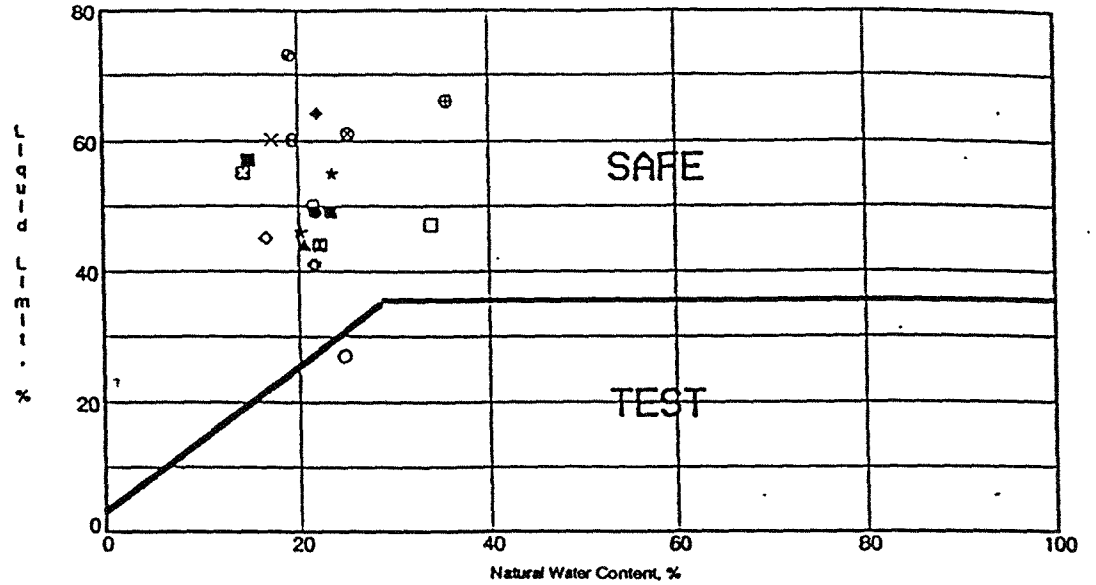


| | Specimen ID | Depth, ft | LL | PI | PL | WC | %Clay |
|---|---|---|---|---|---|---|---|
| ● | H-BOR-23 | 33.9 | 49 | 26 | 23 | 22 | 25.0 |
| ⊡ | H-BOR-23 | 34.5 | 44 | 26 | 18 | 22 | 23.0 |
| ▲ | H-BOR-23 | 40.2 | 44 | 20 | 24 | 21 | 18.0 |
| ★ | H-BOR-23 | 40.8 | 46 | 29 | 17 | 20 | 17.0 |
| ⊙ | H-BOR-23 | 41.4 | 50 | 26 | 24 | 22 | 14.0 |
| ◇ | H-BOR-23 | 43.9 | 41 | 19 | 22 | 22 | 12.0 |
| ○ | H-BOR-23 | 55.1 | 27 | 8 | 19 | 25 | 7.0 |
| △ | H-BOR-23 | 60.6 | 49 | 30 | 19 | 23 | 14.0 |
| ⊗ | H-BOR-23 | 85.0 | 61 | 46 | 15 | 25 | 10.0 |
| ⊕ | H-BOR-23 | 96.9 | 66 | 50 | 16 | 36 | 28.0 |
| □ | H-BOR-23 | 176.2 | 47 | 23 | 24 | 34 | 21.0 |
| ⊖ | H-BOR-29 | 15.4 | 60 | 36 | 24 | 19 | 28.0 |
| ⊘ | H-BOR-29 | 20.0 | 73 | 42 | 31 | 19 | 28.0 |
| ★ | H-BOR-29 | 25.7 | 55 | 32 | 23 | 24 | 39.0 |
| ⊡ | H-BOR-29 | 31.1 | 55 | 29 | 26 | 14 | 39.0 |
| ■ | H-BOR-29 | 35.8 | 57 | 37 | 20 | 15 | 22.0 |
| ✦ | H-BOR-29 | 36.8 | 64 | 43 | 21 | 22 | 28.0 |
| ◇ | H-BOR-29 | 41.1 | 45 | 29 | 16 | 17 | 32.0 |
| × | H-BOR-29 | 46.1 | 60 | 37 | 23 | 17 | 25.0 |
| ■ | H-BOR-29 | 90.5 | 49 | 30 | 19 | 23 | 21.0 |

PROJECT ITP Facility - itp - JOB NO. E3781
DATE 3/23/94

CHINESE CRITERIA FOR CLAYEY SOILS

CHINESE

Westinghouse Savannah River Company
Aiken, South Carolina

ure 7.3-9(c) Application of Chinese criteria to the clayey soils.

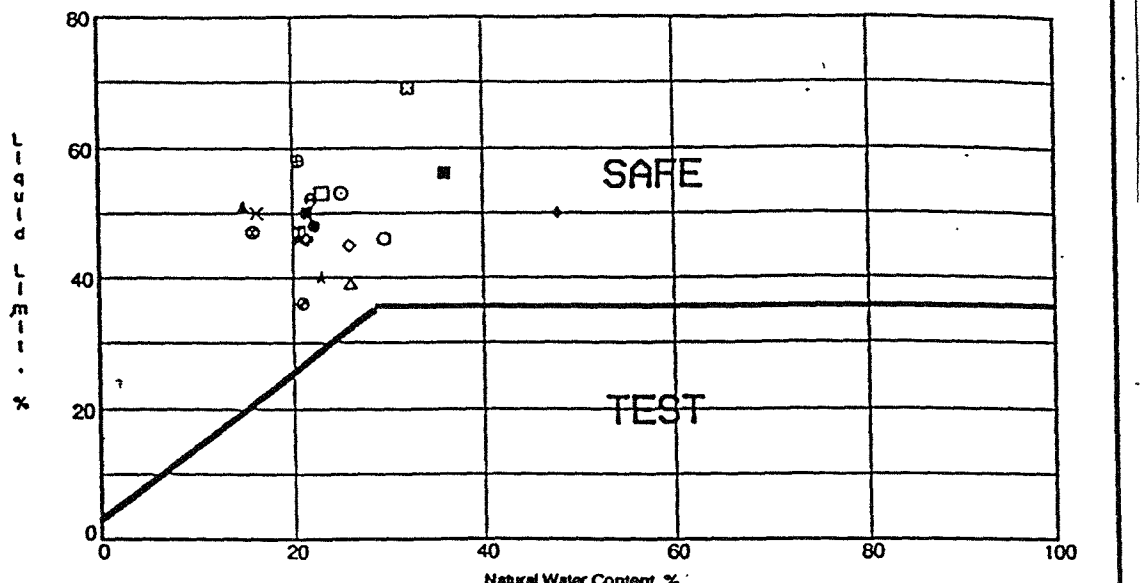


| | Specimen ID | Depth, ft | LL | PI | PL | WC | %Clay |
|---|---|---|---|---|---|---|---|
| ● | H-BOR-29 | 91.1 | 48 | 30 | 18 | 22 | 23.0 |
| ⊟ | H-BOR-29 | 91.7 | 47 | 27 | 20 | 21 | 21.0 |
| ▲ | H-BOR-29 | 92.3 | 51 | 28 | 23 | 15 | 19.0 |
| ★ | H-BOR-29 | 93.4 | 46 | 31 | 15 | 21 | 19.0 |
| ⊙ | H-BOR-29 | 96.0 | 53 | 27 | 26 | 25 | 20.0 |
| ⊕ | H-BOR-29 | 97.1 | 46 | 25 | 21 | 22 | 18.0 |
| ○ | H-BOR-29 | 141.1 | 46 | 25 | 21 | 30 | 11.0 |
| △ | H-BOR-29 | 178.9 | 39 | 18 | 21 | 26 | 13.0 |
| ⊛ | H-SPT-1 | 43.5 | 47 | 21 | 26 | 16 | 12.9 |
| ⊕ | H-SPT-1 | 48.0 | 58 | 32 | 26 | 21 | 24.3 |
| □ | H-SPT-14 | 21.0 | 53 | 28 | 25 | 23 | 7.2 |
| ⊖ | H-SPT-14 | 25.5 | 52 | 27 | 25 | 22 | 8.4 |
| ⊜ | H-SPT-14 | 61.5 | 36 | 14 | 22 | 21 | 2.5 |
| ★ | H-SPT-14 | 69.0 | 40 | 18 | 22 | 23 | 3.6 |
| ⊡ | H-SPT-14 | 122.5 | 69 | 46 | 23 | 32 | 6.8 |
| ■ | H-SPT-14 | 131.5 | 56 | 31 | 25 | 36 | 4.5 |
| ◆ | H-SPT-14 | 142.0 | 50 | 24 | 26 | 48 | 13.1 |
| ◇ | H-SPT-14 | 176.5 | 45 | 22 | 23 | 26 | 9.4 |
| × | H-SPT-18 | 15.0 | 50 | 24 | 26 | 16 | 19.0 |
| ▣ | H-SPT-18 | 27.0 | 50 | 26 | 24 | 22 | 15.9 |

PROJECT ITP Facility - itp - JOB NO. E3781
DATE 3/23/94

CHINESE CRITERIA FOR CLAYEY SOILS

CHINESE

Westinghouse Savannah River Company
Aiken, South Carolina

Figure 7.3-9(d) Application of Chinese criteria to the clayey soils.

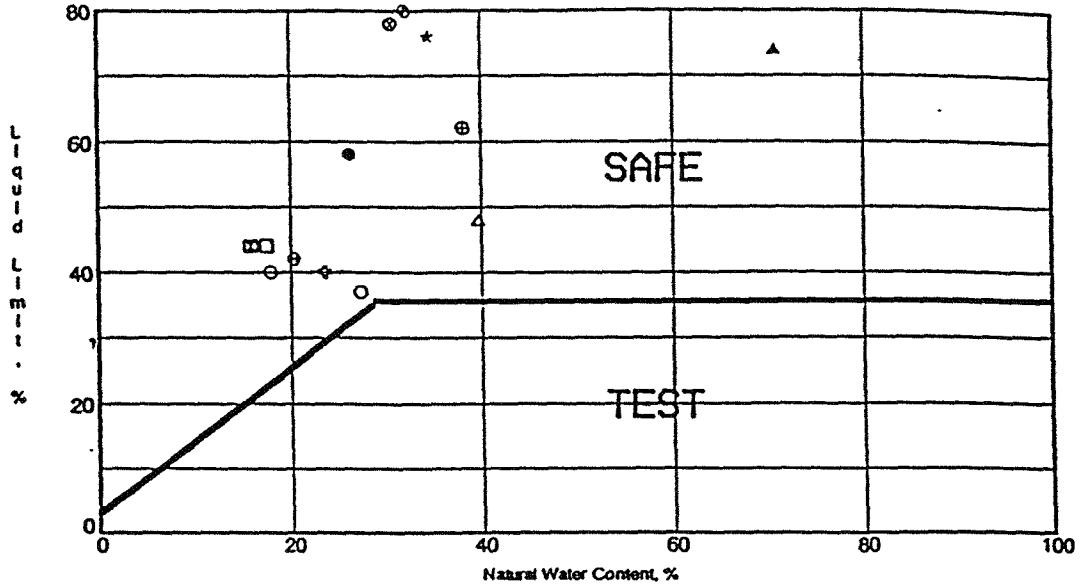


| | Specimen ID | Depth, ft | LL | PI | PL | WC | %Clay |
|---|---|---|---|---|---|---|---|
| ● | H-SPT-18 | 37.5 | 58 | 34 | 24 | 26 | 15.0 |
| ⊞ | H-SPT-18 | 79.5 | 44 | 22 | 22 | 16 | 4.7 |
| ▲ | H-SPT-18 | 132.0 | 74 | 23 | 51 | 71 | 46.6 |
| ★ | H-SPT-18 | 183.5 | 76 | 53 | 23 | 35 | 34.5 |
| ○ | H-SPT-20 | 21.0 | 40 | 20 | 20 | 18 | 2.7 |
| ⊖ | H-SPT-20 | 30.0 | 40 | 18 | 22 | 24 | 13.2 |
| ○ | H-SPT-20 | 55.5 | 37 | 12 | 25 | 27 | 3.0 |
| △ | H-SPT-20 | 84.0 | 48 | 24 | 24 | 40 | 10.8 |
| ⊗ | H-SPT-20 | 106.5 | 78 | 53 | 25 | 31 | 48.8 |
| ⊕ | H-SPT-20 | 180.0 | 62 | 38 | 24 | 38 | 48.5 |
| □ | HBOR23.1 | 17.5 | 44 | 25 | 19 | 17 | 18.0 |
| ⊖ | HBOR23.1 | 28.9 | 42 | 23 | 19 | 20 | 19.0 |
| ⊗ | HBOR23.1 | 97.3 | 80 | 62 | 18 | 32 | 30.0 |

PROJECT ITP Facility - itp - Quik-Gel
JOB NO E3781
DATE 3/23/94

CHINESE CRITERIA FOR CLAYEY SOILS

CHINESE

Westinghouse Savannah River Company
Aiken, South Carolina

Figure 7.3-9(e) Application of Chinese criteria to the clayey soils.

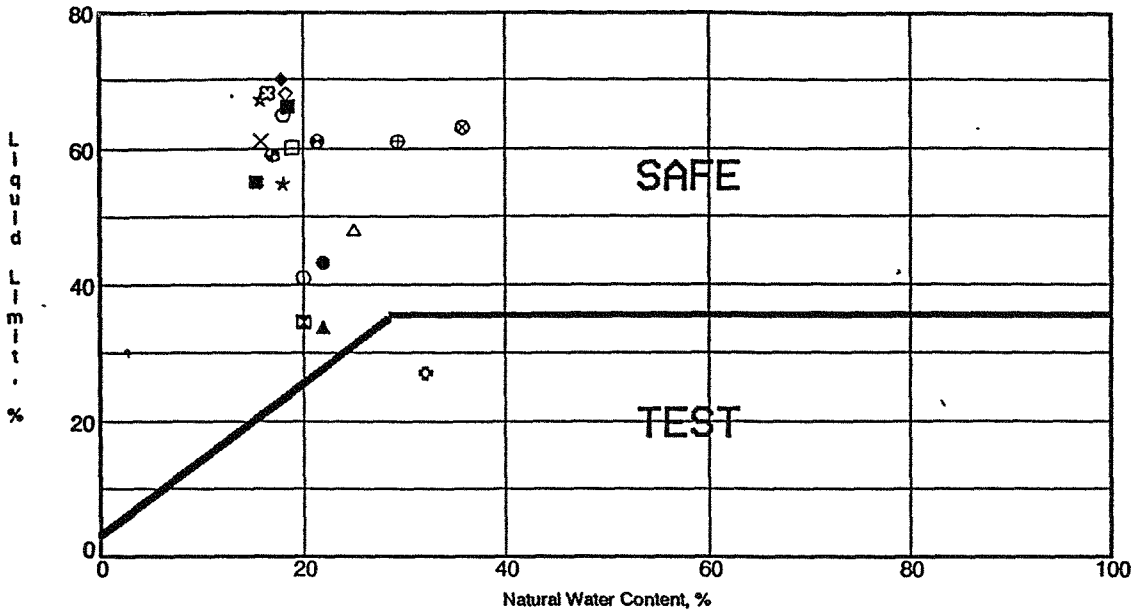


| | Specimen ID | Depth, ft | LL | PI | PL | WC | %Clay |
|---|---|---|---|---|---|---|---|
| ● | 24112H-5 | 24.0 | 43 | 19 | 25 | 22 | |
| ⊠ | 24112H-5 | 68.9 | 35 | 15 | 20 | 20 | |
| ▲ | 24112H-5 | 73.9 | 34 | 11 | 23 | 22 | |
| ★ | 24112H-6 | 24.0 | 55 | 31 | 23 | 18 | |
| ⊙ | 24112H-6 | 79.0 | 65 | 32 | 33 | 18 | |
| ✿ | DH-2 | 90.0 | 27 | 9 | 18 | 32 | |
| ○ | DH-3 | 45.0 | 41 | 17 | 24 | 20 | |
| △ | DH-3 | 95.0 | 48 | 20 | 28 | 25 | |
| ⊗ | H-154U | 10.5 | 63 | 27 | 36 | 36 | |
| ⊕ | H-154U | 13.7 | 61 | 25 | 36 | 29 | |
| □ | H-154U | 17.2 | 60 | 31 | 29 | 19 | |
| ⊖ | H-154U | 72.1 | 61 | 33 | 28 | 21 | |
| ⊛ | HMP-1 | 18.5 | 59 | 38 | 21 | 17 | |
| ★ | HMP-1 | 24.5 | 67 | 44 | 23 | 16 | |
| ⊠ | HMP-1 | 35.5 | 68 | 46 | 22 | 17 | |
| ■ | HMP-2 | 6.0 | 66 | 35 | 31 | 19 | |
| ◆ | HMP-2 | 15.5 | 70 | 43 | 27 | 18 | |
| ◇ | HMP-2 | 26.0 | 68 | 42 | 26 | 18 | |
| × | HMP-2 | 33.5 | 61 | 37 | 24 | 16 | |
| ⊠ | HMP-3 | 35.0 | 55 | 18 | 37 | 15 | |

PROJECT H AREA INVESTIGATION
JOB NO. E3781
DATE 4/20/95

**CHINESE CRITERIA FOR CLAYEY SOILS**

CHINESE

Westinghouse Savannah River Company
Aiken, South Carolina

Figure 7.3-9(f) Application of Chinese criteria to the clayey soils.

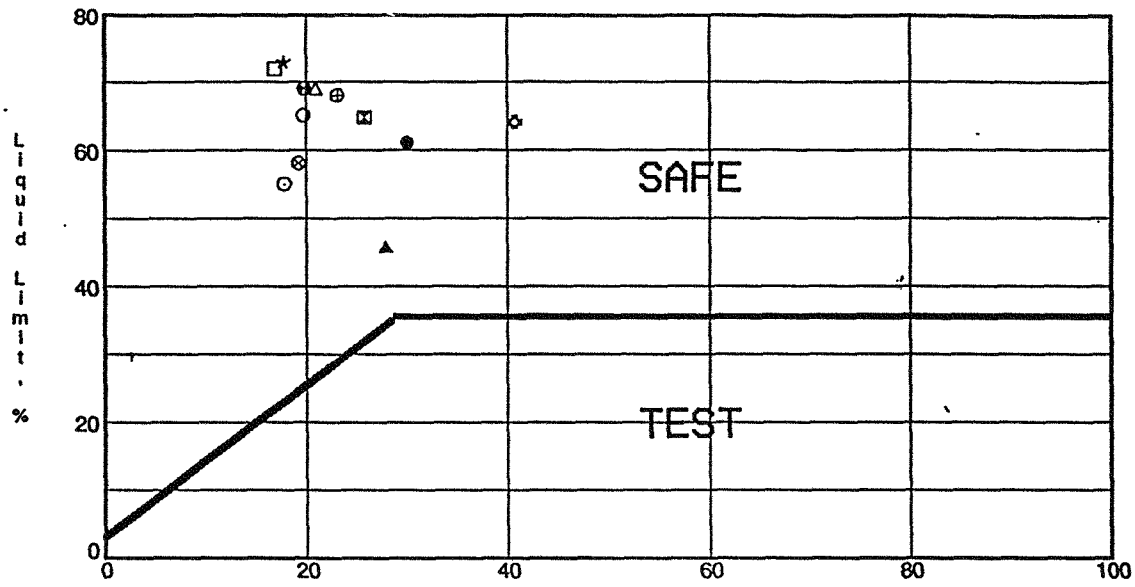


| | Specimen ID | Depth, ft | LL | PI | PL | WC | %Clay |
|---|---|---|---|---|---|---|---|
| ● | HMP-3 | 46.2 | 61 | 31 | 30 | 30 | |
| ⊠ | HMP-3 | 56.1 | 65 | 48 | 17 | 26 | |
| ▲ | HMP-3 | 66.4 | 46 | 26 | 20 | 28 | |
| ★ | HMP-4 | 10.0 | 73 | 56 | 17 | 18 | |
| ⊙ | HMP-4 | 16.0 | 55 | 39 | 16 | 18 | |
| ☼ | HMP-4 | 26.0 | 64 | 46 | 18 | 41 | |
| ○ | HMP-4 | 36.0 | 65 | 45 | 20 | 20 | |
| △ | HMP-5 | 15.5 | 69 | 49 | 20 | 21 | |
| ⊗ | HMP-5 | 26.0 | 58 | 37 | 21 | 19 | |
| ⊕ | HMP-5 | 35.5 | 68 | 45 | 23 | 23 | |
| □ | HMP-6 | 25.0 | 72 | 49 | 23 | 17 | |
| ⊖ | HMP-6 | 35.5 | 69 | 41 | 28 | 20 | |

PROJECT H AREA INVESTIGATION
JOB NO. E3781
DATE 4/20/95

**CHINESE CRITERIA FOR CLAYEY SOILS**

CHINESE

Westinghouse Savannah River Company
Aiken, South Carolina

Figure 7.3-9(g) Application of Chinese criteria to the clayey soils.

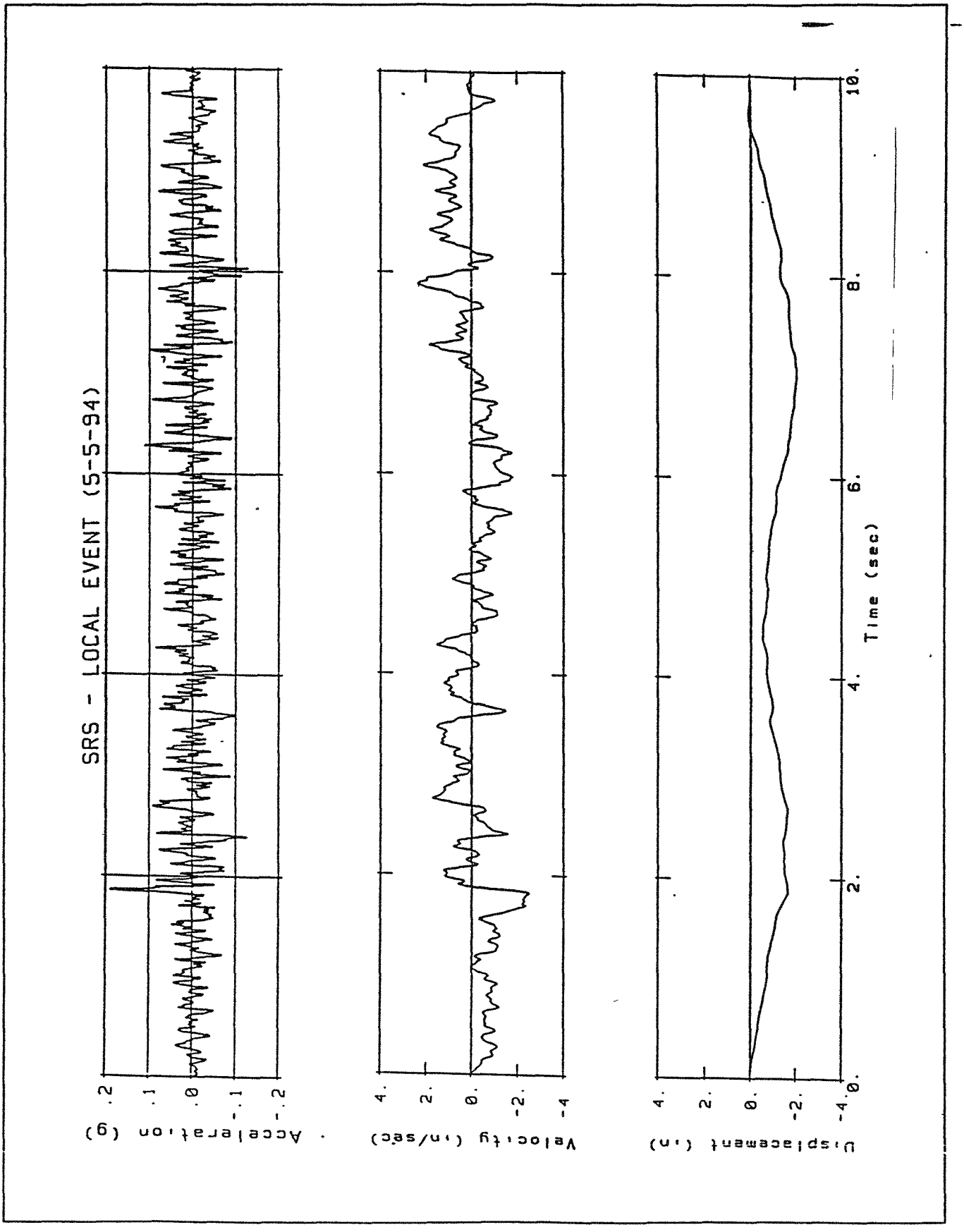


Figure 7.3-10 Acceleration, velocity, and displacement time histories: Local earthquake event.

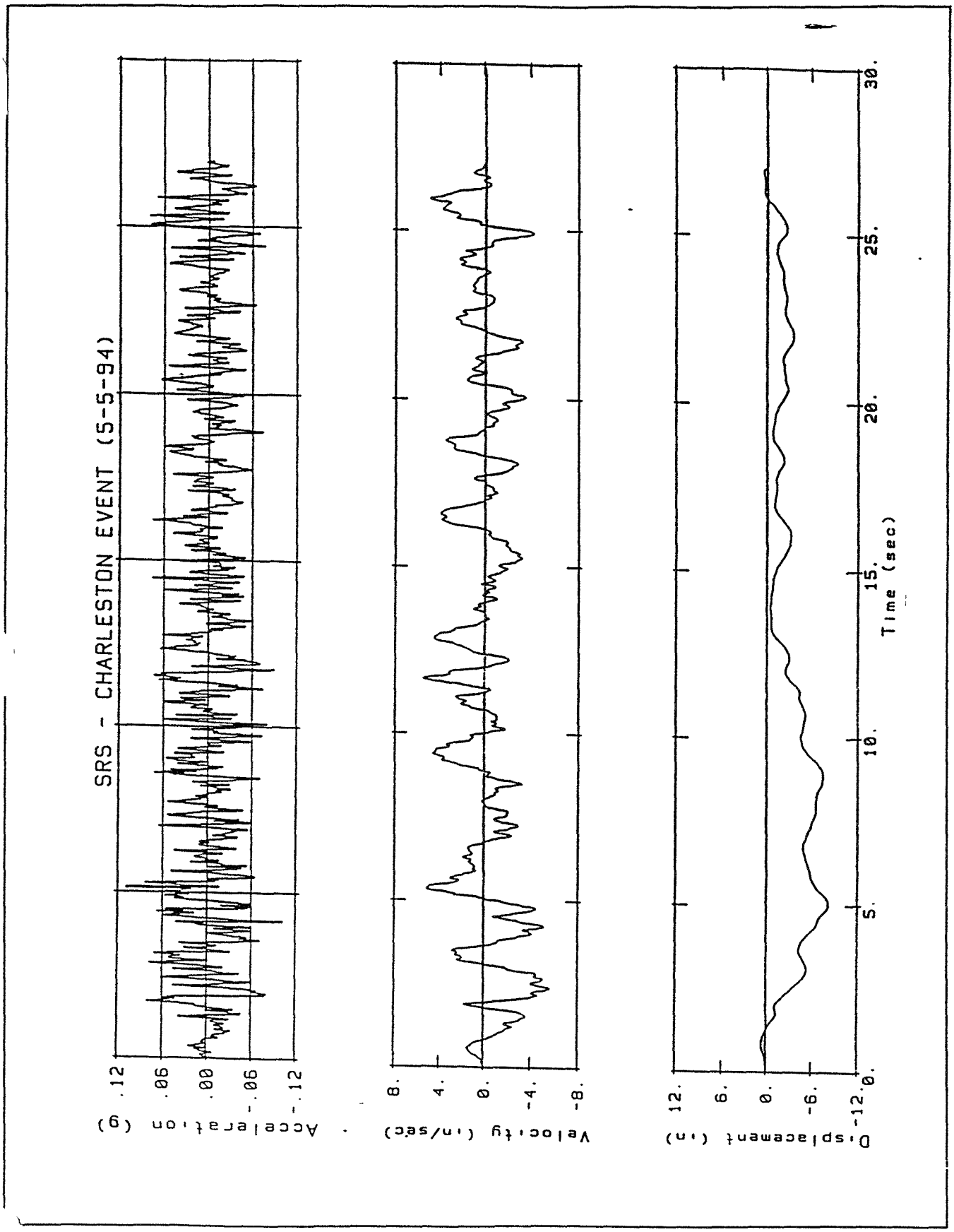


Figure 7.3-11 Acceleration, velocity, and displacement time histories: Distant earthquake event.

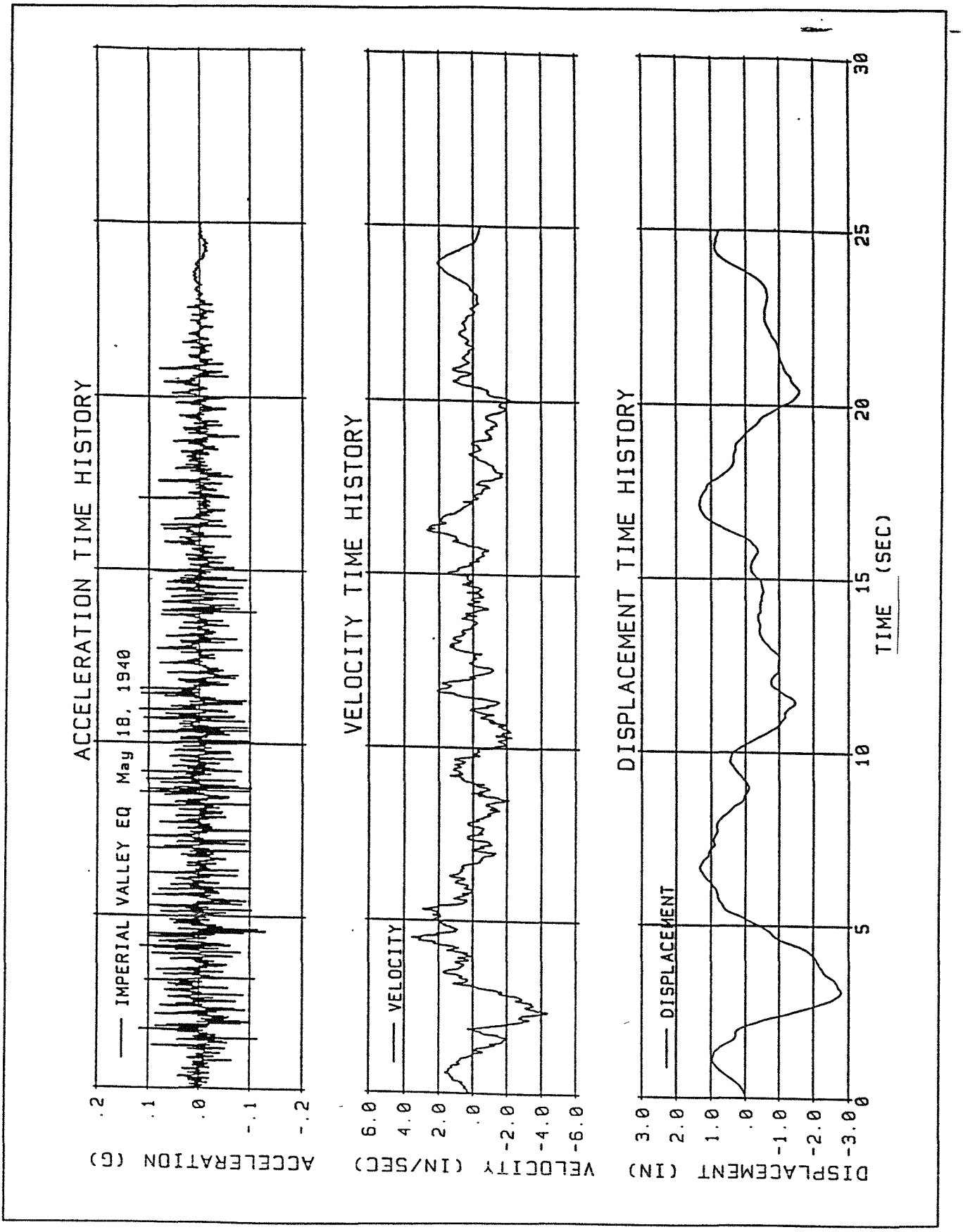


Figure 7.3-12 Acceleration, velocity, and displacement time histories: 84th percentile motion.

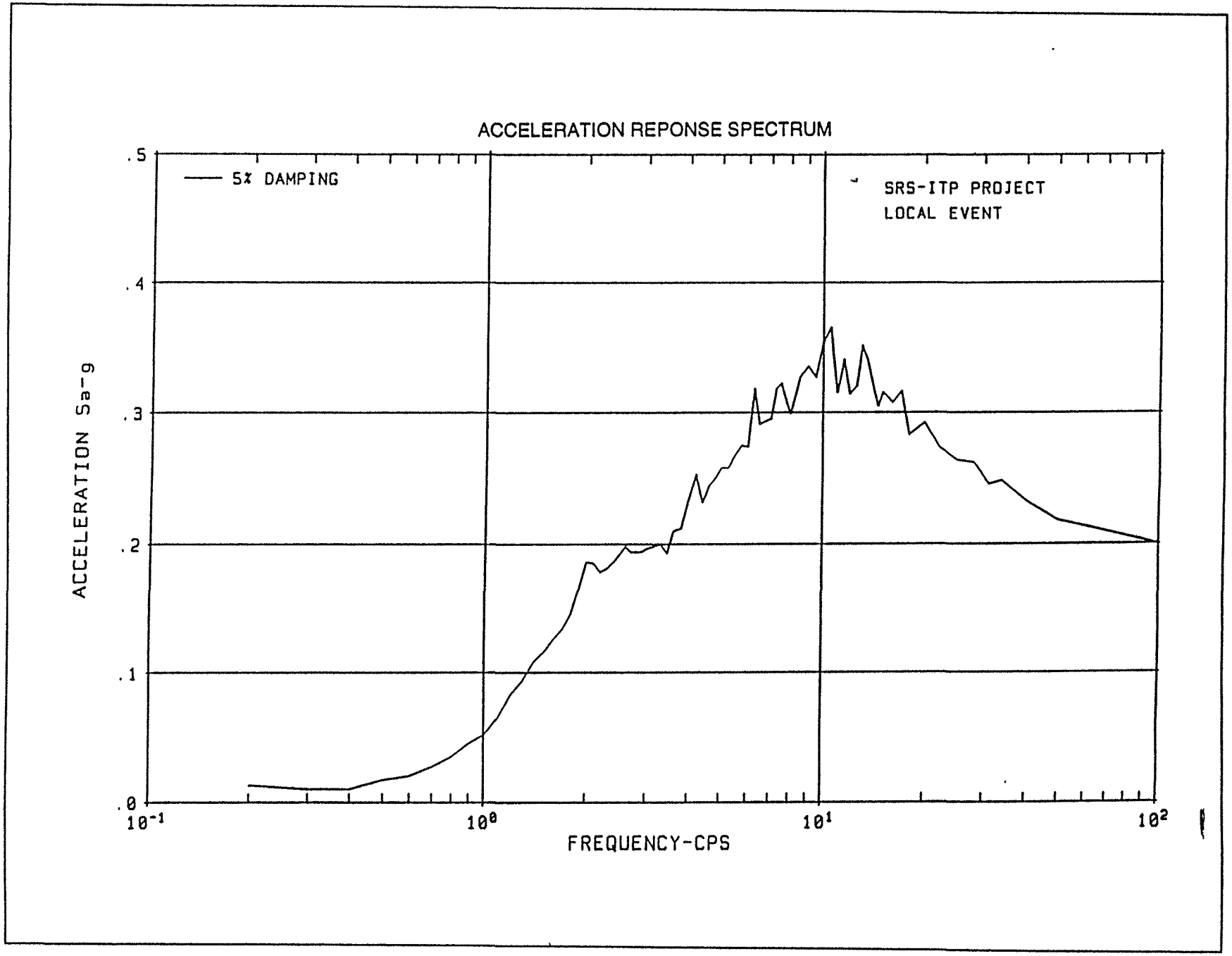


Figure 7.3-13 Acceleration response spectrum: Local earthquake.

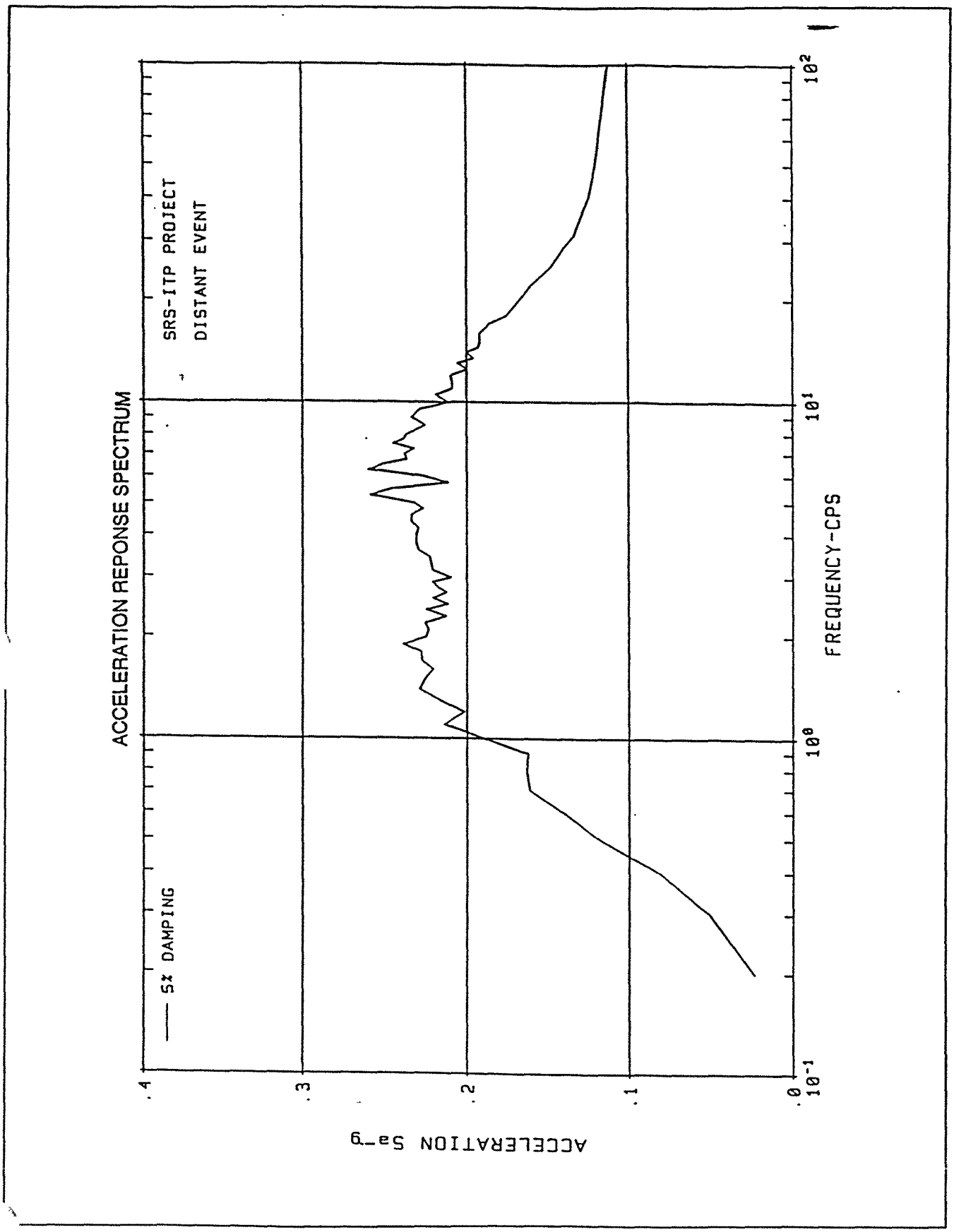


Figure 7.3-14 Acceleration response spectrum: Distant earthquake.

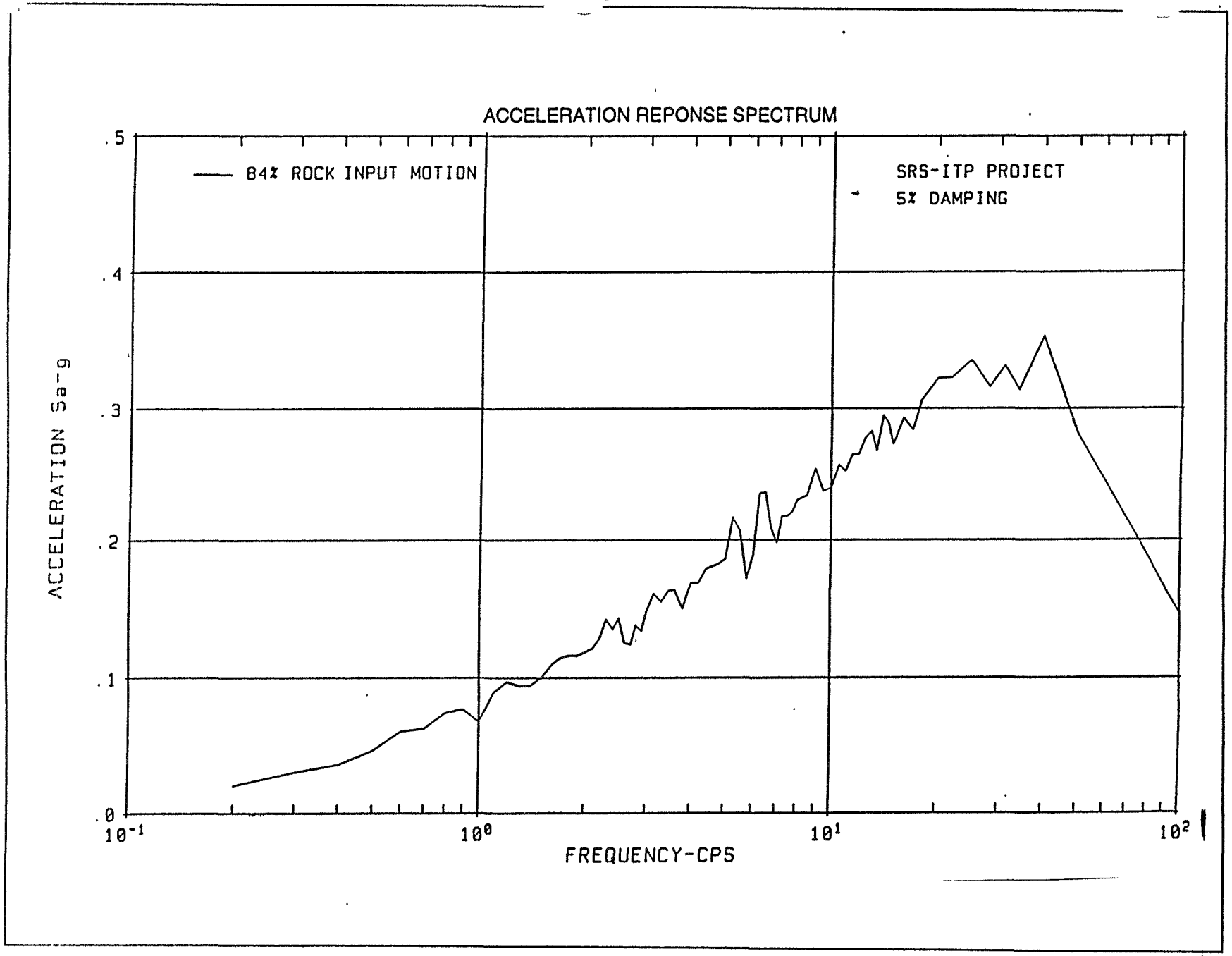


Figure 7.3-15 Acceleration response spectrum: 84th percentile earthquake.

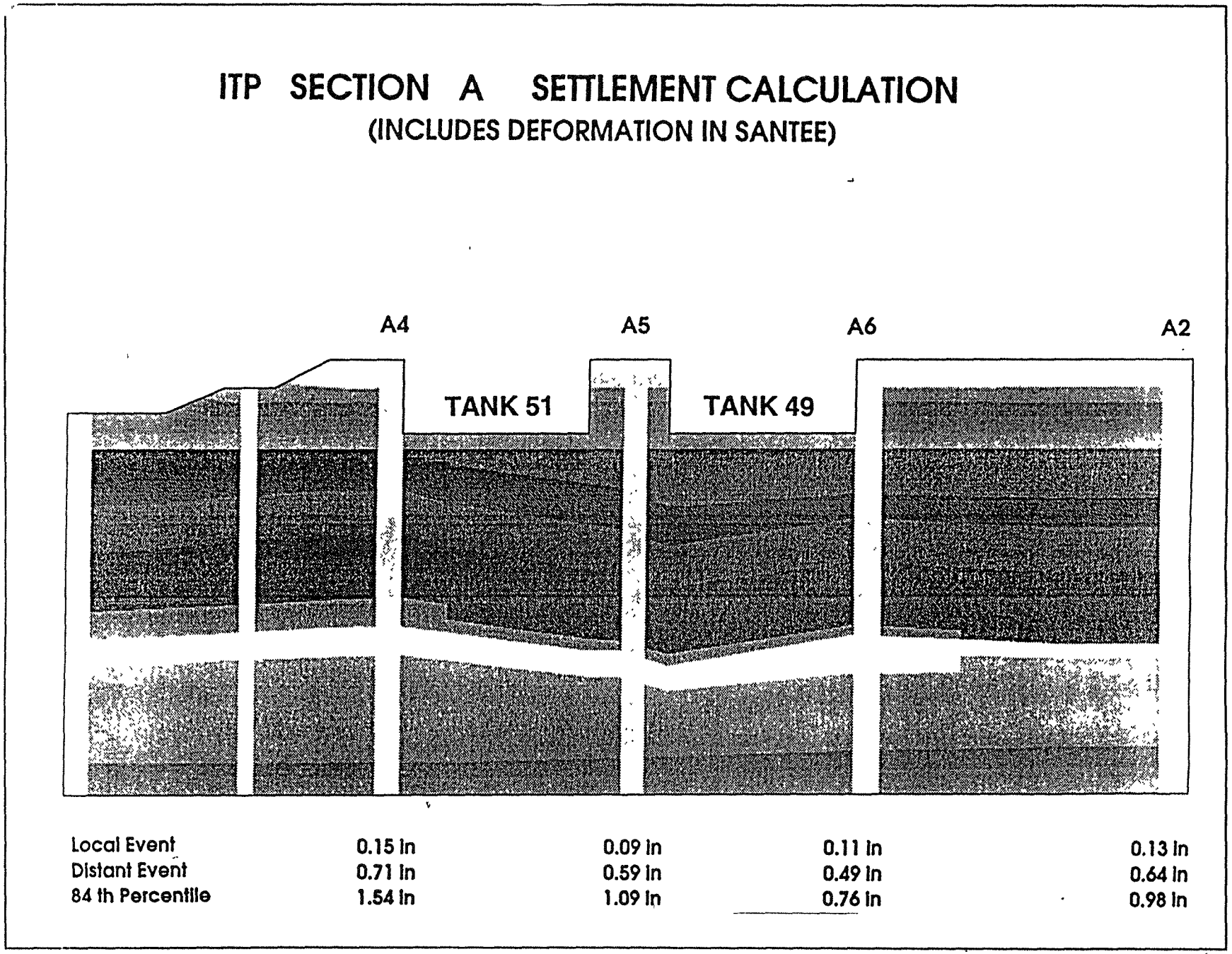


Figure 7.3-16 Subsurface cross-section A used for free field ground response and settlement analyses.

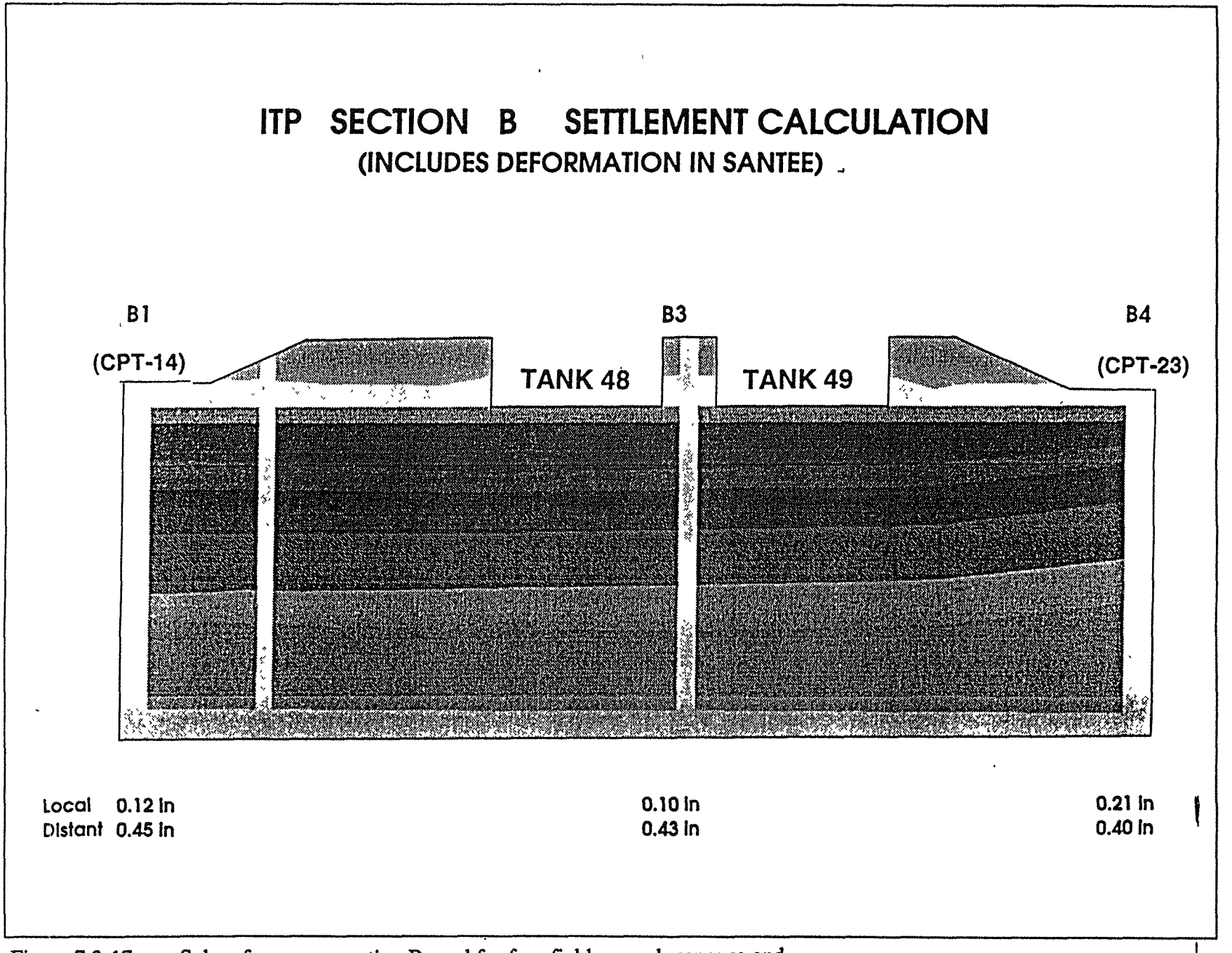


Figure 7.3-17 Subsurface cross-section B used for free-field ground response and settlement analyses.

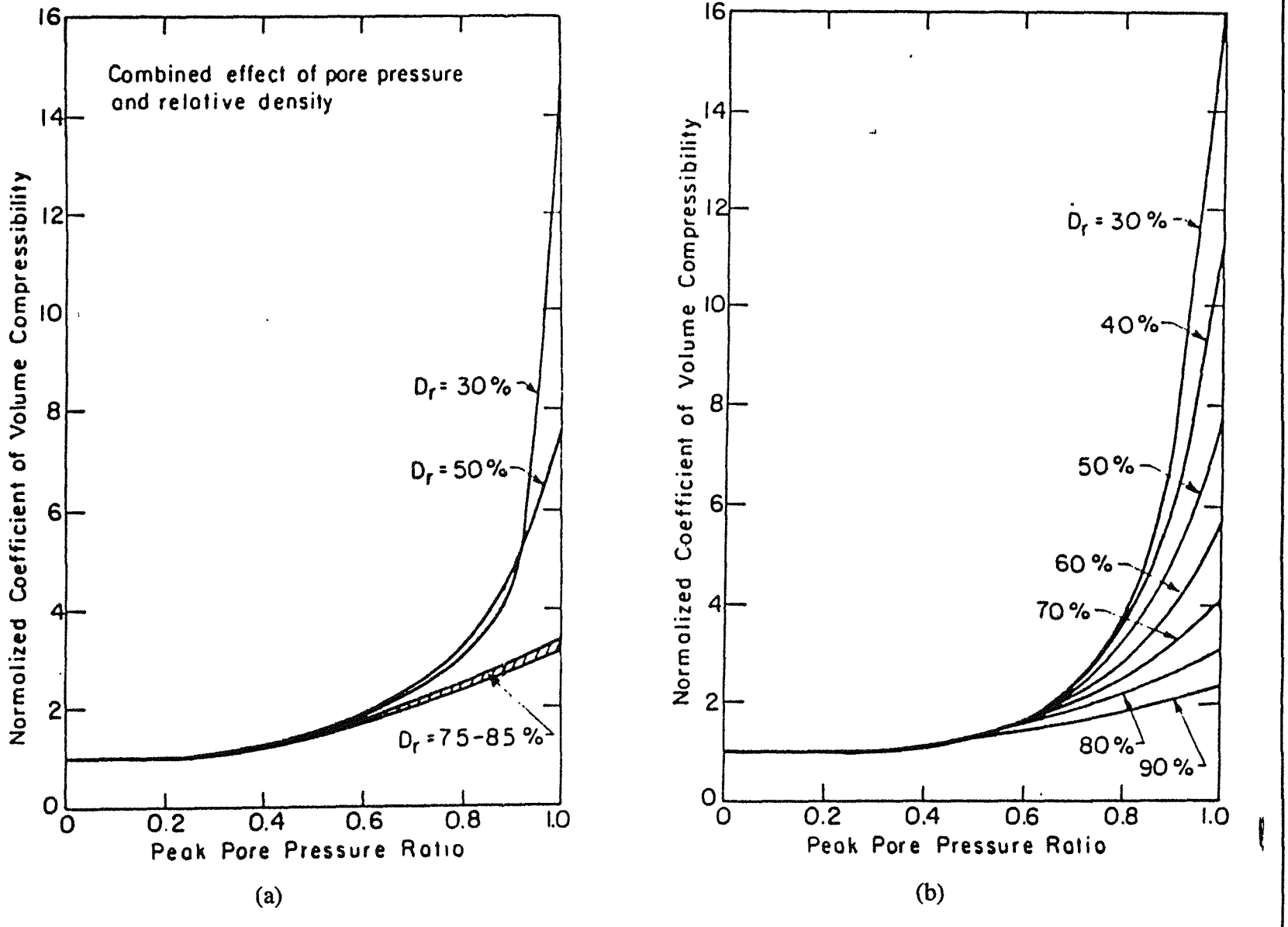


Figure 7.3-18 Relationship between pore pressure build-up and coefficient of volumetric compression - (a) measured; (b) theoretical (Lee and Albaisa, 1974).

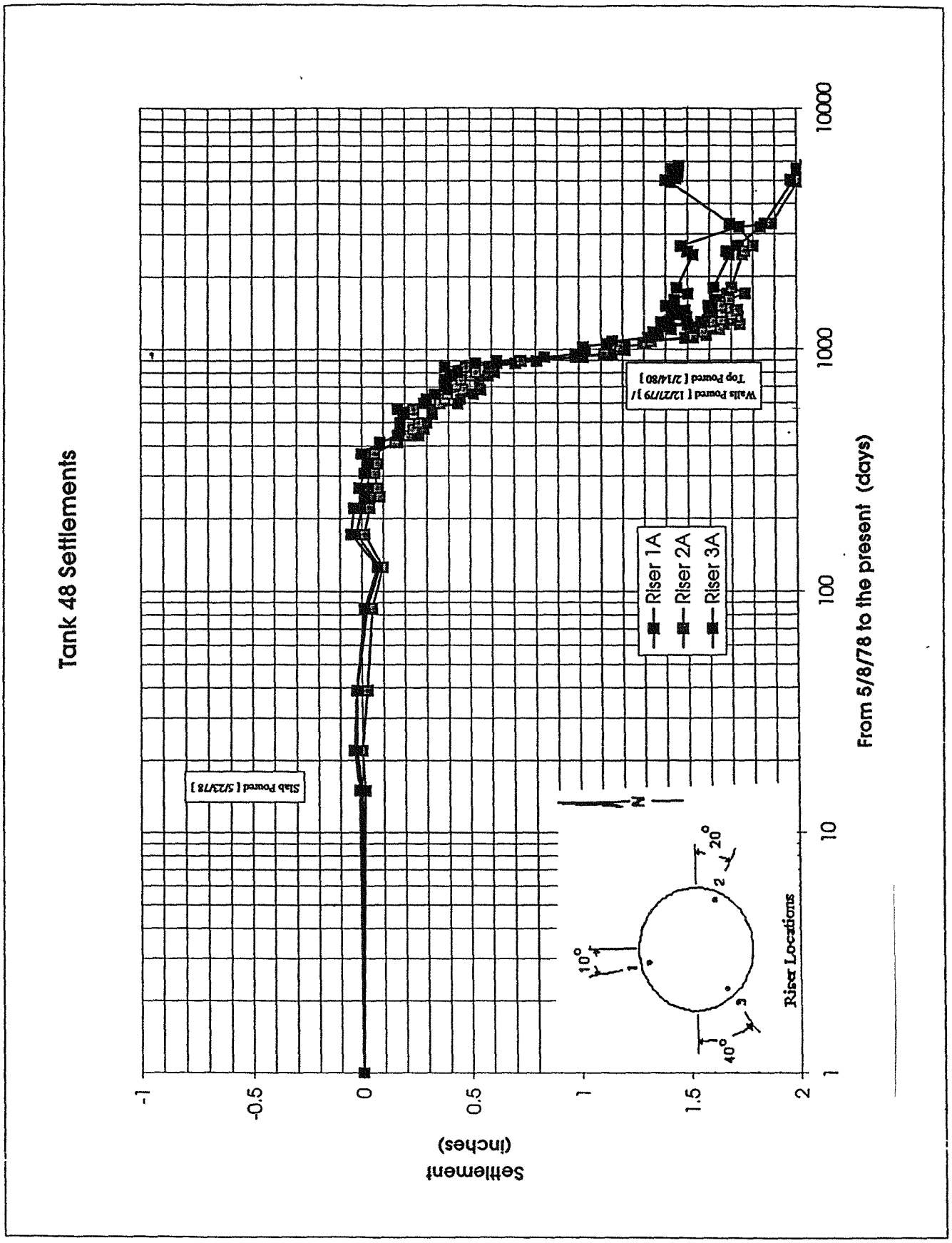


Figure 7 5.1 Tank 48: Observed settlements.

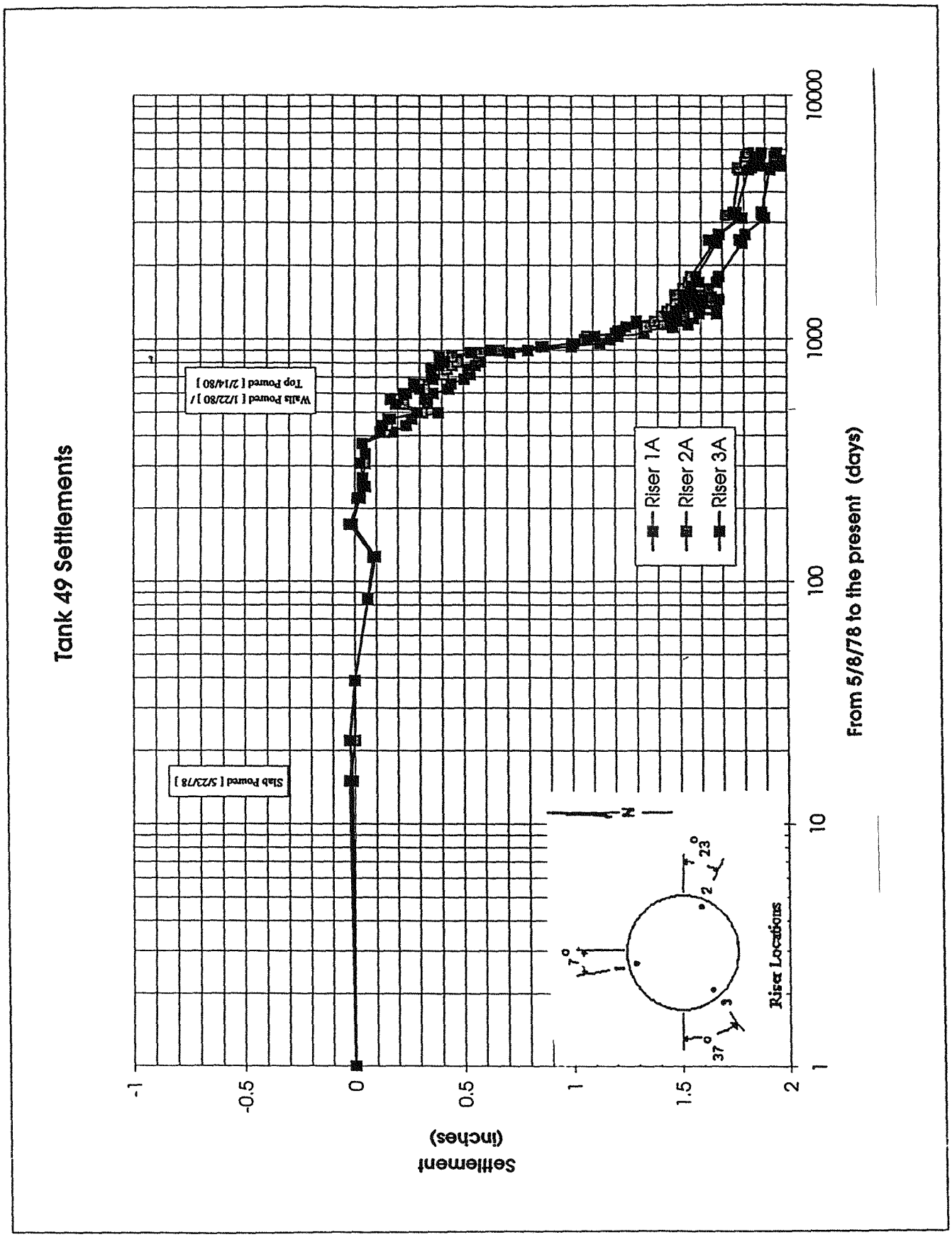


Figure 7.5.2 Tank 49: Observed settlements.

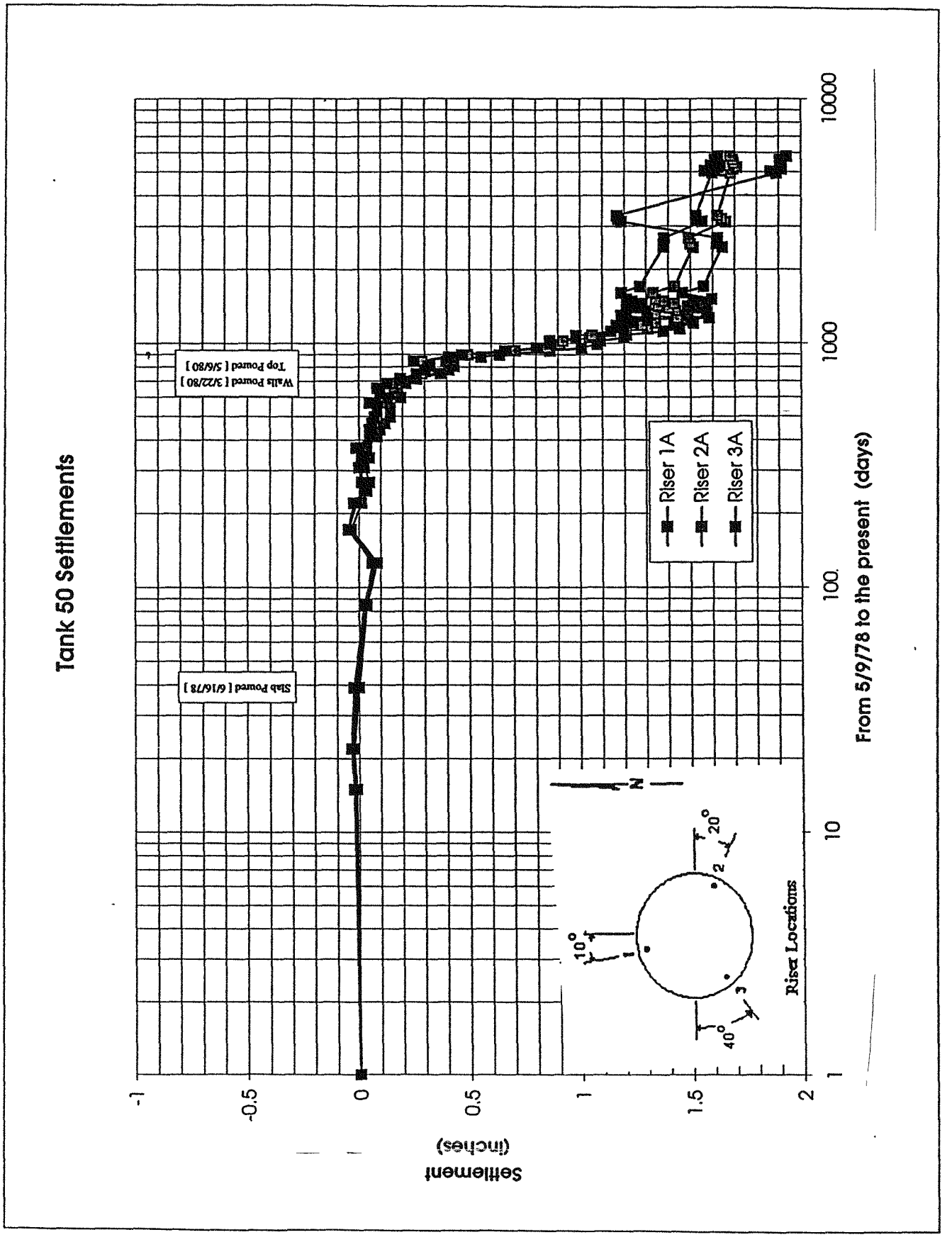


Figure 7.5.3 Tank 50: Observed settlements.

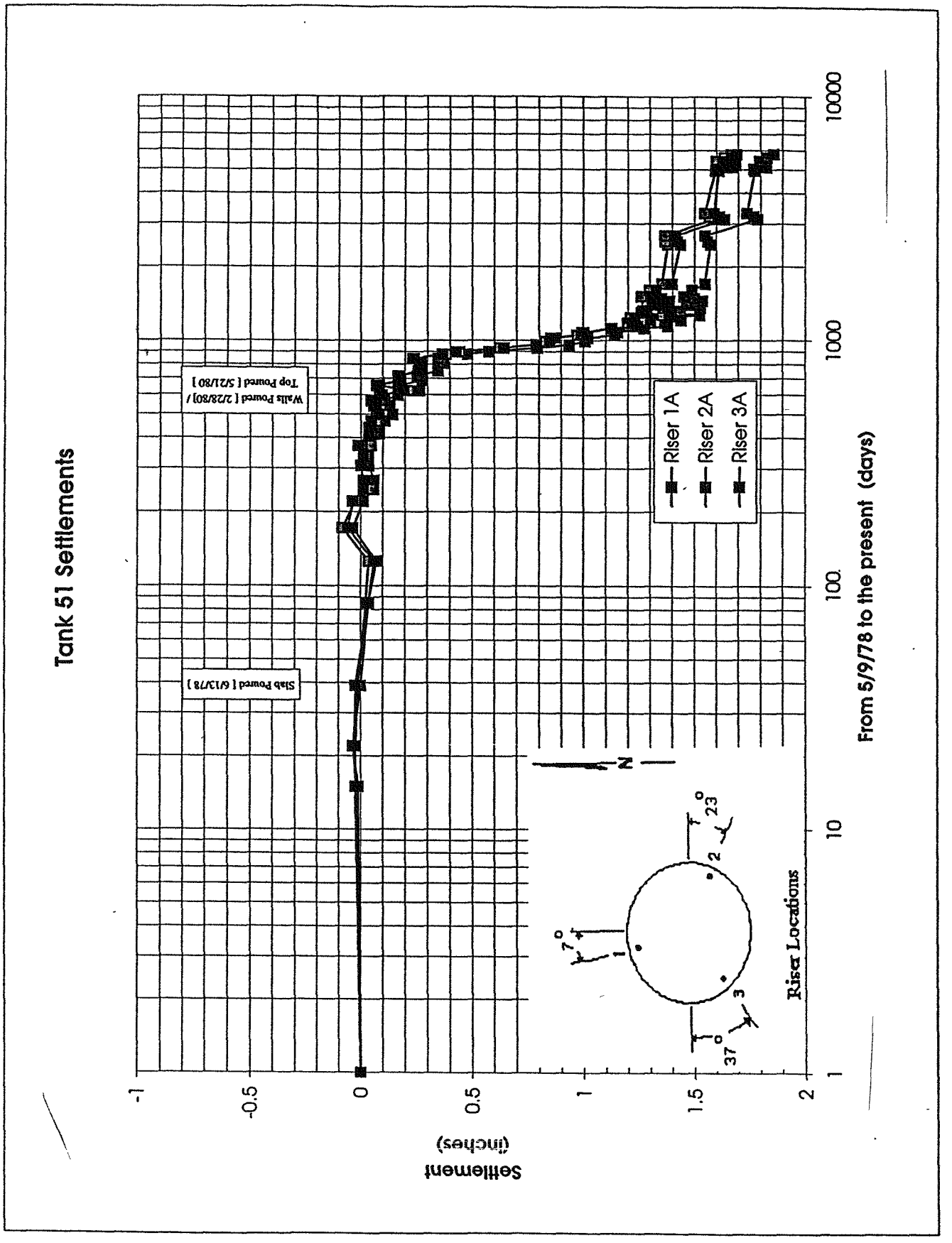


Figure 7.5.4 Tank 51: Observed settlements.

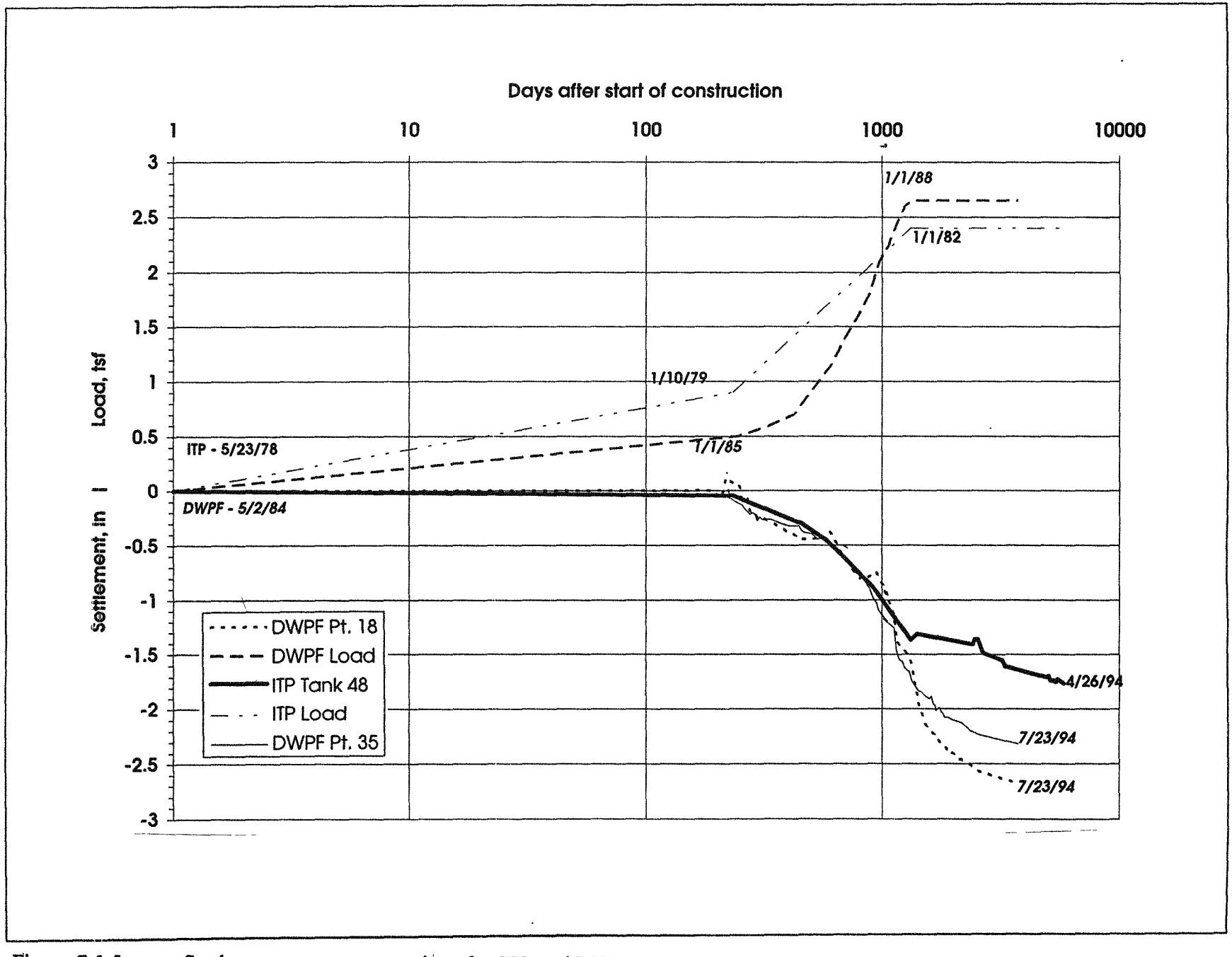


Figure 7.5.5 Settlement pattern comparison for ITP and DWPF.

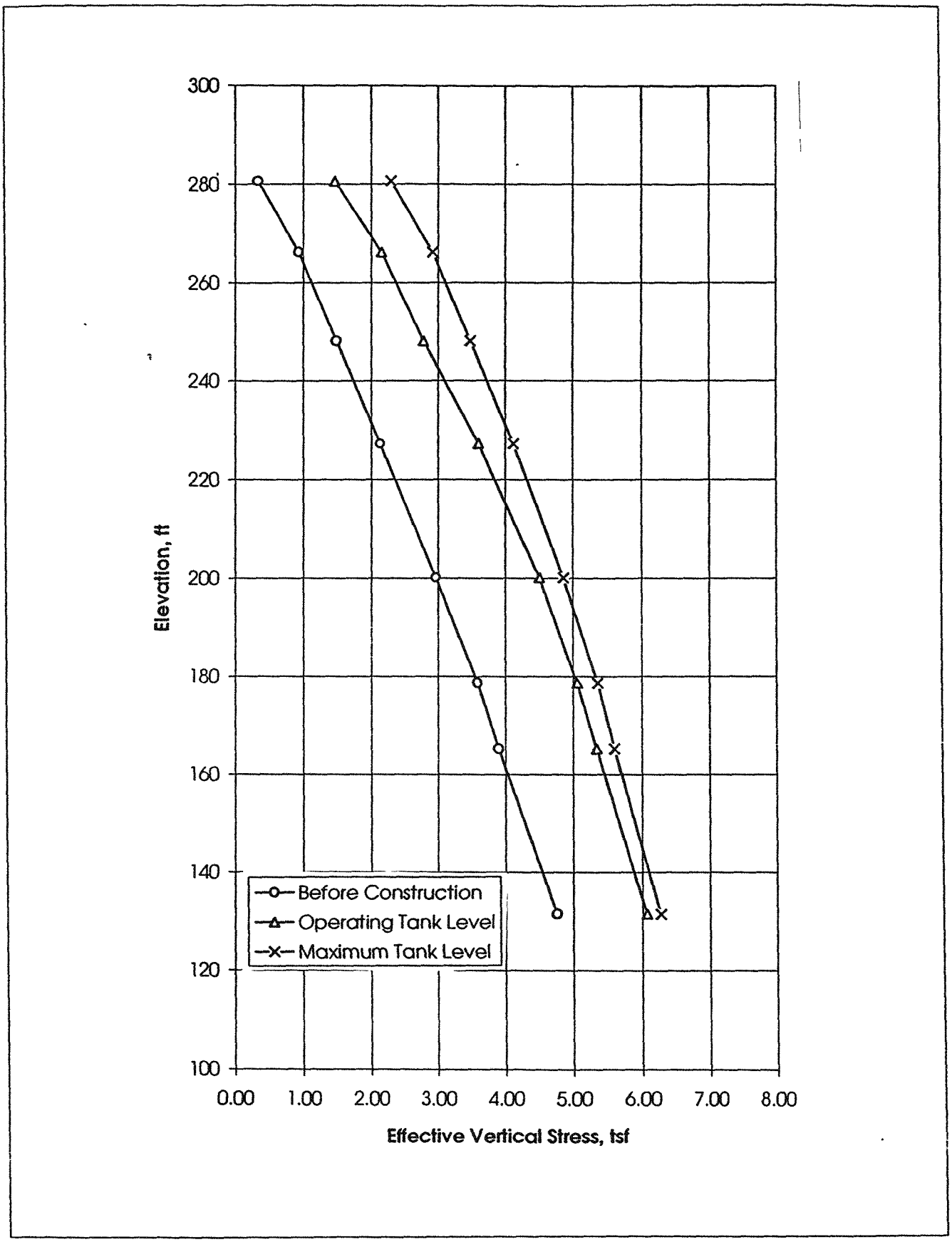


Figure 7.5.6 Distribution of vertical stress at different stages of tank operation.

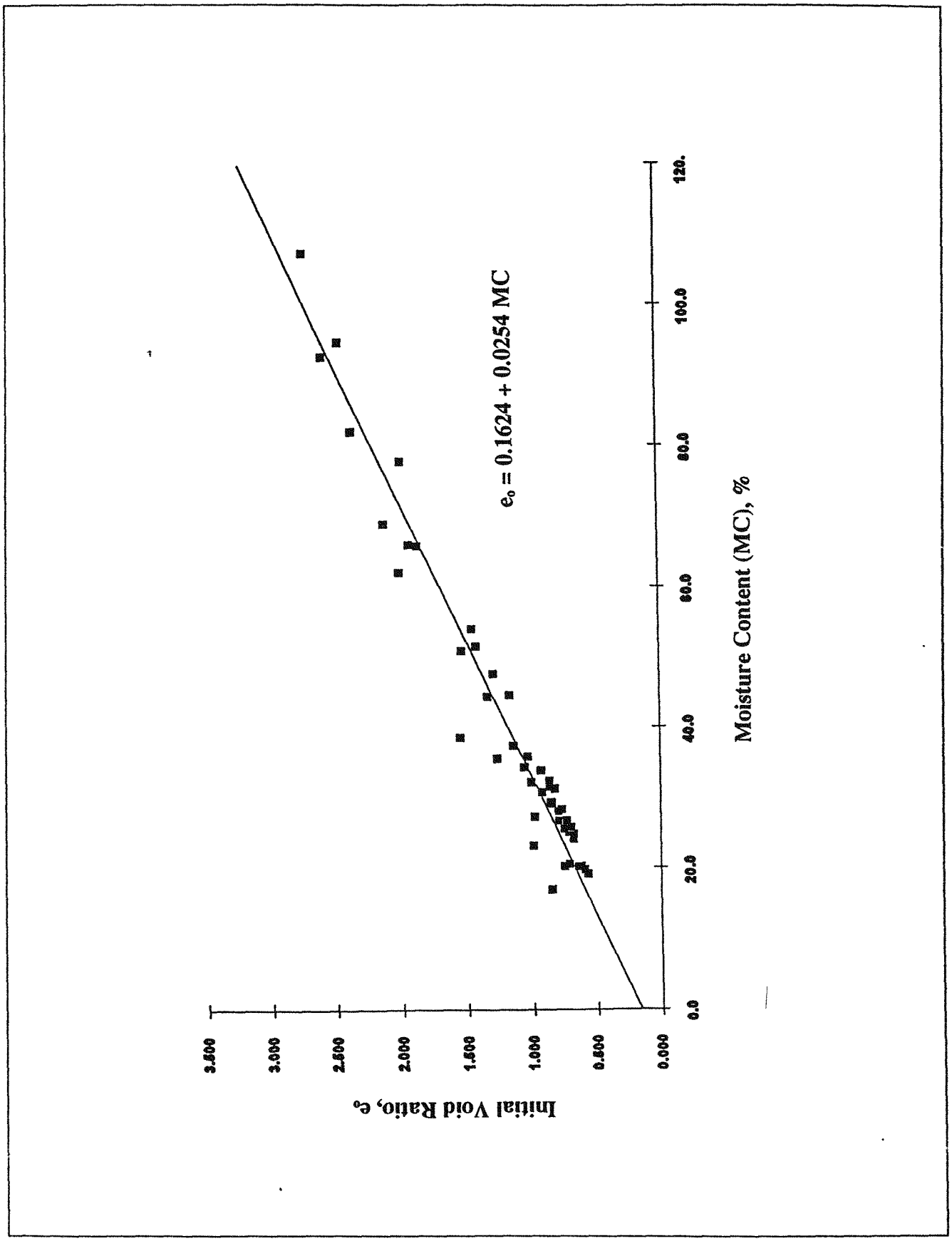


Figure 7.5.7 Correlation between moisture content and initial void ratio.

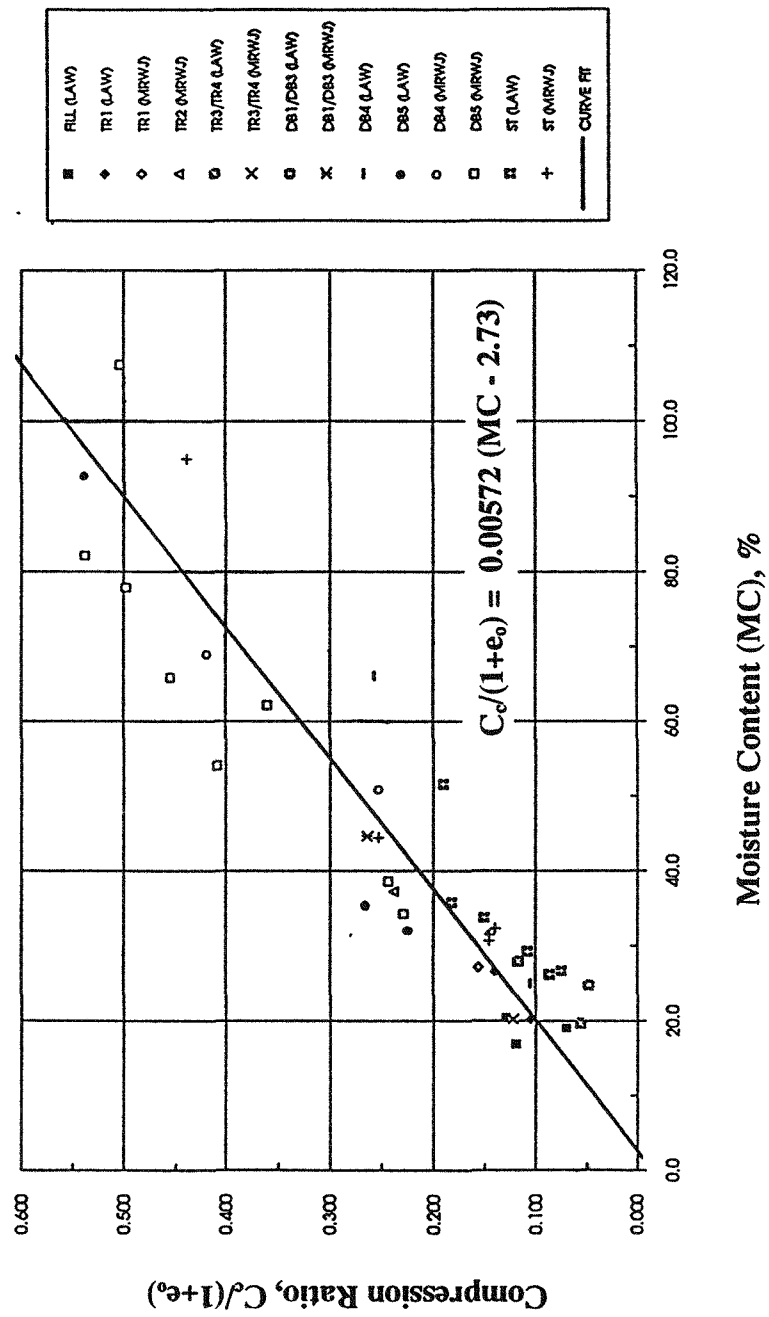


Figure 7.5.8 Correlation between moisture content and compression ratio.

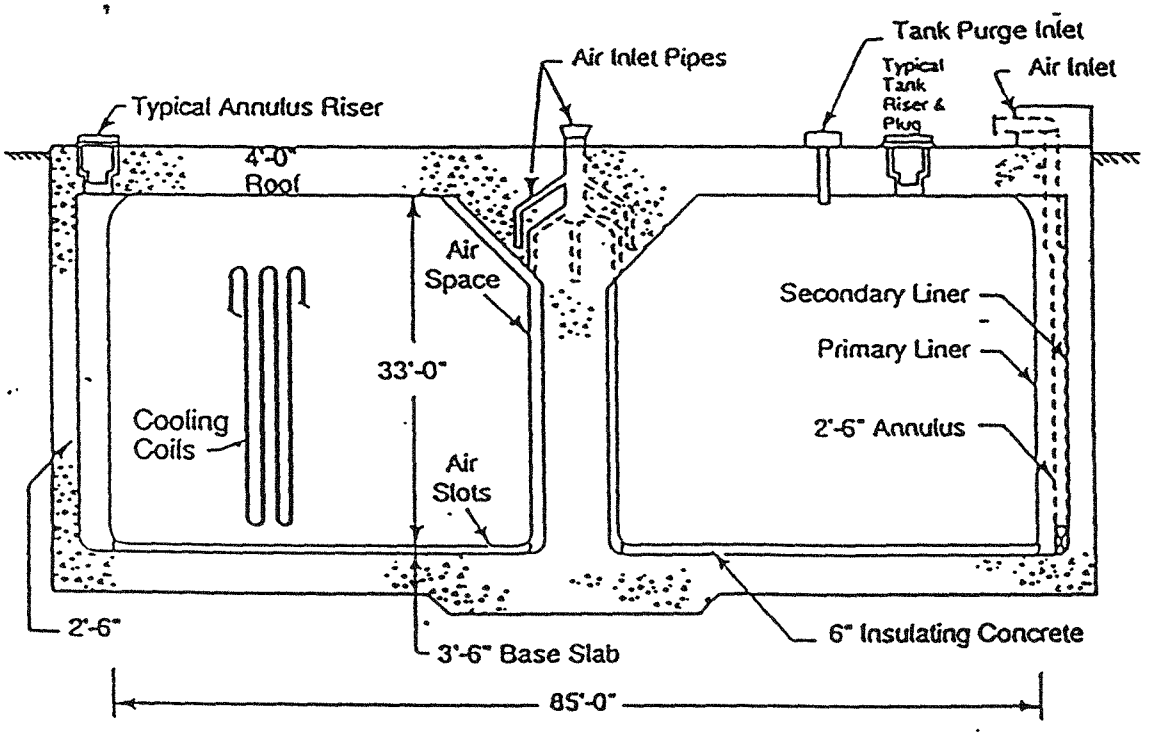


Figure 7.5-9 Tank Type III structure footnote: for Type IIIA tanks, roof is 5 feet thick at the center tapering to 4 feet at edges.

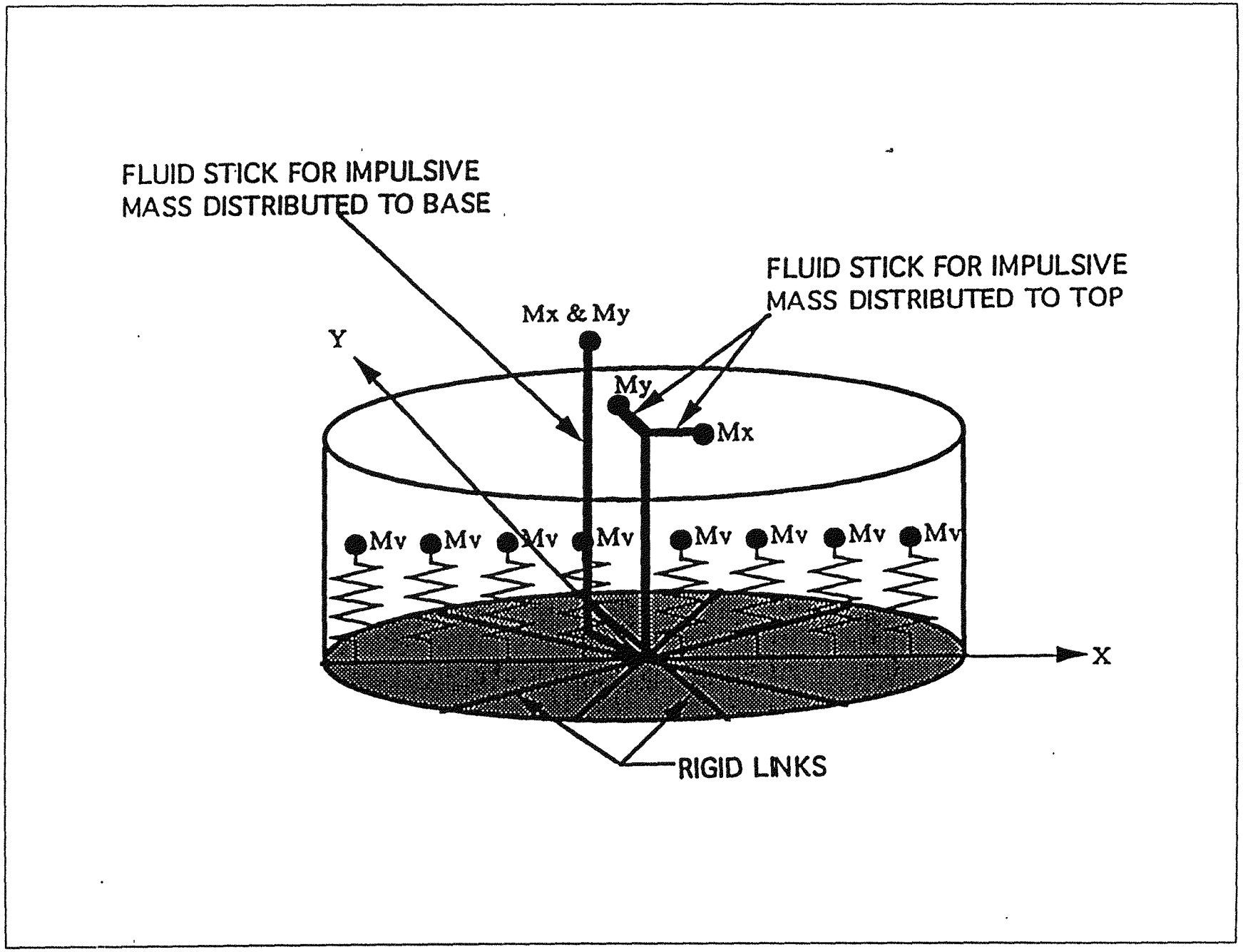


Figure 7.5-10 WSRC tank 3D SASSI model for Type IIIA.

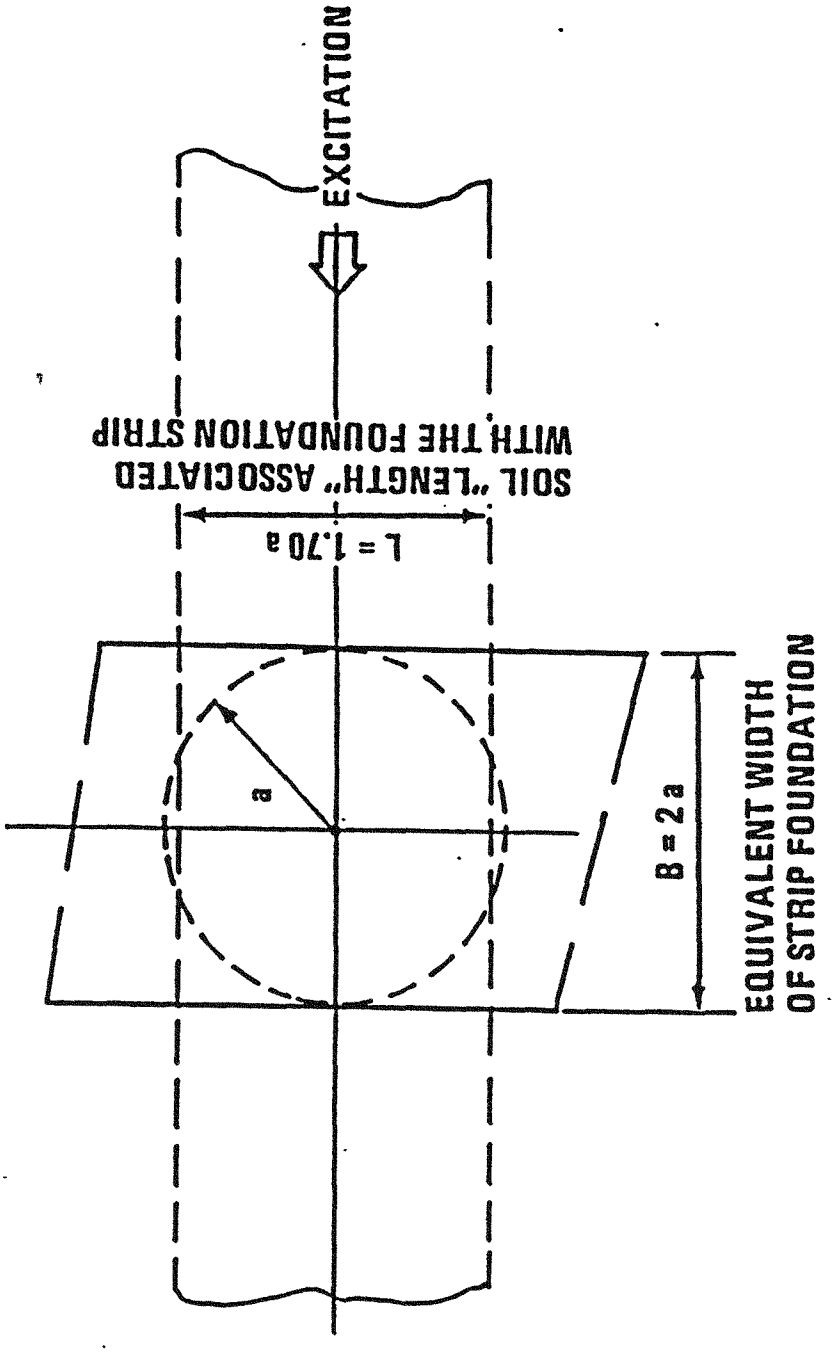


Figure 7 5-11 Criteria for determination of the equivalent length of the 2D model.

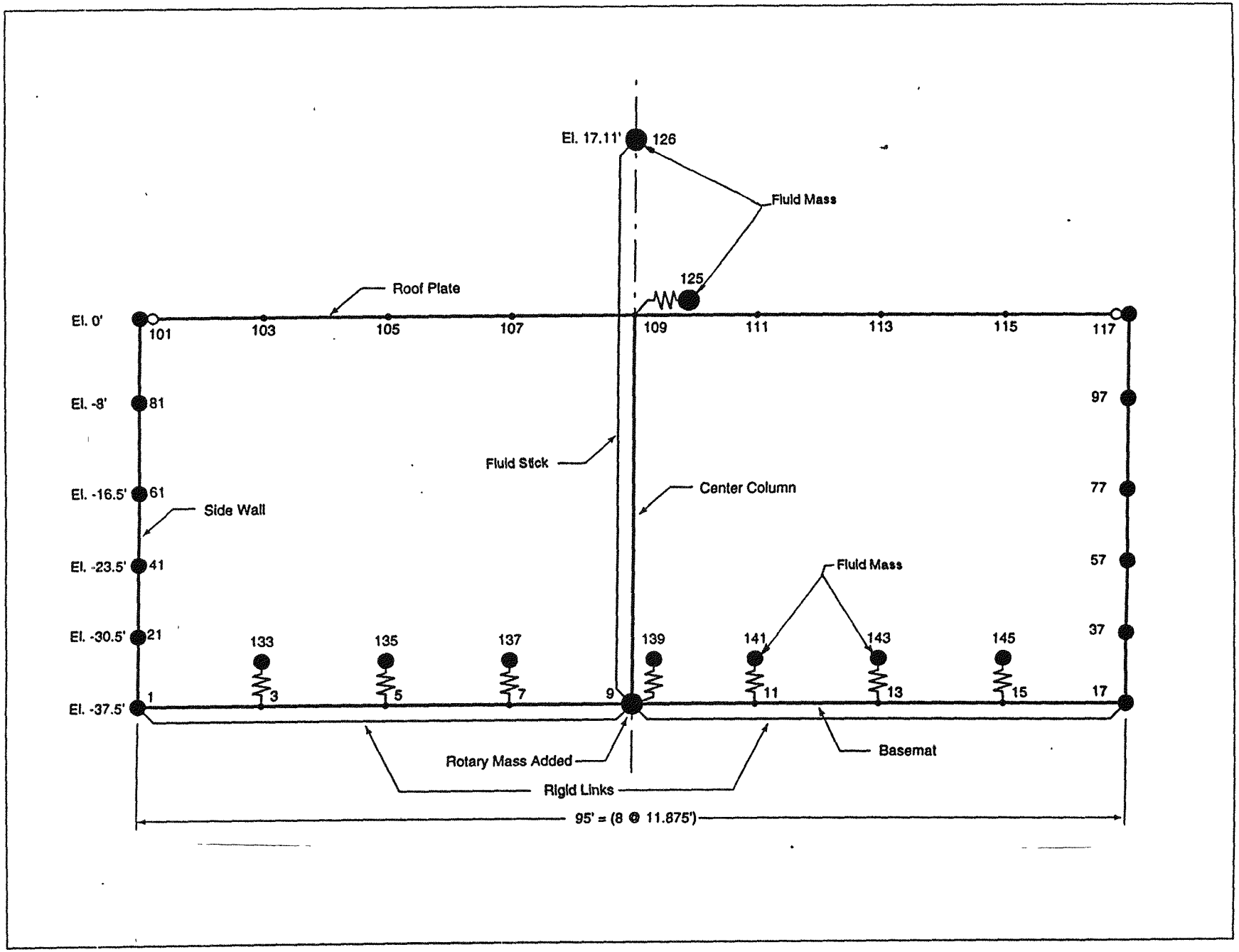


Figure 7 5-12 Tank 2D SASSI model for Type IIIA.

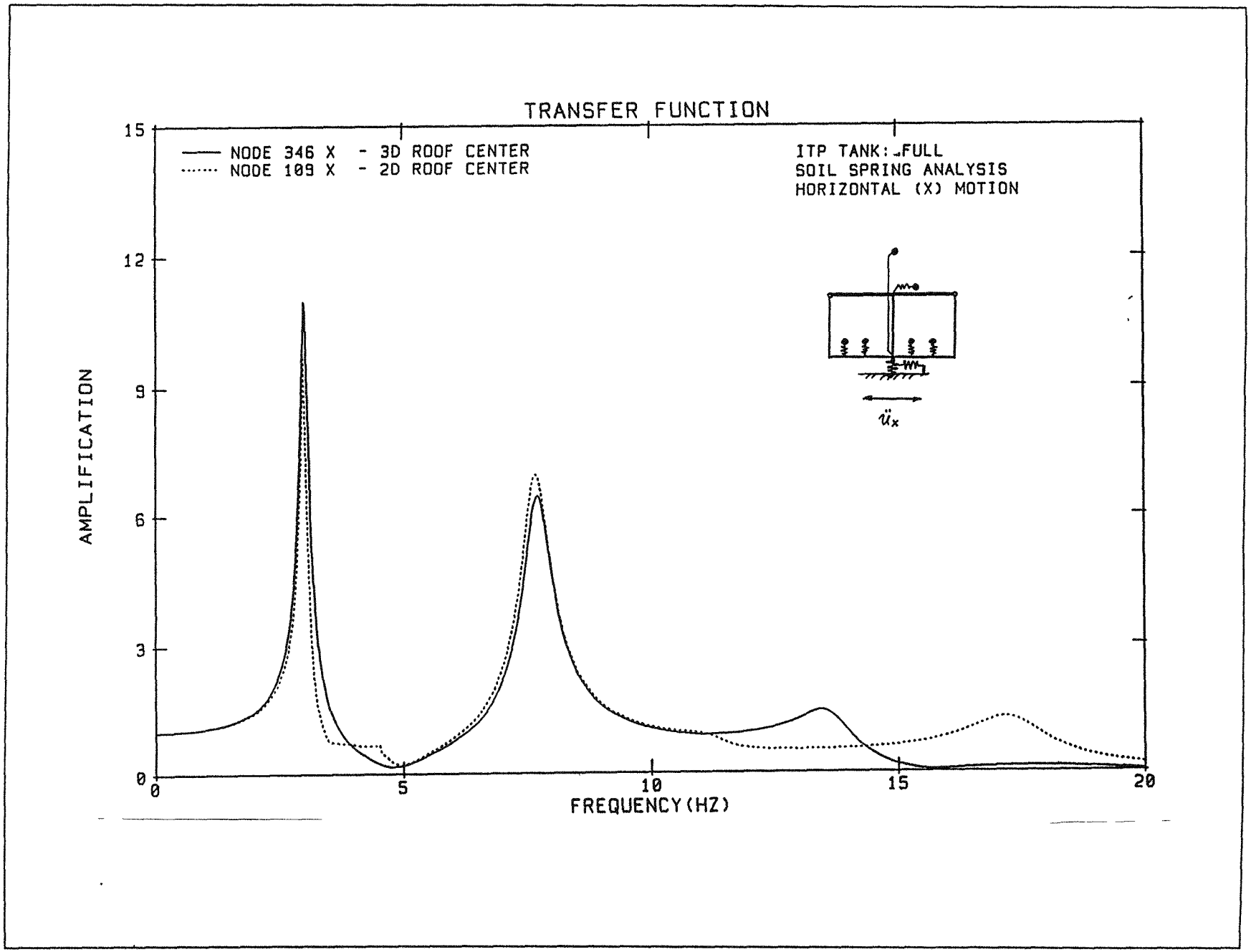


Figure 7.5-13 Comparison of horizontal transfer functions between 2D and 3D models.

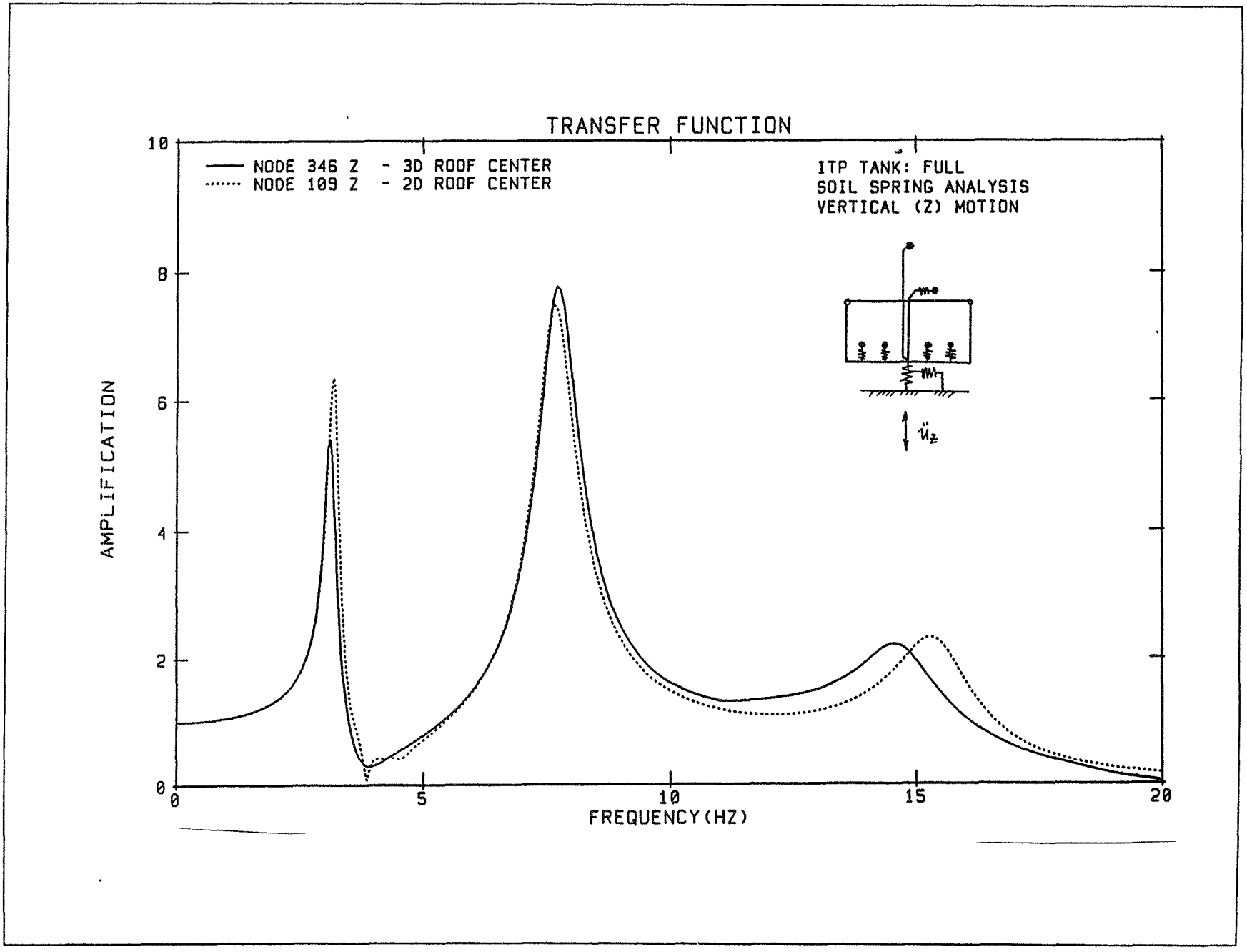


Figure 7.5-14 Comparison of vertical transfer functions between 2D and 3D models.

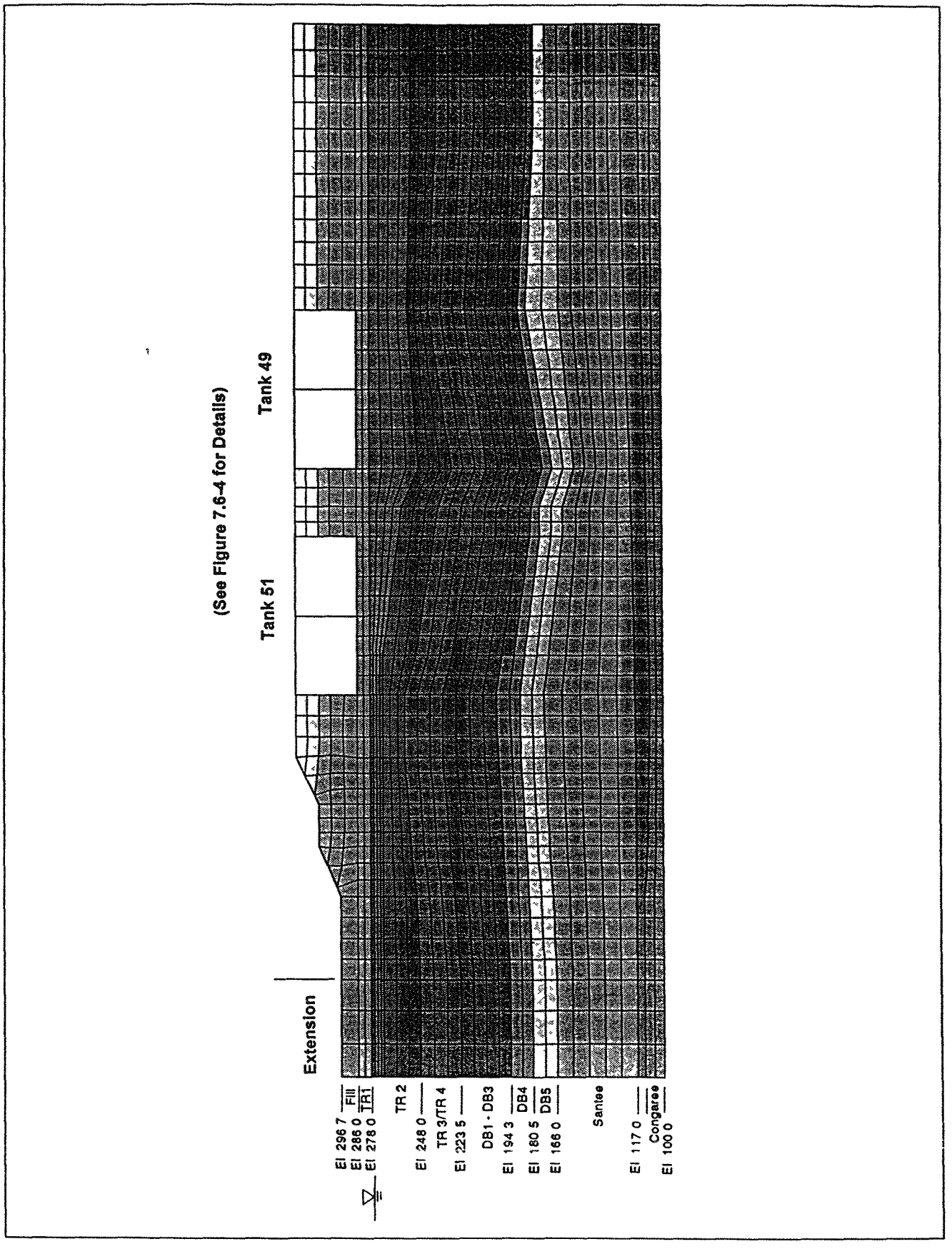


Figure 7.5-15 SASSI 2D model of profile AA'.

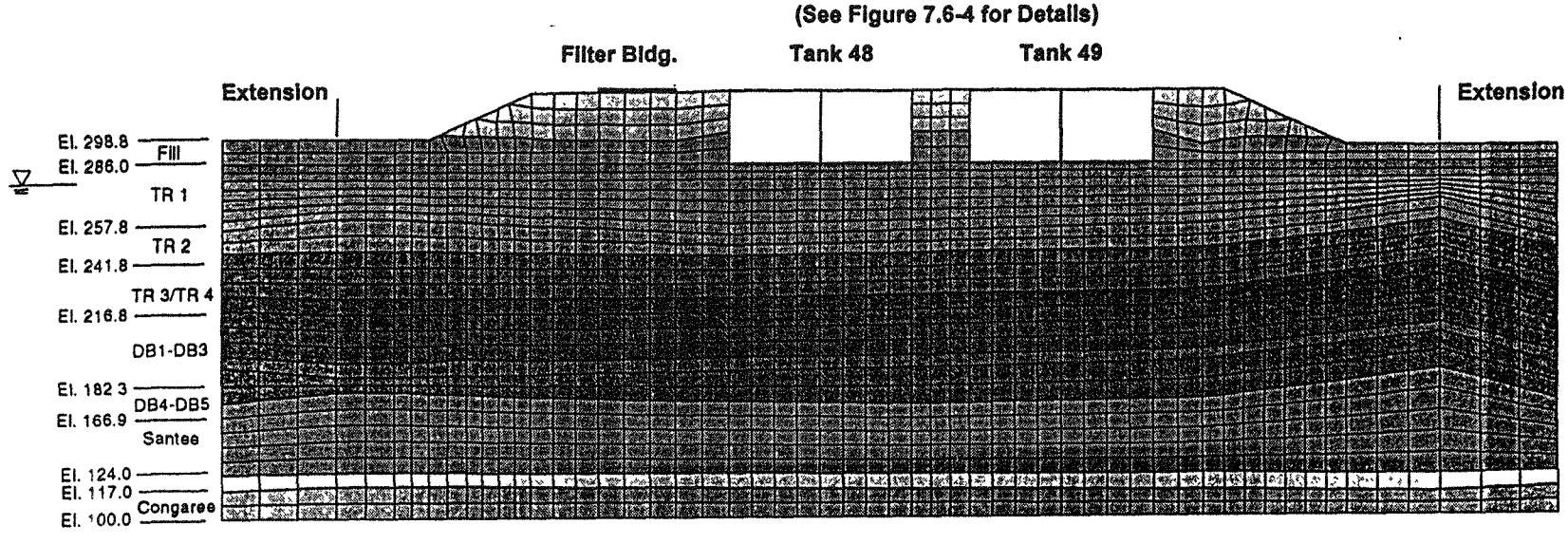


Figure 7.5-16 SASSI 2D model of profile BB'.

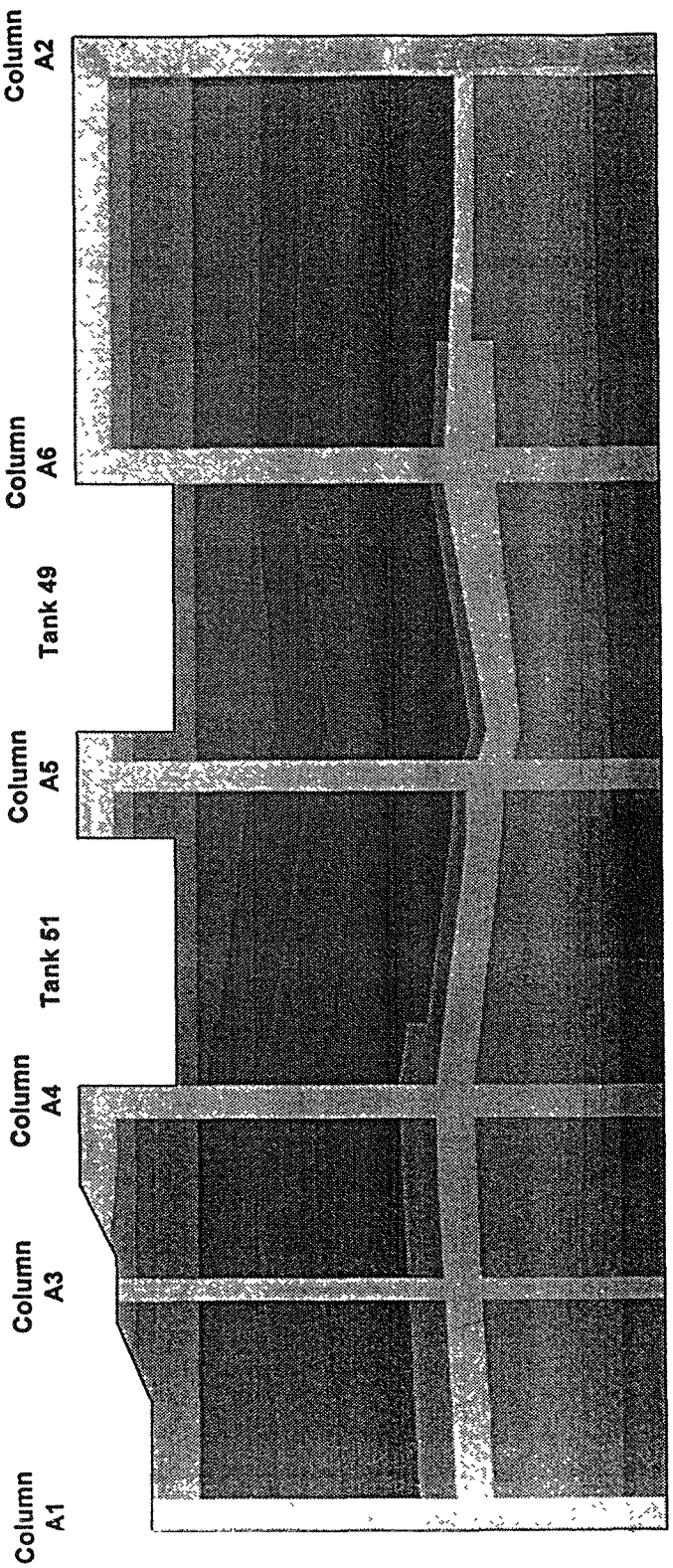


Figure 7.5-17 Comparison of SASSI results with free-field SHAKE results for profile AA' at the location of column A5.

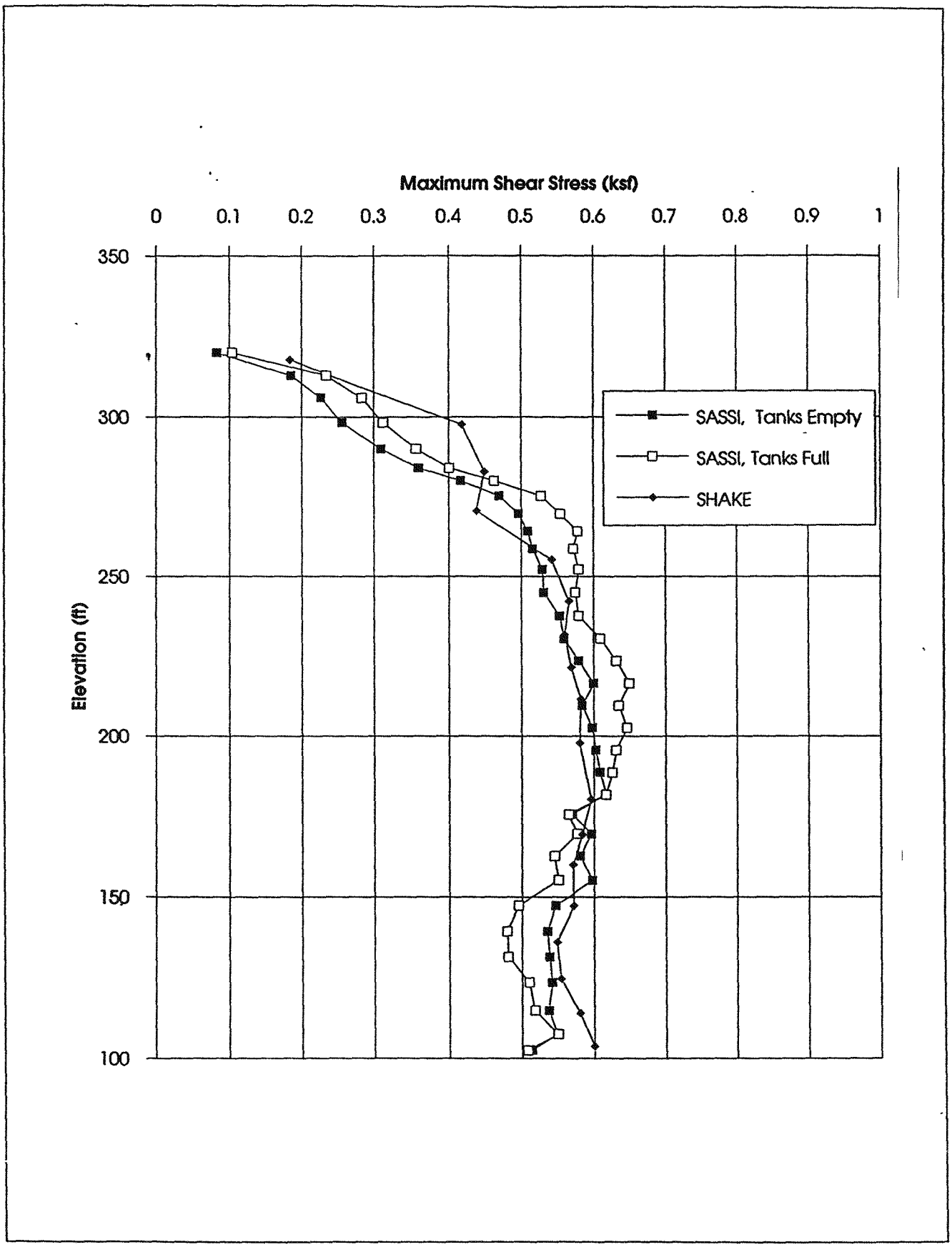


Figure 7.5-18 Comparison of SASSI and SHAKE maximum shear stresses at column A5 for EBE local event.

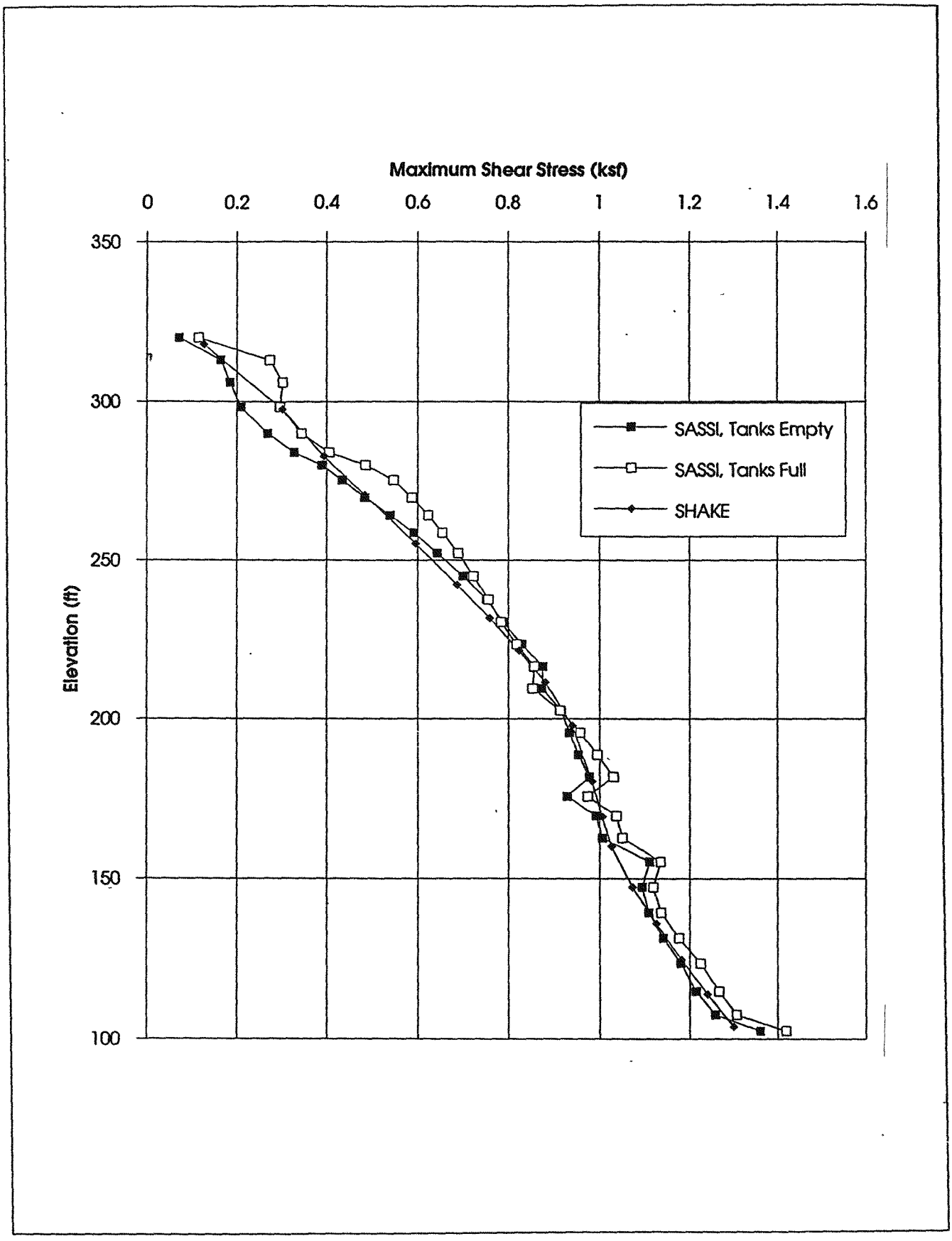


Figure 7.5-19 Comparison of SASSI and SHAKE maximum shear stresses at column A5 for EBE distant event.

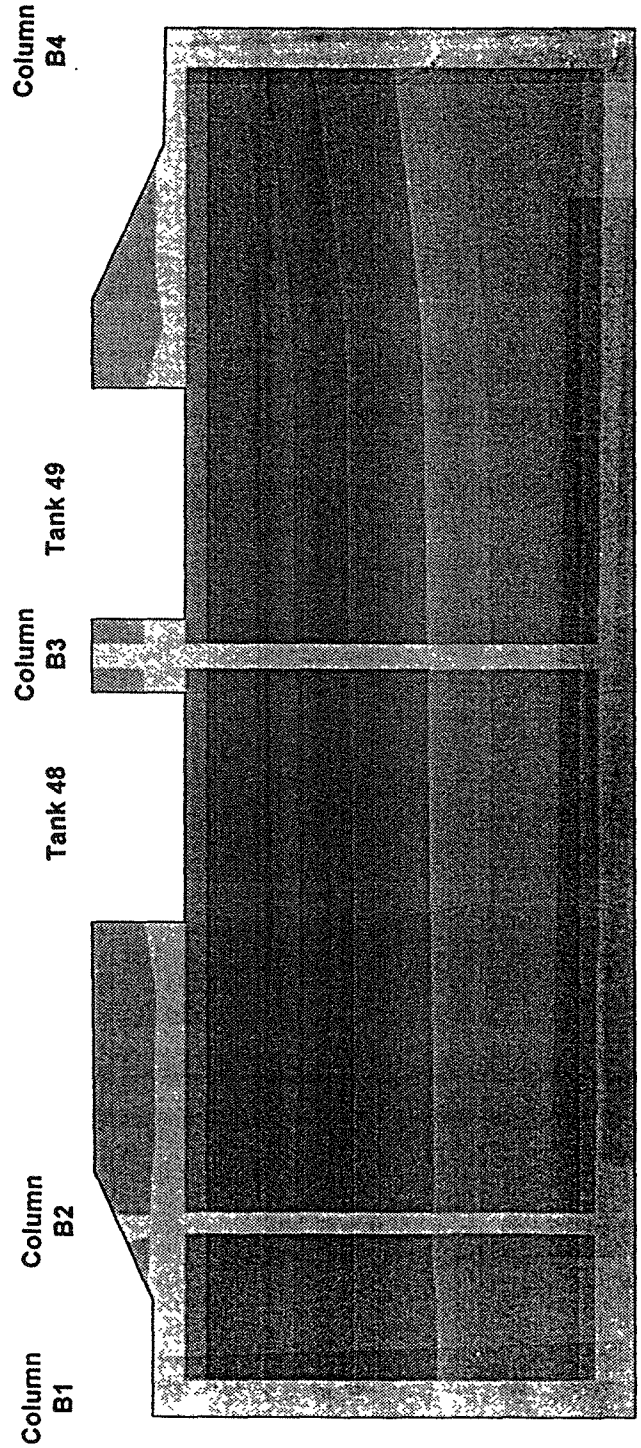


Figure 7.5-20 Comparison of SASSI SSI results with free-field SHAKE results for profile BB' at the location of column B3.

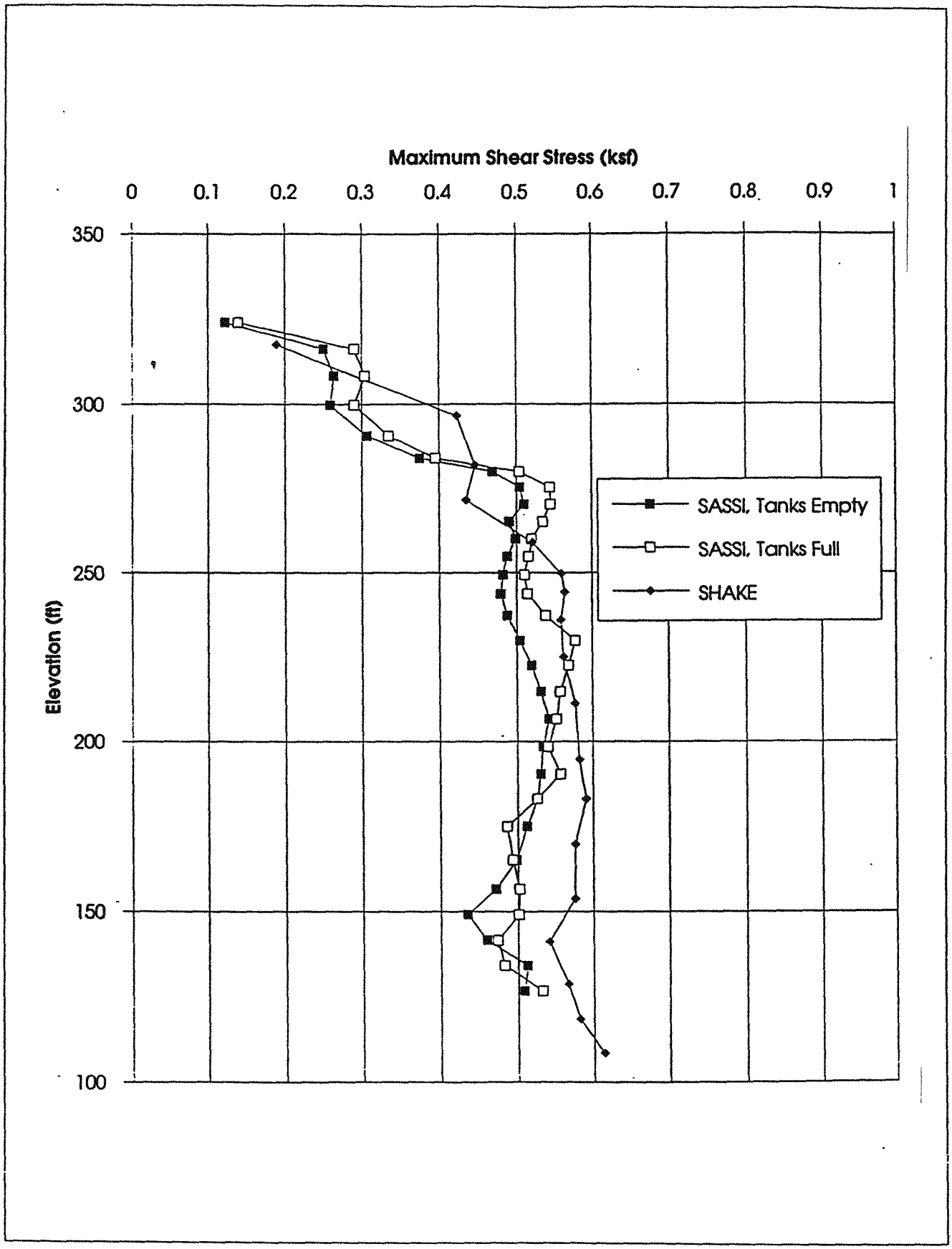


Figure 7.5-21 Comparison of SASSI and SHAKE maximum shear stress results at column B3 for EBE local event.

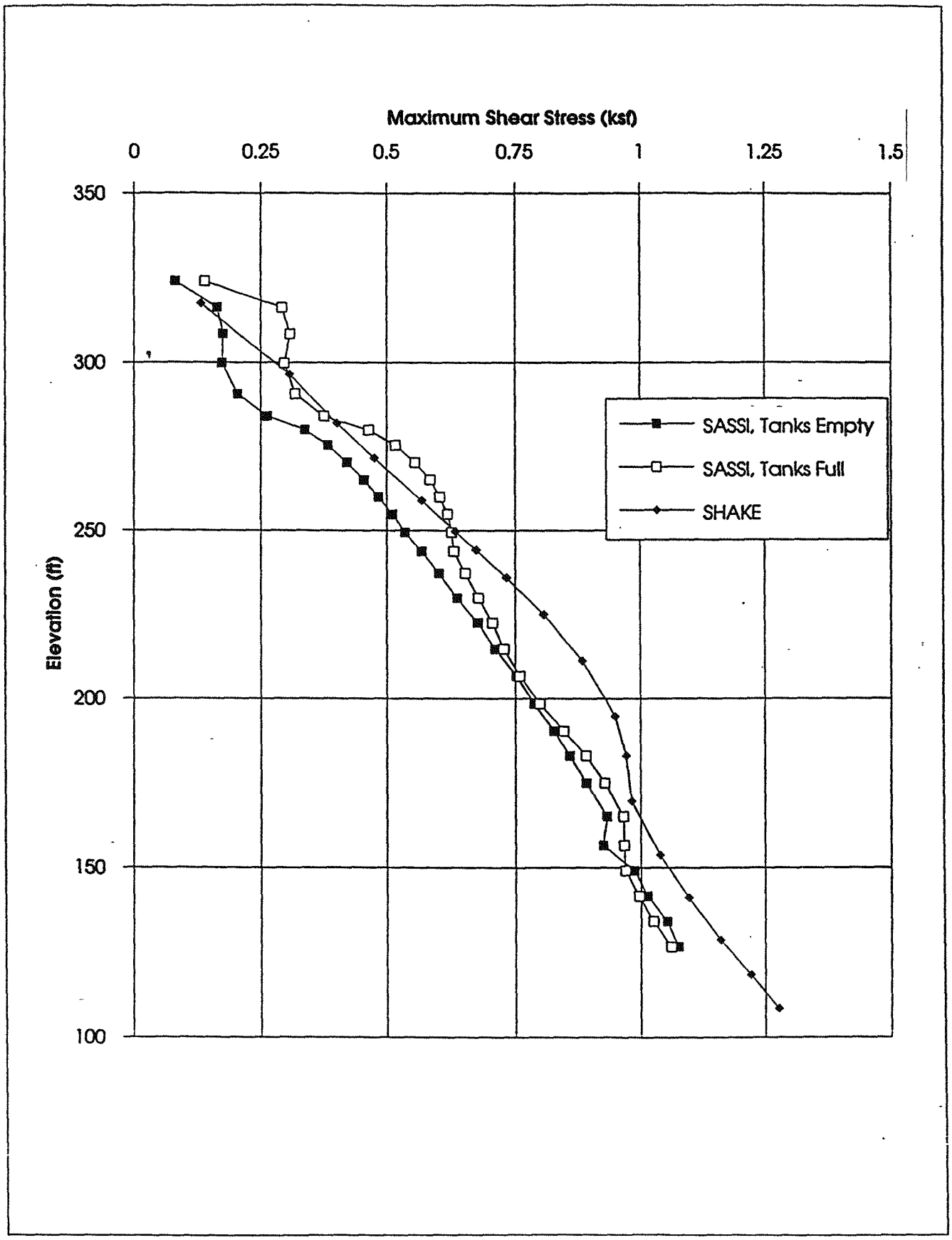


Figure 7.5-22 Comparison of SASSI and SHAKE maximum shear stress results at column B3 for EBE distant event.

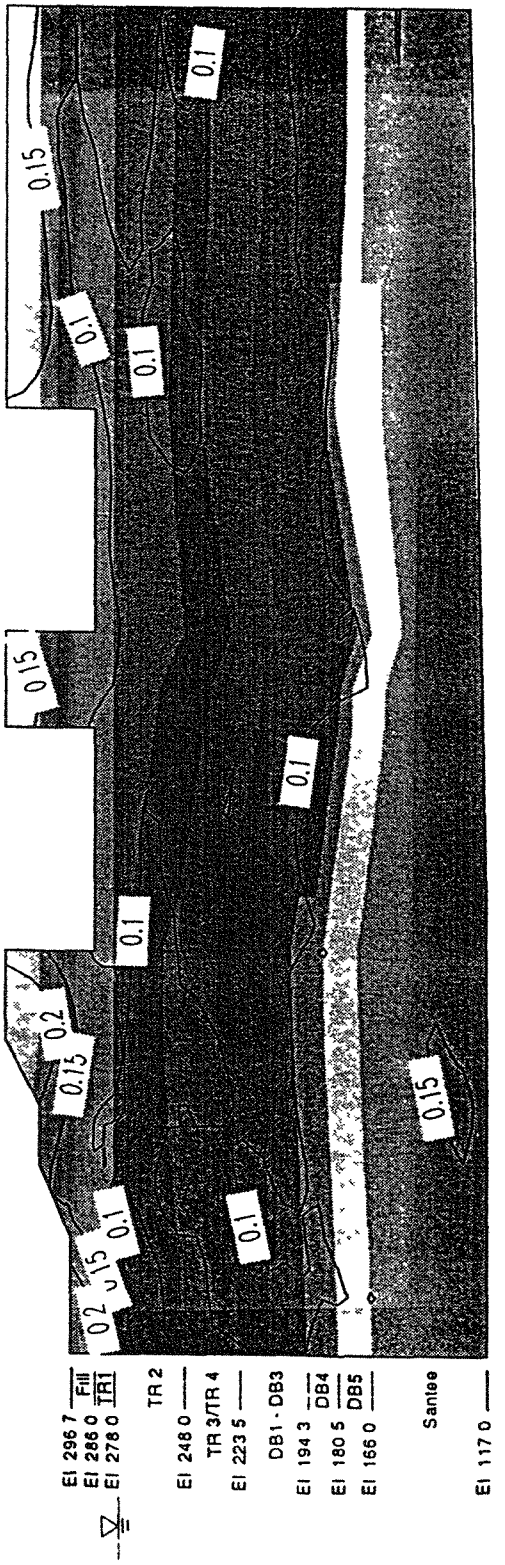


Figure 7 5-23 Maximum horizontal acceleration contours (in g's) for profile AA' from SASSI analysis - EBE local event; full tank condition.

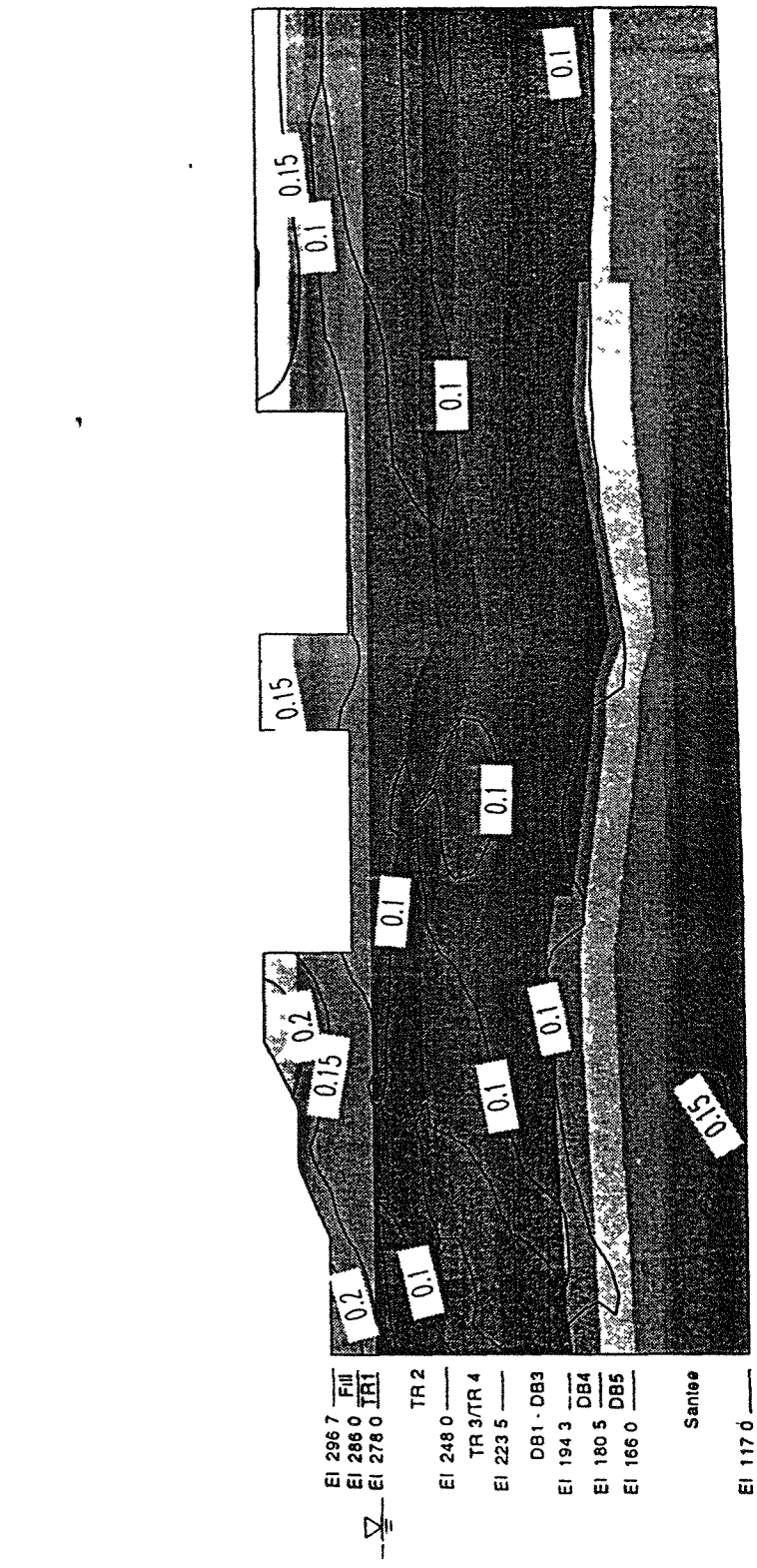


Figure 7.5-24 Maximum horizontal acceleration contours (in g's) for profile AA' from SASSI analysis - EBE local event; empty tank condition.

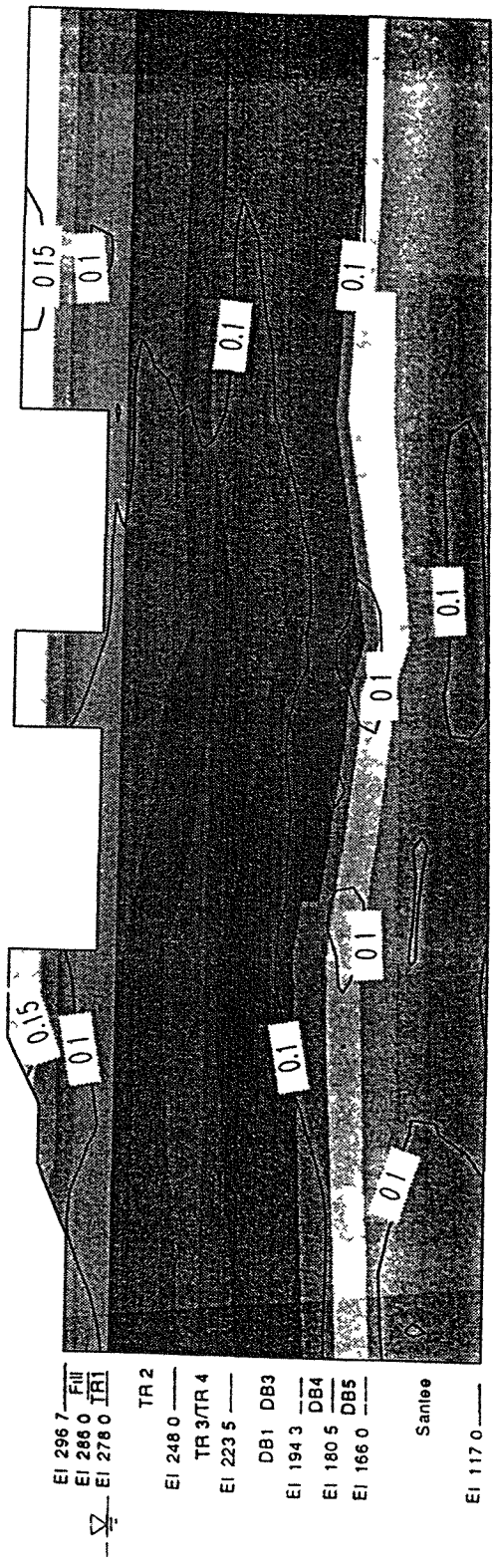


Figure 7.5-25 Maximum horizontal acceleration contours (in g's) for profile AA' from SASSI analysis - EBE distant event; full tank condition.

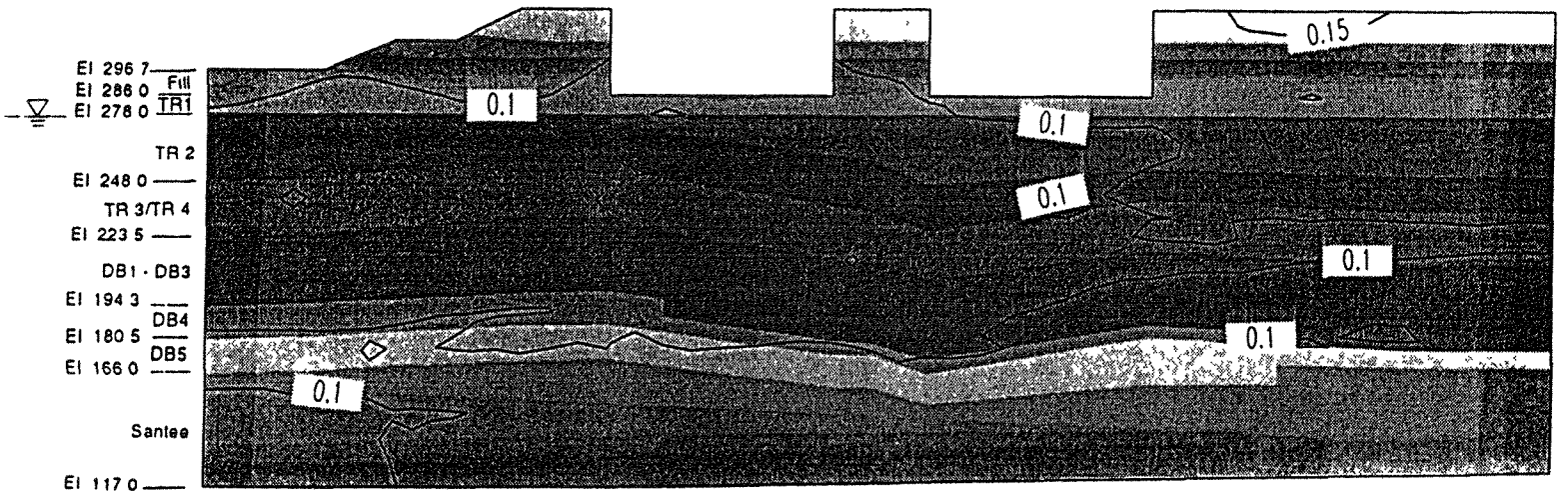


Figure 7.5-26 Maximum horizontal acceleration contours (in g's) for profile AA' from SASSI analysis - EBE distant event; empty tank condition.

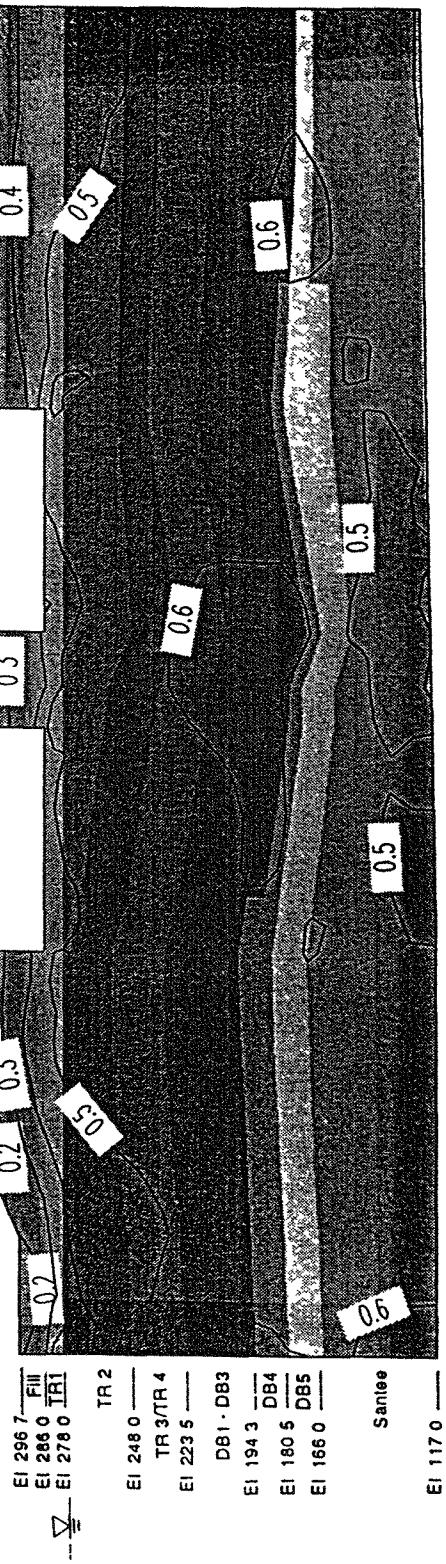


Figure 7.5-27 Maximum shear stress contours (in ksf) for profile AA' from SASSI analysis - EBE local event; full tank condition.

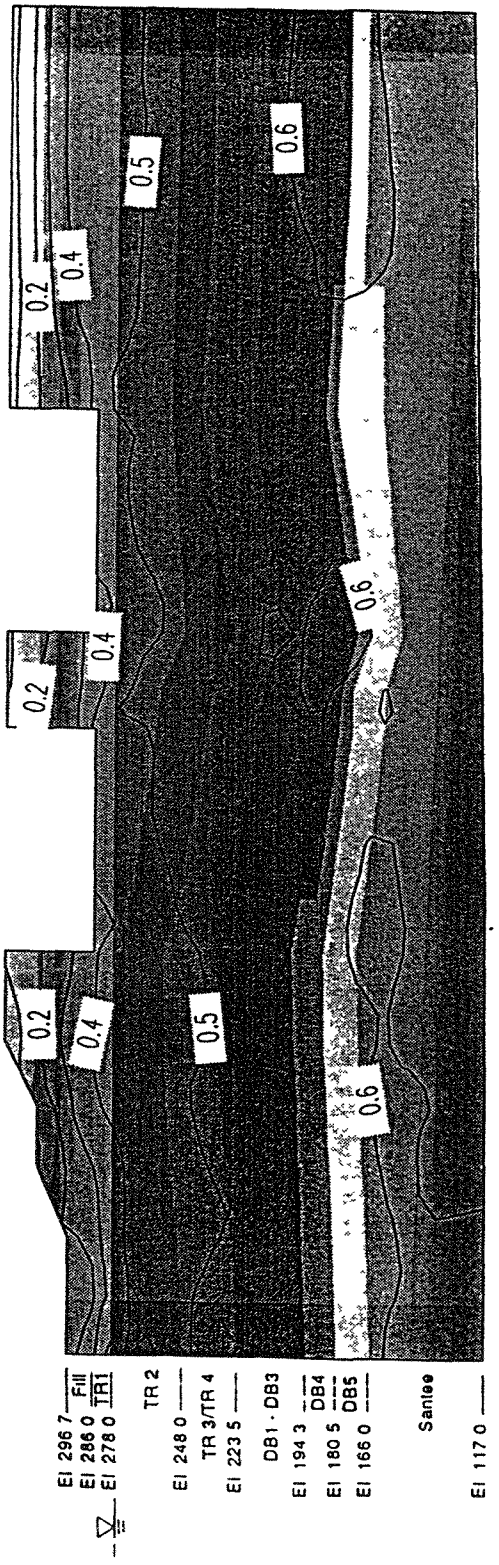


Figure 7.5-28 Maximum shear stress contours (in ksf) for profile AA' from SASSI analysis - EBE local event; empty tank condition.

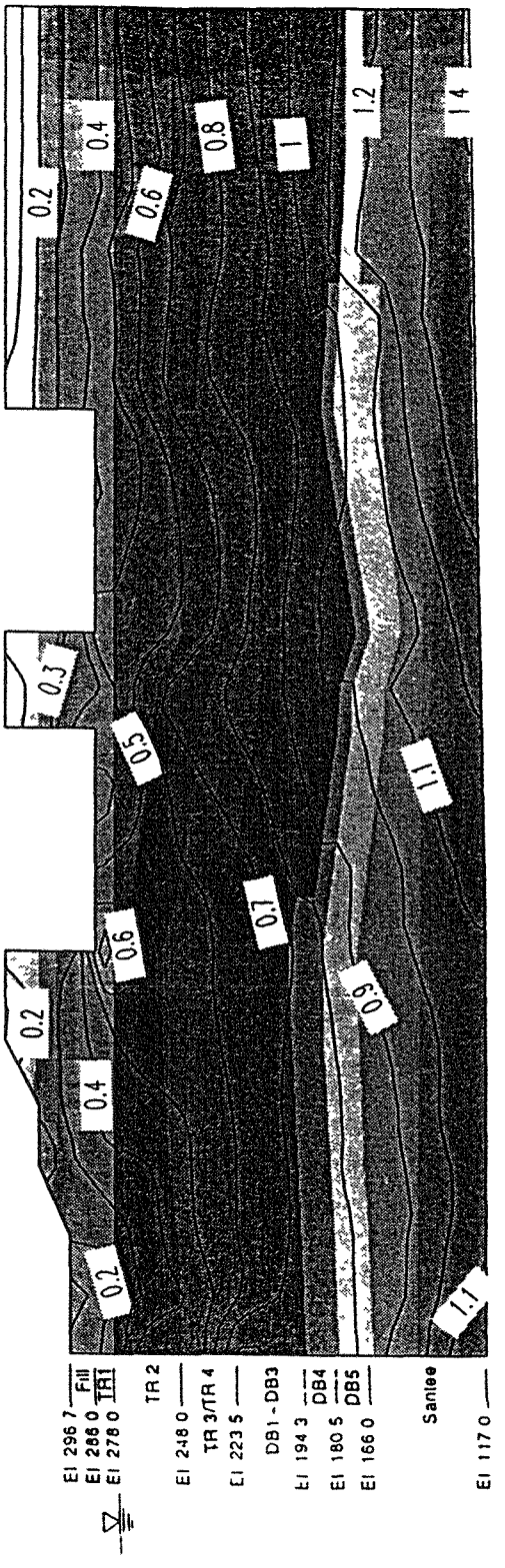


Figure 7.5-29 Maximum shear stress contours (in ksf) for profile AA' from SASSI analysis - EBE distant event; full tank condition.

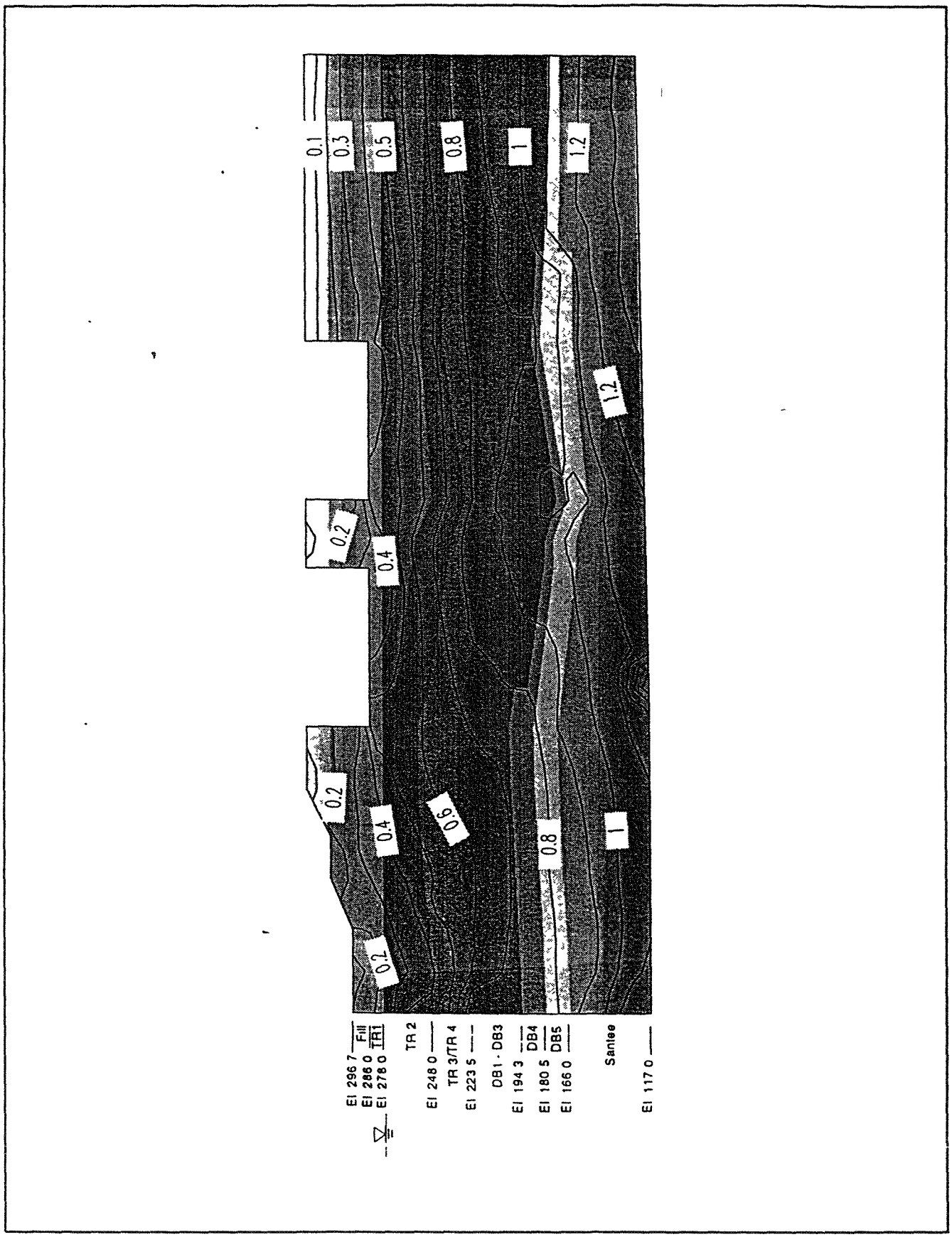


Figure 7.5-30 Maximum shear stress contours (in ksf) for profile AA' from SASSI analysis - EBE distant event; empty tank condition.

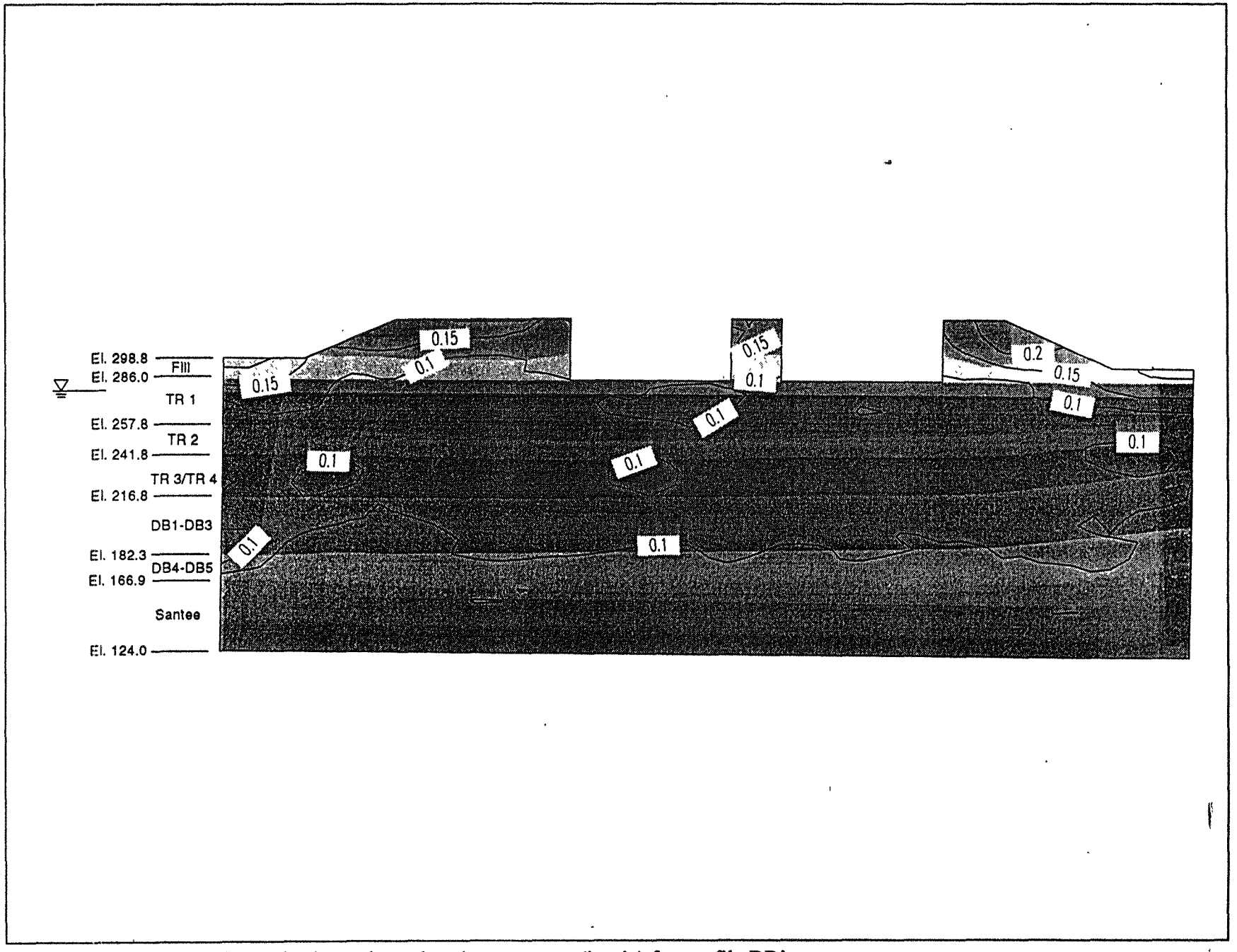


Figure 7.5-31 Maximum horizontal acceleration contours (in g's) for profile BB' from SASSI analysis - EBE local event; full tank condition.

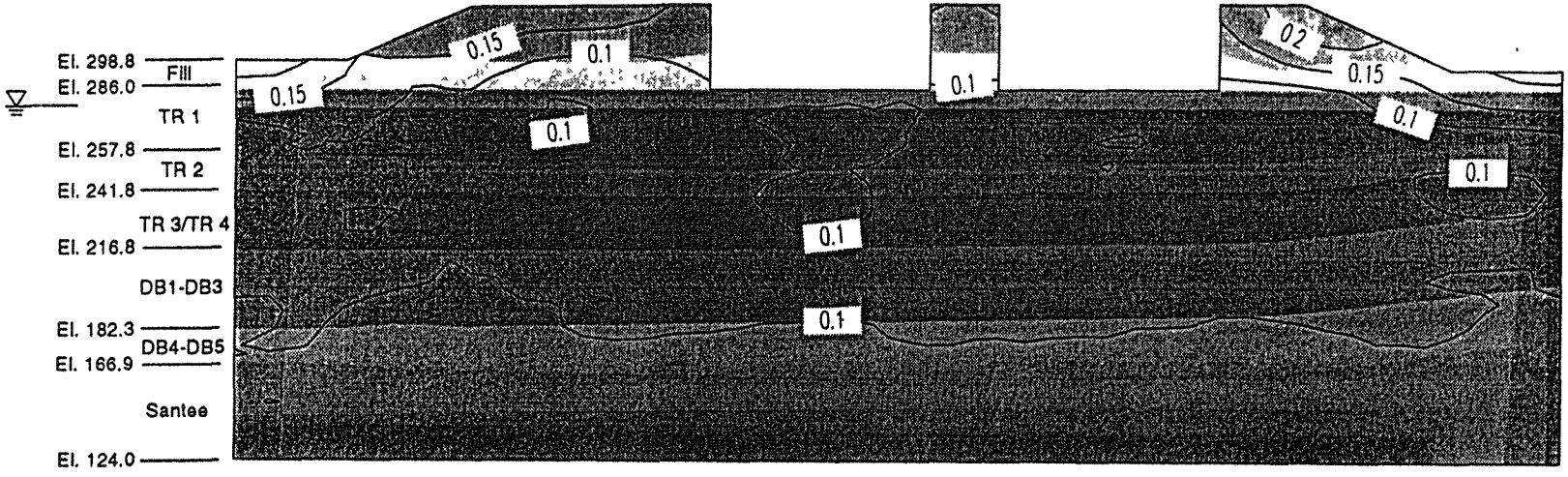


Figure 7.5-32 Maximum horizontal acceleration contours (in g's) for profile BB' from SASSI analysis - EBE local event; empty tank condition.

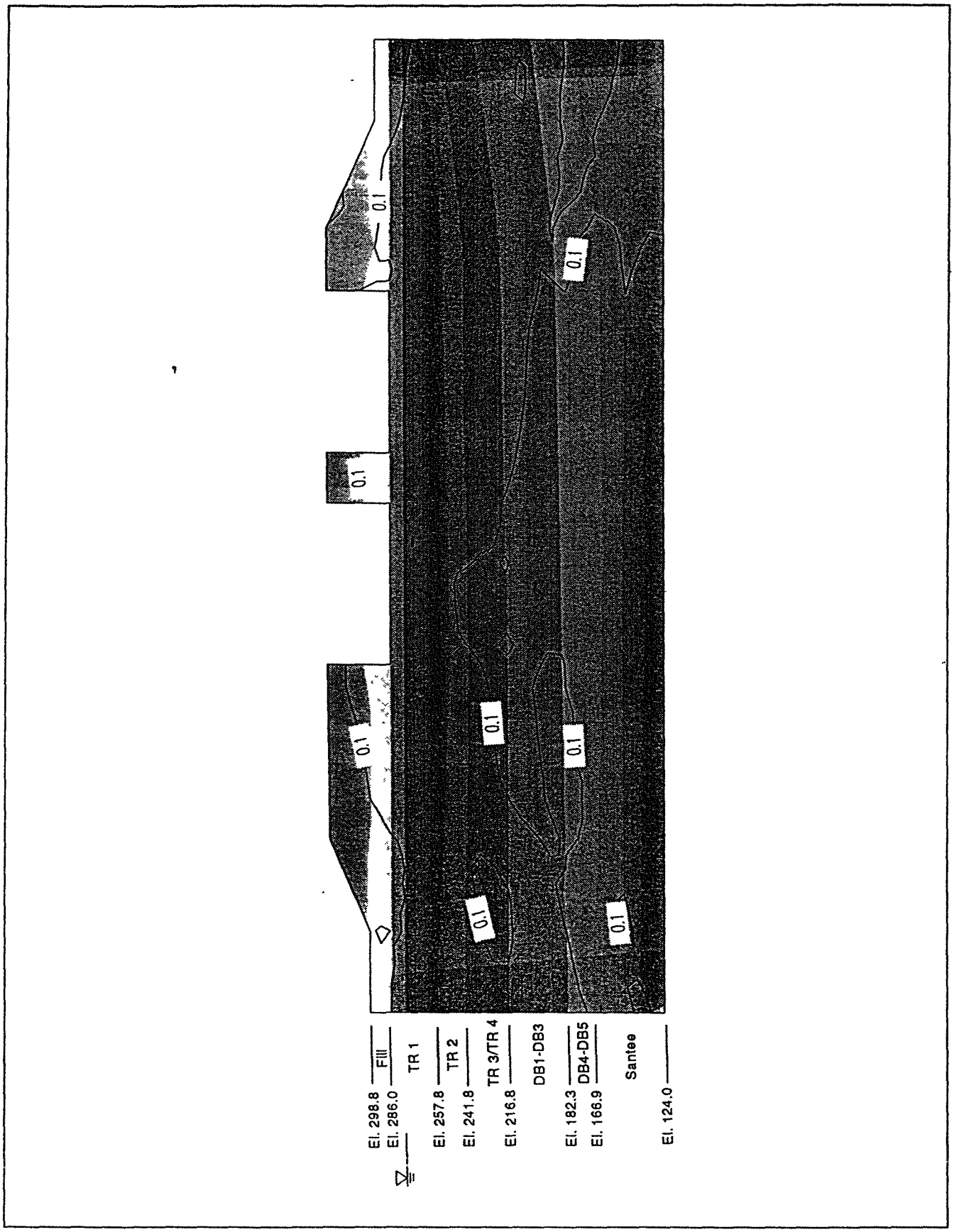


Figure 7.5-33 Maximum horizontal acceleration contours (in g's) for profile BB' from SASSI analysis - EBE distant event; full tank condition.

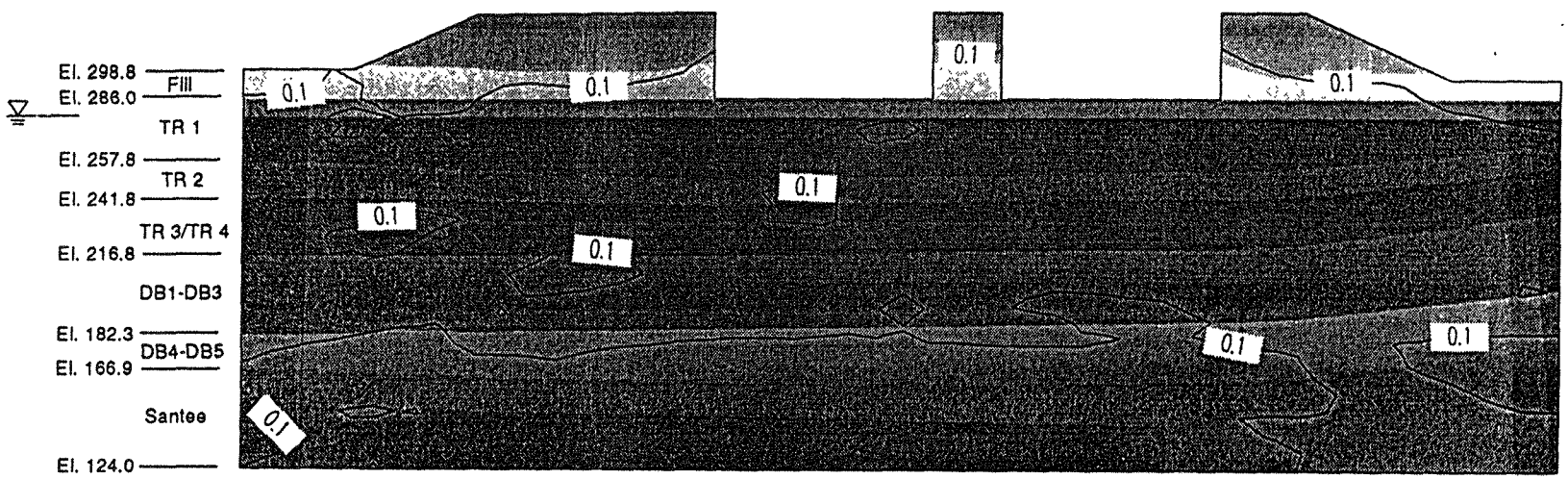


Figure 7.5-34 Maximum horizontal acceleration contours (in g's) for profile BB' from SASSI analysis - EBE distant event; empty tank condition.

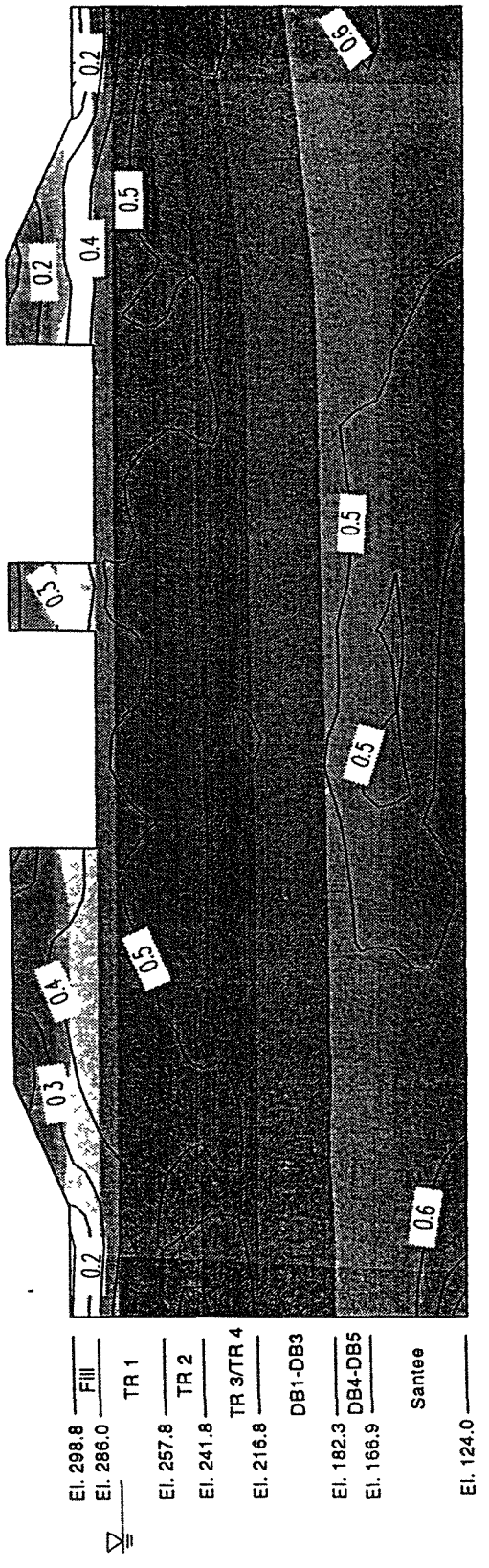


Figure 7.5-35 Maximum shear stress contours (in ksf) for profile BB' from SASSI analysis - EBE local event; full tank condition.

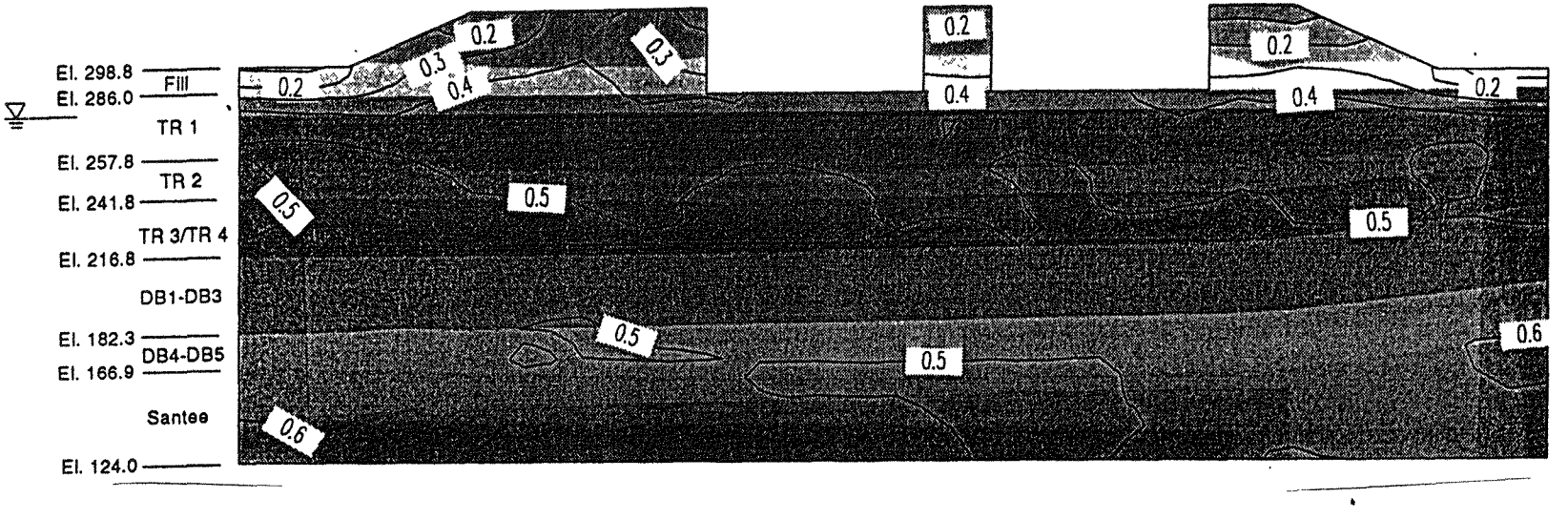


Figure 7.5-36 Maximum shear stress contours (in ksf) for profile BB' from SASSI analysis - EBE local event; empty tank condition.

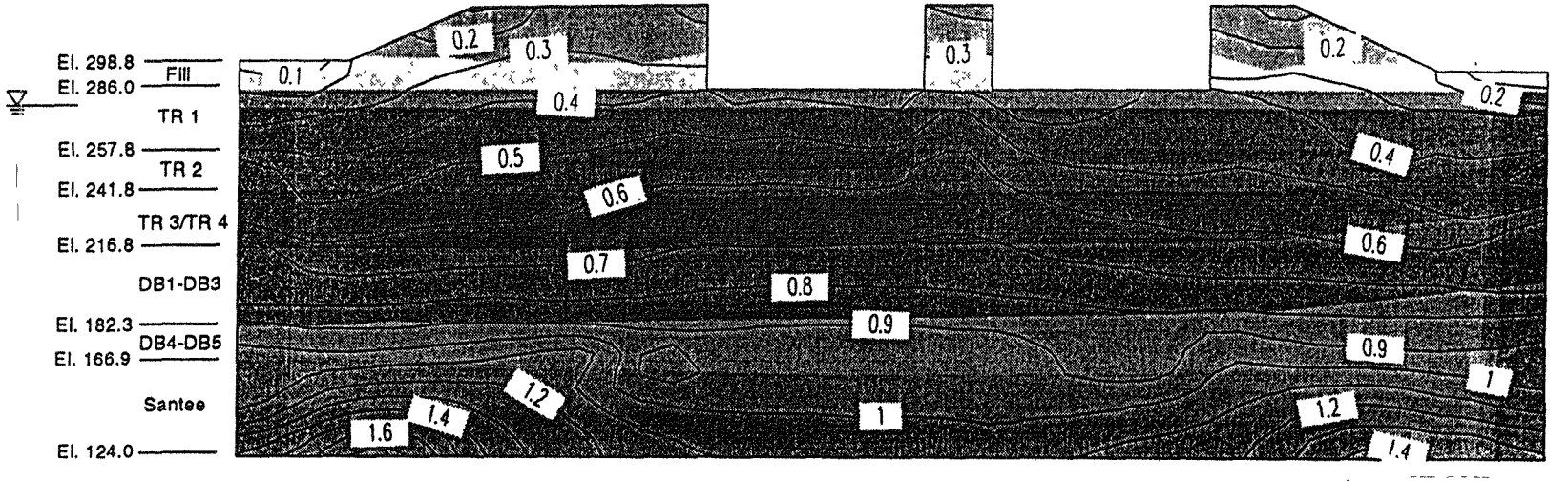


Figure 7.5-37 Maximum shear stress contours (in ksf) for profile BB' from SASSI analysis - EBE distant event; full tank condition.

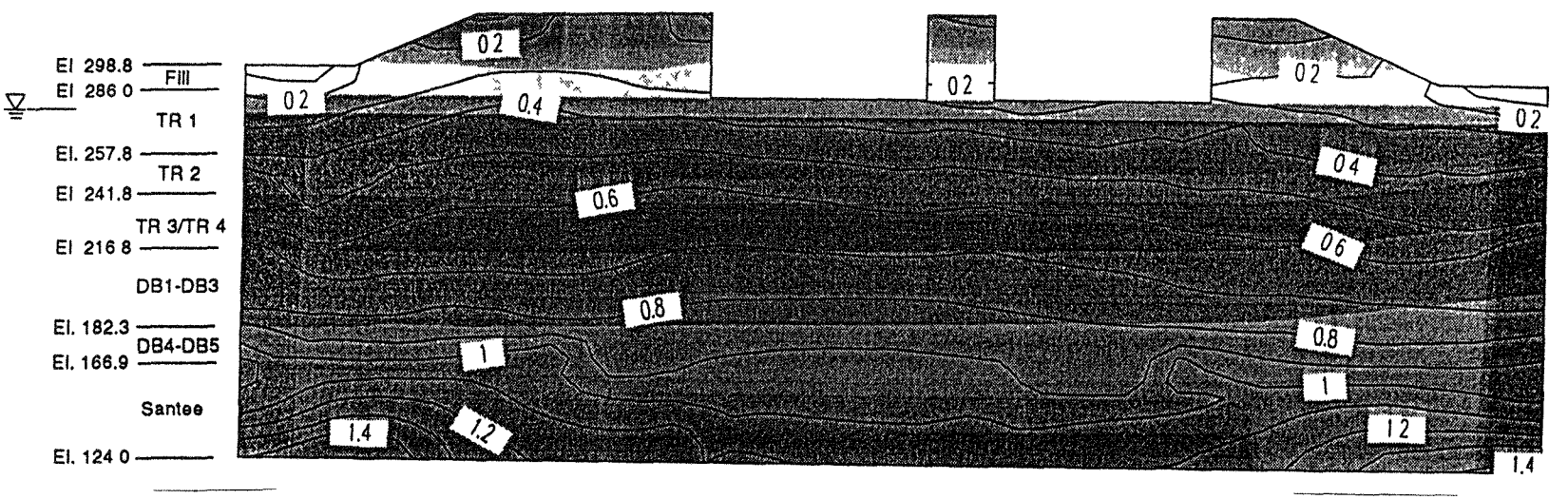


Figure 7.5-38 Maximum shear stress contours (in ksf) for profile BB' from SASSI analysis - EBE distant event; empty tank condition.

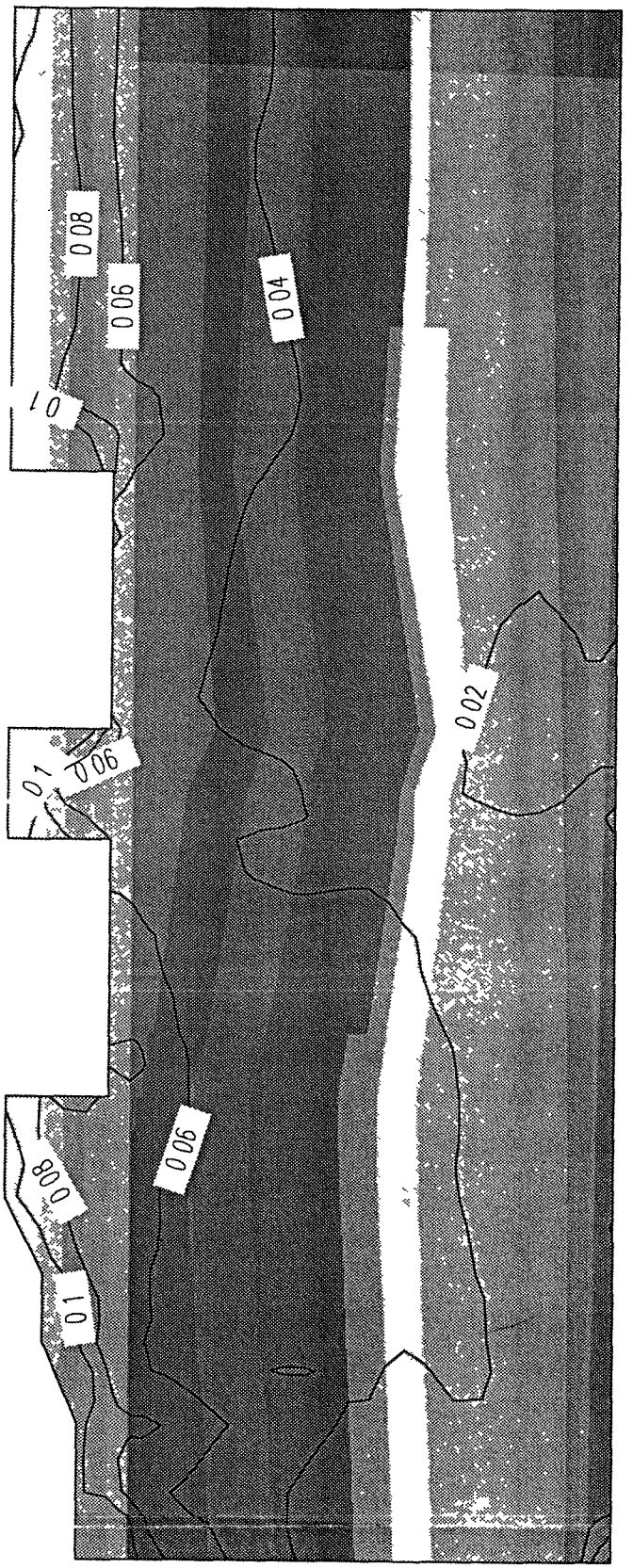


Figure 7.5-39 Effective cyclic shear stress ratio contours for profile AA' from SASSI analysis - EBE local event, full tanks condition.

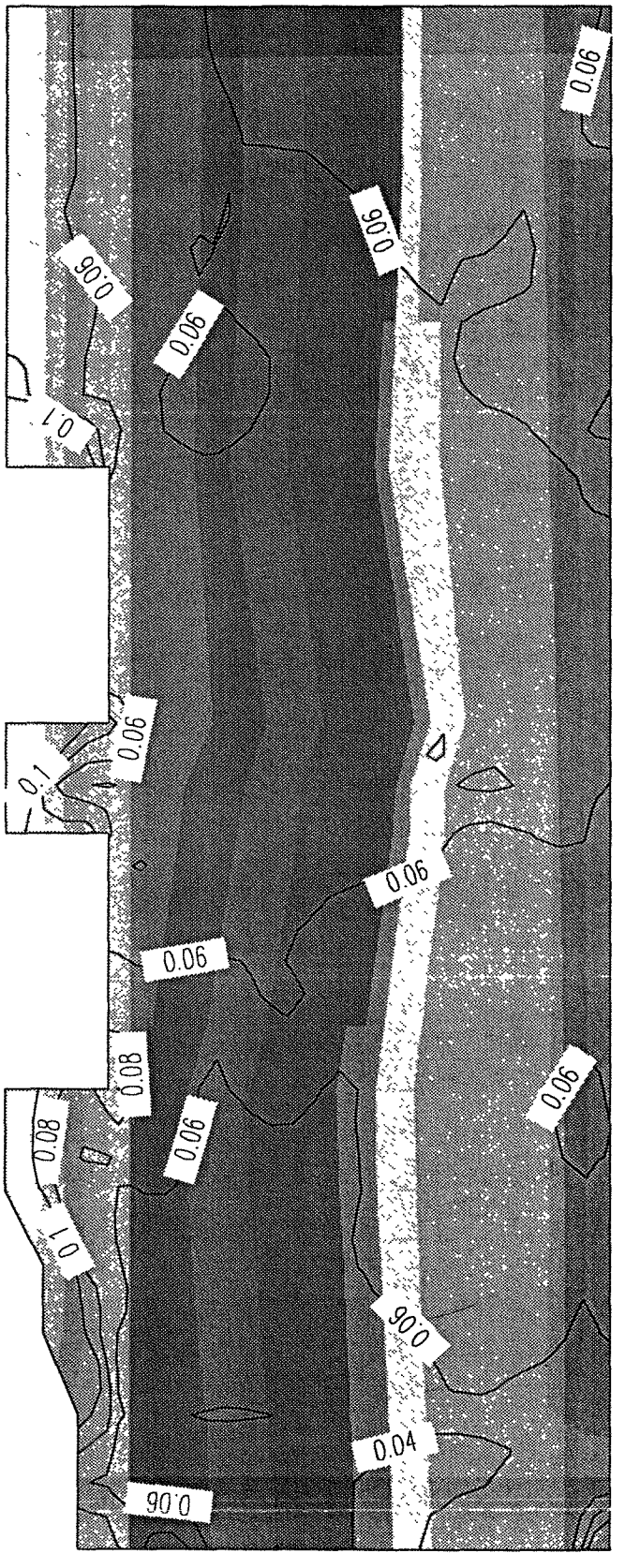


Figure 7.5-40 Effective cyclic shear stress ratio contours for profile AA' from SASSI analysis - EBE distant event, full tanks condition.

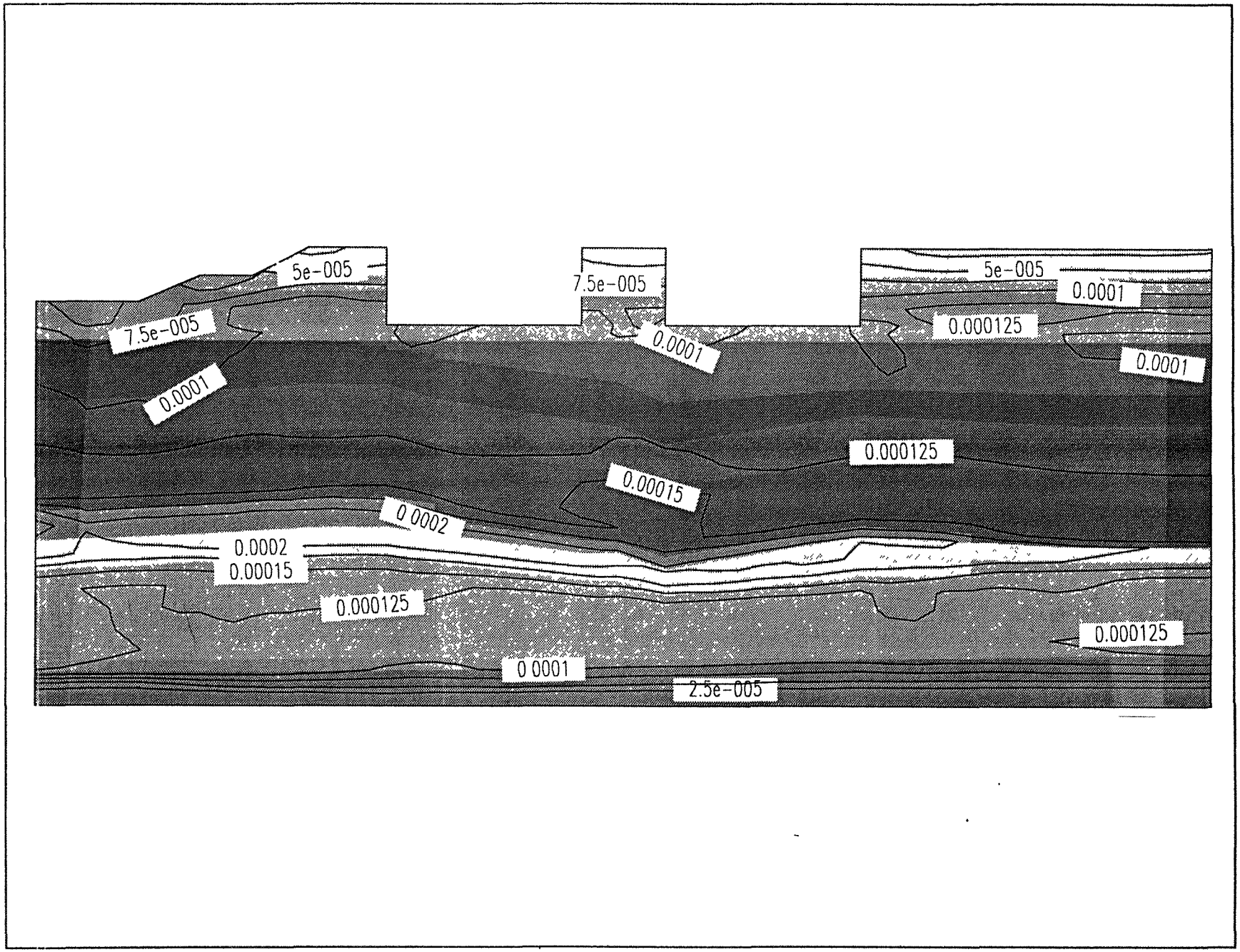


Figure 7.5-41 Maximum shear strain contours for profile AA' form SASSI analysis - EBE local event, full tanks condition.

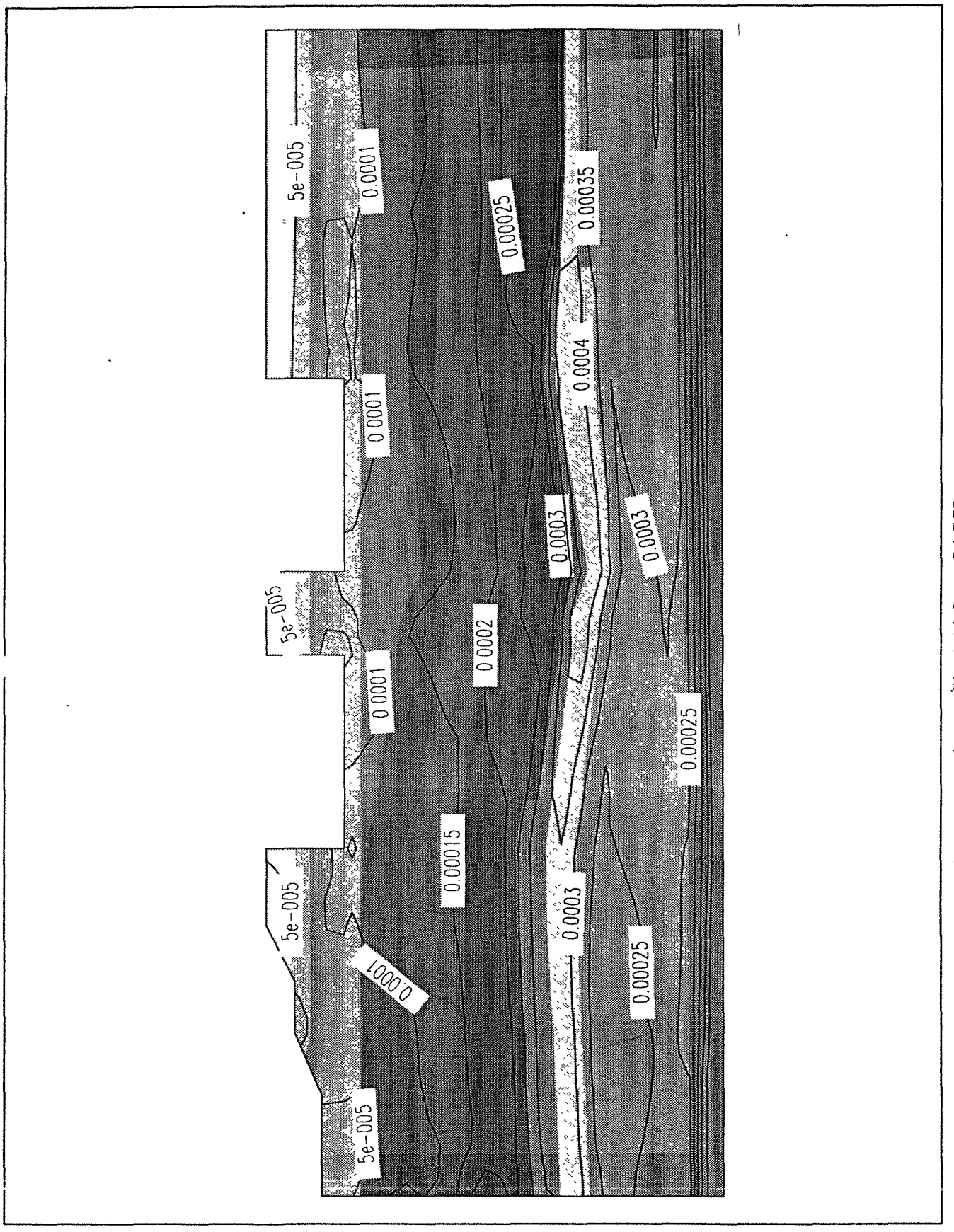


Figure 7.5-42 Maximum shear strain contours for profile AA' form SASSI analysis - EBE distant event, full tanks condition.

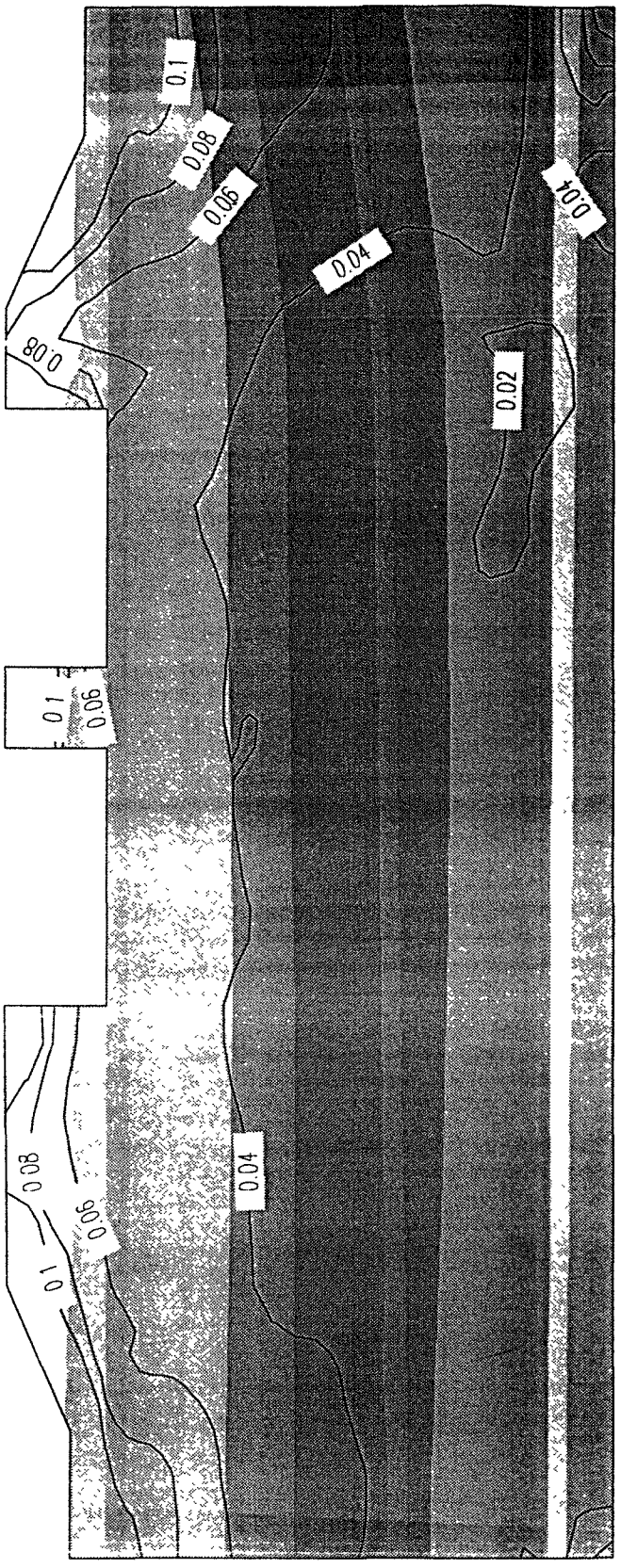


Figure 7.5-43 Effective cyclic shear stress ratio contours for profile BB' from SASSI analysis - EBE local event, full tanks condition.

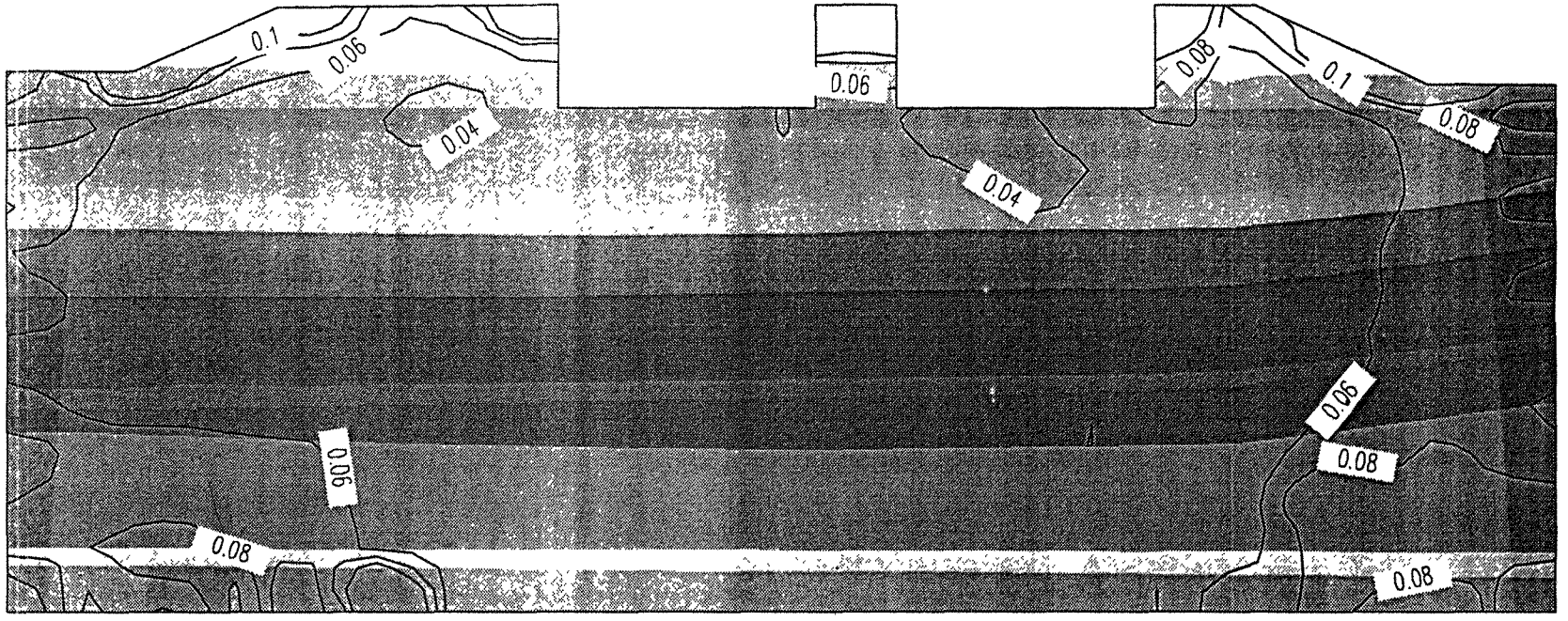


Figure 7.5-44 Effective cyclic shear stress ratio contours for profile BB' from SASSI analysis - EBE distant event, full tanks condition.

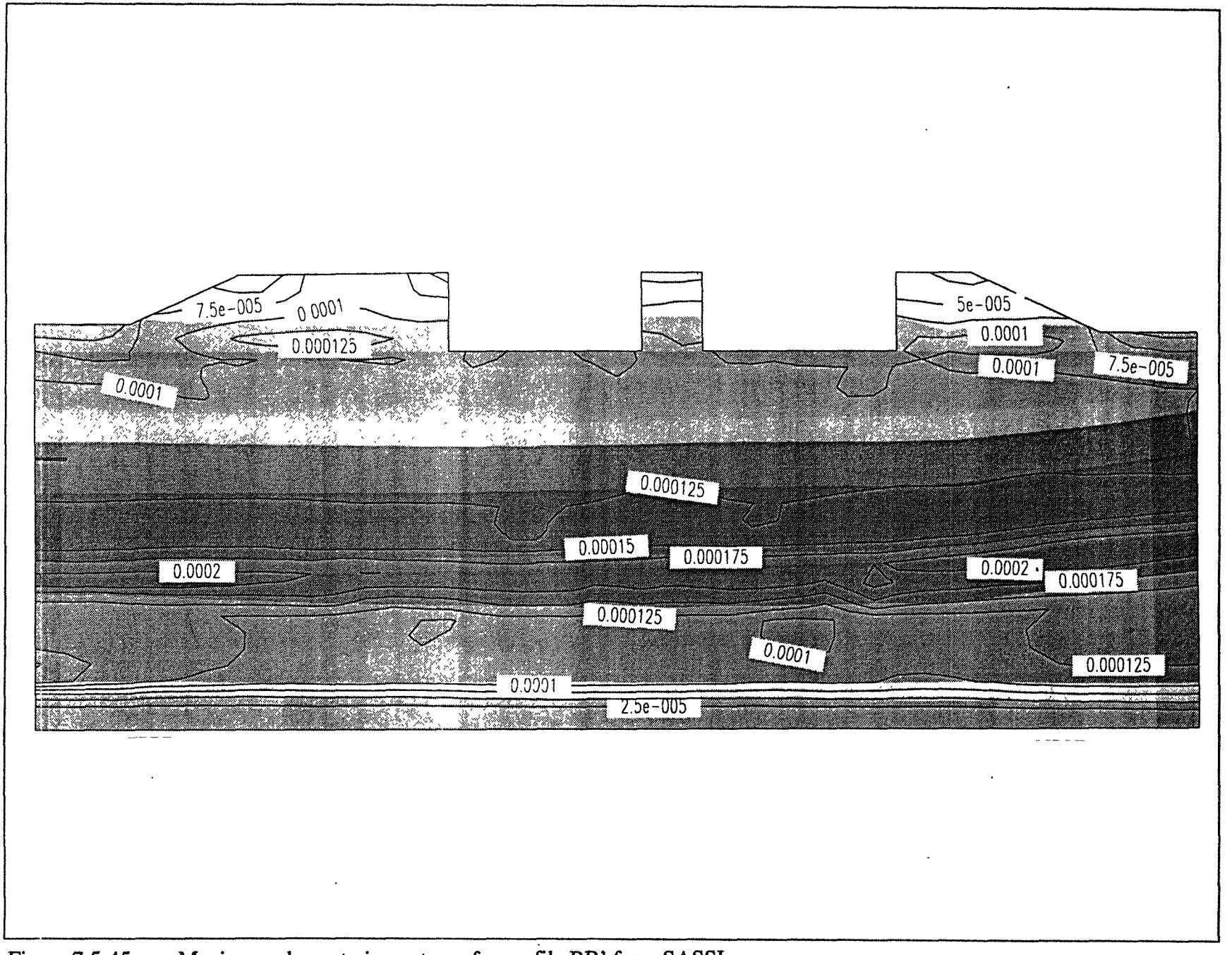


Figure 7.5-45 Maximum shear strain contours for profile BB' form SASSI analysis - EBE local event, full tanks condition.

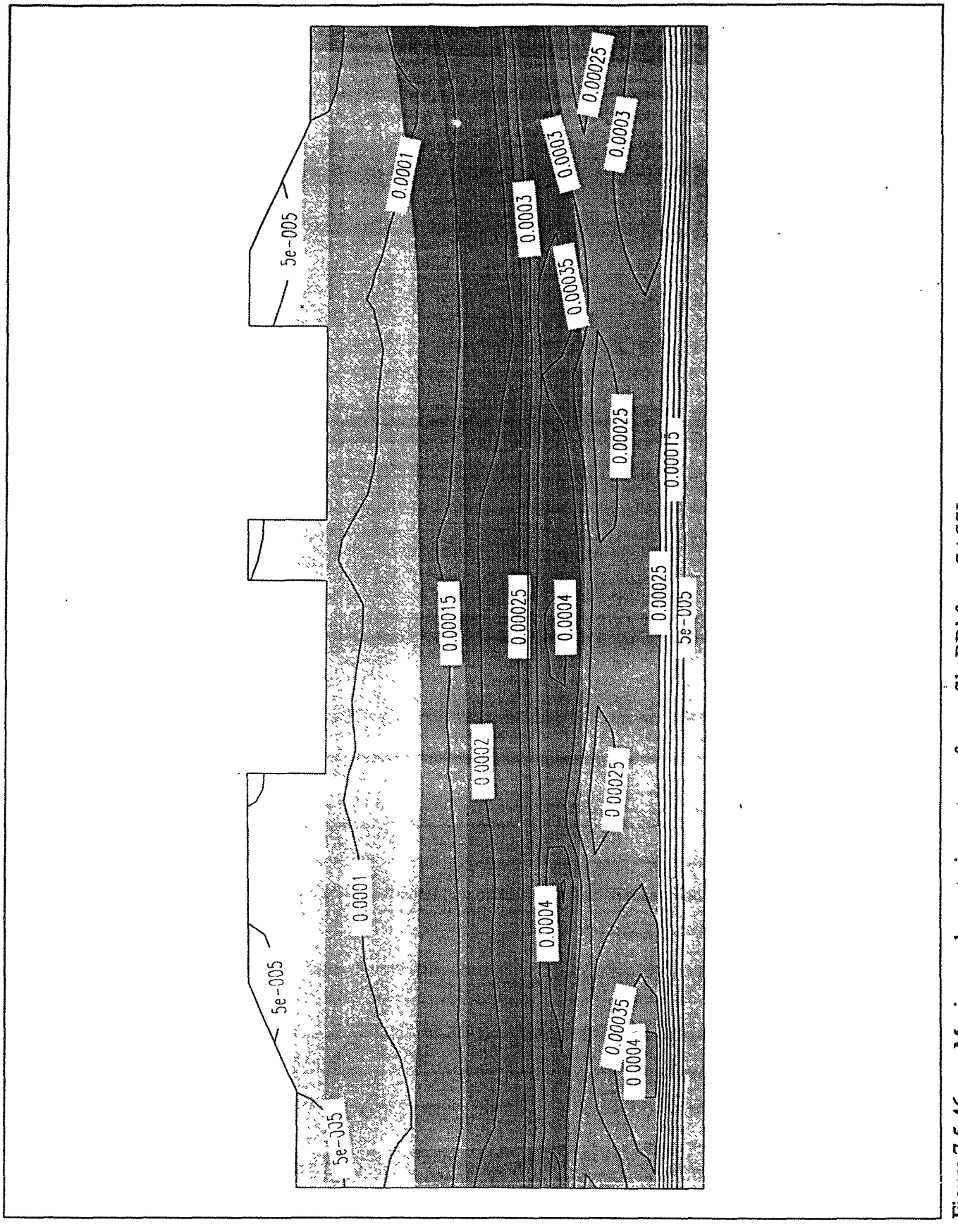


Figure 7.5-46 Maximum shear strain contours for profile BB' form SASSI analysis - EBE distant event, full tanks condition.

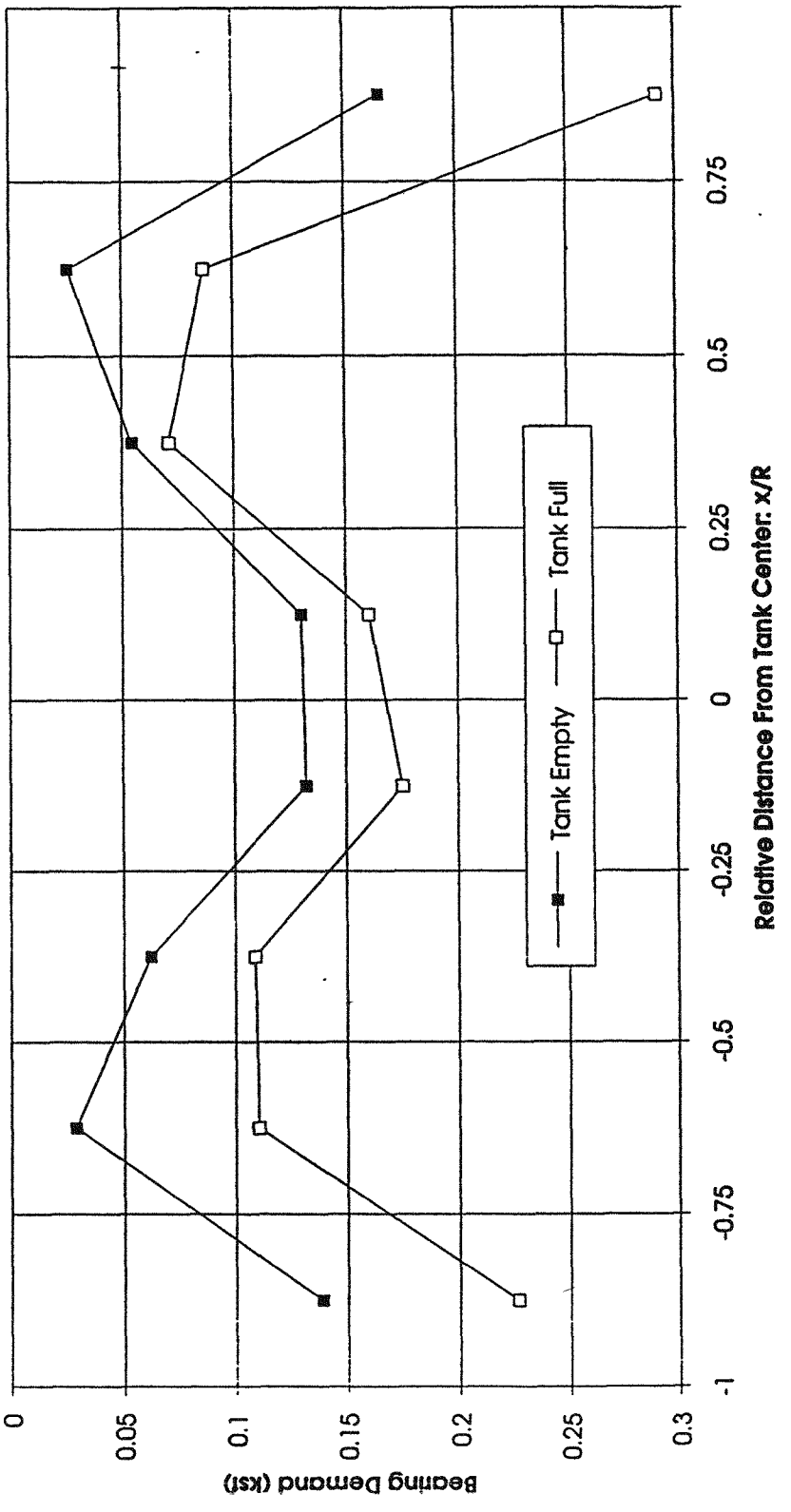


Figure 7.5-47 Maximum seismic soil bearing demand for Tank 48, profile BB', EBE local event.

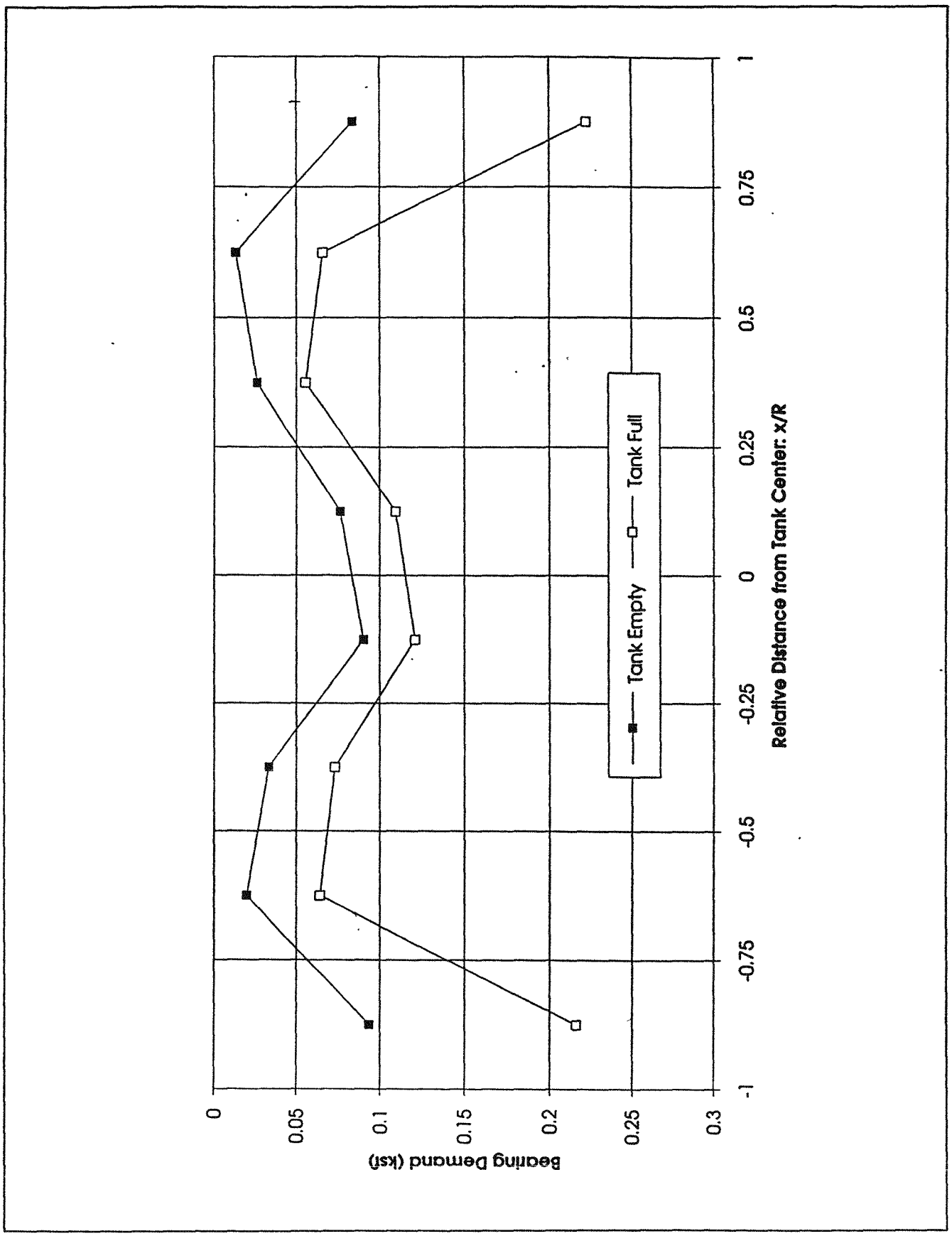


Figure 7.5-48 Maximum seismic soil bearing demand for Tank 48, profile BB', EBE distant event.

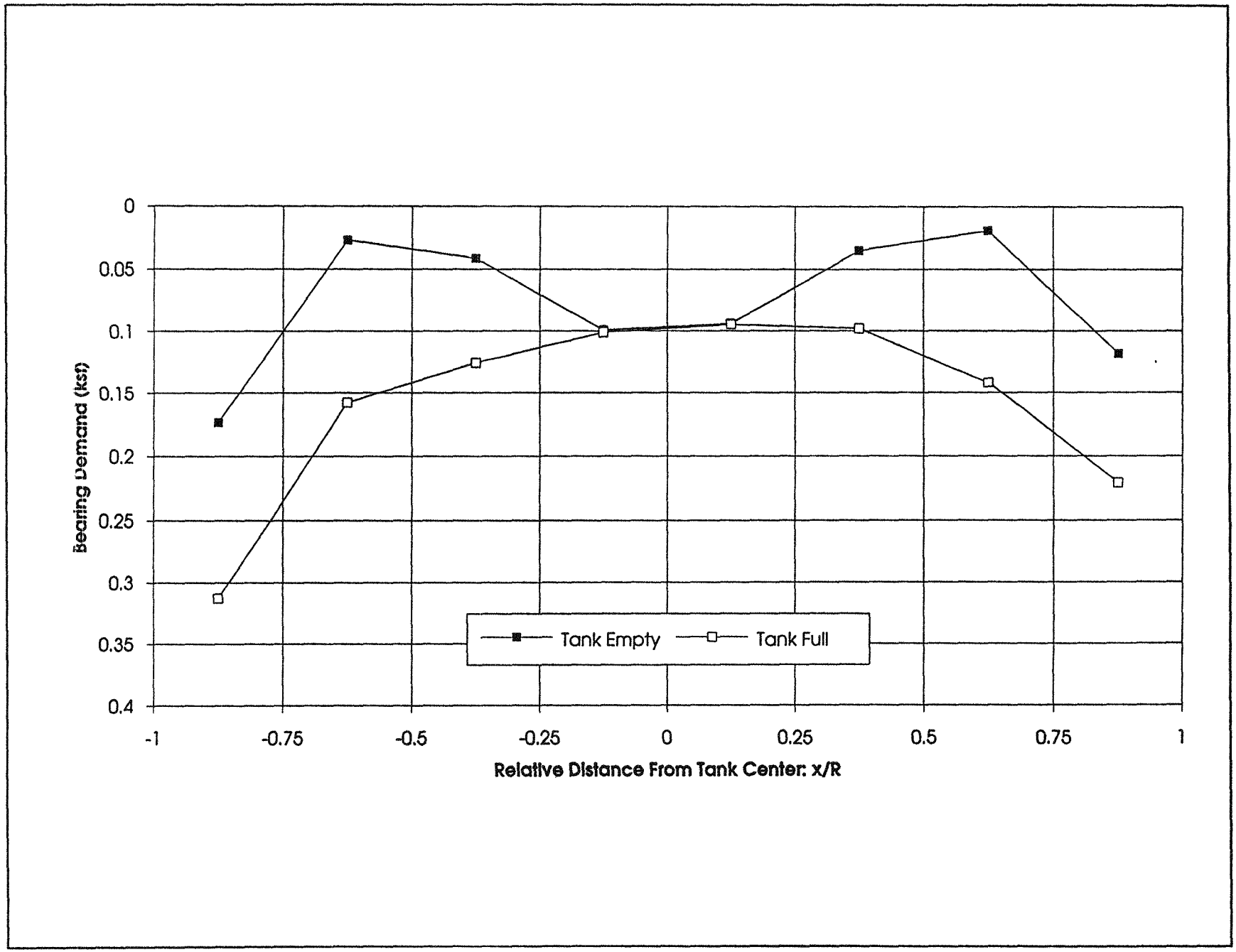


Figure 7.5-49 Maximum seismic soil bearing demand for Tank 49, profile AA', EBE local event.

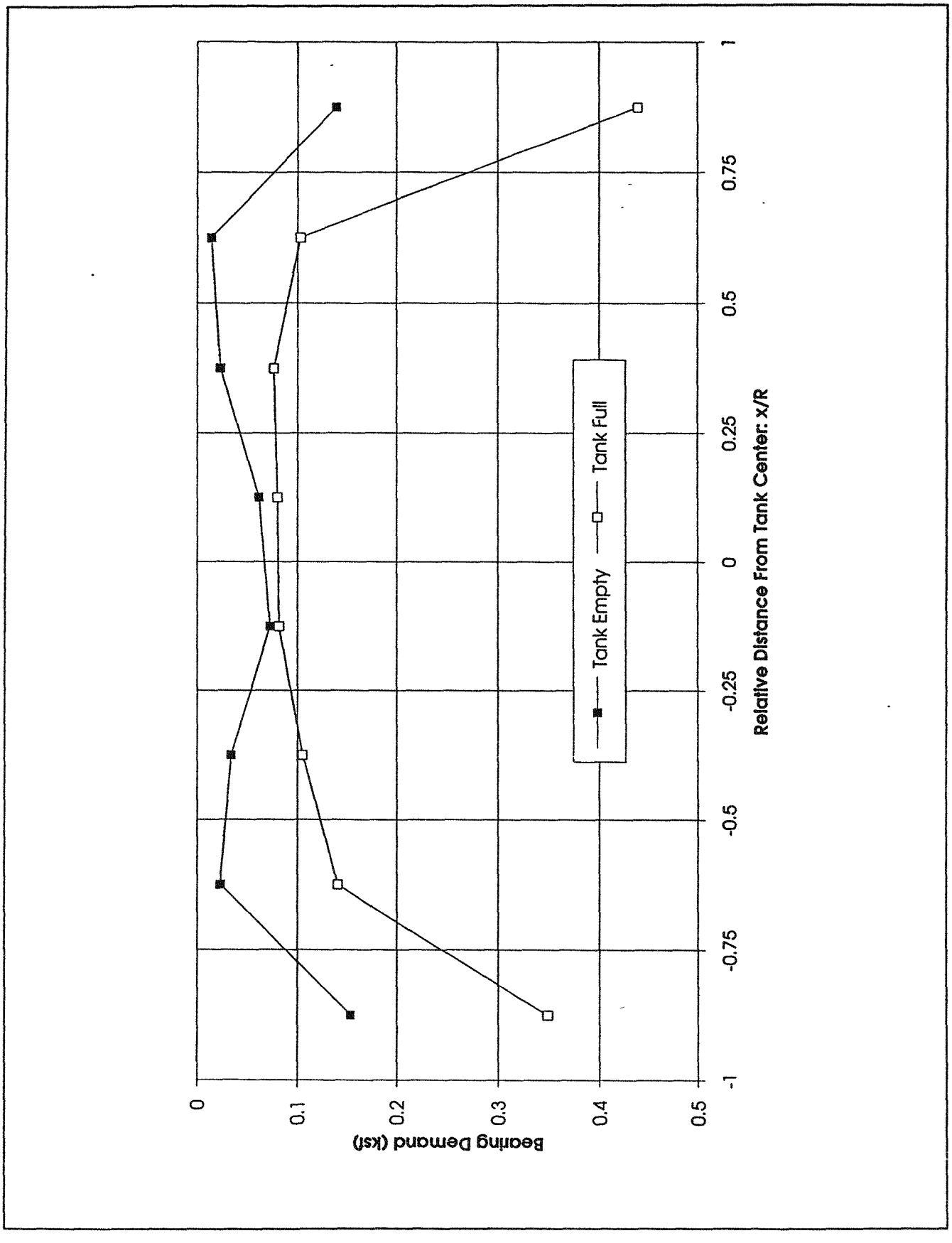


Figure 7.5-50 Maximum seismic soil bearing demand for Tank 49, profile AA', EBE distant event.

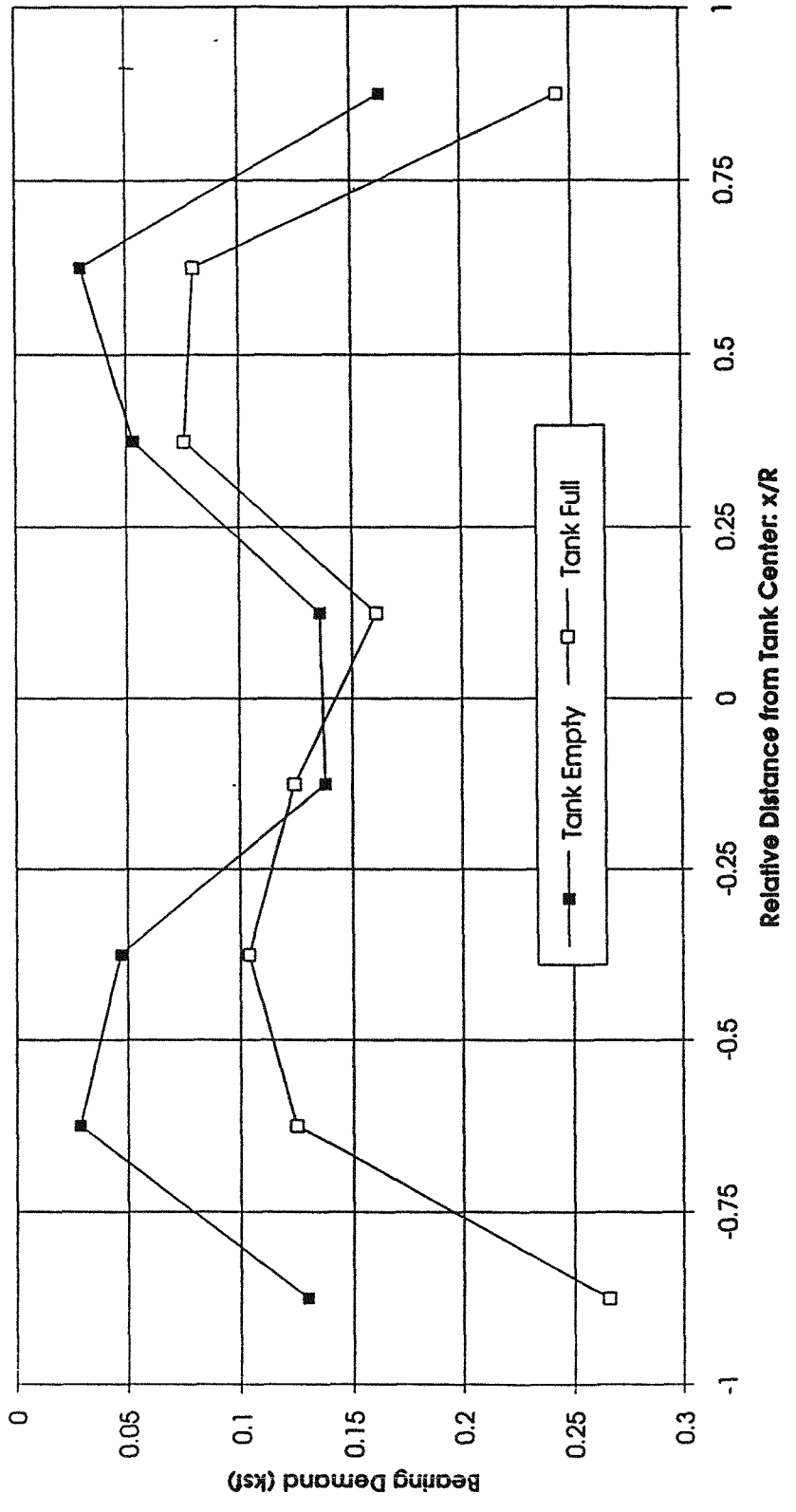


Figure 7.5-51 Maximum seismic soil bearing demand for Tank 49, profile BB', EBE local event.

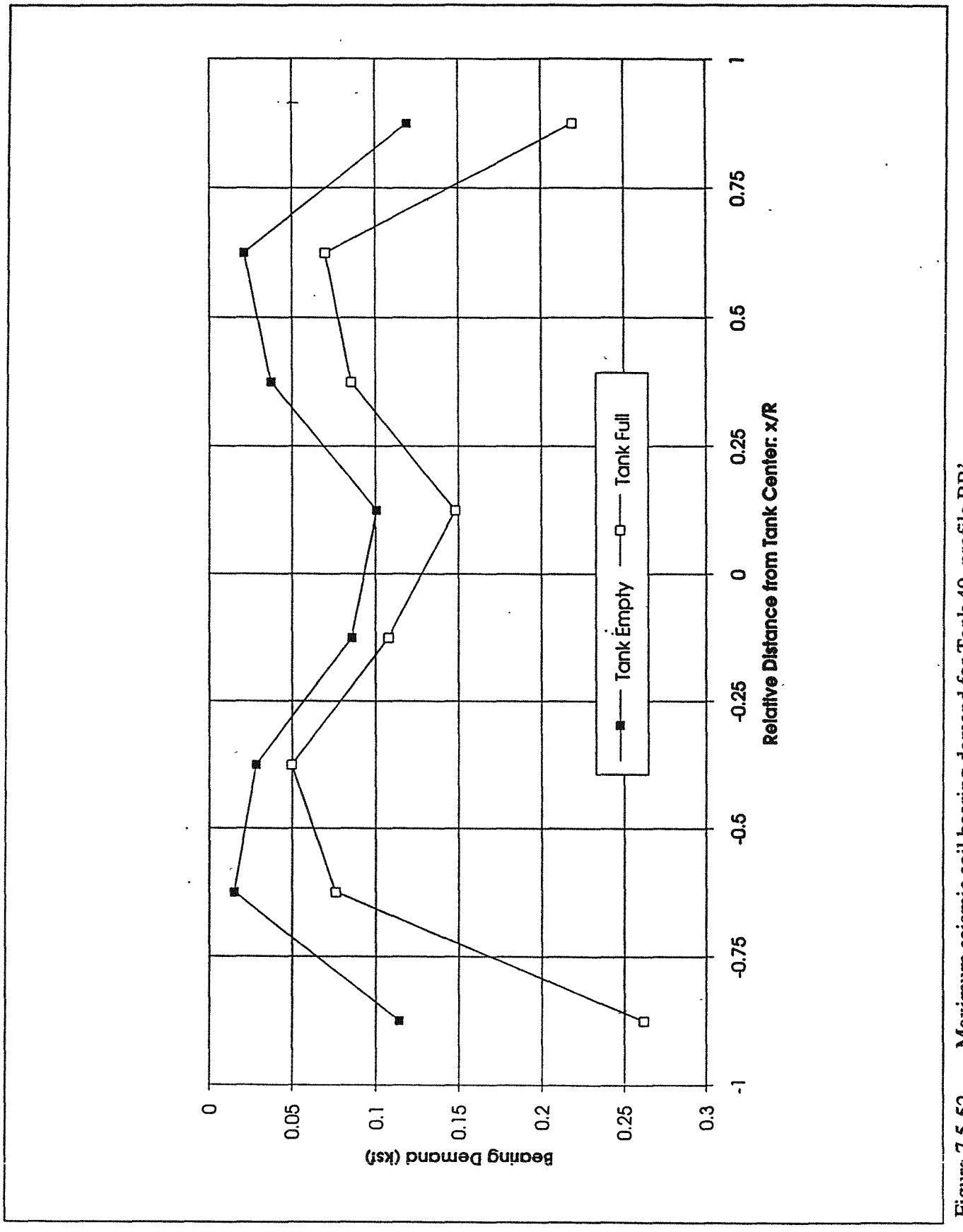


Figure 7.5-52 Maximum seismic soil bearing demand for Tank 49, profile BB', EBE distant event.

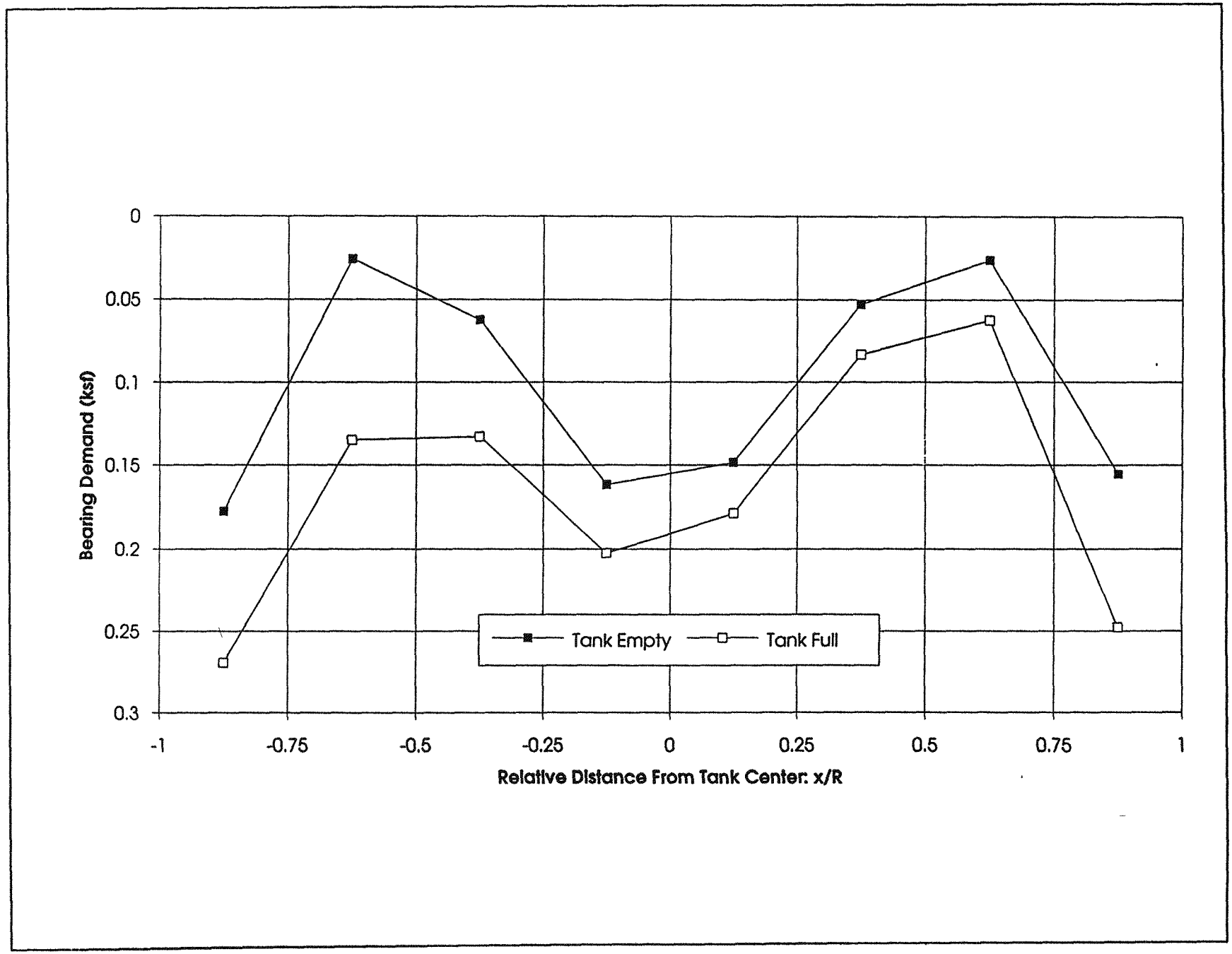


Figure 7.5-53 Maximum seismic soil bearing demand for Tank 51, profile AA', EBE local event.

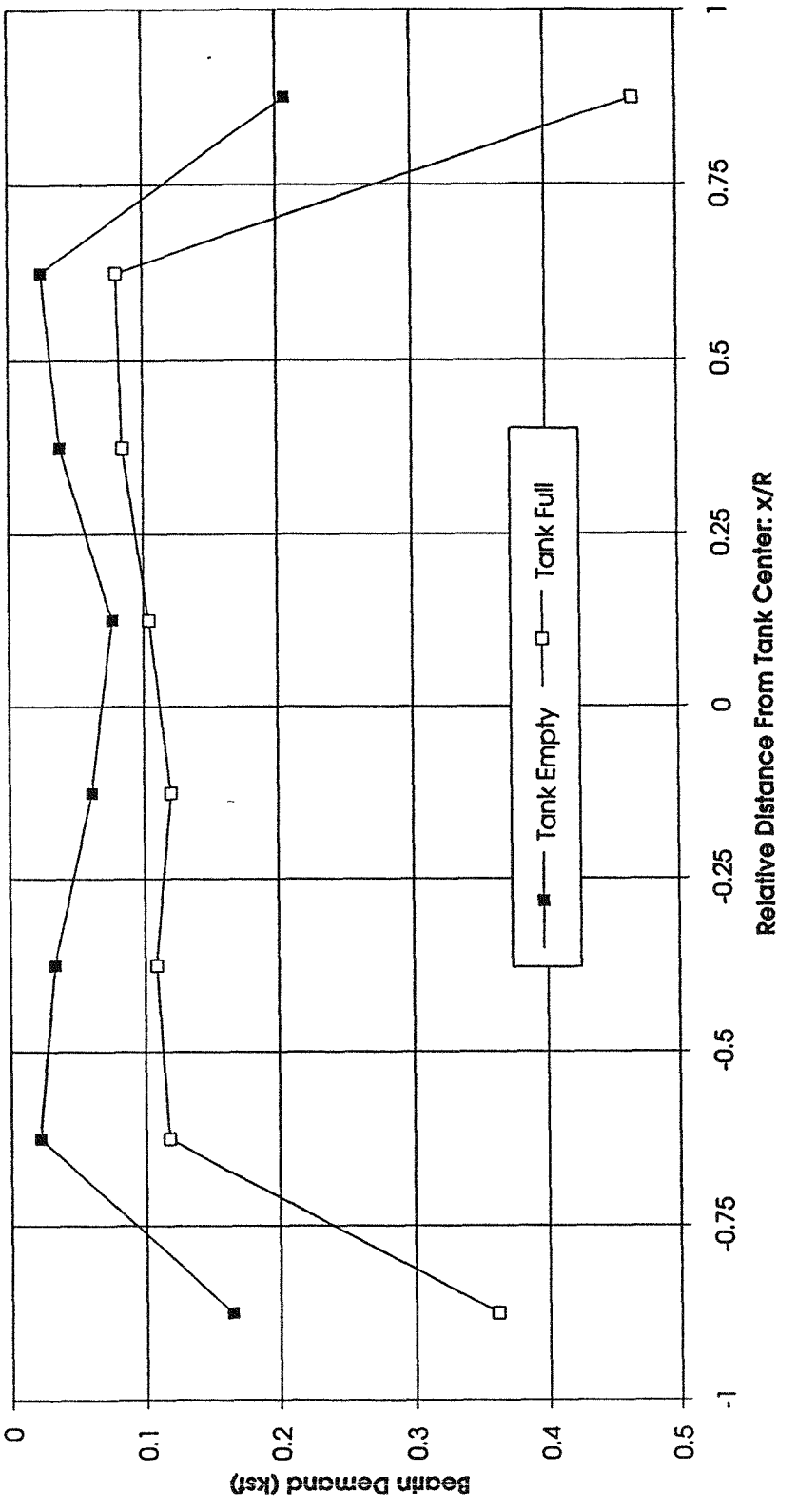


Figure 7.5-54 Maximum seismic soil bearing demand for Tank 51, profile AA', EBE distant event.

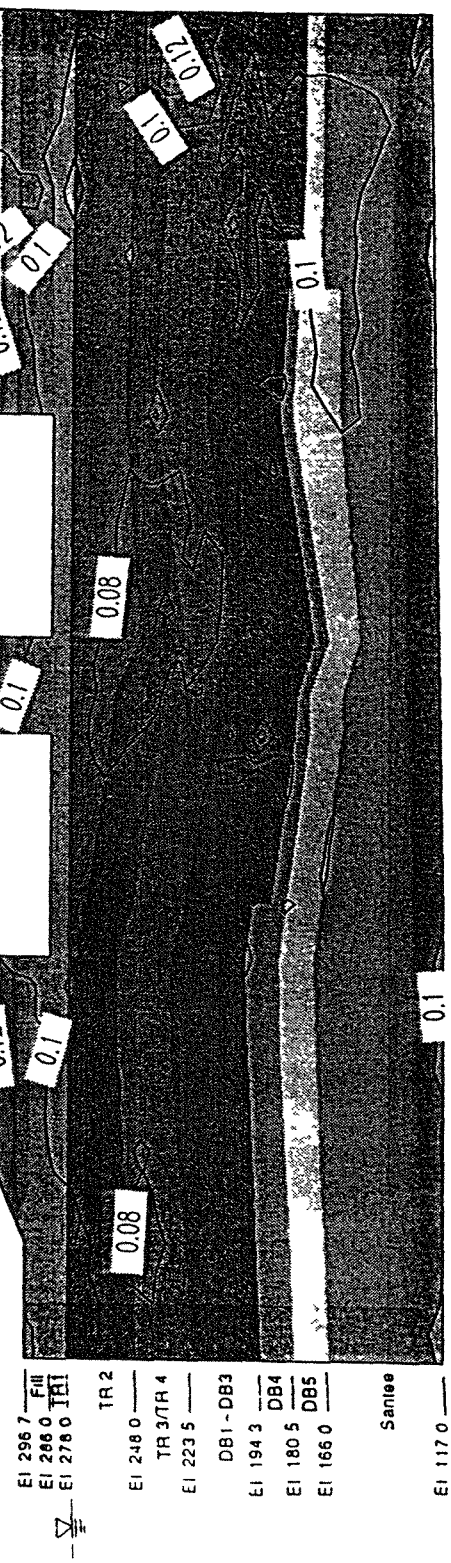


Figure 7 5-55 Maximum horizontal acceleration contours (in g's) for profile AA' from SASSI analysis - 84th percentile motion, full tank condition.

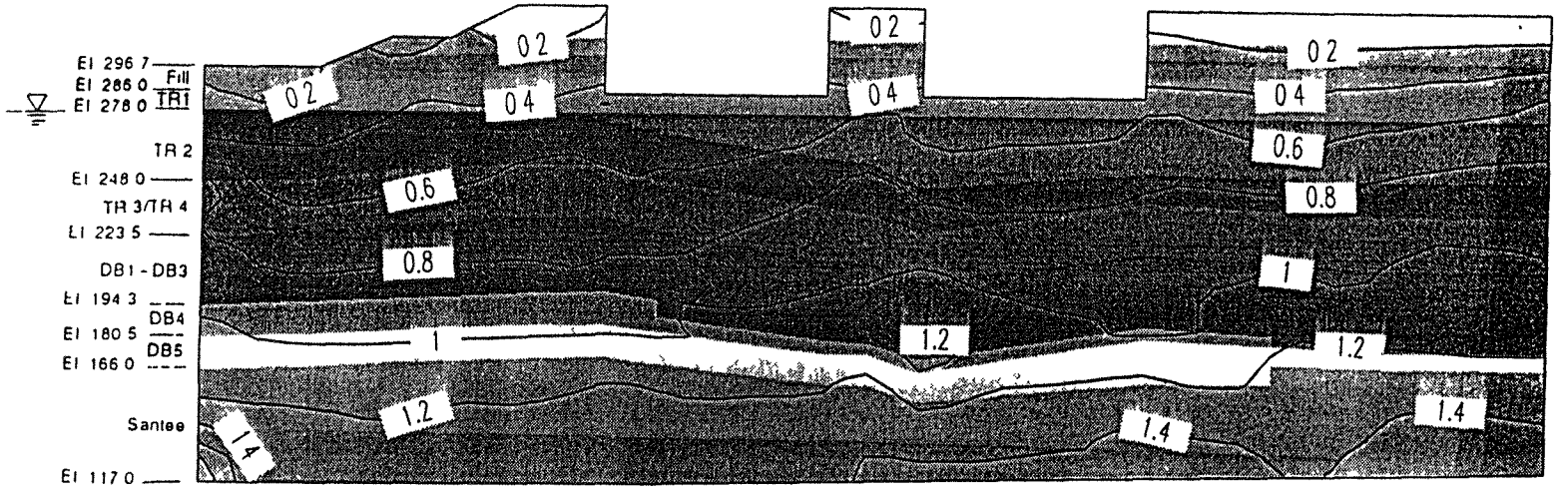


Figure 7.5-56 Maximum shear stress contours ( in ksf) for profile AA' from SASSI analysis - 84th percentile motion; full tank condition.

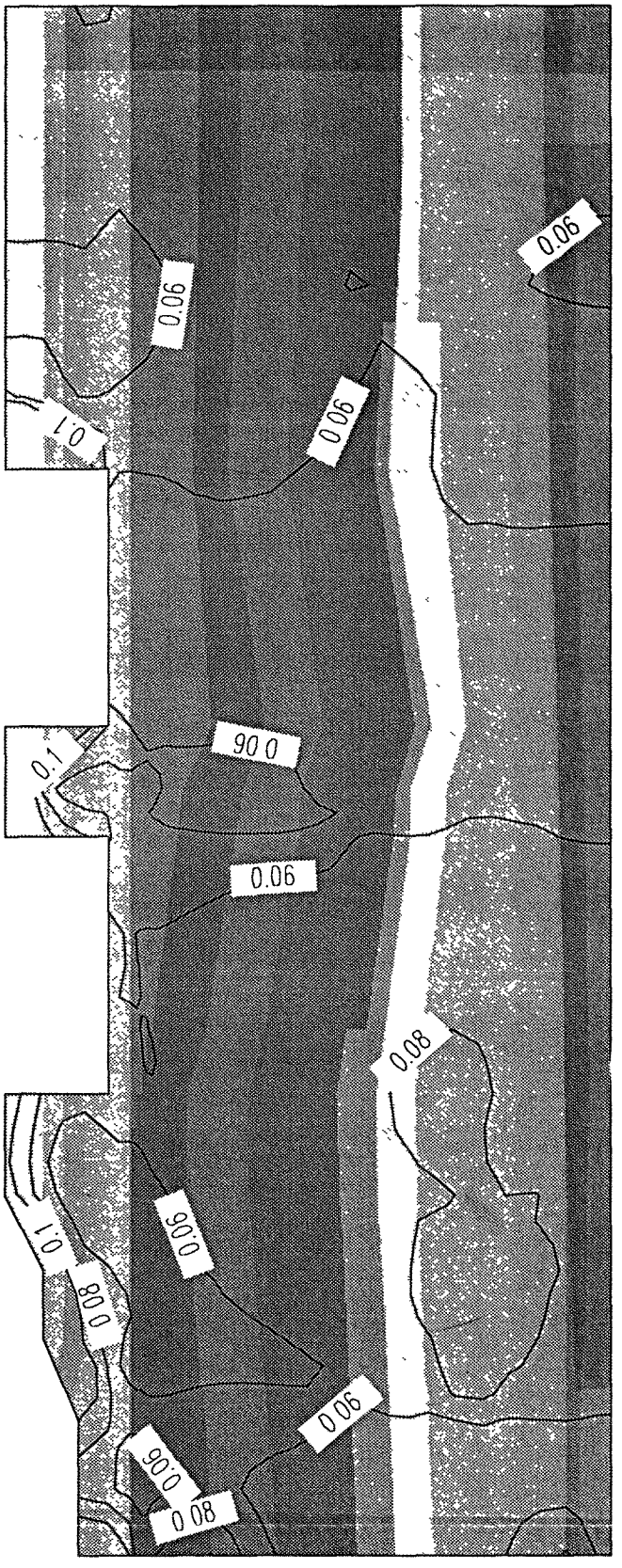


Figure 7.5-57 Effective cyclic stress ratio contours for profile AA' from SASSI analysis - 84th percentile motion; full tank condition.

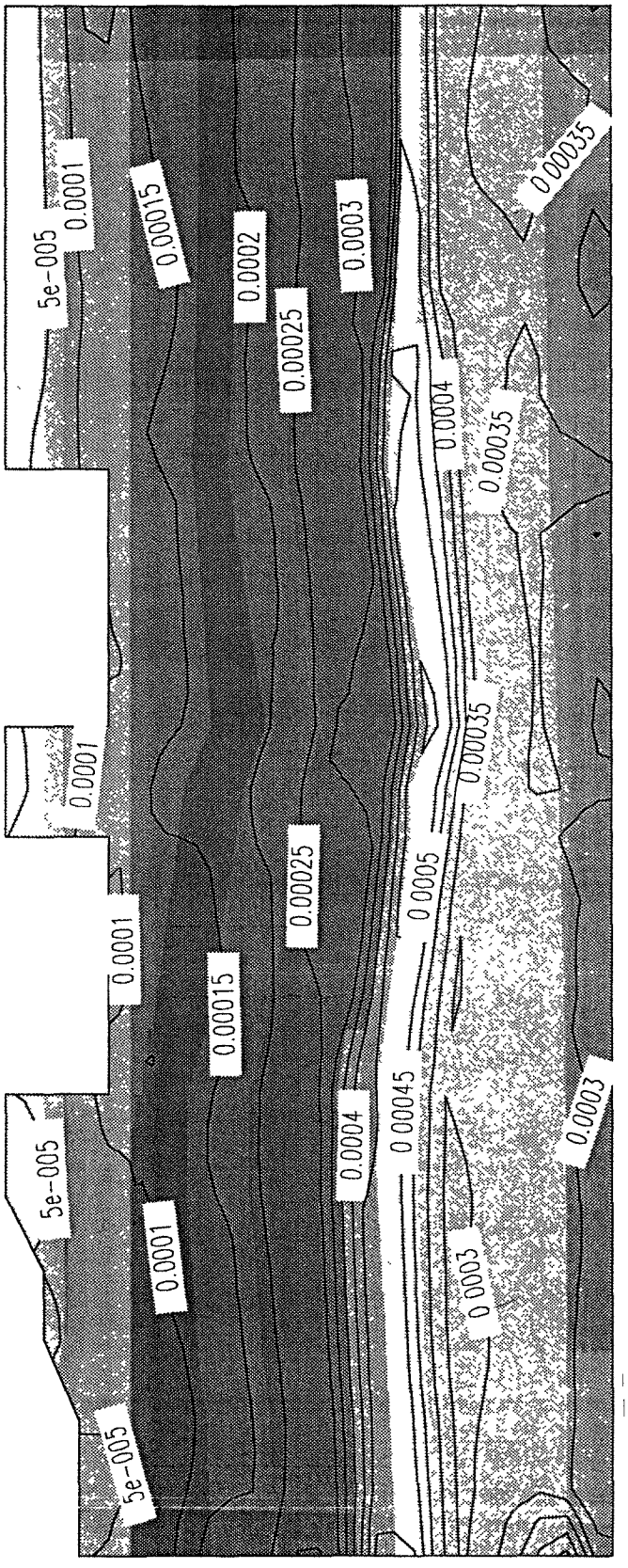


Figure 7.5-58 Maximum shear strain contours for profile AA' from SASSI analysis - 84th percentile motion; full tank condition.

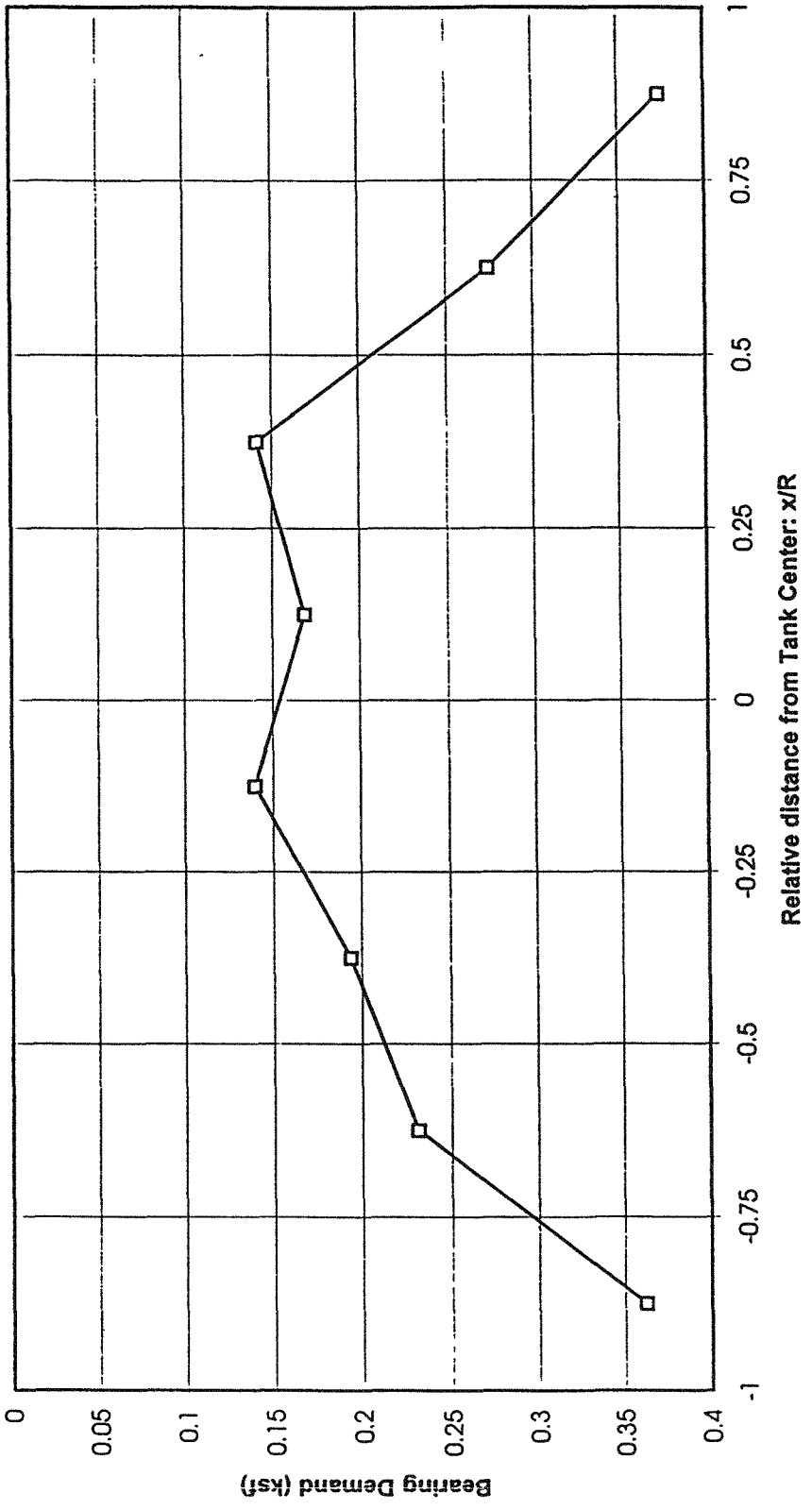


Figure 7.5-59 Maximum seismic soil bearing demand for Tank 49, profile AA', 84th percentile motion.

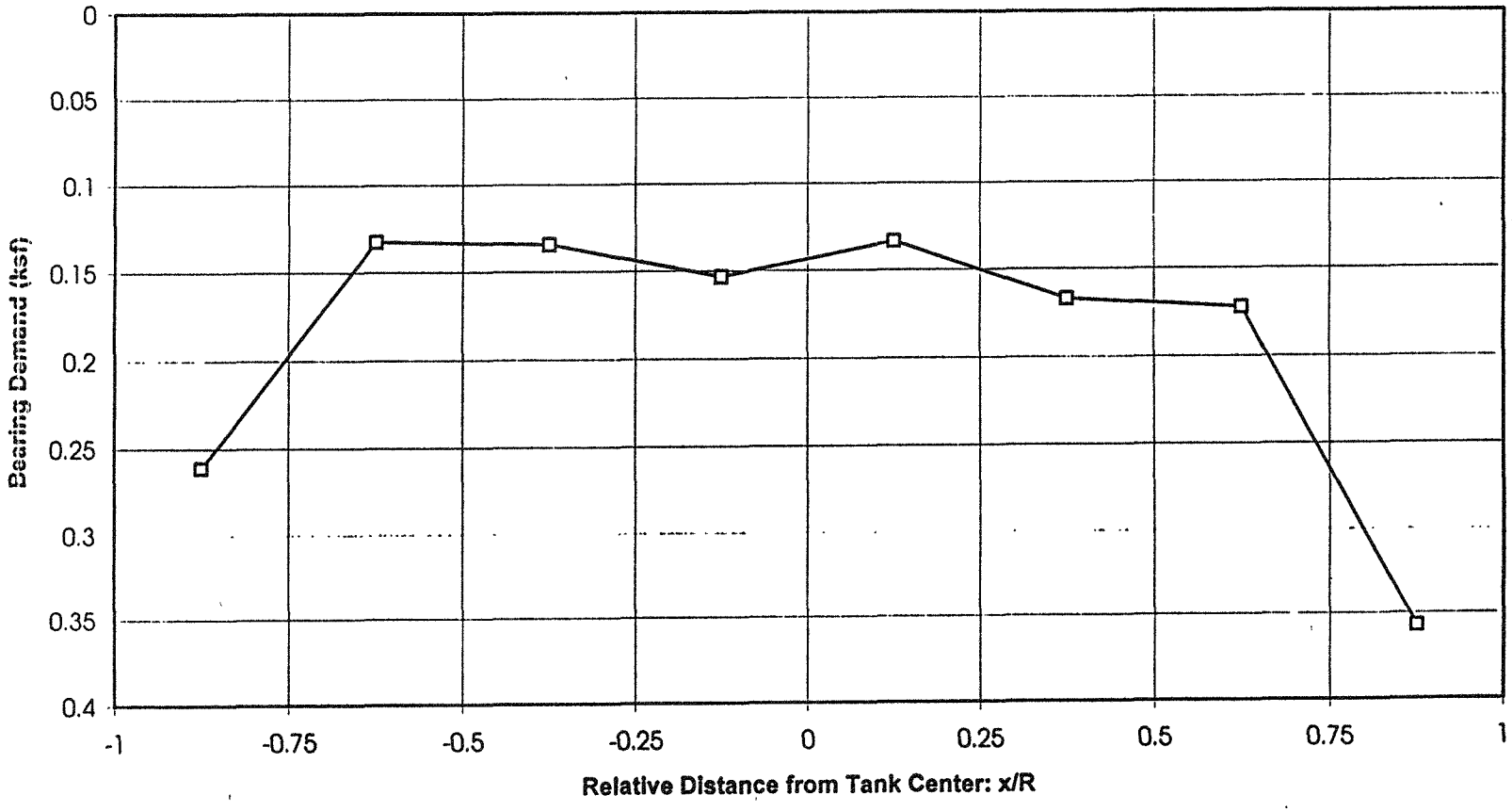


Figure 7.5-60 Maximum seismic soil bearing demand for Tank 51, profile AA', 84th percentile motion.

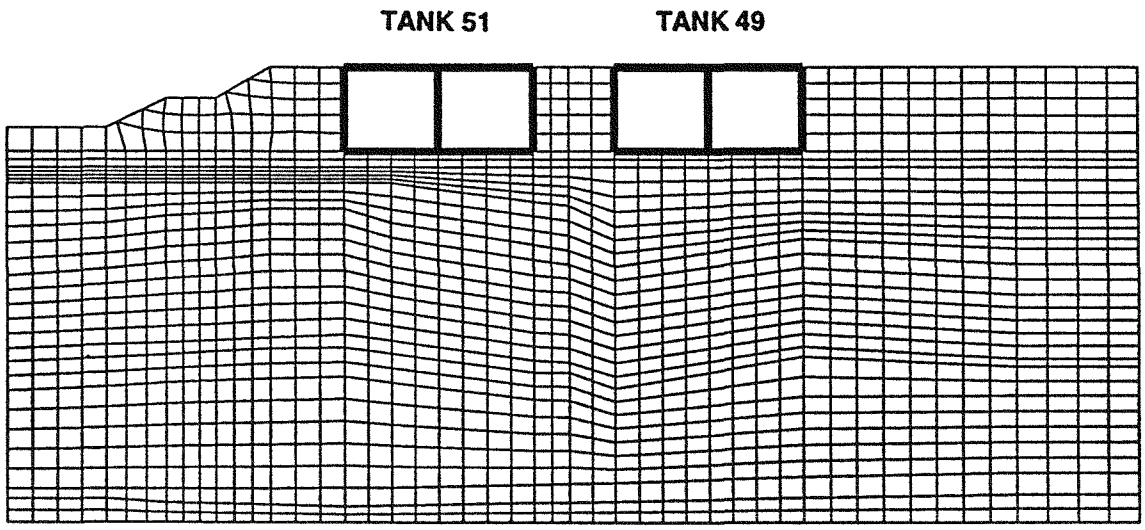


Figure 7.5-61 FLAC discretized elements for profile AA'.

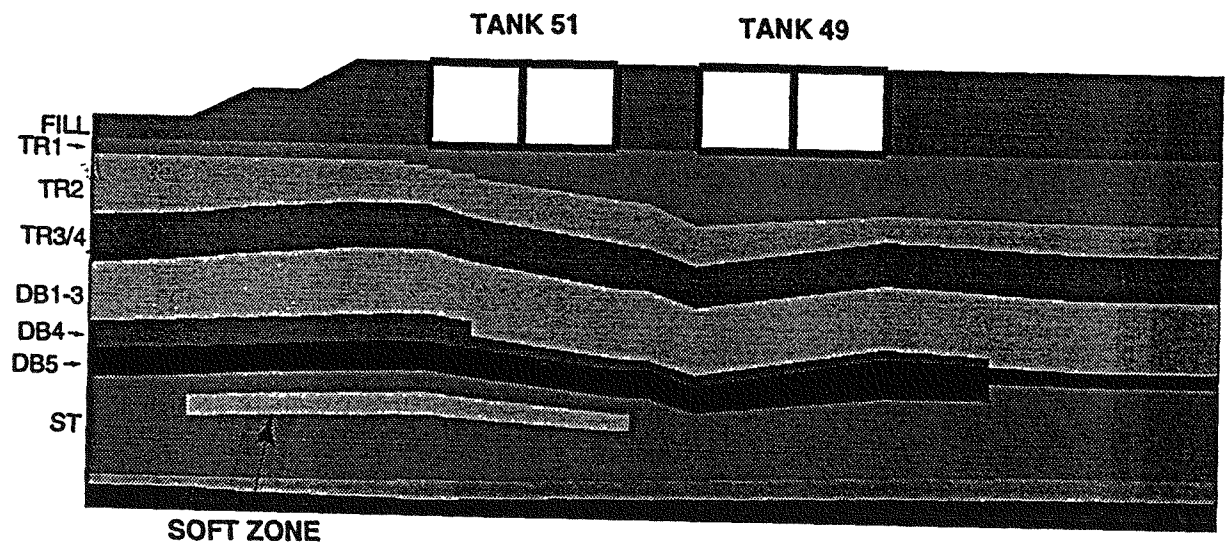


Figure 7.5-62 Soil layers in FLAC model of profile AA'.

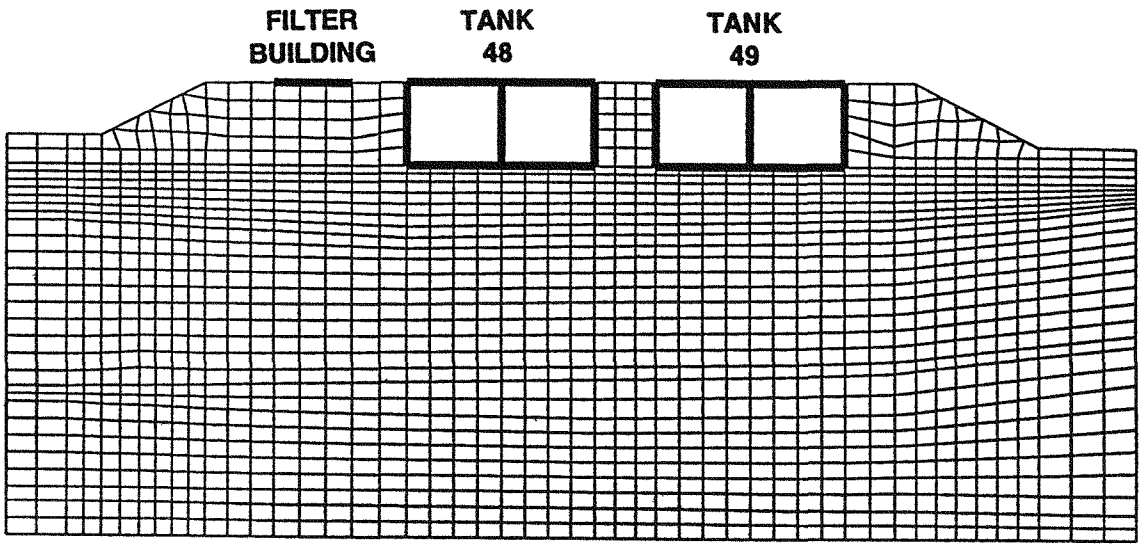


Figure 7.5-63 FLAC discretized elements for profile BB'.

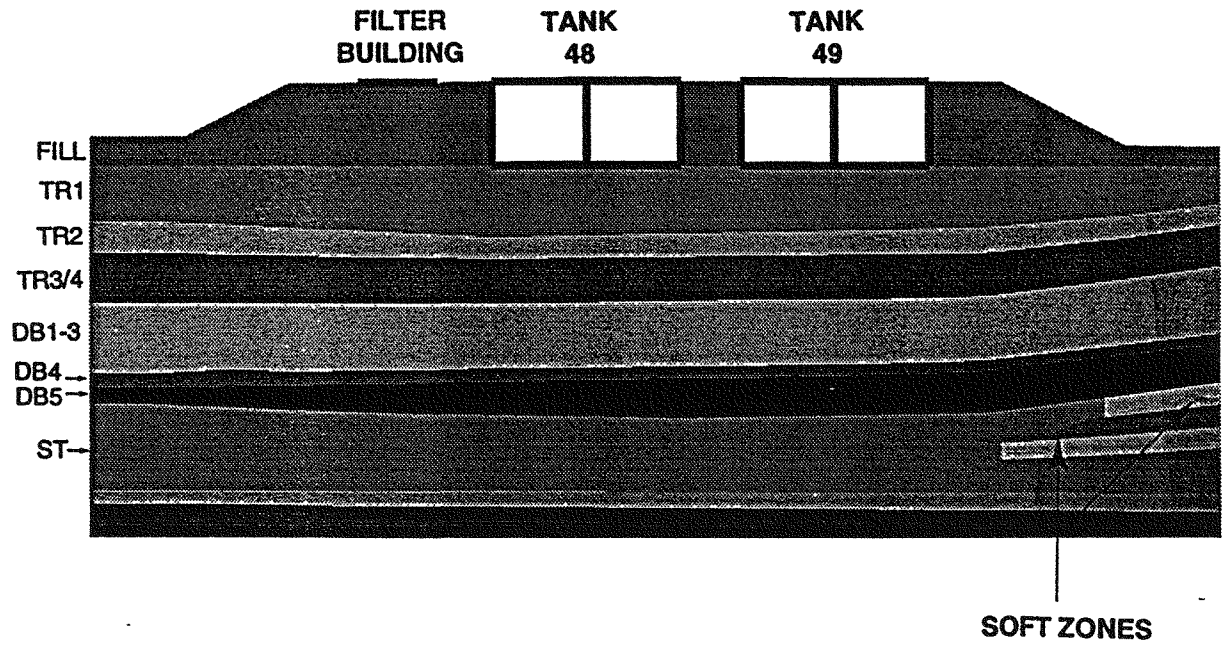


Figure 7.5-64 Soil layers in FLAC model of profile BB'.

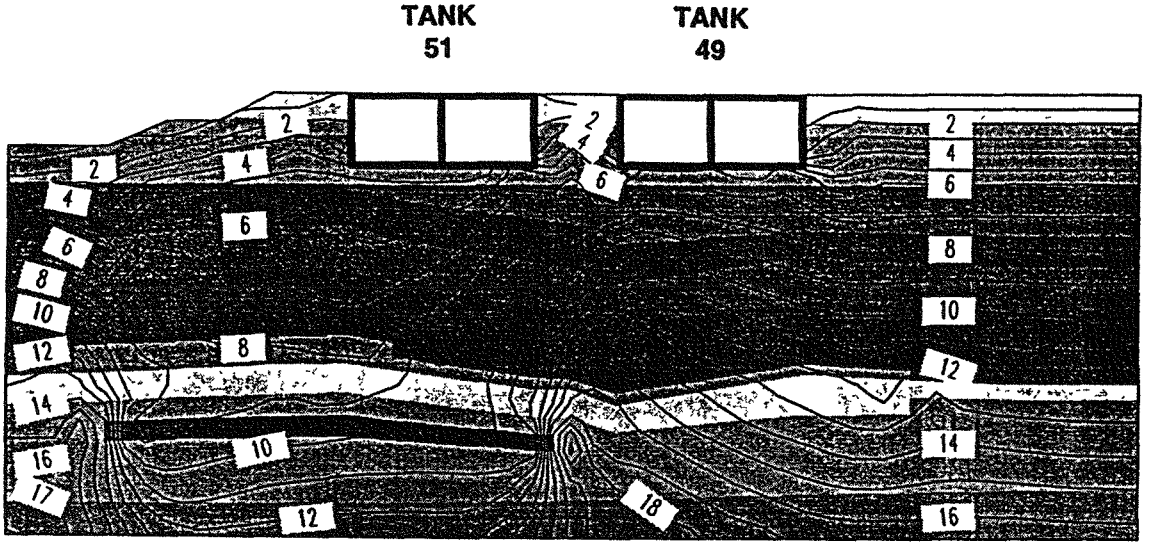


Figure 7.5-65 Contours of effective vertical stresses ( ksf) for profile AA' under full tank condition

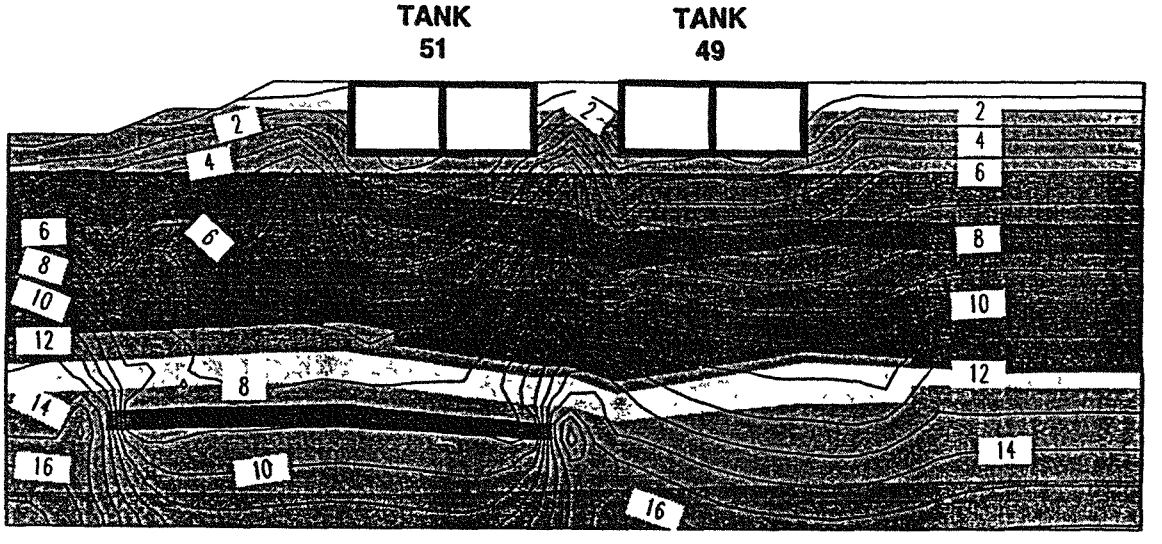


Figure 7.5-66 Contours of effective vertical stresses ( ksf) for profile AA' under empty tank condition.

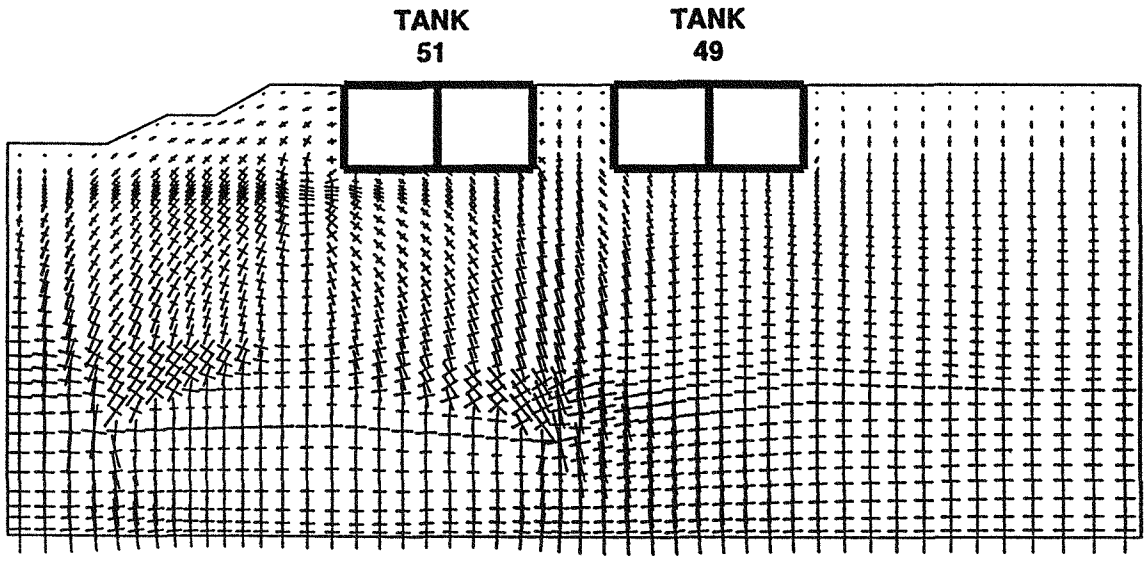


Figure 7.5-67 Orientation of effective principal stresses for profile AA'.

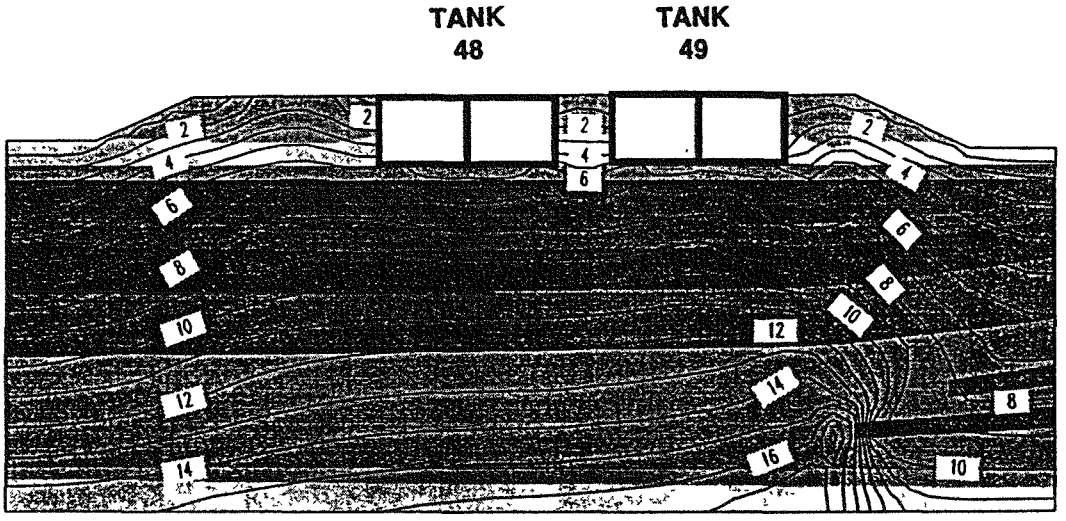


Figure 7.5-68 Contours of effective vertical stresses ( ksf ) for profile BB' under full tank condition.

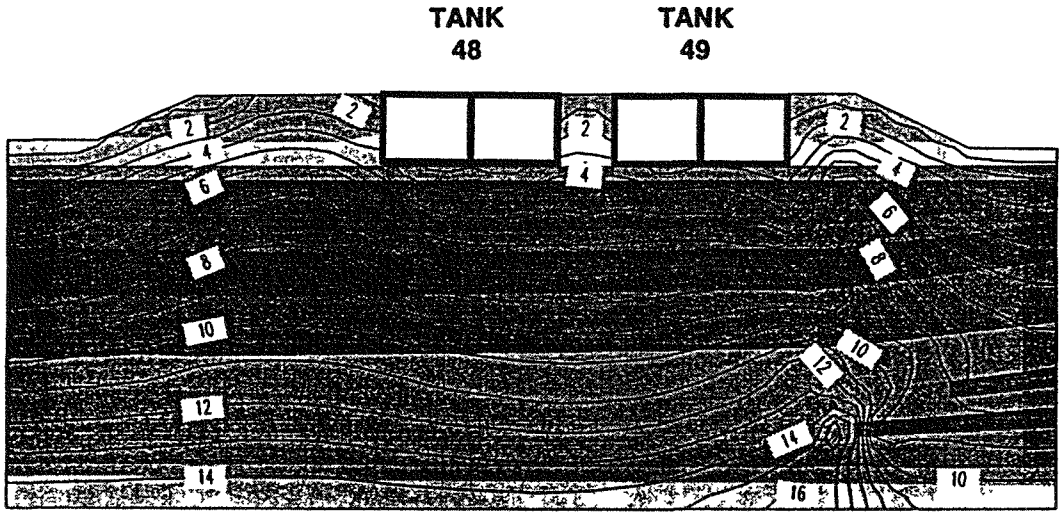


Figure 7.5-69 Contours of effective vertical stresses ( ksf) for profile BB' under empty tank condition.

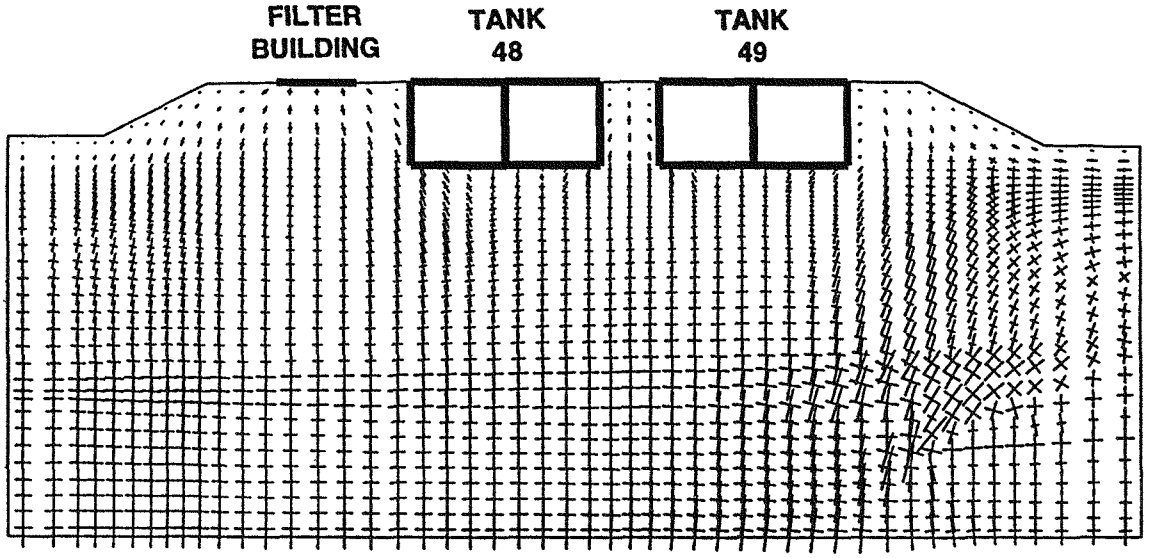


Figure 7.5-70 Orientation of effective principal stresses for profile BB'.

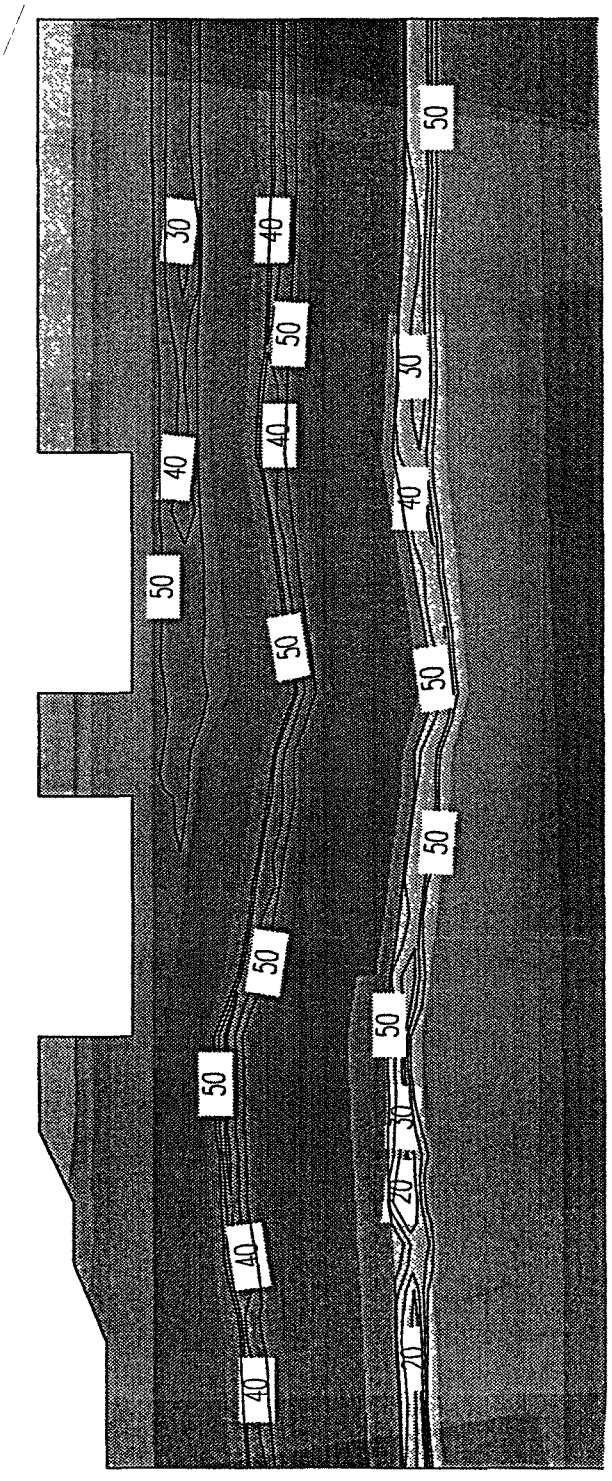


Figure 7.5-71 Kriged CPT tip resistance for profile AA' for tip resistance values less than 50 tsf.

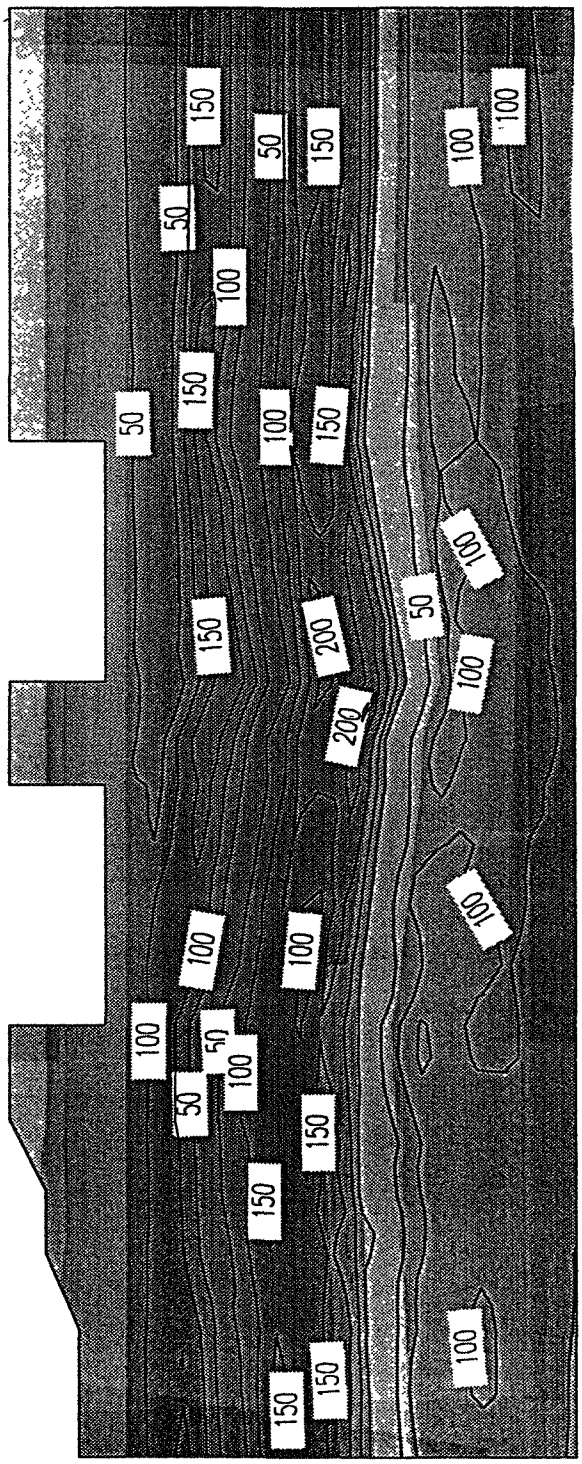


Figure 7.5-72 Kriged CPT tip resistance for profile AA' for tip resistance values greater than 50 tsf.

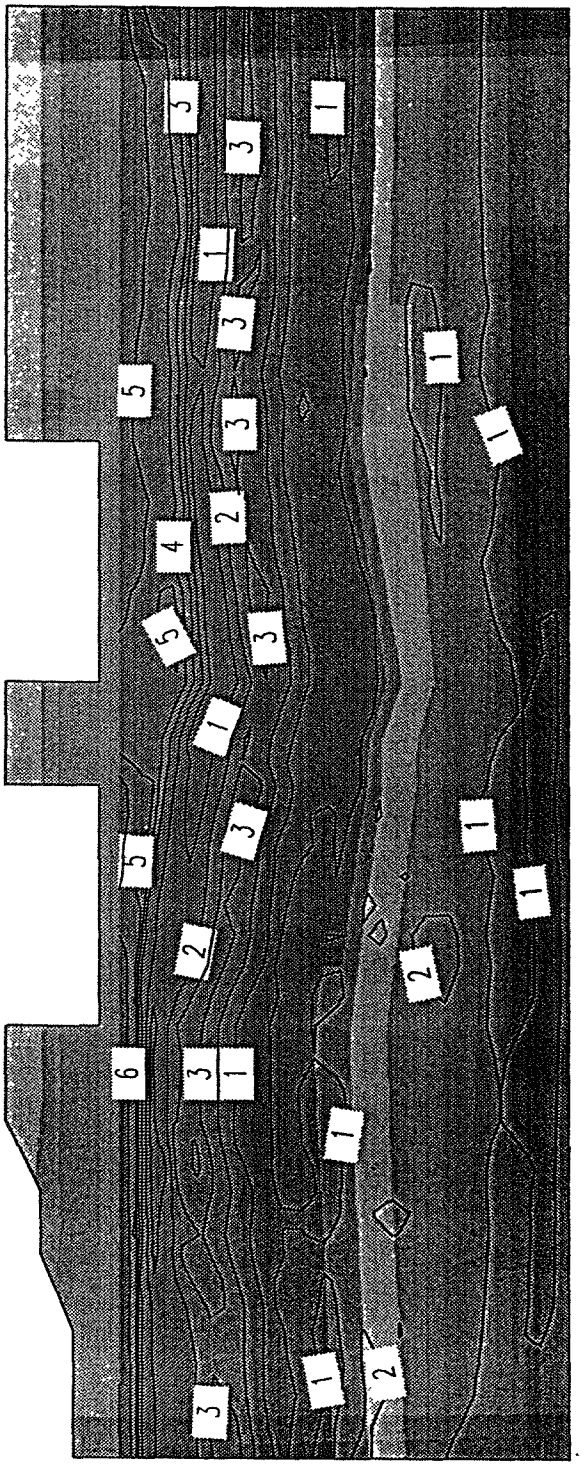


Figure 7.5-73 Kriged CPT friction ratio for profile AA'.

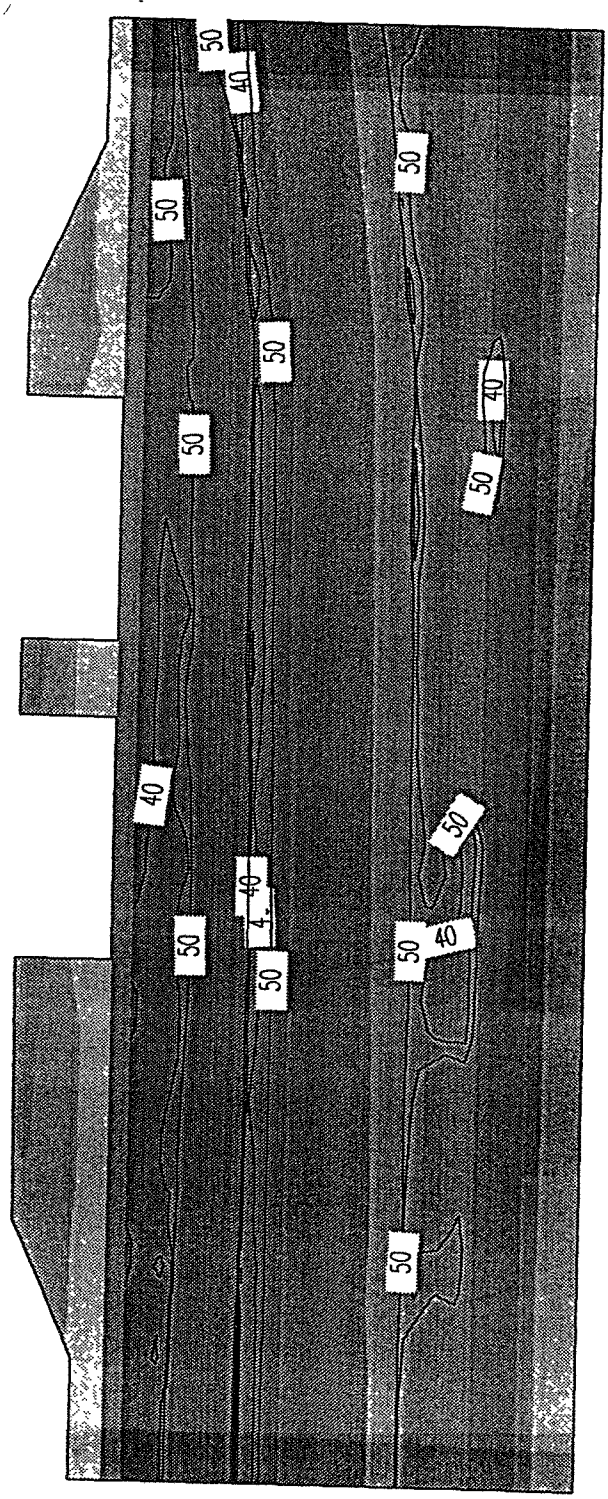


Figure 7.5-74 Kriged CPT tip resistance for profile BB' for tip resistance values less than 50 tsf.

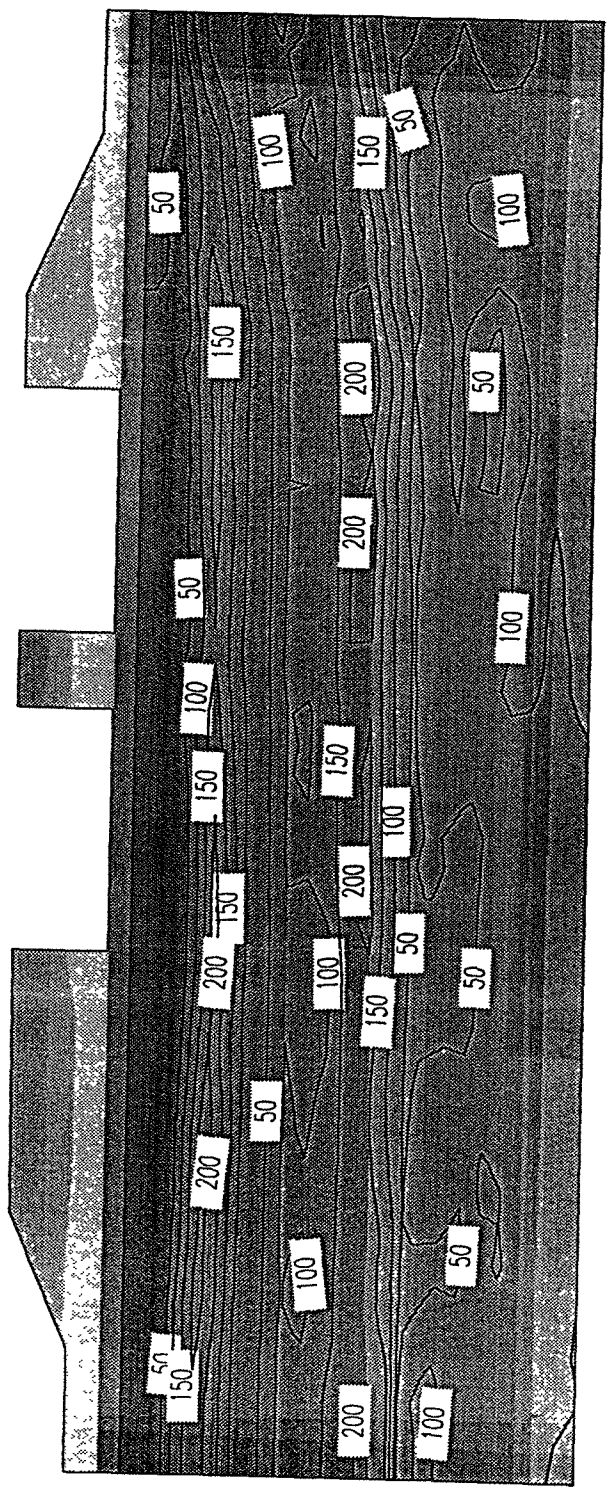


Figure 7.5-75 Kriged CPT tip resistance for profile BB' for tip resistance values greater than 50 tsf.

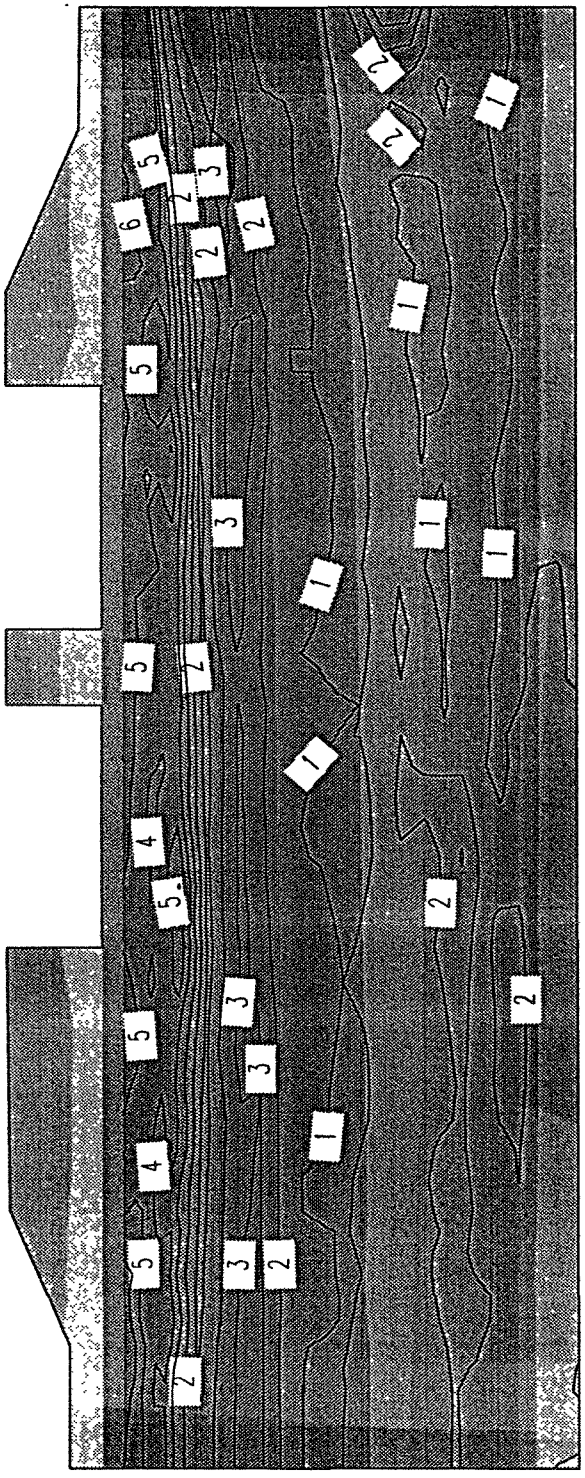

Figure 7.5-76 Kriged CPT friction ratio for profile BB'.

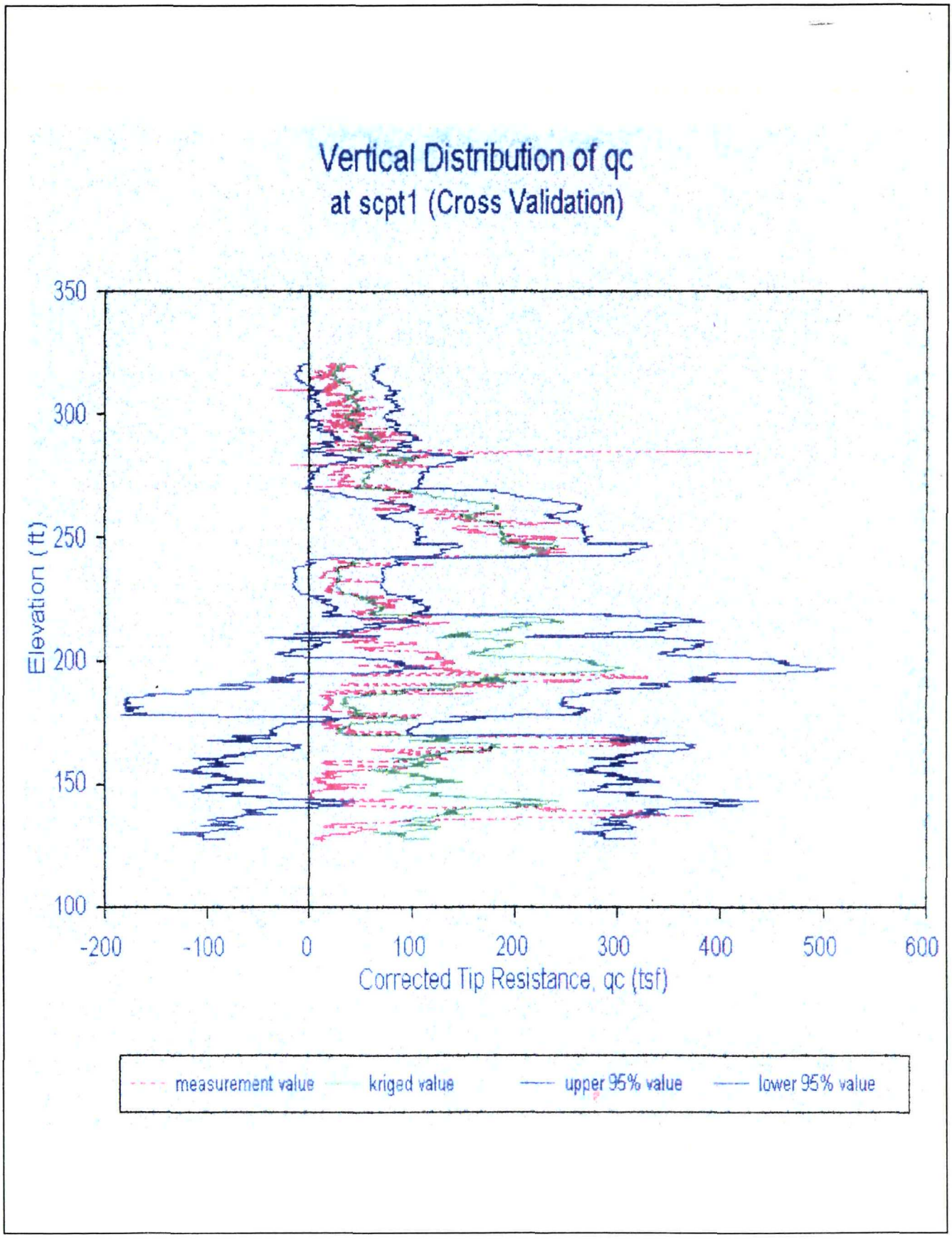


Figure 7.5-77 Cross validation results for borehole SCPT 1

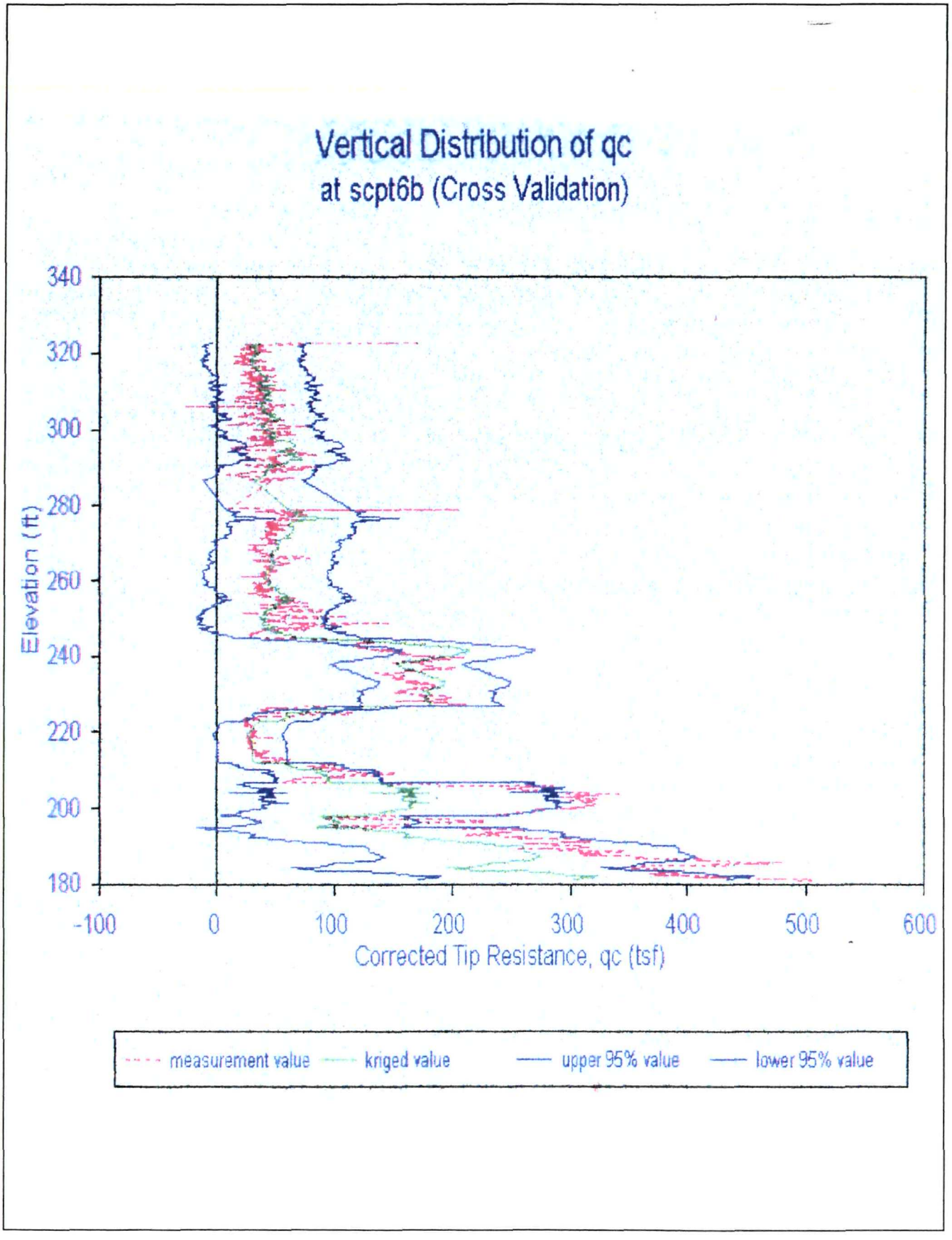


Figure 7.5-78 Cross validation results for borehole SCPT 6B

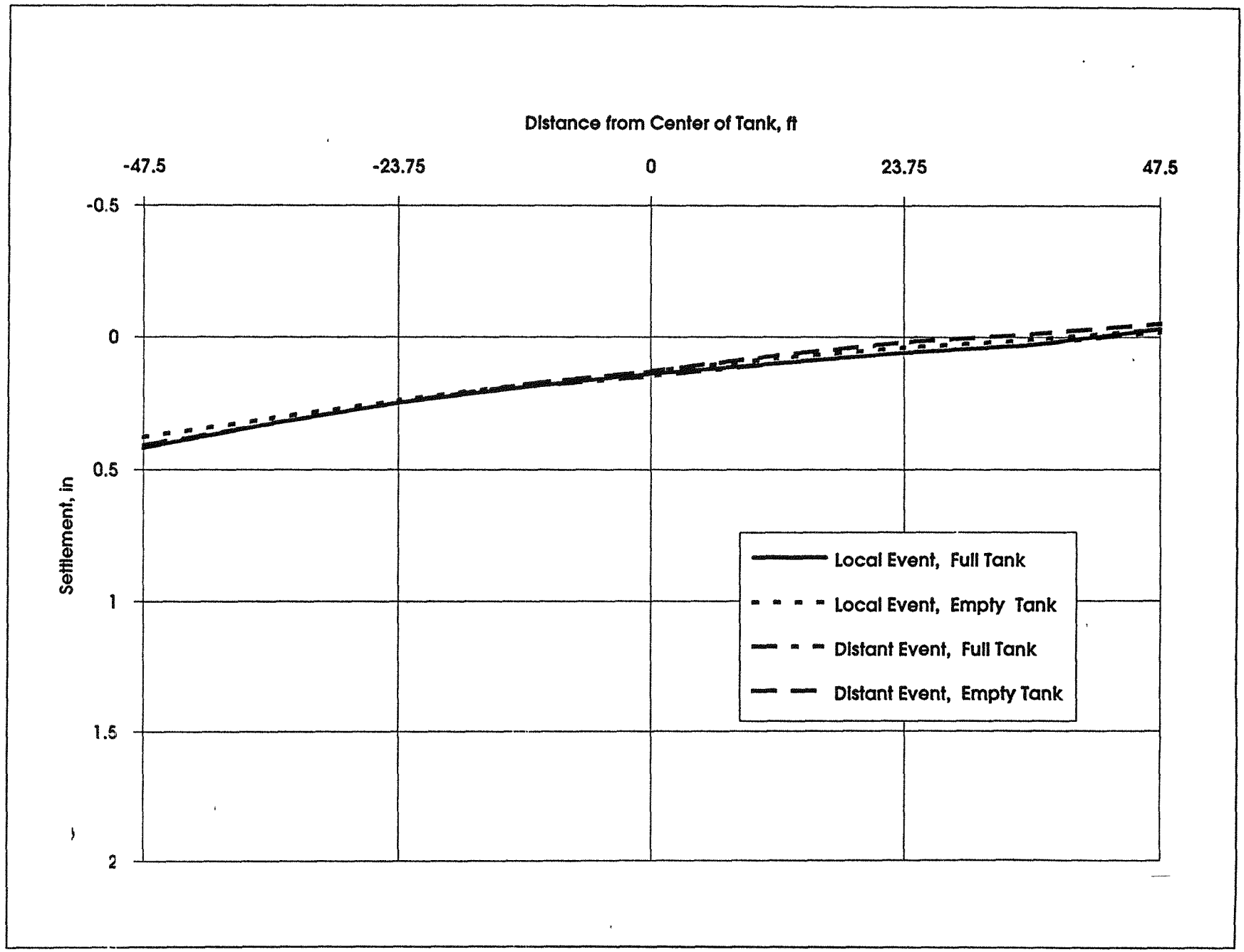


Figure 7.5-79 Settlement profile for Tank 49, EBE local and distant events, with 4.5 in compression of soft zones, tank full and empty conditions, profile A-A'

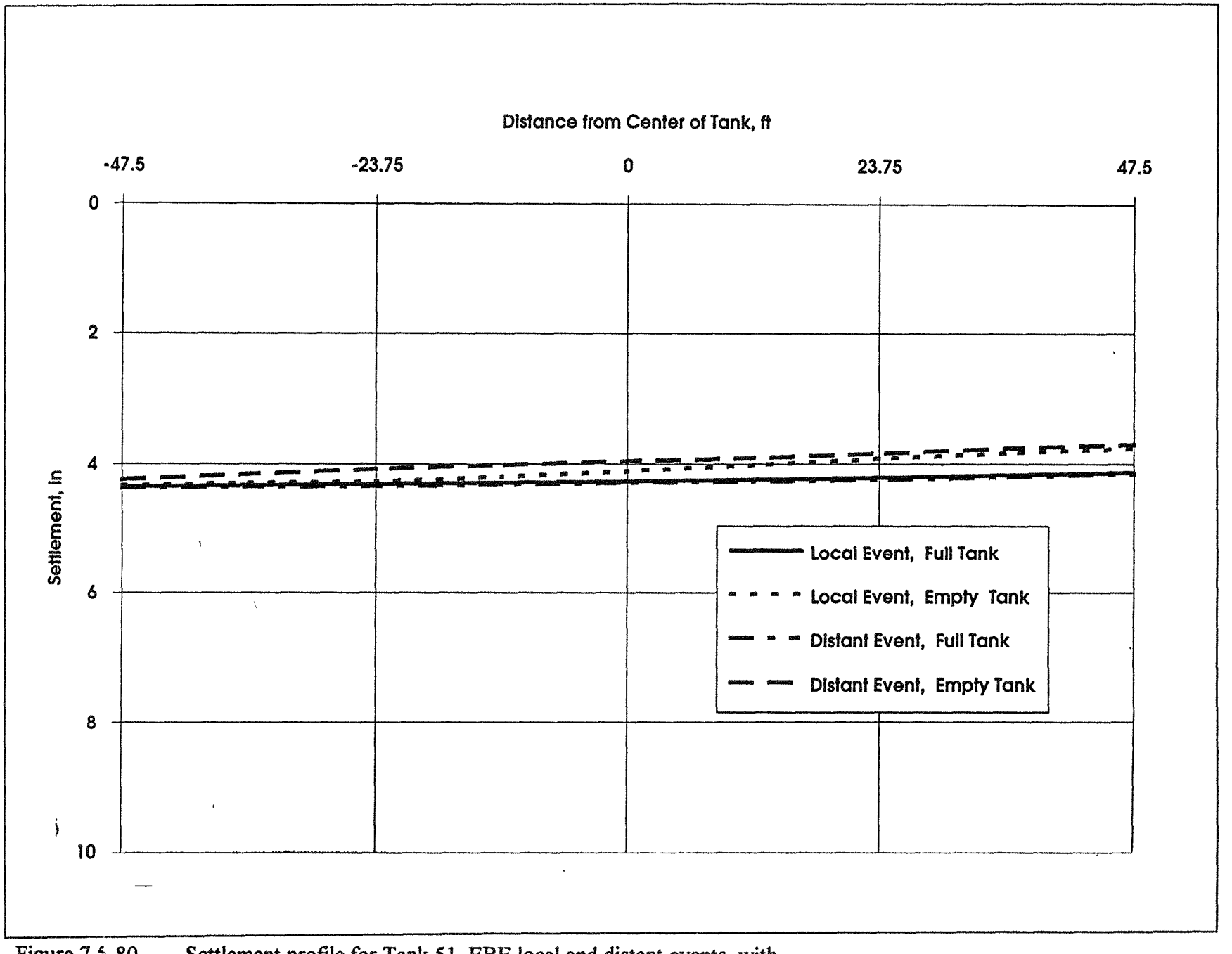


Figure 7.5-80 Settlement profile for Tank 51, EBE local and distant events, with 4.5 in compression of soft zones, tank full and empty conditions, profile A-A'

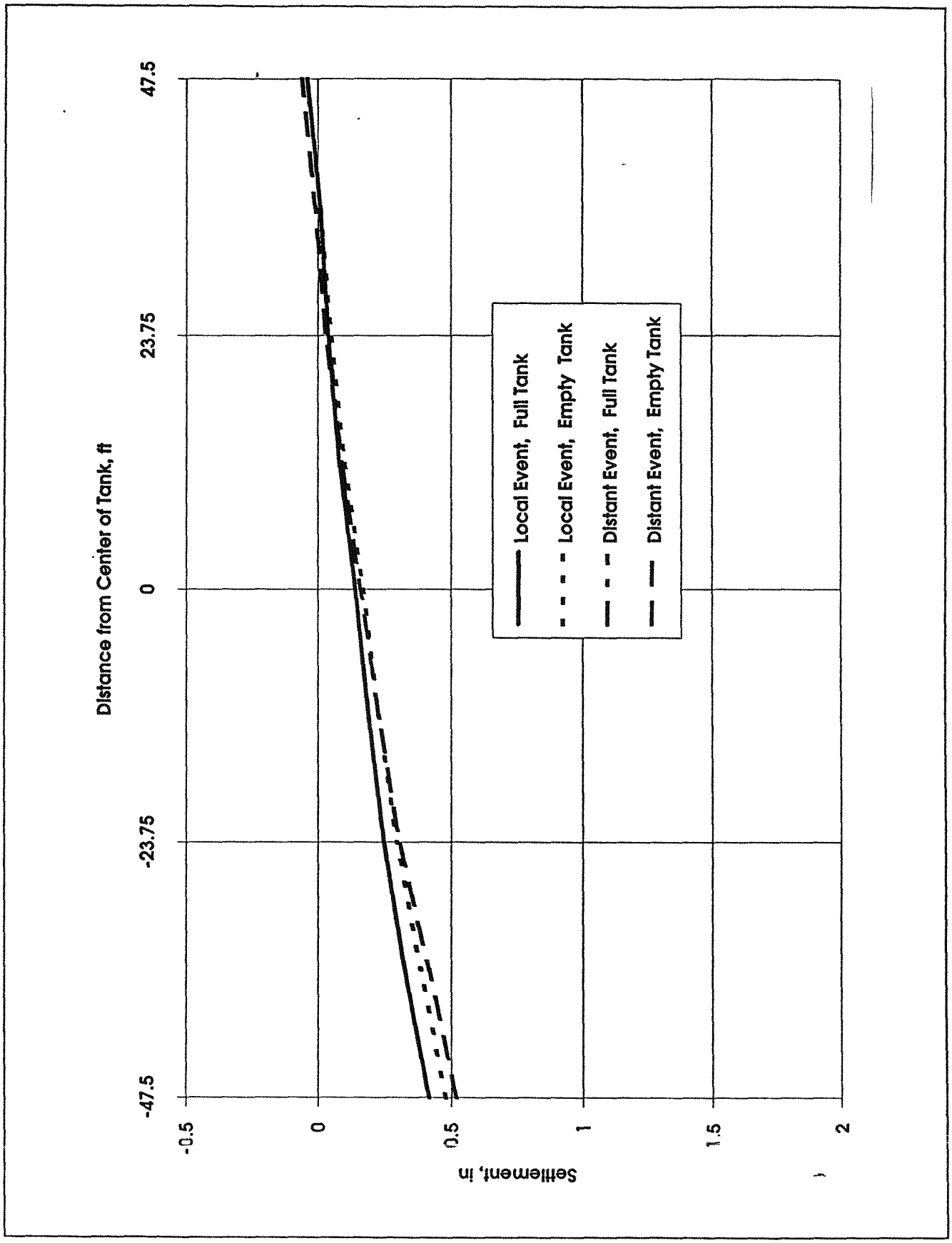


Figure 7.5-81 Settlement profile for Tank 49, EBE local and distant events, with 7 in compression of soft zones, tank full and empty conditions, profile A A'

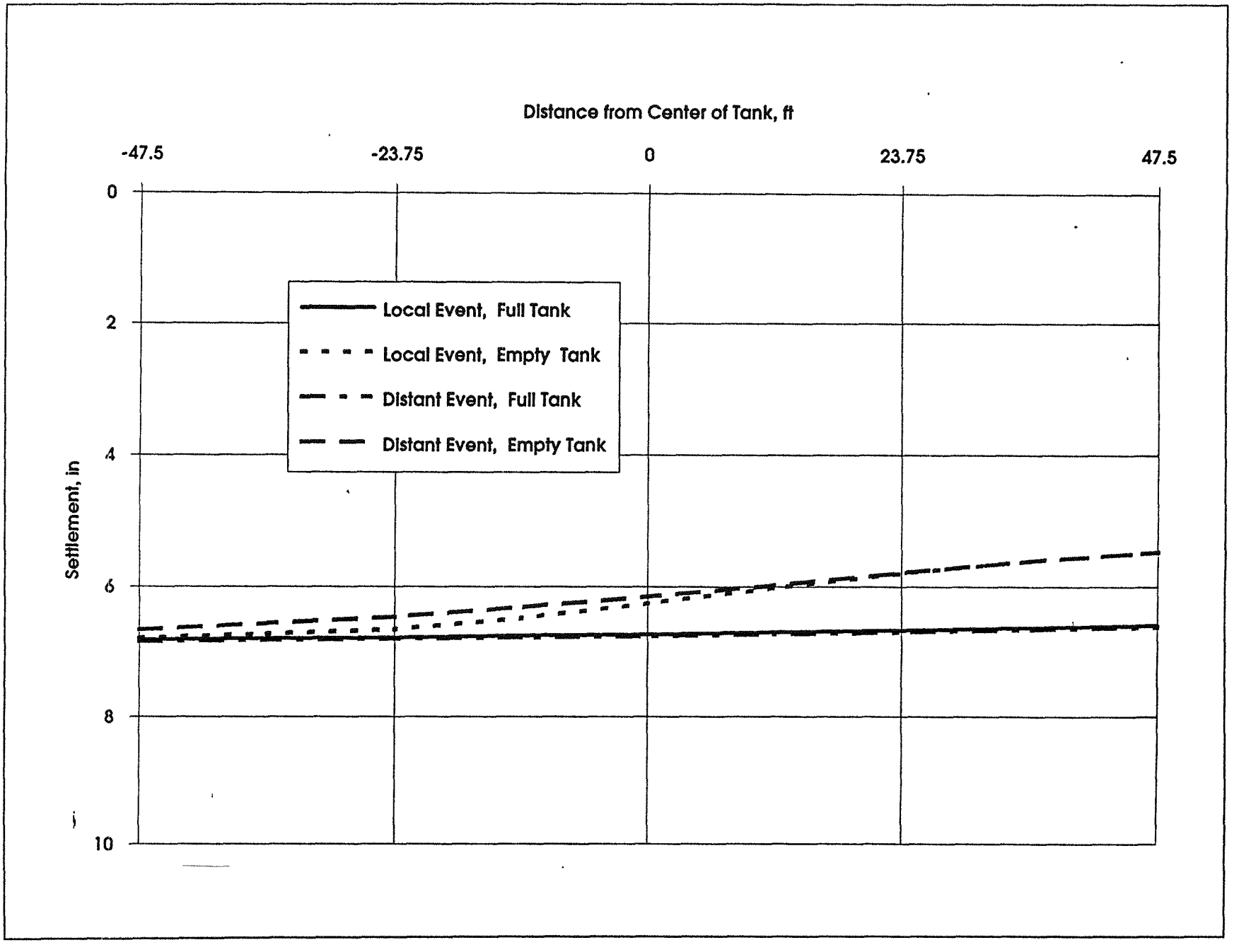


Figure 7.5-82 Settlement profile for Tank 51, EBE local and distant events, with 7 in compression of soft zones, tank full and empty conditions, profile A-A'

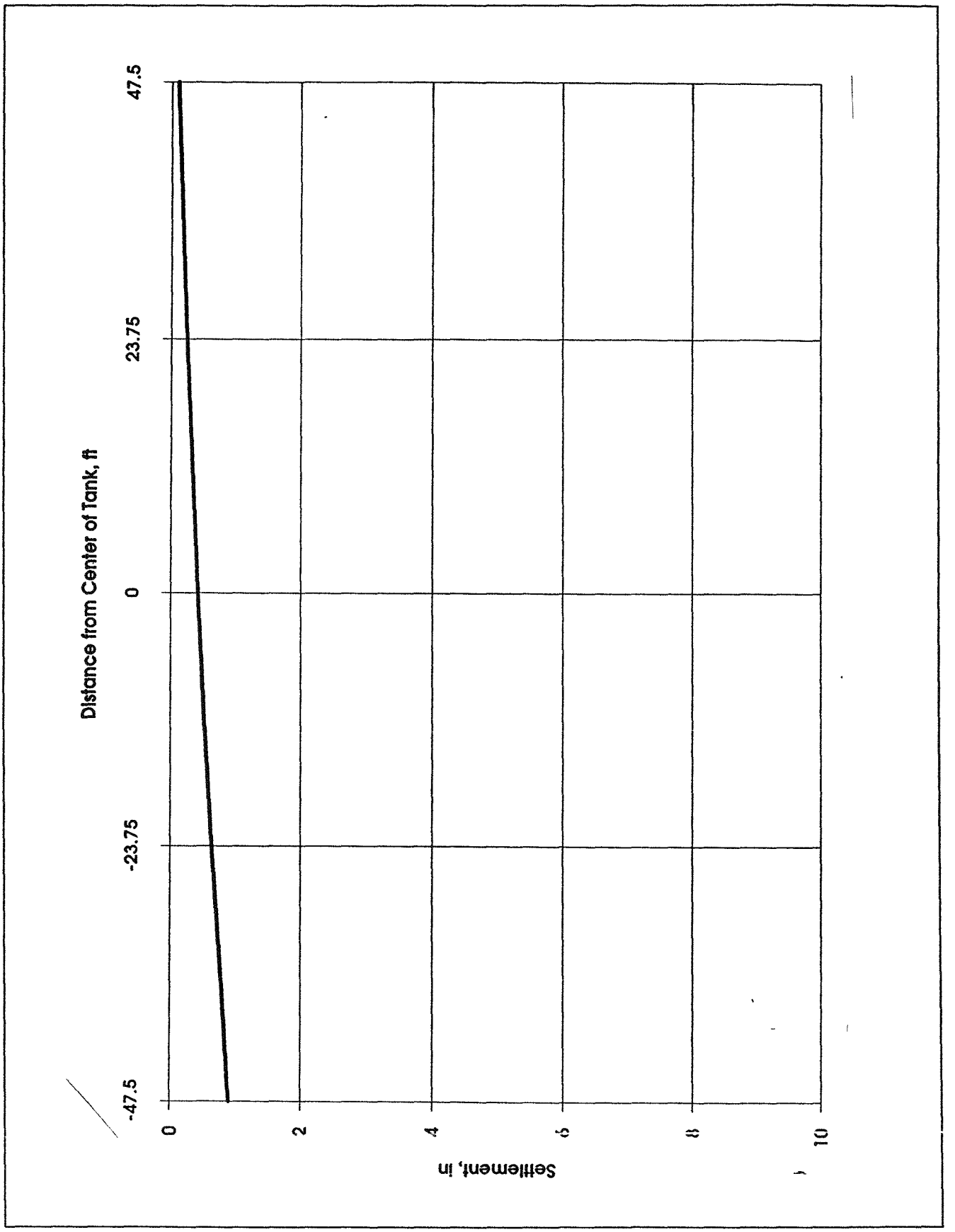


Figure 7.5-83 Settlement profile for Tank 49, EBE local event, with variable compression of soft zones, tank full condition, profile AA'.

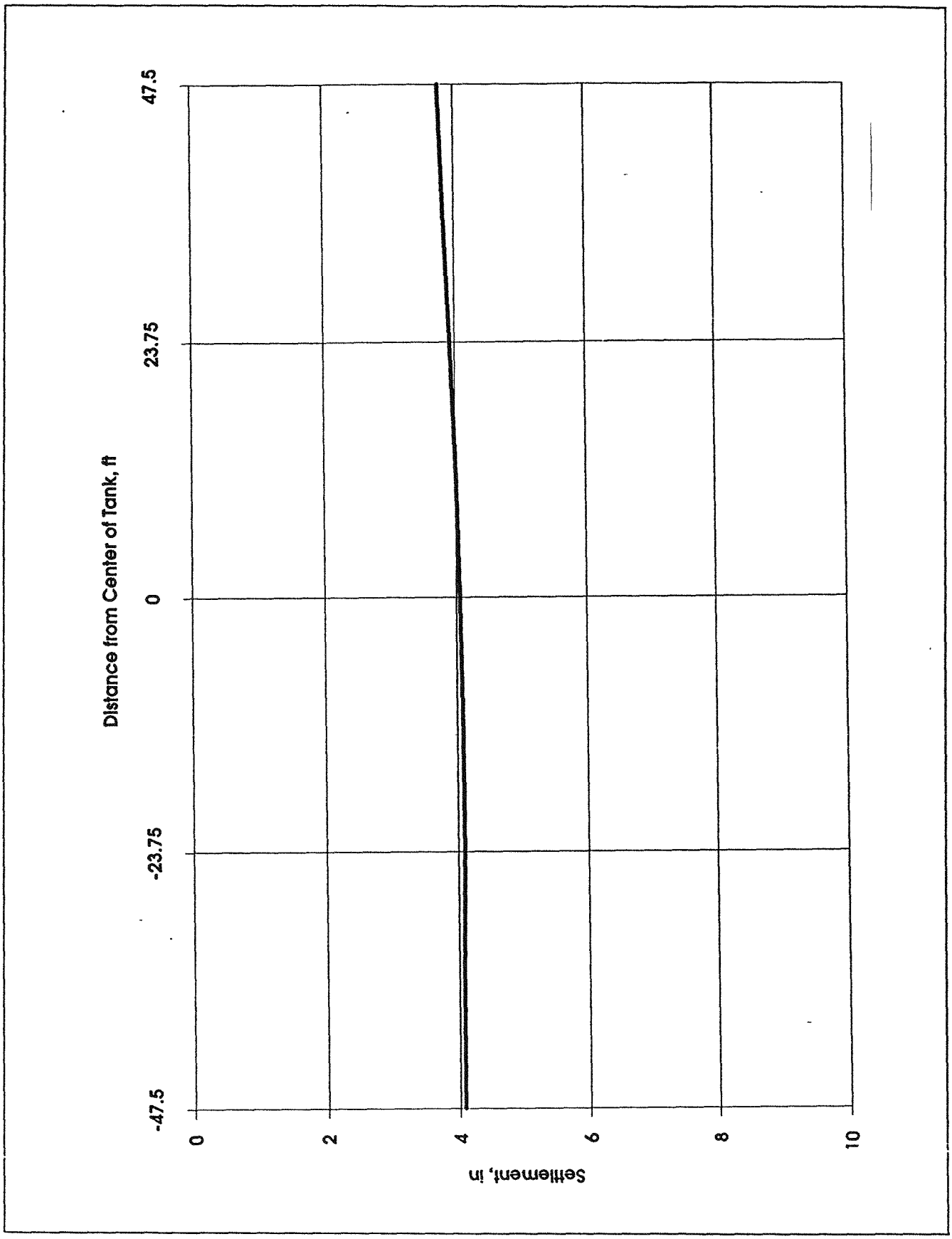


Figure 7.5-84 Settlement profile for Tank 51, EBE local event, with variable compression of soft zones, tank full condition, profile AA'.

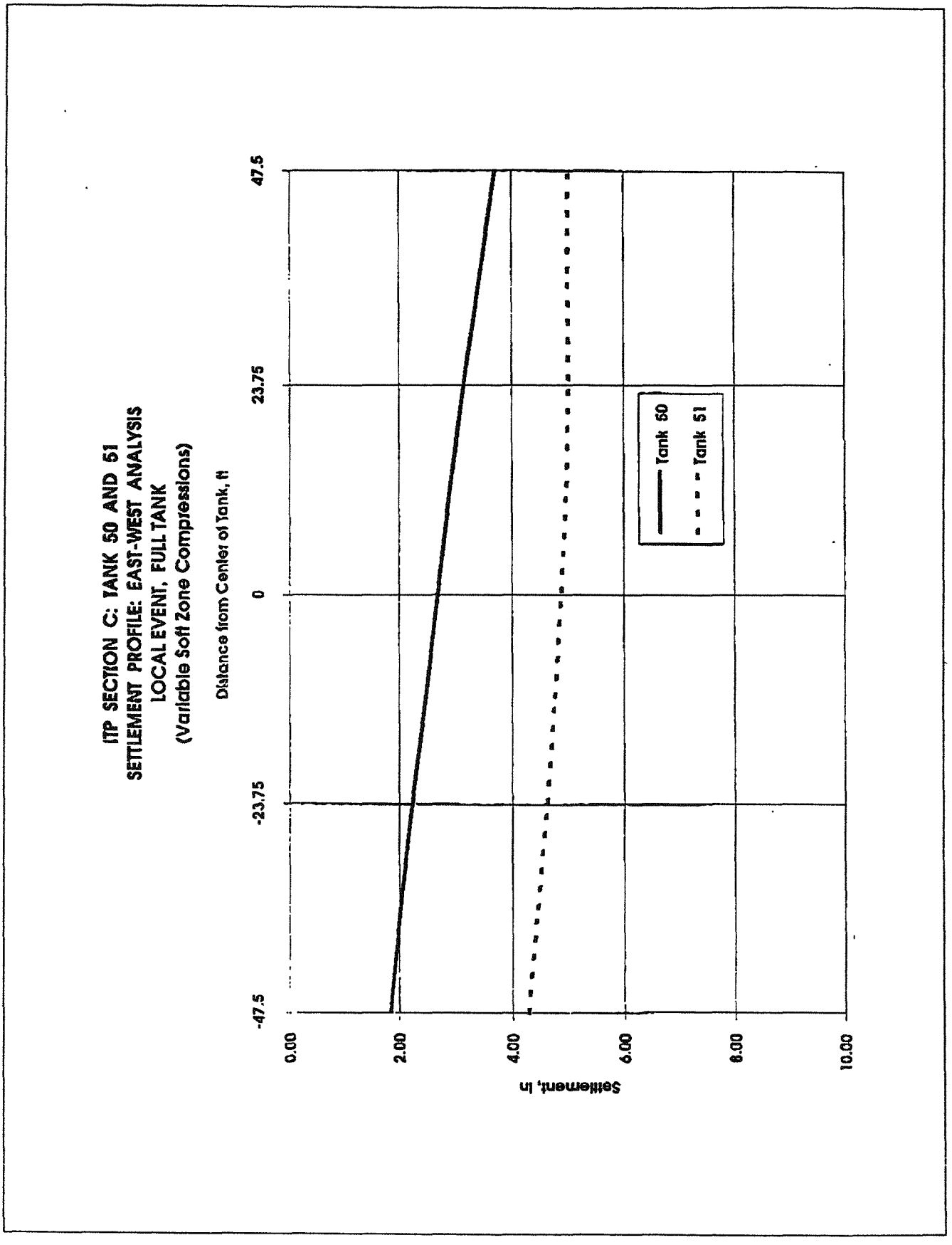


Figure 7.5-85 Settlement profile for Tanks 50 and 51, EBE local event, with variable compression of soft zones, tank full condition, profile CC'.

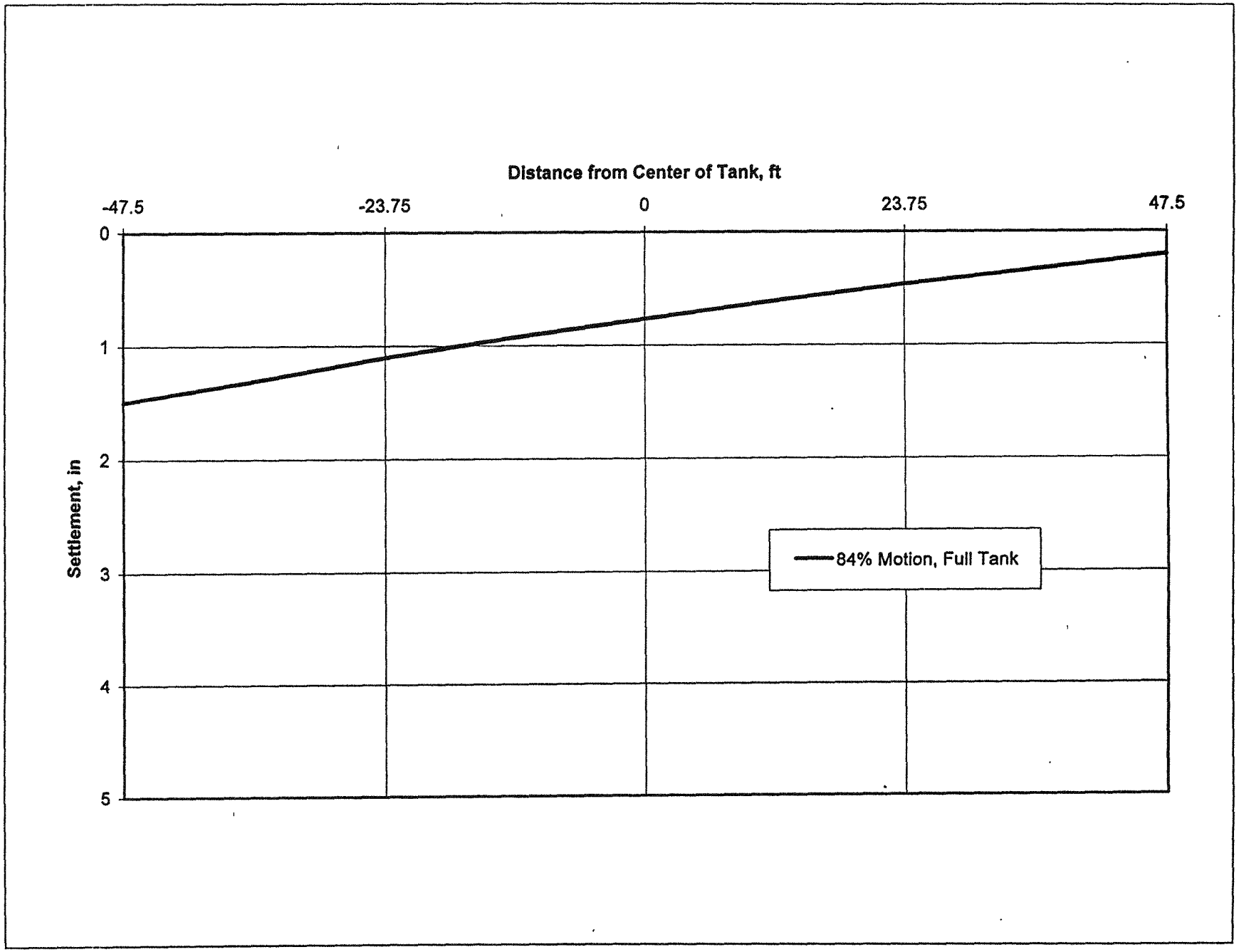


Figure 7.5-86 Settlement profile for Tank 49, 84th percentile motion, with variable compression of soft zones, tank full condition, profile AA'.

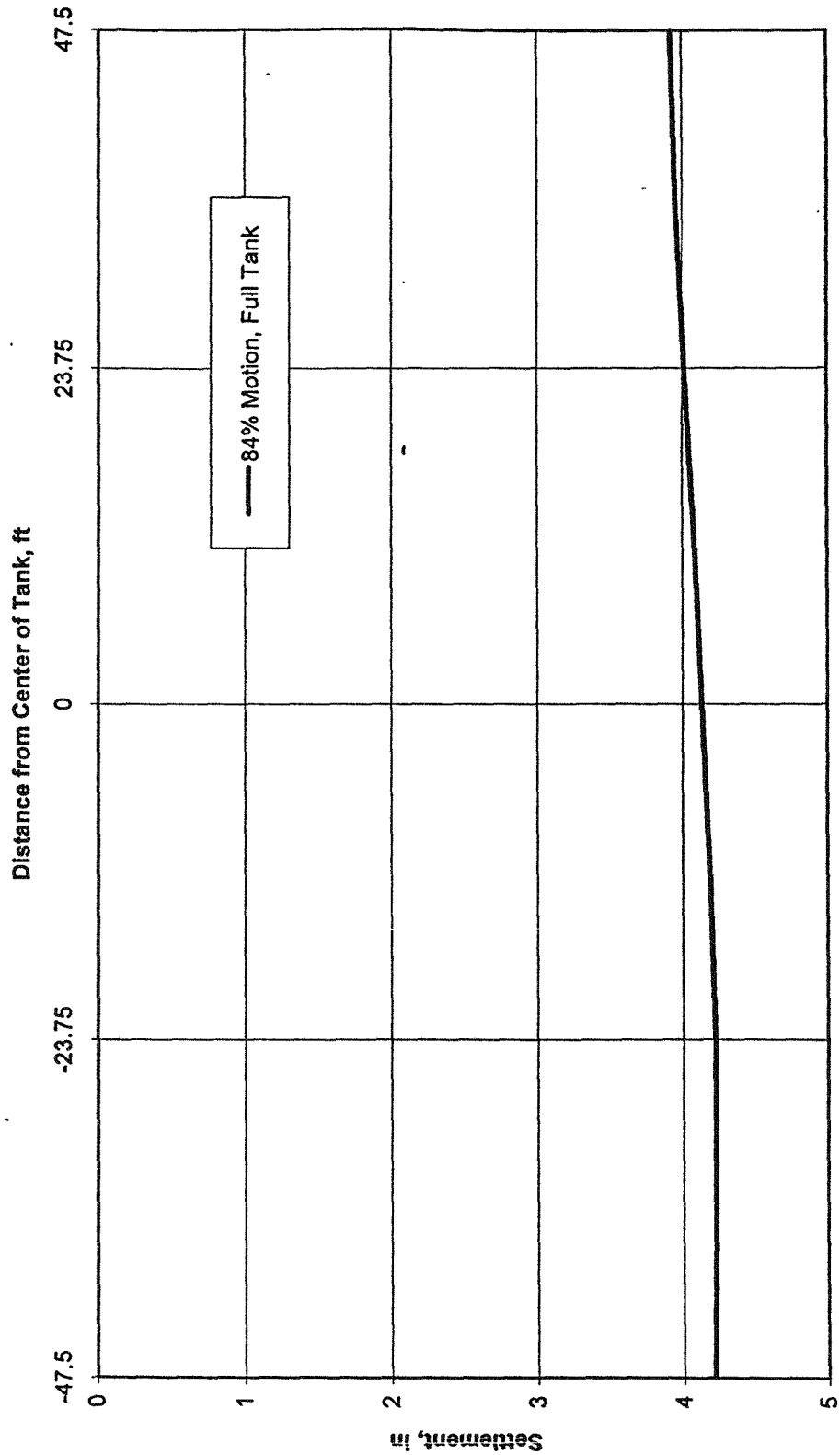


Figure 7.5-87 Settlement profile for Tank 51, 84th percentile motion, with variable compression of soft zones, tank full condition, profile AA'

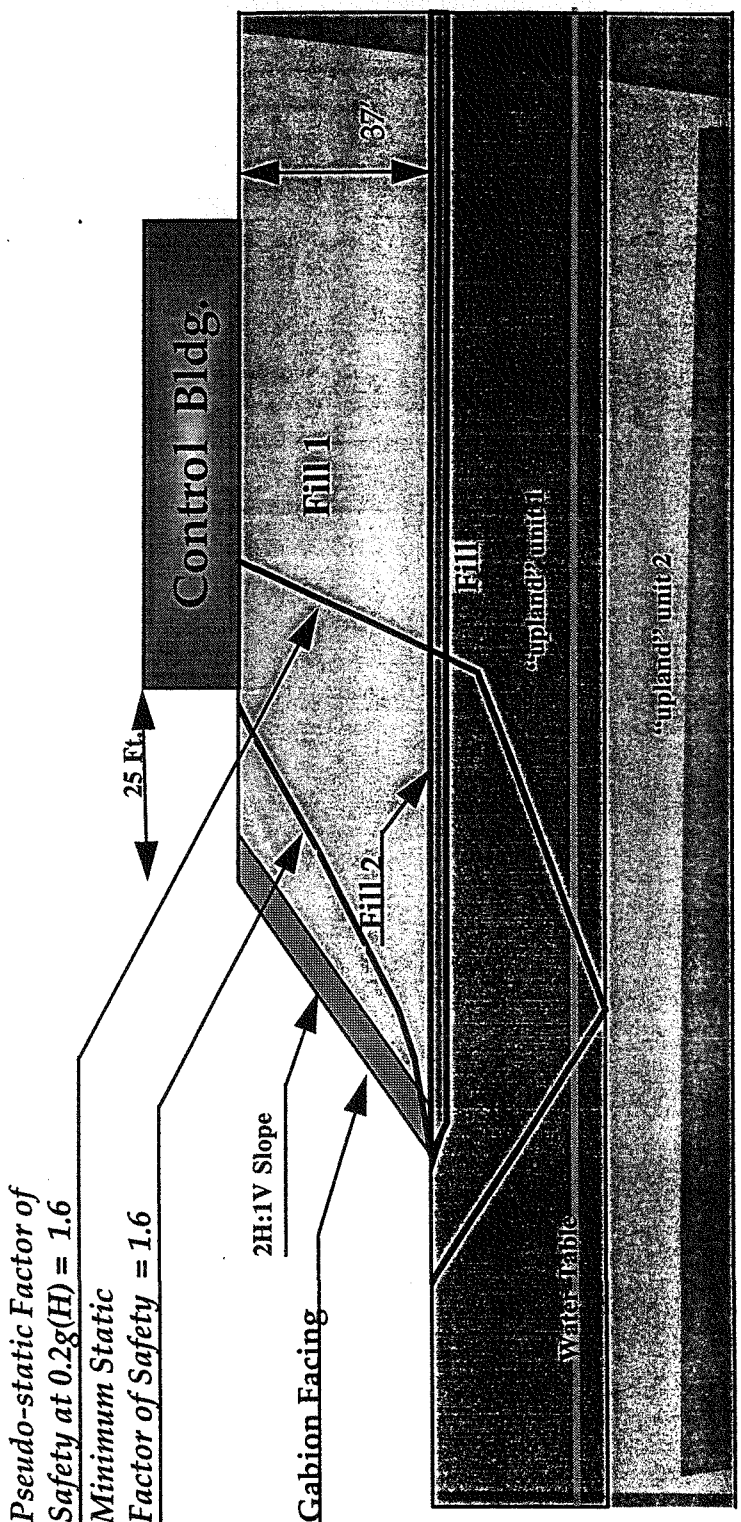


Figure 8.2-1 Slope stability - cross-section 1.

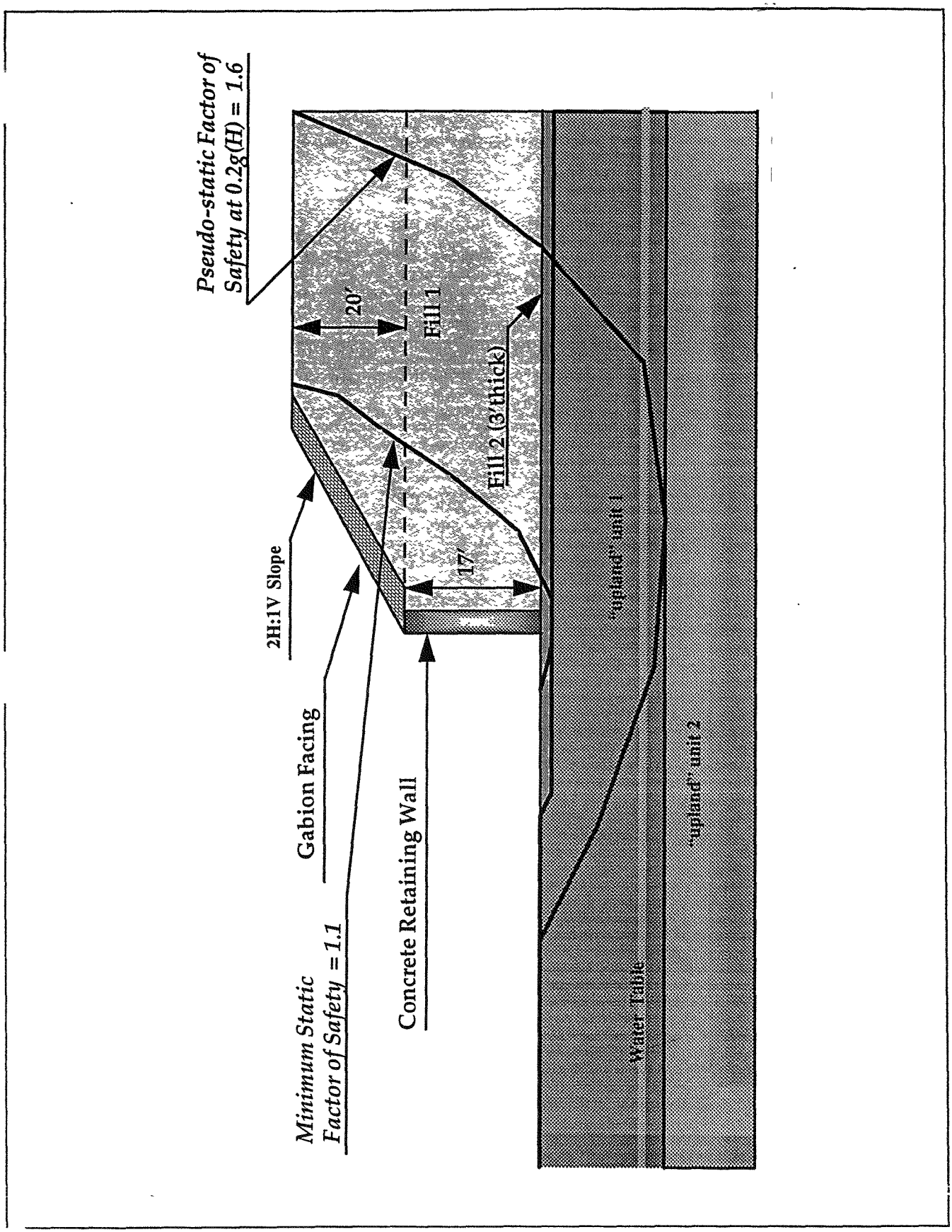


Figure 8.2-2 Slope stability - cross-section 2.

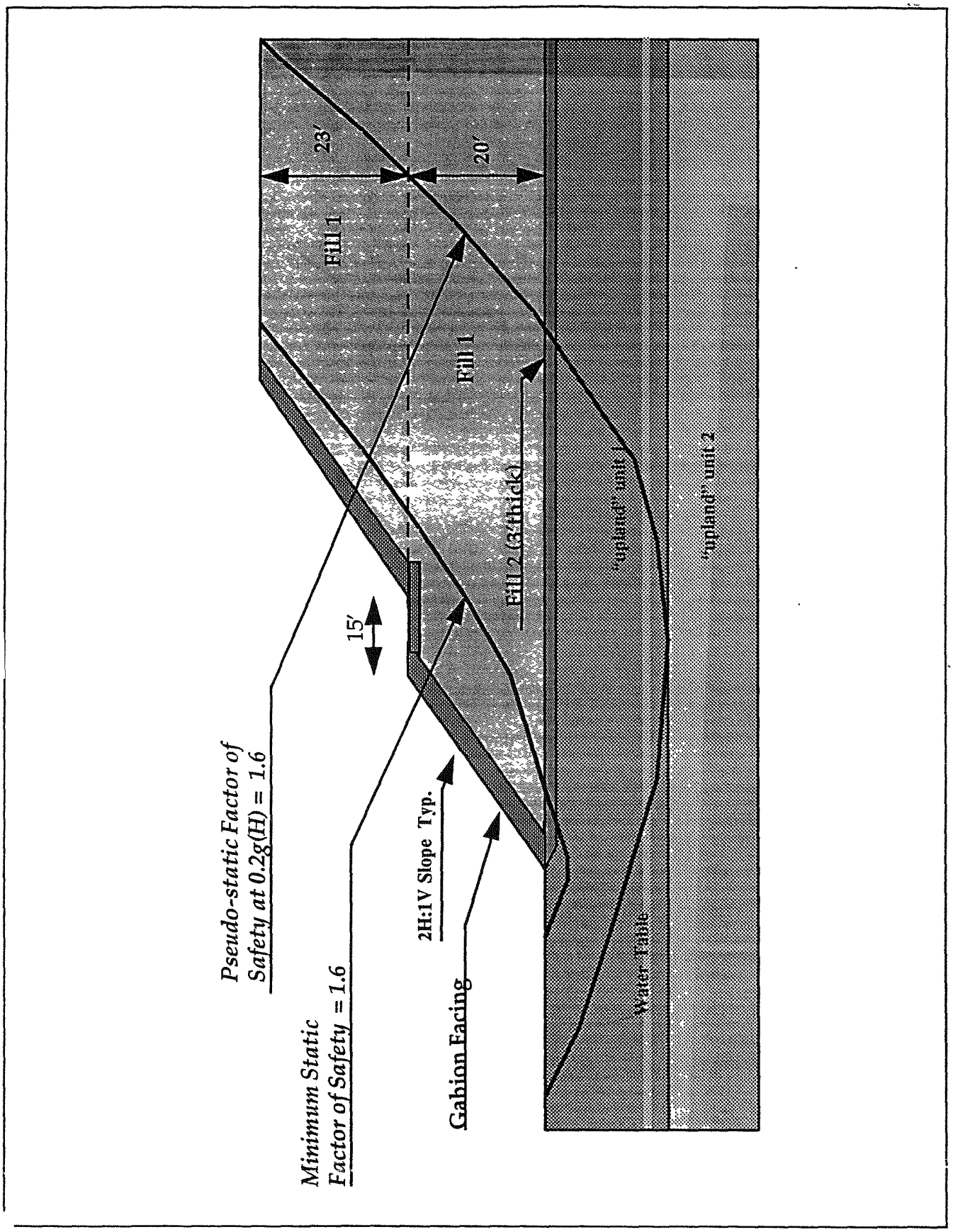


Figure 8.2-3 Slope stability - cross-section 3.

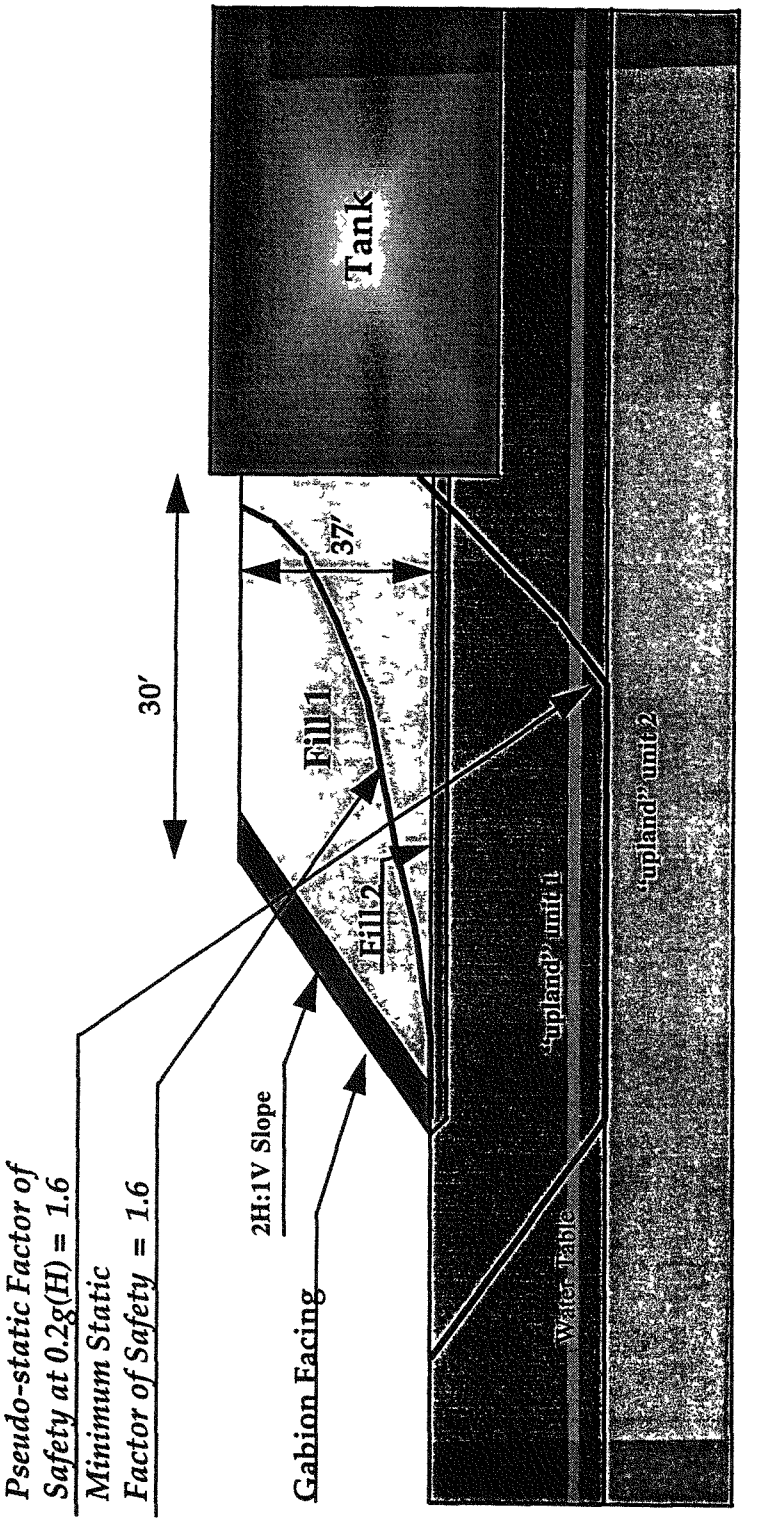


Figure 8.2-4 Slope stability - cross-section 4.

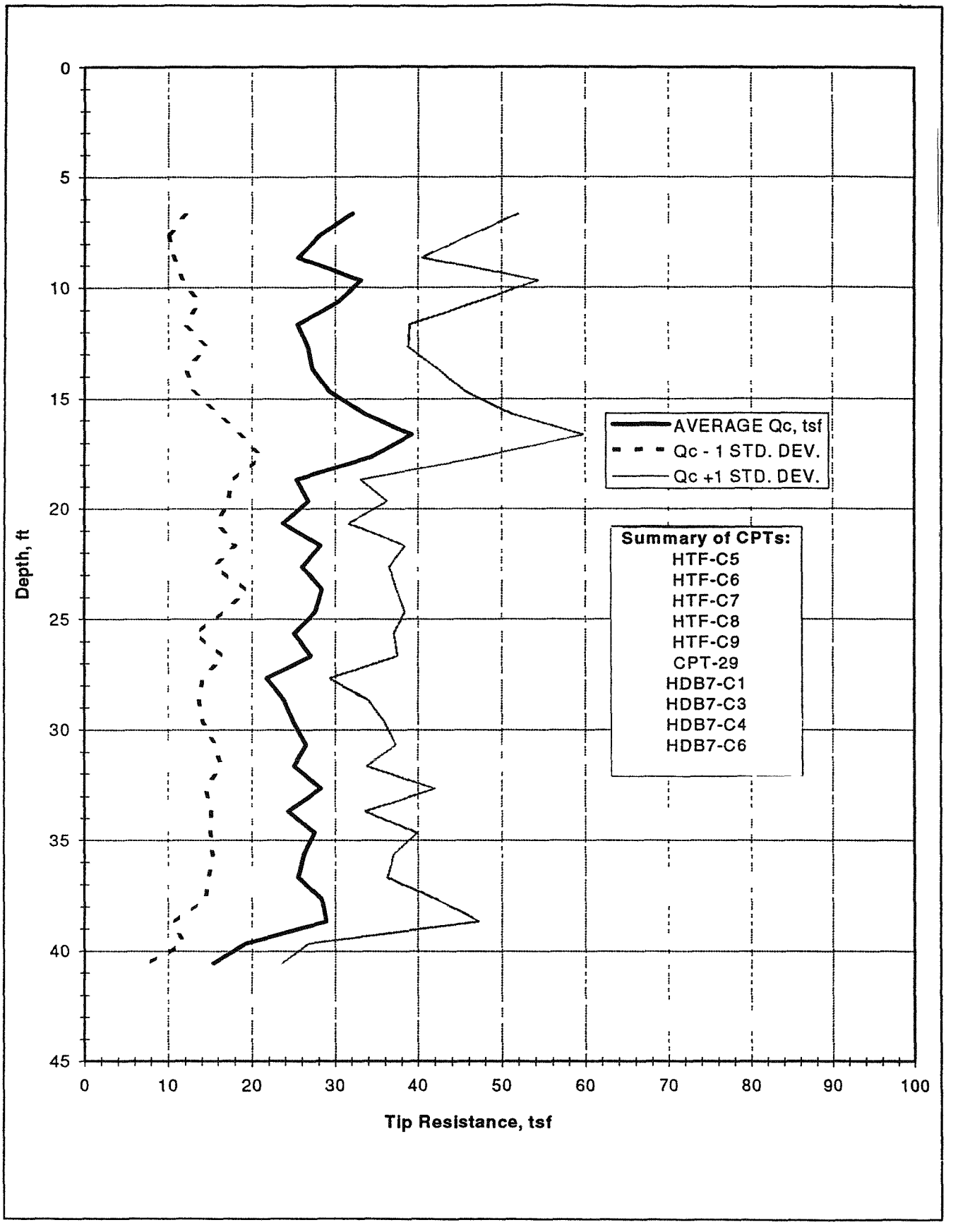


Figure 8.2-5 Summary of tip resistances for CPTs in north hill area.

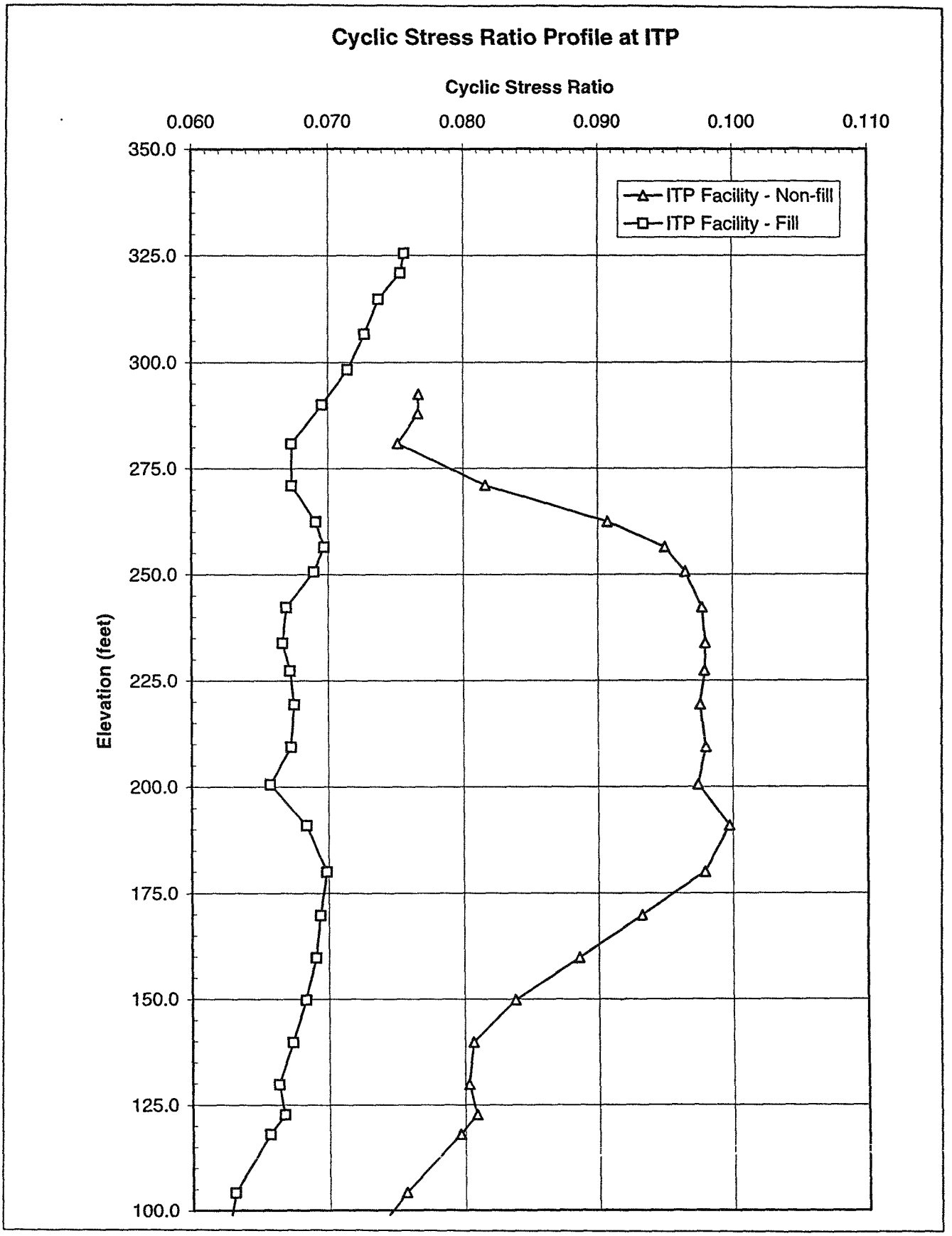


Figure 8.3-1 Cyclic shear stress ratio profile for ITP 1-D liquefaction settlement analysis.

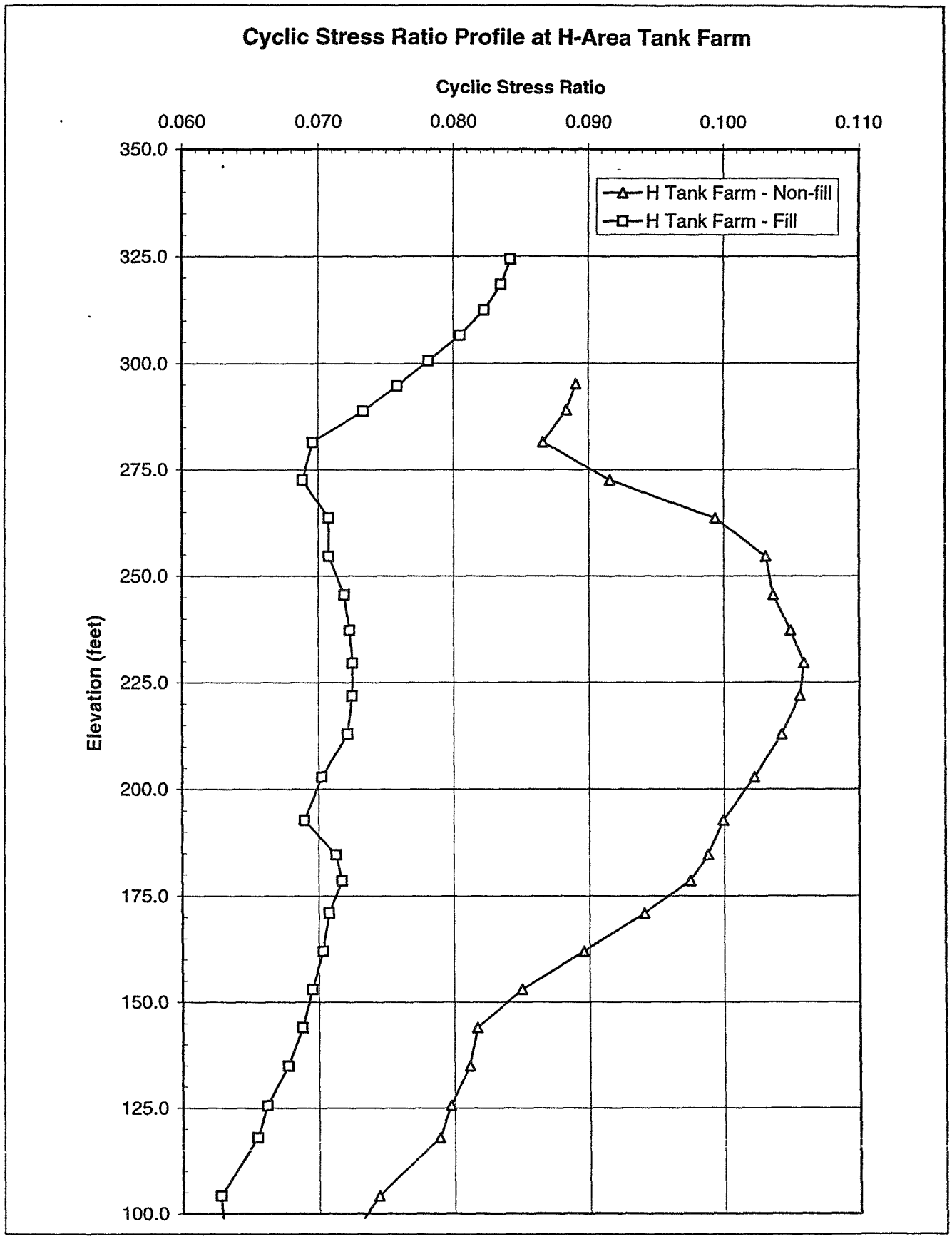


Figure 8.3-2 Cyclic shear stress ratio profile for HTF 1-D liquefaction settlement analysis.

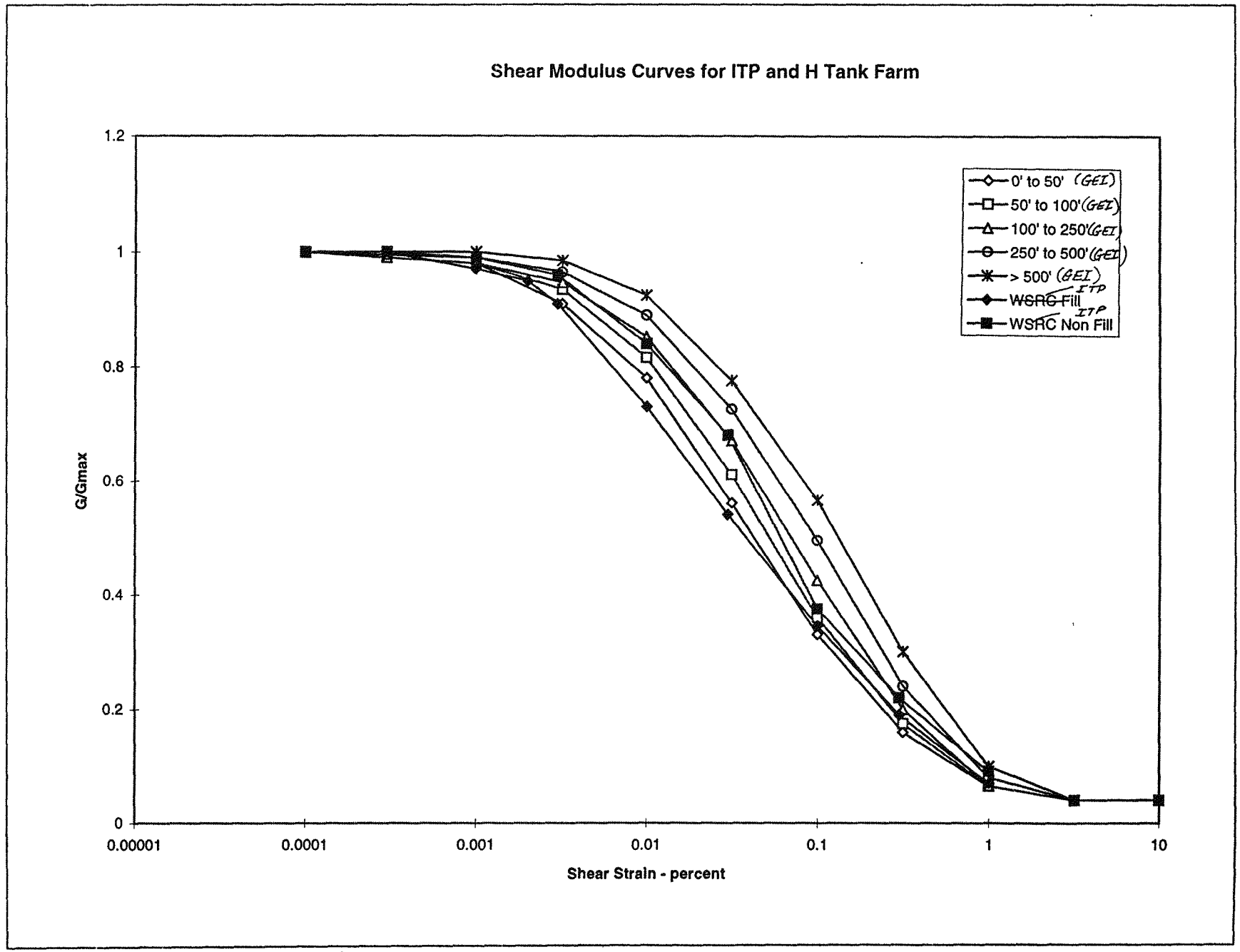


Figure 8.3-3 Comparison of shear modulus curves developed for ITP with those used by GEI.

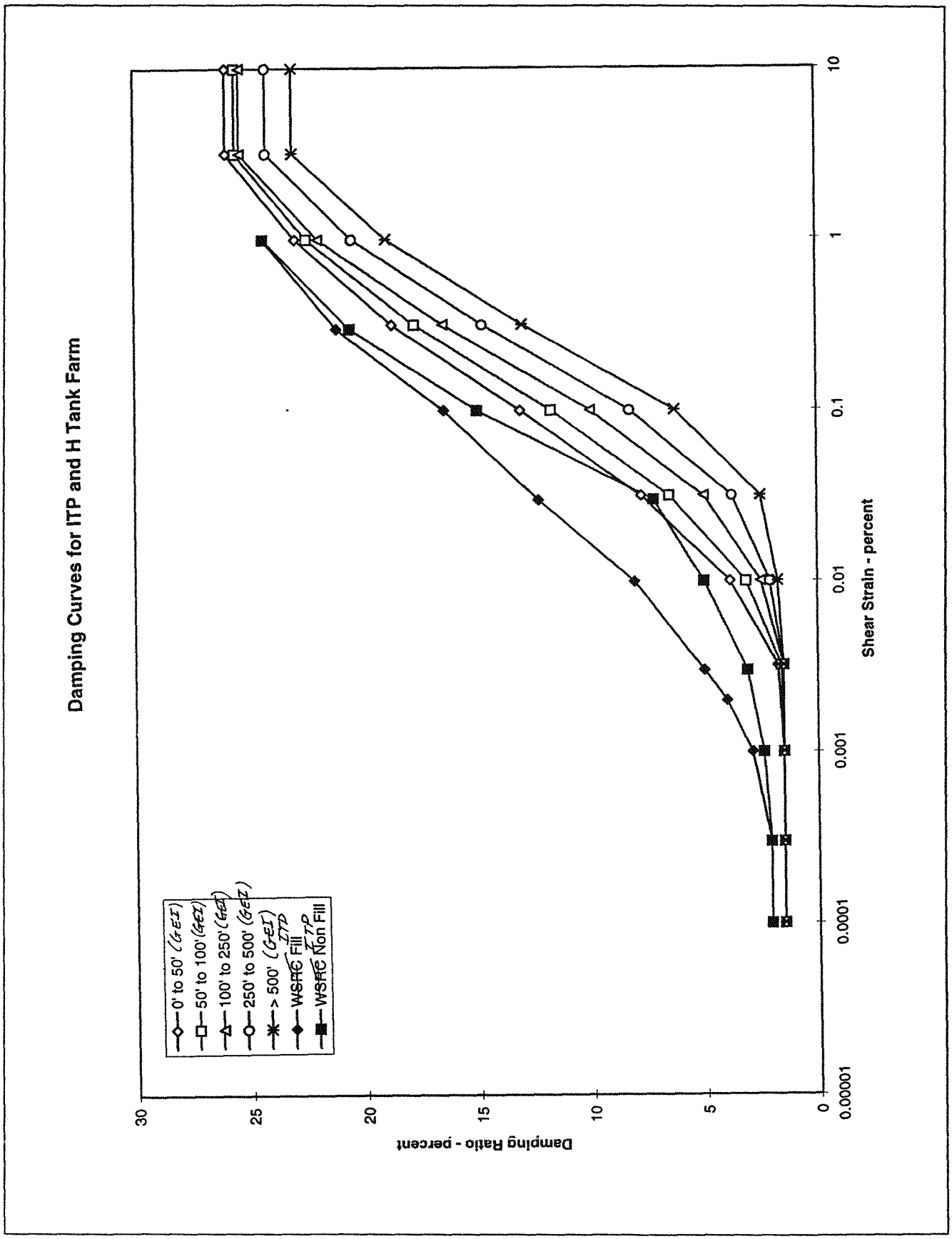


Figure 8.3-4 Comparison of damping curves developed for ITP with those used by GEI.

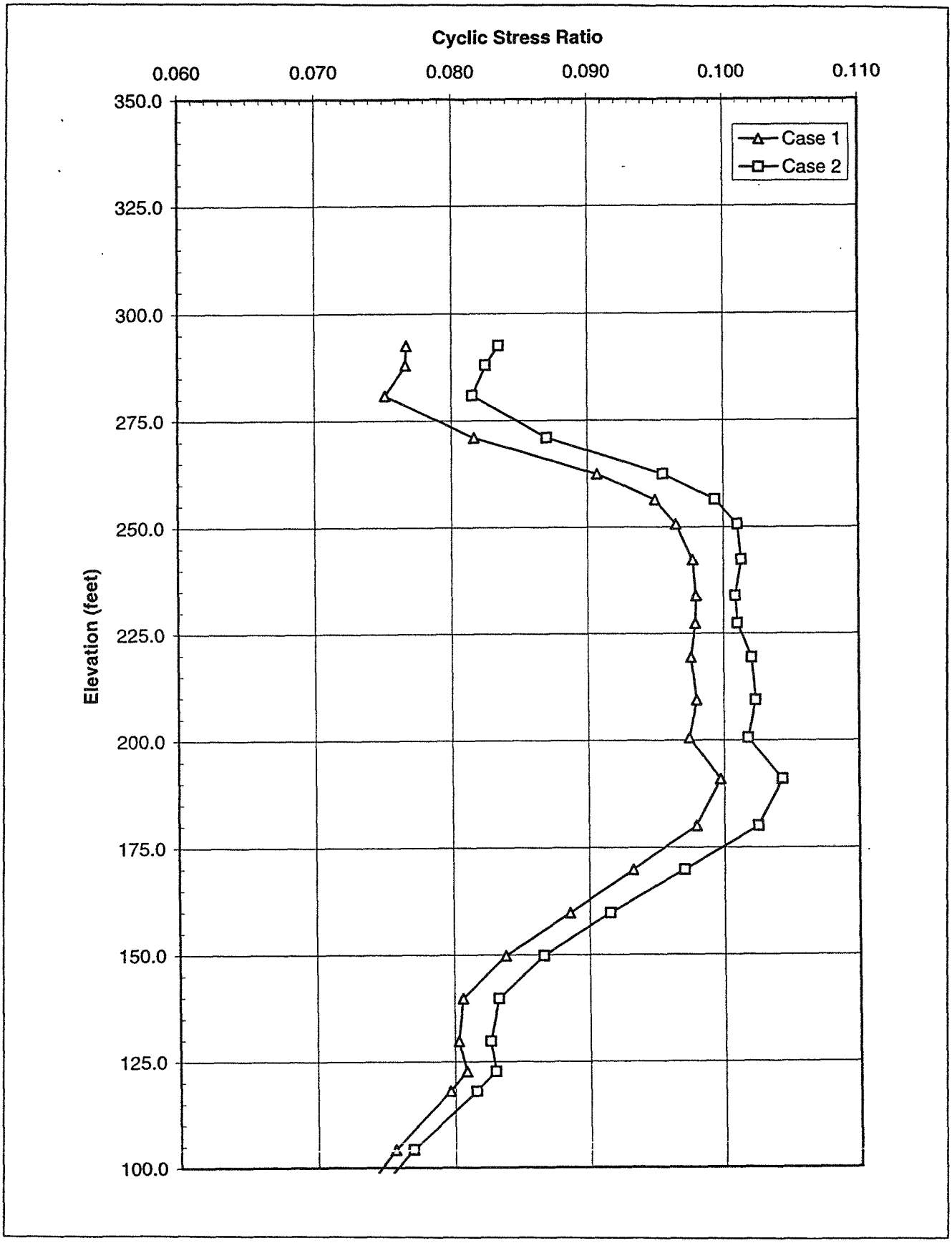


Figure 8.3-5 Comparison of cyclic stress ratio profiles for the 84th percentile ground motion using ITP and GEI dynamic curves.

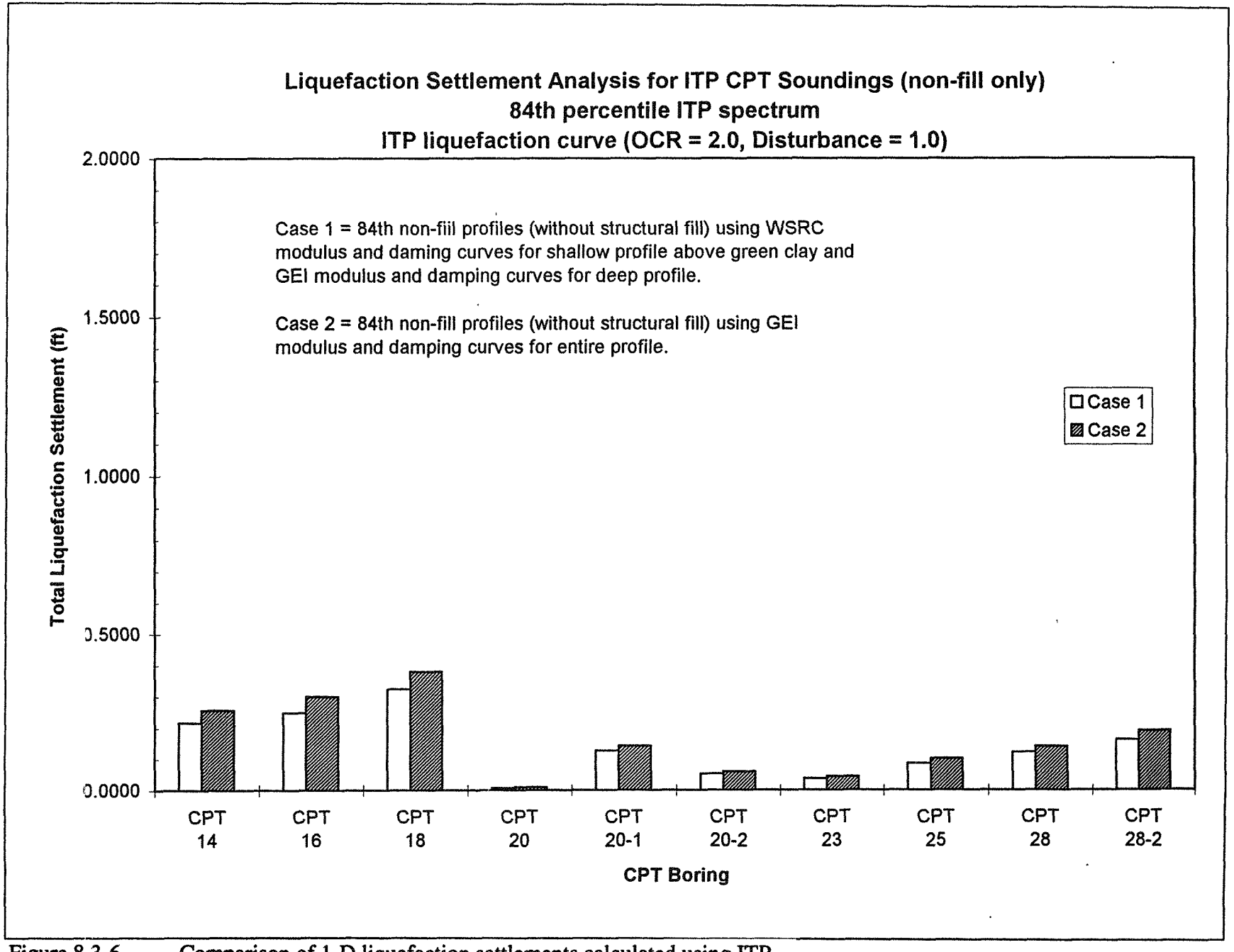


Figure 8.3-6 Comparison of 1-D liquefaction settlements calculated using ITP and GEI dynamic curves for the 84th percentile, non-fill profile at ITP.

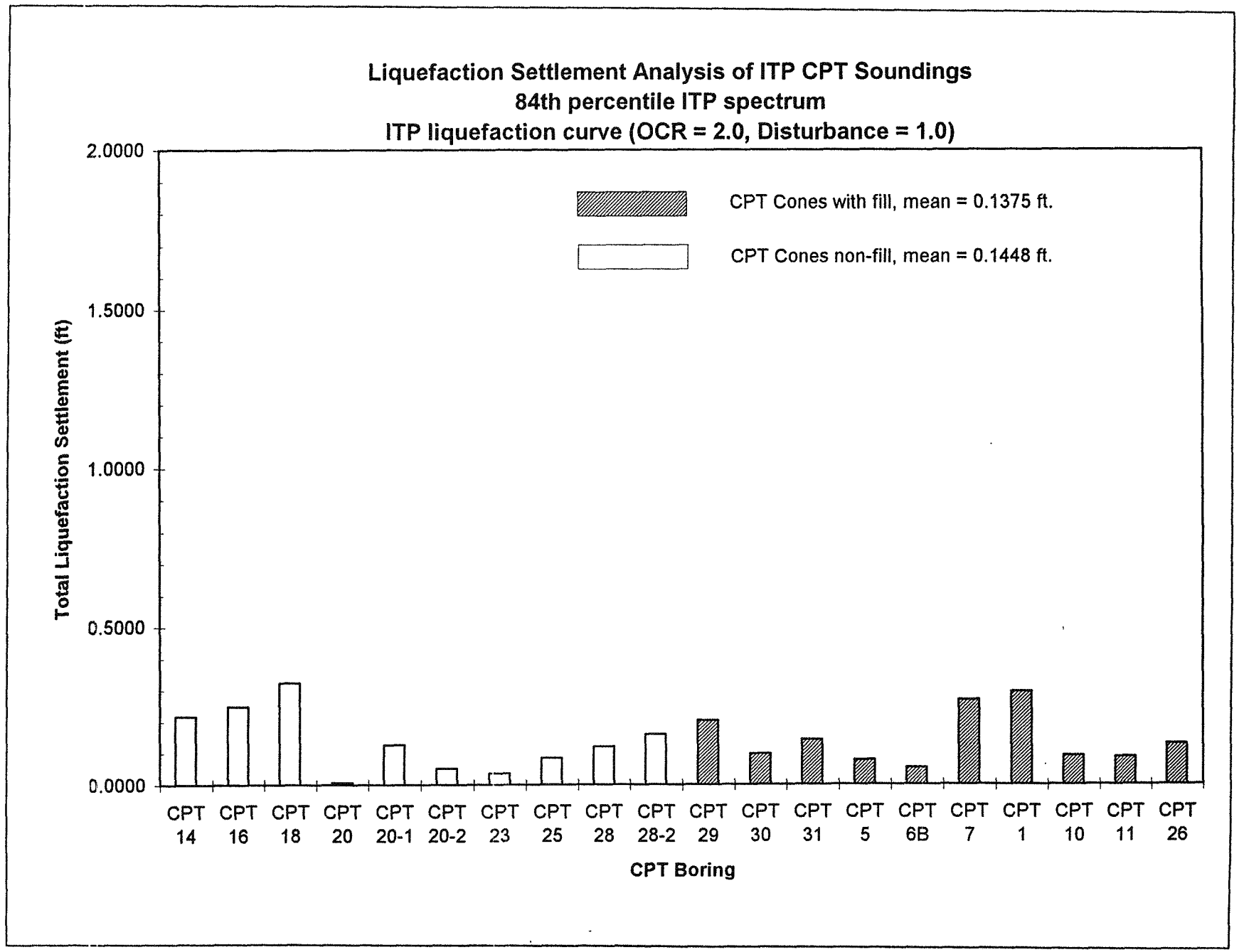


Figure 8.3-7 Summary of 1-D liquefaction settlements calculated for the 84th percentile ground motion at ITP.

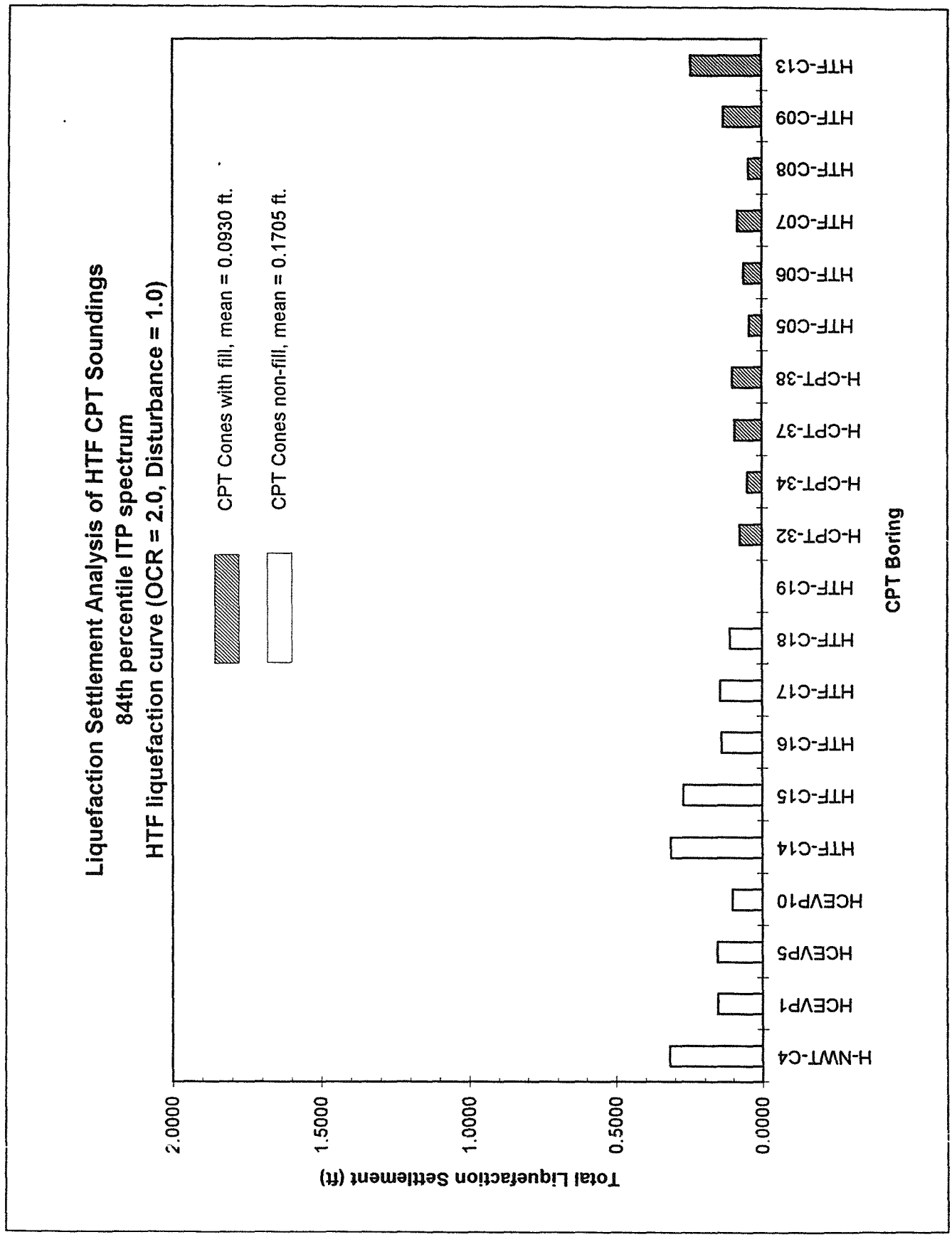


Figure 8.3-8 Summary of 1-D liquefaction settlements calculated for the 84th percentile ground motion at HTF.

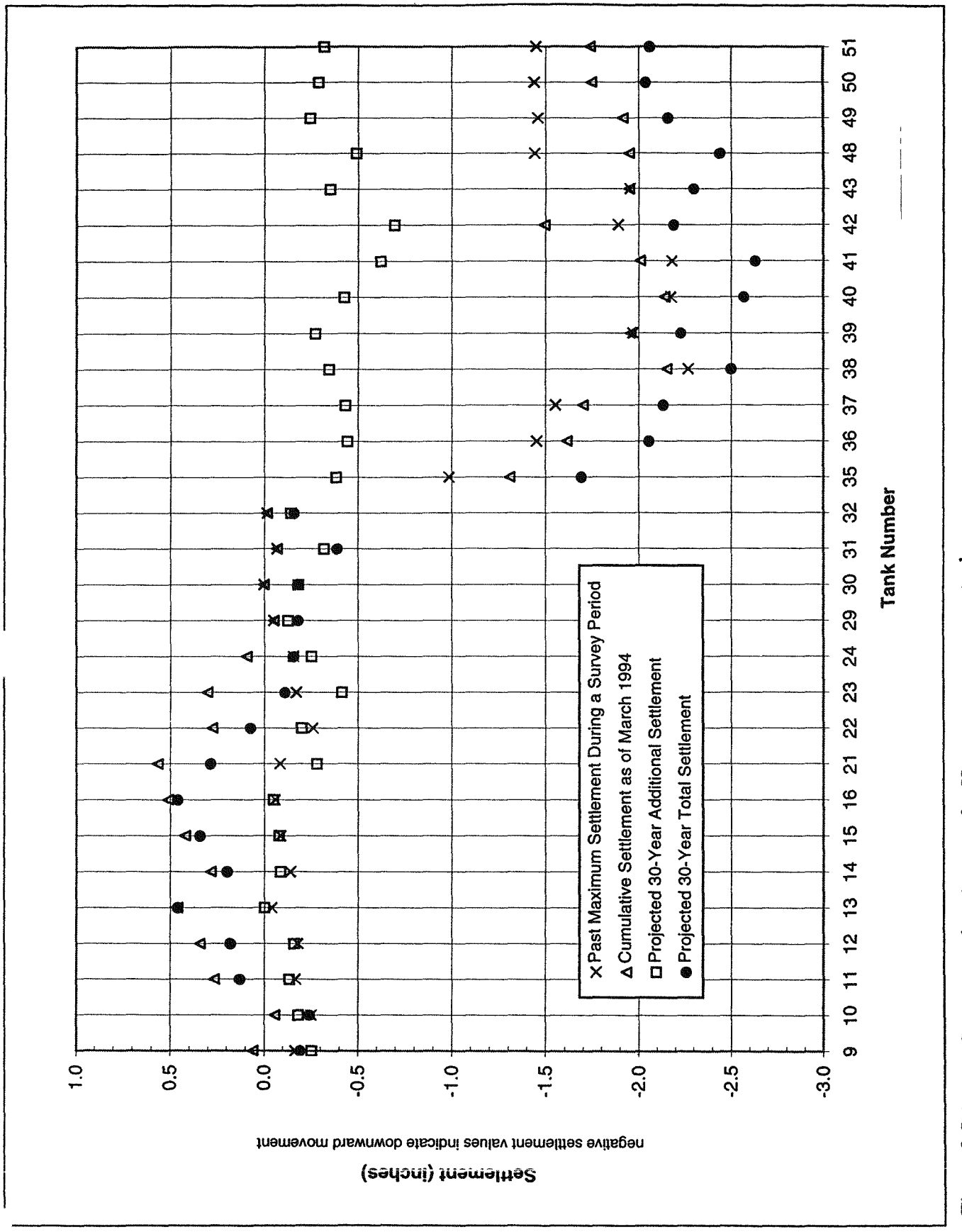


Figure 8.5-1 Summary of settlements for H-area waste storage tanks.

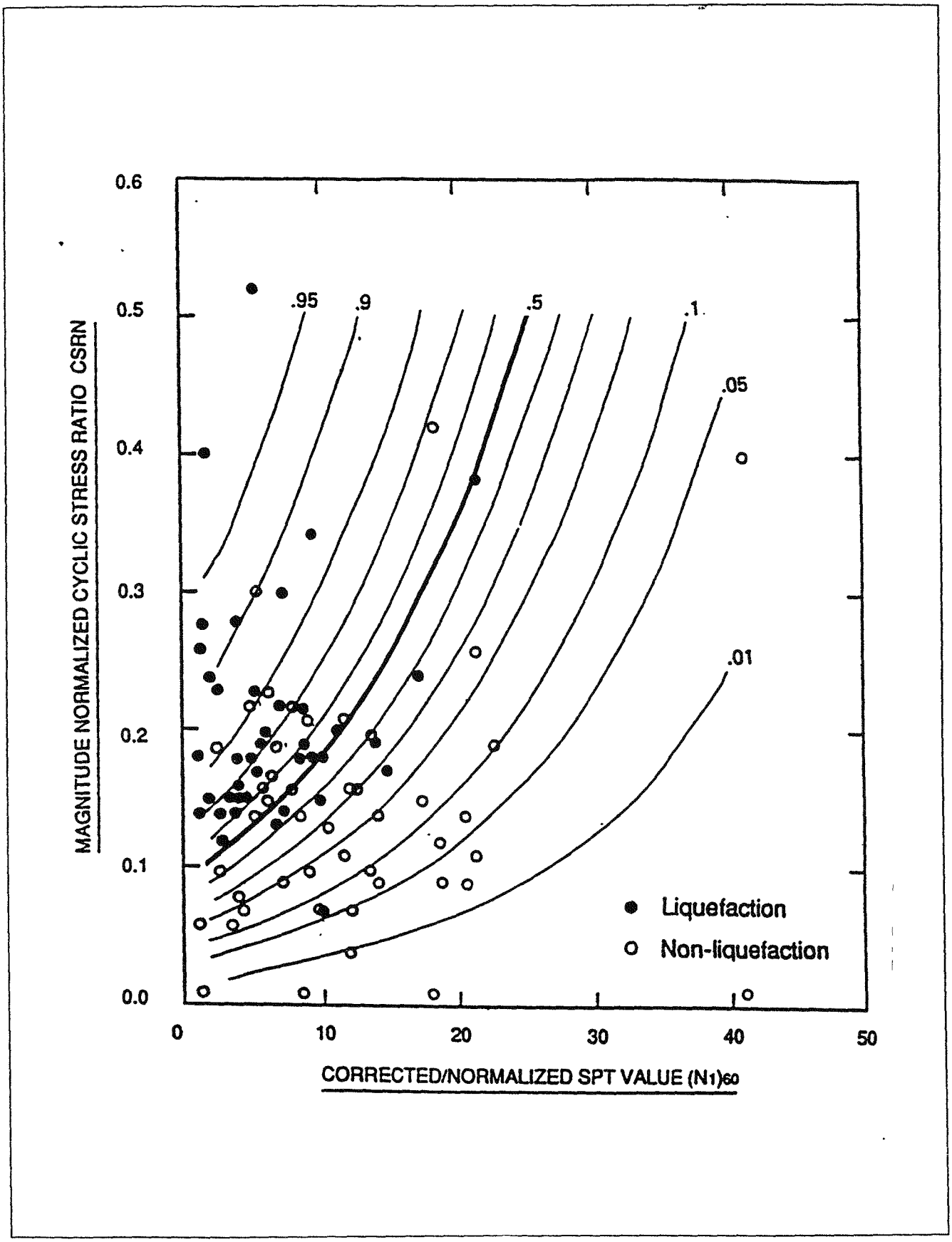


Figure 9.2-1 Contours of equal probability of liquefaction for silty sand - local model ( after Liao et al., 1988 )

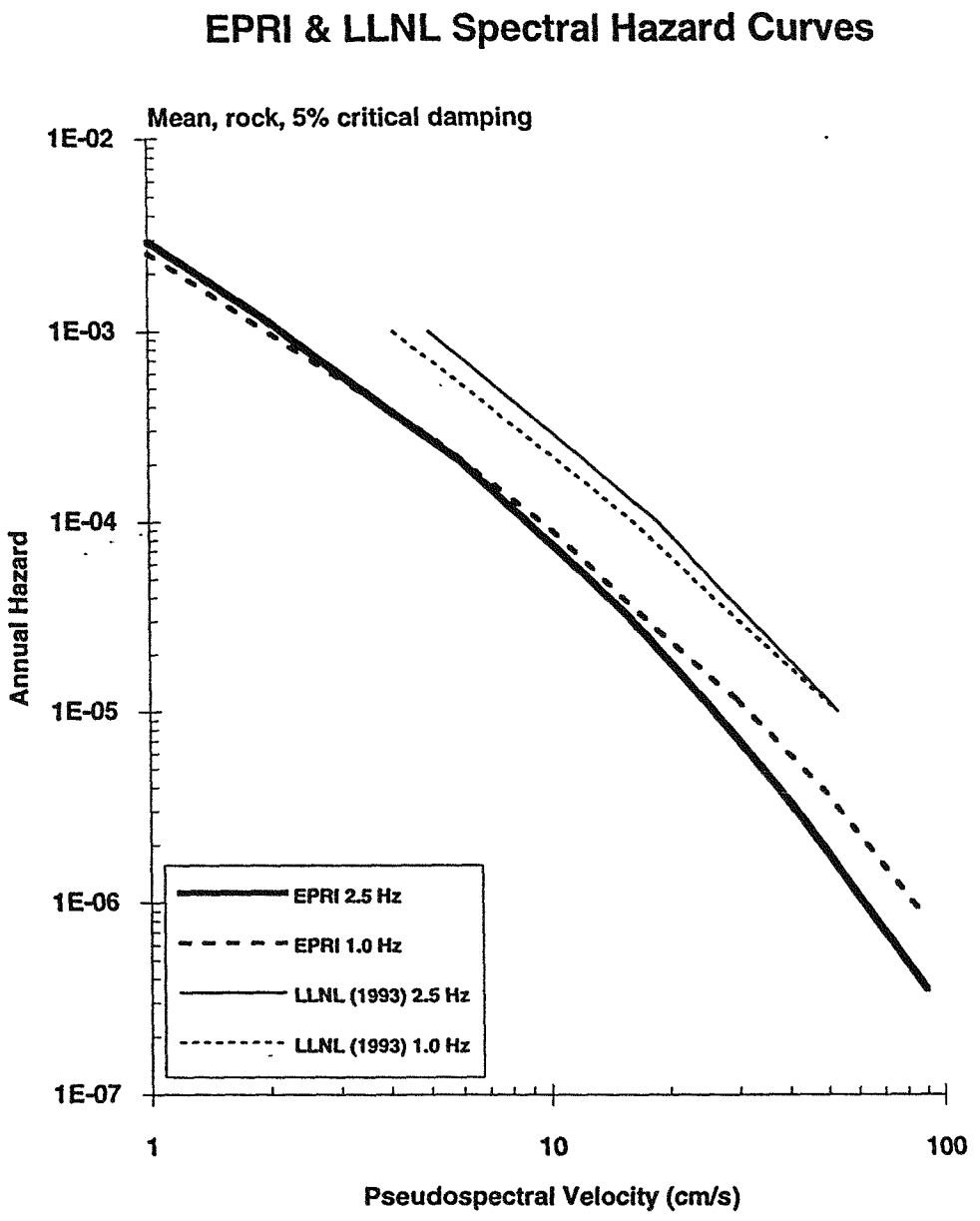


Figure 9.3-1 EPRI and LLNL spectral hazard curves

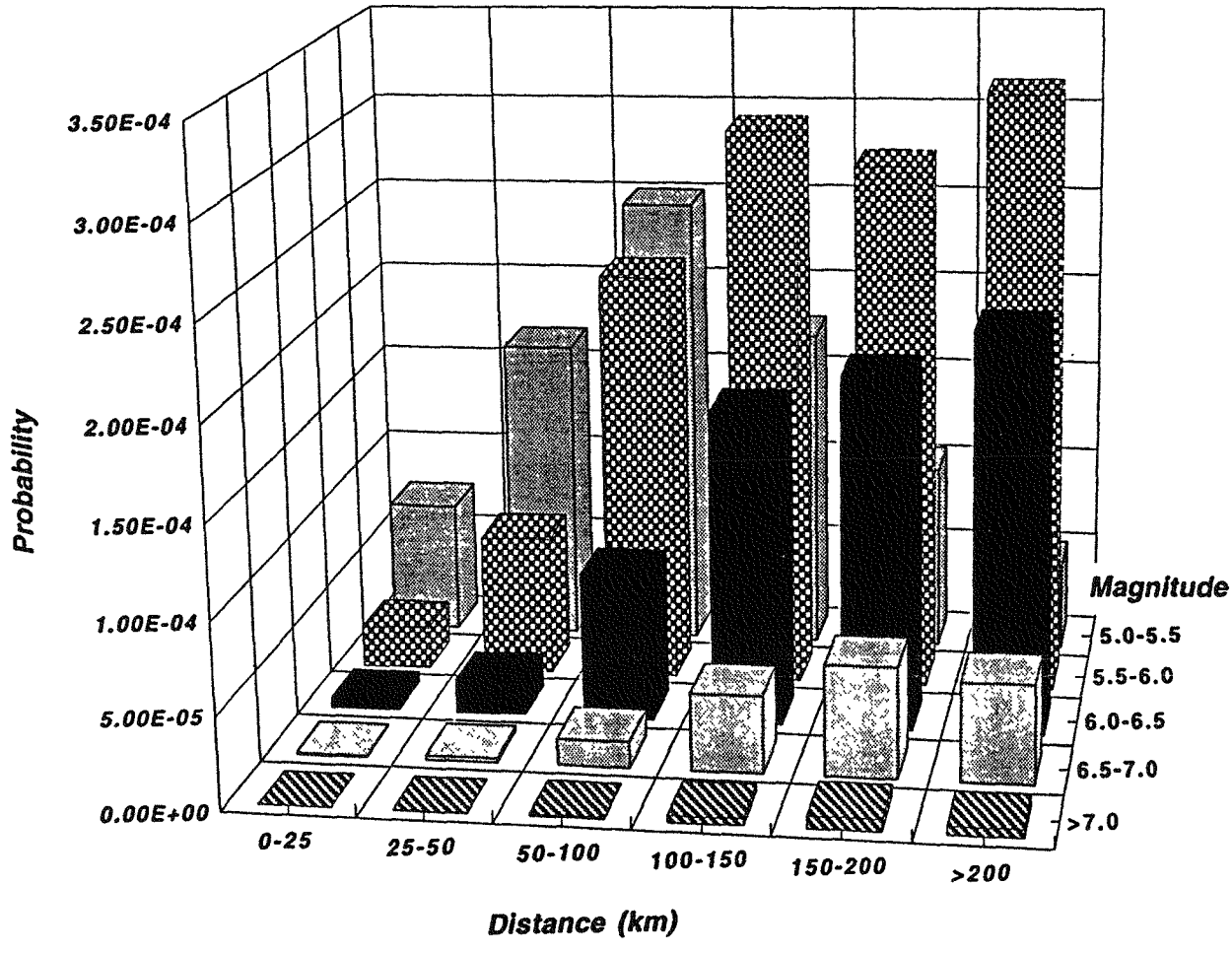


Figure 9.3-2 EPRI Vogtle rock mean hazard - SV(2.5Hz) = 1.0 cm/sec

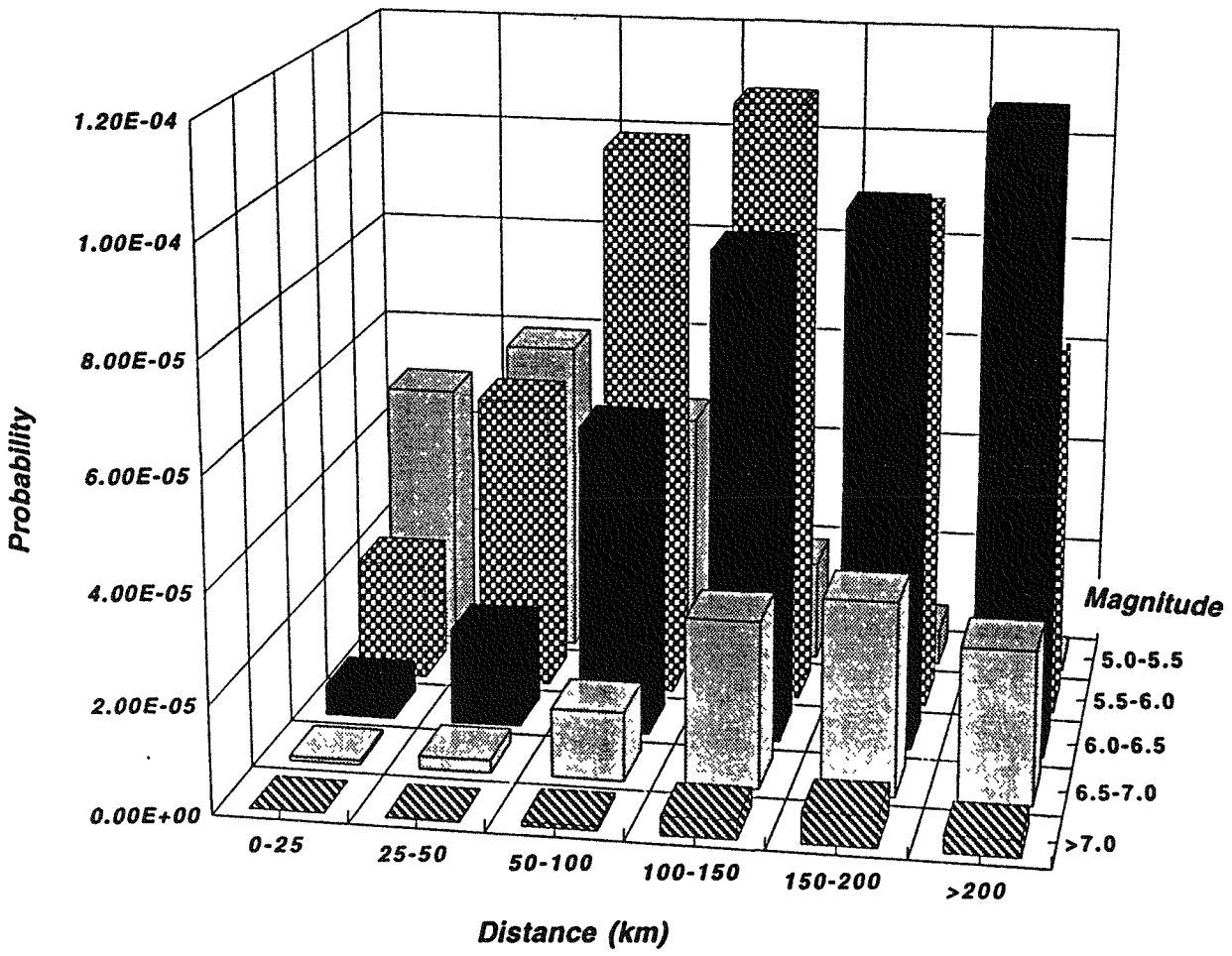


Figure 9.3-3 EPRI Vogtle rock mean hazard - SV(2.5Hz) = 2.0 cm/sec

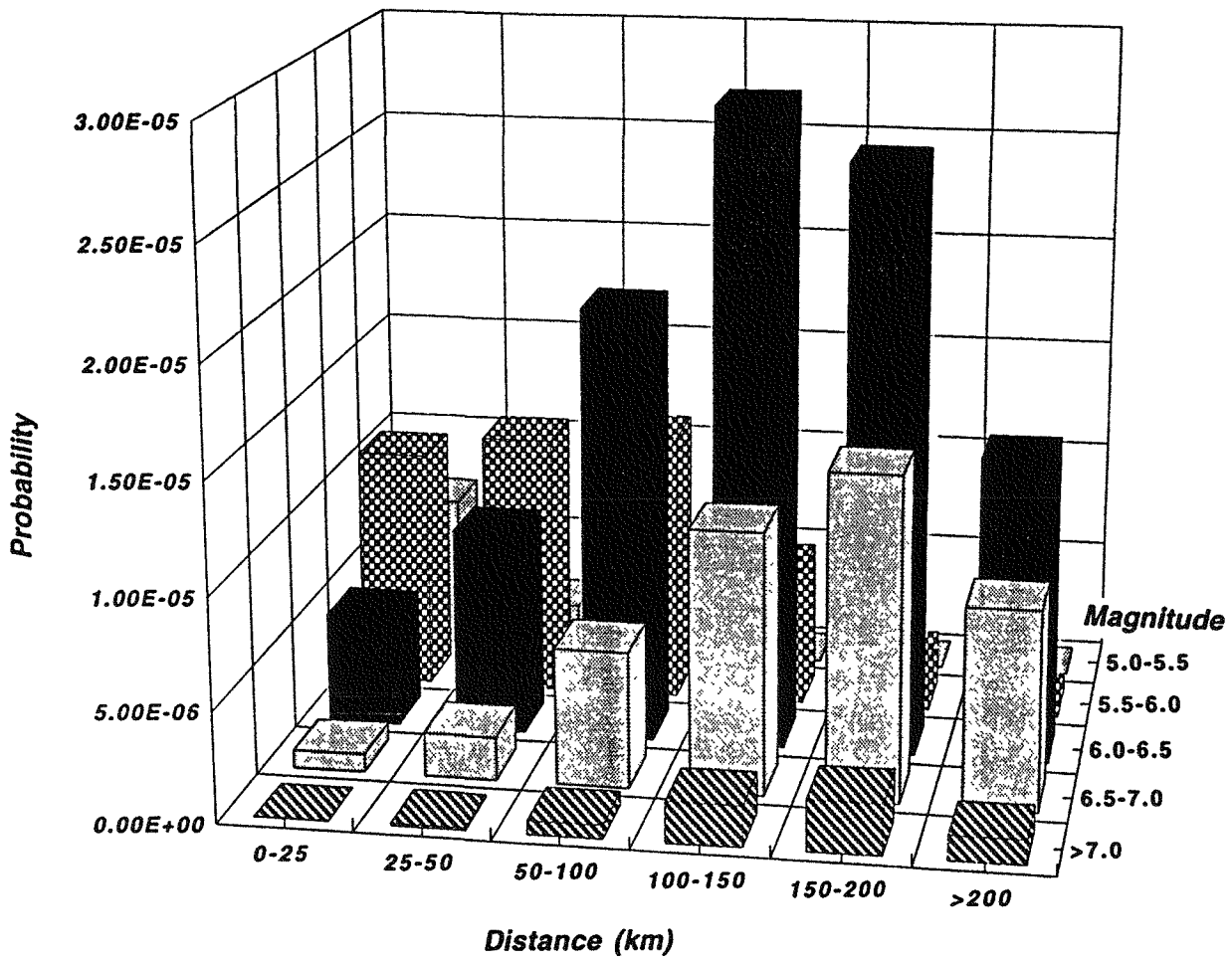


Figure 9.3-4 EPRI Vogtle rock mean hazard - SV(2.5Hz) = 6.0 cm/sec

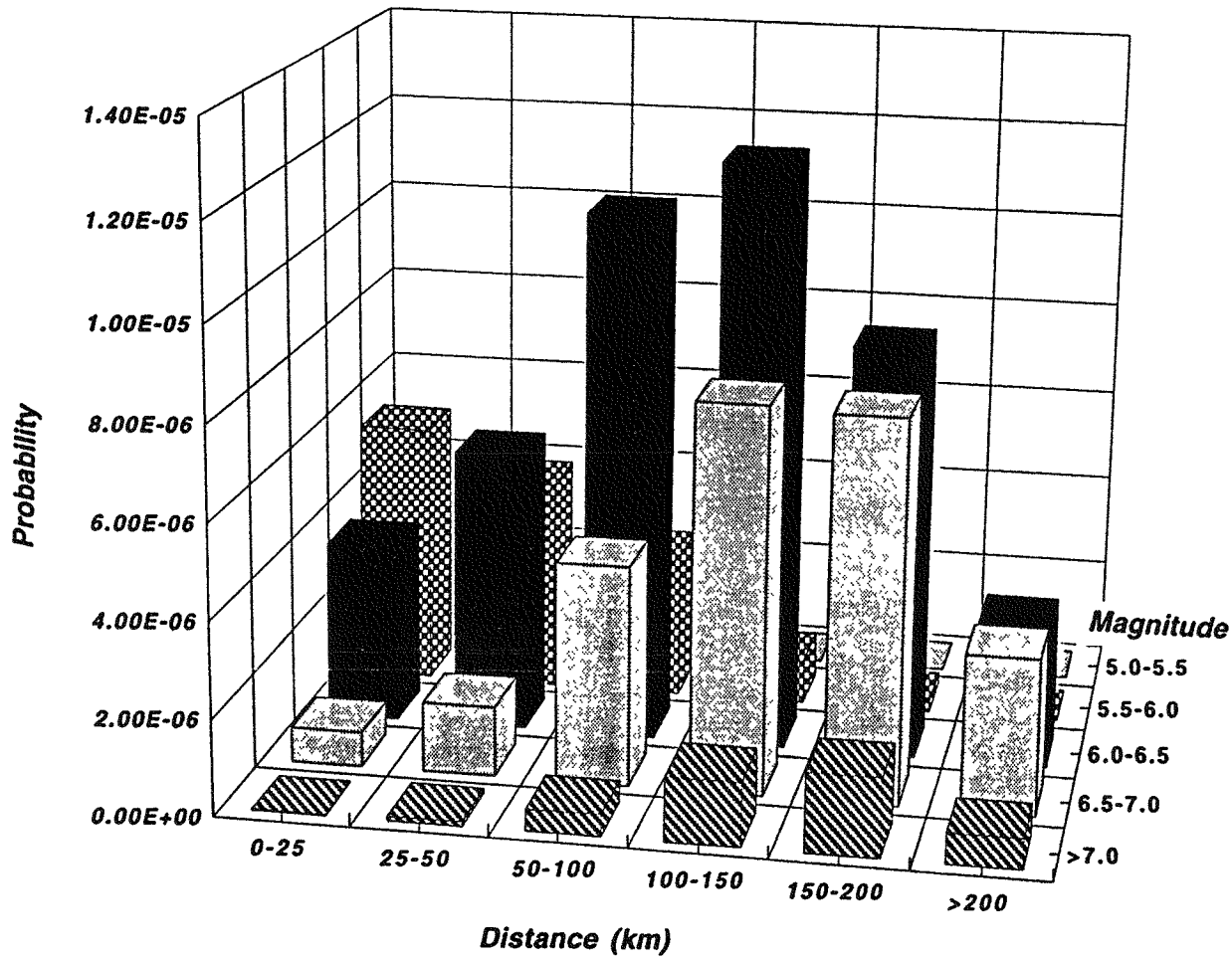


Figure 9.3-5 EPRI Vogtle rock mean hazard - SV(2.5Hz) = 8.7 cm/sec

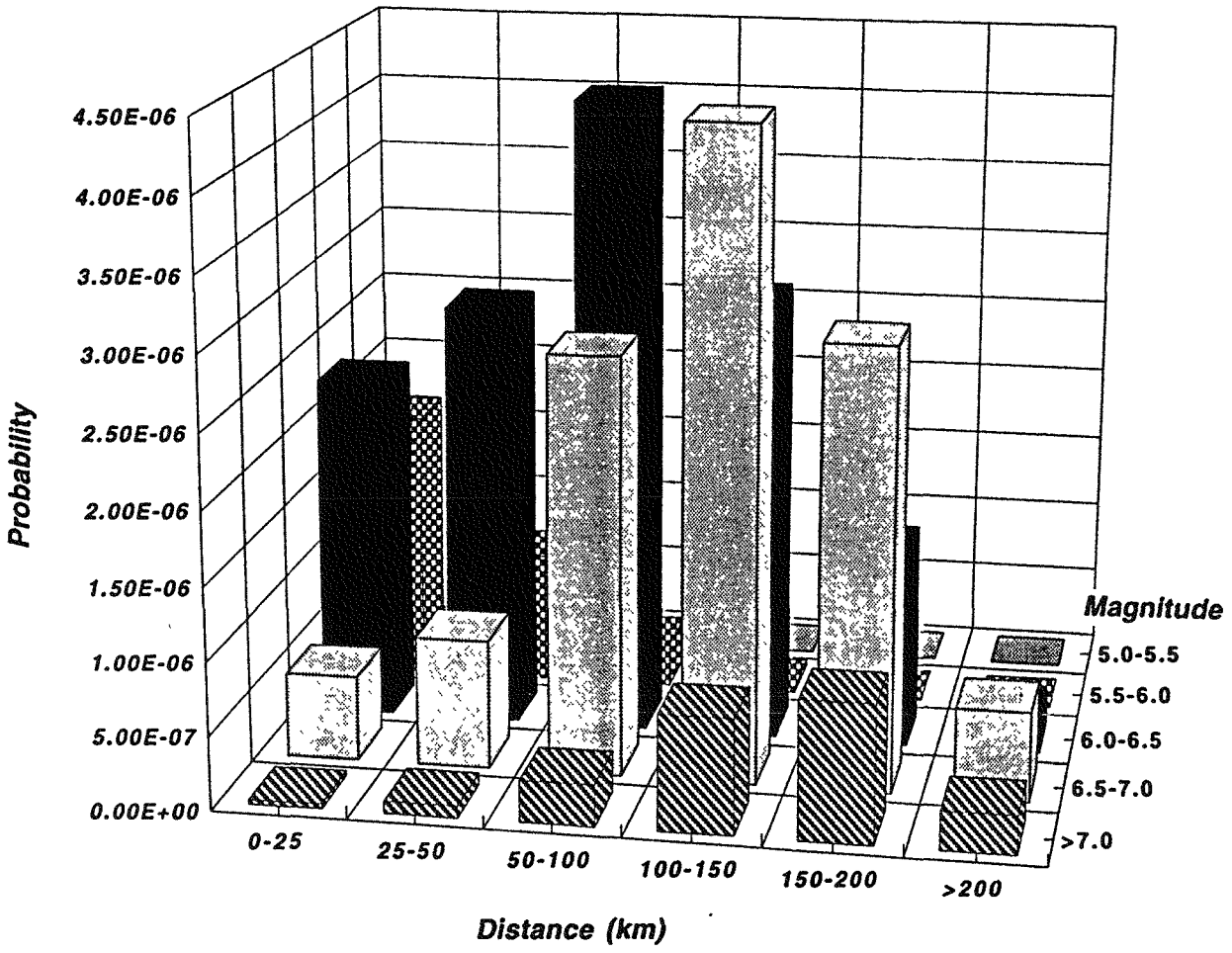


Figure 9.3-6 EPRI Vogtle rock mean hazard - SV(2.5Hz) = 16.0 cm/sec

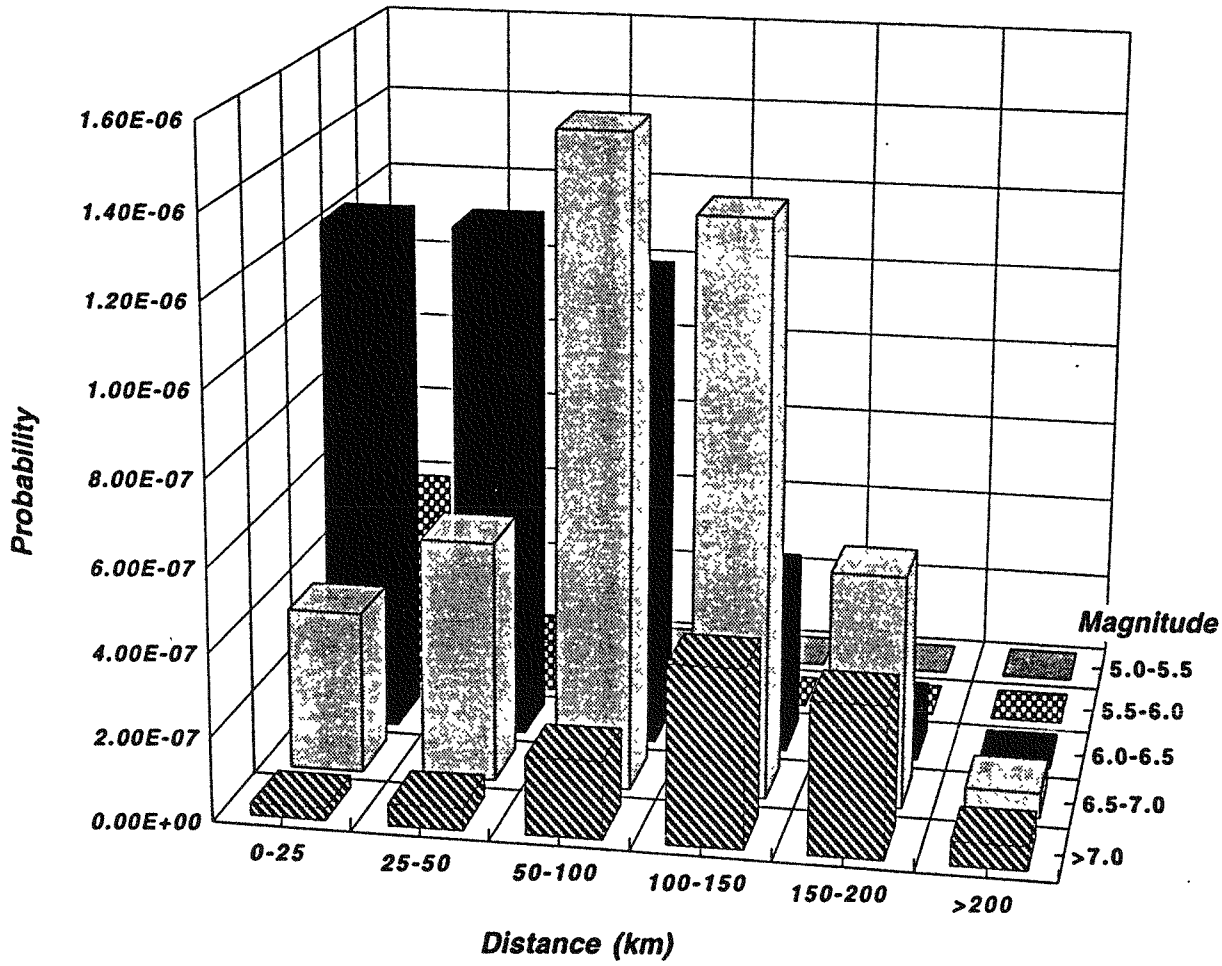


Figure 9.3-7 EPRI Vogtle rock mean hazard - SV(2.5Hz) = 26.0 cm/sec

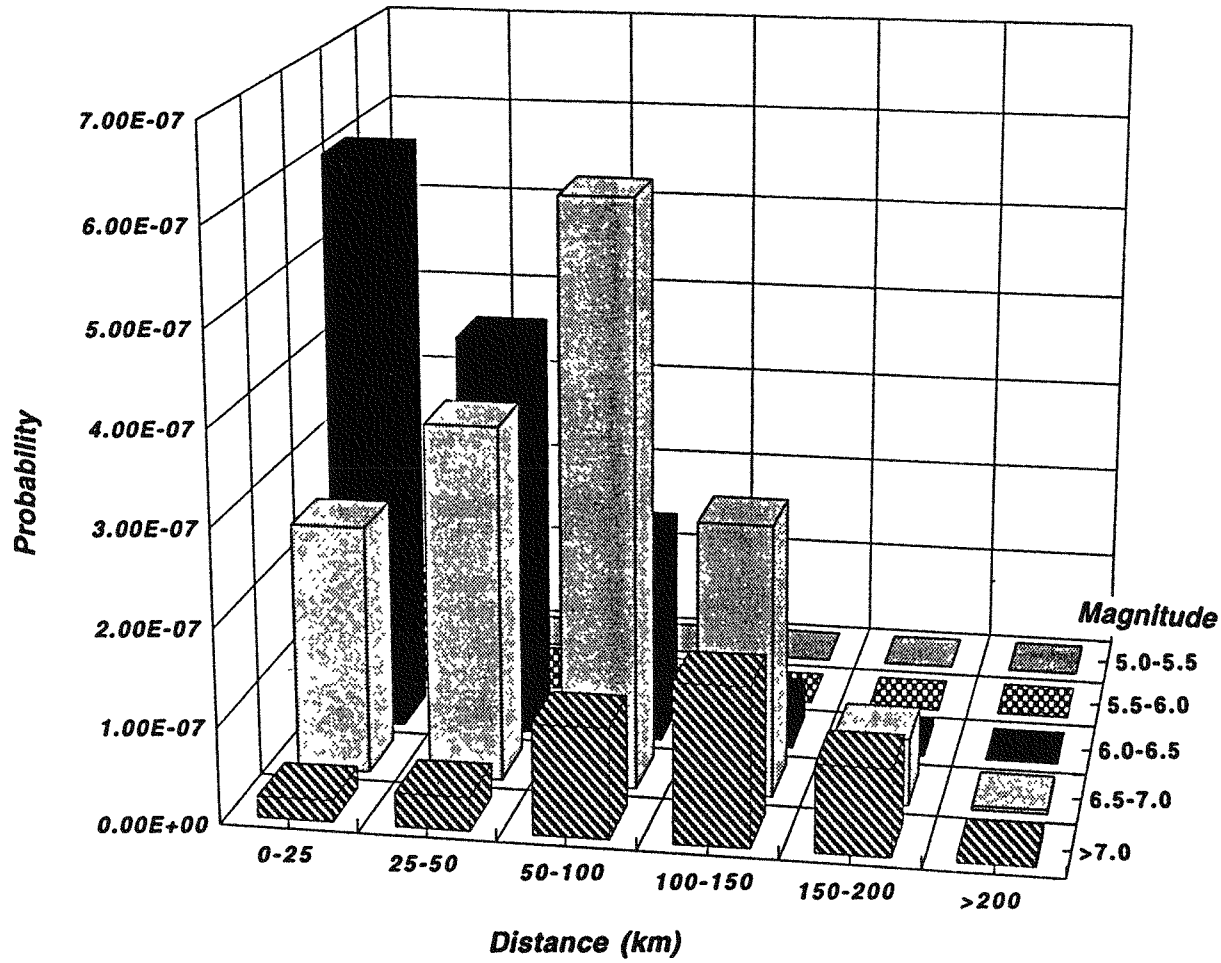


Figure 9.3-8 EPRI Vogtle rock mean hazard - SV(2.5Hz) = 40.0 cm/sec

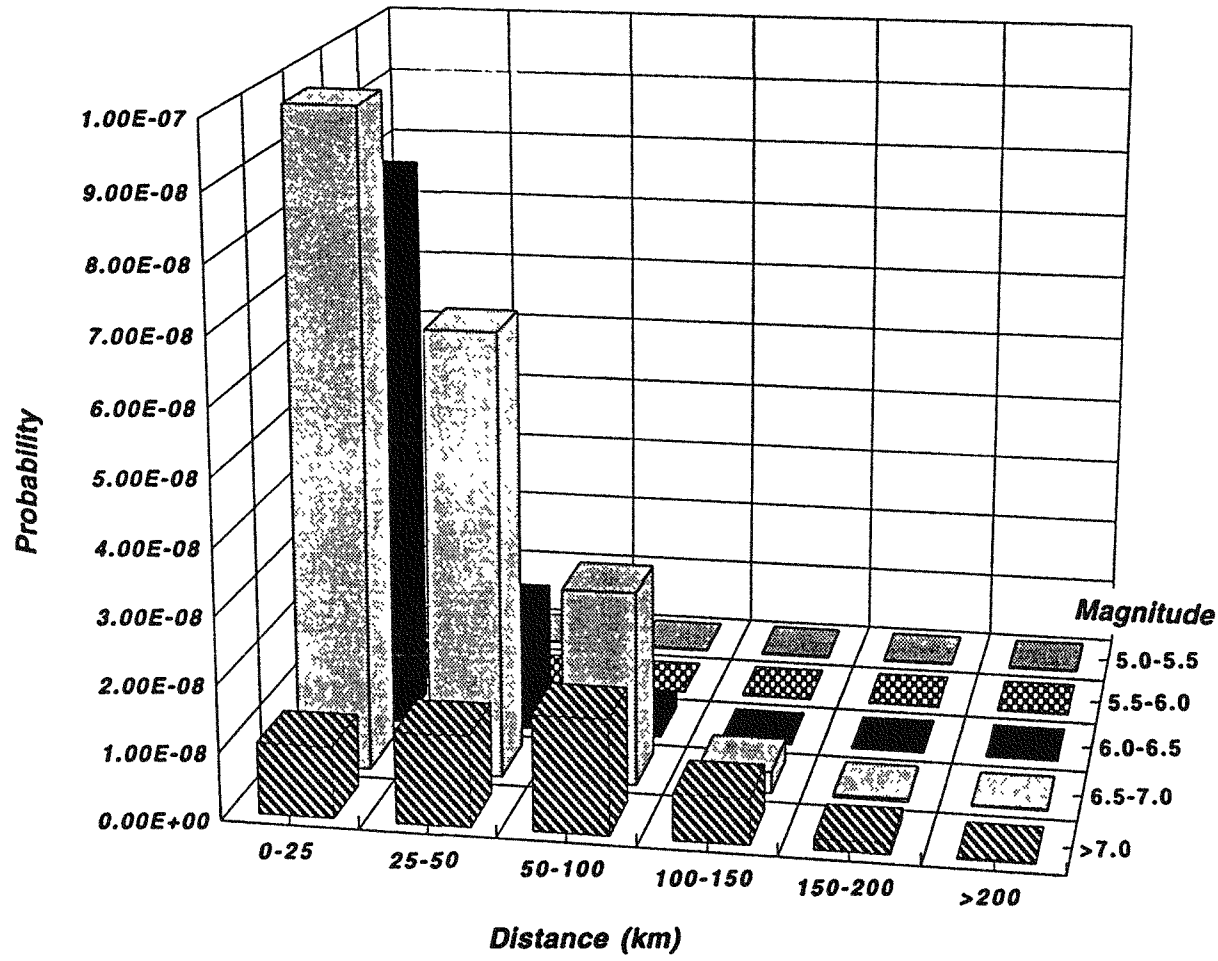


Figure 9.3-9 EPRI Vogtle rock mean hazard - SV(2.5Hz) = 90.0 cm/sec

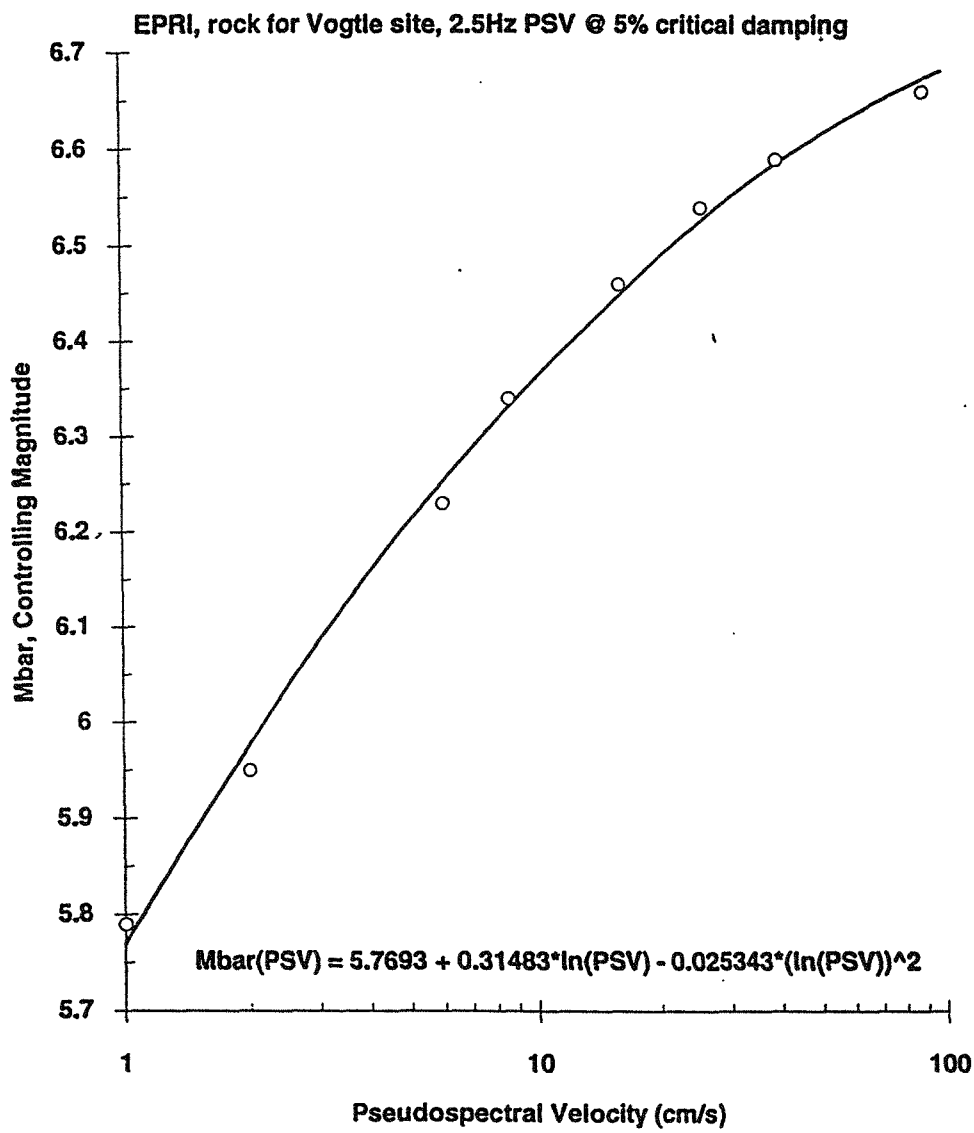


Figure 9.3-10 Functional relationship between Mbar and spectral velocity

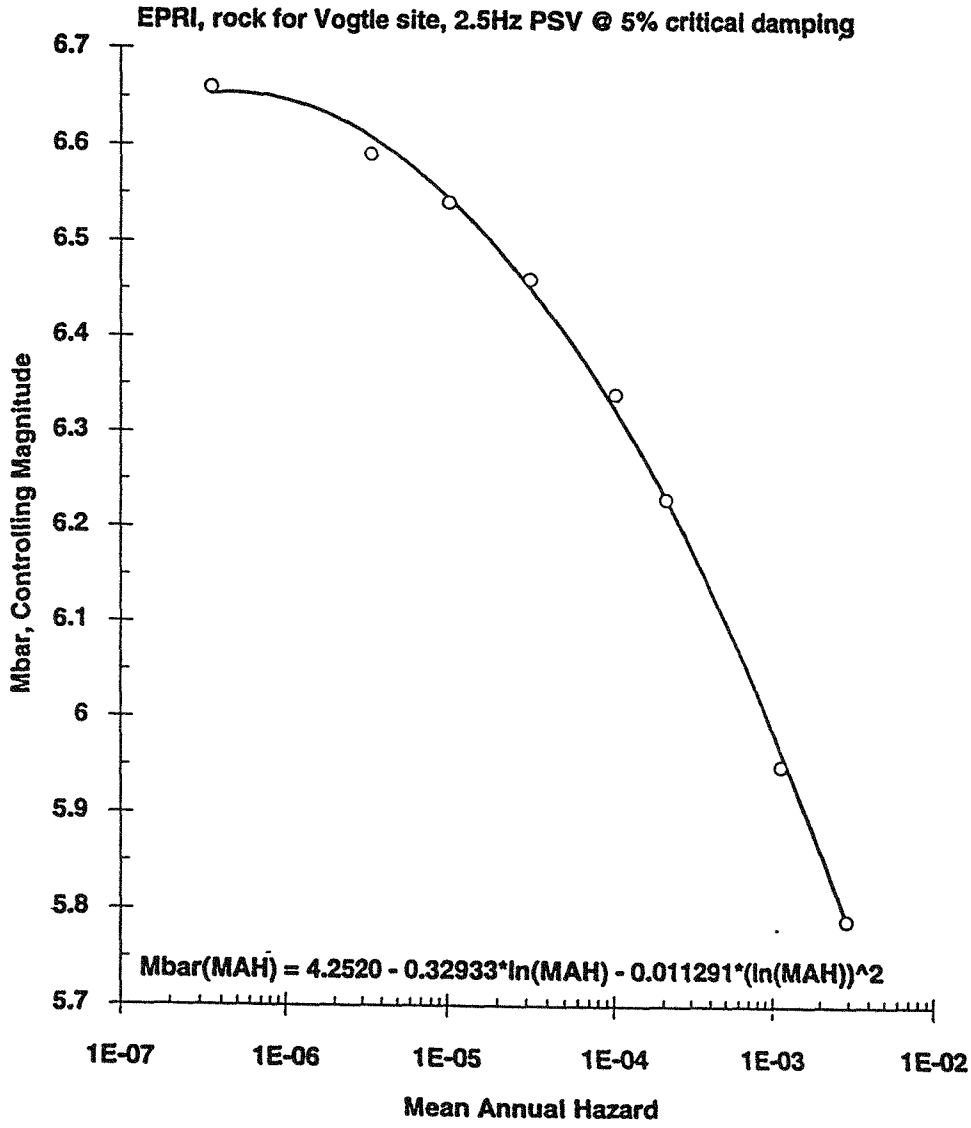


Figure 9.3-11 Functional relationship between Mbar and mean annual hazard

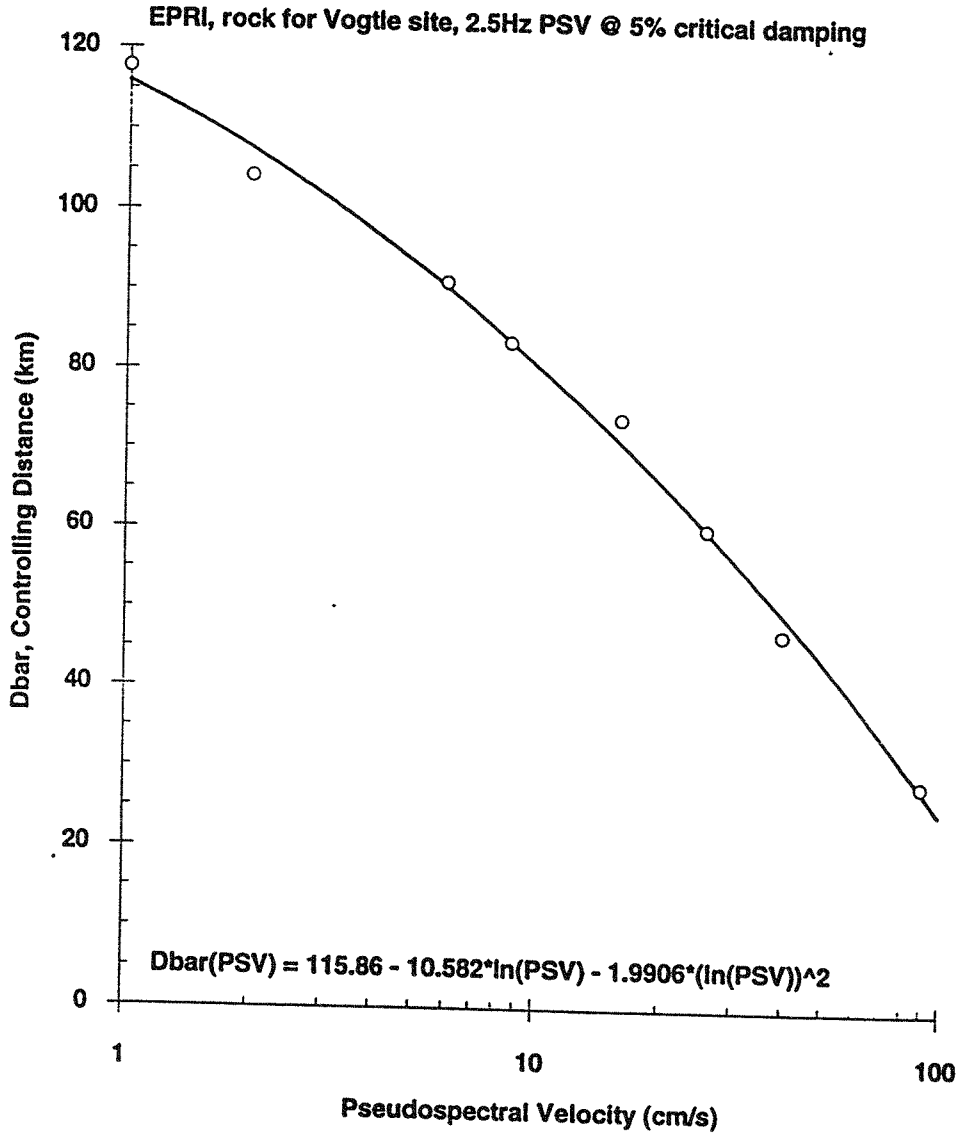


Figure 9.3-12 Functional relationship between Dbar and spectral velocity

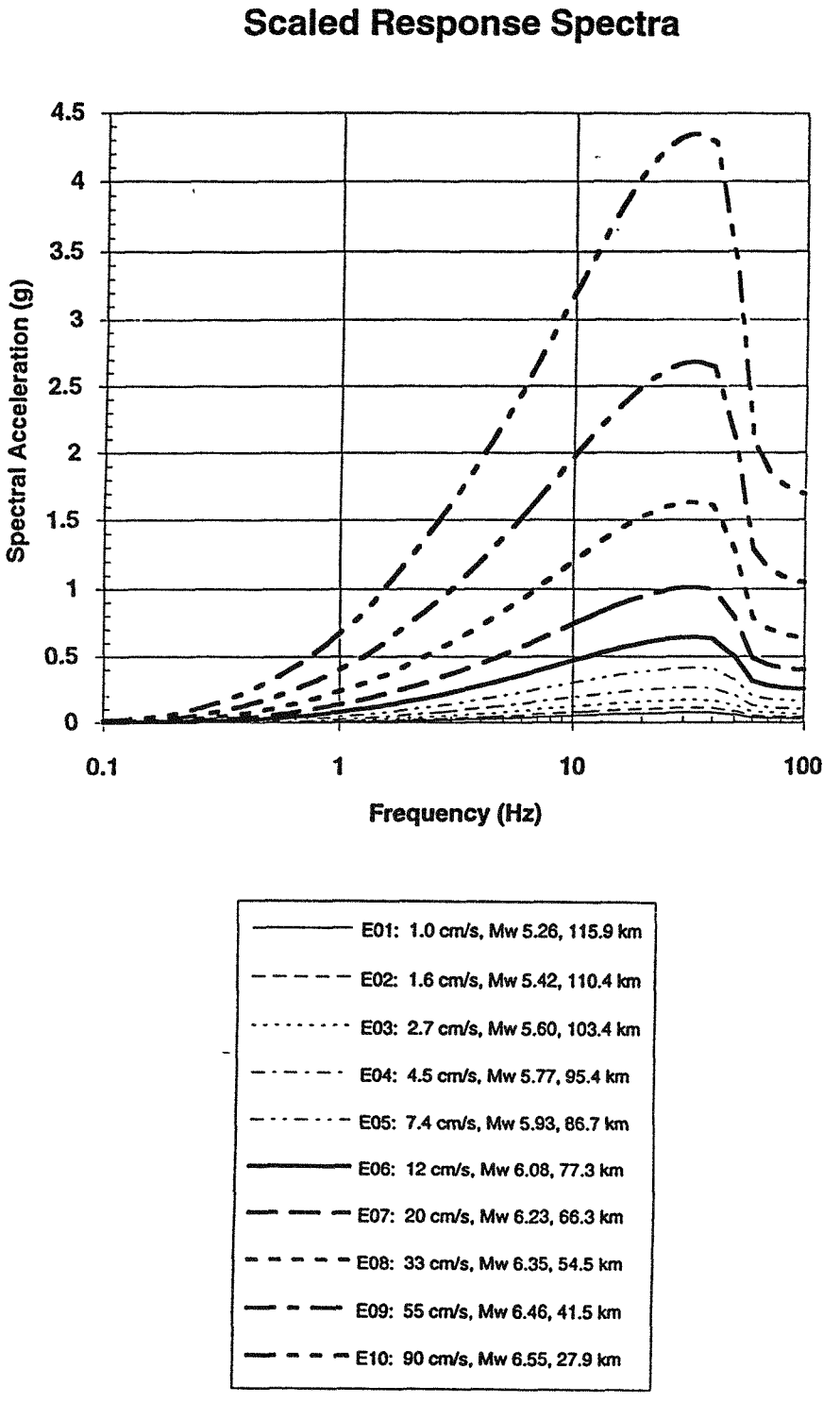


Figure 9.3-13 Ten acceleration response spectra ( 5% damping ) developed for the rock motion

DURATION ENVELOPING FUNCTION PARAMATERS

| Magnitude | Rise Time $t_r$ | Duration of Strong Motion $t_m$ | Decay Time $t_d$ | Total Duration |
|---|---|---|---|---|
| 7.0 - 7.5 | 2 | 13 | 9 | 24 |
| 6.5 - 7.0 | 1.5 | 10 | 7 | 18.5 |
| 6.0 - 6.5 | 1 | 7 | 5 | 13 |
| 5.5 - 6.0 | 1 | 6 | 4 | 11 |
| 5.0 - 5.5 | 1 | 5 | 4 | 10 |

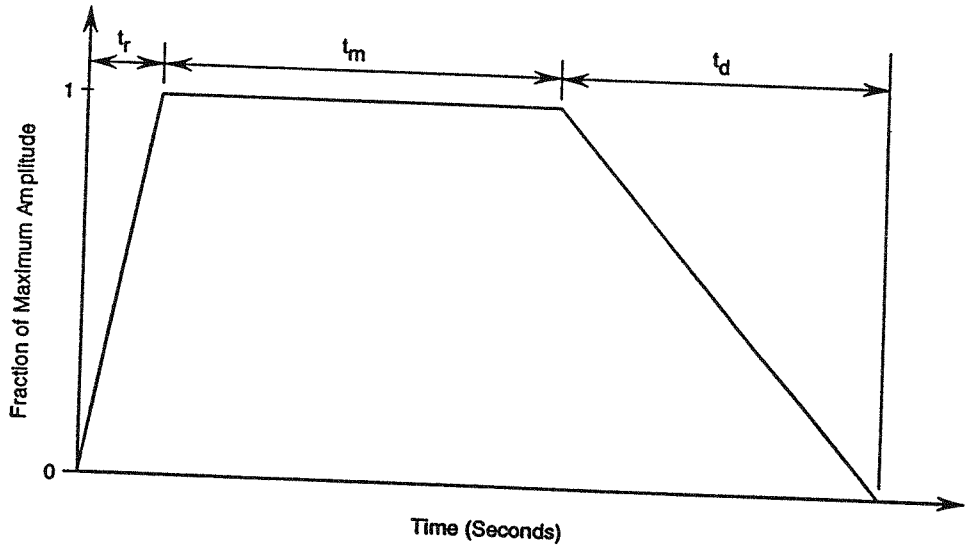


(ASCE, 1986)

Figure 9.3-14 Duration envelope function

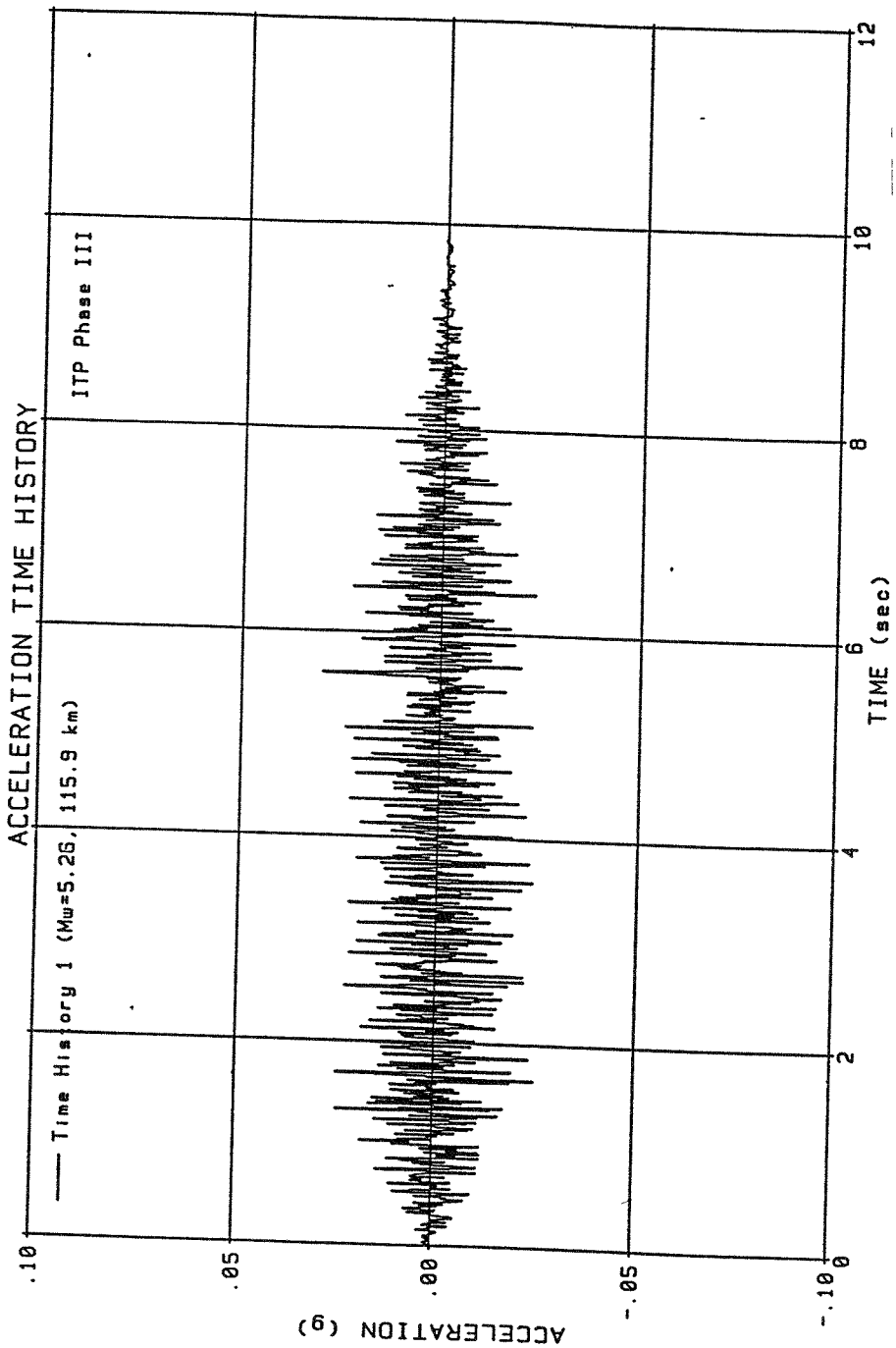


Figure 9.3-15 Acceleration time history for earthquake motion E01

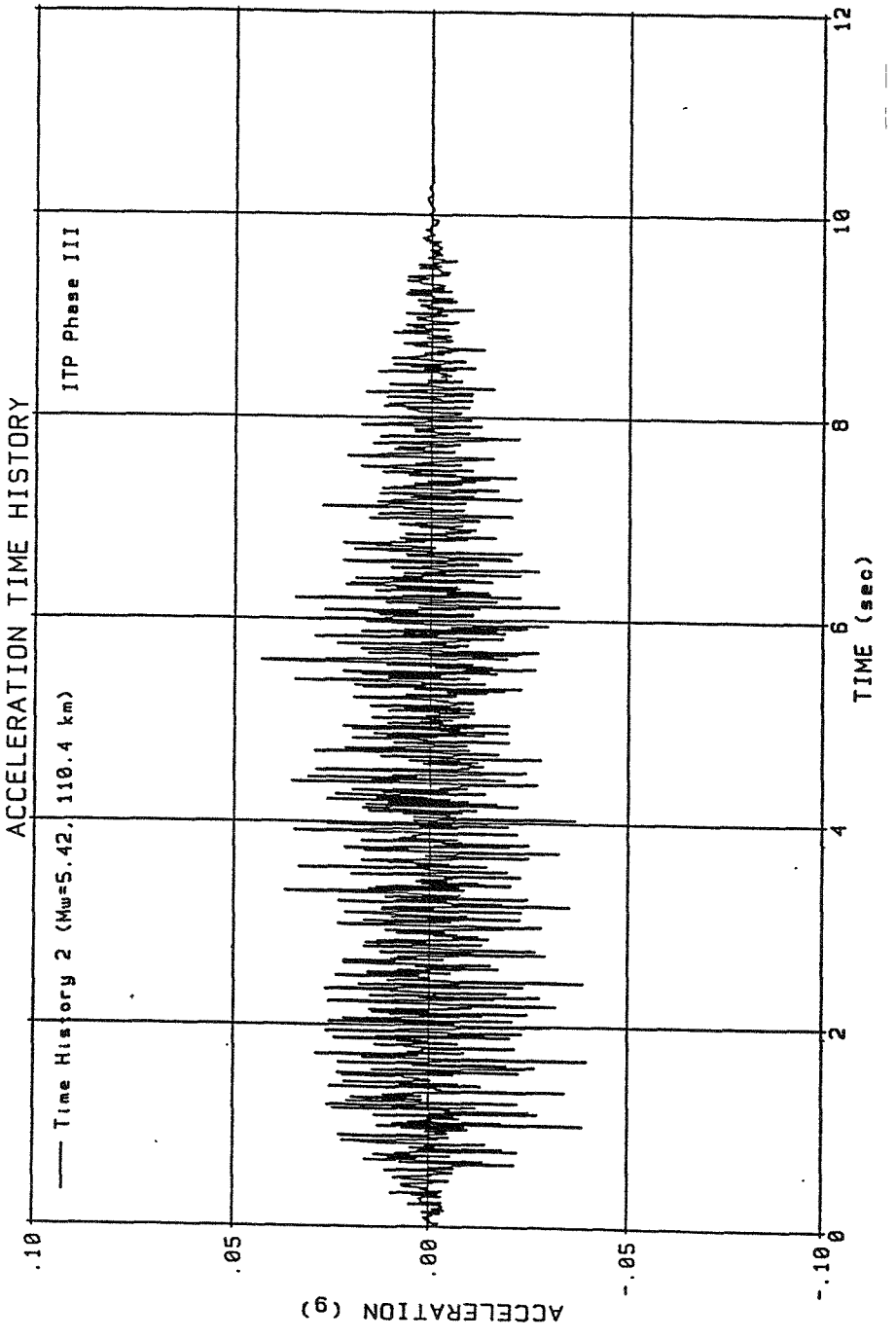


Figure 9.3-16 Acceleration time history for earthquake motion E02

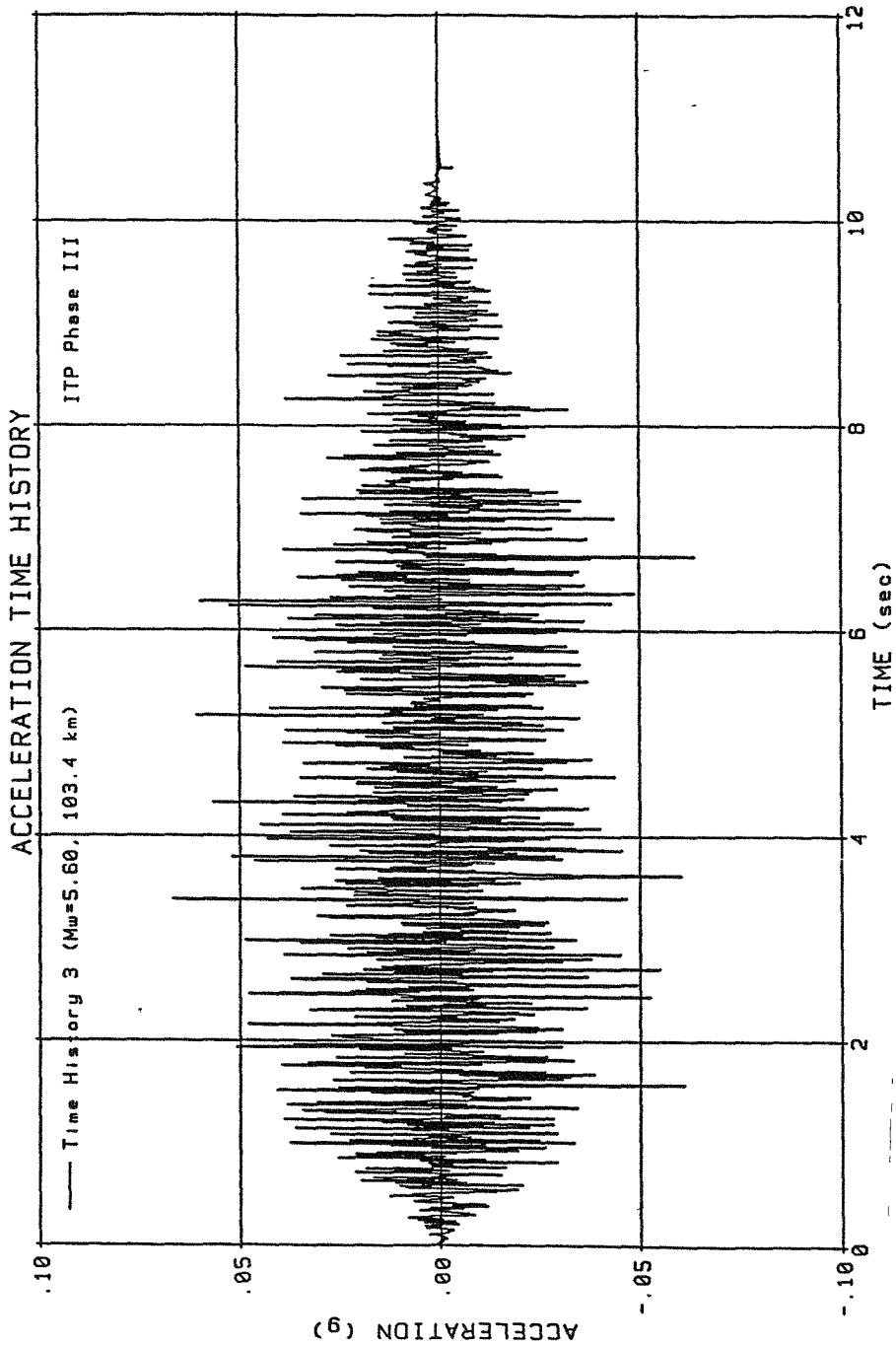


Figure 9.3-17 Acceleration time history for earthquake motion E03

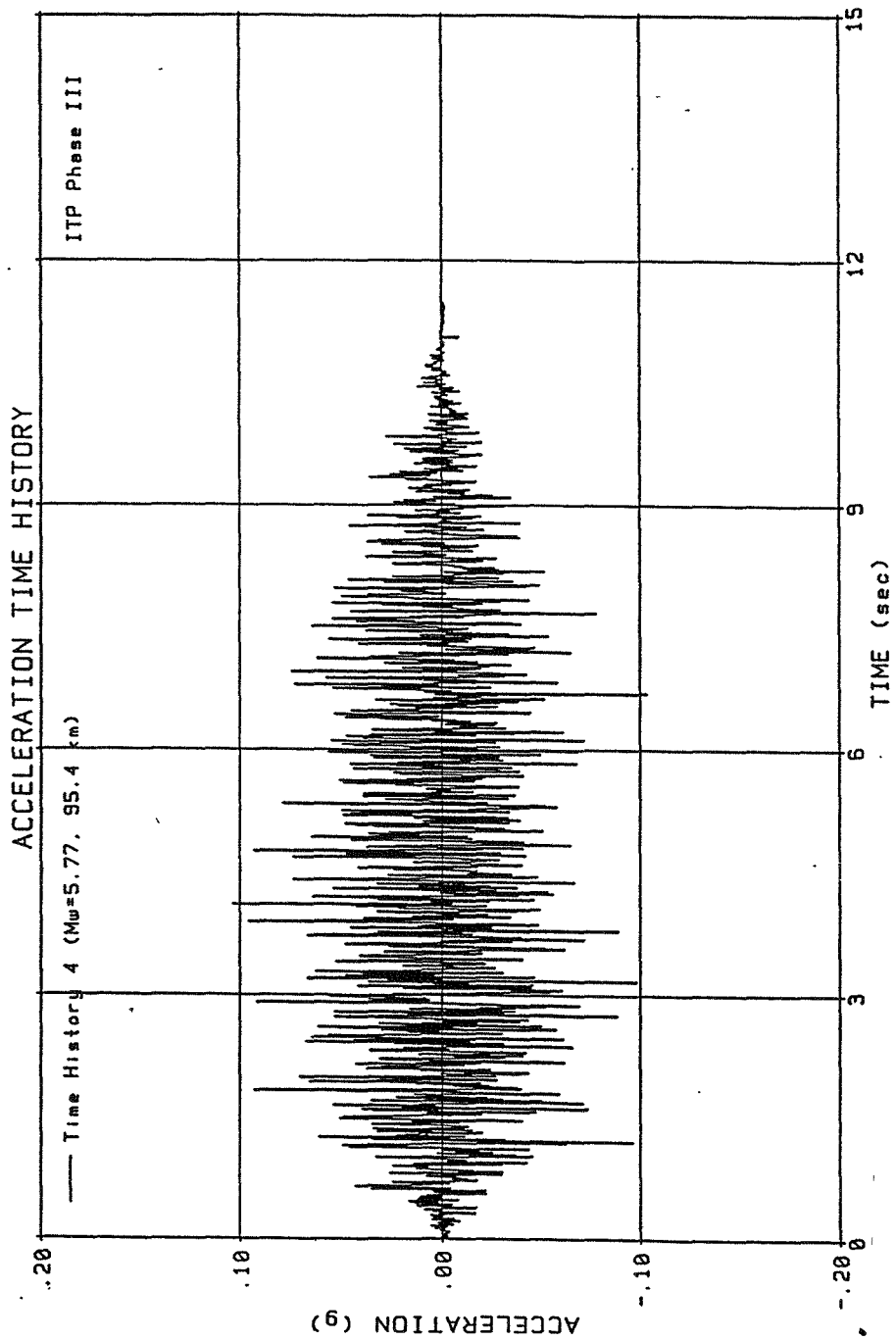


Figure 9.3-18 Acceleration time history for earthquake motion E04

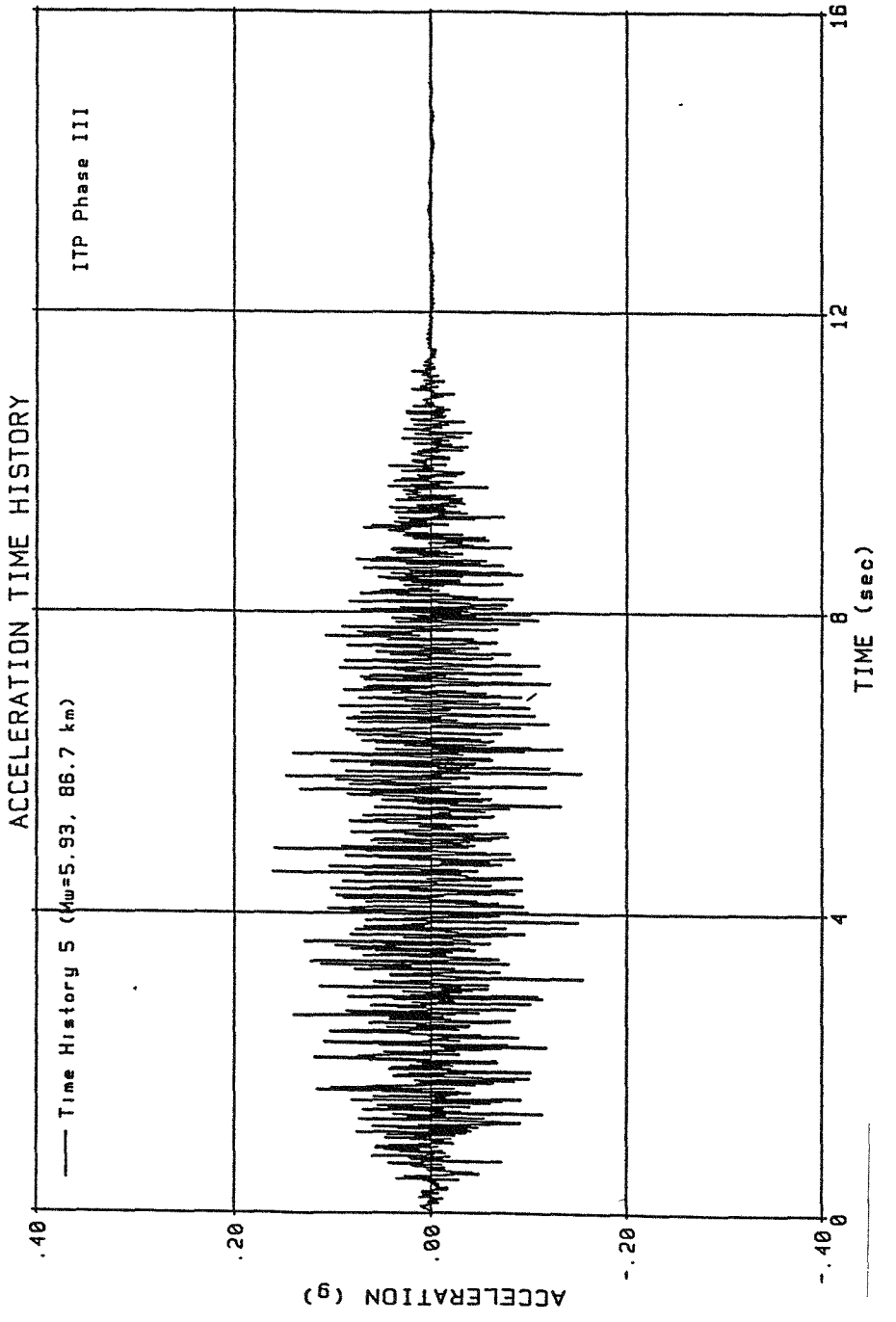


Figure 9.3-19 Acceleration time history for earthquake motion E05

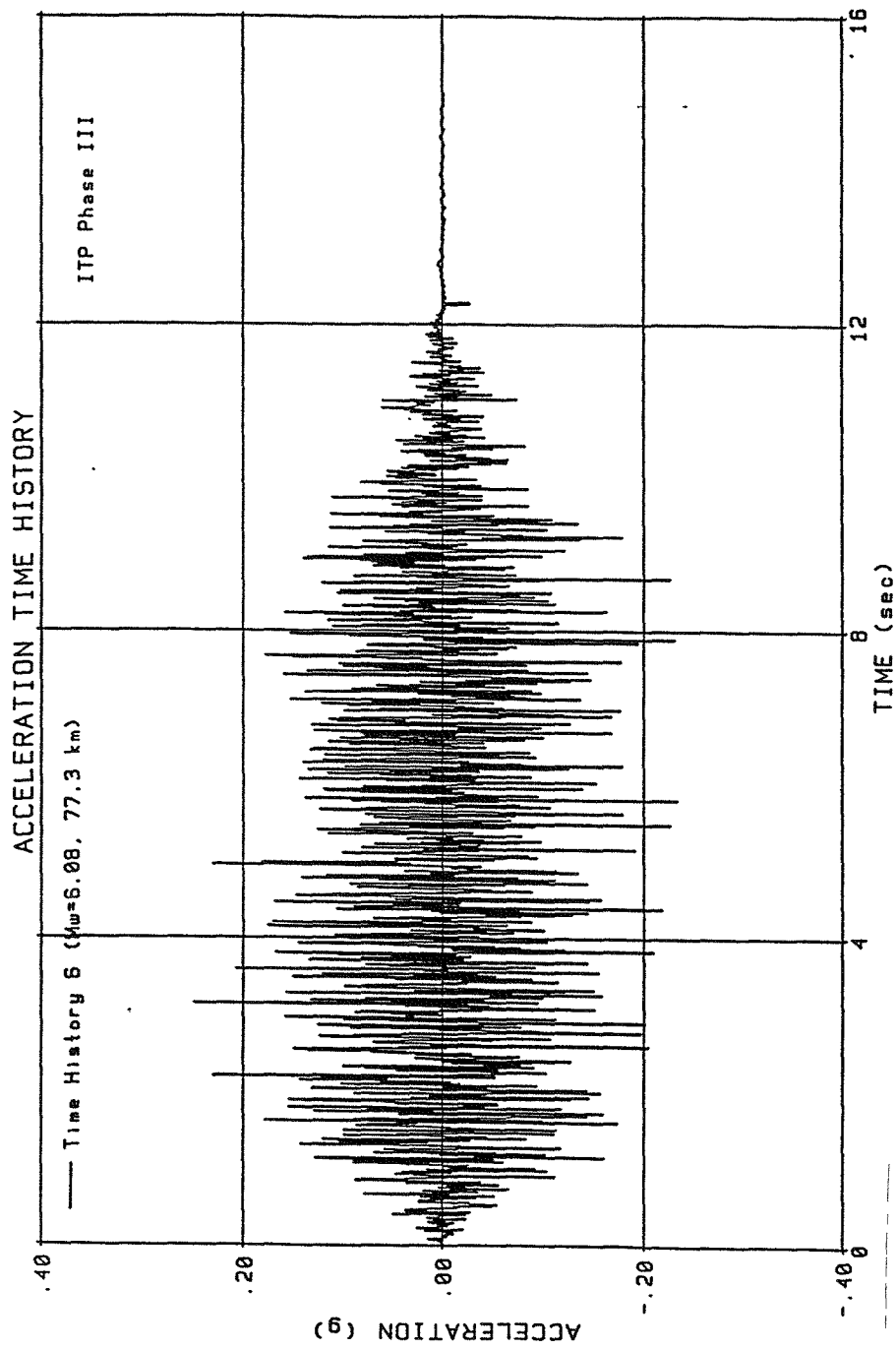


Figure 9.3-20 Acceleration time history for earthquake motion E06

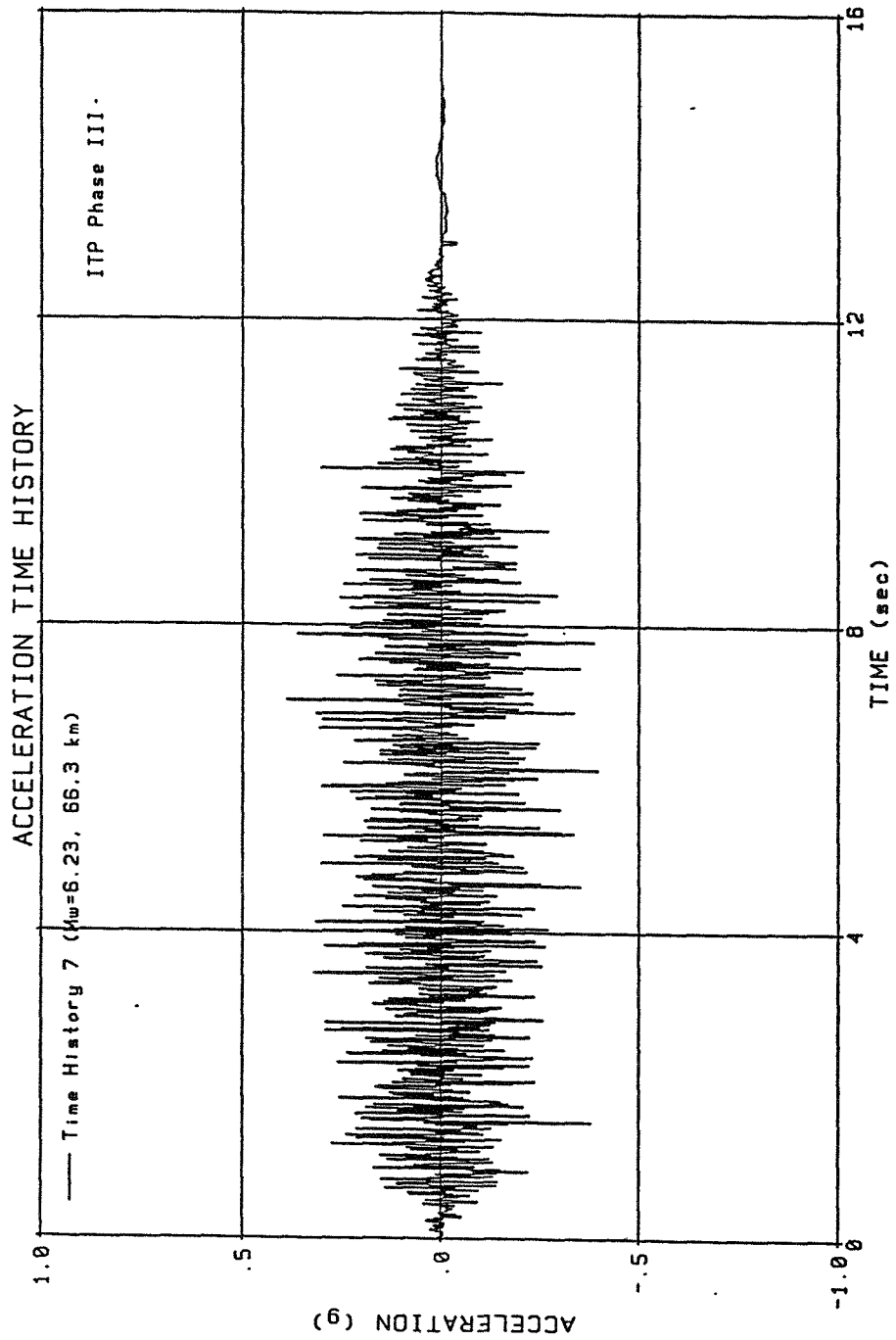


Figure 9.3-21 Acceleration time history for earthquake motion E07

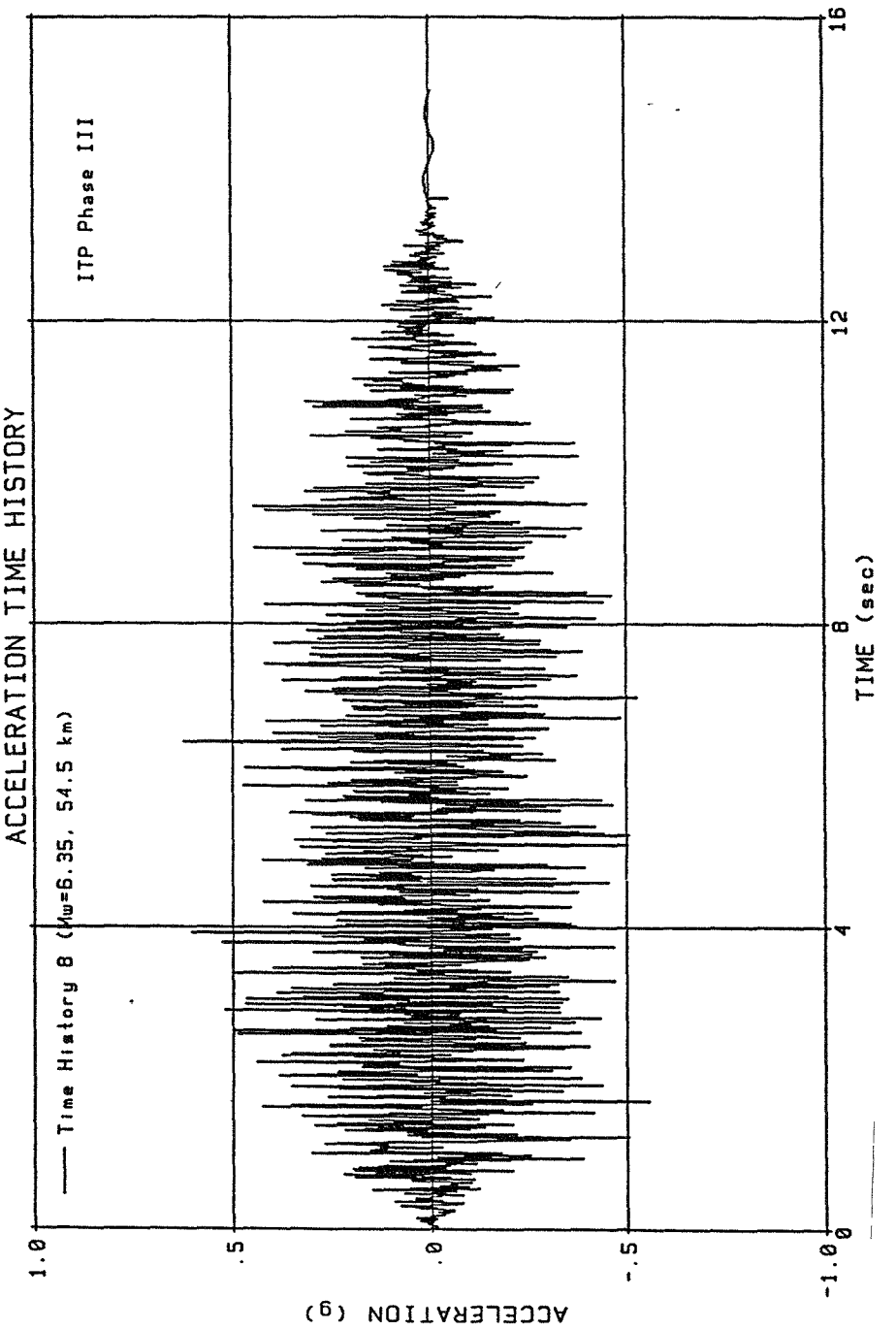


Figure 9.3-22 Acceleration time history for earthquake motion E08

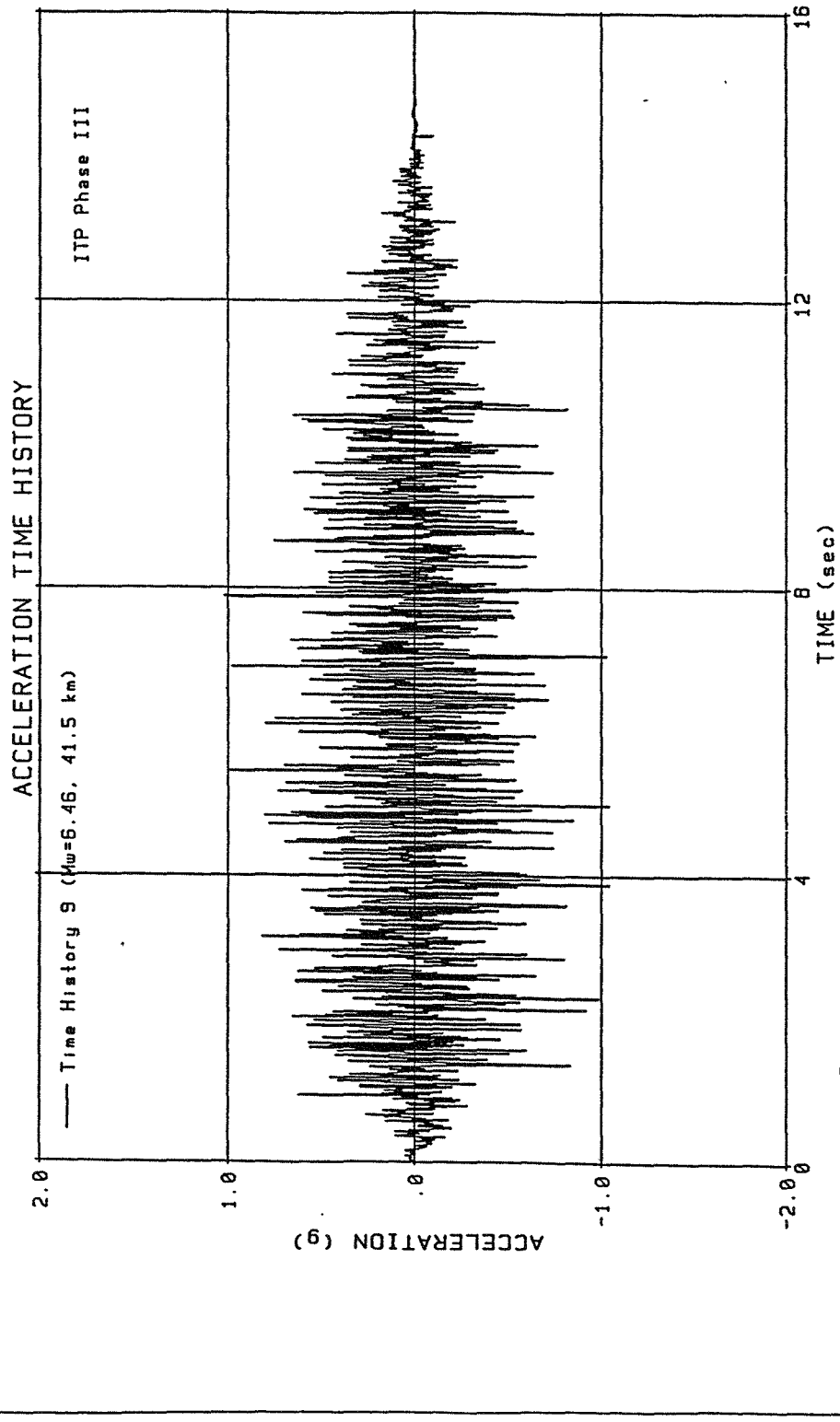


Figure 9.3-23 Acceleration time history for earthquake motion E09

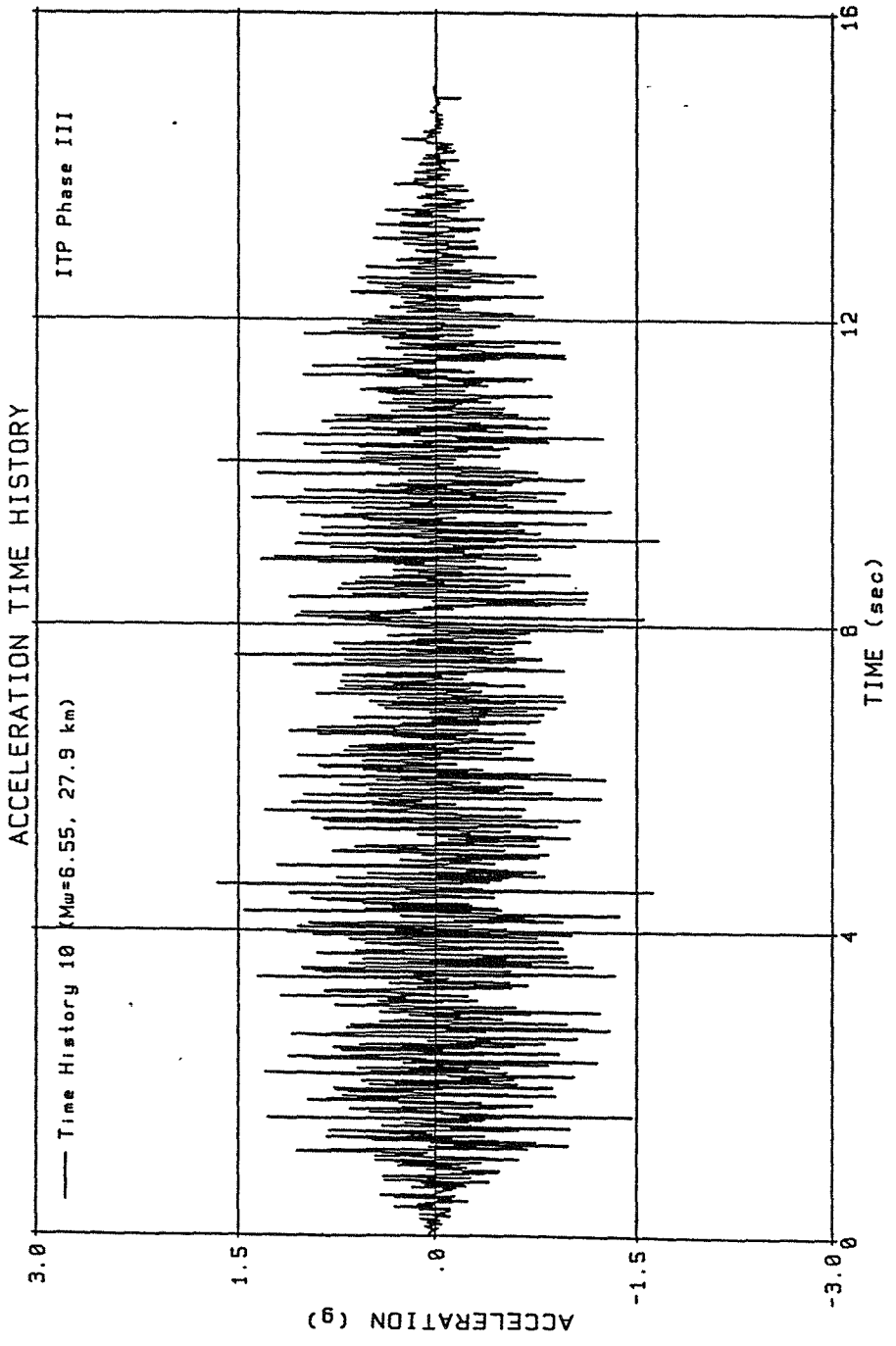


Figure 9.3-24 Acceleration time history for earthquake motion E010

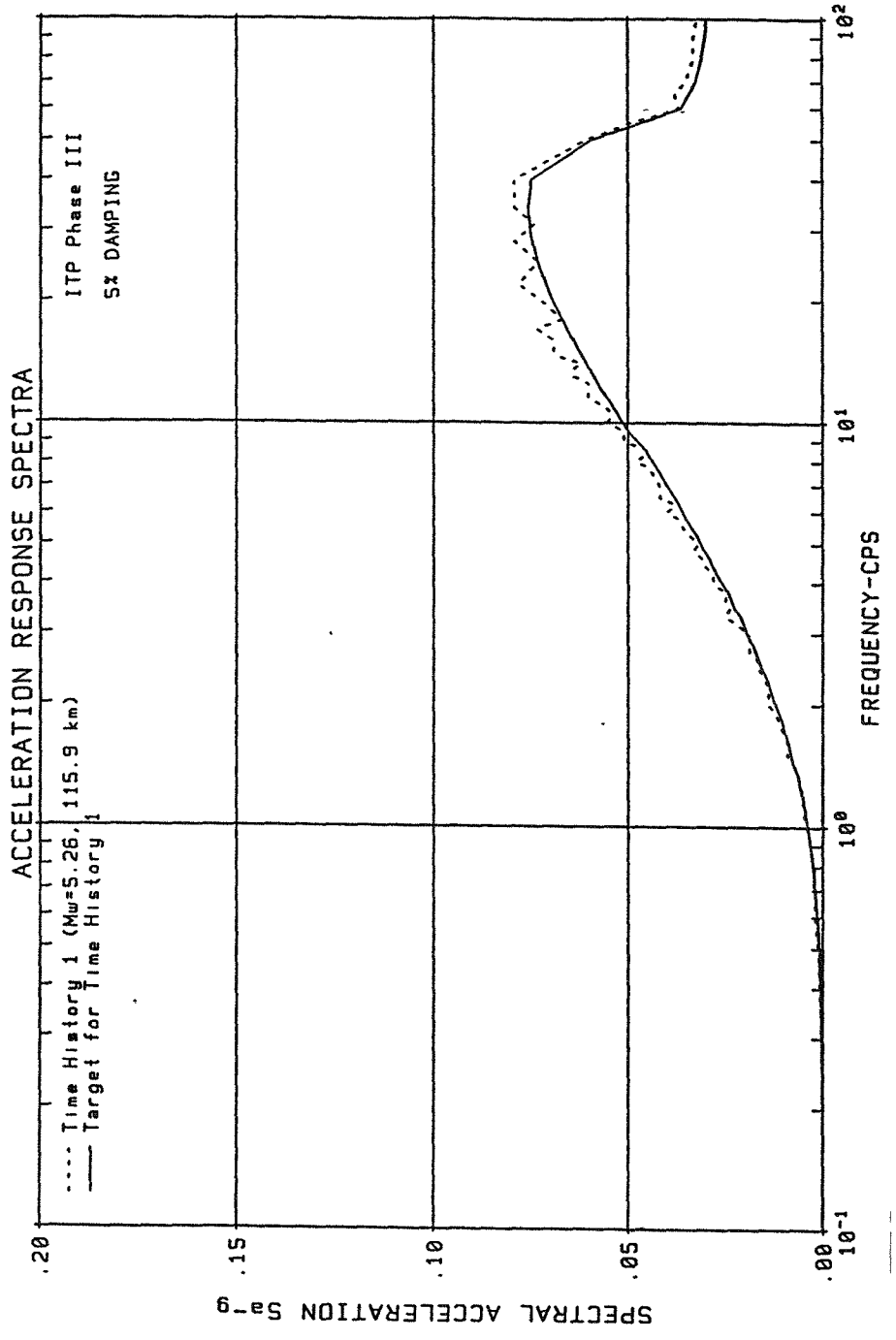


Figure 9.3-25 Acceleration response spectra for earthquake motion E01

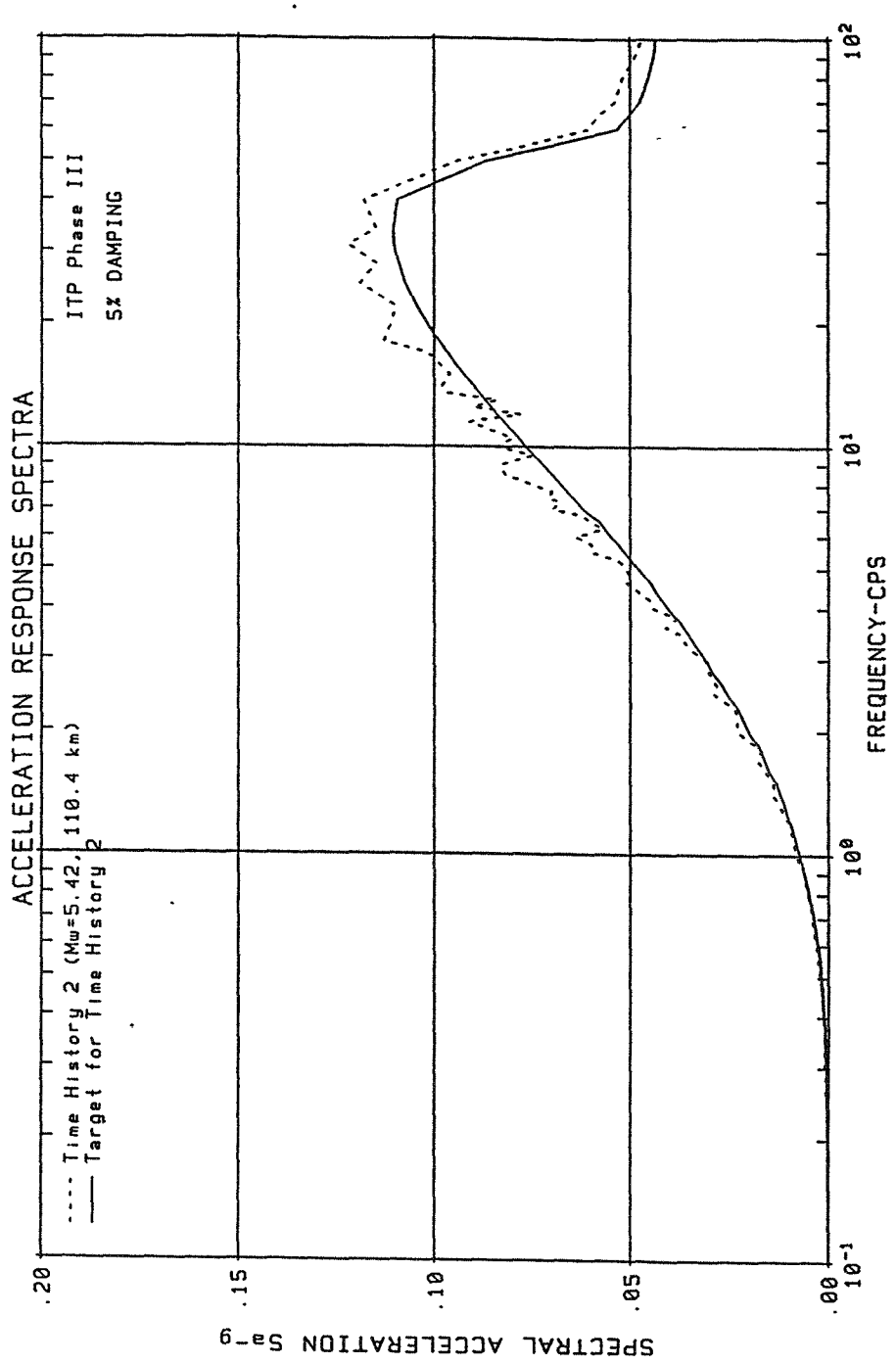


Figure 9.3-26 Acceleration response spectra for earthquake motion E02

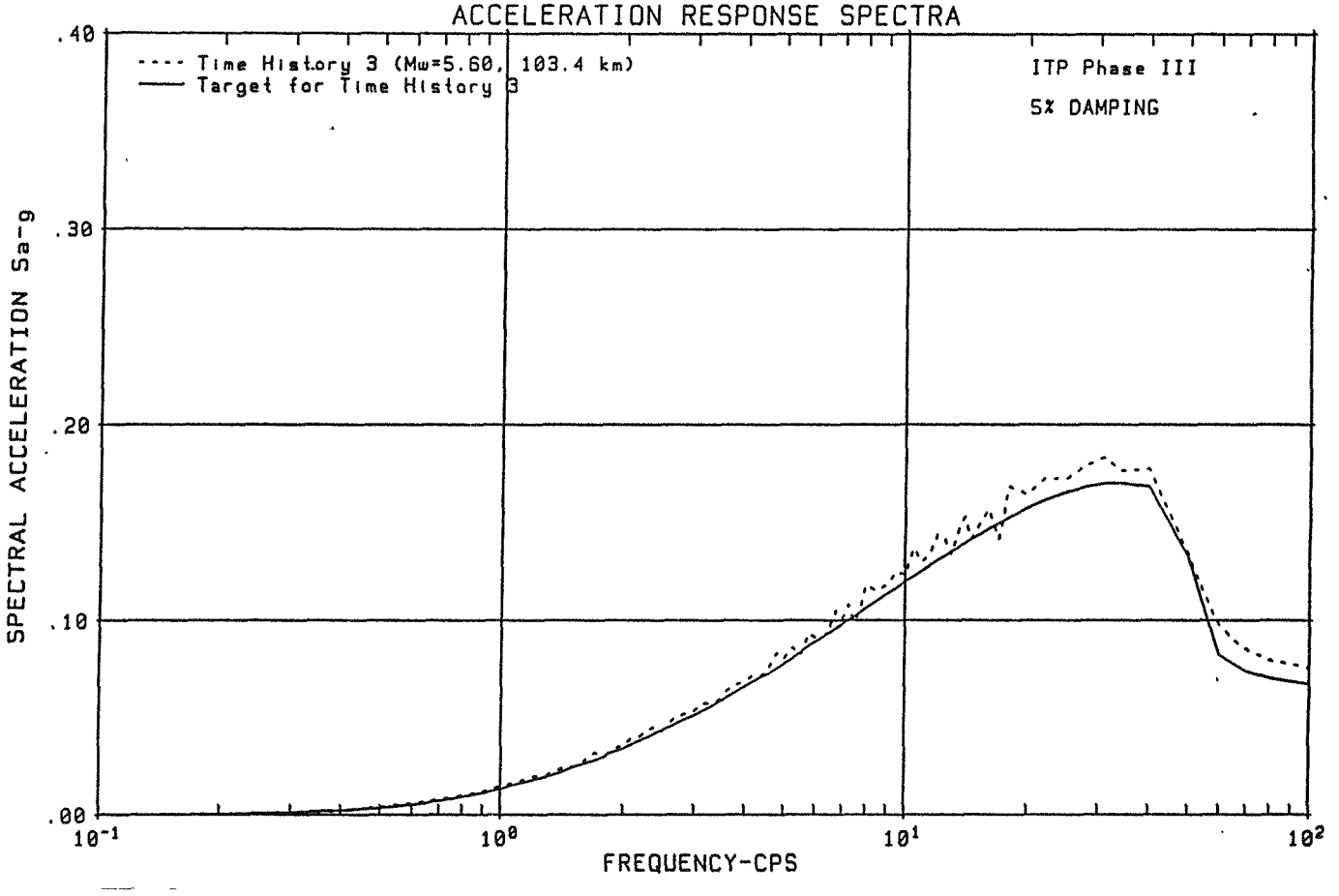


Figure 9.3-27 Acceleration response spectra for earthquake motion E03

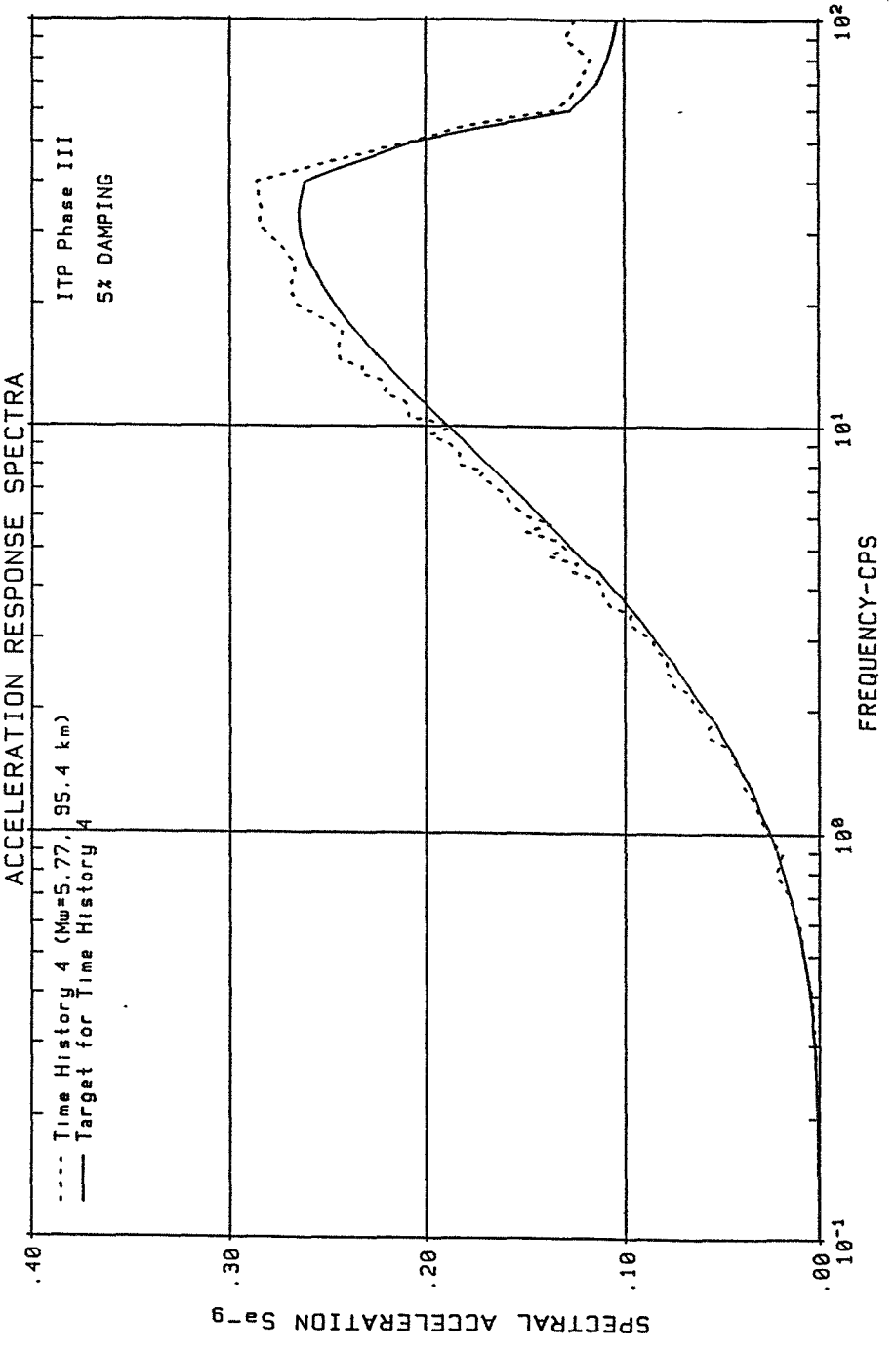


Figure 9.3-28 Acceleration response spectra for earthquake motion E04

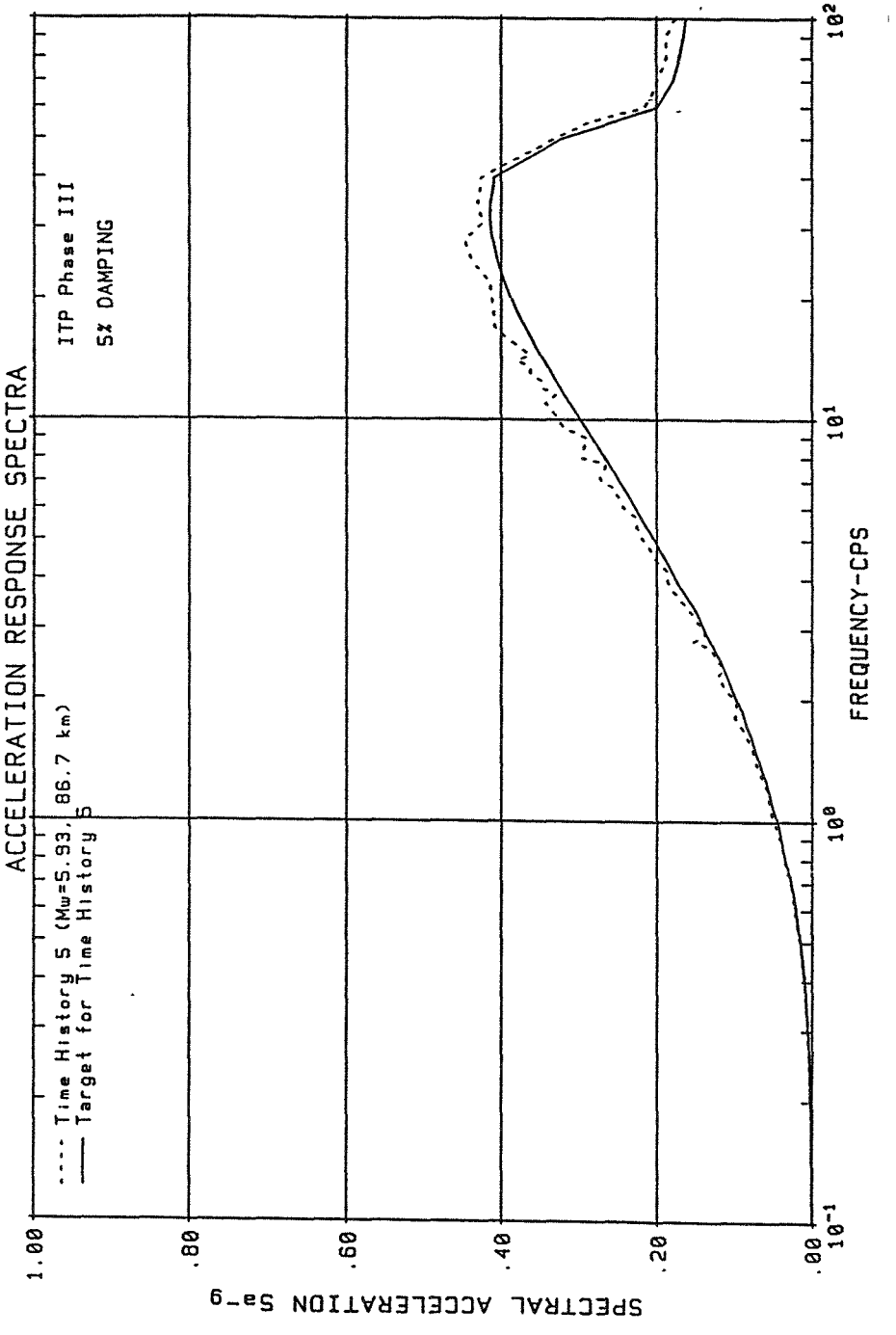


Figure 9.3-29 Acceleration response spectra for earthquake motion E05

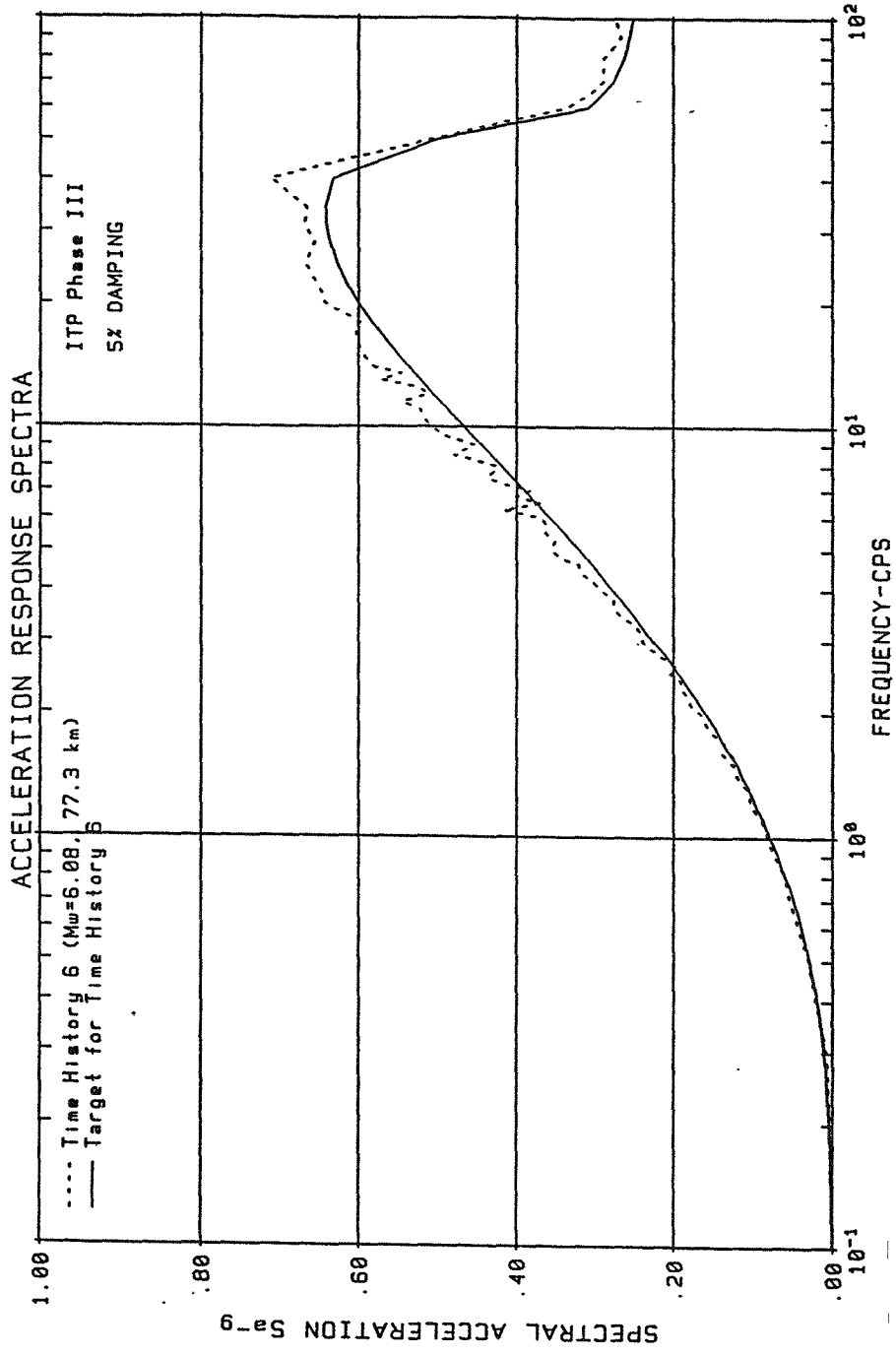


Figure 9.3-30 Acceleration response spectra for earthquake motion E06

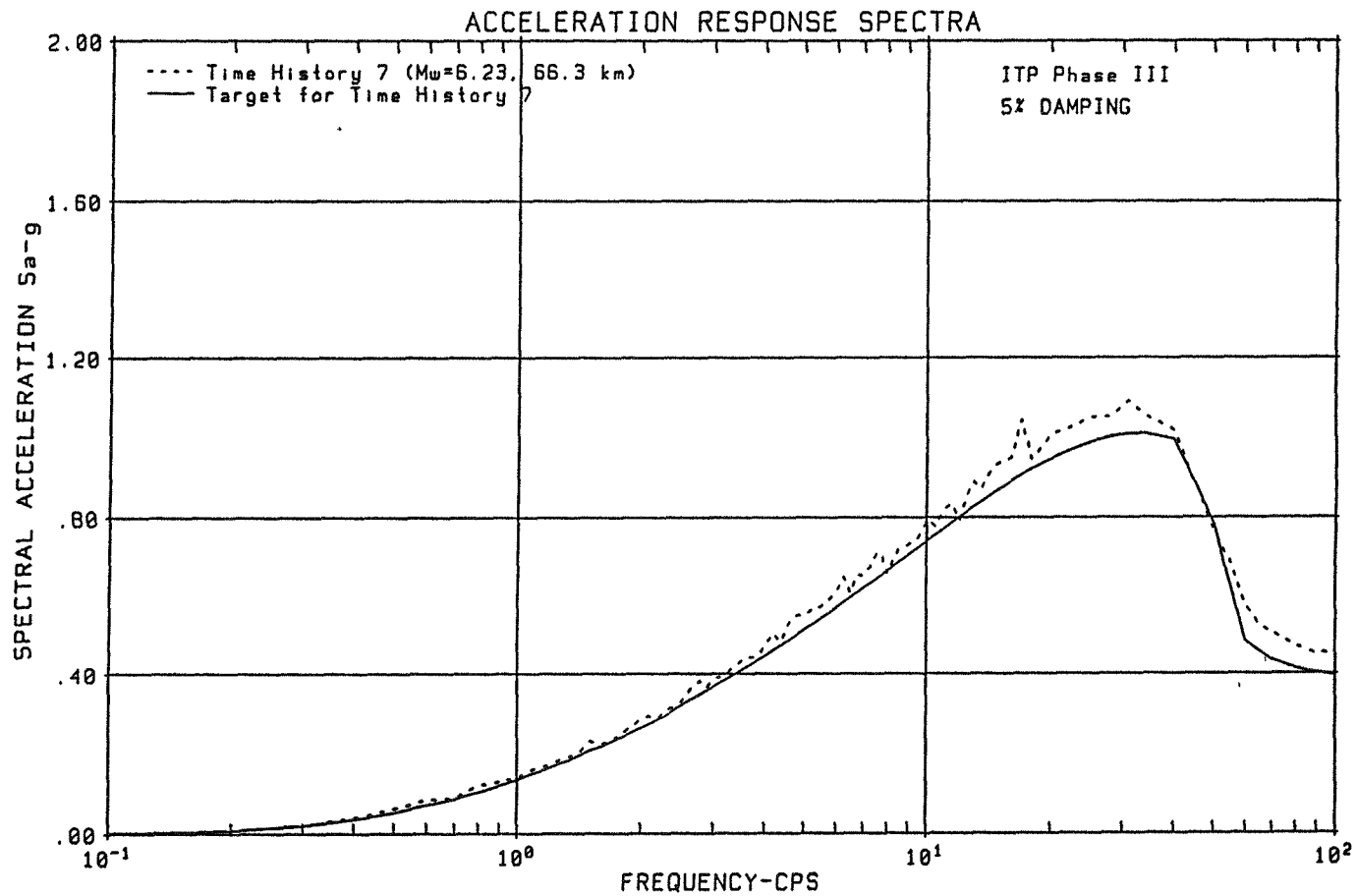


Figure 9.3-31 Acceleration response spectra for earthquake motion E07

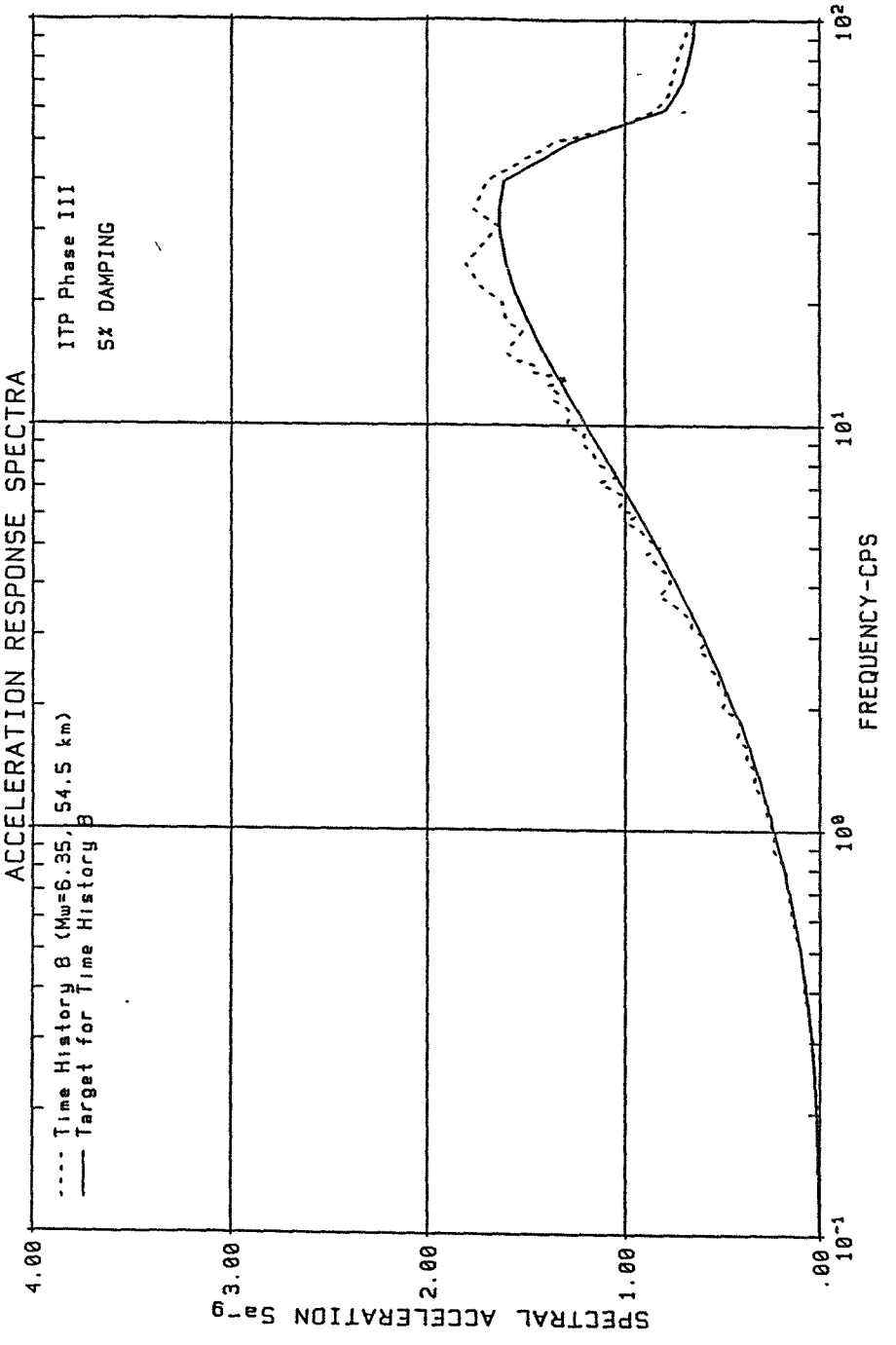


Figure 9.3-32 Acceleration response spectra for earthquake motion E08

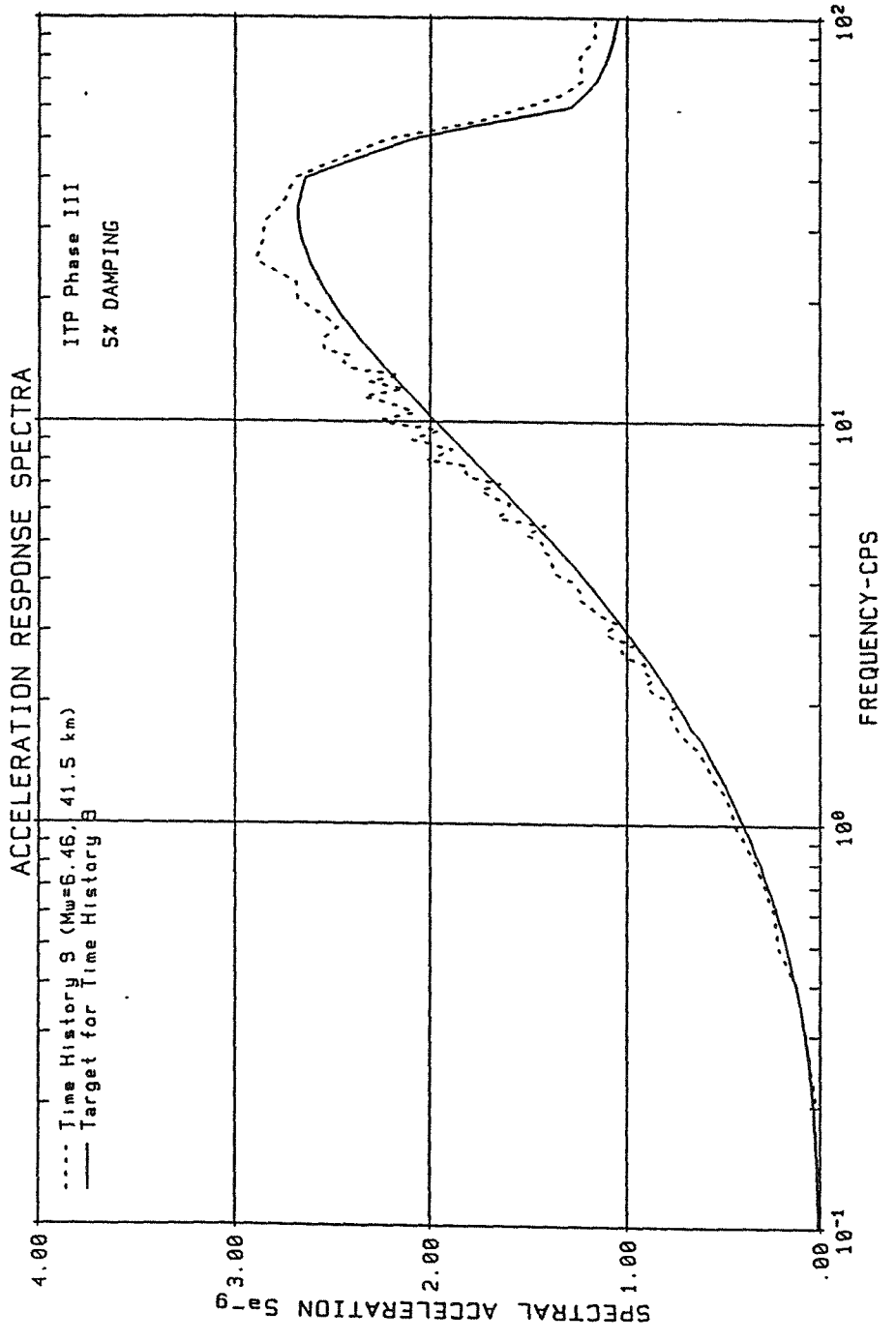


Figure 9.3-33 Acceleration response spectra for earthquake motion E09

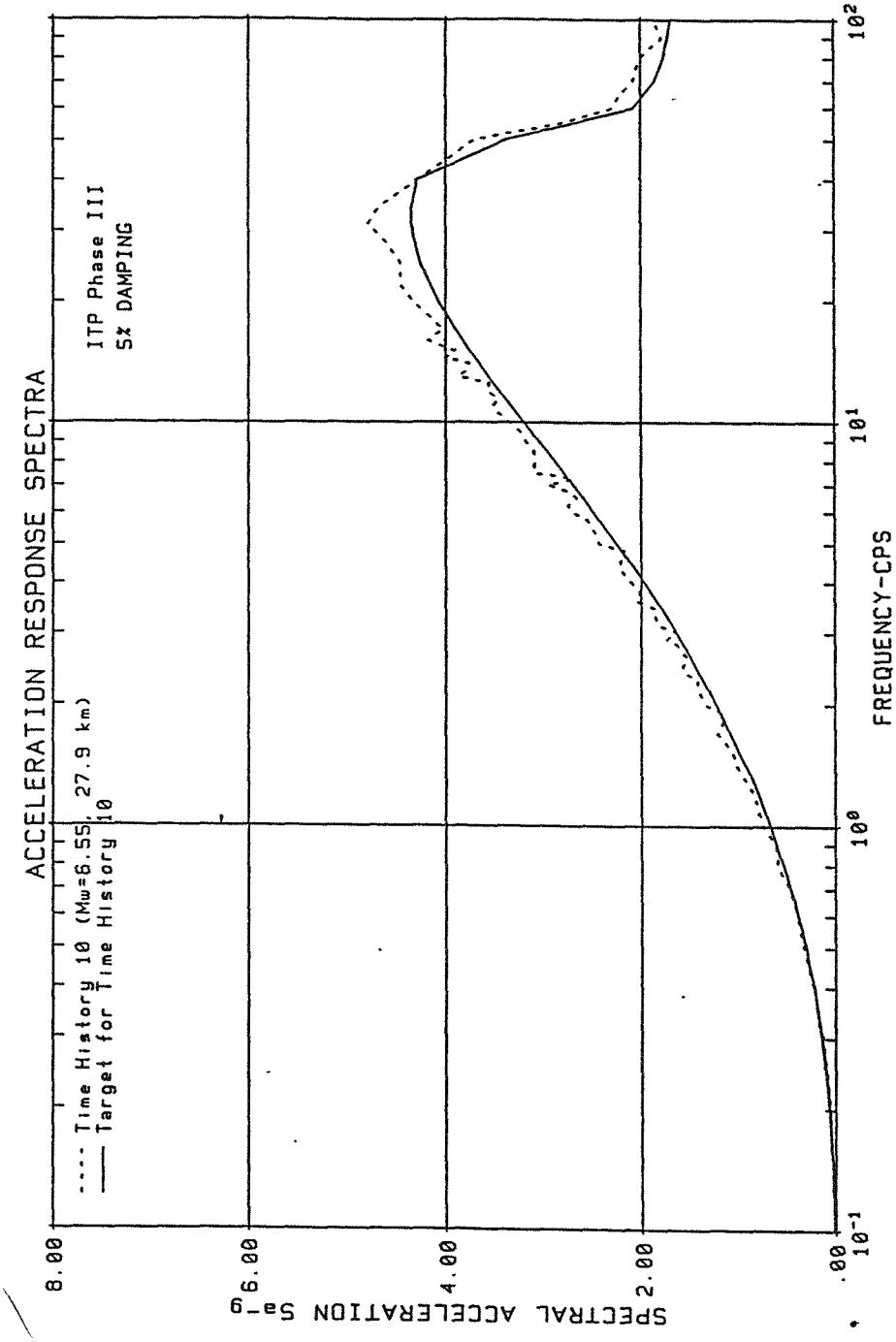


Figure 9.3-34 Acceleration response spectra for earthquake motion E10

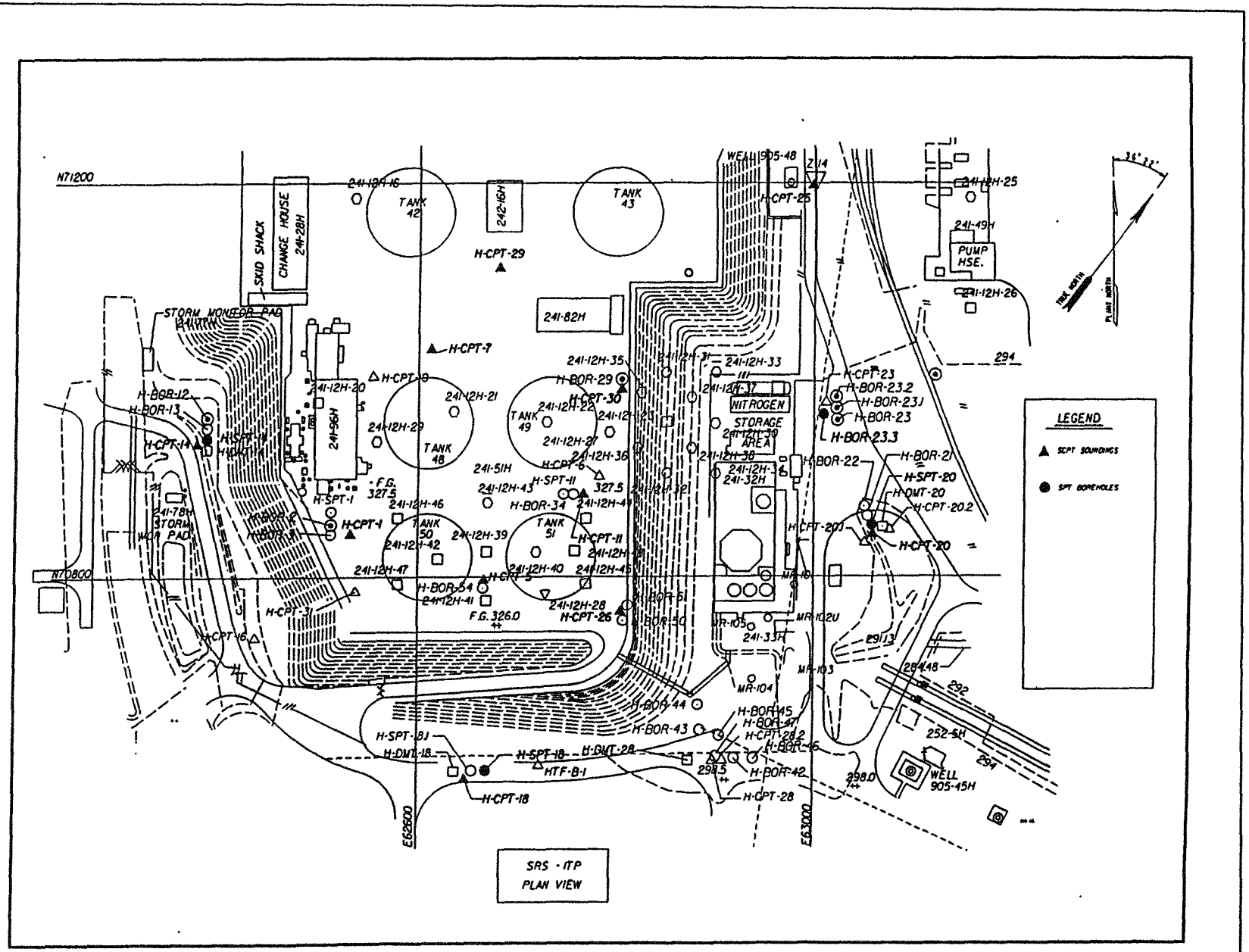


Figure 9.4-1 CPT soundings and SPT boreholes used in probabalistic liquefaction hazard evaluation.

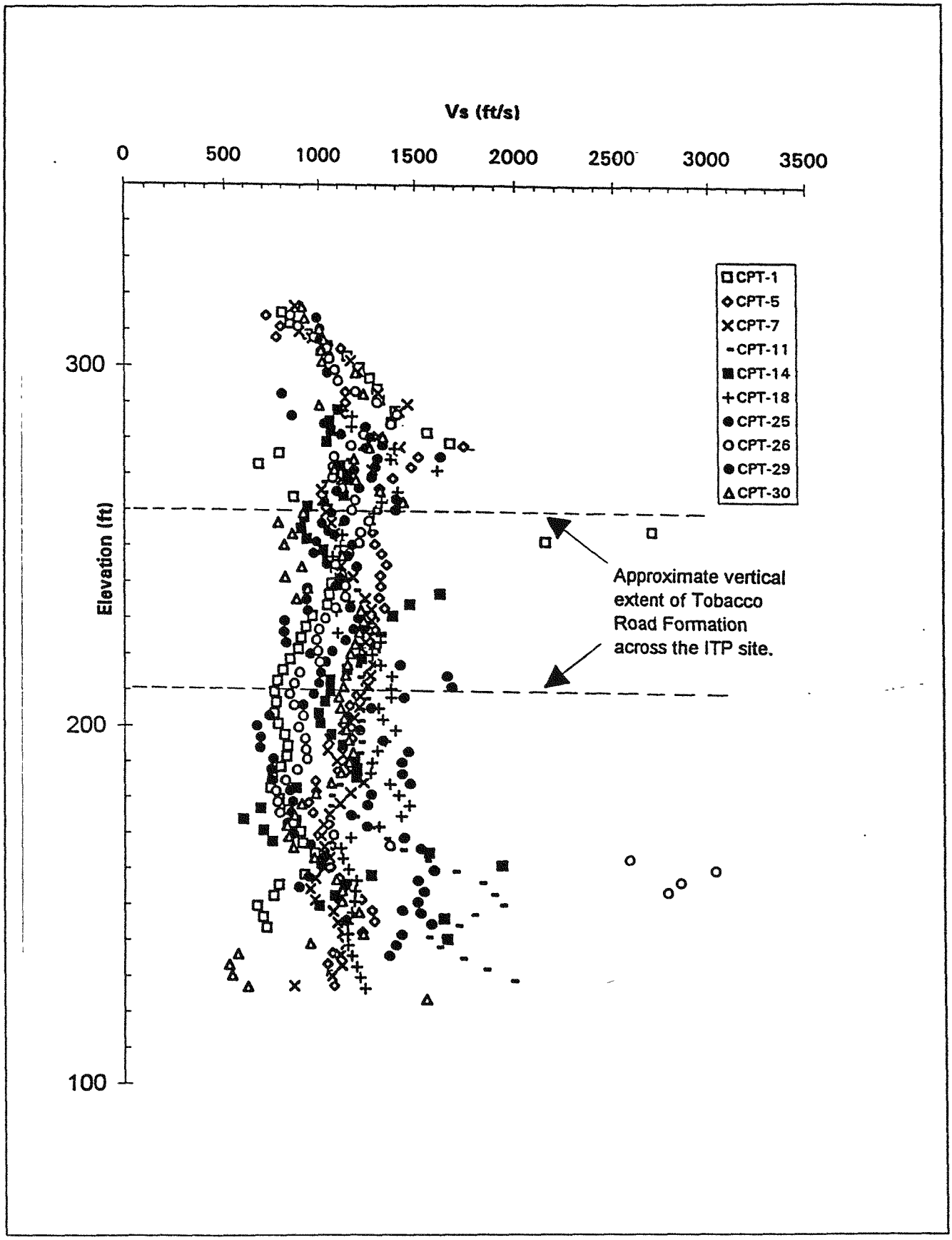


Figure 9.4-2 Shallow Shear Wave velocity profiles at ITP from seismic cone penetrometer.

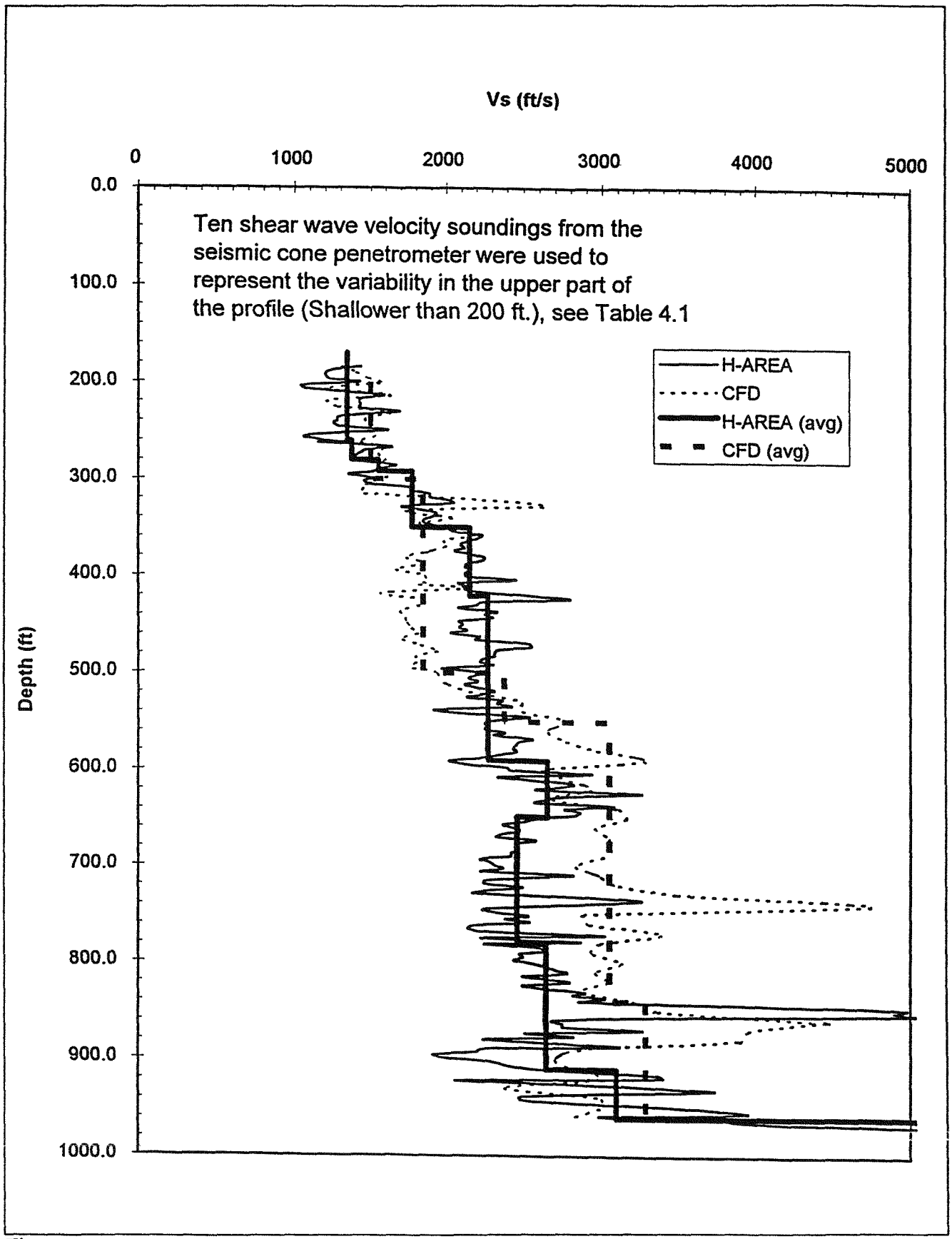


Figure 9.4-3 Comparison of deep shear wave velocity profiles used in dynamic analysis.

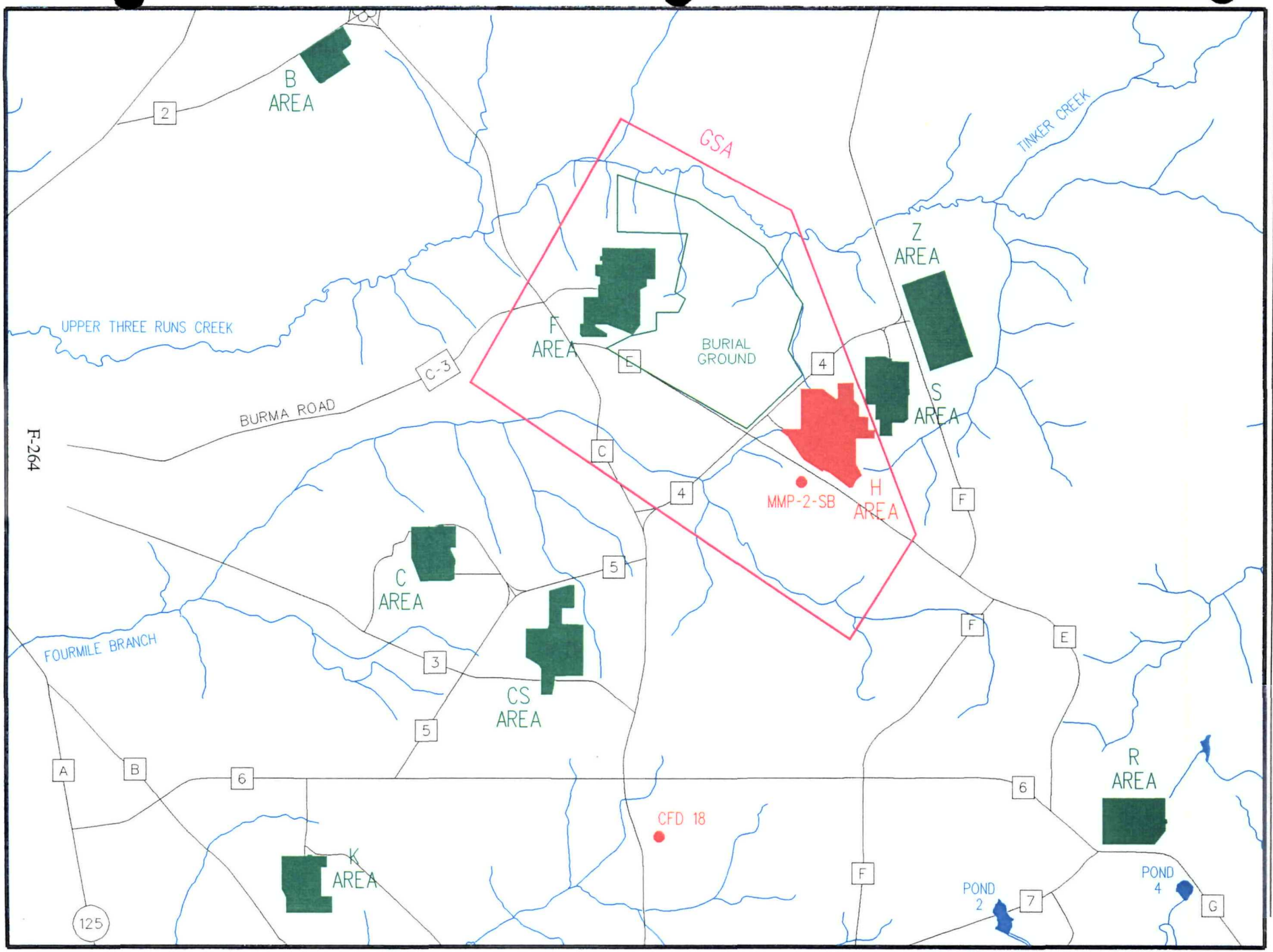


Figure 9.4-4 Map showing 2 OYO™ logged, deep core borings

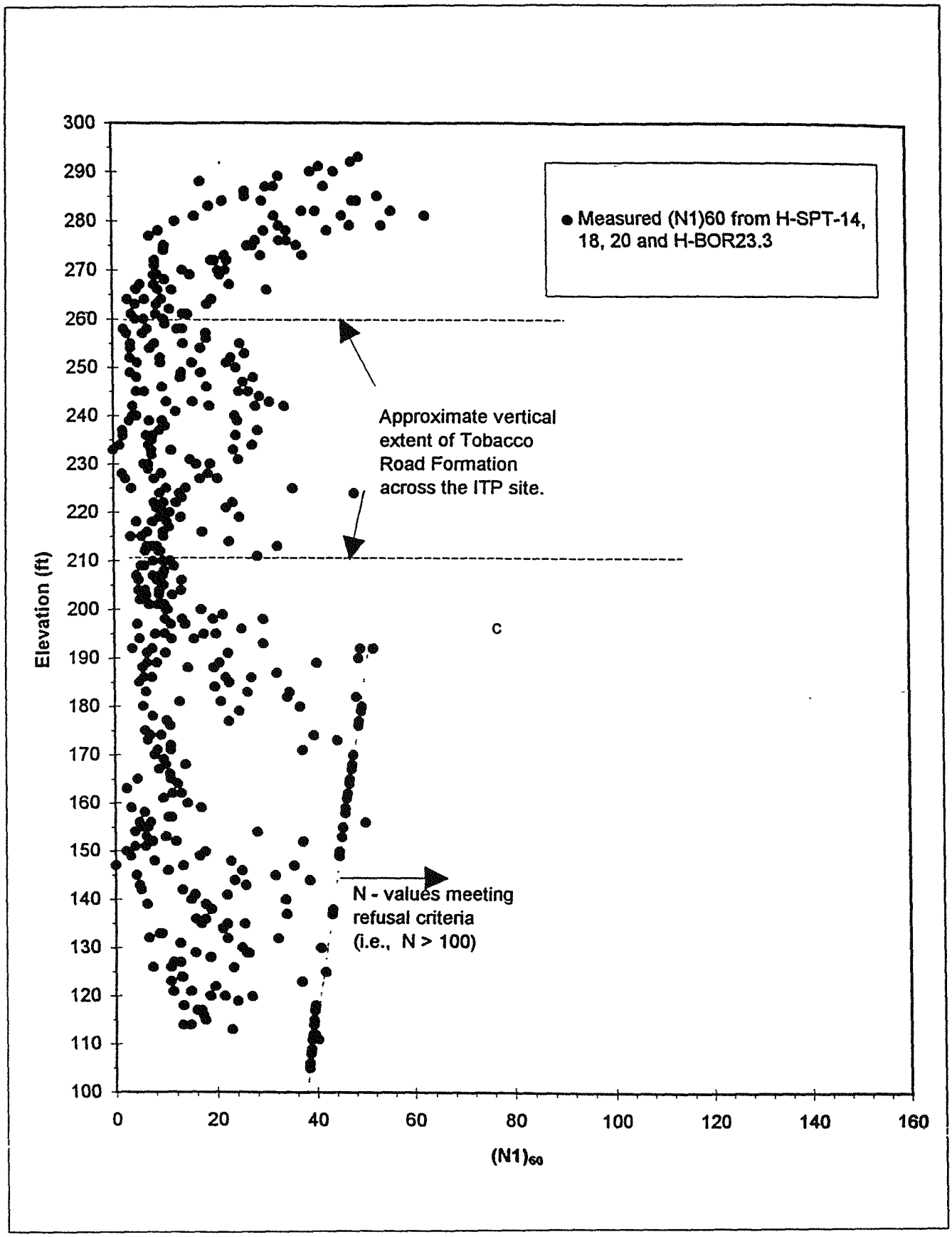


Figure 9.4-5 Measured $(N_1)_{60}$ values for ITP.

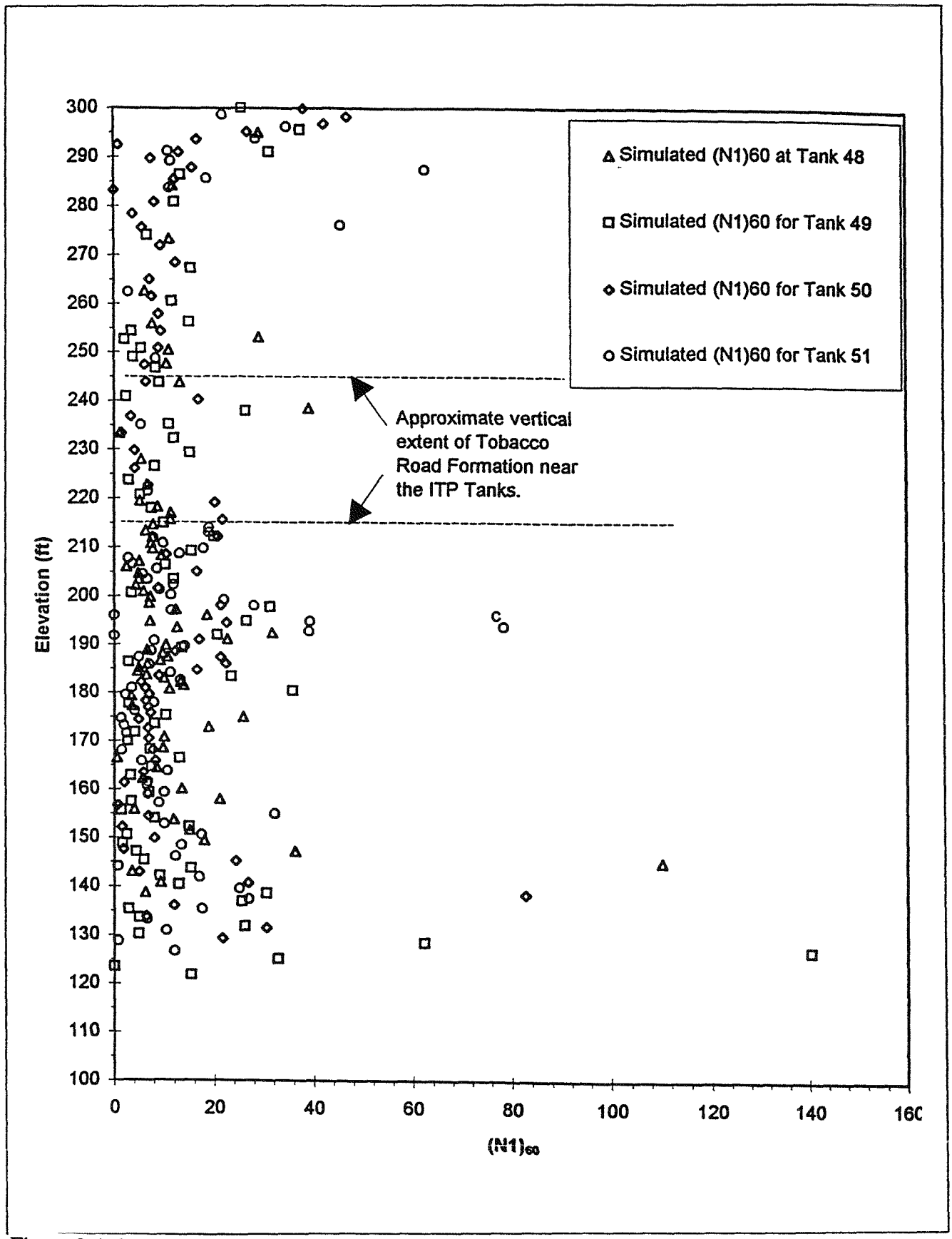


Figure 9.4-6 Simulated $(N_1)_{60}$ values for ITP.

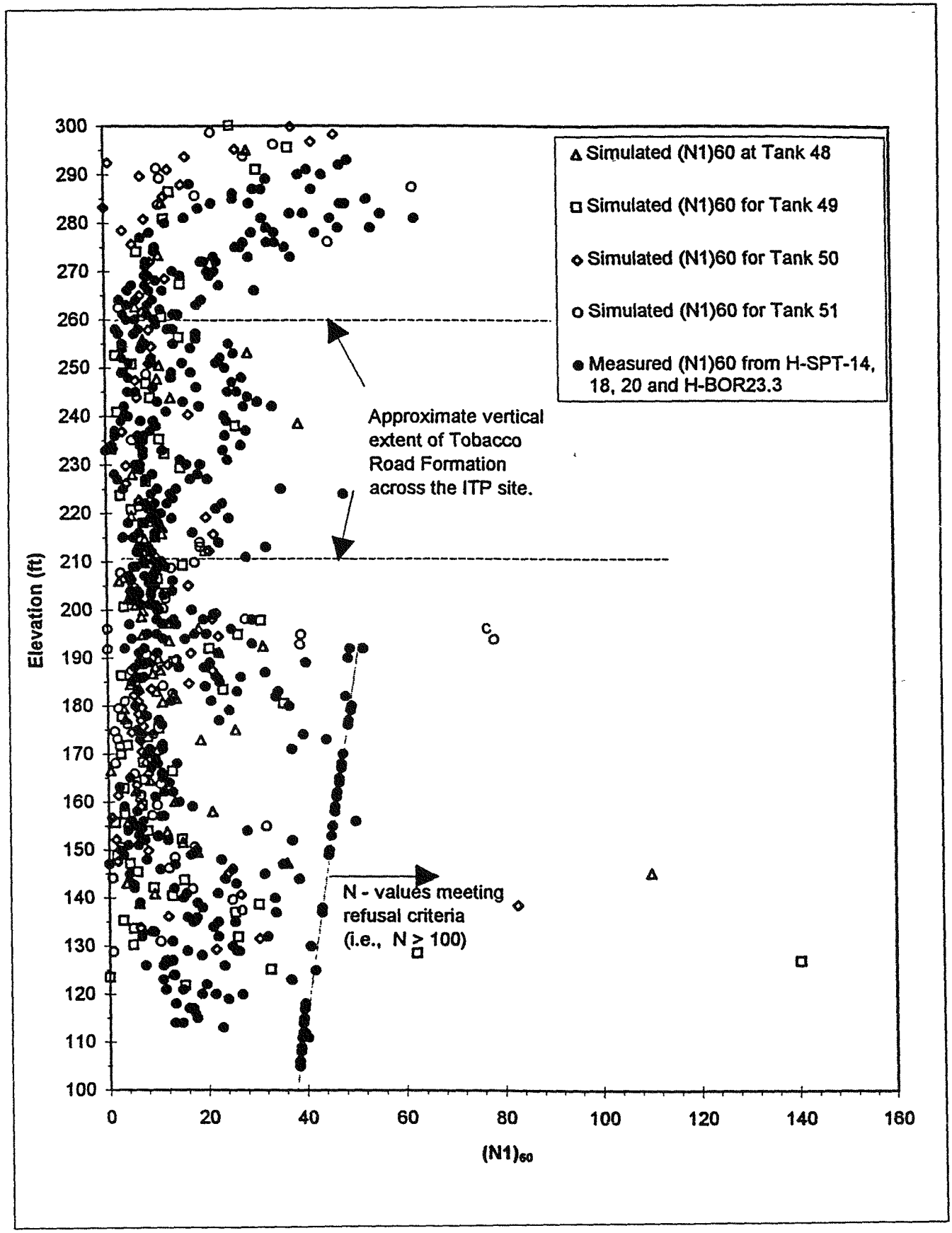


Figure 9.4-7 Measured and simulated $(N_1)_{60}$ values for ITP.

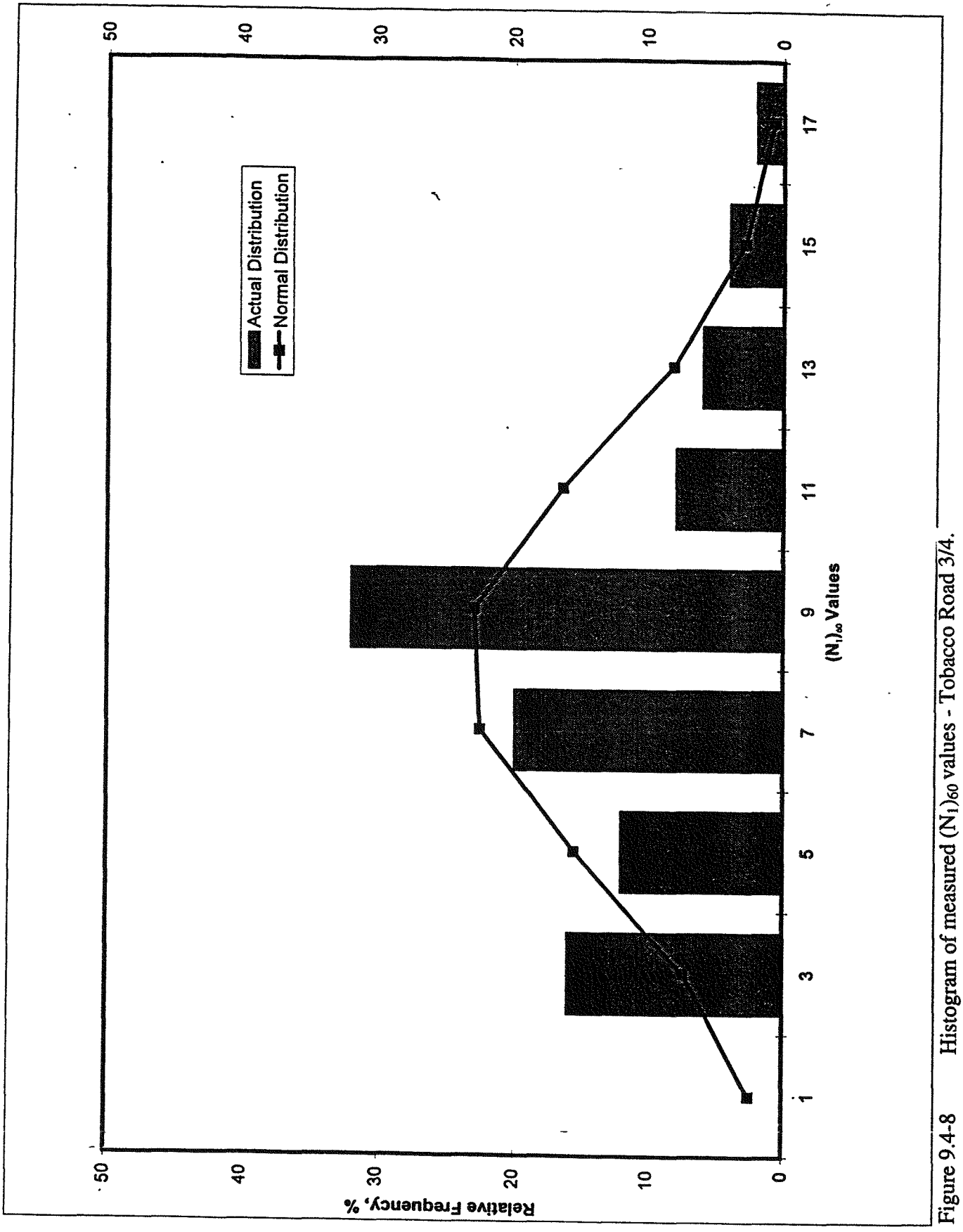


Figure 9.4-8 Histogram of measured $(N_1)_{60}$ values - Tobacco Road 3/4.

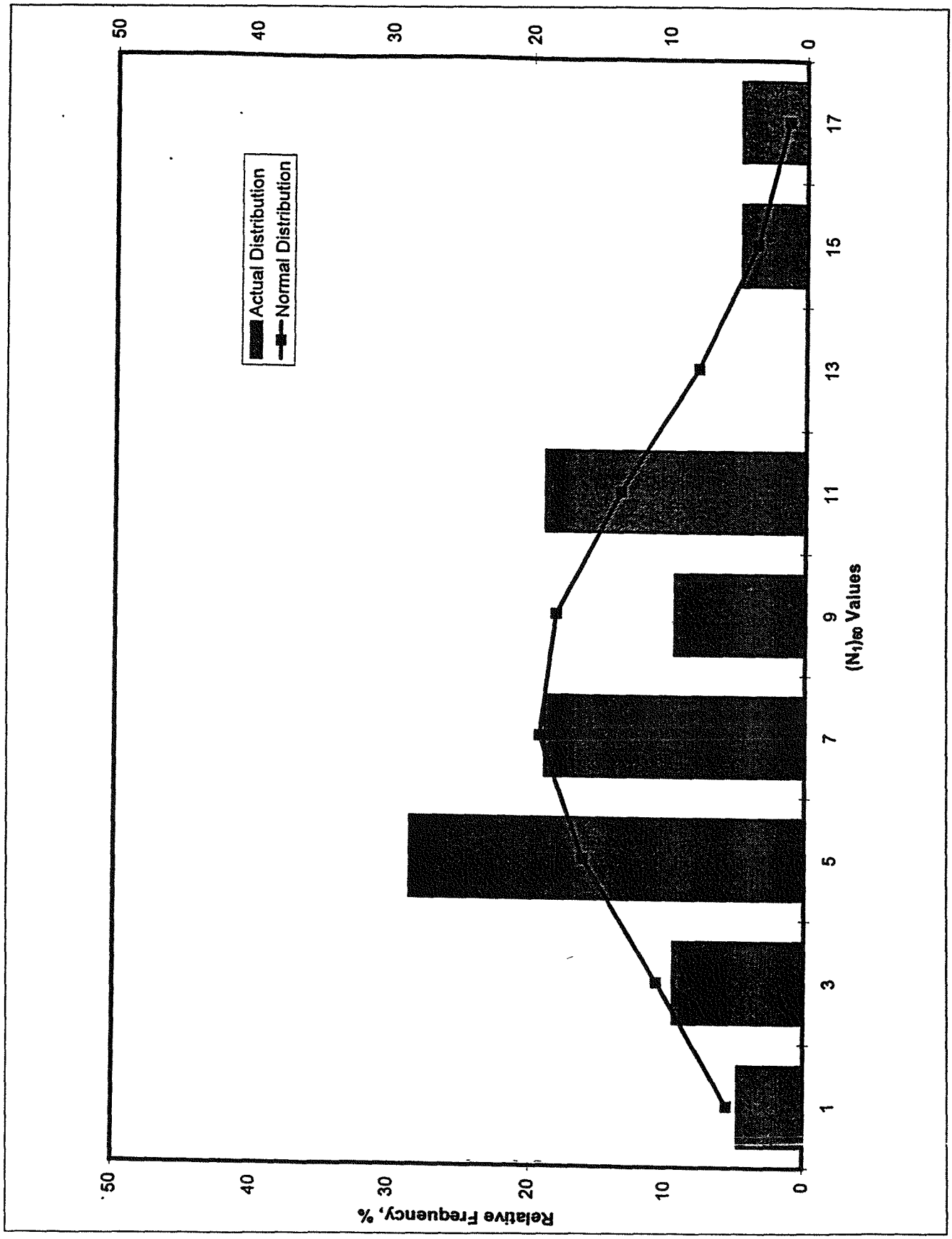


Figure 9.4-9 Histogram of simulated $(N_1)_{60}$ values - Tobacco Road 3/4.

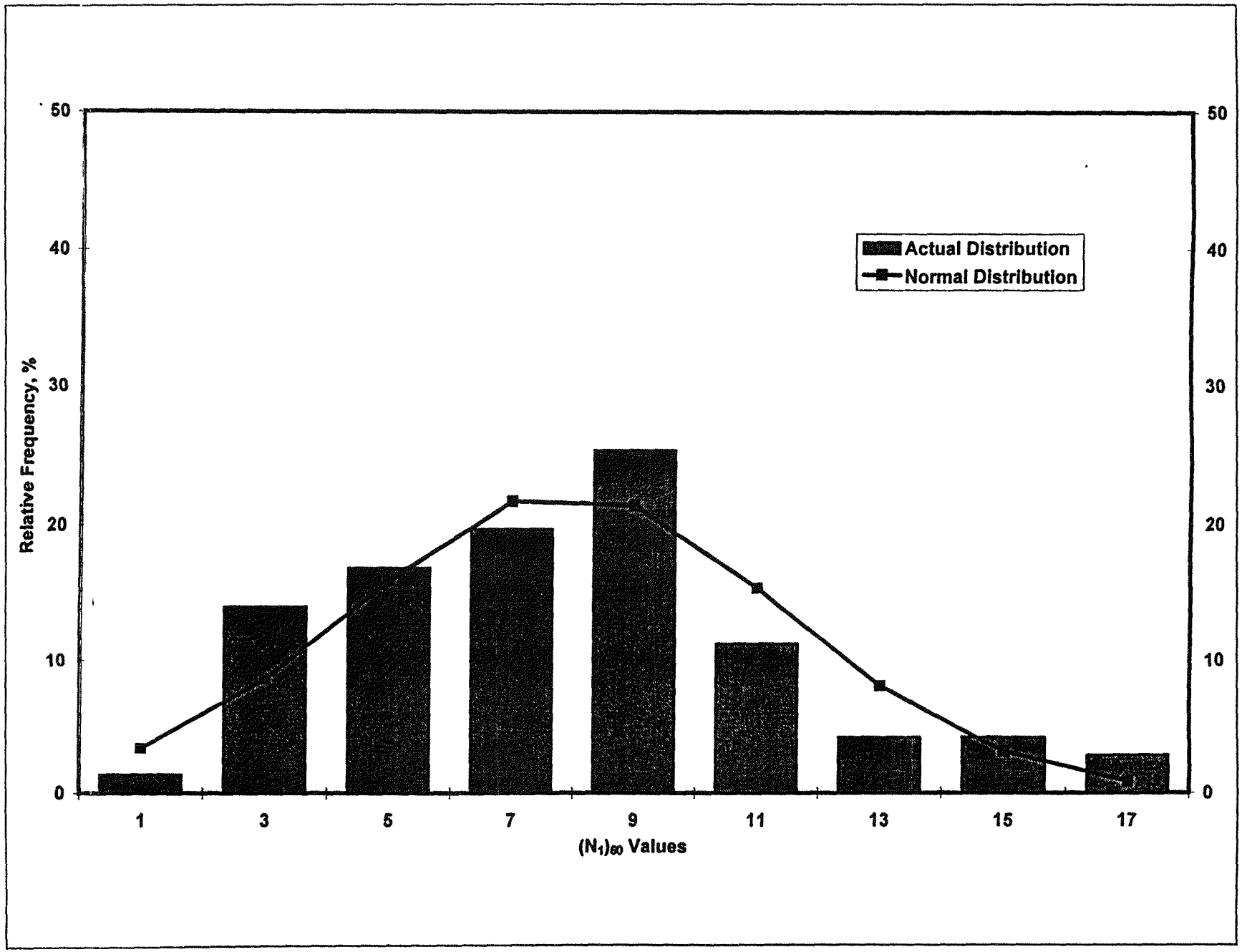


Figure 9.4-10 Histogram of combined (measured and simulated) $(N_1)_{60}$ values - Tobacco Road 3/4.

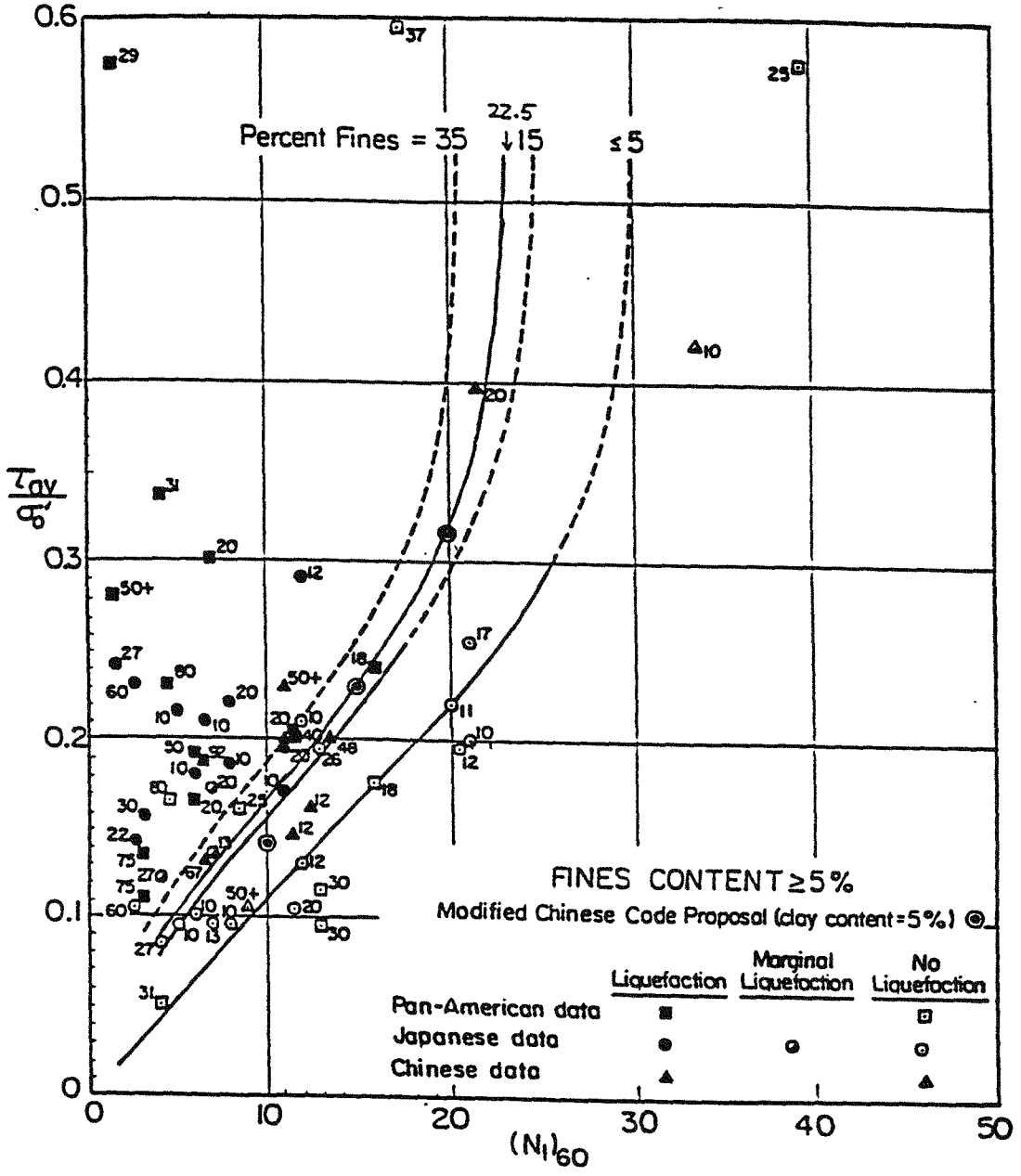


Figure 9.4-11 Relationships between stress ratio causing liquefaction and $(N1_1)_{60}$ values for sands and silty sands in M =7 1/2 earthquakes. (after Seeds et al, 1985)

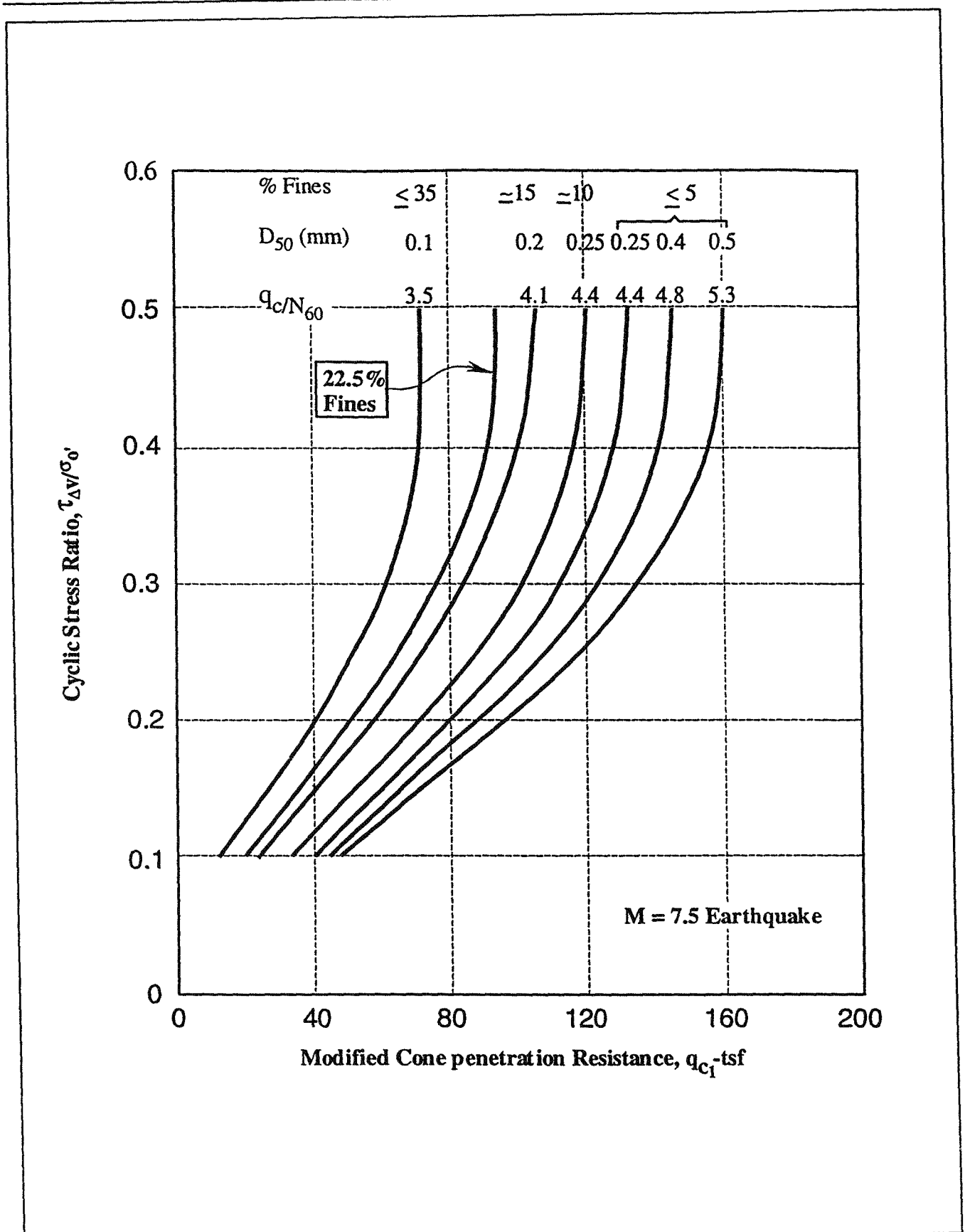


Figure 9.4-12 Relationship between stress ratio causing liquefaction and cone tip resistance for sands and silty sands. (after DeAlba and Seed, 1986)

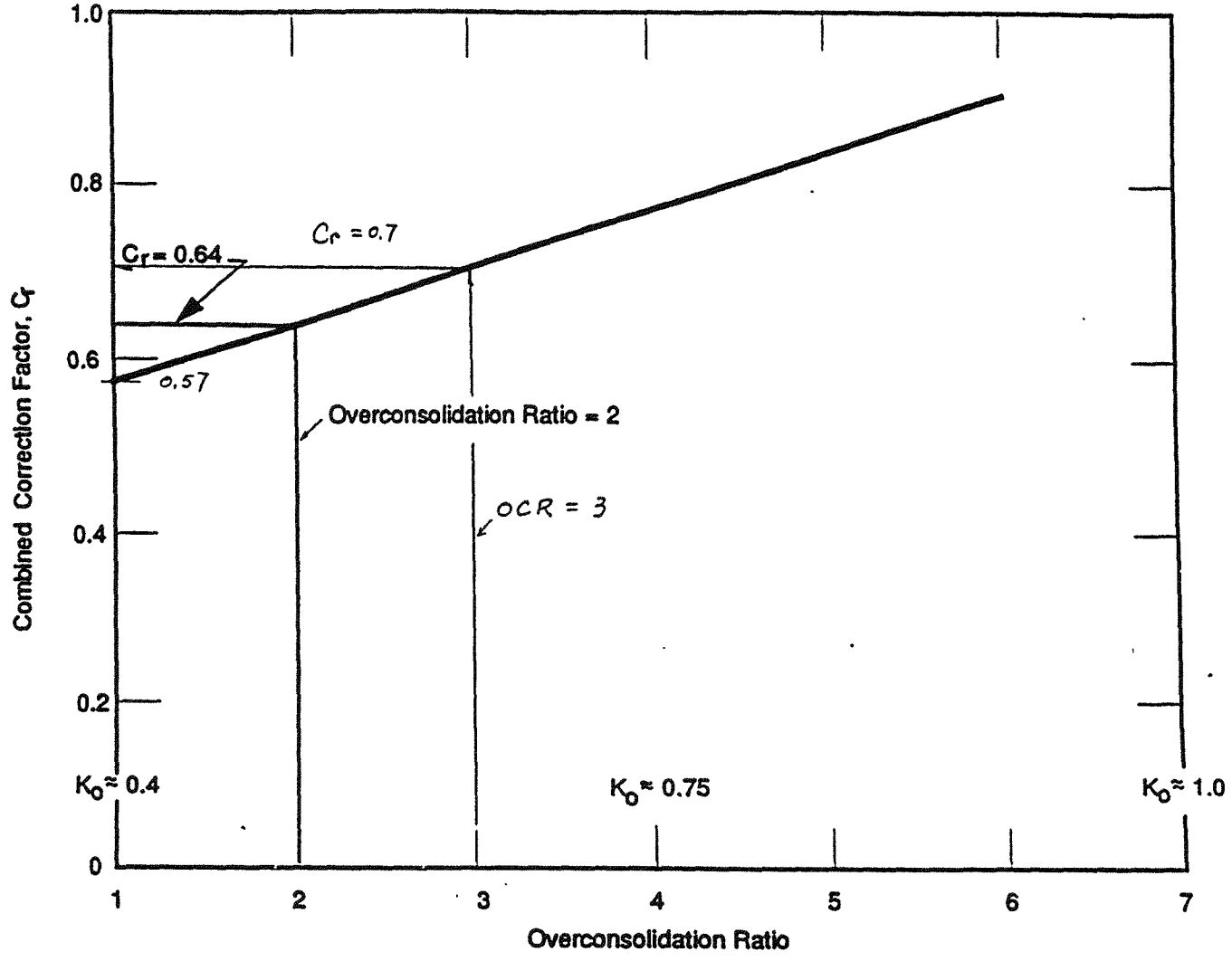


Figure 9.4-13 Relationship between combined correction factor Cr and overconsolidation ratio. (after Seed, Arango and Chan, 1975)

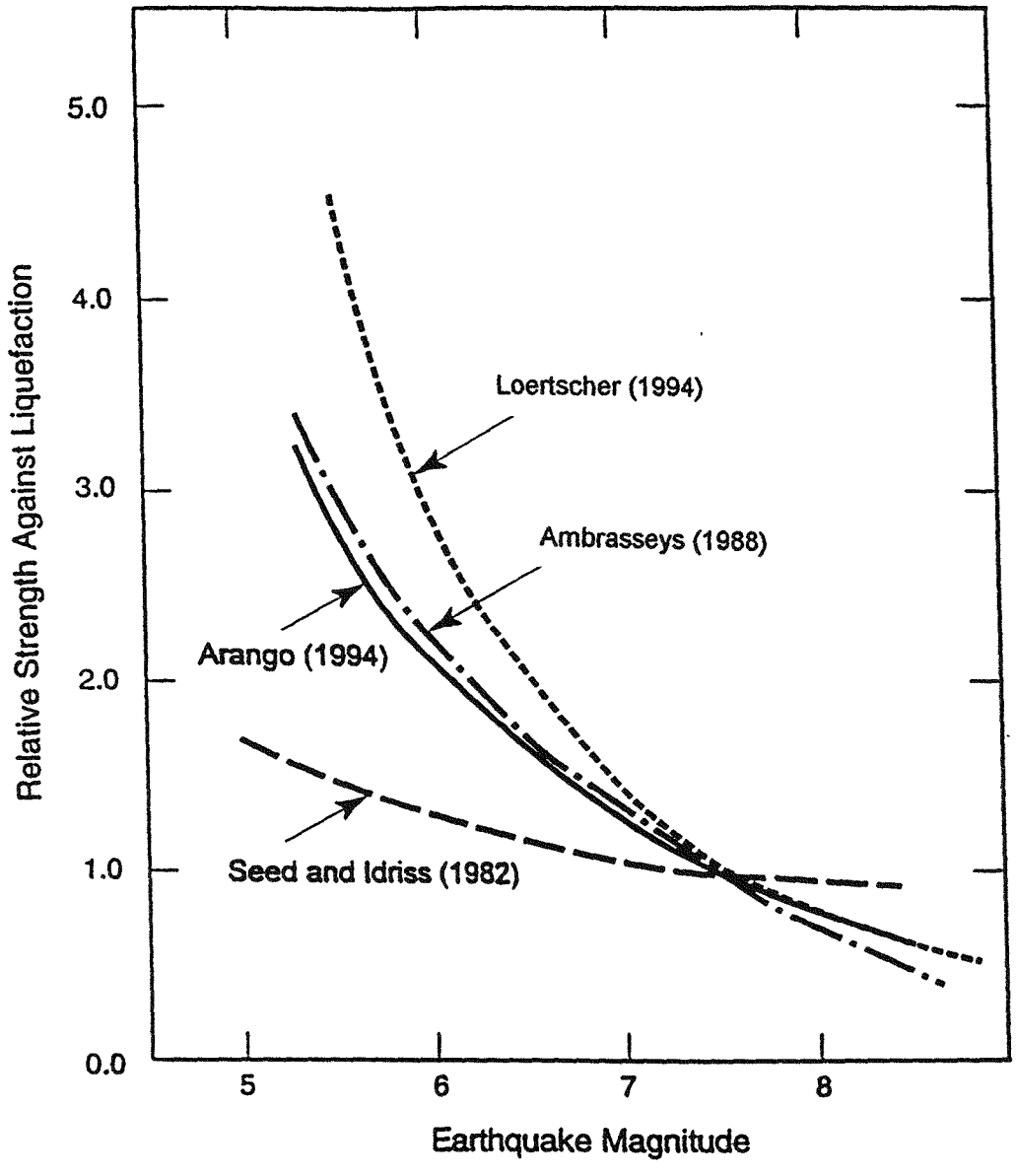


Figure 9.4-14 Comparison of earthquake magnitude correction factors from various sources.

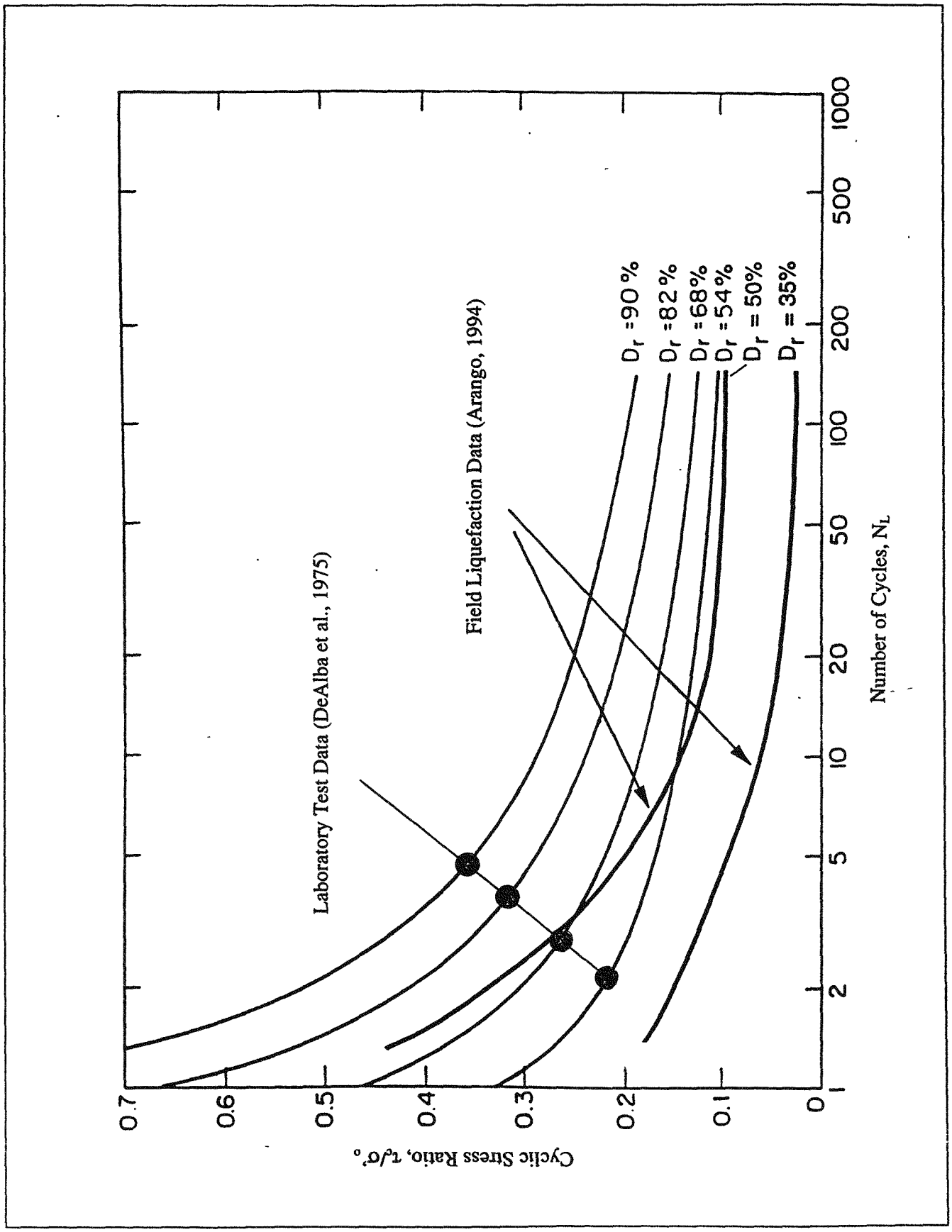


Figure 9.4-15 Liquefaction data: field vs laboratory

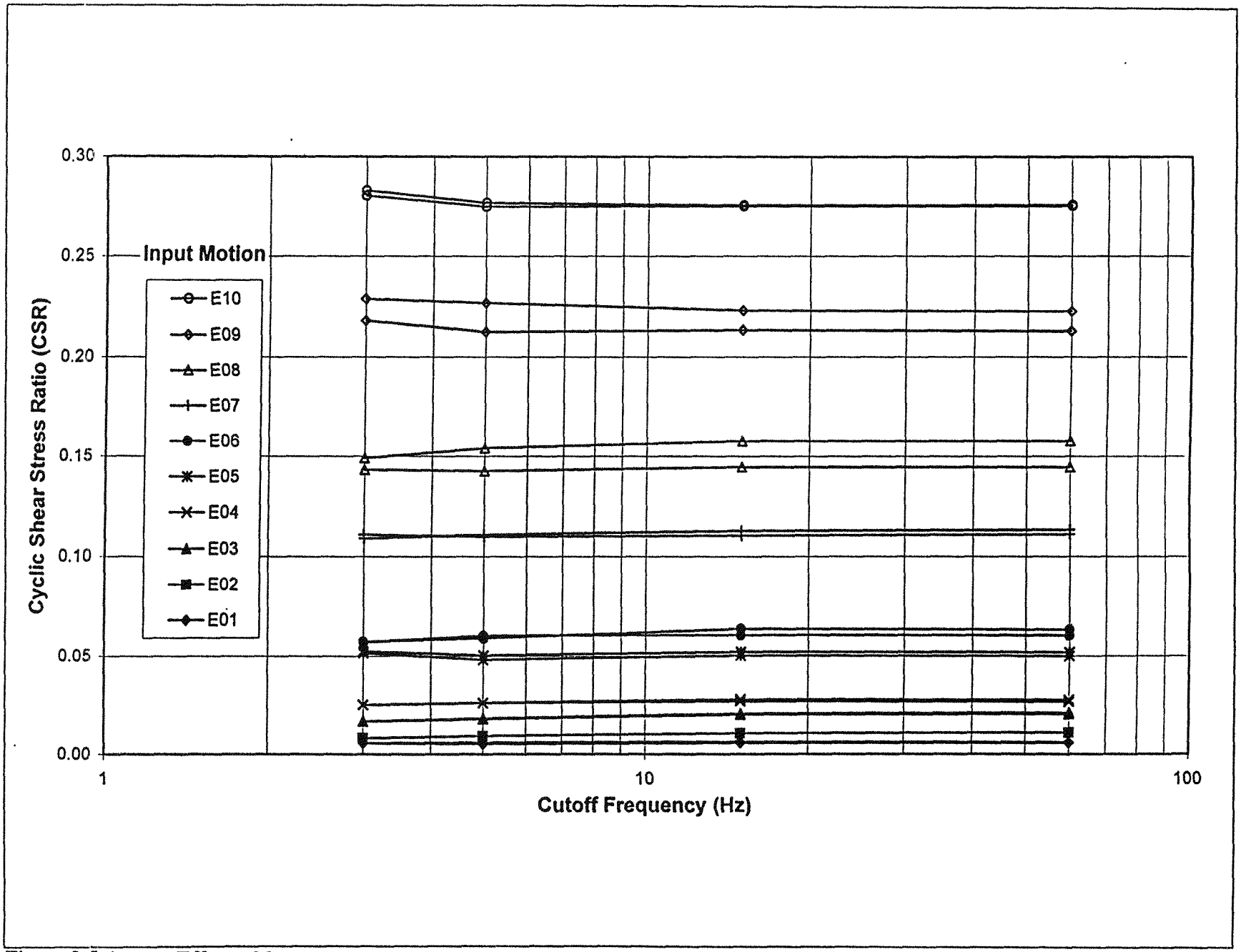


Figure 9.5-1 Effect of frequency content of input motion on the effective cyclic stress ratio (CSR) - Tobacco Road 3/4, Soil Profile CPT11.

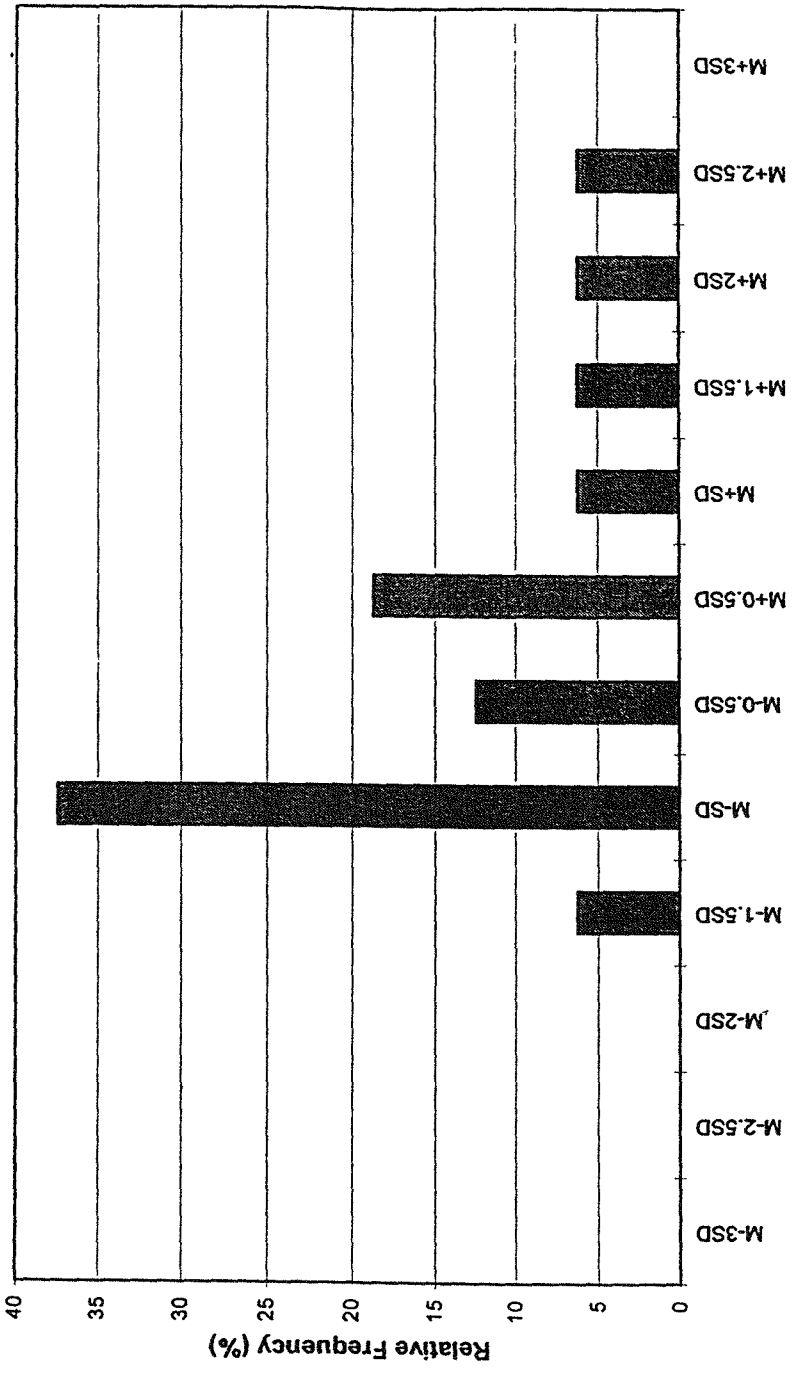


Figure 9.5-2 Relative histogram for effective shear stress ratio - Tobacco Road 3/4, earthquake EO1. Mean = 0.0078, Standard deviation = 0.0018

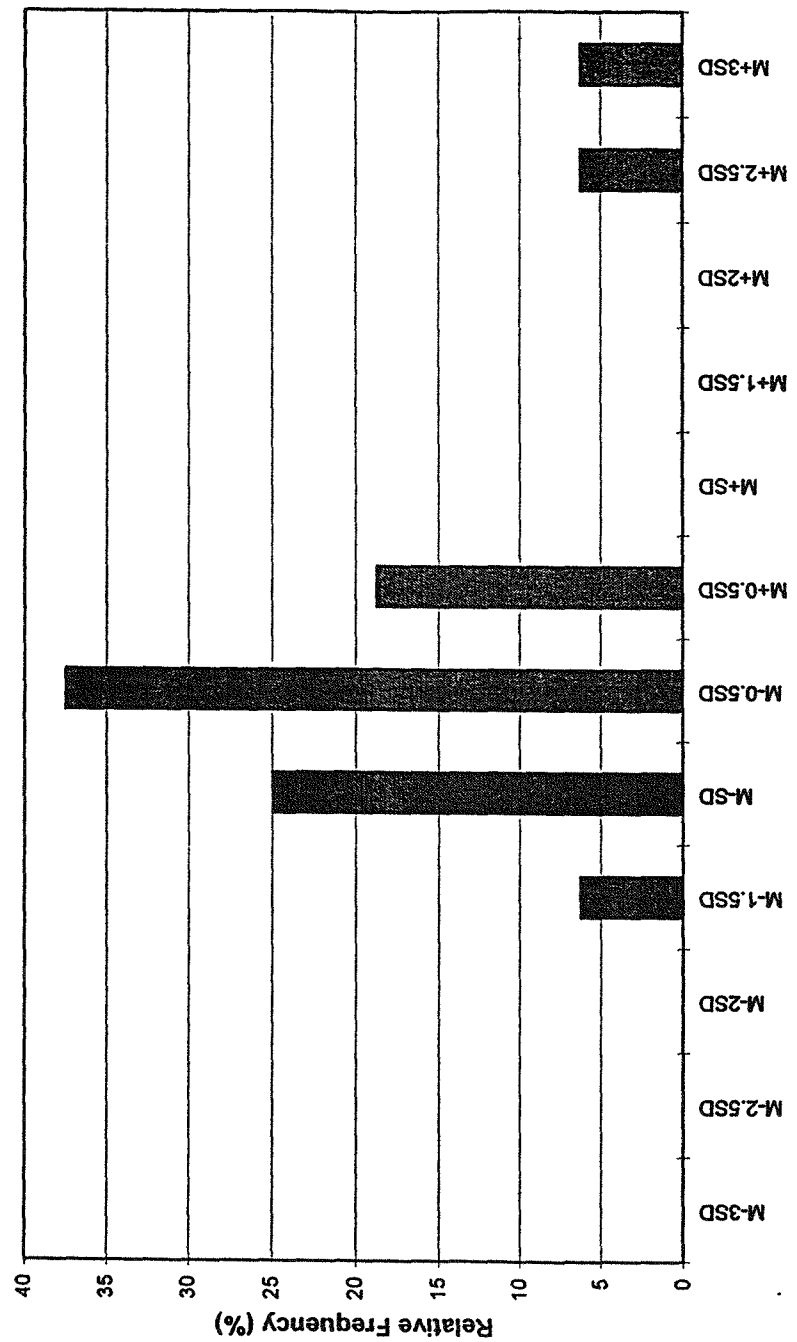


Figure 9.5-3 Relative histogram for effective shear stress ratio - Tobacco Road 3/4, earthquake EO2. Mean = 0.0119, Standard deviation 0.0018.

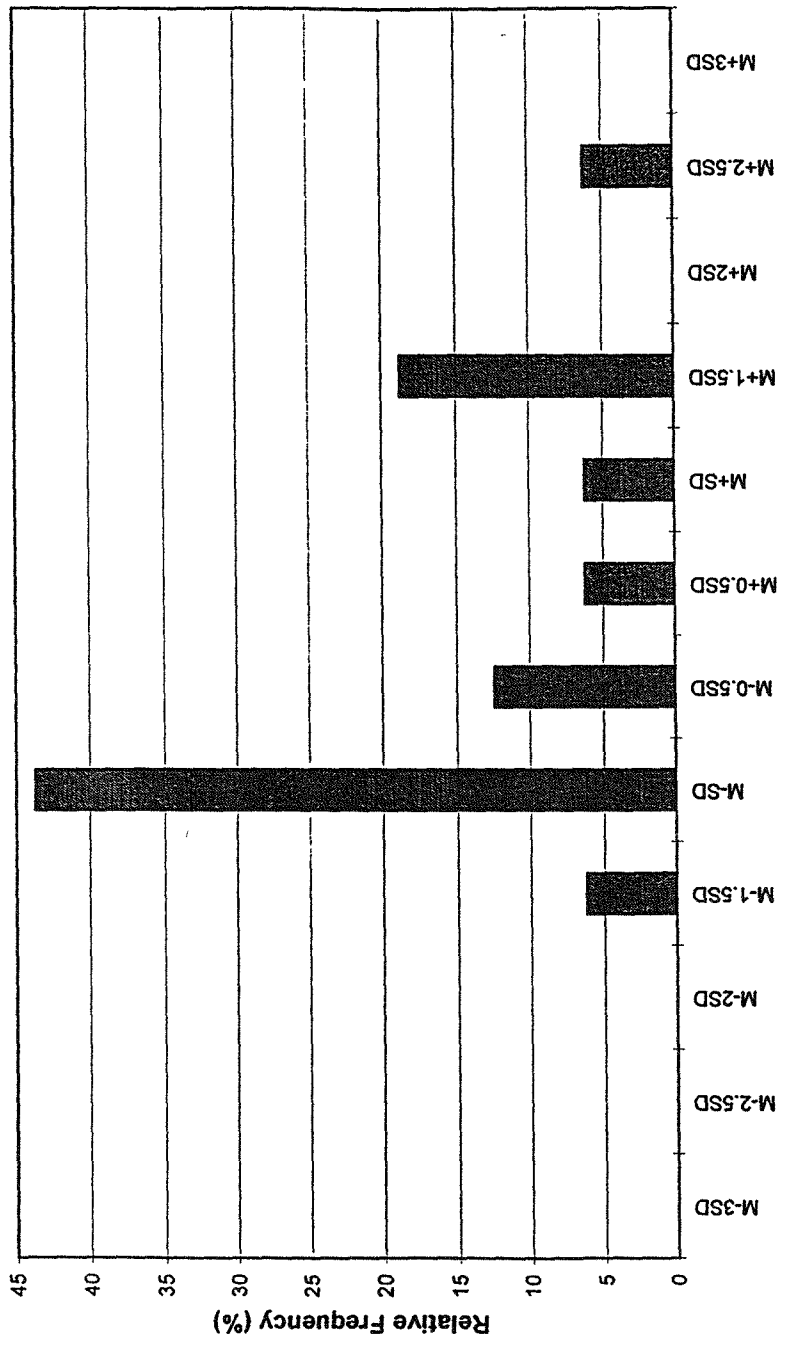


Figure 9.5-4 Relative histogram for effective shear stress ratio - Tobacco Road 3/4, earthquake EO3. Mean = 0.022, Standard deviation = 0.0054.

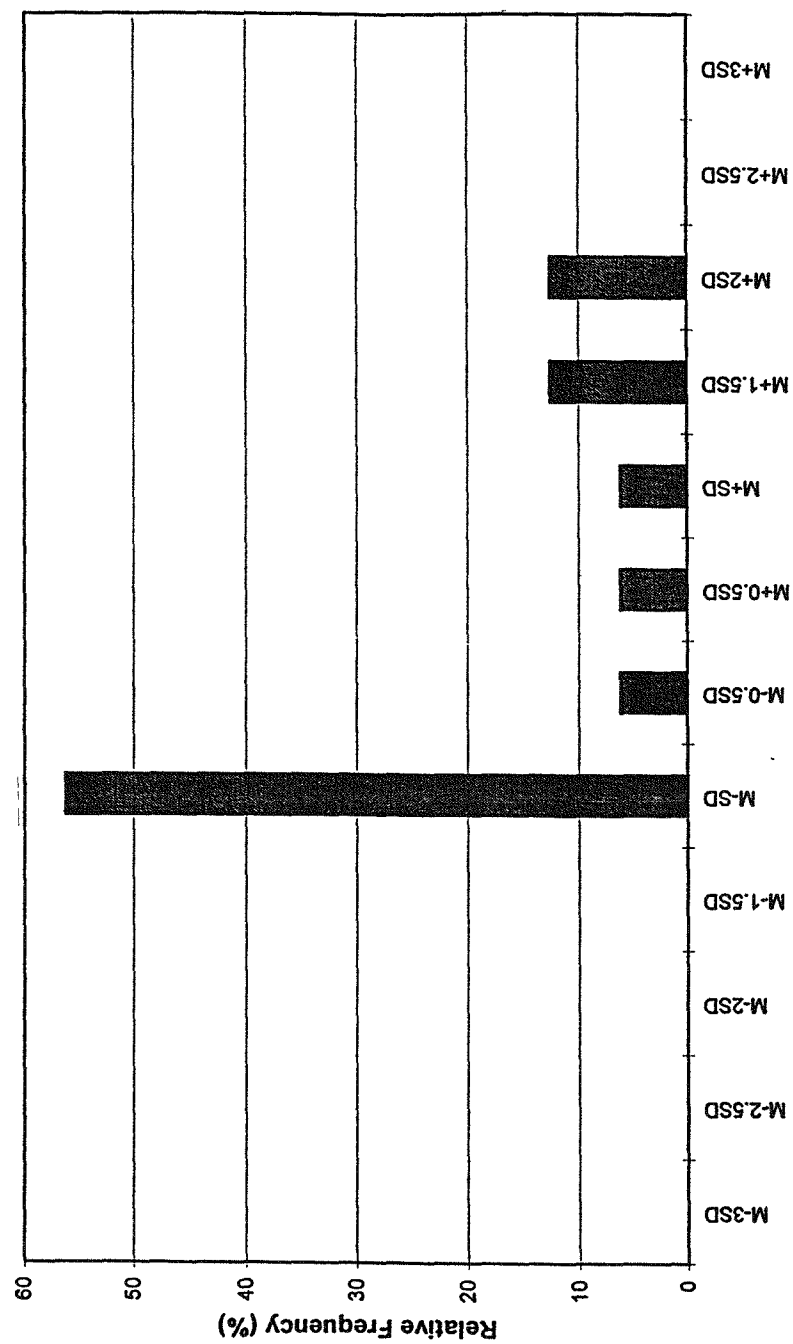


Figure 9.5-5 Relative histogram for effective shear stress ratio - Tobacco Road 3/4, earthquake EO4. Mean = 0.0333 Standard deviation = 0.00922

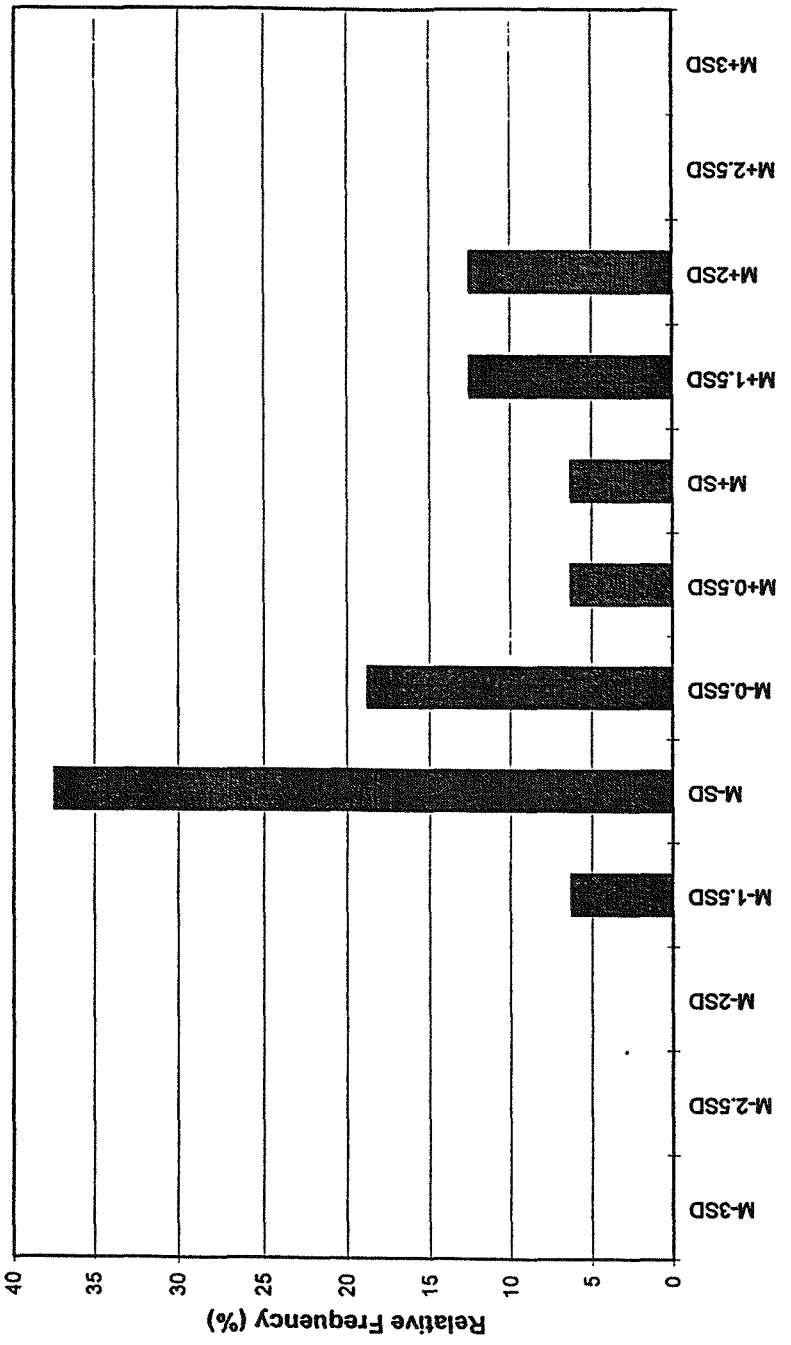


Figure 9.5-6 Relative histogram for effective shear stress ratio - Tobacco Road 3/4, Earthquake E05. Mean = 0.0564, Standard deviation = 0.0124.

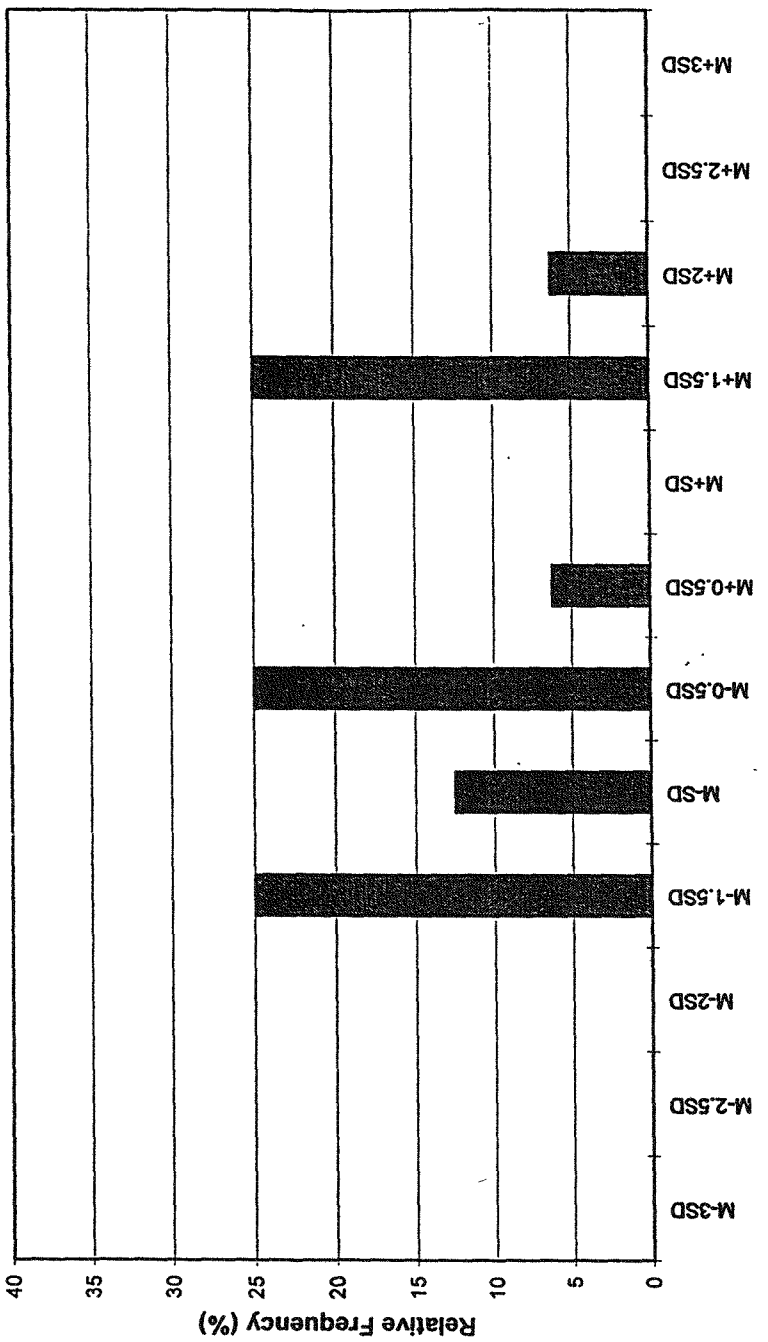


Figure 9.5-7 Relative histogram for effective shear stress ratio - Tobacco Road 3/4, earthquake EO6. Mean = 0.0752, Standard deviation = 0.0116

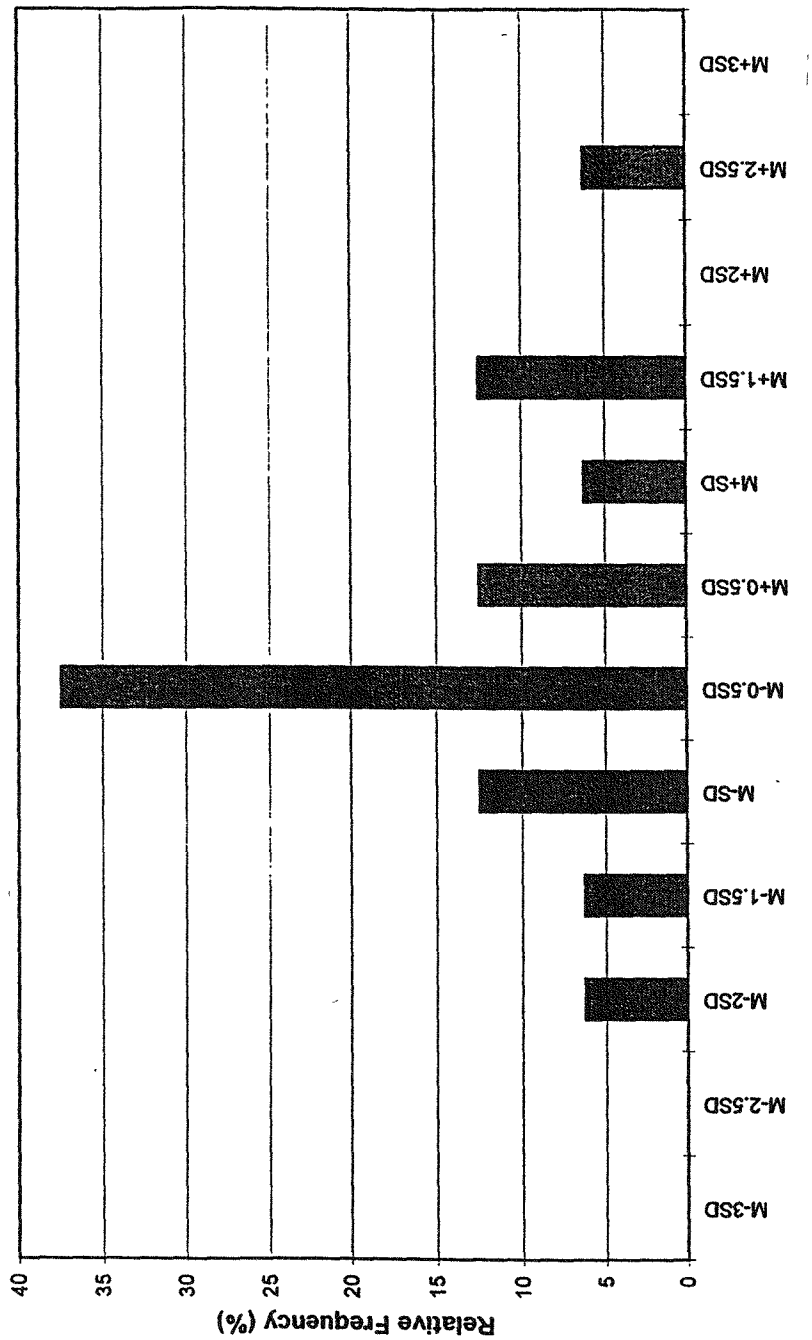


Figure 9.5-8 Relative histogram for effective shear stress ratio - Tobacco Road 3/4, earthquake EO7. Mean = 0.117, standard deviation = 0.021

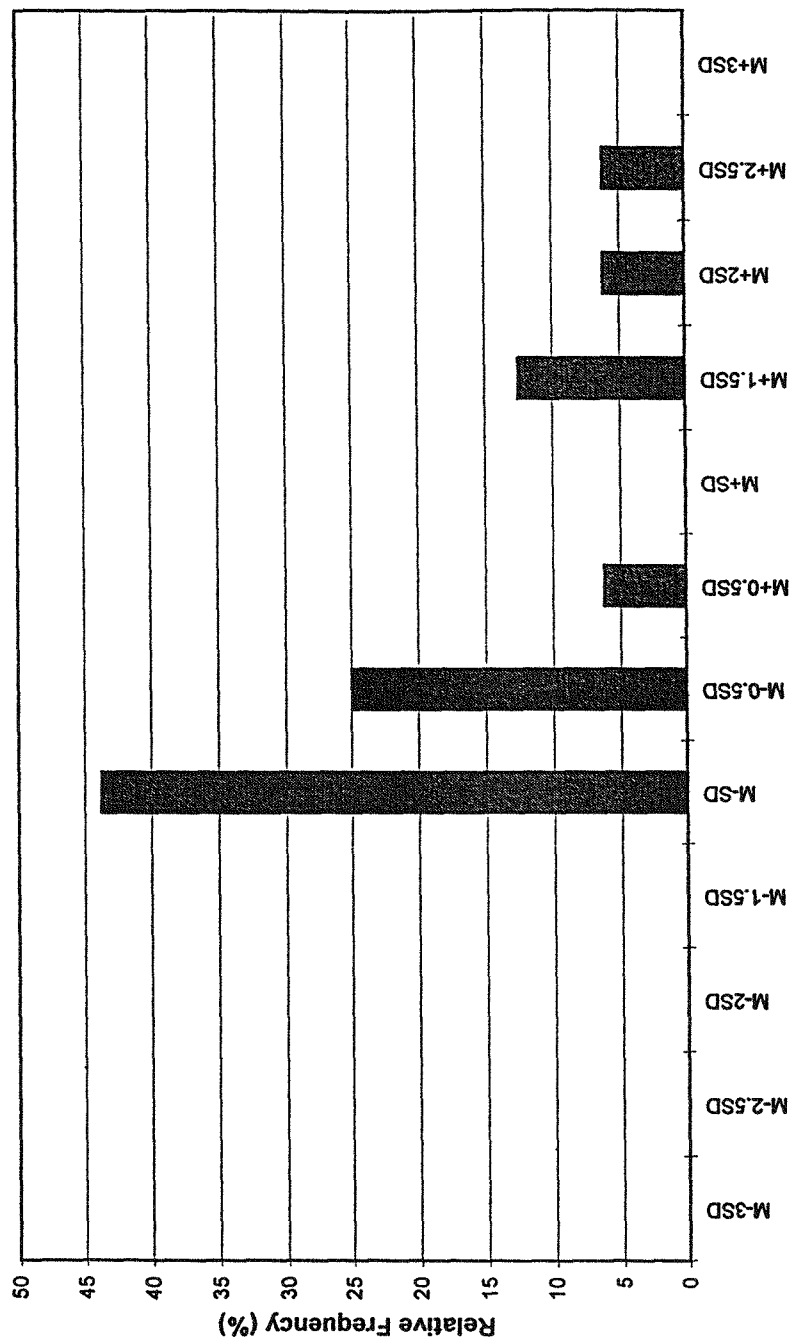


Figure 9 5-9 Relative histogram for effective shear stress ratio - Tobacco Road 3/4, earthquake EO8. Mean = 0.155, Standard deviation = 0.036

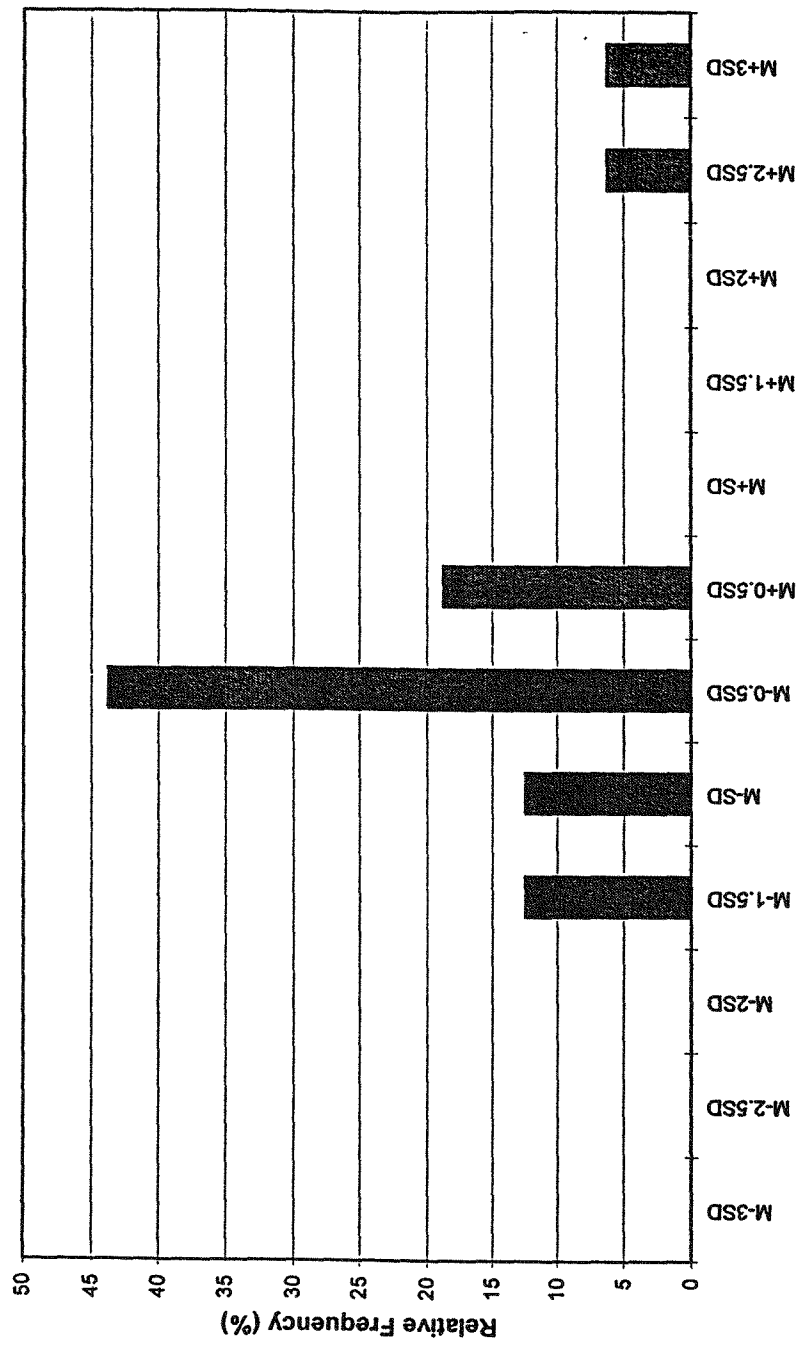


Figure 9.5-10 Relative histogram for effective shear stress ratio - Tobacco Road 3/4, earthquake EO9. Mean 0.205, Standard deviation 0.048.

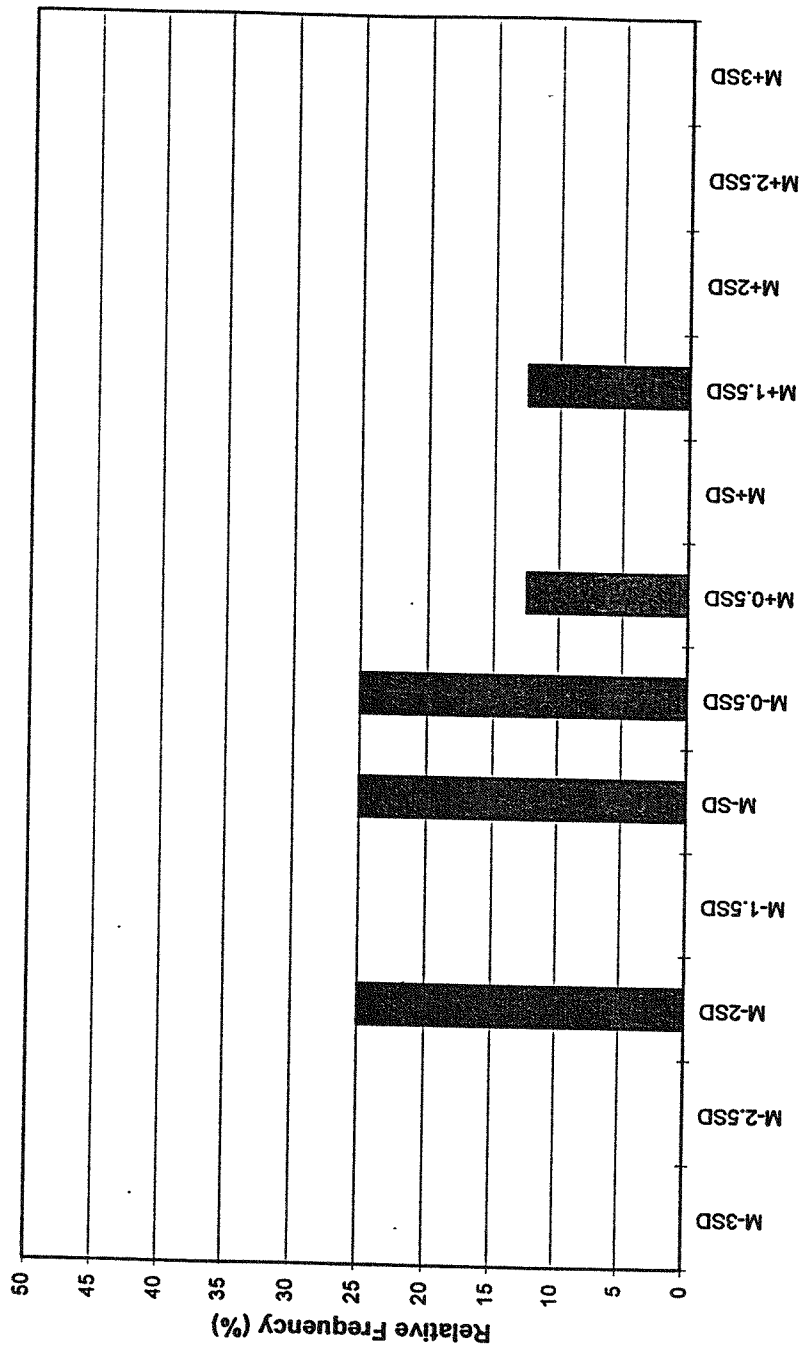


Figure 9.5-11 Relative histogram for effective shear stress ratio - Tobacco Road 3/4, earthquake E10. Mean 0.262, Standard deviation 0.0424.

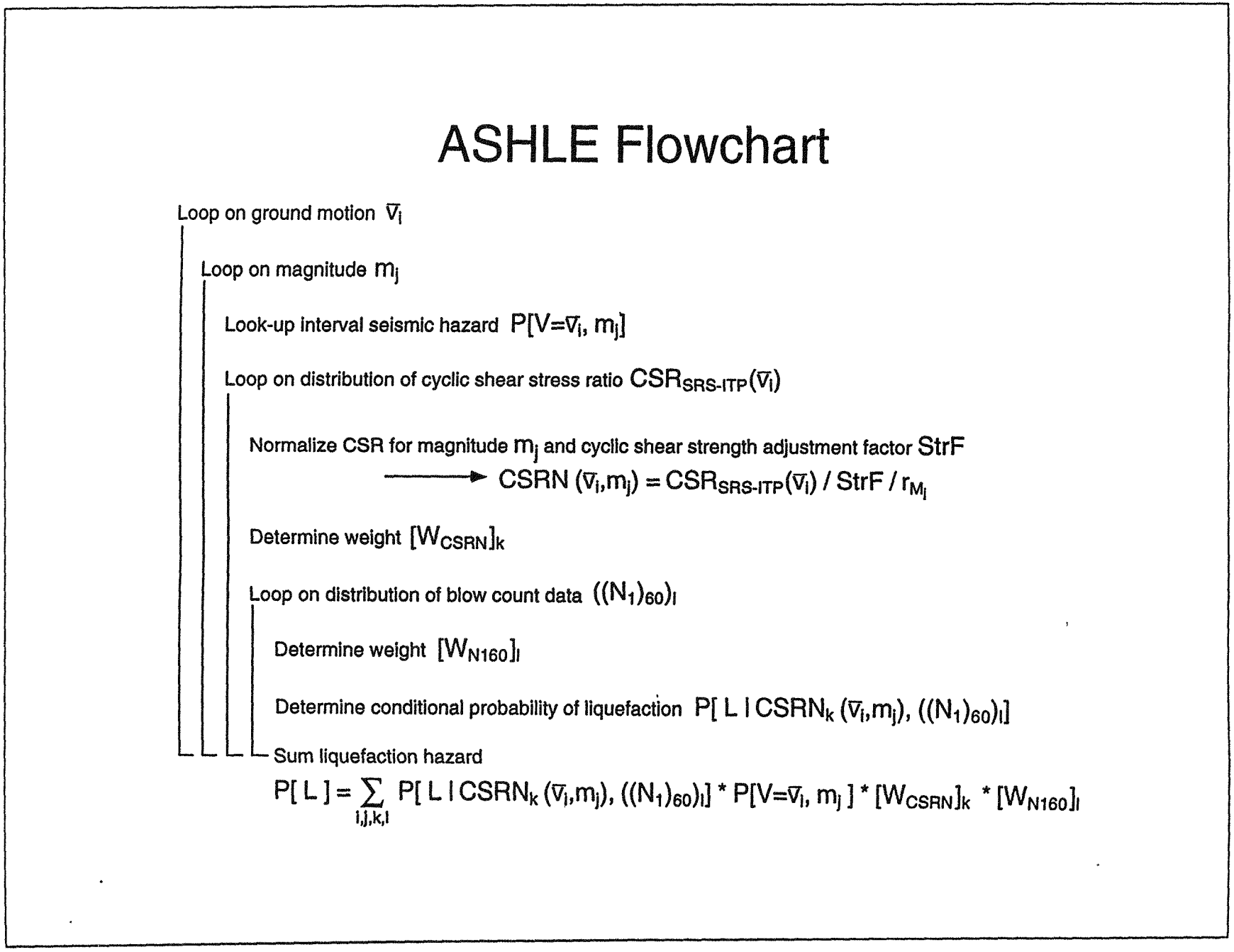


Figure 9.6-1 Flow chart for ASHLE Methodology

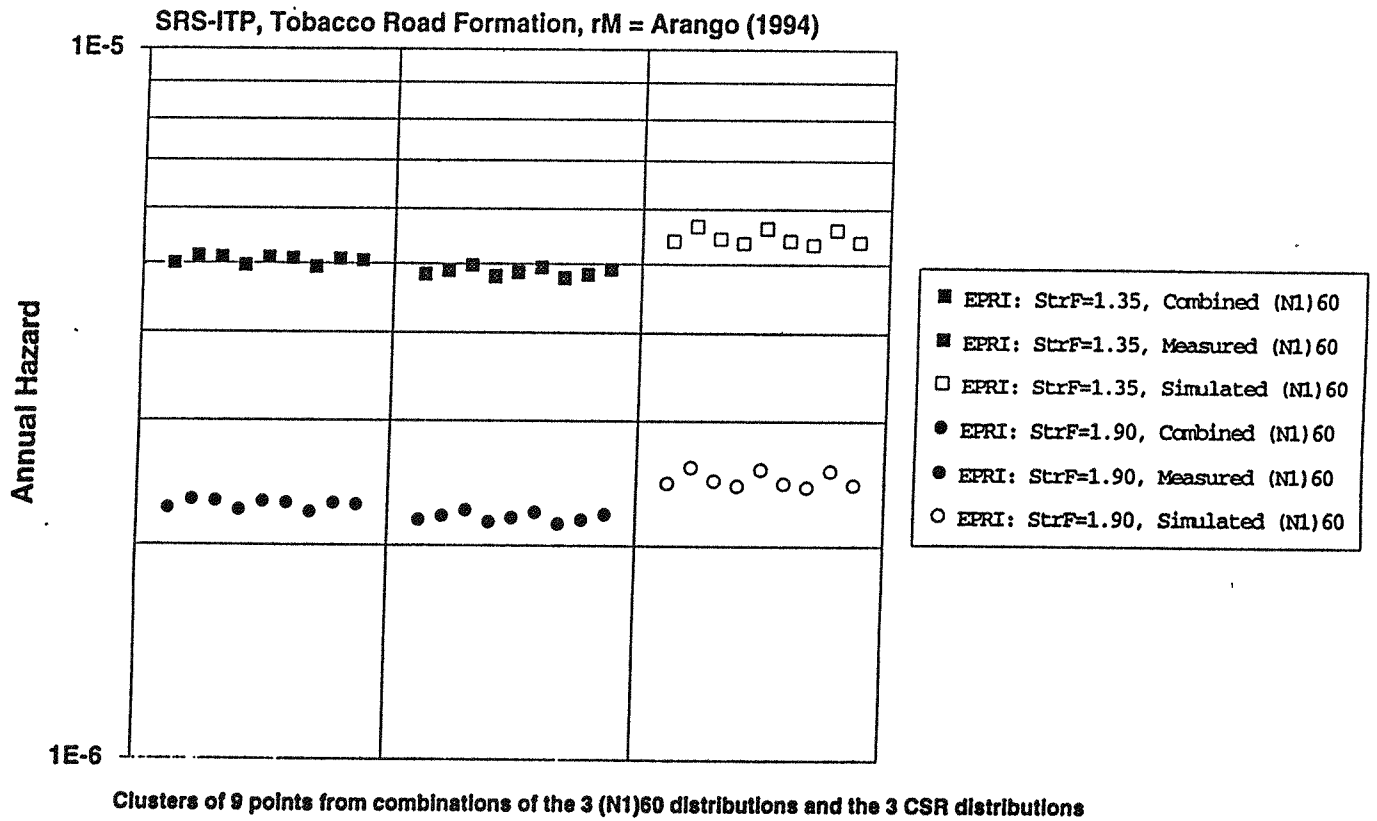


Figure 9.6-2 Annual liquefaction hazard computed by ASHLE